Title

Solar-Reflective “Cool” Walls: Benefits, Technologies, and Implementation

Authors

Levinson, Ronnen
Ban-Weiss, George
Berdahl, Paul
et al.

Publication Date

2019-04-01

DOI

10.20357/B7SP4H

Peer reviewed

doi:10.20357/B7SP4H

LBNL-2001296

BERKELEY LAB

Lawrence Berkeley National Laboratory

Solar-Reflective "Cool" Walls: Benefits, Technologies, and Implementation

Final Project Report

Ronnen Levinson[1]
George Ban-Weiss[2]
Paul Berdahl[1]
Sharon Chen[1]
Hugo Destaillats[1]
Nathalie Dumas[3]
Haley Gilbert[1]
Howdy Goudey[1]
Sébastien Houzé de l'Aulnoit[1]
Jan Kleissl[3]
Benjamin Kurtz[3]
Yun Li[2]
Yan Long[3]
Arash Mohegh[2]
Negin Nazarian[3]
Matteo Pizzicotti[3]
Pablo Rosado[1]
Marion Russell[1]
Jonathan Slack[1]
Xiaochen Tang[1]
Jiachen Zhang[2]
Weilong Zhang[3]

[1] Lawrence Berkeley National Laboratory
[2] University of Southern California
[3] University of California, San Diego

Energy Technologies Area

April 2019

Disclaimer

Energy Research and Development Division

FINAL PROJECT REPORT

Solar-Reflective "Cool" Walls: Benefits, Technologies, and Implementation

California Energy Commission
Gavin Newsom, Governor

April 2019 | CEC-500-2019-040

PREPARED BY:

Authors:

Ronnen Levinson[1,*]
George Ban-Weiss[2]
Paul Berdahl[1]
Sharon Chen[1]
Hugo Destaillats[1]
Nathalie Dumas[3]
Haley Gilbert[1]
Howdy Goudey[1]
Sébastien Houzé de l'Aulnoit[1]
Jan Kleissl[3]
Benjamin Kurtz[3]
Yun Li[2]
Yan Long[3]
Arash Mohegh[2]
Negin Nazarian[3]
Matteo Pizzicotti[3]
Pablo Rosado[1]
Marion Russell[1]
Jonathan Slack[1]
Xiaochen Tang[1]
Jiachen Zhang[2]
Weilong Zhang[3]

* Corresponding author (RMLevinson@LBL.gov)

[1] Lawrence Berkeley National Laboratory
One Cyclotron Road
Berkeley, CA 94720
http://LBL.gov

[2] University of Southern California
3650 McClintock Ave
Los Angeles, CA 90089
http://USC.edu

[3] University of California, San Diego
9500 Gilman Dr
La Jolla, CA 92093
https://UCSD.edu

Contract Number: EPC-14-010

PREPARED FOR:

California Energy Commission

David Hungerford
Project Manager

Virginia Lew
Office Manager
ENERGY EFFICIENCY RESEARCH OFFICE

Laurie ten Hope
Deputy Director
ENERGY RESEARCH AND DEVELOPMENT DIVISION

Drew Bohan
Executive Director

ACKNOWLEDGEMENTS

The authors thank the California Energy Commission for funding this project. We are grateful to David Hungerford of the Energy Commission for his guidance and management of the project. We also thank our industry partners 3M, Behr, Dexerials, Metal Construction Association (MCA), PPG, Saint Gobain, Sherwin Williams, Tex-Cote, and Valspar for supporting this project through donation of product samples, testing, analysis, and guidance. Tim Hebrink at 3M; Ginger Shi and Ming-Ren Tarng at Behr; Hiroko Furumi, Jerry Wu, and Tsutomu Nagahama at Dexerials; Scott Kriner at MCA; Bill Yanetti and Jim Moses, at Mitsubishi Chemical Composites America; Jackie Kulfan, Brian Kornish, David Story, and Michael Zalich at PPG; Olivier Rosseler and Rachel Pytel at Saint Gobain; Morgan Sibbald at Sherwin Williams; Akiko Lovan and Jay Haines at Tex-Cote; and Donde Anderson and Ted Best at Valspar have been extremely engaged and made important contributions to the project. We are also thankful for the expertise and thoughtful reviews from our voluntary Technical Advisory Committee members: Theresa Backus, formerly of United States Green Building Council; Peter Turnbull, Pacific Gas & Electric; Kurt Shickman, Global Cool Cities Alliance; Jeffrey Steuben, Cool Roof Rating Council; Victoria Ludwig, United States Environmental Protection Agency; David Sailor, Arizona State University; Hashem Akbari, Concordia University; Payam Bozorgchami, California Energy Commission; Bahman Habibzadeh, United States Department of Energy; Scott Kriner, MCA; and Ming-Ren Tarng, Behr.

The authors also thank the Cool Walls Working Group members who have volunteered to continue activities to advance the adoption of cool walls. These include Bill Dean, California Environmental Protection Agency; Bill Yanetti and Jim Moses, Mitsubishi Chemical Composites America; Brandon Bethke, Tempo Chemicals and Solutions; Craig Tranby, Los Angeles Department of Water and Power; David Story, PPG; Gary Ilalaole, Hawai'ian homeowner; Gen Minase, Rich Wipfler, and Yisheng Dai, Eastman Chemical; Howard Wiig, State of Hawai'i; Jeffrey Steuben, Cool Roof Rating Council; Jerry Wu, Hiroko Furumi, and Tsutomu Nagahama, Dexerials; Michael Biel, Ultimate Coatings; Olivier Rosseler, Saint Gobain; Peter Turnbull, Pacific Gas & Electric; Tim Hebrink, 3M; Tim Hyer, Gardner-Gibson; and Victoria Ludwig, United States Environmental Protection Agency. We would like to especially thank Dave Speiser of Vitro Architectural Glass for his help in hosting one of our natural exposure sites, and for retrieving and sending samples quarterly. We are very grateful for the assistance and guidance of Martha Van Geem, independent consultant, and Rahul Athalye, Energy Solutions (formerly at Pacific Northwest National Laboratory), to navigate the ASHRAE 90.1 amendment process.

Finally, the authors thank Ellen Thomas of Lawrence Berkeley National Laboratory for coordinating the Cool Walls Stakeholder Workshop.

This project was funded by the California Energy Commission under Contract EPC-14-010. It was also supported by the Assistant Secretary for Energy Efficiency and Renewable Energy, Office of Building Technology, State, and Community Programs, of the United States Department of Energy under Contract No. DE-AC02-05CH11231.

PREFACE

The California Energy Commission's Energy Research and Development Division supports energy research and development programs to spur innovation in energy efficiency, renewable energy and advanced clean generation, energy-related environmental protection, energy transmission and distribution and transportation.

In 2012, the Electric Program Investment Charge (EPIC) was established by the California Public Utilities Commission to fund public investments in research to create and advance new energy solution, foster regional innovation and bring ideas from the lab to the marketplace. The California Energy Commission and the state's three largest investor-owned utilities – Pacific Gas and Electric Company, San Diego Gas & Electric Company and Southern California Edison Company – were selected to administer the EPIC funds and advance novel technologies, tools, and strategies that provide benefits to their electric ratepayers.

The Energy Commission is committed to ensuring public participation in its research and development programs that promote greater reliability, lower costs, and increase safety for the California electric ratepayer and include:

- Providing societal benefits.
- Reducing greenhouse gas emission in the electricity sector at the lowest possible cost.
- Supporting California's loading order to meet energy needs first with energy efficiency and demand response, next with renewable energy (distributed generation and utility scale), and finally with clean, conventional electricity supply.
- Supporting low-emission vehicles and transportation.
- Providing economic development.
- Using ratepayer funds efficiently.

Solar-Reflective "Cool" Walls: Benefits, Technologies, and Implementation is the final report for the Solar-Reflective "Cool" Walls: Benefits, Technologies, and Implementation project (Contract Number EPC-14-010) conducted by Lawrence Berkeley National Laboratory. The information from this project contributes to the Energy Research and Development Division's EPIC Program.

For more information about the Energy Research and Development Division, please visit the Energy Commission's website at www.energy.ca.gov/research/ or contact the Energy Commission at 916-327-1551.

ABSTRACT

Raising the albedo (solar reflectance) of a building's walls reduces unwanted solar heat gain in the cooling season. This saves electricity and lowers peak power demand by decreasing the need for air conditioning. It can also cool the outside air, which can mitigate the urban heat island effect and also improve air quality by slowing the reactions that produce smog. This project quantified the energy savings, peak demand reduction, urban cooling, and air quality improvements attainable from solar-reflective "cool" walls in California; collaborated with industry to assess the performance of existing cool-wall technologies, and to develop innovative cool-wall solutions; and worked with state and federal government agencies, utilities, and industry to create a cool-wall infrastructure, including application guidelines, a product rating program, incentives, and building code credits.

Simulations indicate that cool walls provide annual energy savings, peak demand reduction, annual emission reduction, and summer heat island mitigation benefits comparable to those yielded by cool roofs, and are helpful across California and in most of the southern half of the United States (that is, in U.S. climate zones 1—4). Natural exposure trials conducted at three sites in California and another three sites across the United States indicate that cool-wall materials tend to stay clean and reflective. Significant advances were made in novel cool-wall technologies, such as fluorescent cool pigments that expand the color palette for cool-wall products. We prepared guidelines for the climate- and building-appropriate use of cool walls, convened a stakeholder workshop, and created a working group. Ongoing efforts seek to introduce or expand cool-wall provisions in building energy standards, green building programs, and energy efficiency incentive programs, and to develop a cool-wall product rating system.

Keywords: cool walls, cool roofs, solar reflectance, albedo, energy savings, peak power demand reduction, urban cooling, heat island mitigation, natural exposure, paint, cladding, fluorescent pigments, retroreflectors, guidelines, building energy standards, green building programs, utility incentives, product rating, EnergyPlus, TUF-IOBES, WRF

Please use the following citation for this report:

Levinson, Ronnen, Haley Gilbert, Jiachen Zhang, George Ban-Weiss, Jan Kleissl, Matteo Pizzicotti, Weilong Zhang, Nathalie Dumas, Benjamin Kurtz, Yan Long, Negin Nazarian, Arash Mohegh, Yun Li, Xiaochen Tang, Sharon Chen, Marion Russell, Sébastien Houzé de l'Aulnoit, Paul Berdahl, Pablo Rosado, Jonathan Slack, Howdy Goudey, and Hugo Destaillats. 2019. *Solar-Reflective "Cool" Walls: Benefits, Technologies, and Implementation*. California Energy Commission. Publication Number: CEC-500-2019-040.

TABLE OF CONTENTS

LIST OF FIGURES

Page

LIST OF TABLES

Page

EXECUTIVE SUMMARY

Introduction

California's total consumption of energy is the second highest in the nation, according to the United States Energy Information Administration. However, in terms of energy use per person, California ranked 48th (as of 2016), due in part to the state's aggressive energy efficiency efforts. Over the last 40 years, California's appliance and building efficiency standards have saved consumers billions of dollars in energy costs while helping to reduce greenhouse gas emissions and other pollutants that can harm the environment and human health.

In 2015, California passed the Clean Energy and Pollution Reduction Act (Senate Bill 350, de Leon, Chapter 547, Statutes of 2015) which established new clean energy, clean air, and greenhouse gas reduction goals for 2030 and beyond. Among other things, the act required the state to double statewide energy efficiency savings in electricity and natural gas by 2030.

One way to increase savings in buildings is to improve the efficiency of the building envelope – the roof, subfloor, exterior doors, windows, and exterior walls. For example, since 2005 California's Title 24, Part 6 Building Energy Efficiency Standards have prescribed the use of solar-reflective "cool" roofs. Cool roofs absorb less sunlight than conventional roofs, thereby reducing the need for air conditioning.

The Lawrence Berkeley National Laboratory Heat Island Group has collaborated with the roofing industry and California regulators for two decades to advance the development and climate-appropriate use of cool roofs. These efforts have been supported by the Energy Commission, the California Air Resources Board, Pacific Gas and Electric Company, the United States Environmental Protection Agency, and the United States Department of Energy. There is now a large body of cool-roof science; a well-established cool-roof rating system; cool-roof requirements in building energy standards as well as in voluntary incentive programs like Leadership in Energy and Environmental Design; and thousands of cool roofing products sold in the United States and abroad.

Cool *walls* are also promising. Increasing the solar reflectance, or "albedo," of the building envelope reduces its solar heating, which saves electricity and reduces power demand during peak hours by decreasing the need for air conditioning in warm weather. Raising envelope albedo can also cool the outside air, boosting energy savings and power demand reduction by decreasing the difference between the inside and outside air temperatures. It can also slow global warming by reflecting unwanted solar radiation out of the atmosphere, providing "global cooling."

Lowering urban surface and air temperatures also improves air quality by slowing the reactions that produce smog. High-albedo "cool" surfaces may also increase the need for heating energy (typically natural gas) in the heating season.

Although the solar energy per unit area striking an east or west wall in summer is about half of what hits a horizontal roof, California homes typically have about half as much wall insulation as roof insulation. For example, in a Fresno home with wood-framed walls, 2013 Title 24

requires R-38 (38 h·°F·ft²/BTU) ceiling insulation, but only R-19 wall insulation. Similarly, in a Fresno nonresidential building with light-mass, heavy-mass, or wood-framed walls, 2013 Title 24 requires R-26 roof insulation, but only R-6 to R-17 wall insulation. This suggests that the benefit of raising wall albedo – that is, the extent to which it reduces unwanted heat conducted into the interior space – is comparable to the benefit of increasing roof albedo.

A reflective coating (such as paint or stucco) or cladding (covering with another material) can increase wall albedo. Cool-wall products available today include (1) light-colored paints that reflect 60 percent to 90 percent of sunlight when new, but which may also lose reflectance as they get dirty; and (2) darker "cool-colored" paints that come in a wide palette, but typically reflect less than 50 percent of sunlight when new.

Project Purpose

Prior to this project, cool-wall benefits had not been rigorously quantified and existing studies of the energy-saving potentials of cool walls, and the effects of cool walls on the energy uses of neighboring buildings, or on the urban environment, were limited. The state of cool-wall technology had not been assessed through systematic rating of the initial and long-term performances of cool-wall products, and little infrastructure existed to promote the building- and climate-appropriate use of cool-wall surfaces, such as building energy-efficiency standards and incentive programs prescribing or crediting the use of cool walls.

Therefore, the research team's goals were to:

- Quantify the energy savings, peak demand reduction, urban cooling, and air quality improvements attainable from cool walls in California, through modeling.
- Collaborate with industry to assess the performance of existing cool-wall technologies, and to develop innovative cool-wall solutions.
- Work with state and federal government agencies, utilities, and industry to create a cool-wall infrastructure, including application guidelines, a product rating program, incentives, and building code credits.

Project Process

A team of researchers from Lawrence Berkeley National Laboratory, the University of Southern California, and the University of California at San Diego collaborated with 10 partners from the wall-product industry to advance the science and technology of cool walls. The research team undertook five parallel technical tasks, numbered 2 through 6.

- Task 2 used building-energy simulations to quantify how increasing wall albedo affects the cooling, heating, and lighting energy uses of a building and its neighbors. The simulations examined cool-wall savings for an isolated building and for a central building with neighbors. The researchers analyzed the extent to which the walls of a neighboring building shade and reflect sunlight to those of a central building to develop correction factors that can be applied to cool-wall savings simulated for an isolated building.

- Task 3 quantified the co-benefits (or penalties) of cool walls. The research team used building-, neighborhood-, and city-scale energy simulation models to assess pedestrian comfort, evaluate outdoor air temperature reductions, and explore how cool walls affect the energy-saving benefits of cool pavements. The team also examined air temperature reductions in an unconditioned home. In addition, researchers assessed the ability of a subset of cool-wall coating materials to remove nitrogen oxide pollution from the air in the lab, and estimated air quality impacts in urban areas using wall areas derived from a real-world building dataset.
- Task 4 assessed the performance of available and prototype cool-wall technologies, primarily the ability to reflect sunlight, through field and laboratory measurements. The project team developed metrics and methods to evaluate solar reflectance, de-pollution efficacy, and other material properties, then measured how solar reflectance changed when products were exposed outdoors at sites across California and the United States. Researchers paid special attention to the performance of self-cleaning and de-polluting photocatalytic materials.
- Task 5 explored innovative cool-wall technologies, including self-cleaning materials, fluorescent cool pigments, and retroreflective materials.
- Task 6 promoted the infrastructure needed to advance the climate- and building-appropriate use of cool walls. This included developing cool-wall application guidelines, hosting a cool-wall stakeholder workshop, and exploring and enhancing the treatment of cool walls in building standards and incentive programs.

Project Results

Benefit Analysis

The researchers found that cool walls provide annual energy savings, energy cost savings, peak power demand reduction, annual emission reduction, and summer heat island mitigation benefits comparable to those yielded by cool roofs. Highlights of the researchers' findings include:

- Isolated-building simulations of two residential and eight commercial building prototypes configured according to current, 1980s, and pre-1980 construction practices predicted that raising wall albedo to 0.60 (dull- or off-white wall) from 0.25 (conventional wall) will save energy, reduce energy cost, lower peak power demand, and decrease emissions of greenhouse gases (like carbon dioxide) and criteria pollutants (such as nitrogen oxides and sulfur dioxide) across California. These results are based on total annual heating, ventilation, and air conditioning energy use, and incorporate both cooling savings and heating penalties.
- Cool walls lowered annual heating, ventilation, and air conditioning energy cost per unit modified surface area by $0.07-$1.70 per square meter in single-family homes, $0.10-$2.10 per square meter in medium offices, and $0.00-$4.30 per square meter in stand-alone retail stores. Cool walls also reduced whole-building annual heating, ventilation, and air conditioning energy use by 3 percent to 25 percent in single-family homes, 0.5

percent to 3.7 percent in medium offices, and 0.0 percent to 9.0 percent in stand-alone retail stores. Finally, cool walls decreased annual heating, ventilation, and air conditioning carbon dioxide equivalent emissions per unit modified surface area by 0.0 kilograms to 3.4 kilograms per square meter in single-family homes, 0.17 kilograms to 4.5 kilograms per square meter in medium offices, and 0.16 kilograms to 9.2 kilograms per square meter in stand-alone retail stores.

- The simulations found that energy use, energy cost, and emission savings from the oldest vintage buildings were generally three to six times greater than those from the new vintage. The cool-wall savings from the oldest vintage are important because they represent more than 60 percent of California's existing building stock.
- Isolated-building simulations found that cool walls also save energy, reduce energy cost, lower peak power demand, and decrease emissions in United States climate zones 1 - 4, which is roughly the southern half of the country.
- One can multiply isolated-building cool-wall savings by a "solar availability factor" to account for shading and reflection by neighboring walls. A solar availability factor is the ratio of sunlight striking the central (modeled) building wall in the presence of the neighboring wall to that received in the absence of the neighboring wall. For example, solar availability factors for the walls of a single-family home in a residential neighborhood in Fresno, California range from about 0.5 to 0.9, depending on whether the wall faces a side, back, or front neighbor.
- Simulations of building arrays found that thermal comfort changes for pedestrians walking next to a cool wall are small and will go unnoticed by most people.
- Simulations of building arrays found that cool walls decrease air temperature inside unconditioned buildings. Since buildings without air conditioning generally feel cold at night and warm during the day, the interior air temperature reduction corresponds to a slight worsening of thermal comfort at night and an improvement of thermal comfort during the day. However, the temperature changes are so small that they will go unnoticed by most people.
- Urban climate simulations found that in summer in Los Angeles County, the ratio of the daily average air temperature reduction from cool walls to that from cool roofs is about 86 percent, making their heat island mitigation benefits comparable. Cool walls (roofs) can reduce summertime daily average canyon air temperature – i.e., the temperature of the air in the U-shaped space formed by buildings on opposite sides of a street – by 0.048—0.054 Kelvin (0.058—0.060 Kelvin) per 0.10 increase in wall (roof) albedo.

Technology Assessment

The research team found that there are many cool-wall products available commercially, and that they tend to stay clean and reflective.

- After 24 months of exposure at the three California sites, observed albedo losses for all 69 wall materials did not exceed 0.10, and for 67 of 69 materials did not exceed 0.05. (Albedo is measured on a scale of 0 to 1, where 0 means that no sunlight is reflected

and 1 means that all sunlight is reflected.) After 2 years of exposure at the three United States sites, albedo losses for 51 of 55 wall materials did not exceed 0.05.

- Researchers consider the albedo losses observed to date at the California and United States sites modest when compared to results from similar studies of roofing materials. A 3-year study conducted in 2010 by the same research group (data unpublished) exposed 27 roofing materials at the same three United States sites at 5° tilt (low-slope roofing) and 45° tilt (high-slope roofing). After 24 months of exposure, roof albedo losses ranged as high as 0.28.
- In the 77 materials tested, the researchers observed high albedo retention in fluoropolymer-based coatings and products with "self-cleaning" or "dirt-resistant" formulations.
- Two photocatalytic and self-cleaning architectural fabrics showed excellent year-round retention of initial albedo, in contrast with a non-photocatalytic control that showed significant soiling accumulation during the dry season and modest cleaning during the rainy season. The two photocatalytic fabrics were tested for their ability to remove nitrogen oxides from the urban atmosphere. In most cases, a measurable nitric oxide removal efficiency was partially offset by the formation of nitrogen dioxide as oxidation byproduct. However, a net nitrogen oxide deposition was present in most cases.

Technology Development

Fluorescence (re-emission at longer wavelengths of light absorbed at shorter wavelengths) can expand the palette of colors for cool-wall products, while retroreflection (reflection of light toward its source) can increase the fraction of wall-reflected light that escapes the city.

- The research team built a calorimetric instrument that measures effective solar reflectance, or the fraction of incident solar energy rejected by the combination of reflectance and fluorescence.
- Results showed that pink-red coatings colored with a fluorescent ruby pigment (aluminum oxide doped with chromium) can reject up to 15 percent of incident solar energy by invisibly re-emitting absorbed visible light. Blue, green, and blue-black coatings colored with fluorescent Egyptian blue or Han blue pigments provide a similar benefit.
- The fluorescent blue pigments may also be useful in fabrication of high-performance luminescent solar concentrators for photovoltaic panels.
- The greatest challenge in retroreflective wall design appears to be the need to operate at large incidence angles to reflect a substantial portion of incident sunlight.
- The most promising retroreflector design was a two-surface retroreflector with perpendicular metal mirror faces.

Infrastructure Development

The research team is working to expand and improve building energy standards, green building programs, and energy efficiency inventive programs that already consider cool walls or cool roofs.

- Research showed that there are existing cool-wall measures in building codes/standards, green building programs, and incentive programs. However, these measures should be enhanced to maximize cool-wall benefits by revising specifications and/or expanding to more climate zones.
- There is interest and momentum to develop (a) a cool-wall rating program; (b) new cool-wall measures in building codes/standards, such as California's Building Energy Efficiency Standards; (c) product incentives to manufacturers or consumers; (d) United States Environmental Protection Agency ENERGY STAR® certification; and (e) a United States Green Building Council Leadership in Energy and Environmental Design pilot credit.
- As planned, the researchers hosted a cool walls workshop for stakeholders, and developed cool-wall guidelines to specify the use of and benefits of cool walls.

Benefits to California

Based on this project, the researchers expect cool walls to yield ratepayer benefits such as greater electricity reliability, lower costs, and increased safety by saving energy, reducing peak power demand, cooling the urban environment, and reducing harmful urban air pollution. Results highlighted above show that raising wall albedo lowers annual heating, ventilation, and air conditioning energy cost and emissions for both residential and nonresidential buildings across California, and as a bonus across roughly the southern half of the United States. A case study in Los Angeles County found that the urban heat island mitigation (outside air temperature reduction) benefits of cool walls are comparable to those of cool roofs.

One can ballpark statewide energy cost savings and greenhouse gas emission reductions by focusing on the benefits accrued to single-family homes, which make up the largest share of California's building stock. County assessor records indicate that the combined floor space of single-family homes statewide is about 1.2 billion square meters, while the single-family home prototype used in this project's simulations has a ratio of net wall area (gross wall area minus openings) to floor area of 86 percent. Therefore, the combined net wall area of single-family homes in California is about 1.1 billion square meters. After considering building age and adjusting for shading and reflection by neighboring buildings, the average annual heating, ventilation, and air conditioning energy cost savings and carbon dioxide equivalent emission reduction per unit area of cool wall for single-family homes in California are roughly $0.50 per square meter and 0.5 kilograms per square meter, respectively. Multiplying each rate by the statewide net wall area yields for the stock of single-family homes annual energy cost savings of about $500 million, and annual carbon dioxide equivalent emission reductions of about 0.5 million metric tons. Further savings would accrue from cool walls on other buildings, including but not limited to offices and stores.

The results of this project strongly suggest the need for follow-up studies, including:

- A Code and Standards Enhancement initiative for inclusion of cool walls in the 2022 edition of the California Title 24 building energy efficiency standards.
- Cool-wall measurement and demonstration projects for residential and nonresidential buildings in California.
- Continuation of the United States natural exposure trials through their conclusion in 2021.
- Adaptation to wall materials of the lab-aging practice currently available for roofing products (ASTM Standard D7897).

CHAPTER 1: Introduction

Cool-wall Technology

Increasing the solar reflectance, or albedo, of the building envelope reduces its solar heating, which saves electricity and reduces power demand during peak hours by decreasing the need for air conditioning in warm weather. Raising envelope albedo can also cool the outside air, boosting energy savings and demand reduction by decreasing the difference between the inside and outside air temperatures. It can also slow global warming by reflecting unwanted solar radiation out of the atmosphere, providing "global cooling."

Lowering urban surface and air temperatures also improves air quality by slowing the reactions that produce smog. High-albedo "cool" surfaces may also increase the need for heating energy (typically natural gas) in the heating season.

High wall albedo can be attained with a reflective coating (such as paint or stucco) or cladding. Cool-wall products available today include light-colored paints that reflect 60 percent to 90 percent of sunlight when new, but may lose reflectance as they soil; and darker "cool colored" paints that come in a wide palette, but typically reflect less than 50 percent of sunlight when new.

While the solar energy per unit area striking an east or west wall in summer is about half that incident on a horizontal roof, California homes typically have about half as much wall insulation as roof insulation. For example, in a Fresno home with wood-framed walls, 2013 Title 24 requires R-38 (38 h·°F·ft²/BTU) ceiling insulation, but only R-19 wall insulation. Similarly, in a Fresno nonresidential building with light mass, heavy mass, or wood-framed walls, 2013 Title 24 requires R-26 roof insulation, but only R-6 to R-17 wall insulation. This suggests that the benefit of raising wall albedo – that is, the extent to which it reduces unwanted heat conduction into the conditioned space – is comparable to that of increasing roof albedo.

Project Objective and Scope

Solar reflective "cool" roofs have been established in California as an effective building energy efficiency measure. Cool walls are also promising. However, prior to this project, cool-wall benefits had not been rigorously quantified, the state of cool-wall technology had not been assessed, and little infrastructure for advancing the building- and climate-appropriate use of cool wall surfaces existed. Therefore, the research team set out to (a) through modeling, quantify the energy savings, peak demand reduction, urban cooling, and air quality improvements attainable from cool walls in California; (b) collaborate with industry to assess the performance of existing cool-wall technologies, and to develop innovative cool-wall solutions; and (c) work with state and federal government agencies, utilities, and industry to create a cool-wall infrastructure, including application guidelines, a product rating program, incentives, and building code credits.

The results of this research will provide ratepayer benefits such as greater electricity reliability, lower costs, and increased safety by saving energy, reducing peak power demand, cooling the urban environment, and reducing harmful urban air pollution.

Overview of Project Technical Tasks

This project had five technical tasks, numbered 2 through 6:

- Task 2: Quantify through building-energy simulations how increasing wall albedo affects the cooling, heating, and lighting energy uses of a building and its neighbors.
- Task 3: Quantify through heat transfer analysis and climate modeling how cool walls affect the urban environment (e.g., air temperature, mean radiant temperature, and air quality) and enhance the benefits of solar-reflective pavements.
- Task 4: Assess through field and laboratory measurements the performance (initial albedo, aged albedo, and – where applicable – de-pollution efficacy) of available and prototype cool-wall technologies.
- Task 5: Collaborate with industry to develop innovative cool-wall solutions with higher and/or more directional reflectance.
- Task 6: Promote the infrastructure needed to promote the appropriate use of cool walls, including guidelines, product rating, utility rebates, ENERGY STAR qualification, and credits in building energy standards and energy-efficiency programs.

Task activities and outcomes are summarized in Chapters 2 through 6, with details provided in Appendices A through R.

CHAPTER 2:
Quantifying Cooling, Heating, and Lighting Energy Use Savings (Task 2)

Task 2 quantified how increasing wall albedo affects the cooling, heating, and lighting energy uses of a building and its neighbors through building-energy simulations. The research team simulated cool walls savings for an isolated building with EnergyPlus in Task 2.1, while savings for a building with neighbors were modeled with the Temperature of Urban Facets – Indoor Outdoor Building Energy Simulator (TUF-IOBES) in Task 2.2. Researchers analyzed the extent to which the walls of a neighboring building shaded and reflected sunlight to those of a central building in Task 2.3 to develop correction factors that can be applied to cool-wall savings simulated for an isolated building.

Simulated Heating, Ventilation, and Air Conditioning Energy Savings in an Isolated Building (Task 2.1)

Solar-reflective "cool" walls reduce absorption of sunlight by the building envelope, which may decrease cooling load in warm weather and increase heating load in cool weather. Changes to annual heating, ventilation, and air conditioning (HVAC) energy use depend on climate, wall construction, wall orientation, building geometry, HVAC efficiency, and operating schedule. Changes to annual energy cost and energy-related emissions vary with local energy prices and emission factors. The project researchers used EnergyPlus to perform more than 100,000 building energy simulations, spanning 10 different building categories, three building vintages, 16 California climate zones, and 15 United States climate zones. The simulations varied parameters such as wall albedo (solar reflectance), roof albedo, combination of walls modified, and building orientation. Cool walls yielded annual savings in source energy and energy cost, as well as reductions in emissions (carbon dioxide [CO_2], carbon dioxide equivalent [CO_2e], nitrogen oxide [NO_x], and sulfur dioxide [SO_2]) in all California climate zones and in warm United States (ASHRAE) climate zones. Cool walls also yielded HVAC peak power demand reduction in all California and United States climate zones.

In California, cool walls reduced whole-building annual HVAC energy use 3.0 percent to 25 percent in single-family homes, 0.5 percent to 3.7 percent in medium offices, and 0.0 percent to 9.0 percent in stand-alone retail stores. In warm United States climates – zones 1A (Miami, Florida through 4B (Albuquerque, New Mexico) – cool walls reduced whole-building annual HVAC energy use 2.0 percent to 8.5 percent in single-family homes, 0.0 percent to 4.2 percent in medium offices, and -0.5 percent to 5 percent in stand-alone retail stores. Cool walls also yielded small annual HVAC source energy savings in some cold United States climates – zones 4C (San Francisco, California) through 7 (Duluth, Minnesota) – for certain building categories and vintages. Annual HVAC source energy savings intensities (savings per unit of surface area

modified) from east, south, and west walls were similar, and always larger than those from north walls.

In California, cool walls lowered annual energy cost intensity (per modified surface area) $0.07/square meter (m²) to $1.7/m² in single-family homes, $0.10/m² to $2.1/m² in medium offices, and $0.0/m² to $4.3/m² in stand-alone retail stores. In warm United States climates (zones 1A through 4B) cool walls lowered annual energy cost intensity $0.1/m² to $1.1/m² in single-family homes, $0.0/m² to $1.8/m² in medium offices, and $0.0/m² to $3.7/m² in stand-alone retail stores.

While walls often receive less incident solar energy per unit area than roofs, they are also less insulated than roofs. Therefore, savings intensities from modifying the four walls (albedo increase 0.35) were often comparable to those from modifying the roof (albedo increase 0.30 in residential and 0.40 in commercial). The ratio of whole-building savings from cool walls (raising the albedo of all four walls) to that from a cool roof also depends on the ratio of net wall area (wall area excluding openings) to roof area. In California, the ratio of whole-building cool-wall savings to cool roof savings was 1.5 to 3.5 in single-family homes, 0.40 to 1.0 in medium offices, and 0.20 to 0.85 in stand-alone retail stores. In warm United States climates (zones 1A through 4B), the ratio of whole-building cool-wall savings to cool roof savings was 1.1 to 3.0 in single-family homes, 0.20 to 1.9 in medium offices, and 0.30 to 2.1 in stand-alone retail stores.

Single-family homes are the most common buildings in California and the United States. Figure 1 shows annual whole-building HVAC fractional savings and annual energy cost savings intensity (per unit of modified area) for homes of different vintages in California upon raising the albedo of all walls by 0.35 or upon increasing roof albedo by 0.30. Figure 2 shows the same information for the United States.

The complete study is presented in the Task 2.1 report, Simulated Heating, Ventilation, and Air Conditioning Energy Savings in an Isolated Building (Appendix A). An article based on this work has been published in *Energy and Buildings* (Rosado and Levinson 2019).

Figure 1: Annual Heating, Ventilation, and Air Conditioning Savings for Single-family Homes in California

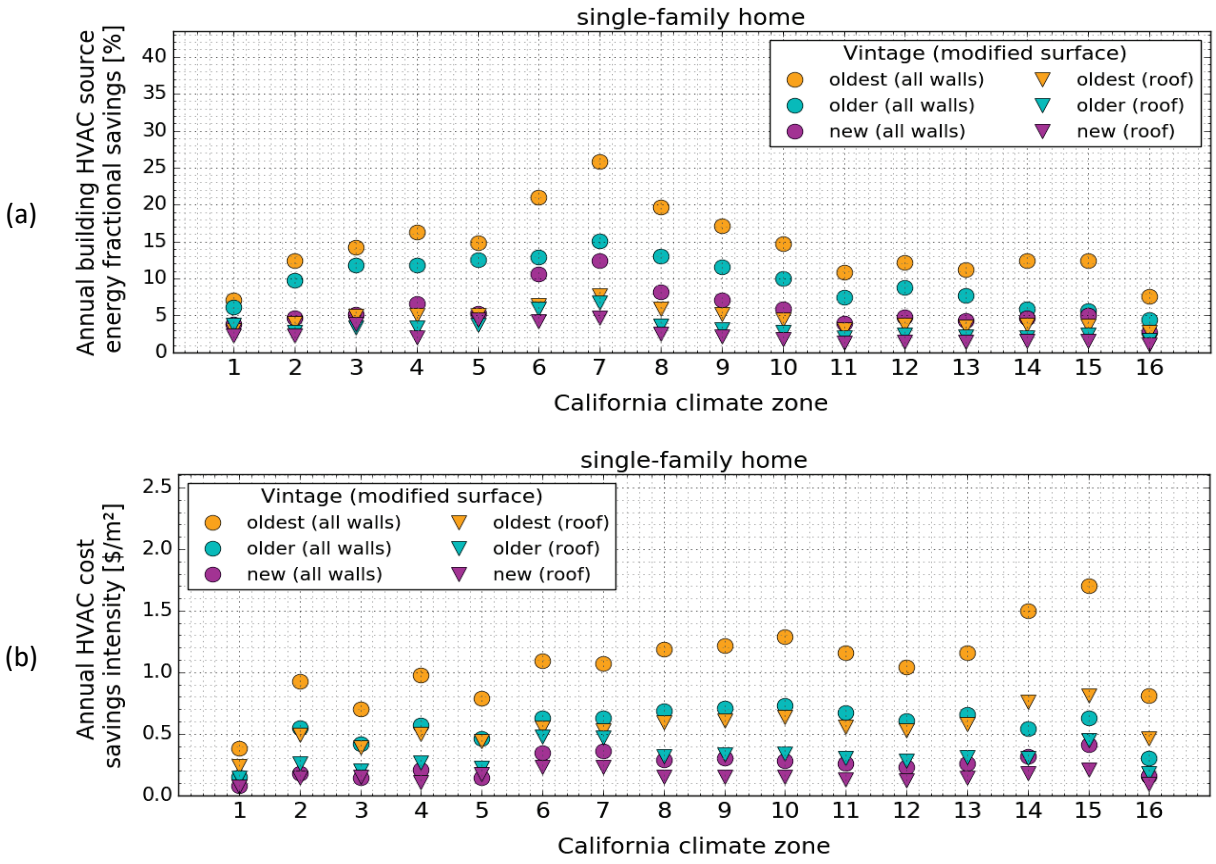

EnergyPlus simulations of annual HVAC savings in California homes by climate zone and vintage, showing (a) whole-building source energy fractional savings and (b) energy cost savings intensity.

Source: Lawrence Berkeley National Laboratory

Figure 2: Annual Heating, Ventilation, and Air Conditioning Savings for Single-family Homes in United States

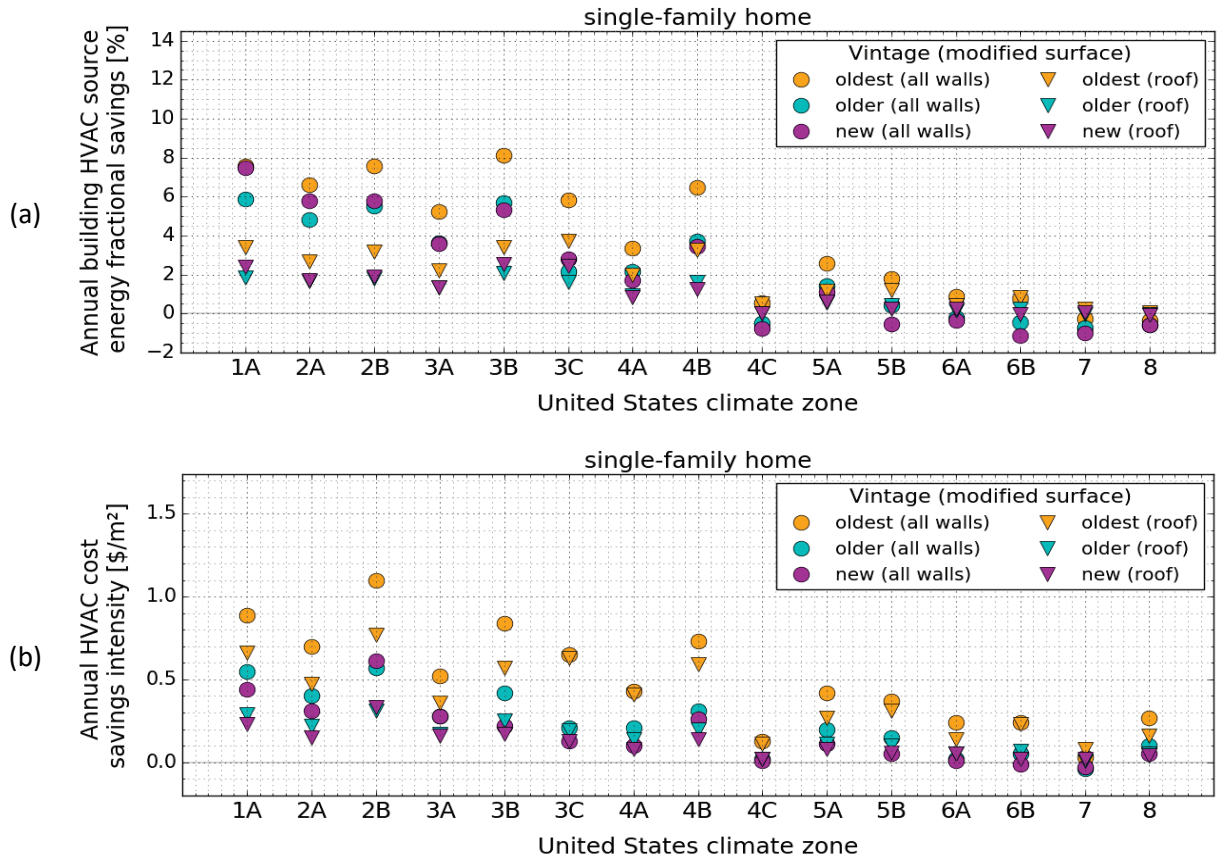

EnergyPlus simulations of annual HVAC savings in United States homes by climate zone and vintage, showing (a) whole-building source energy fractional savings and (b) energy cost savings intensity.

Source: Lawrence Berkeley National Laboratory

Effect of Neighboring Cool Walls on Heating, Ventilation, and Air Conditioning Loads (Task 2.2)

High-albedo ("cool") walls are exterior building walls with surface (usually paint) properties that increase reflection of solar radiation. Cool walls also increase heat transfer between urban surfaces. Consider a central building with neighbors. Raising the albedo of neighboring walls can increase reflection of downwelling sunlight – that is, light traveling downward from the sun or sky – from neighboring walls to the walls and windows of the central building. This can increase cooling load, decrease heating load, and reduce the need for artificial lighting in the central building. Theory shows that the solar heat gain of a central building wall in a regularly spaced array of rectangular buildings is proportional to the area of the modified neighboring building walls, the increase in neighboring wall albedo, the view factor from the neighboring

wall to the central wall, and the solar absorptance[1] (one minus albedo) of the central building wall. This analysis supplements the Task 2.1 report presented in Appendix A by using the Temperature of Urban Facets – Indoor Outdoor Building Energy Simulator (TUF-IOBES) model to account for building-to-building interactions on building heating and cooling loads.

The indoor and outdoor building thermal environments in a three-dimensional urban area with a 5 × 5 array of identical buildings about 23 meters apart are simulated. The indoor and outdoor energy balances are dynamically coupled and forced by outdoor weather conditions, building envelope properties, urban material properties, indoor heat sources, and HVAC systems. Building energy use effects of cool walls are quantified for a pre-1978 apartment building in Fullerton, California (Orange County, California climate zone 8).

Both diffusely reflecting and retroreflective neighboring cool walls are examined. Retro-reflective cool walls improve upon diffusely reflecting cool walls by reflecting incoming beam radiation upwards. Retroreflective walls boost the fraction of sunlight reflected out of the urban canyon.[2]

Figure 3a shows that daytime heating loads are near zero so changing wall albedo does not modify the daytime heating load. Figure 3b shows that nighttime cooling loads are small so changing wall albedo mostly influences the daytime cooling load.

Figure 3: Heating and Cooling Load Cycles for Central Building with Neighbors

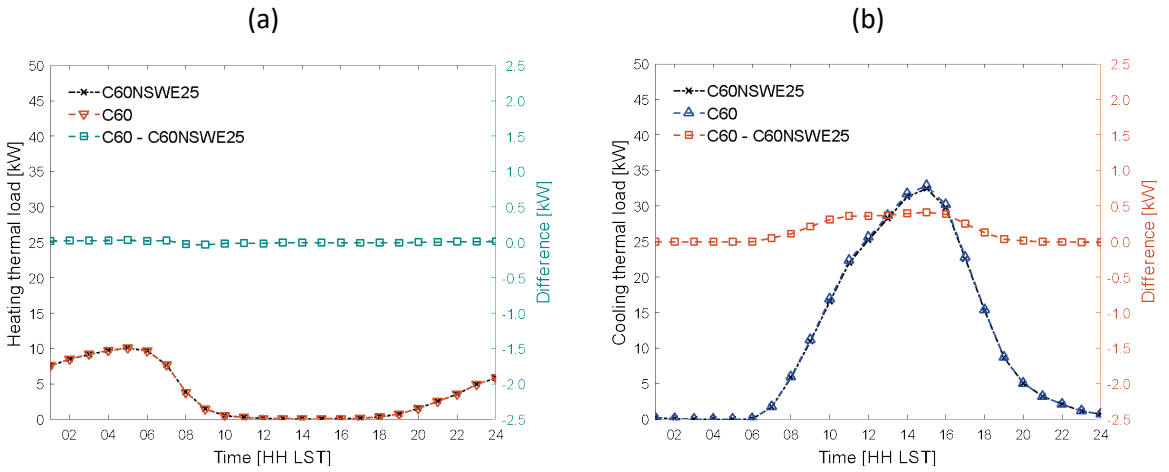

TUF-IOBES simulations of average diurnal cycles of (a) heating load and (b) cooling load for the central building – a pre-1978 apartment building in Fullerton, California. The results show the effect of raising the albedo of the neighboring walls when all central walls are cool. C60NSWE25: All central building walls are cool (diffuse reflectors with albedo 0.60), while neighboring walls are conventional (diffuse reflectors with albedo 0.25). C60: All central and neighboring building walls are cool.

Source: University of California, San Diego

[1] The absorptance of a surface is its effectiveness in absorbing radiant energy. A surface with solar absorptance 0 absorbs no sunlight, while a surface with absorptance 1 absorbs all sunlight.

[2] Lambertian (perfectly diffuse) reflection distributes reflected radiation equally in all directions. Retroreflection reflects radiation back to the source. See Figure 18 for an illustration.

Raising the neighboring wall albedo increases annual cooling load of the central building by 1.2 megawatt hours (MWh) (1.2 percent) due to increased solar radiation reflected from the neighboring buildings towards the central building. The negligible effect of cool walls on annual heating loads is likely an artifact of the way that our model predicts essentially zero daytime heating load.

The cooling-load increase for the central building upon raising the albedo of all neighboring walls (1.2 MWh or 1.2 percent) is smaller than the cooling-load decrease for the central building upon raising the albedo of its own walls (5.0 MWh, or 5.0 percent). Considering the interactions between buildings, the combined cool-wall effect on all buildings is net positive.

Using retroreflective cool walls (albedo 0.60) on all neighboring buildings lowers the annual cooling load of the central building by 3.3 MWh (4.0 percent) with respect to using Lambertian cool walls (also albedo 0.60) on all neighboring buildings. However, the cooling benefit comes at the expense of a 0.9 MWh (2.6 percent) increase in annual heating load. The net effect of changing to a retroreflective wall from a Lambertian wall on the central building is a reduction in average solar radiation incident on walls, which decreases cooling loads and increases heating loads.

The complete study is presented in the Task 2.2 report Effect of Neighboring Cool Walls on Heating, Ventilation, and Air Conditioning Loads (Appendix B).

Using Solar Availability to Scale Heating, Ventilation, and Air Conditioning Energy Savings (Task 2.3)

The solar availability (incident solar radiation) of a central (modeled) building can be reduced by shadows cast by neighboring buildings, and increased by sunlight reflected from neighboring buildings. This study evaluates the solar availability factor of a central building wall, defined as the ratio of sunlight incident on the central building wall in the presence of the neighboring wall to that incident in the absence of the neighboring wall.

One can scale cool-wall cooling savings, heating penalties, or HVAC savings simulated for an isolated central building (no neighbors) by the solar availability factor to account for interaction with the neighboring wall. One can also assess the effect of raising neighboring wall albedo on the solar availability of the central building wall. This analysis emphasizes simplicity, so that its results can be applied knowing only the canyon aspect ratio (ratio of building height to building separation; Figure 4), city, and month. It does not consider shading or reflection by surfaces other than neighboring walls, such as trees.

Monthly values of solar availability factor were evaluated in 17 climates across the United States, including three in California, for north, east, south, and west central walls, over a wide range of canyon aspect ratio (height/width). Figure 5 presents results for four representative aspect ratios – 0.2, 1, 2, and 10.

Figure 4: Canyon Aspect Ratio (Building Height / Separation)

Scale drawings of canyon aspect ratios 0.2, 1, 2, and 10.

Source: Lawrence Berkeley National Laboratory

In Fresno, California, monthly solar availability factor ranges from 0.90 to 0.96 for central walls facing north, east, south, or west when the aspect ratio is 0.2 (two-story single-family homes across a street) and both the central and neighboring walls are conventional (albedo 0.25). These solar availability factors are close to unity because the sun-facing wall is rarely shaded in a canyon with low aspect ratio. Monthly solar availability factors decrease as aspect ratio rises, falling to 0.06 – 0.24 at an aspect ratio of 10 (adjacent 10-story buildings on the same side of the street). Seasonal variation in monthly solar availability factor also increases with aspect ratio, and is greatest for south central walls (Figure 5).

Percentage increases in solar availability factor (equivalent to percentage increases in irradiance) for a central wall upon raising the albedo of a neighboring wall to 0.60 (cool) from 0.25 (conventional) are modest for east, south, and west central walls, ranging 0.9 – 4.1 at aspect ratio 0.2 to 11.0 – 32.9 at aspect ratio 10. Percentage increases for a north central wall are greater because a north wall receives little beam sunlight and faces a well-illuminated south wall.

The complete study is presented in the Task 2.3 report, Using Solar Availability to Scale Heating, Ventilation, and Air Conditioning Energy Savings (Appendix C). An article based on this work has been published in *Solar Energy* (Levinson 2019).

Figure 5: Monthly Solar Availability Factors in Fresno, California

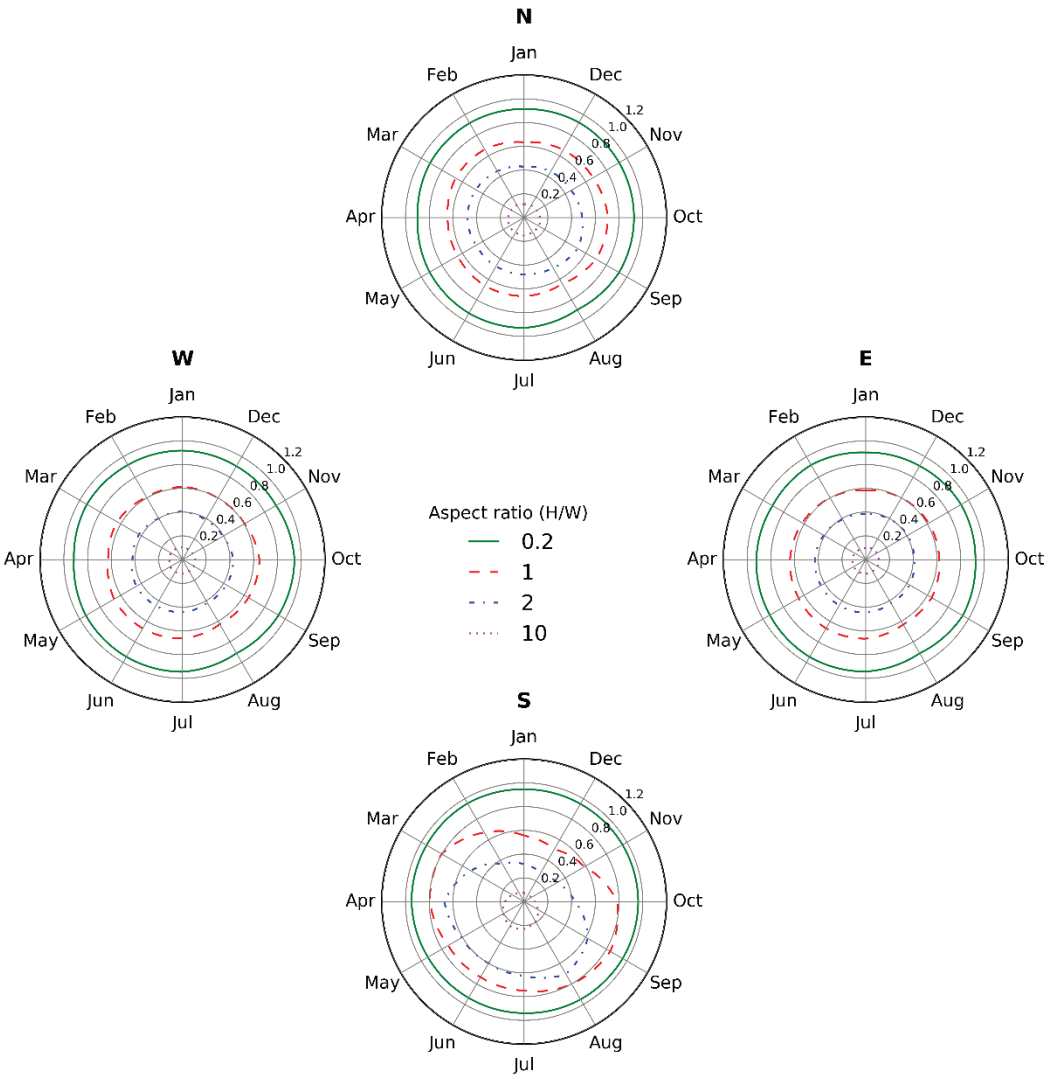

Monthly solar availability factors for a north (N), east (E), south (S), or west (W) conventional central wall (albedo 0.25) with a conventional neighboring wall (albedo 0.25), shown for canyon aspect ratios 0.2, 1, 2, and 10 in Fresno, California. Ground albedo was set to 0.20.

Source: Lawrence Berkeley National Laboratory

CHAPTER 3:
Quantifying the Environmental and Energy Co-benefits of Cool Walls (Task 3)

Task 3 quantified the co-benefits (or penalties) of cool walls. Task 3.1 used the TUF-IOBES model to assess pedestrian comfort, while Task 3.2 applied the Weather Research and Forecasting Model (WRF) to evaluate outdoor air temperature reductions. EnergyPlus simulations in Task 3.3 explored how cool walls affect the energy-saving benefits of cool pavements. Task 3.4 used TUF-IOBES to assess air temperature reductions in an unconditioned home. Task 3.5 assessed the city-level NO_x deposition from adopting self-cleaning walls using laboratory-measured dry deposition velocities and wall area derived from a real-world building dataset.

Pedestrian Mean Radiant Temperature and Thermal Comfort (Task 3.1)

Walls are made more reflective to reduce building solar heat gain, but cool walls also affect the thermal environment of pedestrians by (a) increasing shortwave (solar) radiation striking the pedestrian; (b) decreasing longwave (thermal infrared) radiation incident on the pedestrian; and (c) lowering the outside air temperature. The magnitudes of these sometimes-opposing effects on pedestrians are quantified through human comfort models. Human comfort models attempt to emulate the typical human perception of environmental conditions through thermal comfort indices.

The research team analyzed thermal comfort for homogeneous neighborhoods of either multi-family residences, single-family residences, or medium office buildings. One year of typical weather data was input to a neighborhood microclimate model in three different California climate zones to understand the comfort effects of raising wall albedo on a pedestrian walking parallel to a wall 5 feet away from the central building in a neighborhood. The latest version of the Pierce two-node model was used to compute pedestrian thermal comfort considering radiation from the sun, sky, and surrounding surfaces (for example, walls); wind speed; air temperature; humidity; metabolic activity (walking); and clothing. The principal model output is the Standard Equivalent Temperature, SET*. A higher SET* indicates that a human feels warmer, and a lower SET* indicates feeling cooler.

The insulation provided by clothing is assumed to vary between winter and summer: from November to April, the pedestrian is assumed to wear trousers, a T-shirt, and a long-sleeve sweater; from May to October, the pedestrian is assumed to wear trousers and a T-shirt.

The researchers calculated longwave radiation incident on the pedestrian using wall, window, and ground thermal emittances of 0.90, 0.84, and 0.95, respectively. Conventional (base case)

and cool (reflective) walls were assigned albedos (shortwave reflectances) of 0.25 and 0.60, respectively. The albedo of the ground was set to 0.10 (aged asphalt concrete).

Near a multi-family residence in Fullerton, California (Orange County; California climate zone 8) with conventional walls of albedo 0.25, the annual average hourly SET* is about 18 ˚C at night and up to 30 ˚C during the day. Figure 6 shows that the pedestrian thermal comfort change induced by raising wall albedo is small. During the day, cool walls raise SET* by up to 0.5 ˚C on average over the year. At night, cool walls lower SET* by up to 0.3 ˚C on average over the year. The smallest SET* rise occurs for a pedestrian near the north wall. The largest SET* rise occurs for the pedestrian near the south wall at noon in winter since winter solar irradiation on the south wall is the most of any wall orientation during any season. The absolute SET* difference induced by making walls more reflective is benign at less or equal to 0.2 ˚C over half of the time over the year. While SET* increases over 0.5 ˚C are occasionally observed, they occur exclusively during clear winter days when the pedestrian is more likely to experience a cold sensation. In that situation the SET* increase is beneficial to pedestrian thermal comfort. SET* differences by building type and climate zone were negligible.

Figure 6: Increase in Standard Equivalent Temperature upon Raising Wall Albedo

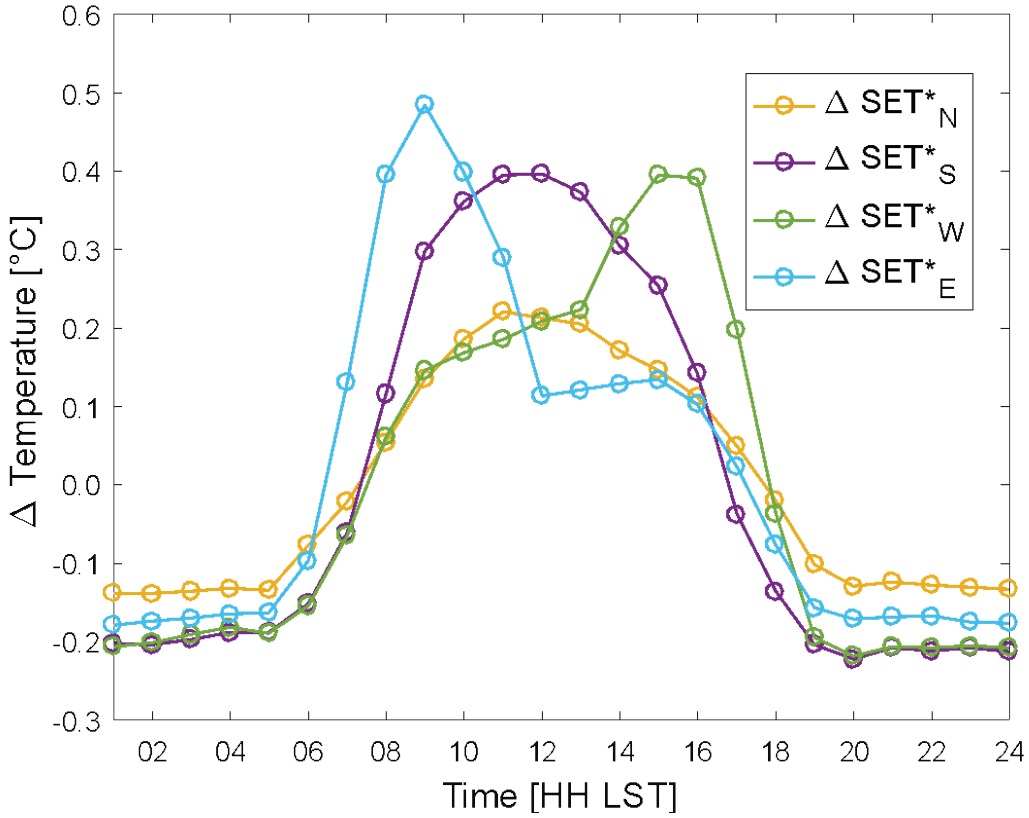

Average (over the year) SET* increase ΔSET^* when raising wall albedo to 0.60 (cool) from 0.25 (conventional) for the multi-family residence in Fullerton, California.

Source: University of California, San Diego

SET* rises during daytime result from increased reflection of solar radiation towards the pedestrian. But cool walls also lower local air temperatures which counteracts radiative effects. The results are sensitive to the pedestrian solar absorptance; on average over the year, a pedestrian with very light-colored clothing and light-colored skin (average solar absorptance 0.40) may even feel colder near a cool wall than near a conventional wall.

Since thermal sensation in California is generally too warm, the SET* rise corresponds to a slight worsening of thermal comfort. However, the SET* rise is so small that it will go unnoticed by most people. Also, the largest daytime SET* increases occur in winter when cool walls improve thermal comfort.

The complete study is presented in the Task 3.1 report, Pedestrian Mean Radiant Temperature and Thermal Comfort (Appendix D).

Urban Climate Impacts of Cool Walls (Task 3.2)

Despite previous studies that examined the urban climate effects of raising albedo of horizontal surfaces (roofs and pavements) in different cities, researchers have not yet systematically investigated the influence of increasing the albedo of vertical surfaces (walls) on urban temperatures. The climate effects of increasing wall albedo are expected to differ from those for cool roofs and pavements for several reasons. First, the diurnal cycle and daily average values of solar irradiance (incident radiative power per unit area) on vertical walls differ from those of solar irradiance on nearly horizontal roofs and pavements. Second, walls make up a different fraction of urban areas than do roofs and pavements. Third, air temperature effects per unit of grid cell albedo increase may differ for walls relative to roofs and pavements. Thus, in this study, the researchers used a regional climate model, coupled to an urban canopy model, to investigate how adopting cool walls influence albedos and near-surface canyon air temperatures in the Los Angeles basin. The team also conducted a suite of cool roof simulations assuming the same facet albedo increases. These simulations allow for systematically comparing the climate effects of cool walls versus cool roofs using a consistent modeling framework.

The research team used the Weather Research and Forecasting model (WRF) version 3.7 to investigate the effects of raising wall albedo on near-surface air temperatures in the Los Angeles basin. The team implemented a new method for selecting parameters to diagnose canyon air temperature, which better represents air temperatures near the ground in cities relative to the model-default near-surface air temperature.

To analyze the influence of cool walls on the climate of the Los Angeles basin, the researchers conducted three cases: CONTROL, in which roof, ground, and wall albedos are each set to 0.10; COOL_WALL_LOW, where wall albedo is raised to 0.50; and COOL_WALL_HIGH, where wall albedo is raised to 0.90. To compare the effect of increasing wall albedo to that of raising roof albedo, the team conducted two additional cases: COOL_ROOF_LOW, where roof albedo is raised to 0.50; and COOL_ROOF_HIGH, where roof albedo is raised to 0.90. Simulations were performed for 14 days (28 June 2012 to 11 July 2012).

Figure 7 shows the diurnal cycle of canyon air temperatures for each simulation, and changes in temperatures upon raising wall or roof albedo, spatially averaged over the urban regions of Los Angeles County. Peak temperature reductions for cool walls (that is, 0.64 K for COOL_WALL_HIGH – CONTROL and 0.28 K for COOL_WALL_LOW – CONTROL) occur at 09:00 local standard time (LST). A local minimum in temperature difference (i.e., maximum in temperature reduction) is also observed around 18:00 LST.

Figure 7: Canyon Air Temperature Change upon Raising Wall or Roof Albedo

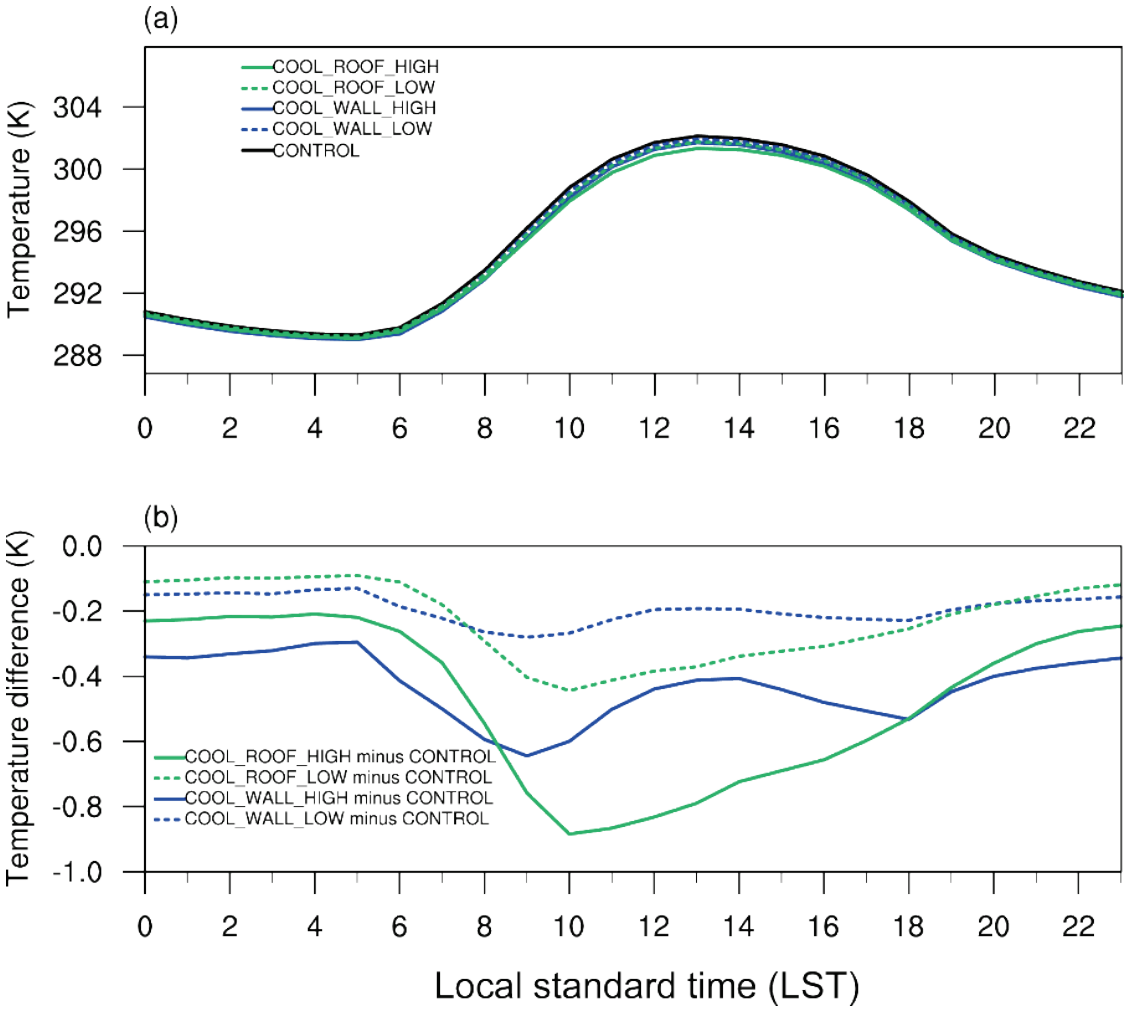

The diurnal cycle of (a) spatially averaged canyon air temperature (K) for CONTROL, COOL_WALL_LOW, COOL_WALL_HIGH, COOL_ROOF_LOW, and COOL_ROOF_HIGH; and (b) differences in canyon air temperatures for COOL_WALL_LOW – CONTROL, COOL_WALL_HIGH – CONTROL, COOL_ROOF_LOW – CONTROL, and COOL_ROOF_HIGH – CONTROL. Values represent spatial averages in Los Angeles County for urban grid cells between July 3 and 12.

Source: University of Southern California

Three factors contribute to the shape of the simulated diurnal cycle for canyon air temperature changes. First, the diurnal cycle of solar irradiance onto walls is concave up, meaning that walls receive the most sunlight in the early morning and late afternoon. Higher solar irradiance leads to larger cool wall induced reductions in solar absorption and heat gain. Second, buildings can retain solar heat gain throughout the day, leading to an accumulation effect of albedo increases

on wall surface temperatures. Third, the height of the planetary boundary layer (PBL) has a diurnal cycle that is concave down, meaning that the boundary layer heights are shallow in the morning and evening, with a maximum generally occurring ~13:00 LST. Shallower PBL heights reduce the volume of air heated by sensible heat fluxes. This means that given reductions in sensible heat flux caused by surface temperature decrease can lead to larger reductions in atmospheric heating rate (temperature/time) in the boundary layer when PBL heights are shallow versus deep. Thus, sensible heat flux decreases from cool-wall adoption are expected to have larger air temperature effects when the PBL is shallow. All three factors contribute to the peak in near-surface air temperature at 09:00 LST, which is two hours after the maximum solar irradiance onto walls occurs and when the PBL height is relatively low.

Figure 7 also shows that the reduction in canyon air temperature from increasing wall albedo is less than that from increasing roof albedo between 09:00 to 17:00, and greater than that from increasing roof albedo at nighttime. This is likely because walls are in the urban canyon, so they can more directly cool canyon air than can roofs. In addition, cool walls lead to a greater cooling at night relative to cool roofs. The atmosphere is stable at night, meaning that there is little vertical mixing. This means that above-canopy air temperature reductions from cool roofs would undergo less mixing into the canyon, and thus have less effect on canyon air temperatures relative to cool walls at night.

The ratio of the daily average temperature reduction for COOL_WALL_HIGH – CONTROL to that for COOL_WALL_LOW – CONTROL (0.43 K / 0.19 K = 2.3) is close to the ratio of the wall albedo rises for the two scenarios (0.80 / 0.40 = 2), indicating that the average temperature reduction induced by cool walls is approximately proportional to increase in wall albedo. A similar linear relationship between facet albedo increase and temperature reduction is also observed for cool roofs (0.48 K / 0.23 K = 2.1). Per 0.10 wall (roof) albedo increase, cool walls (roofs) can reduce summertime daily average canyon air temperature by 0.048–0.054 K (0.058–0.060 K). Thus, results reported here can be interpolated to estimate the effects of increasing wall or roof albedo by other amounts.

The ratio of the daily average air temperature reduction induced by cool walls to that yielded by cool roofs is about 86 percent, making their benefits comparable.

Canyon air temperature reductions from adopting cool walls or roofs in the Los Angeles basin reported in this study can be used to inform policymaking for urban heat island mitigation or climate change adaptation.

The complete study is presented in the Task 3.2 report, Urban Climate Impacts of Cool Walls (Appendix E). An article based on this work has been published in *Environmental Science & Technology* (Zhang et al. 2018).

Effects of Cool Walls on Energy-saving Benefits from Cool Pavements (Task 3.3)

"Heat island" refers to the phenomenon of having higher urban temperatures compared to the temperatures of surrounding suburban and rural areas. In the United States, pavements cover typically up to 30 percent of the urban fabric, and are hot, dry surfaces that can contribute substantially to the heat island effect.

The use of cool pavements is an urban heat island reduction strategy that increases pavement albedo (solar reflectance) to reduce convective heating of the outdoor air. This lowers the air temperature difference across the building envelope, reducing heat gain via conduction and infiltration. This "indirect" effect of reflective pavement can decrease cooling loads in summer and increase heating loads in winter. Raising pavement albedo also increases the solar flux incident on walls and windows, a "direct" effect of reflective pavement that can increase cooling loads in summer and reduce heating loads in winter. The total annual changes in cooling and heating energy loads will depend on the relative magnitudes of the indirect and direct effects. This study explored only the direct effect of cool pavements for buildings in California cities.

The magnitude of the direct effect depends on the design and properties of the building's walls and windows. The research team prepared nine code-compliant building prototypes with external horizontal shading surfaces that represent local roads; examples are shown in Figure 8. To quantify the direct effects of cool pavements, we simulated with EnergyPlus the annual cooling and heating energy uses of each prototype, varying the road albedo, wall absorptance (1 – wall albedo), and window solar heat gain coefficient (SHGC).

Figure 8: Building Prototypes with Adjacent Streets

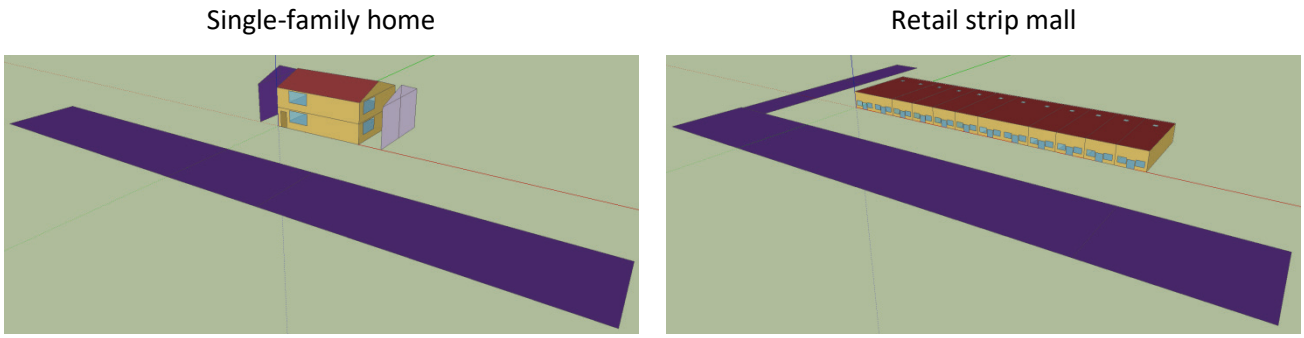

EnergyPlus building prototypes with roads represented by horizontal shading surfaces.

Source: Lawrence Berkeley National Laboratory

The research team used a physical model that relates each heating and cooling energy use to building properties, and to local road albedo. The team used the results from the building simulations to validate the physical model, and to generate relationships that predict the direct effect of pavement albedo change on building energy use.

The study analyzed how the location and dimension of the road with respect to the building affects its direct effect on the building energy use. For this, the researchers compared the

building-to-road view factors to their direct effect and observed a relationship in which the direct effect on cooling increases linearly with the view factor; the direct effect on heating is a linear decrease.

The direct effect from cool pavements is slightly larger through windows than walls. Their individual contributions depend heavily on the window-to-wall ratio, as well as other construction properties. In this case, the latter was similar across prototypes. Hence, after normalizing to a window-to-wall ratio of 0.40, the research team found that windows contribute 1.5 times more to the direct effect than do walls (for the base case values of wall absorptance and window SHGC).

Although increasing the pavement albedo by 0.25 caused net conditioning energy penalties that were as much as 0.80 percent (large office averaged over all climate zones), when reducing the wall absorptance by 0.25 most prototypes experienced net conditioning energy savings (as much as 4.2 percent). Similarly, when researchers reduced window SHGC by 0.05, all prototypes experienced net conditioning energy savings ranging between 0.32 percent and 3.11 percent (Table 1). Hence, the study suggests small modifications to a building's envelope can outweigh the small cooling penalties associated with the direct effect of cool pavements.

The complete study is presented in the Task 3.3 report: Effect of Cool Walls on Energy-saving Benefits from Cool Pavements (Appendix F).

Table 1: Savings from Cool Roads, Walls, and/or Windows

Prototype	Source mean conditioning (cooling + heating) energy intensity savings				
	Base [MJ/m²y]	Savings from road [%]	Savings from road + wall [%]	Savings from road + window [%]	Savings from road, wall, window [%]
Single-family home	146.5	-0.59	4.17	1.64	5.82
Apartment complex	121.6	-0.50	2.20	3.11	5.31
Large hotel	705.0	-0.40	1.14	0.68	1.82
Large office	241.5	-0.80	-0.19	2.94	2.75
Medium office	398.2	-0.29	0.35	2.58	2.93
Primary school	261.3	-0.35	0.59	2.48	3.07
Retail stand-alone	309.6	-0.07	2.00	1.59	3.60
Strip mall retail	350.2	-0.09	1.75	1.39	3.13
Sit-down restaurant	903.6	0.01	0.36	0.32	0.68

Conditioning source energy savings averaged over all California climate zones.

Source: Lawrence Berkeley National Laboratory

Effect of Wall Albedo on the Environment inside an Unconditioned Building (Task 3.4)

Raising a wall's albedo decreases its solar heat gain, which can reduce heat conducted inward through the wall on a hot day, or increase heat conducted outward on a cold day. In buildings without air conditioning, cool walls are expected to affect the interior thermal environment more than in air-conditioned buildings.

The researchers simulated the building outdoor and indoor thermal environment using a building-to-canopy model that simulates heat transfer in a small neighborhood of identical buildings to obtain indoor and outdoor air temperatures; interior and exterior temperatures of walls and ceiling; and radiative, convective, and conductive heat fluxes. The team performed calculations hourly for a year of typical weather conditions for a multi-family residence in a coastal California climate zone in the Greater Los Angeles area (Fullerton).

The human temperature sensation is approximated through thermal comfort models. Such models attempt to emulate the typical human perception of environmental conditions through thermal comfort indices. Thermal comfort depends on clothing and metabolic activity as well as environmental factors including air temperature; radiation from surrounding walls, floor, and ceiling; and humidity. To understand thermal impacts of cool walls on building occupants, calculations are performed for a sitting person. The ASHRAE comfort model based on Fanger's theory expresses thermal comfort as "Predicted Mean Vote" (PMV), which can take on values of -3 (cold), -2 (cool), -1 (slightly cool), 0 (neutral), 1 (slightly warm), 2 (warm), and 3 (hot).

Figure 9 shows that indoor air temperature peaks around 15:00—16:00 LST. The reduction in indoor air temperature with cool walls is between 0.2 ˚C midday and 0.5 ˚C at night.

Figure 9: Change in Indoor Air Temperature and Comfort upon Raising Wall Albedo

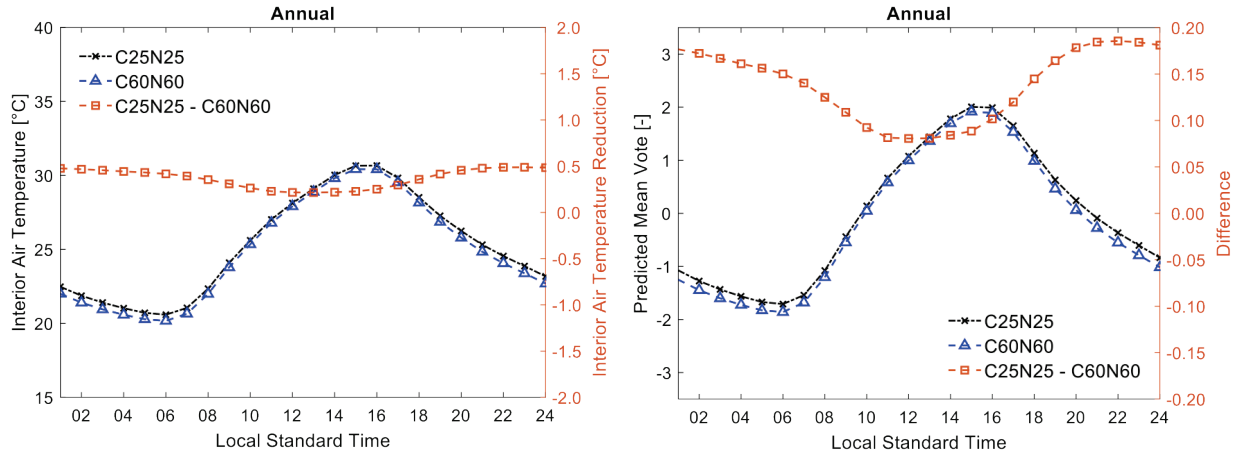

Average (over the year) daily cycle of interior air temperature (left) and predicted mean vote (PMV, right) for the multi-family residence in Fullerton with wall albedos equal to 0.25 (conventional wall, denoted as C25N25) and 0.60 (cool wall, denoted as C60N60). The right axis shows the reduction due to raising wall albedo.

Source: University of California, San Diego

Compared to a conventional wall, during daytime cool walls absorb a smaller fraction of incident solar radiation. This lowers the temperature of the wall's outer surface, reducing heat flux through the wall and the air temperature in the occupied space. The daytime decrease in heat storage in cool walls causes lower wall temperatures and indoor air temperature to persist through the night. The thermal comfort trends during the day follow the indoor air temperature trends. On average, the building occupant tends to be slightly cool to cool during the night and slightly warm to warm during the day.

Since thermal sensation in buildings without air conditioning is generally slightly cold to cold at night and slightly warm to warm during the day, this corresponds to a slight worsening of thermal comfort at night and an improvement of thermal comfort during the day. But since homes without cooling are more common than homes without heating, in practice the worsening of thermal comfort from cool walls during nighttime would not occur and cool walls would then only improve thermal comfort during the day.

The complete study is presented in the Task 3.4 report, Effect of Wall Albedo on the Environment inside an Unconditioned Building (Appendix G).

Effects of Self-cleaning Walls on Urban Air Quality (Task 3.5)

The researchers analyzed total NO_x deposition in Los Angeles County assuming a hypothetical scenario in which all walls are painted with photocatalytic cool paints.[3] We use laboratory-measured dry deposition velocities for NO_x (0.2 – 0.5 centimeters per second [cm s^{-1}]) (Task 4.3), NO_x concentrations measured by ambient air quality stations, and wall-to-urban land area ratios derived from a real-world building dataset. The research team compared total expected deposition to recent (2012) emissions of NO_x in urban Los Angeles County to assess the magnitude of predicted deposition increases.

For a first-order approximation, the team assumed that the deposition velocity onto cool walls was constant throughout the daytime, suggesting that the flux of ultraviolet photons is not the rate-limiting factor. While this is likely not true, the goal was to quantify upper bound estimates of NO_x deposition to compare with total NO_x emissions in Los Angeles County. Figure 10a shows the diurnal cycle of NOx deposition in July. Based on the lower bound of measured NO_x dry deposition velocity (0.02 cm s^{-1}), NO_x deposition ranges 267—709 moles per hour (mol hr^{-1}), depending on time of day. Based on the upper bound of NO_x dry deposition velocity (0.05 cm s^{-1}), NO_x deposition ranges 668 – 1,770 mol hr^{-1}.

Figure 10b shows the hourly NO_x emissions during daytime averaged in July. NO_x emissions reach a maximum at 11:00 LST. NO_x emissions are in the range of $(1.3—2.8) \times 10^5$ mol hr^{-1}. The emissions start to increase with the morning traffic and peak around noon. The diurnal cycle of NO_x emissions is driven by the diurnal variations of on-road and off-road mobile sources and stationary sources (South Coast Air Quality Management District, 2013). Figure 10c shows the diurnal cycle of the ratio of NO_x deposition to emissions. Even when assuming the maximum deposition velocity measured in experiments, the upper-bound daily maximum NO_x deposition is less than 1.1 percent of NO_x emissions.

Daytime (05:00 – 19:00 LST) total NO_x deposition and emissions are 6.6×10^3—1.6×10^4 mol day^{-1} and 3.3×10^6 mol day^{-1}, respectively. Therefore, daytime NO_x deposition is 0.2—0.5% of NO_x emissions in July in Los Angeles County. Thus, adopting photocatalytic cool walls is expected to have small impacts on regional air quality in Los Angeles. Note that this analysis estimates city-level NO_x deposition, and does not consider whether photocatalytic self-cleaning walls may have larger air quality benefits for near-source concentrations in urban canyons. The

[3] Photocatalytic paints contain a catalyst that absorbs UV light to accelerate breakdown of surface pollutants.

researchers suggest future work to estimate the impact of self-cleaning walls on near-source NO_x concentrations.

The complete study is presented in the Task 3.5 report, Effects of Self-cleaning Walls on Urban Air Quality (Appendix H).

Figure 10: Deposition of Nitrogen Oxides in Los Angeles County

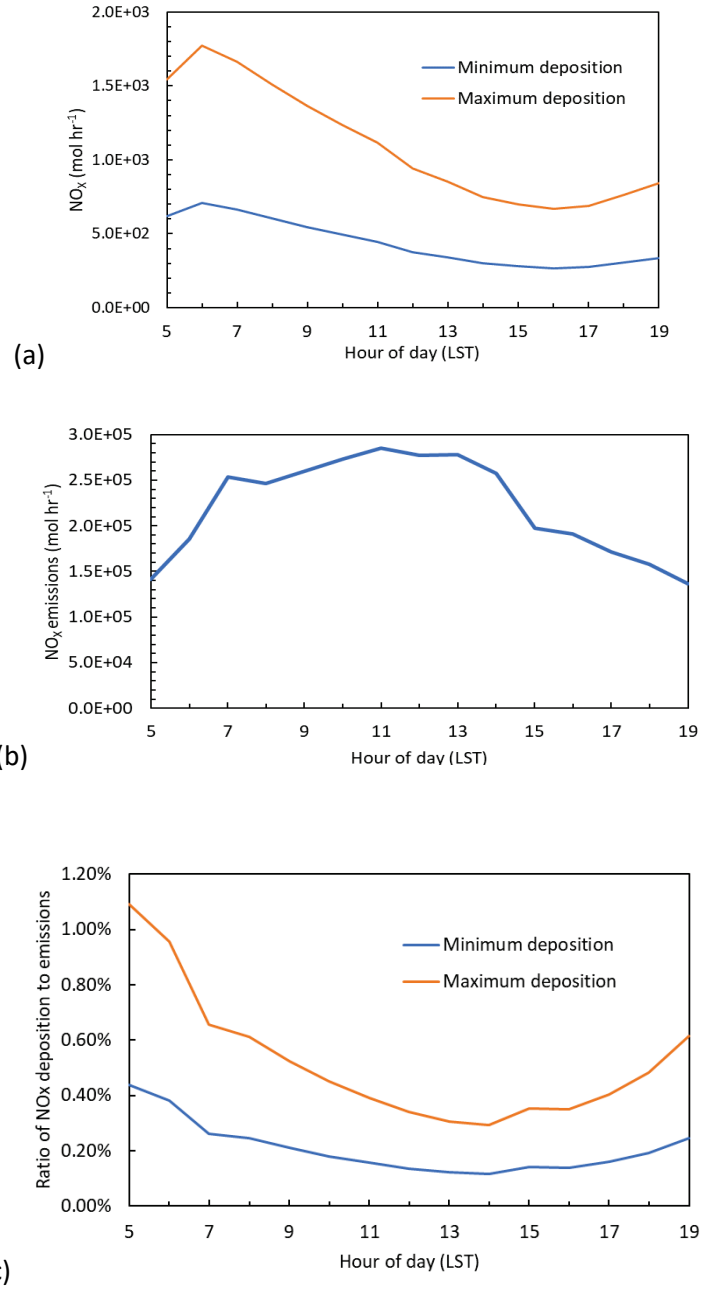

Diurnal cycles for urban Los Angeles County of (a) NO_x deposition (mol hr^{-1}); (b) NO_x emissions (mol hr^{-1}); and (c) the ratio of NO_x deposition to NO_x emissions. Values are averaged for July 2012. Panels (a) and (c) show upper and lower bound estimates based on variations in measured dry deposition velocities.

Source: University of Southern California

CHAPTER 4:
Assessing Performance of Cool-wall Technologies (Task 4)

Task 4 assessed through field and laboratory measurements the performance of available and prototype cool-wall technologies, primarily the ability to reflect sunlight. Task 4.1 developed metrics and methods for evaluation of solar reflectance, de-pollution efficacy, and other material properties, while Task 4.2 measured how solar reflectance changed over time as products were exposed outdoors at sites across California and the United States. Task 4.3 focused on the performance of self-cleaning and de-polluting photocatalytic materials.

Metrics and Methods to Assess Cool-wall Performance (Task 4.1)

The ability of a wall product to stay cool in the sun depends on its solar reflectance and thermal emittance. High solar reflectance reduces solar heat gain (absorption of sunlight), while high thermal emittance can help cool the surface through long-wave radiative exchange with its environment. This report addresses the metrics and methods needed to assess the evolution of the surface properties of a wall product over its service life.

Radiative properties of interest include initial and aged values of solar spectral reflectance (reflectance vs. wavelength); solar reflectance (fraction of incident sunlight that is reflected), thermal emittance (ratio of radiant power emitted to that emitted by a black body radiator, at a temperature near 300 Kelvin); color; effective solar reflectance (fraction of incident sunlight rejected by the combination of reflection and fluorescence), and solar retroreflectance (fraction of incident sunlight reflected to its origin). Nonradiative properties that influence radiative properties include soiling resistance (ability to stay clean), hydrophilicity (attraction of water), and hydrophobicity (repulsion of water).

The research team selected the following metrics and methods:

- Near normal-hemispherical solar spectral reflectance is to be measured over the spectrum 250—2,500 nm using an ultraviolet-visible-near infrared spectrophotometer equipped with an integrating sphere, following ASTM Standard E903. There is also a specified protocol for measuring soiled samples through a protective window, and for correcting those measurements for the influence of the window.
- Air mass 1.5 global-hemispherical solar reflectance is to be measured either (a) by averaging solar spectral reflectance weighted with the air mass 1.5 global solar spectral irradiance incident on a sun-facing vertical surface (AM1.5GV), following ASTM Standard E903; or (b) using the output of a solar spectrum reflectometer that corresponds to this irradiance, following ASTM Standard C1549.

- Hemispherical thermal emittance is to be measured with a portable emissometer following either ASTM Standard C1371 or the Devices & Services "Slide Method," as appropriate to product type.
- Color coordinates are to be calculated from solar spectral reflectance following ASTM Standard E308.
- The effective solar reflectance of a fluorescent surface is to be determined with a custom apparatus developed by LBNL (Figure 11). This calorimetric technique compares the temperature in the sun of a fluorescent specimen to those of non-fluorescent reference specimens of known solar reflectance. It then interpolates effective solar reflectance from the temperature measurements and known solar reflectances.

Figure 11: Apparatus for Measurement of Effective Solar Reflectance

Test and reference specimens on rotating platter pass beneath an IR thermometer (upper right). Apparatus also includes an anemometer (lower left), pyranometer (on same board as anemometer), and control electronics (underneath tripod). An air temperature sensor is hidden below the platter.

Source: Lawrence Berkeley National Laboratory

- Solar retroreflection is assessed with a simple goniometer[4] that compares the intensity of retroreflection to that of first-surface specular reflection, and with an advanced goniometer that measures solar spectral bidirectional reflectance intensity.
- Initial and aged values of solar reflectance and thermal emittance are to be assessed before, during, and after a program of natural exposure at various sites across California and the United States. Aged radiative properties will be measured quarterly, for two years, in the California program, and annually, for five years, in the United States program.
- Relative and absolute values of soiling resistance are to be gauged by comparing aged solar reflectance to initial solar reflectance.
- Hydrophilicity/hydrophobicity is to be determined by measuring water contact angle.

The complete study is presented in the Task 4.1 report, Metrics and Methods to Assess Cool Wall Performance (Appendix I).

Natural Exposure of Wall Products (Task 4.2)

The solar reflectance of wall products can change over time as they soil and weather. The research team collected product samples from its industrial partners, and selected 69 materials to expose in California and 55 to expose across the United States. The exposed set included factory-applied coatings, aluminum-plastic composite cladding, vinyl siding, architectural fabrics, retroreflecting materials, and different types of field-applied coatings. The latter included paint formulations with different surface finishes, some containing cool pigments and/or dirt-resistant formulations. Partners prepared paint samples on different substrates – metal, wood, concrete, and fiber cement – and provided many specimens of each product for use in natural exposure trials and additional lab testing.

The project team exposed specimens vertically, facing west, over two years at three sites in California representing different climate zones and pollution levels:

- Lawrence Berkeley National Laboratory (LBNL) campus in Berkeley (Figure 12).
- An industrial partner facility in Fresno.
- University of Southern California campus in Los Angeles.

The team similarly exposed specimens over a five-year period at three United States sites used by the Cool Roof Rating Council:

- New River, Arizona (near Phoenix; hot and dry weather).
- Miami, Florida (hot and humid weather).
- Medina, Ohio (near Cleveland; temperate weather, more polluted).

For the California exposure program, the team deployed specimens in March/April 2016 that were retrieved quarterly for analysis at LBNL. Specimens used in the United States exposure

[4] A goniometer measures the variation of reflectance with angle.

program were deployed in August 2016 and are being collected annually. Retrieved specimens were photographed, and their solar reflectances were measured with a Devices & Services Solar Spectrum Reflectometer.

Figure 12: Wall Product Racks Used in California Exposure Trials

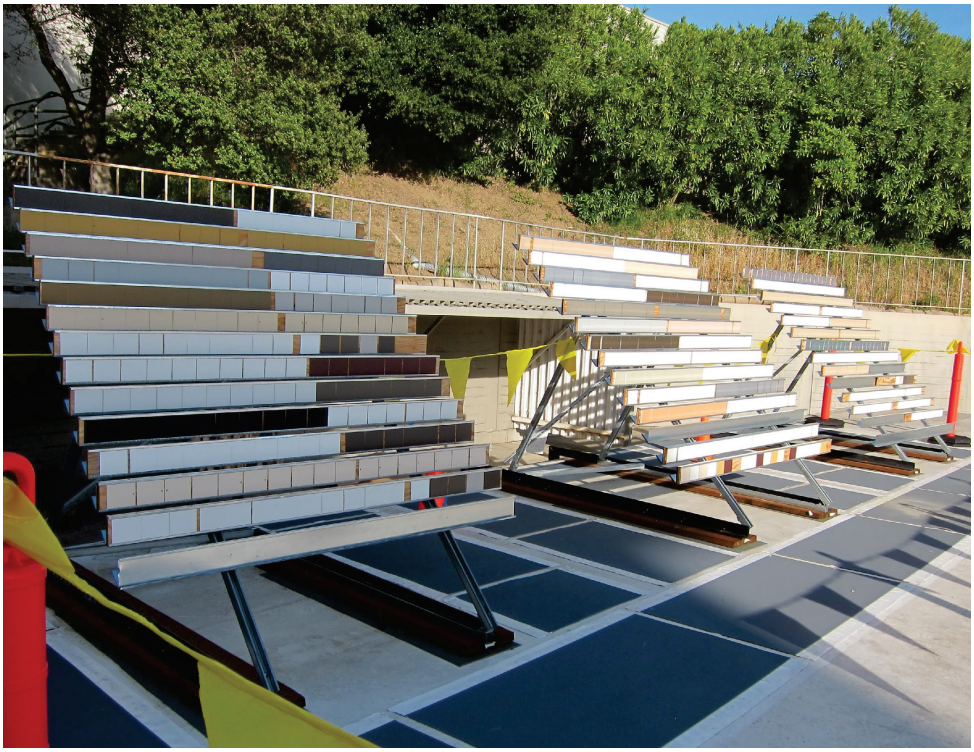

Wall-product exposure rack on building roof at Lawrence Berkeley National Laboratory.

Source: Lawrence Berkeley National Laboratory

Specimens exposed for 24 months in California have been retrieved quarterly and measured. Specimens exposed for 2 years across the United States have been retrieved annually and measured.

Factory-applied coatings have shown excellent performance in all locations used for California and United States exposure, with negligible changes in solar reflectance. Composite metal cladding also exhibited great retention of initial solar reflectance values. In both cases, the use of fluorinated polymers in their formulation may explain the high performance. Factory-applied coatings with textured surfaces (for example, embossed or crinkled) behaved similarly to those with smooth surfaces.

In the case of field-applied coatings, the retention of initial solar reflectance values varied with coating formulation, surface finish, and substrate (Figure 13). Field-applied coatings colored with cool pigments were significantly more reflective than similarly colored products incorporating conventional pigments. Several dirt-resistant field-applied coatings showed a higher retention of solar reflectance than control coatings representing typical formulations.

Specimens with photocatalytic self-cleaning functionalities are detailed in Task 4.3.

The complete study is presented in the Task 4.2 report, Natural Exposure of Wall Products (Appendix J).

Figure 13: Albedo Losses for Naturally Exposed Wall Products

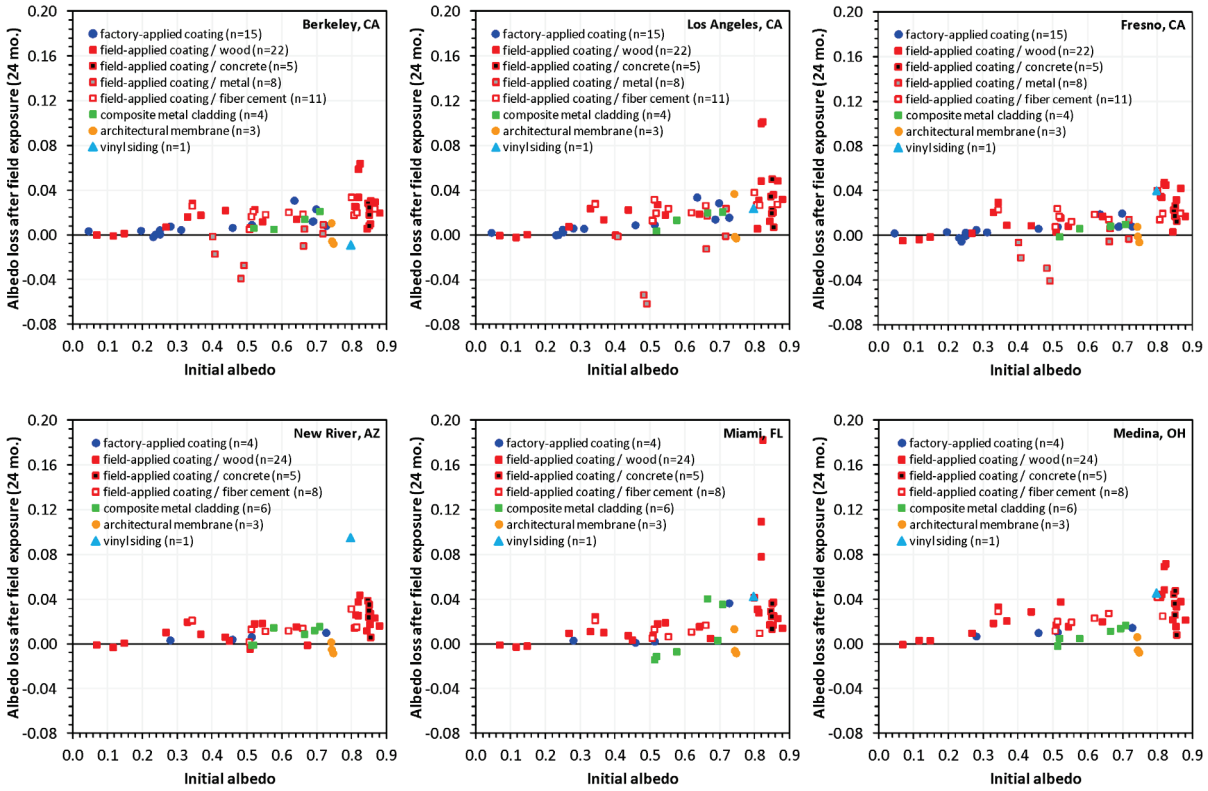

Most wall materials tested experienced minimal to modest albedo losses after 2 years of exposure at three sites in California (top row) and three sites across the United States (bottom row).

Source: Lawrence Berkeley National Laboratory

Self-cleaning and De-polluting Photocatalytic Materials (Task 4.3)

Two of the products evaluated in the California and United States natural exposure trials were architectural fabrics coated with photocatalytic titanium dioxide particles. A third material was an uncoated fabric of identical characteristics, used as a control. The project team evaluated specimens in the field and the laboratory.

The researchers exposed the photocatalytic specimens and their control vertically facing west in three sites in California representing different climate zones and pollution levels (Berkeley, Fresno, and Los Angeles) and in the three United States sites used by the Cool Roof Rating Council (CRRC): Arizona (dry and hot weather), Florida (humid and hot weather), and Ohio (temperate weather with more pollution).

Photocatalytic materials exposed at the California sites showed negligible changes in solar reflectance over the course of two years. During the same period, the solar reflectance of the non-photocatalytic control decreased by 0.01—0.08. These changes reflected seasonal rainfall

patterns, with soiling buildup during the dry season (April—November), and partial recovery of the initial solar reflectance value during the rainy season (December—March). These effects were more marked in Los Angeles and Fresno where ambient particulate matter levels are higher. The measured values are presented in Figure 14 and photos of the specimens collected at 12 months are shown in Figure 15.

Figure 14: Solar Reflectances of Photocatalytic and Control Fabrics

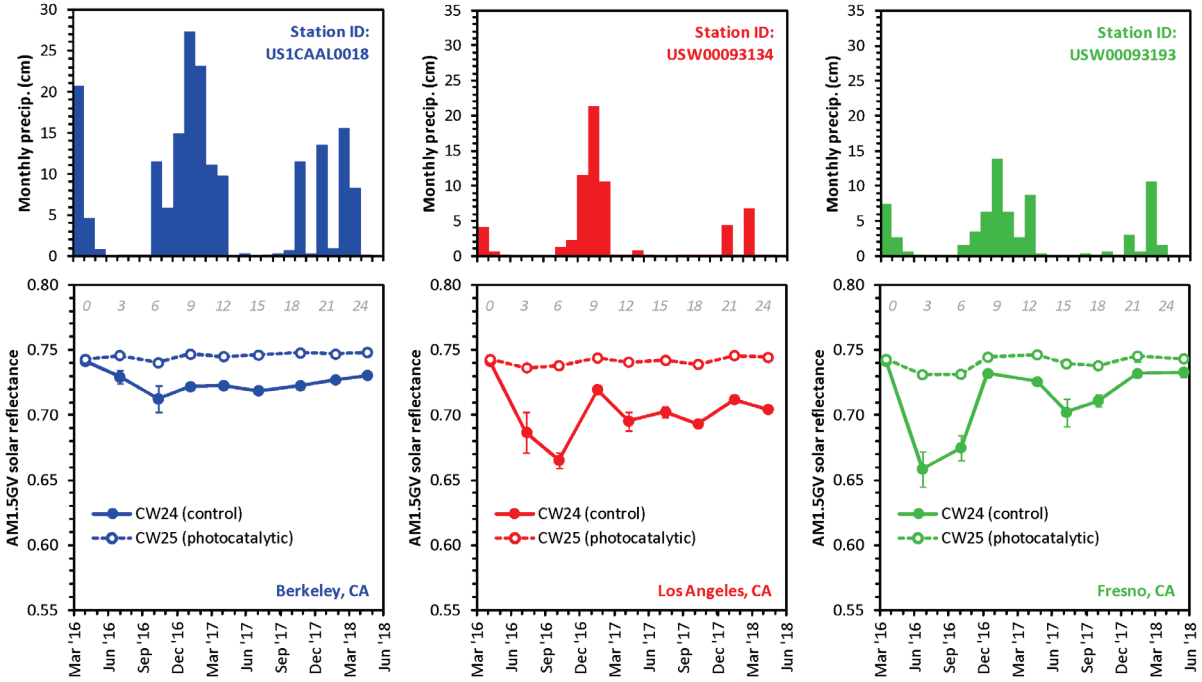

The photocatalytic self-cleaning white fabric experienced less solar reflectance loss than its control.

Source: Lawrence Berkeley National Laboratory

Figure 15: Images of Photocatalytic and Control Fabrics after 1 Year in California

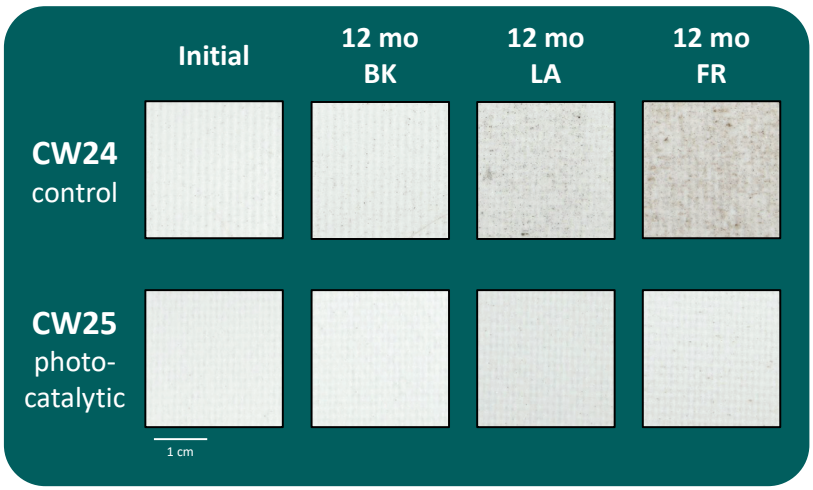

Photos of a photocatalytic self-cleaning fabric (CW25, bottom row) and the control sample (CW24, top row) after 12 months of exposure in Berkeley (BK), Los Angeles (LA), and Fresno (FR).

Source: Lawrence Berkeley National Laboratory

The research team evaluated the de-polluting capacity of each photocatalytic product in the lab by measuring removal of nitrogen oxides (NO_x) from an airstream enriched in nitric oxide (NO). Tested samples included unexposed specimens and those retrieved from the field. The test conditions closely followed ISO Standard 22197-1. The team placed specimens inside a flow chamber in which they were facing a quartz window through which UV light was irradiated continuously for a period of 6 hours. A chemiluminescent NO_x detector was used downstream of the chamber to quantify the concentration of NO_x (NO and NO_2) in real time. From the integration of this signal the researchers could determine the amounts of NO removed and NO_2 formed (as an intermediate byproduct), and, by difference, the amount of nitrate formed as final byproduct. Unexposed samples showed a higher NO_x-removal capacity, on the order of 0.7 micromoles of NO per hour (µmol NO h^{-1}), which was diminished by field exposure to values as low as 0.2 µmol NO h^{-1} for one of the products and 0.1 µmol NO h^{-1} for the other. During the rainy season the research team observed a recovery of the activity associated with a more effective cleaning of the catalyst surface.

The complete study is presented in the Task 4.3 report, Self-cleaning and De-polluting Photocatalytic Materials (Appendix K).

Assessment of Existing and New Retroreflective Materials (Task 4.4)

This activity was merged into Task 5.3 and is discussed in Chapter 5.

CHAPTER 5:
Developing Innovative Cool-wall Solutions (Task 5)

Task 5 explored innovative cool-wall technologies, including self-cleaning materials (Task 5.1, which was merged with Task 4.3), fluorescent cool pigments (Task 5.2), and retroreflective materials (Task 5.3).

Improvement of Self-cleaning Coatings and Claddings (Task 5.1)

This activity was merged into Task 4.3 and is discussed in Chapter 4.

Development of Fluorescent Cool Pigments (Task 5.2)

Various pigments are used to formulate desired non-white colors that stay cooler in the sun than alternatives. These cool pigments provide a high near-infrared (NIR) reflectance in the solar infrared range of 700 nanometers (nm) to 2500 nm, and also a color specified by a reflectance spectrum in the 400 nm to 700 nm visible range. Still cooler materials can be formulated by also utilizing the phenomenon of fluorescence (photoluminescence).

While potential fluorescent cool pigments have been screened during a prior United States Department of Energy funded project with PPG Industries, only a few pigments have demonstrated the potential for efficient fluorescence and also appear to have adequate (low) cost and durability. The first such pigment was ruby, which is composed of aluminum oxide doped with chromium. It can be used to produce red and pink colored materials (Figure 16).

Figure 16: Pink-Red Coatings Incorporating Fluorescent Ruby Pigment

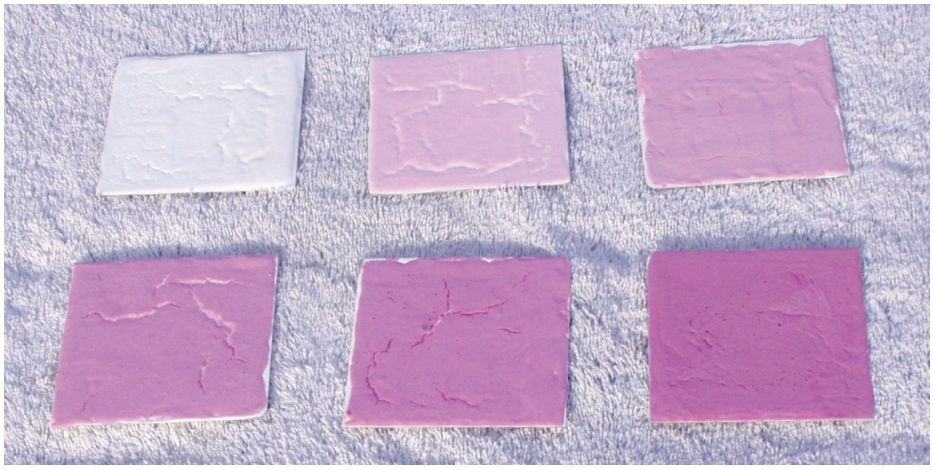

Coatings containing fluorescent ruby powders with 0, 0.2, 1, 2, 3, and 4% doping. The darker coatings contain pigments with more chromium.

Source: Lawrence Berkeley National Laboratory

The second important class of materials includes the ancient pigment Egyptian blue. Egyptian blue has the chemical composition of $CaCuSi_4O_{10}$ – that is, calcium copper tetra-silicate. The most important other members of this class, the Egyptian blue family, have the same formula but with barium (Ba) or strontium (Sr) replacing calcium. The barium variant is also known from ancient times as Han (or Chinese) blue. The strontium variant has no common name. The best performance to date with the Egyptian blue family has been achieved with the calcium and strontium compounds. These blue pigments can also be blended with yellow pigment to achieve a green color, or with an orange pigment to obtain a blue-shade black (Figure 17). The blending process does not diminish the near-infrared fluorescence.

Figure 17: Blue, Green, and Blue-Black Coatings Incorporating Fluorescent Blue Pigment

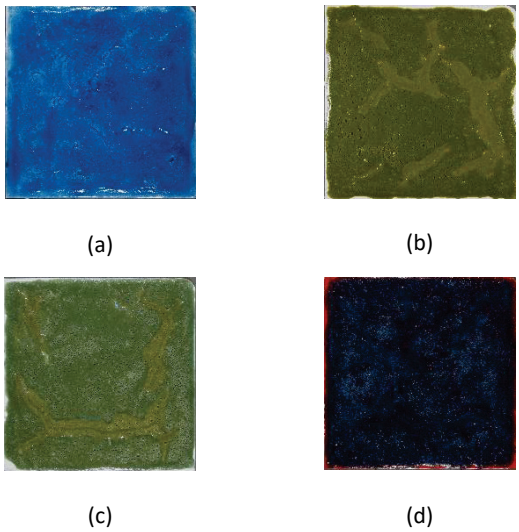

Coatings with a fluorescent blue pigment, each over a bright white undercoat: (a) blue alone, (b) blue mixed with azo yellow, (c) blue mixed with mixed metal oxide yellow, and (d) blue over an orange coating.

Source: Lawrence Berkeley National Laboratory

The research team built a calorimetric instrument that measures effective solar reflectance (ESR), or the fraction of incident solar energy rejected by the combination of reflectance and fluorescence (see Figure 11 in Chapter 4). Laboratory-fabricated coatings have shown that coatings with fluorescent pigments can contribute to, or boost, the ESR up to 0.17 above the ordinary solar reflectance (SR). The target for future commercial coatings is a fluorescence benefit (ESR – SR) of 0.10 to 0.15. The energy flux of full sunlight is roughly 1,000 W m^{-2}, so we can expect that future colored fluorescence materials can reduce peak heat absorption rates by 100 to 150 W m^{-2}.

Even though natural rubies are quite expensive, manufactured rubies with the same properties are not. The wholesale cost of cut and polished manufactured ruby gems for jewelry is about US$0.30 per carat (200 mg). A layer of manufactured rubies has a pleasing dark red color with a fluorescence benefit of 0.30. Also, ruby pigment is not difficult to manufacture; manufacturers can use the same solid-state reaction techniques they currently employ for other mixed metal oxide pigments such as Fe-Cr-O cool black. Unfortunately, prototype coatings colored with ruby pigment are not as dark as desired and have a fluorescence benefit of only 0.15. Future

research may yield further improvements. In the meantime, ruby pigments can provide a dark pink color with high ESR, near 0.80. For comparison, smooth white commercial materials have SR in the range of 0.70 to 0.85 – about the same as the ruby pigment.

The Egyptian blue family of pigments comprises alkaline earth copper silicates usually synthesized by solid-state reaction techniques. Briefly, oxides or carbonates of the component metals are intimately mixed and heated in air for a few hours to a temperature near 900 °C. After the synthesis, copper oxide (CuO), a black compound, is usually present as an impurity. If too much CuO is present, the resulting pigment is gray rather than blue. Egyptian blue is available commercially from Kremer Pigmente. Thus, this company is able to control the CuO concentration to some extent. However, we have found that for fluorescent pigment applications, even more stringent limitations on CuO contamination are needed. We found that washing (leaching) the commercial pigment with hydrochloric acid (HCl) reduces but does not eliminate the CuO. The near-infrared fluorescence is enhanced by up to a factor of 2 with the HCl soak.

The fluorescence benefits of the prototype materials range from about 0.08 up to 0.17. The best material is based on washed Egyptian blue, with pigment amount of 68 g m^{-2}. The visual reflectance (at 550 nm) is only 0.15, a medium dark blue, while the ESR is 0.57. The relatively small amount of pigment needed per unit area indicates that it is a reasonably strong pigment.

The complete study is presented in the Task 5.2 report, Development of Fluorescent Cool Pigments (Appendix N). Articles based on this work have been published in *Solar Energy Materials and Solar Cells* (Berdahl et al. 2016), *Energy and Buildings* (Levinson et al. 2017), and the *Journal of Applied Physics* (Berdahl et al. 2018).

Development of Retroreflective Materials (Task 5.3)

Raising a city's albedo (solar reflectance) increases the amount of incident sunlight returned to outer space, which cools cities and their buildings. Retroreflective cool walls could improve on diffusely reflecting cool walls by reflecting incoming beam radiation to the sun (if the retroreflection is three-dimensional and ideal) or at least upwards (if the retroreflection is two-dimensional and/or imperfect) (Figure 18). For example, a retroreflective wall with albedo 0.60 would reflect 55 percent of incident light out of the city, while a Lambertian (perfectly diffuse) wall with the same albedo would only reflect 36 percent of incident light out of the city.

The greatest challenge in retroreflective wall design appears to be the need to operate at large incidence angles to reflect a substantial portion of incident sunlight. For example, on a summer day in Fresno, California, less than 37 percent of the beam radiation striking an east or west wall, and essentially none of that striking a south wall, will do so at an incidence angle less than or equal to 30° (Figure 19).

The researchers explored wall retroreflector design using first-principle physics, ray-tracing simulations, and goniometer measurements. Physics and simulations suggest that it will be difficult to achieve retroreflection at large incidence angles with surfaces that rely on total internal reflection, such as conventional safety films (Figure 20). This was confirmed with a

simple goniometer that permits comparison of retroreflection to first-surface specular (mirrorlike) reflection (Figure 21), and with an advanced goniometer that measures solar spectral bi-directional reflectance intensity.

The most promising design was a two-surface retroreflector with orthogonal metal mirror faces (Figure 20b). Attempts to fabricate this system by cutting and polishing grooves in an aluminum block indicate that residual surface roughness impedes retroreflection. Ongoing efforts focus on shaping aluminized Mylar film, a material with very high specular reflectance across the solar spectrum (Figure 22).

The complete study is presented in the Task 5.3 report, Development of Retroreflective Materials (Appendix O).

Figure 18: Idealized Reflections: Specular, Lambertian, and Retro

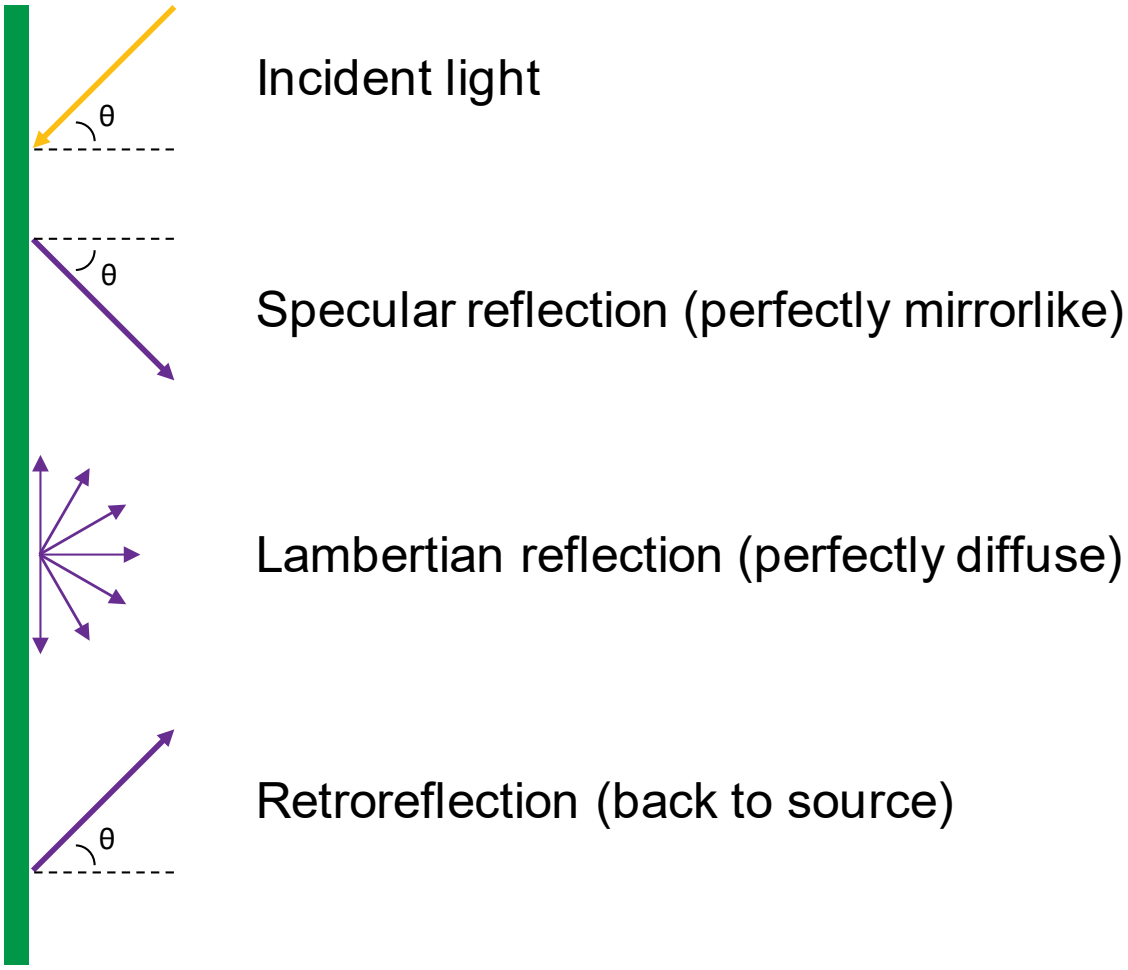

Specular, Lambertian, and retro reflection of beam light striking a vertical surface.

Source: Lawrence Berkeley National Laboratory

Figure 19: Distribution of Beam Solar Irradiance with Solar Altitude Angle

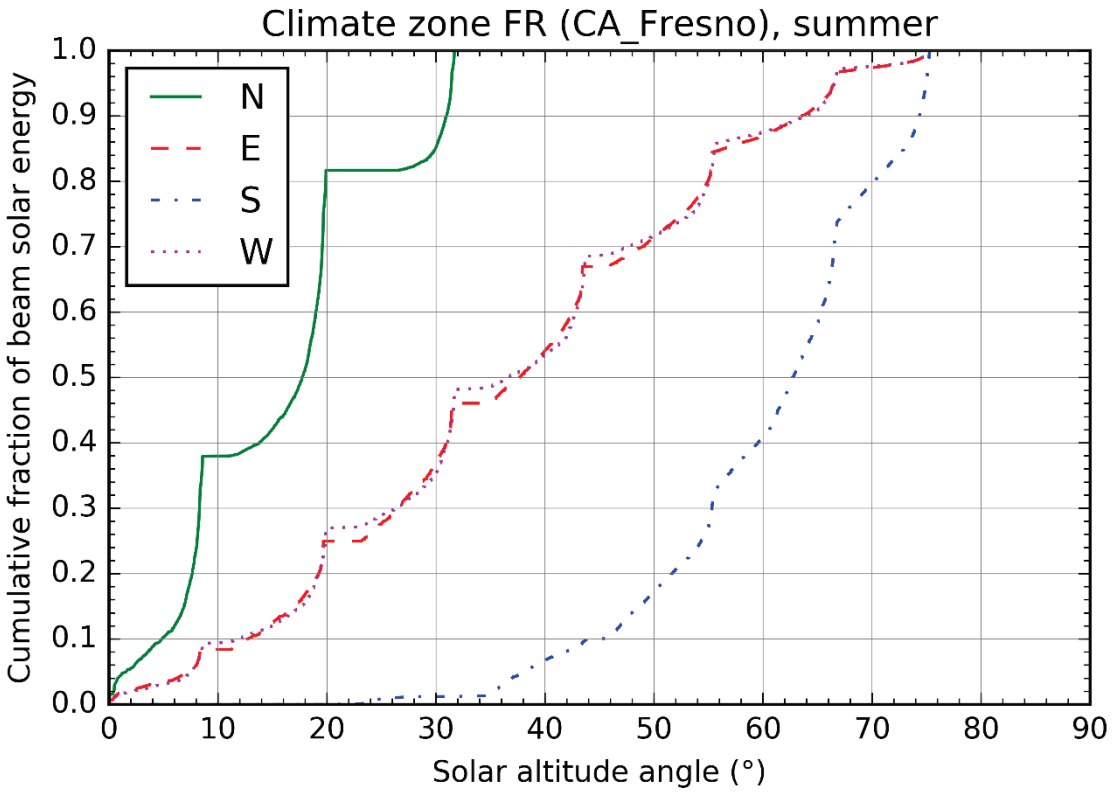

Variation with solar altitude angle of the cumulative fraction of beam solar energy incident on isolated north (N), east (E), south (S), and west (W) walls in Fresno, California, in June-July-August.

Source: Lawrence Berkeley National Laboratory

Figure 20: Simulated Reflections from Wall Retroreflectors

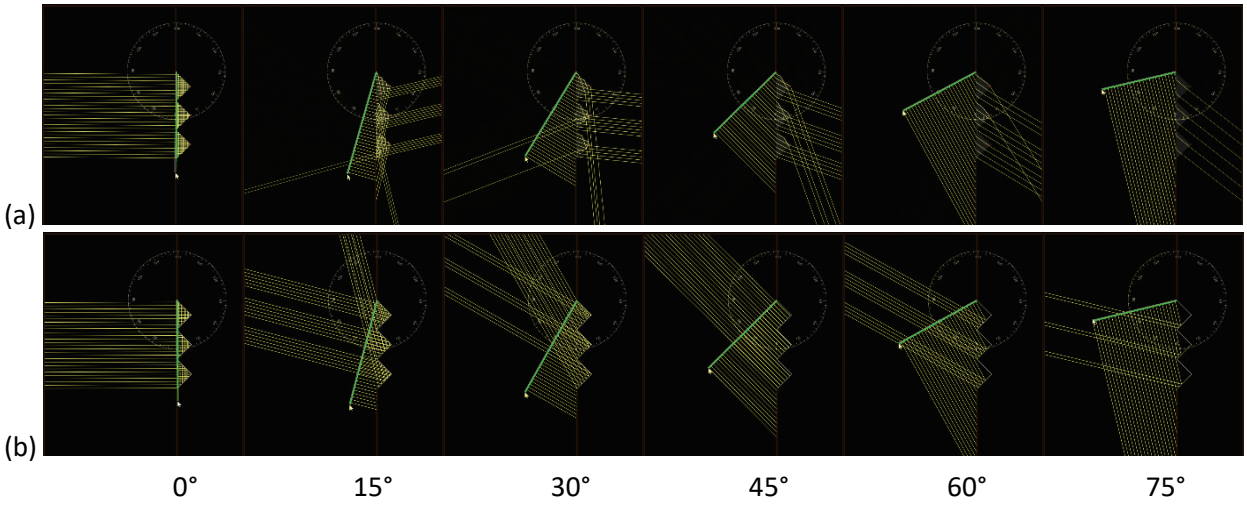

Reflection of beam light as a function of beam altitude angle, shown for (a) symmetric low-index glass (real refractive index 1.5) right triangular prisms, and (b) symmetric empty mirrors.

Source: Lawrence Berkeley National Laboratory

Figure 21: Reflections from a Safety Film

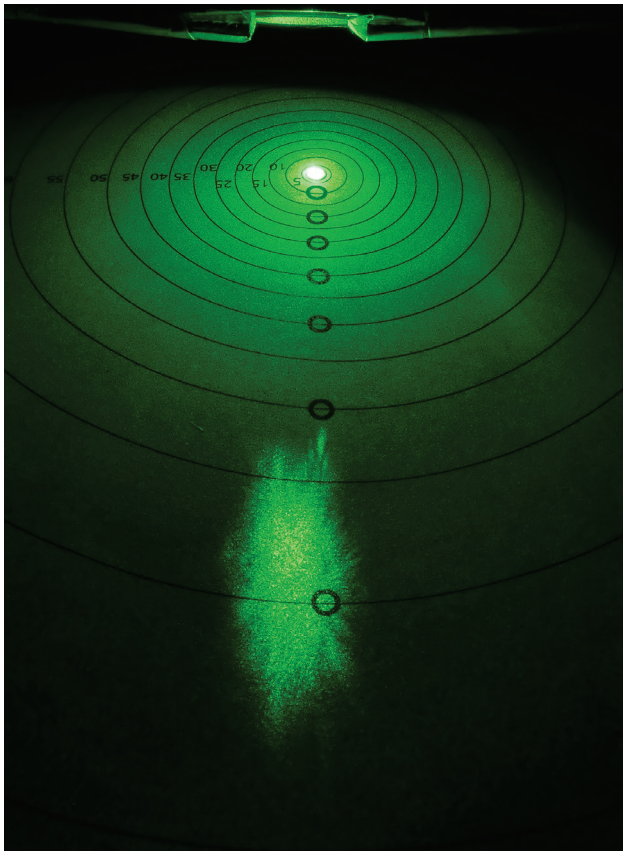

Retroreflection from this safety film is comparable to its specular reflection.

Source: Lawrence Berkeley National Laboratory

Figure 22: Example of Two-Surface Empty Mirror Retroreflector

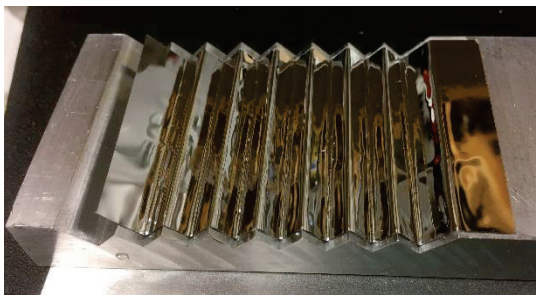

Aluminized Mylar taped to aluminum block with 7-mm pitch orthogonal grooves.

Source: Lawrence Berkeley National Laboratory

CHAPTER 6:
Promoting Cool-Wall Infrastructure (Task 6)

Task 6 promoted the infrastructure needed to advance the climate- and building-appropriate use of cool walls. This included developing cool-wall application guidelines (Task 6.1), hosting a cool-wall stakeholder workshop (Task 6.2), and exploring and enhancing the treatment of cool walls in building standards and incentive programs (Task 6.3).

Cool-wall Application Guidelines (Task 6.1)

This task introduces the concept of solar-reflective "cool" walls, and provides guidelines for their building- and climate-appropriate use to conserve energy and reduce emissions of greenhouse gases and criteria pollutants across California and the United States. First, it explores the nature of cool walls by answering the following questions:

1. What is a cool wall?
2. Why choose a cool wall?
3. Where do cool walls save energy?
4. Is a cool wall like a cool roof?
5. Do cool walls help mitigate the urban heat island effect?
6. How do cool walls affect pedestrian comfort?
7. Are there specifications for cool walls?
8. How can I find a cool-wall product?
9. Will cool walls lose reflectance over time?
10. Do cool walls cost more than conventional products?

Second, the task provides a simple guide to cool-wall effects by detailing the energy cost savings (or penalties) that arise from increasing wall reflectance in three common building categories – single-family home, medium office, and retail stand-alone (Figure 23). This includes identification of building vintage, calculating energy cost savings, and gauging cost effectiveness, with worked examples. The guidelines supply lookup tables and worked examples.

Third, the task provides a detailed guide to these effects by describing the operation and application of the Cool Surface Savings Explorer, a database tool that can report the cool-wall and cool-roof energy, energy cost, peak power demand, and emission savings simulated for many building categories (Figure 24). This includes tool installation, operation, and application.

Fourth, the task discusses how to adjust cool walls savings and penalties to account for shading and reflection by neighboring buildings by applying a "solar availability factor". Lookup tables are provided.

The complete guidelines are presented in the Task 6.1 report, Cool Wall Application Guidelines (Appendix P).

Figure 23: Three Building Prototypes Addressed in the Guidelines

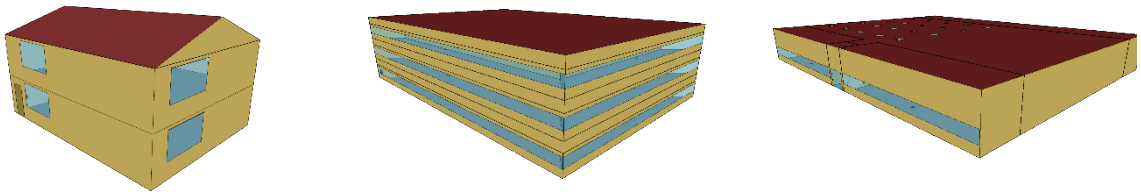

Sketches of the (a) single-family home, (b) medium office, and (c) retail stand-alone building prototypes.

Source: Lawrence Berkeley National Laboratory

Figure 24: Cool Surface Savings Explorer Interface

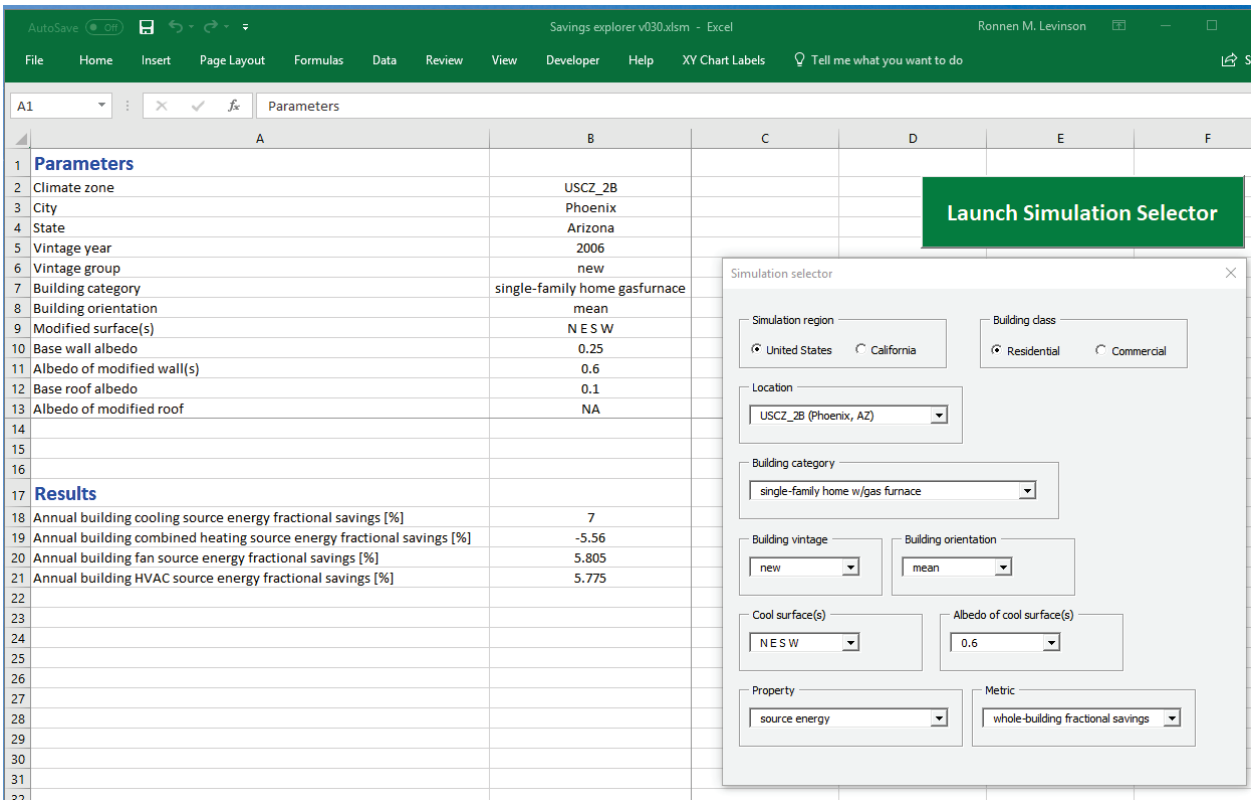

Cool Surface Savings Explorer used to report whole-building source energy fractional savings for a single-family home in Phoenix, Arizona.

Source: Lawrence Berkeley National Laboratory

Cool-wall Stakeholder Workshop (Task 6.2)

The research team hosted a “Cool Wall” stakeholder workshop in October 2017 to review and discuss its research portfolio with interested parties. The one-day event at LBNL was attended by industry, state government, federal government, utility, and building code stakeholders. There were 42 in-person and 6 remote participants. Presentations from the research team addressed energy and emission savings, changes to the urban environment, product aging, novel technologies, and infrastructure. The complete proceedings presented in the Task 6.2 report, Cool Wall Workshop Proceedings (Appendix Q), document the presentations and ensuing discussions.

The morning discussion centered on the underlying assumptions of the research modeling and simulation activities to calculate the building energy, energy cost, and emission savings. There was also discussion on how to interpret the results for specific locations and building/ neighborhood configurations, and discussion related to the cost, cost premium, and availability of cool-wall products.

In the afternoon, the discussion turned to the findings of the urban air temperature reductions from cool-wall deployment. Attendees asked many questions to understand how the results could potentially counter future warming and extreme heat days. They were also interested in discussing the effect of rooftop photovoltaic panels on urban climate.

Attendees posed several questions about the methods used to naturally expose and measure the cool-wall products. They were also interested to learn more about the self-cleaning and de-polluting potential of cool-wall products in the laboratory and from the climate models. Attendees shared insights on the development of retroreflective wall designs and suggested further research into applying metallic mica flakes in wall coatings.

The concluding discussion focused on advancing cool-wall adoption. Attendees inquired how long it would take to have cool-wall measures in building codes and standards, and how those measures would be specified. They expressed concern with specifying cool-wall measures for commercial buildings in which there is such variety in building design. Attendees seemed to agree that if there are cool-wall measures in California’s Building Energy Efficiency Standards, so goes the nation. They requested more field data to corroborate the simulation and modeling findings for building and city benefits.

Manufacturers cautioned that an energy savings claim on a product label has to be substantiated because they are legally liable for the claim and so would like as much concrete data as possible before marketing cool-wall products. They also expressed concern about limiting the color options for cool-wall coatings, noting that while consumers typically select one of about 10 colors, they still like to have many choices.

Figure 25: Cool-wall Stakeholder Workshop

Presentation at the Cool-wall Stakeholder Workshop held at Lawrence Berkeley National Laboratory in October 2017.

Source: Lawrence Berkeley National Laboratory

Advancements in Infrastructure Development: Building Standards and Incentive Programs (Task 6.3)

This task sought to advance the infrastructure needed to promote the appropriate use of cool-wall technologies. Following the model successfully used for cool roofs, activities included developing guidelines, evaluating feasibility of a product rating program, encouraging utility rebates, investigating ENERGY STAR label qualification, and pursuing credits/requirements in building energy standards and energy-efficiency programs (for example, California Title 24, ASHRAE 90.1, and LEED).

Cool roofs can be found on buildings across the United States. They are included in many city, state, and federal building codes/standards. To advance the adoption of cool walls, one can follow and learn from the cool-roof adoption model. Cool roofs were first incorporated in many codes/standards as credits and later became prescribed. The timeline in Figure 26 shows the time taken to adopt cool roofs and the accompanying incentives, such as an ENERGY STAR label and utility rebates. The process was aided by the establishment of the Cool Roof Rating Council (CRRC). The CRRC is an independent organization that has developed methods for evaluating and labeling roofing products for reference by codes, standards, and rebates. It has also propagated the cool roof concept and its rating program.

For cool walls, the research team began by investigating existing references to cool walls. The team found that ASHRAE 90.1 (2016), ASHRAE 189.1 (2014), the California Green Building Standards Code, the Green Building Initiative's Green Building Assessment Protocol for Commercial Buildings, and Hawaii's State Energy Conservation Code already reference cool

walls. The team also found references to cool walls in California's Property Assessed Clean Energy (PACE) program for residential buildings. This is good news because one can build upon these early cool-wall advances to increase inclusion of cool walls in other codes and programs. In addition, the researchers can share their recent findings with these organizations to improve and/or strengthen existing requirements.

Figure 26: Cool-roof Code Development Timeline

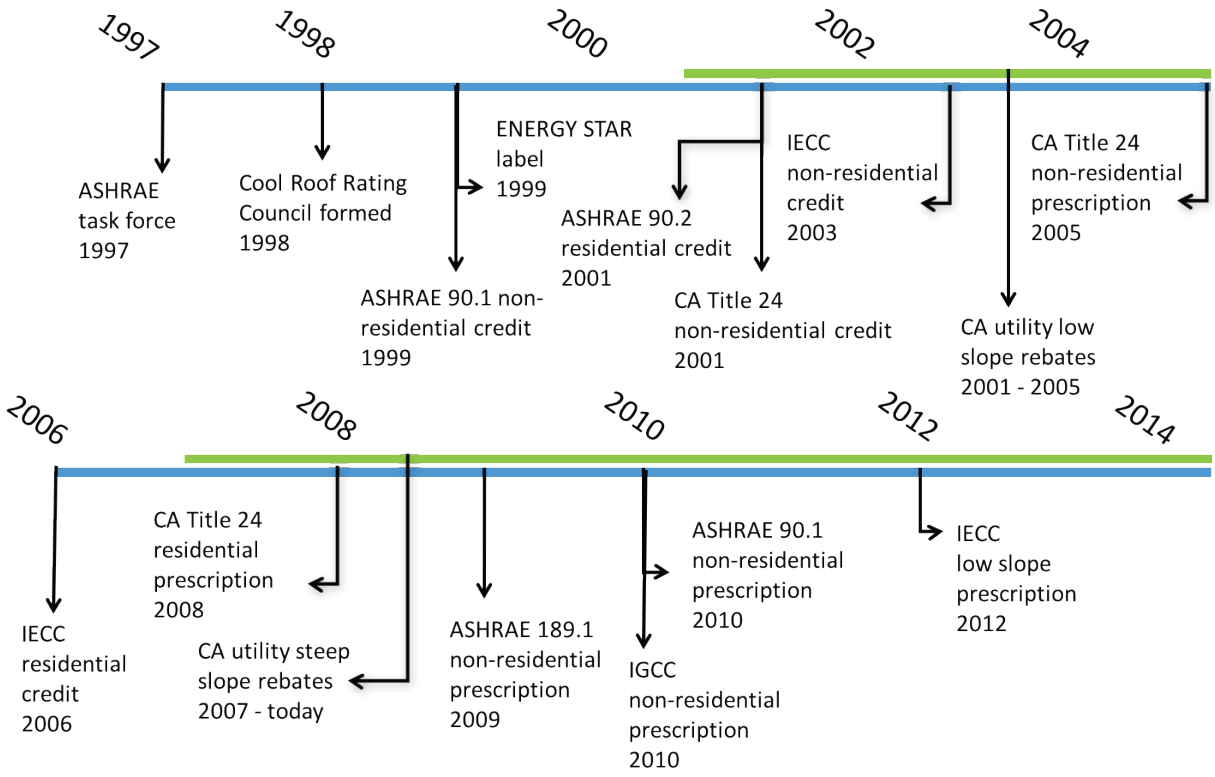

A timeline of the inclusion of cool roofs in major building codes/standards and other milestones.

Source: Lawrence Berkeley National Laboratory

The researchers are developing a pilot credit for the United States Green Building Council's LEED Sustainable Sites category, and exploring the feasibility of creating a rating organization for cool walls like the CRRC, or expanding the scope of the CRRC to include wall products.

However, much additional work beyond the project term will be needed to advance the adoption of cool walls. The researchers would like to collaborate with California utilities to develop cool-wall incentives, and to sponsor a Codes and Standards Enhancement initiative to evaluate how cool walls could be included in California's Title 24 Building Energy Efficiency Standards. In addition, the research team would like to pursue ENERGY STAR certification for cool-wall products.

Increasing the adoption of cool walls requires robust engagement from stakeholders. The adoption of cool walls will take time; thus, long term commitment from stakeholders will be critical. To facilitate stakeholder engagement, the researchers established a working group. The

objective of the working group is to advance appropriate adoption of cool walls by incorporating the technology into building codes and incentive programs, and disseminating information. The team formed the working group in fall 2017 and organized the group's first meeting in winter 2018.

The complete study is presented in the Task 6.3 report, Advancements in Infrastructure Development: Building Standards and Incentive Programs (Appendix R).

CHAPTER 7: Conclusions

Highlights

Energy Savings and Emission Reductions

Simulations indicate that cool walls save energy and reduce emissions in buildings across California and about half of the United States. The savings outlined below assume that the albedos of all four walls are raised simultaneously to 0.60 from 0.25. Each can be scaled by a solar availability factor to account for shading and reflection of sunlight by neighboring buildings.

California

- Cool walls lowered annual HVAC energy cost per unit modified surface area by $0.07/m²—$1.7/m² in single-family homes, $0.10/m²—$2.1/m² in medium offices, and $0.0/m²—$4.3/m² in stand-alone retail stores. They also reduced whole-building annual HVAC energy use by 3.0 percent—25 percent in single-family homes, 0.5 percent—3.7 percent in medium offices, and 0.0 percent—9.0 percent in stand-alone retail stores.
- Cool walls lowered annual HVAC carbon dioxide equivalent emissions per unit modified surface area by 0.0 kg/m²—3.4 kg/m² in single-family homes, 0.17 kg/m²—4.5 kg/m² in medium offices, and 0.16 kg/m²—9.2 kg/m² in stand-alone retail stores.
- Energy use, energy cost, and emission savings from the oldest vintage were generally three to six times greater than those from the new vintage. The cool-wall savings from the oldest vintage are important since they represent over 60 percent of California's building stock.

United States

- In warm United States climates – zones 1A (Miami, FL) through 4B (Albuquerque, NM) – cool walls lowered annual HVAC energy cost per unit modified surface area by $0.1/m²—$1.1/m² in single-family homes, $0.0/m²—$1.8/m² in medium offices, and $0.0/m²—$3.7/m² in stand-alone retail stores. They also reduced whole-building annual HVAC energy use by 2.0 percent—8.5 percent in single-family homes, 0.0 percent—4.2 percent in medium offices, and -0.5 percent—5 percent in stand-alone retail stores.
- In these zones, cool walls lowered annual energy HVAC carbon dioxide equivalent emissions per unit modified surface area by -0.37 kg/m²—5.3 kg/m² in single-family homes, 0.03 kg/m²—10.3 kg/m² in medium offices, and -1.2 kg/m²—20.9 kg/m² in stand-alone retail stores.
- As in California, the oldest vintage yielded greatest cool-wall savings or penalties. This is important since the oldest vintage buildings represent in most United States locations at least 60 percent of the building stock.

Human Comfort

Cool walls had negligible effect on indoor human comfort in an unconditioned building as well as on pedestrians passing by cool walls.

- The typical indoor air temperature reduction inside an unconditioned building with cool walls versus conventional walls was negligible. Since thermal sensation in buildings without air conditioning is generally cold at night and warm during the day this corresponds to a slight worsening of thermal comfort at night and an improvement of thermal comfort during the day.
- Thermal comfort changes for pedestrians walking next to a cool wall are small and will go unnoticed by most people.

Urban Air Temperature Reduction and Air Quality Improvement

Cool walls in Los Angeles provided similar urban air temperature reductions as cool roofs per unit increase in wall or roof albedo.

- The researchers for the first time assessed the influence of employing solar reflective "cool" walls on the urban energy budget and summertime climate of the Los Angeles basin. The team compared the climate effects of hypothetical city-scale cool-wall adoption to cool roof adoption.
- Per 0.10 wall (roof) albedo increase, widespread adoption of cool walls (roofs) can reduce summertime daily average canyon air temperature by 0.048—0.054 K (0.058—0.060 K).

Initial and Long-term Albedos of Wall Materials

After 24 months of natural exposure in California, cool-wall materials exhibited little to no loss in solar reflectance.

- The researchers exposed 69 cool-wall materials at three sites in California and 55 materials in three sites across the United States
- Factory-applied coatings showed excellent performance in all locations used for California and United States exposure, with negligible changes in solar reflectance.
- Field-applied coatings' retention of initial solar reflectance values varied with coating formulation, surface finish, and substrate. Field-applied coatings colored with cool pigments were significantly more reflective than similarly colored products incorporating conventional pigments.

Novel Cool-wall Technologies

Fluorescence (re-emission at longer wavelengths of light absorbed at shorter wavelengths) can expand the palette of colors for cool-wall products, while retroreflection (reflection of incident radiation toward its source) can increase the fraction of wall-reflected light that escapes the city.

- The researchers built a calorimetric instrument that measures effective solar reflectance, or the fraction of incident solar energy rejected by the combination of reflectance and fluorescence.
- Pink-red coatings colored with a fluorescent ruby pigment (aluminum oxide doped with chromium) can reject up to 15 percent of incident solar energy by invisibly re-emitting absorbed visible light. Blue, green, and blue-black coatings colored with fluorescent Egyptian blue or Han blue pigments provide a similar benefit.
- The fluorescent blue pigments may also be useful in fabrication of high-performance luminescent solar concentrators for photovoltaic panels.
- The greatest challenge in retroreflective wall design appears to be the need to operate at large incidence angles to reflect a substantial portion of incident sunlight.
- The most promising retroreflector design was a two-surface retroreflector with perpendicular metal mirror faces.

Infrastructure

There is some existing infrastructure within which to promote cool walls. Developing all necessary infrastructure is a long-term process that must continue after the project is completed.

- The research team developed a cool-wall working group that will continue to advance cool-wall adoption in incentive programs, building codes/standards, and green building programs.
- The research results led the Cool Roof Rating Council to form its own working group to consider expansion to wall products.
- The team developed cool-wall guidelines to identify the building- and climate-appropriate use of cool walls to conserve energy and reduce emissions of greenhouse gases and criteria pollutants across California and the United States.
- Researchers hosted a cool-wall stakeholder workshop to share our research results and solicit feedback from stakeholders.
- The team identified existing cool-wall measures in building codes/standards and ways to expand and enhance their specifications to maximize benefits. In addition, we initiated contact with other building codes/standards, green building programs, and incentive programs to develop new cool-wall measures, pilot credits, certification, and rebates.

California Policy Recommendations

- Incorporate cool-wall measures into California's Title 24 Building Energy Efficiency Standards for 2022. The measures should apply not only to new construction, but also to retrofits, since existing building enjoy the greatest savings.
- Include cool-wall measures in CALGreen's voluntary Tier 1 or 2 requirements for the urban heat island mitigation section for 2022. These voluntary Tier measures can then be easily adopted by local jurisdictions.
- Evaluate the contribution of photocatalytic urban surfaces to help cities, regional Air Quality Management Districts, and the California Air Resources Board meet air quality standards and goals. Analysis should also take into account that photocatalytic self-cleaning urban surfaces are able to maintain high albedo. By staying more reflective over time, the surfaces lead to greater urban temperature reductions than soiled surfaces, and can affect atmospheric chemistry.
- Change research funding structure to enable researchers to serve as technical points-of-contact for policy makers to implement and adopt beneficial EPIC research, such as cool-wall measures.
- Incorporate cool building envelope surfaces (roofs and walls) into low-income weatherization programs in warmer California climate zones to reduce energy demand in residences with air conditioning. This would support the *E-6 Increase climate resiliency in low-income and disadvantaged communities* measure in the Safeguarding California Plan: 2018 Update (CNRA, 2018), and be in coordination with California Department of Community Services and Development.

National Policy Recommendations

- Enhance cool-wall measures in ASHRAE 90.1 and ASHRAE 189.1, revising cool-wall specifications and extending measures to additional climate zones.
- Introduce a federal tax credit to incentivize home and business owners to purchase cool-wall products.

Next Steps

Further Research

While the cool-wall project's research design was comprehensive and evaluated many aspects of this technology and its application, there is need for further research.

- The climate effects of cool walls and roofs are expected to vary depending on building morphology, impervious cover, and the baseline climate of the city under investigation. Therefore, the researchers suggest future work to investigate the effects of cool-wall adoption in areas other than Los Angeles County.

- The research team initiated a 5-year national exposure program as part of this project, and have collected data from years 1 and 2. The team will need to collect data from years 3, 4, and 5 after the conclusion of the current project.
- The analysis presented here estimates city-level NO_x deposition, and does not consider whether photocatalytic self-cleaning walls may have larger air quality benefits for near-source concentrations within urban canyons. The research team suggests future work to estimate the impact of photocatalytic self-cleaning walls on near-source NO_x concentrations. Future work should also assess reactions removing other atmospheric contaminants, and the potential formation of gas- and particle-phase oxidation products by photocatalytic materials.
- The potential for directionally retroreflective walls to cool buildings and the urban environment is a win-win and thus merits further investigation to develop commercially viable prototypes.
- The fluorescence benefits of the prototype materials that were developed are encouraging. However, future work may be required to be apply them within building envelope materials.
- Researchers should develop a cool-wall monitoring and demonstration project that would include several building types in multiple climate zones to validate cool-wall benefits.
- Researchers should adapt to wall materials of the lab-aging practice currently available for roofing products (ASTM Standard D7897).

Advancing Adoption

To further the building- and climate-appropriate adoption of cool walls, the researchers suggest the following action items that build on the research findings:

- Launch California utility incentives for cool-wall products.
- Complete a cool-wall Codes and Standards Enhancement initiative to vet requirements and language for cool-wall measures in California's Title 24 Building Energy Efficiency Standards. An expansion of this initiative could also provide non-energy benefits that would be helpful for CALGreen cool-wall measure improvement.
- Find continued funding to support the cool-wall working group to advance cool-wall measures in incentive programs, building codes/standards, and green building programs, such as ASHRAE 90.1, ASHRAE 189.1, and the United States Green Building Council's LEED.
- Develop a United States Green Building Council's LEED cool-wall pilot credit.
- Improve the existing ASHRAE 90.1 and ASHRAE 189.1 cool-wall measures to expand into United States climate zones.
- Complete United States EPA ENERGY STAR certification of cool-wall products.

- Launch a cool-wall product rating program that would develop credible methods to evaluate and label products.
- Improve the existing State of Hawai'i building energy code to clearly specify cool-wall products.
- Develop case studies of existing buildings with cool walls to note the building owner's (or design team's) decision-making process when selecting cool-wall products.
- Advance inclusion of cool-wall measures in the International Energy Conservation Code.

GLOSSARY AND ACRONYMS

Term	Definition
Albedo	Synonym for “solar reflectance”
ASHRAE	Formerly known as the American Society of Heating, Refrigerating and Air-Conditioning Engineers; in 2012, as part of a rebranding, ASHRAE began doing business as “ASHRAE”.
ASTM	ASTM International, formerly known as American Society for Testing and Materials, is one of the world's largest international standards developing organizations.
Calorimetric	Using change in temperature to assess flow of heat
cm s^{-1}	Centimeters per second
CO_2	Carbon dioxide
CRRC	Cool Roof Rating Council
CuO	Copper oxide
EnergyPlus	A building energy use simulation tool supported by the United States Department of Energy.
EPIC	The Electric Program Investment Charge, created by the California Public Utilities Commission in December 2011, supports investments in clean energy technologies that benefit electricity ratepayers of Pacific Gas and Electric Company, Southern California Edison Company, and San Diego Gas & Electric Company.
ESR	Effective solar reflectance
g m^{-2}	Grams per square meter
Goniometer	An instrument that measures the variation of reflectance with angle
HCl	Hydrochloric acid
HVAC	Heating, ventilation, and air conditioning
ISO	International Organization for Standardization
K	Kelvin
kg	Kilogram
LBNL	Lawrence Berkeley National Laboratory

Term	Definition
LEED	Leadership in Energy and Environmental Design, a green building program operated by the US Green Building Council (USGBC).
LST	Local Standard Time
m^2	Square meter
mg	Milligram
mm	Millimeter
mol hr^{-1}	Moles per hour
MWh	Megawatt-hour
NIR	Near infrared
NO	Nitrogen monoxide
NO_2	Nitrogen dioxide
NO_x	Nitrogen oxides
PACE	Property Assessed Clean Energy, a program to help property owners finance renewable energy and energy efficiency improvements.
PBL	Planetary boundary layer
PMV	Predicted mean vote
SET*	Standard Equivalent Temperature
SHGC	Solar heat gain coefficient
Solar absorptance	Fraction of incident sunlight that is absorbed
Solar reflectance	Fraction of incident sunlight that is reflected
SR	Solar reflectance
TUF-IOBES	Temperature of Urban Facets – Indoor Outdoor Building Energy Simulator, a building energy use simulation tool developed by the University of California at San Diego.
µmol h^{-1}	Micromoles per hour
Urban canyon	The U-shaped space formed by buildings on opposite sides of a street
UV	Ultraviolet

Term	Definition
WRF	Weather Research and Forecasting, a numerical weather prediction system.

REFERENCES

Berdahl, P., Boocock, S. K., Chan, G. C.-Y., Chen, S. S., Levinson, R. M., & Zalich, M. A. (2018). High quantum yield of the Egyptian blue family of infrared phosphors ($MCuSi_4O_{10}$, M = Ca, Sr, Ba). *Journal of Applied Physics*, 123(19), 193103. https://doi.org/10.1063/1.5019808

Berdahl, P., Chen, S. S., Destaillats, H., Kirchstetter, T. W., Levinson, R. M., & Zalich, M. A. (2016). Fluorescent cooling of objects exposed to sunlight – The ruby example. *Solar Energy Materials and Solar Cells*, 157, 312–317. https://doi.org/10.1016/j.solmat.2016.05.058

CNRA. (2018). Safeguarding California: 2018 Update. California Natural Resources Agency. Retrieved from http://resources.ca.gov/docs/climate/safeguarding/update2018/safeguarding-california-plan-2018-update.pdf

Levinson, R. (2019). Using solar availability factors to adjust cool-wall energy savings for shading and reflection by neighboring buildings. *Solar Energy*, 180, 717–734. https://doi.org/10.1016/j.solener.2019.01.023

Levinson, R., Chen, S., Ferrari, C., Berdahl, P., & Slack, J. (2017). Methods and instrumentation to measure the effective solar reflectance of fluorescent cool surfaces. *Energy and Buildings*, 152, 752–765. https://doi.org/10.1016/j.enbuild.2016.11.007

Rosado, P. J., & Levinson, R. (2019). Potential benefits of cool walls on residential and commercial buildings across California and the United States: conserving energy, saving money, and reducing emission of greenhouse gases and air pollutants. *Energy and Buildings*, in press. https://doi.org/10.1016/j.enbuild.2019.02.028

South Coast Air Quality Management District. (2013). Air Quality Management Plan, Appendix V: Modeling and Attainment Demonstrations. Retrieved from http://www.aqmd.gov/docs/default-source/clean-air-plans/air-quality-management-plans/2012-air-quality-management-plan/final-2012-aqmp-(february-2013)/appendix-v-final-2012.pdf

Zhang, J., Mohegh, A., Li, Y., Levinson, R., & Ban-Weiss, G. (2018). Systematic comparison of the influence of cool wall versus cool roof adoption on urban climate in the Los Angeles Basin. *Environmental Science & Technology*, 52(19), 11188–11197. https://doi.org/10.1021/acs.est.8b00732

LIST OF APPENDICES

The following Appendices are available under separate cover:

Appendix A: Simulated Heating, Ventilation, and Air Conditioning Energy Savings in an Isolated Building (Task 2.1 report): See CEC-500-2019-040-APA

Appendix B: Effect of Neighboring Cool Walls on Heating, Ventilation, and Air Conditioning Loads (Task 2.2 report): See CEC-500-2019-040-APB

Appendix C: Using Solar Availability to Scale Heating, Ventilation, and Air Conditioning Energy Savings (Task 2.3 report): See CEC-500-2019-040-APC

Appendix D: Pedestrian Mean Radiant Temperature and Thermal Comfort (Task 3.1 report): See CEC-500-2019-040-APD

Appendix E: Urban Climate Impacts of Cool Walls (Task 3.2 report): See CEC-500-2019-040-APE

Appendix F: Effect of Cool Walls on Energy-saving Benefits from Cool Pavements (Task 3.3 report): See CEC-500-2019-040-APF

Appendix G: Effect of Wall Albedo on the Environment inside an Unconditioned Building (Task 3.4 report): See CEC-500-2019-040-APG

Appendix H: Effects of Self-cleaning Walls on Urban Air Quality (Task 3.5 report): See CEC-500-2019-040-APH

Appendix I: Metrics and Methods to Assess Cool Wall Performance (Task 4.1 report): See CEC-500-2019-040-API

Appendix J: Natural Exposure of Wall Products (Task 4.2 report): See CEC-500-2019-040-APJ

Appendix K: Self-cleaning and De-Polluting Photocatalytic Materials (Task 4.3 report): See CEC-500-2019-040-APK

Appendix L: Assessment of Existing and New Retroreflective Materials (Task 4.4 report): See CEC-500-2019-040-APL

Appendix M: Improvement of Self-cleaning Coatings and Claddings (Task 5.1 report): See CEC-500-2019-040-APM

Appendix N: Development of Fluorescent Cool Pigments (Task 5.2 report): See CEC-500-2019-040-APN

Appendix O: Development of Retroreflective Materials (Task 5.3 report): See CEC-500-2019-040-APO

Appendix P: Cool Wall Application Guidelines (Task 6.1 report): See CEC-500-2019-040-APP

Appendix Q: Cool Wall Workshop Proceedings (Task 6.2 report): See CEC-500-2019-040-APQ

Appendix R: Advancements in Infrastructure Development: Building Standards and Incentive Programs (Task 6.3 report): See CEC-500-2019-040-APR

Energy Research and Development Division

FINAL PROJECT REPORT

Solar-Reflective "Cool" Walls: Benefits, Technologies, and Implementation

Appendix A: Simulated HVAC Energy Savings in an Isolated Building (Task 2.1 Report)

California Energy Commission
Gavin Newsom, Governor

April 2019 | CEC-500-2019-040-APA

Appendix A:
Simulated HVAC energy savings in an isolated building (Task 2.1 report)

Pablo Rosado[1] and Ronnen Levinson[1]

[1] Heat Island Group, Lawrence Berkeley National Laboratory

29 June 2018

Abstract

Solar-reflective “cool” walls reduce absorption of sunlight by the building envelope, which may decrease cooling load in warm weather and increase heating load in cool weather. Changes to annual heating, ventilation, and air conditioning (HVAC) energy use depend on climate, wall construction, wall orientation, building geometry, HVAC efficiency, and operating schedule. Changes to annual energy cost and energy-related emissions vary with local energy prices and emission factors. We used EnergyPlus to perform over 100,000 building energy simulations, spanning 10 different building categories, three building vintages, 16 California climate zones, and 15 United States climate zones. The simulations parametrically varied wall albedo (solar reflectance), roof albedo, combination of walls modified, and building orientation. Cool walls yielded annual source energy, energy cost, and emission savings in all California climate zones and in warm U.S. (ASHRAE) climate zones.

In California, cool walls reduced whole-building annual HVAC energy use 3.0 percent to 25 percent in single-family homes, 0.5 percent to 3.7 percent in medium offices, and 0.0 percent to 9.0 percent in stand-alone retail stores. In warm U.S. climates—zones 1A (Miami, FL) through 4B (Albuquerque, NM)—cool walls reduced whole-building annual HVAC energy use 2.0 percent to 8.5 percent in single-family homes, 0.0 percent to 4.2 percent in medium offices, and -0.5 percent to 5 percent in stand-alone retail stores. Cool walls also yielded small annual HVAC source energy savings in some cold U.S. climates—zones 4C (San Francisco, CA) through 7 (Duluth, MN)—for certain building categories and vintages. Annual HVAC source energy savings intensities (savings per unit surface area modified) from east, south, and west walls were similar, and always greater than those from the north wall.

While walls often receive less incident solar energy per unit area than roofs, they are also less insulated than roofs. Therefore, savings intensities from modifying the four walls (albedo

increase 0.35) were often comparable to those from modifying the roof (albedo increase of 0.30 in residential and 0.40 in commercial). The ratio of whole-building savings from cool walls (raising the albedo of all four walls) to that from a cool roof also depends on the ratio of net wall area (wall area excluding openings) to roof area. In California, the ratio of whole-building cool wall savings to cool roof savings was 1.5 to 3.5 in single-family homes, 0.40 to 1.0 in medium offices, and 0.20 to 0.85 in stand-alone retail stores. In warm U.S. climates (zones 1A through 4B), the ratio of whole-building cool wall savings to cool roof savings was 0.80 to 1.9 in single-family homes, 0.20 to 1.9 in medium offices, and 0.30 to 2.1 in stand-alone retail stores.

1 Introduction

Solar-reflective “cool” walls reduce absorption of sunlight by the building envelope, which may decrease a building’s cooling load in warm weather and increase its heating load in cool weather. The change in a building’s annual heating, ventilation, and air conditioning (HVAC) energy use depends on climate, wall construction, wall geometry, and wall orientation, along with other details of the building, such as HVAC efficiency and operating schedule.

The solar irradiation (solar energy per unit surface area) that strikes a surface decreases with beam incidence angle, or angle between solar beam and surface normal. At noon in summer, the sun is high, and a horizontal roof receives beam (direct) solar irradiation at a small incidence angle. In winter, the sun is lower, the roof’s solar incidence angle is greater, and the days are shorter (Abood 2015); in some climates, winter skies may also be cloudier (Wilcox and Marion 2008). Thus, we expect a horizontal roof to receive more daily solar irradiation in summer than in winter.

The decrease in cooling load and increase in heating load upon raising wall albedo are each proportional to the sunlight intercepted by the walls. Thus, we expect walls that receive more sunlight to contribute more to the changes in cooling and heating loads.

Consider a building in the northern hemisphere with walls that face north, east, south, and west. On a clear day, we expect east and west walls to receive similar daily solar irradiation given the east-west symmetry of the solar path. Beam solar irradiation strikes the east wall in the morning and the west wall in the afternoon. The summer sun rises in the northeast and sets in the northwest. The solar path in summer peaks close to zenith in the southern sky. In winter, the sun rises in the southeast and sets in the southwest; the solar path peaks in the southern sky at a small elevation angle (Abood 2015; Schroeder 2011). Therefore, the north wall receives beam solar irradiation only during early morning and late afternoon of summer days. Under clear skies, the south wall will receive more beam sunlight in winter than in summer because the sun is lower, the wall’s minimum beam incidence angle is smaller, and the wall is exposed to more hours of direct illumination (Abood 2015).

Given the differences in exposure to daily solar irradiation based on orientation, we expect the north wall to yield the smallest summer cooling energy savings and smallest winter heating

energy penalties among all walls. In summer, we expect the east and west walls to yield greater cooling energy savings than the north and south walls. During winter, we expect the south wall to yield the greatest heating energy penalties and the north wall to yield the smallest heating energy penalties. In the United States (U.S.), the first building codes were developed in mid-1970s (Hunn 2010). Before the adoption of the first building codes, residential buildings were erected with little insulation in roofs and often had little to no insulation in walls (Huang et al. 1999). Since then, new codes have been released periodically, often raising insulation requirements. The efficiency of HVAC systems has also increased over time (Table 8-1 in CEC 2016b). The service life of an HVAC system depends on its maintenance but is typically 15 to 25 years (Comfort-Pro 2015). Therefore, we expect cooling savings and heating penalties to be greatest in old buildings that were erected prior to the first building codes and have HVAC systems near end of service life. New buildings comply with the most stringent insulation and HVAC efficiency requirements. Hence, we expect new buildings to yield the smallest cooling savings and heating penalties.

Past and current U.S. building codes prescribe more insulation in roofs than in walls (Table 8-1 in CEC 2016b; Huang et al. 1999; Blum 2007). Therefore, code-complaint walls provide less resistance to heat flow across the envelope than code-compliant roofs. If a building's four walls (considered together) and roof have the same total opaque surface area, receive equal solar energy, and undergo the same increase in albedo (solar reflectance), we expect the walls to yield greater cooling energy savings and heating energy penalties. Of course, cool surface energy savings will also scale with solar irradiation and modified surface area.

Envelope insulation, solar irradiation, and surface area are considered in detail in the current study. However, for a simple example, consider how the ratio of roof area to net wall area (wall area excluding openings, such as windows and doors) can vary between buildings. A one-floor building with a large footprint, such as a single-story box store, will often have a large roof area to net wall area ratio. This ratio decreases with building height since the wall area is proportional to the number of floors while the roof area remains the same. In multi-floor buildings, a cool roof affects the HVAC energy use of only the top floor while cool walls influence the HVAC energy use of every above-grade floor. Thus, all else being equal, we expect cooling savings and heating penalties from cool walls to be greater than those from a roof when the building has a small ratio of roof area to net wall area.

Many workers have simulated cool roof energy savings and penalties in the U.S. (Akbari et al. 1999; Akbari and Konopacki 2005; Levinson and Akbari 2010; Parker et al. 1998), China (Gao et al. 2014); India (Bhatia et al. 2011), Spain (Boixo et al. 2012), and in major cities around the word (Synnefa et al. 2007). However, cool *wall* studies are few and limited in scope. For example, Petrie et al. (2007) used the building energy simulation tool DOE 2.2 to estimate cool-wall energy savings and penalties for a small house in seven U.S. cities, while Moujaes and Brickman (2003) used the 1-D transient heat transfer model RESHEAT to estimate the cool-wall cooling load reduction for a house in Las Vegas, NV.

To quantify the effect of cool walls on individual buildings, we created code-compliant building prototypes representing three vintages of 10 categories of buildings. Using EnergyPlus—a whole building energy use simulation program—we modeled the cooling, heating, and fan energy uses of each prototype to evaluate annual site energy, site peak power demand, source energy, energy cost, and emission savings upon raising wall albedo or roof albedo. Prototype simulations parametrically varied wall albedo or roof albedo, combination of walls modified, and orientation of the building's long axis (east-west or north-south). Simulations spanned climate zones across California and the United States.

We present in this report a subset of the California and U.S. savings and penalties to compare (a) cool wall savings to cool roof savings; (b) cool wall savings between locations; (c) cool wall savings from modifying different wall combinations; (d) savings from different vintages; and (e) the sum of savings from walls modified one at a time to savings from modifying the same set of walls simultaneously.

2 Methodology

2.1 Locations

The effects of cool walls in California were evaluated in the 16 building climate zones established by California Energy Commission (CEC) (CEC 2015). To represent these 16 California climate zones (CACZs), the building energy simulations were executed using weather data from 16 representative cities or towns (Table 1). Figure 1 shows the region covered by each California climate zone.

We also evaluated cool wall effects in 15 ASHRAE climates zones across the United States, which we refer to as United States climate zones (USCZs). Table 2 lists the cities used to represent the U.S. climate zones and Figure 2 shows the region of each U.S. climate zone. The U.S. climate zones are numbered from hottest (USCZ 1A) to coldest (USCZ 8). The letters in the U.S. climate zone name help distinguish between humid (A), dry (B), and marine (C) climates Briggs et al. (2003a,b).

Table 1. Cities or towns in California used to represent its 16 building climate zones.

City or town	CACZ		City or town	CACZ
Arcata	1		Burbank	9
Santa Rosa	2		Riverside	10
Oakland	3		Red bluff	11
San Jose	4		Sacramento	12
Santa Maria	5		Fresno	13
Long Beach	6		China Lake	14
San Diego	7		Imperial	15
Fullerton	8		Mount Shasta	16

Table 2. Cities in United States used to represent ASHRAE climate zones.

City	State	ASHRAE CZ
Miami	Florida	1A
Houston	Texas	2A
Phoenix	Arizona	2B
Memphis	Tennessee	3A
El Paso	Texas	3B
San Francisco	California	3C
Baltimore	Maryland	4A
Albuquerque	New Mexico	4B
Salem [a]	Oregon	4C
Seattle [b]	Washington	4C
Chicago [a]	Illinois	5A
Peoria [b]	Illinois	5A
Boise	Idaho	5B
Burlington	Vermont	6A
Helena	Montana	6B
Duluth	Minnesota	7
Fairbanks	Alaska	8

[a] For commercial prototypes only.

[b] For residential prototypes only.

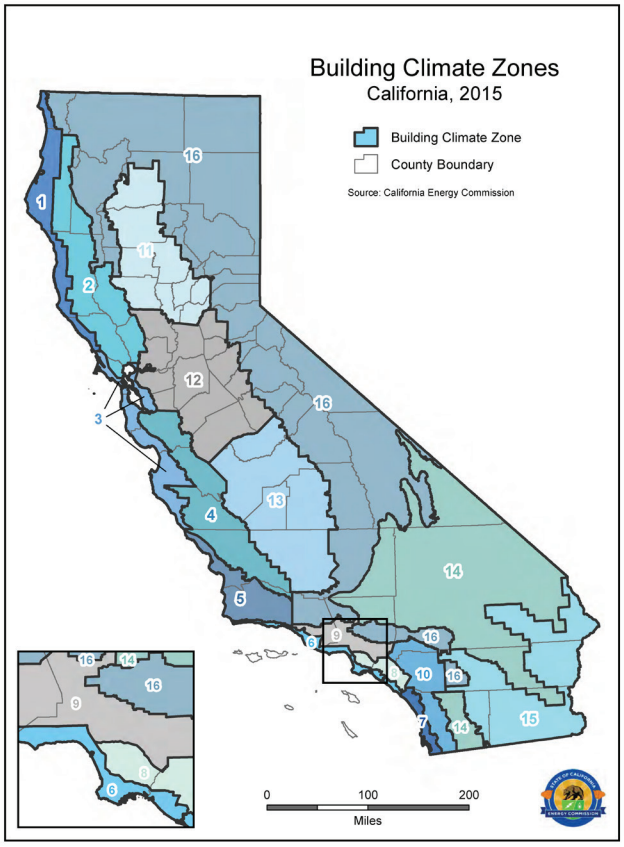

Figure 1. Map of California building climate zones (CEC 2015).

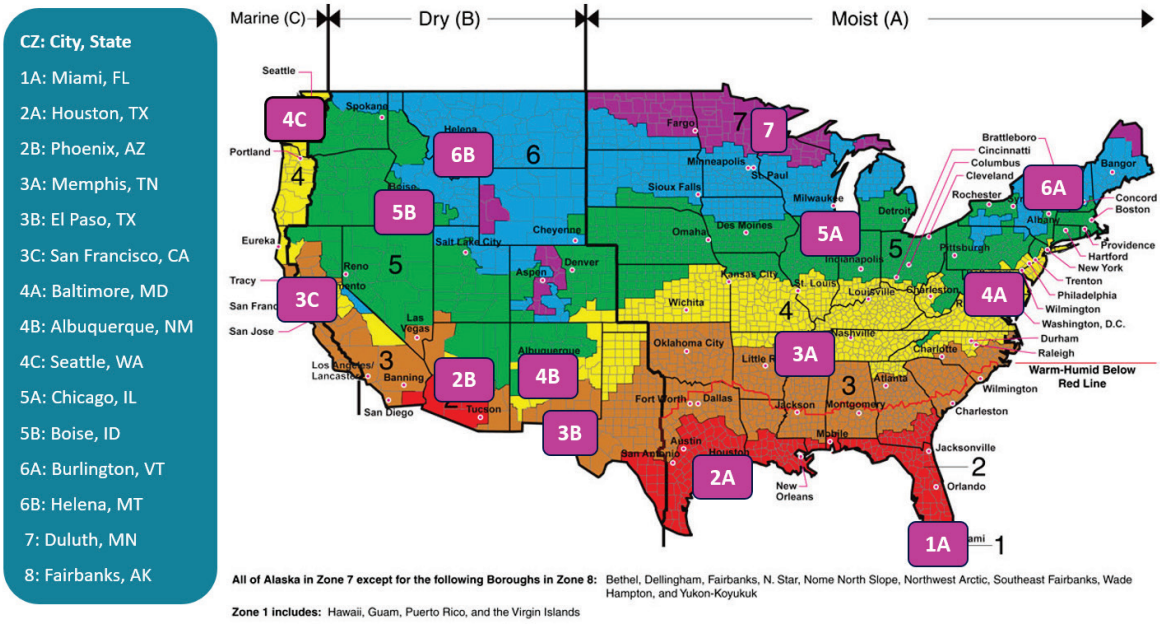

Figure 2. Map of ASHRAE climate zones in the United States, locating representative cities. Adapted from Briggs et al. (2003a,b).

2.2 Representative building vintages

The 2012 Commercial Building Energy Consumption Survey, or CBECS (EIA 2012) and 2009 Residential Energy Consumption Survey, or RECS (EIA 2009) were used to assess the age distribution of the country's current building stock by census division (for commercial buildings) or by state (for residential buildings). In most of the U.S. (including California), 40 percent to 60 percent of the buildings were erected before 1980. The decade of 1980 was typically the next period with significant building construction. In recent years, many states have also experienced rapid construction. Task Report Appendix A details our analysis of the age of U.S. buildings.

To represent California and U.S. building stock, this study analyses the effects of cool walls in three different building vintages: (a) *new* (for construction following current building codes), (b) *older* (for buildings erected in the 1980s), and (c) *oldest* (for pre-1980 buildings). In many U.S. regions, the older and oldest vintage prototypes represent about 75 percent of the residential building stock and 70 percent of the commercial building stock (Task Report Appendix A).

2.3 Building prototypes

2.3.1 Source of residential-building prototypes

The United States Department of Energy (hereafter, DOE) provides through its Building Energy Codes Program (BECP) a collection of prototypes for two building categories: single-family home and apartment building. These prototypes were generated to evaluate the energy and economic savings available by upgrading building energy efficiency standards to the latest version of the International Energy Conservation Code (IECC). BECP provides three sets of prototypes, each following a different IECC edition (year 2006, 2009, or 2012) (PNNL 2016a). BECP's collection of residential prototypes include versions for 199 cities across United States, covering all 15 U.S. climate zones. BECP provides variants of each residential prototype with different building foundations (slab, crawlspace, heated basement, or unheated basement) and heating systems (gas furnace, oil furnace, heat pump, or electric resistance).

To study cool walls in California, we selected BECP single-family home and apartment building prototypes with concrete slab foundation and gas furnace heating. These two prototypes were then modified following HVAC efficiency and building envelope insulation prescriptions in California Title 24 building energy efficiency standards. A version of each prototype was generated for each of California's 16 climate zones. In new construction prototypes, we set the HVAC efficiencies as well as the roof and wall insulations in accordance with 2016 Title 24 (CEC 2016b). Roof and wall insulation levels in older vintage prototypes were assigned following 1988 Title 24 (CEC 1988). Roof and wall insulation in the oldest vintage were set using envelope properties typical of buildings constructed before 1978—the year of the first Title 24 standards. The HVAC efficiencies of the older and oldest California residential prototypes

comply with 2005 Title 24 standards (CEC 2005). California prototype HVAC efficiencies and insulation levels are further detailed in Section 2.3.4 and Section 2.3.5, respectively.

To study cool walls throughout the U.S., we selected BECP prototypes defined in the 15 U.S. climate zones listed in Table 2. Each prototype has a concrete slab foundation. We simulated three heating systems (gas furnace, heat pump, and electric resistance) in each U.S. climate zone. Each of the 15 cities used to represent the 15 ASHRAE climate zones is located in a different U.S. state. Since the rate of IECC adoption varies by state (BCAP 2017), the prototypes selected to represent new residential buildings in each of the 15 cities follow the IECC edition currently mandated in the state containing that city (Table 3).

Starting from these new construction prototypes, we generated the older and oldest vintage prototypes, setting roof and wall insulation following Huang et al. (1999), and HVAC efficiency following IECC 2006. HVAC efficiencies and insulation levels in the U.S. prototypes are further detailed in Section 2.3.4 and Section 2.3.5, respectively.

Table B-2 describes the geometry, envelope construction, and HVAC system for each vintage of the single-family home.

2.3.2 Source of commercial-building prototypes

DOE, in collaboration with three national laboratories[1], developed reference prototypes of 15 commercial building categories that represent realistic building characteristics and construction practices in U.S. (Deru et al. 2011). DOE produced a suite of prototypes that follow pre-1980 construction practices. They generated another version of the prototypes that follow ASHRAE Standard 90.1-1989. To represent new constructions, DOE has periodically released versions of their prototypes that follow recent editions of ASHRAE 90.1 (i.e., 2004, 2007, 2010, and 2013) (PNNL 2016b).

The California Energy Commission (CEC) adapted the prototypes of eight of the 15 DOE commercial building categories to meet 2008 Title 24. For our California study, we modified the CEC prototypes to represent oldest, older, and new vintages in California. The insulation levels in the oldest vintage follow pre-Title 24 construction practices. In the older vintage, insulation levels comply with 1988 Title 24 Standard (CEC 1988). The HVAC efficiencies in the older and oldest vintage meet 2005 Title 24 Standard (CEC 2005). In the new vintage, insulation levels and HVAC efficiencies comply with 2016 Title 24 Standard (CEC 2016a).

For our U.S. study, we selected from DOE prototypes the eight commercial building categories used in the California study. The suite of DOE prototypes that follow pre-1980 construction practices were used to represent oldest vintage. The versions of the DOE prototypes that

[1] The National Renewable Energy Laboratory (NREL), Pacific Northwestern National Laboratory (PNNL), and Lawrence Berkeley National Laboratory (LBNL).

comply with ASHRAE 90.1-1989 were used to represent older vintage. The HVAC efficiencies in the older and oldest vintage comply with ASHRAE 90.1-2001. We simulated new commercial buildings with the prototypes in each of the 15 cities that follow the ASHRAE 90.1 edition currently mandated in the state containing that city (Table 3).

Task Report Appendix B illustrates the 10 building types simulated in this study. Table B-3 and Table B-4 describe for the medium office and stand-alone retail, respectively, the geometry, envelope construction, and HVAC system by vintage.

Table 3. Building codes adopted by state for new residential and commercial buildings (BCAP 2017).

State	ASHRAE CZ	New vintage prototypes meet the following building code	
		ASHRAE 90.1 (for commercial prototypes)	IECC (for residential prototypes)
Florida	1A	2010	2012
Texas	2A	2013	2012
Arizona	2B	2004	2006
Tennessee	3A	2010	2006
Texas	3B	2013	2012
California	3C	2013	2012
Maryland	4A	2013	2012
New Mexico	4B	2007	2009
Oregon	4C	2010	NA [a]
Washington	4C	NA [a]	2012
Illinois	5A	2013	2012
Idaho	5B	2010	2009
Vermont	6A	2013	2012
Montana	6B	2010	2009
Minnesota	7	2010	2012
Alaska	8	2004	2006

[a] BECP provides commercial, but not residential, prototypes for the city of Salem, Oregon. We modeled buildings in USCZ 4C with BECP commercial prototypes specified for Salem, Oregon, and BECP residential prototypes defined for Seattle, Washington (about 300 km north of Salem).

2.3.3 Building category geometry

Table 4 summarizes the geometry of each building category.

Table 4. Geometry of BECP prototypes representing each building category.

Building category	Floors	Conditioned floor area [1000 m²]	Footprint area [1000 m²]	Roof area [1000 m²]	Net wall area [a] [1000 m²]	Window area [1000 m²]	Window-to-wall ratio [b]	Roof-to-wall ratio [c]	Floor-to-wall ratio [d]
Single-family home	2	0.223	0.112	0.118	0.184	0.033	0.15	0.61	1.16
Apartment building	3	2.01	0.669	0.785	1.17	0.247	0.18	0.57	1.72
Large hotel	6	11.4	1.89	1.98	2.81	1.21	0.30	0.70	4.04
Large office	13	46.3	3.56	3.56	6.95	4.64	0.40	0.51	6.66
Medium office	3	4.98	1.66	1.66	1.32	0.653	0.33	1.25	3.77
Small office	1	0.511	0.511	0.599	0.222	0.060	0.21	2.30	2.36
Fast-food restaurant	1	0.232	0.232	0.232	0.160	0.026	0.16	1.45	1.44
Retail stand-alone	1	2.29	2.29	2.29	1.09	0.084	0.07	2.07	2.10
Strip mall retail	1	2.09	2.09	2.09	1.06	0.124	0.10	1.96	1.97
Sit-down restaurant	1	0.511	0.511	0.511	0.229	0.047	0.18	2.24	2.22

[a] Net wall area excludes windows and doors.

[b] Ratio of window area to gross wall area (area of entire wall, including openings).

[c] Ratio of roof area to net wall area.

[d] Ratio of conditioned floor area to net wall area.

2.3.4 HVAC efficiencies

An air conditioner or furnace has a service life of about 15 to 25 years, depending on how well it is maintained (Comfort-Pro 2015). Thus, we expect that HVAC systems in older and oldest vintage buildings have been replaced at least once and their current HVAC system can be anywhere from new to 25 years old. Since the age of the HVAC system in these vintages varies widely, we assume for purposes of this study that the HVAC system in an older or oldest vintage building is on average 10 years old. For such prototypes, we assigned HVAC efficiencies that comply with building codes in effect 10 to 15 years ago.

For the California study, the HVAC efficiencies in the older and oldest vintage prototypes were modified to match 2005 Title 24 standards, which is a 12-year old code (CEC 2005). The HVAC efficiencies of all new prototypes were set to follow 2016 Title 24 standards (CEC 2016c). Table 5 specifies the air conditioner cooling coefficient of performance (COP), and the gas furnace annual fuel utilization efficiency (AFUE) or electric heat pump heating COP, assigned to each vintage and building category in California.

Table 5. HVAC efficiencies and year of Title 24 (T24) standards used in all California prototypes by vintage.

Building category	Air conditioner cooling COP [a]		Gas furnace AFUE or electric heat pump heating COP [b]	
	Older and oldest (2005 T24)	New (2016 T24)	Older and oldest (2005 T24)	New (2016 T24)
Single-family home	2.64	3.69	0.80	0.80
Apartment building	2.64	3.69	0.80	0.80
Large hotel	2.80	2.96	0.75	0.80
Large office	6.10	6.30	0.75	0.80
Medium office	3.78	3.96	0.80	0.80
Small office	2.96	3.49	3.20	3.49
Fast-food restaurant	2.84	3.49	0.80	0.80
Retail stand-alone	2.84	3.49	0.80	0.80
Strip mall retail	2.84	3.49	0.80	0.80
Sit-down restaurant	2.84	3.49	0.80	0.80

[a] Title 24 typically reports Energy Efficiency Ratio (EER) or Seasonal Energy Efficiency Ratio (SEER). To obtain COP, note that 1 EER = COP × 3.413 and 1 SEER = COP × 3.792 (ECOX 2017).

[b] Small office is heated with an electric heat pump, while all other prototypes are heated with a gas furnace.

For the U.S. study, we modified the HVAC efficiencies in the older and oldest vintage prototypes to comply with ASHRAE 90.1-2001 (ASHRAE 2001) in the commercial buildings and with IECC 2006 (IECC 2006) in the residential buildings. In new vintage prototypes, we set the HVAC efficiencies in accordance with the ASHRAE 90.1 edition currently mandated in the state containing the city simulated for each U.S. climate zone. Table 6 and Table 7 give the furnace AFUE, heat pump heating COP, and air conditioner cooling COP by vintage in the residential and commercial buildings, respectively.

Table 6. HVAC efficiencies used in the U.S. residential buildings by vintage. The table also shows the year of the IECC standards from which the efficiencies were obtained.

Building category	Gas furnace AFUE (year of IECC)		Heat pump heating COP (year of IECC)		Air conditioner cooling COP [a] (year of IECC)	
	Older and oldest	New	Older and oldest	New	Older and oldest	New
Single-family home	0.80 (2006)	0.80 (2006, 2009, 2012)	3.04 (2006)	3.04 (2006) 3.26 (2019, 2012)	2.64 (2006)	2.64 (2006) 3.43 (2019, 2012)
Apartment building	0.80 (2006)	0.80 (2006, 2009, 2012)	3.04 (2006)	3.04 (2006) 3.26 (2019, 2012)	2.64 (2006)	2.64 (2006) 3.43 (2019, 2012)

[a] IECC typically reports EER or SEER. To obtain COP, note that 1 EER = COP × 3.413 and 1 SEER = COP × 3.792 (ECOX 2017).

Table 7. HVAC efficiencies used in the U.S. commercial buildings by vintage. The table also shows the year of the ASHRAE 90.1 standards from which the efficiencies were obtained.

Building category	Gas furnace AFUE (year of ASHRAE 90.1)		Heat pump heating COP (year of ASHRAE 90.1)		Air conditioner cooling COP [b] (year of ASHRAE 90.1)	
	Older and oldest	New	Older and oldest	New	Older and oldest	New
Large hotel	0.75 (2001)	0.75 (2004, 2007, 2010) 0.80 (2013)	NA[a]	NA	2.80 (2001)	2.80 (2004, 2007, 2010) 2.96 (2013)
Large office	0.79 (2001)	0.790 (2004) 0.793 (2007, 2010) 0.813 (2013)	NA	NA	6.10 (2001)	6.10 (2004, 2007, 2010) 6.28 (2013)
Medium office	0.80 (2001)	0.80 (2004, 2007, 2010, 2013)	NA	NA	2.84 (2001)	3.23 (2004, 2007) 3.40 (2010, 2013)
Small office	0.80 (2001)	0.80 (2004, 2007, 2010, 2013)	3.00 (2001)	3.00 (2004) 3.29 (2007, 2010) 3.36 (2013)	2.64 (2001)	3.14 (2004) 3.91 (2007, 2010) 4.12 (2013)
Fast-food restaurant	0.80 (2001)	0.80 (2004, 2007, 2010, 2013)	NA	NA	2.84 (2001)	3.30 (2004, 2007) 3.80 (2010, 2013)
Retail stand-alone	0.80 (2001)	0.80 (2004, 2007, 2010, 2013)	NA	NA	2.84 (2001)	3.30 (2004, 2007) 3.80 (2010, 2013)
Strip mall retail	0.80 (2001)	0.80 (2004, 2007, 2010, 2013)	NA	NA	2.84 (2001)	3.30 (2004, 2007, 2010) 3.80 (2013)
Sit-down restaurant	0.80 (2001)	0.80 (2004, 2007, 2010, 2013)	NA	NA	2.84 (2001)	3.30 (2004, 2007) 3.80 (2010, 2013)

[a] NA = Not applicable.

[b] ASHRAE 90.1 typically reports EER or SEER. To obtain COP, note that 1 EER = COP × 3.413 and 1 SEER = COP × 3.792 (ECOX 2017).

2.3.5 Building envelope

2.3.5.1 Envelope construction

All residential prototypes in California and U.S. were simulated with wood frame walls. Their roofs were simulated with a wood frame attic (Table 8 and Table 9).

In California, the envelope construction of each building category did not vary by vintage. Most commercial buildings were simulated with metal frame walls and a metal frame roof. The large hotel had heavy mass walls (Table 8).

Table 8. Types of wall and roof constructions simulated in each of the California building categories for all vintages.

Building category	Walls	Roof
Single-family home	wood frame	attic and wood frame
Apartment building	wood frame	attic and wood frame
Large hotel	heavy mass	metal frame
Large office	metal frame	metal frame
Medium office	metal frame	metal frame
Small office	metal frame	attic and wood frame
Fast-food restaurant	wood frame	attic and wood frame
Retail stand-alone	metal frame	metal frame
Strip mall retail	metal frame	metal frame
Sit-down restaurant	metal frame	attic and wood frame

In the U.S., the large hotel and large office were simulated with heavy mass walls and a metal frame roof in all vintages. Every medium office and strip mall retail building was modeled with metal frame walls and a metal frame roof. The envelope construction of the small office, fast-food restaurant, retail stand-alone, and sit-down restaurant varied by vintage (Table 9). As an example, the oldest retail stand alone was modeled with metal frame walls, while the older and new vintage were modeled with heavy mass walls.

Table 9. Types of wall and roof constructions simulated by vintage in each of the U.S. building categories.

Building category	Oldest		Older		New	
	Walls	Roof	Walls	Roof	Walls	Roof
Single-family home	wood frame	attic and wood frame	wood frame	attic and wood frame	wood frame	attic and wood frame
Apartment building	wood frame	attic and wood frame	wood frame	attic and wood frame	wood frame	attic and wood frame
Large hotel	heavy mass	metal frame	heavy mass	metal frame	heavy mass	metal frame
Large office	heavy mass	metal frame	heavy mass	metal frame	heavy mass	metal frame
Medium office	metal frame	metal frame	metal frame	metal frame	metal frame	metal frame
Small office	metal frame	metal frame	heavy mass	attic and metal frame	metal frame	attic and wood frame
Fast-food restaurant	heavy mass	metal frame	wood frame	attic and metal frame	metal frame	attic and wood frame
Retail stand-alone	metal frame	metal frame	heavy mass	metal frame	heavy mass	metal frame
Strip mall retail	metal frame	metal frame	metal frame	metal frame	metal frame	metal frame
Sit-down restaurant	metal frame	metal frame	metal frame	attic and metal frame	metal frame	attic and wood frame

2.3.5.2 Thermal insulation

EnergyPlus models each envelope assembly (e.g., roof or wall) as a series of spatially uniform layers. We represent each insulated frame (roof joists or wall studs with cavity insulation) as a layer of continuous insulation with thermal resistance equal to that of the insulated frame. Parallel-path calculation of the equivalent thermal resistance R_e of an insulated frame is detailed in Task Report Appendix C.

We computed equivalent thermal resistances of insulated frames for all California prototypes as well as for the oldest residential U.S. prototypes (Task Report Appendix C). The remaining U.S. prototypes were simulated with the equivalent thermal resistances that were already defined in the original EnergyPlus versions provided by DOE.

Table 10 and Table 11 report wall assembly thermal resistance (indoor surface air film to outdoor surface air film, including insulated frame if present) by vintage and climate zone for the single-family home, medium office, and retail stand-alone prototypes in California and the U.S., respectively.

Table 12 and Table 13 do the same for roof assembly thermal resistance.

Table 10. Wall assembly thermal resistance (indoor surface air film to outdoor surface air film) by vintage and California climate zone for the single-family home, medium office, and retail stand-alone California prototypes.

Vintage	Building category	Thermal resistance of wall assembly [ft²·°F·h·BTU-1] a															
		CZ 01	CZ 02	CZ 03	CZ 04	CZ 05	CZ 06	CZ 07	CZ 08	CZ 09	CZ 10	CZ 11	CZ 12	CZ 13	CZ 14	CZ 15	CZ 16
oldest	Single-family home	5.8	5.8	5.8	5.8	5.8	5.8	5.8	5.8	5.8	5.8	5.8	5.8	5.8	5.8	5.8	5.8
	Medium office	2.5	3.9	3.9	4.1	4.1	3.8	3.8	3.8	3.8	3.8	3.6	3.6	3.6	2.5	2.5	2.5
	Retail stand-alone	2.5	3.9	3.9	4.1	4.1	3.8	3.8	3.8	3.8	3.8	3.6	3.6	3.6	2.5	2.5	2.5
older	Single-family home	16.9	11.3	11.3	11.3	11.3	11.3	11.3	11.3	11.3	11.3	11.3	11.3	11.3	16.9	16.9	16.9
	Medium office	7.4	7.6	7.6	8.0	8.0	7.5	7.5	7.5	7.5	7.5	7.0	7.0	7.0	7.2	7.2	7.4
	Retail stand-alone	7.4	7.6	7.6	8.0	8.0	7.5	7.5	7.5	7.5	7.5	7.0	7.0	7.0	7.2	7.2	7.4
new	Single-family home	19.6	19.6	19.6	19.6	19.6	15.4	15.4	19.6	19.6	19.6	19.6	19.6	19.6	19.6	19.6	19.6
	Medium office	14.5	16.1	12.2	16.1	16.1	14.5	14.5	16.1	16.1	16.1	16.1	16.1	16.1	16.1	16.1	16.1
	Retail stand-alone	14.5	16.1	12.2	16.1	16.1	14.5	14.5	16.1	16.1	16.1	16.1	16.1	16.1	16.1	16.1	16.1

[a] To obtain SI thermal resistance, note that 1 ft²·°F·h·BTU-1 = 0.176 m²·K/W²; that is, R-1 = RSI-0.176.

Table 11. Wall assembly thermal resistance (indoor surface air film to outdoor surface air film) by vintage and U.S. climate zone for the single-family home, medium office, and retail stand-alone U.S. prototypes.

Vintage	Building category	Thermal resistance of wall assembly [ft²·°F·h·BTU⁻¹]														
		CZ 1A	CZ 2A	CZ 2B	CZ 3A	CZ 3B	CZ 3C	CZ 4A	CZ 4B	CZ 4C	CZ 5A	CZ 5B	CZ 6A	CZ 6B	CZ 7	CZ 8
oldest	Single-family home	6.5	6.5	6.5	6.5	6.5	6.5	6.5	6.5	6.5	6.5	6.5	6.5	6.5	6.5	6.5
	Medium office	4.3	4.3	4.3	4.4	4.3	4.4	5.6	5.4	5.7	6.4	6.2	6.9	6.9	7.3	8.0
	Retail stand-alone	4.3	4.3	4.3	4.4	4.3	4.4	5.6	5.4	5.7	6.4	6.2	6.9	6.9	7.3	8.0
older	Single-family home	11.3	11.3	12.2	11.3	11.3	11.3	11.3	12.2	11.3	12.2	12.2	12.2	12.2	16.9	11.3
	Medium office	4.3	6.6	4.2	7.7	6.2	7.7	11.2	10.0	10.9	12.2	12.2	15.4	13.9	17.2	22.2
	Retail stand-alone	1.8	2.3	1.8	2.8	2.8	2.8	7.6	4.6	9.3	9.3	6.5	13.4	12.0	15.7	20.6
new	Single-family home	11.5	11.5	11.5	11.5	16.3	16.3	16.3	11.5	16.3	16.3	16.3	16.3	16.3	16.3	16.3
	Medium office	8.0	11.8	8.0	11.8	12.9	12.9	15.5	8.0	15.5	18.1	15.5	20.3	15.5	15.5	15.5
	Retail stand-alone	2.2	6.8	2.2	8.3	8.3	8.3	9.8	6.8	9.8	11.3	11.3	12.7	12.7	14.3	12.7

Table 12. Roof assembly thermal resistance (indoor surface air film to outdoor surface air film) by vintage and by California climate zone for the single-family home, medium office, and retail stand-alone California prototypes.

Vintage	Building category	Thermal resistance of roof assembly [ft²·°F·h·BTU-1]														
		CZ 01	CZ 02	CZ 03	CZ 04	CZ 05	CZ 06	CZ 07	CZ 08	CZ 09	CZ 10	CZ 11	CZ 12	CZ 13	CZ 14	CZ 15	CZ 16
oldest	Single-family home	15.7	15.7	15.7	15.7	15.7	15.7	15.7	15.7	15.7	15.7	15.7	15.7	15.7	15.7	15.7	15.7
	Medium office	6.5	4.9	4.9	4.9	4.9	7.7	7.7	4.9	4.9	4.9	4.9	4.9	4.9	5.1	6.5	5.1
	Retail stand-alone	6.5	4.9	4.9	4.9	4.9	7.7	7.7	4.9	4.9	4.9	4.9	4.9	4.9	5.1	6.5	5.1
older	Single-family home	30.3	30.3	30.3	30.3	30.3	19.3	19.3	30.3	30.3	30.3	30.3	30.3	30.3	38.3	30.3	38.3
	Medium office	12.5	9.5	9.5	9.5	9.5	9.5	9.5	9.5	9.5	9.5	9.5	9.5	9.5	12.5	12.5	12.5
	Retail stand-alone	12.5	9.5	9.5	9.5	9.5	9.5	9.5	9.5	9.5	9.5	9.5	9.5	9.5	12.5	12.5	12.5
new	Single-family home	38.3	38.3	30.3	46.3	30.3	30.3	30.3	46.3	46.3	46.3	46.3	46.3	46.3	46.3	46.3	46.3
	Medium office	29.4	29.4	29.4	29.4	29.4	20.4	20.4	20.4	29.4	29.4	29.4	29.4	29.4	29.4	29.4	29.4
	Retail stand-alone	29.4	29.4	29.4	29.4	29.4	20.4	20.4	20.4	29.4	29.4	29.4	29.4	29.4	29.4	29.4	29.4

Table 13. Roof assembly thermal resistance (indoor surface air film to outdoor surface air film) by vintage and U.S. climate zone for the single-family home, medium office, and retail stand-alone U.S. prototypes.

Vintage	Building category	Thermal resistance of roof assembly [ft²·°F·h·BTU-1]														
		CZ 1A	CZ 2A	CZ 2B	CZ 3A	CZ 3B	CZ 3C	CZ 4A	CZ 4B	CZ 4C	CZ 5A	CZ 5B	CZ 6A	CZ 6B	CZ 7	CZ 8
oldest	Single-family home	10.9	13.3	12.1	13.3	13.3	10.9	10.9	12.1	15.3	15.3	12.1	22.3	12.1	14.8	15.3
	Medium office	9.7	9.7	9.7	9.7	9.7	9.7	11.3	10.9	11.4	13.9	13.1	16.7	16.7	16.3	16.7
	Retail stand-alone	9.7	9.7	9.7	9.7	9.7	9.7	11.3	10.9	11.4	13.9	13.1	16.7	16.7	16.3	16.7
older	Single-family home	27.3	27.3	29.3	27.3	27.3	25.3	27.3	29.3	32.3	32.3	29.3	27.3	29.3	32.3	32.3
	Medium office	13.2	14.8	21.4	13.6	20.5	11.0	16.9	16.6	15.3	18.9	19.6	22.2	20.4	24.7	32.2
	Retail stand-alone	13.2	14.8	21.4	13.6	20.5	11.0	16.9	16.6	15.3	18.9	19.6	22.2	20.4	24.7	32.2
new	Single-family home	27.6	32.4	27.6	27.6	32.4	32.4	37.6	32.4	37.6	37.6	32.4	37.6	37.6	37.6	37.6
	Medium office	15.9	25.6	15.9	20.8	25.6	25.6	31.2	15.9	20.8	31.2	20.8	31.2	20.8	20.8	20.8
	Retail stand-alone	15.9	25.6	15.9	20.8	25.6	25.6	31.2	15.9	20.8	31.2	20.8	31.2	20.8	20.8	20.8

2.3.6 Thermostat schedules

All residential prototypes from DOE had thermostat schedules in which the indoor air cooling temperature setpoint was constant at 24.0˚C and the indoor air heating temperature setpoint was constant at 22.2˚C. These were the thermostat schedules used in our U.S. simulations (Figure 3).

For our California simulations, we adjusted the residential thermostat schedules to match the recommended schedules in the 2016 Title 24 Residential Alternative Calculation Method Reference Manual (CEC 2016d). In the cooling season, the temperature is set to 25.5˚C during the early morning and evening, when residents are expected to be home, and "set up" to a higher value during the day, when residents are expected to be away. In the heating season, the temperature is set to 20.0˚C from morning to evening, and "set back" to a lower value overnight, when residents are expected to be asleep (Figure 3).

In the commercial prototypes, thermostat schedules varied by the type of building and by days of week. For example, the medium and large offices had the weekdays schedules shown in Figure 4. During weekends in the medium and large offices of all California and U.S. prototypes, the indoor air cooling temperature setpoint was constant at 26.7˚C and the indoor air heating temperature setpoint was constant at 15.6˚C.

The retail stand-alone had the weekdays schedules shown in Figure 5. In the weekends, the temperature settings in the retail stand-alone are similar to that in weekdays with the "set up" and "set back" hours shifted to accommodate the operating hours during the weekends. In the U.S. the schedules were identical between the older and oldest vintages, which in turn were slightly different than those in the new vintage. In the California commercial buildings, the

thermostat schedules in all vintages were equal or very close to those of the new U.S. commercial buildings.

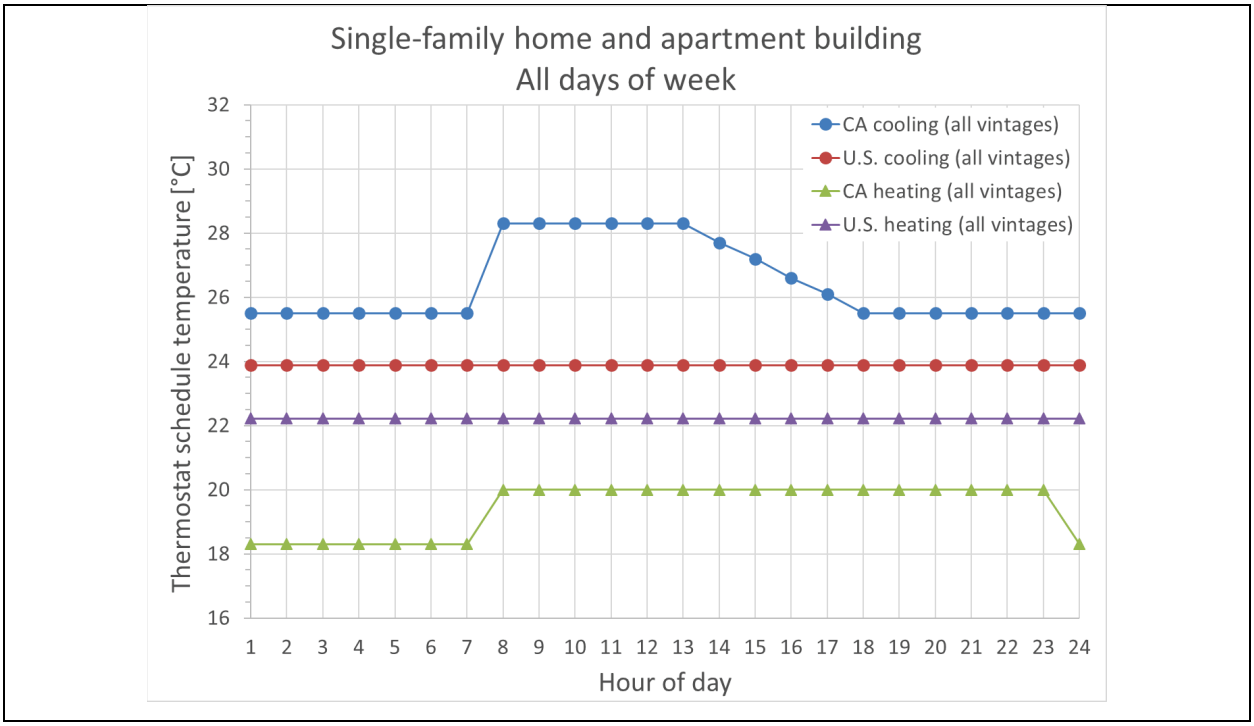

Figure 3. Cooling and heating thermostat schedules in the single-family home and apartment building for California and United States. Thermostat schedules are for every day of the week.

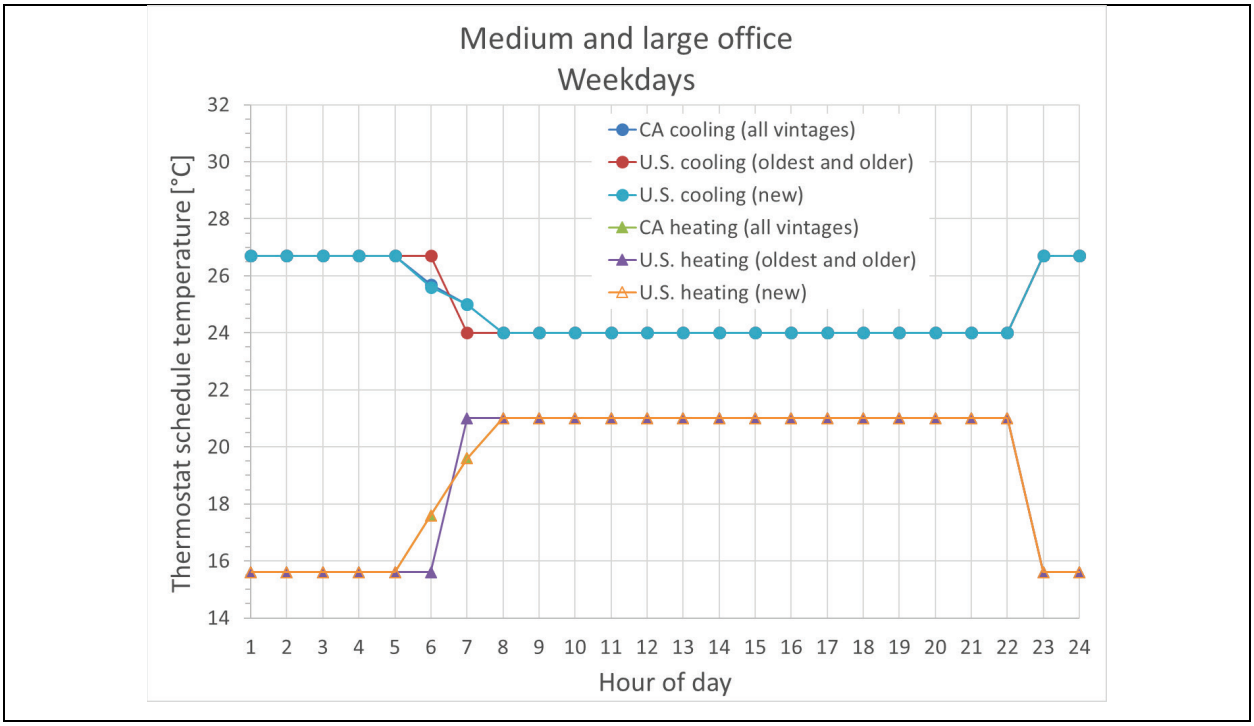

Figure 4. Cooling and heating thermostat schedules for weekdays in the medium and large office for California and United States.

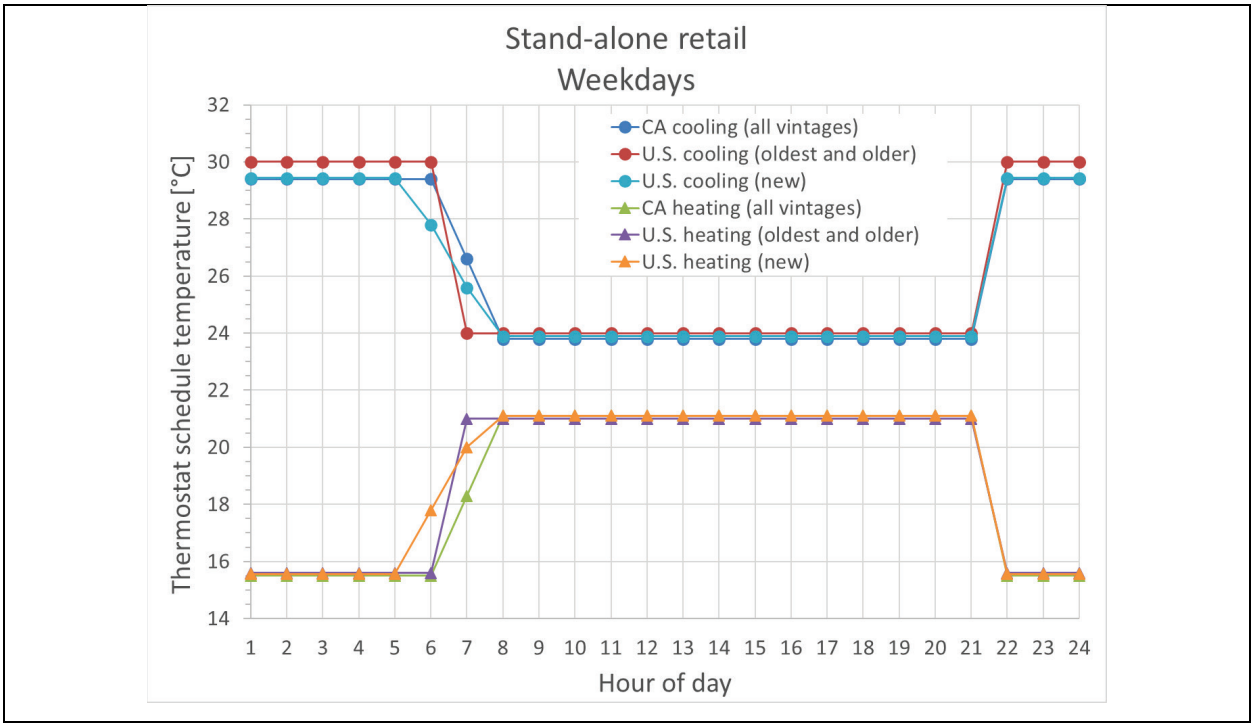

Figure 5. Cooling and heating thermostat schedules for weekdays in the stand-alone retail for California and United States.

2.4 Building energy simulation

2.4.1 Simulation tools

All building energy simulations were performed with EnergyPlus (EnergyPlus 2003), a program designed to model the energy uses of a building, including those for cooling, heating, and ventilation. We used jEPlus (jEPlus 2015), a parametric EnergyPlus simulation manager, to vary wall albedo, roof albedo, and building orientation. All simulations were run on the jEPlus Simulation Server, or JESS, cloud service (JESS 2015).

2.4.2 Parametric analysis

For California, we developed 96 residential building prototypes (2 building categories × 16 California climate zones × 3 vintages) and 384 commercial building prototypes (8 building categories × 16 California climate zones × 3 vintages). Similarly, we developed 270 residential building prototypes (2 building categories × 3 heating systems × 15 U.S. climate zones × 3 vintages) and 360 commercial building prototypes (8 building categories × 15 U.S. climate zones × 3 vintages) for the United States.

We parametrically varied wall and roof albedos to assess changes in annual building cooling, heating, and fan energy consumption. For each building category, climate zone, and vintage, we simulated the following cases.

(a) Base case: base wall albedo 0.25, and base roof albedo 0.10 (residential) or 0.20 (commercial). These base values represent albedos typical of walls and roofs in existing buildings.

(b) Alternative wall cases: a series of alternative albedos (0.10, 0.40, and 0.60) for the modified walls, leaving roof albedo unchanged. This was done for each of the 15 wall combinations in Table 14.

(c) Alternative roof cases: a series of alternative albedos for the roof, leaving wall albedo unchanged. In residential prototypes, the alternative albedos were 0.25, 0.40, and 0.60; in commercial prototypes, the alternative albedos were 0.10, 0.25, 0.40, and 0.60.

Each of these cases was simulated once with the building oriented long axis east-west, and again with the building oriented long axis north-south. Thus, for a given location and vintage, there were 98 simulations per residential prototype [(1 base case + 3 alternative roof albedos + 3 alternative wall albedos × 15 wall combinations) × 2 building orientations] and 100 simulations per commercial prototype [(1 base case + 4 alternative roof albedos + 3 alternative wall albedos × 15 wall combinations) × 2 building orientations].

Table 14. List of simulated wall combinations, taken 1, 2, 3, or 4 walls at a time.

Number of walls modified	Possible wall combinations
1	North (N), East (E), South (S), West (W)
2	NE, ES, EW, NS, NW, SW
3	NES, NEW, ESW, NSW
4	NESW

Therefore, in California we performed 96 residential prototypes × 98 simulations per residential prototype = 9,408 residential simulations, and 384 commercial prototypes × 100 simulations per commercial prototype = 38,400 commercial simulations, for a total of 47,808 California simulations. For the U.S. we performed 270 residential prototypes × 98 simulations per residential prototype = 26,460 residential simulations, and 360 commercial prototypes × 100 simulations per commercial prototype = 36,000 commercial simulations, for a total of 62,460 U.S. simulations.

2.4.3 Weather files

The California simulations were executed with the most recent weather files developed for use in Title 24 compliance simulations. This set of California weather files, called CZ2010, was developed by White Box Technologies (WBT 2011) with funding from the California Energy Commission. CZ2010 replaces the previous set of California weather files, known as CTZ2. The CZ2010 set represents better than CTZ2 the current annual weather in California (Huang 2013), as it includes current actual weather records that span 1998 to 2009, while the CTZ2 set characterized weather records from the 1950s to the 1980s. From the entire CZ2010 set of 85 weather files, we chose the 16 files generated from weather stations located in the 16 representative cities and towns listed in Table 1.

The U.S. simulations were performed using Typical Meteorological Year 3 (TMY3) weather files, which are the latest edition of the typical meteorological year weather files produced by NREL (Wilcox and Marion 2008) and distributed with EnergyPlus. We used the weather files associated with the commercial and residential prototypes from BECP. These were 17 weather files, one per city simulated (Table 2).

2.5 Degree days and annual solar radiation

Cooling degree days at 18˚C (CDD18C) and heating degree days at 18˚C (HDD18C) can be used to predict cooling load and heating load, respectively (EIA 2017). Cool surface energy savings also depend on solar radiation, since changes in cooling and heating loads induced by raising albedo are proportional to incident sunlight. Section 3.1 shows annual CDD18C, annual HDD18C, and annual global horizontal solar radiation (incident solar energy per unit area) computed from the weather files used in the California and U.S. simulations.

2.6 Monthly and seasonal daily sunlight by surface

To understand how daily solar radiation varies by location, season, and orientation, the PVWatts Calculator (NREL 2017) was used to compute for each California and U.S. representative city the monthly and seasonal average values of daily sunlight (solar energy per unit area) incident on a horizontal roof or on a north, east, south, or west exterior wall. We will refer to these five exterior envelope surfaces—roof, north wall, east wall, south wall, and west wall—as building "faces".

Section 3.2 summarizes for each representative city in California and the U.S., respectively, the daily sunlight received by the five building faces in summer and in winter. Task Report Appendix D further summarizes for each simulated location in California and U.S., the monthly and seasonal daily solar radiation intercepted by the five faces. The tables in Task Report Appendix D also show for each face the ratio of sunlight received in winter to that received in summer.

2.7 Energy, peak power, pollution, and energy cost savings

2.7.1 Site energy savings

Consider a building prototype representing a building category, vintage, and location simulated with a given orientation (long axis north-south or east-west). Let E_c, E_h, and E_f represent annual whole-building cooling, heating, and fan site electricity uses, and let G_h represent annual whole-building site gas use, each term evaluated in the base case (i.e., with wall and roof albedos set to prototype-specific base values). When the albedo of the roof or the albedo of one or more walls is raised to an alternative value, the annual whole-building cooling site electricity savings (e_c), heating site electricity *penalty* (e_h), fan site electricity savings (e_f), and heating site gas *penalty* (g_h) are calculated respectively as

$$e_{\mathrm{c}} = E_{\mathrm{c,base}} - E_{\mathrm{c,alternative}} \,, \tag{1}$$

$$e_{\mathrm{h}} = E_{\mathrm{h,alternative}} - E_{\mathrm{h,base}} \,, \tag{2}$$

$$e_{\mathrm{f}} = E_{\mathrm{f,base}} - E_{\mathrm{f,alternative}} \,, \tag{3}$$

and

$$g_{\mathrm{h}} = G_{\mathrm{h,alternative}} - G_{\mathrm{h,base}} \,, \tag{4}$$

where the subscript "alternative" refers to one of the alternative cases of a prototype (see 2.4.2, and the subscript "base" refers to the base case of the same prototype.

2.7.2 Source energy savings

The annual HVAC (cooling + heating + fan) source energy savings is calculated as

$$h_{\mathrm{HVAC}} = s_{\mathrm{e}} \times (e_{\mathrm{c}} + e_{\mathrm{f}} - e_{\mathrm{h}}) - s_{\mathrm{g}} \times g_{\mathrm{h}}\,, \tag{5}$$

where s_e is a state-specific site-to-source conversion factor for electricity, and s_g is a non-regional site-to-source conversion factor for natural gas. These site-to-source conversion factors were obtained from the Source Energy and Emissions Analysis Tool, or SEEAT (GTI 2017). The tool uses current and previous eGRID databases[2] to determine state-specific source energy consumption and greenhouse gas (GHG) emissions associated with annual site electricity consumption and site fuel (natural gas, oil, propane) used. The site-to-source factors for electricity incorporate transmission losses and the gas factors include distribution losses.

[2] The Emissions & Generation Resource Integrated Database (eGRID) is a data source that provides characteristics (e.g., net generation, emission rates, and resource mix) of nearly all electric power generated in the United States (eGRID 2014).

Table 15. Site-to-source electric and natural gas conversion factors (GTI 2017).

	Site-to-source conversion factors	
State	**Electric [BTU/BTU]**	**Natural gas [BTU/BTU]**
Florida	2.94	1.09
Texas	3.25	
Arizona	3.34	
Tennessee	3.18	
Texas	3.25	
California	3.31	
Maryland	3.47	
New Mexico	3.40	
Oregon	2.05	
Washington	1.87	
Illinois	3.44	
Idaho	2.10	
Vermont	3.14	
Montana	2.79	
Minnesota	3.57	
Alaska	2.55	

2.7.3 HVAC peak power demand reduction

In this study, we define *peak hours* as those between 12:00 to 18:00 Clock Time (CT) during the weekdays (Monday to Friday) of June through September. For any given peak hour *i*, the site HVAC peak power demand reduction is calculated as

$$d_{\mathrm{HVAC},i} = \frac{(e_{\mathrm{c},i} + e_{\mathrm{f},i} - e_{\mathrm{h},i})}{1\ \mathrm{hour}}, \tag{6}$$

where $e_{\mathrm{c},i}$, $e_{\mathrm{f},i}$, and $e_{\mathrm{h},i}$ are the peak hour whole-building site cooling energy savings, fan energy savings, and electric heating energy penalty, respectively. Let T be the total number of peak hours in a given year. The annual-average HVAC peak power demand reduction, d_{HVAC}, is calculated by averaging the HVAC power demand over all annual peak hours:

$$d_{\mathrm{HVAC}} = \frac{\sum_{i=1}^{T} d_{\mathrm{HVAC},i}}{T}. \tag{7}$$

2.7.4 Pollution savings

The annual reduction in emission of air pollutant a is calculated as

$$p_a = f_{\mathrm{e},a} \times (e_{\mathrm{c}} + e_{\mathrm{f}} - e_{\mathrm{h}}) - f_{\mathrm{g},a} \times g_{\mathrm{h}} \,. \tag{8}$$

where site electricity emission factor $f_{e,a}$ is the mass of pollutant emitted by power plants per unit of site electricity consumed, and site gas emission factor $f_{g,a}$ is the mass of pollutant emitted by the building's furnace per unit of site gas consumed. This study considers reductions in emission of carbon dioxide (CO_2), carbon dioxide equivalent[3] (CO_2e), nitrogen oxides (NO_x), and sulfur dioxide (SO_2). The emission factors of these four air-pollutants are listed in Table 16 (for site electricity) and in Table 17 (for site gas). These emission factors were also obtained using SEEAT and incorporate transmission and distribution losses.

[3] Carbon dioxide equivalent (CO_2e) is a measure that allows for greenhouse gas emissions other than CO_2 to be expressed in terms of CO_2 based on their global warming potential (GWP) relative to CO_2. Thus, emissions expressed as CO_2e represent the GWP of all greenhouse gases expressed in terms of CO_2 (SBT 2017).

Table 16. State-specific air-pollutant emission factors for site electricity use (GTI 2017).

	Air-pollutant emission rates from generated electricity			
State	**CO_2 [kg/kWh]**	**CO_2e [kg/kWh]**	**NO_x [g/kWh]**	**SO_2 [g/kWh]**
Florida	0.553	0.590	0.435	0.481
Texas	0.631	0.675	0.522	0.844
Arizona	0.553	0.582	0.535	0.272
Tennessee	0.557	0.579	0.354	0.789
California	0.312	0.342	0.308	0.086
Maryland	0.587	0.611	0.562	0.934
New Mexico	0.824	0.868	1.479	0.431
Oregon	0.159	0.172	0.154	0.150
Washington	0.120	0.128	0.109	0.050
Illinois	0.501	0.523	0.327	0.807
Idaho	0.086	0.094	0.086	0.086
Vermont	0.036	0.040	0.109	0.077
Montana	0.646	0.674	0.753	0.540
Minnesota	0.593	0.621	0.549	0.540
Alaska	0.459	0.492	1.878	0.422

Table 17. Non-regional air-pollutant emission factors from site gas use (GTI 2017).

Air-pollutant emission rates from consumed natural gas			
CO_2 [kg/therm]	**CO_2e [kg/therm]**	**NO_X [g/therm]**	**SO_2 [g/therm]**
5.908	6.681	7.802	1.315

2.7.5 Energy cost savings

Annual HVAC energy cost savings are calculated as

$$c = z_{\mathrm{e}} \times (e_{\mathrm{c}} + e_{\mathrm{f}} - e_{\mathrm{h}}) - z_{\mathrm{g}} \times g_{\mathrm{h}} \,, \tag{9}$$

where z_e and z_g are the state-specific annual average prices of electricity and natural gas, respectively. These prices are also dependent on type of building (residential or commercial). The annual average electricity and gas prices used in the study are in Table 18. These prices represent the state-average prices charged to residential and commercial customers in 2015 (EIA 2016a, EIA 2016b).

Table 18. State-specific average price of electricity (EIA 2016a) and natural gas sold to residential and commercial customers in 2015 (EIA 2016b).

	2015 price of electricity [$/kWh]		2015 price of natural gas [$/therm]	
State	Residential customers	Commercial customers	Residential customers	Commercial customers
Florida	0.116	0.095	1.955	1.092
Texas	0.116	0.082	1.062	0.695
Arizona	0.121	0.104	1.704	1.053
Tennessee	0.103	0.102	0.962	0.846
California	0.170	0.157	1.139	0.804
Maryland	0.138	0.110	1.203	0.980
New Mexico	0.125	0.103	0.863	0.632
Oregon	0.107	0.088	1.243	1.009
Washington	0.091	0.082	1.180	0.977
Illinois	0.125	0.090	0.797	0.729
Idaho	0.099	0.078	0.859	0.759
Vermont	0.171	0.145	1.456	0.789
Montana	0.109	0.102	0.826	0.813
Minnesota	0.121	0.094	0.879	0.731
Alaska	0.198	0.174	0.964	0.801

2.7.6 Savings intensity

The savings intensity (savings per unit of modified surface area) for site energy, source energy, emission, or energy cost savings j is calculated as

$$j' = j/A_{\mathrm{m}}\ , \tag{10}$$

where A_{m} is the total surface area modified. For example, if the east and west walls were modified, A_{m} is the sum of the east and west net wall areas.

2.7.7 Averaged savings and savings intensity over two building orientations

Each savings or savings intensity calculated using Eqs. (1) to (10) is for a single building orientation (long axis east-west or north-south). Two-orientation mean savings are calculated as

$$j_{\mathrm{mean}} = (j_{\mathrm{EW}} + j_{\mathrm{NS}})/2\ , \tag{11}$$

where EW and NS refer to the long axis of the building running east-west and north-south, respectively. Two-orientation mean savings intensity is calculated as

$$j'_{\text{mean}} = (j_{\text{EW}} + j_{\text{NS}})/(A_{\text{m,EW}} + A_{\text{m,NS}}). \quad (12)$$

2.8 Tabulating all computed savings

For each prototype and building orientation, the simulations included the base case, alternative wall cases, and alternative roof cases described in Section 2.4.2. These simulations were used to calculate for each prototype the annual whole-building savings in site energy, source energy, emission, energy cost, and site HVAC peak power demand using Eqs. (1) to (9). All saving intensities were calculated using Eq. (10). Savings and savings intensities averaged over the two building orientations were computed using Eqs. (11) and (12), respectively.

All computed savings and savings intensities from every simulated prototype were combined into a savings database, detailed in Task Report Appendix E.

3 Results

3.1 Degree days and annual solar irradiation

Figure 6 and Figure 7 show CDD18C, HDD18C, and annual global horizontal solar radiation (incident solar energy per unit area) calculated from the weather files used in the California and U.S. simulations.

In California (Figure 6), the warmest climate zone is CACZ15 (Imperial; 2,700 CDD18C), which represents the state's southeastern deserts. California climate zones located in the state's Central Valley (CACZs 11, 12, 13, and 14) have warm summers as well as cool winters. The coastal climates zones (CACZs 1, 2, 3, and 5) have cool climates and have high HDD18C. The coldest climate zone is CACZ 16 (Mount Shasta; 3,400 HDD18C), which represents the mountainous regions of the state.

California has limited variation in annual global horizontal solar radiation, ranging from 1.45 MWh/m² (Arcata; CACZ 1) to 2.1 MWh/m² (China Lake; CACZ 14).

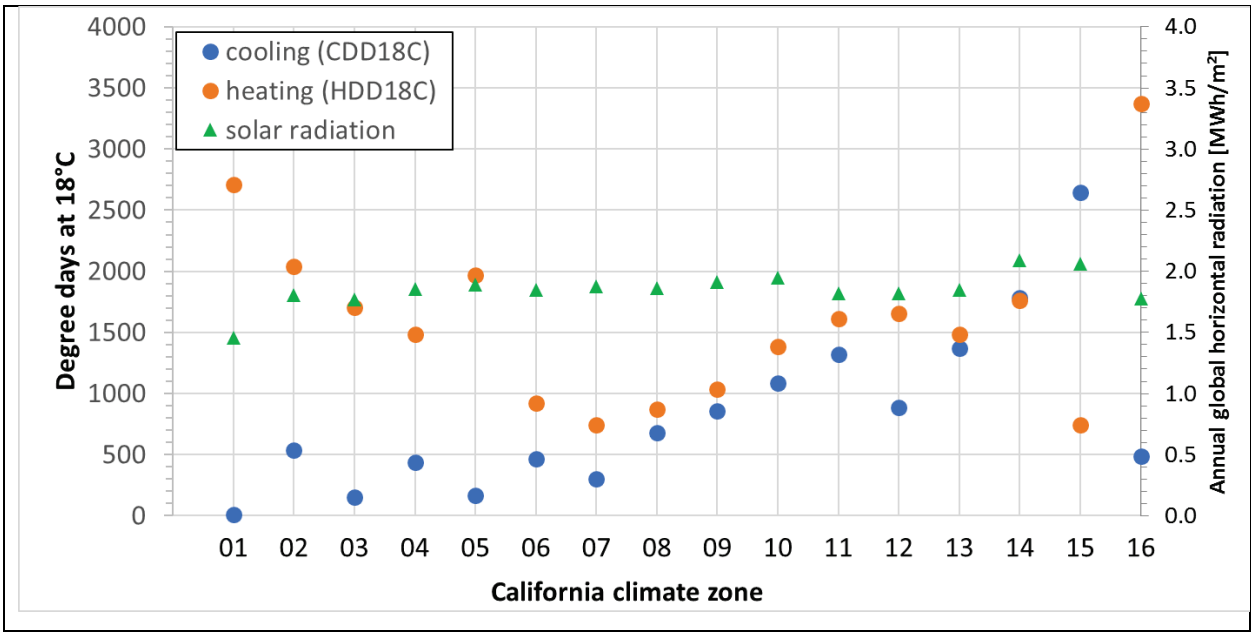

Figure 6. Cooling degree days at 18°C (CDD18C), heating degree days at 18°C (HDD18C), and annual global horizontal solar radiation by California climate zone, computed from CZ2010 weather files.

In the U.S. (Figure 7) the U.S. climate zone with the greatest CDD18C is 2B (Phoenix; 2,800 CDD18C) followed by USCZ 1A (Miami; 2,500 CDD18C). All U.S. climate zones from 3C onward had CDD18C below 1,000. HDD18C increased with U.S. climate zone number, ranging from 140 HDD18C (Miami; USCZ 1A) to 7,200 HDD18C (Fairbanks; USCZ 8).

USCZs 3B (El Paso) and 4B (Albuquerque) receive the most sunlight, getting nearly 2.1 MWh/m² annually. USCZ 8 (Fairbanks) receives the least sunlight (950 MWh/m²).

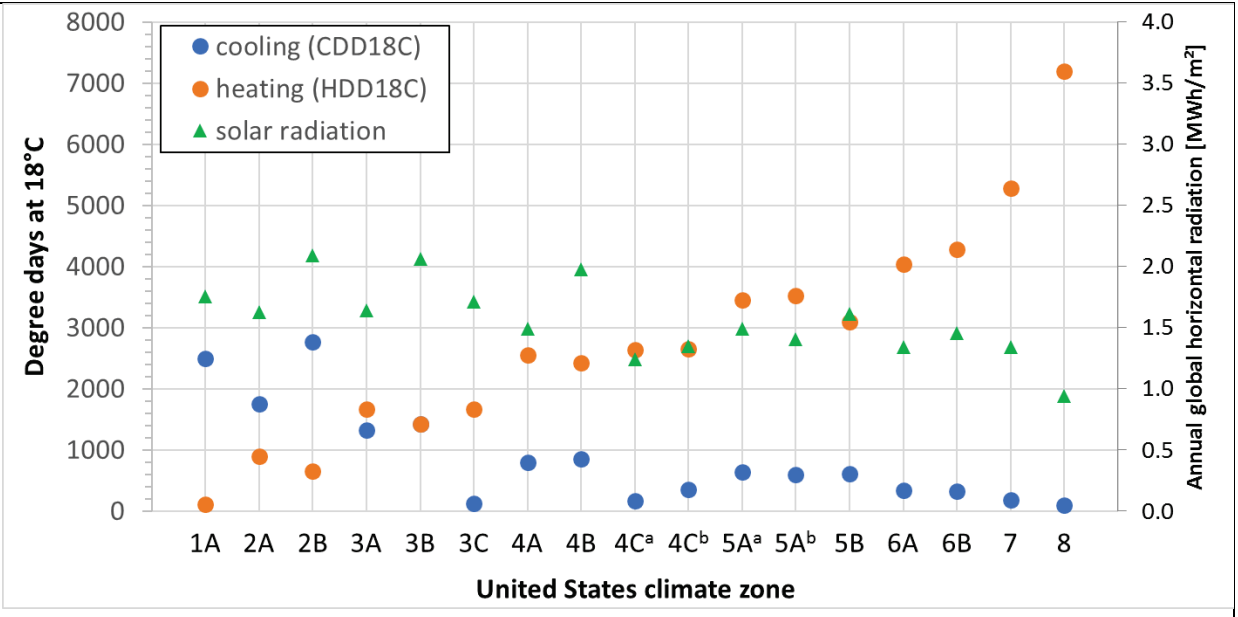

[a] From weather files used for residential prototypes.

[b] From weather files used for commercial prototypes.

Figure 7. Cooling degree days at 18°C (CDD18C), heating degree days at 18°C (HDD18C), and annual global horizontal solar radiation by United States climate zone, computed from TMY3 weather files.

3.2 Monthly and seasonal daily sunlight by face

Table 19 and Table 20 give for the representative cities in California and the U.S., respectively, the ratios of daily sunlight on each vertical face (north, east, south, or west) to that on the horizontal roof. Each ratio is evaluated in summer (June-July-August) and winter (December-January-February) as seasonal-average vertical sunlight to seasonal-average horizontal sunlight.

During the summer in all California locations, the roof receives the most sunlight, followed in descending order by the west, east, south, and north walls. During summer, the west-to-horizontal ratios range from 53 percent to 65 percent; the east-to-horizontal ratios range from 43 percent to 58 percent; the south-to-horizontal ratios range from 34 percent to 46 percent; and the north-to-horizontal ratios range from 23 percent to 31 percent (Table 19).

During winter in California, the south wall always receives more sunlight than all other faces, while the north wall once again receives the least solar radiation. During winter, the west-to-horizontal ratios range from 62 percent to 75 percent; the east-to-horizontal ratios range from 59 percent to 71 percent; the south-to-horizontal ratios range from 129 percent to 169 percent; and the north-to-horizontal ratios range from 22 percent to 32 percent (Table 19).

Table 19. Ratios of daily sunlight over a surface facing north (N), east (E), south (S), or west (W) to daily sunlight over a horizontal (H) roof. The table includes ratios computed for summer days and winter days in each of California's representative cities.

City or town in California	CAC Z	Summer (Jun, Jul, and Aug)				Winter (Dec, Jan, and Feb)			
		N-to-H ratio	E-to-H ratio	S-to-H ratio	W-to-H ratio	N-to-H ratio	E-to-H ratio	S-to-H ratio	W-to-H ratio
Arcata	1	31%	44%	46%	65%	32%	68%	148%	66%
Santa Rosa	2	23%	49%	40%	55%	32%	64%	136%	66%
Oakland	3	24%	45%	40%	55%	29%	61%	139%	65%
San Jose	4	23%	51%	39%	54%	28%	66%	146%	67%
Santa Maria	5	24%	42%	37%	59%	24%	65%	144%	65%
Long Beach	6	25%	43%	36%	59%	25%	59%	134%	62%
San Diego	7	24%	43%	34%	56%	22%	60%	138%	63%
Fullerton	8	25%	47%	36%	56%	26%	61%	137%	64%
Burbank	9	24%	52%	35%	53%	24%	63%	139%	63%
Riverside	10	25%	52%	35%	54%	25%	63%	141%	66%
Beale (for Red bluff) [a]	11	24%	56%	41%	54%	31%	63%	144%	69%
Sacramento	12	23%	57%	39%	54%	32%	61%	139%	68%
Fresno	13	24%	56%	37%	56%	32%	64%	129%	64%
China Lake	14	23%	58%	34%	55%	23%	71%	158%	69%
Palm Springs (for Imperial) [a]	15	26%	57%	34%	57%	24%	66%	148%	68%
Montague (for Mount Shasta) [a]	16	23%	58%	42%	55%	26%	67%	169%	75%
Minimum		**23%**	**43%**	**34%**	**53%**	**22%**	**59%**	**129%**	**62%**
Maximum		**31%**	**58%**	**46%**	**65%**	**32%**	**71%**	**169%**	**75%**

[a] Calculated for town that is near the climate zone's representative city.

During the summer in all U.S. locations, the roof receives the most sunlight, followed in descending order by the east, west, south, and north walls. In lower-latitude cities, such as Miami and Houston, the surfaces facing N and S receive similar solar radiation. The solar radiation received by the south wall increases with latitude. During summer and excluding Fairbanks, the west-to-horizontal ratios range from 46 percent to 61 percent; the east-to-horizontal ratios range from 46 percent to 62 percent; the south-to-horizontal ratios range from 31 percent to 53 percent; and the north-to-horizontal ratios range from 19 percent to 31 percent (Table 20).

In winter across the U.S., the south wall always receives more sunlight than the horizontal surface. The north wall once again receives the least sunlight. During winter and excluding

Fairbanks, the west-to-horizontal ratios range from 56 percent to 86 percent; the east-to-horizontal ratios range from 57 percent to 79 percent; the south-to-horizontal ratios range from 107 percent to 195 percent; and the north-to-horizontal ratios range from 21 percent to 37 percent (Table 20).

Table 20. Ratios of daily sunlight over a surface facing north (N), east (E), south (S), or west (W) to daily sunlight over a horizontal (H) roof. The table includes ratios computed for summer days and winter days in each of the U.S. representative cities.

City, State	USCZ	Summer (Jun, Jul, and Aug)				Winter (Dec, Jan, and Feb)			
		N-to-H ratio	E-to-H ratio	S-to-H ratio	W-to-H ratio	N-to-H ratio	E-to-H ratio	S-to-H ratio	W-to-H ratio
Miami, FL	1A	31%	52%	31%	48%	25%	58%	107%	58%
Houston, TX	2A	29%	54%	33%	50%	29%	57%	114%	64%
Phoenix, AZ	2B	25%	54%	34%	54%	23%	65%	144%	68%
Memphis, TN	3A	27%	53%	39%	54%	27%	64%	136%	64%
El Paso, TX	3B	25%	54%	32%	52%	24%	66%	138%	64%
San Francisco, CA	3C	25%	49%	40%	56%	29%	64%	144%	66%
Baltimore, MD	4A	29%	56%	43%	53%	29%	69%	150%	67%
Albuquerque, NM	4B	26%	58%	36%	50%	22%	65%	153%	69%
Salem, OR	4C	28%	56%	50%	61%	36%	65%	144%	70%
Seattle, WA	4C	28%	55%	53%	57%	37%	68%	157%	70%
Chicago, IL	5A	31%	57%	48%	56%	33%	67%	152%	68%
Peoria, IL	5A	19%	46%	36%	46%	21%	59%	141%	56%
Boise, ID	5B	25%	58%	46%	57%	32%	68%	159%	71%
Burlington, VT	6A	31%	58%	51%	58%	34%	68%	147%	66%
Helena, MT	6B	28%	62%	52%	57%	36%	79%	195%	86%
Duluth, MN	7	28%	55%	51%	58%	32%	72%	176%	72%
Fairbanks, AK	8	42%	79%	77%	61%	38%	131%	323%	69%
Minimum [a]		**19%**	**46%**	**31%**	**46%**	**21%**	**57%**	**107%**	**56%**
Maximum [a]		**31%**	**62%**	**53%**	**61%**	**37%**	**79%**	**195%**	**86%**

[a] Excluding USCZ 8 (Fairbanks, AK).

Table 21 and Table 22 give for the representative cities in California and U.S., respectively, the ratio of winter to summer daily sunlight for each of the five surfaces (roof, north wall, east wall, south wall, and west wall) and for the four-wall average. In California as well as the U.S., the roof, north wall, east wall, and west wall always receive more sunlight in summer than in winter. Changes to cooling and heating loads from modifying the albedo of an exterior surface are proportional to the sunlight intercepted by the modified surface. Therefore, since the roof, north wall, east wall, and west wall receive more sunlight during summer than in winter, we expect that modifying any of these four surfaces would yield cooling load changes in summer that are greater than the heating load changes in winter.

In the northern hemisphere, the sun in summer rises in the northeast and sets in the northwest. The solar altitude peaks close to zenith from the south. During winter, the sun rises in the southeast and sets in the southwest; the solar altitude peaks in the southern sky at a low

elevation (Abood 2015; Schroeder 2011). As an example, in Fresno, the peak solar altitude at the summer solstice is 77˚, and the peak solar altitude in the winter solstice is 30˚ (Figure 8). Thus, the south wall in summer receives direct solar irradiation only from mid-morning to mid-afternoon and at a large incidence angle. In winter, the south wall is exposed to beam solar irradiation all day, and at a smaller incidence angle than in summer. At a surface, the beam solar irradiation increases inversely with incidence angle. Therefore, under clear skies the south wall receives more solar irradiation in winter than in summer. In China Lake, CA; Palm Springs, CA; Miami, FL; Phoenix, AZ; El Paso, TX; and Albuquerque, NM the south wall receives twice or more sunlight in winter than in summer. Since the south wall receives more sunlight in winter than in summer, we expect heating load changes in winter from a cool wall to be greater than the cooling load changes in summer.

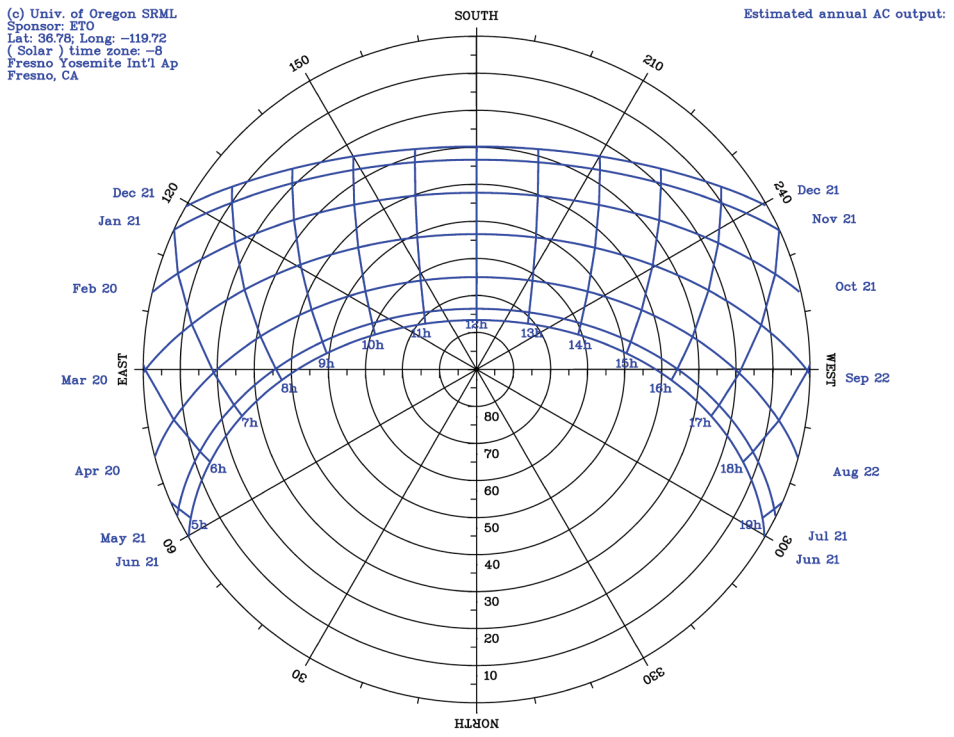

Figure 8. Sun path chart for Fresno, California (UO SRML 2008).

Table 21. Ratios of sunlight striking a face during a winter day to that of a summer day for each representative city in California. The table include ratios for a horizontal (H) roof, north (N) wall, east (E) wall, south (S) wall, west (W) wall, and the four-wall average.

City or town in California	CACZ	Winter to summer ratio					
		H	N	E	S	W	Four-wall average
Arcata	1	35%	36%	53%	110%	35%	58%
Santa Rosa	2	27%	37%	36%	94%	33%	49%
Oakland	3	33%	40%	45%	116%	39%	60%
San Jose	4	32%	40%	42%	123%	40%	60%
Santa Maria	5	43%	41%	66%	166%	47%	78%
Long Beach	6	41%	41%	57%	154%	44%	71%
San Diego	7	47%	43%	65%	188%	52%	84%
Fullerton	8	43%	45%	56%	162%	49%	76%
Burbank	9	39%	40%	47%	157%	46%	69%
Riverside	10	42%	43%	51%	169%	51%	75%
Beale (for Red Bluff) [a]	11	30%	39%	34%	104%	38%	52%
Sacramento	12	27%	37%	29%	96%	34%	47%
Fresno	13	30%	39%	34%	103%	34%	50%
China Lake	14	42%	42%	51%	194%	53%	79%
Palm Springs (for Imperial) [a]	15	46%	41%	53%	197%	54%	80%
Montague (for Mount Shasta) [a]	16	30%	35%	35%	120%	41%	57%
Minimum		**27%**	**35%**	**29%**	**94%**	**33%**	**47%**
Maximum		**47%**	**45%**	**66%**	**194%**	**54%**	**84%**

[a] Calculated for town that is near the climate zone's representative city.

Table 22. Ratios of sunlight striking a face during a winter day to that of a summer day for each U.S. representative city. The table include ratios for a horizontal (H) roof, north (N) wall, east (E) wall, south (S) wall, west (W) wall, and the four-wall average.

City, State	USCZ	Winter to summer ratio					
		H	N	E	S	W	Four-wall average
Miami, FL	1A	64%	52%	71%	221%	78%	98%
Houston, TX	2A	50%	50%	52%	172%	64%	79%
Phoenix, AZ	2B	46%	42%	55%	192%	58%	82%
Memphis, TN	3A	38%	37%	45%	131%	45%	63%
El Paso, TX	3B	51%	48%	62%	220%	64%	91%
San Francisco, CA	3C	36%	42%	46%	130%	43%	64%
Baltimore, MD	4A	37%	38%	46%	130%	47%	65%
Albuquerque, NM	4B	47%	41%	52%	197%	64%	85%
Salem, OR	4C	23%	30%	27%	67%	27%	38%
Seattle, WA	4C	22%	29%	27%	64%	27%	37%
Chicago, IL	5A	33%	35%	38%	104%	40%	54%
Peoria, IL	5A	35%	37%	45%	135%	42%	65%
Boise, ID	5B	26%	33%	30%	89%	32%	46%
Burlington, VT	6A	31%	34%	36%	88%	34%	48%
Helena, MT	6B	26%	35%	33%	99%	40%	52%
Duluth, MN	7	32%	36%	41%	108%	39%	58%
Fairbanks, AK	8	6%	6%	10%	27%	7%	14%
Minimum [a]		**22%**	**33%**	**27%**	**64%**	**27%**	**37%**
Maximum [a]		**64%**	**52%**	**71%**	**221%**	**78%**	**98%**

[a] Excluding USCZ 8 (Fairbanks, AK).

Task Report Appendix D further summarizes for each simulated location in California and U.S., the monthly and seasonal daily solar radiation intercepted by the five faces. In addition to the monthly and seasonal solar radiation, the tables in Task Report Appendix D show for each face the ratio of sunlight received in winter to that received in summer.

3.3 California case studies

This section uses some of the California simulations to evaluate the effects of raising wall albedo. We use the simulations from the single-family home to represent residential buildings, and those of the medium office building and stand-alone retail building to represent commercial buildings.

Cool roofing products for pitched roofs on homes (e.g., concrete tiles, clay tiles, and high-performance asphalt shingles) are typically rated with an aged albedo around 0.40, while cool roofing products for low-slope roofs on commercial buildings are typically rated with an aged albedo of at least 0.60 (Sleiman et al. 2011). In the case of walls, an aged albedo of at least 0.60 can be currently obtained with light-colored paints (Task 4.2 report: *Natural exposure of wall products*). We assume that a conventional residential roofing product (e.g., a dark asphalt shingle) has an aged albedo of about 0.10; that a conventional commercial roofing product (e.g., a dark gray membrane) has an aged albedo of about 0.20; and that a conventional wall coating (e.g., a dark to medium color paint) has an aged albedo of about 0.25. Thus, in these case studies, we present cool wall savings from increasing wall albedo by 0.35 (to 0.60 from 0.25) in both residential and commercial buildings, and from increasing roof albedo by 0.30 (to 0.40 from 0.10) in residential buildings and by 0.40 (to 0.60 from 0.20) in commercial buildings.

We compare savings between cool walls and cool roofs, and explore how the cool wall savings vary by location, vintage, and combination of modified walls. Finally, we investigate whether the sum of savings from walls modified one at a time equals the savings from modifying the same set of walls simultaneously.

All savings and penalties shown here are average values from the two building orientations (east-west and north-south). Values by orientation are available in the savings database.

3.3.1 California source energy savings intensity (per unit surface area modified) of the new single-family home by climate zone and modified surface

This section shows the annual source cooling, fan, and HVAC savings intensity and heating penalty intensity of the new single-family home by California climate zone from individually increasing the albedo by 0.35 (to 0.60 from 0.25) of the north wall, east wall, south wall, west wall, and roof, and of the roof by 0.30 (to 0.40 from 0.10). We choose to present the savings in the single-family home because it is the most common building type in California and has the most floor area in the state (Section 6.7.5 in Rosado 2016). Savings from the older and oldest single-family home show similar behavior to those from the new vintage but of different magnitudes.

3.3.1.1 Source energy changes by California climate zone

Figure 9 shows annual source values of cooling savings intensity, heating penalty intensity, fan savings intensity, and HVAC savings intensity for the new single-family home in California. In every California climate zone, raising wall or roof albedo reduced cooling and fan energy uses and increased heating energy use. However, every face (walls or roof) yielded source energy savings from cooling and fan that exceeded the heating penalties, leading to HVAC source energy savings in every California climate zone. CACZs 1 (Arcata) and 16 (Mount Shasta) had the smallest HVAC source energy savings intensities. The first (CACZ 1), was the location with the smallest source cooling savings intensities; it is also the location with the fewest CDD18C

(8). Arcata also yielded large heating penalties when compared to most other locations; it was the location with the second highest HDD18C (2,700). Mount Shasta (CACZ 16) experienced the most HDD18C in all California (nearly 3,400 HDD18C), yielding large heating source penalties.

The greatest HVAC source energy savings intensities were in CACZs 6 (Long Beach), 7 (San Diego), and 15 (Imperial). The first two (CACZs 6 and 7) were locations with small CDD18C and HDD18C when compared to the other California locations. However, low requirements for roof and wall insulation in the single-family home helped make annual HVAC source energy savings intensities in CACZs 6 and 7 larger than those in the other California climate zones. Specifically, the new single-family prototypes from CACZs 6 and 7 were simulated with less wall insulation than all other CACZs; the wall assembly thermal resistance in CACZs 6 and 7 was R-15.4 (Table 10), which is 79 percent of the R-19.6 that was used in all other CACZs (R-15.4 / R-19.6 = 79 percent). The roof assembly thermal resistance in CACZs 6 and 7 was R-30.3 (Table 12), which is 66 percent of the R-46.2 that what was used in many other CACZs (4, 8-16).

The third location (CACZ 15) is the location with the most CDD18C (2,650) and fewest HDD18C (740); it is also one of the most sunlit locations in California (Figure 9d). This CACZ 15 climate led to the largest HVAC source energy savings intensities.

3.3.1.2 Source energy changes by face

Changes in HVAC energy use are proportional to changes in heat conducted through the building envelope, which in turn scale with changes in wall solar heat gain. Wall solar heat gain depends on orientation. Thus, all else being equal, we expect changes in HVAC energy use to be greater from modified external surfaces that receive more sunlight (solar energy per unit area).

Of all four walls, the north wall was the one that yielded in all California climate zones the lowest annual cooling and fan source energy savings intensities (Figure 9a,c) because it received the least sunlight. As an example, consider CACZ 13 (Fresno), in which the north wall yields annual cooling source energy savings intensity 9.5 MJ/m², or 42 percent of that from the east wall (22.5 MJ/m²). From Table D-13 in Task Report Appendix D, we find that the summer daily solar irradiation on the north wall was 1.89 kWh/m², which is 44 percent of that from the east wall (4.33 kWh/m²). During winter, the north wall again received the least sunlight, yielding the smallest annual heating source energy penalty intensity (Figure 9b).

In all California climate zones, the annual cooling and fan source energy savings intensities from the roof were generally as small as those from the north wall. The roof and north wall savings intensities were in turn smaller than those from the east, south, and west walls. However, the roof (if assumed to be horizontal) was the face that received the most summer daily solar irradiation (Table D-13). The key is that the thermal resistance of the wall is less than half that of the roof. For example, in CACZs 4 and 8-16, the thermal resistance of the wall assembly was R-19.6, which is 42 percent of the roof thermal resistance in the roof of the same California climate zones (Table 10 and Table 12).

During winter, the annual heating source energy penalties from the roof were once again smaller than those from the east, south, and west walls, and similar to those from the north wall.

The wall that receives the most summer daily solar radiation is the west wall, followed by the east wall (Table 19). However, in many California climate zones the south wall yielded the greatest annual cooling and fan source energy savings intensities. In the remaining California climate zones, the greatest annual cooling and fan energy savings intensities were from the east wall. The savings intensities from the west wall were always 70 percent to 90 percent of those from the east wall.

In all California climate zones, the south wall received more sunlight during winter than any of the other surfaces (including the roof). Thus, in all locations, the south wall yielded annual heating source energy penalty intensities greater than those from any of the other surfaces (Table 21). In most locations, the south wall received more sunlight during winter than in summer, causing its heating penalties to be in some locations nearly as much as its cooling savings. The face yielding the largest annual HVAC source energy savings intensities varied by location, but was usually either the east wall or south wall (Figure 9d).

(a)

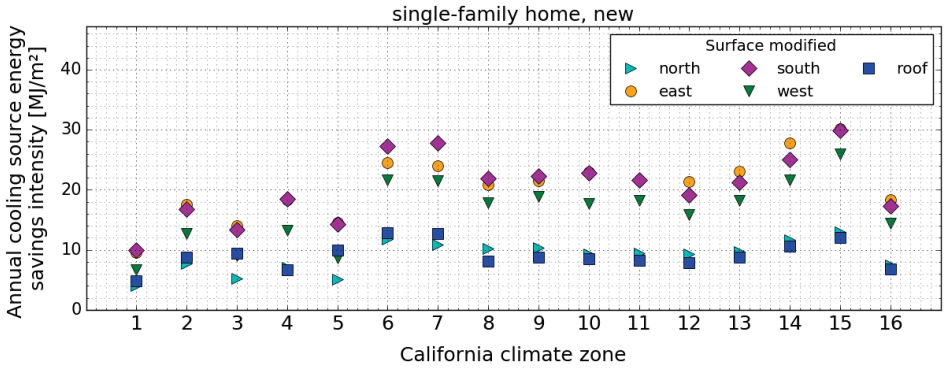

(b)

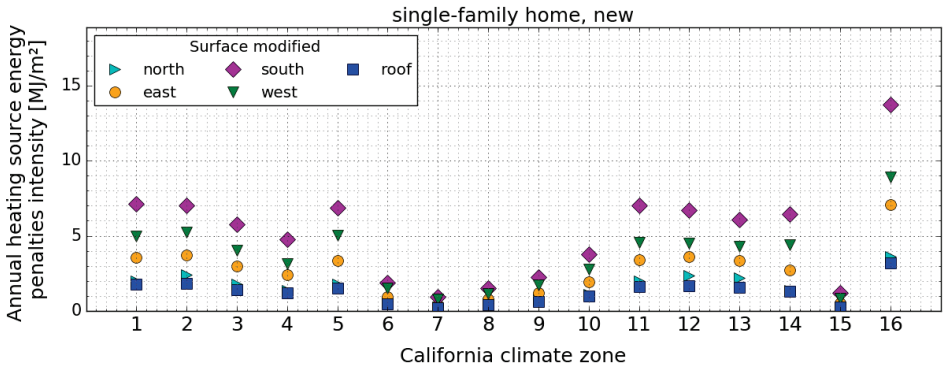

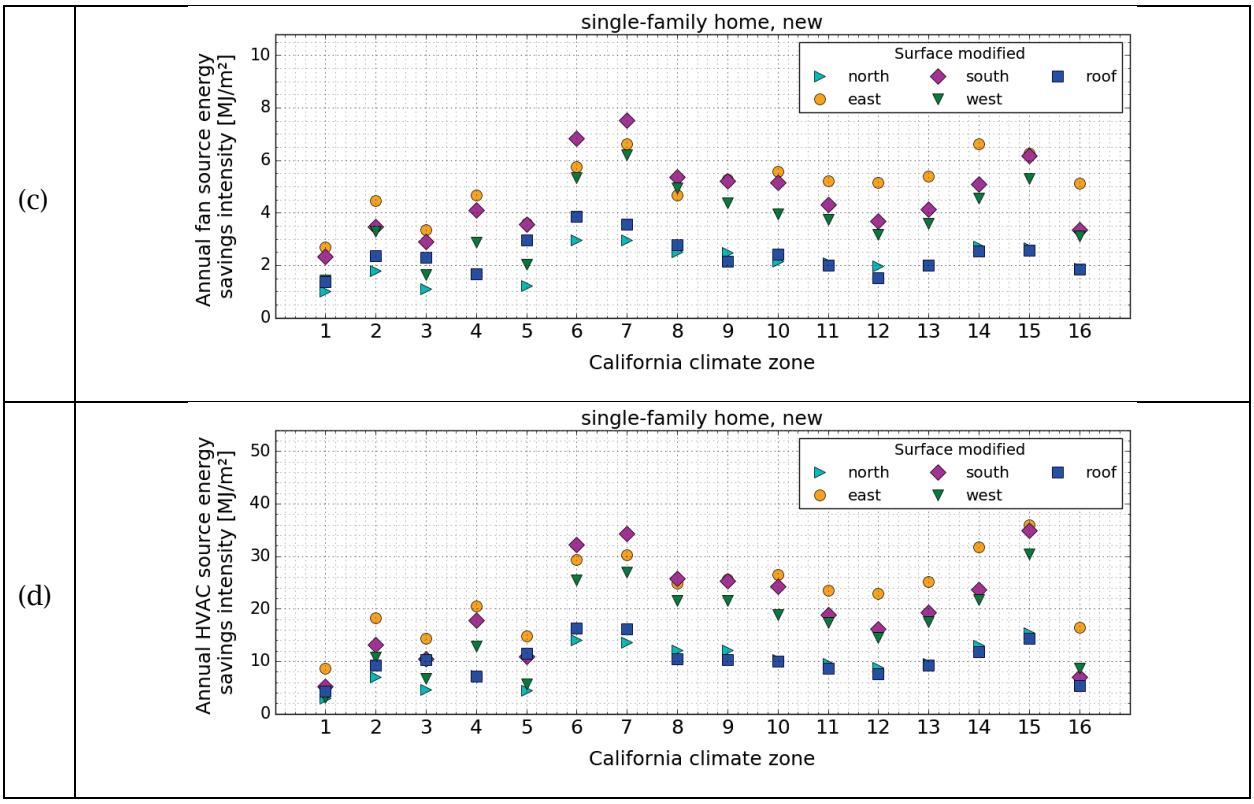

Figure 9. Annual source energy savings and penalty intensities of the new single-family home by California climate zone. The plots show (a) cooling savings, (b) heating penalties, (c) fan savings, and (d) HVAC savings.

3.3.2 Correlation of savings in California to outdoor air temperature and to changes in solar absorptance

Annual cooling savings and heating penalties vary by location, which is in part due to differences in climate between locations. This section investigates for the oldest single-family home the correlation of the annual cooling savings or heating penalties to two drivers: (a) change in absorbed solar radiation and (b) annual degree days. We used the coefficient of determination (R^2) to assess the fractions of variation in savings and penalties that can be explained by either driver.

Figure 10a and Figure 10b show how annual cooling site energy savings intensity from each modified face vary with changes in absorbed summer solar radiation and with annual CDD18C, respectively, in the oldest single-family home. Since the insulation in the building envelope and the efficiency of the AC system often vary by location, the changes in absorbed radiation were normalized by the face's thermal resistance and by the cooling efficiency (Figure 10a). annual CDD18C were normalized in the same manner (Figure 10b).

The annual site cooling savings from the south wall were essentially uncorrelated (R^2=0.03) with the change in absorbed irradiation (Figure 10a). Annual cooling savings for the other four

faces—north wall (R^2=0.48), east wall (R^2=0.60), west wall (R^2=0.42), and roof (R^2=0.57)—showed considerably better correlation with change in absorbed irradiation. Figure 10b shows that for every modified face, the annual cooling savings intensity correlates very well with annual CDD18C (from R^2=0.76 for south wall to R^2=0.86 for east wall). The graph clearly shows how cooling savings intensity increases with annual CDD18C.

Figure 10c and Figure 10d show the correlation of annual site gas heating energy penalty intensity to changes in absorbed solar radiation to annual HDD18C, respectively, for the oldest single-family home. The changes in winter solar radiation and annual HDD18C were normalized by the envelope's thermal resistance and the heating efficiency.

Annual site gas heating energy penalty intensities correlated poorly with changes in winter solar radiation (R^2=0.02 for east wall, west wall, and roof; R^2=0.11 for north wall). However, the annual site gas heating energy penalty intensities correlated very well with annual HDD18C (from R^2=0.90 for north wall to R^2=0.98 for west wall). Thus, annual heating penalty intensity increases with annual HDD18C.

	Changes in site energy vs changes in absorbed sunlight	Changes in site energy vs degree days
	(a)	(b)
Cooling	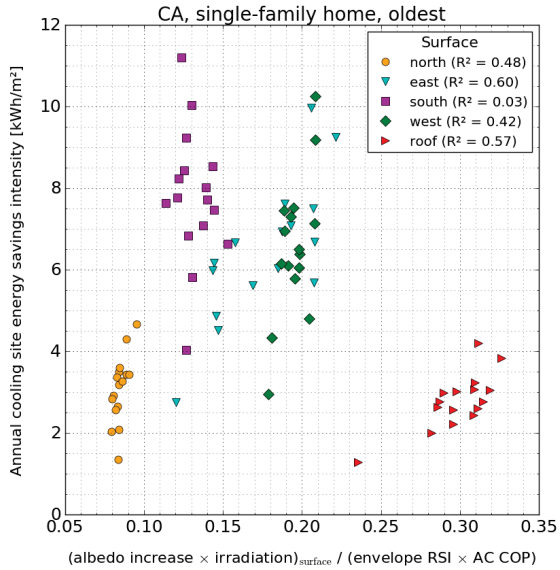	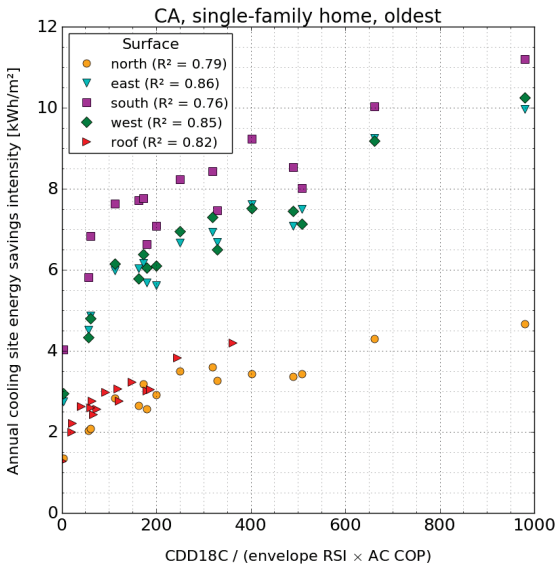
	(c)	(d)
Heating	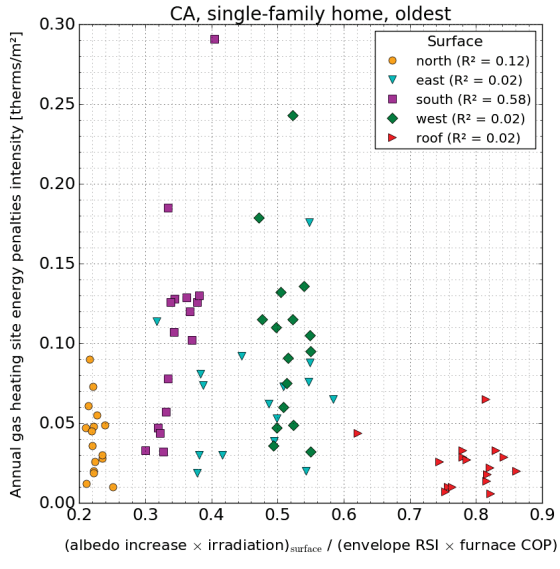	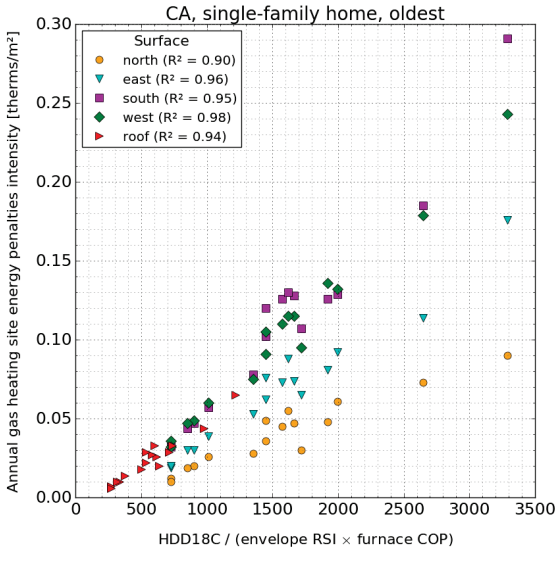

Figure 10. Correlation of changes in site energy use in California to changes in absorbed sunlight and to degree days, including (a) correlation of annual cooling site energy savings to change in absorbed sunlight during summer; (b) correlation of annual cooling site energy savings to annual CDD18C; (c) correlation of annual heating site energy penalties to change in absorbed sunlight during winter; and (d) correlation of annual heating site energy penalties to annual HDD18C.

We applied a multivariate linear regression analysis to investigate whether the correlations of cooling energy savings to either changes in absorbed sunlight or to annual CDD18C improved when both drivers (change in absorbed sunlight and annual CDD18C) were considered simultaneously.

Table 23 shows for all modified faces of the single-family home, medium office, and retail stand-alone the coefficient of determination from the correlation analysis of annual site cooling savings (a) to annual cooling degree days (CDD18C), (b) to change in absorbed summer sunlight, and (c) simultaneously to annual CDD18C and change in absorbed summer sunlight. For all buildings and faces, cooling savings correlated better with cooling degree days than with change in absorbed summer sunlight. When both metrics were considered simultaneously, the correlation improved the most—compared to the individual correlations to both drivers (change in absorbed summer sunlight and annual CDD18C)—for the south wall and the roof in the new vintage of the three building categories. The multivariate linear regression yielded little to no improvement—compared to the individual correlations to each driver—for the north wall, east wall, and west wall.

We repeated this analysis to investigate whether the correlation of annual site heating energy penalties to changes in absorbed winter sunlight or to heating degree days heating improved when both metrics are considered simultaneously. Table 24 shows for all modified faces of the single-family home, medium office, and retail stand-alone, the coefficient of determination from the correlation analysis of annual site heating penalties (a) to heating degree days, (b) to change in absorbed winter sunlight, and (c) simultaneously to heating degree days and change in absorbed winter sunlight. Heating penalties usually correlated better with heating degree days than with change in absorbed winter sunlight. When both metrics were considered simultaneously, the correlations improved significantly (increased by > 0.20) only in some vintages of the medium office, specifically for the north wall, east wall, and roof. This improvement of more than 0.20 was relative to the largest correlation to the individual metrics.

Table 23. Coefficient of determination (R^2) from the correlations of annual cooling savings to annual cooling degree days at 18°C ("cdd"), annual cooling savings to change in absorbed summer sunlight ("sun"), and annual cooling savings to cdd and sun. The coefficients of determination are for all vintages in California of the single-family home, medium office, and retail stand-alone.

Building	Vintage	Coefficient of determination (R^2)														
		north wall			east wall			south wall			west wall			roof		
		cdd	sun	cdd + sun	cdd	sun	cdd + sun	cdd	sun	cdd + sun	cdd	sun	cdd + sun	cdd	sun	cdd + sun
single-family home	oldest	0.79	0.48	0.80	0.86	0.60	0.88	0.76	0.03	0.79	0.85	0.42	0.86	0.82	0.57	0.89
	older	0.21	0.09	0.23	0.32	0.31	0.36	0.12	0.03	0.15	0.23	0.09	0.23	0.35	0.66	0.96
	new	0.51	0.28	0.53	0.66	0.38	0.66	0.43	0.16	0.60 [a]	0.55	0.24	0.55	0.17	0.42	0.87 [a]
medium office	oldest	0.89	0.60	0.89	0.86	0.43	0.86	0.83	0.03	0.87	0.85	0.39	0.85	0.70	0.41	0.82
	older	0.85	0.53	0.85	0.82	0.47	0.82	0.72	0.06	0.80	0.83	0.35	0.83	0.43	0.47	0.79
	new	0.69	0.42	0.70	0.63	0.32	0.63	0.41	0.20	0.63 [a]	0.62	0.21	0.62	0.32	0.72	0.94 [a]
retail stand-alone	oldest	0.89	0.59	0.89	0.88	0.51	0.88	0.84	0.01	0.85	0.84	0.42	0.85	0.75	0.44	0.88
	older	0.77	0.48	0.78	0.84	0.49	0.84	0.72	0.03	0.76	0.78	0.37	0.78	0.60	0.40	0.88
	new	0.42	0.31	0.42	0.70	0.20	0.76	0.31	0.20	0.53 [a]	0.50	0.22	0.50	0.43	0.64	0.95 [a]

[a] Coefficient of determination that significantly improved in the multivariate linear regression.

Table 24. Coefficient of determination (R^2) from the correlations of annual heating penalty to annual heating degree days at 18°C ("hdd"), annual heating penalty to change in absorbed winter sunlight ("sun"), and annual heating penalty to hdd and sun. The coefficients of determination are for all vintages in California of the single-family home, medium office, and retail stand-alone.

Building	Vintage	Coefficient of determination (R^2)														
		north wall			east wall			south wall			west wall			roof		
		hdd	sun	hdd + sun	hdd	sun	hdd + sun	hdd	sun	hdd + sun	hdd	sun	hdd + sun	hdd	sun	hdd + sun
single-family home	oldest	0.90	0.12	0.91	0.96	0.02	0.97	0.95	0.58	0.97	0.98	0.02	0.98	0.94	0.02	0.94
	older	0.64	0.09	0.64	0.83	0.05	0.86	0.86	0.74	0.97	0.78	0.00	0.80	0.74	0.35	0.79
	new	0.81	0.08	0.81	0.88	0.06	0.93	0.89	0.69	0.97	0.90	0.00	0.92	0.66	0.05	0.78
medium office	oldest	0.79	0.16	0.81	0.06	0.36	0.43	0.14	0.16	0.18	0.40	0.07	0.43	0.16	0.08	0.39 [a]
	older	0.66	0.24	0.73	0.26	0.47	0.71 [a]	0.16	0.31	0.32	0.02	0.38	0.38	0.19	0.23	0.34
	new	0.44	0.43	0.67 [a]	0.26	0.36	0.60 [a]	0.18	0.22	0.24	0.00	0.49	0.49	0.47	0.23	0.50
retail stand-alone	oldest	0.85	0.03	0.86	0.84	0.04	0.87	0.84	0.33	0.84	0.85	0.00	0.85	0.96	0.17	0.96
	older	0.87	0.04	0.88	0.93	0.05	0.97	0.93	0.51	0.94	0.91	0.00	0.92	0.95	0.04	0.95
	new	0.11	0.02	0.11	0.72	0.09	0.79	0.90	0.44	0.90	0.88	0.00	0.89	0.89	0.16	0.89

[a] Coefficient of determination that significantly improved in the multivariate linear regression.

3.3.3 Savings in California by climate zone and vintage

This section reports annual HVAC source energy, energy cost, CO_2e, NO_x, SO_2, and peak power demand savings for the single-family home, the medium office, and the stand-alone retail buildings upon (a) increasing the albedo of all four walls simultaneously by 0.35 (to 0.60 from 0.25) or (b) increasing the albedo of the roof to 0.40 from 0.10 (single-family home) or to 0.60 from 0.20 (medium office and retail stand-alone). Each metric is compared by vintage and by California climate zone.

3.3.3.1 Annual HVAC source energy savings

Figure 11 shows annual HVAC source energy savings intensity by vintage and by California climate zone for the single-family home (Figure 11a), medium office (Figure 11b), and stand-alone retail (Figure 11c).

In the single-family home (Figure 11a) the increase in roof albedo (0.30) was 86 percent of that of walls (0.35). In each vintage, the thermal resistance of the roof assembly was much greater than that of the wall assembly; in older and oldest vintages, the thermal resistance of the roof assembly was 2.7 times greater than that of the wall assembly, and in the new vintage, the thermal resistance of the roof assembly insulation was 1.5 to 2.4 times greater than that of walls (Table 10 and Table 12). Hence, these differences between roof and wall thermal resistance are a major reason why the four-walls annual HVAC source energy savings intensities were generally at least twice than those from the roof.
In the single-family home (Figure 11a), the thermal resistance of the wall assembly in the new vintage was 3.4 times that in the oldest vintage, while the cooling efficiency in the new vintage was 1.4 times that in the oldest vintage. Thus, we would expect the HVAC savings intensity from cool walls in the oldest single-family home to be about $3.4 \times 1.4 = 4.75$ times that of the new home. This estimate matches well with what we observe in Figure 11a and calculated in Table 25, where the cool wall savings intensity from the oldest vintage is about 5 times that of the new vintage. In the case of older single-family home, the HVAC savings intensity were about 2.5 times that of the new vintage (Table 26).

The medium-office savings (Figure 11b) were from increasing the wall albedo by 0.35 (to 0.60 from 0.25), and from increasing the roof albedo by 0.40 (to 0.60 from 0.20). Thus, the increase in roof albedo was 1.14 times that of walls. The thermal resistance of the roof assembly in the oldest medium office was from 1.2 to 1.4 times that of the wall assembly in CACZs 2-5 and 8-13; however, the thermal resistance of the roof assembly was 2.0 to 2.6 times that of the wall assembly in the remaining CACZs (1, 6-7, and 14-16) (Table 10 and Table 12). In these California climate zones with large ratio of roof thermal resistance to wall thermal resistance, annual HVAC savings intensity from the walls were greater than those from the roof (Figure 11b).
In the medium office (Figure 11b), the ratio of wall thermal resistances of new to oldest vintage varies by location but ranges from 3.8 to 6.4. Additionally, the cooling efficiency in the new vintage was only 1.1 times that of the oldest vintage. Thus, we would expect the HVAC savings

from cool walls in the oldest single-family home to be between 4.2 (3.8 × 1.1) to 7.0 (6.4 × 1.1) times that of the new medium office. This estimate matches well with what we observe in Figure 11a and calculated in Table 25, where the cool walls savings intensity from the oldest vintage were on average, 5.2 times that of the new vintage. In the case of older medium office, the annual HVAC savings intensity were on average, 2.0 times that of the new vintage (Table 26)

In the retail stand-alone, the cool wall savings throughout California from the oldest vintage were on average 5.8 times that of the new vintage (Figure 11c; Table 25); the wall savings from the older vintage were on average 2.6 times that of the new vintage (Figure 11c; Table 26). These oldest-to-new and older-to-new savings ratios of the stand-alone retail were greater than those of the medium office even though the thermal resistance of the retail stand-alone and medium office were very similar (identical in most cases). That is because the air conditioner efficiency in the stand-alone retail increased 23 percent (to 3.49 from 2.84) between the old vintages and the new vintage, while in the medium office, the air conditioner efficiency increased only 5.0 percent (to 3.96 from 3.78) (Table 5).

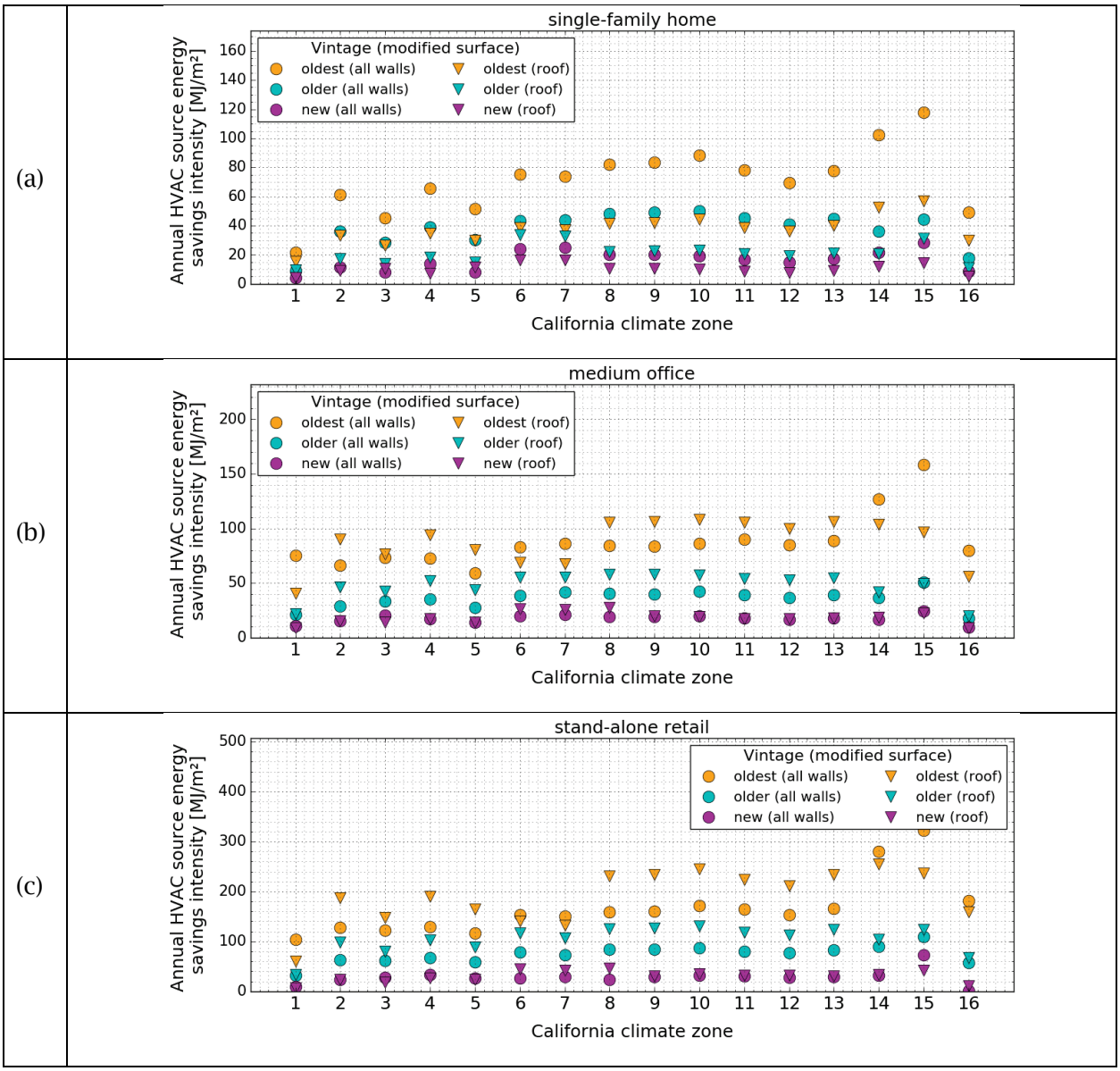

Figure 11. Annual HVAC source energy savings intensity by vintage and by California climate zone for the (a) single-family home, (b) medium office, and (c) retail stand-alone. The plots compare the savings intensity from increasing the albedo of all walls by 0.35 tothat from increasing the roof albedo by 0.30 (residential) or 0.40 (commercial).

The fractional savings (absolute savings / base value) of the energy, energy cost, and emission metrics were influenced not only by the absolute savings but also by the energy consumed in the base case. When comparing cool walls to a cool roof, the differences in fractional savings

were driven by the envelope characteristics (e.g., differences in surface albedo change and in insulation) as well as by the envelope geometry (e.g., ratio of roof area to net wall area).

Figure 12 shows the annual HVAC source energy fractional savings by vintage and by California climate zone for the single-family home (Figure 12a), medium office (Figure 12b), and stand-alone retail (Figure 12c). For the single-family home (Figure 12a), CACZ 7 (San Diego) had the greatest cool walls and cool roof fractional savings in all vintages, reaching up to 25 percent (oldest vintage) when all walls were made cool and 8.0 percent (oldest vintage) when the roof was made cool. Low requirements for roof and wall insulation helped make annual HVAC source energy savings intensity in CACZ 7 larger than those in the other CACZs. San Diego also experienced fewer CDD18C and HDD18C than other locations, requiring lower-than-average baseline conditioning energy consumption. CACZs 14 (China Lake) and 15 (Imperial) were the locations with the greatest annual HVAC source energy savings intensity, but yielded less than the CA-average annual HVAC energy fractional savings; savings in CACZs 14 and 15 were up to 12 percent (oldest vintage) from when all walls were made cool and 4.0 percent (oldest vintage) when the roof was made cool.

In the single-family home, annual HVAC source energy savings intensity from the walls were about 2 times that of the roof (Figure 11a). However, the HVAC fractional savings from the walls were from 2.2 to 3.3 times that of the roof. The walls-to-roof ratio in fractional savings was greater than the ratio in savings intensity because the net wall area is greater than the roof area. From Table 4, we gather that the net wall area is 1.6 times that of the roof area. Thus, the ratio of wall savings intensity to roof savings intensity adjusted by the wall-to-roof area ratio is $2 \times 1.6 = 3.2$. This adjusted wall-to-roof savings ratio is similar to the ratio of 2.2 to 3.5 we observed for HVAC energy fractional savings Figure 12a.

For the medium office (Figure 12b), we saw once again that CACZ 15 (Imperial), which was the location with greatest annual HVAC energy savings intensity, yielded fractional savings that were close to the average fractional savings for California; fractional savings in CACZ 15 were 3.7 percent (oldest vintage) when all walls were made cool and 3.0 percent (older and oldest vintage) when the roof was made cool.

When analyzing the annual HVAC source energy savings intensity of the medium office (Figure 11b), we observed that in most California climate zones and vintages, the savings intensity from the roof were slightly greater than those from the walls. In the case of fractional savings (Figure 12b) the ratio of roof-to-wall savings were greater than those from the savings intensity. This difference is due in part because the modified roof area is 1.3 times that of the modified net wall area. Although the medium office is three stories high, its large window area (ratio of window to gross wall area = 0.33) gives it more roof area than net wall area.

In the case of retail stand-alone (Figure 12c), the roof-to-wall ratios of annual HVAC fractional savings were even greater than those observed in the medium office. That is because the stand-alone retail is a single-story building with a large footprint (2,290 m²), and has more than twice

as much roof area as wall area (roof area to net wall area ratio = 2.1) (Table 4). Hence, the difference in cool roof fractional savings to those from the cool walls was significantly influenced by the large ratio of roof area to net wall area.

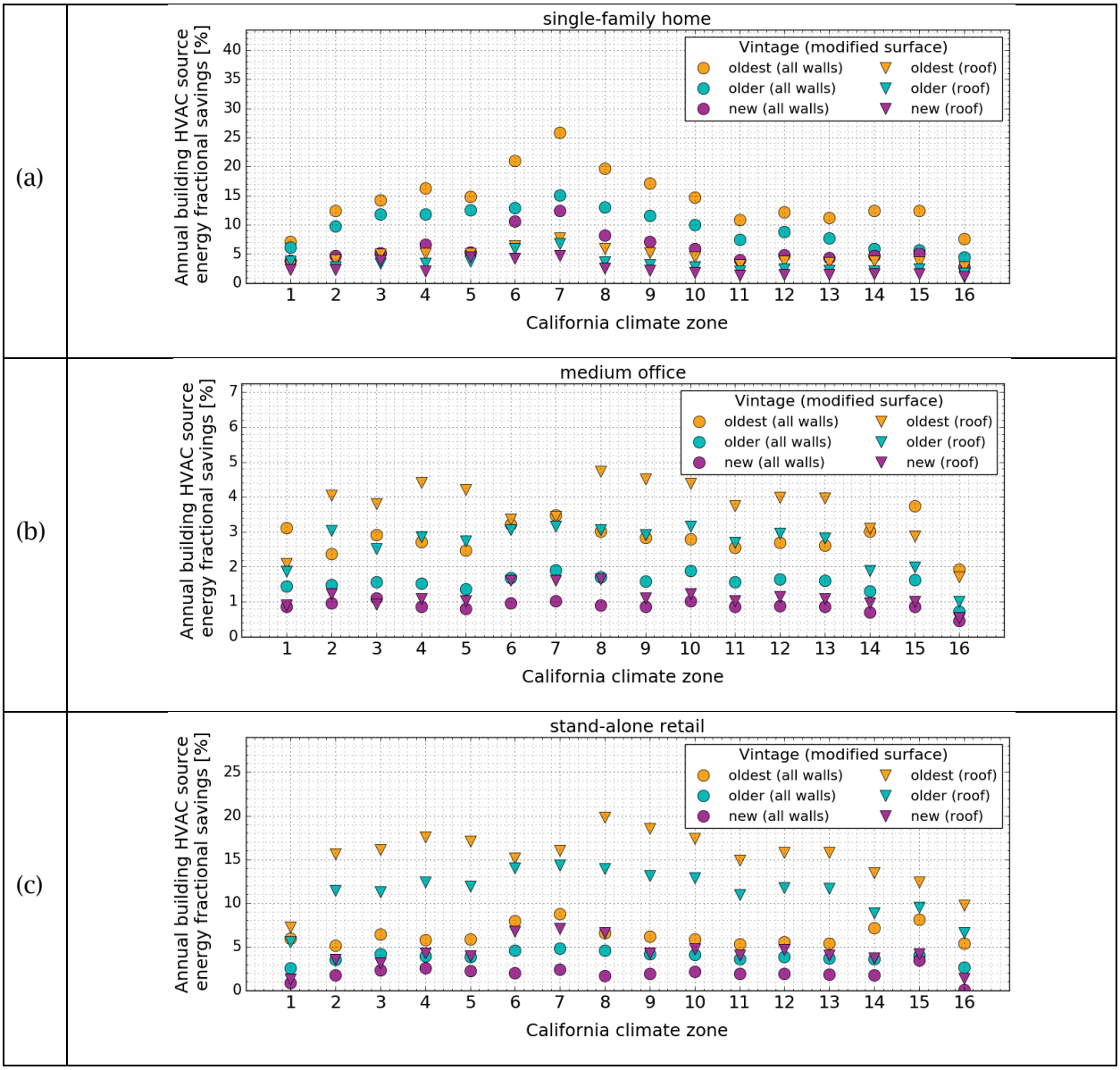

Figure 12. Annual HVAC source energy fractional savings by vintage and by California climate zone for the (a) single-family home, (b) medium office, and (c) retail stand-alone. The plots compare the fractional savings from increasing the albedo of all walls by 0.35 to that from increasing the roof albedo by 0.30 (residential) or 0.40 (commercial).

3.3.3.2 Annual HVAC energy cost savings

Figure 13 shows annual HVAC energy cost savings intensity by vintage and by California climate zone for the single-family home (Figure 13a), medium office (Figure 13b), and stand-alone retail (Figure 13c). These annual HVAC energy cost savings intensities were computed using Eq. (9) and California's electricity and gas prices from Table 18. For the single-family home, we used the prices for residential buildings; for the medium office and retail stand-alone, we used the prices for commercial buildings.

The annual HVAC energy cost savings intensities show the same trend between California climate zones and between vintages that those we observed for the HVAC source energy savings intensities. The proportions of cool roof energy cost savings intensities to those from cool walls were very similar to those we observed for annual HVAC energy savings intensities. These similarities happen because HVAC energy cost savings intensities and HVAC energy savings intensities are affected equally by climate (i.e., solar radiation, CDD18C, and HDD18C) and building properties (i.e., envelope insulation).
In the single-family home (Figure 13a), cool walls generated greater annual HVAC energy cost savings intensities than did cool roof. The greatest annual HVAC energy cost savings intensities when all walls were made cool were $1.7/m² (oldest, CACZ 15, Imperial) and $1.5/m² (oldest; CACZ 14, China Lake). CACZ 1 (Arcata) yielded the smallest annual HVAC energy cost savings intensities. The cool wall HVAC energy cost savings intensity from the oldest vintage were on average, 4.5 times that those of the new vintage (Table 25). In the case of older single-family home, the HVAC energy cost savings intensity were about 2.4 times that of the new vintage (Table 26).

Note that for a given building category and vintage, the only difference between locations in wall construction is the climate-specific insulation requirements. Thus, the variations in wall thermal resistance between locations stem from the insulation requirements. In the oldest medium office (Figure 13b), the wall thermal resistance was smaller in CACZs 1, 6-7, and 14-16 than in the other California climate zones. These locations with lower wall thermal resistance yielded wall annual HVAC energy cost savings intensities greater than those from the roof. For the medium office, the cool wall annual HVAC energy cost savings intensity from the oldest vintage was on average 5.1 times those of the new vintage (Table 25). The annual HVAC energy cost savings intensity from the older vintage was on average, 2.0 times that of the new vintage (Table 26).

Trends for the stand-alone retail (Figure 13c) were similar to those observed for the medium office because the roof and wall thermal resistances of these two buildings were nearly identical. However, the wall annual HVAC energy cost savings throughout California from the oldest vintage were on average 5.8 times that of the new vintage (Table 25); the wall savings from the older vintage were on average 3.6 times that of the new vintage (Table 26). Oldest-to-new and older-to-new savings ratios of the stand-alone retail were greater than those of the medium office even though the insulation between the retail stand-alone and medium office were mostly identical. That is because the air conditioner efficiency in the stand-alone retail

increased 23 percent between the old vintages and the new vintage, while in the medium office, the air conditioner efficiency increased only 5.0 percent (Table 5).

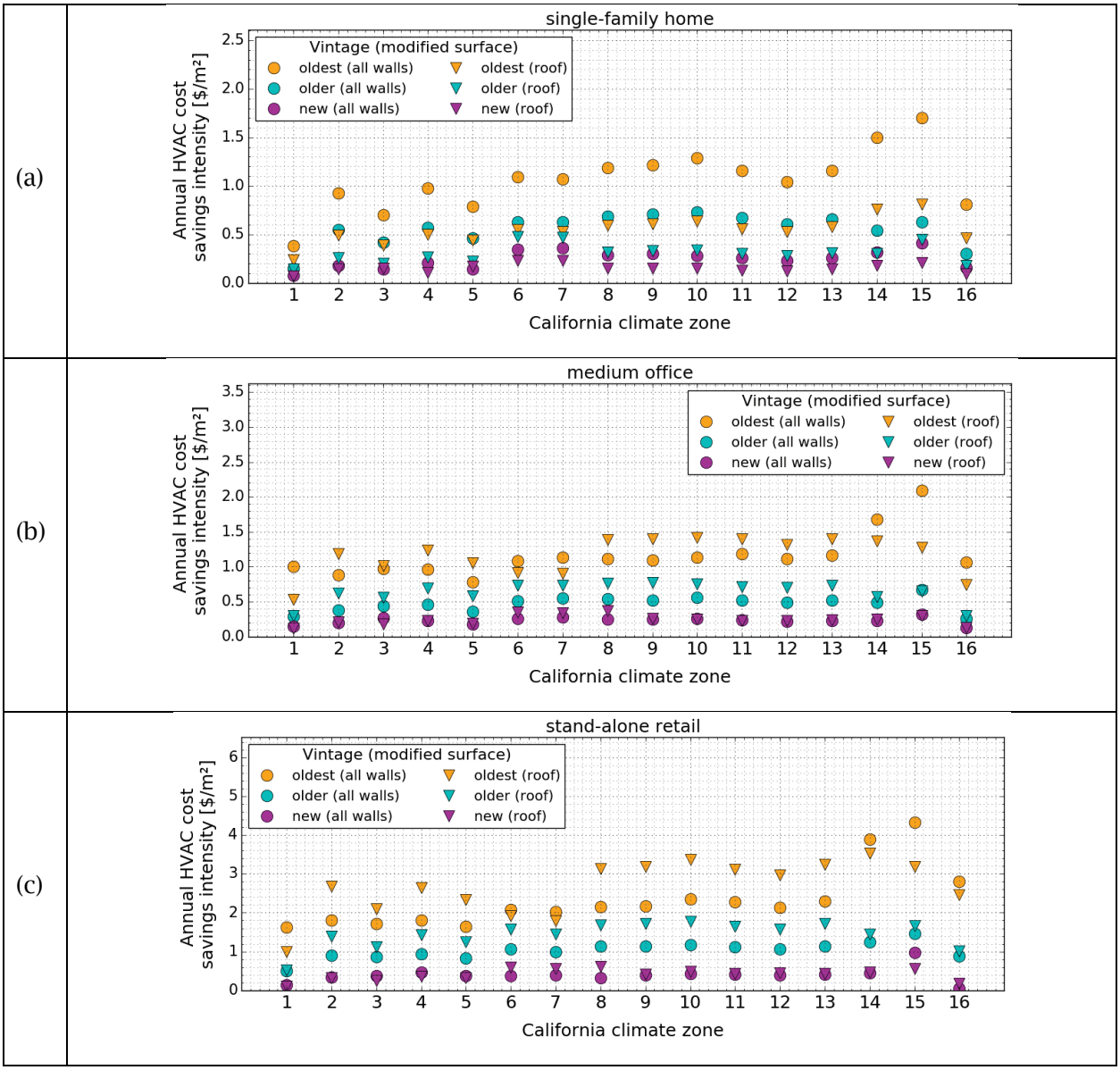

Figure 13. Annual HVAC energy cost savings intensity by vintage and by California climate zone for the (a) single-family home, (b) medium office, and (c) retail stand-alone. The plots compare the savings intensity from increasing the albedo of all walls by 0.35 to that from increasing the roof albedo by 0.30 (residential) or 0.40 (commercial).

Figure 14 shows HVAC energy cost fractional savings by vintage and by California climate zone for the single-family home (Figure 14a), medium office (Figure 14b), and stand-alone retail (Figure 14c). Similar to what we observed between annual HVAC source energy and energy cost

savings intensities, the annual HVAC source energy and energy cost savings intensities are affected equally by climate and building properties (Section 3.3.3.1).

For the single-family home (Figure 14a), CACZ 7 (San Diego) had the greatest cool walls and cool roof fractional savings in all vintages, reaching up to 27 percent (oldest vintage) when all walls were made cool and 8.5 percent (oldest vintage) when the roof was made cool. Low requirements for roof and wall insulation and small base HVAC energy cost helped make annual HVAC energy cost fractional savings in CACZ 7 larger than those in the other California climate zones. CACZs 14 (China Lake) and 15 (Imperial) were the locations with the greatest annual HVAC energy cost savings intensities, but yielded less than CA-averaged energy cost fractional savings; savings in CACZs 14 and 15 were up to 14 percent (oldest vintage) from when all walls were made cool and 4.0 percent (oldest vintage) when the roof was made cool.

In the single-family home (Figure 14a), the annual HVAC energy cost fractional savings from the walls were from 2.0 to 3.3 times that of the roof. These wall-to-roof ratios of fractional savings were greater than those of savings intensities due to the wall area being 1.64 times that of the roof.

In the oldest medium office (Figure 14b), the wall thermal resistance was greater in CACZs 2-5 and 8-13, when compared to the other California climate zones. These locations with more wall thermal resistance yielded roof annual HVAC energy cost fractional savings that were greater than those from the walls. This three-story building has more roof area than net wall area (ratio 1.3), which further increased the roof-to-wall ratio of annual HVAC energy cost fractional savings.

For the medium office (Figure 14b), the greatest cool roof annual HVAC energy cost fractional savings was 4.8 percent and occurred from the oldest vintage in CACZ 8 (Fullerton). In the case of walls, the greatest annual HVAC energy cost fractional savings was 3.8 percent and occurred from the oldest vintage in CACZ 15 (Imperial).

As discussed earlier, the roof-to-wall ratios of HVAC fractional savings in the retail stand-alone (Figure 14c) were even greater than those observed in the medium office, even though both buildings have nearly identical envelope thermal resistances in all locations. That is because the stand-alone retail is a single-story building with a very large footprint (2,290 m^2), and has more than twice as much roof area as wall area (ratio of roof area to net wall area = 2.1) (Table 4).

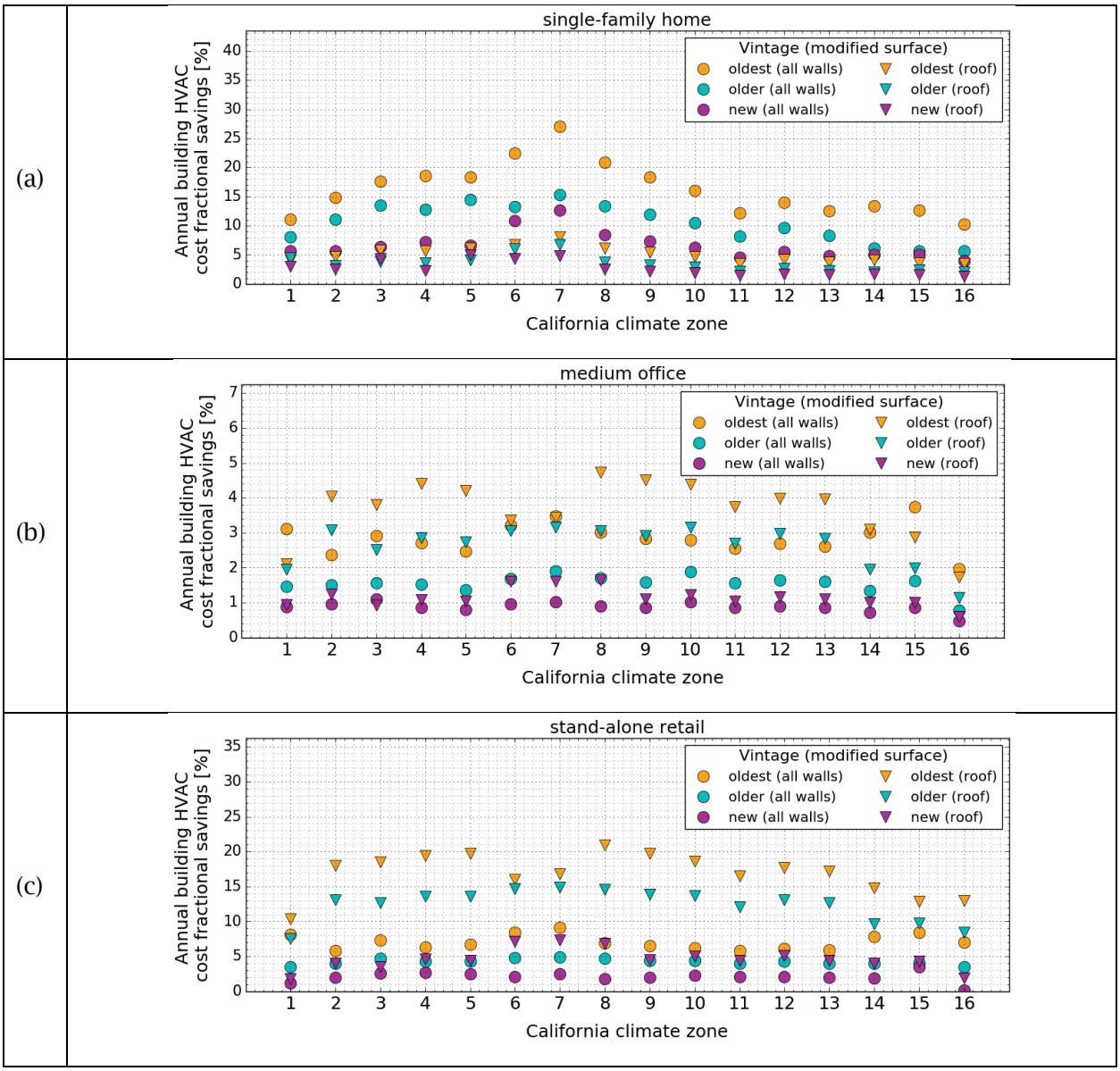

Figure 14. Annual HVAC energy cost fractional savings by vintage and by California climate zone for the (a) single-family home, (b) medium office, and (c) retail stand-alone. The plots compare the fractional savings from increasing the albedo of all walls by 0.35 to that from increasing the roof albedo by 0.30 (residential) or 0.40 (commercial).

3.3.3.3 Annual CO_2e emissions reduction

Figure 15 shows annual CO_2e emissions reduction intensities by vintage and by California climate zone for the single-family home (Figure 15a), medium office (Figure 15b), and stand-alone retail (Figure 15c). These emissions reduction intensities were computed using Eq. (8) and California's CO_2e emissions rate of generated electricity (Table 16) and of consumed gas (Table 17). This study included calculations of CO_2, which are available in the savings database.

The annual CO_2e emissions reduction intensities exhibit the same trend between California climate zones and between vintages that those we observed for the annual HVAC source energy and energy cost savings intensities. The ratios of cool roof CO_2e reduction intensities to those from cool walls were very similar to those we observed for annual HVAC energy and energy cost savings intensities. These similarities happen because emissions reduction intensities, HVAC source energy savings intensity, and energy cost savings intensities are affected equally by climate (i.e., solar radiation, CDD18C, and HDD18C) and building properties (i.e. envelope insulation) (see Section 3.3.3.1).

In the single-family home (Figure 15a), the walls generated higher annual CO_2e emissions reduction intensities than did the roof. The greatest CO_2e emissions reduction intensities were 3.3 kg/m² (oldest, CACZ 15, Imperial) and 2.6 kg/m² (oldest; CACZ 14, China Lake). CACZ 1 (Arcata) and CACZ 16 (Mount Shasta) yielded the smallest annual CO_2e emissions reduction intensities. In California, the four-wall CO_2e emissions reduction intensity from the oldest vintage was on average, 5.4 times that of the new vintage (Table 25). In the case of older single-family home in California, the CO_2e emissions reduction intensity was on average, 3.1 times that of the new vintage (Table 26).

As noted earlier, the wall thermal resistance in the oldest medium office was smaller in CACZs 1, 6-7, and 14-16 than in the other CACZs (Figure 15b). These locations with less wall thermal resistance yielded wall CO_2e emissions reduction intensities greater than those from the roof. For the medium office in California, the wall CO_2e emissions reduction intensity from the oldest vintage were on average, 5.1 times that of the new vintage (Table 25). The CO_2e emissions reduction intensity from the older vintage were on average, 2.0 times that of the new vintage (Table 26).

In the stand-alone retail (Figure 15c), the greatest annual CO_2e emissions reduction intensities were 9.3 kg/m² (oldest, CACZ 15, Imperial) and 7.5 kg/m² (oldest; CACZ 14, China Lake). CACZ 1 (Arcata) and CACZ 16 (Mount Shasta) yielded the smallest annual CO_2e emissions reduction intensities. For the stand-alone retail in California, the wall CO_2e emissions reduction intensities from the oldest vintage were 6.0 times that of the new vintage (Table 25); the wall emissions reduction from the older vintage were on average, 2.7 times that of the new vintage (Table 26).

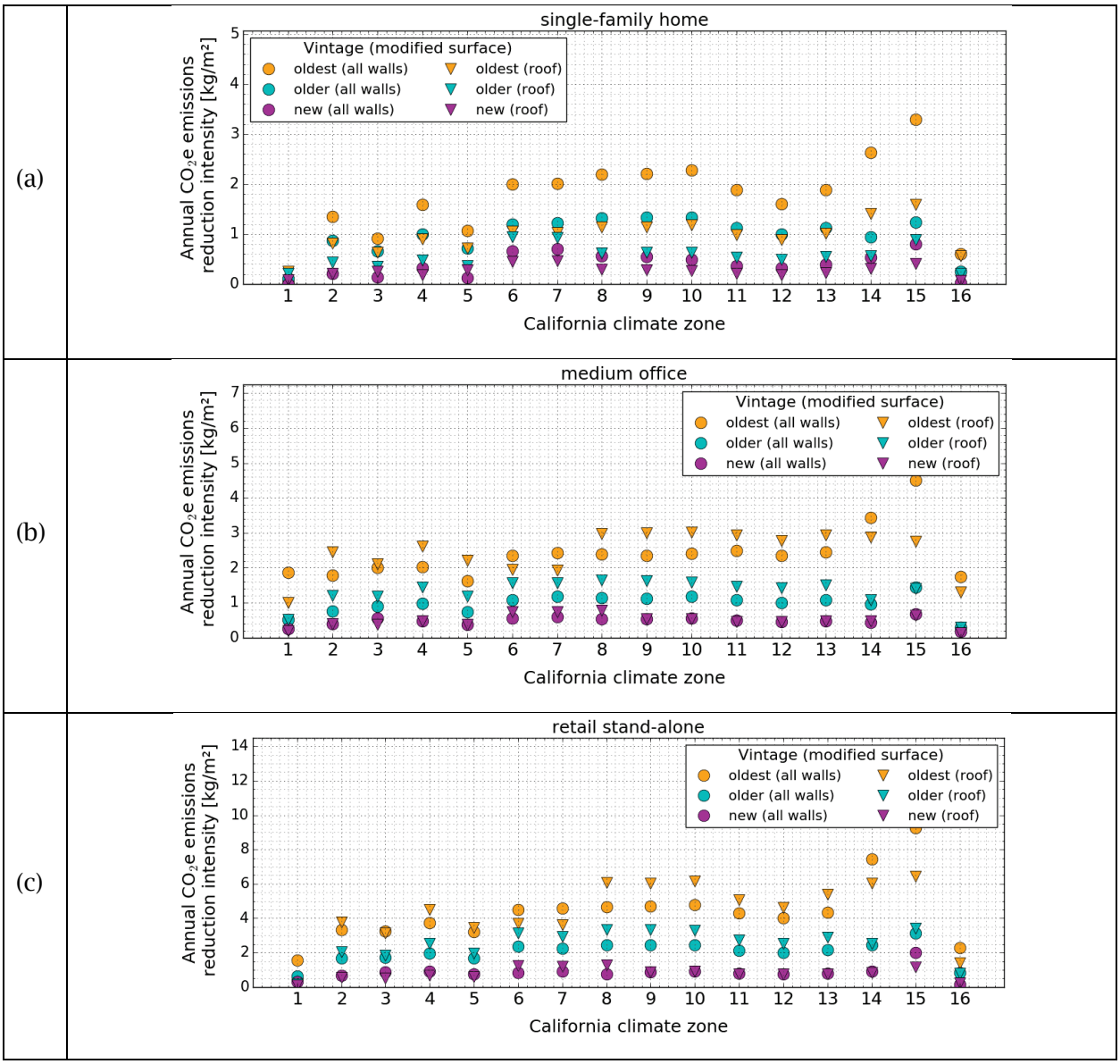

Figure 15. Annual CO_2e emissions reduction intensity by vintage and by California climate zone for the (a) single-family home, (b) medium office, and (c) retail stand-alone. The plots compare the reduction intensity from increasing the albedo of all walls by 0.35 to that from increasing the roof albedo by 0.30 (residential) or 0.40 (commercial).

Figure 16 shows fractional reductions in CO_2e emissions by vintage and by California climate zone for the single-family home (Figure 16a), medium office (Figure 16b), and stand-alone retail (Figure 16c). The annual CO_2e emission fractional reductions have the same trend between California climate zones and between vintages that those we observed for the annual HVAC source energy and energy cost fractional savings. The ratios of cool roof CO_2e fractional reductions to those from cool walls were very similar to those we observed for annual HVAC energy and energy cost fractional savings. These similarities happen because emissions

fractional reduction, HVAC source energy fractional savings, and HVAC energy cost fractional savings are affected equally by climate (i.e., solar radiation, CDD18C, and HDD18C) and building properties (i.e. envelope insulation, envelope geometry) (see in Section 3.3.3.1).

In all vintages of the single-family home (Figure 16a), CACZ 7 (San Diego) had the greatest cool walls and cool roof fractional savings of annual CO_2e emissions, reaching up to 23 percent (oldest vintage) when all walls were made cool and 7.0 percent (oldest vintage) when the roof was made cool. Low requirements for roof and wall insulation and small base whole-building CO_2e emissions helped make annual fractional savings of CO_2e emissions in CACZ 7 larger than those in the other California climate zones.

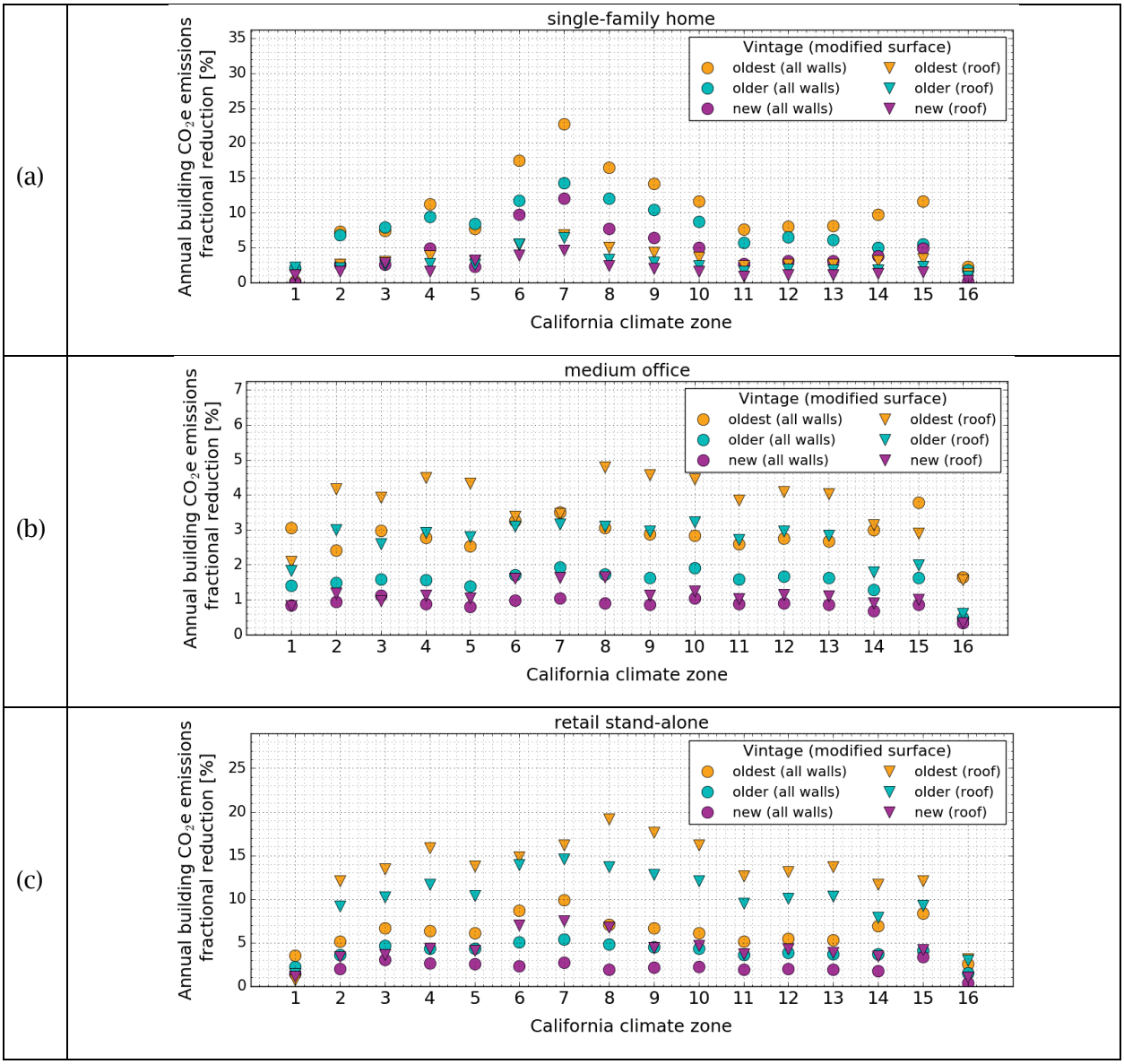

Figure 16. Annual CO_2e emissions fractional reduction by vintage and by California climate zone for the (a) single-family home, (b) medium office, and (c) retail stand-alone. The plots compare the fractional reduction from increasing the albedo of all walls by 0.35 to that from increasing the roof albedo by 0.30 (residential) or 0.40 (commercial).

3.3.3.4 Annual NO_x emissions reduction

Figure 17 and Figure 18 show annual NO_x emissions reduction intensities and fractional reductions, respectively, by vintage and by California climate zone for the single-family home (Figure 17a and Figure 18a), medium office (Figure 17b and Figure 18b), and stand-alone retail (Figure 17c and Figure 18c). These emissions reduction intensities were computed using Eq. (8) and (10), and the fractional reductions were computed using Eq. (8). These emission reductions

were calculated using California's NO_X emissions rate of generated electricity (Table 16) and of consumed gas (Table 17).

The annual NO_X emissions reduction intensities and fractional reductions exhibit the same trend between California climate zones and between vintages that those we observed for the annual savings intensity and fractional savings of annual CO_2e emissions. The ratios of cool roof NO_X reductions to those from cool walls were very similar to those we observed for annual CO_2e emissions reductions. These similarities happen because NO_X and CO_2e emission reductions are affected equally by climate (i.e., solar radiation, CDD18C, and HDD18C) and building properties (i.e. envelope thermal resistance) (see Section 3.3.3.1). Fractional savings are also affected by building geometry (e.g., net wall area and roof area).

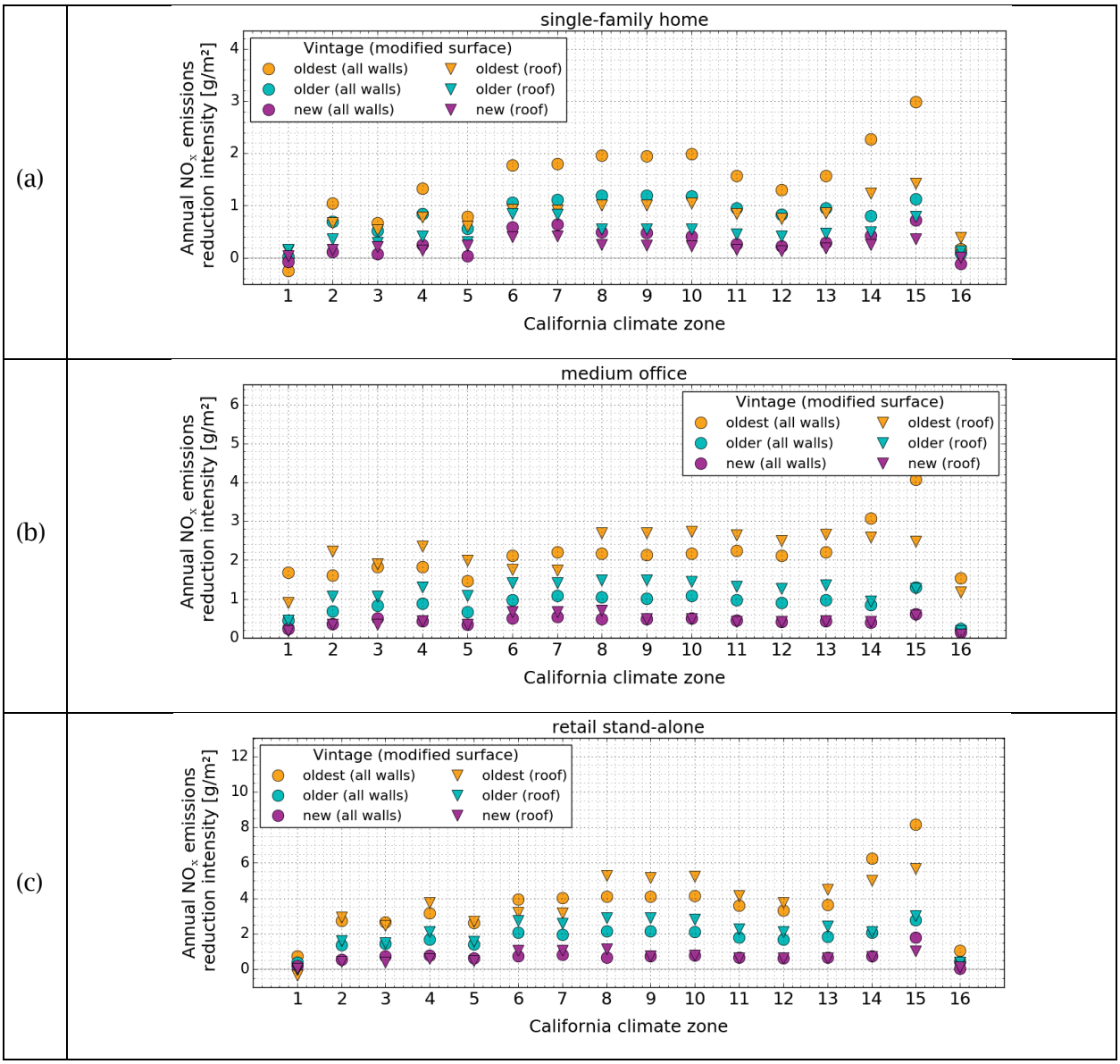

Figure 17. Annual NO_X emissions reduction intensity by vintage and by California climate zone for the (a) single-family home, (b) medium office, and (c) retail stand-alone. The plots compare the reduction intensity from increasing the albedo of all walls by 0.35 to that from increasing the roof albedo by 0.30 (residential) or 0.40 (commercial).

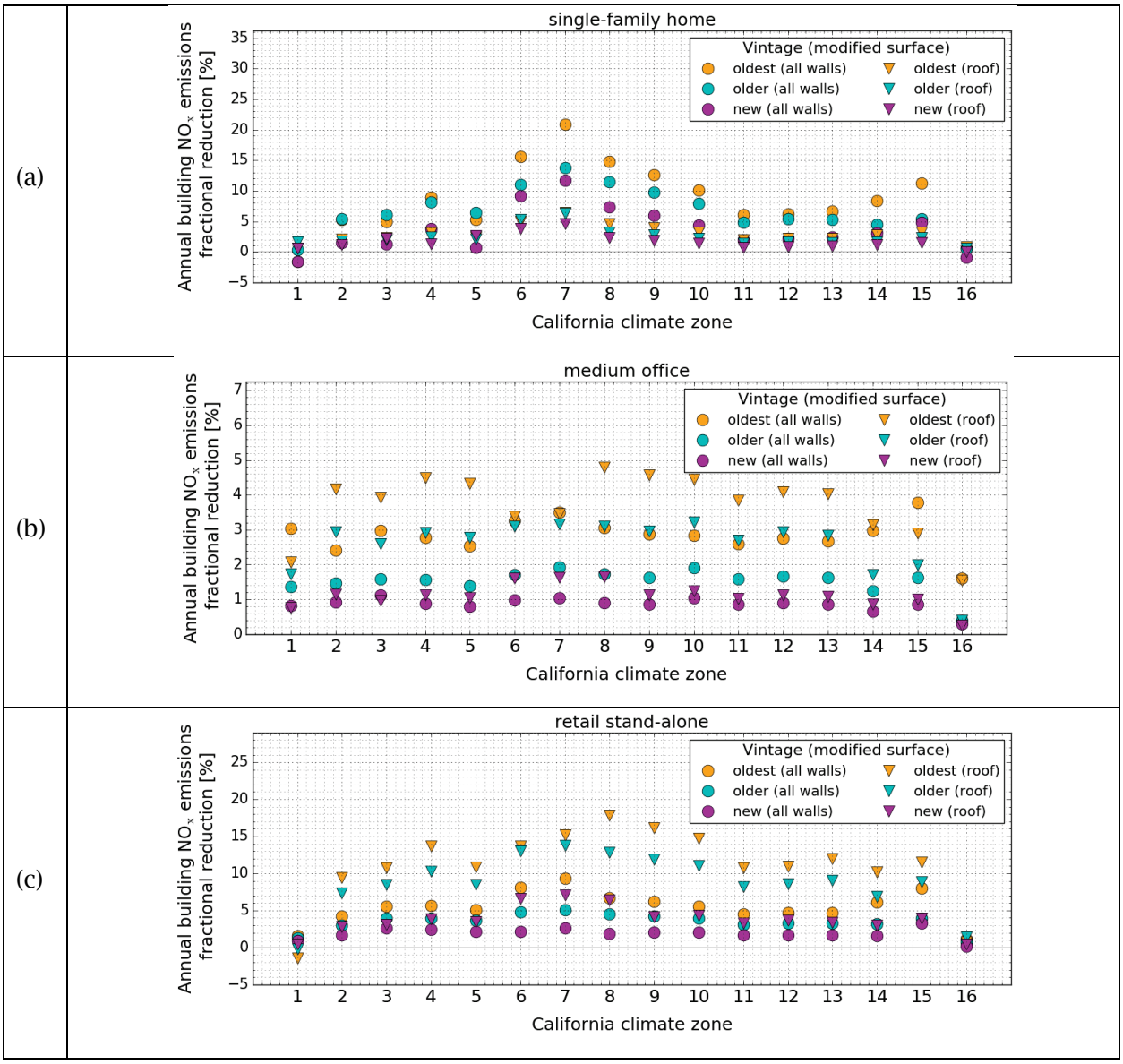

Figure 18. Annual NO_X emissions fractional reduction by vintage and by California climate zone for the (a) single-family home, (b) medium office, and (c) retail stand-alone. The plots compare the fractional reduction from increasing the albedo of all walls by 0.35 to that from increasing the roof albedo by 0.30 (residential) or 0.40 (commercial).

3.3.3.5 Annual SO_2 emissions reduction

Figure 19 and Figure 20 show annual SO_2 emissions reduction intensities and fractional reductions, respectively, by vintage and by California climate zone for the single-family home (Figure 19a and Figure 20a), medium office (Figure 19b and Figure 20b), and stand-alone retail (Figure 19c and Figure 20c). These emissions reduction intensities were computed using Eq. (8) and (10), and the fractional reductions were computed using Eq. (8). These emission reductions

were calculated using California's SO_2 emissions rate of generated electricity (Table 16) and of consumed gas (Table 17).

The annual SO_2 emissions reduction intensities and fractional reductions have the same trend between California climate zones and between vintages that those we observed for the annual savings intensity and fractional savings of annual CO_2e emissions. The ratios of cool roof SO_2 reductions to those from cool walls were very similar to those we observed for annual CO_2e emissions reductions. These similarities happen because SO_2 and CO_2e emissions reductions are affected equally by climate (i.e., solar radiation, CDD18C, and HDD18C) and building properties (i.e. envelope thermal resistance) (see Section 3.3.3.1). Fractional savings are also affected by building geometry (e.g., net wall area and roof area).

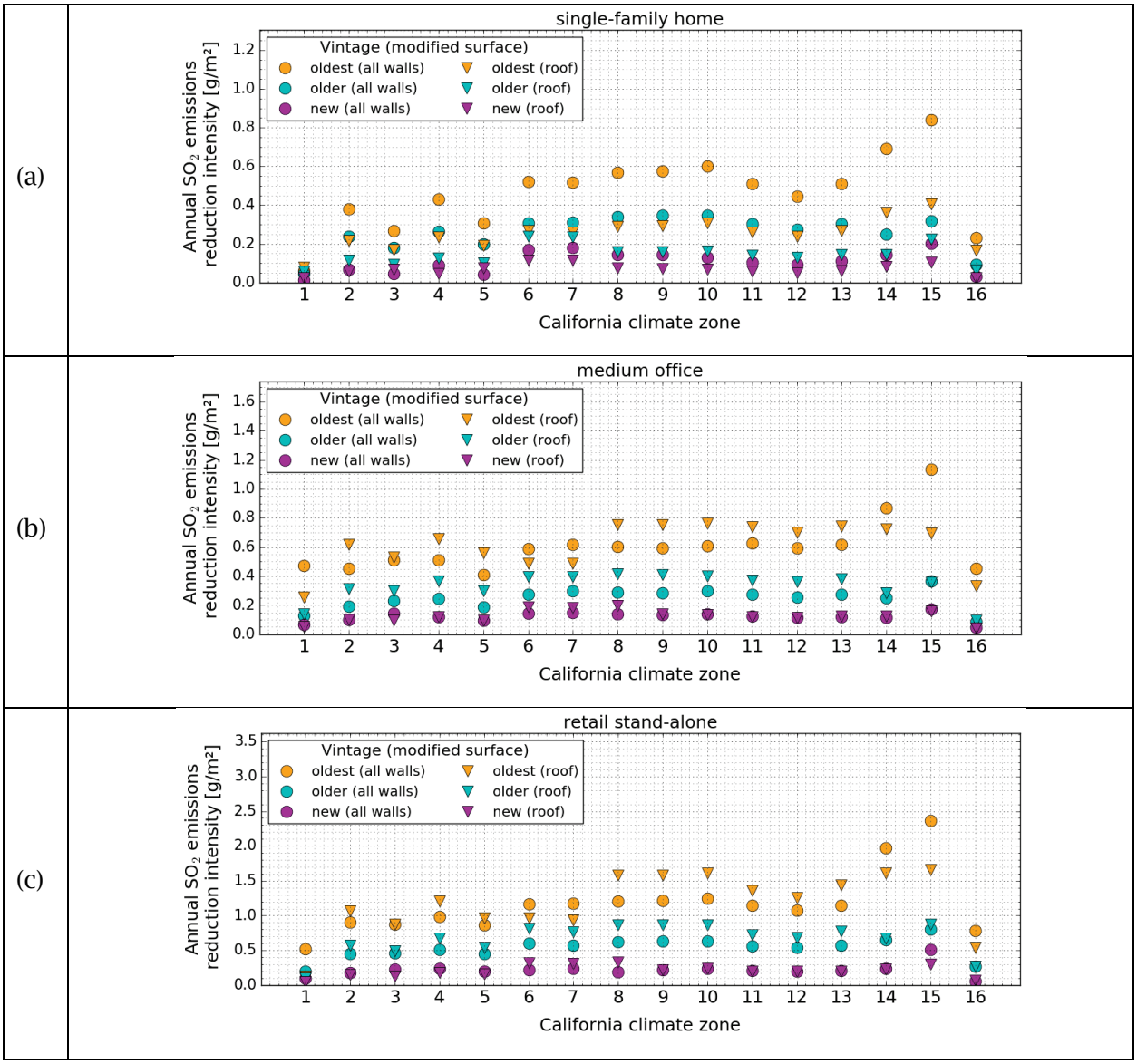

Figure 19. Annual SO_2 emissions reduction intensity by vintage and by California climate zone for the (a) single-family home, (b) medium office, and (c) retail stand-alone. The plots compare the reduction intensity from increasing the albedo of all walls by 0.35 to that from increasing the roof albedo by 0.30 (residential) or 0.40 (commercial).

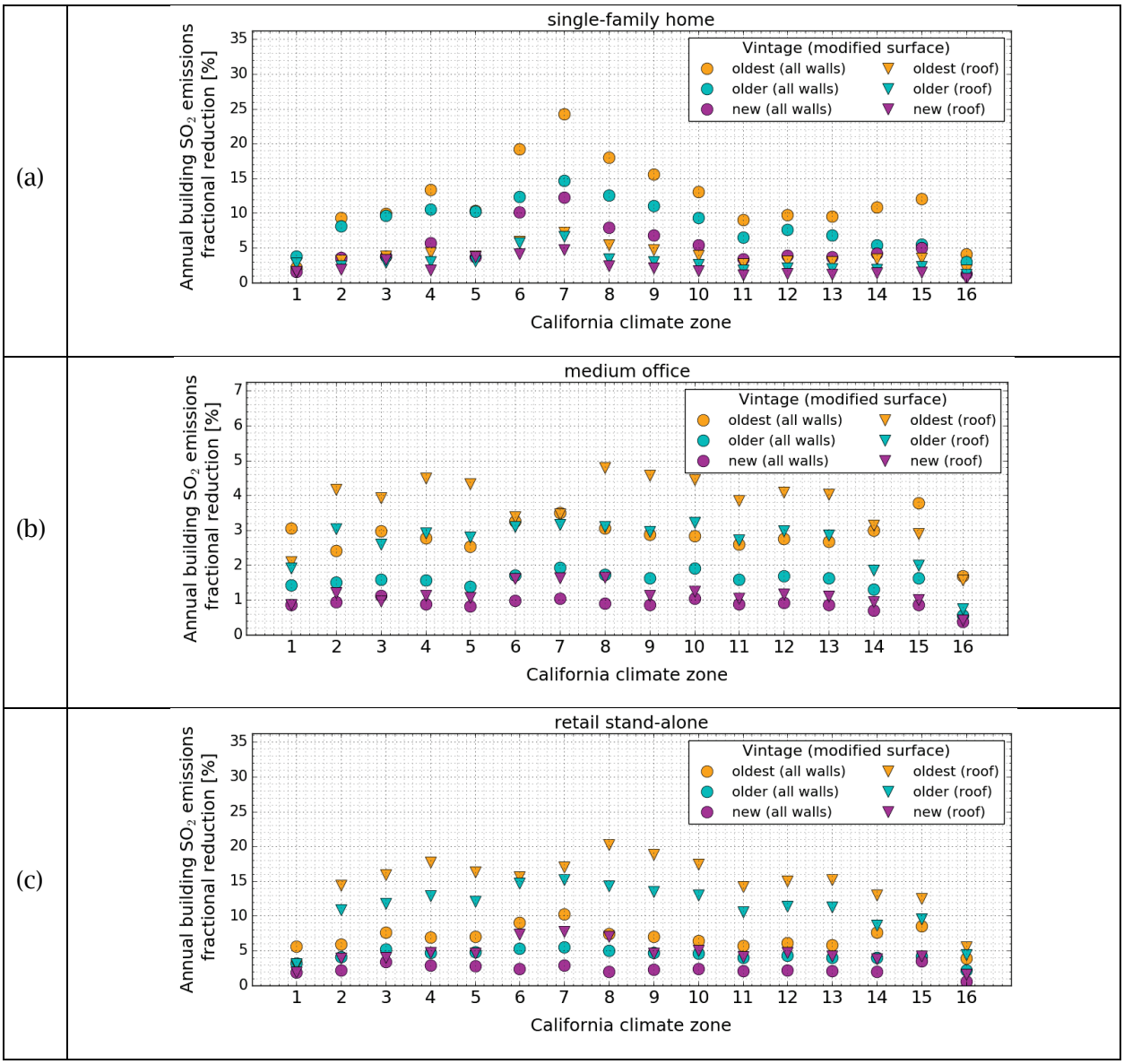

Figure 20. Annual SO_2 emissions fractional reduction by vintage and by California climate zone for the (a) single-family home, (b) medium office, and (c) retail stand-alone. The plots compare the fractional reduction from increasing the albedo of all walls by 0.35 to that from increasing the roof albedo by 0.30 (residential) or 0.40 (commercial).

3.3.3.6 HVAC peak power demand reduction

Figure 21 and Figure 22 show annual-average HVAC peak power demand reduction intensity and fractional reduction, respectively, by vintage and by California climate zone for the single-family home (Figure 21a and Figure 22a), medium office (Figure 21b and Figure 22b), and stand-alone retail (Figure 21c and Figure 22c). The peak power demand reduction intensity were computed using Eqs. (7), (10), and (12).

The annual-average HVAC peak power demand reduction intensity and fractional reduction show a similar trend between vintages that those observed for HVAC source energy, energy cost, and emissions. When comparing between California climate zones, the trends observed for peak power demand reduction intensity and fractional reduction are somewhat different than those of HVAC source energy, energy cost, and emissions. These differences in trends happen because HVAC peak power demand is affected only by the summer climate (i.e. peak hours solar radiation and CDD18C), while HVAC source energy, energy cost, and emissions are affected by the annual climate (i.e. solar radiation, CDD18C, and HDD18C).

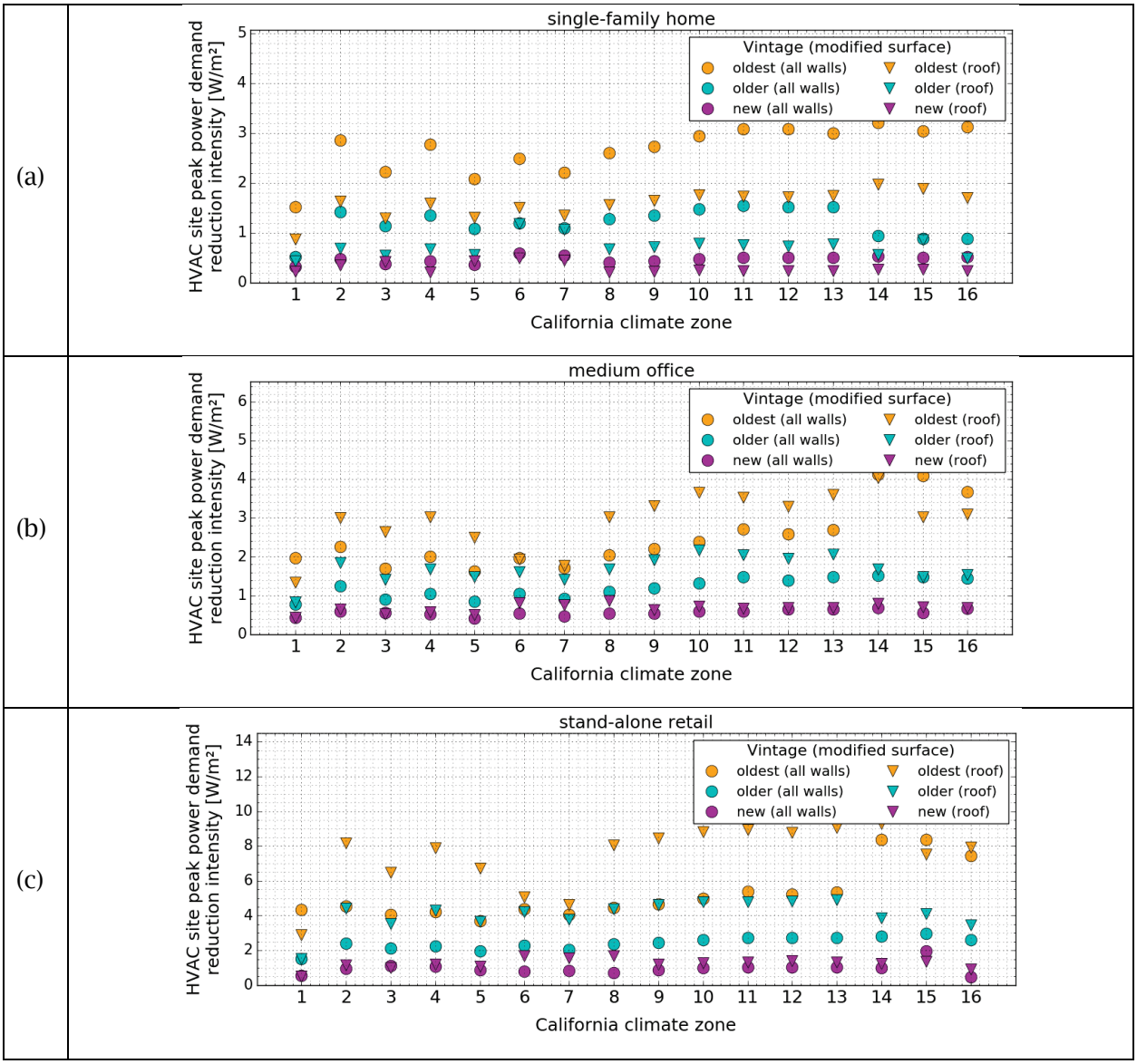

Figure 21. Annual-average HVAC peak power demand reduction intensity by vintage and by California climate zone for the (a) single-family home, (b) medium office, and (c) retail stand-alone. The plots compare the reduction intensity from increasing the albedo of all walls by 0.35 to that from increasing the roof albedo by 0.30 (residential) or 0.40 (commercial).

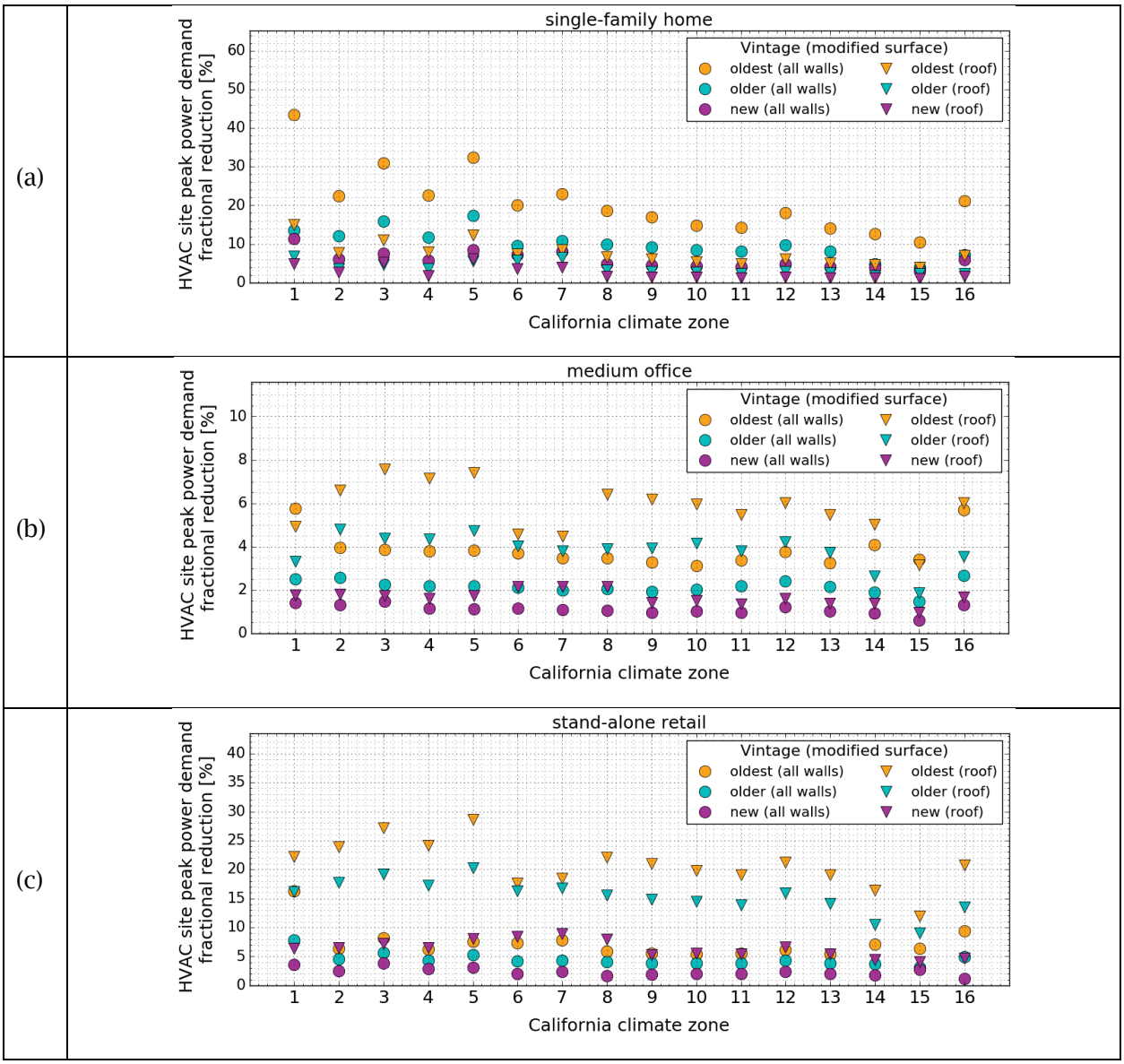

Figure 22. Annual-average HVAC peak power demand fractional reduction by vintage and by California climate zone for the (a) single-family home, (b) medium office, and (c) retail stand-alone. The plots compare the fractional reduction from increasing the albedo of all walls by 0.35 to that from increasing the roof albedo by 0.30 (residential) or 0.40 (commercial).

3.3.3.7 Comparing savings between vintages

Table 25 and Table 26 report oldest-to-new vintage and older-to-new vintage ratios respectively, of annual HVAC source energy savings, emissions reductions, and HVAC energy cost savings. The savings were from increasing the albedo of all walls by 0.35 (to 0.60 from 0.25). The ratios are given by building type and are the mean of both building orientations. The calculations omit ratios that were negative to exclude the few instances where the new vintage generated small annual penalties, while the older and oldest vintages generated annual savings.

In the case of oldest-to-new vintage (Table 25), savings from the oldest vintage were usually between 3.0 to 6.0 times that of the new vintage. In the case of older-to-new vintage (Table 26), savings from the older vintage were typically between 2.0 to 3.0 times that of the new vintage.

Table 25. California average ratios of oldest vintage to new vintage savings by building type and metric. Values are the mean from the two building orientations (east-west and north-south).

	CA average annual savings ratios (oldest-to-new)				
Prototype building	**HVAC source energy [MJ/MJ]**	**CO_2e [kg/kg]**	**NOx [g/g]**	**SO_2 [g/g]**	**HVAC energy cost [$/$]**
Single-family home	4.6	5.4	5.5	5.3	4.5
Apartment building	3.3	3.1	3.1	3.1	3.4
Large hotel	1.7	1.9	1.5	1.7	1.8
Large office	5.2	5.3	5.4	5.3	5.1
Medium office	5.2	5.3	5.3	5.2	5.1
Small office	5.0	4.9	4.9	5.0	5.0
Fast-food restaurant	7.0	5.8	5.8	6.3	7.9
Retail stand-alone	5.8	6.0	5.3	5.9	5.8
Strip mall retail	5.0	5.3	5.2	5.1	5.0
Sit-down restaurant	5.3	6.1	7.6	5.4	5.6

Table 26. California average ratios of older vintage to new vintage savings by building type and metric. Values are the mean from the two building orientations (east-west and north-south).

Prototype building	CA average annual saving ratios (older-to-new)				
	HVAC source energy [MJ/MJ]	CO_2e [kg/kg]	NOx [g/g]	SO_2 [g/g]	HVAC energy cost [$/$]
Single-family home	2.5	3.1	3.5	2.9	2.4
Apartment building	2.0	2.1	2.2	2.1	2.0
Large hotel	1.2	1.2	1.3	1.1	1.2
Large office	2.4	2.4	2.5	2.4	2.4
Medium office	2.0	2.0	2.0	2.0	2.0
Small office	2.2	2.2	2.2	2.2	2.2
Fast-food restaurant	3.0	2.4	2.5	2.6	2.9
Retail stand-alone	2.6	2.7	3.0	2.7	3.6
Strip mall retail	2.5	2.6	2.5	2.5	2.5
Sit-down restaurant	2.4	2.8	4.1	2.5	2.3

3.3.4 Savings from modifying multiple walls simultaneously to sum of savings from modifying same set of walls one at a time (California)

This section compares the savings obtained from modifying a group of walls simultaneously (e.g., east and west) to the sum of the savings from modifying the walls one at a time. These comparisons are presented for whole-building annual values of (a) source cooling savings, (b) heating penalties, (c) fan savings, and (d) HVAC savings. Energy savings and penalties are shown for the new single-family home (Figure 23), new medium office (Figure 24), and new stand-alone retail (Figure 25). The plots include all the 15 wall combinations simulated in each California climate zone; the values are the average of the two building orientations (east-west and north-south).

If the energy savings from simultaneously modifying a group of walls equals the sum of the individual contributions from each wall, we refer to this behavior as the savings being linearly *additive* (hereafter, simply "additive"). These plots help visualize for each prototype and energy metric whether the additive behavior holds for all wall combinations and climate zones. In the plots, the savings of a prototype are additive in all locations if the slope of the linear regression and the coefficient of determination, or R^2, equal unity and the intercept of the regression is zero. (Visually, this means all savings fall along the $y=x$ line.)

In the single-family home, the annual cooling source energy savings were nearly perfectly additive (Figure 23a). In some cases, savings from adding individual walls were slightly smaller than those from a group of walls. In the case of annual heating source energy, the penalties from adding individual walls were typically smaller than those from a modifying a group of

walls (Figure 23b). As the number of combined walls increases (e.g., modifying all four walls), the heating savings get less additive. In the case of annual fan source energy, the savings were not additive for just some wall combinations in some of the California climate zones (Figure 23c). The annual HVAC source energy savings were nearly perfectly additive (Figure 23d).

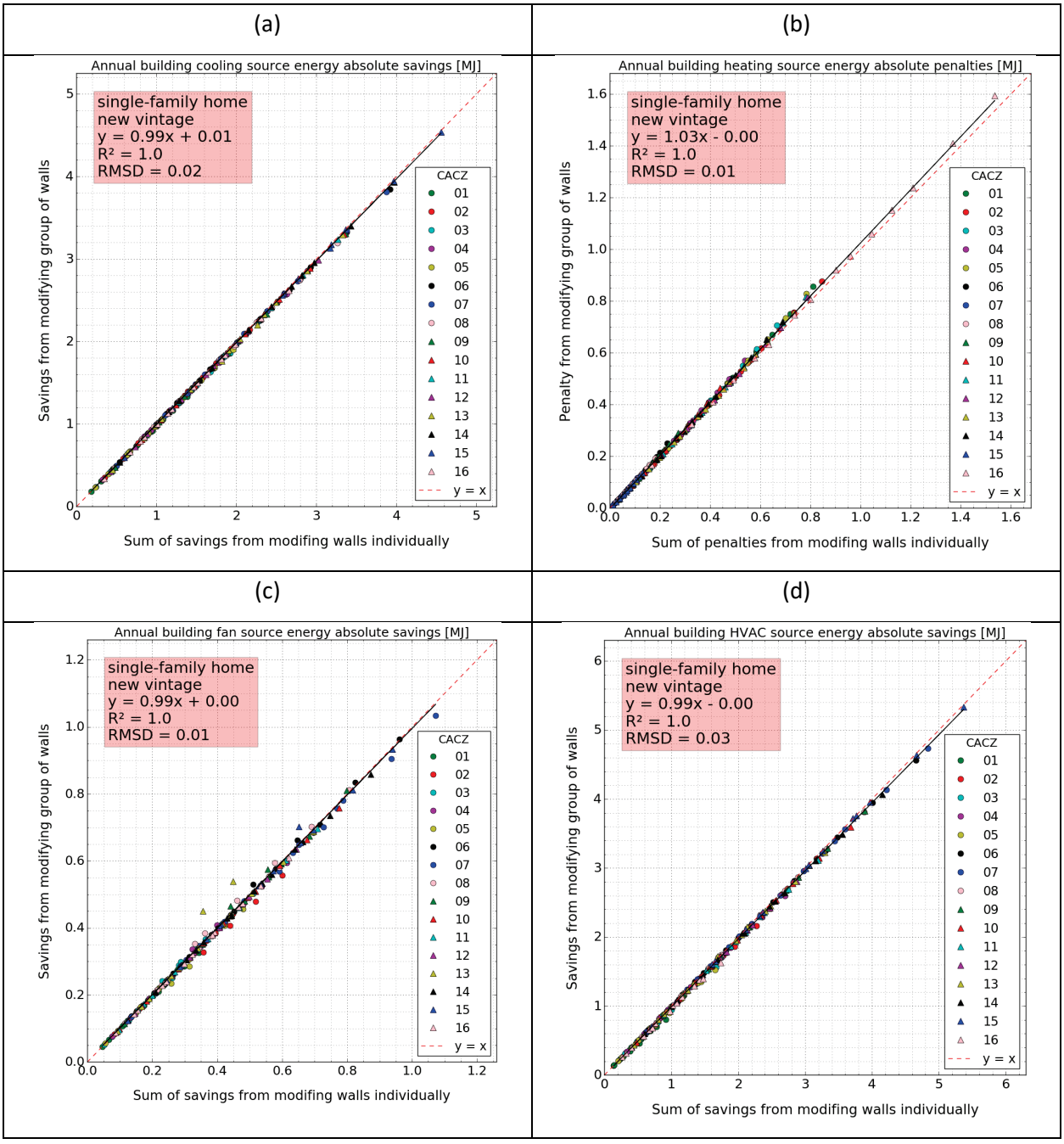

Figure 23. Comparing changes in annual whole-building source energies for the new vintage of single-family home in California climate zones from walls modified one at a time to savings from modifying multiple walls simultaneously. The plots show (a) cooling savings, (b) heating penalties, (c) fan savings, and (d) HVAC savings.

The regressions in the additive test of the medium office were very similar to those of the single-family home. In all California climate zones, the annual cooling source energy savings of the medium office were almost perfectly additive (Figure 24a). In the case of annual heating

source energy, the savings and penalties from adding individual walls were close to additive in most California climate zones, except in some wall combinations in CACZ 16 (Mount Shasta) (Figure 24b). Annual fan source energy savings were mostly additive except for a few wall combinations in a few climate zones, most noticeably in CACZ 1 (Figure 24c). The annual HVAC source energy savings were nearly perfectly additive (Figure 24d).

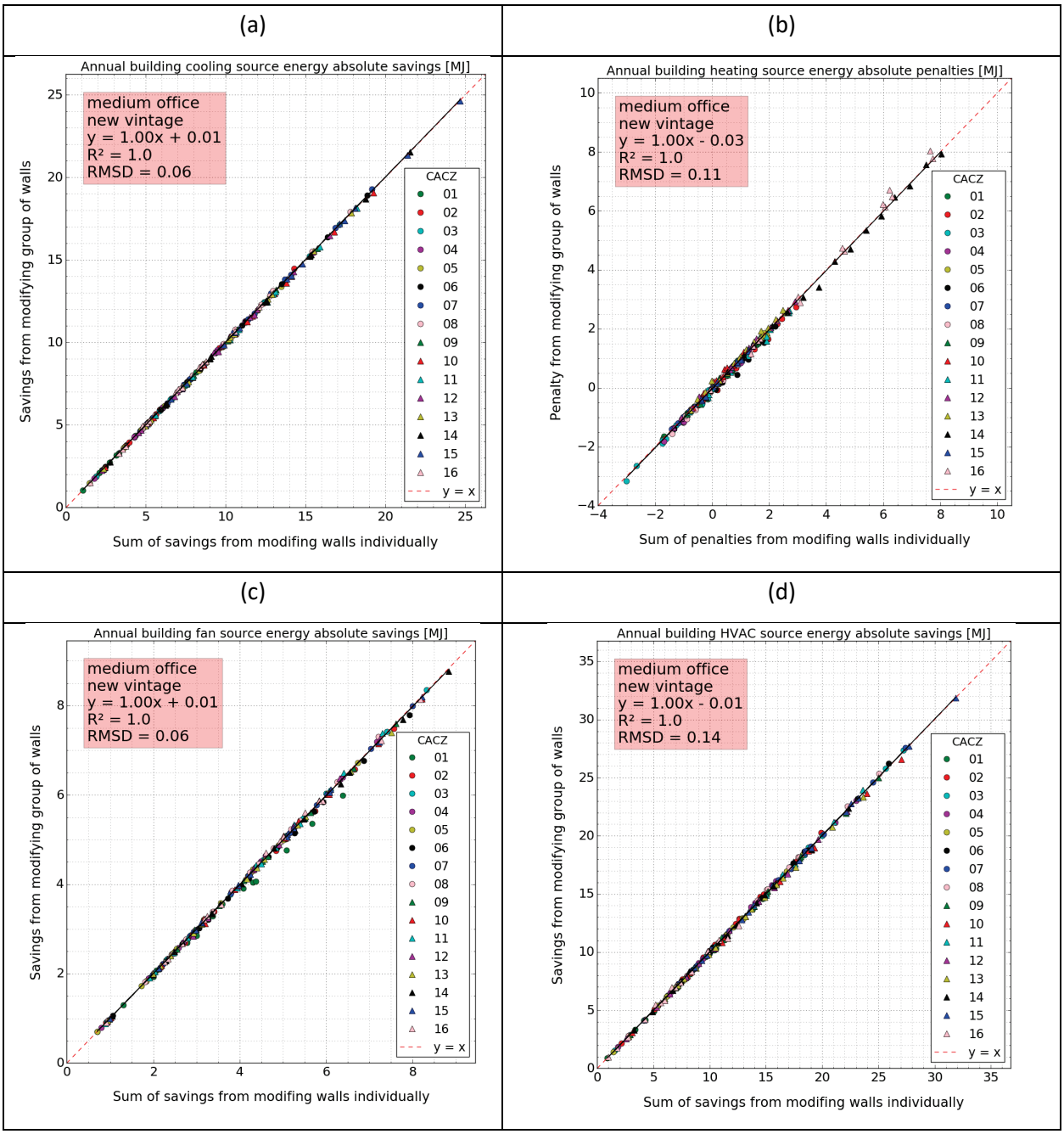

Figure 24. Comparing changes in annual whole-building source energies for the new vintage of medium office in California climate zones from walls modified one at a time to savings from modifying multiple walls simultaneously. The plots show (a) cooling savings, (b) heating penalties, (c) fan savings, and (d) HVAC savings.

Like the medium office, the annual cooling source energy savings of the stand-alone retail were additive, except for two instances of wall combinations in CACZ 8 (Figure 25a). In the case of annual heating source energy, the penalties from adding individual walls were often slightly less than those from modifying a group of walls (Figure 25b). For the case of annual fan source

energy savings, some California climate zones were more additive than others; CACZs 4, 5, 6, and 15 had wall combinations that were less additive than in the other California climate zones (Figure 25c).

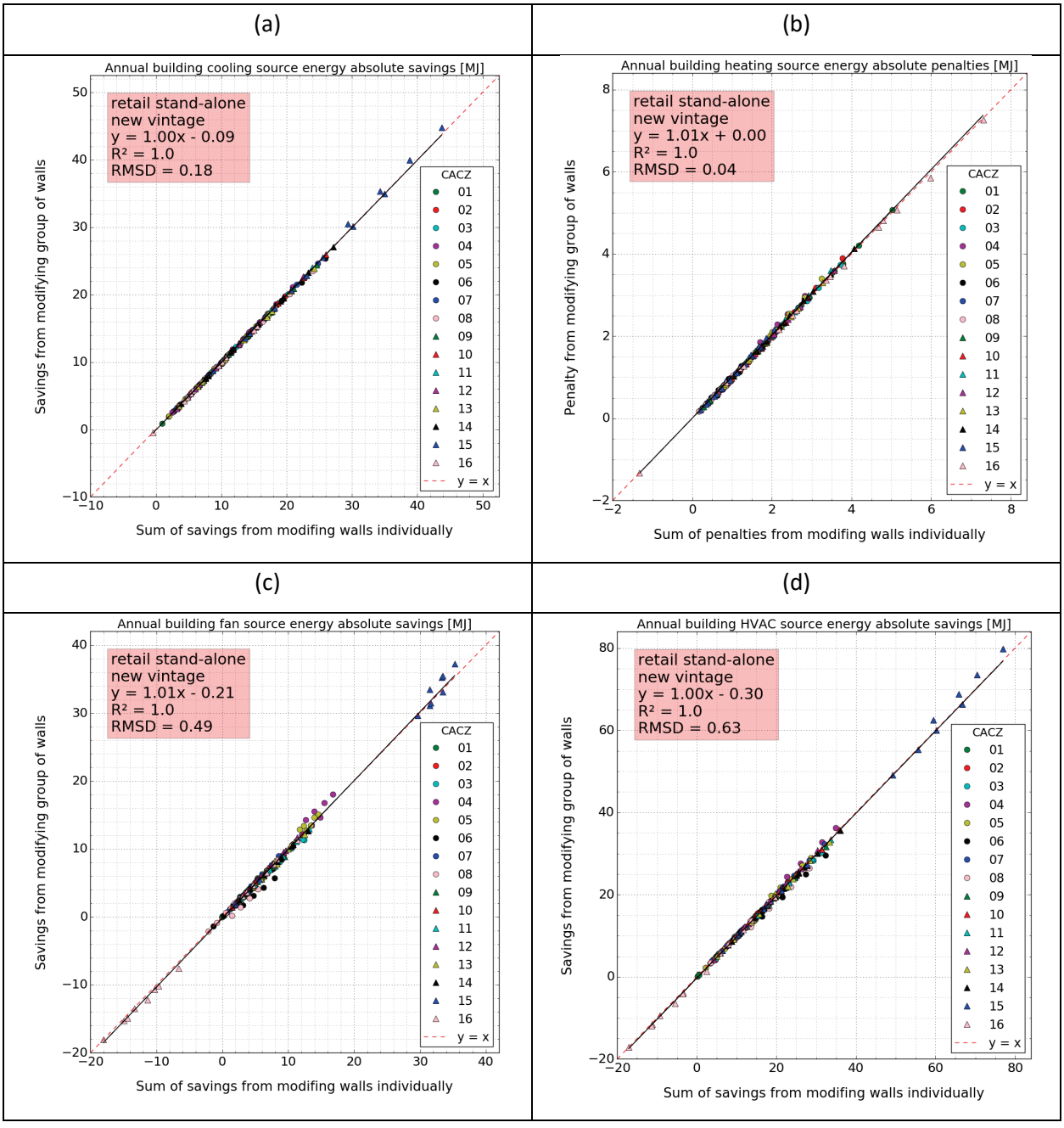

Figure 25. Comparing changes in annual whole-building source energies for the new vintage of stand-alone retail in California climate zones from walls modified one at a time to savings from modifying multiple walls simultaneously. The plots show (a) cooling savings, (b) heating penalties, (c) fan savings, and (d) HVAC savings.

Table 27 summarizes for the California prototypes, the slope, intercept, coefficient of determination (R^2), and root mean square difference (RMSD) of linear regression comparing HVAC source energy savings from modifying multiple walls simultaneously (dependent variable) to the sum of savings from walls modified one at a time (independent variable). The HVAC source energy savings from a given building category are perfectly additive in all locations when the slope = 1, R^2 = 1, and intercept = 0. There was no building category in any vintage in which the HVAC savings were perfectly additive for every wall combination and climate zone.

For almost all prototypes and climate zones in California, annual cooling energy savings were additive. However, for most prototypes, annual heating (electric or gas) energy savings and fan energy savings were additive only in some climate zones and for some wall orientations. Thus, when combining the savings from the different HVAC components (cooling, heating, and fan), there is no prototype in any vintage in which the HVAC system is perfectly additive in all locations and for all wall combinations.

In many prototypes, the fan drew constant load irrespective of changes to cooling or heating load. Therefore, fan energy use lacked any sensitivity to changes in cooling and heating energy changes, which resulted in the fan being non-additive. In these cases, annual HVAC energy changes were close to additive when fan energy was not included.

Table 27. Slope, intercept, coefficient of determination (R^2), and root mean square difference (RMSD) of linear regression comparing HVAC source energy savings from modifying multiple walls simultaneously (dependent variable) to the sum of savings from walls modified one at a time (independent variable). These results include all California climate zones and wall combinations of each prototype, and are the average values from both building orientations (E-W and N-S).

	Regression slope [MJ/MJ]			Regression intercept [MJ]			Coefficient of determination (R^2)			RMSD [MJ]		
Prototype building	**oldest**	**older**	**new**	**oldest**	**older**	**new**	**oldest**	**older**	**new**	**oldest**	**older**	**new**
Single-family home	0.96	0.99	0.99	0.12	0.01	0.00	0.97	1.00	1.00	0.80	0.07	0.03
Apartment building	1.00	1.00	1.00	-0.11	-0.06	-0.02	1.00	1.00	1.00	0.25	0.12	0.05
Large hotel	1.06	1.00	1.00	-3.65	-2.63	-2.88	1.00	1.00	0.99	14.5	7.33	11.4
Large office	1.01	0.99	0.97	1.78	1.60	2.95	1.00	0.99	0.98	12.5	6.60	5.16
Medium office	1.00	0.99	1.00	-0.05	0.11	-0.01	1.00	1.00	1.00	0.65	0.45	0.14
Small office	1.00	0.99	0.99	0.09	0.04	0.02	1.00	1.00	1.00	0.20	0.10	0.06
Fast-food restaurant	0.98	1.00	1.00	0.10	0.03	0.00	0.99	0.99	0.99	0.66	0.18	0.11
Retail stand-alone	1.00	1.00	1.00	-0.12	-0.07	-0.30	1.00	1.00	1.00	1.10	0.39	0.63
Strip mall retail	1.00	1.00	1.01	-0.46	0.05	0.35	1.00	1.00	0.99	1.62	1.41	1.09
Sit-down restaurant	0.98	0.98	1.00	0.15	0.06	0.04	1.00	1.00	0.99	0.54	0.21	0.14

3.4 United States case studies

This section uses some of the U.S. simulations to evaluate the effects of cool walls. As in the California case studies, we discuss outcomes for a single-family home, a medium office building, and a stand-alone retail building, each with a gas furnace. We present cool wall savings from increasing wall albedo by 0.35 (to 0.60 from 0.25) in both residential and commercial buildings, and from increasing roof albedo by 0.30 (to 0.40 from 0.10) in residential buildings and by 0.40 (to 0.60 from 0.20) in commercial buildings.

We compare savings between cool walls and cool roofs, and show how the cool wall savings vary by location, vintage, and combination of modified walls. Finally, we investigate where the sum of savings from walls modified one at a time equals the savings from modifying the same set of walls simultaneously. All savings and penalties shown here are the average values from the two building orientations (east-west and north-south).

3.4.1 United States source energy savings intensity (per unit surface area modified) of the new single-family home by climate zone and modified surface

This section shows the annual source cooling, fan, and HVAC savings intensity and heating penalty intensity of the new single-family home by U.S. climate zone from individually increasing the albedo by 0.35 (to 0.60 from 0.25) of the north wall, east wall, south wall, west wall, and roof, and of the roof by 0.30 (to 0.40 from 0.10). We chose to present the savings of the new single-family home because it is the most common building type in the U.S. and with the most floor area in the country (EIA 2009, EIA 2012). Savings from the older and oldest single-family home show similar behavior to those from the new vintage but of different magnitudes.

3.4.1.1 Source energy changes by United States climate zone

First, note that in the new single-family home, the wall assembly thermal resistance in USCZs 1A, 2A, 2B, 3A, and 4B was R-11.5 (Table 11), which is 71 percent of the R-16.3 that was used in all other U.S. climate zones (R-11.5 / R-16.3 = 71 percent). The roof assembly thermal resistance in USCZs 1A, 2B, and 3A was R-27.6 (Table 13), which is 85 percent of the R-32.4 that was used in USCZs 2A, 3B, 3C, 4B, and 5B (R-27.6 / R-32.4 = 85 percent), and which is 73 percent of the R-37.6 that was used in USCZs 4A, 4C, 5A, 6A, 6B, 7, and 8 (R-27.6 / R-37.6 = 73 percent).

Figure 26 shows annual source values of cooling savings intensity, heating penalty intensity, fan savings intensity, and HVAC savings intensity for the new single-family home in U.S. In every U.S. climate zone, raising wall or roof albedo reduced cooling and fan energy uses (Figure 26a,b) and increased heating energy use (Figure 26b). However, 9 out of 15 U.S. climate zones (USCZs 1A, 2A, 2B, 3A, 3B, 3C, 4A, 4B and 5A) yielded annual HVAC source energy savings intensities from each of the five surfaces (Figure 26d). From these 9 U.S. climate zones, USCZ 2B (Phoenix) benefited the most from cool walls and cool roofs, yielding significantly greater HVAC savings intensities than all other climate zones. USCZ 2B was the climate zone with the most CDD18C (2,800), received the most sunlight, and had few HDD18C (700). Additionally, Phoenix was one of the locations with the lowest wall and roof thermal resistances. USCZ 1A (Miami) had the second largest HVAC savings intensities; it had large CDD18C (2,500) and the fewest HDD18C (100) (Figure 7). In Miami, wall and roof thermal resistances were as low as those from Phoenix. From these 9 U.S. climate zones, USCZ 5A (Peoria) had the smallest HVAC source energy savings intensities; in this location, CDD18C were 5 times that of HDD18C, and had more wall and roof thermal resistances than the other 8 USCZs yielding HVAC savings intensities. USCZs 4C (Seattle), 5B (Boise), and 6A (Burlington) yielded small annual HVAC source energy savings intensities from some surfaces and HVAC source energy penalty intensities from the other surfaces. USCZs 6B (Helena), 7 (Duluth), and 8 (Fairbanks) yielded HVAC source energy penalty intensities from all five surfaces (Figure 26d). All these USCZs that yield HVAC energy penalty intensities experienced significantly more HDD18C than CDD18C. Fairbanks, AK (USCZ 8) had the lowest CDD18C (50) and the highest HDD18C (7,100). Still, USCZ 8 yielded very similar

HVAC source energy penalty intensities than USCZ 6B (Helena), which had 4,150 HDD18C (42 percent less HDD18C than those in USCZ 8). However, the magnitudes of all HVAC source energy savings and penalty intensities from USCZs 4C, 5B, 6A, 6B, 7, and 8 were half or less than the magnitude of those from USCZs 1A (Miami), 2B (Phoenix), 3A (Memphis), and 3B (El Paso) (Figure 26d).

3.4.1.2 Source energy changes by face

As described in Section 3.3.1.2, changes in HVAC energy use are proportional to changes in heat conducted through the building envelope, which in turn scale with changes in wall solar heat gain. Wall solar heat gain depends on orientation. Thus, all else being equal, we expect changes in HVAC energy use to be greater from modified external surfaces that receive more sunlight (solar energy per unit area).

Of all four walls, the north wall was the one that yielded in all U.S. climate zones the lowest annual cooling and fan source energy savings intensities (Figure 26a,c) due to being the face that received the least sunlight. As an example, let us consider USCZ 2B (Phoenix), in which the north wall yields annual cooling source energy savings intensity 30 MJ/m², or 41 percent of that from the east wall (68 MJ/m²). From Table D-19 in Task Report Appendix D, we gather that the summer daily solar irradiation on the north wall was 1.95 kWh/m², which is 47 percent of that from the east wall (4.13 kWh/m²). During winter, the north wall again received the least sunlight, yielding the smallest annual heating source energy penalty intensity (Figure 26b).

The annual source cooling energy savings intensities from the roof were never greater than those from any of the four walls, and in most cases, were less than those from the east, south, and west walls. However, in all U.S. climate zones, the roof (if assumed to be horizontal) was the face that received the most summer daily solar irradiation (Table 20). The key is that the thermal resistance of the roof is at least twice that of the wall. For example, in USCZs 1A, 3B, and 3A, the thermal resistance of the wall assembly was R-11.5, which is 42 percent of the roof thermal resistance in the roof of the same U.S. climate zones (Table 11 and Table 13). During winter, the annual heating source energy penalties from the roof were once again smaller than those from the east, south, and west walls, and slightly greater than those from the north wall.

The wall that receives the most summer daily solar radiation varied by U.S. climate zone, but was either the east wall or the west wall (Table 20). However, in some locations, the south wall yielded the greatest annual cooling energy savings intensities. In the rest of the U.S. climate zones, either the east or the west wall yielded the greatest annual cooling energy savings intensities. Still, in all locations, the annual cooling energy savings intensities from the east, south, and west walls were very similar.

In all U.S. climate zones, the south wall received more sunlight during winter than any of the other surfaces (including the roof) (Table 20). Thus, in all locations, the south wall yielded annual heating source energy penalty intensities greater than those from any of the other faces (Figure 26b).

In the majority of U.S. locations, the south wall received at least as much sunlight in winter as in summer (Table 22). Additionally, from USCZ 4C onward, each location experienced significantly more HDD18C than CDD18C. Thus, the magnitude of the annual heating penalties from the south wall were up to twice as much as the magnitude of the annual cooling savings in locations with cold climates (Figure 26a,b).

(a)

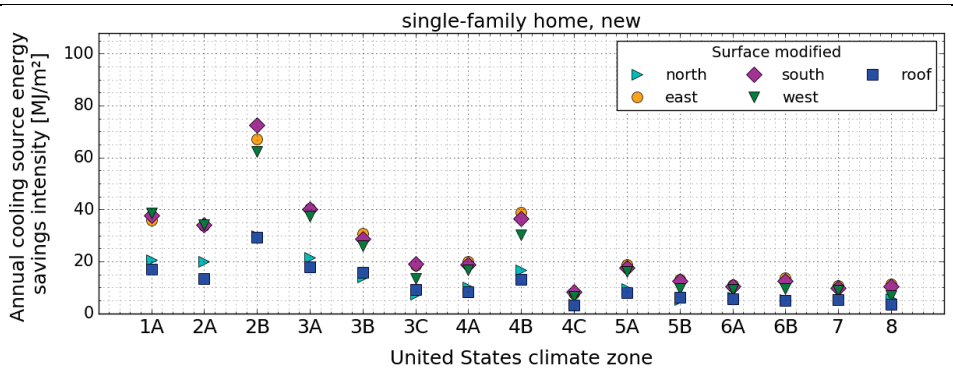
single-family home, new
Annual cooling source energy savings intensity [MJ/m²]
Surface modified
north
south
roof
east
west
0
20
40
60
80
100
1A
2A
2B
3A
3B
3C
4A
4B
4C
5A
5B
6A
6B
7
8
United States climate zone

(b)

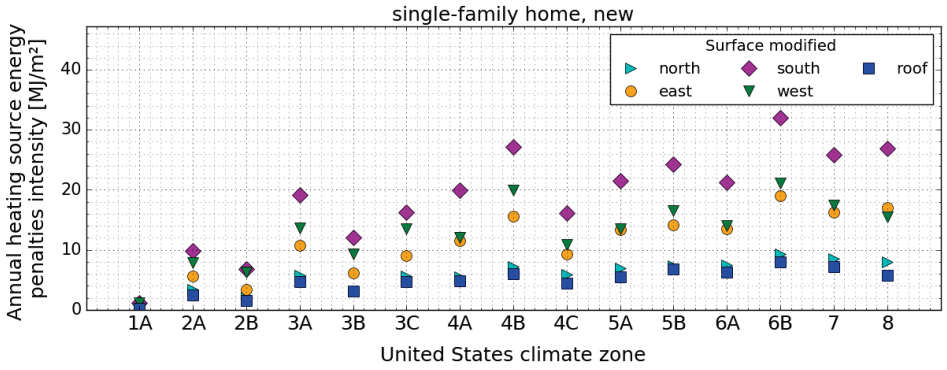
single-family home, new
Annual heating source energy penalties intensity [MJ/m²]
Surface modified
north
south
roof
east
west
0
10
20
30
40
1A
2A
2B
3A
3B
3C
4A
4B
4C
5A
5B
6A
6B
7
8
United States climate zone

(c)

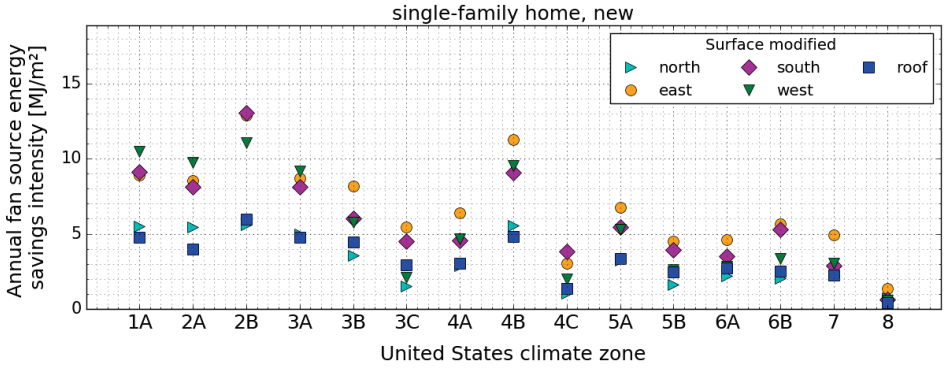
single-family home, new
Annual fan source energy savings intensity [MJ/m²]
Surface modified
north
south
roof
east
west
0
5
10
15
1A
2A
2B
3A
3B
3C
4A
4B
4C
5A
5B
6A
6B
7
8
United States climate zone

(d)

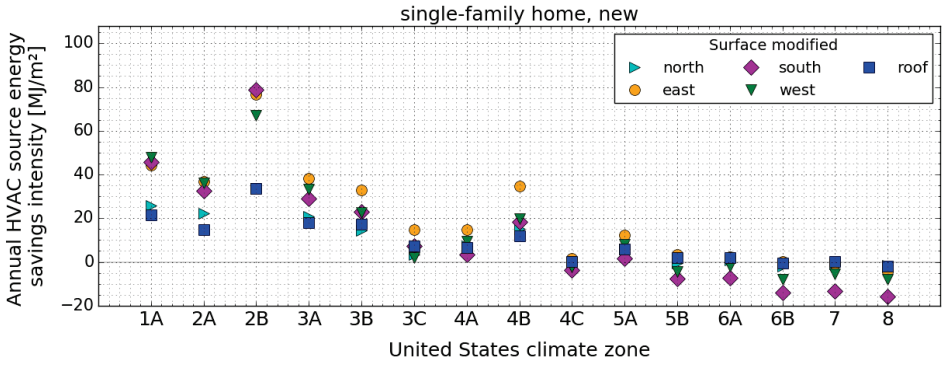
single-family home, new
Annual HVAC source energy savings intensity [MJ/m²]
Surface modified
north
south
roof
east
west
−20
0
20
40
60
80
100
1A
2A
2B
3A
3B
3C
4A
4B
4C
5A
5B
6A
6B
7
8
United States climate zone

Figure 26. Annual source energy savings and penalty intensities of the new single-family home by U.S. climate zone. The plots show (a) cooling savings, (b) heating penalties, (c) fan savings, and (d) HVAC savings.

3.4.2 Correlation of savings in United States to outdoor air temperature and to changes in solar absorptance

Annual cooling savings and heating penalties vary by location, which is in part due to the variation in climate between locations. This section investigates for the oldest single-family home the correlation of the annual cooling savings or heating penalties to two drivers: (a) change in absorbed solar radiation and (b) annual degree days. As done in the California case study, we used the coefficient of determination (R^2) to assess the fractions of variation in savings and penalties that can be explained by either driver.

Figure 27a and Figure 27b show how annual cooling site energy savings intensity from each modified face vary with changes in absorbed summer solar radiation and with annual CDD18C, respectively, in the oldest single-family home. Since the insulation in the building envelope and the efficiency of the air conditioner often vary by location, the changes in absorbed radiation were normalized by the face's thermal resistance and by the cooling efficiency (Figure 27a). Annual CDD18C were normalized in the same manner (Figure 27b).

The annual site cooling savings from the north (R^2=0.05) and west (R^2=0.03) walls were essentially uncorrelated with the change in absorbed irradiation (Figure 27a). Annual cooling savings for the east (R^2=0.17) and south (R^2=0.28) walls correlated poorly with absorbed irradiation. Only the roof (R^2=0.62) had better correlation with change in absorbed irradiation. Figure 27b shows that for every modified surface, the annual cooling savings intensity correlates well with annual CDD18C (from R^2=0.70 for south wall to R^2=0.90 for north and west walls). The graph demonstrates how cooling savings intensity increases with annual CDD18C.

Figure 27c and Figure 27d show the correlation of annual site gas heating energy penalty intensity to changes in absorbed solar radiation to annual HDD18C, respectively, for the oldest single-family home. The changes in winter solar radiation and annual HDD18C were normalized by the envelope's thermal resistance and the heating efficiency.

Annual site gas heating energy penalty intensities were essentially uncorrelated with changes in winter solar radiation for the north wall, east wall, west wall, and roof, ranging from R^2=0.00 (east wall) to R^2=0.06 (north wall). Only the south wall (R^2=0.58) showed considerably better correlation with change in absorbed irradiation. The annual site gas heating energy penalty intensities correlated well with annual HDD18C (from R^2=0.58 for west wall to R^2=0.84 for east wall). Thus, annual heating penalty intensity increased with annual HDD18C.

	Changes in site energy vs changes in absorbed sunlight	Changes in site energy vs degree days
	(a)	(b)
Cooling	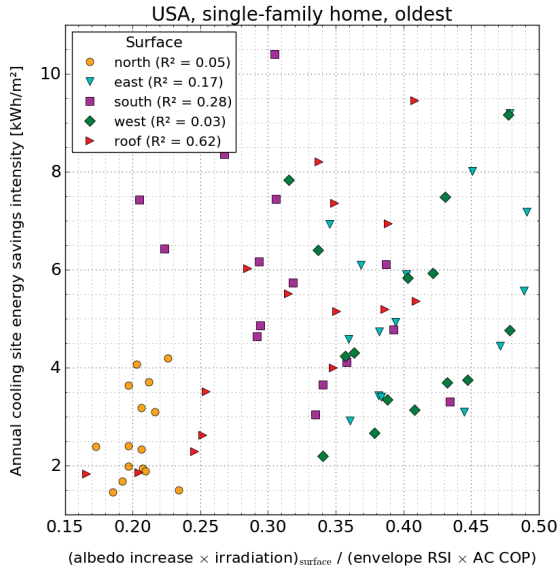	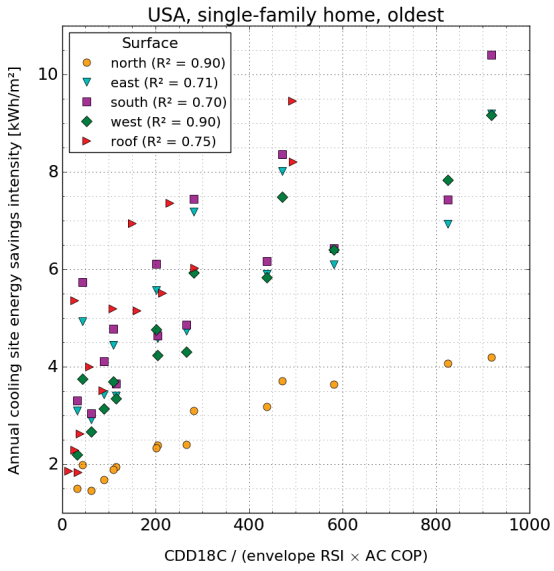
	(c)	(d)
Heating	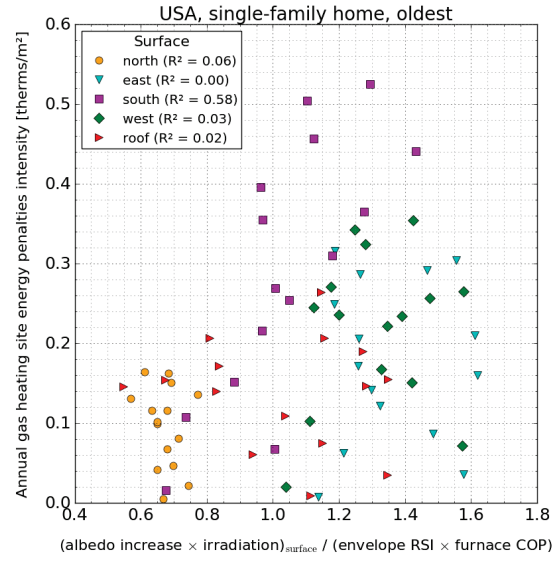	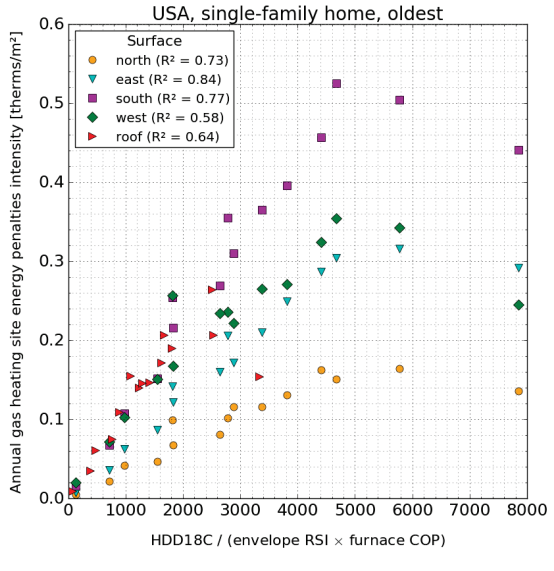

Figure 27. Correlation of changes in site energy use in United States to changes in absorbed sunlight and to degree days, including (a) correlation of annual cooling site energy savings to change in absorbed sunlight during summer; (b) correlation of annual cooling site energy savings to annual CDD18C; (c) correlation of annual heating site energy penalties to change in absorbed sunlight during winter; and (d) correlation of annual heating site energy penalties to annual HDD18C.

We applied a multivariate linear regression analysis to investigate if the correlations of cooling energy savings to either changes in absorbed sunlight or to annual CDD18C improved when both metrics (change in absorbed sunlight and annual CDD18C) were considered simultaneously.

Table 28 shows for all modified surfaces of the single-family home, medium office, and retail stand-alone, the coefficient of determination from the correlation analysis of annual site cooling savings (a) to cooling degree days (CDD18C), (b) to change in absorbed summer sunlight, and (c) simultaneously to annual CDD18C and change in absorbed summer sunlight. For all buildings and surfaces, cooling savings correlated better with cooling degree days than with change in absorbed sunlight. When both metrics were considered simultaneously, the correlation improved the most—compared to the individual correlations to both metrics (change in absorbed sunlight and annual CDD18C)—for the east wall and the roof in the oldest and older vintage of the single-family home. The multivariate linear regression caused little to no improvement—compared to the individual correlations to both metrics—in any of the other cases.

Similarly, we applied a multivariate linear regression analysis to investigate if the correlation of annual site heating energy penalties to changes in absorbed sunlight or to heating degree days heating improved when both metrics were considered simultaneously. Table 29 shows for all modified surfaces of the single-family home, medium office, and retail stand-alone, the coefficient of determination from the correlation analysis of annual site heating penalties (a) to heating degree days, (b) to change in absorbed winter sunlight, and (c) simultaneously to heating degree days and change in absorbed sunlight. Heating penalties always correlated better with heating degree days than with change in absorbed sunlight. When both metrics were considered simultaneously, the correlations improved by more than 0.10 only for the east wall in the new medium office and for the roof of the oldest and older retail stand-alone. This improvement of more than 0.10 was relative to the largest correlation from both individual metrics.

Table 28. Coefficient of determination (R^2) from the correlations of annual cooling savings to annual cooling degree days at 18°C (cdd), annual cooling savings to change in absorbed summer sunlight (sun), and annual cooling savings to cdd and sun. The coefficients of determination are for all vintages in U.S. of the single-family home, medium office, and retail stand-alone.

Building	vintage	Coefficient of determination (R^2)														
		north wall			east wall			south wall			west wall			roof		
		cdd	sun	cdd + sun	cdd	sun	cdd + sun	cdd	sun	cdd + sun	cdd	sun	cdd + sun	cdd	sun	cdd + sun
single-family home	oldest	0.90	0.05	0.89	0.71	0.17	0.84 [a]	0.70	0.28	0.66	0.90	0.03	0.93	0.75	0.62	0.95 [a]
	older	0.91	0.18	0.92	0.79	0.22	0.90 [a]	0.83	0.16	0.83	0.93	0.06	0.95	0.85	0.44	0.96 [a]
	new	0.94	0.71	0.95	0.89	0.72	0.94	0.92	0.18	0.93	0.96	0.66	0.97	0.93	0.79	0.97
medium office	oldest	0.96	0.71	0.96	0.96	0.53	0.96	0.94	0.06	0.94	0.95	0.46	0.97	0.95	0.52	0.96
	older	0.87	0.74	0.86	0.86	0.67	0.85	0.87	0.66	0.84	0.87	0.63	0.85	0.87	0.25	0.90
	new	0.98	0.68	0.98	0.99	0.53	0.99	0.99	0.29	0.99	0.99	0.51	0.99	0.96	0.57	0.98
retail stand-alone	oldest	0.94	0.65	0.93	0.97	0.50	0.97	0.97	0.05	0.97	0.97	0.34	0.97	0.98	0.50	0.99
	older	0.87	0.70	0.84	0.89	0.68	0.88	0.91	0.61	0.89	0.91	0.59	0.90	0.90	0.22	0.92
	new	0.99	0.97	0.99	1.00	0.97	1.00	0.95	0.97	0.99	0.72	0.86	0.87	0.98	0.52	0.99

[a] Coefficient of determination that improved in the multivariate linear regression by more than 0.10.

Table 29. Coefficient of determination (R^2) from the correlations of annual heating penalty to annual heating degree days at 18°C (hdd), heating penalty to change in absorbed winter sunlight (sun), and heating penalty to hdd and sun. The coefficients of determination are for all vintages in U.S. of the single-family home, medium office, and retail stand-alone.

Build-ing	vintage	Coefficient of determination (R^2)														
		north wall			east wall			south wall			west wall			roof		
		hdd	sun	hdd + sun	hdd	sun	hdd + sun	hdd	sun	hdd + sun	hdd	sun	hdd + sun	hdd	sun	hdd + sun
single-	oldest	0.73	0.06	0.81	0.84	0.00	0.81	0.77	0.58	0.75	0.58	0.03	0.62	0.64	0.02	0.62
family	older	0.63	0.08	0.66	0.74	0.00	0.69	0.66	0.44	0.62	0.44	0.01	0.45	0.56	0.04	0.62
home	new	0.72	0.27	0.73	0.77	0.05	0.74	0.70	0.16	0.66	0.54	0.02	0.53	0.62	0.19	0.57
mediu	oldest	0.75	0.80	0.81	0.76	0.66	0.79	0.85	0.19	0.87	0.68	0.52	0.66	0.52	0.37	0.44
m	older	0.48	0.61	0.55	0.53	0.60	0.60	0.60	0.61	0.68	0.53	0.60	0.61	0.74	0.40	0.78
office	new	0.25	0.61	0.64	0.70	0.29	0.82 [a]	0.58	0.03	0.60	0.71	0.36	0.81	0.55	0.15	0.56
retail	oldest	0.48	0.37	0.39	0.45	0.09	0.45	0.58	0.00	0.54	0.17	0.01	0.36	0.16	0.02	0.49 [a]
stand-	older	0.42	0.00	0.32	0.45	0.00	0.37	0.43	0.00	0.34	0.43	0.03	0.34	0.35	0.11	0.77 [a]
alone	new	0.04	0.03	-0.10	0.09	0.01	-0.01	0.03	0.04	-0.10	0.04	0.15	0.14	0.14	0.12	0.20

[a] Coefficient of determination that improved in the multivariate linear regression by more than 0.10.

3.4.3 Savings in United States by climate zone and vintage

This section reports annual HVAC source energy, energy cost, CO_2e, NO_x, SO_2, and peak power demand savings for the single-family home, the medium office, and the stand-alone retail buildings upon (a) increasing the albedo of all four walls simultaneously by 0.35 (to 0.60 from 0.25) or (b) increasing the albedo of the roof to 0.40 from 0.10 (single-family home) or to 0.60 from 0.20 (medium office and retail stand-alone). Each metric is compared by vintage and by U.S. climate zone.

We have omitted all results for the new stand-alone retail building in USCZ 1A (Miami) because modifying the albedo of its back wall yielded unrealistically large changes in annual fan energy use.

3.4.3.1 Annual HVAC source energy savings

First, note that in all locations except USCZ 8 (Fairbanks), the annual daily solar irradiation received by the roof was 1.7 to 2.0 times the four-wall average received solar irradiation.

Figure 28 shows annual HVAC source energy savings intensity by vintage and by U.S. climate zone for the single-family home (Figure 28a), medium office (Figure 28b), and stand-alone retail (Figure 28c). In the single-family home (Figure 28a) the increase in roof albedo (0.30) was 86 percent of that of walls (0.35). Additionally, in each vintage, the thermal resistance of the roof assembly was much greater than that of the wall assembly; in all vintages, the thermal

resistance of the roof assembly was 1.7 to 3.4 times that of walls (Table 11 and Table 13). Hence, although the roof receives about twice more solar irradiation than the average of all walls, the large thermal resistance in roofs led to annual HVAC source energy savings intensities that were often similar or slightly greater than those from the average of all walls.

In the single-family home (Figure 28a), the differences in cool walls annual HVAC savings intensities between vintages is related to the differences in wall assembly thermal resistance and cooling efficiency between vintages. As an example, in USCZ 1A (Miami), the thermal resistance of the wall assembly in the new vintage was 1.8 times that in the oldest vintage; the ratio of cooling efficiency of new to oldest vintage was 1.3. Thus, we would expect the HVAC savings intensity from cool walls in the oldest single-family home to be about $1.8 \times 1.3 = 2.3$ times that of the new home. This estimate matches well with what we observe in Figure 28a, where the cool wall savings intensity from the oldest single-family home in USCZ 1A is about 2.1 times that of the new vintage. This ratio varied by U.S. location, but on average, the annual HVAC source energy savings intensities from the oldest home were 3.0 times that of the new home (Table 30). In the case of older single-family home, the annual HVAC savings intensity were on average 1.3 times that of the new home (Table 31).

The savings of the medium office (Figure 28b) were from increasing the wall albedo by 0.35 (to 0.60 from 0.25), and from increasing the roof albedo by 0.40 (to 0.60 from 0.20). Thus, the increase in roof albedo was 1.14 times that of walls. The thermal resistance of the roof assembly in the oldest medium office was about 2.0 to 2.4 times that of the wall assembly (Table 11 and Table 13). Hence, even though the roof receives about twice solar irradiation than the walls, the large thermal resistance in roofs led to annual HVAC source energy savings intensities that were equal or less than those from the average of all walls (Figure 28b).

In the medium office (Figure 28b), the thermal resistance of the wall assembly in the new vintage ranged from 1.5 to 3.0 times that in the oldest vintage, while the cooling efficiency ratio of wall thermal resistances of new to oldest vintage varies by location but ranges from 1.5 to 3.0. Additionally, the cooling efficiency in the new vintage was 1.1 to 1.2 times that in the oldest vintage. As an example, in USCZ 2B (Phoenix), the ratio of wall thermal resistance of new to oldest vintage was 1.9 and the ratio of cooling efficiency of new to oldest vintage was 1.1. Thus, we would expect the annual HVAC savings intensity from cool walls in the oldest medium office to be $1.9 \times 1.1 = 2.1$ times that of the new medium office. This estimate is similar to what we observe in Figure 28b where the cool walls savings intensity from the oldest vintage were 1.8 times that of the new vintage. This ratio varied by U.S. location, but on average, the annual HVAC source energy savings intensities from the oldest home were 1.5 to 8 times that of the new home in USCZs 1A to 4B and 5A, which were the U.S. climate zones that yielded annual HVAC source energy savings in both vintages. In the case of older medium office, the annual HVAC savings intensity were on average 4.1 times that of the new medium office in locations that yielded savings in both vintages (Table 31).

In the stand-alone retail (Figure 28c), the differences in annual HVAC source energy savings intensities from the walls to those of the roof were related to the differences in albedo change, thermal resistance and annual daily solar irradiation between walls and roof. However, in the stand-alone retail, the oldest vintage didn't present the largest annual HVAC source energy savings or penalty intensities. As an example, in USCZ 2B (Phoenix), the annual HVAC source energy savings intensity when all walls were made cool in the new vintage was 410 MJ/m², which is about 2.2 times that of the oldest vintage. The reason the new vintage in USCZ 2B yielded about twice the wall savings than those in the oldest vintage is that the wall thermal resistance in the new vintage was half of that in the oldest vintage. The oldest stand-alone retail was simulated with metal frame walls, while the new stand-alone retail was simulated with heavy mass walls. In warm climates (e.g., USCZ 2B) the walls of the new stand-alone retail were simulated with no additional wall insulation. Thus, in some locations, the resistance of the wall assembly in the new stand-alone retail was less than that of the oldest vintage. Note that the older stand-alone retail was also simulated with heavy mass walls.

(a)

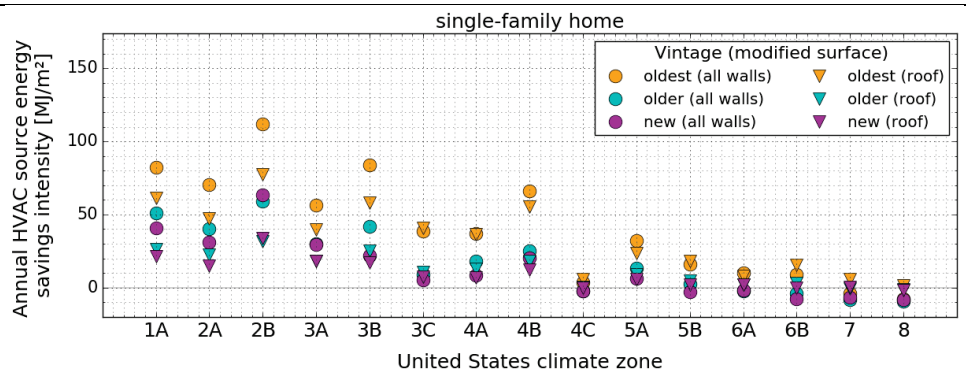

(b)

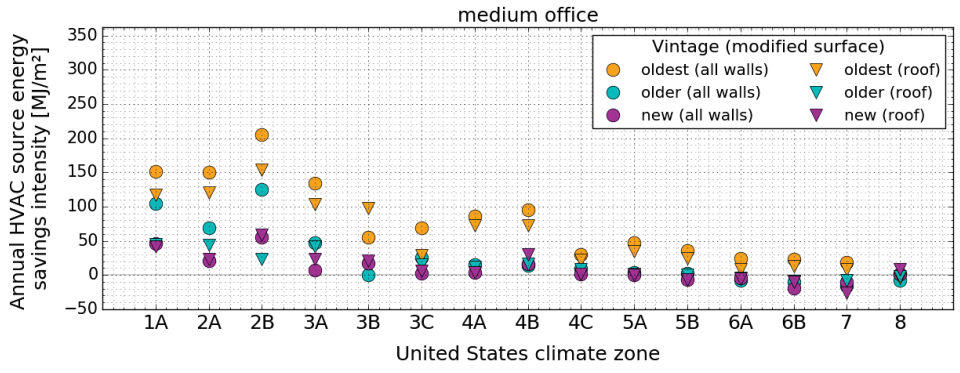

(c)

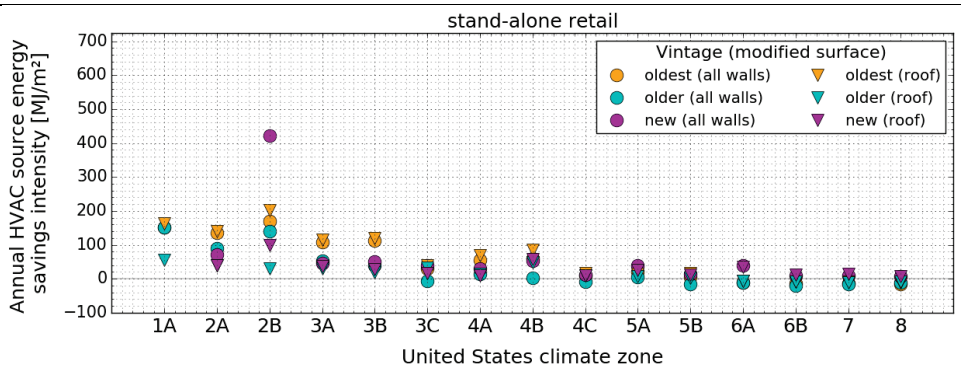

Figure 28. Annual HVAC source energy savings intensity by vintage and by U.S. climate zone for the (a) single-family home, (b) medium office, and (c) retail stand-alone. The plots compare the savings intensity from increasing the albedo of all walls by 0.35 to that from increasing the roof albedo by 0.30 (residential) or 0.40 (commercial).

The fractional savings (absolute savings / base value) of the energy, energy cost, and emission metrics were influenced not only by the absolute savings but also by the energy consumed in the base case. When comparing cool walls to a cool roof, the differences in fractional savings were driven by the envelope characteristics (e.g., differences in surface albedo change and in insulation) as well as by the envelope geometry (e.g., ratio of roof area to net wall area).

Figure 29 shows the annual HVAC source energy fractional savings by vintage and by U.S. climate zone for the single-family home (Figure 29a), medium office (Figure 29b), and stand-alone retail (Figure 29c). For the single-family home (Figure 29a), the greatest HVAC source energy fractional savings when all walls were made cool were 8.3 percent (oldest, USCZ 3B, El Paso), followed in descending order by 7.7 percent (oldest, USCZ 2B, Phoenix), 7.5 percent (oldest and new, USCZ 1A, Miami), and 6.7 percent (oldest, USCZ 2A, Houston). The greatest cool roof fractional savings were from the oldest vintage in USCZ 3C (San Francisco), followed in descending order by the oldest vintages in USCZs 1A (Miami), 3B (El Paso), 2B (Phoenix), and 4B (Albuquerque). In U.S. climate zones 4C (Salem), 5B (Boise), 6A (Burlington), and 6B (Helena), the walls in the oldest home yielded fractional savings of 0.5 percent to 2.0 percent while the walls in the new home led to fractional penalties of 0.2 percent to 1.2 percent.

In the single-family home, the walls-to-roof ratio in fractional savings was always greater than 1.0, and often up to 2.0 (Figure 28a), because the net wall area is greater than the roof area. As an example, consider the oldest home in USCZ 2B (Phoenix). The annual HVAC source energy savings intensity from the walls were about 1.4 times that from the roof. From Table 4, we gather that the net wall area is 1.6 times that of the roof area. Thus, the ratio of wall savings intensity to roof savings intensity adjusted by the wall-to-roof area ratio is $1.4 \times 1.6 = 2.2$. This adjusted wall-to-roof savings ratio is close to the ratio of about 2.3 we observed for HVAC energy fractional savings Figure 29a for the oldest home in USCZ 2B.

For the medium office (Figure 29b), we see that USCZ 2B (Phoenix) was the location with greatest annual HVAC source energy savings intensity for roof and walls, and for all vintages. However, the largest HVAC source energy fractional savings were from the walls of the oldest medium office in USCZ 3C (San Francisco), yielding 4.5 percent savings. Although USCZ 3C had small HVAC source energy savings intensities for all vintages, it yielded large HVAC source energy fractional savings from having small base energy use compared to the other locations.

When analyzing annual HVAC source energy savings intensity of the medium office (Figure 28b), we observed that in most U.S. climate zones and vintages, the savings intensity from the walls were slightly greater than those from the roof. However, the roof area in the medium office is greater than the net wall area (roof area to net wall area ratio 1.3). Since fractional savings relate to the surface area modified, the fractional savings from the roof were often similar or greater than those from the walls (Figure 29b). The walls and roof fractional savings from the oldest vintage were greater than those from the older and new vintages, and yielded about 3.5 percent savings from USCZ 1A (Miami) to 3A (Memphis). The oldest vintage led to HVAC source energy fractional savings from walls and roof in all locations, but the fractional savings decreased as U.S. climate zones increased. The new medium office yielded HVAC source energy fractional savings from walls of up to 2 percent (USCZs 1A and 2B), but led to HVAC fractional penalties of up to 1.6 percent between USCZs 5B (Boise) to 7 (Duluth).

In the case of retail stand-alone (Figure 29c), the roof-to-wall ratios of annual HVAC source energy fractional savings were even greater than those observed in the medium office. That is because the stand-alone retail is a single-story building with a large footprint area (2,290 m²), and has more than twice as much roof area as wall area (roof area to net wall area ratio = 2.1) (Table 4). Hence, the difference in cool roof fractional savings to those from the cool walls was significantly influenced by the large roof area to net wall area ratio. leading to HVAC source energy fractional savings from the roof being in most cases greater than those from the walls.

In the new retail stand-alone, making all walls cool led to HVAC source energy fractional savings in all U.S. climate zones, yielding up to 11 percent in USCZ 2B (Phoenix), and nearly 5.0 percent in USCZ 2A (Houston). The older retail stand-alone in USCZ 5B (Boise) yielded the largest HVAC fractional penalties (1.0 percent). The older retail stand-alone also led to less than 1.0 percent HVAC fractional penalties in USCZs 3C (San Francisco), 4C (Salem), 6A (Burlington), 6B (Helena), 7 (Duluth), and 8 (Fairbanks).

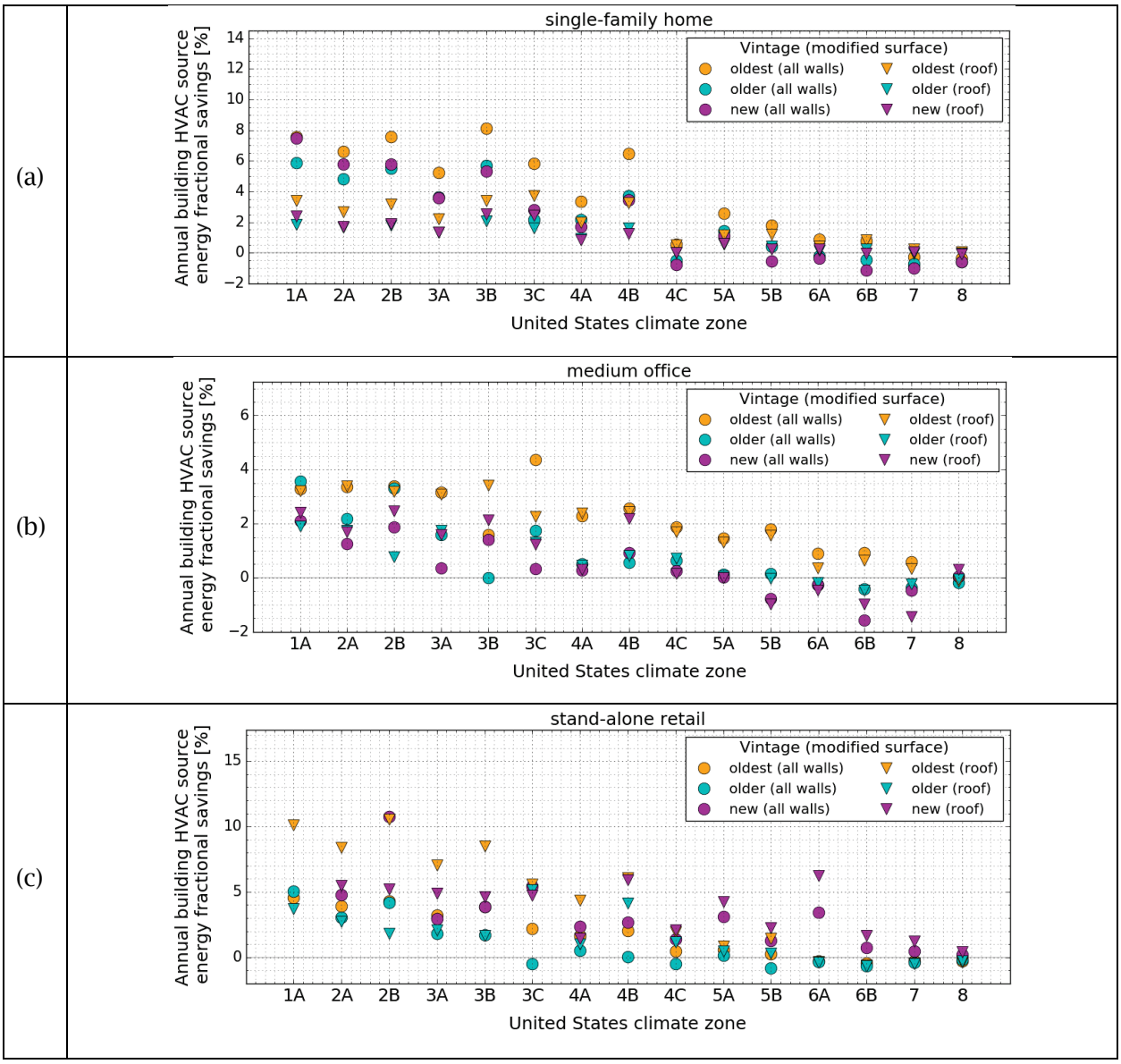

Figure 29. Annual HVAC source energy fractional savings by vintage and by U.S. climate zone for the (a) single-family home, (b) medium office, and (c) retail stand-alone. The plots compare the fractional savings from increasing the albedo of all walls by 0.35 to that from increasing the roof albedo by 0.30 (residential) or 0.40 (commercial).

3.4.3.2 Annual HVAC energy cost savings

Figure 30 shows annual HVAC energy cost savings intensity by vintage and by California climate zone for the single-family home (Figure 30a), medium office (Figure 30b), and stand-alone retail (Figure 30c). These annual HVAC energy cost savings intensities were computed using Eq. (9) and the state-dependent electricity and gas prices from Table 18. For the single-family home, we used the prices for residential buildings; for the medium office and retail stand-alone, we used the prices for commercial buildings.

The annual HVAC energy cost savings intensities show a similar trend between U.S. climate zones and between vintages that those we observed for the annual HVAC source energy savings intensities. Additionally, the proportions of cool walls energy cost savings intensities to those from cool roof were very similar to those we observed for annual HVAC energy savings intensities. These similarities happen because HVAC energy cost savings intensities and HVAC energy savings intensities are affected equally by climate (i.e., solar radiation, CDD18C, and HDD18C) and building properties (i.e., envelope insulation).

The small trend differences in savings and penalty intensities between HVAC source energy and energy cost relate to the variations in electricity and gas prices between states. As an example, making all walls cool in the new single-family home in USCZ 8 (Fairbanks) yielded an annual HVAC source energy *penalty* intensity of 10 MJ/m² (Figure 28a), but an annual HVAC energy cost *savings* intensity of $0.10/m² (Figure 30a). The price of electricity in Fairbanks, AK, is the highest of all represented states (Table 18), which gives larger cooling energy cost savings per unit of saved cooling energy compared to the other locations. Thus, in Fairbanks, AK, while the cool walls led to annual HVAC source energy penalty (heating source energy penalty exceeds cooling source energy savings), cool walls yield annual HVAC energy cost savings (cooling energy cost savings were greater than the heating energy cost penalties).

In the single-family home (Figure 30a), cool roofs generated greater annual HVAC energy cost savings intensities than did cool walls in most locations and vintages. The new home in all vintages led to HVAC cost savings from cool walls. The savings intensity from the oldest vintage were on average, 4.8 times that those of the new vintage (Table 30). The greatest wall annual HVAC energy cost savings intensities were $1.1/m² (oldest, USCZ 2B, Phoenix), $0.88/m² (oldest, USCZ 1A, Miami), and $0.85/m² (oldest, USCZ 3B, El Paso). HVAC energy cost penalties were less than $0.1/m² and happened only in the new home in USCZs 4C (Seattle), 6B (Helena), and 7 (Duluth).

In the oldest medium office (Figure 30b), every location yielded cool walls HVAC energy cost savings intensity, which in turn were greater than those from the cool roof. These cool walls HVAC energy cost savings were greater in warm U.S. climate zones (i.e., USCZs 1A to 4B) and were smallest in the coldest climates (e.g., USCZs 7 and 8). The greatest HVAC energy cost savings when making all walls cool were $1.8/m² (oldest, USCZ 2B, Phoenix), $1.4/m² (oldest, USCZ 1A, Miami), and $1.2/m² (oldest, USCZ 3A, Memphis). In USCZs 5B (Boise), 6A (Burlington), 6B (Helena), 7 (Duluth), and 8 (Fairbanks), the older and new medium offices yielded HVAC energy cost penalties of no more than $0.20/m². The HVAC energy cost savings intensities from the oldest vintage were on average, 7.6 times that those of the new vintage (Table 30).

In the retail stand-alone (Figure 30c), the oldest vintage didn't always yield the largest annual HVAC energy cost savings or penalty intensities. As an example, in the new vintage in USCZ 2B (Phoenix), the annual HVAC energy cost savings intensity when all walls were made cool was $3.7/m², which is about 2.5 times that of the oldest vintage. The new vintage had greater energy cost savings than the oldest vintage because the wall thermal resistance in the new

vintage was half of that in the oldest vintage. The oldest retail stand-alone was simulated with metal frame walls, while the new stand-alone retail was simulated with heavy mass walls. In warm climates (e.g., USCZ 2B) the walls of the new stand-alone retail were simulated with no additional wall insulation. Thus, in some locations, the resistance of the wall assembly in the new stand-alone retail was less than that of the oldest vintage.

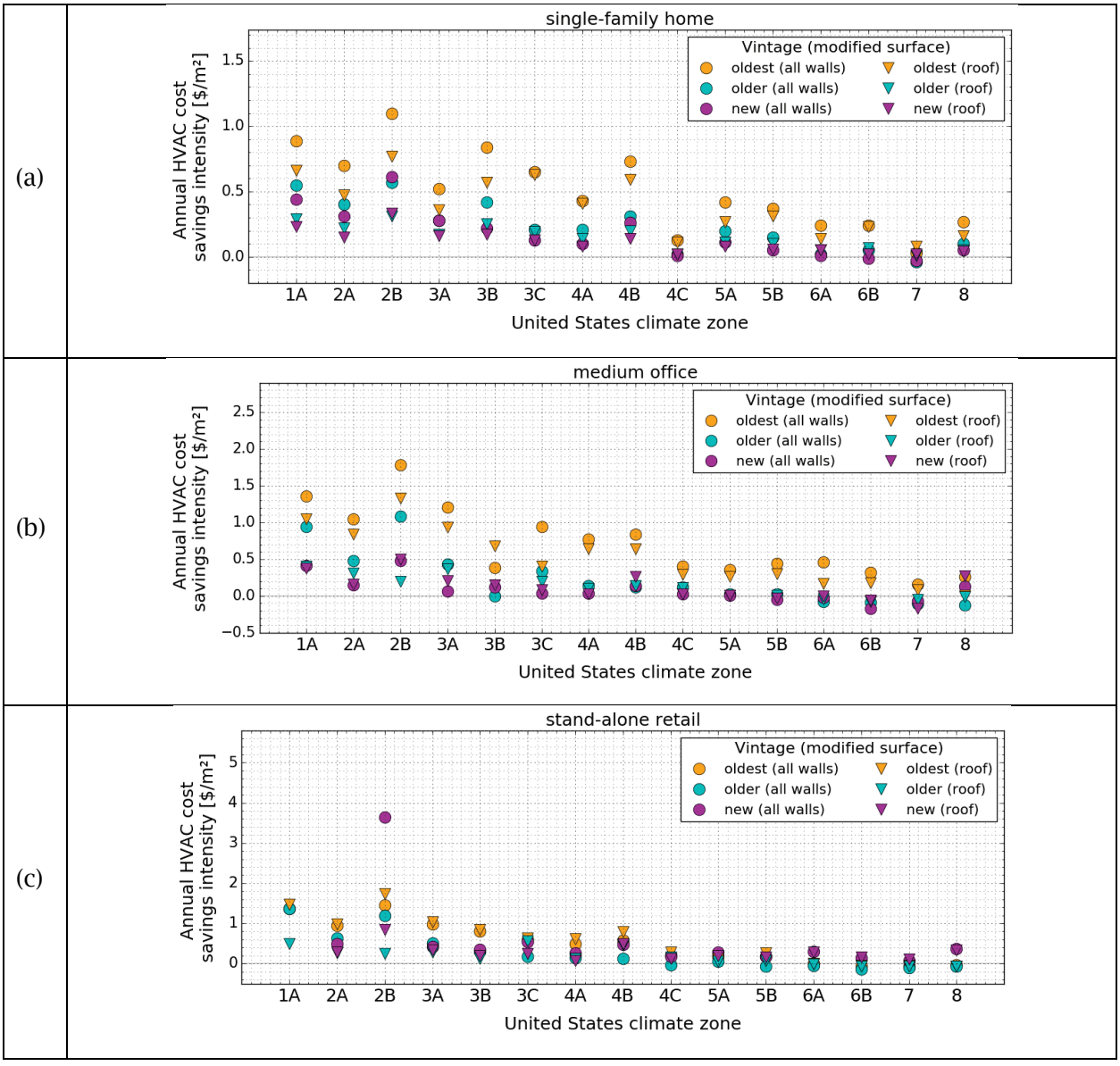

Figure 30. Annual HVAC energy cost savings intensity by vintage and by U.S. climate zone for the (a) single-family home, (b) medium office, and (c) retail stand-alone. The plots compare the savings intensity from increasing the albedo of all walls by 0.35 to that from increasing the roof albedo by 0.30 (residential) or 0.40 (commercial).

Figure 31 shows HVAC energy cost fractional savings by vintage and by U.S. climate zone for the single-family home (Figure 31a), medium office (Figure 31b), and stand-alone retail (Figure 31c). Similar to what we observed between annual HVAC source energy and energy cost savings intensities, the annual HVAC source energy and energy cost fractional savings are affected equally by climate and building properties.

For the single-family home (Figure 31a), the greatest HVAC energy cost fractional savings when all walls were made cool were 8.3 percent (oldest, USCZ 3B, El Paso), followed in descending order by 8.2 percent (oldest, USCZ 3C, San Francisco), 8.0 percent (oldest, USCZ 4B, Albuquerque), and 7.5 percent (oldest and new, USCZ 1A, Miami). In seven U.S. climate zones (1A, 2A, 2B, 3A, 3B, 3C, and 4B) making all walls cool led to HVAC energy cost savings of 4.0 percent or greater from all vintages. HVAC energy cost fractional penalties occurred only in the new vintage in USCZs 6B (Helena) and 7 (Duluth); the HVAC energy cost penalties were 0.2 percent and 0.7 percent, respectively.

In most locations and vintages of the single-family home, the annual HVAC energy cost savings intensity from the walls were equal or greater than those from the roof (Figure 30a). The HVAC energy cost fractional savings from the walls were often up to twice that of roof because the net wall area is greater than the roof area (roof-to-wall ratio 0.61, Table 4).

For the medium office (Figure 31b), USCZ 2B (Phoenix) yielded the greatest annual HVAC energy cost savings intensity for roof and walls, and for all vintages. However, the largest HVAC energy cost fractional savings were from the walls of the oldest medium office in USCZ 3C (San Francisco), yielding 4.5 percent savings. Although USCZ 3C had small HVAC energy cost savings intensities for all vintages, it yielded large HVAC energy cost fractional savings from having small base energy use compared to the other locations.

In most locations and vintages, annual HVAC energy cost savings intensity from the walls of the medium office were slightly greater than those from the roof (Figure 30b). However, the roof area in the medium office is greater than the net wall area (roof area to net wall area ratio 1.3, Table 4). Since fractional savings relate to the surface area modified, the HVAC energy cost fractional savings from the roof were often similar or greater than those from the walls (Figure 31b). The cool walls and cool roof in the oldest medium office always led to HVAC energy cost savings, and were in most cases greater than the HVAC energy cost savings from the older and new vintage. Making all walls cool in the oldest medium office led to HVAC energy cost savings of more than 3.0 percent from USCZ 1A to 3C. The largest HVAC energy cost penalties were 1.5 percent (new, USCZ 6B, Helena) and 0.70 percent (new, USCZ 5B, Boise).

The retail stand-alone is a single-story building with a large footprint area (2,290 m^2), and has more than twice as much roof area as wall area (roof area to net wall area ratio = 2.1) (Table 4). This large roof area to net wall area ratio led to annual HVAC energy cost fractional savings from the roof that were greater than those from the walls (Figure 31c).

The new retail stand-alone led to HVAC energy cost fractional savings in all U.S. climate zones from cool walls and cool roof; the HVAC energy cost fractional savings from the new vintage when all walls were made cool were up to 11 percent in USCZ 2B (Phoenix), and 6.0 percent in USCZ 3C (San Francisco). The largest HVAC energy cost fractional penalties were 0.50 percent (older, USCZ 6B, Helena).

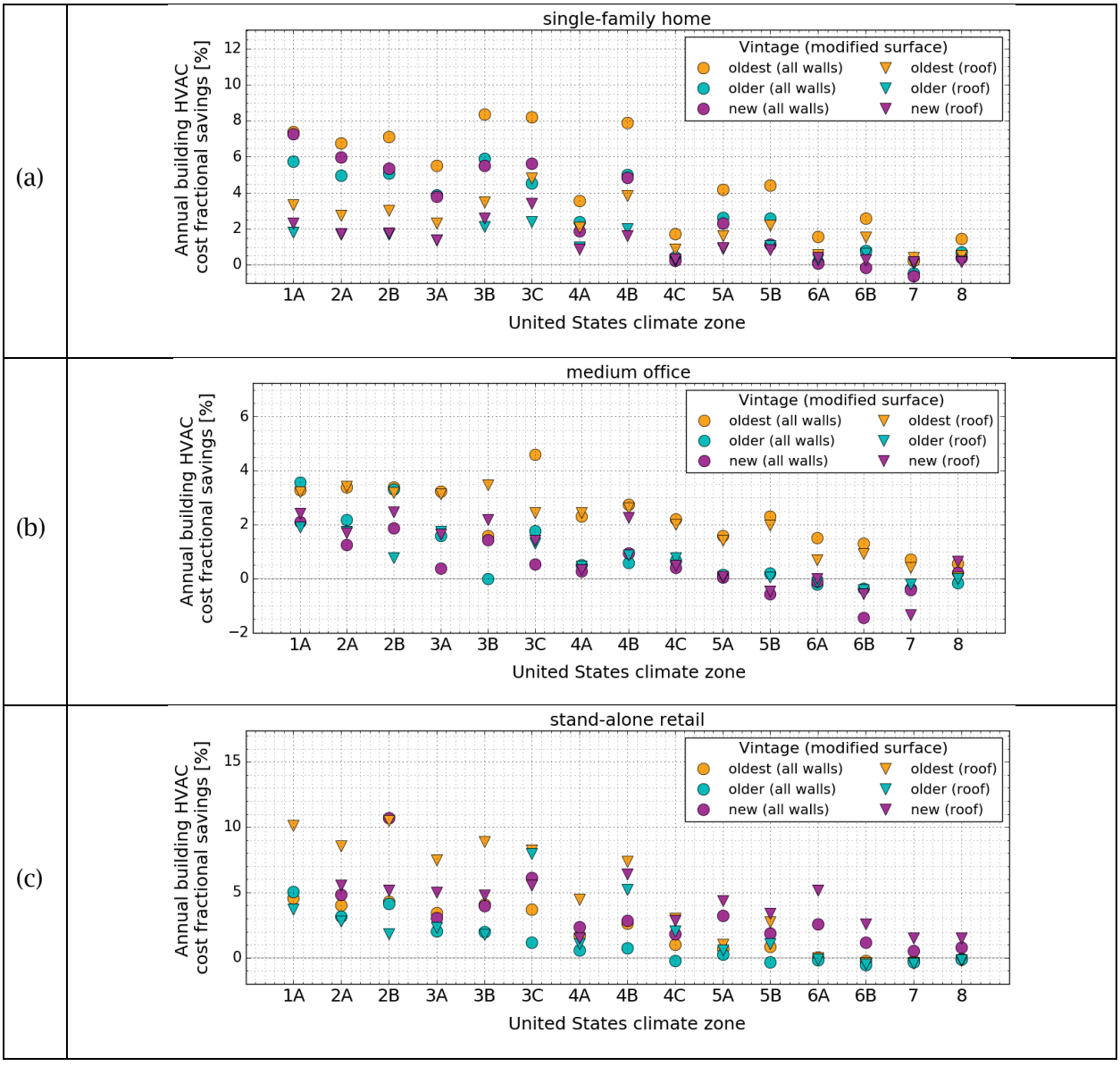

Figure 31. Annual HVAC energy cost fractional savings by vintage and by U.S. climate zone for the (a) single-family home, (b) medium office, and (c) retail stand-alone. The plots compare the fractional savings from increasing the albedo of all walls by 0.35 to that from increasing the roof albedo by 0.30 (residential) or 0.40 (commercial).

3.4.3.3 Annual CO_2e emissions reduction

Figure 32 shows annual CO_2e emissions reduction intensity by vintage and by U.S. climate zone for the single-family home (Figure 32a), medium office (Figure 32b), and stand-alone retail (Figure 32c). These emissions reduction intensities were computed using Eq. (8) and state-dependent CO_2e emissions rate of generated electricity (Table 16) and non-regional emission rates of consumed gas (Table 17). For the single-family home, we used the emissions rate for residential buildings; for the medium office and retail stand-alone, we used the emissions rate for commercial buildings.

Climate zone and vintage trends for annual CO_2e emissions reduction intensities were similar to those observed for annual HVAC source energy savings intensities. These similarities happen because CO_2e emissions reductions and HVAC energy savings are affected equally by climate (i.e., solar radiation, CDD18C, and HDD18C) and building properties (i.e., envelope insulation).

Variations in electricity emission rates between states led to the trend differences between CO_2e emissions reductions and HVAC source energy savings. For example, the cool walls and cool roof in the older and oldest single-family home in USCZ 5B (Boise) yielded annual HVAC source energy savings intensity (Figure 28a). However, in the same U.S. climate zone and vintages, the cool walls and cool roof led to CO_2e emissions increase intensity (Figure 32a). The CO_2e emissions rate from electricity in Boise, ID is among the lowest of all represented states (Table 16), which leads to small cooling CO_2e emissions reduction per unit of saved cooling energy compared to the other locations. Thus, in Boise, while the cool walls and cool roof led to annual HVAC energy savings (cooling energy savings exceed heating energy penalty), they yield annual CO_2e emissions increases (heating CO_2e emissions increase exceeds cooling CO_2e emissions reduction).

In the single-family home (Figure 32a), cool walls generated equal or greater annual CO_2e emissions reduction intensities than did cool roofs in most locations and vintages. The greatest CO_2e emissions reduction intensities when all walls were made cool were 5.3 kg/m² (oldest, USCZ 2B, Phoenix), 4.7 kg/m² (oldest, USCZs 3B and 4B, El Paso and Albuquerque), and 4.6 kg/m² (oldest, USCZ 1A, Miami). USCZs 4C (Seattle), 5B (Boise), and 6A (Burlington), have cool climates, which led to small home cooling energy savings intensities compared to the homes in warm climates. Additionally, CO_2e emissions rates from electricity were smaller in Seattle (Washington), Boise (Idaho), and Burlington (Vermont) than for cities in other states. Thus, cooling CO_2e emissions reduction from cool walls and cool roof in these three locations were small. This led to annual CO_2e emissions increase from cool walls and cool roof in all vintages.

In the medium office (Figure 32b), the cool walls CO_2e emissions reduction intensities were greatest in the oldest vintage in USCZs 1A (Miami), 2A (Houston), 2B (Phoenix), 3A (Memphis), and 4B (Albuquerque). In all U.S. climate zones that yielded CO_2e emissions reduction from the new and oldest vintages, the reductions from the oldest vintage were about 4.4 times that of the new vintage (Table 30).

In the retail stand-alone (Figure 32c), the oldest vintage didn't always lead to the largest annual CO_2e emissions reduction or increase intensities. As an example, in USCZ 2B (Phoenix), the annual CO_2e emissions reduction intensity when all walls were made cool in the new vintage was 21 kg/m², which is about 2.3 times that of the oldest vintage. The new vintage had greater CO_2e emissions reduction than the oldest vintage because the wall thermal resistance in the new vintage was half of that in the oldest vintage, leading to more annual HVAC energy savings in the new vintage. The oldest retail stand-alone was simulated with metal frame walls, while the new stand-alone retail was simulated with heavy mass walls. In warm climates (e.g., USCZ 2B) the walls of the new stand-alone retail were simulated with no additional wall insulation. Thus, in some locations, the resistance of the wall assembly in the new stand-alone retail was less than that of the oldest vintage.

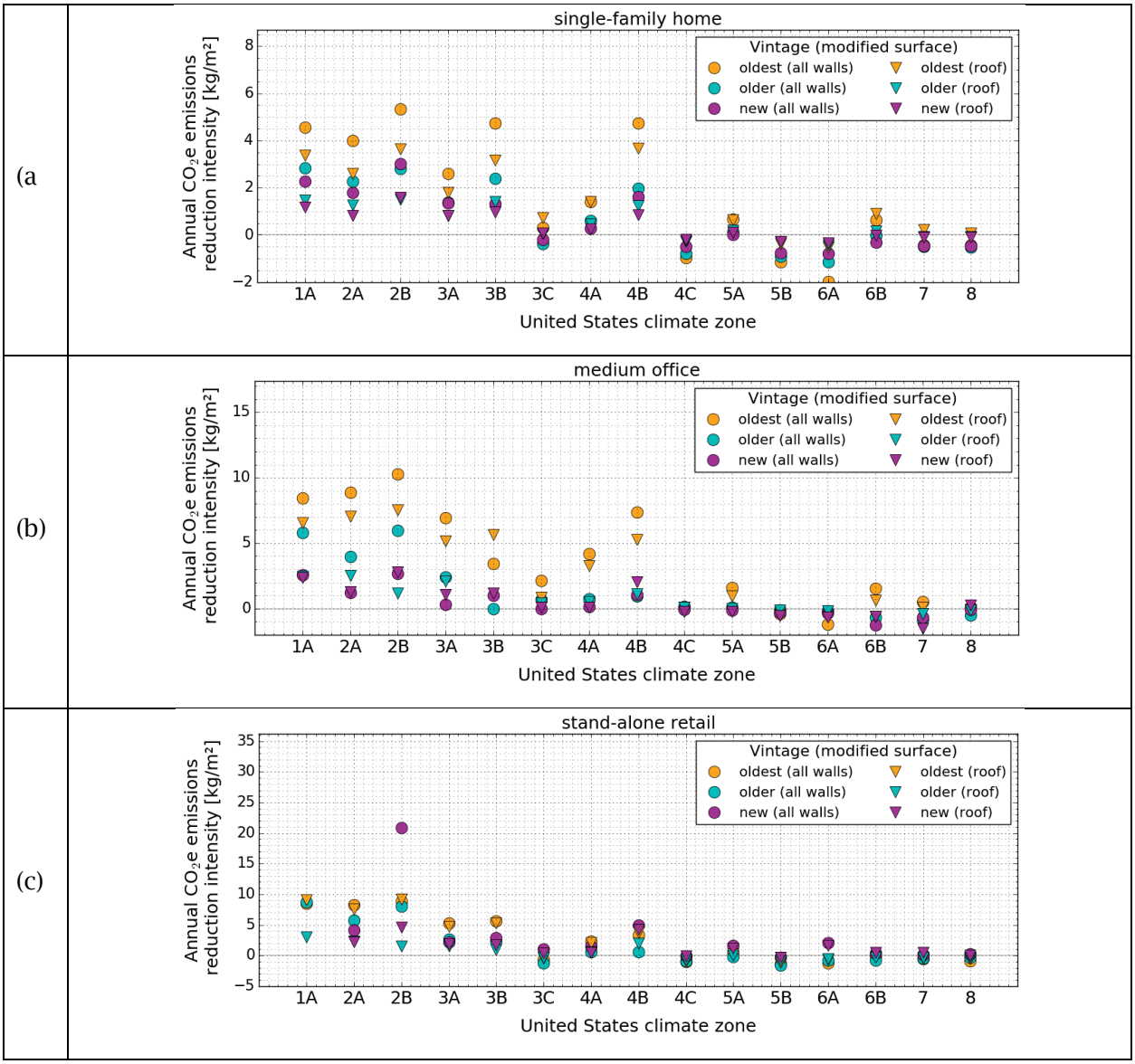

Figure 32. Annual CO_2e emissions reduction intensity by vintage and by U.S. climate zone for the (a) single-family home, (b) medium office, and (c) retail stand-alone. The plots compare the reduction intensity from increasing the albedo of all walls by 0.35 to that from increasing the roof albedo by 0.30 (residential) or 0.40 (commercial).

Figure 33 shows CO_2e emissions fractional reduction by vintage and by U.S. climate zone for the single-family home (Figure 33a), medium office (Figure 33b), and stand-alone retail (Figure 33c). Similar to what we observed between annual HVAC source energy and energy cost fractional savings, the annual CO_2e emissions fractional reduction are affected equally by climate and building properties.

When all walls were made cool in the single-family home (Figure 33a), the greatest CO_2e emission fractional reductions were 8.3 percent (oldest, USCZ 3B, El Paso), followed by 8.0 percent (oldest, USCZ 4B, Albuquerque), 7.5 percent (oldest and new, USCZ 1A, Miami), and 7.5 percent (oldest, USCZ 2B, Phoenix). In 7 U.S. climate zones (1A, 2A, 2B, 3A, 3B, 4A, and 4B) making all walls cool led to CO_2e emissions reduction of 2.0 percent or greater from all vintages. In USCZs 4C (San Francisco), 5B (Boise), and 6A (Burlington), making all walls cool led to CO_2e emissions increased from all vintages, reaching increases of up to 3.8 percent (oldest, USCZ 6A, Burlington).

Similar to the case of HVAC source energy and energy cost fractional savings, the annual CO_2e emissions reductions from increasing the albedo of all walls were often much greater than those from cool roof because a) the thermal resistance in walls is less than that of walls, and b) the net wall area is greater than the roof area (roof-to-wall ratio 0.61, Table 4).

In most locations and vintages of the single-family home, the annual CO_2e emissions reductions or penalty intensities from the roof were greater than those from the walls (Figure 32a). However, the annual CO_2e emissions fractional reductions or increases from the walls were mostly greater than those from the roof because the net wall area was greater than the roof area (roof area to net wall area ratio 0.61) (Table 4).

For the medium office (Figure 32b), we see that USCZ 2B (Phoenix) was the location with greatest cool walls annual CO_2e emissions reduction intensity for all vintages. However, the largest cool walls annual CO_2e emissions fractional reductions were in the oldest medium office in USCZ 3C (San Francisco), which led to a 6.0 percent reduction (Figure 33b). Although USCZ 3C had small CO_2e emissions savings intensity for all vintages, the small base CO_2e emissions led to large CO_2e emissions fractional reductions.

In most locations and vintages, annual CO_2e emissions reduction or increase intensities from the walls of the medium office were slightly greater than those from the roof (Figure 32b). However, since the roof area in the medium office is greater than the net wall area (roof area to net wall area ratio 1.3) (Table 4), the CO_2e emissions fractional reductions or increases from the roof were often similar or greater than those from the walls (Figure 33b).

The retail stand-alone is a single-story building with a large footprint area (2,290 m²), and has more than twice as much roof area as wall area (roof area to net wall area ratio = 2.1) (Table 4). In most U.S. climate zones, this large roof area to net wall area ratio led to annual CO_2e emissions fractional savings or penalties from the roof that were greater than those from the walls (Figure 33c). The greatest CO_2e emissions fractional reductions when all walls were made cool were 11.9 percent (new, USCZ 2B, Phoenix). In USCZs 4C (San Francisco), 5B (Boise), and 6A (Burlington), making all walls cool led to CO_2e emissions increased from all vintages, reaching increases of up to 2.5 percent (older, USCZ 5B, Boise). In USCZs 7 and 8, raising wall albedo yielded almost no change to CO_2e emissions.

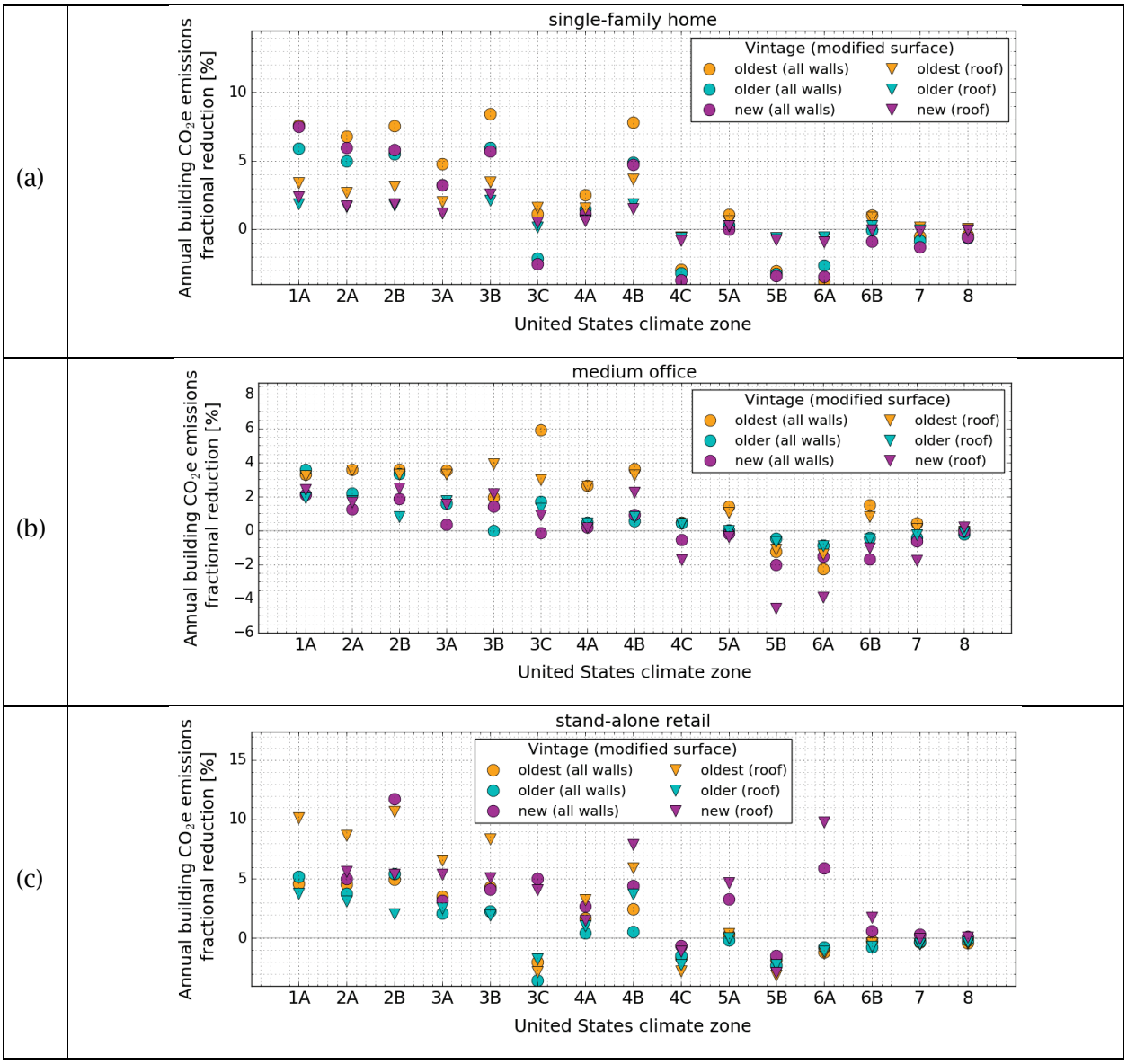

Figure 33. Annual CO_2e emissions fractional reduction by vintage and by U.S. climate zone for the (a) single-family home, (b) medium office, and (c) retail stand-alone. The plots compare the fractional reduction from increasing the albedo of all walls by 0.35 to that from increasing the roof albedo by 0.30 (residential) or 0.40 (commercial).

3.4.3.4 Annual NO_x emissions reduction

Figure 34 and Figure 35 show annual NO_x emissions reduction intensities and fractional reductions, respectively, by vintage and by U.S. climate zone for the single-family home (Figure 34a and Figure 35a), medium office (Figure 34b and Figure 35b), and stand-alone retail (Figure 34c and Figure 35c). These emissions reduction intensities were computed using Eq. (8) and (10), and the fractional reductions were computed using Eq. (8). These emission reductions were

calculated using the state-dependent NO_X emissions rate of generated electricity (Table 16) and the non-regional emissions rate of consumed gas (Table 17).

The annual NO_x emissions reduction intensities and fractional reductions have the same trend between U.S. climate zones and between vintages that those we observed for the annual savings intensity and fractional savings of annual CO_2e emissions. The proportions of cool walls NO_x reductions to those from cool roof were very similar to those we observed for annual CO_2e emissions reductions. These similarities happen because NO_x and CO_2e emissions reductions are affected equally by climate (i.e., solar radiation, CDD18C, and HDD18C) and building properties (i.e. envelope thermal resistance) (see Section 3.3.3.1). All fractional savings are also affected equally by building geometry.

(a)

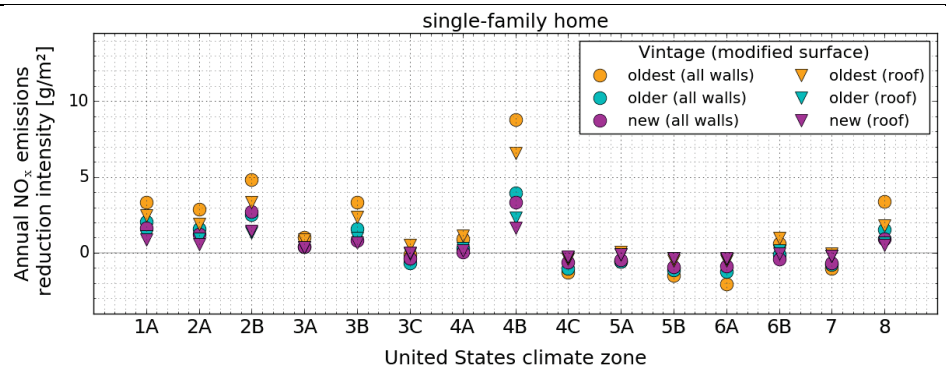

(b)

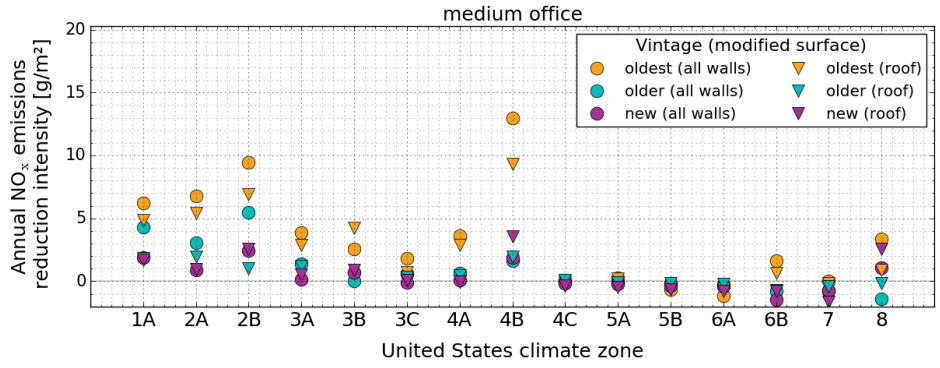

(c)

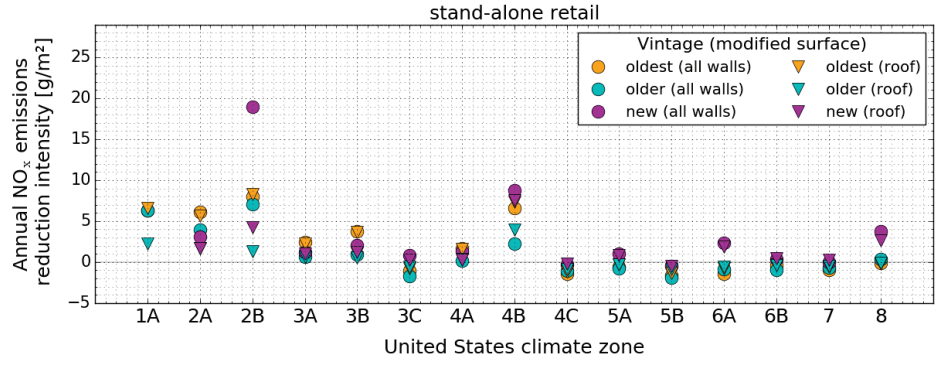

Figure 34. Annual NO_x emissions reduction intensity by vintage and by U.S. climate zone for the (a) single-family home, (b) medium office, and (c) retail stand-alone. The plots compare the reduction intensity from increasing the albedo of all walls by 0.35 to that from increasing the roof albedo by 0.30 (residential) or 0.40 (commercial).

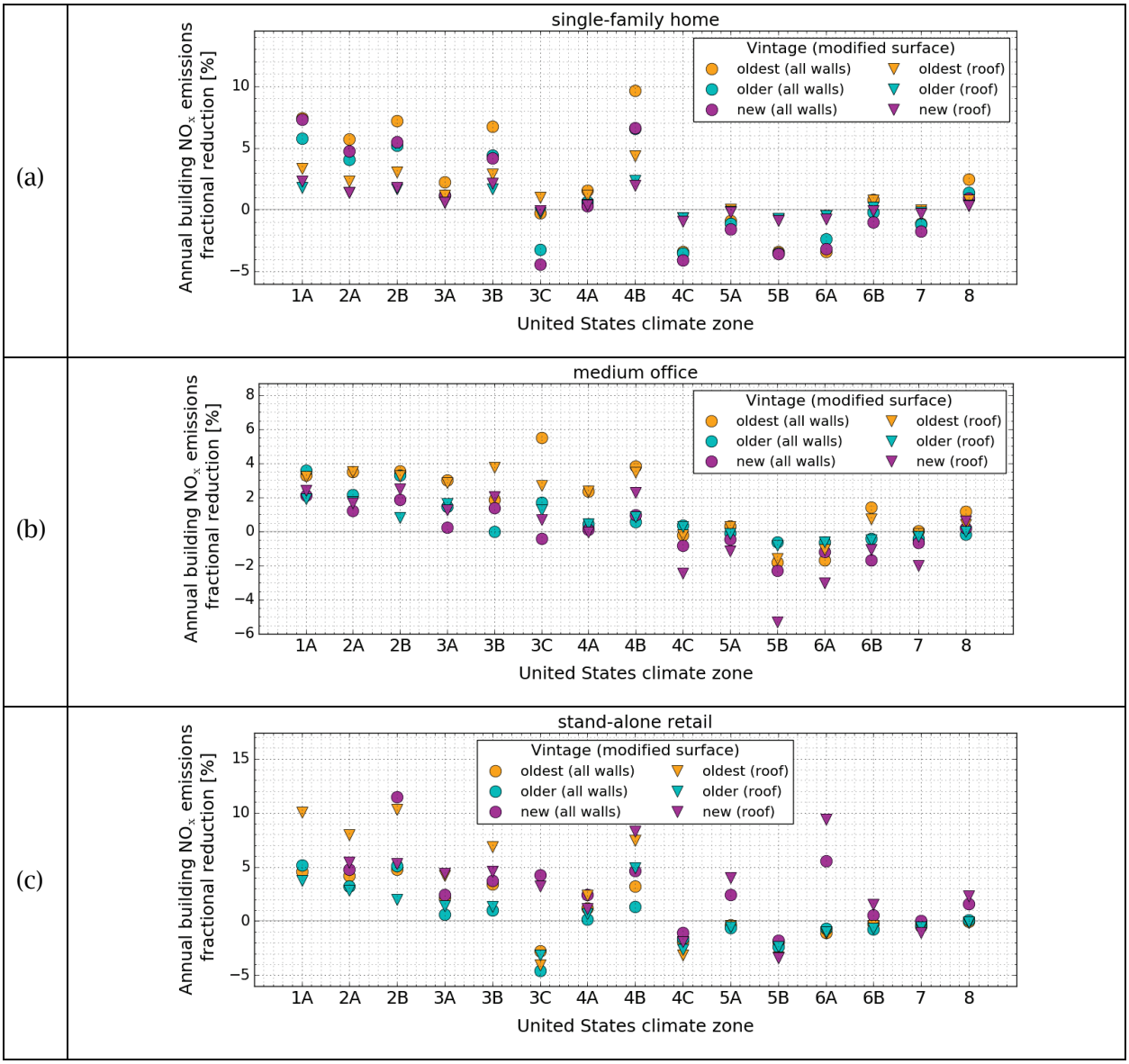

Figure 35. Annual NO_x emissions fractional reduction by vintage and by U.S. climate zone for the (a) single-family home, (b) medium office, and (c) retail stand-alone. The plots compare the fractional reduction from increasing the albedo of all walls by 0.35 to that from increasing the roof albedo by 0.30 (residential) or 0.40 (commercial).

3.4.3.5 Annual SO_2 emissions reduction

Figure 36 and Figure 37 show annual SO_2 emissions reduction intensities and fractional reductions, respectively, by vintage and by U.S. climate zone for the single-family home (Figure 36a and Figure 37a), medium office (Figure 36b and Figure 37b), and stand-alone retail (Figure 36c and Figure 37c). These emissions reduction intensities were computed using Eq. (8) and (10), and the fractional reductions were computed using Eq. (8). These emission reductions were calculated using the state-dependent SO_2 emissions rate of generated electricity (Table 16) and the non-regional emissions rate of consumed gas (Table 17).

The annual SO_2 emissions reduction intensities and fractional reductions have the same trend between U.S. climate zones and between vintages that those we observed for the annual savings intensity and fractional savings of annual CO_2e emissions. The ratios of SO_2 reductions from cool walls to those from a cool roof were very similar to those we observed for CO_2e because these reductions are affected equally by climate (i.e., solar radiation, CDD18C, and HDD18C) and building properties (i.e. envelope thermal resistance) (see Section 3.3.3.1). All fractional savings are also affected equally by building geometry.

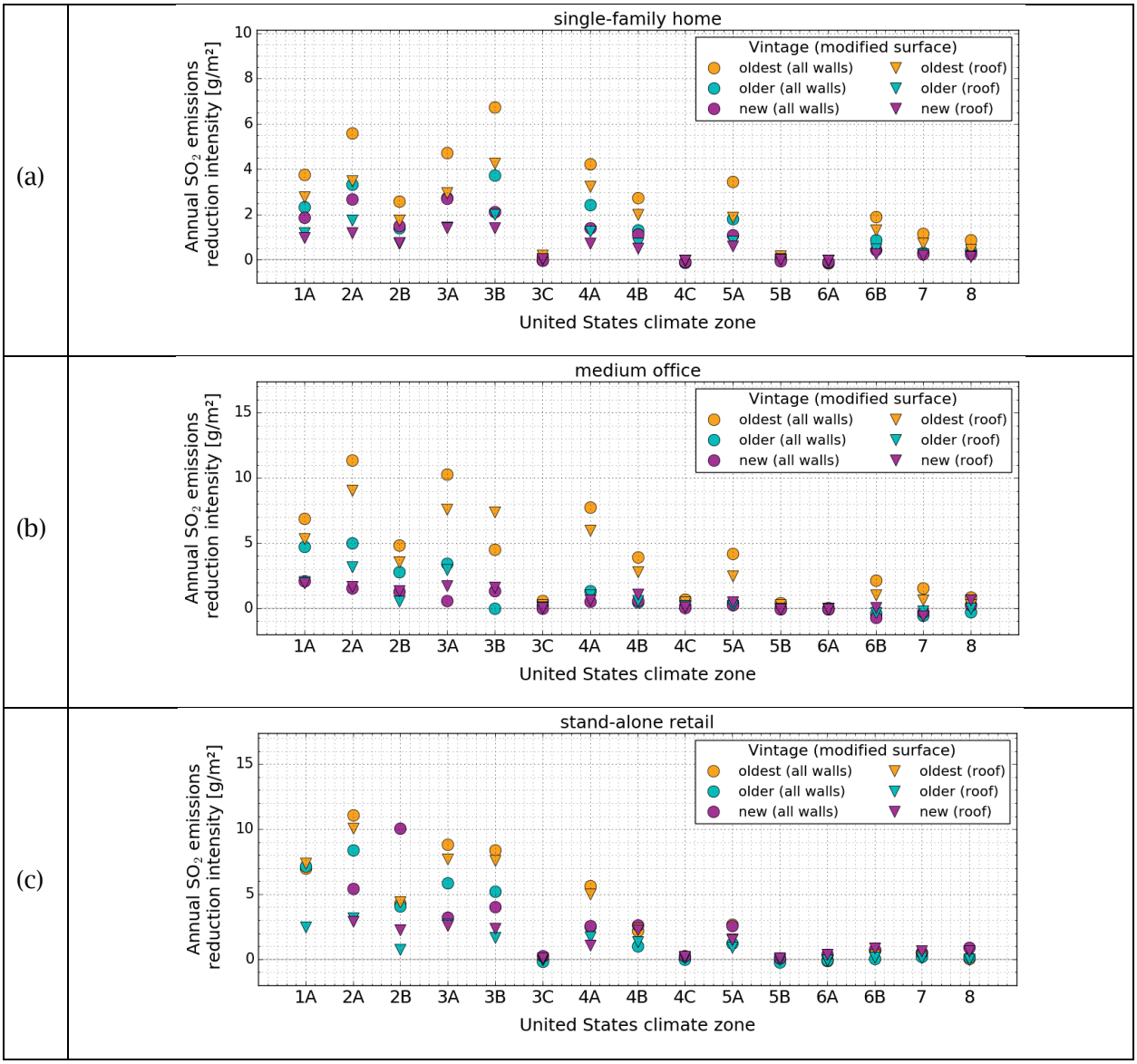

Figure 36. Annual SO_2 emissions reduction intensity by vintage and by U.S. climate zone for the (a) single-family home, (b) medium office, and (c) retail stand-alone. The plots compare the reduction intensity from increasing the albedo of all walls by 0.35 to that from increasing the roof albedo by 0.30 (residential) or 0.40 (commercial).

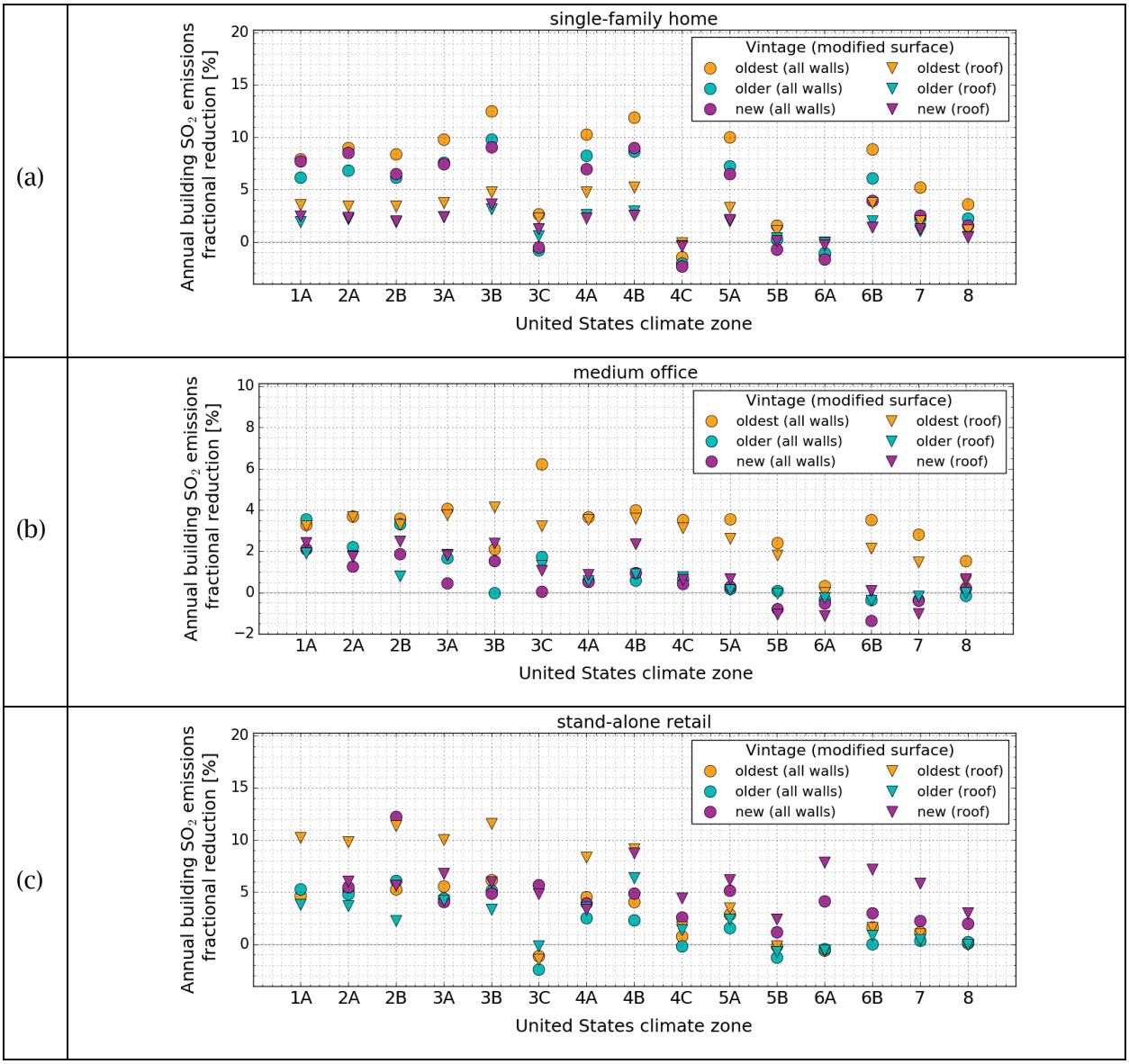

Figure 37. Annual SO_2 emissions fractional reduction by vintage and by U.S. climate zone for the (a) single-family home, (b) medium office, and (c) retail stand-alone. The plots compare the fractional reduction from increasing the albedo of all walls by 0.35 to that from increasing the roof albedo by 0.30 (residential) or 0.40 (commercial).

3.4.3.6 HVAC peak power demand reduction

Figure 38 and Figure 39 show annual-average HVAC peak power demand reduction intensity and fractional reduction, respectively, by vintage and by California climate zone for the single-family home (Figure 38a and Figure 39a), medium office (Figure 38b and Figure 39b), and stand-alone retail (Figure 38c and Figure 39c). The peak power demand reduction intensity were computed using Eqs. (7), (10), and (12).

When comparing between vintages, the reduction intensities and fractional reduction in annual-average HVAC peak power demand have a similar trend to those we observed for the annual savings intensity and fractional savings of HVAC source energy, energy cost, and emissions. However, when comparing between U.S. climate zones, the reduction intensities and fractional reduction in annual-average HVAC peak power demand show a different trend that those observed for HVAC source energy, energy cost, and emissions. These differences in trends happen because HVAC peak power demand is affected only by the summer climate (i.e. peak hours solar radiation and CDD18C), while HVAC source energy, energy cost, and emissions are affected by the annual climate (i.e. solar radiation, CDD18C, and HDD18C).

HVAC source energy, energy cost, and emissions sometimes yielded small penalty intensities and fractional penalties in cold U.S. climate zones. However, HVAC peak power demand yielded reduction intensities and fractional reduction in all U.S. climate zones. Furthermore, in the single-family home (Figure 38a), the peak power demand reduction intensities in cold U.S. climate zones were similar to those from warm U.S. climate zones. Additionally, the peak power demand fractional reduction in the single-family home (Figure 39a) increased slightly with U.S. climate zone.

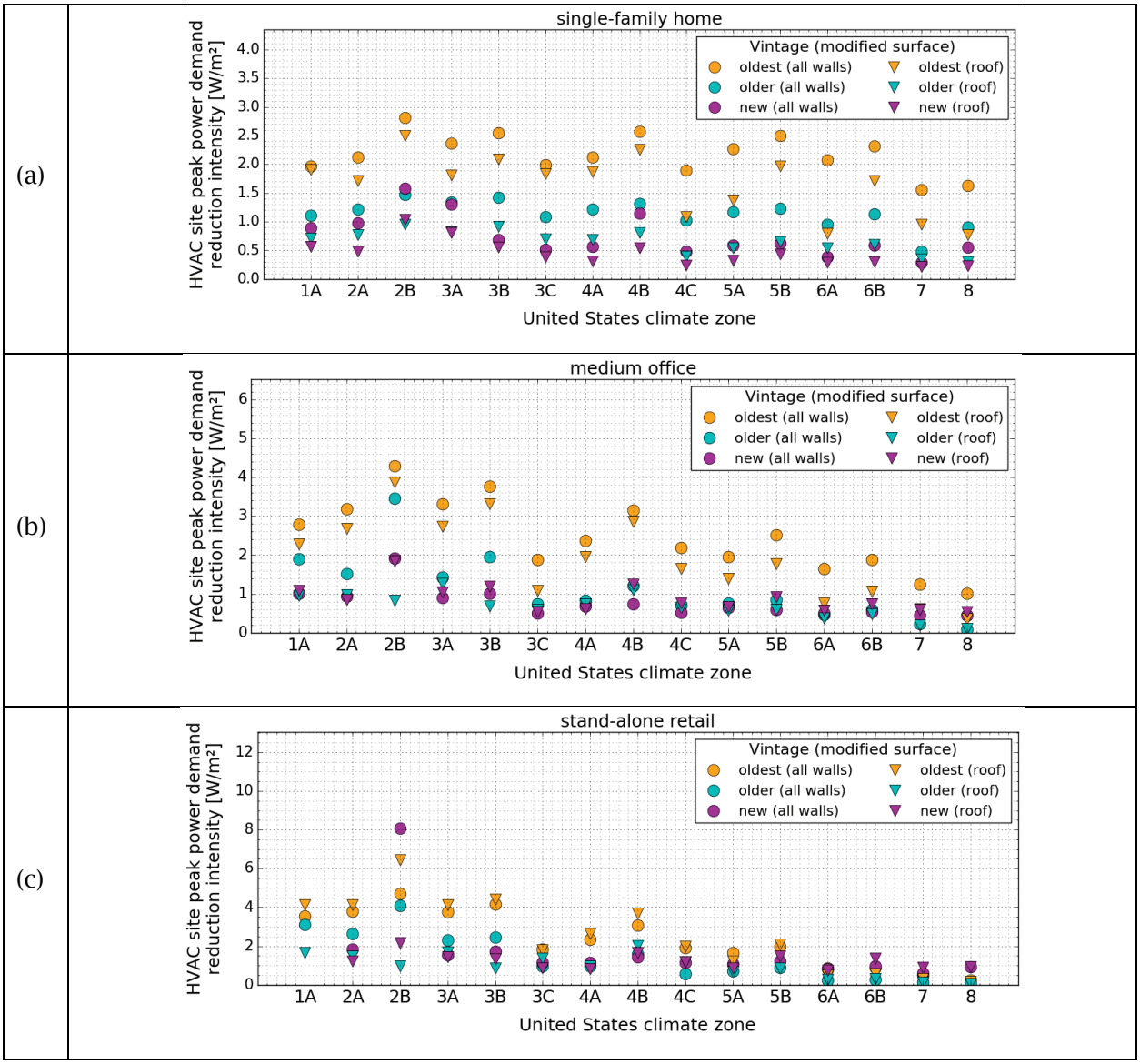

Figure 38. Annual-average HVAC peak power demand reduction intensity by vintage and by U.S. climate zone for the (a) single-family home, (b) medium office, and (c) retail stand-alone. The plots compare the reduction intensity from increasing the albedo of all walls by 0.35 to that from increasing the roof albedo by 0.30 (residential) or 0.40 (commercial).

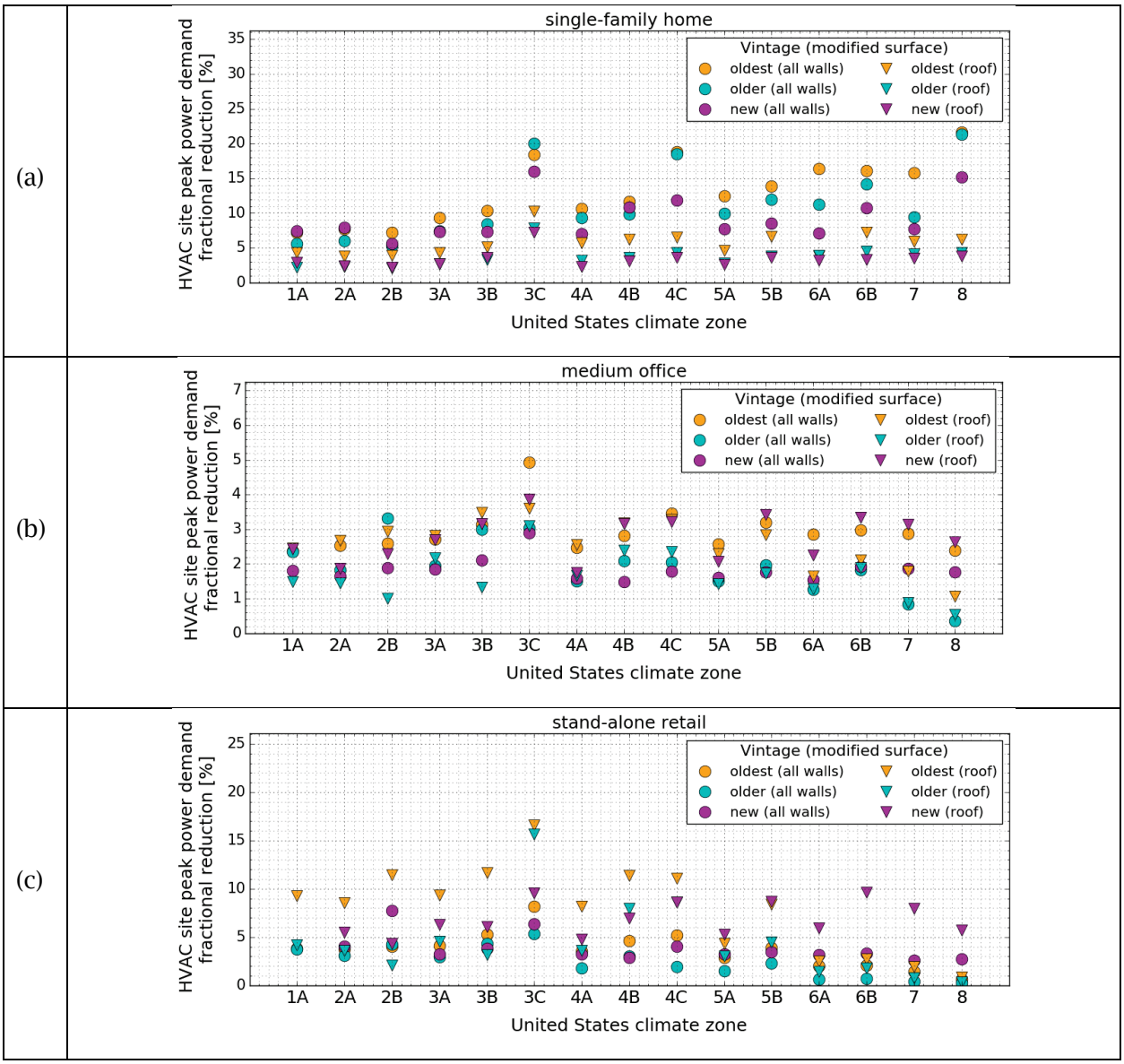

Figure 39. Annual-average HVAC peak power demand fractional reduction by vintage and by U.S. climate zone for the (a) single-family home, (b) medium office, and (c) retail stand-alone. The plots compare the fractional reduction from increasing the albedo of all walls by 0.35 to that from increasing the roof albedo by 0.30 (residential) or 0.40 (commercial).

3.4.3.7 Comparing savings between vintages

Table 30 and Table 31 give oldest-to-new vintage and older-to-new vintage ratios respectively, of annual HVAC source energy savings, emissions reductions, and HVAC energy cost savings. The savings were from increasing the albedo of all walls by 0.35 (to 0.60 from 0.25). The ratios are given by building type and are the mean of both building orientations. The calculations omit ratios that were negative to exclude the few instances where the new vintage generated small annual penalties, while the older and oldest vintages generated annual savings.

In the case of oldest-to-new vintage (Table 30), the oldest-to-new ratios vary widely by building category. In the residential building categories, the oldest-to-new ratio were mostly between 2.0 and 3.0. The medium office yielded the greatest oldest-to-new ratios. The large hotel was the only building category where the energy and energy cost savings as well as the emissions reductions in the oldest vintage were less than those in the new vintage.

In the case of older-to-new vintage (Table 31), savings from the older vintage of residential buildings were typically between 1.2 to 2.0 times that of the new vintage. The medium office yielded the greatest older-to-new ratios. For the large hotel, the savings and reductions from the older vintage were about 0.10 times that of the new vintage.

Table 30. United States average ratios of oldest vintage to new vintage savings by building type and metric for the mean values of the two building orientations.

	U.S. average annual savings ratios (oldest-to-new)				
Prototype building	HVAC source energy [MJ/MJ]	CO_2e [kg/kg]	NO_x [g/g]	SO_2 [g/g]	HVAC energy cost [$/$]
Single-family home (gas furnace)	3.0	2.3	2.9	2.7	4.8
Single-family home (heat pump)	2.5	2.5	2.5	2.5	2.5
Single-family home (electric resistance)	1.9	1.9	1.9	1.9	1.9
Apartment building (gas furnace)	3.0	2.7	2.5	2.8	5.1
Apartment building (heat pump)	2.9	2.9	2.9	2.9	2.9
Apartment building (electric resistance)	2.0	2.0	2.0	2.0	2.0
Large hotel	0.5	0.4	0.7	0.4	0.4
Large office	2.4	1.2	1.5	1.4	0.7
Medium office	8.0	4.4	3.7	9.7	7.6
Small office	4.8	5.0	4.6	4.9	4.4
Fast-food restaurant	3.2	5.2	4.8	3.9	2.4
Retail stand-alone	1.1	2.1	1.9	1.1	1.1
Strip mall retail	3.9	4.0	2.6	2.2	3.8
Sit-down restaurant	6.6	4.0	3.6	5.0	8.1

Table 31. United States average ratios of older vintage to new vintage savings by building type and metric for the mean values of the two building orientations.

Prototype building	U.S. average annual saving ratios (older-to-new)				
	HVAC source energy [MJ/MJ]	CO_2e [kg/kg]	NO_x [g/g]	SO_2 [g/g]	HVAC energy cost [$/$]
Single-family home (gas furnace)	1.3	1.3	1.5	1.6	1.8
Single-family home (heat pump)	1.6	1.6	1.6	1.6	1.6
Single-family home (electric resistance)	1.2	1.2	1.2	1.2	1.2
Apartment building (gas furnace)	1.3	1.8	1.5	1.4	2.0
Apartment building (heat pump)	1.3	1.3	1.3	1.3	1.3
Apartment building (electric resistance)	1.4	1.4	1.4	1.4	1.4
Large hotel	0.1	0.1	0.2	0.1	0.1
Large office	1.5	0.9	1.0	1.0	0.6
Medium office	4.1	2.8	2.6	2.2	3.2
Small office	1.9	3.0	3.7	2.3	1.8
Fast-food restaurant	1.8	2.1	2.5	1.9	1.7
Retail stand-alone	0.5	1.6	1.1	0.6	0.5
Strip mall retail	2.0	2.1	2.4	1.1	1.7
Sit-down restaurant	3.4	2.2	2.2	2.7	3.7

3.4.4 Sum of savings from walls modified one at a time to savings from modifying multiple walls simultaneously (United States)

This section compares the savings obtained from modifying a group of walls simultaneously (e.g., east and west) to the sum of the savings from modifying the walls one at a time. These comparisons are presented for whole-building annual values of (a) source cooling savings, (b) heating penalties, (c) fan savings, and (d) HVAC savings. These energy savings and penalties are shown for the new single-family home (Figure 40), new medium office (Figure 41), and new stand-alone retail (Figure 42). The plots include all the 15 wall combinations simulated in each U.S. climate zone; the values are the average of the two building orientations (east-west and north-south).

In the single-family home, the annual cooling source energy savings were nearly perfectly additive (Figure 40a). In the case of annual heating source energy, the penalties from adding individual walls were additive in many of the wall combinations of all U.S. climate zones (Figure 40b). The remaining wall combinations were close to additive. In the case of annual fan source energy, the savings were not additive for USCZs 6B (Helena) and 7 (Duluth) (Figure 40c). The annual HVAC source energy savings were nearly perfectly additive in the majority of the wall combinations and U.S. climate zones (Figure 40d).

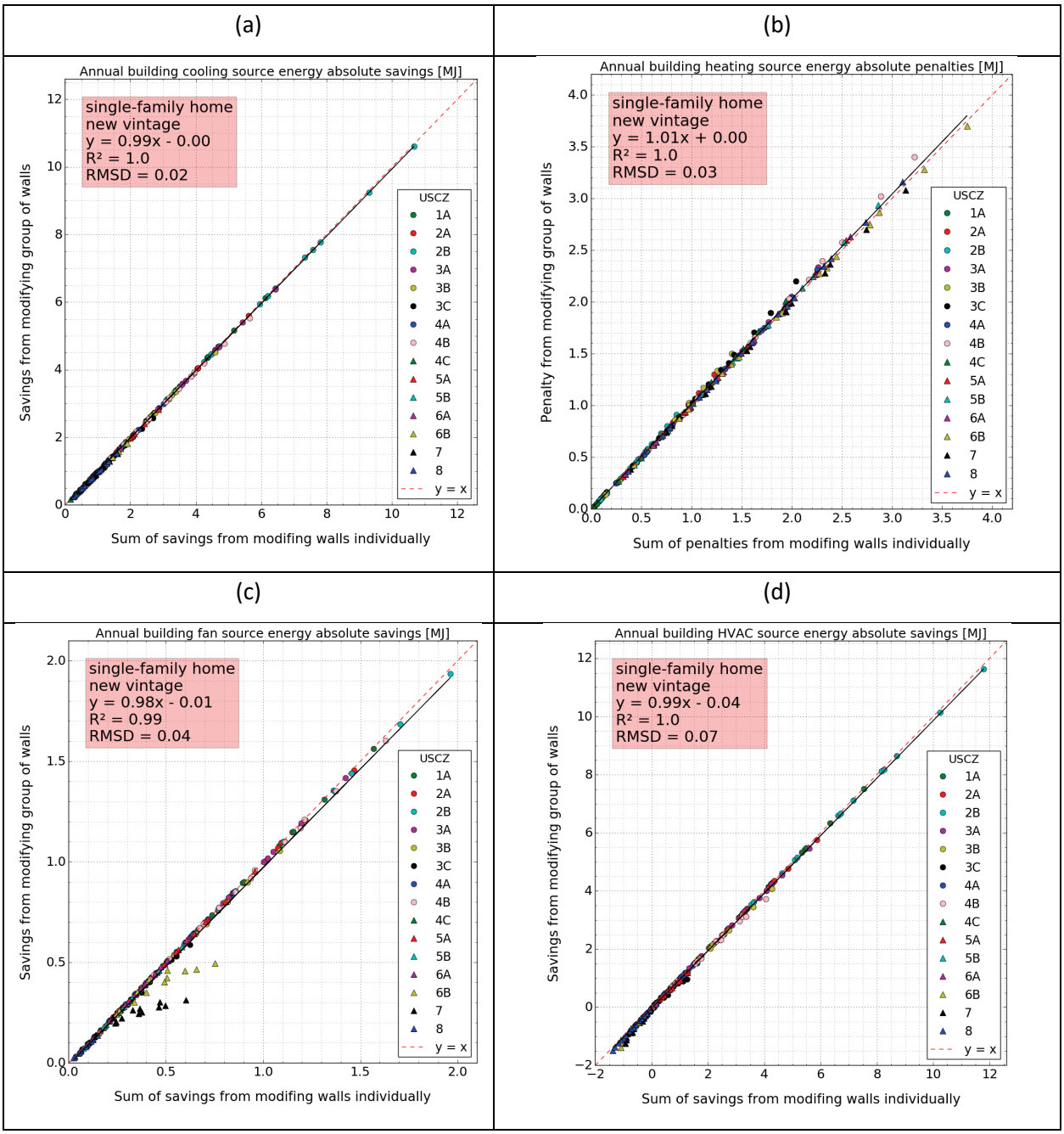

Figure 40. Comparing changes in annual whole-building source energies for the new vintage of single-family home in California climate zones from modifying group of walls simultaneously to those from adding changes from individual walls. The plots show (a) cooling savings, (b) heating penalties, fan savings, and HVAC savings.

In all U.S. climate zones, the annual cooling source energy savings of the medium office were almost perfectly additive (Figure 41a). In the case of annual heating source energy savings, the penalties from adding individual walls were not additive in USCZs 3A (Memphis) and 5B (Boise) and for one wall combination in USCZ 6B (Helena) (Figure 41b). Annual fan source energy

savings were not additive for most wall combinations in USCZ 5B (Boise) (Figure 41c). The cases in which heating and fan were not additive led to HVAC source energy savings not being additive in USCZs 3A (Memphis) and 5B (Boise).

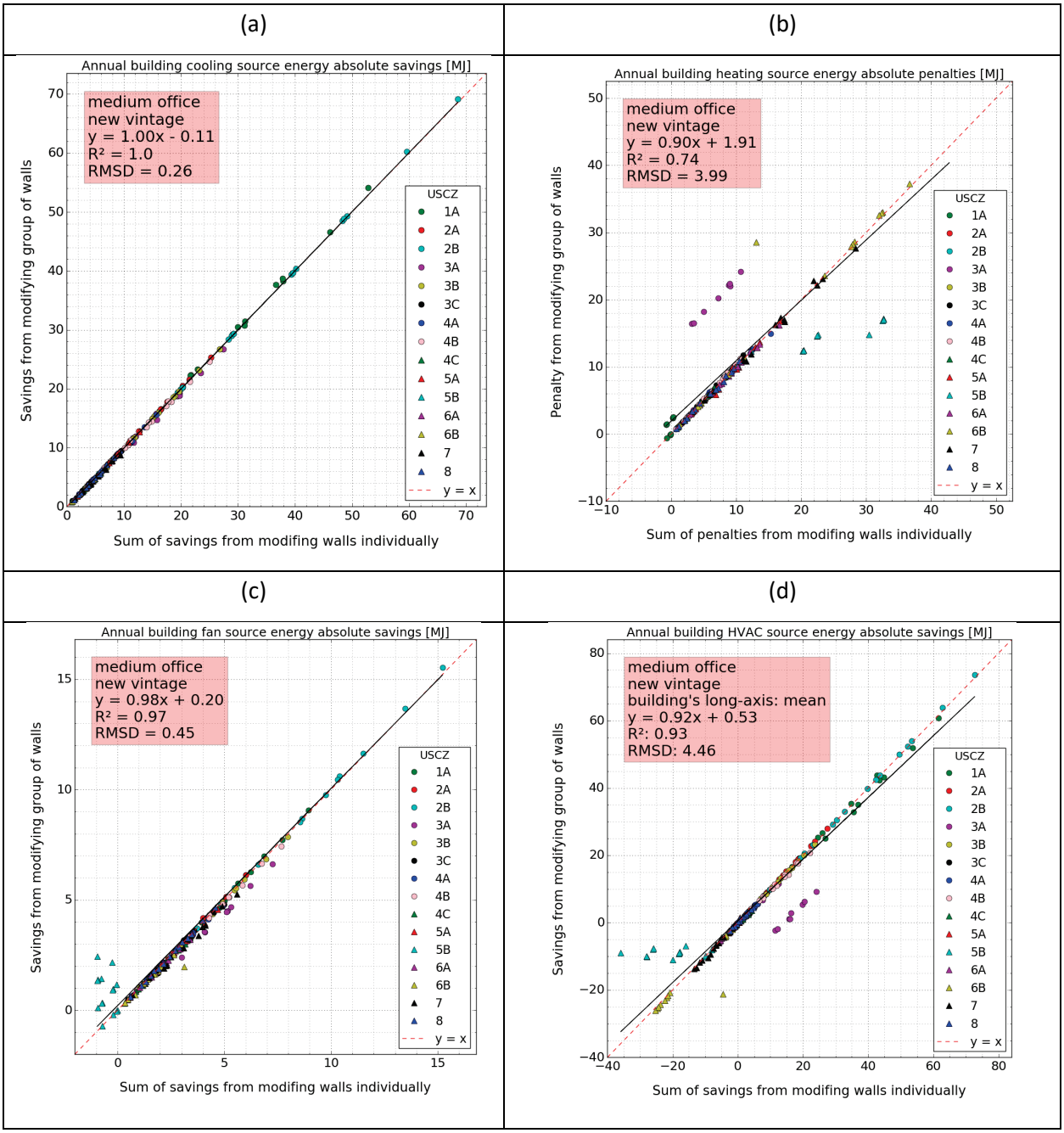

Figure 41. Comparing changes in annual whole-building source energies for the new vintage of medium office in California climate zones from modifying group of walls simultaneously to those from adding changes from individual walls. The plots show (a) cooling savings, (b) heating penalties, fan savings, and HVAC savings.

The new retail stand-alone was the only building category and vintage in which the wall combinations were mostly none additive (Table 32). Source heating and fan energy savings were far from additive in a few USCZs (Figure 42b,c). Thus, HVAC source energy savings ended up being additive only in some U.S. climate zones (Figure 42d).

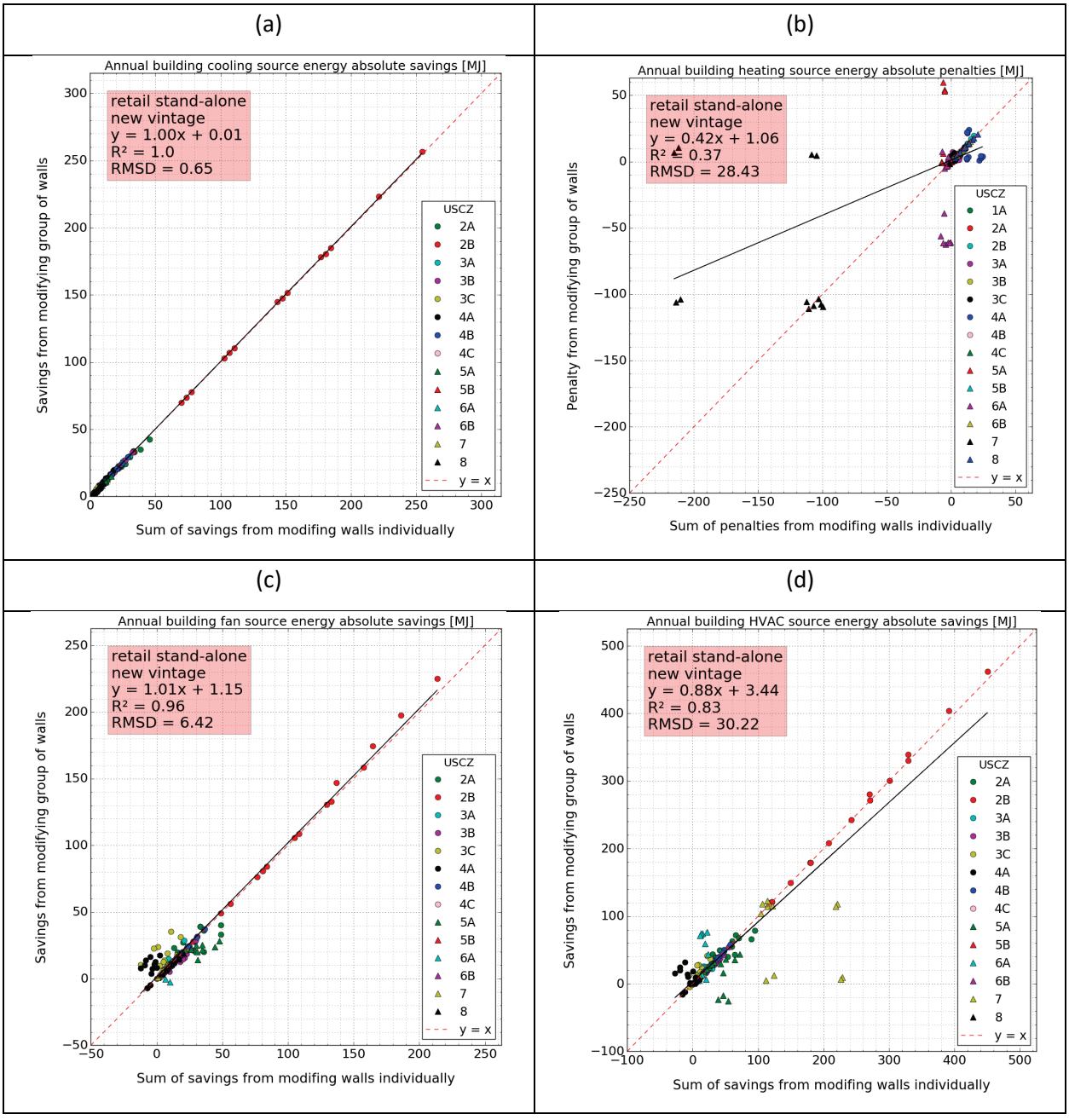

Figure 42. Comparing changes in annual whole-building source energies for the new vintage of stand-alone retail in California climate zones from modifying group of walls simultaneously to

those from adding changes from individual walls. The plots show (a) cooling savings, (b) heating penalties, fan savings, and HVAC savings.

Table 32 summarizes for the U.S. prototypes, the slope, intercept, coefficient of determination (R^2), and root mean square difference (RMSD) of linear regression comparing HVAC source energy savings from modifying multiple walls simultaneously (dependent variable) to the sum of savings from walls modified one at a time (independent variable). There was no building category in which the HVAC savings were perfectly additive for every wall combination and climate zone. However, all vintages of every residential building category show savings that were nearly perfectly additive.

Similar to what was obtained from California simulations, for almost all prototypes and climate zones in U.S., annual cooling energy savings were additive. However, for most prototypes, annual heating (electric or gas) and fan energy savings were additive only in some climate zones and for some wall orientations. Thus, when combining the savings from the different HVAC components (cooling, heating, and fan), there is no prototype in any vintage in which the HVAC system is perfectly additive in all locations and for all wall combinations.

Table 32. Slope, intercept, coefficient of determination (R^2), and root mean square difference (RMSD) of linear regression comparing HVAC source energy savings from modifying multiple walls simultaneously (dependent variable) to the sum of savings from walls modified one at a time (independent variable). These results include all U.S. climate zones and wall combinations of each prototype, and are the average values from both building orientations (E-W and N-S).

	Regression slope [MJ/MJ]			Regression intercept [MJ]			Coefficient of determination (R^2)			RMSD [MJ]		
Prototype building	**oldest**	**older**	**new**	**oldest**	**older**	**new**	**oldest**	**older**	**new**	**oldest**	**older**	**new**
Single-family home (gas furnace)	0.99	0.99	0.99	-0.06	-0.05	-0.04	1.00	1.00	1.00	0.14	0.09	0.07
Single-family home (heat pump)	0.99	0.98	0.99	-0.16	-0.02	-0.02	1.00	1.00	1.00	0.24	0.15	0.10
Single-family home (electric resistance)	1.00	1.00	1.00	-0.16	-0.07	-0.06	1.00	1.00	1.00	0.25	0.13	0.11
Apartment building (gas furnace)	1.00	1.00	1.00	-0.14	-0.07	-0.05	1.00	1.00	1.00	0.19	0.12	0.09
Apartment building (heat pump)	1.00	1.00	1.00	-0.14	-0.07	-0.04	1.00	1.00	1.00	0.23	0.11	0.08
Apartment building (electric resistance)	1.01	1.01	1.01	-0.22	-0.11	-0.08	1.00	1.00	1.00	0.38	0.22	0.16
Large hotel	1.00	0.99	1.01	0.14	0.03	-0.95	1.00	1.00	1.00	0.69	0.90	4.58
Large office	1.03	1.02	0.98	0.86	0.50	0.44	1.00	1.00	1.00	4.82	5.24	10.38
Medium office	1.00	1.00	0.92	-0.13	0.00	0.53	1.00	1.00	0.93	0.69	0.35	4.46
Small office	1.00	0.99	1.00	0.06	0.03	-0.01	1.00	1.00	1.00	0.10	0.12	0.06
Fast-food restaurant	1.00	0.97	1.00	0.02	0.05	0.02	1.00	1.00	1.00	0.25	0.28	0.08
Retail stand-alone	1.00	0.99	0.88	0.00	0.02	3.44	1.00	1.00	0.83	0.68	1.12	30.22
Strip mall retail	0.99	0.99	1.01	-0.06	0.08	0.24	1.00	1.00	0.95	0.81	1.10	3.18
Sit-down restaurant	1.00	0.99	0.99	0.03	0.08	0.01	1.00	0.99	1.00	0.50	0.96	0.21

4 Discussion

4.1 Location-dependent savings

4.1.1 California

We investigated whether annual cooling energy savings intensities and heating energy penalty intensities correlated with cooling degree days and heating degree days, respectively, as well as with absorbed sunlight. Since the insulation in the building envelope and the efficiency of the air conditioner system often vary by location, we normalized cooling degree days, heating degree days, and absorbed sunlight by the face's thermal resistance and by the air conditioner efficiency. Annual cooling energy savings and heating energy penalties increased with annual cooling degree days and annual heating degree days, respectively. However, we observed that these savings and penalties often correlated poorly with changes in absorbed summer and winter sunlight, respectively, possibly because solar irradiation is similar throughout California. Using multivariate linear regression, we investigated whether the energy savings and penalties correlated better with degree days and changes in absorbed sunlight when these two metrics were considered simultaneously. The multivariate linear regression showed that the correlation of cooling and heating energy savings to both metrics did not improve significantly, except in a few instances.

In the older and new vintage prototypes, the requirements in envelope thermal resistances varied by location. These variation in thermal resistances were an additional key factor to how cooling and heating energy savings varied by location.

The warmest California locations—those with the most cooling degree days—yielded the greatest annual cooling savings. CACZ 15 is the climate region in California that would yield the greatest cooling savings intensities from cool walls. CACZs 1 and 16 are the coldest zones in California—highest heating degree days and lowest cooling degree days—leading to the smallest annual cooling savings intensities and greatest annual heating penalty intensities of all climate zones.

Even in the coldest regions, cool walls yielded annual HVAC energy savings and peak power demand reduction in all prototypes and locations, except in the new stand-alone retail in CACZ 16. Thus, the annual cooling savings from cool walls nearly always exceeded the annual heating penalties.

CACZs 14 and 15 were the zones that benefited the most from cool walls. These are the warmest zones in California. However, CACZs 6 through 13, which had similar cooling degree days and heating degree days, also yielded large annual HVAC energy savings. Thus, the zones having similar or greater cooling degree days than heating degree days benefited the most in HVAC energy savings from cool walls. Furthermore, all CACZs greatly benefited in HVAC peak power demand reduction from cool walls.

4.1.2 United States

In the U.S., the warm climates benefitted the most from cool walls. In the case of new prototypes in the U.S., the differences in cool wall savings between locations also depended in the year of building code adopted by the states. For example, Phoenix, AZ (USCZ 2B), which has a warm climate, follows a building code that is 10+ years old. Thus, the prototypes simulated for USCZ 2B followed less stringent wall construction and HVAC efficiencies than the prototypes simulated in states that mandate newer building codes. Thus, climate zone 2B (Phoenix) benefitted the most from cool walls because it has a warm climate and the state follow 10+ year old building codes. USCZs 1A (Miami), 2A (Houston), 3A (Memphis), 3B (El Paso), 3C (San Francisco), 4A (Baltimore), and 4B (Albuquerque), were locations that also yielded cool wall savings from all vintages. The remaining U.S. climate zones are the coldest locations in the country, and experienced small cool wall energy savings and often yielded small energy penalties. However, all USCZs experienced cool wall HVAC peak power demand reduction.

4.2 Cool wall savings versus cool roof savings

Recall that in the California and U.S. case studies, the simulated increase in wall albedo (0.35) was 0.05 (16.7 percent) more than the increase in residential roof albedo (0.30), and was 0.05 (12.5 percent) less than the increase in commercial roof albedo (0.40). Thus, the differences in energy savings between cool walls and cool roofs were in part due to these differences in albedo increase.

4.2.1 California

In the older and oldest vintages of all prototypes, the east, south, and west walls yielded greater annual HVAC source energy savings intensities (per area of surface modified) than those from the roof. In these vintages, walls were built with significantly less thermal resistance than the roofs. Hence, although the roof in summer received more sunlight than any of the walls, the savings intensities from the roof were as small as those from the north wall, which was the wall that received the least sunlight in summer. In the new vintage prototypes, the wall annual HVAC savings intensities were greater than the roof savings in some of the prototypes.

The annual savings and penalty intensities were also influenced by the solar irradiation received by the individual faces. In summer, while the roof receives more daily solar irradiation than any of the four walls, the combined daily solar irradiation intercepted by the four walls was often equal or greater than the daily solar irradiation received by the roof. In winter, the solar path peaks in the southern sky at a small elevation angle; therefore, the roof receives less solar irradiation in winter than it does in summer and the south wall receives significantly more solar irradiation than it does in summer. Thus, the differences in savings and penalty intensities from the walls to those from the roof were influenced by the differences in thermal resistance and incident solar irradiation.

In prototypes with a large ratio of roof area to net wall area, whole-building annual HVAC savings from raising the albedo of all four walls were smaller than those from increasing roof albedo. The two retail prototypes and the sit-down restaurant had the largest roof area to net wall area ratios, which were at least 200 percent. In these three prototypes, the whole-building savings from the four walls were smaller than those from the roof in all three vintages. Conversely, buildings with a small roof area to net wall area ratio (e.g., the single-family home and apartment building) typically yielded whole-building wall savings that were greater than the roof savings. In the oldest vintage, the whole-building wall savings in the single-family home were up to 3.0 times that of the roof. In the new vintage, buildings with small roof area to net wall area ratio still had whole-building wall savings that were equal or greater than those from the roof.

4.2.2 United States

In all vintages, the magnitude of HVAC source energy changes from the east, south, and west walls yielded were always greater than that from the roof. In locations with warm climates (USCZ 1 to USCZ 4B), the east, south, and west walls in the single-family home yielded greater annual HVAC source energy savings intensities than those from the roof; savings intensities from the roof were similar to those from the north wall. In the U.S., the ratio of roof thermal resistance to wall thermal resistance varies widely between locations. The ratio of solar irradiation intercepted by the roof to that by each wall also varies widely between locations. Thus, the differences in HVAC savings intensities from the east, south, or west wall to those from the roof varied widely between USCZs. In locations with cold climates, the annual HVAC source energy penalty intensities from the north, east, and west wall were similar to those from the roof.

In the warm climates, increasing the albedo of all four walls led to annual HVAC source energy savings intensity that were comparable to those from increasing roof albedo. The differences in savings between the four-walls and the roof varied by building category, vintage, and location. In cold climates [USCZs 5B (Boise) to 8 (Fairbanks)], the changes (savings or penalties) in annual HVAC source energy from the north, east, or west walls were similar to those from the roof. In these cold climates, the south wall yielded annual HVAC source energy penalties greater than those from any other face.

As in California, the differences in whole-building savings from increasing the albedo of all walls to those from increasing the albedo of the roof were influenced by the roof area to net wall area ratio. In building prototypes with small roof area to net wall area ratio (e.g. single-family home), savings from increasing albedo of all walls were up to 2.5 times that from roofs.

4.3 Savings by wall orientation

All walls within a given prototype have the same thermal resistance. If each modified wall undergoes the same albedo change, differences by orientation in savings or penalty intensities

are driven by the differences in absorbed solar irradiation. For example, consider a building in the northern hemisphere. In summer, the east and west walls receive the most solar irradiation followed in descending order by the south wall and north wall. Under clear skies, the south wall will receive more beam sunlight in winter than in summer because the sun is lower, the wall's minimum beam incidence angle is smaller, and the wall is exposed to more hours of direct (beam) illumination.

4.3.1 California

The north wall always had the smallest cooling savings and heating penalty intensities. During the heating season, the north wall rarely yielded heating penalties; north wall generated heating penalties only in a few cases in CACZ 16.

The south wall was typically the wall with the greatest cooling savings intensity, followed closely by the west and east walls. However, the south wall typically had the greatest heating penalty intensities.

When considering the entire year, the wall with the greatest HVAC savings intensity varied by prototype and climate zone. In the commercial prototypes, the west wall, followed by the east wall, were typically the surfaces with the greatest annual HVAC saving intensities. In the residential prototypes, the greatest savings were from the south wall. However, the savings from the three walls (east, south, and west) were very similar to each other; thus, all three walls yielded significant savings from cool walls.

4.3.2 United States

As in California, the north wall in the single-family home always had the smallest cooling savings and heating penalty intensities, leading to the smallest annual HVAC savings or penalties. During the cooling season, all walls in every U.S. climate zone yielded cooling savings. The wall orientation with the greatest cooling savings varied by location, but it was either the east, south, or west wall. However, these three wall orientations typically yielded similar cooling savings. During the heating season, all walls in every U.S. climate zone yielded heating penalties; however, the penalties were significantly greater from the south wall compared to those from the other walls.

When considering annual HVAC source energy, all walls in the single-family home yielded savings from USCZ 1A (Miami) to USCZ 4B (Albuquerque). In USCZs 6B (Helena), 7 (Duluth), and 8 (Fairbanks), every wall led to annual HVAC energy penalties or to no change in HVAC energy. The south wall led to annual HVAC energy penalties from USCZ 4C (Seattle) to USCZ 8 (Fairbanks).

4.4 Savings by vintage and building geometry

4.4.1 California

The oldest vintage always yielded the greatest cool wall savings intensities, followed by the older vintage. As mentioned before, this is because walls in these vintages were built with substantially less insulation that required in new construction. The older and oldest vintages were also simulated with HVAC efficiencies that comply with 10+ year old building codes. These older and oldest vintage results are important because in California, they represent over 75 percent of the current residential building stock and about 70 percent of the commercial building stock. Cool walls in the new vintage prototypes still yielded significant annual HVAC savings intensities, which were comparable to the savings intensities from cool roofs.

Whole-building savings scale with wall area. Thus, whole-building wall savings will increase with building height. Even prototypes with a large window-to-wall area ratio (i.e., medium and large offices) benefited from cool walls since these were tall multi-level buildings with a large net wall area.

4.4.2 United States

For most building categories in the U.S., the oldest vintage yielded greater cool wall savings or penalty intensities than the other vintages. In buildings like the retail stand-alone, which the wall type and wall construction varied by vintage, the vintage yielding the greatest annual HVAC energy changes varied by U.S. climate zone.

For the case of new vintage, some U.S. climate zones were simulated in states which mandate building codes that are 10 to 13 years old (Table 3). In these U.S. climate zones, the prototypes were simulated with HVAC efficiencies comparable to those used in the older and oldest vintages. Additionally, the prototypes in these U.S. climate zones were simulated with less envelope thermal resistances than those used in the rest of the U.S. climate zones. Thus, in these U.S. climate zones that follow 10+ year old building codes, the annual HVAC source energy savings from the new vintage were often close to those from the older vintage.

4.5 Additive property of cool wall savings

4.5.1 California and United States

While the annual cooling savings were usually additive, the annual heating penalties and fan savings were sometimes non-additive. When investigating why the gas heating and fan were often non-additive, we delved into a few analyses that considered (a) auto-sized vs fixed size HVAC system and (b) hourly energy uses from each HVAC component.

In many prototypes, the fan drew constant load irrespective of changes to cooling or heating load. Therefore, fan energy use lacked any sensitivity to changes in cooling and heating energy

changes. In these cases, annual HVAC energy changes were close to additive when fan energy was not included.

The additive tests indicate that it is worth exploring further this matter, since for most prototypes and in most locations, annual HVAC energy savings were close to being fully additive. If savings from individual walls are in fact additive, this will simplify estimation of cool wall savings for any of the 15 possible wall combinations. As an example, assume we are interested in knowing the savings from modifying all walls of a building. If savings are additive, the savings from modifying all walls are obtained by adding the individual savings from each of the four walls. The same approach can be applied to obtain the savings from any other wall combination.

5 Conclusions

This report presents an exhaustive study on the effects of cool walls in individual buildings in all California and U.S. climate zones. The work investigated how cool walls may lead to changes in site energy use, source energy use, pollutant emissions, energy cost, and HVAC peak power demand. As we expected, the magnitude of savings and penalties from cool walls depend on key factors, including climate, wall construction, wall orientation, building orientation, and HVAC efficiency. The influence of each of these factors on cool wall savings were investigated by simulating: (a) 31 different climate zones across California and U.S.; (b) three different building vintages (oldest, older, and new) that followed building codes adopted in each location and vintage; (c) 15 different wall combinations; and (d) two different building orientations.

5.1 California

In California, cool walls led to annual HVAC source energy savings in all 16 climate zones. Consequently, all California climate zones also yielded savings in pollutant emissions and energy cost. All CACZs also experienced HVAC peak power demand reduction. The locations that yielded the greatest cool wall savings intensities were climate zones 14 (China Lake) and 15 (Imperial), which are locations with a long and warm cooling season, and short and mild heating season. The smallest cool wall savings intensities were from California climate zones 1 (Arcata) and 16 (Mount Shasta), which are the two coldest locations in the state.

Cool walls benefitted the oldest vintage prototypes significantly more than the older and new vintage prototypes; cool walls in the oldest single-family home led up to 25 percent (CACZ 7, San Diego) in annual HVAC source energy savings. Among all vintages, cool walls reduced whole-building annual HVAC energy use 3.0 percent to 25 percent in single-family homes, 0.5 percent to 3.7 percent in medium offices, and 0.0 percent to 9.0 percent in stand-alone retail stores. Energy use, emissions, and energy cost savings from the oldest vintage were generally three to six times greater than those from the new vintage. The cool wall savings from the oldest vintage are important since they represent over 60 percent of California's building stock.

Past and present California building codes prescribe more insulation in roofs than in walls. Additionally, in any annual season, the combined solar energy received by the four walls is more than the solar energy received by the roof. Hence, the energy use, emissions, and energy cost savings from cool walls are comparable to those from cool roofs even in buildings with a large ratio of roof area to net wall area. In buildings with small ratio of roof area to net wall area, the savings from cool walls were often significantly greater than those from cool roof. In the single-family home, which had small ratio of roof area to net wall area, the whole-building cool walls to cool roof HVAC source energy savings ratio were 1.5 to 3.5. The medium office and stand-alone retail had large ratio of roof area to net wall area; the whole-building cool walls to cool roof HVAC source energy savings ratio were 0.40 to 1.0 in medium offices, and 0.20 to 0.85 in stand-alone retail stores. Thus, the differences in savings between cool walls and cool roofs are highly dependent on two building characteristics: (a) roof and wall insulation, and (b) ratio of roof area to net wall area.

The south wall always led to the largest heating penalties; however, it also led to large savings during the cooling season. Annually, the savings from the south wall were similar to those from the east wall and west wall. These savings from the east, south, and west walls were always greater than those from the north wall. Therefore, the east, south, and west walls are the most crucial when considering adopting cool walls in any region in California.

5.2 United States

In the U.S., climate zone 2B (Phoenix) benefitted the most from cool walls because it has a warm climate and the state follows 10+ year old building codes. USCZs 1A (Miami), 2A (Houston), 3A (Memphis), 3B (El Paso), 3C (San Francisco), 4A (Baltimore), and 4B (Albuquerque), were locations that also yielded cool wall whole-building savings and savings intensities from all vintages. The remaining U.S. climate zones are the coldest locations in the country, and experienced small cool wall savings and often yielded small penalties.

As in California, the oldest vintage yielded greater cool wall savings or penalties than the other vintages. This is important since the oldest vintage buildings represent in most U.S. locations at least 60 percent of the building stock. In warm U.S. climate zones [1A (Miami, FL) to 4B (Albuquerque, NM)], cool walls in all vintages reduced whole-building annual HVAC energy use 2.0 percent to 8.5 percent in single-family homes, 0.0 percent to 4.2 percent in medium offices, and -0.5 percent to 5 percent in stand-alone retail stores. Cool walls also led to small annual HVAC source energy savings in cold United States climate zones [4C (San Francisco, CA) to 7 (Duluth, MN)] in some building categories and vintages.

The east, south, and west walls typically had similar savings, which in turn were greater than those from the north wall. Additionally, cool wall savings were similar, and sometimes much greater, than those from the cool roof. In warm U.S. climate zones [1A (Miami, FL) to 4B (Albuquerque, NM)], the ratio of whole-building cool wall savings to cool roof savings were 1.1

to 3.0 in single-family homes, 0.20 to 1.9 in medium offices, and 0.30 to 2.1 in stand-alone retail stores

This study demonstrated that in the U.S., all buildings of any vintage from USCZ 1A (Miami) to USCZ 4B (Albuquerque) would benefit from cool walls, especially on the east, south, and west faces. Additionally, all USCZs will benefit from a reduction in HVAC peak power demand.

6 Future work

Future work should further investigate the additive nature of cool wall savings, examining those simulations in which the cool wall savings were not additive. It should also explore how shadows casted and sunlight reflected by neighboring buildings influence cool wall savings.

The current study also provides the foundation for two new Codes and Standards Enhancement (CASE) studies for California's Title 24 building energy efficiency standards. The first CASE study should evaluate the prescription of cool walls for commercial and residential buildings. The second CASE study should consider the prescription of cool roofs for residential cool roof retrofits.

Finally, the current study can serve as a roadmap to any future work interested in the effect of cool walls in regions outside of U.S.

7 References

Abood AA. 2015. A comprehensive solar angles simulation and calculation using MATLAB *International Journal of Energy and Environment* 6(4), 367-376.

Akbari H, Konopacki S, Pomerantz M. 1999. Cooling energy savings potential of reflective roofs for residential and commercial buildings in the United States. *Energy* 24, 391 – 407. https://doi.org/10.1016/S0360-5442(98)00105-4

Akbari H, Konopacki S. 2005. Calculating energy-saving potentials of heat-island reduction strategies. *Energy Policy* 33, 721 – 756. https://doi.org/10.1016/j.enpol.2003.10.001

ASHRAE. 2001. ANSI/ASHRAE/*IES Standard 90.1-2001—Energy Standard for Buildings Except Low-Rise Residential Buildings*. American Society of Heating, Refrigerating, and Air-Conditioning Engineers. Atlanta, GA.

ASHRAE. 2002. ASHRAE Guideline 14-2002, Measurement of Energy and Demand Savings, American Society of Heating, Refrigerating, and Air-Conditioning Engineers, Atlanta, GA.

Bhatia A, Mathur J, Garg V. 2011. Calibrated simulation for estimating energy savings by the use of cool roof in five Indian climatic zones. *Journal of Renewable Sustainable Energy* 3, 023108. http://dx.doi.org/10.1063/1.3582768

BCAP 2017. Code Status Maps. Building Codes Assistance Project (BCAP). Retrieved 2017-01 from https://bcapcodes.org/code-status/

Blum J. 2007. Roof insulation R-values for commercial buildings under ASHRAE and "above-code" standards. *RCI Interface*, 31-36. November 2007. Retrieved from http://rci-online.org/wp-content/uploads/2016/04/2007-11-blum.pdf

Boixo S, Diaz-Vicente M, Colmenar A, Castro MA. 2012. Potential energy savings from cool roofs in Spain and Andalusia. *Energy* 38, 425 – 438. https://doi.org/10.1016/j.energy.2011.11.009

Briggs RL, Lucas RG, Taylor ZT. 2003a. Climate Classification for Building Energy Codes and Standards: Part 1—Development Process. ASHRAE Transactions, 109(1).

Briggs RL, Lucas RG, Taylor ZT. 2003b. Climate Classification for Building Energy Codes and Standards: Part 2—Zone Definitions, Maps, and Comparisons. ASHRAE Transactions 109(2).

CEC. 1988. 1988 Building Energy Efficiency Standards. Publication CEC-400-1988-001, California Energy Commission, Sacramento, CA. Retrieved 2015-12-10 from http://www.energy.ca.gov/title24/standards_archive/

CEC. 2005. 2005 Building Energy Efficiency Standards for Residential and Nonresidential Buildings. Publication CEC-400-2006-015, California Energy Commission, Sacramento, CA. Retrieved 2015-12-10 from http://www.energy.ca.gov/title24/standards_archive/

CEC. 2015. California Building Climate Zone Areas. California Energy Commission, Sacramento, CA. Retrieved 2015-12-10 from http://www.energy.ca.gov/maps/renewable/building_climate_zones.html

CEC. 2016a. 2016 Nonresidential compliance manual. Publication CEC-400-2015-033-CMF, California Energy Commission, Sacramento, CA. Retrieved 2016-01 from http://www.energy.ca.gov/title24/

CEC. 2016b. 2016 Residential compliance manual. Publication CEC-400-2015-032-CMF, California Energy Commission, Sacramento, CA. Retrieved 2016-01 from http://www.energy.ca.gov/title24/

CEC. 2016c. 2016 Building Energy Efficiency Standards for Residential and Nonresidential Buildings. Publication CEC-400-2015-037-CMF, California Energy Commission, Sacramento, CA. Retrieved 2016-01 from http://www.energy.ca.gov/title24/

CEC. 2016d. 2016 Reference Appendices. Publication CEC-400-2015-038-CMF, California Energy Commission, Sacramento, CA. Retrieved 2016-01 from http://www.energy.ca.gov/title24/

CEC. 2016d. 2016 Residential Alternative Calculation Method (ACM) Reference Manual. Publication CEC-400-2015-024-CMF-REV3, California Energy Commission, Sacramento, CA. Retrieved 2016-06 from http://www.energy.ca.gov/title24/

Comfort-Pro. 2015. What is the Life Expectancy of My HVAC System? [Blog post]. Posted March 12, 2015. Retrieved from https://www.comfort-pro.com/2015/03/what-is-the-life-expectancy-of-my-hvac-system/

Deru M, Field K, Studer D, Benne K, Griffith B, Torcellini P, Liu B, Halverson M, Winiarski D, Rosenberg M, Yazdanian M, Huang J, Crawley D. 2011. US Department of Energy commercial reference building models of the national building stock. Technical report NREL/TP-5500-46861, National Renewable Energy Laboratory, Golden, CO. Retrieved 2015-12 from http://energy.gov/eere/buildings/commercial-reference-buildings

ECOX. 2017. What is seasonal efficiency ratio (SEER)? – Technical Information Bulletin No. E-004-EN. ECOX Line. Retrieved from www.galpaexport.com/media/downloads/45.pdf

EIA. 2009. Residential energy consumption survey (RECS) – public use microdata. US Energy Information Administration Washington, DC. Retrieved 2015-12-10 from http://www.eia.gov/consumption/residential/data/2009/

EIA. 2012. Commercial Building Energy Consumption Survey (CBECS) – public use microdata. US Energy Information Administration, Washington, DC. Retrieved 2016-09-01 from http://www.eia.gov/consumption/commercial/data/2012/

EIA 2016a. Annual average retail price of electricity to ultimate customers by state, sector, and year. US Energy Information Administration, Washington, DC. Retrieved from https://www.eia.gov/electricity/data.php#sales

EIA 2016b. Annual natural gas price by state and year. US Energy Information Administration, Washington, DC. Retrieved from https://www.eia.gov/naturalgas/data.cfm

EIA 2017. Units and Calculators – Degree Days. US Energy Information Administration, Washington, DC. Retrieved 2017-06-30 from https://www.eia.gov/energyexplained/index.cfm?page=about_degree_days

eGRID 2014. 2014 Emissions & Generation Resource Integrated Database (eGRID). United States Environmental Protection Agency (EPA). Retrieved from https://www.epa.gov/energy/emissions-generation-resource-integrated-database-egrid

EnergyPlus. 2003. EnergyPlus version 8.5. Downloaded from https://energyplus.net/

Gao Y, Xu J, Yang S, Tang X, Zhou Q, Ge J, Xu T, Levinson R. 2014. Cool roofs in China: Policy review, building simulations, and proof-of-concept experiments. *Energy Policy* 74, 190 – 214. https://doi.org/10.1016/j.enpol.2014.05.036

Huang J, Hanford JW, and Yang F. 1999. Residential heating and cooling loads component analysis. LBNL-44636. Lawrence Berkeley National Laboratory, Berkeley CA.

Huang J. 2013. Explanation of California Energy Commission's new CZ2010 weather files [Blog post]. Posted July 13, 2013 in Energy Models – Instruction and Discussion for Energy Modelers. Retrieved from http://energy-models.com/forum/explanation-california-energy-commissions-new-cz2010-weather-files

Hunn BD. 2010. 35 Years of Standard 90.1. ASHRAE Journal. American Society of Heating, Refrigerating, and Air-Conditioning Engineers. March 2010. Retrieved from https://www.ashrae.org/resources--publications/bookstore/90-1---celebrating-35-years-of-energy-efficiency

IECC. 2006. 2006 International Energy Conservation Code. International Code Consortium. January 2006. Retrieved from https://archive.org/details/gov.law.icc.iecc.2006

jEPlus. 2015. jEPlus v1.6.0 – An EnergyPlus simulation manager for parametrics. Downloaded 2015-12 from http://www.jeplus.org/wiki/doku.php

JESS. 2015. JESS – jEPlus Simulation Server. Downloaded 2015-12 from http://www.jeplus.org/wiki/doku.php

Levinson R, Akbari H. 2010. Potential benefits of cool roofs on commercial buildings: conserving energy, saving money, and reducing emission of green-house gases and air pollutants. *Energy Efficiency* 3(1), 53 – 109. https://doi.org/10.1007/s12053-008-9038-2

Moujaes SF, Brickman R. 2003. Thermal performance analysis of highly reflective coating on residences in hot and arid climates. *Journal of Energy Engineering* 129, 56 – 68. https://doi.org/10.1061/(ASCE)0733-9402(2003)129:2(56)

NREL 2017. PVWatts Calculator Model. National Renewable Energy Laboratory (NREL). Retrieved from http://pvwatts.nrel.gov/.

Parker D, Huang Y, Konopacki S, Gartland L, Sherwin J, Gu L. 1998. Measured and simulated performance of reflective roofing systems in residential buildings. *ASHRAE Transactions* 104(1), 963 – 975. http://www.fsec.ucf.edu/en/publications/html/FSEC-PF-331-98

Petrie TW, Atchley JA; Childs PW, Desjarlais AO. 2007. Energy savings for stucco walls coated with cool colors. Proceedings of Thermal Performance of Exterior Envelopes of Whole Buildings

X, December 2 – 7, Clearwater, FL. https://www.coolrooftoolkit.org/knowledgebase/energy-savings-for-stucco-walls-coated-with-cool-colors/

PNNL. 2016a. Residential Prototype Building Models. Pacific Northwest National Laboratory, Richland, WA. Retrieved 2015-10 from https://www.energycodes.gov/development/residential/iecc_models

PNNL. 2016b. Commercial Prototype Building Models. Pacific Northwest National Laboratory, Richland, WA. Retrieved 2015-10 from https://www.energycodes.gov/development/commercial/prototype_models

Rosado PJ. 2016. *Evaluating Cool Impervious Surfaces: Application to an Energy-Efficient Residential Roof and to City Pavements* (Doctoral dissertation). University of California, Mechanical Engineering Department. Retrieved from http://escholarship.org/uc/item/6bf80485

SBT 2017. What is the difference between CO2 and CO2e?. Sustainable Business Toolkit. Retrieved from https://www.sustainablebusinesstoolkit.com/difference-between-co2-and-co2e/

Schroeder DV. 2011. Understanding the seasons: the sun and the seasons. College of Science, Weber State University. Retrieved from http://physics.weber.edu/schroeder/ua/sunandseasons.html

GTI. 2017. Carbon Management Information Center Source Energy and Emissions Analysis Tool (SEEAT), Version 7.3, Gas Technology Institute. Copyright 2017. Retrieved 2017-05 from http://www.cmictools.com/cmicec/default.aspx

Sleiman M, Ban-Weiss G, Gilbert HE, Francois D, Berdahl P, Kirchstetter TW, Destaillats H, Levinson R. 2011. Soiling of building envelope surfaces and its effect on solar reflectance—Part I: Analysis of roofing product databases. *Solar Energy Materials & Solar Cells* 95, 3385-3399.

Synnefa A, Santamouris M, Akbari H. 2007. Estimating the effect of using cool coatings on energy loads and thermal comfort in residential buildings in various climatic conditions. *Energy and Buildings* 39, 1167 – 1174. https://doi.org/10.1016/j.enbuild.2007.01.004

UO SRML. 2008. Polar sun chart program. University of Oregon Solar Radiation Monitoring Laboratory. Retrieved from http://solardat.uoregon.edu/PolarSunChartProgram.html

WBT. 2011. White Box Technologies – weather data for energy calculations. Retrieved 2015-12-10 from http://weather.whiteboxtechnologies.com/

Wikipedia. 2017. Thermal bridge. Retrieved 2017-06 from https://en.wikipedia.org/wiki/Thermal_bridge

Wilcox S, Marion W. 2008. User's Manual for TMY3 Data Sets, NREL/TP-581-43156. April 2008. Golden, Colorado: National Renewable Energy Laboratory.

Task Report Appendix A: Building stock age distribution

The latest available version of the Commercial Building Energy Consumption Survey (CBECS) is 2012 (EIA 2012). We used the microdata from CBECS 2012 to calculate the age distribution of existing commercial buildings in different U.S. locations. Table A-2 through Table A-6 give the age distribution of different building types related to the commercial prototypes used in this study. All buildings were grouped into four age periods (<1980, 1980-1989, 1990-1999, and 2000-2012). The darkness of the green in the cells of the tables increases with the number of buildings in the age group (see color legend in Table A-1). The tables show that in most locations and for most building types, the majority of the buildings are from <1980, 1980-1989, and 2000-2012.

The latest version of the Residential Energy Consumption Survey (RECS) available with microdata when our study began was 2009 (EIA 2009). We used the microdata from RECS 2009 to calculate the age distribution of existing single-family home (Table A-7) and apartment buildings (Table A-8) in different U.S. states. All buildings were grouped into five age periods (<1980, 1980-1989, 1990-1999, 2000-2004, and 2005-2009). As done with the commercial buildings, the darkness of the green in the table cells increases with the number buildings in each age group.

Table A-1. Legend for color scheme in Table A-2 through Table A-8.

Color	Fraction of existing buildings [%]
	> 30
	20-30
	10-20
	< 10

Table A-2. Age distribution of offices by U.S. census division computed using CBECS 2012.

CBECS building category: office **Related EnergyPlus building categories: small office, medium office, large office**					
Census Division	**Representative cities (USCZ)**	**< 1980 [%]**	**1980-1989 [%]**	**1990-1999 [%]**	**2000-2012 [%]**
South Atlantic	Miami (1A) Baltimore (4A)	43	24	11	21
West South Central	Houston (2A) El Paso (3B)	39	26	11	24
Mountain	Phoenix (2B) Albuquerque (4B) Boise (5B) Helena (6B)	40	13	19	28
East South Central	Memphis (3A)	51	22	11	17
Pacific	San Francisco (3C) Salem (4C) Fairbanks (8)	51	23	15	11
East North Central	Chicago (5A)	59	12	18	12
New England	Burlington (6A)	60	18	9	13
West North Central	Duluth (7)	58	15	14	13

Table A-3. Age distribution of retail stores (no malls) by U.S. census division computed using CBECS 2012.

CBECS building category: retail other than mall Related EnergyPlus building category: stand-alone retail					
Census Division	**Representative cities (USCZ)**	**< 1980 [%]**	**1980-1989 [%]**	**1990-1999 [%]**	**2000-2012 [%]**
South Atlantic	Miami (1A) Baltimore (4A)	46	20	12	23
West South Central	Houston (2A) El Paso (3B)	47	9	21	24
Mountain	Phoenix (2B) Albuquerque (4B) Boise (5B) Helena (6B)	35	33	12	19
East South Central	Memphis (3A)	45	21	23	11
Pacific	San Francisco (3C) Salem (4C) Fairbanks (8)	68	7	12	13
East North Central	Chicago (5A)	50	22	8	20
New England	Burlington (6A)	69	7	15	10
West North Central	Duluth (7)	63	18	5	14

Table A-4. Age distribution of strip shopping malls by U.S. census division computed using CBECS 2012.

CBECS building category: strip shopping mall Related EnergyPlus building category: retail strip mall					
Census Division	**Representative cities (USCZ)**	**< 1980 [%]**	**1980-1989 [%]**	**1990-1999 [%]**	**2000-2012 [%]**
South Atlantic	Miami (1A) Baltimore (4A)	38	25	9	28
West South Central	Houston (2A) El Paso (3B)	54	8	12	26
Mountain	Phoenix (2B) Albuquerque (4B) Boise (5B) Helena (6B)	32	6	1	62
East South Central	Memphis (3A)	11	49	22	18
Pacific	San Francisco (3C) Salem (4C) Fairbanks (8)	43	13	11	34
East North Central	Chicago (5A)	45	12	29	14
New England	Burlington (6A)	65	11	15	10
West North Central	Duluth (7)	49	39	7	5

Table A-5. Age distribution of sit-down and fast-food restaurants by U.S. census division computed using CBECS 2012.

CBECS building category: Food service Related EnergyPlus building categories: sit-down restaurant, fast-food restaurant					
Census Division	**Representative cities (USCZ)**	**< 1980 [%]**	**1980-1989 [%]**	**1990-1999 [%]**	**2000-2012 [%]**
South Atlantic	Miami (1A) Baltimore (4A)	39	15	19	27
West South Central	Houston (2A) El Paso (3B)	40	16	30	14
Mountain	Phoenix (2B) Albuquerque (4B) Boise (5B) Helena (6B)	57	15	8	20
East South Central	Memphis (3A)	42	26	13	20
Pacific	San Francisco (3C) Salem (4C) Fairbanks (8)	64	10	17	9
East North Central	Chicago (5A)	54	19	17	9
New England	Burlington (6A)	66	10	17	8
West North Central	Duluth (7)	48	7	16	29

Table A-6. Age distribution of hotels by U.S. census division computed using CBECS 2012.

CBECS building category: lodging Related EnergyPlus building category: large hotel					
Census Division	**Representative cities (USCZ)**	**< 1980 [%]**	**1980-1989 [%]**	**1990-1999 [%]**	**2000-2012 [%]**
South Atlantic	Miami (1A) Baltimore (4A)	60	21	5	15
West South Central	Houston (2A) El Paso (3B)	39	23	26	12
Mountain	Phoenix (2B) Albuquerque (4B) Boise (5B) Helena (6B)	61	6	17	15
East South Central	Memphis (3A)	76	4	14	6
Pacific	San Francisco (3C) Salem (4C) Fairbanks (8)	58	21	10	11
East North Central	Chicago (5A)	36	9	19	35
New England	Burlington (6A)	32	7	12	49
West North Central	Duluth (7)	40	18	2	39

Table A-7. Age distribution of detached single-family homes by state or group of states computed using RECS 2009.

RECS building category: single-family detached Related EnergyPlus building category: single-family home						
RECS reported state or group of states	**Representative cities (USCZ)**	**< 1980 [%]**	**1980-1989 [%]**	**1990-1999 [%]**	**2000-2004 [%]**	**2005-2009 [%]**
Florida	Miami (1A)	45	17	16	14	8
Texas	Houston (2A) El Paso (3B)	50	16	15	11	8
Arizona	Phoenix (2B)	30	16	31	15	8
Tennessee	Memphis (3A)	51	10	18	11	10
California	San Francisco (3C)	67	13	12	5	4
Delaware, District of Columbia, Maryland, Virginia	Baltimore (4A)	59	16	19	4	2
Nevada, New Mexico	Albuquerque (4B)	36	21	25	7	10
Alaska, Hawaii, Oregon, Washington	Seattle (4C) Fairbanks (8)	51	14	17	10	8
Illinois	Peoria (5A)	66	10	8	13	2
Idaho, Montana, Utah, Wyoming	Boise (5B) Helena (6B)	47	25	15	3	10
Connecticut, Maine, New Hampshire, Rhode Island, Vermont	Burlington (6A)	69	13	8	8	3
Iowa, Minnesota, North Dakota, South Dakota	Duluth (7)	64	11	13	6	6

Table A-8. Age distribution of apartment buildings by state or group of states computed using RECS 2009.

RECS building category: apartment building with 5+ units Related EnergyPlus building category: apartment building						
RECS reported state or group of states	**Representative cities (USCZ)**	**< 1980 [%]**	**1980-1989 [%]**	**1990-1999 [%]**	**2000-2004 [%]**	**2005-2009 [%]**
Florida	Miami (1A)	46	25	13	8	8
Texas	Houston (2A) El Paso (3B)	56	24	9	5	7
Arizona	Phoenix (2B)	29	26	17	11	19
Tennessee	Memphis (3A)	43	18	30	4	5
California	San Francisco (3C)	65	19	10	3	3
Delaware, District of Columbia, Maryland, Virginia	Baltimore (4A)	56	7	10	18	8
Nevada, New Mexico	Albuquerque (4B)	0	14	0	29	57
Alaska, Hawaii, Oregon, Washington	Seattle (4C) Fairbanks (8)	52	22	18	7	1
Illinois	Peoria (5A)	62	5	20	3	9
Idaho, Montana, Utah, Wyoming	Boise (5B) Helena (6B)	9	73	18	0	0
Connecticut, Maine, New Hampshire, Rhode Island, Vermont	Burlington (6A)	67	29	1	3	0
Iowa, Minnesota, North Dakota, South Dakota	Duluth (7)	55	22	13	5	6

Task Report Appendix B: Building prototype characteristics

Table B-1 illustrates the 10 prototypes used in the study.

Table B-1. Sketches of building category prototypes.

Single-family home	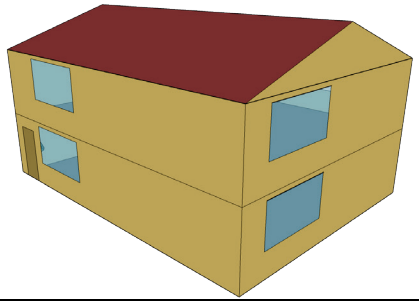
Apartment building	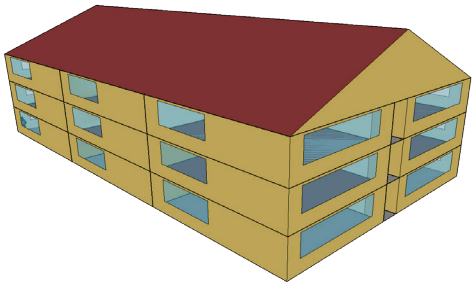
Large hotel	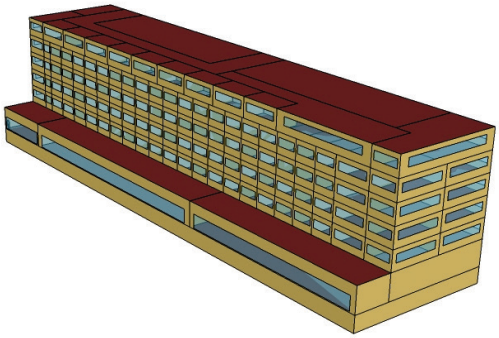
Large office	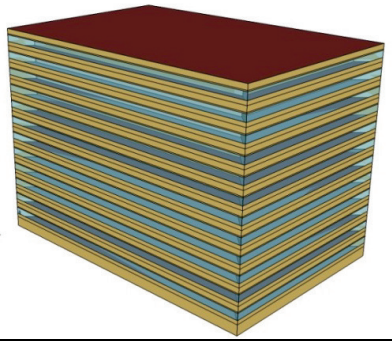

Medium office	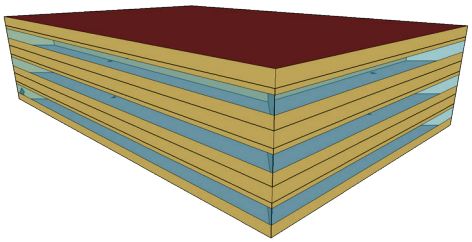
Small office	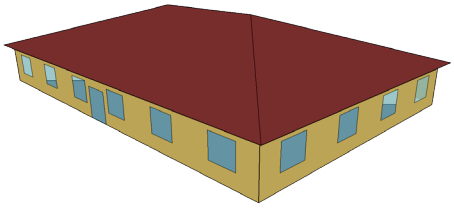
Fast-food restaurant	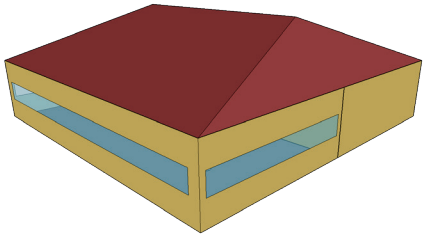
Sit-down restaurant	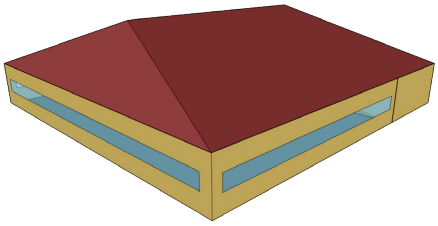
Retail stand-alone	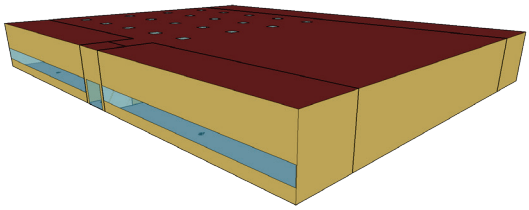
Strip mall retail	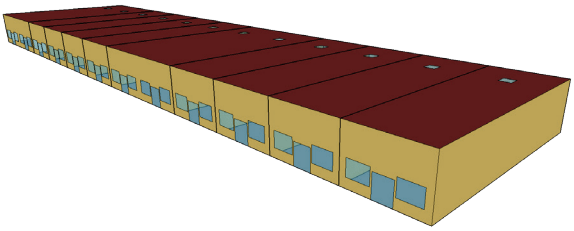

Table B-2 describes the geometry, envelope construction, and HVAC system for each vintage of the single-family home. Details of the internal loads (e.g. persons, lighting, equipment) and their hourly schedules are further described in the EnergyPlus single-family home prototypes.

Table B-2. Geometry, envelope construction, and HVAC system for each vintage of the single-family home.

Property	Oldest vintage	Older vintage	New vintage
General building characteristics			
Conditioned floor area (m²)	223	Same	Same
Roof area (m²)	118	Same	Same
Number of stories	2	Same	Same
Ratio of roof area to net wall area [a]	0.61	Same	Same
Ratio of window area to net wall area	0.15	Same	Same
Roof albedo			
Base case	0.10	Same	Same
Alternative cases	0.25, 0.40, and 0.60	Same	Same
Roof thermal emittance	0.90	Same	Same
Roof construction			
Thermal resistance (m²·K/W) [ft²·°F·h/BTU]			
Asphalt shingles	0.077 [0.440]	Same	Same
1/2” oriented strand board (OSB)	0.109 [0.620]	Same	Same
Attic			
Rise to run [slope]	4:12 [18.4°]	Same	Same
Ceiling construction (top to bottom)			
Thermal resistance (m²·K/W) [ft²·°F·h/BTU]			
Insulated wood frame (10% framing factor)	Varies by climate zone (Table C-3 &Table C-6)	Same	Same
1/2” drywall	0.079 [0.450]	Same	Same
Wall construction (outside to inside)			
Thermal resistance (m²·K/W) [ft²·°F·h/BTU]			
Stucco	0.018 [0.103]	Same	Same
Paper felt	0.011 [0.060]	Same	Same
Sheathing	0.135 [0.767]	Same	Same
5/8” OSB	0.137 [0.775]	Same	Same

Insulated wood frame (15% framing factor)		Varied by climate zone (Table C-2 &Table C-5)		Same		Same
1/2” drywall		0.079 [0.450]		Same		Same
Net wall area when long-axis of building extends east-west (m²)						
North		52.9		Same		Same
East		39.2		Same		Same
South		52.9		Same		Same
West		39.2		Same		Same
Foundation		Slab		Same		Same
Windows						
Thermal transmittance (W/m²·K)		Varies by climate zone and orientation		Same		Same
Visible transmittance		Varies by climate zone and orientation		Same		Same
Window area when long-axis of building extends east-west (m²)						
North		8.29		Same		Same
East		8.29		Same		Same
South		8.29		Same		Same
West		8.29		Same		Same
Effective air leakage area (cm²)						
Living unit		842		Same		Same
Attic		370		Same		Same
HVAC system						
Air conditioner		Direct expansion unitary system		Same		Same
California						
SEER (BTU/Wh)		10		10		14
Estimated COP [b] (Wh/Wh)		2.64		2.64		3.69
U.S.						
SEER (BTU/Wh)		10		10		10 to 13 (varies by climate zone)
Estimated COP [b] (Wh/Wh)		2.64		2.64		2.64 to 3.43 (varies by climate zone)
Gas furnace (California and U.S.)						
Annual Fuel Utilization Efficiency (AFUE) (%)		0.80		Same		Same
Electric heating (U.S.)						
COP		3.04		3.04		3.04 to 3.26 (varies by climate zone)

Distribution						
Type		Single-zone constant air volume		Same		Same
Design flow rate (m^3/s)		0.0283		Same		Same
Maximum number of occupants		3		Same		Same

[a] Net wall area excludes windows and doors.

[b] To obtain COP, divide SEER by 3.79 (ECOX 2017).

Table B-3 describes the geometry, envelope construction, and HVAC system for each vintage of the medium office. Details of the internal loads (e.g. persons, lighting, equipment) and their hourly schedules are further described in the EnergyPlus medium office prototypes.

Table B-3. Details on the geometry, envelope construction, and HVAC system for each vintage of the medium office.

Property		Oldest vintage		Older vintage		New vintage
General building characteristics						
Conditioned floor area (m^2)		4,980		Same		Same
Roof area (m^2)		1,660		Same		Same
Number of stories		3		Same		Same
Ratio of roof area to net wall area [a]		1.25		Same		Same
Ratio of window area to net wall area		0.33		Same		Same
Roof albedo						
Base case		0.20		Same		Same
Alternative cases		0.10, 0.25, 0.40, and 0.60		Same		Same
Roof thermal emittance		0.90		Same		Same
Roof construction						
Thermal resistance ($m^2 \cdot K/W$) [$ft^2 \cdot °F \cdot h/BTU$]						
Built-up roofing		0.059 [0.337]		Same		Same
Insulation above deck		Varies by climate zone (Table C-3 &Table C-6)		Same		Same
Metal surface		0.000 [0.000]		Same		Same
Wall construction (outside to inside)						
Thermal resistance ($m^2 \cdot K/W$) [$ft^2 \cdot °F \cdot h/BTU$]						
Stucco		0.035 [0.200]		Same		Same
Gypsum board		0.079 [0.451]		Same		Same
Insulated metal frame		Varies by climate zone (Table C-2 &Table C-5)		Same		Same

Gypsum board		0.079 [0.451]		Same		Same
Net wall area when long-axis of building extends east-west (m^2)						
North		398		Same		Same
East		265		Same		Same
South		398		Same		Same
West		265		Same		Same
Foundation type		Slab		Same		Same
Windows						
Thermal transmittance ($W/m^2 \cdot K$)		Varies by climate zone and orientation		Same		Same
Visible transmittance		Varies by climate zone and orientation		Same		Same
Window area when long-axis of building extends east-west (m^2)						
North		0.00		Same		Same
East		0.00		Same		Same
South		83.9		Same		Same
West		0.00		Same		Same
HVAC system						
Air conditioner						
California						
SEER (BTU/Wh)						
Estimated COP [b] (Wh/Wh)		Precision air conditioning unit		Same		Same
U.S.						
Estimated SEER [b] (BTU/Wh)		14		14		15
COP (Wh/Wh)		3.78		3.78		3.95
Gas furnace						
Annual Fuel Utilization Efficiency (AFUE) (%)		11		11		12 to 13 (varies by climate zone)
Electric heating		2.84		2.84		3.23 to 3.40 (varies by climate zone)
COP						
Distribution		0.80		Same		Same
Type						
		3.78		3.78		3.95
		Multi-zone variable air volume		Same		Same

[a] Net wall area excludes windows and doors.

[b] To obtain COP, divide SEER by 3.79 (ECOX 2017).

Table B-4 describes the geometry, envelope construction, and HVAC system for each vintage of the stand-alone retail. Details of the internal loads (e.g. persons, lighting, equipment) and their hourly schedules are further described in the EnergyPlus stand-alone retail prototypes.

Table B-4. Details on the geometry, envelope construction, and HVAC system for each vintage of the stand-alone retail.

Property	Oldest vintage	Older vintage	New vintage
General building characteristics			
Conditioned floor area (m^2)	2,290	Same	Same
Roof area (m^2)	2,290	Same	Same
Number of stories	1	Same	Same
Ratio of roof area to net wall area [a]	2.07	Same	Same
Ratio of window area to net wall area	0.07	Same	Same
Roof albedo			
Base case	0.20	Same	Same
Alternative cases	0.10, 0.25, 0.40, and 0.60	Same	Same
Roof thermal emittance	0.90	Same	Same
Roof construction			
Thermal resistance ($m^2 \cdot K/W$) [$ft^2 \cdot °F \cdot h/BTU$]			
Built-up roofing	0.059 [0.337]	Same	Same
Insulation above deck	Varies by climate zone (Table C-3 &Table C-6)	Same	Same
Metal surface	0.000 [0.000]	Same	Same
Wall construction in California (outside to inside)			
Thermal resistance ($m^2 \cdot K/W$) [$ft^2 \cdot °F \cdot h/BTU$]			
Stucco	0.035 [0.200]	Same	Same
Gypsum board	0.079 [0.451]	Same	Same
Insulated metal frame	Varies by climate zone (Table C-2 &Table C-5)	Same	Same
Gypsum board	0.079 [0.451]	Same	Same
Wall construction in U.S. (outside to inside)			
Thermal resistance ($m^2 \cdot K/W$) [$ft^2 \cdot °F \cdot h/BTU$]			
Oldest vintage			
Wood siding	0.091 [0.516]	NA [b]	NA

Insulated metal frame		Varied by climate zone (Table C-2 &Table C-5)		NA		NA
Gypsum board		0.079 [0.451]		NA		NA
Older vintage						
Stucco		NA		0.037 [0.208]		NA
Heavy-weight concrete		NA		0.155 [0.880]		NA
Wall insulation		NA		Varies by climate zone (Table C-2 &Table C-5)		NA
Gypsum board		NA		0.079 [0.451]		NA
New vintage						
Normal-weight concrete		NA		NA		0.088 [0.499]
Wall insulation		NA		NA		Varies by climate zone (Table C-2 & Table C-5)
Gypsum board		NA		NA		0.079 [0.451]
Net wall area when long-axis of building extends east-west (m^2)						
North		331		Same		Same
East		258		Same		Same
South		247		Same		Same
West		258		Same		Same
Foundation type		Slab		Same		Same
Windows						
Thermal transmittance ($W/m^2 \cdot K$)		Varies by climate zone and orientation		Same		Same
Visible transmittance		Varies by climate zone and orientation		Same		Same
Window area when long-axis of building extends east-west (m^2)						
North		0.00		Same		Same
East		0.00		Same		Same
South		83.9		Same		Same
West		0.00		Same		Same
HVAC system						
Air conditioner						
California						
SEER (BTU/Wh)						
Estimated COP [c] (Wh/Wh)		Precision air conditioning unit		Same		Same
U.S.						
Estimated SEER [c] (BTU/Wh)		11		11		13

COP (Wh/Wh)		2.84		2.84		3.49
Gas furnace						
Annual Fuel Utilization Efficiency (AFUE) (%)		11		11		12 to 14 (varies by climate zone)
Electric heating		2.84		2.84		3.23 to 3.8 (varies by climate zone)
COP						
Distribution		0.80		Same		Same
Type						
		Single-zone constant air volume		Same		Same

[a] Net wall area excludes windows and doors.

[b] NA = not applicable.

[c] To obtain COP, divide SEER by 3.79 (ECOX 2017).

Task Report Appendix C: Estimation of wall and roof thermal resistances

Each roof and wall in EnergyPlus is modeled as a series of layers; each layer represents one type of material. In an actual building, envelope insulation is usually placed in the cavities formed by wood or metal frames. Thus, a fraction of the wall's cross section is wood (or metal) and the remainder is insulation. In this scenario, conduction through the wood (or metal) lowers the thermal resistance of the insulated frame; this effect is commonly known as thermal bridging.

In EnergyPlus, thermal bridging can be addressed by calculating the equivalent (parallel path) thermal resistance (R_e) of the insulated studded frame. This equivalent thermal resistance is then assigned to the EnergyPlus envelope layer that describes the insulated studded frame.

The following example assumes a wood frame, although it is also applicable to a metal frame. If fraction f of the wall cross section is wood (W) and the remainder is insulation (I), the equivalent thermal resistance of the insulated wood-studded frame will be

$$R_{\mathrm{e}} = \frac{R_{\mathrm{I}} \times R_{\mathrm{W}}}{f \times R_{\mathrm{I}} + (1 - f) \times R_{\mathrm{W}}} \tag{13}$$

where R_{I} and R_{W} are the thermal resistances of the insulating material and of the stud of the wood frame, respectively. f is commonly referred to as the "framing factor". Assuming frame is made of Douglas fir wood, which has a thermal resistance of R-0.99 per inch (Table 4.1.1 in 2016 Title 24 Reference Appendices) (CEC 2016d), a two-by-four wood stud has a thermal resistance (R_{W}) of R-3.5 (3.5 $ft^2 \cdot {}^\circ F \cdot h \cdot BTU^{-1}$) or RSI-0.62 (0.62 $m^2 \cdot K \cdot W^{-1}$).

In a wood-framed roof, a portion of the required insulation is placed between the rafters; the remaining insulation is typically placed over the insulated wood frame. In this scenario, the equivalent thermal resistance is computed as

$$R_{\mathrm{e}} = (R_{\mathrm{I}} - R_{\mathrm{I,\,cavity}}) \frac{R_{\mathrm{I,\,cavity}} \times R_{\mathrm{W}}}{f \times R_{\mathrm{I}} + (1 - f) \times R_{\mathrm{W}}} \tag{14}$$

where $R_{\mathrm{I,\,cavity}}$ is the maximum insulation that fits in the frame cavities.

C.1 California

The equivalent thermal resistances we calculated for each California prototype was computed so that the thermal resistance of the building envelope comply with California building codes. This section details the methods taken to calculate the equivalent thermal resistance by building type (commercial or residential) and by vintage. Section C.1.1 and Section C.1.2 summarize the methods we used to calculate the equivalent thermal resistances of our California residential and commercial prototypes, respectively. Section C.1.3 gives all the California equivalent thermal resistances that were calculated in this study.

C.1.1 Residential prototypes

C.1.1.1 New vintage

In 2016 Title 24 Building Energy Efficiency Standards (CEC 2016c), Table 150.1-A prescribes by California climate zone the thermal transmittance ("U-factor") requirements for different building envelope construction types (e.g., wood frame, metal frame, heavy mass) and for different envelope assemblies (e.g. roof, walls). The thermal transmittances given in Table 150.1-A describe the entire assembly, from indoor surface air film to outdoor surface air film.

We selected from Table 150.1-A the assembly thermal transmittances for wood-framed roof and wood-framed walls required in each California climate zone. For every location, the thermal resistances of the roof assembly ($R_{\text{roof, assembly}}$) and of the wall assembly ($R_{\text{wall, assembly}}$) were obtained as the reciprocals of the corresponding thermal transmittances.[4]

Let $R_{\text{roof, no\_I}}$ represent the thermal resistance of the roof excluding the insulating layer and $R_{\text{wall, no\_I}}$ represent the thermal resistance of the wall excluding the insulating layer. We calculated $R_{\text{roof, no\_I}}$ and $R_{\text{wall, no\_I}}$ for each new residential prototype. Then, we computed the equivalent thermal resistance R_{e} of the roof's insulating layer by subtracting $R_{\text{roof, no\_I}}$ from $R_{\text{roof, assembly}}$. Similarly, we calculated the equivalent thermal resistance R_{e} of the walls' insulating layer by subtracting $R_{\text{wall, no\_I}}$ from $R_{\text{wall, assembly}}$.

C.1.1.2 Older vintage

The 1988 Title 24 Building Energy Efficiency Standards (CEC 1988) prescribe for each California climate zone the minimum thermal resistance ("R-value") of insulation between wood framing members in roofs and walls. We selected the thermal resistances of ceiling and wall insulation prescribed for residential buildings in Alternative Package A (see Table 2-43Z1 through Table 2-43Z16 in 1988 Title 24 Standards).

A wood frame with two-by-four wood studs (actual dimensions 1.5" by 3.5") can typically contain up to R-13 of cavity insulation [see Table 4.3.1 in 2016 Title 24 Reference Appendices (CEC 2016d)]. Thus, for California climate zones in which the prescribed wall insulation was equal to or less than R-13, we computed the wall equivalent thermal resistance using Eq. (13), assuming two-by-four wood studs spaced 16" center-to-center (framing factor f approximately 0.15). For locations with prescribed wall insulation greater than R-13, the wall equivalent thermal resistance was computed with Eq. (13) assuming two-by-six wood studs (actual dimensions 1.5" by 5.5") with framing factor 0.15.

---

[4] Strictly speaking, thermal resistance is the reciprocal of thermal conductance (measured from surface to surface) rather than that of thermal transmittance (measured from air film to air film). We neglect that minor difference.

For roofs in the older residential buildings, we assumed two-by-four wood rafters following the recommendations in Section JA4.2 of 2016 Title 24 Reference Appendices (CEC 2016d). From the prescribed ceiling insulations in 1988 Title 24 Standards, only R-13 insulation fits in the frame cavity. Thus, the equivalent thermal resistances were computed using Eq. (14) with $R_{\text{I, cavity}} = 13$.

C.1.1.3 Oldest vintage

In the 2016 Title 24 Residential Compliance Manual (CEC 2016b), Table 8-1 gives default assumptions of insulation thermal transmittance ("U-factor"), that can be found in different vintages of residential buildings. We assumed these thermal transmittances in Table 8-1 refer to that of only the insulation layer in the assembly. For pre-1978 buildings, the default insulation U-factor of a ceiling is U-0.079 [0.079 BTU/(ft²·°F·h)] and of a wall is U-0.356. Treating thermal resistance as the reciprocal of thermal transmittances, the insulation thermal resistance of the roof is R-12.7 and of the wall is R-2.8. In our simulations of the oldest residential building categories, these thermal resistances were used as the equivalent thermal resistance assigned to the wood-framed insulating layer in EnergyPlus.

C.1.2 Commercial prototypes

C.1.2.1 New vintage

To compute the equivalent thermal resistances of the new commercial prototype in California, we followed the same process used for the new residential prototypes (Section C.1.1.1). From the prescriptive requirements in Component Package A (see Table 150.1-A in 2016 Title 24 Building Energy Efficiency Standards), we selected the assembly thermal transmittances for roof and walls that matched the construction type of our commercial prototypes. As an example, for the large hotel walls, we used the thermal transmittances for heavy mass walls.

The thermal resistance of the roof assembly ($R_{\text{roof, assembly}}$) and of the wall assembly ($R_{\text{wall, assembly}}$) were obtained as the inverse of the thermal transmittances. We then calculated $R_{\text{roof, no\_I}}$ and $R_{\text{wall, no\_I}}$ for each new commercial prototype. The equivalent thermal resistances, R_{e}, of the roof's insulating layer were computed by subtracting $R_{\text{roof, no\_I}}$ from $R_{\text{roof, assembly}}$; R_{e} of the walls' insulating layer was calculated by subtracting $R_{\text{wall, no\_I}}$ from $R_{\text{wall, assembly}}$.

C.1.2.2 Older vintage

The 1988 Title 24 Building Energy Efficiency Standards (CEC 1988) provide prescriptive standards for three types of commercial buildings: low-rise office buildings, high-rise office buildings, and retail and whole-sale stores. These standards define minimum thermal resistances ("R-values") for different building envelope assemblies (e.g., roof and walls). First, we matched each of our commercial building categories to one of the commercial building types detailed in 1988 Title 24 Standards. Later, we selected the roof and wall assembly thermal

resistances prescribed in Alternative Package A. Table C-1 shows how we mapped the building types in 1988 Title 24 Standards to our building categories.

Table C-1. Building types from 1988 Title 24 Standards mapped to each of our simulated building categories.

Building category	Building type from 1988 Title 24 Standards		Building category	Building type from 1988 Title 24 Standards
Large office	high-rise office [a]		Sit-down restaurant	retail and wholesale store [d]
Medium office	low-rise office [b]		Fast-food restaurant	retail and wholesale store [d]
Small office	low-rise office [b]		Stand-alone retail	retail and wholesale store [d]
Large hotel	high-rise office [c]		Retail strip mall	retail and wholesale store [d]

[a] 1988 T24 Standards; Tables 2-53W1 to 2-53W16; Package A; wall heat capacity 4-10 BTU/R·ft².

[b] 1988 T24 Standards; Tables 2-53V1 to 2-53V16; Package A; wall heat capacity 4-10 BTU/R·ft².

[c] 1988 T24 Standards; Tables 2-53W1 to 2-53W16; Package A; wall heat capacity 15-20 BTU/R·ft².

[d] 1988 T24 Standards; Tables 2-53WA1 to 2-53WA16; Package A; wall heat capacity 4-10 BTU/R·ft².

From the prescriptive requirement tables in 1988 Title 24 Standards, we obtained for each prototype the roof assembly thermal resistance ($R_{\text{roof, no\_I}}$) and the wall assembly thermal resistance ($R_{\text{wall, no\_I}}$). We then computed the equivalent thermal resistances following the same process used for the older residential prototypes (Section C.1.1.2). The equivalent thermal resistance of the roof's insulating layer was calculated by subtracting $R_{\text{roof, no\_I}}$ from $R_{\text{roof, assembly}}$. Similarly, we computed the equivalent thermal resistance of the walls' insulating layer by subtracting $R_{\text{wall, no\_I}}$ from $R_{\text{wall, assembly}}$.

C.1.2.3 Oldest vintage

We did not find a reference that provided estimates of thermal insulation typically installed in pre-1978 commercial buildings in California. To estimate the equivalent thermal resistances for our oldest commercial prototypes, we first calculated the equivalent thermal resistance ratio of oldest to older residential prototype. This ratio was computed for each California climate zone and used to scale down the equivalent thermal resistances from the older commercial prototypes. These scaled-down equivalent thermal resistances were used in the oldest commercial prototypes.

As an example, the wall equivalent thermal resistances in the oldest residential prototypes in CACZ 1 was R-2.8, and that in the older residential prototypes was R-13.9. The ratio of wall equivalent thermal resistances of oldest to older prototype is 0.20 (R-2.8 / R-13.9). The wall equivalent thermal resistances in the older medium office in CACZ 1 is R-5.4. Thus, for the oldest medium office in CACZ 1, the estimated wall equivalent thermal resistances is R-0.6 (R-5.4 × 0.20).

C.1.3 Equivalent thermal resistances used in the California commercial and residential prototypes

Table C-2 gives the equivalent thermal resistance used in the walls of all California prototypes.

Table C-2. Equivalent thermal resistance, R_e, of the insulated wall frame by vintage and by California climate zone for all prototypes.

Vintage	Prototype	Equivalent thermal resistance of the insulated wall frame, R [ft²·°F·h·BTU⁻¹]															
		CZ 01	CZ 02	CZ 03	CZ 04	CZ 05	CZ 06	CZ 07	CZ 08	CZ 09	CZ 10	CZ 11	CZ 12	CZ 13	CZ 14	CZ 15	CZ 16
oldest	Single-family home	2.8	2.8	2.8	2.8	2.8	2.8	2.8	2.8	2.8	2.8	2.8	2.8	2.8	2.8	2.8	2.8
	Apartment building	2.8	2.8	2.8	2.8	2.8	2.8	2.8	2.8	2.8	2.8	2.8	2.8	2.8	2.8	2.8	2.8
	Large office	0.3	1.4	1.4	1.5	1.5	1.3	1.3	1.3	1.3	1.3	1.4	1.4	1.4	0.3	0.3	0.3
	Medium office	0.6	1.9	1.9	2.1	2.1	1.9	1.9	1.9	1.9	1.9	1.6	1.6	1.6	0.5	0.5	0.6
	Small office	0.6	1.9	1.9	2.1	2.1	1.9	1.9	1.9	1.9	1.9	1.6	1.6	1.6	0.5	0.5	0.6
	Large hotel	0.01	0.01	0.01	0.01	0.01	0.01	0.01	0.01	0.01	0.01	0.01	0.01	0.01	0.01	0.01	0.01
	Sit-down restaurant	0.6	2.0	2.0	2.2	2.2	2.0	2.0	2.0	2.0	2.0	1.7	1.7	1.7	0.6	0.6	0.6
	Fast-food restaurant	0.4	1.7	1.7	1.9	1.9	1.7	1.7	1.7	1.7	1.7	1.4	1.4	1.4	0.3	0.3	0.4
	Retail stand-alone	0.6	1.9	1.9	2.1	2.1	1.9	1.9	1.9	1.9	1.9	1.6	1.6	1.6	0.5	0.5	0.6
	Strip mall retail	0.6	1.9	1.9	2.1	2.1	1.9	1.9	1.9	1.9	1.9	1.6	1.6	1.6	0.5	0.5	0.6
older	Single-family home	13.9	8.3	8.3	8.3	8.3	8.3	8.3	8.3	8.3	8.3	8.3	8.3	8.3	13.9	13.9	13.9
	Apartment building	13.9	8.3	8.3	8.3	8.3	8.3	8.3	8.3	8.3	8.3	8.3	8.3	8.3	13.9	13.9	13.9
	Large office	4.5	4.5	4.5	4.6	4.6	4.3	4.3	4.3	4.3	4.3	4.4	4.4	4.4	4.5	4.5	4.5
	Medium office	5.4	5.6	5.6	6.0	6.0	5.5	5.5	5.5	5.5	5.5	5.0	5.0	5.0	5.3	5.3	5.4
	Small office	5.4	5.6	5.6	6.0	6.0	5.5	5.5	5.5	5.5	5.5	5.0	5.0	5.0	5.3	5.3	5.4
	Large hotel	1.9	1.0	1.0	1.2	1.2	0.6	0.6	0.6	0.6	0.6	1.0	1.0	1.0	1.9	1.9	1.9
	Sit-down restaurant	5.4	5.6	5.6	6.0	6.0	5.5	5.5	5.5	5.5	5.5	5.0	5.0	5.0	5.3	5.3	5.4
	Fast-food restaurant	5.3	5.5	5.5	5.9	5.9	5.4	5.4	5.4	5.4	5.4	4.9	4.9	4.9	5.1	5.1	5.3
	Retail stand-alone	5.4	5.6	5.6	6.0	6.0	5.5	5.5	5.5	5.5	5.5	5.0	5.0	5.0	5.3	5.3	5.4
	Strip mall retail	5.4	5.6	5.6	6.0	6.0	5.5	5.5	5.5	5.5	5.5	5.0	5.0	5.0	5.3	5.3	5.4
new	Single-family home	16.6	16.6	16.6	16.6	16.6	12.4	12.4	16.6	16.6	16.6	16.6	16.6	16.6	16.6	16.6	16.6

	Apartment building	16.6	16.6	16.6	16.6	16.6	12.4	12.4	16.6	16.6	16.6	16.6	16.6	16.6	16.6	16.6	16.6	
	Large office	12.5	14.2	10.2	14.2	14.2	12.5	12.5	14.2	14.2	14.2	14.2	14.2	14.2	14.2	14.2	14.2	
	Medium office	12.5	14.2	10.2	14.2	14.2	12.5	12.5	14.2	14.2	14.2	14.2	14.2	14.2	14.2	14.2	14.2	
	Small office	12.5	14.2	10.2	14.2	14.2	12.5	12.5	14.2	14.2	14.2	14.2	14.2	14.2	14.2	14.2	14.2	
	Large hotel	2.0	0.01	0.01	0.01	0.01	0.01	0.01	0.01	0.01	0.01	3.4	2.0	2.7	3.4	3.4	4.2	
	Sit-down restaurant	12.5	14.2	10.2	14.2	14.2	12.5	12.5	14.2	14.2	14.2	14.2	14.2	14.2	14.2	14.2	14.2	
	Fast-food restaurant	8.4	14.8	7.0	14.8	7.7	7.0	7.0	7.7	14.8	14.8	20.1	14.8	14.8	14.8	21.7	14.8	
	Retail stand-alone	12.5	14.2	10.2	14.2	14.2	12.5	12.5	14.2	14.2	14.2	14.2	14.2	14.2	14.2	14.2	14.2	
	Strip mall retail	12.5	14.2	10.2	14.2	14.2	12.5	12.5	14.2	14.2	14.2	14.2	14.2	14.2	14.2	14.2	14.2	

Table C-3 gives the equivalent thermal resistance used in the roof of all California prototypes.

Table C-3. Equivalent thermal resistance, R_e, of the insulated roof frame by vintage and by California climate zone for all prototypes.

Vintage	Prototype	Equivalent thermal resistance of the insulated roof frame, R [ft²·°F·h·BTU⁻¹]															
		CZ 01	CZ 02	CZ 03	CZ 04	CZ 05	CZ 06	CZ 07	CZ 08	CZ 09	CZ 10	CZ 11	CZ 12	CZ 13	CZ 14	CZ 15	CZ 16
oldest	Single-family home	12.7	12.7	12.7	12.7	12.7	12.7	12.7	12.7	12.7	12.7	12.7	12.7	12.7	12.7	12.7	12.7
	Apartment building	12.7	12.7	12.7	12.7	12.7	12.7	12.7	12.7	12.7	12.7	12.7	12.7	12.7	12.7	12.7	12.7
	Large office	6.7	6.7	6.7	6.7	6.7	11.1	11.1	6.7	6.7	6.7	6.7	6.7	6.7	5.0	6.7	5.0
	Medium office	5.4	3.8	3.8	3.8	3.8	6.6	6.6	3.8	3.8	3.8	3.8	3.8	3.8	4.0	5.4	4.0
	Small office	2.8	1.2	1.2	1.2	1.2	4.1	4.1	1.2	1.2	1.2	1.2	1.2	1.2	1.4	2.8	1.4
	Large hotel	6.7	6.7	6.7	6.7	6.7	11.1	11.1	6.7	6.7	6.7	6.7	6.7	6.7	5.0	6.7	5.0
	Sit-down restaurant	2.1	0.6	0.6	0.6	0.6	3.4	3.4	0.6	0.6	0.6	0.6	0.6	0.6	0.8	2.1	0.8
	Fast-food restaurant	2.1	0.6	0.6	0.6	0.6	3.4	3.4	0.6	0.6	0.6	0.6	0.6	0.6	0.8	2.1	0.8
	Retail stand-alone	5.4	3.8	3.8	3.8	3.8	6.6	6.6	3.8	3.8	3.8	3.8	3.8	3.8	4.0	5.4	4.0
	Strip mall retail	5.4	3.8	3.8	3.8	3.8	6.6	6.6	3.8	3.8	3.8	3.8	3.8	3.8	4.0	5.4	4.0
older	Single-family home	27.2	27.2	27.2	27.2	27.2	16.2	16.2	27.2	27.2	27.2	27.2	27.2	27.2	35.2	27.2	35.2
	Apartment building	27.2	27.2	27.2	27.2	27.2	16.2	16.2	27.2	27.2	27.2	27.2	27.2	27.2	35.2	27.2	35.2
	Large office	13.9	13.9	13.9	13.9	13.9	13.9	13.9	13.9	13.9	13.9	13.9	13.9	13.9	13.9	13.9	13.9
	Medium office	11.4	8.4	8.4	8.4	8.4	8.4	8.4	8.4	8.4	8.4	8.4	8.4	8.4	11.4	11.4	11.4
	Small office	8.8	5.8	5.8	5.8	5.8	5.8	5.8	5.8	5.8	5.8	5.8	5.8	5.8	8.8	8.8	8.8
	Large hotel	13.9	13.9	13.9	13.9	13.9	13.9	13.9	13.9	13.9	13.9	13.9	13.9	13.9	13.9	13.9	13.9
	Sit-down restaurant	8.2	5.1	5.1	5.1	5.1	5.1	5.1	5.1	5.1	5.1	5.1	5.1	5.1	8.1	8.1	8.1
	Fast-food restaurant	8.2	5.1	5.1	5.1	5.1	5.1	5.1	5.1	5.1	5.1	5.1	5.1	5.1	8.1	8.1	8.1
	Retail stand-alone	11.4	8.4	8.4	8.4	8.4	8.4	8.4	8.4	8.4	8.4	8.4	8.4	8.4	11.4	11.4	11.4
	Strip mall retail	11.4	8.4	8.4	8.4	8.4	8.4	8.4	8.4	8.4	8.4	8.4	8.4	8.4	11.4	11.4	11.4
new	Single-family home	35.2	35.2	27.2	43.2	27.2	27.2	27.2	43.2	43.2	43.2	43.2	43.2	43.2	43.2	43.2	43.2
	Apartment building	35.2	35.2	27.2	43.2	27.2	27.2	27.2	43.2	43.2	43.2	43.2	43.2	43.2	43.2	43.2	43.2
	Large office	28.3	28.3	28.3	28.3	28.3	19.3	19.3	19.3	28.3	28.3	28.3	28.3	28.3	28.3	28.3	28.3
	Medium office	28.3	28.3	28.3	28.3	28.3	19.3	19.3	19.3	28.3	28.3	28.3	28.3	28.3	28.3	28.3	28.3
	Small office	25.7	25.7	25.7	25.7	25.7	16.7	16.7	16.7	25.7	25.7	25.7	25.7	25.7	25.7	25.7	25.7
	Large hotel	28.3	28.3	28.3	28.3	28.3	19.3	19.3	19.3	28.3	28.3	28.3	28.3	28.3	28.3	28.3	28.3
	Sit-down restaurant	25.1	25.1	25.1	25.1	25.1	16.1	16.1	16.1	25.1	25.1	25.1	25.1	25.1	25.1	25.1	25.1
	Fast-food restaurant	25.1	25.1	25.1	25.1	25.1	16.1	16.1	16.1	25.1	25.1	25.1	25.1	25.1	25.1	25.1	25.1
	Retail stand-alone	28.3	28.3	28.3	28.3	28.3	19.3	19.3	19.3	28.3	28.3	28.3	28.3	28.3	28.3	28.3	28.3
	Strip mall retail	28.3	28.3	28.3	28.3	28.3	19.3	19.3	19.3	28.3	28.3	28.3	28.3	28.3	28.3	28.3	28.3

Table C-4. Ratios of thermal resistances for roof assembly to wall assembly by vintage and by California climate zone for all prototypes. The thermal resistances consider the entire envelope construction from indoor surface air film to outdoor surface air film.

Vintage	Prototype	Thermal resistance ratio of roof assembly to wall assembly, [R/R]															
		CZ 01	CZ 02	CZ 03	CZ 04	CZ 05	CZ 06	CZ 07	CZ 08	CZ 09	CZ 10	CZ 11	CZ 12	CZ 13	CZ 14	CZ 15	CZ 16
oldest	Single-family home	2.7															
	Apartment building	2.7															
	Large office	3.5	2.3	2.3	2.3	2.3	3.8	3.8	2.4	2.4	2.4	2.4	2.4	2.4	2.7	3.5	2.7
	Medium office	2.6	1.3	1.3	1.2	1.2	2.0	2.0	1.3	1.3	1.3	1.4	1.4	1.4	2.1	2.6	2.0
	Small office	2.6	1.3	1.3	1.2	1.2	2.0	2.0	1.3	1.3	1.3	1.4	1.4	1.4	2.1	2.6	2.0
	Large hotel	5.9	5.1	5.1	4.8	4.8	9.3	9.3	6.0	6.0	6.0	5.1	5.1	5.1	4.7	5.9	4.7
	Sit-down restaurant	2.5	1.2	1.2	1.2	1.2	2.0	2.0	1.3	1.3	1.3	1.3	1.3	1.3	2.0	2.6	2.0
	Fast-food restaurant	2.6	1.3	1.3	1.2	1.2	2.1	2.1	1.3	1.3	1.3	1.4	1.4	1.4	2.1	2.7	2.1
	Retail stand-alone	2.6	1.3	1.3	1.2	1.2	2.0	2.0	1.3	1.3	1.3	1.4	1.4	1.4	2.1	2.6	2.0
	Strip mall retail	2.6	1.3	1.3	1.2	1.2	2.0	2.0	1.3	1.3	1.3	1.4	1.4	1.4	2.1	2.6	2.0
older	Single-family home	1.8	2.7	2.7	2.7	2.7	1.7	1.7	2.7	2.7	2.7	2.7	2.7	2.7	2.3	1.8	2.3
	Apartment building	1.8	2.7	2.7	2.7	2.7	1.7	1.7	2.7	2.7	2.7	2.7	2.7	2.7	2.3	1.8	2.3
	Large office	2.3	2.3	2.3	2.3	2.3	2.4	2.4	2.4	2.4	2.4	2.3	2.3	2.3	2.3	2.3	2.3
	Medium office	1.7	1.3	1.3	1.2	1.2	1.3	1.3	1.3	1.3	1.3	1.4	1.4	1.4	1.7	1.7	1.7
	Small office	1.7	1.3	1.3	1.2	1.2	1.3	1.3	1.3	1.3	1.3	1.4	1.4	1.4	1.7	1.7	1.7
	Large hotel	3.9	5.1	5.1	4.8	4.8	5.9	5.9	5.9	5.9	5.9	5.1	5.1	5.1	3.9	3.9	3.9
	Sit-down restaurant	1.7	1.2	1.2	1.2	1.2	1.2	1.2	1.2	1.2	1.2	1.3	1.3	1.3	1.7	1.7	1.7
	Fast-food restaurant	1.7	1.3	1.3	1.2	1.2	1.3	1.3	1.3	1.3	1.3	1.4	1.4	1.4	1.8	1.8	1.7
	Retail stand-alone	1.7	1.3	1.3	1.2	1.2	1.3	1.3	1.3	1.3	1.3	1.4	1.4	1.4	1.7	1.7	1.7
	Strip mall retail	1.7	1.3	1.3	1.2	1.2	1.3	1.3	1.3	1.3	1.3	1.4	1.4	1.4	1.7	1.7	1.7
new	Single-family home	2.0	2.0	1.5	2.4	1.5	2.0	2.0	2.4	2.4	2.4	2.4	2.4	2.4	2.4	2.4	2.4
	Apartment building	2.0	2.0	1.5	2.4	1.5	2.0	2.0	2.4	2.4	2.4	2.4	2.4	2.4	2.4	2.4	2.4
	Large office	2.0	1.8	2.4	1.8	1.8	1.4	1.4	1.3	1.8	1.8	1.8	1.8	1.8	1.8	1.8	1.8
	Medium office	2.0	1.8	2.4	1.8	1.8	1.4	1.4	1.3	1.8	1.8	1.8	1.8	1.8	1.8	1.8	1.8
	Small office	2.0	1.8	2.4	1.8	1.8	1.4	1.4	1.3	1.8	1.8	1.8	1.8	1.8	1.8	1.8	1.8
	Large hotel	7.4	15.0	15.0	15.0	15.0	10.4	10.4	10.4	15.0	15.0	5.5	7.5	6.3	5.5	5.5	4.7
	Sit-down restaurant	2.0	1.8	2.4	1.8	1.8	1.4	1.4	1.3	1.8	1.8	1.8	1.8	1.8	1.8	1.8	1.8
	Fast-food restaurant	2.8	1.8	3.3	1.8	3.0	2.3	2.3	2.1	1.8	1.8	1.3	1.8	1.8	1.8	1.2	1.8
	Retail stand-alone	2.0	1.8	2.4	1.8	1.8	1.4	1.4	1.3	1.8	1.8	1.8	1.8	1.8	1.8	1.8	1.8
	Strip mall retail	2.0	1.8	2.4	1.8	1.8	1.4	1.4	1.3	1.8	1.8	1.8	1.8	1.8	1.8	1.8	1.8

C.2 United States

We calculated the effective thermal resistance for the roof and walls for the older and oldest residential U.S. prototypes so that the thermal properties of the building envelope follow typical residential construction practices of older and oldest vintage residential buildings. In the remaining U.S. prototypes, we did not make any changes to the roof and wall thermal resistances. Section C.2.1 summarizes the methods we used to calculate the equivalent thermal resistances of the older and oldest U.S. residential prototypes. Section C.2.2 gives all the U.S. equivalent thermal resistances that were either calculated in this study or already defined in the prototypes.

C.2.1 Residential prototypes

C.2.1.1 Older vintage

Huang et al. (1999) compiled U.S. residential building characteristics from the 1984 Residential Energy Consumption Survey (RECS), the Census Bureau, and the 1987 National Association of Homebuilders Annual Survey, then tabulated typical construction practices by U.S. Census Division and for three periods of construction (pre-1940, 1950-1970, and 1980s). The study provides the thermal resistance of the insulation present in the roof and walls of single-family homes and multi-family buildings.

To calculate the equivalent thermal resistance for our U.S. older residential prototypes, we used the insulation thermal resistances provided by Huang et al. (1999) for the 1980s period. For each of our prototypes, we used the insulation values from the Census Division that contains the city simulated by the prototype.

The wall equivalent thermal resistances were calculated with Eq. (13) and assuming wood frame with two-by-four studs. The roof equivalent thermal resistances were computed with Eq. (14) and assuming wood frame with two-by-four rafters.

C.2.1.2 Oldest vintage

To calculate the equivalent thermal resistances for our U.S. oldest residential prototypes, we used the insulation thermal resistances provided by Huang et al. (1999) for the period 1950-1970. For this period, Huang's study provided building characteristics for retrofitted and non-retrofitted buildings.

We averaged the retrofitted and non-retrofitted values of insulation thermal resistances. We used the average values to calculate: (a) wall equivalent thermal resistances using Eq. (13) and assuming wood frame with two-by-four studs, and (b) roof equivalent thermal resistances using Eq. (14) and assuming wood frame with two-by-four rafters.

C.2.2 Equivalent thermal resistances used in the U.S. commercial and residential prototypes

Table C-5 gives the equivalent thermal resistance used in the walls of all U.S. prototypes.

Table C-5. Equivalent thermal resistance, R_e, of the insulated wall frame by vintage and by U.S. climate zone for all prototypes.

Vintage	Prototype	Equivalent thermal resistance of the insulated wall frame, R [ft²·°F·h·BTU⁻¹]														
		CZ 1A	CZ 2A	CZ 2B	CZ 3A	CZ 3B	CZ 3C	CZ 4A	CZ 4B	CZ 4C	CZ 5A	CZ 5B	CZ 6A	CZ 6B	CZ 7	CZ 8
oldest	Single-family home	3.5	3.5	3.5	3.5	3.5	3.5	3.5	3.5	3.5	3.5	3.5	3.5	3.5	3.5	3.5
	Apartment building	3.5	3.5	3.5	3.5	3.5	3.5	3.5	3.5	3.5	3.5	3.5	3.5	3.5	3.5	3.5
	Large office	2.0	2.0	2.0	2.1	2.0	2.1	3.2	3.0	3.3	4.0	3.8	4.5	4.5	5.0	5.6
	Medium office	2.5	2.5	2.5	2.6	2.5	2.6	3.8	3.6	3.9	4.6	4.4	5.1	5.1	5.5	6.2
	Small office	2.5	2.5	2.5	2.6	2.5	2.6	3.8	3.6	3.9	4.6	4.4	5.1	5.1	5.5	6.2
	Large hotel	2.0	2.0	2.0	2.1	2.0	2.1	3.2	3.0	3.3	4.0	3.8	4.5	4.5	5.0	5.6
	Sit-down restaurant	2.5	2.5	2.5	2.6	2.5	2.6	3.8	3.6	3.9	4.6	4.4	5.1	5.1	5.5	6.2
	Fast-food restaurant	2.0	2.0	2.0	2.1	2.0	2.1	3.2	3.0	3.3	4.0	3.8	4.5	4.5	5.0	5.6
	Retail stand-alone	2.5	2.5	2.5	2.6	2.5	2.6	3.8	3.6	3.9	4.6	4.4	5.1	5.1	5.5	6.2
	Strip mall retail	2.5	2.5	2.5	2.6	2.5	2.6	3.8	3.6	3.9	4.6	4.4	5.1	5.1	5.5	6.2
older	Single-family home	8.3	8.3	9.2	8.3	8.3	8.3	8.3	9.2	8.3	9.2	9.2	9.2	9.2	13.9	8.3
	Apartment building	8.3	8.3	9.2	8.3	8.3	8.3	8.3	9.2	8.3	9.2	9.2	9.2	9.2	13.9	8.3
	Large office	2.0	0.6	0.1	1.1	1.1	1.1	5.9	2.9	7.6	7.6	4.8	11.7	10.3	14.0	18.9
	Medium office	2.5	4.8	2.4	5.9	4.4	5.9	9.4	8.2	9.1	10.4	10.4	13.6	12.1	15.4	20.4
	Small office	0.1	0.6	0.1	1.1	1.1	1.1	5.9	2.9	7.6	7.6	4.8	11.7	10.3	14.0	18.9
	Large hotel	2.0	0.6	0.1	1.1	1.1	1.1	5.9	2.9	7.6	7.6	4.8	11.7	10.3	14.0	18.9
	Sit-down restaurant	2.5	4.8	2.4	5.9	4.4	5.9	9.4	8.2	9.1	10.4	10.4	13.6	12.1	15.4	20.4
	Fast-food restaurant	1.2	4.8	2.4	5.9	4.4	5.9	9.4	8.2	9.1	10.4	10.4	13.6	12.1	15.4	20.4
	Retail stand-alone	0.1	0.6	0.1	1.1	1.1	1.1	5.9	2.9	7.6	7.6	4.8	11.7	10.3	14.0	18.9
	Strip mall retail	2.5	4.8	2.4	5.9	4.4	5.9	9.4	8.2	9.1	10.4	10.4	13.6	12.1	15.4	20.4
new	Single-family home	8.5	8.5	8.5	8.5	13.3	13.3	13.3	8.5	13.3	13.3	13.3	13.3	13.3	13.3	13.3
	Apartment building	8.5	8.5	8.5	8.5	13.3	13.3	13.3	8.5	13.3	13.3	13.3	13.3	13.3	13.3	13.3
	Large office	0.2	4.8	0.2	6.3	6.3	6.3	7.8	4.8	7.8	9.3	9.3	10.7	10.7	12.3	10.7
	Medium office	5.9	9.7	5.9	9.7	10.8	10.8	13.4	5.9	13.4	16.0	13.4	18.2	13.4	13.4	13.4
	Small office	9.1	9.1	9.1	9.1	9.1	9.1	13.4	9.1	9.1	17.4	13.4	17.4	17.4	17.4	17.4
	Large hotel	0.2	4.8	0.2	6.3	6.3	6.3	7.8	4.8	7.8	9.3	9.3	10.7	10.7	12.3	10.7
	Sit-down restaurant	5.9	9.7	5.9	9.7	10.8	10.8	13.4	5.9	13.4	16.0	13.4	18.2	13.4	13.4	13.4
	Fast-food restaurant	9.1	9.1	9.1	9.1	9.1	9.1	13.4	9.1	9.1	17.4	13.4	17.4	17.4	17.4	17.4
	Retail stand-alone	0.2	4.8	0.2	6.3	6.3	6.3	7.8	4.8	7.8	9.3	9.3	10.7	10.7	12.3	10.7
	Strip mall retail	5.9	9.7	5.9	9.7	10.8	10.8	13.4	5.9	13.4	16.0	13.4	18.2	13.4	13.4	13.4

Table C-6 gives the equivalent thermal resistance used in the roof of all U.S. prototypes.

Table C-6. Equivalent thermal resistance, R_e, of the insulated roof frame by vintage and by U.S. climate zone for all prototypes.

Vintage	Prototype	Equivalent thermal resistance of the insulated roof frame, R [ft²·°F·h·BTU⁻¹]														
		CZ 1A	CZ 2A	CZ 2B	CZ 3A	CZ 3B	CZ 3C	CZ 4A	CZ 4B	CZ 4C	CZ 5A	CZ 5B	CZ 6A	CZ 6B	CZ 7	CZ 8
oldest	Single-family home	7.8	10.2	9.1	10.2	10.2	7.8	7.8	9.1	12.2	12.2	9.1	19.2	9.1	11.7	12.2
	Apartment building	7.8	10.2	9.1	10.2	10.2	7.8	7.8	9.1	12.2	12.2	9.1	19.2	9.1	11.7	12.2
	Large office	8.6	8.6	8.6	8.6	8.6	8.6	10.2	9.8	10.3	12.8	12.0	15.6	15.6	15.2	15.6
	Medium office	8.6	8.6	8.6	8.6	8.6	8.6	10.2	9.8	10.3	12.8	12.0	15.6	15.6	15.2	15.6
	Small office	8.6	8.6	8.6	8.6	8.6	8.6	10.2	9.8	10.3	12.8	12.0	15.6	15.6	15.2	15.6
	Large hotel	8.6	8.6	8.6	8.6	8.6	8.6	10.2	9.8	10.3	12.8	12.0	15.6	15.6	15.2	15.6
	Sit-down restaurant	8.6	8.6	8.6	8.6	8.6	8.6	10.2	9.8	10.3	12.8	12.0	15.6	15.6	15.2	15.6
	Fast-food restaurant	8.6	8.6	8.6	8.6	8.6	8.6	10.2	9.8	10.3	12.8	12.0	15.6	15.6	15.2	15.6
	Retail stand-alone	8.6	8.6	8.6	8.6	8.6	8.6	10.2	9.8	10.3	12.8	12.0	15.6	15.6	15.2	15.6
	Strip mall retail	8.6	8.6	8.6	8.6	8.6	8.6	10.2	9.8	10.3	12.8	12.0	15.6	15.6	15.2	15.6
older	Single-family home	24.2	24.2	26.2	24.2	24.2	22.2	24.2	26.2	29.2	29.2	26.2	24.2	26.2	29.2	29.2
	Apartment building	24.2	24.2	26.2	24.2	24.2	22.2	24.2	26.2	29.2	29.2	26.2	24.2	26.2	29.2	29.2
	Large office	12.1	13.7	20.3	12.5	19.4	9.9	15.8	15.5	14.2	17.8	18.5	21.1	19.3	23.6	31.1
	Medium office	12.1	13.7	20.3	12.5	19.4	9.9	15.8	15.5	14.2	17.8	18.5	21.1	19.3	23.6	31.1
	Small office	11.2	12.9	19.5	11.6	18.6	9.1	15.0	14.7	13.3	16.9	17.6	20.3	18.4	22.7	30.3
	Large hotel	12.1	13.7	20.3	12.5	19.4	9.9	15.8	15.5	14.2	17.8	18.5	21.1	19.3	23.6	31.1
	Sit-down restaurant	11.2	12.9	19.5	11.6	18.6	9.1	15.0	14.7	13.3	16.9	17.6	20.3	18.4	22.7	30.3
	Fast-food restaurant	11.2	12.9	19.5	11.6	18.6	9.1	15.0	14.7	13.3	16.9	17.6	20.3	18.4	22.7	30.3
	Retail stand-alone	12.1	13.7	20.3	12.5	19.4	9.9	15.8	15.5	14.2	17.8	18.5	21.1	19.3	23.6	31.1
	Strip mall retail	12.1	13.7	20.3	12.5	19.4	9.9	15.8	15.5	14.2	17.8	18.5	21.1	19.3	23.6	31.1
new	Single-family home	24.5	29.3	24.5	24.5	29.3	29.3	34.5	29.3	34.5	34.5	29.3	34.5	34.5	34.5	34.5
	Apartment building	26.3	32.9	26.3	26.3	32.9	32.9	41.2	32.9	41.2	41.2	32.9	41.2	41.2	41.2	41.2
	Large office	14.8	24.5	14.8	19.7	24.5	24.5	30.1	14.8	19.7	30.1	19.7	30.1	19.7	19.7	19.7
	Medium office	14.8	24.5	14.8	19.7	24.5	24.5	30.1	14.8	19.7	30.1	19.7	30.1	19.7	19.7	19.7
	Small office	27.8	35.4	27.8	35.4	35.4	35.4	46.0	27.8	35.4	46.0	35.4	46.0	35.4	35.4	35.4
	Large hotel	14.8	24.5	14.8	19.7	24.5	24.5	30.1	14.8	19.7	30.1	19.7	30.1	19.7	19.7	19.7
	Sit-down restaurant	27.8	35.4	27.8	35.4	35.4	35.4	46.0	27.8	35.4	46.0	35.4	46.0	35.4	35.4	35.4
	Fast-food restaurant	27.8	35.4	27.8	35.4	35.4	35.4	46.0	27.8	35.4	46.0	35.4	46.0	35.4	35.4	35.4
	Retail stand-alone	14.8	24.5	14.8	19.7	24.5	24.5	30.1	14.8	19.7	30.1	19.7	30.1	19.7	19.7	19.7
	Strip mall retail	14.8	24.5	14.8	19.7	24.5	24.5	30.1	14.8	19.7	30.1	19.7	30.1	19.7	19.7	19.7

Table C-7. Ratios of thermal resistances for roof assembly to wall assembly by vintage and by U.S. climate zone for all prototypes. The thermal resistances consider the entire envelope construction from indoor surface air film to outdoor surface air film.

Vintage	Prototype	Thermal resistance ratio of roof assembly to wall assembly, [R/R]														
		CZ 1A	CZ 2A	CZ 2B	CZ 3A	CZ 3B	CZ 3C	CZ 4A	CZ 4B	CZ 4C	CZ 5A	CZ 5B	CZ 6A	CZ 6B	CZ 7	CZ 8
oldest	Single-family home	1.7	2.0	1.9	2.0	2.0	1.7	1.7	1.9	2.4	2.4	1.9	3.4	1.9	2.3	2.4
	Apartment building	1.7	2.0	1.9	2.0	2.0	1.7	1.7	1.9	2.4	2.4	1.9	3.4	1.9	2.3	2.4
	Large office	2.6	2.6	2.6	2.6	2.6	2.6	2.3	2.3	2.3	2.4	2.4	2.7	2.7	2.4	2.3
	Medium office	2.3	2.3	2.3	2.2	2.3	2.2	2.0	2.0	2.0	2.2	2.1	2.4	2.4	2.2	2.1
	Small office	2.3	2.3	2.3	2.2	2.3	2.2	2.0	2.0	2.0	2.2	2.1	2.4	2.4	2.2	2.1
	Large hotel	2.6	2.6	2.6	2.6	2.6	2.6	2.3	2.3	2.3	2.4	2.4	2.7	2.7	2.4	2.3
	Sit-down restaurant	2.3	2.3	2.3	2.2	2.3	2.2	2.0	2.0	2.0	2.2	2.1	2.4	2.4	2.2	2.1
	Fast-food restaurant	2.6	2.6	2.6	2.6	2.6	2.6	2.3	2.3	2.3	2.4	2.4	2.7	2.7	2.4	2.3
	Retail stand-alone	2.3	2.3	2.3	2.2	2.3	2.2	2.0	2.0	2.0	2.2	2.1	2.4	2.4	2.2	2.1
	Strip mall retail	2.3	2.3	2.3	2.2	2.3	2.2	2.0	2.0	2.0	2.2	2.1	2.4	2.4	2.2	2.1
older	Single-family home	2.4	2.4	2.4	2.4	2.4	2.2	2.4	2.4	2.9	2.6	2.4	2.2	2.4	1.9	2.9
	Apartment building	2.4	2.4	2.4	2.4	2.4	2.2	2.4	2.4	2.9	2.6	2.4	2.2	2.4	1.9	2.9
	Large office	3.6	6.4	11.8	4.8	7.3	3.9	2.2	3.6	1.6	2.0	3.0	1.7	1.7	1.6	1.6
	Medium office	3.1	2.2	5.1	1.8	3.3	1.4	1.5	1.7	1.4	1.5	1.6	1.4	1.5	1.4	1.5
	Small office	8.3	7.2	12.8	5.5	7.9	4.6	2.5	4.0	1.8	2.2	3.3	1.8	1.8	1.7	1.7
	Large hotel	3.6	6.4	11.8	4.8	7.3	3.9	2.2	3.6	1.6	2.0	3.0	1.7	1.7	1.6	1.6
	Sit-down restaurant	3.5	2.5	5.5	2.0	3.6	1.7	1.7	1.8	1.6	1.7	1.7	1.6	1.6	1.5	1.5
	Fast-food restaurant	4.9	2.5	5.5	2.0	3.6	1.7	1.7	1.8	1.6	1.7	1.7	1.6	1.6	1.5	1.5
	Retail stand-alone	7.3	6.4	11.8	4.8	7.3	3.9	2.2	3.6	1.6	2.0	3.0	1.7	1.7	1.6	1.6
	Strip mall retail	3.1	2.2	5.1	1.8	3.3	1.4	1.5	1.7	1.4	1.5	1.6	1.4	1.5	1.4	1.5
new	Single-family home	2.4	2.8	2.4	2.4	2.0	2.0	2.3	2.8	2.3	2.3	2.0	2.3	2.3	2.3	2.3
	Apartment building	2.6	3.1	2.6	2.6	2.2	2.2	2.7	3.1	2.7	2.7	2.2	2.7	2.7	2.7	2.7
	Large office	7.3	3.8	7.3	2.5	3.1	3.1	3.2	2.4	2.1	2.8	1.8	2.5	1.6	1.5	1.6
	Medium office	2.0	2.2	2.0	1.8	2.0	2.0	2.0	2.0	1.3	1.7	1.3	1.5	1.3	1.3	1.3
	Small office	2.8	3.5	2.8	3.5	3.5	3.5	3.2	2.8	3.5	2.6	2.5	2.6	2.0	2.0	2.0
	Large hotel	7.3	3.8	7.3	2.5	3.1	3.1	3.2	2.4	2.1	2.8	1.8	2.5	1.6	1.5	1.6
	Sit-down restaurant	4.0	3.3	4.0	3.3	3.1	3.1	3.2	4.0	2.5	2.8	2.5	2.5	2.5	2.5	2.5
	Fast-food restaurant	2.8	3.5	2.8	3.5	3.5	3.5	3.2	2.8	3.5	2.6	2.5	2.6	2.0	2.0	2.0
	Retail stand-alone	7.3	3.8	7.3	2.5	3.1	3.1	3.2	2.4	2.1	2.8	1.8	2.5	1.6	1.5	1.6
	Strip mall retail	2.0	2.2	2.0	1.8	2.0	2.0	2.0	2.0	1.3	1.7	1.3	1.5	1.3	1.3	1.3

Task Report Appendix D: Solar radiation in representative cities

The monthly and seasonal daily solar radiations for each of the cities simulated in this study are summarized for California (Table D-1 through Table D-16) and U.S. (Table D-17 through Table D-33).

Table D-1. Monthly and seasonal daily solar irradiation in Arcata, California (city representing California building climate zone 1).

		Solar Radiation [kWh/m²·day]						
		Horizontal (H)	North wall (N)	East wall (E)	South wall (S)	West wall (W)	Four-wall average (NESW)	Ratio of NESW to H
Month	January	1.68	0.59	1.12	2.46	1.09	1.31	78%
	February	2.67	0.82	1.73	3.40	1.75	1.92	72%
	March	3.62	0.93	2.13	3.13	2.16	2.09	58%
	April	4.60	1.19	2.52	2.74	2.62	2.27	49%
	May	5.62	1.52	2.71	2.42	3.19	2.46	44%
	June	6.17	1.95	2.82	2.49	3.91	2.79	45%
	July	5.98	1.83	2.55	2.63	3.87	2.72	46%
	August	5.08	1.49	2.15	2.85	3.45	2.48	49%
	September	4.15	1.19	2.24	3.31	2.84	2.40	58%
	October	3.03	0.90	1.81	3.38	2.12	2.05	68%
	November	2.13	0.65	1.40	3.31	1.51	1.72	81%
	December	1.59	0.49	1.18	2.92	1.08	1.42	89%
Season	Winter (DJF)	1.98	0.63	1.34	2.92	1.31	1.55	78%
	Spring (MAM)	4.61	1.21	2.45	2.76	2.66	2.27	49%
	Summer (JJA)	5.74	1.75	2.51	2.65	3.74	2.66	46%
	Fall (SON)	3.10	0.92	1.82	3.33	2.16	2.06	66%
Ratio	Winter / Summer	35%	36%	53%	110%	35%	58%	

Table D-2. Monthly and seasonal daily solar irradiation in Santa Rosa, California (city representing California building climate zone 2).

		Solar Radiation [kWh/m²·day]						
		Horizontal (H)	North wall (N)	East wall (E)	South wall (S)	West wall (W)	Four-wall average (NESW)	Ratio of NESW to H
Month	January	1.90	0.61	1.11	2.62	1.22	1.39	73%
	February	2.47	0.73	1.61	2.94	1.60	1.72	70%
	March	3.33	0.87	1.93	2.58	1.91	1.82	55%
	April	5.96	1.29	3.03	3.36	3.65	2.83	47%
	May	7.34	1.61	3.63	2.89	3.93	3.01	41%
	June	7.65	1.91	3.86	2.48	4.08	3.08	40%
	July	7.38	1.75	3.49	2.75	4.10	3.02	41%
	August	6.59	1.40	3.23	3.37	3.80	2.95	45%
	September	5.44	1.16	2.92	4.30	3.39	2.94	54%
	October	3.58	0.89	2.11	4.04	2.28	2.33	65%
	November	2.39	0.63	1.58	3.70	1.56	1.87	78%
	December	1.55	0.54	1.08	2.52	1.09	1.31	84%
Season	Winter (DJF)	1.98	0.63	1.27	2.69	1.31	1.47	75%
	Spring (MAM)	5.54	1.26	2.86	2.94	3.16	2.55	46%
	Summer (JJA)	7.21	1.69	3.53	2.87	4.00	3.02	42%
	Fall (SON)	3.80	0.90	2.20	4.01	2.41	2.38	63%
Ratio	Winter / Summer	27%	37%	36%	94%	33%	49%	

Table D-3. Monthly and seasonal daily solar irradiation in Oakland, California (city representing California building climate zone 3).

		Solar Radiation [kWh/m²·day]						Ratio of NESW to H
		Horizontal (H)	North wall (N)	East wall (E)	South wall (S)	West wall (W)	Four-wall average (NESW)	
Month	January	2.17	0.62	1.37	3.23	1.38	1.65	76%
	February	2.65	0.75	1.45	2.91	1.68	1.70	64%
	March	3.44	0.90	1.93	2.58	1.93	1.84	53%
	April	6.21	1.29	3.21	3.41	3.59	2.88	46%
	May	6.71	1.58	3.33	2.57	3.45	2.73	41%
	June	7.64	1.89	3.47	2.48	4.11	2.99	39%
	July	6.82	1.70	2.92	2.58	3.73	2.73	40%
	August	6.17	1.38	2.82	3.13	3.49	2.71	44%
	September	5.51	1.23	3.07	4.20	3.33	2.96	54%
	October	3.56	0.92	2.07	3.89	2.30	2.29	64%
	November	2.67	0.70	1.75	3.93	1.65	2.01	75%
	December	2.01	0.63	1.37	3.37	1.38	1.69	84%
Season	Winter (DJF)	2.28	0.67	1.40	3.17	1.48	1.68	74%
	Spring (MAM)	5.45	1.26	2.82	2.85	2.99	2.48	46%
	Summer (JJA)	6.88	1.66	3.07	2.73	3.78	2.81	41%
	Fall (SON)	3.91	0.95	2.29	4.01	2.42	2.42	62%
Ratio	Winter / Summer	33%	40%	45%	116%	39%	60%	

Table D-4. Monthly and seasonal daily solar irradiation in San Jose, California (city representing California building climate zone 4).

		Solar Radiation [kWh/m²·day]						Ratio of NESW to H
		Horizontal (H)	North wall (N)	East wall (E)	South wall (S)	West wall (W)	Four-wall average (NESW)	
Month	January	2.25	0.64	1.42	3.40	1.45	1.73	77%
	February	2.96	0.81	1.97	3.57	1.90	2.06	70%
	March	3.45	0.96	2.03	2.60	2.00	1.90	55%
	April	6.07	1.33	3.36	3.42	3.46	2.89	48%
	May	7.31	1.68	3.74	2.84	3.96	3.06	42%
	June	8.10	2.01	4.22	2.55	4.17	3.24	40%
	July	7.72	1.80	3.78	2.75	4.18	3.13	41%
	August	6.94	1.42	3.59	3.48	3.92	3.10	45%
	September	5.68	1.23	3.12	4.38	3.46	3.05	54%
	October	4.07	0.98	2.41	4.54	2.55	2.62	64%
	November	2.70	0.69	1.76	4.15	1.80	2.10	78%
	December	2.17	0.61	1.45	3.84	1.60	1.88	86%
Season	Winter (DJF)	2.46	0.69	1.61	3.60	1.65	1.89	77%
	Spring (MAM)	5.61	1.32	3.05	2.95	3.14	2.61	47%
	Summer (JJA)	7.59	1.74	3.86	2.93	4.09	3.16	42%
	Fall (SON)	4.15	0.97	2.43	4.35	2.61	2.59	62%
Ratio	Winter / Summer	32%	40%	42%	123%	40%	60%	

Table D-5. Monthly and seasonal daily solar irradiation in Santa Maria, California (city representing California building climate zone 5).

		Solar Radiation [kWh/m²·day]						
		Horizontal (H)	North wall (N)	East wall (E)	South wall (S)	West wall (W)	Four-wall average (NESW)	Ratio of NESW to H
Month	January	2.88	0.57	1.81	4.46	1.82	2.16	75%
	February	3.70	0.94	2.35	4.29	2.34	2.48	67%
	March	4.54	1.15	2.79	3.67	2.78	2.60	57%
	April	6.33	1.41	3.33	3.48	3.72	2.99	47%
	May	7.18	1.51	3.36	2.35	3.70	2.73	38%
	June	7.38	1.95	3.04	2.30	4.42	2.93	40%
	July	7.40	1.84	3.04	2.50	4.43	2.95	40%
	August	6.84	1.47	3.05	3.24	3.98	2.94	43%
	September	5.68	1.20	2.63	4.13	3.64	2.90	51%
	October	4.27	0.99	2.44	4.57	2.80	2.70	63%
	November	3.20	0.76	2.20	4.82	2.05	2.46	77%
	December	2.67	0.67	1.85	4.57	1.82	2.23	83%
Season	Winter (DJF)	3.08	0.73	2.00	4.44	1.99	2.29	74%
	Spring (MAM)	6.01	1.36	3.16	3.17	3.40	2.77	46%
	Summer (JJA)	7.21	1.76	3.04	2.68	4.28	2.94	41%
	Fall (SON)	4.38	0.98	2.42	4.50	2.83	2.69	61%
Ratio	Winter / Summer	43%	41%	66%	166%	47%	78%	

Table D-6. Monthly and seasonal daily solar irradiation in Long Beach, California (city representing California building climate zone 6).

		Solar Radiation [kWh/m²·day]						Ratio of NESW to H
		Horizontal (H)	North wall (N)	East wall (E)	South wall (S)	West wall (W)	Four-wall average (NESW)	
Month	January	2.61	0.65	1.51	3.74	1.66	1.89	72%
	February	3.46	0.83	1.89	3.67	2.02	2.10	61%
	March	4.64	1.20	2.48	3.73	2.91	2.58	56%
	April	5.95	1.46	2.89	3.17	3.63	2.79	47%
	May	6.56	1.78	3.09	2.46	3.78	2.78	42%
	June	7.06	1.94	2.85	2.17	4.26	2.81	40%
	July	7.30	1.82	3.06	2.40	4.25	2.88	39%
	August	6.65	1.53	3.16	3.02	3.94	2.91	44%
	September	5.46	1.27	2.77	3.72	3.35	2.78	51%
	October	4.17	1.06	2.24	4.22	2.64	2.54	61%
	November	3.21	0.81	1.94	4.55	2.17	2.37	74%
	December	2.64	0.70	1.75	4.28	1.76	2.12	80%
Season	Winter (DJF)	2.90	0.73	1.71	3.90	1.81	2.04	70%
	Spring (MAM)	5.72	1.48	2.82	3.12	3.44	2.72	47%
	Summer (JJA)	7.00	1.76	3.02	2.53	4.15	2.87	41%
	Fall (SON)	4.28	1.05	2.32	4.17	2.72	2.56	60%
Ratio	Winter / Summer	41%	41%	57%	154%	44%	71%	

Table D-7. Monthly and seasonal daily solar irradiation in San Diego, California (city representing California building climate zone 7).

		Solar Radiation [kWh/m²·day]						
		Horizontal (H)	North wall (N)	East wall (E)	South wall (S)	West wall (W)	Four-wall average (NESW)	Ratio of NESW to H
Month	January	3.01	0.67	1.84	4.46	1.92	2.22	74%
	February	3.85	0.84	2.16	4.30	2.26	2.39	62%
	March	4.87	1.20	2.69	3.81	3.10	2.70	55%
	April	6.08	1.45	3.29	3.17	3.46	2.84	47%
	May	6.46	1.70	2.83	2.35	3.53	2.60	40%
	June	6.97	1.72	2.86	1.93	3.67	2.54	36%
	July	7.19	1.82	3.06	2.25	4.24	2.84	40%
	August	6.75	1.47	3.08	2.97	3.82	2.84	42%
	September	5.73	1.21	2.83	3.81	3.53	2.84	50%
	October	4.28	1.03	2.21	4.23	2.69	2.54	59%
	November	3.54	0.82	2.17	4.99	2.32	2.58	73%
	December	2.88	0.66	1.90	4.71	1.95	2.30	80%
Season	Winter (DJF)	3.25	0.72	1.96	4.49	2.04	2.30	71%
	Spring (MAM)	5.80	1.45	2.94	3.11	3.36	2.71	47%
	Summer (JJA)	6.97	1.67	3.00	2.38	3.91	2.74	39%
	Fall (SON)	4.52	1.02	2.40	4.35	2.85	2.65	59%
Ratio	Winter / Summer	47%	43%	65%	188%	52%	84%	

Table D-8. Monthly and seasonal daily solar irradiation in Fullerton, California (city representing California building climate zone 8).

		Solar Radiation [kWh/m²·day]						Ratio of NESW to H
		Horizontal (H)	North wall (N)	East wall (E)	South wall (S)	West wall (W)	Four-wall average (NESW)	
Month	January	3.06	0.72	1.90	4.51	1.85	2.25	73%
	February	3.21	0.93	1.92	3.37	2.06	2.07	64%
	March	4.47	1.05	2.26	3.38	2.76	2.36	53%
	April	6.53	1.40	3.54	3.34	3.63	2.98	46%
	May	6.52	1.73	3.14	2.36	3.70	2.73	42%
	June	7.19	1.87	3.14	2.20	3.90	2.78	39%
	July	7.28	1.87	3.25	2.41	4.28	2.95	41%
	August	6.72	1.54	3.52	3.06	3.66	2.95	44%
	September	5.71	1.29	3.04	4.03	3.39	2.94	51%
	October	3.75	1.01	2.08	3.72	2.30	2.27	61%
	November	3.21	0.83	2.02	4.36	2.12	2.33	73%
	December	2.81	0.74	1.76	4.53	1.93	2.24	80%
Season	Winter (DJF)	3.03	0.80	1.86	4.14	1.95	2.19	72%
	Spring (MAM)	5.84	1.39	2.98	3.03	3.36	2.69	46%
	Summer (JJA)	7.06	1.76	3.30	2.55	3.95	2.89	41%
	Fall (SON)	4.22	1.04	2.38	4.04	2.60	2.52	60%
Ratio	Winter / Summer	43%	45%	56%	162%	49%	76%	

Table D-9. Monthly and seasonal daily solar irradiation in Burbank, California (city representing California building climate zone 9).

		Solar Radiation [kWh/m²·day]						
		Horizontal (H)	North wall (N)	East wall (E)	South wall (S)	West wall (W)	Four-wall average (NESW)	Ratio of NESW to H
Month	January	2.97	0.65	1.96	4.56	1.81	2.25	76%
	February	3.19	0.81	1.82	3.33	1.88	1.96	61%
	March	4.99	0.99	2.68	3.76	2.81	2.56	51%
	April	6.42	1.26	3.28	3.06	3.59	2.80	44%
	May	6.74	1.70	3.53	2.30	3.62	2.79	41%
	June	7.79	1.90	3.70	2.17	4.06	2.96	38%
	July	7.60	1.91	4.14	2.43	3.98	3.11	41%
	August	7.23	1.51	3.92	3.26	4.05	3.19	44%
	September	5.36	1.22	3.11	3.77	3.28	2.84	53%
	October	3.90	0.96	2.47	4.02	2.24	2.42	62%
	November	3.56	0.79	2.23	5.15	2.38	2.64	74%
	December	2.66	0.67	1.79	4.41	1.84	2.18	82%
Season	Winter (DJF)	2.94	0.71	1.86	4.10	1.84	2.13	72%
	Spring (MAM)	6.05	1.31	3.17	3.04	3.34	2.71	45%
	Summer (JJA)	7.54	1.77	3.92	2.62	4.03	3.09	41%
	Fall (SON)	4.27	0.99	2.60	4.31	2.63	2.63	62%
Ratio	Winter / Summer	39%	40%	47%	157%	46%	69%	

Table D-10. Monthly and seasonal daily solar irradiation in Riverside, California (city representing California building climate zone 10).

		Solar Radiation [kWh/m²·day]						
		Horizontal (H)	North wall (N)	East wall (E)	South wall (S)	West wall (W)	Four-wall average (NESW)	Ratio of NESW to H
Month	January	3.09	0.75	1.87	4.62	2.06	2.33	75%
	February	3.51	0.92	2.14	3.93	2.21	2.30	66%
	March	4.87	1.07	2.42	3.69	2.96	2.54	52%
	April	6.17	1.39	3.46	3.15	3.38	2.84	46%
	May	6.91	1.77	3.36	2.45	3.89	2.87	41%
	June	7.92	2.02	3.76	2.26	4.24	3.07	39%
	July	7.61	1.98	4.14	2.46	4.04	3.16	41%
	August	7.12	1.59	3.96	3.24	3.93	3.18	45%
	September	4.93	1.22	2.90	3.42	2.95	2.62	53%
	October	3.83	0.99	2.28	3.84	2.27	2.34	61%
	November	3.55	0.82	2.20	5.06	2.34	2.60	73%
	December	2.94	0.73	2.02	4.95	1.98	2.42	82%
Season	Winter (DJF)	3.18	0.80	2.01	4.50	2.09	2.35	74%
	Spring (MAM)	5.98	1.41	3.08	3.10	3.41	2.75	46%
	Summer (JJA)	7.55	1.86	3.95	2.65	4.07	3.14	42%
	Fall (SON)	4.10	1.01	2.46	4.11	2.52	2.52	62%
Ratio	Winter / Summer	42%	43%	51%	169%	51%	75%	

Table D-11. Monthly and seasonal daily solar irradiation in Beale, California (city located in California building climate zone 11, 105 miles south of Red Bluff, CA, which is the city representing CACZ 11).

		Solar Radiation [kWh/m²·day]						
		Horizontal (H)	North wall (N)	East wall (E)	South wall (S)	West wall (W)	Four-wall average (NESW)	Ratio of NESW to H
Month	January	1.87	0.59	1.19	2.78	1.22	1.44	77%
	February	2.53	0.82	1.52	2.87	1.70	1.73	68%
	March	3.93	1.05	2.43	3.32	2.31	2.28	58%
	April	5.16	1.27	2.87	3.02	3.04	2.55	49%
	May	7.42	1.68	4.20	2.96	3.87	3.18	43%
	June	7.15	1.94	3.83	2.51	3.82	3.03	42%
	July	7.53	1.87	4.22	2.81	4.11	3.25	43%
	August	7.11	1.40	4.05	3.68	3.90	3.26	46%
	September	5.72	1.19	3.60	4.66	3.38	3.21	56%
	October	3.36	0.90	2.20	3.66	2.01	2.19	65%
	November	2.12	0.66	1.33	2.96	1.28	1.56	74%
	December	2.08	0.63	1.39	3.71	1.52	1.81	87%
Season	Winter (DJF)	2.16	0.68	1.37	3.12	1.48	1.66	77%
	Spring (MAM)	5.50	1.34	3.16	3.10	3.07	2.67	48%
	Summer (JJA)	7.26	1.73	4.03	3.00	3.94	3.18	44%
	Fall (SON)	3.73	0.91	2.38	3.76	2.22	2.32	62%
Ratio	Winter / Summer	30%	39%	34%	104%	38%	52%	

Table D-12. Monthly and seasonal daily solar irradiation in Sacramento, California (city representing California building climate zone 12).

		Solar Radiation [kWh/m²·day]						Ratio of NESW to H
		Horizontal (H)	North wall (N)	East wall (E)	South wall (S)	West wall (W)	Four-wall average (NESW)	
Month	January	1.74	0.55	0.97	2.50	1.24	1.31	76%
	February	2.64	0.81	1.70	3.12	1.64	1.82	69%
	March	4.73	1.06	2.88	4.07	2.62	2.66	56%
	April	6.40	1.38	3.82	3.71	3.73	3.16	49%
	May	7.35	1.69	4.18	2.93	3.85	3.16	43%
	June	8.09	2.07	4.49	2.62	4.28	3.37	42%
	July	7.87	1.92	4.40	2.85	4.28	3.37	43%
	August	7.05	1.40	4.17	3.58	3.87	3.25	46%
	September	5.42	1.19	3.42	4.40	3.26	3.07	57%
	October	3.65	0.90	2.37	4.16	2.34	2.44	67%
	November	2.51	0.72	1.64	3.69	1.58	1.91	76%
	December	1.88	0.62	1.16	3.06	1.35	1.55	82%
Season	Winter (DJF)	2.09	0.66	1.28	2.89	1.41	1.56	75%
	Spring (MAM)	6.16	1.38	3.63	3.57	3.40	2.99	49%
	Summer (JJA)	7.67	1.80	4.35	3.02	4.14	3.33	43%
	Fall (SON)	3.86	0.94	2.47	4.09	2.39	2.47	64%
Ratio	Winter / Summer	27%	37%	29%	96%	34%	47%	

Table D-13. Monthly and seasonal daily solar irradiation in Sacramento, California (city representing California building climate zone 12).

		Solar Radiation [kWh/m²·day]						Ratio of NESW to H
		Horizontal (H)	North wall (N)	East wall (E)	South wall (S)	West wall (W)	Four-wall average (NESW)	
Month	January	1.86	0.67	1.16	2.28	1.11	1.31	70%
	February	3.19	0.95	2.10	3.74	2.06	2.21	69%
	March	4.72	1.23	2.76	3.95	2.90	2.71	57%
	April	6.53	1.48	3.75	3.82	3.77	3.21	49%
	May	7.35	1.84	4.12	2.83	3.90	3.17	43%
	June	8.18	2.14	4.52	2.49	4.40	3.39	41%
	July	7.84	1.99	4.33	2.67	4.38	3.34	43%
	August	7.31	1.56	4.15	3.58	4.28	3.39	46%
	September	5.73	1.20	3.51	4.33	3.43	3.12	54%
	October	4.36	1.03	2.80	4.82	2.60	2.81	65%
	November	2.73	0.77	1.60	3.80	1.87	2.01	74%
	December	1.92	0.61	1.19	2.95	1.25	1.50	78%
Season	Winter (DJF)	2.32	0.74	1.48	2.99	1.48	1.67	72%
	Spring (MAM)	6.20	1.52	3.55	3.53	3.52	3.03	49%
	Summer (JJA)	7.78	1.89	4.33	2.91	4.35	3.37	43%
	Fall (SON)	4.28	1.00	2.64	4.32	2.63	2.65	62%
Ratio	Winter / Summer	30%	39%	34%	103%	34%	50%	

Table D-14. Monthly and seasonal daily solar irradiation in China Lake, California (city representing California building climate zone 14).

		Solar Radiation [kWh/m²·day]						Ratio of NESW to H
		Horizontal (H)	North wall (N)	East wall (E)	South wall (S)	West wall (W)	Four-wall average (NESW)	
Month	January	3.19	0.74	2.33	5.41	2.13	2.65	83%
	February	4.02	0.94	2.77	5.13	2.69	2.89	72%
	March	5.60	1.08	3.48	4.72	3.49	3.20	57%
	April	6.98	1.50	4.32	3.73	3.84	3.34	48%
	May	8.08	1.97	4.57	2.85	4.55	3.49	43%
	June	8.55	2.16	4.81	2.36	4.57	3.47	41%
	July	7.91	1.91	4.61	2.49	4.16	3.29	42%
	August	7.41	1.50	4.46	3.31	4.35	3.41	46%
	September	6.15	1.14	3.87	4.59	3.82	3.35	55%
	October	4.79	0.95	3.20	5.42	3.09	3.17	66%
	November	3.45	0.73	2.33	5.55	2.55	2.79	81%
	December	2.81	0.65	2.02	5.26	2.12	2.51	89%
Season	Winter (DJF)	3.34	0.78	2.38	5.27	2.32	2.68	80%
	Spring (MAM)	6.88	1.52	4.12	3.77	3.96	3.34	49%
	Summer (JJA)	7.96	1.86	4.63	2.72	4.36	3.39	43%
	Fall (SON)	4.80	0.94	3.14	5.19	3.15	3.10	65%
Ratio	Winter / Summer	42%	42%	51%	194%	53%	79%	

Table D-15. Monthly and seasonal daily solar irradiation in Palm Springs, California (city located in California building climate zone 15, 100 miles north of Imperial, California, which is the city representing CACZ 15).

		Solar Radiation [kWh/m²·day]						
		Horizontal (H)	North wall (N)	East wall (E)	South wall (S)	West wall (W)	Four-wall average (NESW)	Ratio of NESW to H
Month	January	3.24	0.75	2.23	5.09	2.12	2.55	79%
	February	3.92	0.98	2.49	4.55	2.59	2.65	68%
	March	5.20	1.05	3.20	4.15	3.11	2.88	55%
	April	6.82	1.48	4.08	3.46	3.74	3.19	47%
	May	7.85	2.03	4.48	2.71	4.42	3.41	43%
	June	8.09	2.35	4.44	2.26	4.66	3.43	42%
	July	7.66	2.10	4.30	2.38	4.42	3.30	43%
	August	7.06	1.53	4.17	3.14	4.01	3.21	45%
	September	5.89	1.20	3.73	4.23	3.54	3.17	54%
	October	4.59	0.97	3.00	4.86	2.71	2.89	63%
	November	3.66	0.78	2.36	5.49	2.57	2.80	76%
	December	3.23	0.73	2.17	5.71	2.39	2.75	85%
Season	Winter (DJF)	3.46	0.82	2.30	5.12	2.37	2.65	77%
	Spring (MAM)	6.62	1.52	3.92	3.44	3.76	3.16	48%
	Summer (JJA)	7.60	1.99	4.30	2.59	4.36	3.31	44%
	Fall (SON)	4.71	0.98	3.03	4.86	2.94	2.95	63%
Ratio	Winter / Summer	46%	41%	53%	197%	54%	80%	

Table D-16. Monthly and seasonal daily solar irradiation in Montague Siskiyou County airport, which is 30 miles north of Mount Shasta, California (city representing California building climate zone 16).

		Solar Radiation [kWh/m²·day]						
		Horizontal (H)	North wall (N)	East wall (E)	South wall (S)	West wall (W)	Four-wall average (NESW)	Ratio of NESW to H
Month	January	1.94	0.56	1.33	3.45	1.49	1.71	88%
	February	2.97	0.69	1.88	4.20	2.15	2.23	75%
	March	4.41	0.93	2.73	4.27	2.86	2.70	61%
	April	5.60	1.25	3.41	3.47	3.27	2.85	51%
	May	6.87	1.65	4.02	2.92	3.61	3.05	44%
	June	7.59	2.01	4.23	2.69	4.11	3.26	43%
	July	7.82	1.81	4.44	2.98	4.28	3.38	43%
	August	7.19	1.32	4.34	3.92	4.04	3.41	47%
	September	5.69	1.00	3.62	4.91	3.69	3.30	58%
	October	3.51	0.80	2.41	4.44	2.26	2.48	71%
	November	1.95	0.56	1.26	3.11	1.35	1.57	80%
	December	1.89	0.54	1.33	3.86	1.49	1.81	95%
Season	Winter (DJF)	2.27	0.60	1.51	3.84	1.71	1.91	84%
	Spring (MAM)	5.63	1.28	3.39	3.55	3.25	2.87	51%
	Summer (JJA)	7.53	1.71	4.34	3.20	4.14	3.35	44%
	Fall (SON)	3.72	0.79	2.43	4.15	2.43	2.45	66%
Ratio	Winter / Summer	30%	35%	35%	120%	41%	57%	

Table D-17. Monthly and seasonal daily solar irradiation in Miami, Florida (city representing ASHRAE climate zone 1A).

		Solar Radiation [kWh/m²·day]						Ratio of NESW to H
		Horizontal (H)	North wall (N)	East wall (E)	South wall (S)	West wall (W)	Four-wall average (NESW)	
Month	January	3.49	0.83	2.15	4.05	1.93	2.24	64%
	February	4.25	1.09	2.54	3.87	2.47	2.49	59%
	March	5.16	1.30	3.03	3.31	3.03	2.67	52%
	April	5.93	1.28	3.08	2.34	3.11	2.45	41%
	May	5.81	1.78	3.13	1.83	3.05	2.45	42%
	June	5.54	1.93	3.07	1.59	2.59	2.30	41%
	July	6.01	1.92	3.18	1.77	2.89	2.44	41%
	August	5.49	1.40	2.68	1.94	2.67	2.17	40%
	September	4.88	1.41	2.80	2.78	2.47	2.36	48%
	October	4.32	1.03	2.43	3.42	2.33	2.30	53%
	November	3.54	1.03	2.13	3.72	2.06	2.23	63%
	December	3.22	0.83	1.67	3.83	1.97	2.08	65%
Season	Winter (DJF)	3.65	0.92	2.12	3.92	2.12	2.27	62%
	Spring (MAM)	5.63	1.46	3.08	2.49	3.06	2.52	45%
	Summer (JJA)	5.68	1.75	2.98	1.77	2.72	2.30	41%
	Fall (SON)	4.25	1.15	2.45	3.30	2.29	2.30	54%
Ratio	Winter / Summer	64%	52%	71%	221%	78%	98%	

Table D-18. Monthly and seasonal daily solar irradiation in Houston, Texas (city representing ASHRAE climate zone 2A).

		Solar Radiation [kWh/m²·day]						
		Horizontal (H)	North wall (N)	East wall (E)	South wall (S)	West wall (W)	Four-wall average (NESW)	Ratio of NESW to H
Month	January	2.83	0.82	1.66	3.42	1.81	1.93	68%
	February	3.29	0.97	1.81	3.15	2.06	2.00	61%
	March	4.27	1.16	2.33	3.03	2.55	2.27	53%
	April	4.92	1.43	2.56	2.41	2.70	2.27	46%
	May	5.44	1.70	2.90	1.94	2.91	2.36	43%
	June	5.95	1.90	3.27	1.71	2.94	2.46	41%
	July	6.18	1.82	3.27	1.88	3.04	2.50	41%
	August	5.47	1.39	2.99	2.19	2.75	2.33	43%
	September	5.05	1.30	2.93	3.18	2.87	2.57	51%
	October	4.22	1.06	2.46	3.90	2.53	2.49	59%
	November	3.17	0.88	1.90	3.75	1.94	2.12	67%
	December	2.60	0.78	1.52	3.40	1.70	1.85	71%
Season	Winter (DJF)	2.91	0.86	1.67	3.32	1.86	1.93	66%
	Spring (MAM)	4.88	1.43	2.60	2.46	2.72	2.30	47%
	Summer (JJA)	5.87	1.70	3.18	1.93	2.91	2.43	41%
	Fall (SON)	4.15	1.08	2.43	3.61	2.45	2.39	58%
Ratio	Winter / Summer	50%	50%	52%	172%	64%	79%	

Table D-19. Monthly and seasonal daily solar irradiation in Phoenix, Arizona (city representing ASHRAE climate zone 2B).

		Solar Radiation [kWh/m²·day]						Ratio of NESW to H
		Horizontal (H)	North wall (N)	East wall (E)	South wall (S)	West wall (W)	Four-wall average (NESW)	
Month	January	3.29	0.78	2.07	5.08	2.39	2.58	78%
	February	4.18	0.97	2.72	4.84	2.57	2.77	66%
	March	5.34	1.12	3.19	4.18	3.27	2.94	55%
	April	7.12	1.49	4.22	3.64	3.91	3.31	47%
	May	7.85	1.98	4.36	2.64	4.28	3.31	42%
	June	8.31	2.29	4.50	2.29	4.41	3.37	41%
	July	7.60	1.96	3.95	2.42	3.92	3.06	40%
	August	7.12	1.60	3.95	3.18	4.02	3.19	45%
	September	6.31	1.28	3.71	4.38	3.73	3.28	52%
	October	4.78	1.03	3.14	5.07	2.86	3.03	63%
	November	3.75	0.83	2.57	5.55	2.48	2.86	76%
	December	3.07	0.72	2.06	5.25	2.19	2.56	83%
Season	Winter (DJF)	3.52	0.82	2.28	5.06	2.38	2.64	75%
	Spring (MAM)	6.77	1.53	3.92	3.48	3.82	3.19	47%
	Summer (JJA)	7.68	1.95	4.13	2.63	4.12	3.21	42%
	Fall (SON)	4.95	1.05	3.14	5.00	3.02	3.05	62%
Ratio	Winter / Summer	46%	42%	55%	192%	58%	82%	

Table D-20. Monthly and seasonal daily solar irradiation in Memphis, Tennessee (city representing ASHRAE climate zone 3A).

		Solar Radiation [kWh/m²·day]						
		Horizontal (H)	North wall (N)	East wall (E)	South wall (S)	West wall (W)	Four-wall average (NESW)	Ratio of NESW to H
Month	January	2.29	0.59	1.41	3.35	1.52	1.72	75%
	February	2.82	0.77	1.76	3.09	1.65	1.82	64%
	March	4.25	1.06	2.40	3.32	2.68	2.36	56%
	April	5.34	1.28	2.99	2.85	3.04	2.54	48%
	May	5.99	1.80	3.40	2.38	3.21	2.70	45%
	June	6.65	1.96	3.48	2.25	3.49	2.79	42%
	July	6.64	1.83	3.53	2.32	3.40	2.77	42%
	August	6.19	1.56	3.39	3.03	3.56	2.88	47%
	September	4.85	1.26	2.85	3.45	2.83	2.60	54%
	October	3.86	1.02	2.29	3.98	2.46	2.44	63%
	November	2.66	0.77	1.66	3.53	1.73	1.92	72%
	December	2.21	0.64	1.51	3.48	1.51	1.79	81%
Season	Winter (DJF)	2.44	0.67	1.56	3.31	1.56	1.77	73%
	Spring (MAM)	5.19	1.38	2.93	2.85	2.97	2.53	49%
	Summer (JJA)	6.49	1.78	3.47	2.53	3.48	2.82	43%
	Fall (SON)	3.79	1.02	2.27	3.65	2.34	2.32	61%
Ratio	Winter / Summer	38%	37%	45%	131%	45%	63%	

Table D-21. Monthly and seasonal daily solar irradiation in El Paso, Texas (city representing ASHRAE climate zone 3B).

		Solar Radiation [kWh/m²·day]						Ratio of NESW to H
		Horizontal (H)	North wall (N)	East wall (E)	South wall (S)	West wall (W)	Four-wall average (NESW)	
Month	January	3.44	0.81	2.16	5.06	2.28	2.58	75%
	February	4.33	1.02	2.87	5.01	2.62	2.88	66%
	March	5.80	1.27	3.48	4.36	3.39	3.12	54%
	April	7.07	1.53	4.10	3.41	3.87	3.23	46%
	May	7.67	1.99	4.27	2.53	4.23	3.26	42%
	June	8.04	2.17	4.29	2.11	4.11	3.17	39%
	July	7.00	1.87	3.79	2.09	3.59	2.84	40%
	August	6.54	1.44	3.58	2.73	3.44	2.80	43%
	September	6.12	1.26	3.63	4.06	3.60	3.14	51%
	October	4.72	1.04	2.80	4.83	3.10	2.94	62%
	November	3.86	0.84	2.54	5.42	2.66	2.86	74%
	December	3.25	0.80	2.20	5.18	2.20	2.60	80%
Season	Winter (DJF)	3.67	0.88	2.41	5.08	2.37	2.68	73%
	Spring (MAM)	6.85	1.60	3.95	3.43	3.83	3.20	47%
	Summer (JJA)	7.19	1.83	3.89	2.31	3.72	2.94	41%
	Fall (SON)	4.90	1.05	2.99	4.77	3.12	2.98	61%
Ratio	Winter / Summer	51%	48%	62%	220%	64%	91%	

Table D-22. Monthly and seasonal daily solar irradiation in San Francisco, California (city representing ASHRAE climate zone 3C).

		Solar Radiation [kWh/m²·day]						
		Horizontal (H)	North wall (N)	East wall (E)	South wall (S)	West wall (W)	Four-wall average (NESW)	Ratio of NESW to H
Month	January	2.14	0.64	1.35	3.10	1.35	1.61	75%
	February	3.18	0.87	1.91	3.89	2.10	2.19	69%
	March	4.41	0.98	2.37	3.69	2.55	2.40	54%
	April	5.68	1.32	3.01	3.08	3.21	2.65	47%
	May	6.42	1.49	3.16	2.50	3.31	2.61	41%
	June	7.15	1.75	3.47	2.28	3.71	2.80	39%
	July	7.12	1.84	3.42	2.69	4.12	3.02	42%
	August	6.38	1.51	3.31	3.29	3.76	2.97	47%
	September	5.47	1.15	2.77	4.19	3.36	2.87	52%
	October	3.76	0.99	2.28	4.07	2.43	2.44	65%
	November	2.53	0.72	1.68	3.60	1.56	1.89	75%
	December	2.13	0.63	1.47	3.75	1.50	1.84	86%
Season	Winter (DJF)	2.48	0.71	1.58	3.58	1.65	1.88	76%
	Spring (MAM)	5.50	1.26	2.85	3.09	3.02	2.56	46%
	Summer (JJA)	6.88	1.70	3.40	2.75	3.86	2.93	43%
	Fall (SON)	3.92	0.95	2.24	3.95	2.45	2.40	61%
Ratio	Winter / Summer	36%	42%	46%	130%	43%	64%	

Table D-23. Monthly and seasonal daily solar irradiation in Baltimore, Maryland (city representing ASHRAE climate zone 4A).

		Solar Radiation [kWh/m²·day]						Ratio of NESW to H
		Horizontal (H)	North wall (N)	East wall (E)	South wall (S)	West wall (W)	Four-wall average (NESW)	
Month	January	2.02	0.59	1.43	3.35	1.37	1.69	84%
	February	2.75	0.78	1.95	3.45	1.71	1.97	72%
	March	3.90	1.04	2.42	3.55	2.31	2.33	60%
	April	5.10	1.37	2.95	3.14	2.89	2.59	51%
	May	5.64	1.67	3.14	2.55	3.11	2.62	46%
	June	6.46	1.94	3.69	2.49	3.36	2.87	44%
	July	5.97	1.82	3.32	2.49	3.33	2.74	46%
	August	5.26	1.35	2.89	2.65	2.74	2.41	46%
	September	4.29	1.19	2.64	3.21	2.51	2.39	56%
	October	3.44	0.92	2.10	3.94	2.11	2.27	66%
	November	2.21	0.65	1.49	3.39	1.57	1.77	80%
	December	1.82	0.56	1.17	3.11	1.31	1.54	84%
Season	Winter (DJF)	2.20	0.64	1.52	3.30	1.46	1.73	79%
	Spring (MAM)	4.88	1.36	2.83	3.08	2.77	2.51	52%
	Summer (JJA)	5.90	1.70	3.30	2.54	3.14	2.67	45%
	Fall (SON)	3.31	0.92	2.08	3.51	2.06	2.14	65%
Ratio	Winter / Summer	37%	38%	46%	130%	47%	65%	

Table D-24. Monthly and seasonal daily solar irradiation in Albuquerque, New Mexico (city representing ASHRAE climate zone 4B).

		Solar Radiation [kWh/m²·day]						Ratio of NESW to H
		Horizontal (H)	North wall (N)	East wall (E)	South wall (S)	West wall (W)	Four-wall average (NESW)	
Month	January	3.16	0.74	2.13	5.06	2.18	2.53	80%
	February	4.15	0.92	2.52	5.16	2.73	2.83	68%
	March	5.08	1.16	3.24	4.23	2.98	2.90	57%
	April	6.80	1.43	4.19	3.55	3.67	3.21	47%
	May	7.18	1.63	3.98	2.50	3.49	2.90	40%
	June	7.59	2.12	4.47	2.20	3.82	3.15	42%
	July	7.37	1.85	4.15	2.46	3.51	2.99	41%
	August	6.96	1.63	4.11	3.26	3.59	3.15	45%
	September	5.78	1.23	3.44	4.19	3.25	3.03	52%
	October	4.55	0.88	3.01	5.04	2.94	2.97	65%
	November	3.41	0.75	2.36	5.23	2.36	2.67	78%
	December	2.93	0.63	2.01	5.41	2.12	2.54	87%
Season	Winter (DJF)	3.41	0.76	2.22	5.21	2.35	2.63	77%
	Spring (MAM)	6.35	1.41	3.80	3.43	3.38	3.00	47%
	Summer (JJA)	7.31	1.87	4.24	2.64	3.64	3.10	42%
	Fall (SON)	4.58	0.95	2.94	4.82	2.85	2.89	63%
Ratio	Winter / Summer	47%	41%	52%	197%	64%	85%	

Table D-25. Monthly and seasonal daily solar irradiation in Salem, Oregon (city representing ASHRAE climate zone 4C, used for commercial prototypes).

		Solar Radiation [kWh/m²·day]						
		Horizontal (H)	North wall (N)	East wall (E)	South wall (S)	West wall (W)	Four-wall average (NESW)	Ratio of NESW to H
Month	January	1.33	0.49	0.89	2.07	0.92	1.09	82%
	February	1.99	0.69	1.21	2.38	1.39	1.42	71%
	March	3.11	0.86	1.87	2.84	1.89	1.86	60%
	April	4.34	1.36	2.44	2.94	2.74	2.37	55%
	May	5.46	1.76	2.91	2.89	3.35	2.73	50%
	June	6.26	2.00	3.36	2.81	3.75	2.98	48%
	July	6.78	1.96	3.88	3.20	4.13	3.29	49%
	August	5.57	1.25	3.17	3.35	3.41	2.79	50%
	September	4.55	1.14	2.79	4.14	3.04	2.78	61%
	October	2.56	0.70	1.53	3.10	1.72	1.77	69%
	November	1.35	0.52	0.84	1.79	0.89	1.01	75%
	December	1.01	0.38	0.73	1.79	0.73	0.91	90%
Season	Winter (DJF)	1.45	0.52	0.94	2.08	1.02	1.14	79%
	Spring (MAM)	4.30	1.33	2.41	2.89	2.66	2.32	54%
	Summer (JJA)	6.20	1.74	3.47	3.12	3.77	3.02	49%
	Fall (SON)	2.82	0.79	1.72	3.01	1.88	1.85	66%
Ratio	Winter / Summer	23%	30%	27%	67%	27%	38%	

Table D-26. Monthly and seasonal daily solar irradiation in Seattle, Washington (city representing ASHRAE climate zone 4C, used for residential prototypes).

		Solar Radiation [kWh/m²·day]						Ratio of NESW to H
		Horizontal (H)	North wall (N)	East wall (E)	South wall (S)	West wall (W)	Four-wall average (NESW)	
Month	January	1.02	0.40	0.66	1.61	0.70	0.84	83%
	February	1.80	0.62	1.19	2.51	1.22	1.39	77%
	March	2.83	0.86	1.69	2.72	1.63	1.72	61%
	April	4.35	1.31	2.64	3.16	2.53	2.41	55%
	May	5.49	1.71	2.84	3.09	3.23	2.72	50%
	June	5.93	1.68	3.24	2.78	2.98	2.67	45%
	July	6.19	1.77	3.17	3.23	3.81	3.00	48%
	August	5.05	1.28	2.95	3.16	3.04	2.61	52%
	September	3.68	0.98	2.23	3.34	2.54	2.27	62%
	October	2.27	0.68	1.50	2.83	1.50	1.63	72%
	November	1.16	0.45	0.77	1.66	0.77	0.91	79%
	December	0.89	0.36	0.68	1.72	0.69	0.86	96%
Season	Winter (DJF)	1.24	0.46	0.84	1.95	0.87	1.03	83%
	Spring (MAM)	4.22	1.29	2.39	2.99	2.46	2.29	54%
	Summer (JJA)	5.72	1.58	3.12	3.06	3.28	2.76	48%
	Fall (SON)	2.37	0.70	1.50	2.61	1.60	1.61	68%
Ratio	Winter / Summer	22%	29%	27%	64%	27%	37%	

Table D-27. Monthly and seasonal daily solar irradiation in Chicago, Illinois (city representing ASHRAE climate zone 5A, used for commercial prototypes).

		Solar Radiation [kWh/m²·day]						
		Horizontal (H)	North wall (N)	East wall (E)	South wall (S)	West wall (W)	Four-wall average (NESW)	Ratio of NESW to H
Month	January	1.76	0.58	1.17	2.88	1.24	1.47	83%
	February	2.50	0.80	1.59	3.20	1.65	1.81	72%
	March	3.45	1.05	2.15	3.16	2.04	2.10	61%
	April	4.39	1.18	2.51	2.72	2.50	2.23	51%
	May	5.98	1.75	3.39	2.88	3.31	2.83	47%
	June	6.29	1.98	3.65	2.64	3.43	2.93	47%
	July	6.17	1.88	3.40	2.83	3.46	2.89	47%
	August	5.14	1.52	3.05	2.96	2.98	2.63	51%
	September	4.17	1.16	2.67	3.40	2.49	2.43	58%
	October	2.92	0.87	1.99	3.47	1.84	2.04	70%
	November	1.80	0.63	1.17	2.53	1.12	1.36	75%
	December	1.49	0.49	1.09	2.67	1.02	1.32	88%
Season	Winter (DJF)	1.92	0.62	1.29	2.92	1.30	1.53	80%
	Spring (MAM)	4.61	1.32	2.68	2.92	2.62	2.39	52%
	Summer (JJA)	5.87	1.79	3.37	2.81	3.29	2.82	48%
	Fall (SON)	2.96	0.89	1.94	3.13	1.82	1.94	66%
Ratio	Winter / Summer	33%	35%	38%	104%	40%	54%	

Table D-28. Monthly and seasonal daily solar irradiation in Peoria, Illinois (city representing ASHRAE climate zone 5A, used for residential prototypes).

		Solar Radiation [kWh/m²·day]						Ratio of NESW to H
		Horizontal (H)	North wall (N)	East wall (E)	South wall (S)	West wall (W)	Four-wall average (NESW)	
Month	January	1.85	0.41	1.15	2.84	1.02	1.36	74%
	February	2.93	0.55	1.66	3.56	1.59	1.84	63%
	March	3.78	0.72	2.09	2.99	1.76	1.89	50%
	April	4.59	0.82	2.19	2.40	2.38	1.95	43%
	May	5.87	1.13	2.89	2.18	2.46	2.16	37%
	June	6.62	1.38	3.11	1.97	3.01	2.37	36%
	July	6.29	1.23	2.95	2.11	2.87	2.29	36%
	August	5.60	0.95	2.47	2.61	2.73	2.19	39%
	September	4.48	0.73	2.43	3.12	2.21	2.12	47%
	October	3.21	0.56	1.87	3.54	1.69	1.91	60%
	November	2.04	0.45	1.16	2.70	1.19	1.37	67%
	December	1.65	0.37	1.00	2.66	0.96	1.25	76%
Season	Winter (DJF)	2.14	0.44	1.27	3.02	1.19	1.48	69%
	Spring (MAM)	4.75	0.89	2.39	2.53	2.20	2.00	42%
	Summer (JJA)	6.17	1.19	2.84	2.23	2.87	2.28	37%
	Fall (SON)	3.24	0.58	1.82	3.12	1.70	1.80	56%
Ratio	Winter / Summer	35%	37%	45%	135%	42%	65%	

Table D-29. Monthly and seasonal daily solar irradiation in Boise, Idaho (city representing ASHRAE climate zone 5B).

		Solar Radiation [kWh/m²·day]						Ratio of NESW to H
		Horizontal (H)	North wall (N)	East wall (E)	South wall (S)	West wall (W)	Four-wall average (NESW)	
Month	January	1.69	0.59	1.16	2.69	1.18	1.40	83%
	February	2.50	0.76	1.62	3.42	1.79	1.90	76%
	March	3.66	0.91	2.42	3.48	2.22	2.26	62%
	April	5.46	1.43	3.49	3.71	3.12	2.94	54%
	May	6.31	1.67	3.57	3.04	3.50	2.94	47%
	June	7.56	2.09	4.37	2.92	4.17	3.39	45%
	July	7.62	1.81	4.29	3.20	4.11	3.35	44%
	August	6.60	1.46	4.00	3.91	4.11	3.37	51%
	September	5.00	1.05	3.32	4.58	3.24	3.05	61%
	October	3.40	0.79	2.51	4.39	2.17	2.47	72%
	November	1.83	0.55	1.25	3.08	1.29	1.54	84%
	December	1.40	0.44	1.00	2.78	1.00	1.30	93%
Season	Winter (DJF)	1.86	0.59	1.26	2.96	1.32	1.53	82%
	Spring (MAM)	5.14	1.34	3.16	3.41	2.95	2.71	53%
	Summer (JJA)	7.26	1.78	4.22	3.34	4.13	3.37	46%
	Fall (SON)	3.41	0.80	2.36	4.02	2.24	2.35	69%
Ratio	Winter / Summer	26%	33%	30%	89%	32%	46%	

Table D-30. Monthly and seasonal daily solar irradiation in Burlington, Vermont (city representing ASHRAE climate zone 6A).

		Solar Radiation [kWh/m²·day]						Ratio of NESW to H
		Horizontal (H)	North wall (N)	East wall (E)	South wall (S)	West wall (W)	Four-wall average (NESW)	
Month	January	1.71	0.63	1.14	2.56	1.19	1.38	81%
	February	2.45	0.78	1.65	3.13	1.50	1.77	72%
	March	3.37	0.94	2.11	3.08	2.21	2.08	62%
	April	4.81	1.34	3.08	3.27	2.93	2.65	55%
	May	5.37	1.55	3.05	2.68	3.01	2.57	48%
	June	6.04	2.02	3.51	2.71	3.50	2.94	49%
	July	5.89	1.84	3.30	2.85	3.34	2.83	48%
	August	5.26	1.52	3.13	3.26	3.20	2.78	53%
	September	3.80	1.18	2.28	3.17	2.25	2.22	58%
	October	2.59	0.83	1.69	3.04	1.69	1.81	70%
	November	1.58	0.54	1.05	2.35	1.11	1.26	80%
	December	1.11	0.39	0.77	2.03	0.77	0.99	89%
Season	Winter (DJF)	1.75	0.60	1.18	2.57	1.15	1.38	79%
	Spring (MAM)	4.52	1.28	2.74	3.01	2.72	2.44	54%
	Summer (JJA)	5.73	1.79	3.31	2.94	3.35	2.85	50%
	Fall (SON)	2.66	0.85	1.67	2.86	1.68	1.77	67%
Ratio	Winter / Summer	31%	34%	36%	88%	34%	48%	

Table D-31. Monthly and seasonal daily solar irradiation in Helena, Montana (city representing ASHRAE climate zone 6B).

		Solar Radiation [kWh/m²·day]						Ratio of NESW to H
		Horizontal (H)	North wall (N)	East wall (E)	South wall (S)	West wall (W)	Four-wall average (NESW)	
Month	January	1.48	0.47	1.16	3.14	1.14	1.48	100%
	February	2.38	1.00	1.96	3.92	2.26	2.29	96%
	March	3.58	0.99	2.27	3.78	2.49	2.38	67%
	April	4.97	1.37	3.20	3.67	3.05	2.82	57%
	May	5.87	1.85	3.76	3.08	3.48	3.04	52%
	June	6.72	1.98	4.08	2.96	3.68	3.17	47%
	July	7.14	1.95	4.34	3.49	4.09	3.47	49%
	August	5.75	1.49	3.79	3.72	3.41	3.10	54%
	September	4.30	1.08	2.94	4.08	2.83	2.73	64%
	October	2.66	0.74	1.87	3.70	1.91	2.06	77%
	November	1.69	0.53	1.21	3.21	1.33	1.57	93%
	December	1.30	0.41	0.96	2.98	1.04	1.35	103%
Season	Winter (DJF)	1.72	0.63	1.36	3.35	1.48	1.70	99%
	Spring (MAM)	4.81	1.40	3.07	3.51	3.01	2.75	57%
	Summer (JJA)	6.54	1.81	4.07	3.39	3.73	3.25	50%
	Fall (SON)	2.88	0.78	2.01	3.67	2.02	2.12	73%
Ratio	Winter / Summer	26%	35%	33%	99%	40%	52%	

Table D-32. Monthly and seasonal daily solar irradiation in Duluth, Minnesota (city representing ASHRAE climate zone 7).

		Solar Radiation [kWh/m²·day]						
		Horizontal (H)	North wall (N)	East wall (E)	South wall (S)	West wall (W)	Four-wall average (NESW)	Ratio of NESW to H
Month	January	1.64	0.54	1.21	3.14	1.18	1.52	92%
	February	2.49	0.78	1.67	3.71	1.78	1.98	80%
	March	3.63	1.02	2.42	3.76	2.35	2.39	66%
	April	4.95	1.25	3.16	3.42	3.02	2.71	55%
	May	5.86	1.79	3.32	3.20	3.73	3.01	51%
	June	6.08	1.92	3.46	2.75	3.45	2.89	48%
	July	5.80	1.61	3.22	2.77	3.34	2.74	47%
	August	4.99	1.27	2.66	3.15	3.02	2.52	51%
	September	3.71	1.06	2.24	3.26	2.49	2.26	61%
	October	2.20	0.65	1.40	2.67	1.47	1.55	71%
	November	1.53	0.54	1.09	2.58	1.14	1.34	88%
	December	1.19	0.41	0.95	2.55	0.90	1.20	101%
Season	Winter (DJF)	1.78	0.57	1.28	3.13	1.28	1.57	88%
	Spring (MAM)	4.82	1.35	2.97	3.46	3.03	2.70	56%
	Summer (JJA)	5.63	1.60	3.11	2.89	3.27	2.72	48%
	Fall (SON)	2.48	0.75	1.57	2.84	1.70	1.72	69%
Ratio	Winter / Summer	32%	36%	41%	108%	39%	58%	

Table D-33. Monthly and seasonal daily solar irradiation in Fairbanks, Alaska (city representing ASHRAE climate zone 8).

		Solar Radiation [kWh/m²·day]						
		Horizontal (H)	North wall (N)	East wall (E)	South wall (S)	West wall (W)	Four-wall average (NESW)	Ratio of NESW to H
Month	January	0.14	0.06	0.21	0.65	0.10	0.26	178%
	February	0.74	0.27	0.95	2.16	0.52	0.97	132%
	March	2.25	0.70	2.48	3.80	1.46	2.11	94%
	April	4.27	1.79	3.70	5.29	3.76	3.63	85%
	May	5.25	2.00	4.55	4.17	3.15	3.47	66%
	June	5.62	2.54	4.24	3.86	3.47	3.53	63%
	July	5.05	2.14	4.03	3.69	2.93	3.20	63%
	August	3.88	1.39	3.25	3.70	2.42	2.69	69%
	September	2.18	0.75	2.07	2.90	1.47	1.80	82%
	October	0.97	0.36	1.16	2.07	0.61	1.05	108%
	November	0.26	0.16	0.32	1.15	0.31	0.48	189%
	December	0.04	0.02	0.04	0.17	0.02	0.06	157%
Season	Winter (DJF)	0.31	0.12	0.40	1.00	0.21	0.43	140%
	Spring (MAM)	3.92	1.50	3.57	4.42	2.79	3.07	78%
	Summer (JJA)	4.85	2.02	3.84	3.75	2.94	3.14	65%
	Fall (SON)	1.14	0.42	1.18	2.04	0.80	1.11	98%
Ratio	Winter / Summer	6%	6%	10%	27%	7%	14%	

Task Report Appendix E: Cool surface savings database fields

Table E-1 lists the building properties and saving metrics recorded in the savings database.

Table E-1. List of simulation properties and saving metrics recorded in the savings database.

Category		Property	Units [a]
Building and simulation properties		Year of building code	NA [b]
		Vintage	NA
		State	NA
		Representative location	NA
		Climate zone	NA
		Building category	NA
		Building orientation	NA
		Modified surfaces	NA
		Total modified surface area	m²
		Base wall albedo	NA
		Modified wall albedo	NA
		Base roof albedo	NA
		Modified roof albedo	NA
Annual building base	Site energy use	Cooling electricity	MWh
		Heating electricity	MWh
		Heating gas	therm
		Fan electricity	MWh
	Site peak power demand	HVAC electricity	W
Annual building absolute savings, fractional savings, and savings intensity	Site energy [c]	Cooling electricity	kWh
		Heating electricity	kWh
		Heating gas	therm
		Fan electricity	kWh
	Site peak power demand reduction [c]	HVAC electricity	W
	Source energy [c]	Cooling	MJ
		Heating	MJ
		Fan	MJ
		HVAC	MJ
	Emissions reduction [c]	CO_2	kg
		CO_2e	kg
		NO_x	g
		SO_2	g
	Energy cost [c]	Cooling	$

		Heating	$
		Fan	$
		HVAC	$

[a] Fractional values are dimensionless; intensities are per square meter of modified surface.

[b] NA = not applicable.

[c] The savings database reports positive penalties as negative savings.

Energy Research and Development Division

FINAL PROJECT REPORT

Solar-Reflective "Cool" Walls: Benefits, Technologies, and Implementation

Appendix B: Effect of Neighboring Cool Walls on Heating, Ventilation, and Air Conditioning Loads (Task 2.2 Report)

California Energy Commission
Gavin Newsom, Governor

April 2019 | CEC-500-2019-040-APB

Appendix B:
Effect of neighboring cool walls on HVAC loads (Task 2.2 report)

Weilong Zhang[1], Matteo Pizzicotti[1], Ronnen Levinson[2], Nathalie Dumas[1], Benjamin Kurtz[1], Yan Long[1], Negin Nazarian[1], Jan Kleissl[1]

[1] Center for Energy Research, University of California, San Diego

[2] Heat Island Group, Lawrence Berkeley National Laboratory

28 February 2018

Abstract

High albedo ("cool") walls are exterior building walls with surface (usually paint) properties that increase reflection of solar radiation. Consider a central building with neighbors. Raising the albedo of neighboring walls can increase reflection of downwelling sunlight from neighboring walls to the walls and windows of the central building. The indoor and outdoor building thermal environments in a three-dimensional urban area with a 5×5 array of identical buildings about 23 m apart are simulated. Building energy use effects of cool walls are quantified for a pre-1978 apartment building in Fullerton, CA (Orange County; California climate zone 8).

Daytime heating loads are near zero and changing wall albedo therefore does not modify the daytime heating load. Nighttime cooling loads are small and changing wall albedo therefore mostly influences the daytime cooling load. Raising the neighboring wall albedo increases annual cooling load of the central building by 1.2 MWh (1.2 percent) due to increased solar radiation reflected from the neighboring buildings towards the central building. The cooling load increase for the central building upon raising the albedo of all neighboring walls (1.2 MWh or 1.2 percent) is smaller than the cooling load decrease for the central building upon raising the albedo of its own walls (5.0 MWh, or 5.0 percent). The combined cool wall effect on all buildings is net positive.

Using retroreflective cool walls (albedo 0.60) on all neighboring buildings lowers the annual cooling load of the central building by 3.3 MWh (4.0 percent) with respect to using Lambertian cool walls (also albedo 0.60) on all neighboring buildings. However,

the cooling benefit comes at the expense of a 0.9 MWh (2.6 percent) increase in annual heating load. The net effect of changing to a retroreflective wall from a Lambertian wall on the central building is a reduction in average solar radiation incident on walls, which decreases cooling loads and increases heating loads.

1 Introduction

Global energy consumption increased considerably in the last 20 years and the U.S Energy Information Administration's projections show a continuing upward trend into the future (EIA, 2017). For residential buildings in California and the U.S., 30 percent and 47 percent, respectively, of the total energy consumed is related to heating, ventilation, and air conditioning, or HVAC (EIA, 2009). HVAC is on average the largest energy expense (EIA, 2009).

Increasing the albedo (solar reflectance) of roof or wall surfaces can cool the building envelope by reducing its solar heat gain. This decreases conduction of heat from the envelope to the building's conditioned space on a warm, sunny day, reducing the need for air conditioning. It also lessens convection of heat from the envelope to city air, mitigating the urban heat island effect (UHIE), or elevation of urban air temperature above that in surrounding rural areas. Cooling the outside air furthers decreases the air conditioning demand.

Reflective (cool) roofs are a common example of cool urban surfaces and are already prescribed by building energy standards in California and other U.S. states (Akbari and Levinson, 2010; CRRC, 2017). Little of the sunlight reflected by a roof will strike neighboring buildings unless the surrounding buildings are substantially taller. This allows cool roof effects to be evaluated by considering a single building in isolation. Cool urban surfaces other than roofs, such as high-albedo walls and pavements, will reflect sunlight to other elements of the city, including neighboring walls, neighboring windows, and pedestrians.

Yaghoobian et al. (2012) examined such effects on building energy use of cool pavements in an urban canyon using the Temperature of Urban Facets – Indoor Outdoor Building Energy Simulator (TUF-IOBES). Annual heating and cooling loads (quantities of heat added to or removed from the conditioned space to regulate indoor temperature) were simulated for pre-1980 and 1990s office buildings with window-to-wall ratio (net glazed area / gross wall area) 0.47, canyon aspect ratio (building height divided by inter-building separation) 0.37 – 1.5, and pavement albedo 0.10 – 0.50. As expected, they found reduced pavement temperature that led to a lower canopy air temperature. On the other hand, reflecting more sunlight from the pavement heated the walls of adjacent buildings, and increased solar radiation incident on and through windows. This raised summer cooling loads and lowered winter heating loads. Depending on building type and canyon aspect ratio, annual cooling loads increased by 2.2 – 8.3 kWh per square

meter of building floor area for every 0.10 increase in pavement albedo. The overall effect for Phoenix, Arizona was an increase in annual building energy use. However, in Yaghoobian et al. (2012) the effects of cool pavements on daylighting and lighting energy use were neglected.

Cool walls also increase heat transfer between urban surfaces. Consider a central building with neighbors. Raising the albedo of neighboring walls can increase reflection of downwelling sunlight from neighboring walls to the walls and windows of the central building. Raising the albedo of walls on the central building, on neighboring buildings, or on both can increase reflection of sunlight from the central building to neighboring buildings back to the central building. Either mechanism can increase cooling load, decrease heating load, and reduce need for artificial lighting in the central building. Raising central or neighboring building wall albedo also lowers the solar absorptance of the urban canyon, cooling the air within.

The Center for Energy Research at the University of California, San Diego (UCSD) partnered with Lawrence Berkeley National Laboratory (LBNL) to quantify the effect of cool walls on building energy use. The current report extends the analysis in the Task 2.1 report: *Simulated HVAC energy savings in an isolated building* to account for building-to-building interactions on building heating and cooling loads. It considers both diffusely reflecting walls and retroreflective walls. Building-to-building interaction on lighting loads will be analyzed in future work.

The report is structured as follows. Section 2 (Theory) contains a theoretical analysis of radiative interaction within an array of buildings. Section 3 (Methodology) starts with a description of the computer model in Section 3.1. Section 3.2 describes how we calculate the effect on the thermal load of a central building of changing the albedo of neighboring walls, in the common case where all walls reflect diffusely. Section 3.3 presents a variation in which the walls are retroreflective. Section 3.4 details the simulation setup, including weather, building thermal properties, and building equipment. Section 4 (Results and Discussion) contains the outcomes, and the take-away is provided in Section 5 (Conclusions).

2 Theory

Here we assess how reflection from the walls of neighboring buildings contributes to the wall solar heat gain of a central building. We also consider how that solar heat gain is affected by changes in the albedos of walls on the central building and on the neighboring buildings.

The buildings are assumed to be rectangular, cardinally oriented, and regularly spaced. In the first scenario, the buildings are square, with equal north-south and east-west

separations. The second scenario relaxes the requirements of the first scenario, but orients half the buildings with long axis north-south, and half with long axis east-west.

2.1 Central-building wall solar heat gain in regularly spaced array of rectangular buildings

Consider a regularly spaced array of cardinally oriented rectangular buildings—that is, buildings with outer walls facing due north (N), east (E), south (S), and west (W)—with separation δ_{NS} between the N and S walls of adjacent buildings, and separation δ_{EW} between the E and W walls of adjacent buildings. If each wall of the central building (subscript c) sees parallel, but not perpendicular, walls of neighboring buildings (subscript n), the total wall solar heat gain (power) of the central building will be

$$\begin{aligned} K = (1-\rho_{\mathrm{c}}) \big[& \left(A_{\mathrm{N,c}}\, I_{\mathrm{N}} + A_{\mathrm{E,c}}\, I_{\mathrm{E}} + A_{\mathrm{S,c}}\, I_{\mathrm{S}} + A_{\mathrm{W,c}}\, I_{\mathrm{W}}\right) \\ & + \rho_{\mathrm{n}} \left(A_{\mathrm{N,n}}\, I_{\mathrm{N}}\, F_{\mathrm{N,n\to S,c}} + A_{\mathrm{E,n}}\, I_{\mathrm{E}}\, F_{\mathrm{E,n\to W,c}} + A_{\mathrm{S,n}}\, I_{\mathrm{S}}\, F_{\mathrm{S,n\to N,c}} \right. \\ & \left. + A_{\mathrm{W,n}}\, I_{\mathrm{W}}\, F_{\mathrm{W,n\to E,c}}\right) \big] . \end{aligned} \tag{1}$$

where ρ is wall albedo; A is wall area; I is wall irradiance (power/area), assumed spatially uniform; and $F_{X\to Y}$ is the view factor from surface X to surface Y. Here subscript "D,c" denotes the central building wall facing direction D, while the subscript "D,n" refers to the multi-element surface comprising all neighboring walls that face direction D and see the central building. The first term in the bracket sums downwelling incident solar radiation, while the second term sums diffuse reflection to the central walls of downwelling sunlight incident on the neighboring walls.[1] Applying the view factor reciprocity relationship

$$A_X\, F_{X\to Y} = A_Y\, F_{Y\to X} \tag{2}$$

and rearranging,

$$\begin{aligned} K = (1-\rho_{\mathrm{c}}) \big[& A_{\mathrm{N}}\, I_{\mathrm{N}} \left(1 + \rho_{\mathrm{n}}\, F_{\mathrm{N,c\to S,n}}\right) + A_{\mathrm{E}}\, I_{\mathrm{E}} \left(1 + \rho_{\mathrm{n}}\, F_{\mathrm{E,c\to W,n}}\right) + A_{\mathrm{S}}\, I_{\mathrm{S}} \left(1 + \right. \\ & \left. \rho_{\mathrm{n}}\, F_{\mathrm{S,c\to N,n}}\right) + A_{\mathrm{W}}\, I_{\mathrm{W}} \left(1 + \rho_{\mathrm{n}}\, F_{\mathrm{W,c\to E,n}}\right) \big]. \end{aligned} \tag{3}$$

[1] Light reflected from central building to neighboring walls and back to the central building is neglected; the ratio of this flux to that in the second term of Eq. (1) would be equal to $\rho_{\mathrm{c}}\, F_{D\mathrm{,c}\to D\mathrm{,n}}$, which tends to be small (typically < 20 percent). If, say, $F_{D\mathrm{,c}\to D\mathrm{,n}} = 0.13$ as for the multifamily building array in this report, the ratio will be 3.3 percent for a conventional central wall ($\rho_{\mathrm{c}} = 0.25$) or 7.8 percent for a cool central wall ($\rho_{\mathrm{c}} = 0.60$).

2.2 Scenario 1: Evenly spaced array of square buildings

If the buildings are square and have equal N-S and E-W spacings, the total wall solar heat gain can be expressed as

$$K_0 = (1 - \rho_c)\,(I_N + I_E + I_S + I_W)\,A_0\,(1 + F_0\,\rho_n)\,, \tag{4}$$

where A_0 is the area of each wall and F_0 is the view factor from each central wall to the extended surface comprised of all parallel neighboring walls. F_0 is most sensitive to the distance $\delta_{NS} = \delta_{EW}$ between the central wall and the neighboring wall. Since the adjacent wall dominates the view factor towards all walls, the view factor to all walls decreases approximately as δ_{NS}^2 following the Nusselt analog for view factors[2].

Raising the albedo of neighboring walls by $\Delta\rho_n$ will increase the central building's total wall solar heat gain by

$$\Delta K_0 = (1 - \rho_c)\,(I_N + I_E + I_S + I_W)\,A_0\,F_0\,\Delta\rho_n\,. \tag{5}$$

Using view factor reciprocity [Eq. (2)], we can also express this increase in terms of the area A_n of the extended surface comprised of all parallel neighboring walls, and the view factor F_n from this surface to the central wall:

$$\Delta K_0 = (1 - \rho_c)\,(I_N + I_E + I_S + I_W)\,A_n\,F_n\,\Delta\rho_n\,. \tag{6}$$

This alternative formulation shows that the increase in the central building's total wall solar heat gain is proportional to the area A_n of the modified neighboring wall.

Returning to the original formulation, the fractional increase in K will be

$$f_{K_0} \equiv \frac{\Delta K_0}{K_0} = \frac{F_0\,\Delta\rho_n}{1 + F_0\,\rho_n}\,. \tag{7}$$

where ρ_n is the initial (pre-raise) albedo of the neighboring wall. We can compare the absolute increase in K_0 on raising the albedo of neighboring walls to the absolute *decrease* in K_0 upon raising the albedo of the central building walls. The ratio of the former to the latter will be

---

[2] Nusselt (1928) proposed to calculate view factors as the conical projection of the receiving surface on a unit sphere around the emitting surface. The view factor from the emitting surface to the receiving surface is then the fraction of the circle occupied by the conical projection.

$$g \equiv \frac{(1-\rho_c)\,(I_N + I_E + I_S + I_W)\,A_0\,F_0\,\Delta\rho_n}{(I_N + I_E + I_S + I_W)\,A_0\,(1+F_0\,\rho_n)\,\Delta\rho_c} = \frac{F_0\,(1-\rho_c)\,\Delta\rho_n}{(1+F_0\,\rho_n)\,\Delta\rho_c}\,. \tag{8}$$

where ρ_c is the initial (pre-raise) albedo of the central wall. If $\Delta\rho_n = \Delta\rho_c$,

$$g = \frac{F_0\,(1-\rho_c)}{1+F_0\,\rho_n}\,. \tag{9}$$

2.3 Scenario 2: Half the buildings oriented N-S, half oriented E-W

We relax the requirements of the first scenario, but divide the buildings into two side-by-side sets of equal population, each set contiguous. In set A, where streets run N-S, the long axis of each building extends N-S, making the E and W walls longer than the N and S walls. The buildings in set B, where streets run E-W, are rotated 90˚ from those in set A, with the long axis extending E-W, and the N and S walls longer than the E and W walls. Differences in building-to-building shading may cause wall irradiances to vary by set.

Let A_1 and A_2 represent the area of each long wall and each short wall, respectively, and F_1 and F_2 represent the view factors from each central long wall to its parallel neighboring walls and from each central short wall to its parallel neighboring walls, respectively. In set A, $A_E = A_W = A_1$, $A_N = A_S = A_2$, $F_{E,c\to W,n} = F_{W,c\to E,n} = F_1$, and $F_{N,c\to S,n} = F_{S,c\to N,n} = F_2$. In set B, $A_N = A_S = A_1$, $A_E = A_W = A_2$, $F_{N,c\to S,n} = F_{S,c\to N,n} = F_1$, and $F_{E,c\to W,n} = F_{W,c\to E,n} = F_2$. Hence for a central building in set A,

$$K_A = (1-\rho_c)\left[A_1\,(1+\rho_n\,F_1)\left(I_{E,A} + I_{W,A}\right) + A_2\,(1+\rho_n\,F_2)\left(I_{N,A} + I_{S,A}\right)\right], \tag{10}$$

and for a central building in set B,

$$K_B = (1-\rho_c)\left[A_1\,(1+\rho_n\,F_1)\left(I_{N,B} + I_{S,B}\right) + A_2\,(1+\rho_n\,F_2)\left(I_{E,B} + I_{W,B}\right)\right]. \tag{11}$$

Averaging over the two sets yields the population average total wall solar heat gain

$$\bar{K} \equiv \frac{K_A + K_B}{2} = \frac{(1-\rho_c)}{2}\left[A_1\,(1+\rho_n\,F_1)\left(I_{N,B} + I_{E,A} + I_{S,B} + I_{W,A}\right) + A_2\,(1+\rho_n\,F_2)\left(I_{N,A} + I_{E,B} + I_{S,A} + I_{W,B}\right)\right]. \tag{12}$$

Raising the albedo of neighboring walls by $\Delta\rho_n$ will increase $\bar{K}$ by

$$\Delta\bar{K} = \frac{(1-\rho_c)}{2}\left[A_1\,F_1\,\Delta\rho_n\left(I_{N,B} + I_{E,A} + I_{S,B} + I_{W,A}\right) + A_2\,F_2\,\Delta\rho_n\left(I_{N,A} + I_{E,B} + I_{S,A} + I_{W,B}\right)\right]. \tag{13}$$

The fractional increase in $\bar{K}$ will be

$$f_{\bar{K}} = \frac{\Delta\bar{K}}{\bar{K}} = \frac{A_1\,F_1\,\Delta\rho_n\,(I_{N,B}+I_{E,A}+I_{S,B}+I_{W,A})+A_2\,F_2\,\Delta\rho_n\,(I_{N,A}+I_{E,B}+I_{S,A}+I_{W,B})}{A_1\,(1+\rho_n\,F_1)\,(I_{N,B}+I_{E,A}+I_{S,B}+I_{W,A})+A_2\,(1+\rho_n\,F_2)\,(I_{N,A}+I_{E,B}+I_{S,A}+I_{W,B})}. \quad (14)$$

where ρ_n is the initial (pre-raise) albedo of the neighboring wall. As before, we can compare the absolute increase in $\bar{K}$ on raising the albedo of neighboring walls to the *decrease* in $\bar{K}$ upon raising the albedo of the central building walls. The ratio of the former to the latter will be

$$g = \frac{\frac{(1-\rho_c)}{2}[A_1\,F_1\,\Delta\rho_n\,(I_{N,B}+I_{E,A}+I_{S,B}+I_{W,A})+A_2\,F_2\,\Delta\rho_n\,(I_{N,A}+I_{E,B}+I_{S,A}+I_{W,B})]}{\frac{1}{2}[A_1\,(1+\rho_n\,F_1)\,(I_{N,B}+I_{E,A}+I_{S,B}+I_{W,A})+A_2\,(1+\rho_n\,F_2)\,(I_{N,A}+I_{E,B}+I_{S,A}+I_{W,B})]\,\Delta\rho_c}. \quad (15)$$

where ρ_c is the initial (pre-raise) albedo of the central wall. In the special case in which neighboring walls on the same side of the street are close enough to keep each other in shadow and to have small view factors to the sky, $I_{N,A} = I_{E,B} = I_{S,A} = I_{W,B} \approx 0$. Then

$$f_{\bar{K}} \equiv \frac{\Delta\bar{K}}{\bar{K}} = \frac{A_1\,F_1\,\Delta\rho_n\,(I_{N,B}+I_{E,A}+I_{S,B}+I_{W,A})}{A_1\,(1+\rho_n\,F_1)\,(I_{N,B}+I_{E,A}+I_{S,B}+I_{W,A})} = \frac{F_1\,\Delta\rho_n}{(1+F_1\,\rho_n)} \quad (16)$$

and

$$g = \frac{\frac{(1-\rho_c)}{2}[A_1\,F_1\,\Delta\rho_n\,(I_{N,B}+I_{E,A}+I_{S,B}+I_{W,A})]}{\frac{1}{2}[A_1\,(1+\rho_n\,F_1)\,(I_{N,B}+I_{E,A}+I_{S,B}+I_{W,A})]\,\Delta\rho_c} = \frac{F_1\,\Delta\rho_n(1-\rho_c)}{(1+F_1\,\rho_n)\,\Delta\rho_c}. \quad (17)$$

If $\Delta\rho_n = \Delta\rho_c$,

$$g = \frac{F_1\,(1-\rho_c)}{1+F_1\,\rho_n}. \quad (18)$$

Note how $f_{\bar{K}}$ and g take the same form as in Scenario 1, changing only the view factor to F_1 from F_0.

3 Simulation methodology

3.1 Temperature of Urban Facets Indoor – Outdoor Building Energy Simulator

The simulations in this chapter employ the TUF-IOBES model that simulates indoor and outdoor building surface and air temperatures and heat fluxes in a three-dimensional urban area with a 5×5 array of identical buildings. The indoor and outdoor energy balances are dynamically coupled and forced by outdoor weather conditions, building envelope properties, urban material properties, indoor heat sources, and HVAC systems (Figure 1).

Any (indoor or outdoor) surface energy balance can include shortwave (SW) and longwave (LW) radiation, conduction, convection of sensible and latent heat, and phase change. Beam (a.k.a. direct) and diffuse solar radiation and downwelling longwave radiation from the sky, as well as sunlight reflected by and LW radiation emitted by the ground and neighboring buildings, are partly absorbed by exterior wall and roof surfaces. This heat is then transferred through the wall or roof via conduction, to the outside air via convection, or to the surroundings via longwave radiation. Windows also admit sunlight.

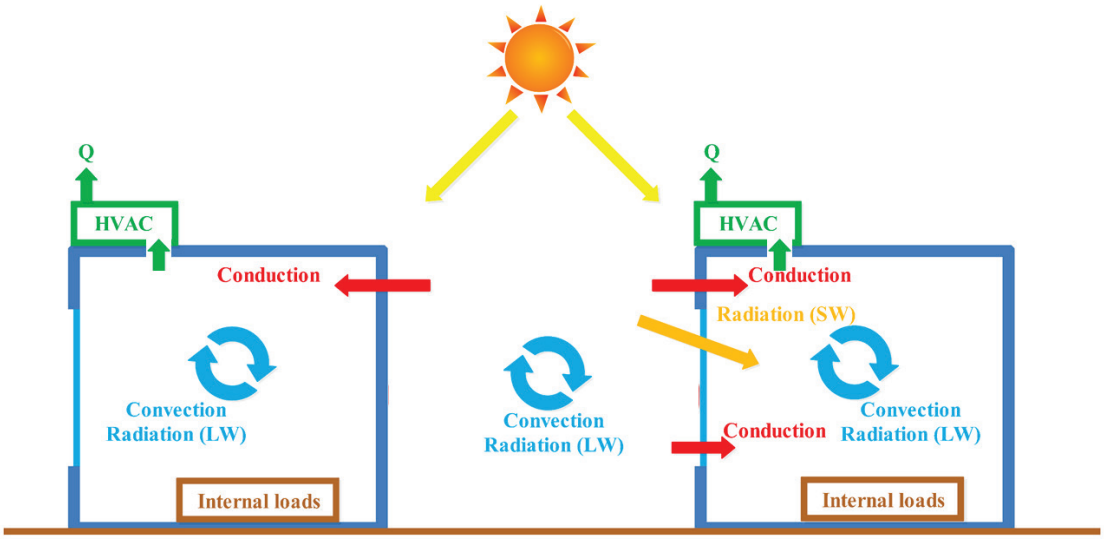

Figure 1. Illustration of the heat transfer process in the TUF-IOBES building-to-canopy model during the cooling season. Q is heat exhaust from the HVAC. TUF-IOBES simulates a 3D domain with an array of 5 × 5 buildings, but here only a cross section through two buildings is shown.

The interior wall or ceiling surface energy balance includes conduction through the building envelope, convection to the room air, absorption of shortwave radiation, and longwave radiation exchange between indoor surfaces. Shortwave (solar spectrum) radiation comes from windows and lamps, while longwave (thermal infrared) radiation emits from interior envelope surfaces, equipment, and occupants.

The outdoor energy balance yields the canopy air and urban surface temperatures and is forced by weather data. In turn, outdoor conditions affect the indoor environment. The internal surface temperatures, indoor air temperature, and building thermal loads are obtained from the indoor energy balance model. If the indoor air temperature is outside the setpoint range, thermal energy (heat) is added or removed to bring the temperature within the setpoint range; this thermal energy constitutes the heating or cooling load. The air-conditioning (AC) system transfers the cooling load waste heat from the indoor to the outdoor environment, increasing the canopy air temperature. Heating equipment

is assumed to be electric resistance and all heat produced by the heating equipment increases interior air temperature; i.e. the heating equipment does not exhaust waste heat to the outside air. The TUF-IOBES model has been described and validated in detail by Yaghoobian and Kleissl (2012).

3.2 Effects of raising neighboring building wall albedo on the heat balance of the central building

Raising the albedo of walls on neighboring buildings affects the heat balance of the central building. A cool (high albedo) wall of a neighboring building increases shortwave irradiance and decreases longwave irradiance on the opposing wall of the central building compared to the case with conventional (lower albedo) walls on the neighboring building. The widespread use of cool walls may also reduce canyon air temperature. However, this effect is expected to be minor if only a few buildings are assigned cool walls, and is neglected here.[3]

The TUF-3D radiation model in TUF-IOBES uses periodic boundary conditions on a single building (the central building unit, or CBU) to simulate a 5×5 array of buildings.[4] This setup does not allow wall albedo to vary building to building. Therefore, a workaround was devised to examine the effect of neighboring buildings with cool walls on a CBU with conventional walls, or that of neighboring buildings with conventional walls on a CBU with cool walls. The following cases are simulated for the 5×5 array of buildings:

- C25N25: All central ("C") and neighboring ("N") building walls are conventional (albedo 0.25). Note the use of "N" to mean "neighboring", rather than "north", in the case labels.

- C60N60: All central and neighboring building walls are cool (albedo 0.60).

- C25N60: All central and neighboring building walls are conventional (albedo 0.25), but shortwave and longwave irradiances on every wall of the CBU are assigned values consistent with facing a cool neighboring wall of albedo 0.60. That is, irradiances on CBU walls are taken from the C60N60 simulation.

---

[3] The Task 3.2 report: *Urban climate impacts of cool walls* assesses canyon air temperature reduction upon raising wall albedo.

[4] The TUF-3D solver imitates periodic boundary conditions by solving for reflected radiances only for patches in the central urban unit, and setting radiative and energy balance exchanges of all other patches equal to those of the corresponding patch within the central urban unit (Krayenhoff and Voogt, 2007).

- C60N25: All central and neighboring building walls are cool (albedo 0.60), but shortwave and longwave irradiances on every wall of the CBU are assigned values consistent with facing a conventional neighboring wall of albedo 0.25. That is, irradiances on CBU walls are taken from the C25N25 simulation.

We can use these load profiles to evaluate four albedo-change scenarios:

a) raising the albedo of all central walls, leaving all neighboring walls conventional (C60N25 – C25N25);

b) raising the albedo of all neighboring walls when all central walls remain conventional (C25N60 – C25N25);

c) raising the albedo of all neighboring walls when all central walls are cool (C60N60 – C60N25); and

d) raising the albedo of all central walls and all neighboring walls (C60N60 – C25N25).

The workaround incorporates the following assumptions:

i. The component of central wall irradiance due to reflection from central wall to opposing neighboring wall back to central wall is small. This is reasonable if the wall-to-wall view factor F_0 (the view factor from each central wall to the extended surface comprised of all parallel neighboring walls) is modest, because the wall-to-walls-to-wall reflection would be proportional to the square of this view factor. For example, if $F_o = 0.13$, then F^2 is 0.017. This wall-to-walls-to-wall radiation is further diminished by absorption at the neighboring walls.

ii. Spatial variations in wall irradiance (that is, variations across the face of a given wall) induced by partial shading are neglected. The average shortwave and longwave irradiances across each wall are input to the heterogeneous simulations. Intra-wall differences are expected to be small except when parts of the wall are shaded by surrounding buildings shortly after sunrise or shortly before sunset.

3.3 Retroreflector analysis

In this section, the methodology for studying the effect of retroreflective (RR) walls on building energy use is presented. Retroreflective cool walls improve upon diffusely reflecting cool walls by reflecting incoming beam radiation toward the solar disc (if a retroreflection is three dimensional) or at least upwards (if the retroreflection is two dimensional). This can increase the fraction of sunlight reflected out of the urban canyon.

Depending on the canyon aspect ratio, a large fraction of the sunlight reflected by diffusely reflecting cool walls could remain trapped between buildings due to reflection towards ground or neighboring wall surfaces with low albedo. For example, consider an isolated building with 0.60 wall albedo and 0.10 ground albedo, each surface a perfectly diffuse reflector. About 33 percent of the sunlight incident on the wall would return to the sky [0.60 wall albedo × (0.5 sky view factor + 0.5 ground view factor × 0.10 ground albedo)]. If the wall were instead covered with a 2D retroreflector (pairs of orthogonal surfaces, each of albedo 0.775, with a two-bounce albedo of $0.775^2 = 0.60$), it would reflect upward 60 percent of incident beam sunlight, and about 30 percent of the incident diffuse sunlight (of the 60 percent of diffuse light that is reflected, half will go up, and half will go down). If 20 percent of the incident sunlight is diffuse, the final fraction returned to the sky would be 80 percent × 0.60 wall solar retroreflectance + 20 percent × [0.60 wall solar diffuse reflectance × (0.5 sky view factor + 0.5 ground view factor × 0.10 ground albedo)] = 55 percent. Retroreflection can thereby reduce the solar heat gain of other urban surfaces, including ground, opposing walls, and pedestrians. However, retroreflective cool walls would provide less daylighting to neighboring buildings than would diffusely reflecting cool walls.

The retroreflector simulation setup is based on C60N60, but all walls of the neighboring and central buildings become retroreflective (C60rrN60rr). The effect of retroreflection on building energy use is also estimated using TUF-IOBES by comparing C60rrN60rr to C60N60 and the same building layout described in Section 3.2. TUF-IOBES uses a view-factor based radiation model which assumes all surfaces to be Lambertian (perfectly diffuse) reflectors. While this assumption is diametrically opposed to the working principle of a retroreflector, the effects of retroreflective materials can be approximated as shown in Figure 2. The wall is assumed to be a retroreflector for the beam solar radiation, but it is assumed to be a Lambertian reflector for the diffuse sky and ground reflected radiation. Retroreflectance of beam radiation is achieved by zeroing out wall beam reflection in the radiation model as the reflected radiative energy exits the simulation domain.

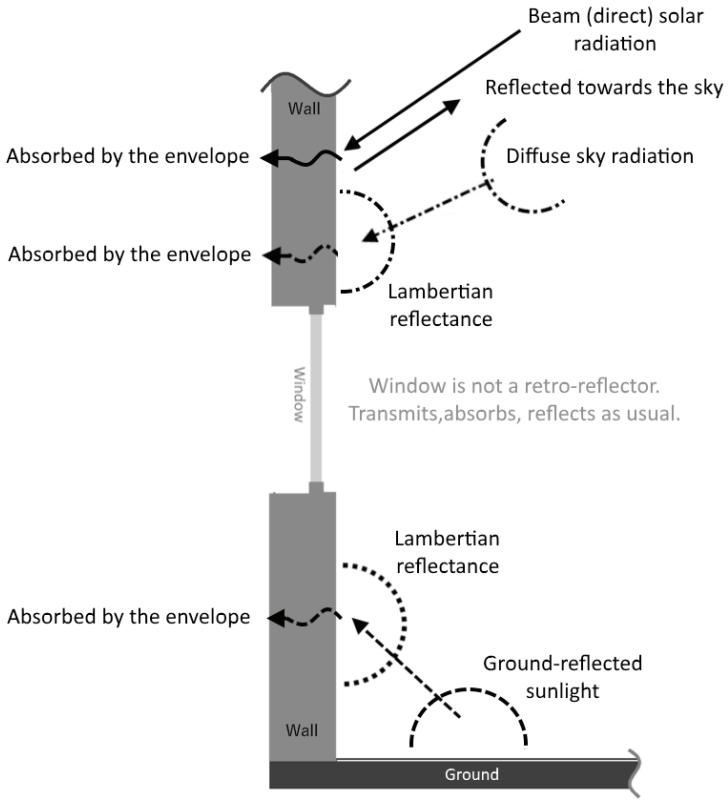

Figure 2. Sketch of TUF-IOBES radiation model for retroreflective wall simulations.

3.4 Simulation setup

3.4.1 Climate zones

Building energy use effects of cool walls are quantified in the coastal building climate zone 8 in California (California Energy Commission, 2017) represented by Fullerton in Orange County. Environmental conditions, including dry-bulb and wet-bulb air temperatures; global, beam, and diffuse solar irradiances; and wind speed are input from Typical Meteorological Year 3 (TMY3), weather data (NREL 2017). The ground albedo is set to 0.10 (asphalt concrete).

3.4.2 Other meteorological boundary conditions

In TUF-IOBES, the deep-ground temperature is set as the mean dry-bulb air temperature of the whole year from TMY3. The TMY3 air temperature and wind speed are applied at twice the building height. For wind speed, a logarithmic profile is assumed down to the building height. The wind speed at canyon half height is then estimated as $U_{\mathrm{can}} = U_{\mathrm{top}} \exp(-N/2)$, where U_{top} is the wind speed at the building height and N is half the canyon aspect ratio (defined as building height divided by inter-building spacing). For details see section 2.9.5 in Masson (2000). The canyon air temperature is computed from an energy balance in the urban canyon.

On outdoor surfaces, available energy (net radiation minus conduction) is converted to sensible and latent heat fluxes. Since most of the areas in California are semi-arid, a Bowen ratio of 5 is used (Taha, 1997). The Bowen ratio is the ratio of the sensible heat flux to the latent heat flux.

3.4.3 Building prototypes

Building categories. Offices are the most common type of commercial building in California comprising 1.7 percent to 21.9 percent of total building floor area depending on climate zone (Rosado, 2016). For the DOE prototype office building model (DOE, 2017), the deadband of HVAC temperature setpoints is wider at night and on weekends than during business hours (Table 1). Therefore, nighttime heating and cooling energy use is small as the building interior temperature first adjusts from the narrow deadband to the wide deadband before the HVAC systems incurs heating or cooling energy use. A large fraction of the energy use then occurs in the early morning when the building needs to be brought from the wider night-time deadband to the tighter temperature deadband for business hours. This period of morning heating and cooling is therefore coincident with cool wall effects. However, in TUF-IOBES temperature setpoints for heating and cooling cannot be varied by time of day or day of the week. Therefore TUF-IOBES is expected to overestimate nighttime HVAC energy consumption and underestimate daytime HVAC energy use. Since cool wall effects predominantly occur during the day, simulating the timing of HVAC energy accurately is critical to understanding the real impacts of cool walls on building energy use. Therefore the project team decided against simulating office buildings.

Residential buildings constitute 78 percent of the building stock in California (Rosado, 2016). In large metropolitan areas residential buildings are about evenly split between single and multi-family residences (e.g., 62 percent single-family homes versus 36 percent apartment buildings in San Diego in Table 6.7 of Rosado, 2016), while single-family residences dominate in rural areas (e.g., 94 percent single-family homes versus 4 percent apartment buildings in Lancaster in Table 6.8 of Rosado, 2016). Since the solar heat gain on neighboring walls is a function of wall-to-wall view factors (Section 2) and the wall area of the prototype multi-family residence is 4 times the wall area of the prototype single-family residence (Table A-1 of Task Report Appendix A), the multi-family residence was chosen for further study. Cool wall effects between neighboring single-family residences are expected to be smaller than the multi-family residence results in this report. Building geometrical specifications are provided in Table A-1.

Table 1. Variation with hour of week of the HVAC setpoint deadband in a DOE-supplied prototype office building model (DOE, 2017). In TUF-IOBES deadbands are constant across time of day and day of the week.

	Weekday (business hours)	Weekday (outside of business hours)	Weekend (business closed)
Day	Mon - Fri	Mon - Fri	Sat, Sun
Time (local)	07:00 – 22:00	22:00 – 07:00	00:00 – 24:00
HVAC setpoint deadband	21.0 ˚C to 24.0 ˚C	15.6 ˚C to 26.7 ˚C	15.6 ˚C to 26.7 ˚C

Adaptation of DOE residential prototype building model for use in TUF-IOBES. The multi-family residence prototype was based on a template from the U.S. Department of Energy (DOE, 2017) that was modified to follow California's Title 24 building energy efficiency standards as described in the Task 2.1 report: *Simulated HVAC energy savings in an isolated building*. Since TUF-IOBES can only simulate simple building geometries, the original U.S. DOE building prototype as simulated in EnergyPlus in the Task 2.1 report were modified as follows.

1. In TUF-IOBES, buildings must have square footprints. Therefore, the footprint is simplified as a square that is dimensioned to match the total footprint area in EnergyPlus. The footprint area in TUF-IOBES and EnergyPlus differs by 2 percent because the TUF-IOBES wall and ground surfaces are discretized into square, equal-sized sub-areas (patches). Computational costs dictate a small number of patches; typically width and height of each building face is subdivided into two to five patches.

2. In EnergyPlus, the multi-family residence roof is pitched and the pitched roof rise (roof peak height – roof base height) is 4.1 m. TUF-IOBES can only simulate flat roofs. The height of the flat roof in TUF-IOBES was set equal to the roof base height in EnergyPlus.

3. Any façade patch has to be either a wall or a window. Therefore only discrete values of window-to-wall ratio (WWR; ratio of window area to gross wall area) can be chosen in TUF-IOBES. The WWR is 29 percent in TUF-IOBES and 28 percent in EnergyPlus.

4. In TUF-IOBES all building facades must be of identical geometry. Therefore the window size, number, and location cannot be varied by aspect. A single window near the center of each façade is assumed.

5. Exterior sunshades and interior blinds are not modeled in TUF-IOBES. All window-transmitted solar irradiance is absorbed inside the building.

6. Intermediate floors and internal mass are not considered in TUF-IOBES. That is, the buildings are empty and do not store heat in the interior space. For comparison to EnergyPlus some of the thermal loads are still reported by floor area, where floor area is the product of TUF-IOBES building footprint and EnergyPlus number of floors.

EnergyPlus and TUF-IOBES building prototype geometry, including footprint, height, length, width, window area, gross wall area, and canyon width, are compared in Table A-2.

Building vintages. The Task 2.1 report: *Simulated HVAC energy savings in an isolated building* simulates three building vintages—pre-1978, 1988, and 2016. In this report only pre-1978 buildings are simulated. As stricter building energy efficiency standards were first introduced around 1980, pre-1978 buildings have little insulation, while 1988 and 2016 buildings follow progressively stricter building energy efficiency standards with more insulation. Effects of cool walls on thermal loads of neighboring buildings are expected to be largest for the pre-1978 buildings.

Construction. Floor construction is a layer of plywood over a concrete slab over a layer of crushed rock (Yaghoobian and Kleissl, 2012). Roof, wall, building floor, and street construction are detailed in Table A-3; material properties are summarized in Table A-4 and Table A-5. Double-pane windows are chosen from the International Glazing Database (IGDB) in the Berkeley Lab WINDOW (2017) software to match EnergyPlus prototypes of overall solar heat gain coefficient (SHGC) and thermal transmittance. Angular and diffuse SHGC, absorptance, and transmittance of window glasses also derived from Berkeley Lab WINDOW are shown in Table A-6.

Equipment and people settings. Internal loads including lighting, equipment, and occupants play an important role in building energy use. The technical parameters are based on the simulations of the DOE prototype building using the DOE EnergyPlus building energy simulation model detailed in Rosado et al. (2017). Specifically, the lighting, equipment, and infiltration schedules are based on the EnergyPlus output files and the occupancy schedule is based on the EnergyPlus input files. Figure A-1 shows the TUF-IOBES inputs for lighting, equipment, occupancy, and infiltration schedules per footprint area of the multi-family residence, respectively. The conversion of lighting, equipment, and occupancy loads to conduction, convection, and radiation heat flows is shown in Table A-7. Specifications for people, equipment, and lighting follow the same scheme. First the total emitted power is split into latent and sensible fractions. Then the sensible fraction is further split into longwave, convective, and shortwave (only for lighting) fractions. People power is computed from the occupancy in Figure A-1 multiplied by the activity level in Table A-7.

HVAC is simulated simplistically in TUF-IOBES assuming (i) continuous HVAC operation with fixed temperature setpoints of 22.2 ˚C and 23.9 ˚C; (ii) constant coefficient of performance (COP = 2.64); and (iii) unlimited HVAC capacity. Therefore the heat transfer to/from the HVAC system always satisfies the air heat balance to keep the room temperature between the minimum and maximum setpoints. The constant TUF-IOBES setpoints are obtained by averaging the hourly EnergyPlus HVAC schedules over the year (Table A-7). Dividing TUF-IOBES cooling load by COP yields the cooling site energy use.

3.5 Limitations

The magnitude of cool wall effects on neighboring buildings was only analyzed for one particular building configuration. Cool wall effects are expected to be a function of the window solar heat gain coefficient, wall insulation, inter-building spacing, and window-to-wall ratio. Pre-1978 buildings with a window-to-wall ratio of 29 percent were simulated. For newer buildings with reduced window solar heat gain coefficient and improved wall insulation the cool wall effects on thermal loads of the central buildings would be smaller.

Inter-building spacing modifies the view factor from the neighboring cool wall to the central building wall. The view factor effect is difficult to test in simulations since changes to the inter-building spacing also change the view factor from ground to wall. Theory (Section 2) suggests that the increase in wall solar heat gain of the central building is proportional to the modified wall area of the neighboring buildings (A_n), the view factor to the central building wall from the extended surface comprised of all parallel neighboring walls (F_n), the increase in the albedo of the neighboring wall, and one minus the albedo of the central wall. Since view factors between two surfaces are proportional to the square of their distance, the cool wall effects reported here can be scaled to estimate gains for different inter-building spacings. However, note that F_n does not decrease with inter-building distance squared as it describes the joint view factor to the central wall from an extended surface comprised of several surfaces.

Window-to-wall ratios have different effects depending on the building where they are applied. On the neighboring building, larger window-to-wall ratios reduce the cool wall area and linearly decrease the sunlight reflected onto the central building wall. On the central building, larger window-to-wall ratios increase the solar heat gain through windows and increase cool wall effects. The window solar heat gain coefficient for diffuse sunlight is 0.52 (Table A-6), indicating that 52 percent of the solar radiation reflected from neighboring cool walls towards a window on the central building reaches the conditioned space. While conventional walls absorb 75 percent of the solar radiation reflected from neighboring cool walls, the majority of the absorbed heat is removed to the canopy air as sensible heat flux. Only a small fraction is conducted through the wall

and reaches the conditioned spaces. Therefore central-building windows increase the effects of neighboring cool walls.

A caveat to this analysis is that the daylighting effects of cool walls were ignored. However, most likely this will not impact the conclusions since residential lighting loads during daytime are small (see Figure A-1). The effect of daylighting energy savings may be significant for office buildings with large window-to-wall ratios, but office buildings are not studied in this report.

4 Results and discussion

4.1 Comparison between TUF-IOBES and EnergyPlus results

While this report focuses on *changes* in thermal loads with changing wall albedo, a brief comparison of absolute thermal loads in this report to the Task 2.1 report: *Simulated HVAC energy savings in an isolated building* is presented in this section. As described in Section 3 perfect agreement is not expected, because (i) the simulated multi-family building is different (see also Table A-2); and (ii) simplifying assumptions had to be made to run the TUF-IOBES building energy simulator compared to the more realistic building operation in EnergyPlus.

The C25N25 and C60N25 cases in TUF-IOBES are similar to the cases in EnergyPlus where a single building with all conventional and all cool walls is simulated, respectively. While neighboring buildings are not represented in EnergyPlus, a fixed reflectance of the surrounding pavements and buildings is assumed to obtain ground-reflected diffuse solar irradiance onto walls.

Table 2 shows agreement within 38 percent for cooling loads, but heating loads differ by a factor of about 5. The reasons for the differences are not well understood at present.

Relative changes in the magnitude of cooling loads are larger in EnergyPlus (-14.1 percent) than TUF-IOBES (-5.0 percent). Relative changes in heating loads are similar in EnergyPlus (10.0 percent) and TUF-IOBES (13.6 percent). The consistency in the direction and order of magnitude of the trends is encouraging, but the underestimation of cooling load savings in Table 2 suggests that TUF-IOBES cooling load savings reported for different scenarios in the following sections may be biased low.

Table 2. Annual thermal loads for the pre-1978 multi-family residence in CZ8 (Fullerton) from TUF-lOBES (this report) and EnergyPlus (Task 2.1 report: *Simulated HVAC energy savings in an isolated building*).

	Annual heating load [MWh]		Annual cooling load [MWh]	
	TUF-IOBES	EnergyPlus	TUF-IOBES	EnergyPlus
C25N25	28.7	4.6	101.3	81.2
C60N25	32.6	5.1	96.2	69.8
(a) C60N25 – C25N25	+3.9 MWh (+13.6 %)	+0.5 MWh (+10.0%)	-5.0 MWh (-5.0 %)	-11.4 MWh -14.1 %

4.2 Building-to-building interaction effect

Figure 3 (left column, i) shows that daytime heating loads are near zero for all scenarios and changing wall albedo therefore does not modify the daytime heating load. Heating load at night increases, however, when the central wall albedo is raised (C60N25 – C25N25 and C60N60 – C25N25). During the day conventional walls store more heat than cool walls. The stored heat provides a heat flux into the conditioned space and reduces heating load by up to 1 kW.

Figure 3 (right column, ii) shows that nighttime cooling loads are small and changing wall albedo therefore mostly influences the daytime cooling load. Raising the neighboring wall albedo increases cooling load of the central building due to increased solar radiation reflected from the neighboring buildings towards the central building (C25N60 – C25N25). Raising the central wall albedo reduces cooling loads due to a decrease in absorbed solar radiation (C60N25 – C25N25 and C60N60 – C25N25); the decrease in cooling loads also persists into the night due to reduced wall heat storage.

Examining the scenarios (a – d) described in Section 3.2 one by one reveals the following changes in annual thermal loads (Figure 3; Table 3):

a) **Raising the albedo of all central walls while leaving all neighboring walls conventional (C60N25 – C25N25)** decreases annual cooling load by 5.0 MWh (5.0 percent), while annual heating load increases by 3.6 MWh (13.9 percent). Raising wall albedo of a building reduces its absorption of sunlight which reduces cooling loads and increases heating loads.

b) **Raising the albedo of all neighboring walls when all central walls remain conventional (C25N60 – C25N25)** increases annual cooling load by 1.5 MWh (1.5 percent). The annual heating load reductions (0.1 MWh, or 0.3 percent) are negligible. These changes are small (less than 1.5 percent) compared with the

total annual heating and cooling loads of 28.7 MWh and 101.3 MWh, respectively. The negligible effect of cool walls on heating loads is likely an artifact of the way that TUF-IOBES predicts essentially zero daytime heating load. In scenario (a) the central wall heat gain is reduced by $(0.75 - 0.40)/0.75 = 47$ percent. The reduced heat storage in the walls of the central building then increases nighttime cooling loads. In scenario (b) the fractional increase in solar heat gain on the central building is only 4.3 percent (see below), which is too small to significantly influence heat storage and nighttime heating loads.

The annual cooling load increases can be compared to the fractional increase in solar heat gain predicted by Eq. (7). With $F_0 = 0.127$, $\Delta\rho_n = 0.35$, and $\rho_n = 0.25$, f_{K_0} is 4.3 percent. The fractional cooling load increase is less than the fractional solar heat gain increase, because (i) not all increase in solar heat gain incurs a cooling load, as for example on cold winter days; and (ii) cooling load depends on multiple heat transfer processes, including wall conduction (dependent on wall solar heat gain), window transmission (dependent on wall irradiance, but not on wall solar absorption), infiltration (independent of wall solar heat gain), and occupant and equipment loads (also independent of wall solar heat gain).

We can also compare the absolute increase in central building total wall solar heat gain K_0 on raising the albedo of neighboring walls to the absolute *decrease* in K_0 upon raising the albedo of the central building walls. This ratio is defined as g in Eq. (9). For the parameters in the simulations, $g = 0.09$, while the cooling load change ratio $-(\mathrm{C25N60} - \mathrm{C25N25})/(\mathrm{C60N25} - \mathrm{C25N25}) = 0.30$. The cooling load change ratio is not expected to match the solar heat gain change ratio, but may allow scaling the simulation results obtained here to other building geometries and/or cool wall albedos.

c) **Raising the albedo of all neighboring walls when all central walls are cool (C60N60 – C60N25)** increases annual cooling load by 1.2 MWh (1.2 percent). Scenario (c) is similar to scenario (b), but the effect of neighboring cool walls on annual cooling load is diminished by the high albedo of the central building walls. That is, 60 percent, rather than 25 percent, of the additional sunlight that is reflected towards the central building is reflected away from the central building, reducing the increase in annual cooling load to 1.2 MWh (1.2 percent) from 1.5 MWh (1.5 percent).

d) **Raising the albedo of all central walls and all neighboring walls (C60N60 – C25N25)** is similar to scenario (a). But since the neighboring walls' albedos are also increased, cool walls on the central building are less effective than in case (a). The neighboring walls reflect more sunlight towards the central building. The cool walls on the central building reflect 60 percent of that sunlight, but 40 percent is absorbed. Annual cooling load in scenario (d) decreases only by 3.8

MWh (3.8 percent) versus 5.0 MWh (5.0 percent) for scenario (a). Annual heating load in scenario (d) increases by 3.9 MWh (13.7 percent), which is almost identical to scenario (a). The lack of heating load differences between scenarios (a) and (d) is consistent with scenario (b)—that is, raising the albedo of neighboring walls does not influence heating loads.

When thermal loads are only averaged over winter and summer (Figure 4), the effects of wall modifications on thermal loads are enhanced, because these limited datasets contain more days when heating and cooling are required, respectively. The wall modifications then influence the thermal loads on a larger fraction of days compared to when the entire year is considered (Figure 3).

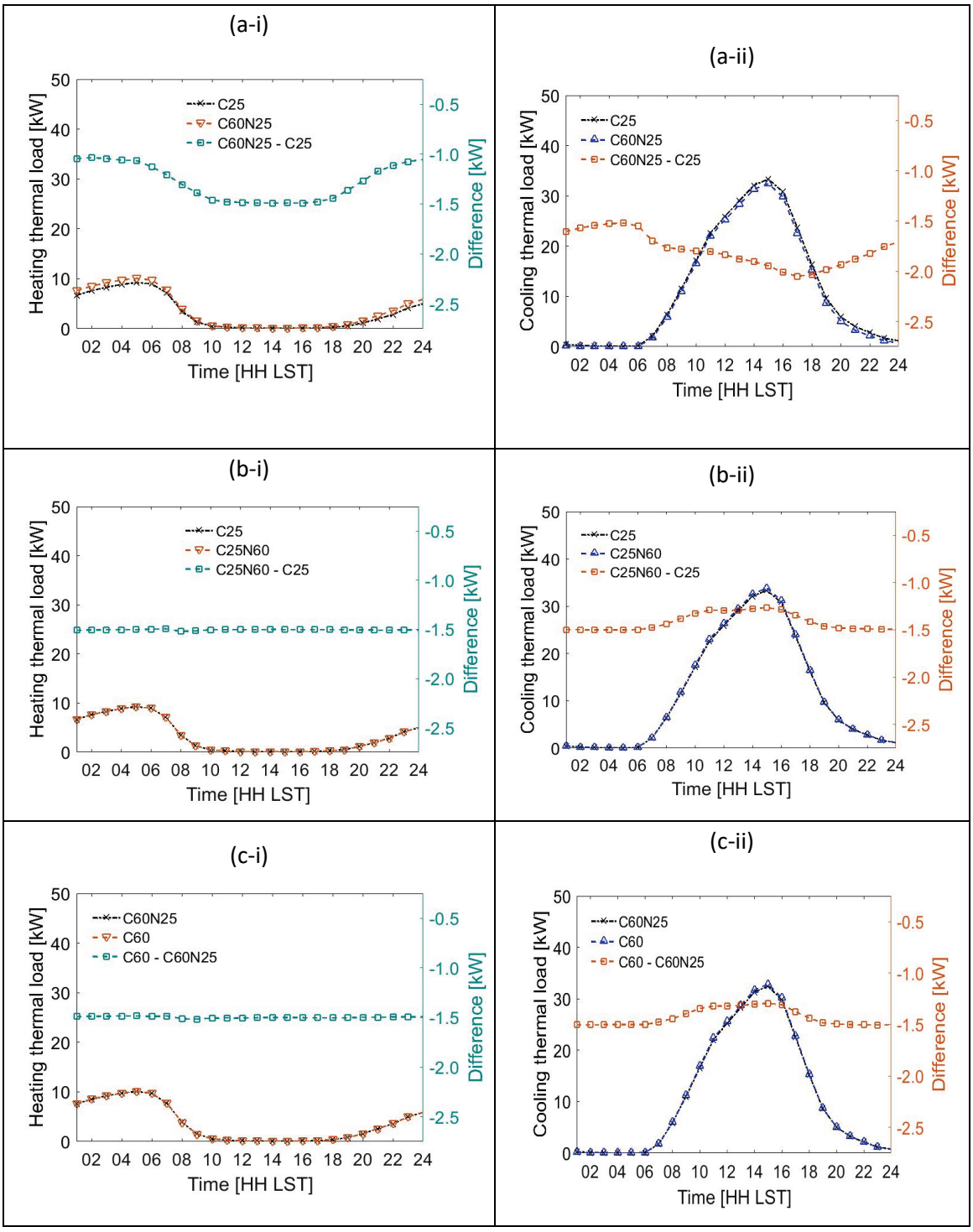
(a-i)
Heating thermal load [kW]
Difference [kW]
Time [HH LST]
C25
C60N25
C60N25 - C25
(a-ii)
Cooling thermal load [kW]
Difference [kW]
Time [HH LST]
C25
C60N25
C60N25 - C25
(b-i)
Heating thermal load [kW]
Difference [kW]
Time [HH LST]
C25
C25N60
C25N60 - C25
(b-ii)
Cooling thermal load [kW]
Difference [kW]
Time [HH LST]
C25
C25N60
C25N60 - C25
(c-i)
Heating thermal load [kW]
Difference [kW]
Time [HH LST]
C60N25
C60
C60 - C60N25
(c-ii)
Cooling thermal load [kW]
Difference [kW]
Time [HH LST]
C60N25
C60
C60 - C60N25

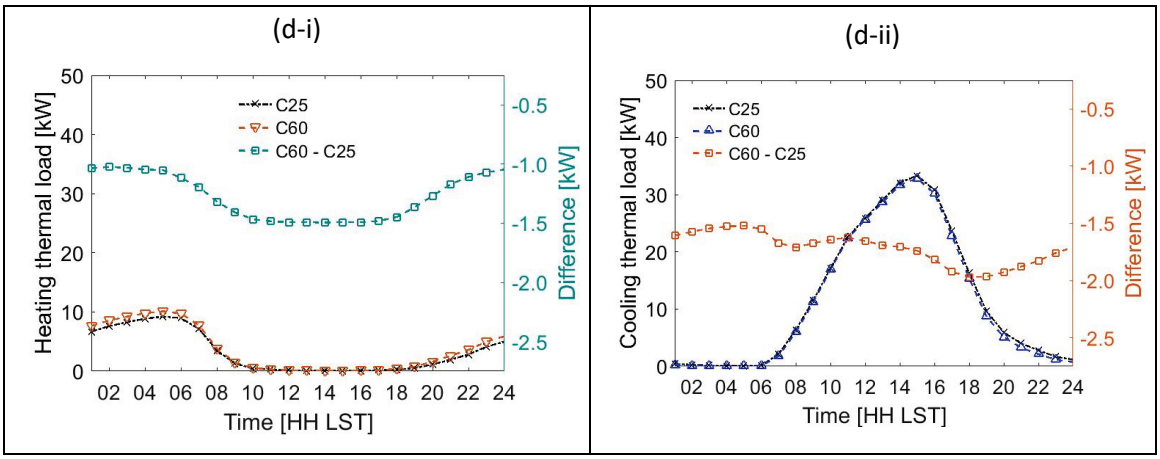

Figure 3. Average diurnal cycles of heating load (column i, left) and cooling load (column ii, right) for the central building—a pre-1978 multi-family residence in CZ8 (Fullerton)—surrounded by buildings with the same or different wall albedo. Shown are results for (a) raising the albedo of all central walls, leaving all neighboring walls conventional (C60N25 – C25N25); (b) raising the albedo of all neighboring walls when all central walls remain conventional (C25N60 – C25N25); (c) raising the albedo of the neighboring walls when all central walls are cool (C60N60 – C60N25); and (d) raising the albedo of all central walls and all neighboring walls (C60N60 – C25N25).

Table 3. Annual thermal loads for the pre-1978 multi-family residence in CZ8. The top group of four rows shows the annual results for homogeneous simulations with all-cool (C60N60) or all-conventional (C25N25) walls and combinations of cool and conventional walls. The second group of four rows shows differences in thermal loads in MWh and percent in the same order as in Figure 3.

	Annual heating load [MWh]	Annual cooling load [MWh]
C25N25	28.7	101.3
C60N60	32.7	97.5
C25N60	28.7	102.7
C60N25	32.6	96.2
(a) C60N25 – C25N25	+3.9 MWh (+13.6 %)	-5.0 MWh (+5.0 %)
(b) C25N60 – C25N25	-0.1 MWh (-0.3 %)	+1.5 MWh (+1.5 %)
(c) C60N60 – C60N25	-0.0 MWh (-0.0 %)	+1.2 MWh (+1.3 %)
(d) C60N60 – C25N25	+3.9 MWh (+13.7 %)	-3.8 MWh (+3.8 %)

(a-i)

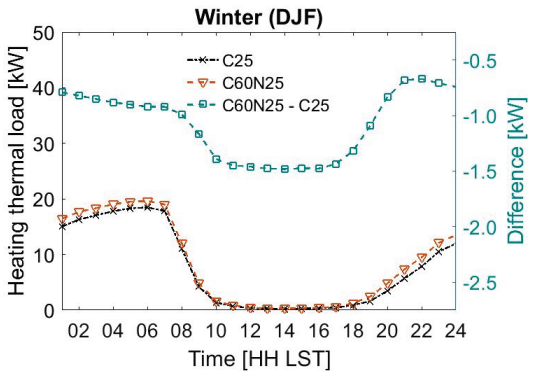

(a-ii)

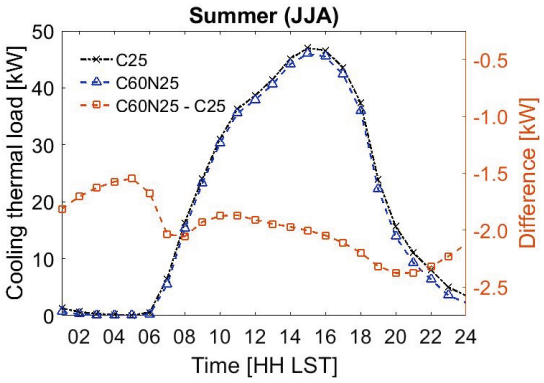

(b-i)

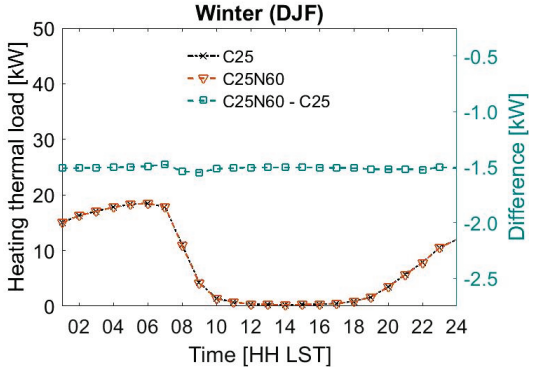

(b-ii)

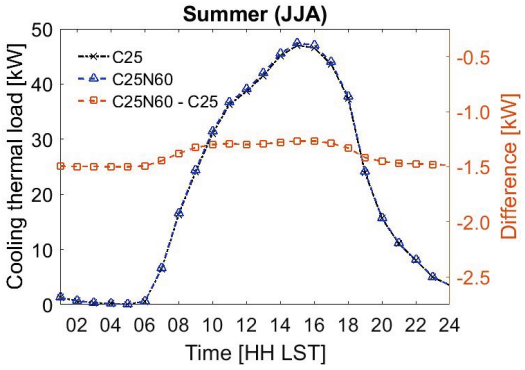

(c-i)

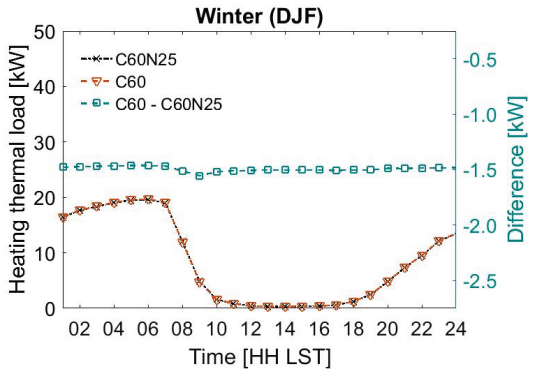

(c-ii)

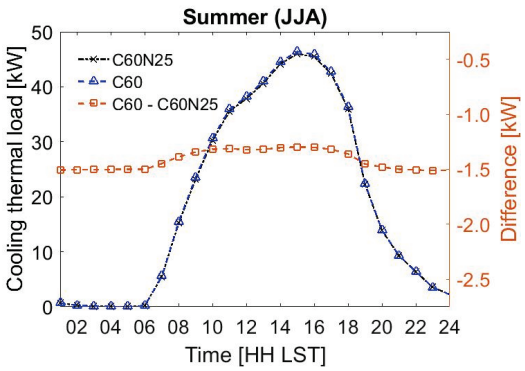

(d-i)

(d-ii)

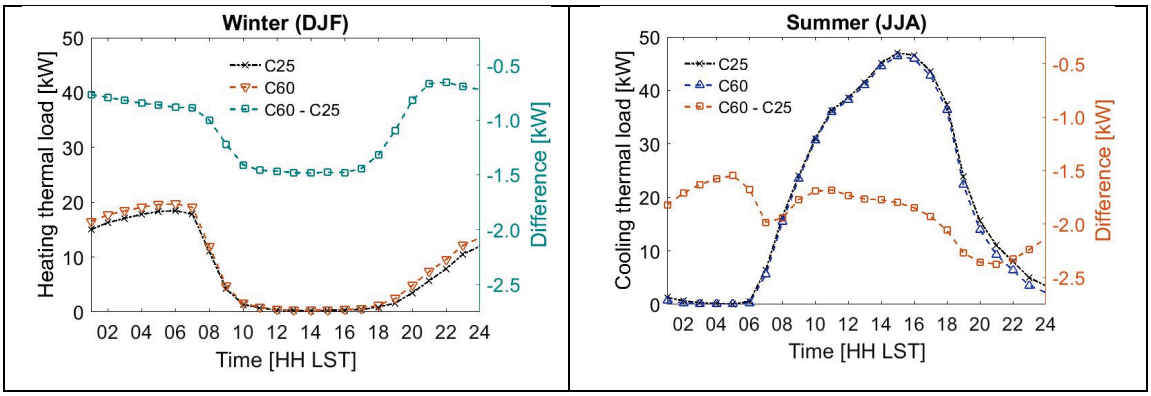

Figure 4. Seasonal analogs of Figure 3 for summer (June to August) and winter (December to February).

4.3 Retroreflective versus Lambertian Walls

For the pre-1978 multi-family residence in Fullerton retroreflective walls on all (neighboring and central) building walls (C60rrN60rr) increase heating load and decrease cooling load with respect to the C60N60 case of Lambertian cool walls on all building walls (Figure 5). Retroreflective walls completely remove the reflected beam component while Lambertian cool walls partially reflect it towards other urban surfaces. The net effect of changing to a retroreflective wall from a Lambertian wall is a reduction in average solar radiation incident on walls, which decreases cooling loads and increases heating loads.

The effect on cooling loads is largest during the day, while the effect on heating loads is largest shortly after sunrise. Shortly after sunrise, Lambertian cool walls reflect more solar radiation to surroundings walls and windows; this passive heating reduces the need for electric heating to maintain temperature setpoints. These effects are more expressed when only heating loads in winter and cooling loads in summer are considered (Figure 6).

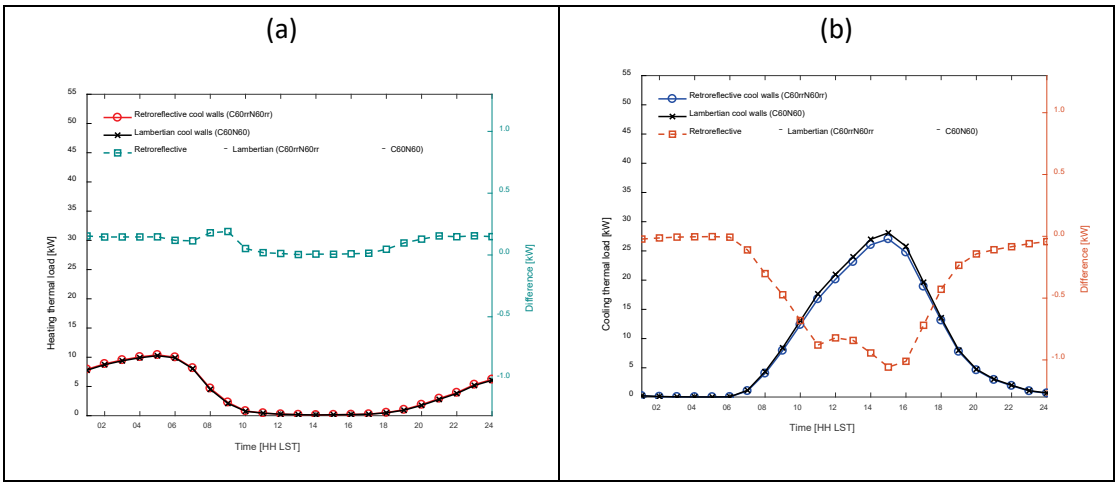

Figure 5. Comparison of the average diurnal cycle of heating (left, a) and cooling (right, b) loads for buildings with Lambertian reflector walls with wall albedo of 0.60 (C60N60) and walls with retroreflectors with wall albedo of 0.60 (C60rrN60rr). Results are averaged over the year for the pre-1978 multi-family residence in CZ8 (Fullerton).

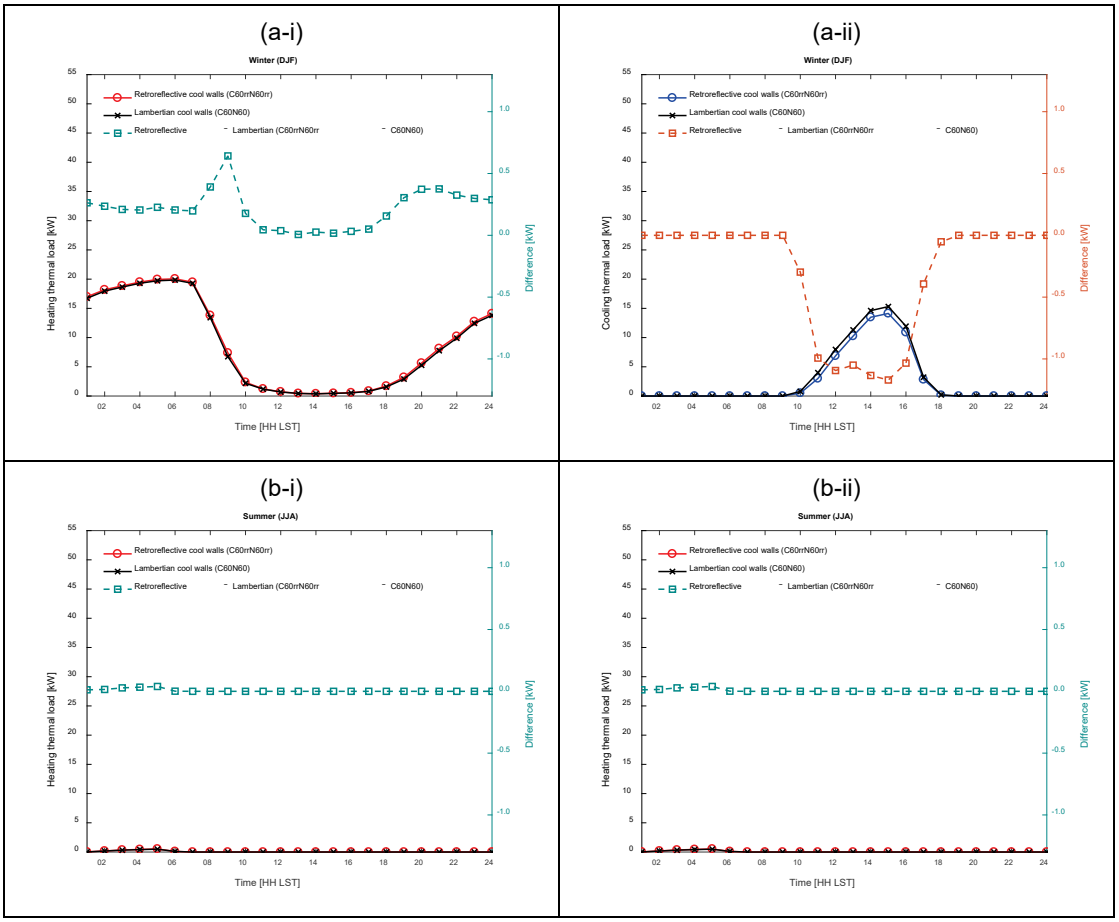

Figure 6. Seasonal analogs of Figure 5 for winter (December to February, a) and summer (June to August, b).

Table 4 shows the thermal loads for buildings with retroreflective walls and the change with respect to a multi-family residence with Lambertian cool walls. Retroreflective walls (C60rrN60rr) decrease annual cooling energy use by 3.3 MWh (4.0 percent) with respect to buildings with Lambertian cool walls (C60N60). The cooling benefit comes at the expense of a 0.9 MWh (2.6 percent) increase in annual heating load.

Table 4. Seasonal and annual heating and cooling loads for pre-1978 multi-family residence in CZ8 with Lambertian cool walls (C60N60) and retroreflective walls (C60rrN60rr). The retroreflective wall results are reported as load with retroreflective walls of albedo 0.60 minus the load with Lambertian walls of albedo 0.60.

	Heating load			Cooling load		
	Lambertian cool walls (C60N60)	Change due to retroreflective walls (C60rrN60rr – C60N60)		Lambertian cool walls (C60N60)	Change due to retroreflective walls (C60rrN60rr – C60N60)	
	[MWh]	[MWh]	[%]	[MWh]	[MWh]	[%]
Winter (DJF)	19.1	+0.5	+2.6	6.2	-0.7	-11.3
Summer (JJA)	0.1	+0.0	+9.4	37.9	-1.0	-2.6
Year	34.3	+0.9	+2.6	81.6	-3.3	-4.0

5 Conclusions

This report investigates the effects of reflective (cool) walls on building thermal loads for multi-family residences in California. The annual cooling load decreases but the annual heating load increases with increasing wall albedo. More detailed results on cool wall effects on the building where the cool wall is applied can be found in the Task 2.1 report: *Simulated HVAC energy savings in an isolated building.*

The unique analysis in this report is the interaction effect between buildings with and without cool walls. For this discussion the neighboring building is the building where the cool wall is applied, while the central building receives the sunlight reflected by the neighboring cool wall. Raising the albedo of neighboring walls reflects more sunlight onto the central building, which can increase its cooling load and reduce its heating load. Central building thermal loads and the outdoor thermal environment were simulated for a 5×5 array of multi-family residences separated by 23.3 m in California climate zone 8 (Fullerton).

In the first analysis set, all walls were assumed to be perfectly diffuse (Lambertian) reflectors. When the central building has conventional walls (albedo 0.25), raising the albedo of all neighboring walls to 0.60 (cool) from 0.25 (conventional) increases the central building's cooling load by 1.5 MWh (1.5 percent); the central building's heating

load is unaffected. If the central building also has cool walls (albedo 0.60), the central building's cooling load only increased by 1.2 MWh (1.3 percent). The negligible effect of cool walls on heating loads is likely an artifact of the way that TUF-IOBES predicts essentially zero daytime heating load. The cooling load increase for the central building upon raising the albedo of all neighboring walls are smaller than the cooling load decreases for the central building upon raising the albedo of its own walls (5.0 MWh, or 5.0 percent). Considering interactions between buildings therefore does not change the direction of the cool wall effects on all buildings combined. The equations derived in the theory section may allow scaling the simulation results obtained here to other building geometries and/or cool wall albedos.

In the second analysis set, all walls are assumed to retroreflected beam (direct) sunlight. Retroreflectors further enhance the cool wall effects, because retroreflective walls completely remove the reflected beam component while Lambertian cool walls partially reflect it towards other urban surfaces. Retroreflector effects were simulated in homogeneous arrays of buildings where all wall albedos are 0.60, but all walls are either retroreflective or Lambertian reflectors. Retroreflective walls decrease annual cooling loads by 3.3 MWh (4.0 percent) with respect to buildings with Lambertian cool walls. However, the cooling benefit comes at the expense of a 0.9 MWh (2.6 percent) increase in annual heating load.

6 References

Akbari H, Levinson R. 2008. Evolution of cool roof standards in the United States. *Advances in Building Energy Research* 2, 1-32, http://doi.org/10.3763/aber.2008.0201

American Society of Heating, Refrigerating and Air-conditioning Engineers Inc. ANSI/ASHRAE/IESNA Standard 90.1-2004.

Berkeley Lab WINDOW v.7.4.8.0. 2017. https://windows.lbl.gov/software/window/window.html, accessed May 15, 2017

Building in California, California Climate Zone, http://buildingincalifornia.com/california-climate-zones/, Accessed July 11, 2017.

California Energy Commission. 2017. California Energy Maps. http://www.energy.ca.gov/maps/renewable/building_climate_zones.html. Accessed May 15, 2017.

CRRC. 2017. Cool roof rebates and codes. Cool Roof Rating Council. Retrieved 2017-08-05 from http://coolroofs.org/resources/rebates-and-codes .

Energy Information Administration. 2017. https://www.eia.gov/outlooks/ieo/world.cfm, accessed May 15, 2017.

Energy Information Administration. 2009. Household Energy Use in California, 2009, https://www.eia.gov/consumption/residential/reports/2009/state_briefs/pdf/CA.pdf, accessed May 15, 2017

Masson V. 2000. A physically-based scheme for the urban energy budget in atmospheric models. *Boundary-Layer Meteorology* 94: 357-397, https://doi.org/10.1023/A:1002463829265.

National Renewable Energy Laboratory. 2017. National Solar Radiation Data Base, 1991-2005 Update: Typical Meteorological Year 3. http://rredc.nrel.gov/solar/old_data/nsrdb/1991-2005/tmy3/. Accessed May 15, 2017.

Rosado PJ. 2016. Evaluating cool impervious surfaces: application to an energy-efficient residential roof and to city pavements. Ph.D. dissertation, UC Berkeley. http://escholarship.org/uc/item/6bf80485 .

Taha H. 1997. Urban Climates and Heat Islands: Albedo, Evapotranspiration, and Anthropogenic Heat. *Energy and Buildings* 25: 99-103, https://doi.org/10.1016/S0378-7788(96)00999-1 .

U.S. Department of Energy (2017), https://www.energycodes.gov/development/, accessed May 15, 2017.

Yaghoobian N, Kleissl J. 2012. An indoor-outdoor building energy simulator to study urban modification effects on building energy use – Model description and validation. *Energy and Buildings* 54: 407-417, https://doi.org/10.1016/j.enbuild.2012.07.019 .

Yaghoobian N, Kleissl J. 2012. Effect of reflective pavements on building energy use. *Urban Climate* 2: 25-42, https://doi.org/10.1016/j.uclim.2012.09.002 .

Task Report Appendix A: Building Specifications

The appendix contains details of the building specifications discussed in Section 3.4.

Table A-1. Geometric parameters for each U.S. DOE building prototype as simulated in EnergyPlus in the Task 2.1 report: *Simulated HVAC energy savings in an isolated building*. TUF-IOBES parameters are shown in Table A-2.

Building type	Prototype sketches	Footprint area [m^2] [a]	Roof area [m^2]	Building height [m]	Building length × width [m]	Floors [b]	Whole-building window to wall ratio [%] [c]	Whole-building gross wall area [m^2]	Whole-building window area [m^2]
Single-family residence	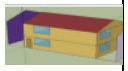	112	118	5.2	12.2 × 9.2	2	14	235	33
Multi-family residence	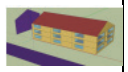	725	785	7.8	36.5 × 19.8	3	26	958	246

[a] Since in TUF-IOBES only buildings with square footprints can be simulated, footprint area is taken as the similarity parameter and building length is taken as the square root of the footprint area.

[b] The number of floors refers to the EnergyPlus setup, while in TUF-IOBES the building is simulated as an empty shell.

[c] Window-to-wall ratio is defined as the ratio of window area to gross wall area.

Table A-2. Comparison of the building geometrical properties between the EnergyPlus (E+) simulations in the Task 2.1 report: *Simulated HVAC energy savings in an isolated building* and TUF-lOBES. Only single-family and multi-family residences are considered in this chapter.

Building type	Footprint area [m^2]		Height *H* [m]		Length × width [m × m]		Whole-building gross wall area [m^2]		Whole-building window area [m^2]		Window-to-wall ratio [a] [%]		Canyon width W_c [b] [m]	Canyon aspect ratio H / W_c [b] [-]
	E+	TUF-lOBES	E+	TUF-lOBES	E+	TUF-lOBES	E+	TUF-lOBES	E+	TUF-lOBES	E+	TUF-lOBES	TUF-lOBES	TUF-lOBES
Multi-family residence	723	740	7.8	7.8	36.5 × 19.8	27.2 × 27.2	878	849	246	242	28	29	23.3	0.33

[a] Window-to-wall ratio is defined as the ratio of window area to gross wall area.

[b] Canyon width and canyon aspect ratio are not shown for EnergyPlus since EnergyPlus simulates an isolated building.

Table A-3. Roof, walls, building floor, and street construction. [a]

Surface	Layer	Multi-family residence
Roof	Top	Asphalt shingle
	2	OSB_1/2 in
	3	Roof insulation [b]
	4	½ in drywall
Walls	Outside	25 mm stucco
	2	200 mm normal weight concrete wall
	3	Wall insulation [b]
	4	13 mm gypsum board
Floor	Top	Plywood
	2	Concrete
	3	Crushed rock
Street	Top	Asphalt concrete
	2	Crushed rock

[a] The thermal and roughness material properties are defined in Table A-4 and Table A-5.

[b] The thickness of walls and roof insulation varies by building vintage and climate zone.

Table A-4. Material properties.

Materials	Thickness [m]	Conductivity [W/m · K]	Density [kg/m³]	Specific heat [kJ/kg · K]	Thermal resistance [m² · K/W]	Thermal emittance [-]	Solar absorptance [-] [b]	Texture
Metal surface	0.001	45.28	7,824	0.50	0.000018	0.90	0.70	Smooth
25 mm stucco	0.025	0.72	1,856	0.84	0.035	0.90	0.75	Smooth
200 mm normal weight concrete wall	0.203	2.31	2,322	0.83	0.088	0.90	0.70	Medium rough
13mm gypsum board	0.013	0.16	800	1.09	0.079	0.90	0.70	Smooth
Wall insulation [a]	Table A-5	0.06	43	1.21	Table A-5	0.90	0.70	Medium rough
Asphalt shingle	0.006	0.08	1,121	1.26	0.077	0.90	0.80	Medium rough
OSB_1/2 in	0.013	0.12	545	1.21	0.109	0.90	0.70	Medium smooth
Roof insulation [a]	Table A-5	0.06	42	0.78	Table A-5	0.90	0.70	Rough
Drywall_1/2 in	0.013	0.16	801	1.09	0.079	0.90	0.70	Medium smooth
Asphalt	0.070	0.75	2,110	0.92	0.093	0.95	0.82	Very rough
Concrete	0.070	1.51	2,400	0.88	0.046	0.95	0.82	Very rough
Plywood	0.019	0.12	545	1.22	0.158	0.90	0.80	Medium smooth
Crushed rock	0.200	0.95	1,200	1.05	0.211	0.90	0.65	Medium smooth

[a] Wall and roof insulation properties depend on the climate zone and are provided in Table A-5.

[b] If the material is opaque to sunlight, solar absorptance = 1 – solar reflectance.

Table A-5. Wall and roof insulation thickness and thermal resistance for the pre-1978 multi-family residences in CZ8. [a]

Vintage	Pre-1978
Wall insulation thickness [m]	0.05
Wall insulation thermal resistance [m^2·K/W]	0.82
Roof insulation thickness [m]	0.15
Roof insulation thermal resistance [m^2·K/W]	2.51

[a] For insulation materials, $L = R \times k$, where L = thickness [m], R = thermal resistance [m^2·K/W], and k = thermal conductivity [W/m·K].

Table A-6. Angular solar heat gain coefficient (SHGC), visible transmittance, and visible absorptance of window glass for pre-1978 buildings [a,b].

Incident angle (°)	SHGC	Transmittance	Absorptance (first pane)	Absorptance (second pane)
0	0.611	0.346	0.053	0.513
10	0.609	0.348	0.053	0.511
20	0.605	0.353	0.053	0.506
30	0.597	0.362	0.054	0.496
40	0.583	0.373	0.055	0.478
50	0.555	0.388	0.055	0.477
60	0.500	0.403	0.053	0.390
70	0.393	0.411	0.046	0.386
80	0.123	0.370	0.031	0.123
90	0.611	0.346	0.053	0.513
Diffuse	0.522	0.420	0.375	0.051

[a] Window properties are simulated by the Berkeley Lab WINDOW v.7.4.8.0 (2017) software.

[b] Window is opaque to thermal infrared radiation. Thermal transmittance $U = 1/(R_{\text{in}} + R_{\text{window}} + R_{\text{out}}) = 3.65$ W/(m2·K) for the pre-1978 building, where R_{in}, R_{window}, and R_{out} are the thermal resistances of the inside air film, window, and outside air film, respectively.

Table A-7. Lighting splits, equipment splits, and occupancy splits from the U.S. DOE building prototypes as simulated in this report and the Task 2.1 report: *Simulated HVAC energy savings in an isolated building*.

Splits			Multi-family residence
People splits	Activity Level [W / person]		134
	Latent fraction		0.38
	Sensible fraction		0.62
	split into:	LW radiant fraction	0.00
		Convective fraction	1.00
Equipment splits	Latent fraction		0.12
	Sensible fraction		0.88
	split into:	LW radiant fraction	0.48
		Convective fraction	0.52
Lighting splits	Sensible fraction		1.00
	split into:	SW radiant fraction	0.20
		LW radiant fraction	0.60
		Convective fraction	0.20
	Fraction of heat return air duct		0.00

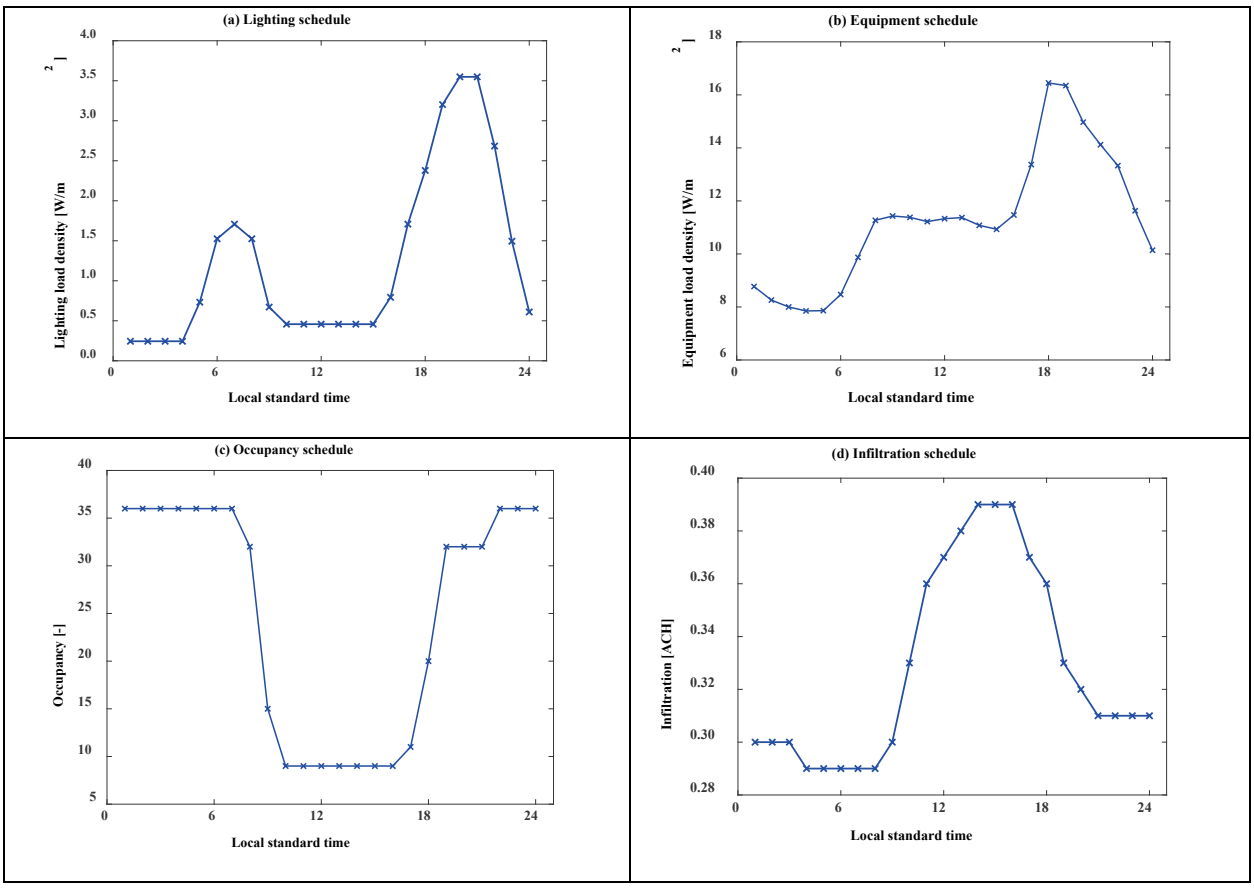

Figure A-1. Lighting load density, equipment load density, occupancy, and infiltration schedules for the multi-family residence in EnergyPlus and TUF-IOBES. Lighting and equipment load densities shown here were calculated by normalizing whole-building loads to TUF-IOBES building footprint area.

Energy Research and Development Division

FINAL PROJECT REPORT

Solar-Reflective "Cool" Walls: Benefits, Technologies, and Implementation

Appendix C: Using Solar Availability to Scale Heating, Ventilation, and Air Conditioning Savings (Task 2.3 Report)

California Energy Commission
Gavin Newsom, Governor

April 2019 | CEC-500-2019-040-APC

Appendix C:
Using solar availability to scale HVAC savings (Task 2.3 report)

Ronnen Levinson[1]

[1] Heat Island Group, Lawrence Berkeley National Laboratory

28 February 2018

Abstract

To assess how the solar availability (incident solar radiation) of a central (modeled) building is affected by a neighboring wall across a canyon, we calculate its solar availability factor (SAF), defined as the ratio of sunlight incident on the central building wall in the presence of the neighboring wall to that incident in the absence of the neighboring wall. Cool-wall cooling savings, heating penalties, or HVAC savings simulated for an isolated central building (no neighbors) can be scaled by SAF to account for interaction with the neighboring wall.

Monthly values of SAF were evaluated in 17 climates across the United States, including three in California, for north, east, south, and west central walls, over a wide range of canyon aspect ratio (height/width). Results for four representative aspect ratios—0.2, 1, 2, and 10—are presented.

In Fresno, CA, monthly SAF ranges from 0.90 to 0.96 for central walls facing north, east, south west when the aspect ratio is 0.2 (two-story single-family homes across a street) and both the central and neighboring walls are conventional (albedo 0.25). Monthly SAFs decrease as aspect ratio rises, falling to 0.06 – 0.24 at an aspect ratio of 10 (adjacent 10-story buildings on the same side of the street).

1 Introduction

The solar availability (incident solar radiation) of a central (modeled) building can be reduced by shadows cast by neighboring buildings, and increased by sunlight reflected from neighboring buildings. This study evaluates the solar availability factor of a central building wall, defined as the ratio of sunlight incident on the central building wall in the presence of the neighboring wall to that incident in the absence of the neighboring wall. We can scale cool-wall cooling savings, heating penalties, or HVAC savings simulated for an isolated central building (no neighbors) by the solar availability factor to account for interaction with the neighboring wall. We can also

assess the effect of raising neighboring wall albedo on the solar availability of the central building wall.

This analysis emphasizes simplicity, so that its results can be applied knowing only the canyon aspect ratio (ratio of building height to building separation), city, and month. It does not consider shading or reflection by surfaces other than neighboring walls, such as trees.

2 Theory

2.1 Geometry

Consider a two-dimensional canyon formed by a pair of adjacent buildings of equal height and infinite extent (Figure 1). Let H = building height, W = ground (canyon floor) width, L = canyon depth, and J = ground shadow length, all dimensional. Let θ_z = solar zenith angle and ϕ = solar azimuth angle. Azimuth angles are measured clockwise from north, such that 0° is north and 90° is east.

Let subscripts LW, RW, SFW, G, and C designate the canyon's left wall, right wall, sun-facing wall, ground, and ceiling, respectively. Let ψ represent wall azimuth angle, and let wall surface-solar azimuth angle $\gamma = \phi - \psi$. When the solar beam is normal to the wall, $\gamma = 0$ and $\cos\gamma = 1$; when the solar beam is parallel to the wall, $\gamma = \pm 90°$ and $\cos\gamma = 0$; and when the solar beam is behind the wall, $\gamma < -90°$ or $\gamma > 90°$, and $\cos\gamma < 0$.

Let I_{BH} = beam (direct) horizontal irradiance; I_{DH} = diffuse horizontal irradiance; ρ = albedo (solar reflectance), $R \equiv H/W$ = canyon aspect ratio; and ground shadow length (normal to wall)

$$J = \min(H \times \tan\theta_z \times \cos\gamma_{SFW}, W). \quad (1)$$

It follows from Eq. (1) that the shadow will not cross the canyon when $\tan\theta_z \times \cos\gamma_{SFW} < 1/R$, and that the sun-facing wall will be unshaded when the solar zenith angle

$$\theta_z < \text{atan}[1/(R \times \cos\gamma_{SFW})]. \quad (2)$$

Since $0 < \cos\gamma_{SFW} \leq 1$, the sun-facing wall will also be unshaded during the subset of these times when

$$\theta_z < \text{atan}(1/R). \quad (3)$$

We show in Task Report Appendix A that the cumulative irradiance (solar power per unit area) striking the left wall after no more than two reflections off canyon surfaces will be

$$I_{LW} = a \times Q''_{i,LW} + b \times Q''_{i,RW} + c \times Q''_{i,G}, \quad (4)$$

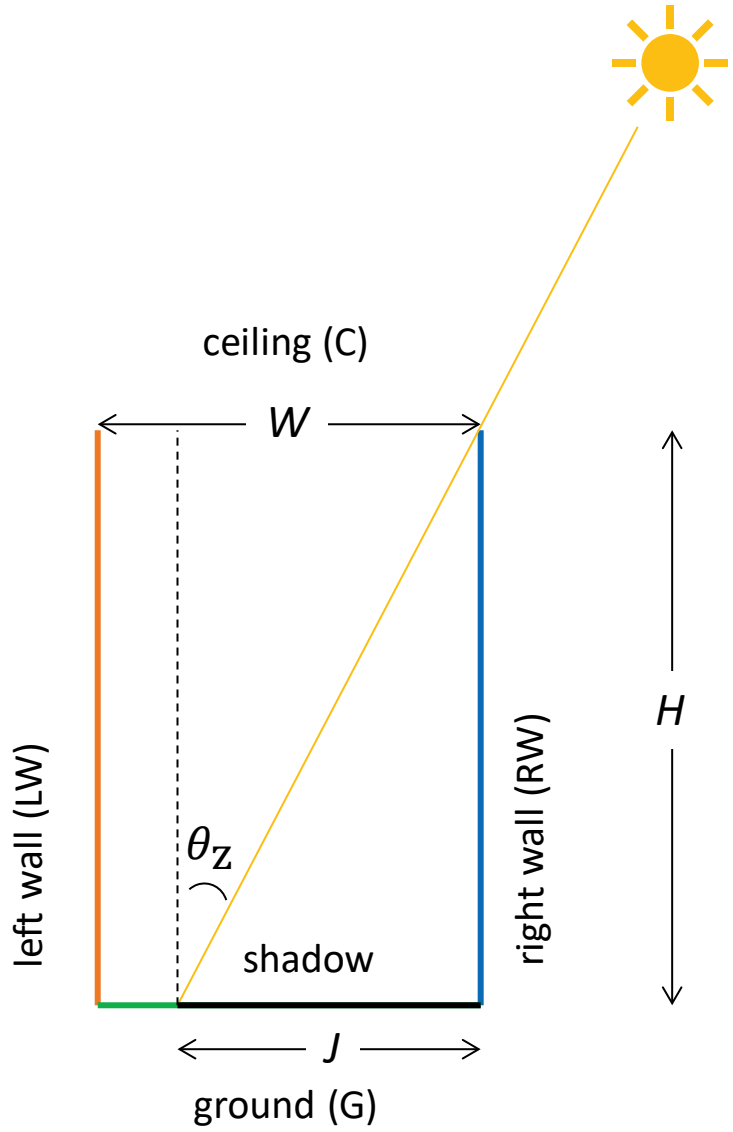

Figure 1. Canyon of width W formed by walls of adjacent buildings of equal height H and infinite extent into page. Ground shadow length is J and solar zenith angle is θ_z.

where

$$a = 1 + \rho_{LW} \times (F_{LW\to G} \times \rho_G \times F_{G\to LW} + F_{LW\to RW} \times \rho_{RW} \times F_{RW\to LW}) \quad (5)$$

$$b = \rho_{RW} \times (F_{RW\to LW} + F_{RW\to G} \times \rho_G \times F_{G\to LW}) \quad (6)$$

$$c = \rho_G \times (F_{G\to LW} + F_{G\to RW} \times \rho_{RW} \times F_{RW\to LW}) \quad (7)$$

are reflection multipliers and

$$Q''_{\mathrm{i,LW}} = [I_{\mathrm{BH}} \times (J/H) + I_{\mathrm{DH}} \times F_{\mathrm{C}\to\mathrm{LW}}/R] \text{ if } \cos\gamma_{\mathrm{LW}} > 0, \text{ or } (I_{\mathrm{DH}} \times F_{\mathrm{C}\to\mathrm{LW}}/R) \text{ otherwise} \quad (8)$$

$$Q''_{\mathrm{i,RW}} = [I_{\mathrm{BH}} \times (J/H) + I_{\mathrm{DH}} \times F_{\mathrm{C\to RW}}/R] \text{ if } \cos\gamma_{\mathrm{RW}} > 0, \text{ or } (I_{\mathrm{DH}} \times F_{\mathrm{C\to RW}}/R) \text{ otherwise} \quad (9)$$

$$Q''_{\mathrm{i,G}} = I_{\mathrm{BH}} \times [(1/R) - (J/H)] + (I_{\mathrm{DH}} \times F_{\mathrm{C\to G}})/R \quad (10)$$

are the initial radiative powers per unit left wall area incident on the left wall, right wall, and ground, respectively. View factors

$$F_{\mathrm{C\to G}} = \sqrt{1 + R^2} - R \quad (11)$$

$$F_{\mathrm{C\to LW}} = F_{\mathrm{C\to RW}} = (1 - F_{\mathrm{C\to G}})/2 \quad (12)$$

$$F_{\mathrm{G\to LW}} = F_{\mathrm{G\to RW}} = F_{\mathrm{C\to LW}} \quad (13)$$

$$F_{\mathrm{LW\to G}} = F_{\mathrm{G\to LW}}/R \quad (14)$$

$$F_{\mathrm{RW\to G}} = F_{\mathrm{G\to RW}}/R \quad (15)$$

$$F_{\mathrm{LW\to RW}} = F_{\mathrm{RW\to LW}} = 1 - (2/R) \times F_{\mathrm{C\to LW}}. \quad (16)$$

2.2 Isolated-wall irradiance

Following the standard isotropic sky model (Duffie and Beckman 2006), the global irradiance on an isolated wall is

$$I_{\mathrm{W,isolated}} = I_{\mathrm{BN}} \times \cos\theta + \frac{I_{\mathrm{DH}} + (I_{\mathrm{BH}} + I_{\mathrm{DH}})\rho_{\mathrm{G}}}{2} \text{ if } \cos\theta > 0, \text{ or } \frac{I_{\mathrm{DH}} + (I_{\mathrm{BH}} + I_{\mathrm{DH}})\rho_{\mathrm{G}}}{2} \text{ otherwise;} \quad (17)$$

where beam-normal solar irradiance

$$I_{\mathrm{BN}} = I_{\mathrm{BH}}/\cos\theta_{\mathrm{z}}; \quad (18)$$

and the solar beam's incidence angle θ is given by

$$\cos\theta = \sin\theta_{\mathrm{z}} \cos\gamma. \quad (19)$$

Combining,

$$I_{\mathrm{W,isolated}} = I_{\mathrm{BN}} \times \tan\theta_{\mathrm{z}} \times \cos\gamma + \frac{I_{\mathrm{DH}} + (I_{\mathrm{BH}} + I_{\mathrm{DH}})\,\rho_{\mathrm{G}}}{2} \text{ if } \cos\theta > 0, \text{ or } \frac{I_{\mathrm{DH}} + (I_{\mathrm{BH}} + I_{\mathrm{DH}})\rho_{\mathrm{G}}}{2} \text{ otherwise.} \quad (20)$$

We can compare this to the left-wall irradiance predicted by our canyon model, I_{LW}, when $W \to \infty$ and the sun is above the horizon (keeping $\tan\theta_{\mathrm{z}}$ finite and less than $1/R$). If the left wall faces the sun,

$$\lim_{R\to 0} I_{\mathrm{LW}} = I_{\mathrm{BH}} \times \tan\theta_{\mathrm{z}} \times \cos\gamma_{\mathrm{LW}} + \frac{I_{\mathrm{DH}} + (I_{\mathrm{BH}} + I_{\mathrm{DH}})\,\rho_{\mathrm{G}}}{2}, \quad (21)$$

while if it opposes the sun,

$$\lim_{R\to 0} I_{\mathrm{LW}} = \frac{I_{\mathrm{DH}} + (I_{\mathrm{BH}} + I_{\mathrm{DH}})\,\rho_{\mathrm{G}}}{2}. \quad (22)$$

Each limiting result agrees with the corresponding isolated-wall irradiance predicted by the isotropic sky model.

2.3 Solar availability factor

We can now calculate the left wall's hourly solar availability factor (SAF)

$$f = I_{\mathrm{LW}}/I_{\mathrm{W,isolated}} \tag{23}$$

or its daily SAF

$$f_{\mathrm{daily}} = \frac{\int\limits_{\mathrm{day}} dt\, I_{\mathrm{LW}}}{\int\limits_{\mathrm{day}} dt\, I_{\mathrm{W,isolated}}} \tag{24}$$

where t is time, and the left wall and isolated wall face the same direction.

We can compute monthly SAF from monthly mean values of left-wall and isolated wall daily irradiation:

$$f_{\mathrm{monthly}} = \frac{\text{mean daily left wall irradiation}}{\text{mean daily isolated wall irradiation}}. \tag{25}$$

2.4 Applications of solar availability factor

If f_{monthly} is roughly constant over the course of the year, we can scale both the cooling savings and heating penalties simulated for an isolated building by a single value of f_{monthly}. If there is substantial variation in f_{monthly}, we will need to consider its values in both the heating and cooling seasons.

We can also use SAF to assess the effect of raising neighboring wall albedo on the sunlight incident on the central building wall. For example, the fractional increase in monthly sunlight incident on the central wall building is

$$g_{\mathrm{monthly}} \equiv \frac{\text{mean daily left wall irradiation, high-albedo neighbor}}{\text{mean daily left wall irradiation, low-albedo neighbor}} - 1 = \frac{f_{\text{monthly, high-albedo neighbor}}}{f_{\text{monthly, low-albedo neighbor}}} - 1. \tag{26}$$

3 Methodology

Hourly and monthly SAFs were evaluated for 17 locations across the United States, including three in California: Burbank, Fresno, and San Francisco (Figure 2). Hourly values of diffuse horizontal irradiance I_{DH} and beam horizontal irradiance I_{BH} (calculated as global horizontal irradiance – diffuse horizontal irradiance) were obtained from the Typical Meteorological Year 3 (TMY3) weather file (NREL 2018b) representing each location (Table 1). Mid-hour values of solar position were computed with the Measurement and Information Data Center Solar Position and

Intensity (MIDC SOLPOS) Calculator provided by the National Renewable Energy Laboratory (NREL 2018a). Solar positions were evaluated in year 2015 to avoid leap days and leap seconds.

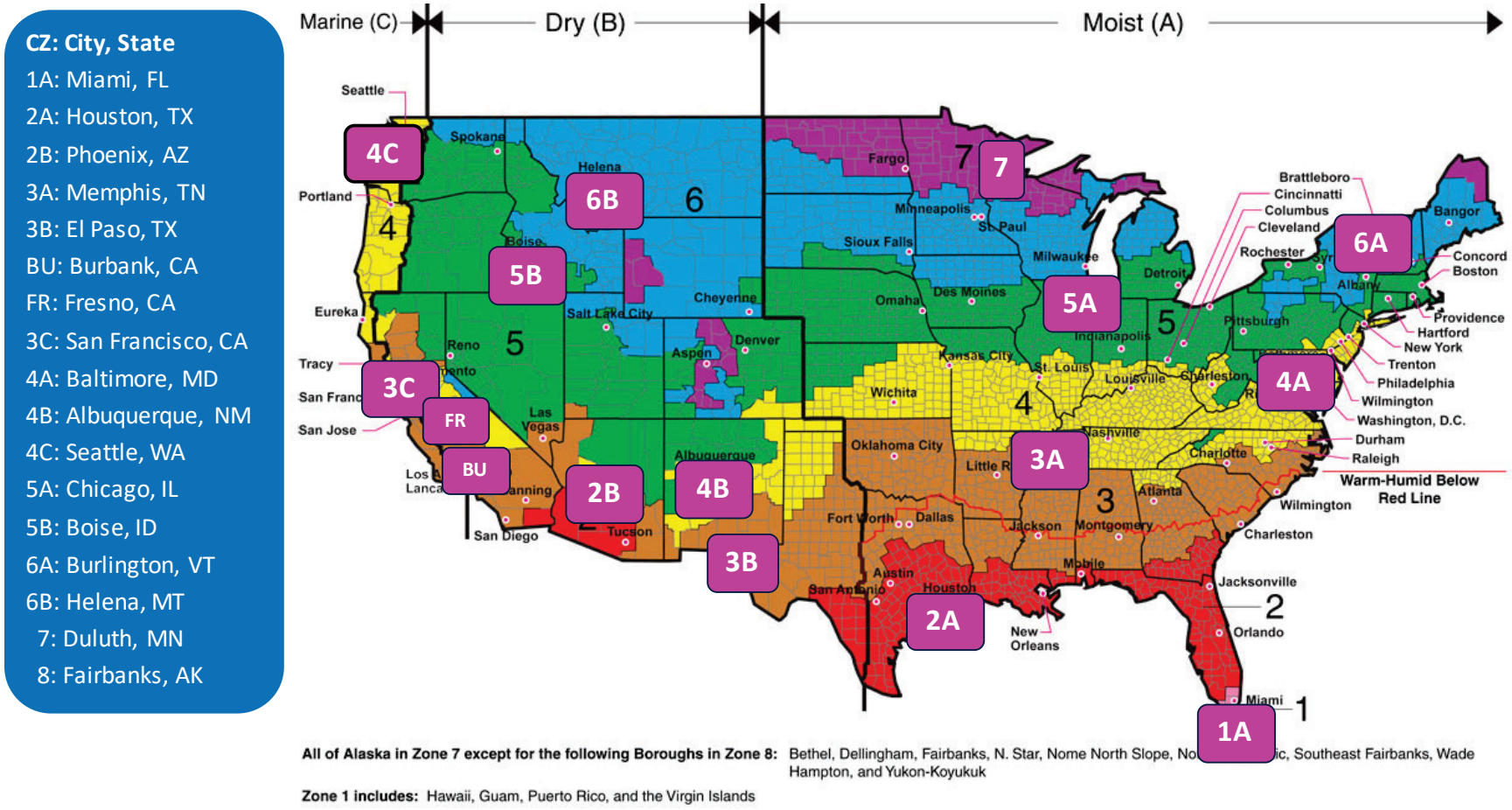

Figure 2. Map of U.S. climates in which solar availability factors were calculated. Climate 8 (Fairbanks, AK) is not shown.

Table 1. Location, site name, and site code of Typical Meteorological Year 3 (TMY3) weather file used to characterize each climate.

Climate	City, State	USAF [a]	Site Name	Latitude (°N)	Longitude (°W)
1A	Miami, FL	722020	MIAMI INTL AP	25.817	-80.3
2A	Houston, TX	722430	HOUSTON BUSH INTERCONTINENTAL	30.0	-95.367
2B	Phoenix, AZ	722780	PHOENIX SKY HARBOR INTL AP	33.45	-111.983
3A	Memphis, TN	723340	MEMPHIS INTERNATIONAL AP	35.067	-89.983
3B	El Paso, TX	722700	EL PASO INTERNATIONAL AP [UT]	31.77	-106.5
FR	Fresno, CA	723890	FRESNO YOSEMITE INTL AP	36.783	-119.717
BU	Burbank, CA	722880	BURBANK-GLENDALE-PASSADENA AP	34.2	-118.35
3C	San Francisco, CA	724940	SAN FRANCISCO INTL AP	37.617	-122.4
4A	Baltimore, MD	724060	BALTIMORE BLT-WASHNGTN INT'L	39.167	-76.683
4B	Albuquerque, NM	723650	ALBUQUERQUE INTL ARPT [ISIS]	35.04	-106.62
4C	Seattle, WA	727930	SEATTLE SEATTLE-TACOMA INTL A	47.467	-122.317
5A	Chicago, IL	725300	CHICAGO OHARE INTL AP	41.983	-87.917
5B	Boise, ID	726810	BOISE AIR TERMINAL [UO]	43.62	-116.21
6A	Burlington, VT	726170	BURLINGTON INTERNATIONAL AP	44.467	-73.15
6B	Helena, MT	727720	HELENA REGIONAL AIRPORT	46.6	-111.967
7	Duluth, MN	727450	DULUTH INTERNATIONAL ARPT	46.833	-92.217
8	Fairbanks, AK	702610	FAIRBANKS INTL ARPT	64.817	-147.85

[a] United States Air Force (USAF) code identifying Typical Meteorological Year 3 (TMY3) weather file.

SAFs were computed for central building walls facing north, east, south, and west in canyons with 29 aspect ratios ranging from 0 (infinitely wide canyon) to 90 (extremely narrow canyon). For simplicity, we focus on the results for four aspect ratios:

- R=0.2, representing two-story single-family homes across a residential street (H=6 m, W=30 m);
- R=1, representing two-story single-family across small back yards (H=6 m, W=6 m);
- R=2, representing adjacent two-story single-family homes on the same side of a street (H=6 m, W=3 m); and
- R=10, representing adjacent 10-story office buildings on the same side of the street (H=30 m, W=3 m).

Canyons with these four aspect ratios are drawn to scale in Figure 3.

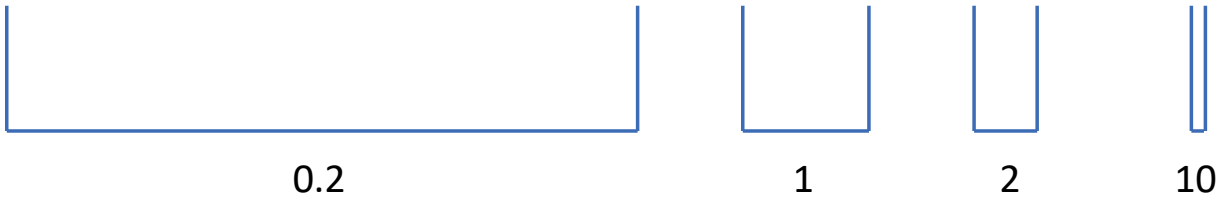

Figure 3. Canyon aspect ratio $R = H/W$ = 0.2, 1, 2, or 10.

SAFS were computed in four scenarios:

(1) conventional central wall with conventional neighboring wall;

(2) conventional central wall with cool neighboring wall;

(3) cool central wall with conventional neighboring wall; and

(4) cool central wall with cool neighboring wall.

Conventional and cool walls were assigned albedos 0.25 (dark-to-medium color) and 0.60 (off-white color), respectively. Ground albedo was fixed at 0.20, representing a lawn or aged pavement.

Fractional increases in monthly central wall irradiance upon raising neighboring-wall albedo were computed from monthly SAFs following Eq. (26).

4 Results and discussion

4.1 Monthly SAF

Trends in monthly SAF are illustrated for Fresno, CA in Figure 4. Variation of monthly SAF in Fresno with central wall orientation (N, E, S, or W) and aspect ratio (0.2, 1, 2, or 10) is plotted for Scenario 1 (conventional central wall with conventional neighboring wall) in Figure 4a, and for Scenario 2 (conventional central wall with cool neighboring wall) in Figure 4b. Analogous plots spanning all 17 climates are presented in Figure B-1 and Figure B-2 of Task Report Appendix B.

In Scenario 1, monthly SAFs in Fresno for the set of north, east, and west central walls range annually from 0.90 to 0.95 for R=0.2, 0.58 to 0.71 for R=1, 0.38 to 0.52 for R=2, and 0.10 to 0.15 for R=10. Ranges for the south central wall are in some cases wider: 0.94 to 0.96 for R=0.2, 0.51 to 0.84 for R=1, 0.28 to 0.71 for R=2, and 0.06 to 0.24 for R=10 (row "FR" in panels a - d of Table 2).

Eq. (3) predicts that for canyon aspect ratios of 0.2, 1, 2, or 10, the sun-facing wall is unshaded when the solar altitude angle $\alpha = 90° - \theta_z$ exceeds 11.3˚, 45.0˚, 63.4˚, or 84.3˚, respectively. [It will also be unshaded at lower solar altitudes that satisfy Eq. (2).] The high values of Fresno monthly SAF for R=0.2 (0.90 to 0.96 over all four orientations) in Scenario 1 result from minimal shading of the sun-facing wall. Inspection of the Fresno sun path shows that across the year, the solar altitude rises above 11.3˚ within about an hour of sunrise, and remains above that value until about an hour before sunset (Figure 5). Monthly SAFs diminish as the aspect ratio grows because the sun-facing wall spends more time in the shade.

Seasonal variations in monthly SAF are greatest for south central walls (Figure 4a) because the Fresno midday sun is much higher in summer than in winter (Figure 5). For example, the solar altitude angle at noon on June 21 (summer solstice) is 76.7˚, while that on December 21 (winter solstice) is 29.8˚.

Table 2 reports for all 17 climates the annual mean, minimum, maximum, and range (maximum – minimum) values of monthly SAF in scenario 1 (conventional central wall with conventional neighboring wall) by climate, central wall orientation, and aspect ratio. Corresponding values for the three remaining scenarios are presented in Table C-1 through Table C-3 of Task Report Appendix C.

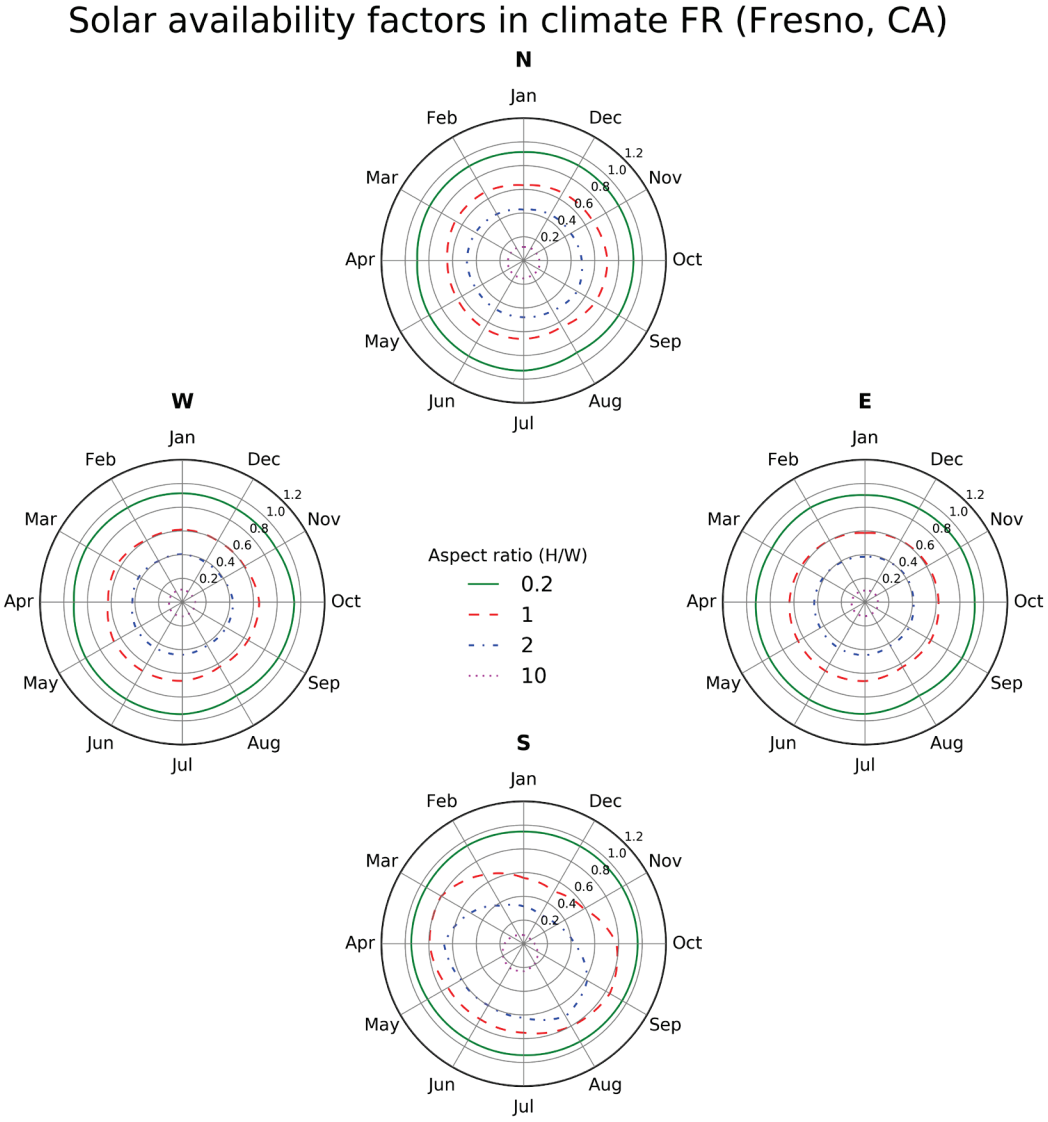

ground albedo = 0.20, central wall albedo = 0.25, neighboring wall albedo = 0.25

(a)

Figure 4. Monthly SAFs for a north (N), east (E), south (S), or west (W) conventional central wall (ρ=0.25) with (a) conventional neighboring wall (ρ=0.25) and (b) cool neighboring wall (ρ=0.25). Results shown for aspect ratios 0.2, 1, 2, and 10 in Fresno, CA.

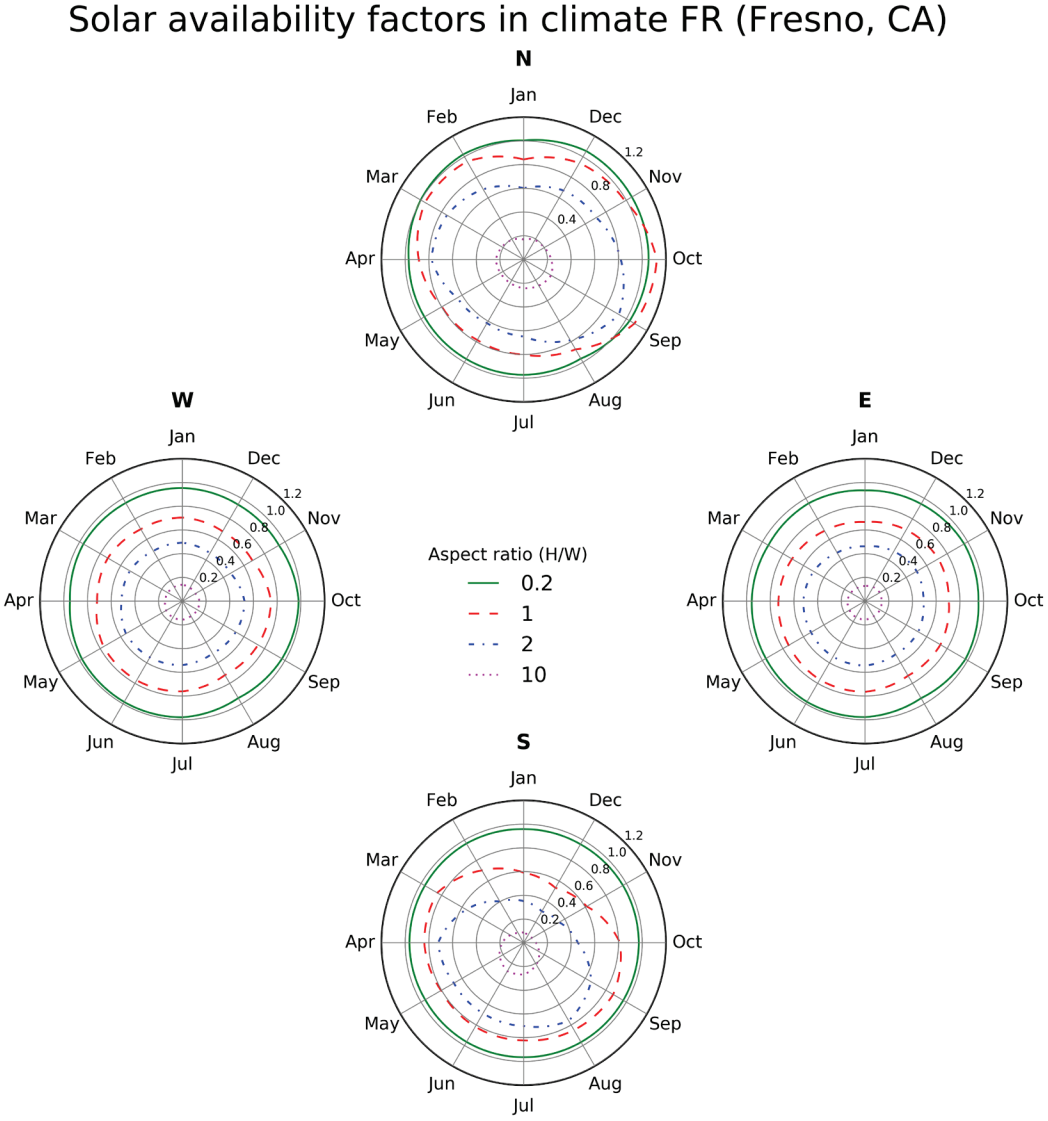

ground albedo = 0.20, central wall albedo = 0.25, neighboring wall albedo = 0.60

(b)

Figure 4 (continued)

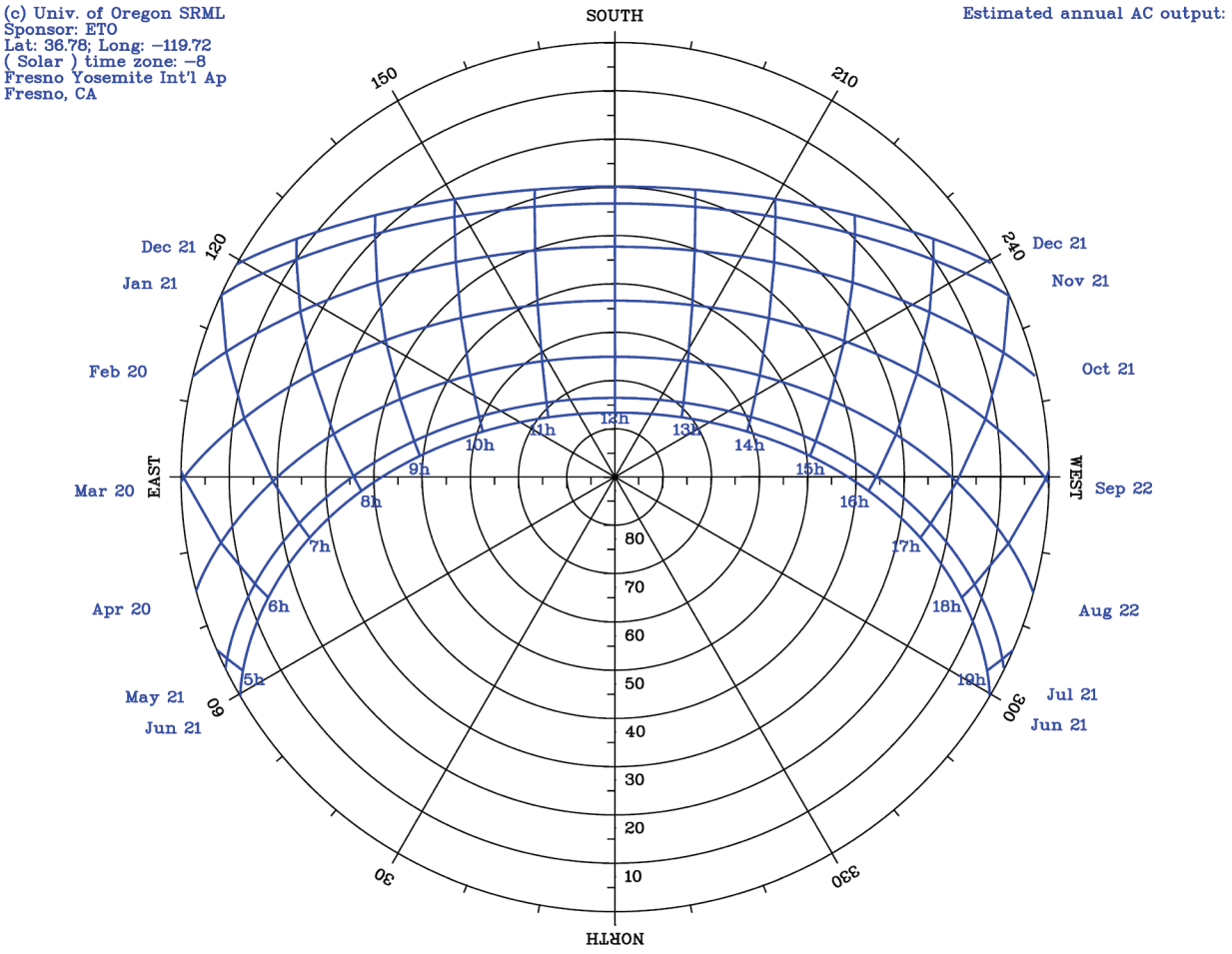

Figure 5. Solar path in climate FR (Fresno, CA).

Table 2. Annual mean, minimum, maximum, and range (maximum – minimum) values of monthly SAF for a north (N), east (E), south (S), or west (W) conventional central wall (ρ=0.25) with a conventional neighboring wall (ρ=0.25). Results shown by climate for aspect ratios of (a) R=0.2, (b) R=1, (c) R=2, and (d) R=10.

(a) aspect ratio R=0.2

	N				E				S				W			
	mean	min	max	range	mean	min	max	range	mean	min	max	range	mean	min	max	range
1A (Miami, FL)	0.91	0.91	0.92	0.02	0.92	0.89	0.94	0.05	0.93	0.91	0.96	0.05	0.91	0.84	0.94	0.10
2A (Houston, TX)	0.91	0.89	0.92	0.03	0.91	0.86	0.94	0.07	0.93	0.91	0.95	0.04	0.91	0.86	0.93	0.07
2B (Phoenix, AZ)	0.92	0.86	0.95	0.09	0.91	0.87	0.95	0.08	0.95	0.93	0.97	0.04	0.92	0.88	0.95	0.06
3A (Memphis, TN)	0.92	0.90	0.93	0.03	0.92	0.85	0.94	0.08	0.94	0.92	0.96	0.04	0.91	0.84	0.94	0.10
3B (El Paso, TX)	0.93	0.91	0.95	0.04	0.94	0.88	0.96	0.07	0.95	0.93	0.97	0.04	0.93	0.90	0.94	0.04
BU (Burbank, CA)	0.92	0.91	0.94	0.03	0.93	0.89	0.94	0.06	0.95	0.93	0.96	0.04	0.93	0.90	0.95	0.05
FR (Fresno, CA)	0.92	0.90	0.93	0.03	0.92	0.90	0.95	0.04	0.95	0.94	0.96	0.03	0.93	0.91	0.95	0.04
3C (San Francisco, CA)	0.91	0.88	0.94	0.06	0.92	0.87	0.94	0.07	0.95	0.93	0.96	0.03	0.92	0.89	0.94	0.05
4A (Baltimore, MD)	0.91	0.88	0.93	0.06	0.90	0.74	0.94	0.19	0.94	0.91	0.96	0.05	0.90	0.83	0.93	0.10
4B (Albuquerque, NM)	0.93	0.88	0.97	0.09	0.92	0.87	0.95	0.08	0.95	0.93	0.97	0.03	0.92	0.89	0.95	0.06
4C (Seattle, WA)	0.91	0.90	0.92	0.03	0.91	0.85	0.94	0.08	0.94	0.91	0.96	0.05	0.90	0.82	0.93	0.12
5A (Chicago, IL)	0.91	0.91	0.93	0.02	0.91	0.86	0.94	0.08	0.94	0.92	0.95	0.03	0.91	0.84	0.94	0.10
5B (Boise, ID)	0.92	0.90	0.94	0.03	0.91	0.86	0.94	0.08	0.95	0.92	0.96	0.04	0.91	0.86	0.95	0.09
6A (Burlington, VT)	0.91	0.87	0.93	0.06	0.90	0.82	0.93	0.11	0.94	0.90	0.95	0.05	0.90	0.85	0.93	0.08
6B (Helena, MT)	0.92	0.88	0.94	0.06	0.91	0.86	0.94	0.08	0.95	0.91	0.96	0.05	0.90	0.80	0.95	0.15
7 (Duluth, MN)	0.91	0.86	0.93	0.07	0.90	0.83	0.94	0.11	0.94	0.91	0.96	0.05	0.90	0.84	0.94	0.10
8 (Fairbanks, AK)	0.88	0.77	0.94	0.16	0.77	0.56	0.92	0.36	0.79	0.24	0.96	0.72	0.91	0.70	0.94	0.24

Table 2 (continued)

(b) aspect ratio R=1

	N				E				S				W			
	mean	min	max	range	mean	min	max	range	mean	min	max	range	mean	min	max	range
1A (Miami, FL)	0.65	0.62	0.69	0.08	0.63	0.59	0.66	0.07	0.70	0.61	0.80	0.19	0.63	0.57	0.66	0.09
2A (Houston, TX)	0.65	0.61	0.69	0.07	0.62	0.57	0.66	0.09	0.70	0.59	0.80	0.21	0.62	0.57	0.66	0.09
2B (Phoenix, AZ)	0.68	0.61	0.75	0.14	0.61	0.56	0.65	0.09	0.72	0.54	0.83	0.30	0.62	0.57	0.67	0.10
3A (Memphis, TN)	0.66	0.63	0.69	0.06	0.62	0.56	0.67	0.10	0.69	0.50	0.80	0.29	0.61	0.55	0.67	0.12
3B (El Paso, TX)	0.69	0.65	0.75	0.10	0.64	0.60	0.69	0.09	0.73	0.57	0.82	0.26	0.63	0.58	0.69	0.11
BU (Burbank, CA)	0.68	0.64	0.72	0.08	0.63	0.59	0.68	0.10	0.71	0.53	0.82	0.29	0.64	0.58	0.69	0.11
FR (Fresno, CA)	0.66	0.63	0.71	0.07	0.63	0.58	0.67	0.09	0.71	0.51	0.84	0.33	0.63	0.60	0.67	0.07
3C (San Francisco, CA)	0.66	0.62	0.69	0.07	0.63	0.56	0.68	0.12	0.70	0.47	0.83	0.36	0.63	0.58	0.66	0.09
4A (Baltimore, MD)	0.65	0.61	0.69	0.08	0.60	0.47	0.65	0.19	0.67	0.44	0.81	0.36	0.60	0.54	0.65	0.12
4B (Albuquerque, NM)	0.70	0.62	0.77	0.15	0.61	0.55	0.67	0.11	0.71	0.51	0.83	0.32	0.62	0.56	0.69	0.13
4C (Seattle, WA)	0.64	0.62	0.67	0.05	0.60	0.55	0.65	0.11	0.64	0.37	0.80	0.42	0.59	0.51	0.65	0.14
5A (Chicago, IL)	0.64	0.63	0.67	0.04	0.60	0.53	0.64	0.12	0.65	0.42	0.80	0.38	0.61	0.53	0.65	0.12
5B (Boise, ID)	0.67	0.64	0.72	0.08	0.59	0.51	0.65	0.13	0.68	0.39	0.85	0.46	0.60	0.53	0.66	0.14
6A (Burlington, VT)	0.63	0.59	0.66	0.07	0.59	0.52	0.64	0.12	0.65	0.39	0.78	0.40	0.59	0.53	0.64	0.11
6B (Helena, MT)	0.66	0.63	0.70	0.06	0.59	0.51	0.64	0.14	0.64	0.34	0.82	0.48	0.58	0.47	0.65	0.18
7 (Duluth, MN)	0.64	0.59	0.67	0.08	0.58	0.50	0.64	0.13	0.63	0.35	0.80	0.45	0.58	0.52	0.63	0.12
8 (Fairbanks, AK)	0.60	0.49	0.66	0.17	0.42	0.25	0.56	0.31	0.47	0.10	0.79	0.69	0.58	0.36	0.64	0.27

Table 2 (continued)

(c) aspect ratio R=2

	N				E				S				W			
	mean	min	max	range	mean	min	max	range	mean	min	max	range	mean	min	max	range
1A (Miami, FL)	0.45	0.43	0.48	0.05	0.42	0.39	0.44	0.06	0.48	0.36	0.62	0.26	0.42	0.38	0.45	0.07
2A (Houston, TX)	0.45	0.43	0.48	0.06	0.42	0.38	0.44	0.07	0.47	0.32	0.63	0.31	0.41	0.37	0.45	0.07
2B (Phoenix, AZ)	0.49	0.44	0.52	0.08	0.41	0.37	0.44	0.07	0.51	0.28	0.70	0.42	0.41	0.36	0.45	0.09
3A (Memphis, TN)	0.46	0.44	0.48	0.03	0.41	0.37	0.45	0.08	0.47	0.27	0.63	0.36	0.41	0.36	0.45	0.10
3B (El Paso, TX)	0.50	0.46	0.53	0.07	0.42	0.39	0.46	0.07	0.51	0.30	0.68	0.38	0.42	0.38	0.47	0.09
BU (Burbank, CA)	0.48	0.45	0.50	0.05	0.42	0.38	0.47	0.08	0.50	0.28	0.67	0.39	0.43	0.38	0.47	0.09
FR (Fresno, CA)	0.47	0.43	0.52	0.09	0.42	0.38	0.45	0.07	0.50	0.28	0.71	0.43	0.42	0.39	0.45	0.06
3C (San Francisco, CA)	0.46	0.44	0.50	0.06	0.42	0.36	0.47	0.11	0.48	0.26	0.66	0.41	0.42	0.37	0.45	0.07
4A (Baltimore, MD)	0.46	0.43	0.47	0.05	0.40	0.30	0.44	0.14	0.45	0.24	0.62	0.38	0.40	0.34	0.44	0.10
4B (Albuquerque, NM)	0.50	0.45	0.54	0.09	0.41	0.36	0.45	0.09	0.50	0.26	0.68	0.42	0.41	0.36	0.47	0.11
4C (Seattle, WA)	0.44	0.42	0.46	0.04	0.40	0.35	0.44	0.09	0.43	0.21	0.65	0.44	0.39	0.33	0.44	0.11
5A (Chicago, IL)	0.45	0.43	0.46	0.02	0.40	0.34	0.43	0.09	0.44	0.23	0.60	0.37	0.40	0.34	0.44	0.10
5B (Boise, ID)	0.47	0.43	0.52	0.09	0.39	0.33	0.43	0.10	0.47	0.21	0.69	0.48	0.39	0.34	0.45	0.10
6A (Burlington, VT)	0.44	0.42	0.46	0.04	0.39	0.33	0.42	0.09	0.44	0.22	0.60	0.38	0.39	0.34	0.43	0.08
6B (Helena, MT)	0.46	0.44	0.49	0.04	0.38	0.32	0.42	0.10	0.44	0.18	0.69	0.50	0.37	0.29	0.43	0.14
7 (Duluth, MN)	0.45	0.43	0.47	0.04	0.38	0.32	0.42	0.10	0.43	0.20	0.63	0.43	0.38	0.33	0.42	0.09
8 (Fairbanks, AK)	0.40	0.33	0.45	0.12	0.26	0.15	0.36	0.20	0.28	0.06	0.51	0.45	0.38	0.23	0.42	0.19

Table 2 (continued)

(d) aspect ratio R=10

	N				E				S				W			
	mean	min	max	range	mean	min	max	range	mean	min	max	range	mean	min	max	range
1A (Miami, FL)	0.13	0.12	0.13	0.01	0.11	0.10	0.11	0.02	0.13	0.08	0.19	0.11	0.11	0.10	0.12	0.02
2A (Houston, TX)	0.13	0.12	0.13	0.01	0.11	0.09	0.11	0.02	0.13	0.07	0.18	0.11	0.11	0.09	0.11	0.02
2B (Phoenix, AZ)	0.14	0.14	0.14	0.01	0.10	0.09	0.11	0.02	0.14	0.06	0.25	0.19	0.10	0.09	0.11	0.03
3A (Memphis, TN)	0.13	0.12	0.13	0.01	0.11	0.10	0.12	0.03	0.13	0.06	0.19	0.13	0.11	0.09	0.12	0.03
3B (El Paso, TX)	0.14	0.14	0.16	0.02	0.11	0.10	0.12	0.03	0.15	0.06	0.25	0.18	0.11	0.10	0.13	0.03
BU (Burbank, CA)	0.14	0.12	0.15	0.02	0.11	0.10	0.13	0.03	0.14	0.06	0.23	0.17	0.11	0.09	0.12	0.03
FR (Fresno, CA)	0.13	0.11	0.15	0.04	0.11	0.10	0.12	0.02	0.14	0.06	0.24	0.17	0.11	0.10	0.12	0.02
3C (San Francisco, CA)	0.13	0.12	0.14	0.02	0.11	0.09	0.12	0.03	0.13	0.06	0.21	0.16	0.11	0.10	0.12	0.02
4A (Baltimore, MD)	0.13	0.12	0.13	0.01	0.10	0.07	0.11	0.04	0.12	0.05	0.19	0.14	0.10	0.09	0.12	0.03
4B (Albuquerque, NM)	0.14	0.13	0.15	0.02	0.10	0.09	0.12	0.03	0.14	0.06	0.25	0.19	0.11	0.09	0.13	0.04
4C (Seattle, WA)	0.12	0.11	0.13	0.02	0.10	0.09	0.11	0.03	0.10	0.05	0.16	0.11	0.10	0.09	0.12	0.03
5A (Chicago, IL)	0.12	0.11	0.13	0.01	0.10	0.09	0.11	0.03	0.11	0.05	0.18	0.13	0.10	0.09	0.12	0.03
5B (Boise, ID)	0.13	0.11	0.14	0.03	0.10	0.09	0.11	0.03	0.11	0.05	0.20	0.15	0.10	0.08	0.12	0.03
6A (Burlington, VT)	0.12	0.11	0.12	0.01	0.10	0.09	0.11	0.03	0.11	0.05	0.16	0.11	0.10	0.08	0.11	0.03
6B (Helena, MT)	0.13	0.12	0.14	0.02	0.09	0.08	0.10	0.02	0.10	0.04	0.18	0.14	0.09	0.08	0.11	0.03
7 (Duluth, MN)	0.12	0.11	0.13	0.01	0.10	0.08	0.11	0.03	0.10	0.04	0.16	0.12	0.10	0.08	0.11	0.03
8 (Fairbanks, AK)	0.11	0.09	0.12	0.03	0.06	0.04	0.09	0.05	0.06	0.02	0.12	0.10	0.10	0.06	0.11	0.05

4.2 Increase in monthly SAF

Figure 6 plots by central wall orientation and aspect ratio the percentage increases in monthly SAF of a conventional central wall in Fresno upon raising the albedo of its neighboring wall to 0.60 (cool) from 0.25 (conventional). This represents the shift to scenario 2 from scenario 1. Analogous graphs spanning all 17 climates are presented in Figure D-1 of Task Report Appendix D.

Percentage increases in monthly SAF in Fresno for the set of east, south, and west central walls range annually from 0.9 to 4.1 for R=0.2, 3.6 to 15.3 for R=1, 14.5 to 23.4 for R=2, and 11.0 to 32.9 for R=10. Ranges for the north central wall are wider: 4.2 to 14.2 for R=0.2, 18.4 to 59.1 for R=1, 30.7 to 77.9 for R=2, and 49.4 to 85.4 for R=10 (row "FR" in panels a - d of Table 3).

Percentage increases in Fresno monthly SAF upon raising neighboring wall albedo are greatest for north central walls (Figure 6) because a north wall, receiving little beam sunlight and facing a well-illuminated south wall, receives a higher fraction of its irradiance via reflection that do walls pointing east, south, or west. Between March 20 (spring equinox) and Sep 22 (autumn equinox) in Fresno, the sun is 0 to 30˚ north of east for up to about 4 hours after sunrise, and 0 to 30˚ north of west for up to about 4 hours before sunset; at all other hours of the year, the sun lies between east and west, at least partially illuminating the south wall.

4.3 Application of monthly SAFs to cool-wall energy savings simulated for an isolated central building

The results for Fresno can illustrate the application of SAF to adjust cool-wall cooling energy savings and heating energy penalties for shading and reflection by a neighboring building. Consider a two-story single-family home (central building) on the south side of an east-west street in Fresno. Assume that it forms a canyon of aspect ratio 0.2 with its front (N) neighbor, a canyon of aspect ratio 1 with its back (S) neighbor, and canyons of aspect ratio 2 with its right and left (E, W) neighbors. Table 2 indicates that over the course of the year, the monthly SAF for the front (N) wall will range from 0.90 to 0.93 (mean 0.92, range 0.03). Meanwhile, that for the back (S) wall will range from 0.51 to 0.84 (mean 0.72, range 0.33); that for the right (E) wall will range from 0.38 to 0.45 (mean 0.42, range 0.07); and that for the left (W) wall will range from 0.39 to 0.45 (mean 0.42, range 0.06). Since the ranges for the north, east, and west walls (0.03, 0.07, and 0.06) are narrow, we can apply the wall-specific annual mean values of monthly SAF (0.92, 0.42, and 0.42) to the cooling savings, heating penalty, and annual metrics based on these two terms, such as heating, ventilation, and air conditioning (HVAC) energy cost savings and HVAC source energy savings.

The range for the south wall (0.33) is substantially greater, warranting inspection of the south-wall plot in Figure 4a. With aspect ratio 1 (dashed red line), monthly SAF for the south wall ranges from about 0.6 to 0.8 between November and March (heating season), and from about

0.75 to 0.84 between May and September (cooling season). This suggests applying a mean SAF of about 0.7 to the heating penalty, and a mean SAF of about 0.8 to the cooling savings. Since the cooling-season mean SAF exceeds the heating-season mean SAF (as it generally will for an east, west, or south wall, because the sun is highest in summer), we can conservatively estimate HVAC energy cost or source energy savings by applying the cooling-season mean SAF. This approach will overestimate the heating penalty and underestimate the annual HVAC savings, but is convenient.

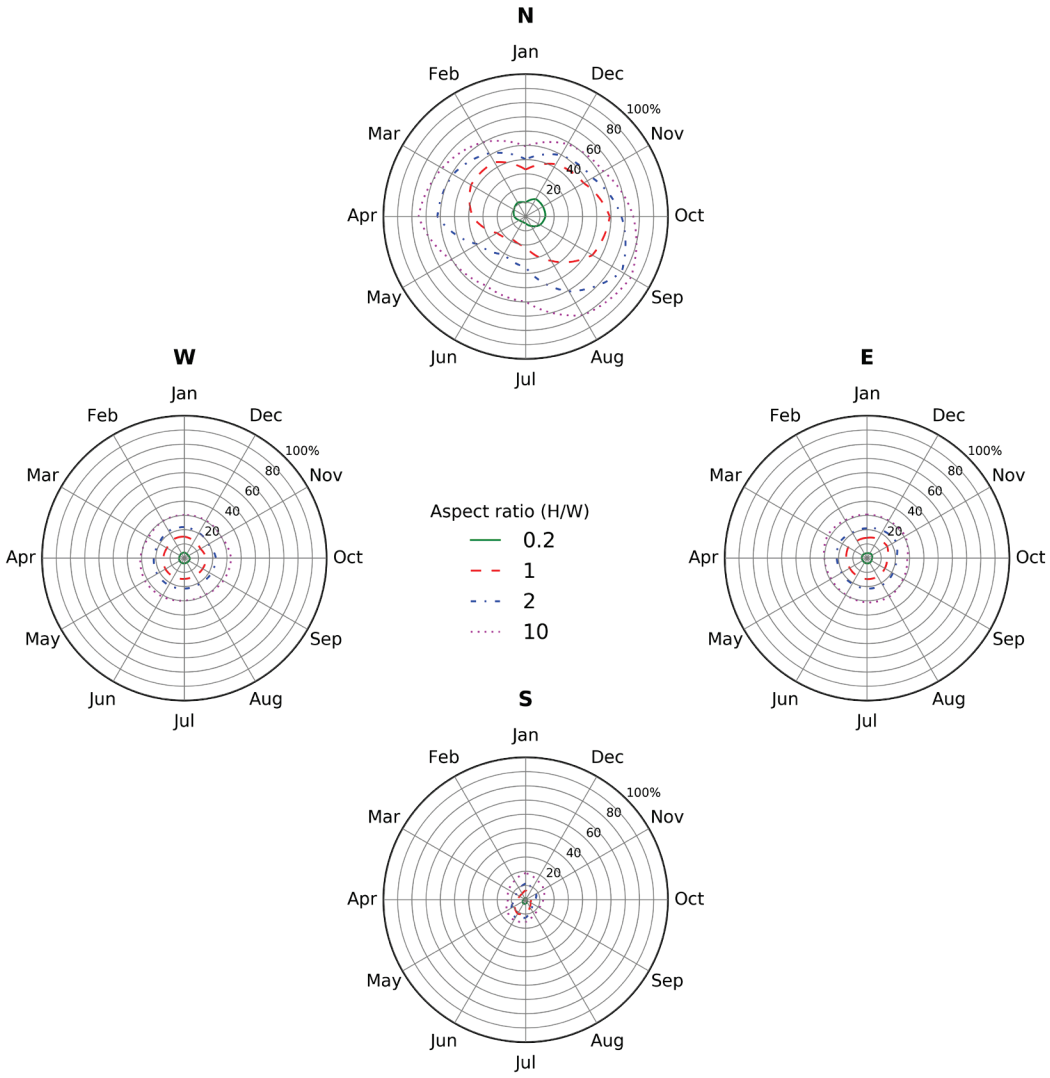

ground albedo = 0.20, central wall albedo = 0.25, neighboring wall albedo ratio = 0.60 / 0.25

Figure 6. Percentage increases in monthly SAFs for a north (N), east (E), south (S), or west (W) conventional central wall (ρ=0.25) upon raising the albedo of its neighboring wall to 0.60 (cool) from 0.25 (conventional). Results shown for aspect ratios 0.2, 1, 2, and 10 in Fresno, CA.

Table 3. Annual mean, minimum, maximum, and range (maximum – minimum) percentage increases in monthly SAF for a north (N), east (E), south (S), or west (W) conventional central wall (ρ=0.25) upon raising the albedo of its neighboring wall to 0.60 (cool) from 0.25 (conventional). Results shown by climate for aspect ratios of (a) R=0.2, (b) R=1, (c) R=2, and (d) R=10.

(a) aspect ratio R=0.2

	N				E				S				W			
	mean	min	max	range	mean	min	max	range	mean	min	max	range	mean	min	max	range
1A (Miami, FL)	7.5	3.2	13.6	10.3	3.6	3.1	4.3	1.2	2.3	1.0	4.1	3.2	3.8	3.1	4.3	1.2
2A (Houston, TX)	8.1	3.4	13.5	10.1	3.8	3.4	4.1	0.7	2.1	1.0	3.9	2.9	3.6	3.3	4.0	0.7
2B (Phoenix, AZ)	12.4	3.6	24.1	20.5	3.6	3.3	4.0	0.7	1.6	0.5	3.6	3.0	3.7	3.4	4.1	0.7
3A (Memphis, TN)	9.6	4.0	17.5	13.5	3.7	3.4	4.0	0.6	1.8	0.8	3.3	2.5	3.6	3.4	3.9	0.6
3B (El Paso, TX)	11.8	3.6	21.7	18.1	3.6	3.3	4.1	0.8	1.7	0.6	3.7	3.1	3.8	3.3	4.1	0.8
BU (Burbank, CA)	10.8	4.0	20.0	16.0	3.7	3.4	4.0	0.6	1.6	0.7	3.3	2.6	3.6	3.4	4.0	0.6
FR (Fresno, CA)	9.5	4.2	14.2	10.0	3.7	3.4	4.1	0.7	1.7	0.9	3.1	2.2	3.7	3.3	3.9	0.6
3C (San Francisco, CA)	10.0	4.4	18.5	14.0	3.9	3.4	4.4	1.0	1.6	0.7	3.0	2.2	3.5	3.0	4.0	0.9
4A (Baltimore, MD)	10.4	4.4	18.2	13.9	3.6	3.2	4.2	0.9	1.7	0.7	3.0	2.3	3.8	3.3	4.2	0.9
4B (Albuquerque, NM)	13.5	3.8	29.9	26.0	3.4	3.0	4.1	1.0	1.5	0.4	3.4	3.0	4.0	3.3	4.4	1.1
4C (Seattle, WA)	9.2	5.3	14.0	8.7	3.8	3.4	4.3	1.0	1.6	1.0	2.5	1.6	3.6	3.1	4.0	0.9
5A (Chicago, IL)	9.4	4.5	16.5	11.9	3.6	3.4	3.8	0.5	1.7	0.8	2.9	2.1	3.8	3.5	4.0	0.5
5B (Boise, ID)	11.6	4.9	19.3	14.4	3.6	3.2	4.0	0.8	1.4	0.7	2.7	2.0	3.8	3.4	4.3	0.8
6A (Burlington, VT)	9.0	4.5	15.3	10.7	3.7	3.4	3.9	0.5	1.7	0.9	2.9	2.1	3.7	3.4	4.0	0.5
6B (Helena, MT)	12.3	5.0	21.8	16.7	3.7	3.3	4.2	0.9	1.4	0.6	2.6	2.0	3.7	3.2	4.1	0.9
7 (Duluth, MN)	10.5	4.9	18.2	13.3	3.8	3.5	4.1	0.6	1.5	0.7	2.7	2.0	3.6	3.3	3.9	0.6
8 (Fairbanks, AK)	11.2	5.1	20.7	15.7	2.5	1.9	3.8	1.9	1.4	0.7	2.7	2.0	5.6	3.6	7.1	3.5

Table 3 (continued)

(b) aspect ratio R=1

	N				E				S				W			
	mean	min	max	range	mean	min	max	range	mean	min	max	range	mean	min	max	range
1A (Miami, FL)	31.9	12.4	54.1	41.6	14.3	12.8	16.5	3.7	8.6	4.0	16.9	13.0	15.1	13.1	16.8	3.7
2A (Houston, TX)	33.7	13.6	51.7	38.1	14.9	13.4	16.1	2.7	7.9	4.1	15.4	11.3	14.5	13.3	16.0	2.6
2B (Phoenix, AZ)	47.1	15.6	72.8	57.2	14.5	13.6	15.4	1.8	5.9	2.9	13.3	10.3	14.8	14.0	15.7	1.8
3A (Memphis, TN)	37.5	17.0	55.2	38.3	14.7	13.9	15.8	1.9	6.7	3.9	12.4	8.5	14.6	13.6	15.4	1.8
3B (El Paso, TX)	45.8	14.5	74.2	59.7	14.4	13.9	15.6	1.7	6.3	2.9	14.2	11.4	14.9	13.8	15.5	1.7
BU (Burbank, CA)	41.8	16.9	63.6	46.7	15.0	14.0	15.8	1.8	6.2	3.4	12.3	9.0	14.4	13.6	15.3	1.7
FR (Fresno, CA)	38.3	18.4	59.1	40.7	14.7	14.0	16.5	2.5	6.2	3.6	11.3	7.7	14.6	13.1	15.3	2.3
3C (San Francisco, CA)	38.8	19.3	52.6	33.3	15.5	14.0	17.2	3.1	6.2	4.1	10.8	6.8	13.9	12.5	15.4	2.9
4A (Baltimore, MD)	38.4	18.9	54.0	35.1	14.3	13.4	16.3	2.9	6.4	4.0	11.1	7.2	15.1	13.2	16.1	2.9
4B (Albuquerque, NM)	49.1	16.6	78.5	61.9	13.8	12.7	15.7	3.0	5.6	2.7	12.5	9.8	15.6	13.7	16.8	3.2
4C (Seattle, WA)	33.5	23.9	45.8	22.0	15.0	13.4	16.9	3.5	6.6	4.7	8.9	4.2	14.4	12.7	16.0	3.3
5A (Chicago, IL)	34.4	19.9	46.2	26.3	14.3	13.6	15.2	1.6	6.7	4.6	10.6	6.0	15.1	14.2	15.9	1.7
5B (Boise, ID)	42.2	22.5	64.2	41.7	14.3	13.3	15.3	2.0	5.5	3.3	9.4	6.1	15.1	14.1	16.2	2.1
6A (Burlington, VT)	33.2	20.2	43.7	23.5	14.5	13.6	15.6	1.9	6.8	4.9	10.5	5.6	14.9	13.8	15.8	1.9
6B (Helena, MT)	41.1	22.5	54.4	31.8	14.5	13.4	16.4	3.0	5.6	3.9	9.4	5.5	14.9	13.2	16.1	2.9
7 (Duluth, MN)	36.3	22.4	48.2	25.8	15.1	13.9	16.3	2.4	6.2	4.4	9.5	5.0	14.3	13.2	15.5	2.3
8 (Fairbanks, AK)	32.4	19.3	46.6	27.3	11.8	10.1	15.0	4.9	7.0	4.6	11.2	6.6	18.5	14.4	21.4	6.9

Table 3 (continued)

(c) aspect ratio R=2

	N				E				S				W			
	mean	min	max	range	mean	min	max	range	mean	min	max	range	mean	min	max	range
1A (Miami, FL)	43.3	17.7	61.6	43.9	20.9	18.9	23.8	4.9	12.6	7.4	25.2	17.7	22.0	19.2	24.2	5.0
2A (Houston, TX)	45.2	20.2	64.3	44.1	21.6	19.8	23.3	3.5	11.6	7.1	22.1	15.0	21.2	19.6	23.1	3.4
2B (Phoenix, AZ)	61.0	24.8	79.3	54.5	21.2	20.0	22.2	2.2	8.7	5.8	17.9	12.1	21.6	20.6	22.8	2.3
3A (Memphis, TN)	49.7	27.1	62.3	35.2	21.4	20.4	22.9	2.5	9.9	7.3	16.5	9.2	21.3	20.0	22.4	2.4
3B (El Paso, TX)	59.3	23.1	80.6	57.5	21.1	20.6	22.4	1.8	9.1	5.7	19.1	13.4	21.7	20.4	22.2	1.7
BU (Burbank, CA)	55.4	27.4	70.5	43.1	21.8	20.6	22.9	2.3	9.1	6.5	16.2	9.7	21.0	19.9	22.2	2.3
FR (Fresno, CA)	52.3	30.7	77.9	47.3	21.4	20.5	23.4	2.9	9.3	5.9	14.5	8.6	21.4	19.5	22.3	2.7
3C (San Francisco, CA)	52.0	31.8	72.4	40.6	22.4	20.5	24.1	3.6	9.2	6.3	14.1	7.8	20.4	18.9	22.4	3.4
4A (Baltimore, MD)	50.3	30.9	61.4	30.4	20.9	19.9	23.3	3.4	9.5	7.5	14.5	7.1	21.9	19.6	23.0	3.3
4B (Albuquerque, NM)	62.7	27.5	84.9	57.4	20.4	18.9	22.8	3.8	8.2	5.4	16.1	10.7	22.5	20.1	24.1	4.0
4C (Seattle, WA)	45.3	35.9	56.0	20.1	21.6	19.7	23.4	3.8	10.3	8.2	12.8	4.6	21.2	19.5	23.2	3.8
5A (Chicago, IL)	46.0	32.7	55.7	23.0	21.0	19.9	22.1	2.2	10.1	8.2	13.8	5.6	21.8	20.7	22.9	2.2
5B (Boise, ID)	55.7	38.6	78.9	40.3	21.1	19.6	22.4	2.8	8.5	5.8	11.7	5.9	21.7	20.4	23.3	2.9
6A (Burlington, VT)	44.7	33.3	54.5	21.2	21.2	19.9	22.7	2.8	10.4	8.4	13.6	5.2	21.6	20.2	23.0	2.8
6B (Helena, MT)	53.7	39.2	65.4	26.2	21.1	19.7	23.0	3.4	8.7	7.0	11.6	4.6	21.8	19.9	23.3	3.3
7 (Duluth, MN)	48.2	38.0	56.3	18.3	21.8	20.3	23.7	3.3	9.6	8.1	12.0	3.8	21.1	19.3	22.5	3.2
8 (Fairbanks, AK)	40.8	26.2	55.0	28.8	18.0	15.7	21.7	6.0	11.7	8.3	17.5	9.2	25.7	21.1	29.2	8.1

Table 3 (continued)

(d) aspect ratio R=10

	N				E				S				W			
	mean	min	max	range	mean	min	max	range	mean	min	max	range	mean	min	max	range
1A (Miami, FL)	56.0	26.1	70.2	44.2	30.2	27.8	34.6	6.8	18.2	13.3	35.0	21.7	30.7	26.8	33.3	6.5
2A (Houston, TX)	58.5	37.5	72.8	35.3	31.0	28.9	33.4	4.5	16.5	12.8	24.6	11.7	29.9	27.7	31.9	4.2
2B (Phoenix, AZ)	75.0	49.0	87.5	38.5	30.5	27.8	32.4	4.6	12.9	10.7	18.9	8.2	30.4	28.7	33.4	4.7
3A (Memphis, TN)	62.9	49.7	70.9	21.1	30.6	28.5	33.4	4.9	15.0	13.2	18.6	5.4	30.4	27.8	32.6	4.8
3B (El Paso, TX)	74.0	46.9	87.9	41.0	30.7	29.7	32.1	2.4	13.1	10.7	19.7	9.0	30.3	28.9	31.2	2.3
BU (Burbank, CA)	69.8	53.2	78.6	25.3	30.3	28.7	31.9	3.2	13.6	11.9	17.4	5.5	30.6	29.1	32.2	3.1
FR (Fresno, CA)	66.0	49.4	85.4	36.1	30.3	28.2	32.1	3.9	14.5	11.0	18.8	7.8	30.7	28.9	32.9	4.0
3C (San Francisco, CA)	65.1	55.1	80.7	25.5	32.3	28.7	34.2	5.5	14.5	11.6	16.8	5.2	28.8	27.1	32.3	5.2
4A (Baltimore, MD)	62.2	50.8	70.0	19.2	30.4	29.2	32.8	3.6	15.1	13.3	18.3	4.9	30.5	28.2	31.7	3.5
4B (Albuquerque, NM)	76.6	54.1	92.0	37.9	30.0	28.4	33.2	4.8	12.5	10.2	17.1	6.9	31.0	27.9	32.7	4.8
4C (Seattle, WA)	55.5	45.1	65.1	20.0	31.3	29.2	33.5	4.3	17.0	14.3	20.6	6.3	29.6	27.7	31.7	4.1
5A (Chicago, IL)	57.4	50.7	64.7	13.9	29.5	28.2	31.4	3.2	16.3	14.4	18.3	3.9	31.5	29.6	32.9	3.3
5B (Boise, ID)	67.0	51.0	86.7	35.7	29.3	28.2	31.1	2.9	14.2	10.8	18.2	7.4	31.6	29.8	32.8	3.0
6A (Burlington, VT)	55.5	45.7	63.8	18.1	29.7	27.8	31.6	3.8	16.9	14.6	20.3	5.7	31.3	29.3	33.4	4.0
6B (Helena, MT)	63.9	54.8	74.0	19.2	30.3	28.3	34.0	5.8	14.7	12.6	17.0	4.3	30.7	27.2	32.7	5.5
7 (Duluth, MN)	58.5	51.4	65.1	13.7	31.7	30.0	34.6	4.6	16.0	14.3	18.1	3.8	29.3	26.8	30.9	4.1
8 (Fairbanks, AK)	50.0	35.3	64.0	28.7	26.2	23.2	30.0	6.8	19.0	14.6	26.2	11.7	35.6	30.9	40.0	9.1

5 Summary

This study evaluates the solar availability factor (SAF) of a central building wall, or ratio of sunlight incident on the central building wall in the presence of the neighboring wall to that incident in the absence of the neighboring wall. The theory considers shading and reflection by neighboring buildings, as well as reflection from the ground between the buildings. SAF can be used to scale cool-wall cooling savings, heating penalties, or HVAC savings simulated for an isolated central building (no neighbors) to account for interaction with the neighboring wall.

Monthly values of SAF were evaluated in 17 climates across the United States, including three in California, for north, east, south, and west central walls, over a wide range of canyon aspect ratio (height/width). Results for four representative aspect ratios—0.2, 1, 2, and 10—are presented.

In Fresno, CA, monthly SAF ranges from 0.90 to 0.96 for central walls facing north, east, south, or west when the aspect ratio is 0.2 (two-story single-family homes across a street) and both the central and neighboring walls are conventional (albedo 0.25). These SAFs are close to unity because the sun-facing wall is rarely shaded in a canyon with low aspect ratio. Monthly SAFs decrease as aspect ratio rises, falling to 0.06 – 0.24 at an aspect ratio of 10 (adjacent 10-story buildings on the same side of the street). Seasonal variation in monthly SAF also increases with aspect ratio, and is greatest for south central walls.

Percentage increases in SAF (equivalent to percentage increases in irradiance) for a central wall upon raising the albedo of a neighboring wall to 0.60 (cool) from 0.25 (conventional) are modest for east, south, and west central walls, ranging 0.9 – 4.1 at aspect ratio 0.2 to 11.0 – 32.9 at aspect ratio 10. Percentage increases for a north central wall are greater because a north wall receives little beam sunlight, and faces a well-illuminated south wall.

6 References

Duffie JA, Beckman WA. 2006. *Solar Engineering of Thermal Processes*, 3rd ed. Wiley.

Howell, JR. A catalog of radiation heat transfer configuration factors. Retrieved 2018-01-09 from http://thermalradiation.net/indexCat.html .

NREL. 2018a. Measurement and Information Data Center Solar Position and Intensity (MIDC SOLPOS) Calculator. National Renewable Energy Laboratory. https://midcdmz.nrel.gov/solpos/solpos.html .

NREL. 2018b. National Solar Radiation Data Base, 1991- 2005 Update: Typical Meteorological Year 3. National Renewable Energy Laboratory. http://rredc.nrel.gov/solar/old_data/nsrdb/1991-2005/tmy3 .

Task Report Appendix A: Derivation of canyon irradiances

A.1 Initial solar powers incident on canyon surfaces

All beam sunlight (power) downwelling through the canyon ceiling,

$$Q_{\mathrm{C,B}} = I_{\mathrm{BH}} \times W \times L, \tag{A-1}$$

will strike either the ground or the sun-facing wall. Therefore, all beam sunlight that enters the canyon, but does not strike the ground, will strike the sun-facing wall. The beam solar power incident on the sun-facing wall (SFW) will be

$$Q_{\mathrm{SFW,B}} = I_{\mathrm{BH}} \times J \times L, \tag{A-2}$$

where ground shadow length (normal to wall)

$$J = \min(H \times \tan\theta_{\mathrm{z}} \times \cos\gamma_{\mathrm{SFW}}, W). \tag{A-3}$$

The beam solar power incident on the ground will be

$$Q_{\mathrm{G,B}} = I_{\mathrm{BH}} \times (W - J) \times L, \tag{A-4}$$

and that incident on the sun-opposing wall will be zero.

The diffuse sunlight (power) downwelling through the canyon ceiling,

$$Q_{\mathrm{C,D}} = I_{\mathrm{DH}} \times W \times L, \tag{A-5}$$

will strike the walls and ground in proportion to the view factor from the canyon ceiling to each surface.

Let $Q_{\mathrm{i,B}}$, $Q_{\mathrm{i,D}}$, and $Q_{\mathrm{i}} = Q_{\mathrm{i,B}} + Q_{\mathrm{i,D}}$ represent the initial beam, diffuse, and global solar powers—that is, those downwelling through the canyon ceiling—incident on each canyon surface (LW, RW, or G). Then

$$Q_{\mathrm{i,LW,B}} = Q_{\mathrm{SFW,B}} \text{ if } \cos\gamma_{\mathrm{LW}} > 0, \text{ or } 0 \text{ otherwise} \tag{A-6}$$

$$Q_{\mathrm{i,RW,B}} = Q_{\mathrm{SFW,B}} \text{ if } \cos\gamma_{\mathrm{RW}} > 0, \text{ or } 0 \text{ otherwise} \tag{A-7}$$

$$Q_{\mathrm{i,G,B}} = Q_{\mathrm{G,B}} \tag{A-8}$$

$$Q_{\mathrm{i,LW,D}} = Q_{\mathrm{C,D}} \times F_{\mathrm{C\to LW}} \tag{A-9}$$

$$Q_{\mathrm{i,RW,D}} = Q_{\mathrm{C,D}} \times F_{\mathrm{C\to RW}} \tag{A-10}$$

$$Q_{\mathrm{i,G,D}} = Q_{\mathrm{C,D}} \times F_{\mathrm{C\to G}} \tag{A-11}$$

A.2 View factors

The view factor from ceiling to ground is

$$F_{\mathrm{C}\to\mathrm{G}} = \sqrt{1+R^2} - R \tag{A-12}$$

where canyon aspect ratio $R \equiv H/W$ (Howell 2018, entry C-1).

Since the ceiling does not see itself, $F_{\mathrm{C}\to\mathrm{LW}} + F_{\mathrm{C}\to\mathrm{RW}} + F_{\mathrm{C}\to\mathrm{G}} = 1$; by symmetry, $F_{\mathrm{C}\to\mathrm{LW}} = F_{\mathrm{C}\to\mathrm{RW}}$. Hence the view factor from the ceiling to either wall is

$$F_{\mathrm{C}\to\mathrm{LW}} = F_{\mathrm{C}\to\mathrm{RW}} = (1 - F_{\mathrm{C}\to\mathrm{G}})/2. \tag{A-13}$$

By symmetry, the view factor from the ground to either wall equals that from the ceiling to either wall:

$$F_{\mathrm{G}\to\mathrm{LW}} = F_{\mathrm{G}\to\mathrm{RW}} = F_{\mathrm{C}\to\mathrm{LW}}. \tag{A-14}$$

Applying view factor reciprocity ($A_{\mathrm{X}}\, F_{\mathrm{X}\to\mathrm{Y}} = A_{\mathrm{Y}}\, F_{\mathrm{Y}\to\mathrm{X}}$), the view factor from the left wall to the ground is

$$F_{\mathrm{LW}\to\mathrm{G}} = (A_{\mathrm{G}}/A_{\mathrm{LW}})\, F_{\mathrm{G}\to\mathrm{LW}}, \tag{A-15}$$

where ground area

$$A_{\mathrm{G}} = W \times L \tag{A-16}$$

and left wall area

$$A_{\mathrm{LW}} = H \times L. \tag{A-17}$$

Simplifying,

$$F_{\mathrm{LW}\to\mathrm{G}} = F_{\mathrm{G}\to\mathrm{LW}}/R. \tag{A-18}$$

Similarly, the view factor from the right wall to the ground is

$$F_{\mathrm{RW}\to\mathrm{G}} = F_{\mathrm{G}\to\mathrm{RW}}/R. \tag{A-19}$$

The left wall does not see itself, and by symmetry, its view factor to the ground equals that to the ceiling. Hence, the view factor from the left wall to the right wall is

$$F_{\mathrm{LW}\to\mathrm{RW}} = 1 - (F_{\mathrm{LW}\to\mathrm{G}} + F_{\mathrm{LW}\to\mathrm{C}}) = 1 - 2 \times F_{\mathrm{LW}\to\mathrm{C}}. \tag{A-20}$$

Applying view factor reciprocity,

$$F_{\mathrm{LW}\to\mathrm{C}} = (A_{\mathrm{C}}/A_{\mathrm{LW}})\, F_{\mathrm{C}\to\mathrm{LW}} = F_{\mathrm{C}\to\mathrm{LW}}/R \tag{A-21}$$

where ceiling area

$$A_{\mathrm{C}} = W \times L. \tag{A-22}$$

Since by symmetry $F_{\mathrm{LW}\to\mathrm{RW}} = F_{\mathrm{RW}\to\mathrm{LW}}$,

$$F_{\mathrm{LW}\to\mathrm{RW}} = F_{\mathrm{RW}\to\mathrm{LW}} = 1 - (2/R) \times F_{\mathrm{C}\to\mathrm{LW}}. \tag{A-23}$$

Note that each view factor depends only on canyon aspect ratio R.

A.3 Cumulative irradiance incident on left wall

The cumulative solar power that strikes the left wall after no more than two reflections off canyon surfaces will be

$$Q_{LW} = a \times Q_{\mathrm{i,LW}} + b \times Q_{\mathrm{i,RW}} + c \times Q_{\mathrm{i,G}} \tag{A-24}$$

where reflection multipliers

$$a = 1 + \rho_{\mathrm{LW}} \times (F_{\mathrm{LW}\to\mathrm{G}} \times \rho_{\mathrm{G}} \times F_{\mathrm{G}\to\mathrm{LW}} + F_{\mathrm{LW}\to\mathrm{RW}} \times \rho_{\mathrm{RW}} \times F_{\mathrm{RW}\to\mathrm{LW}}) \tag{A-25}$$

$$b = \rho_{\mathrm{RW}} \times (F_{\mathrm{RW}\to\mathrm{LW}} + F_{\mathrm{RW}\to\mathrm{G}} \times \rho_{\mathrm{G}} \times F_{\mathrm{G}\to\mathrm{LW}}) \tag{A-26}$$

$$c = \rho_{\mathrm{G}} \times (F_{\mathrm{G}\to\mathrm{LW}} + F_{\mathrm{G}\to\mathrm{RW}} \times \rho_{\mathrm{RW}} \times F_{\mathrm{RW}\to\mathrm{LW}}) \tag{A-27}$$

and ρ is albedo (solar reflectance). This sum (Q_{LW}) includes power transmitted from

- ceiling to left wall,
- ceiling to left wall to ground to left wall,
- ceiling to left wall to right wall to left wall,
- ceiling to ground to left wall,
- ceiling to ground to right wall to left wall,
- ceiling to right wall to left wall, and
- ceiling to right wall to ground to left wall.

Note that multipliers a, b, and c depend only on canyon surface albedos and canyon view factors, and that the view factors depend only on canyon's aspect ratio R.

The cumulative irradiance on the left wall is

$$I_{\mathrm{LW}} = \frac{Q_{\mathrm{LW}}}{A_{\mathrm{LW}}} = Q''_{\mathrm{LW}} = a \times Q''_{\mathrm{i,LW}} + b \times Q''_{\mathrm{i,RW}} + c \times Q''_{\mathrm{i,G}}, \tag{A-28}$$

where double prime means normalized to left wall area $A_{\mathrm{LW}} = H \times L$. Starting with the first term of I_{LW} (left wall contribution), the left wall's initial global power $Q_{\mathrm{i,LW}}$ is the sum of its beam component $Q_{\mathrm{i,LW,B}}$ and its diffuse component $Q_{\mathrm{i,LW,D}}$. Recall that $Q_{\mathrm{i,LW,B}} = Q_{\mathrm{SFW,B}} = I_{\mathrm{BH}} \times J \times L$ if $\cos\gamma_{\mathrm{LW}} > 0$, or zero otherwise. Hence

$$Q''_{\mathrm{i,LW,B}} = I_{\mathrm{BH}} \times (J/H) \text{ if } \cos\gamma_{\mathrm{LW}} > 0, \text{ or zero otherwise.} \tag{A-29}$$

Since $J = \min(H \times \tan\theta_z \times \cos\gamma_{SFW}, W)$,

$$J/H = \min(\tan\theta_z \times \cos\gamma_{SFW}, 1/R). \tag{A-30}$$

Note that J/H can be fully predicted from θ_z, γ_{LW}, and R.

Since $Q_{i,LW,D} = Q_{C,D} \times F_{C\to LW}$ and $Q_{C,D} = I_{DH} \times W \times L$,

$$Q''_{i,LW,D} = I_{DH} \times W \times L \times F_{C\to LW}/(H \times L) = I_{DH} \times F_{C\to LW}/R. \tag{A-31}$$

Summing beam and diffuse components,

$$\begin{gathered} Q''_{i,LW} = [I_{BH} \times (J/H) + I_{DH} \times F_{C\to LW}/R] \text{ if } \cos\gamma_{LW} > 0, \\ \text{or } (I_{DH} \times F_{C\to LW}/R) \text{ otherwise.} \end{gathered} \tag{A-32}$$

The derivation of the second term of I_{LW} (right wall contribution) is analogous to that of the first term (left wall contribution), yielding

$$\begin{gathered} Q''_{i,RW} = [I_{BH} \times (J/H) + I_{DH} \times F_{C\to RW}/R] \text{ if } \cos\gamma_{RW} > 0, \\ \text{or } (I_{DH} \times F_{C\to RW}/R) \text{ otherwise.} \end{gathered} \tag{A-33}$$

In the third term of I_{LW} (ground contribution), the ground's initial global power $Q_{i,G}$ is the sum of its initial beam power $Q_{i,G,B} = I_{BH} \times (W - J) \times L$ and its initial diffuse power $Q_{i,G,D} = Q_{C,D} \times F_{C\to G}$. Thus

$$Q''_{i,G,B} = I_{BH} \times (W - J)/H = I_{BH} \times [(W/H) - (J/H)] = I_{BH} \times [(1/R) - (J/H)] \tag{A-34}$$

and

$$Q''_{i,G,D} = (I_{DH} \times W \times L \times F_{C\to G})/(H \times L) = (I_{DH} \times F_{C\to G})/R. \tag{A-35}$$

Summing beam and diffuse contributions,

$$Q''_{i,G} = I_{BH} \times [(1/R) - (J/H)] + (I_{DH} \times F_{C\to G})/R. \tag{A-36}$$

Thus, the cumulative global irradiance on the left wall after no more than two reflections off canyon surfaces, I_{LW}, is computed from Eqs. (A-28), (A-32), (A-33), and (A-36), with coefficients a, b, and c from Eqs. (A-25) - (A-27); normalized shadow length J/H from Eq. (A-30); and assorted view factors from Eqs. (A-12), (A-13), (A-18), (A-19), (A-21), and (A-23). Each term in I_{LW} can be predicted from I_{BH}, I_{DH}, θ_z, γ_{LW}, γ_{RW}, and/or R.

Note that the sun-facing wall is that for which $\cos\gamma > 0$. If neither wall faces the sun, then $J/H = 0$.

Task Report Appendix B: Monthly SAF plots by climate zone

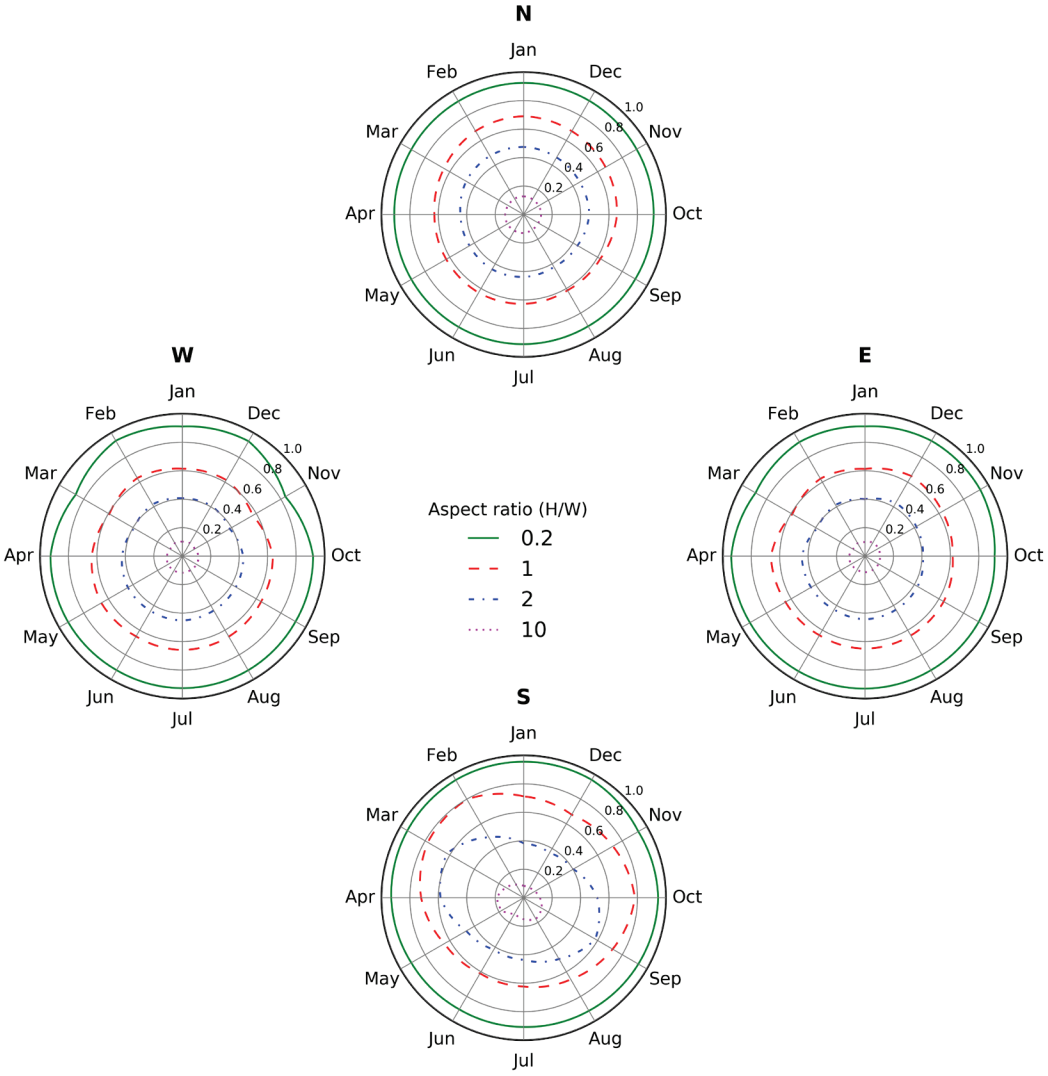

Figure B-1. Monthly SAFs for a north (N), east (E), south (S), or west (W) conventional central wall (ρ=0.25) with a conventional neighboring wall (ρ=0.25). Results shown for aspect ratios 0.2, 1, 2, and 10 in each of 17 climates (panels a through q).

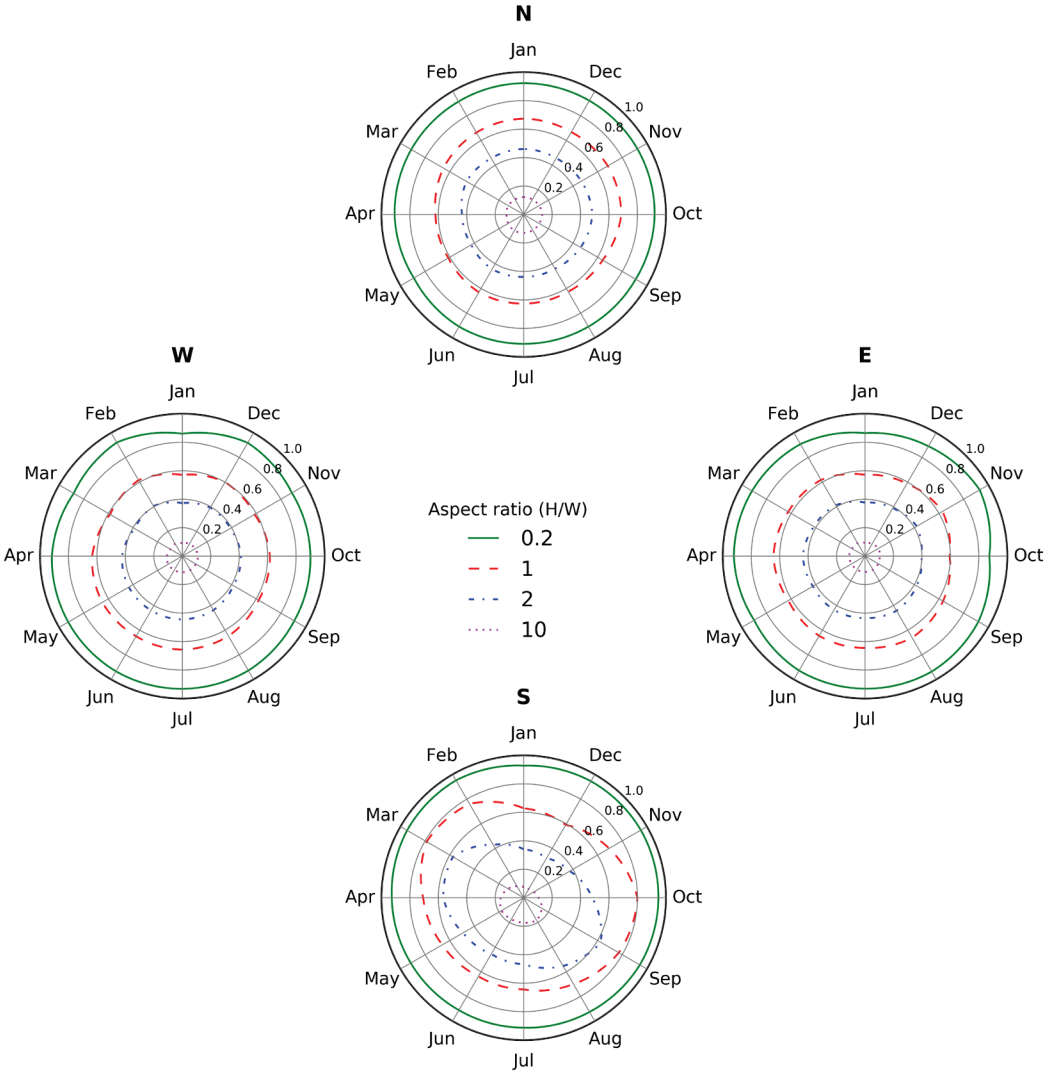

ground albedo = 0.20, central wall albedo = 0.25, neighboring wall albedo = 0.25

(b)

Figure B-1 (continued)

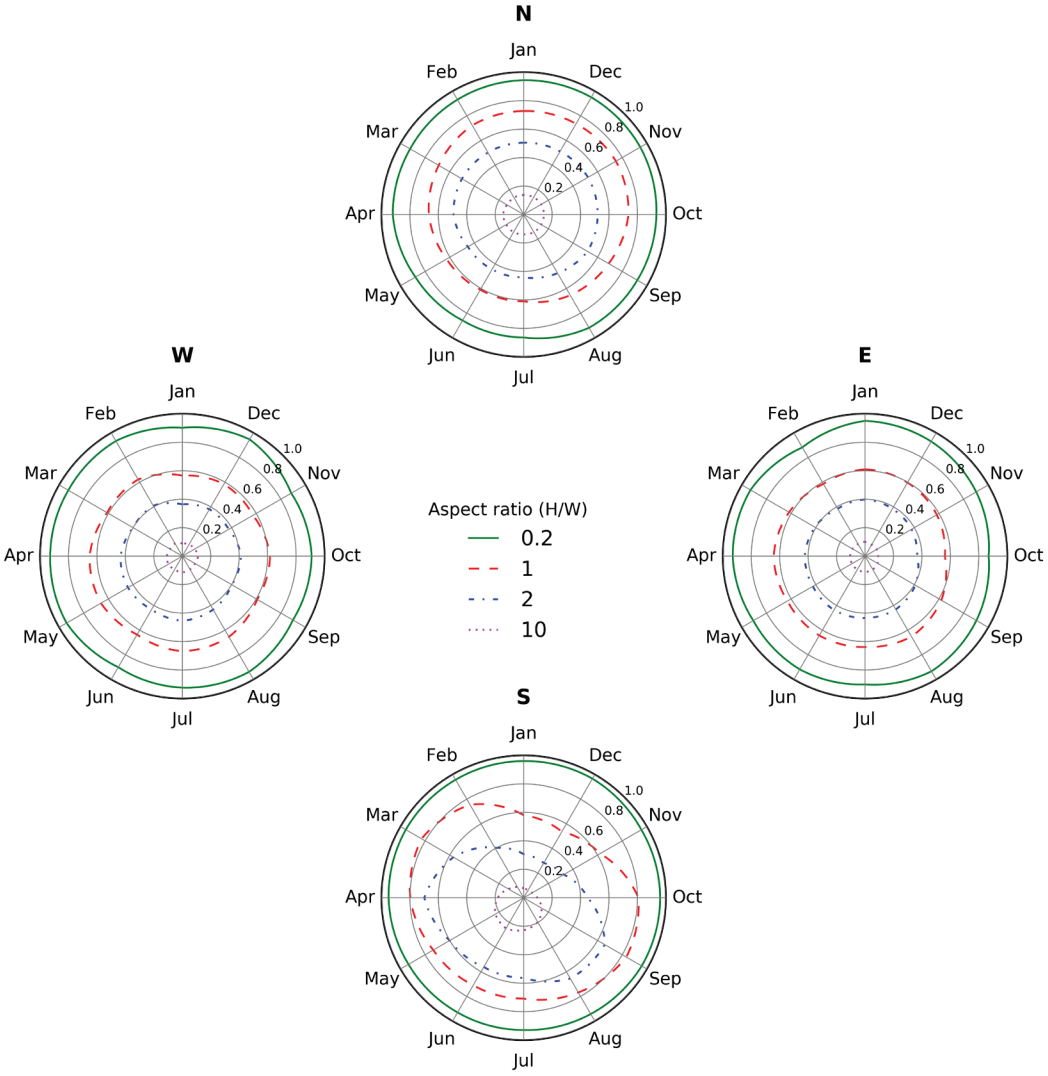

ground albedo = 0.20, central wall albedo = 0.25, neighboring wall albedo = 0.25

(c)

Figure B-1 (continued)

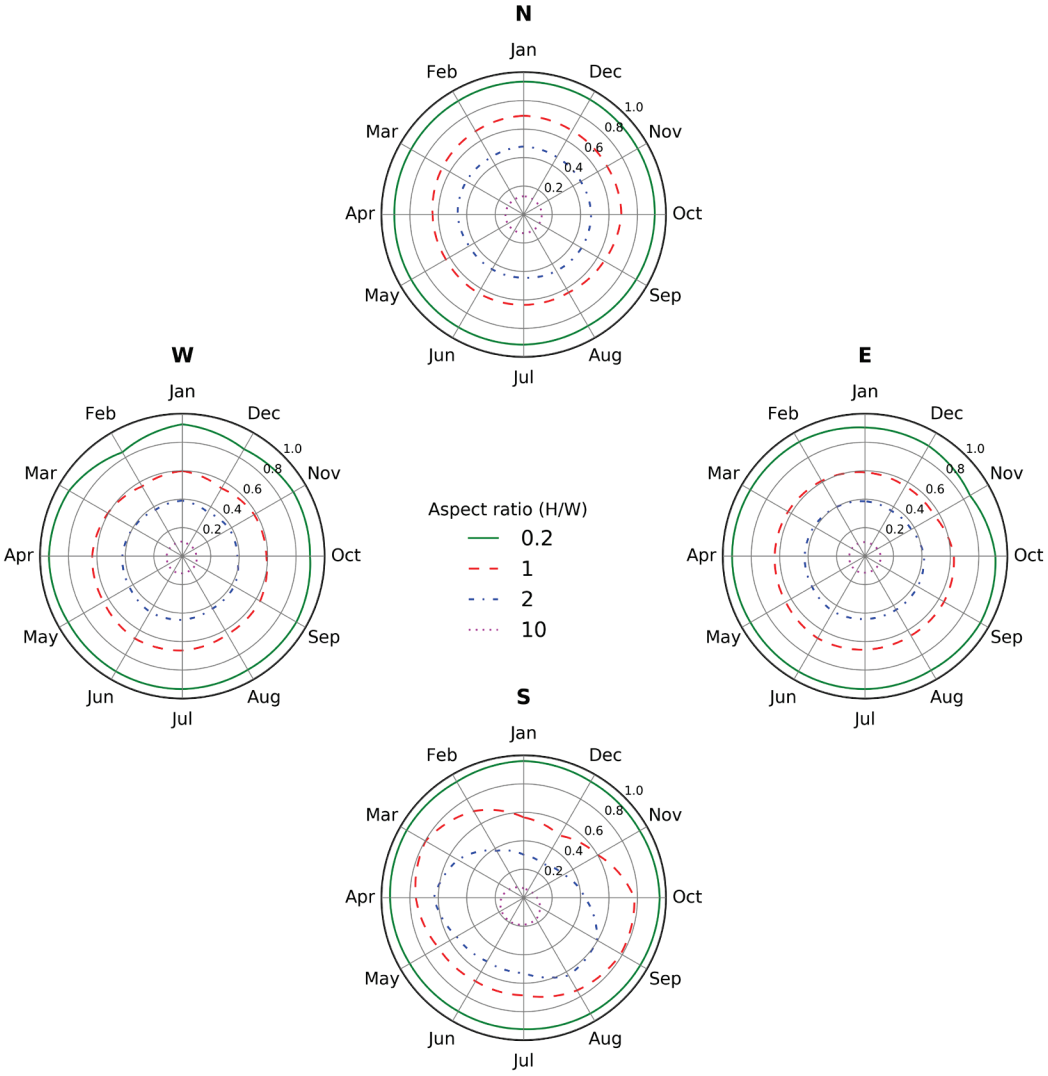

ground albedo = 0.20, central wall albedo = 0.25, neighboring wall albedo = 0.25

(d)

Figure B-1 (continued)

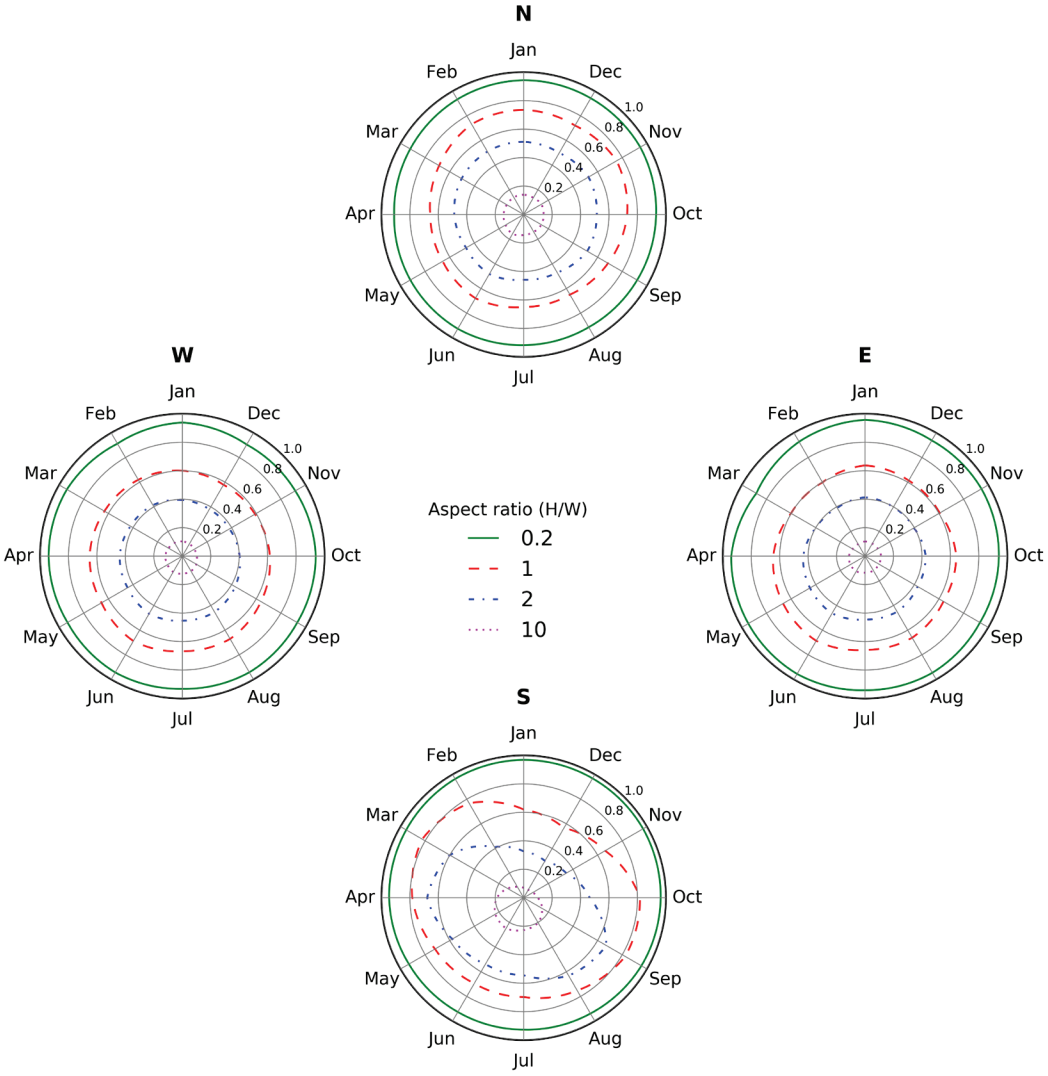

ground albedo = 0.20, central wall albedo = 0.25, neighboring wall albedo = 0.25

(e)

Figure B-1 (continued)

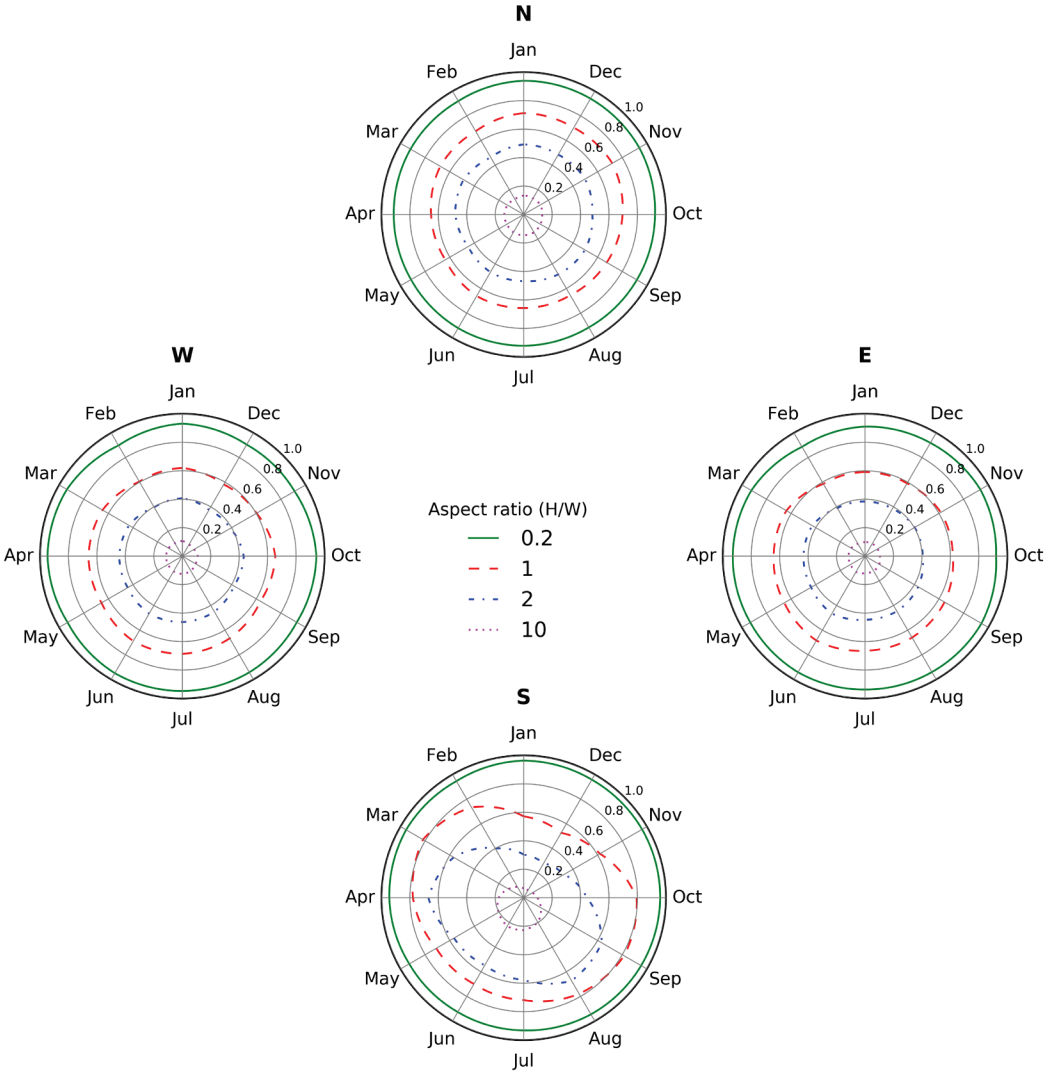

ground albedo = 0.20, central wall albedo = 0.25, neighboring wall albedo = 0.25

(f)

Figure B-1 (continued)

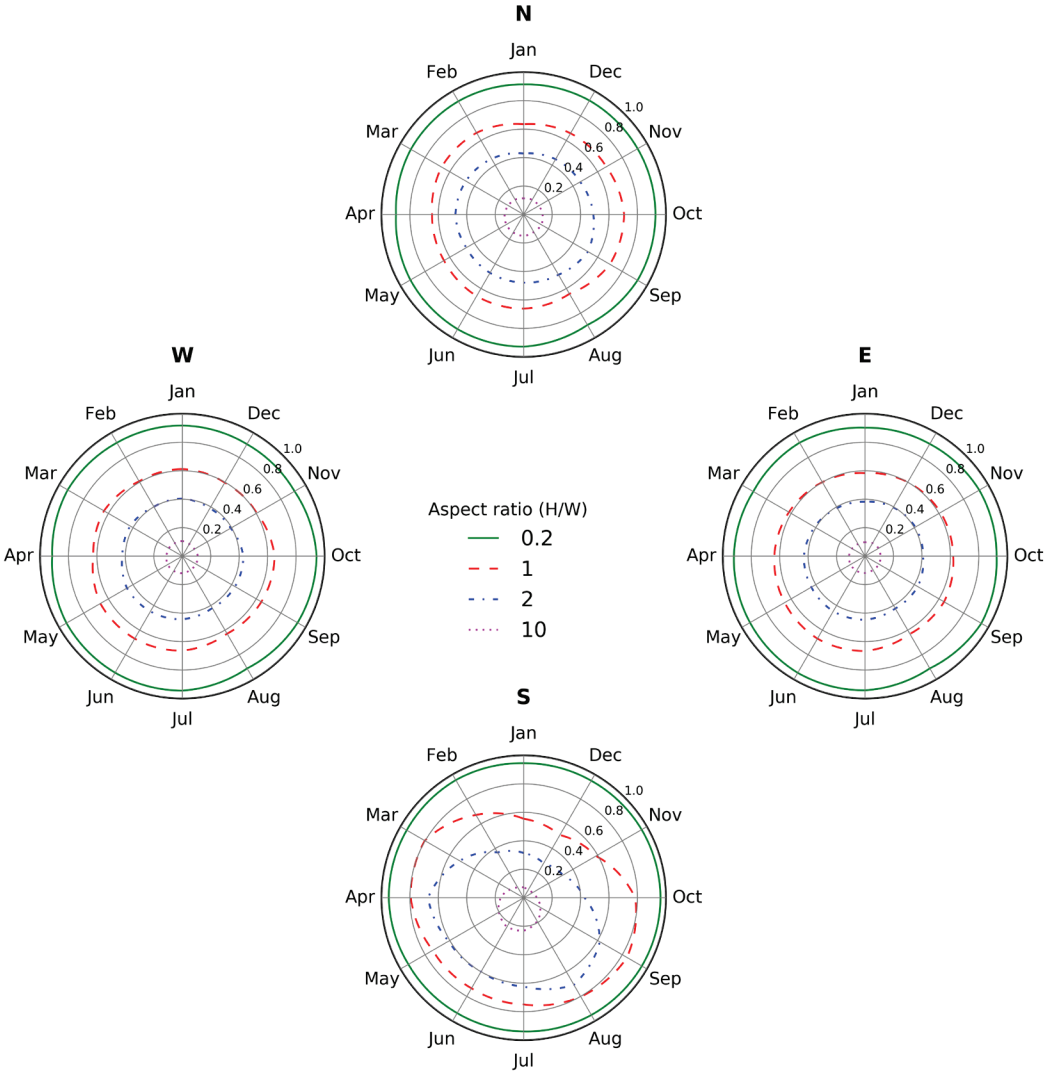

ground albedo = 0.20, central wall albedo = 0.25, neighboring wall albedo = 0.25

(g)

Figure B-1 (continued)

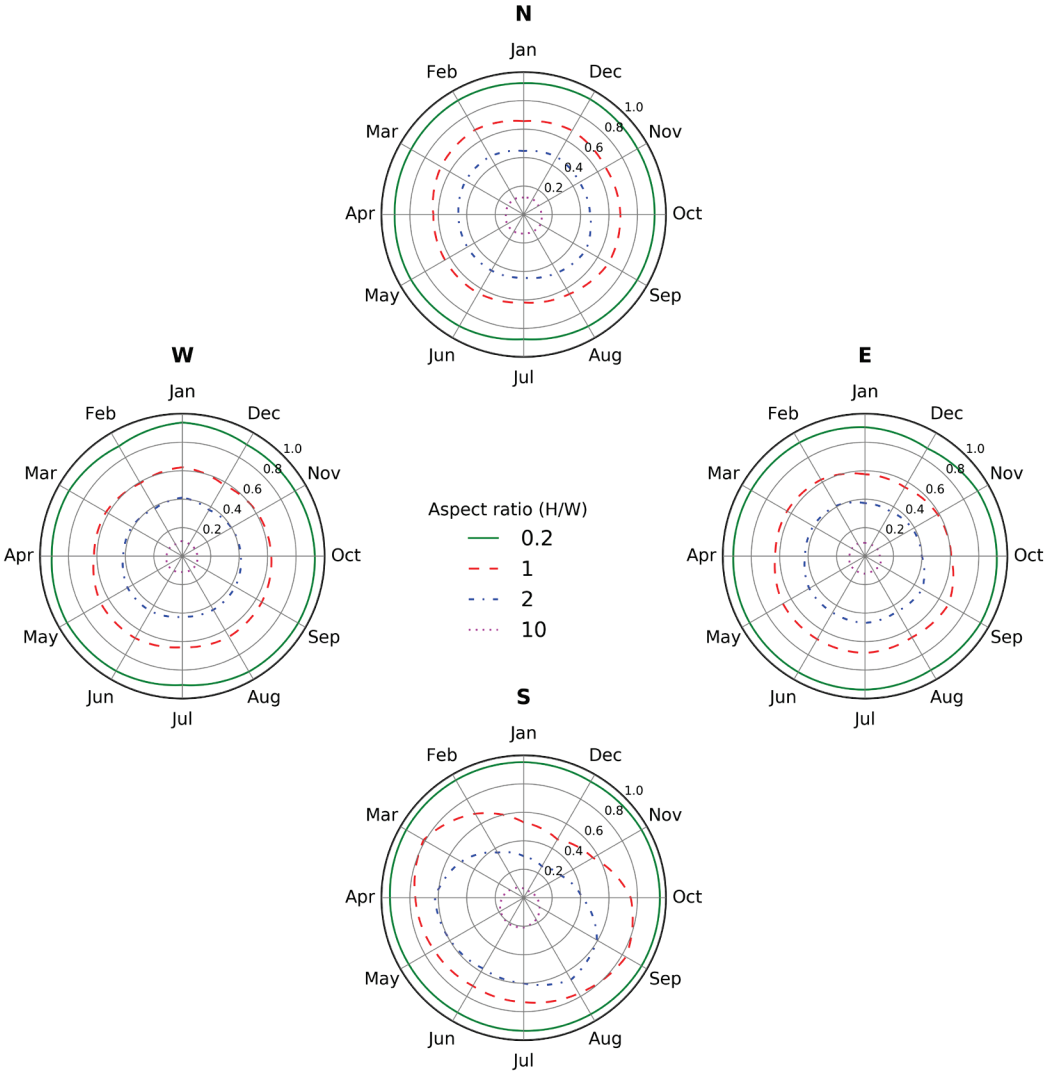

(h)

Figure B-1 (continued)

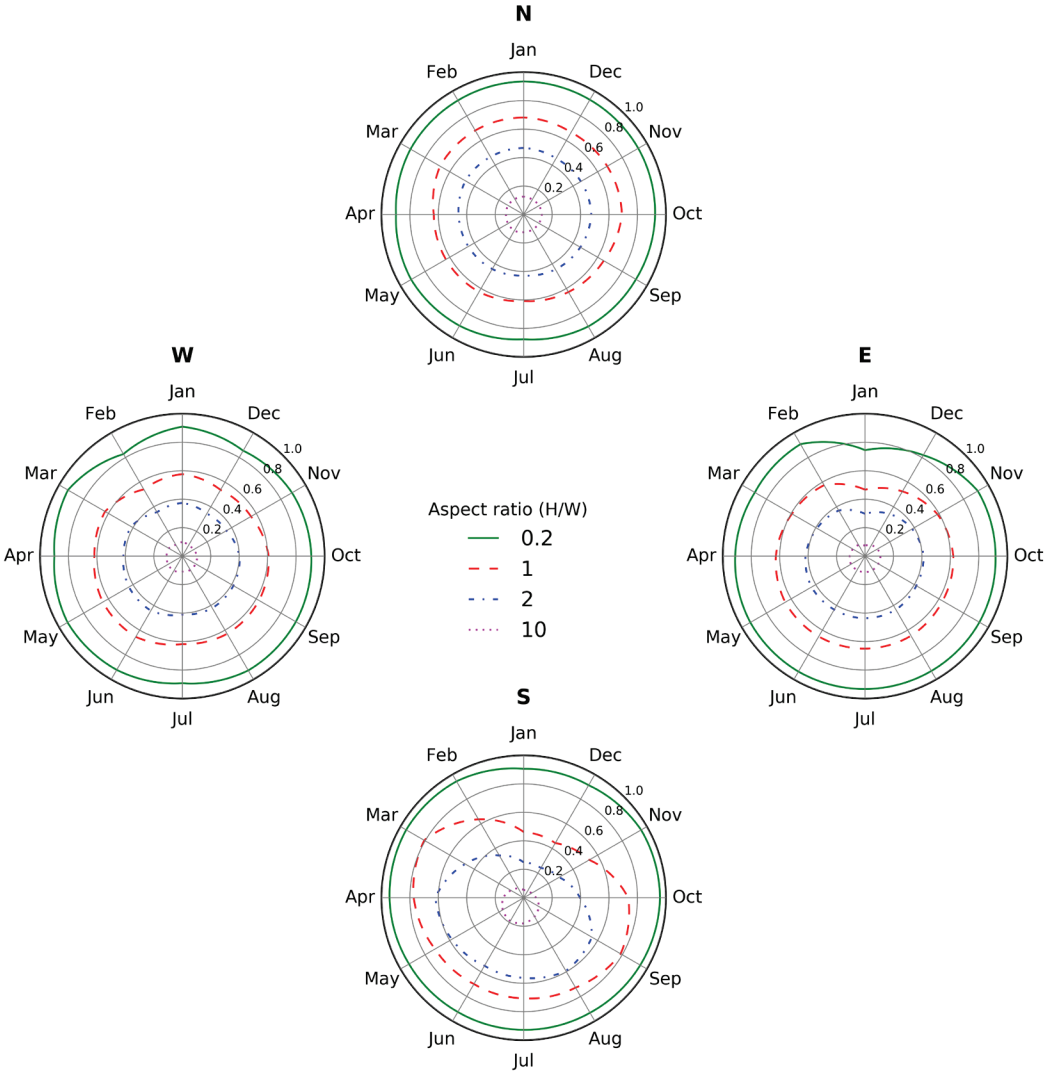

(i)

Figure B-1 (continued)

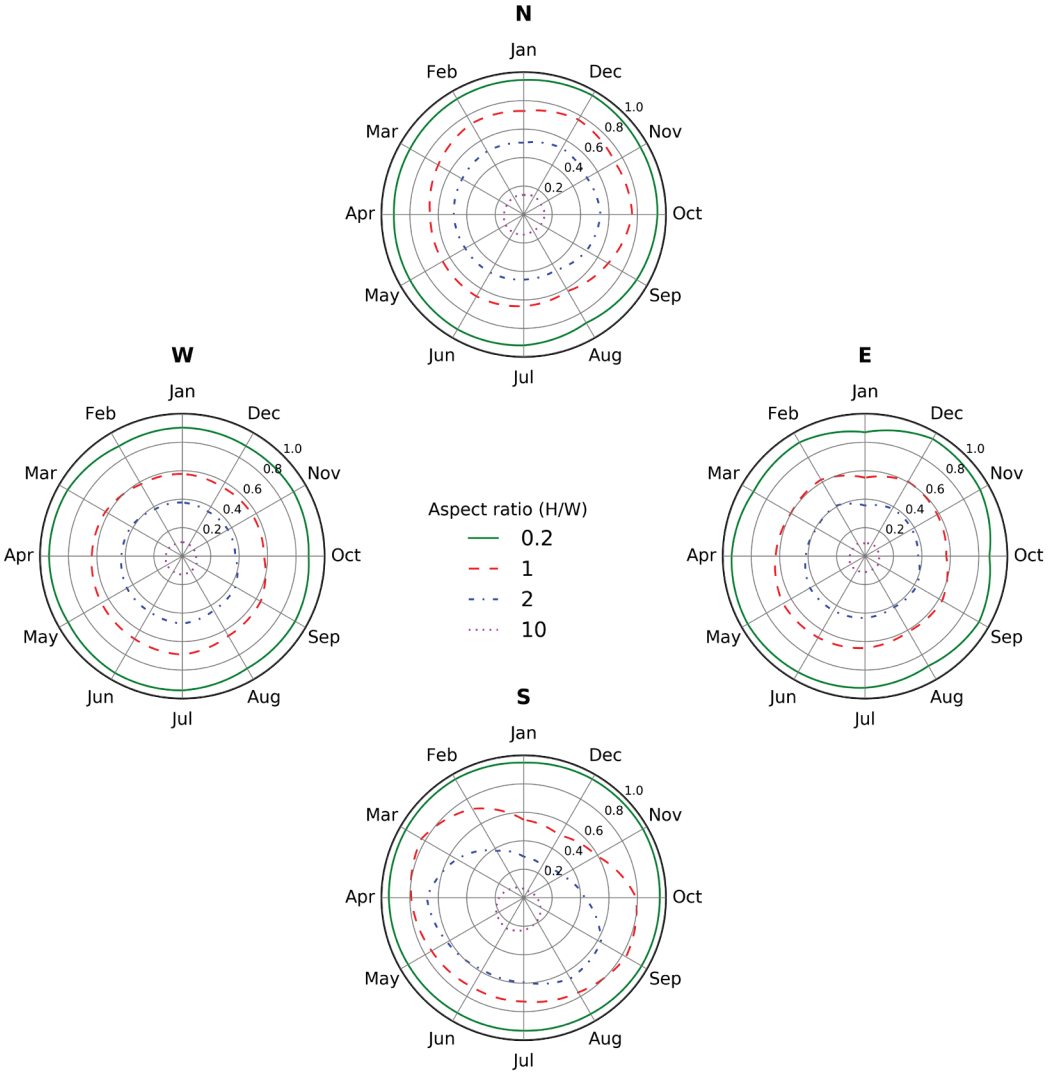

Figure B-1 (continued)

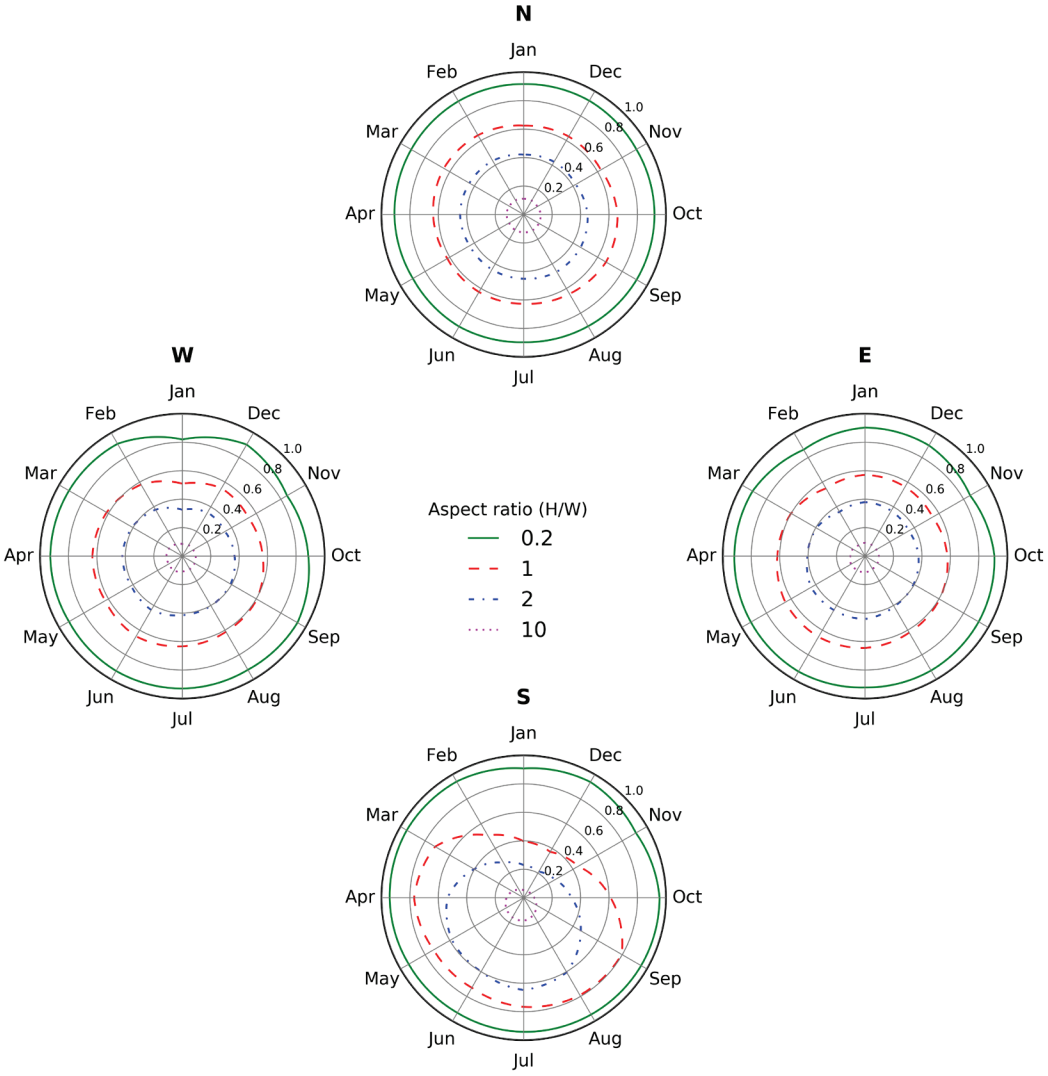

ground albedo = 0.20, central wall albedo = 0.25, neighboring wall albedo = 0.25

(k)

Figure B-1 (continued)

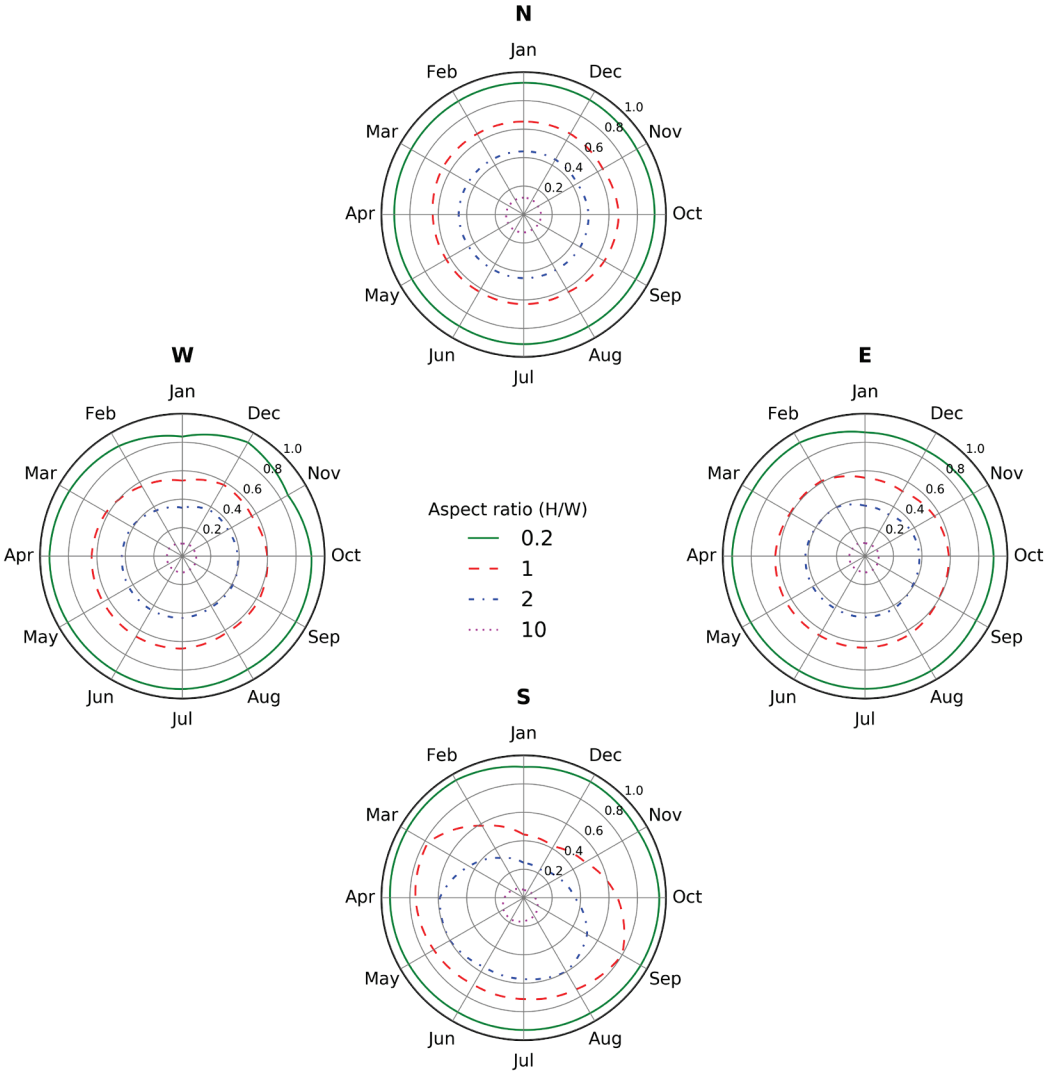

ground albedo = 0.20, central wall albedo = 0.25, neighboring wall albedo = 0.25

(l)

Figure B-1 (continued)

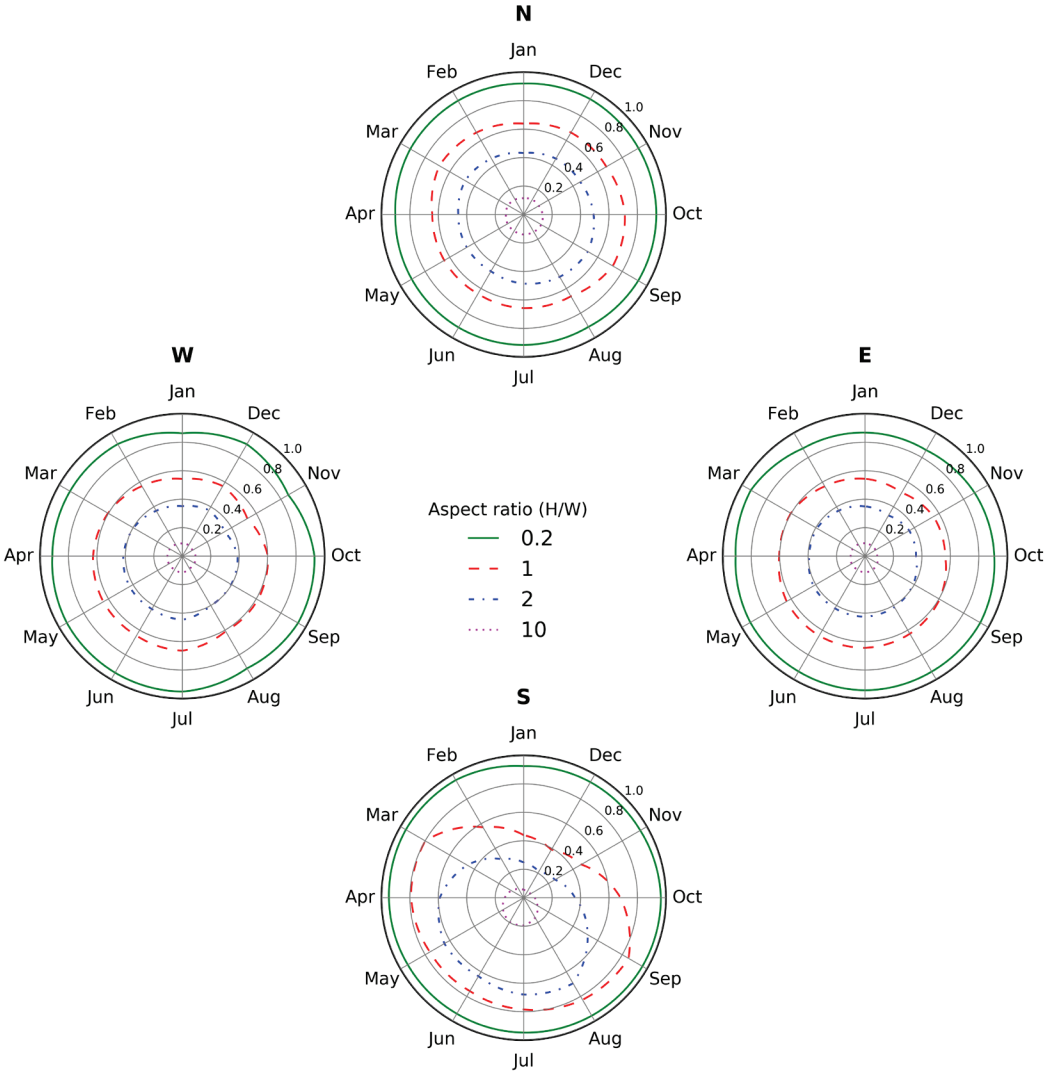

ground albedo = 0.20, central wall albedo = 0.25, neighboring wall albedo = 0.25

(m)

Figure B-1 (continued)

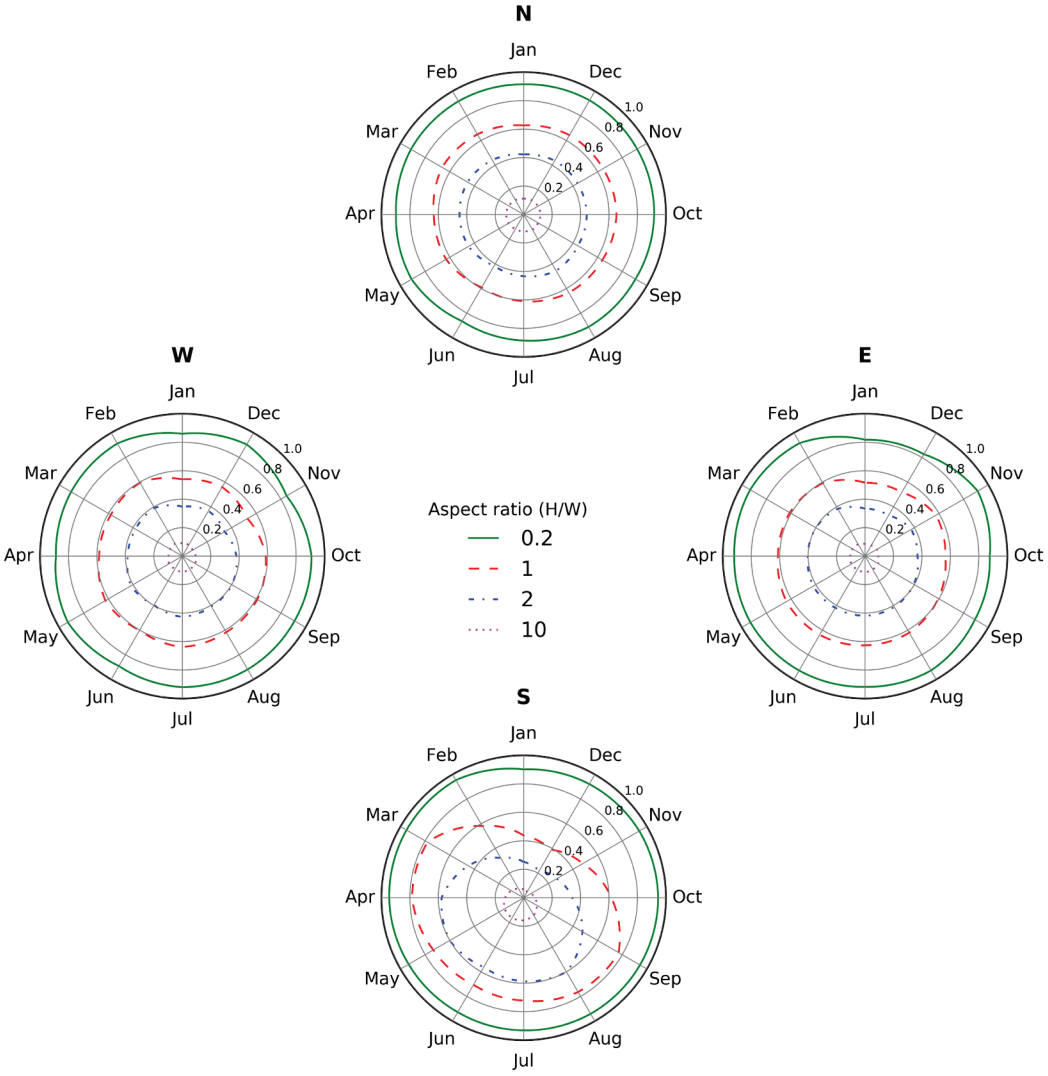

ground albedo = 0.20, central wall albedo = 0.25, neighboring wall albedo = 0.25

(n)

Figure B-1 (continued)

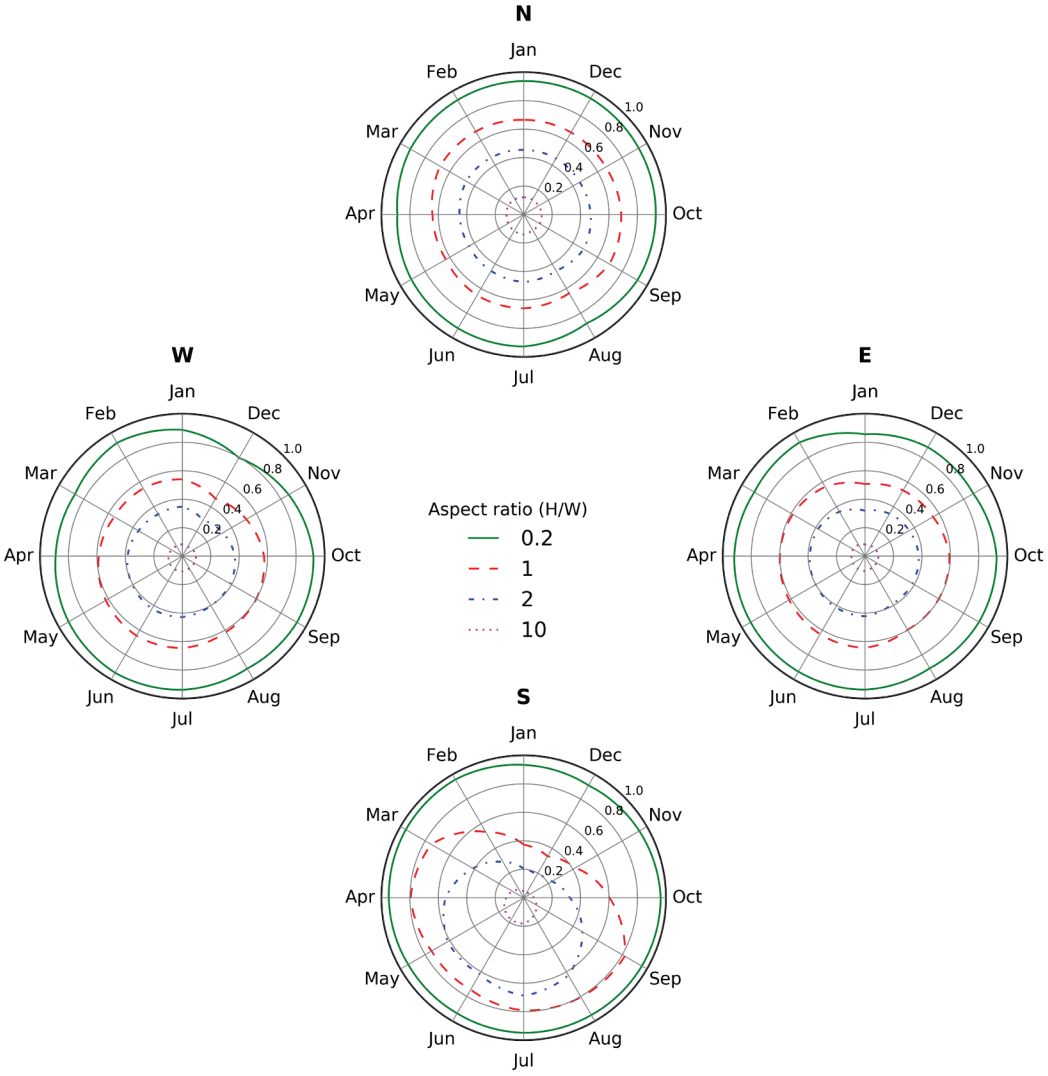

ground albedo = 0.20, central wall albedo = 0.25, neighboring wall albedo = 0.25

(o)

Figure B-1 (continued)

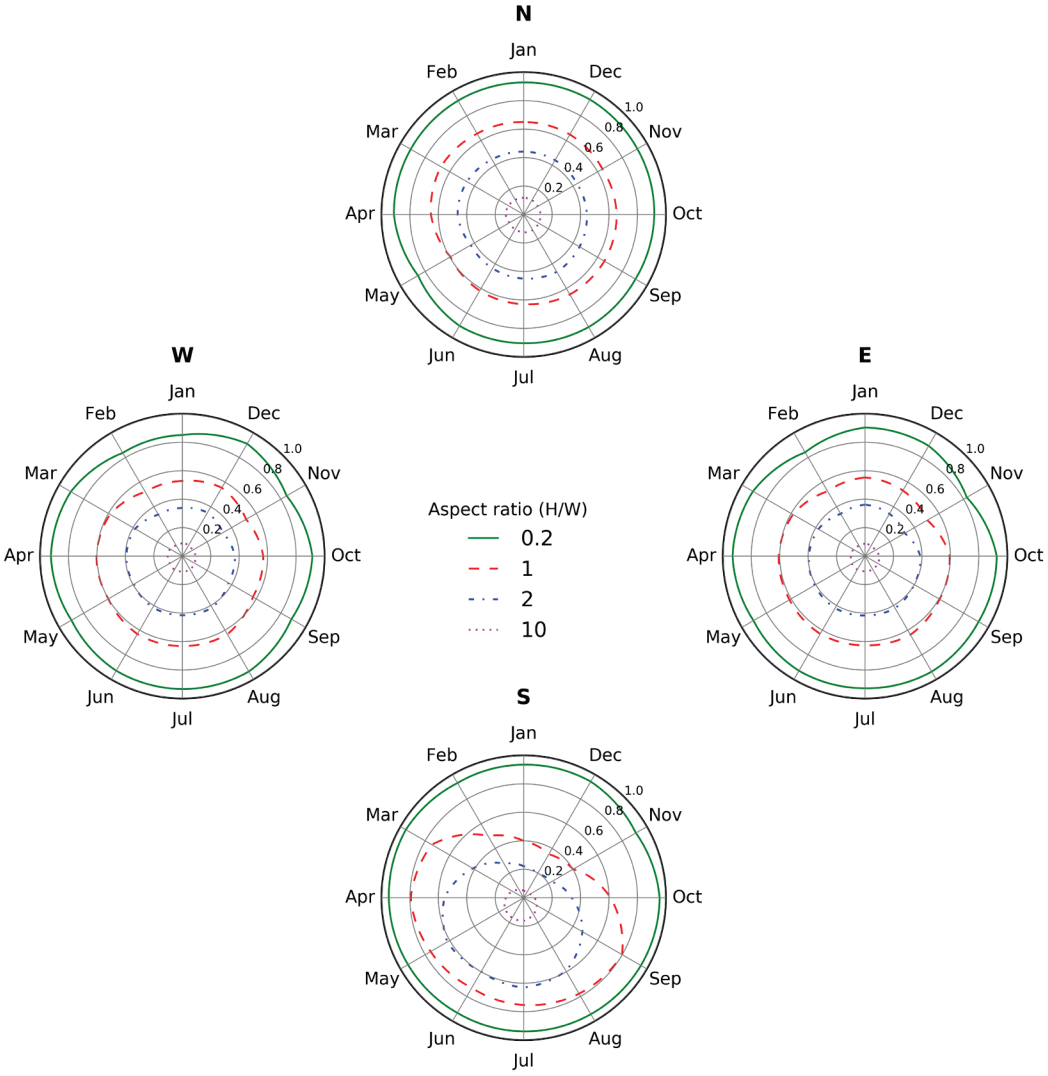

ground albedo = 0.20, central wall albedo = 0.25, neighboring wall albedo = 0.25

(p)

Figure B-1 (continued)

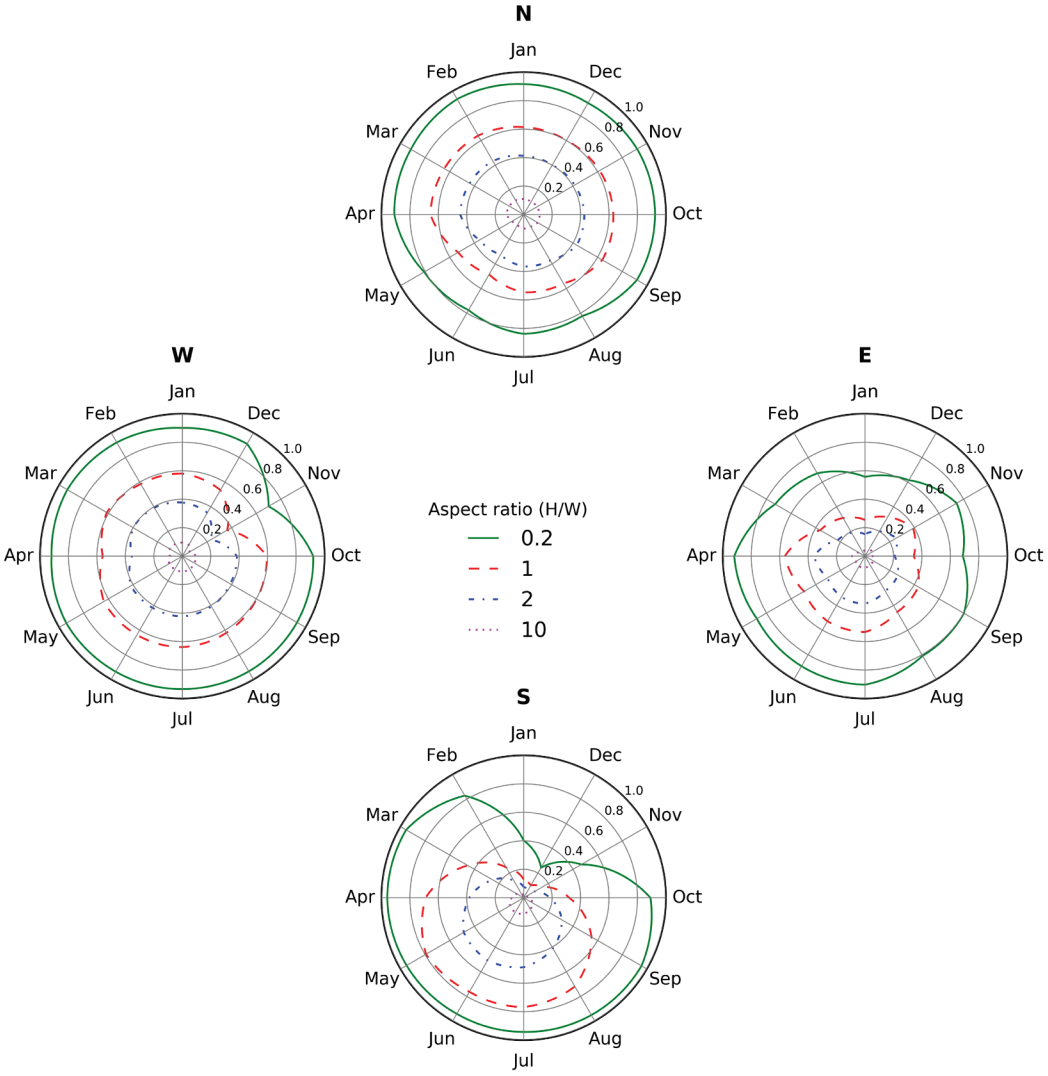

ground albedo = 0.20, central wall albedo = 0.25, neighboring wall albedo = 0.25

(q)

Figure B-1 (continued)

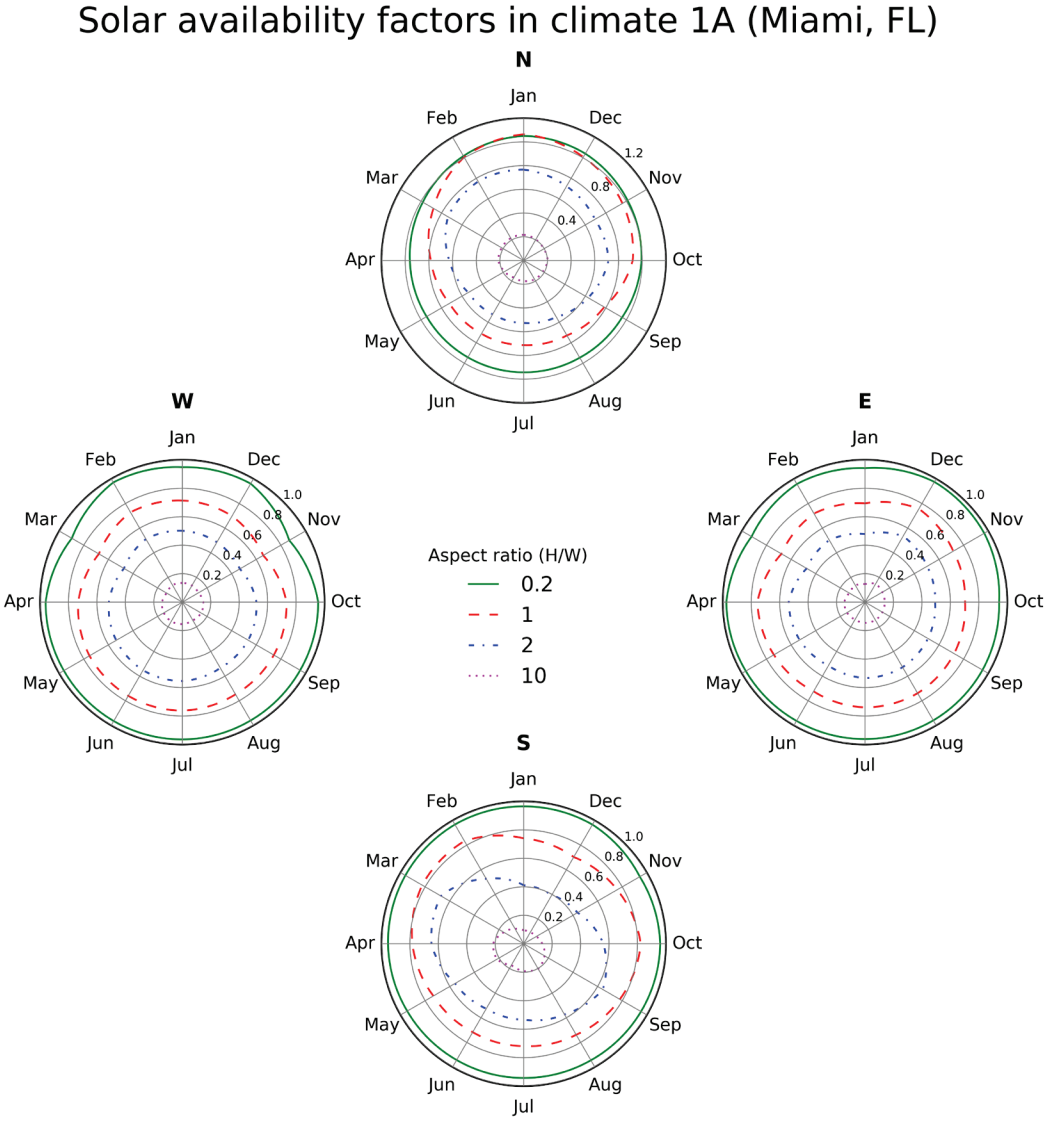

Figure B-2. Monthly SAFs for a north (N), east (E), south (S), or west (W) conventional central wall (ρ=0.25) with a cool neighboring wall (ρ=0.60). Results shown for aspect ratios 0.2, 1, 2, and 10 in each of 17 climates (panels a through q).

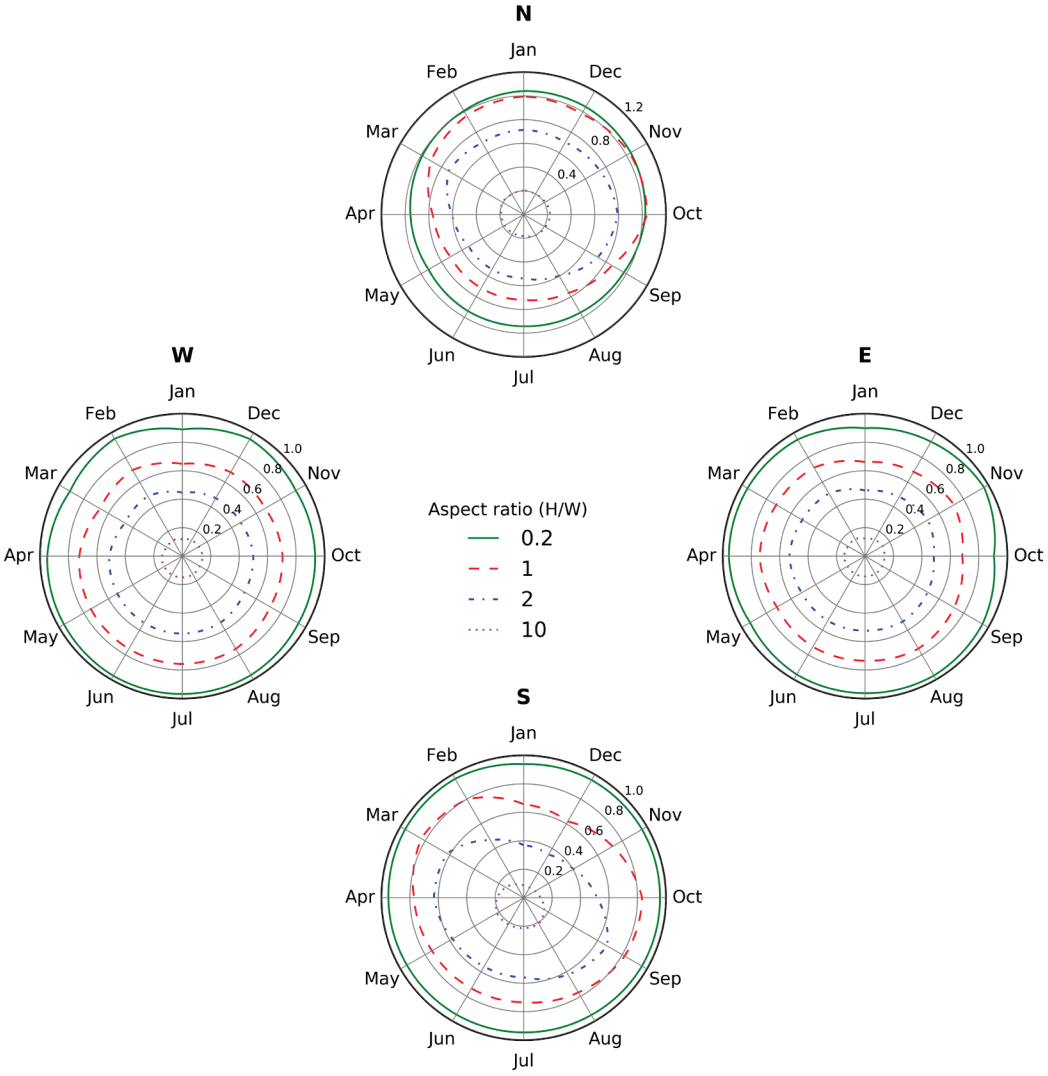

ground albedo = 0.20, central wall albedo = 0.25, neighboring wall albedo = 0.60

(b)

Figure B-2 (continued)

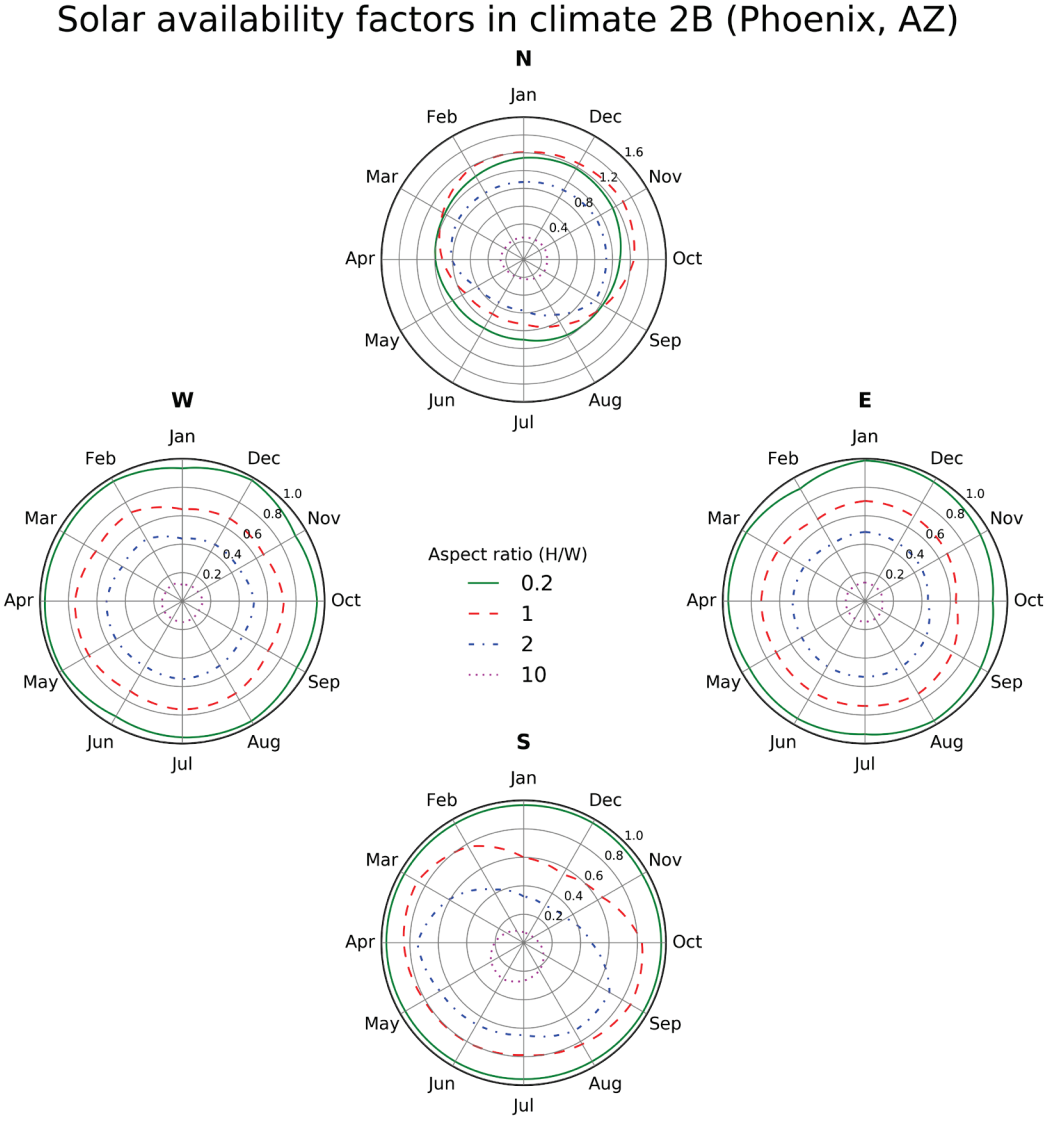

ground albedo = 0.20, central wall albedo = 0.25, neighboring wall albedo = 0.60

(c)

Figure B-2 (continued)

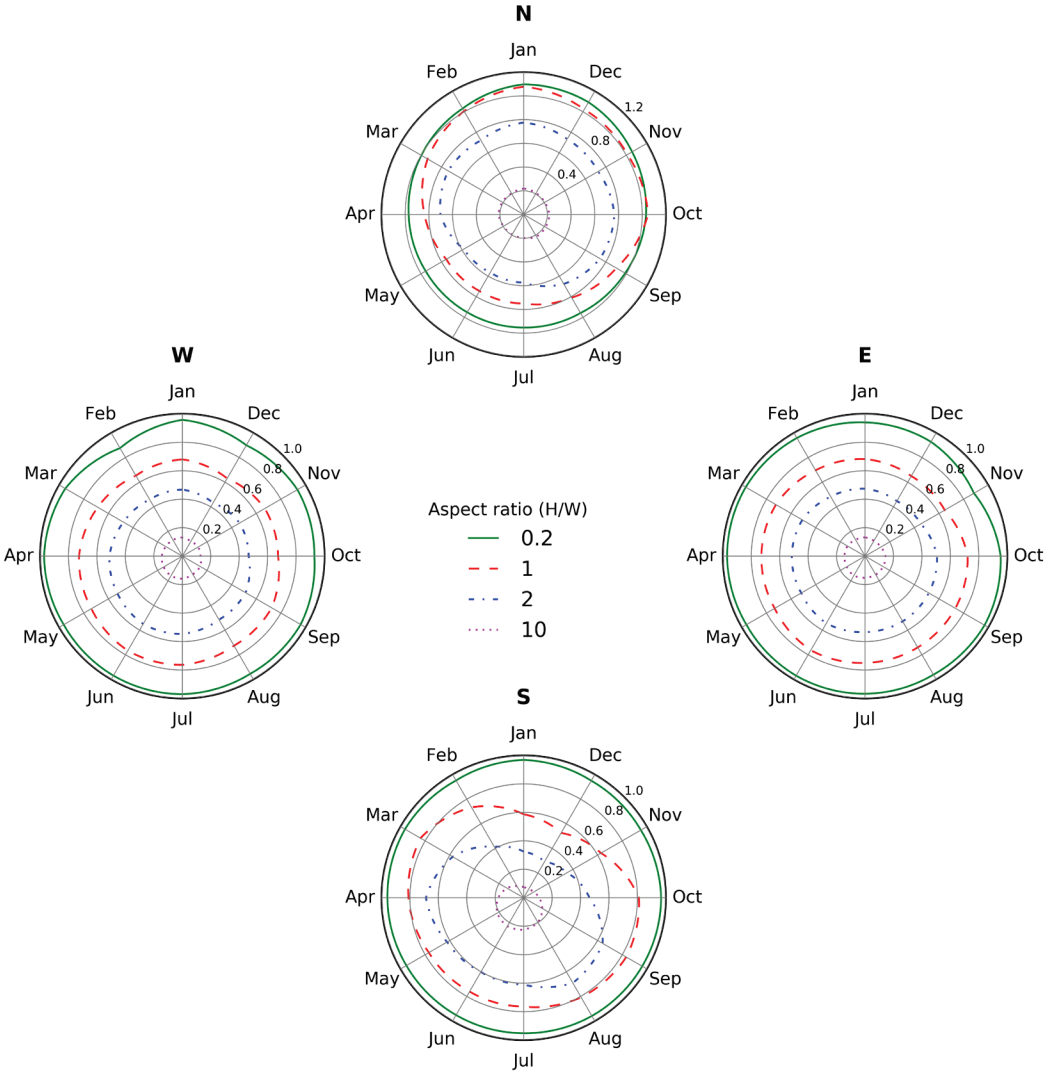

ground albedo = 0.20, central wall albedo = 0.25, neighboring wall albedo = 0.60

(d)

Figure B-2 (continued)

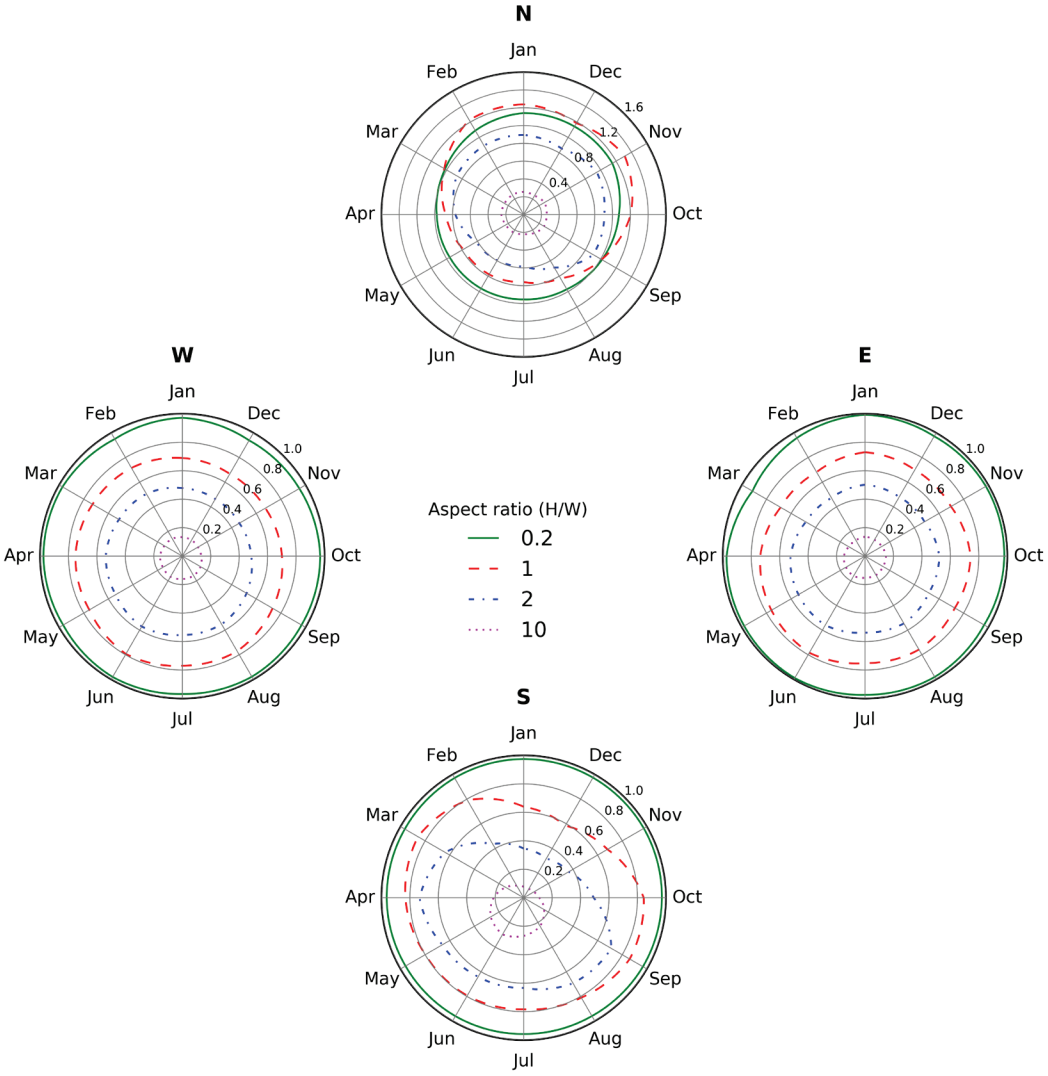

ground albedo = 0.20, central wall albedo = 0.25, neighboring wall albedo = 0.60

(e)

Figure B-2 (continued)

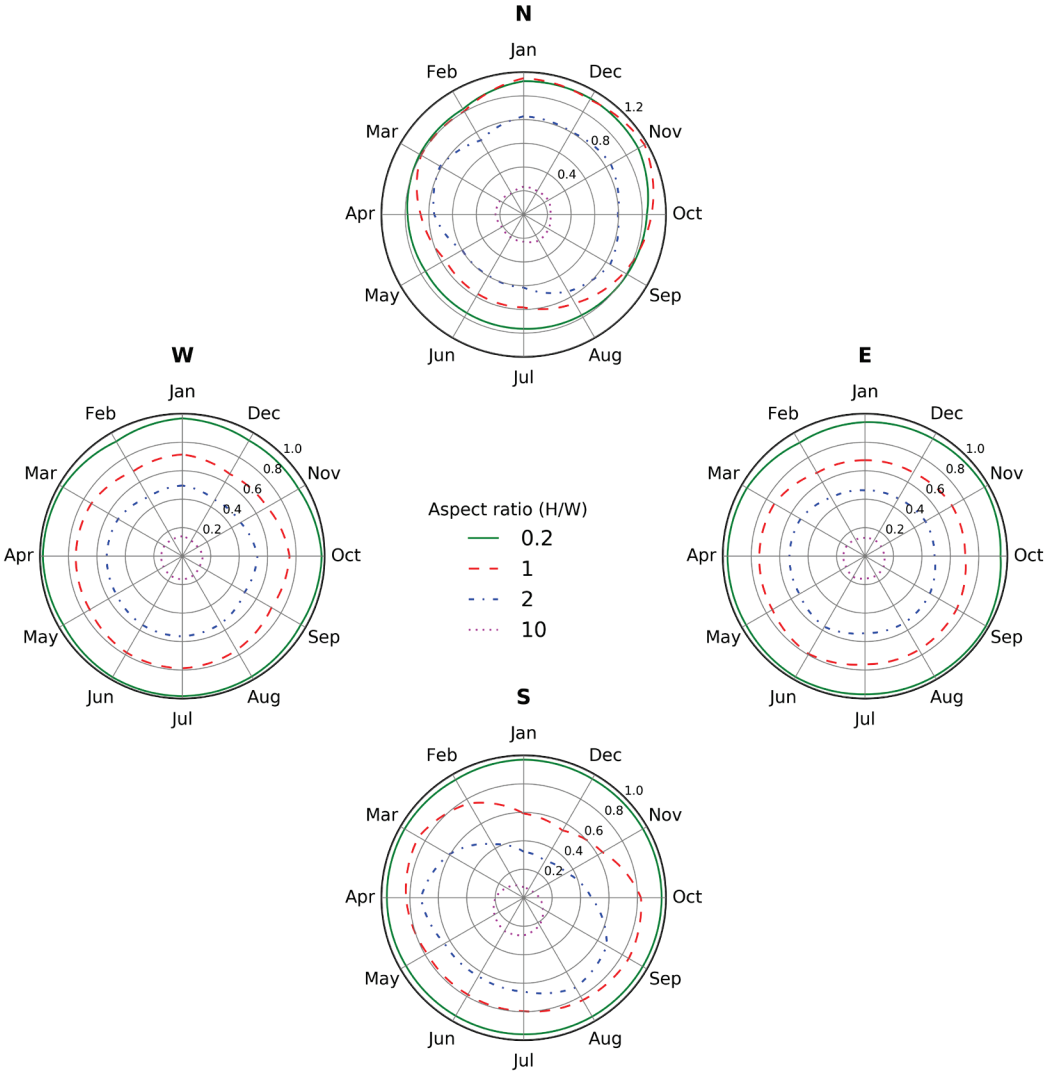

ground albedo = 0.20, central wall albedo = 0.25, neighboring wall albedo = 0.60

(f)

Figure B-2 (continued)

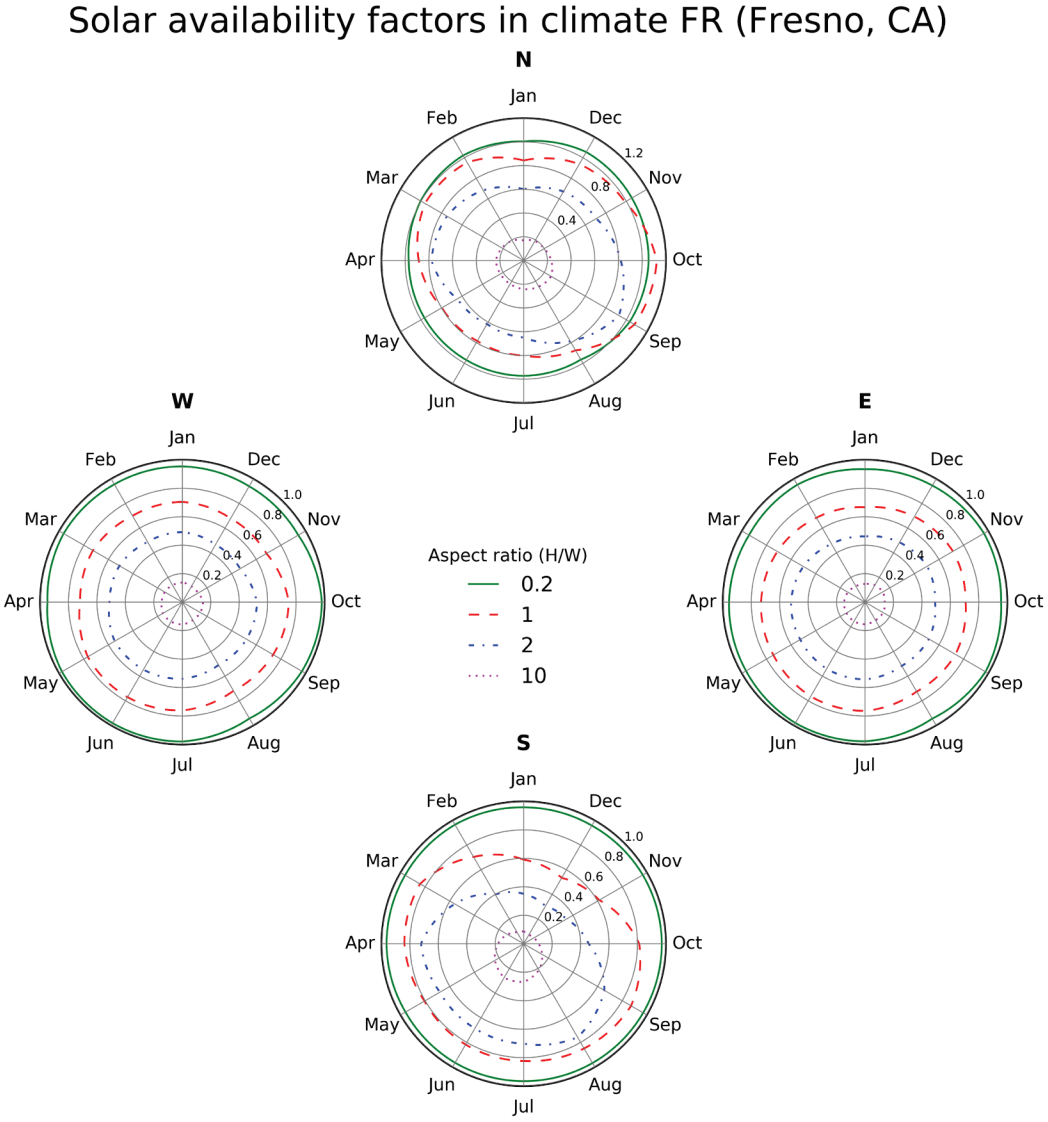

ground albedo = 0.20, central wall albedo = 0.25, neighboring wall albedo = 0.60

(g)

Figure B-2 (continued)

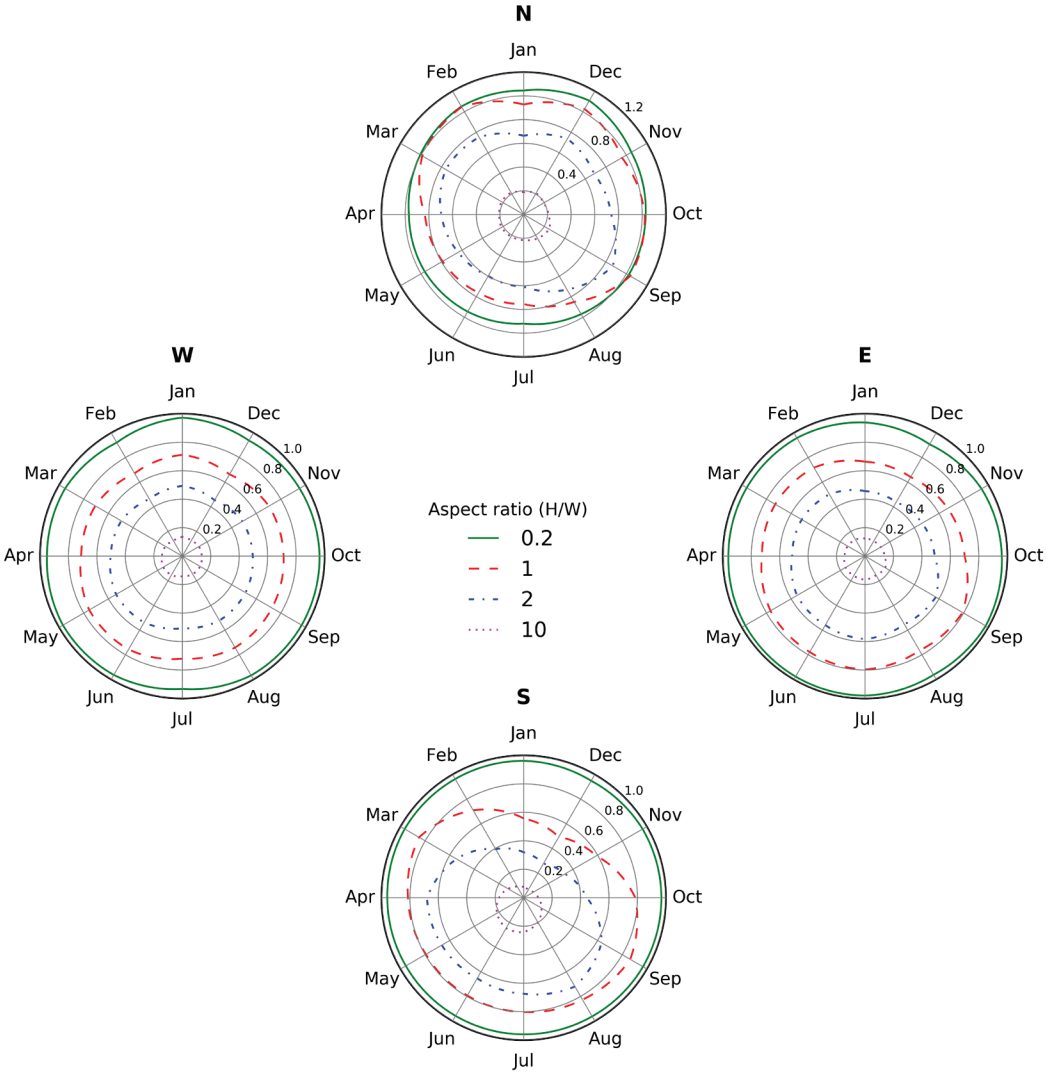

ground albedo = 0.20, central wall albedo = 0.25, neighboring wall albedo = 0.60

(h)

Figure B-2 (continued)

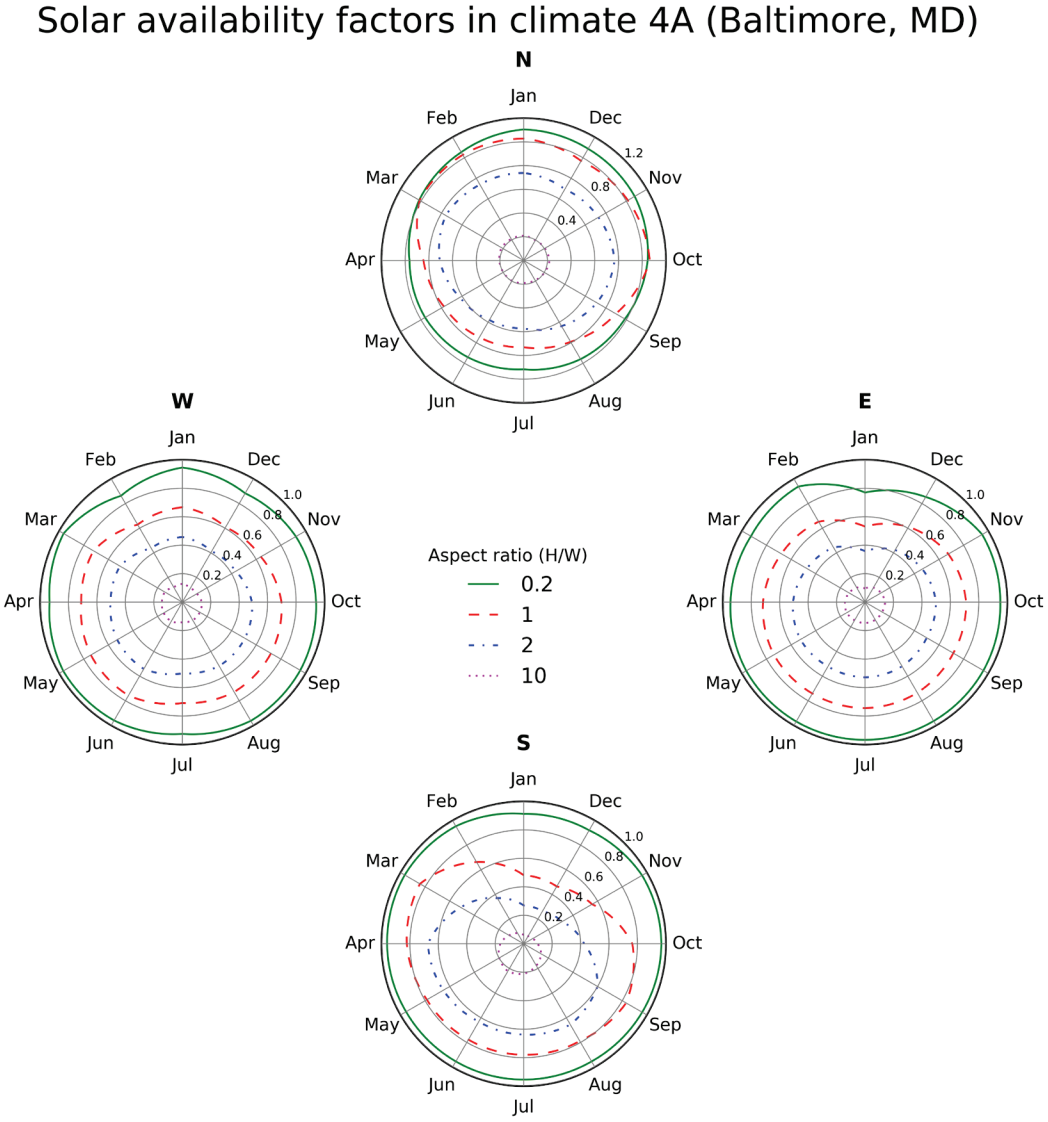

ground albedo = 0.20, central wall albedo = 0.25, neighboring wall albedo = 0.60

(i)

Figure B-2 (continued)

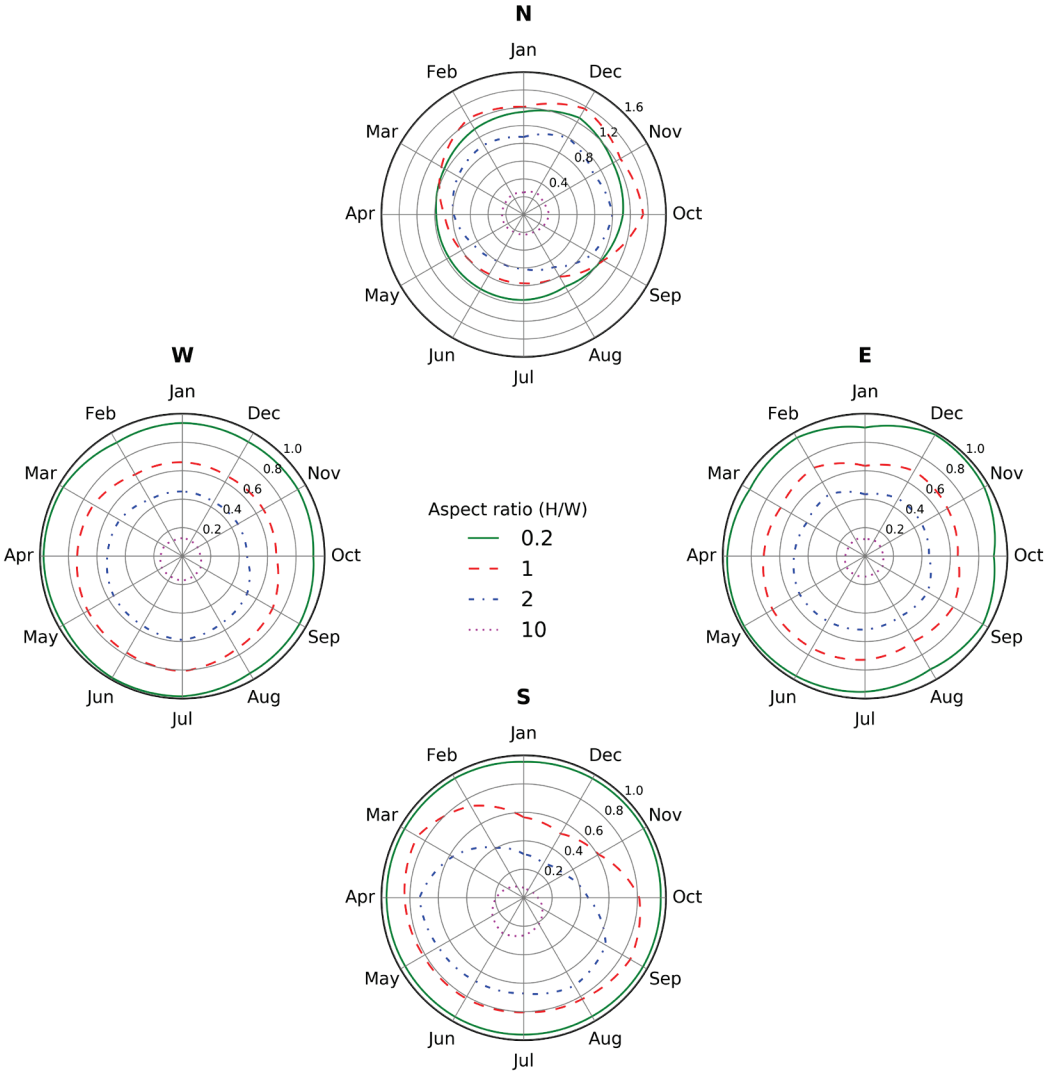

ground albedo = 0.20, central wall albedo = 0.25, neighboring wall albedo = 0.60

(j)

Figure B-2 (continued)

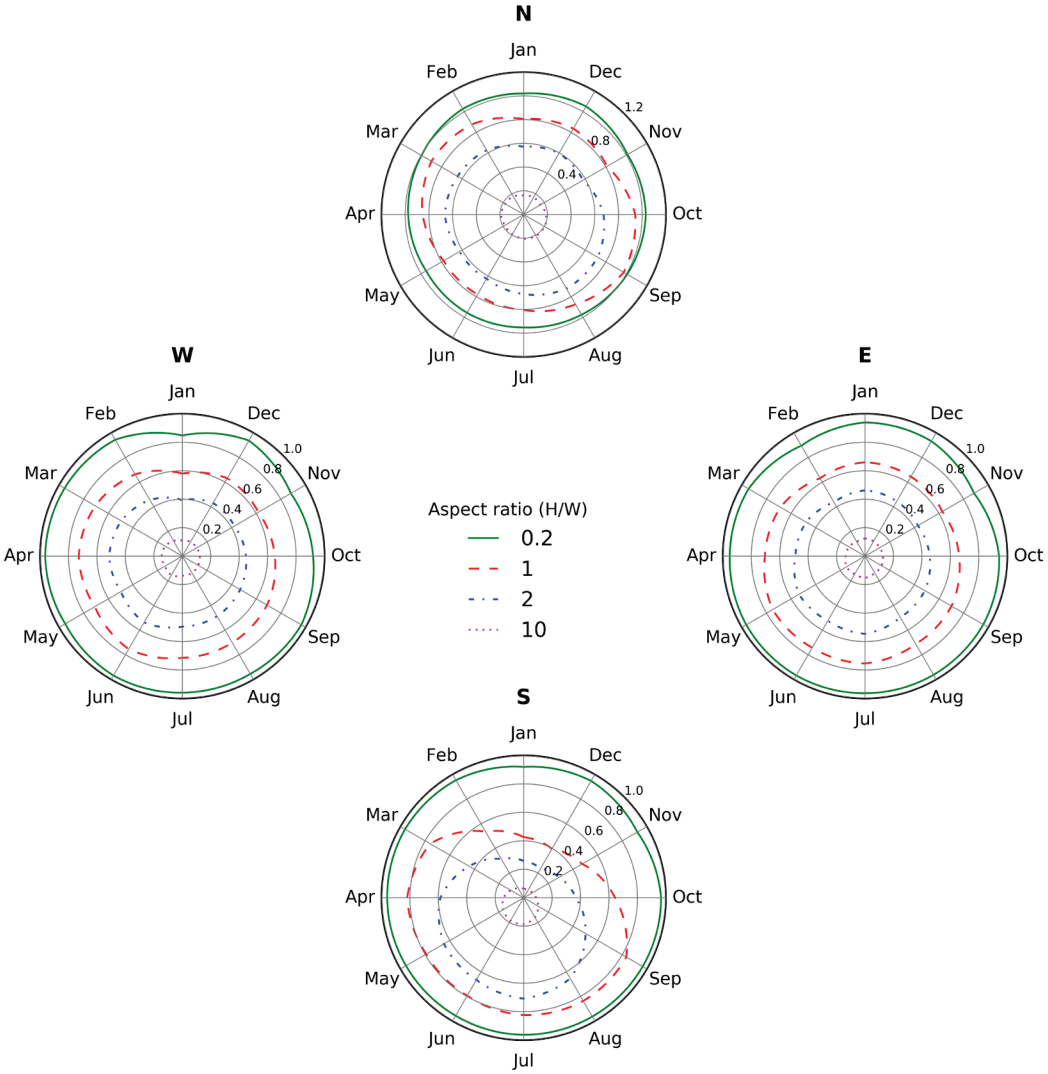

ground albedo = 0.20, central wall albedo = 0.25, neighboring wall albedo = 0.60

(k)

Figure B-2 (continued)

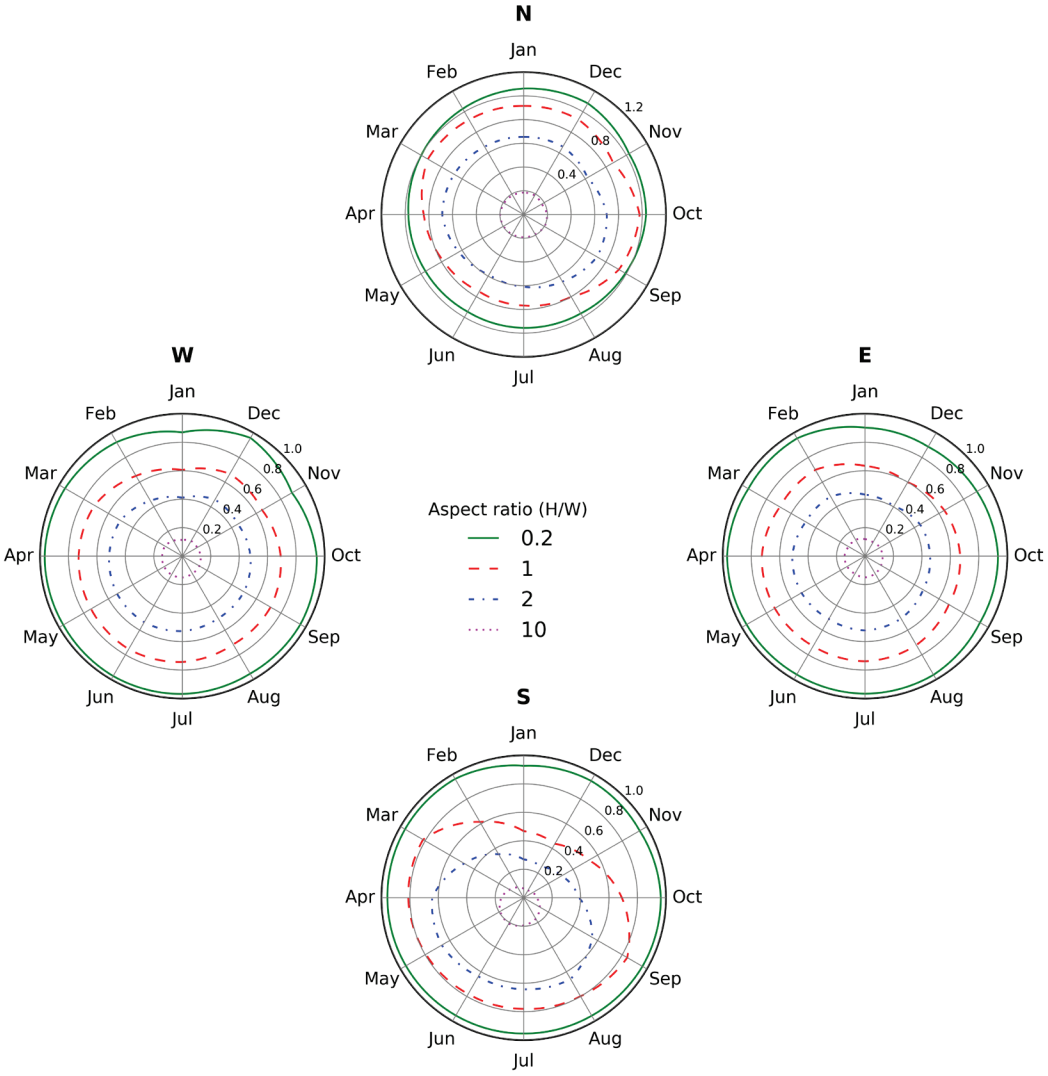

ground albedo = 0.20, central wall albedo = 0.25, neighboring wall albedo = 0.60

(l)

Figure B-2 (continued)

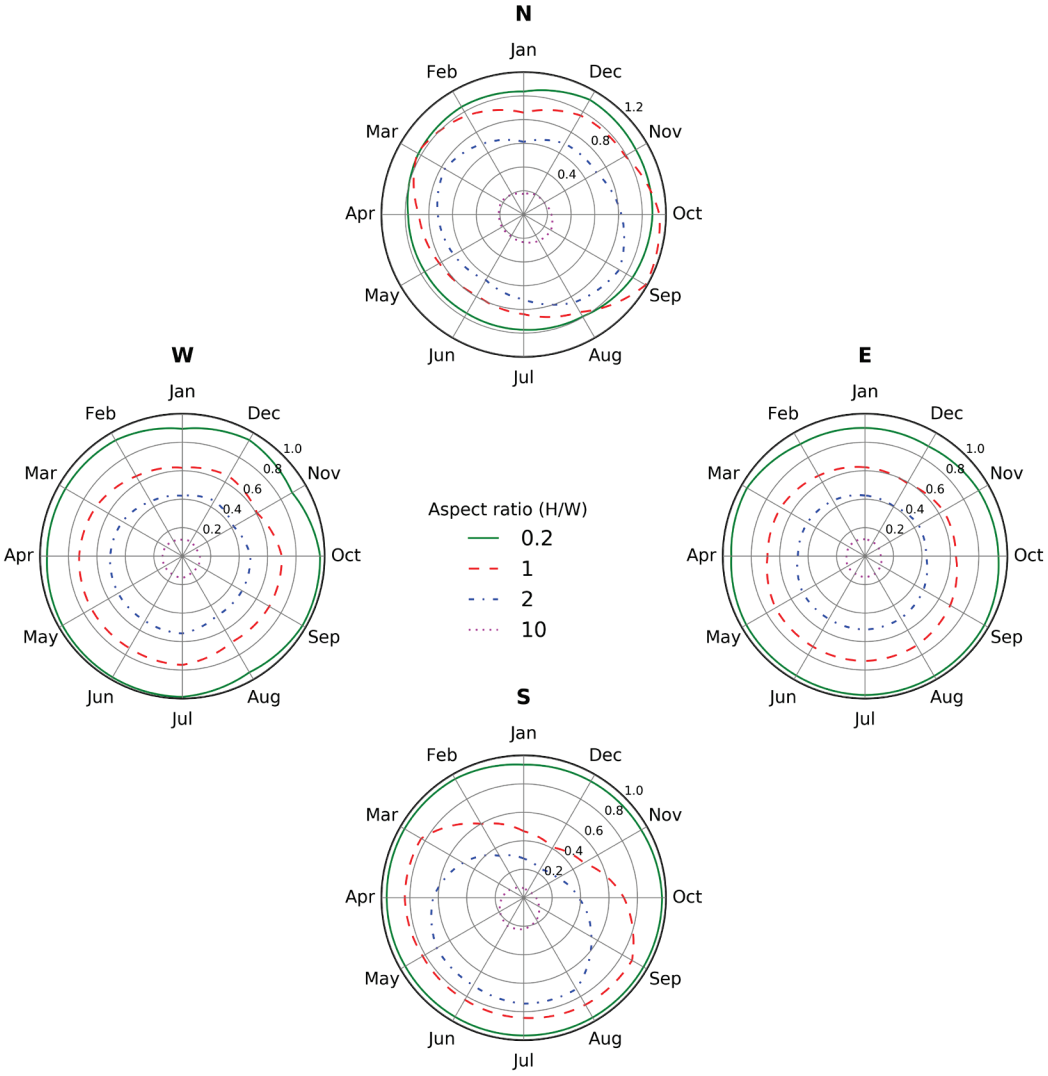

Figure B-2 (continued)

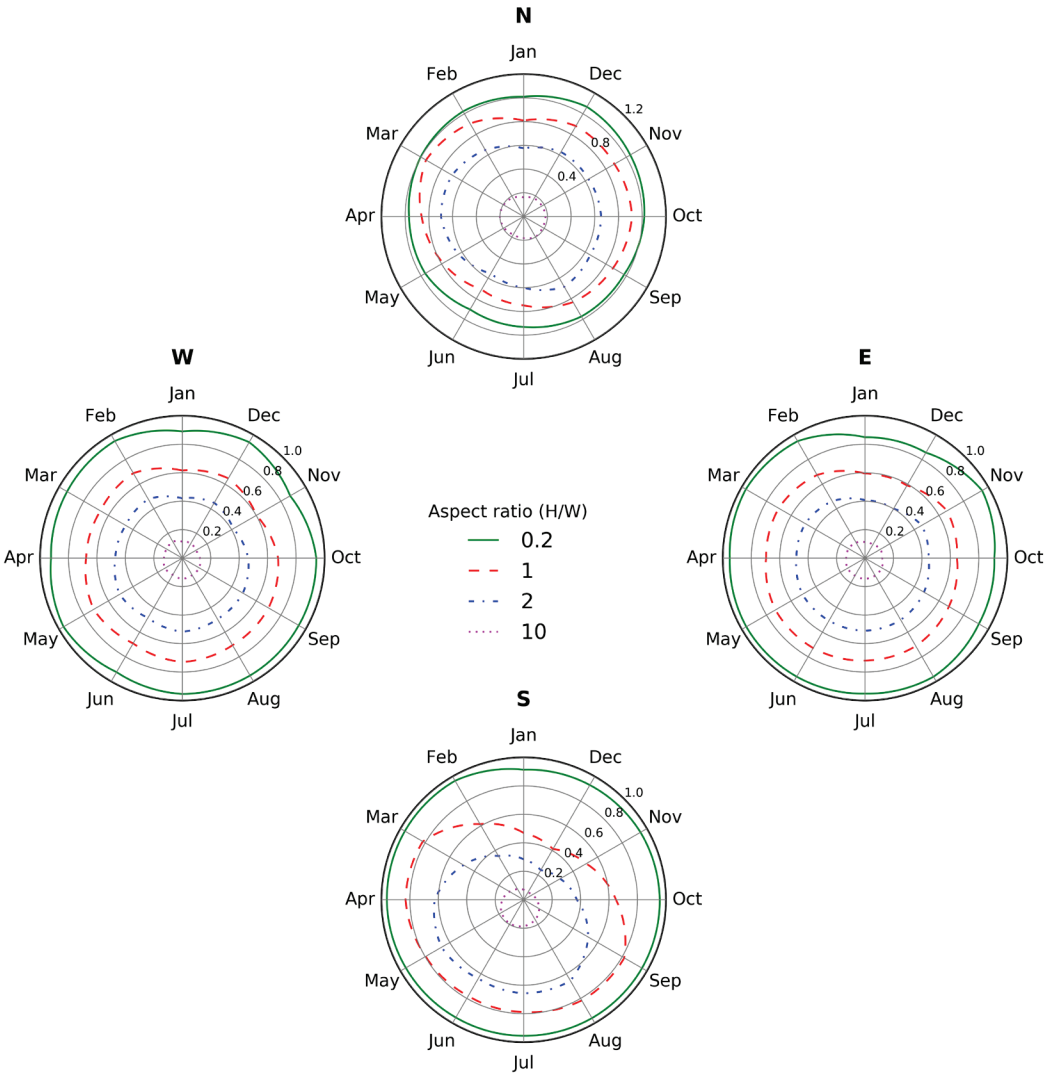

ground albedo = 0.20, central wall albedo = 0.25, neighboring wall albedo = 0.60

(n)

Figure B-2 (continued)

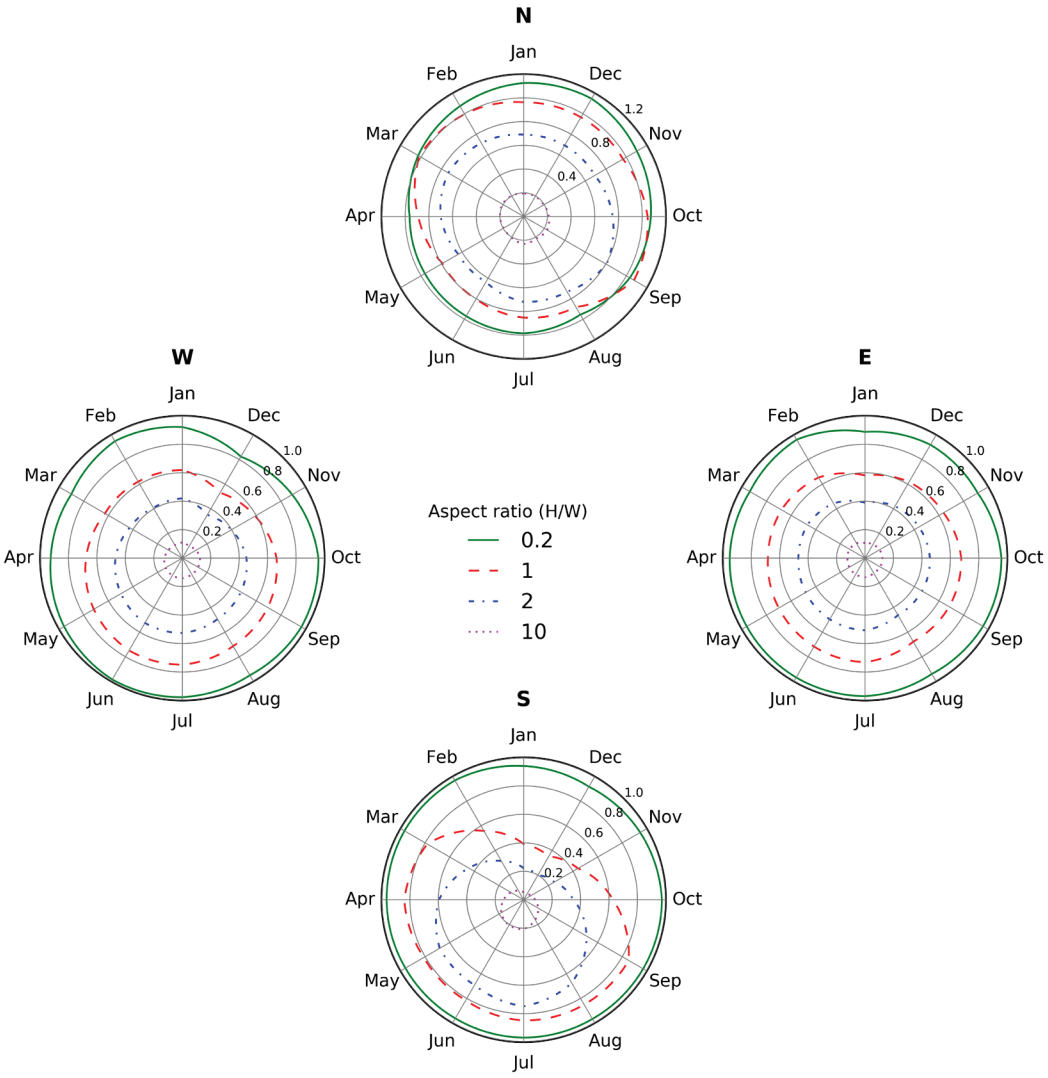

ground albedo = 0.20, central wall albedo = 0.25, neighboring wall albedo = 0.60

(o)

Figure B-2 (continued)

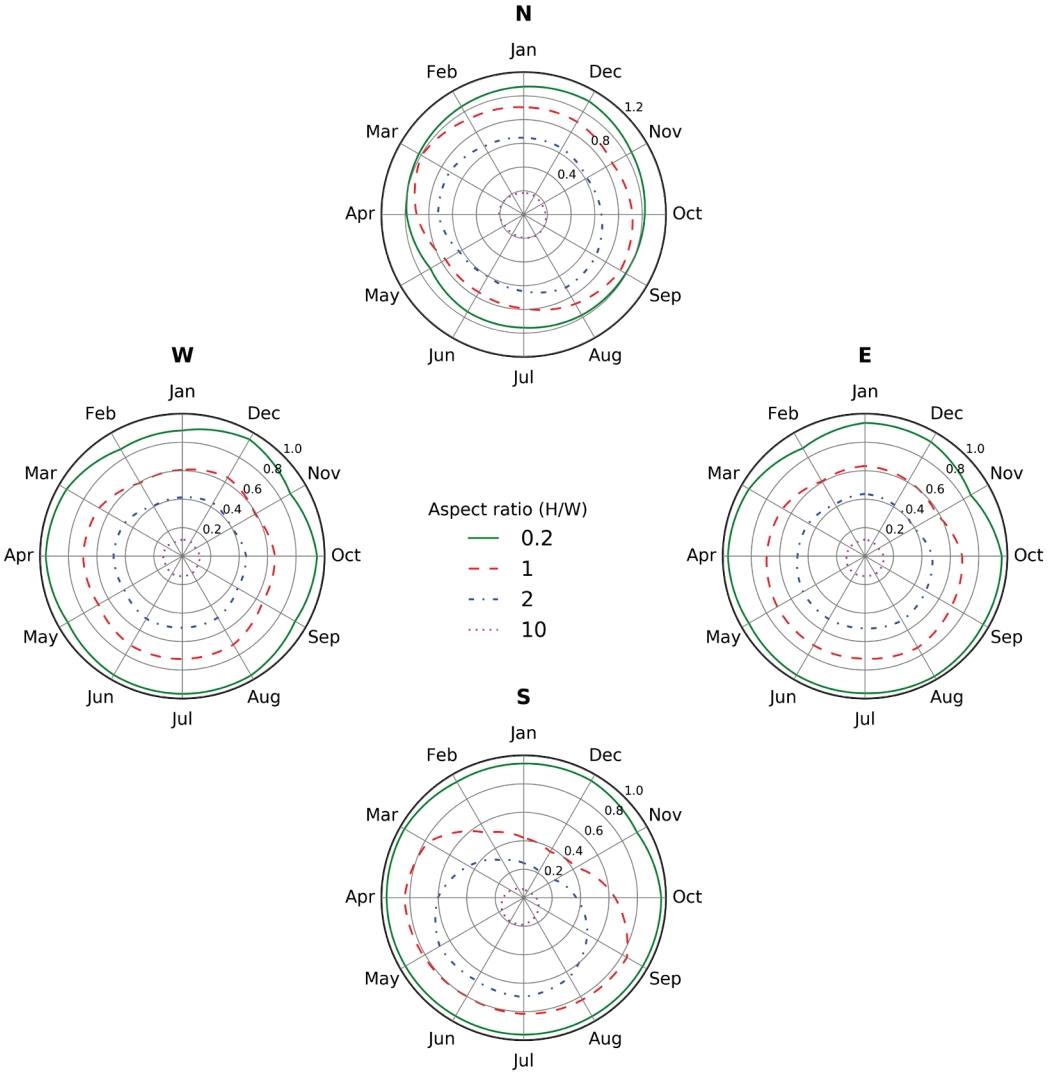

ground albedo = 0.20, central wall albedo = 0.25, neighboring wall albedo = 0.60

(p)

Figure B-2 (continued)

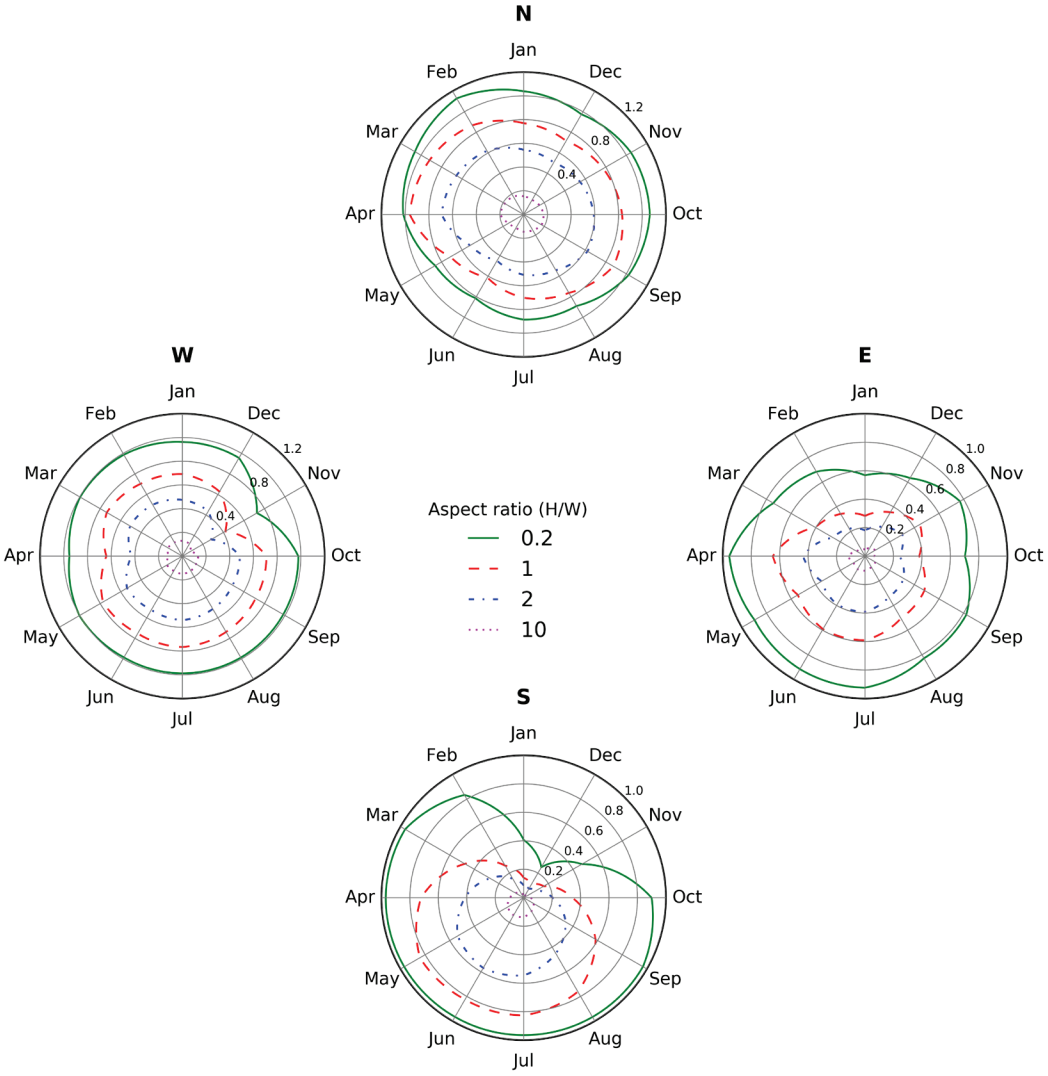

ground albedo = 0.20, central wall albedo = 0.25, neighboring wall albedo = 0.60

(q)

Figure B-2 (continued)

Task Report Appendix C: SAF tables for Scenarios 2 – 4

Table C-1. Annual mean, minimum, maximum, and range (maximum – minimum) values of monthly SAF for a north (N), east (E), south (S), or west (W) conventional central wall (ρ=0.25) with a cool neighboring wall (ρ=0.60). Results shown by climate for aspect ratios of (a) R=0.2, (b) R=1, (c) R=2, and (d) R=10.

(a) aspect ratio R=0.2

	N				E				S				W			
	mean	min	max	range	mean	min	max	range	mean	min	max	range	mean	min	max	range
1A (Miami, FL)	0.98	0.94	1.05	0.11	0.96	0.92	0.98	0.05	0.95	0.94	0.97	0.02	0.95	0.87	0.97	0.10
2A (Houston, TX)	0.99	0.93	1.05	0.12	0.94	0.90	0.97	0.07	0.95	0.94	0.96	0.03	0.94	0.89	0.97	0.08
2B (Phoenix, AZ)	1.03	0.89	1.18	0.29	0.95	0.90	0.99	0.09	0.96	0.96	0.97	0.01	0.95	0.92	0.98	0.06
3A (Memphis, TN)	1.01	0.95	1.10	0.14	0.95	0.88	0.97	0.09	0.96	0.95	0.97	0.02	0.94	0.88	0.97	0.10
3B (El Paso, TX)	1.04	0.95	1.15	0.20	0.97	0.91	0.99	0.08	0.97	0.96	0.98	0.02	0.97	0.94	0.98	0.04
BU (Burbank, CA)	1.02	0.96	1.13	0.17	0.96	0.92	0.98	0.06	0.96	0.96	0.97	0.01	0.96	0.93	0.98	0.05
FR (Fresno, CA)	1.01	0.96	1.06	0.09	0.96	0.93	0.98	0.05	0.96	0.96	0.97	0.01	0.96	0.94	0.98	0.04
3C (San Francisco, CA)	1.01	0.92	1.11	0.19	0.96	0.91	0.98	0.07	0.96	0.95	0.97	0.02	0.95	0.92	0.97	0.05
4A (Baltimore, MD)	1.01	0.92	1.10	0.19	0.93	0.77	0.97	0.20	0.95	0.91	0.97	0.06	0.94	0.86	0.97	0.10
4B (Albuquerque, NM)	1.05	0.94	1.25	0.32	0.95	0.90	0.99	0.08	0.96	0.95	0.97	0.02	0.95	0.92	0.99	0.07
4C (Seattle, WA)	1.00	0.95	1.05	0.10	0.94	0.88	0.97	0.08	0.95	0.92	0.97	0.05	0.94	0.85	0.97	0.12
5A (Chicago, IL)	1.00	0.95	1.08	0.14	0.94	0.89	0.97	0.08	0.95	0.93	0.96	0.04	0.94	0.87	0.97	0.10
5B (Boise, ID)	1.03	0.96	1.12	0.16	0.94	0.89	0.98	0.08	0.96	0.93	0.97	0.04	0.95	0.89	0.99	0.10
6A (Burlington, VT)	0.99	0.90	1.07	0.16	0.93	0.85	0.97	0.12	0.95	0.91	0.97	0.05	0.93	0.88	0.96	0.09
6B (Helena, MT)	1.03	0.96	1.15	0.19	0.94	0.89	0.97	0.08	0.96	0.92	0.97	0.05	0.93	0.82	0.98	0.16
7 (Duluth, MN)	1.01	0.91	1.10	0.19	0.94	0.86	0.98	0.12	0.95	0.92	0.97	0.05	0.93	0.87	0.97	0.10
8 (Fairbanks, AK)	0.98	0.81	1.13	0.32	0.79	0.57	0.95	0.39	0.80	0.25	0.97	0.72	0.96	0.73	1.00	0.28

Table C-1 (continued)

(b) aspect ratio R=1

	N				E				S				W			
	mean	min	max	range	mean	min	max	range	mean	min	max	range	mean	min	max	range
1A (Miami, FL)	0.86	0.71	1.06	0.35	0.72	0.68	0.76	0.08	0.76	0.70	0.83	0.13	0.73	0.66	0.76	0.11
2A (Houston, TX)	0.87	0.71	1.04	0.33	0.72	0.66	0.75	0.09	0.75	0.62	0.83	0.21	0.71	0.65	0.76	0.11
2B (Phoenix, AZ)	1.02	0.70	1.29	0.59	0.70	0.64	0.75	0.11	0.77	0.55	0.87	0.31	0.71	0.64	0.76	0.12
3A (Memphis, TN)	0.91	0.75	1.08	0.33	0.71	0.65	0.76	0.12	0.74	0.53	0.84	0.31	0.70	0.63	0.77	0.14
3B (El Paso, TX)	1.02	0.76	1.31	0.55	0.73	0.68	0.78	0.10	0.77	0.58	0.86	0.28	0.73	0.67	0.79	0.13
BU (Burbank, CA)	0.96	0.76	1.18	0.41	0.73	0.67	0.79	0.12	0.76	0.55	0.85	0.31	0.73	0.67	0.79	0.12
FR (Fresno, CA)	0.92	0.78	1.12	0.34	0.72	0.67	0.76	0.10	0.76	0.53	0.87	0.34	0.73	0.68	0.77	0.09
3C (San Francisco, CA)	0.92	0.75	1.05	0.29	0.73	0.64	0.80	0.16	0.74	0.49	0.86	0.37	0.72	0.66	0.76	0.09
4A (Baltimore, MD)	0.91	0.73	1.06	0.33	0.69	0.53	0.74	0.21	0.71	0.46	0.84	0.38	0.69	0.61	0.76	0.15
4B (Albuquerque, NM)	1.05	0.77	1.37	0.60	0.70	0.63	0.75	0.12	0.76	0.52	0.87	0.35	0.72	0.64	0.81	0.16
4C (Seattle, WA)	0.85	0.78	0.97	0.20	0.69	0.63	0.75	0.13	0.68	0.40	0.84	0.44	0.68	0.58	0.75	0.17
5A (Chicago, IL)	0.87	0.75	0.98	0.23	0.69	0.60	0.74	0.14	0.70	0.44	0.84	0.40	0.70	0.61	0.75	0.15
5B (Boise, ID)	0.95	0.79	1.19	0.40	0.68	0.59	0.74	0.14	0.71	0.41	0.88	0.47	0.69	0.61	0.76	0.16
6A (Burlington, VT)	0.85	0.71	0.95	0.24	0.68	0.59	0.73	0.14	0.69	0.41	0.83	0.42	0.68	0.60	0.73	0.13
6B (Helena, MT)	0.94	0.79	1.07	0.28	0.67	0.58	0.73	0.15	0.68	0.35	0.85	0.50	0.66	0.53	0.75	0.22
7 (Duluth, MN)	0.88	0.76	1.00	0.24	0.67	0.58	0.74	0.16	0.67	0.37	0.84	0.47	0.66	0.59	0.72	0.13
8 (Fairbanks, AK)	0.79	0.61	0.96	0.35	0.46	0.28	0.65	0.37	0.50	0.11	0.84	0.73	0.69	0.42	0.77	0.35

Table C-1 (continued)

(c) aspect ratio R=2

	N				E				S				W			
	mean	min	max	range	mean	min	max	range	mean	min	max	range	mean	min	max	range
1A (Miami, FL)	0.65	0.52	0.77	0.25	0.51	0.47	0.54	0.06	0.54	0.39	0.67	0.28	0.52	0.47	0.55	0.09
2A (Houston, TX)	0.66	0.53	0.79	0.26	0.51	0.46	0.53	0.07	0.53	0.35	0.68	0.33	0.50	0.45	0.54	0.10
2B (Phoenix, AZ)	0.80	0.56	0.94	0.38	0.49	0.44	0.53	0.09	0.55	0.30	0.75	0.45	0.50	0.44	0.55	0.11
3A (Memphis, TN)	0.69	0.56	0.77	0.21	0.50	0.45	0.54	0.10	0.52	0.29	0.69	0.40	0.49	0.43	0.55	0.12
3B (El Paso, TX)	0.79	0.58	0.95	0.37	0.51	0.47	0.56	0.09	0.56	0.32	0.73	0.41	0.52	0.46	0.57	0.11
BU (Burbank, CA)	0.75	0.60	0.85	0.25	0.51	0.46	0.57	0.11	0.55	0.30	0.73	0.43	0.52	0.46	0.56	0.11
FR (Fresno, CA)	0.72	0.60	0.93	0.33	0.51	0.46	0.54	0.08	0.55	0.31	0.76	0.45	0.51	0.47	0.55	0.08
3C (San Francisco, CA)	0.71	0.60	0.87	0.27	0.52	0.44	0.58	0.14	0.53	0.28	0.72	0.44	0.50	0.45	0.54	0.08
4A (Baltimore, MD)	0.69	0.57	0.77	0.19	0.48	0.36	0.53	0.17	0.50	0.26	0.67	0.41	0.49	0.41	0.54	0.13
4B (Albuquerque, NM)	0.81	0.60	1.00	0.40	0.49	0.43	0.53	0.10	0.54	0.28	0.73	0.45	0.51	0.44	0.59	0.15
4C (Seattle, WA)	0.64	0.57	0.72	0.15	0.48	0.43	0.55	0.12	0.47	0.24	0.71	0.47	0.47	0.39	0.54	0.14
5A (Chicago, IL)	0.65	0.59	0.71	0.13	0.48	0.41	0.52	0.12	0.49	0.25	0.67	0.41	0.49	0.41	0.54	0.12
5B (Boise, ID)	0.74	0.61	0.93	0.32	0.47	0.40	0.52	0.11	0.51	0.23	0.74	0.51	0.48	0.42	0.54	0.13
6A (Burlington, VT)	0.64	0.55	0.70	0.14	0.47	0.40	0.51	0.11	0.48	0.24	0.67	0.43	0.47	0.41	0.52	0.10
6B (Helena, MT)	0.71	0.64	0.81	0.17	0.46	0.39	0.51	0.12	0.47	0.20	0.75	0.55	0.45	0.35	0.53	0.18
7 (Duluth, MN)	0.66	0.60	0.72	0.12	0.47	0.39	0.52	0.13	0.47	0.22	0.70	0.48	0.46	0.40	0.51	0.11
8 (Fairbanks, AK)	0.57	0.45	0.69	0.24	0.31	0.18	0.44	0.26	0.31	0.07	0.57	0.50	0.48	0.28	0.54	0.26

Table C-1 (continued)

(d) aspect ratio R=10

	N				E				S				W			
	mean	min	max	range	mean	min	max	range	mean	min	max	range	mean	min	max	range
1A (Miami, FL)	0.20	0.17	0.22	0.05	0.14	0.13	0.15	0.02	0.16	0.09	0.22	0.13	0.14	0.13	0.16	0.03
2A (Houston, TX)	0.20	0.18	0.22	0.04	0.14	0.12	0.15	0.02	0.15	0.08	0.22	0.14	0.14	0.12	0.15	0.03
2B (Phoenix, AZ)	0.25	0.21	0.27	0.05	0.13	0.12	0.15	0.02	0.16	0.07	0.30	0.23	0.14	0.12	0.15	0.03
3A (Memphis, TN)	0.21	0.20	0.22	0.02	0.14	0.12	0.16	0.03	0.15	0.07	0.23	0.16	0.14	0.12	0.16	0.04
3B (El Paso, TX)	0.25	0.22	0.27	0.05	0.14	0.13	0.16	0.03	0.17	0.07	0.30	0.23	0.15	0.13	0.17	0.04
BU (Burbank, CA)	0.23	0.20	0.25	0.05	0.15	0.13	0.17	0.04	0.16	0.07	0.27	0.20	0.14	0.12	0.16	0.04
FR (Fresno, CA)	0.22	0.17	0.27	0.10	0.14	0.13	0.16	0.03	0.16	0.07	0.28	0.20	0.14	0.13	0.16	0.03
3C (San Francisco, CA)	0.21	0.19	0.25	0.06	0.14	0.12	0.16	0.04	0.15	0.06	0.25	0.18	0.14	0.12	0.15	0.03
4A (Baltimore, MD)	0.20	0.19	0.22	0.03	0.13	0.10	0.15	0.05	0.13	0.06	0.22	0.16	0.14	0.11	0.16	0.04
4B (Albuquerque, NM)	0.25	0.22	0.28	0.06	0.14	0.12	0.15	0.03	0.16	0.06	0.29	0.23	0.14	0.12	0.17	0.05
4C (Seattle, WA)	0.18	0.16	0.21	0.05	0.13	0.12	0.15	0.04	0.12	0.06	0.19	0.13	0.13	0.11	0.16	0.05
5A (Chicago, IL)	0.19	0.17	0.20	0.03	0.13	0.11	0.15	0.04	0.13	0.06	0.21	0.15	0.14	0.11	0.15	0.04
5B (Boise, ID)	0.22	0.17	0.27	0.09	0.13	0.11	0.15	0.04	0.13	0.05	0.23	0.17	0.13	0.11	0.15	0.05
6A (Burlington, VT)	0.18	0.16	0.20	0.04	0.13	0.11	0.15	0.03	0.12	0.06	0.19	0.14	0.13	0.11	0.15	0.04
6B (Helena, MT)	0.21	0.19	0.23	0.04	0.12	0.11	0.13	0.03	0.12	0.05	0.21	0.16	0.12	0.10	0.14	0.04
7 (Duluth, MN)	0.19	0.17	0.21	0.04	0.13	0.11	0.14	0.04	0.12	0.05	0.19	0.14	0.13	0.11	0.14	0.04
8 (Fairbanks, AK)	0.16	0.13	0.20	0.07	0.08	0.05	0.12	0.07	0.08	0.02	0.14	0.12	0.13	0.08	0.15	0.07

Table C-2. Same as Table C-1, but for cool central wall (ρ=0.60) with a conventional neighboring wall (ρ=0.25).

(a) aspect ratio R=0.2

	N				E				S				W			
	mean	min	max	range	mean	min	max	range	mean	min	max	range	mean	min	max	range
1A (Miami, FL)	0.92	0.91	0.93	0.02	0.93	0.89	0.94	0.05	0.94	0.91	0.96	0.05	0.92	0.84	0.94	0.10
2A (Houston, TX)	0.92	0.89	0.93	0.03	0.91	0.87	0.94	0.07	0.94	0.91	0.96	0.04	0.91	0.86	0.94	0.07
2B (Phoenix, AZ)	0.92	0.86	0.95	0.09	0.92	0.87	0.95	0.08	0.95	0.93	0.97	0.04	0.92	0.89	0.95	0.06
3A (Memphis, TN)	0.92	0.91	0.94	0.03	0.92	0.85	0.94	0.08	0.94	0.92	0.96	0.04	0.91	0.85	0.94	0.10
3B (El Paso, TX)	0.93	0.91	0.95	0.03	0.94	0.89	0.96	0.07	0.95	0.93	0.97	0.04	0.93	0.91	0.95	0.04
BU (Burbank, CA)	0.93	0.92	0.94	0.03	0.93	0.89	0.95	0.06	0.95	0.93	0.97	0.04	0.93	0.90	0.95	0.05
FR (Fresno, CA)	0.92	0.90	0.93	0.03	0.93	0.90	0.95	0.04	0.95	0.94	0.96	0.03	0.93	0.91	0.95	0.04
3C (San Francisco, CA)	0.92	0.88	0.94	0.06	0.93	0.88	0.94	0.07	0.95	0.93	0.96	0.03	0.93	0.89	0.94	0.05
4A (Baltimore, MD)	0.92	0.88	0.94	0.06	0.90	0.75	0.94	0.19	0.94	0.91	0.96	0.05	0.90	0.83	0.93	0.10
4B (Albuquerque, NM)	0.93	0.88	0.97	0.09	0.92	0.87	0.96	0.08	0.95	0.94	0.97	0.04	0.92	0.89	0.95	0.06
4C (Seattle, WA)	0.91	0.90	0.93	0.03	0.91	0.86	0.94	0.08	0.94	0.91	0.96	0.05	0.91	0.82	0.94	0.12
5A (Chicago, IL)	0.92	0.91	0.93	0.02	0.91	0.86	0.94	0.08	0.94	0.92	0.96	0.03	0.91	0.84	0.94	0.10
5B (Boise, ID)	0.92	0.90	0.94	0.03	0.91	0.86	0.95	0.08	0.95	0.93	0.97	0.04	0.92	0.86	0.95	0.09
6A (Burlington, VT)	0.91	0.87	0.93	0.06	0.90	0.82	0.94	0.12	0.94	0.91	0.96	0.05	0.90	0.85	0.93	0.08
6B (Helena, MT)	0.92	0.89	0.94	0.06	0.91	0.86	0.94	0.08	0.95	0.91	0.97	0.05	0.90	0.80	0.95	0.15
7 (Duluth, MN)	0.91	0.86	0.93	0.07	0.91	0.83	0.94	0.11	0.94	0.91	0.96	0.05	0.90	0.84	0.94	0.10
8 (Fairbanks, AK)	0.88	0.78	0.94	0.16	0.77	0.56	0.92	0.36	0.79	0.24	0.96	0.72	0.91	0.70	0.94	0.24

Table C-2 (continued)

(b) aspect ratio R=1

	N				E				S				W			
	mean	min	max	range	mean	min	max	range	mean	min	max	range	mean	min	max	range
1A (Miami, FL)	0.66	0.62	0.70	0.07	0.64	0.60	0.67	0.07	0.72	0.62	0.81	0.19	0.64	0.58	0.67	0.09
2A (Houston, TX)	0.66	0.62	0.69	0.07	0.63	0.58	0.67	0.09	0.71	0.60	0.82	0.21	0.63	0.58	0.67	0.09
2B (Phoenix, AZ)	0.69	0.62	0.76	0.14	0.63	0.57	0.66	0.09	0.74	0.55	0.85	0.30	0.63	0.58	0.68	0.10
3A (Memphis, TN)	0.67	0.64	0.70	0.06	0.63	0.57	0.68	0.10	0.70	0.51	0.81	0.30	0.62	0.56	0.68	0.12
3B (El Paso, TX)	0.70	0.66	0.76	0.10	0.65	0.61	0.70	0.09	0.74	0.58	0.84	0.26	0.65	0.59	0.70	0.11
BU (Burbank, CA)	0.68	0.64	0.73	0.08	0.64	0.60	0.70	0.10	0.73	0.54	0.83	0.30	0.65	0.59	0.70	0.11
FR (Fresno, CA)	0.67	0.64	0.71	0.07	0.64	0.59	0.68	0.09	0.73	0.52	0.86	0.34	0.64	0.61	0.68	0.07
3C (San Francisco, CA)	0.67	0.63	0.70	0.07	0.64	0.57	0.69	0.12	0.71	0.48	0.85	0.36	0.64	0.59	0.68	0.09
4A (Baltimore, MD)	0.66	0.62	0.70	0.08	0.61	0.47	0.66	0.19	0.68	0.45	0.82	0.37	0.61	0.55	0.67	0.12
4B (Albuquerque, NM)	0.70	0.63	0.78	0.15	0.62	0.56	0.68	0.12	0.73	0.52	0.85	0.33	0.63	0.57	0.70	0.13
4C (Seattle, WA)	0.65	0.63	0.68	0.05	0.61	0.56	0.67	0.11	0.65	0.38	0.81	0.43	0.60	0.52	0.66	0.14
5A (Chicago, IL)	0.65	0.63	0.68	0.04	0.61	0.53	0.65	0.12	0.66	0.42	0.82	0.39	0.62	0.54	0.66	0.12
5B (Boise, ID)	0.68	0.65	0.73	0.08	0.60	0.52	0.66	0.13	0.69	0.40	0.87	0.47	0.61	0.54	0.68	0.14
6A (Burlington, VT)	0.64	0.60	0.67	0.07	0.60	0.53	0.65	0.12	0.66	0.40	0.80	0.40	0.60	0.54	0.65	0.11
6B (Helena, MT)	0.67	0.64	0.70	0.06	0.60	0.51	0.66	0.14	0.66	0.34	0.84	0.49	0.59	0.47	0.66	0.18
7 (Duluth, MN)	0.65	0.60	0.68	0.08	0.59	0.51	0.65	0.13	0.65	0.36	0.81	0.45	0.59	0.53	0.65	0.12
8 (Fairbanks, AK)	0.61	0.49	0.66	0.17	0.42	0.26	0.57	0.32	0.48	0.10	0.81	0.71	0.59	0.37	0.65	0.28

Table C-2 (continued)

(c) aspect ratio R=2

	N				E				S				W			
	mean	min	max	range	mean	min	max	range	mean	min	max	range	mean	min	max	range
1A (Miami, FL)	0.46	0.44	0.49	0.05	0.44	0.40	0.46	0.06	0.50	0.38	0.65	0.27	0.44	0.40	0.47	0.07
2A (Houston, TX)	0.46	0.44	0.49	0.05	0.43	0.39	0.46	0.07	0.49	0.33	0.65	0.32	0.43	0.38	0.46	0.07
2B (Phoenix, AZ)	0.50	0.45	0.53	0.08	0.42	0.38	0.45	0.07	0.52	0.29	0.72	0.43	0.42	0.37	0.47	0.09
3A (Memphis, TN)	0.47	0.45	0.49	0.03	0.43	0.38	0.46	0.08	0.49	0.28	0.65	0.37	0.42	0.37	0.47	0.10
3B (El Paso, TX)	0.51	0.47	0.53	0.06	0.44	0.40	0.48	0.08	0.52	0.31	0.70	0.39	0.44	0.39	0.48	0.09
BU (Burbank, CA)	0.49	0.46	0.51	0.05	0.43	0.40	0.48	0.08	0.52	0.29	0.70	0.41	0.44	0.39	0.48	0.09
FR (Fresno, CA)	0.48	0.44	0.53	0.09	0.43	0.39	0.46	0.07	0.52	0.29	0.73	0.44	0.43	0.40	0.46	0.06
3C (San Francisco, CA)	0.47	0.45	0.51	0.06	0.43	0.37	0.48	0.11	0.50	0.26	0.69	0.42	0.43	0.39	0.46	0.07
4A (Baltimore, MD)	0.47	0.44	0.48	0.05	0.41	0.31	0.45	0.14	0.47	0.25	0.64	0.39	0.41	0.36	0.46	0.10
4B (Albuquerque, NM)	0.51	0.46	0.55	0.09	0.42	0.37	0.46	0.09	0.52	0.27	0.71	0.43	0.43	0.37	0.49	0.12
4C (Seattle, WA)	0.45	0.43	0.47	0.04	0.41	0.37	0.46	0.09	0.44	0.22	0.67	0.45	0.40	0.34	0.45	0.11
5A (Chicago, IL)	0.46	0.45	0.47	0.02	0.41	0.35	0.44	0.10	0.46	0.24	0.62	0.38	0.41	0.35	0.45	0.10
5B (Boise, ID)	0.48	0.44	0.53	0.09	0.40	0.34	0.44	0.10	0.48	0.22	0.72	0.50	0.41	0.35	0.46	0.11
6A (Burlington, VT)	0.45	0.43	0.47	0.04	0.40	0.34	0.43	0.09	0.45	0.22	0.62	0.40	0.40	0.35	0.44	0.09
6B (Helena, MT)	0.47	0.45	0.50	0.04	0.39	0.33	0.44	0.11	0.45	0.19	0.71	0.52	0.38	0.30	0.44	0.14
7 (Duluth, MN)	0.46	0.44	0.48	0.04	0.40	0.33	0.43	0.10	0.44	0.20	0.65	0.45	0.39	0.34	0.43	0.09
8 (Fairbanks, AK)	0.41	0.33	0.46	0.12	0.27	0.16	0.37	0.21	0.29	0.06	0.53	0.46	0.39	0.24	0.44	0.20

Table C-2 (continued)

(d) aspect ratio R=10

	N				E				S				W			
	mean	min	max	range	mean	min	max	range	mean	min	max	range	mean	min	max	range
1A (Miami, FL)	0.13	0.12	0.14	0.02	0.11	0.10	0.12	0.02	0.14	0.09	0.20	0.12	0.12	0.10	0.12	0.02
2A (Houston, TX)	0.13	0.13	0.14	0.01	0.11	0.10	0.12	0.02	0.14	0.08	0.19	0.12	0.11	0.10	0.12	0.02
2B (Phoenix, AZ)	0.15	0.14	0.15	0.01	0.11	0.10	0.12	0.02	0.15	0.06	0.26	0.20	0.11	0.09	0.12	0.03
3A (Memphis, TN)	0.13	0.13	0.14	0.01	0.11	0.10	0.13	0.03	0.13	0.06	0.21	0.14	0.11	0.10	0.13	0.03
3B (El Paso, TX)	0.15	0.14	0.17	0.03	0.12	0.10	0.13	0.03	0.16	0.07	0.26	0.20	0.12	0.10	0.14	0.03
BU (Burbank, CA)	0.14	0.13	0.15	0.02	0.12	0.10	0.14	0.03	0.15	0.06	0.24	0.18	0.12	0.10	0.13	0.03
FR (Fresno, CA)	0.14	0.12	0.16	0.04	0.12	0.10	0.13	0.02	0.15	0.07	0.25	0.18	0.12	0.10	0.13	0.02
3C (San Francisco, CA)	0.13	0.12	0.14	0.02	0.12	0.10	0.13	0.03	0.14	0.06	0.23	0.17	0.11	0.10	0.13	0.02
4A (Baltimore, MD)	0.13	0.13	0.14	0.01	0.11	0.08	0.12	0.04	0.12	0.06	0.20	0.14	0.11	0.09	0.13	0.03
4B (Albuquerque, NM)	0.15	0.14	0.15	0.02	0.11	0.09	0.13	0.03	0.15	0.06	0.26	0.20	0.12	0.10	0.14	0.04
4C (Seattle, WA)	0.12	0.12	0.13	0.02	0.11	0.09	0.12	0.03	0.11	0.05	0.17	0.12	0.11	0.09	0.12	0.03
5A (Chicago, IL)	0.13	0.12	0.13	0.01	0.11	0.09	0.12	0.03	0.12	0.05	0.19	0.13	0.11	0.09	0.12	0.03
5B (Boise, ID)	0.13	0.12	0.15	0.03	0.10	0.09	0.12	0.03	0.12	0.05	0.21	0.16	0.10	0.09	0.12	0.04
6A (Burlington, VT)	0.12	0.12	0.13	0.01	0.11	0.09	0.12	0.03	0.11	0.05	0.17	0.12	0.10	0.09	0.12	0.03
6B (Helena, MT)	0.13	0.13	0.15	0.02	0.10	0.09	0.11	0.02	0.11	0.04	0.19	0.15	0.10	0.08	0.11	0.03
7 (Duluth, MN)	0.13	0.12	0.13	0.01	0.10	0.09	0.12	0.03	0.11	0.05	0.17	0.13	0.10	0.09	0.12	0.03
8 (Fairbanks, AK)	0.11	0.09	0.12	0.03	0.07	0.04	0.10	0.06	0.07	0.02	0.13	0.11	0.10	0.06	0.11	0.05

Table C-3. Same as Table B-1, but for cool central wall (ρ=0.60) with a cool neighboring wall (ρ=0.25).

(a) aspect ratio R=0.2

	N				E				S				W			
	mean	min	max	range	mean	min	max	range	mean	min	max	range	mean	min	max	range
1A (Miami, FL)	0.99	0.95	1.05	0.11	0.96	0.92	0.98	0.05	0.96	0.95	0.97	0.03	0.95	0.87	0.97	0.10
2A (Houston, TX)	0.99	0.93	1.05	0.12	0.95	0.90	0.97	0.07	0.96	0.94	0.97	0.03	0.95	0.89	0.97	0.08
2B (Phoenix, AZ)	1.03	0.89	1.18	0.29	0.95	0.90	0.99	0.09	0.97	0.96	0.98	0.02	0.96	0.92	0.98	0.06
3A (Memphis, TN)	1.01	0.96	1.10	0.14	0.96	0.89	0.97	0.09	0.96	0.95	0.97	0.02	0.95	0.88	0.98	0.10
3B (El Paso, TX)	1.04	0.96	1.15	0.20	0.98	0.92	1.00	0.08	0.97	0.96	0.98	0.02	0.97	0.94	0.98	0.04
BU (Burbank, CA)	1.03	0.96	1.13	0.17	0.96	0.92	0.98	0.06	0.97	0.96	0.97	0.02	0.97	0.93	0.99	0.05
FR (Fresno, CA)	1.01	0.97	1.06	0.09	0.96	0.94	0.98	0.05	0.97	0.96	0.98	0.01	0.96	0.94	0.98	0.04
3C (San Francisco, CA)	1.01	0.92	1.11	0.19	0.96	0.91	0.98	0.07	0.97	0.95	0.97	0.02	0.96	0.92	0.98	0.05
4A (Baltimore, MD)	1.01	0.92	1.11	0.19	0.93	0.77	0.97	0.20	0.96	0.92	0.97	0.06	0.94	0.87	0.97	0.10
4B (Albuquerque, NM)	1.06	0.94	1.26	0.32	0.95	0.91	0.99	0.08	0.97	0.96	0.98	0.02	0.96	0.92	0.99	0.07
4C (Seattle, WA)	1.00	0.95	1.06	0.10	0.95	0.89	0.97	0.08	0.96	0.92	0.97	0.05	0.94	0.85	0.97	0.12
5A (Chicago, IL)	1.00	0.95	1.09	0.14	0.94	0.89	0.97	0.08	0.96	0.93	0.97	0.04	0.95	0.87	0.98	0.10
5B (Boise, ID)	1.03	0.96	1.12	0.16	0.95	0.89	0.98	0.08	0.97	0.94	0.98	0.04	0.95	0.90	0.99	0.10
6A (Burlington, VT)	0.99	0.91	1.07	0.16	0.94	0.85	0.97	0.12	0.96	0.92	0.97	0.05	0.94	0.88	0.97	0.09
6B (Helena, MT)	1.04	0.96	1.15	0.19	0.95	0.89	0.97	0.08	0.96	0.92	0.98	0.05	0.94	0.83	0.99	0.16
7 (Duluth, MN)	1.01	0.91	1.11	0.19	0.94	0.86	0.98	0.12	0.96	0.92	0.97	0.05	0.93	0.87	0.97	0.10
8 (Fairbanks, AK)	0.99	0.82	1.13	0.32	0.79	0.57	0.96	0.39	0.81	0.25	0.97	0.73	0.96	0.73	1.01	0.28

Table C-3 (continued)

(b) aspect ratio R=1

	N				E				S				W			
	mean	min	max	range	mean	min	max	range	mean	min	max	range	mean	min	max	range
1A (Miami, FL)	0.87	0.73	1.08	0.35	0.75	0.70	0.78	0.08	0.79	0.73	0.86	0.13	0.75	0.68	0.78	0.11
2A (Houston, TX)	0.89	0.73	1.06	0.32	0.74	0.68	0.77	0.09	0.78	0.64	0.86	0.22	0.73	0.67	0.78	0.11
2B (Phoenix, AZ)	1.03	0.72	1.31	0.59	0.73	0.66	0.77	0.12	0.79	0.57	0.90	0.33	0.73	0.66	0.79	0.12
3A (Memphis, TN)	0.93	0.76	1.09	0.33	0.74	0.67	0.79	0.12	0.76	0.55	0.87	0.32	0.72	0.65	0.79	0.14
3B (El Paso, TX)	1.04	0.78	1.33	0.55	0.75	0.70	0.81	0.10	0.80	0.61	0.89	0.28	0.75	0.69	0.82	0.13
BU (Burbank, CA)	0.98	0.78	1.19	0.41	0.75	0.69	0.82	0.12	0.78	0.57	0.89	0.32	0.76	0.69	0.81	0.12
FR (Fresno, CA)	0.94	0.80	1.14	0.34	0.74	0.69	0.79	0.10	0.79	0.55	0.90	0.35	0.75	0.70	0.79	0.09
3C (San Francisco, CA)	0.93	0.77	1.06	0.29	0.75	0.66	0.82	0.16	0.77	0.51	0.90	0.38	0.74	0.68	0.78	0.10
4A (Baltimore, MD)	0.93	0.75	1.08	0.33	0.71	0.55	0.77	0.22	0.74	0.48	0.87	0.39	0.71	0.63	0.78	0.15
4B (Albuquerque, NM)	1.06	0.79	1.39	0.60	0.72	0.65	0.77	0.12	0.78	0.54	0.90	0.36	0.74	0.66	0.83	0.17
4C (Seattle, WA)	0.87	0.80	0.99	0.19	0.71	0.65	0.78	0.13	0.70	0.41	0.87	0.45	0.70	0.60	0.78	0.18
5A (Chicago, IL)	0.89	0.77	0.99	0.23	0.71	0.62	0.76	0.14	0.72	0.45	0.87	0.42	0.72	0.62	0.78	0.15
5B (Boise, ID)	0.97	0.81	1.20	0.40	0.70	0.61	0.76	0.15	0.74	0.42	0.91	0.49	0.71	0.62	0.79	0.16
6A (Burlington, VT)	0.86	0.73	0.97	0.24	0.70	0.61	0.75	0.14	0.72	0.43	0.86	0.43	0.70	0.62	0.75	0.13
6B (Helena, MT)	0.95	0.81	1.09	0.28	0.69	0.60	0.75	0.16	0.71	0.37	0.89	0.52	0.68	0.55	0.77	0.22
7 (Duluth, MN)	0.90	0.77	1.01	0.24	0.69	0.60	0.76	0.16	0.70	0.39	0.87	0.48	0.68	0.61	0.75	0.14
8 (Fairbanks, AK)	0.81	0.63	0.98	0.35	0.48	0.29	0.67	0.38	0.52	0.12	0.87	0.76	0.71	0.43	0.79	0.36

Table C-3 (continued)

(c) aspect ratio R=2

	N				E				S				W			
	mean	min	max	range	mean	min	max	range	mean	min	max	range	mean	min	max	range
1A (Miami, FL)	0.67	0.55	0.79	0.24	0.54	0.50	0.57	0.07	0.58	0.42	0.72	0.30	0.54	0.49	0.58	0.09
2A (Houston, TX)	0.68	0.56	0.81	0.25	0.54	0.49	0.56	0.07	0.56	0.37	0.73	0.35	0.53	0.47	0.57	0.10
2B (Phoenix, AZ)	0.82	0.58	0.95	0.37	0.52	0.47	0.56	0.09	0.59	0.32	0.80	0.48	0.53	0.46	0.58	0.11
3A (Memphis, TN)	0.71	0.59	0.80	0.21	0.53	0.47	0.58	0.10	0.56	0.32	0.74	0.42	0.52	0.46	0.58	0.12
3B (El Paso, TX)	0.81	0.61	0.97	0.36	0.54	0.50	0.59	0.09	0.59	0.34	0.78	0.44	0.54	0.49	0.60	0.11
BU (Burbank, CA)	0.77	0.62	0.87	0.25	0.54	0.49	0.60	0.11	0.58	0.32	0.78	0.46	0.55	0.48	0.59	0.11
FR (Fresno, CA)	0.74	0.63	0.95	0.32	0.54	0.49	0.57	0.08	0.59	0.33	0.81	0.49	0.54	0.49	0.58	0.09
3C (San Francisco, CA)	0.73	0.62	0.89	0.26	0.55	0.46	0.61	0.15	0.57	0.30	0.77	0.48	0.53	0.48	0.57	0.09
4A (Baltimore, MD)	0.71	0.60	0.79	0.19	0.51	0.38	0.56	0.18	0.53	0.28	0.72	0.44	0.51	0.44	0.57	0.14
4B (Albuquerque, NM)	0.83	0.63	1.01	0.39	0.52	0.46	0.56	0.10	0.58	0.30	0.79	0.49	0.53	0.46	0.62	0.15
4C (Seattle, WA)	0.67	0.60	0.74	0.15	0.51	0.45	0.58	0.12	0.51	0.25	0.76	0.51	0.50	0.42	0.57	0.15
5A (Chicago, IL)	0.68	0.61	0.74	0.12	0.51	0.43	0.55	0.12	0.52	0.27	0.71	0.44	0.52	0.43	0.57	0.13
5B (Boise, ID)	0.76	0.64	0.95	0.31	0.49	0.43	0.55	0.12	0.54	0.25	0.80	0.55	0.51	0.44	0.57	0.13
6A (Burlington, VT)	0.66	0.58	0.72	0.14	0.50	0.42	0.54	0.12	0.52	0.26	0.71	0.46	0.50	0.44	0.55	0.11
6B (Helena, MT)	0.73	0.66	0.83	0.17	0.48	0.41	0.54	0.12	0.51	0.21	0.80	0.59	0.48	0.37	0.56	0.18
7 (Duluth, MN)	0.69	0.63	0.74	0.12	0.49	0.42	0.55	0.13	0.50	0.23	0.74	0.51	0.48	0.42	0.54	0.12
8 (Fairbanks, AK)	0.59	0.47	0.71	0.25	0.32	0.19	0.46	0.27	0.33	0.08	0.61	0.53	0.50	0.30	0.57	0.27

Table C-3 (continued)

(d) aspect ratio R=10

	N				E				S				W			
	mean	min	max	range	mean	min	max	range	mean	min	max	range	mean	min	max	range
1A (Miami, FL)	0.21	0.18	0.23	0.05	0.15	0.14	0.16	0.02	0.18	0.10	0.24	0.14	0.16	0.14	0.17	0.03
2A (Houston, TX)	0.21	0.20	0.24	0.04	0.15	0.14	0.16	0.03	0.17	0.09	0.24	0.15	0.15	0.13	0.17	0.03
2B (Phoenix, AZ)	0.26	0.23	0.28	0.05	0.15	0.13	0.16	0.03	0.19	0.08	0.33	0.26	0.15	0.13	0.16	0.04
3A (Memphis, TN)	0.22	0.21	0.23	0.02	0.16	0.14	0.17	0.04	0.17	0.08	0.26	0.18	0.15	0.13	0.18	0.04
3B (El Paso, TX)	0.26	0.23	0.28	0.05	0.16	0.14	0.18	0.04	0.19	0.08	0.33	0.25	0.16	0.14	0.18	0.05
BU (Burbank, CA)	0.24	0.22	0.27	0.05	0.16	0.14	0.19	0.04	0.18	0.08	0.30	0.23	0.16	0.14	0.18	0.04
FR (Fresno, CA)	0.23	0.18	0.28	0.10	0.16	0.14	0.17	0.03	0.18	0.08	0.31	0.23	0.16	0.14	0.17	0.03
3C (San Francisco, CA)	0.22	0.20	0.26	0.06	0.16	0.13	0.18	0.05	0.17	0.07	0.28	0.21	0.15	0.14	0.17	0.03
4A (Baltimore, MD)	0.22	0.20	0.23	0.03	0.15	0.11	0.16	0.06	0.15	0.07	0.25	0.18	0.15	0.13	0.17	0.05
4B (Albuquerque, NM)	0.26	0.24	0.29	0.06	0.15	0.13	0.17	0.04	0.18	0.07	0.33	0.26	0.16	0.13	0.19	0.05
4C (Seattle, WA)	0.20	0.17	0.22	0.05	0.15	0.13	0.17	0.04	0.13	0.07	0.21	0.15	0.14	0.12	0.17	0.05
5A (Chicago, IL)	0.20	0.19	0.21	0.03	0.15	0.12	0.16	0.04	0.15	0.07	0.24	0.17	0.15	0.12	0.17	0.04
5B (Boise, ID)	0.23	0.18	0.27	0.09	0.14	0.12	0.16	0.04	0.15	0.06	0.26	0.20	0.14	0.12	0.17	0.05
6A (Burlington, VT)	0.20	0.17	0.21	0.04	0.14	0.12	0.16	0.04	0.14	0.07	0.22	0.15	0.14	0.12	0.16	0.04
6B (Helena, MT)	0.22	0.21	0.24	0.04	0.13	0.12	0.15	0.03	0.14	0.05	0.23	0.18	0.13	0.11	0.15	0.05
7 (Duluth, MN)	0.20	0.19	0.22	0.03	0.14	0.12	0.16	0.04	0.13	0.06	0.22	0.16	0.14	0.12	0.16	0.04
8 (Fairbanks, AK)	0.17	0.14	0.21	0.07	0.09	0.05	0.13	0.08	0.09	0.02	0.16	0.14	0.14	0.08	0.16	0.08

Task Report Appendix D: Monthly SAF increase plots by climate zone

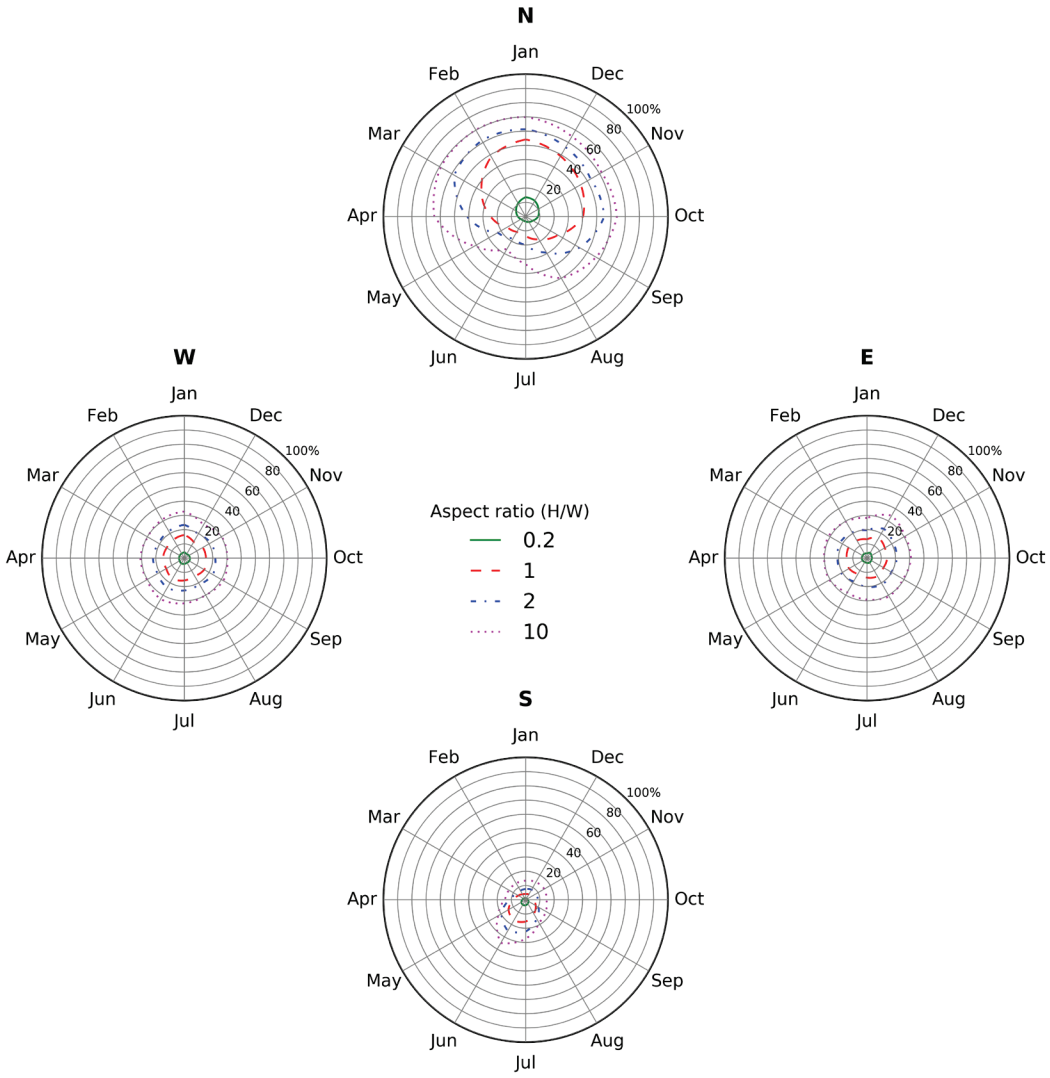

ground albedo = 0.20, central wall albedo = 0.25, neighboring wall albedo ratio = 0.60 / 0.25

(a)

Figure D-1. Percentage increases in monthly SAFs for a north (N), east (E), south (S), or west (W) conventional central wall (ρ=0.25) upon raising the albedo of its neighboring wall to 0.60 (cool) from 0.25 (conventional). Results shown for aspect ratios 0.2, 1, 2, and 10 in each of 17 climates (panels a through q).

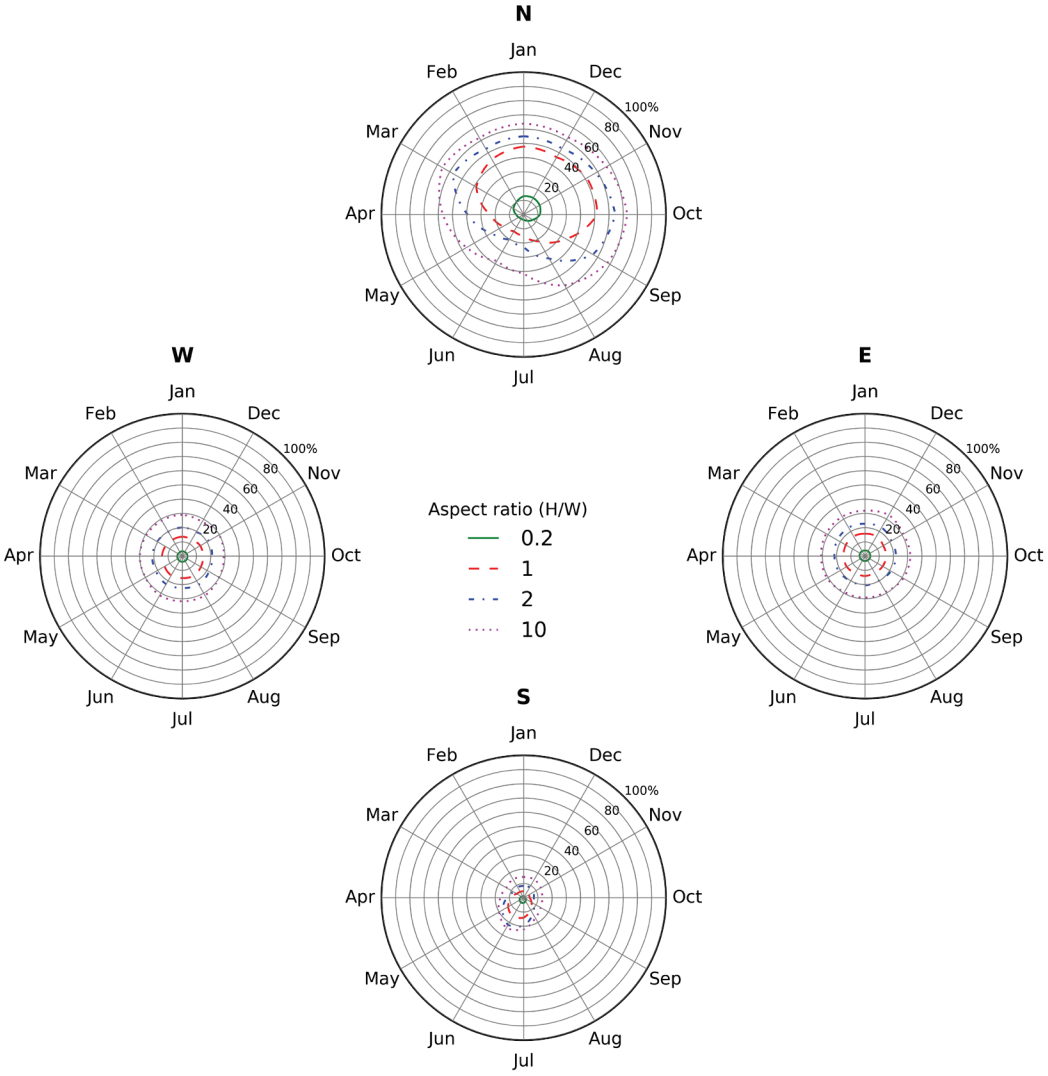

ground albedo = 0.20, central wall albedo = 0.25, neighboring wall albedo ratio = 0.60 / 0.25

(b)

Figure D-1 (continued)

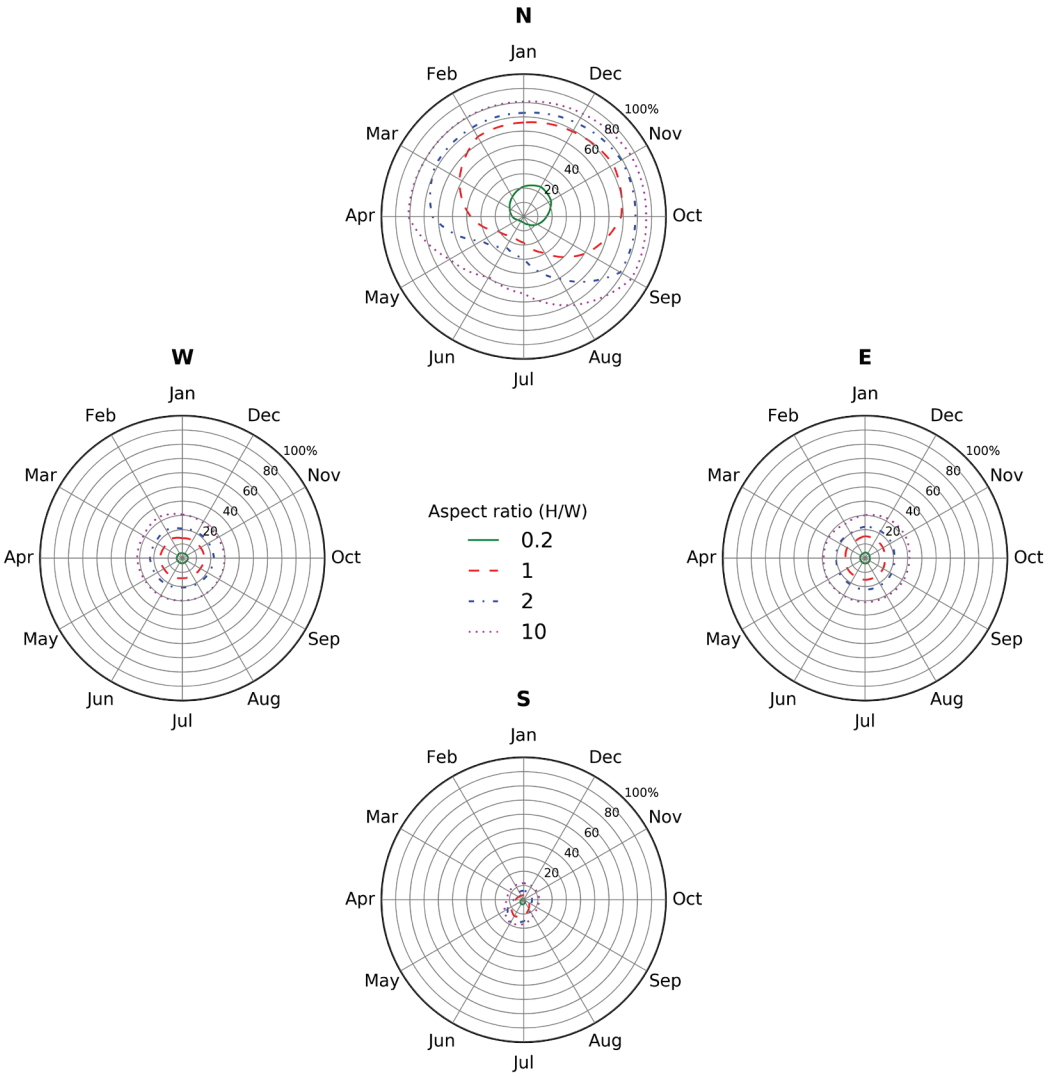

ground albedo = 0.20, central wall albedo = 0.25, neighboring wall albedo ratio = 0.60 / 0.25

(c)

Figure D-1 (continued)

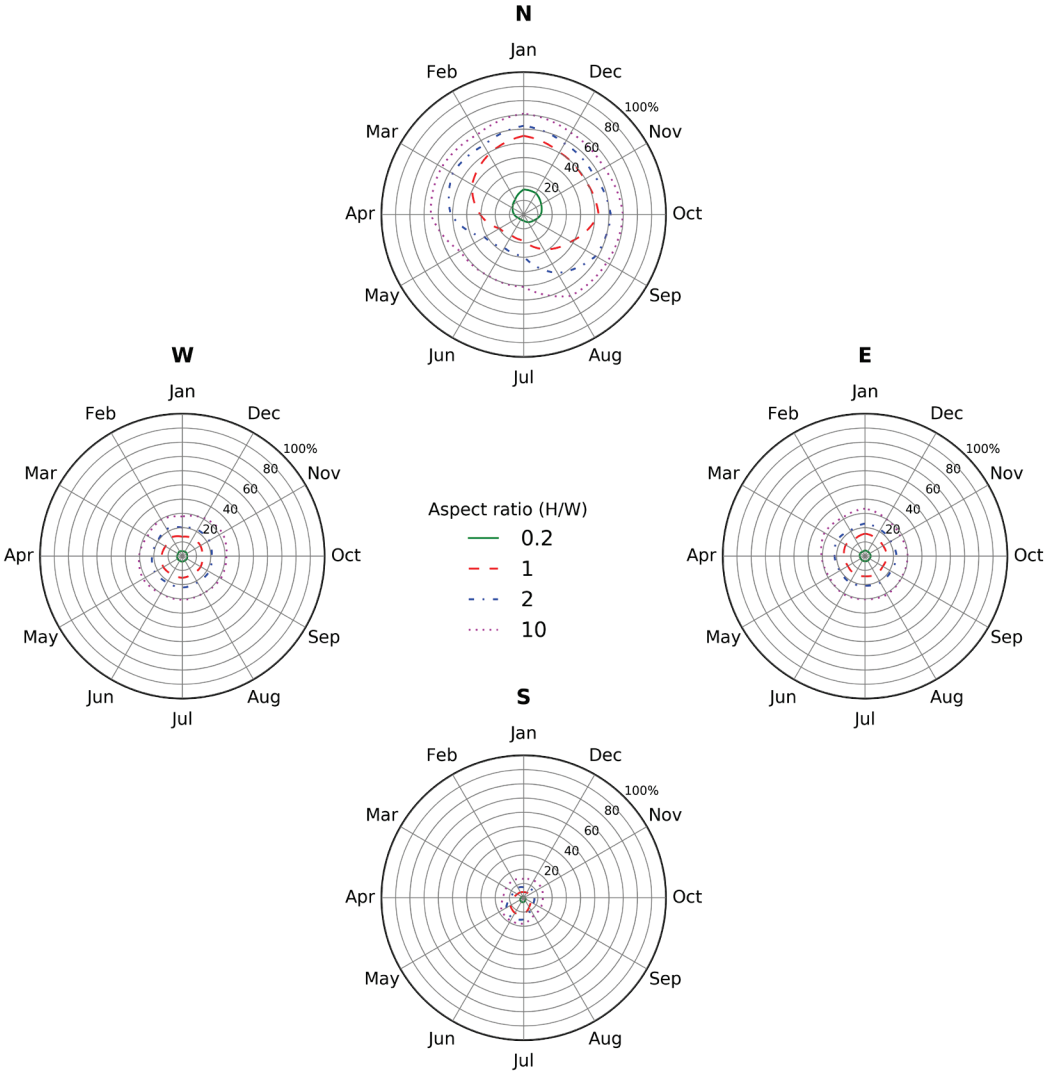

ground albedo = 0.20, central wall albedo = 0.25, neighboring wall albedo ratio = 0.60 / 0.25

(d)

Figure D-1 (continued)

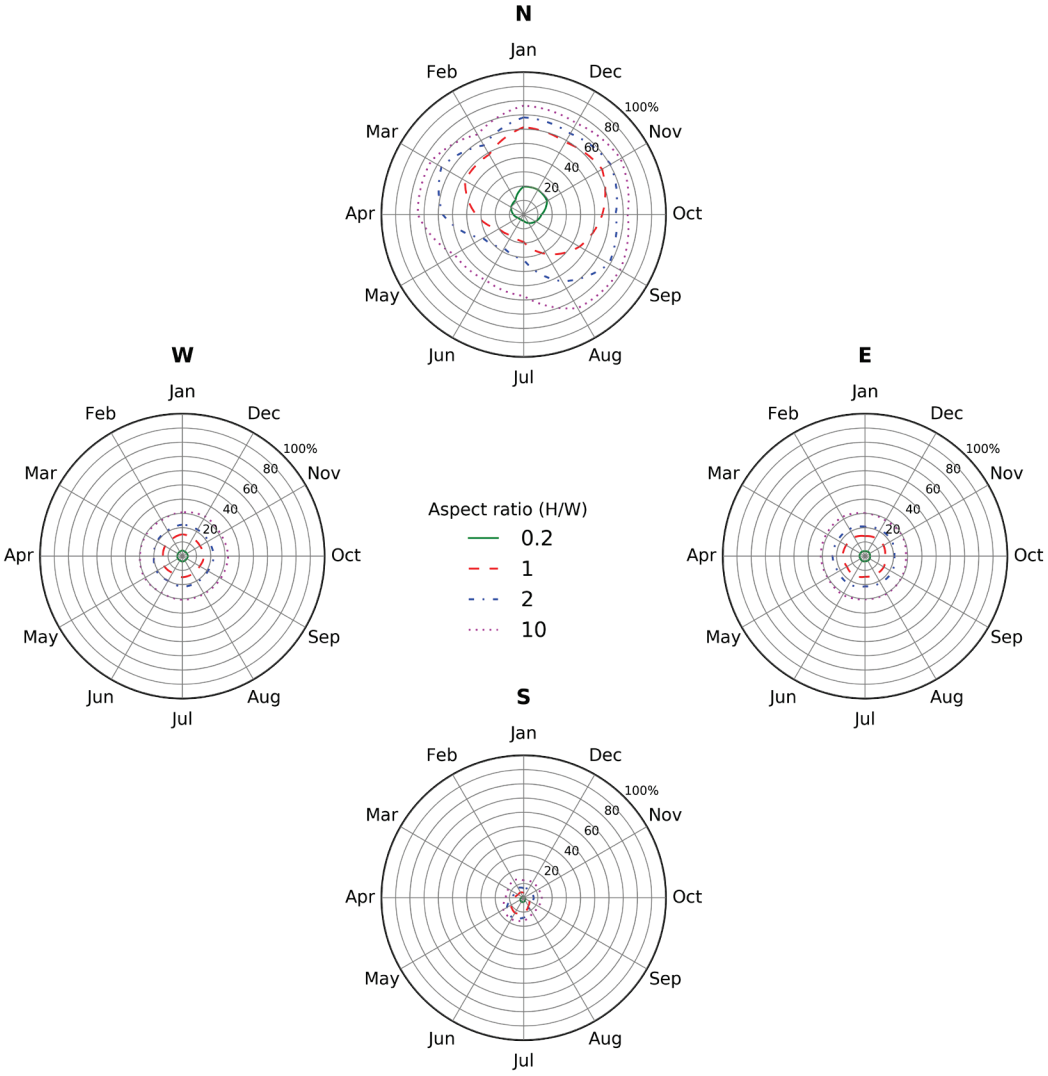

ground albedo = 0.20, central wall albedo = 0.25, neighboring wall albedo ratio = 0.60 / 0.25

(e)

Figure D-1 (continued)

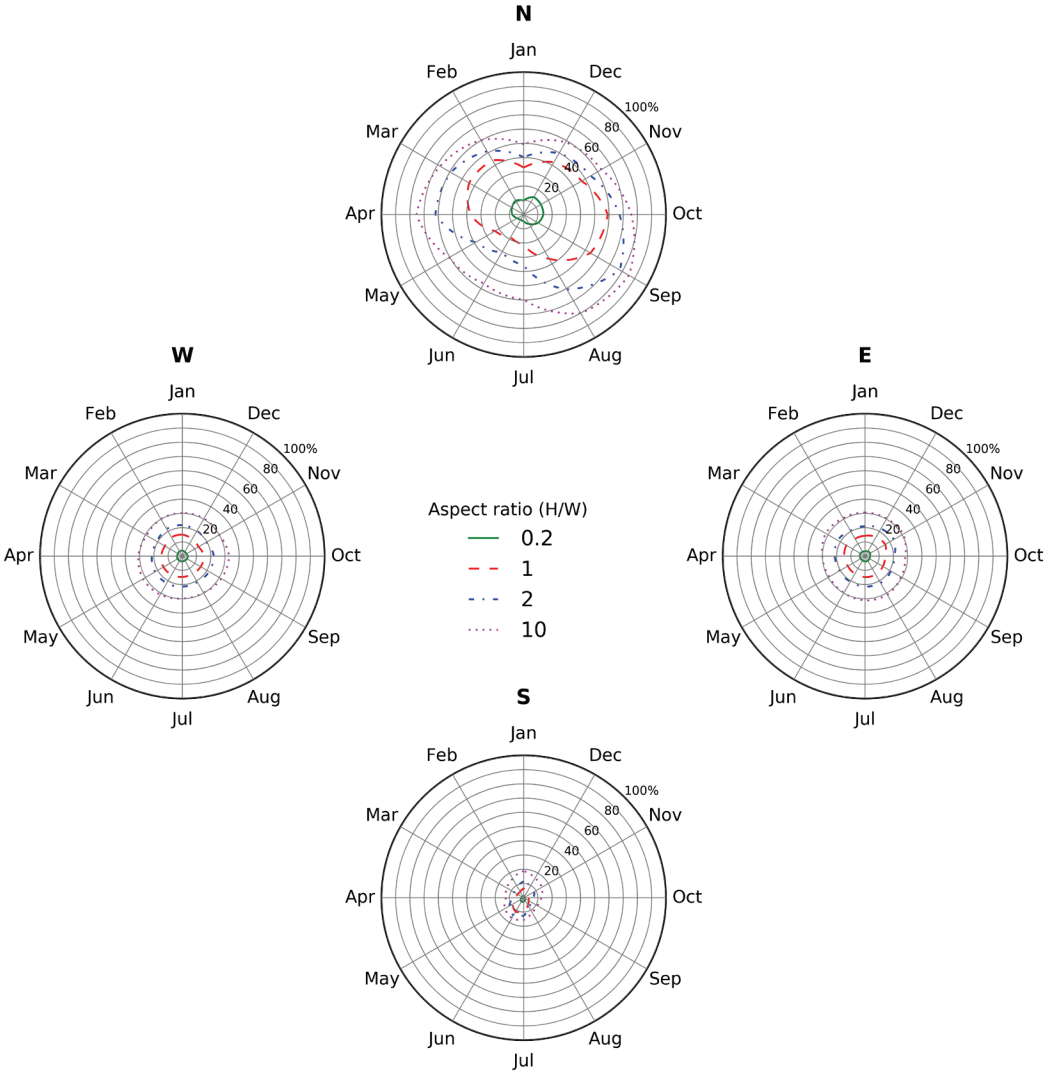

ground albedo = 0.20, central wall albedo = 0.25, neighboring wall albedo ratio = 0.60 / 0.25

(f)

Figure D-1 (continued)

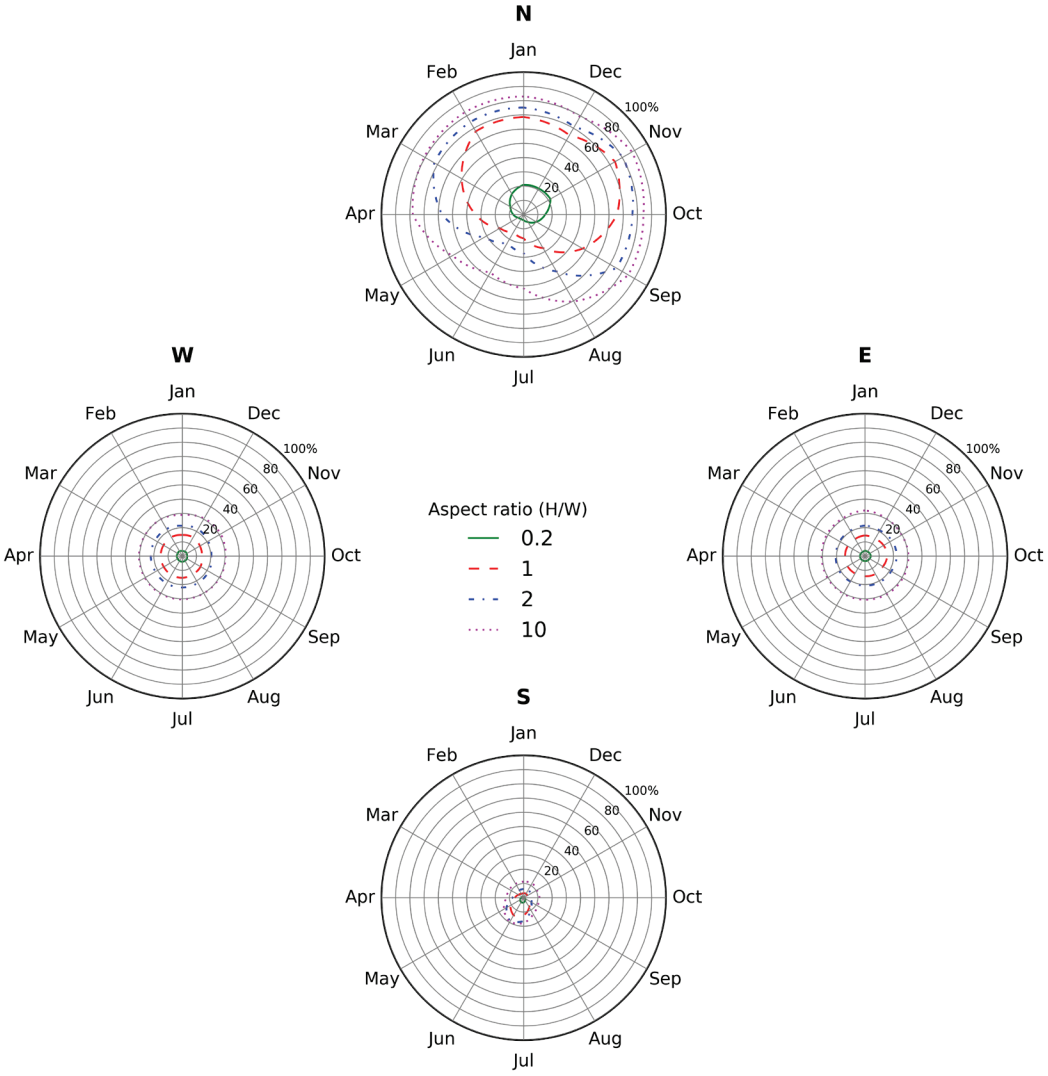

ground albedo = 0.20, central wall albedo = 0.25, neighboring wall albedo ratio = 0.60 / 0.25

(g)

Figure D-1 (continued)

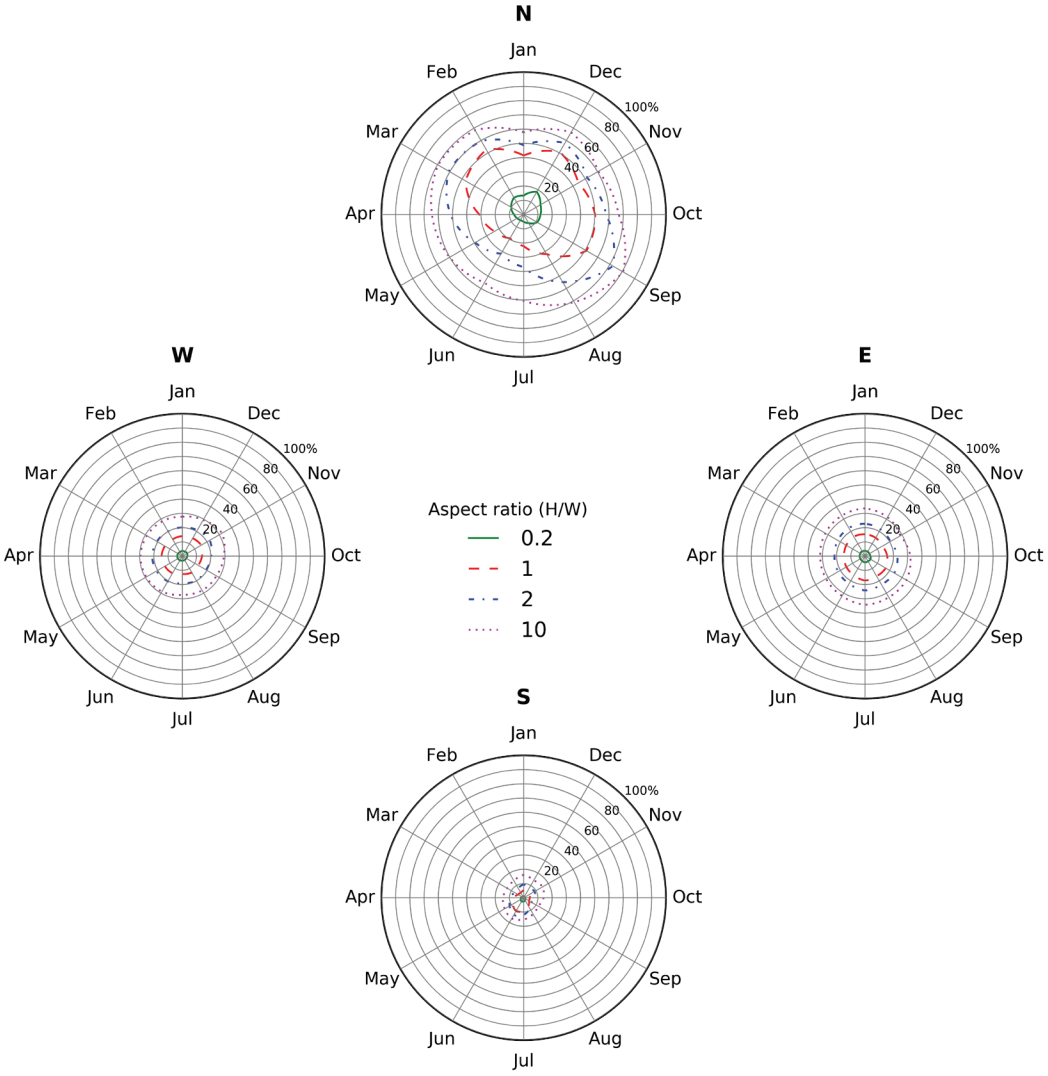

ground albedo = 0.20, central wall albedo = 0.25, neighboring wall albedo ratio = 0.60 / 0.25

(h)

Figure D-1 (continued)

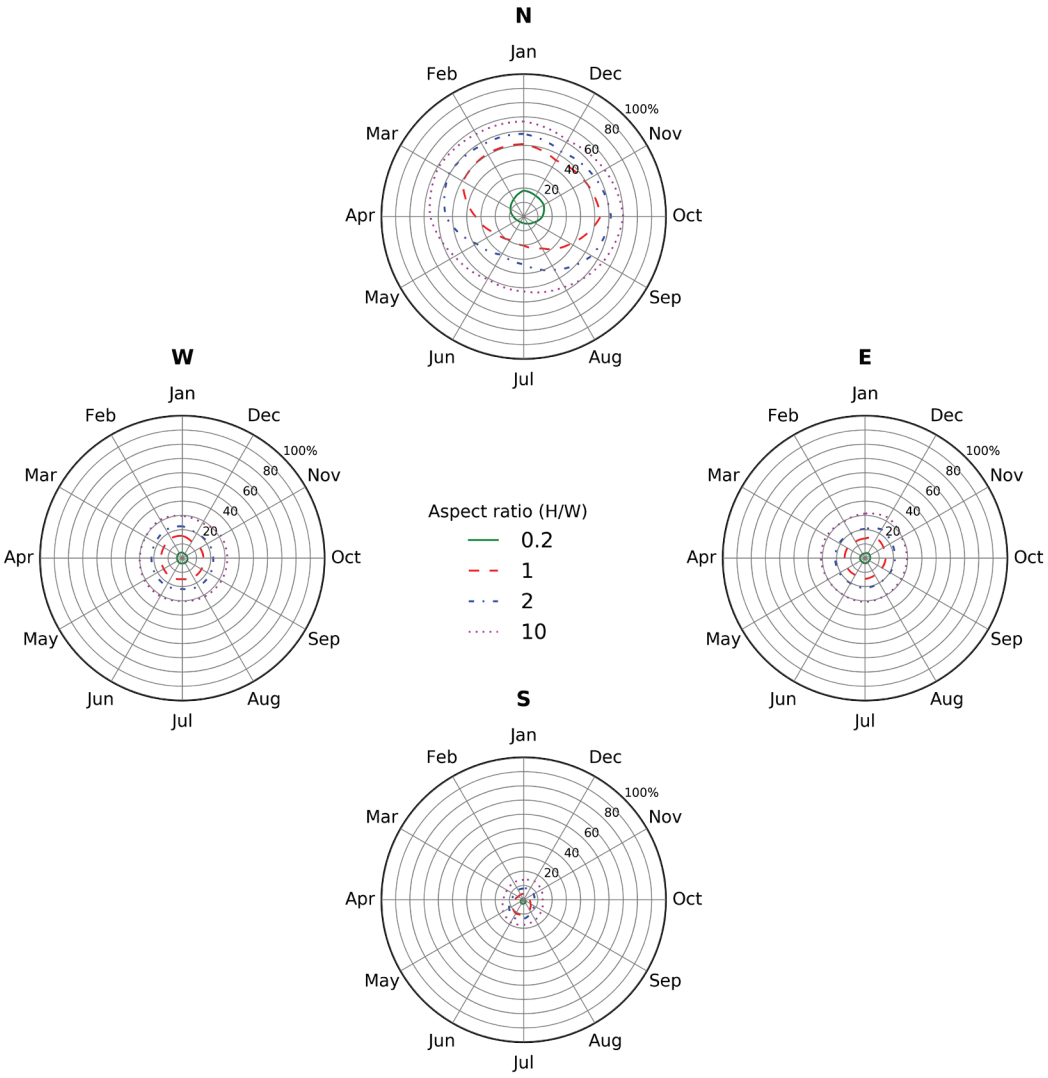

ground albedo = 0.20, central wall albedo = 0.25, neighboring wall albedo ratio = 0.60 / 0.25

(i)

Figure D-1 (continued)

Solar availability factor increases in climate 4B (Albuquerque, NM)

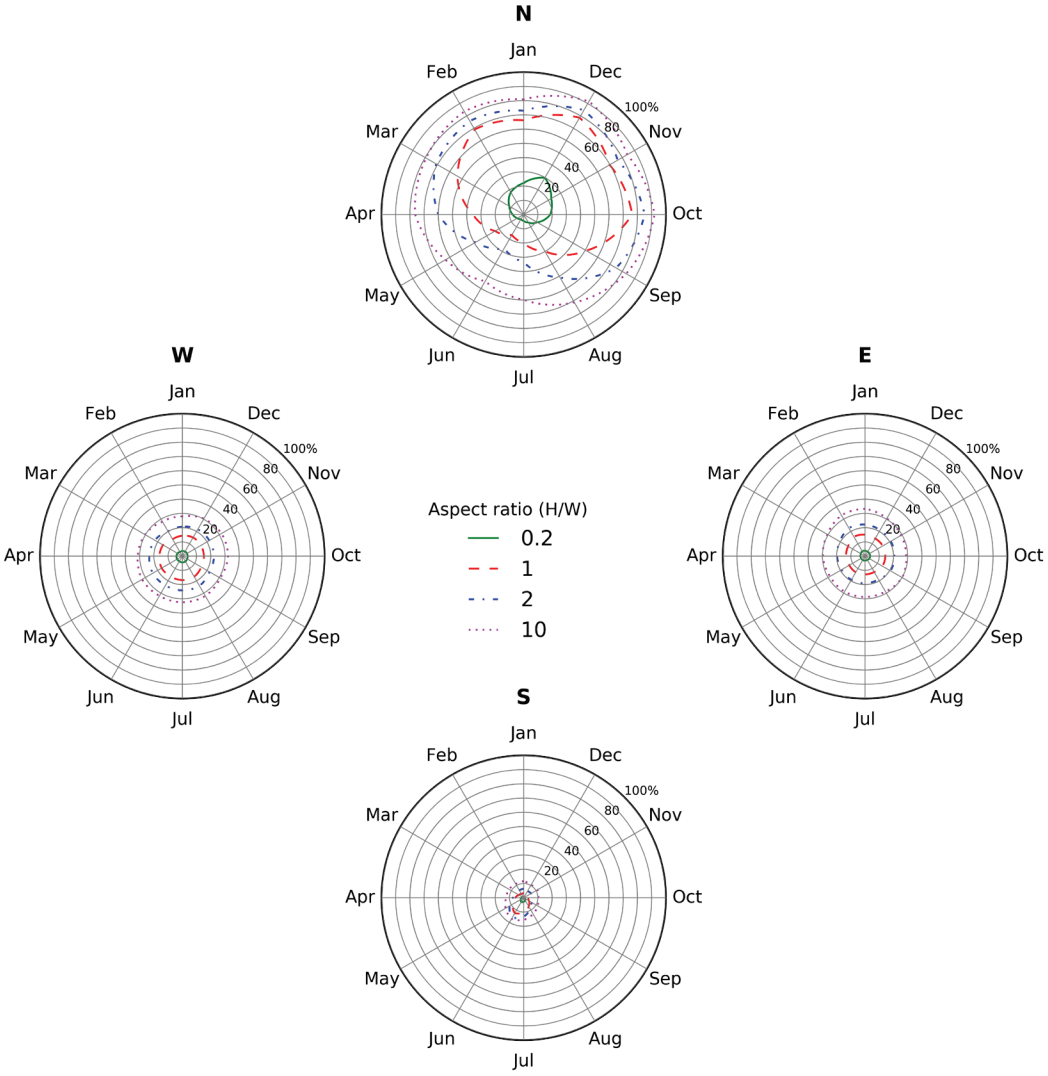

ground albedo = 0.20, central wall albedo = 0.25, neighboring wall albedo ratio = 0.60 / 0.25

(j)

Figure D-1 (continued)

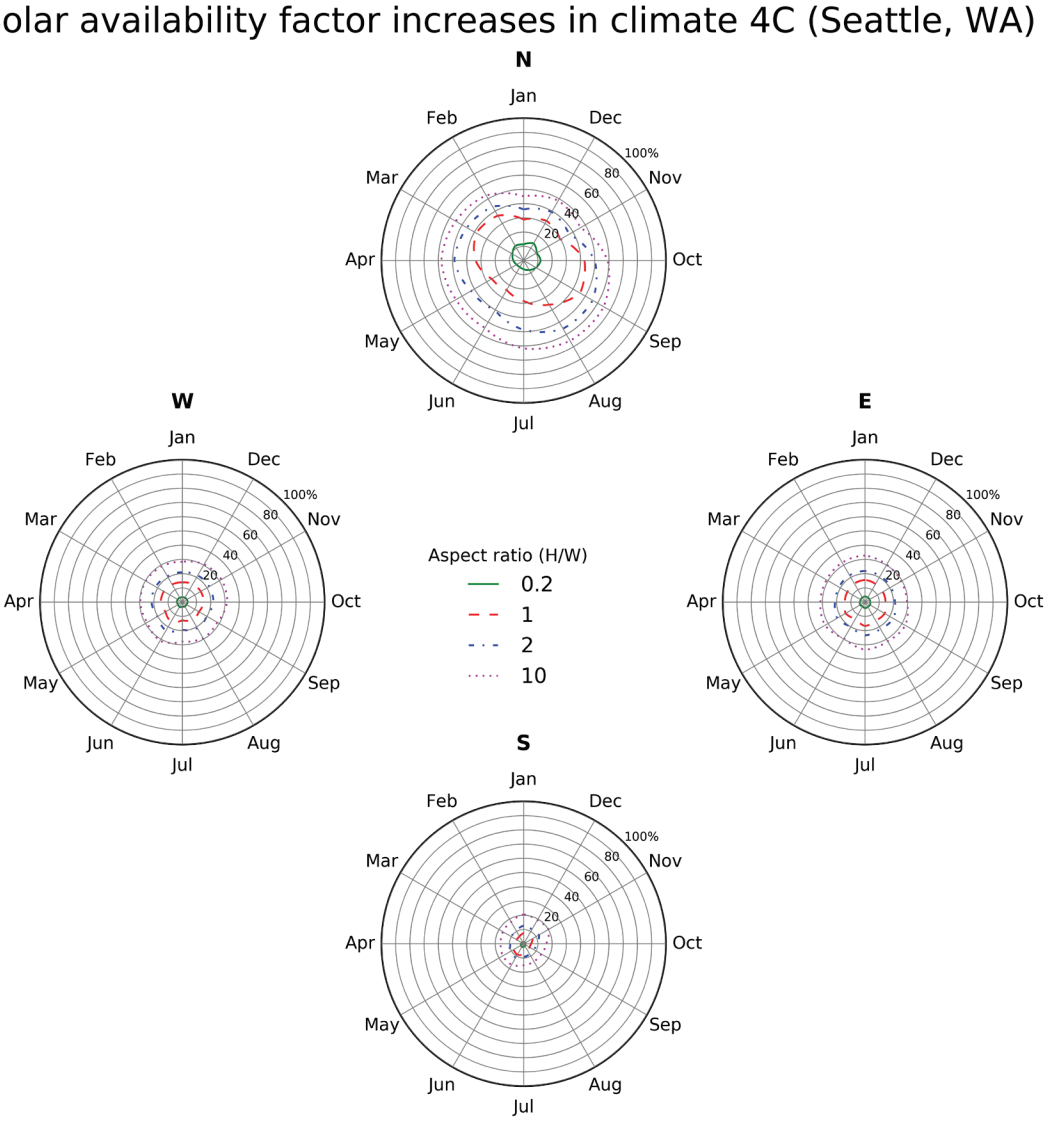

ground albedo = 0.20, central wall albedo = 0.25, neighboring wall albedo ratio = 0.60 / 0.25

(k)

Figure D-1 (continued)

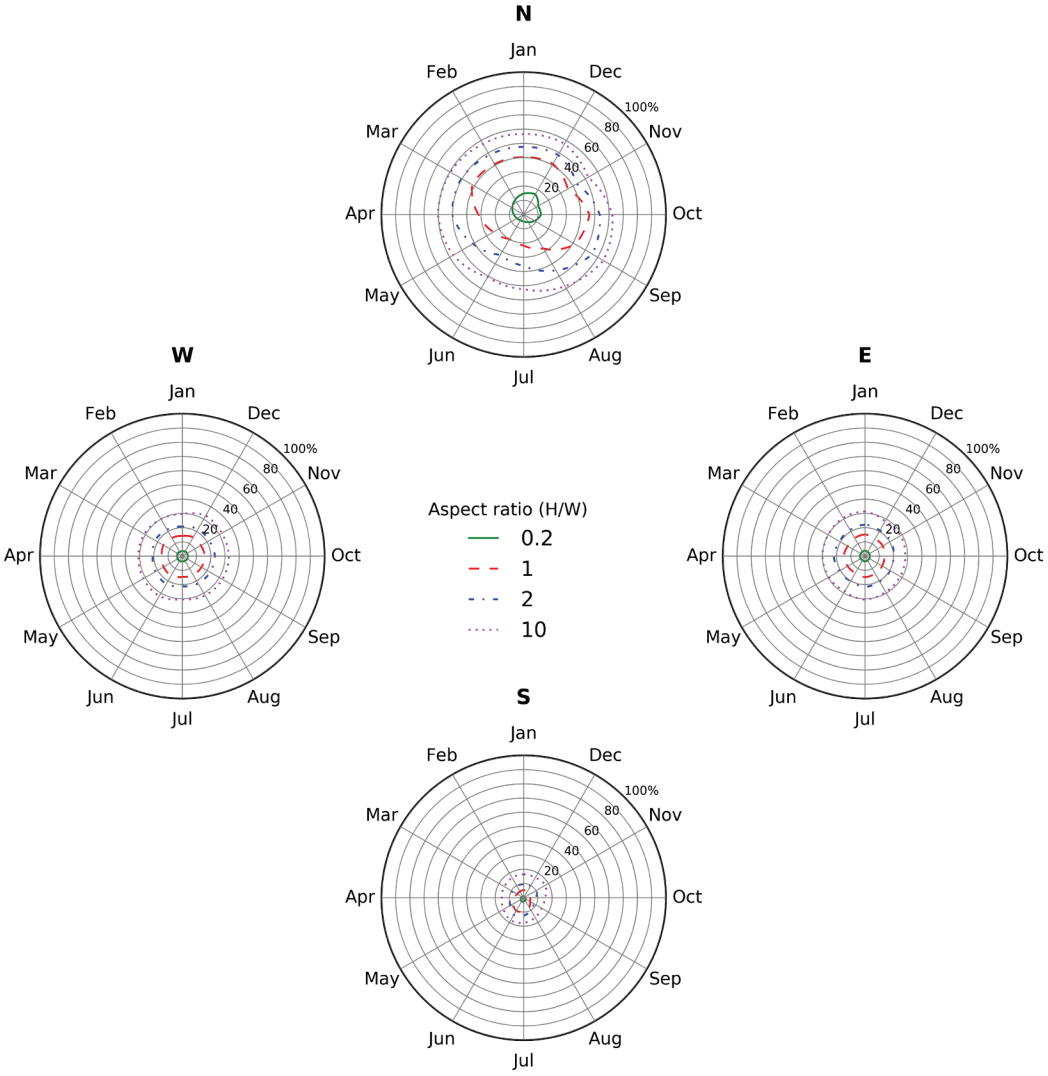

ground albedo = 0.20, central wall albedo = 0.25, neighboring wall albedo ratio = 0.60 / 0.25

(l)

Figure D-1 (continued)

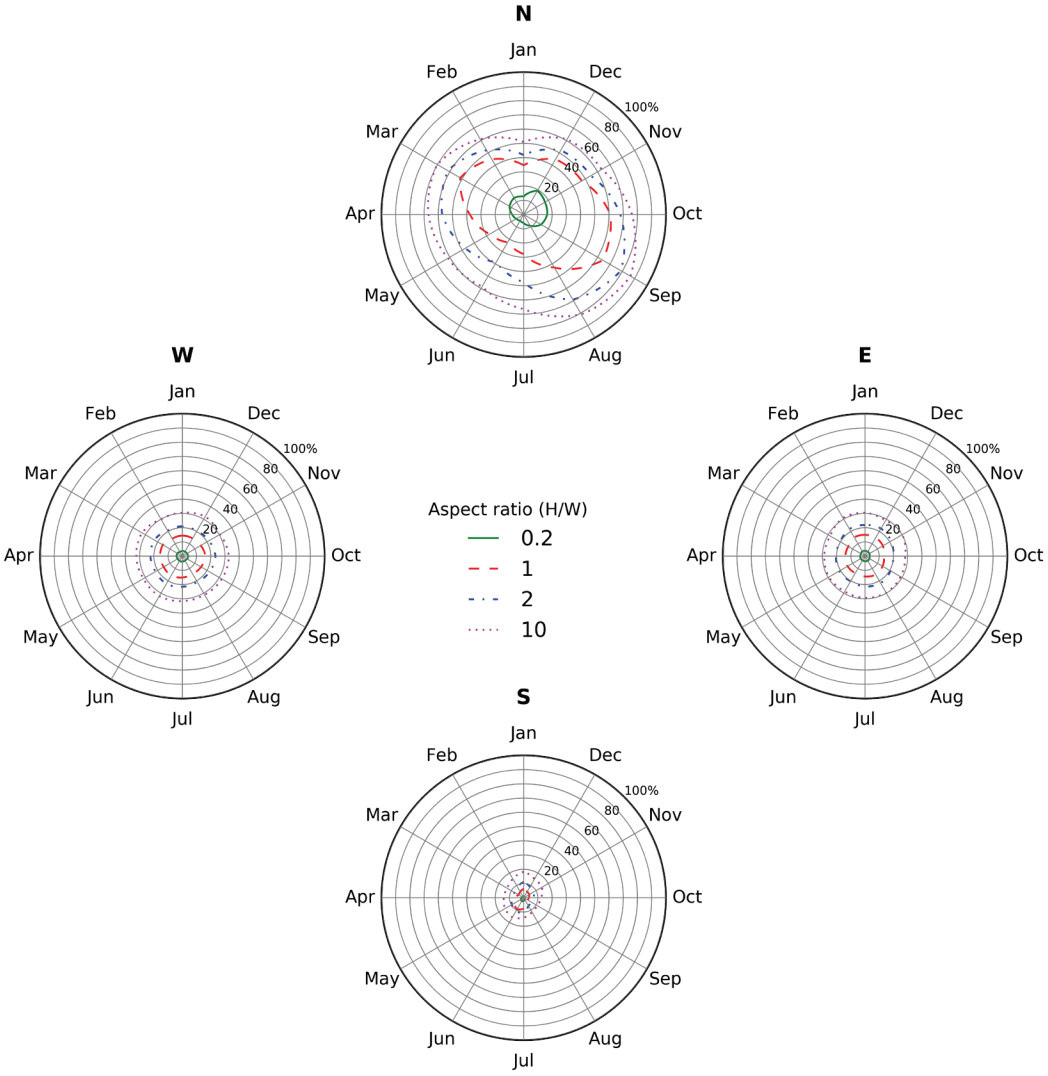

ground albedo = 0.20, central wall albedo = 0.25, neighboring wall albedo ratio = 0.60 / 0.25

(m)

Figure D-1 (continued)

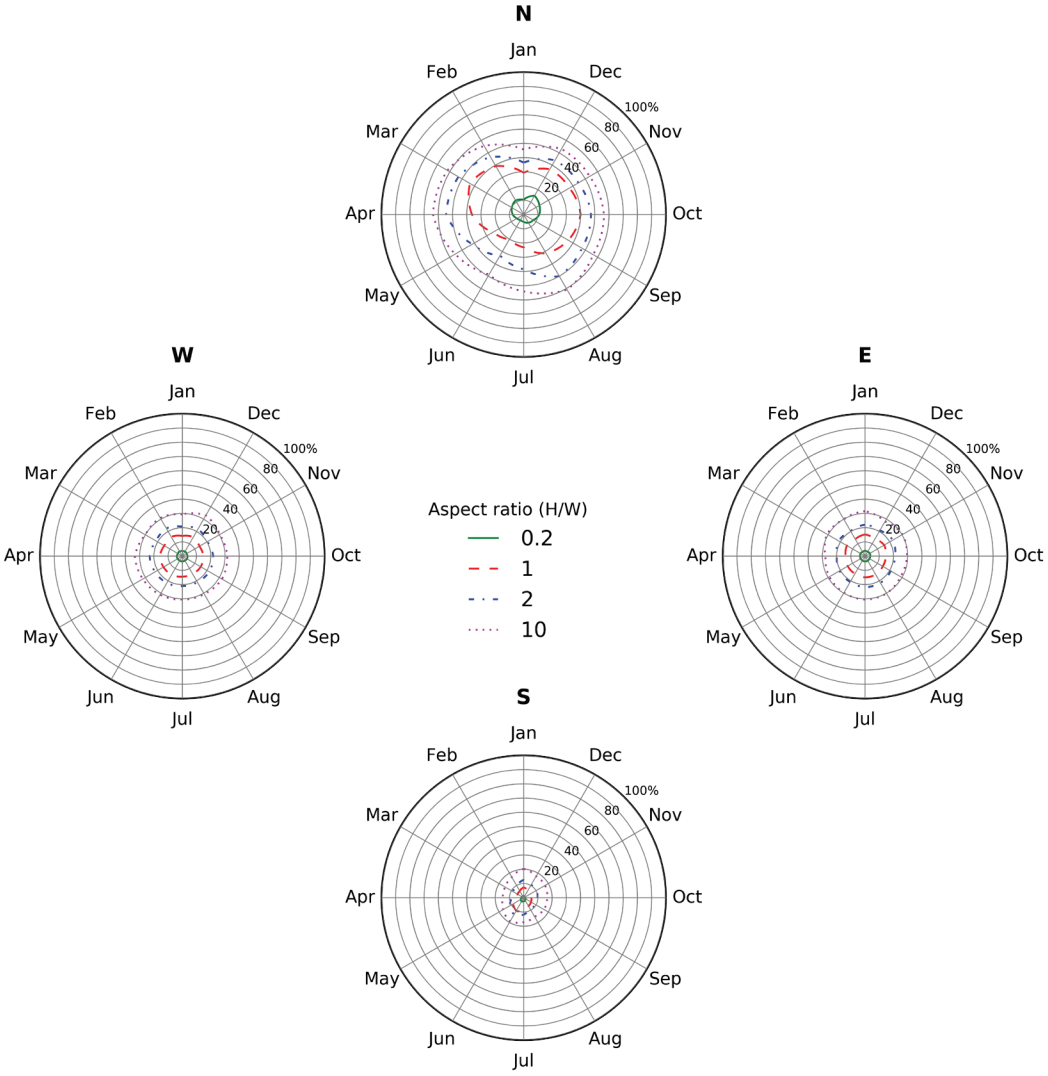

ground albedo = 0.20, central wall albedo = 0.25, neighboring wall albedo ratio = 0.60 / 0.25

(n)

Figure D-1 (continued)

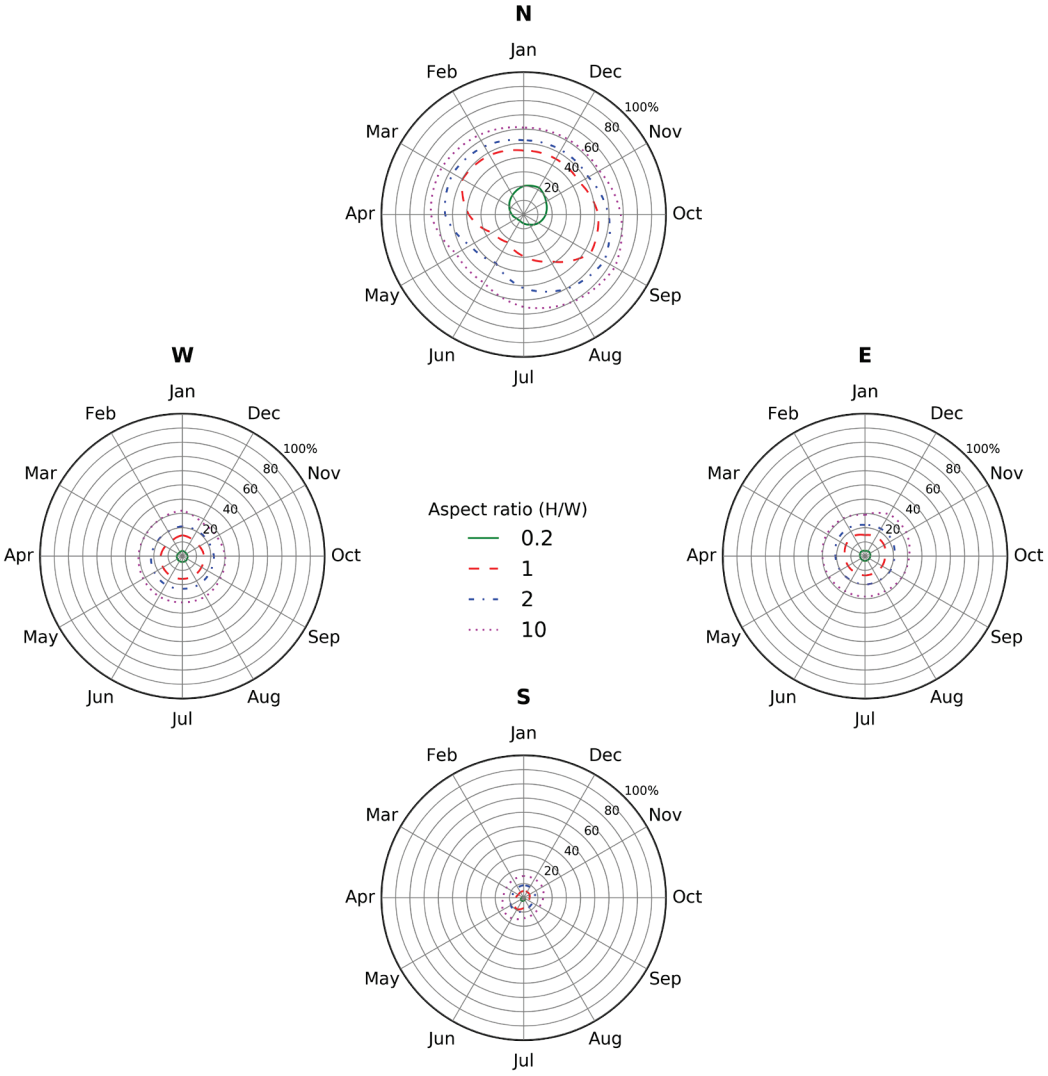

ground albedo = 0.20, central wall albedo = 0.25, neighboring wall albedo ratio = 0.60 / 0.25

(o)

Figure D-1 (continued)

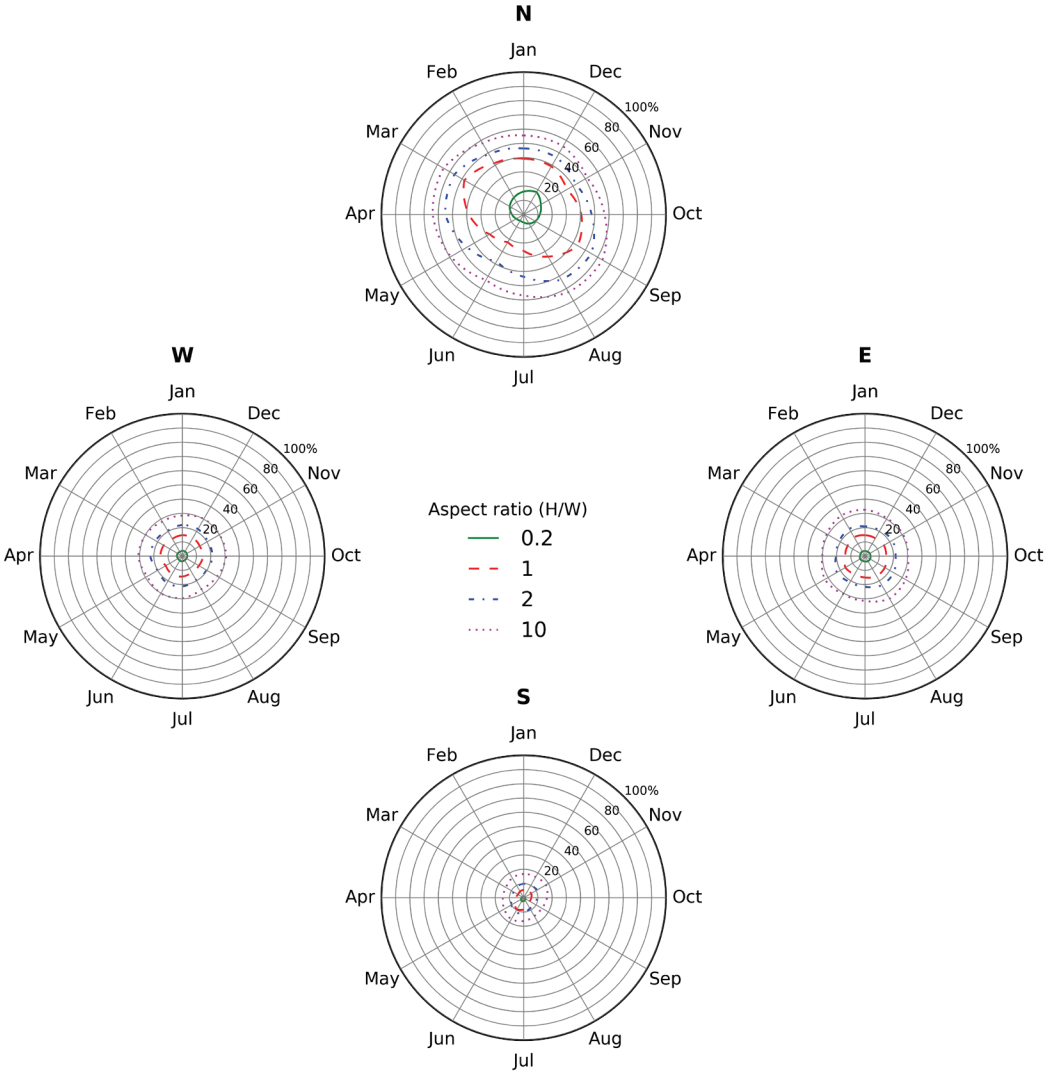

ground albedo = 0.20, central wall albedo = 0.25, neighboring wall albedo ratio = 0.60 / 0.25

(p)

Figure D-1 (continued)

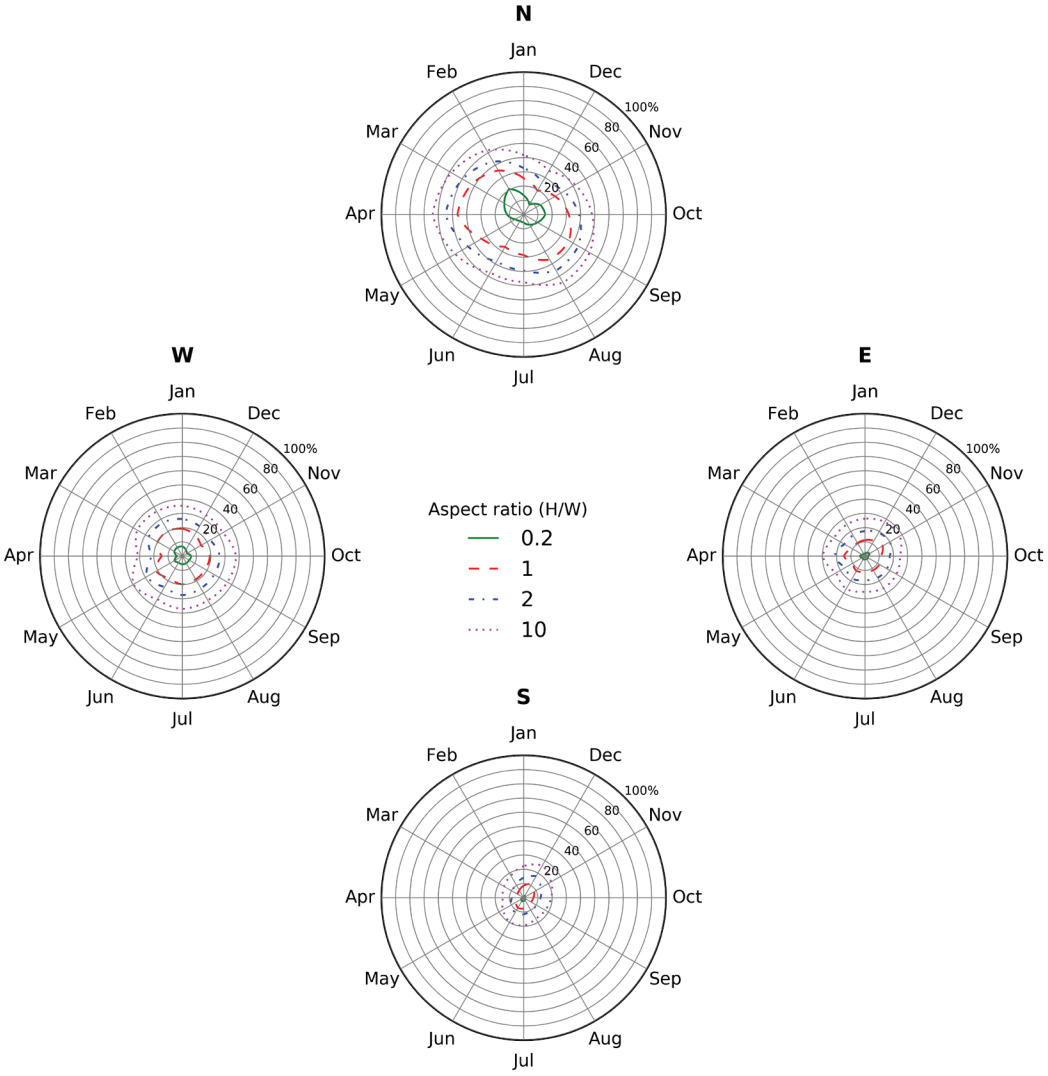

ground albedo = 0.20, central wall albedo = 0.25, neighboring wall albedo ratio = 0.60 / 0.25

(q)

Figure D-1 (continued)

Energy Research and Development Division

FINAL PROJECT REPORT

Solar-Reflective "Cool" Walls: Benefits, Technologies, and Implementation

Appendix D: Pedestrian Mean Radiant Temperature and Thermal Comfort (Task 3.1 Report)

California Energy Commission
Gavin Newsom, Governor

April 2019 | CEC-500-2019-040-APD

Appendix D: Pedestrian mean radiant temperature and thermal comfort (Task 3.1 report)

Matteo Pizzicotti[1], Ronnen Levinson[2], Nathalie Dumas[1], Benjamin Kurtz[1], Yan Long[1], Negin Nazarian[1], Weilong Zhang[1], Jan Kleissl[1]

[1] Center for Energy Research, University of California, San Diego

[2] Heat Island Group, Lawrence Berkeley National Laboratory

28 February 2018

Abstract

Cool walls affect the thermal environment of pedestrians by (a) increasing shortwave (solar) radiation striking the pedestrian; (b) decreasing longwave (thermal infrared) radiation incident on the pedestrian; and (c) lowering the outside air temperature. Human thermal comfort was quantified through the Standard Equivalent Temperature, SET* for homogeneous neighborhoods of different building types with cool walls. For reference, near a conventional-wall of albedo 0.25 the average diurnal cycle shows a SET* of about 18 ˚C at night and up to 30 ˚C during the day. The pedestrian thermal comfort change due to cool walls is small. During daytime, cool walls raise SET* by up to 0.5 ˚C on average over the year. At night, cool walls lower SET* by up to 0.3 ˚C on average over the year. Since thermal sensation in California is generally too warm the daytime SET* rise corresponds to a slight worsening of thermal comfort. However, the SET* rise is so small that it will go unnoticed by most people. While SET* increases over 0.5 ˚C are occasionally observed, they occur exclusively during clear winter days when the SET* increase is beneficial to pedestrian thermal comfort. SET* differences by building type and climate zone were negligible.

1 Introduction and scope

High albedo (“cool”) walls are exterior building walls with surface (usually paint) properties that increase reflection of solar radiation. Albedo is the fraction of incident sunlight reflected, or “solar reflectance”, of a material. Cool walls reduce the wall’s solar heat gain, which can reduce heat conducted inward through the wall on a hot day, or increase heat conducted outward on a cold day. Cool walls also affect the thermal environment of pedestrians by (a) increasing

shortwave (solar) radiation striking the pedestrian; (b) decreasing longwave (thermal infrared) radiation incident on the pedestrian; and (c) lowering the outside air temperature. The magnitudes of these sometimes-opposing effects on pedestrians are quantified in this report.

The human temperature sensation is approximated through thermal comfort models. Pedestrian thermal comfort depends on clothing and activity as well as meteorological factors including mean radiant temperature (MRT), air temperature, humidity, and wind speed. Raising wall albedo is expected to raise MRT and lower urban air temperature.

MRT and a thermal comfort index are calculated using a building-to-canopy model called TUF-IOBES (Temperature of Urban Facets – Indoor Outdoor Building Energy Simulator). TUF-IOBES simulates heat transfer in a small neighborhood of identical buildings to obtain indoor air, outdoor air, façade, and roof temperatures, and radiative, convective, and conductive heat fluxes. To understand thermal impact on pedestrians, calculations are performed for a person walking near the center of the base of each wall of the central building unit, as shown in Figure 1. Calculations are performed hourly for a typical meteorological year (TMY).

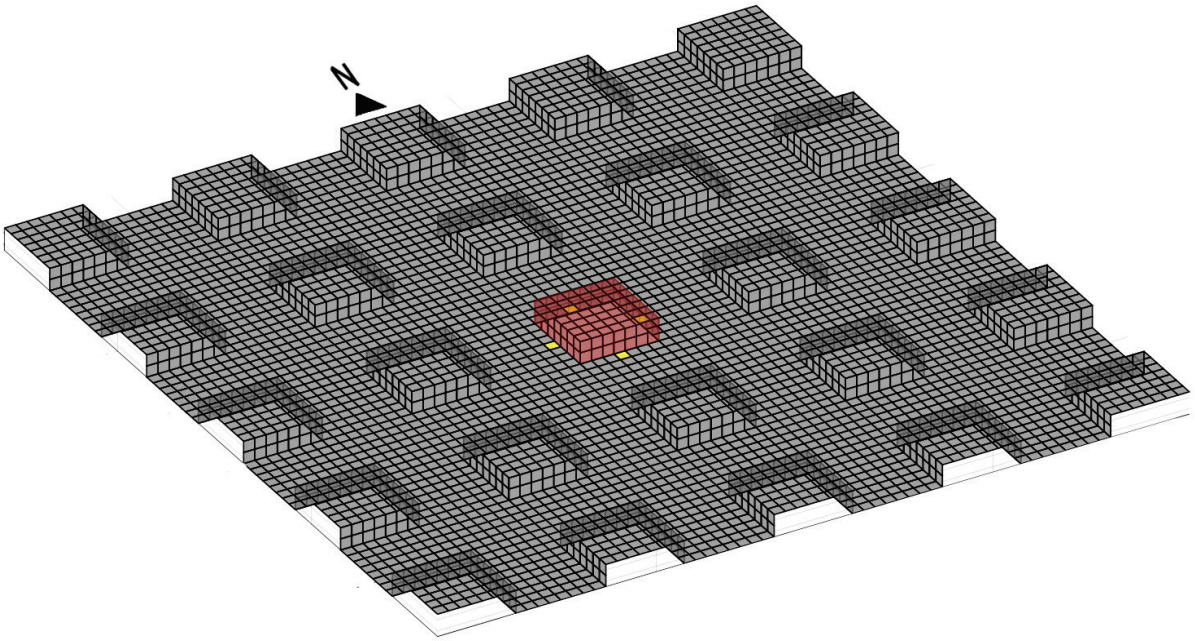

Figure 1. Example of the calculation domain for multi-family residences. The locations of the pedestrian are shown in yellow. The central building unit is highlighted in red.

The results for different California building climate zones (Table 1) and for different building categories (Table 2) will be reported. Three building categories have been chosen that correspond to the most prevalent categories in California: multi-family residence, single-family residence, and medium office building. The climate zones represent a coastal to inland gradient from CZ8 (Fullerton) to CZ10 (Riverside) to CZ13 (Fresno).

Table 1. Climate zones in California with their representative weather stations (California Energy Commission, 2017).

Climate Zone	City	Weather station	Latitude [°N]	Longitude [°W]
CZ8	Fullerton	Fullerton Municipal	33.867	117.983
CZ10	Riverside	Riverside Muni	33.950	117.450
CZ13	Fresno	Fresno-Yosemite-IAP	36.783	119.717

Table 2. Building category and geometrical properties. All facades are identical. *L*, *W*, *H* are building length, width, and height.

Building category	Building footprint dimension $L \times W$ [m × m]	Building height [m]	Building aspect ratio L/H [-]	Ratio of window area to gross wall area [-]	Canyon width [m]	Canyon aspect ratio [-]
Multi-family	27.2 × 27.2	7.8	0.29	0.29	31.1	0.25
Single-family	10.4 × 10.4	5.2	0.50	0.13	28.5	0.18
Medium office	41.6 × 41.6	11.9	0.29	0.32	33.2	0.36

This report is structured as follows. Sections 2 and 3 contain the methodology for the canyon air temperature and MRT calculation. Section 4 contains the methodology for the thermal comfort calculation. Results for different building categories, climate zones, and seasons are presented and discussed in Section 5 separately for mean radiant temperature, canyon air temperature, and thermal comfort. Section 6 concludes the report.

2 Canyon air temperature calculation

In TUF-IOBES, the canyon air temperature is defined as the average temperature of all exterior air space below the building height. Canyon air temperature change is calculated from an energy balance. The control volume is the entire exterior air space below the building height. Heat fluxes into and out of the control volume are (i) convection between canopy air and air above the buildings, in which the air temperature above the buildings is assumed to equal the TMY air temperature; (ii) convection from urban surfaces including pavements and walls; and (iii) heating, ventilation, and air conditioning (HVAC) waste heat.

Switching to cool walls (albedo 0.60, attained with off-white surfaces) from conventional walls (albedo 0.25, typically of dark to medium colors) is expected to lower canyon air temperature. Two factors are at work. First, cool walls absorb less sunlight and remain at a lower temperature than conventional walls. The lower wall temperature reduces convection heat fluxes to the canopy air. Second, building with cool walls require less air conditioning, reducing HVAC waste heat flux into the canyon air.

It is important to disclose a limitation of the TUF-IOBES model. Since the simulation is forced with TMY data above the urban canopy, the canopy air temperature cooling effect of cool walls

is underestimated in TUF-IOBES. A better estimate of city-wide air temperature effects is available in a separate report generated under this contract. However, since these more accurate estimates are only available for two weeks of the year, a comprehensive analysis of seasonal effects was not possible at this time.

3 Mean radiant temperature calculation

3.1 Mean radiant temperature

Mean radiant temperature (MRT) is defined as the uniform surface temperature of an imaginary enclosure in which the human body will exchange the same amount of radiant heat energy as in the actual non-uniform enclosure (ASHRAE Standard 55, 2010). MRT is calculated using the mean radiant flux density (S_{rad}) from the Stefan-Boltzmann equation

$$S_{\mathrm{rad}} = \varepsilon_{\mathrm{body}}\, \sigma\, T_{\mathrm{MRT}}^4, \tag{1}$$

as (VDI 3787 part 2, 2008)

$$T_{\mathrm{MRT}} = \sqrt[4]{\frac{S_{\mathrm{rad}}}{\varepsilon_{\mathrm{body}}\sigma}}, \tag{2}$$

where σ is the Stefan-Boltzmann constant and $\varepsilon_{\mathrm{body}}$ is the thermal emittance of the human body.

The mean radiant flux density is the mean radiant energy passing through a normal section of the imaginary enclosure per unit time. While radiation is a flux, to make its values more intuitive the flux is expressed as a temperature state utilizing the Stefan-Boltzmann law. The exact threshold for which warm sensation turns into cold sensation depends on the clothing and activity level, but generally if the MRT exceeds the human skin temperature, then a person would experience a warm sensation and vice versa. For an outdoor environment the mean radiant flux density is defined as the summation of shortwave (K) and longwave (L) irradiances weighted by view factors (F) plus the direct contribution from the sun as (VDI 3787 part 2, 2008), such that

$$S_{\mathrm{rad}} = \alpha_{\mathrm{SW}} \left(\sum_j K_j\, F_{\mathrm{body}\to j} + I_{\mathrm{d}}\, F_{\mathrm{sky}} + I_{\mathrm{b}}\, f_{\mathrm{p}} \right) + \alpha_{\mathrm{LW}} \left(\sum_j L_j\, F_{\mathrm{body}\to j} + L_{\mathrm{atm}}\, F_{\mathrm{sky}} \right), \tag{3}$$

where α_{SW} is the pedestrian's shortwave absorptance and α_{LW} is the pedestrian's longwave absorptance[1]. The index *i* indexes surfaces including all walls (e.g., the ten walls in Figure 2) and ground. View factors are defined directionally as the fraction of radiation leaving surface A that strikes surface B.

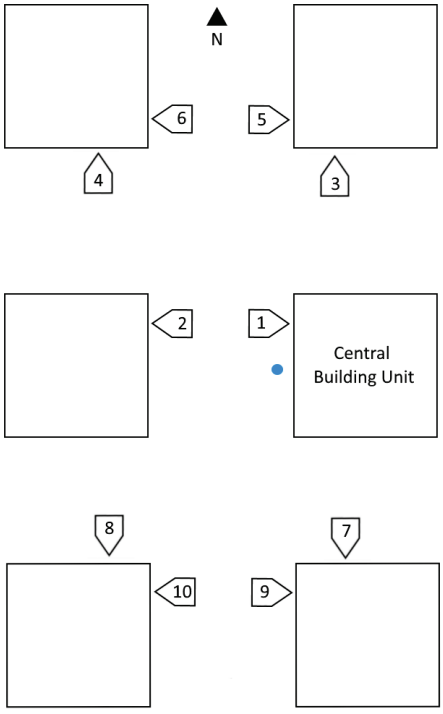

Figure 2. Plan view (not to scale) of a section of the domain identifying the walls that are assumed to contribute to the mean radiant flux. The blue dot to the left of the central building unit locates the pedestrian. Since the domain is symmetric about the center of the central building unit, analogous geometries exist for the other pedestrian locations.

The mean radiant flux density includes the radiation reflected by or emitted from the surrounding surfaces (K_i, L_i); downwelling solar irradiance, both beam (I_b) and diffuse (I_d); and the downwelling atmospheric longwave irradiance (L_{atm}). Shade provided by surrounding buildings is considered by multiplying the beam irradiance (I_b) with a variable that assumes values between 0 (when the patch in which the pedestrian is located is completely shaded) and 1 (when the patch is completely exposed to the sun). The sky and solar terms in Equation (3) are identical for the simulations with different wall albedo. MRT changes resulting from raising wall albedo are solely due to changes in the radiation reflected by or emitted from wall and ground. For simplicity, spatial averages of shortwave and longwave irradiance for each flat surface (i.e., ground, and north, south, east, and west building facades) are used. The radiative

[1] By Kirchhoff's law, pedestrian thermal absorptance α_{LW} is equal to pedestrian thermal emittance ε_{body}. The sensitivity of MRT and thermal comfort to pedestrian solar absorptance is analyzed in Section5.5.

contributions from the façade surfaces (each including walls and windows) of the six buildings surrounding each pedestrian location (Figure 2) are aggregated. Longwave radiation incident on the pedestrian is calculated using wall, window, and ground thermal emittances of 0.90, 0.84, and 0.95, respectively. Conventional (base case) and cool (reflective) walls are assigned albedos (shortwave reflectances) of 0.25 and 0.60, respectively. The albedo of the ground is set to 0.10.

3.2 View factors

The view factor from a person to a surface is the fraction of radiation leaving the person that strikes the surface. The approach by Johnson and Watson (1984) is adopted for view factor calculations. The human body is assumed to be a right circular cylinder with height $H_{\text{body}} = 1.8$ m and radius $r = 0.15$ m. The base of the cylinder is on the ground. The cylinder has three surfaces: a circular top plate, a circular bottom plate, and a curved side wall. The view factors from the cylinder surfaces and the entire cylinder to wall, sky, and ground are derived in Task Report Appendix A.

3.3 Solar projection

The surface projection factor for the beam irradiation (I_{b}) is assumed to be equal to the ratio of A_{sol} , the projection of the human body surface exposed to the solar beam[2], to the total surface area of the human body ($A_{\text{body}} = 1.8\,\text{m}^2$), such that

$$f_{\text{p}} = \frac{A_{\text{sol}}}{A_{\text{body}}} \tag{4}$$

A_{sol} is calculated using the simplified approach in Underwood et al. (1966)

$$A_{\text{sol}} = 0.0429\ \text{m}^2\ \sin\alpha_{\text{sol}} + 0.3845\ \text{m}^2 \cos\ \alpha_{\text{sol}}, \qquad [\text{m}^2] \tag{5}$$

where α_{sol} is the solar altitude angle.

3.4 Pedestrian longwave and shortwave absorptances

Longwave absorptances for skin and clothing range from 0.95 to 0.99 and the average of 0.97 is used here (Table 3). Shortwave absorptances vary significantly based on skin color and clothing. The standard shortwave absorptance of 0.70 recommended by Höppe is used here (Table 3), but

[2] $A_{\text{sol,}}$ is the area of the erected human body projected in the direction normal to the solar rays. More intuitively, the A_{sol} is proportional to the length of the shadow of the human body. Per Eq. (5) A_{sol} of a given body depends only the solar altitude angle. A_{sol} decreases with increasing solar altitude angle.

the sensitivity of MRT and thermal comfort to shortwave absorptance is also investigated in Section 5.5.

Table 3. Shortwave and longwave absorptances of skin and clothing (Hoppe, 1992), and the values assigned to the pedestrian.

	Skin	Clothing	Pedestrian
Shortwave absorptance	0.55 to 0.85	0.40 to 0.90	0.70
Longwave absorptance	0.99	0.95	0.97

4 Thermal comfort

MRT is just one input to the thermal comfort of pedestrians. The latest version of the Pierce two-node model (Gagge et al., 1986) is used to compute pedestrian thermal comfort considering MRT, wind speed, air temperature, humidity, metabolic activity, and clothing. Biological and behavioral differences between people make estimation of human comfort more complicated than calculation of MRT, which is derived from first principles in physics. Human comfort models, on the other hand, attempt to emulate the typical human perception of environmental conditions through thermal comfort indices.

Outdoor environmental comfort is more dynamic than indoor comfort, and pedestrians experience a wide range of temperatures. Therefore, body thermoregulatory responses such as shivering and sweating must be considered. The Pierce two-node model captures these responses and is therefore suitable to model outdoor human thermal comfort.

The principal model output is the Standard Equivalent Temperature, SET*. SET* is defined as the air and radiant temperature of a standard isothermal environment that would cause the same thermal stress to the human body as the test environment. A larger SET* indicates that a human feels warmer and vice versa. The human body is modeled as two isothermal concentric compartments, the skin and the core.

The heat balance between the skin and the environment can be written as

$$H_{\mathrm{sk}} = H_{\mathrm{flow}} + Q_{\mathrm{r}} + Q_{\mathrm{c}} + E_{\mathrm{sk}}, \qquad [\mathrm{W/m^2}] \qquad (6)$$

where H_{sk} is the heat stored in the skin (positive for a body that is heating up), Q_{r} and Q_{c} are the radiative and convective heat losses through skin and clothing, E_{sk} is the evaporative heat loss from the skin, and H_{flow} is heat exchange rate from core to skin. All heat flows and storage are defined per unit area of skin. The heat balance between the skin and the core is

$$H_{\mathrm{cr}} = M - H_{\mathrm{flow}} - (E_{\mathrm{res}} + C_{\mathrm{res}}), \qquad [\mathrm{W/m^2}] \qquad (7)$$

where H_{cr} is heat stored in the core (positive for a body that is heating up), M is the metabolic activity, and E_{res} and C_{res} are respectively the latent and sensible parts of the respiratory heat losses. To reach thermal equilibrium body thermoregulatory mechanisms, such as vasodilation in warm weather, or vasoconstriction in cold weather, can increase or decrease the heat exchange between core and skin, by adjusting the blood flow rate. If despite adjustments of the blood flow rate, the temperature of the core or skin exceeds a threshold, sweating removes heat. Instead, if the core or skin temperature falls below a threshold, shivering produces additional heat.

Several assumptions about metabolic activity and clothing are needed. A metabolic activity of 115 W/m^2 corresponding to the heat produced by a person walking on level surface at 3.2 km/h (ASHRAE Standard 55, 2010) is assumed. The insulation provided by clothing is assumed to vary between winter and summer: from November to April, thermal resistance equals 0.155 m²·K/W, corresponding to trousers, a T-shirt, and a long-sleeve sweater; from May to October, clothing thermal resistance equals 0.088 m²·K/W, corresponding to trousers and a T-shirt (ASHRAE Standard 55, 2010). Heat balances, skin temperature, thermoregulatory strain, and the SET* are calculated as the air and radiant temperature of an isothermal environment with 50% relative humidity and 0.15 m/s wind speed (Gagge et al., 1986) in which the human body would have the same skin temperature and the same thermoregulatory mechanism as in the TUF-IOBES environment.

5 Results and Discussion

5.1 Computed view factors

View factors from the pedestrian to individual building walls, all walls, sky, and ground are reported in Table 4. Note that since windows comprise a portion of the façade area (gross wall area), and window thermal properties are the same for the conventional (albedo 0.25) and cool (albedo 0.60) walls, the view factor from the pedestrian to the modified wall surface is smaller than the façade view factor in Table 4.

For multi-family residence, single-family residence, and medium office building the view factors from the pedestrian to the set of all 10 walls are 34.6%, 29.5%, and 37.9%, respectively. The view factors to the set of all walls are dominated by the view factors to the wall immediately adjacent to the pedestrian which are 30.9%, 27.5%, and 32.1%. View factors to any wall are most sensitive to the distance D of the pedestrian from the wall. Since the adjacent wall (wall 1)

dominates the view factor towards all walls when the pedestrian stands close to it, the view factor to all walls decreases approximately as D^2 following the Nusselt analog for view factors[3].

Table 4. View factor from the pedestrian to each gross wall (façade), sky, and ground by building category. The wall reference numbers are given in Figure 2. By symmetry, the view factors to walls 7, 8, 9, and 10 are equal to those to walls 3, 4, 5, and 6, respectively.

	Multi-family residence	Single-family residence	Medium-office
$F_{\text{body}\to\text{wall},1}$	30.9%	27.5%	32.1%
$F_{\text{body}\to\text{wall},2}$	2.0%	0.7%	3.8%
$F_{\text{body}\to\text{wall},3}$	0.1%	0.3%	0.1%
$F_{\text{body}\to\text{wall},4}$	0.4%	0.2%	0.6%
$F_{\text{body}\to\text{wall},5}$	0.0%	0.0%	0.0%
$F_{\text{body}\to\text{wall},6}$	0.2%	0.1%	0.3%
$F_{\text{body}\to\text{walls}}$	33.6%	28.9%	36.9%
$F_{\text{body}\to\text{sky}}$	25.0%	29.4%	21.5%
$F_{\text{body}\to\text{ground}}$	40.7%	41.1%	40.6%

5.2 Mean Radiant Temperature (MRT)

MRTs for different wall albedos, building types, and climate zones are compared. The multi-family residence in climate zone 8 (Fullerton) with conventional walls (albedo 0.25) is arbitrarily chosen as the reference case.

Figure 3 shows the results averaged over the entire year for the reference case. In TUF-IOBES T_{air} is the forcing (TMY) temperature above the canyon and T_{can} is the simulated air temperature inside the canyon. The MRT follows the trend of air and canyon temperatures, but with larger amplitude. At night T_{MRT} is lower than T_{can} because of the longwave radiation exchanged by the pedestrian with the cool sky and with urban surfaces, which tend to be cooler than the canyon air. During the day T_{MRT} is higher than T_{can} because of beam solar radiation and diffuse solar radiation from the sky, solar radiation reflected by surrounding walls and ground surfaces, and longwave radiation emitted by surrounding walls and ground surfaces. Therefore during the day the only environmental factor that provides sustained radiative cooling is the longwave exchange with the sky.

[3] Nusselt (1928) proposed to calculate view factors as the conical projection of the receiving surface on a unit sphere around the emitting surface. The view factor from the emitting surface to the receiving surface is then the fraction of the circle occupied by the conical projection.

The MRT differences between pedestrian locations stem from building shadows, shortwave radiation reflected by walls, and longwave radiation emitted by walls. For example, a pedestrian to the east of the building records higher MRT during the morning in direct sun exposure. A pedestrian to the west of the building is in shadow during the early morning but experiences the highest MRT in the afternoon. The pedestrian in the south location experiences the maximum daily MRT while the pedestrian in the north location experiences the lowest MRT on average. The pedestrian in the north location is often shaded, primarily receiving radiation reflected by and emitted from the north building wall. For example for Fullerton, the north wall only receives 1.3 kWh/m^2·day of solar radiation on average during the year, while the south wall receives 3.4 kWh/m^2·day of solar radiation.

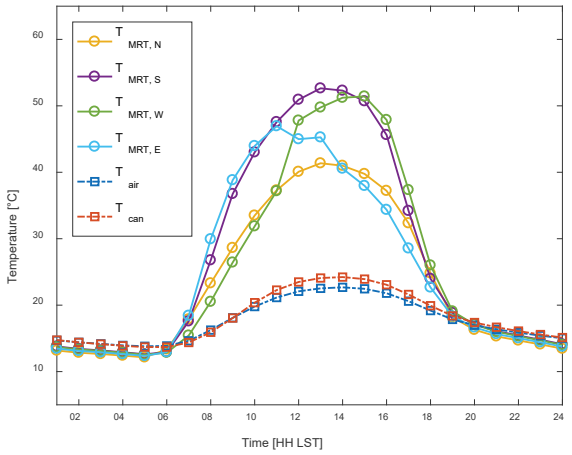

Figure 3. Average (over the year) daily cycle of air and mean radiant temperatures in four locations for the multi-family residence in Fullerton (CZ8) with (conventional) wall albedo equal to 0.25. T_{air} is the forcing air temperature above the urban canopy, T_{can} is the average air temperature in the urban canyon, and $T_{\mathrm{MRT},i}$ is the mean radiant temperature experienced by the pedestrian north, south, west and east of the building (façade i = N, S, W, E). LST is Local Standard Time.

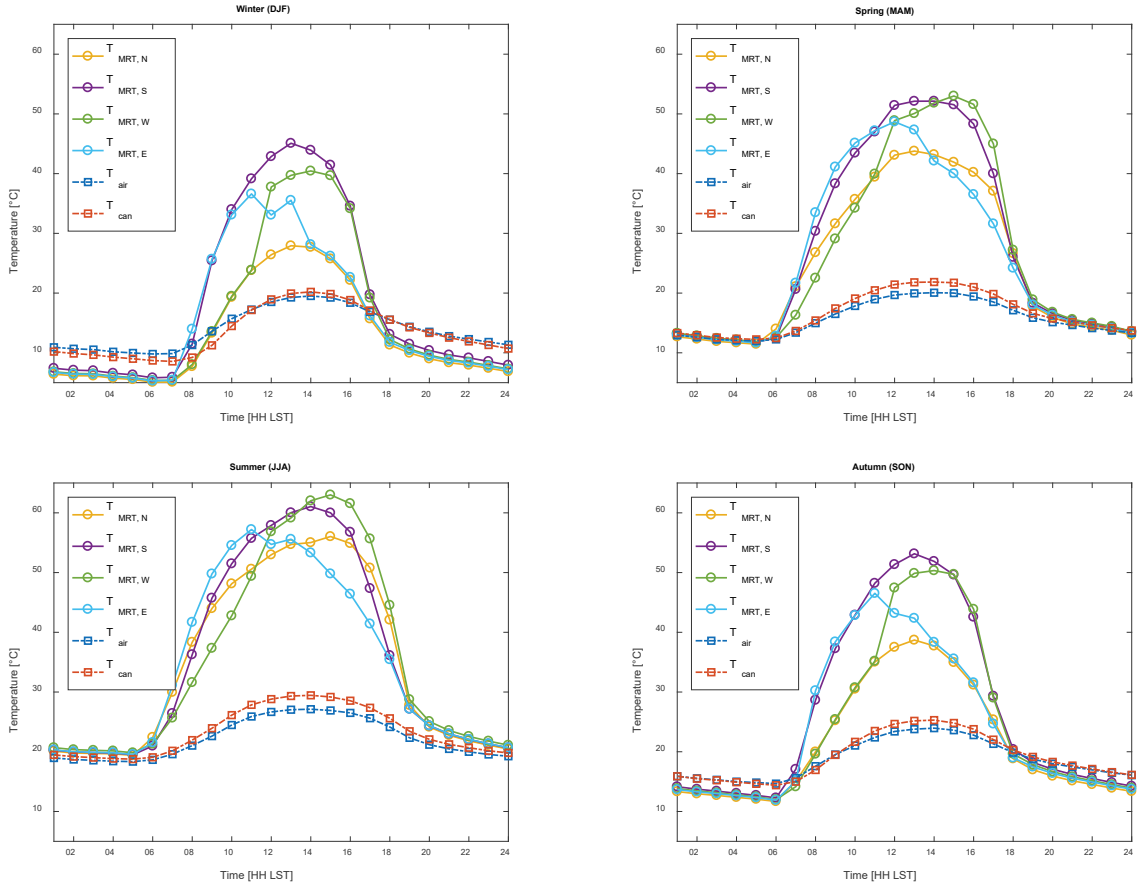

Figure 4. Seasonal analogs of Figure 3 (winter = Dec/Jan/Feb, spring = Mar/Apr/May, summer = Jun/Jul/Aug, and autumn = Sep/Oct/Nov).

MRT differences by building aspect are consistent across the seasons (Figure 4). The MRT for the pedestrian on the west and south sides are largest with seasonally averaged early afternoon peaks up to 63 ˚C in summer and 45 ˚C in winter.

Figure 5 shows the annual average rise in MRT ($\Delta T_{\mathrm{MRT}} = T_{\mathrm{MRT,modified}} - T_{\mathrm{MRT,base}}$) upon switching to a cool wall (albedo 0.60) from a conventional wall (albedo 0.25). Seasonal rises are presented in Figure 6. Increasing wall albedo raises daytime MRT. Compared to a conventional wall, during daytime cool walls reflect a larger fraction of incident solar radiation to the surroundings leading to an increase in pedestrian MRT. While the high albedo also lowers wall surface temperature, the associated reduction in emission of longwave radiation from the wall is not sufficient to balance the shortwave increase. On the other hand, at night the MRT is lower in neighborhoods with cool walls, since a decrease in wall heat storage in cool walls during daytime causes lower wall temperatures to persist through the night. The timing of the peak rise of MRT with wall albedo in Figure 5 depends on pedestrian location and coincides with the MRT peaks in Figure 3.

For any seasonal average and the annual average, the east location experiences the peak MRT rise shortly after sunrise, due to the reflection from the strongly irradiated east facing walls; at the west location the peak MRT rise is recorded just before sunset. The MRT rise at the south and north locations is close to symmetric about noon LST and peaks around noon because of the reflection from the south-facing wall for both locations. The pedestrian near the south wall receives sunlight diffusely reflected from the south wall (pedestrian to south wall view factor 30.9%) that arrived at the south wall as beam radiation from the solar disc. The pedestrian near the north wall receives (i) sunlight diffusely reflected from the north wall (pedestrian to north wall view factor is also 30.9%) that arrived at the north wall as diffuse shortwave radiation from the sky; (ii) sunlight diffusely reflected from the south wall (pedestrian to south wall view factor 2.0%) that arrived at the south wall as beam radiation from the solar disc; (iii) sunlight diffusely reflected from the north wall that arrived at the north wall as diffuse radiation reflected from the south wall (south wall to the north wall view factor 5.6%).

Switching to cool walls from conventional walls increases substantially the shortwave contribution to the MRT, but this is partly offset by a reduction in longwave emission from the now-cooler wall. The pedestrian-to-gross wall view factors are only 33.6% (Table 4), and windows comprise 29% of the façade area (gross wall area) in the multi-family residence, further reducing the view factor from the pedestrian to the modified (net) wall surface area. To illustrate cool wall effects on pedestrian MRT a sample calculation is provided for a clear day on March 22 in Fullerton with a pedestrian walking 1.5 m from a multi-family residence. Daytime mean global horizontal irradiance and mean beam-normal irradiance are 473 W/m^2 and 651 W/m^2, respectively. Averaging over daytime and all walls, switching to cool walls from conventional walls increases reflected radiation to 119 W/m^2 from 49 W/m^2, while decreasing longwave emission to 420 W/m^2 (corresponding to 20.5 ˚C) from 444 W/m^2 (24.9 ˚C). The net increase in all-wave radiation is 46 W/m^2. However, the change in pedestrian MRT depends also on the pedestrian shortwave absorptance, as analyzed in Section 5.5.

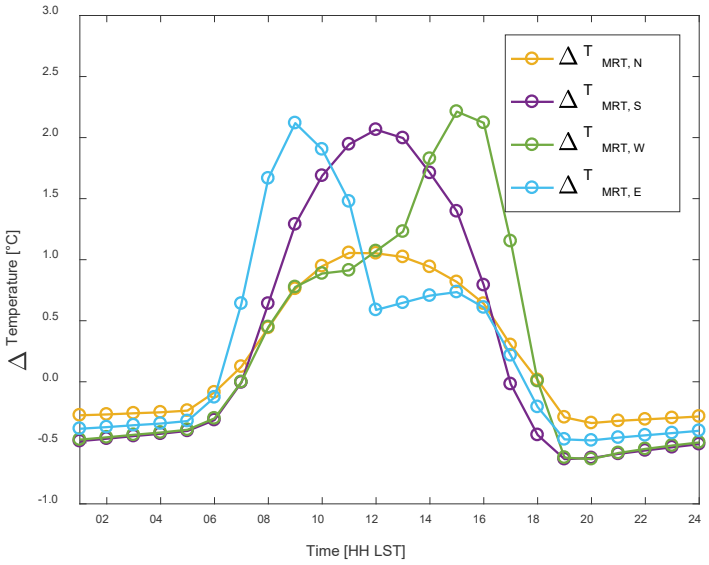

Figure 5. Average (over the year) MRT rise ΔT_{MRT} when switching to cool walls (albedo 0.60) from conventional walls (albedo 0.25) for the multi-family residence in Fullerton (CZ8).

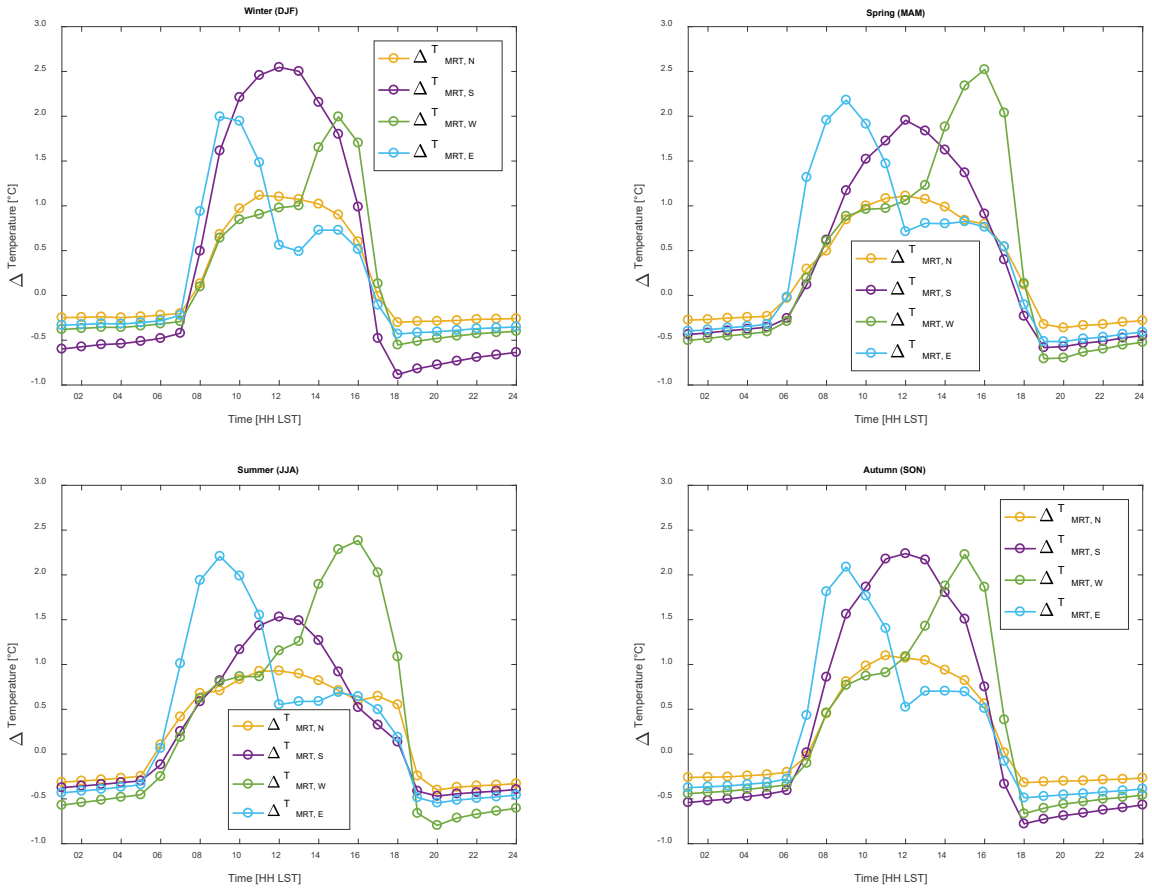

Figure 6. Seasonal analogs of Figure 5 (winter = Dec/Jan/Feb, spring = Mar/Apr/May, summer = Jun/Jul/Aug, and autumn = Sep/Oct/Nov).

The same procedure illustrated above for the multi-family in CZ8 was repeated for the various climate zones and building categories tabulated in Table 1 and Table 2, respectively. The mean MRT and canopy air temperature during the day and the mean daytime increase in MRT and canopy air temperature are shown in Table 5 through Table 13. Section 5.3 discusses the canyon air temperature results.

The earlier finding for the multi-family residence in Fullerton (CZ8) holds for all building categories and climate zones: cool wall MRTs are largest for the pedestrian on the south side, followed by about equal MRT on the east and west sides, and the MRT is lowest for the pedestrian on the north side. The MRT trend with CZ is inconsistent (for examples, see Table 5, Table 6, and Table 7), presumably due to different patterns in the diurnal cycle of cloudiness in the different climate zones. For example the coastal CZ8 tends to be more cloudier in the morning than in the afternoon, especially in summer. Morning cloud cover manifests in a smaller average daily peak MRT for the pedestrian on the east side compared to the west side, because morning cloud cover greatly reduces sunlight incident on the east wall, which in turn reduces reflected sunlight incident on the pedestrian walking next to it. On the other hand, for

CZ10 and CZ13, the average MRT tends to be nearly identical for the pedestrian in the east and west locations, indicating similar solar irradiance for mornings and afternoons.

Pedestrian MRTs are higher in cool-wall neighborhoods with MRT increases ranging from 0.5 to 0.9 ˚C for a pedestrian at the north wall to 0.6 to 2.0˚C for a pedestrian at the south wall depending on season, building type, and climate zone. The largest MRT increases occur on the south wall for the coastal climate zones in the winter.

The results are consistent with the distribution of sunlight on the different facades and seasons. Facades that receive more sunlight also reflect more sunlight toward the pedestrian. As cool walls have larger solar reflectance, they augment this increase in reflection of sunlight to the pedestrian, further increasing MRT. Daytime global irradiance on walls is largest in the winter for the south façade, while it is largest in summer for the east and west façades.

Table 5. Seasonal mean values of daytime canyon air temperature and MRT with conventional walls, and corresponding increases when switching to cool walls (albedo 0.60) from conventional walls (albedo 0.25), shown for the multi-family residence in CZ8. Note that 0.0 is a rounded result with a value between -0.05 °C and 0.05 °C.

	T_{can} [°C]	ΔT_{can} [°C]	$T_{\mathrm{MRT,N}}$ [°C]	$\Delta T_{\mathrm{MRT,N}}$ [°C]	$T_{\mathrm{MRT,S}}$ [°C]	$\Delta T_{\mathrm{MRT,S}}$ [°C]	$T_{\mathrm{MRT,W}}$ [°C]	$\Delta T_{\mathrm{MRT,W}}$ [°C]	$T_{\mathrm{MRT,E}}$ [°C]	$\Delta T_{\mathrm{MRT,E}}$ [°C]
Winter (DJF)	16.6	-0.2	21.0	0.8	33.7	1.6	27.6	1.0	27.1	0.9
Spring (MAM)	19.2	0.0	35.1	0.7	40.5	1.0	38.1	1.2	37.2	1.0
Summe r (JJA)	25.9	0.0	45.4	0.6	46.5	0.7	46.2	1.1	44.8	0.9
Autumn (SON)	22.2	-0.1	30.5	0.7	41.5	1.3	36.3	1.1	35.7	1.0
Year	21.3	-0.1	34.1	0.7	41.1	1.1	37.8	1.1	36.9	1.0

Table 6. Analog of Table 5 for multi-family residence in CZ10.

	T_{can} [°C]	ΔT_{can} [°C]	$T_{\mathrm{MRT,N}}$ [°C]	$\Delta T_{\mathrm{MRT,N}}$ [°C]	$T_{\mathrm{MRT,S}}$ [°C]	$\Delta T_{\mathrm{MRT,S}}$ [°C]	$T_{\mathrm{MRT,W}}$ [°C]	$\Delta T_{\mathrm{MRT,W}}$ [°C]	$T_{\mathrm{MRT,E}}$ [°C]	$\Delta T_{\mathrm{MRT,E}}$ [°C]
Winter (DJF)	15.8	-0.1	19.0	0.8	33.2	1.8	26.1	1.1	26.1	1.1
Spring (MAM)	20.2	0.0	36.0	0.7	41.6	1.0	38.9	1.2	38.5	1.1
Summer (JJA)	28.0	0.0	47.0	0.7	48.0	0.8	47.0	1.2	47.0	1.1
Autumn (SON)	22.6	-0.1	28.7	0.7	40.0	1.3	34.2	1.0	34.2	0.9

Year	22.1	-0.1	33.9	0.7	41.3	1.2	37.4	1.1	37.3	1.0

Table 7. Analog of Table 5 for multi-family residence in CZ13.

	T_{can} [°C]	ΔT_{can} [°C]	$T_{\mathrm{MRT,N}}$ [°C]	$\Delta T_{\mathrm{MRT,N}}$ [°C]	$T_{\mathrm{MRT,S}}$ [°C]	$\Delta T_{\mathrm{MRT,S}}$ [°C]	$T_{\mathrm{MRT,W}}$ [°C]	$\Delta T_{\mathrm{MRT,W}}$ [°C]	$T_{\mathrm{MRT,E}}$ [°C]	$\Delta T_{\mathrm{MRT,E}}$ [°C]
Winter (DJF)	11.3	-0.1	16.0	0.7	24.4	1.2	20.3	0.8	20.0	0.8
Spring (MAM)	20.7	0.0	34.3	0.7	40.8	1.1	37.3	1.2	37.3	1.1
Summer (JJA)	31.2	0.0	46.9	0.6	48.2	0.7	47.0	1.1	47.2	1.0
Autumn (SON)	22.3	-0.1	28.7	0.7	41.1	1.4	35.0	1.1	34.8	1.0
Year	22.3	0.0	33.1	0.7	39.7	1.1	36.2	1.0	36.2	1.0

Table 8. Analog of Table 5 for single-family residence in CZ8.

	T_{can} [°C]	ΔT_{can} [°C]	$T_{\mathrm{MRT,N}}$ [°C]	$\Delta T_{\mathrm{MRT,N}}$ [°C]	$T_{\mathrm{MRT,S}}$ [°C]	$\Delta T_{\mathrm{MRT,S}}$ [°C]	$T_{\mathrm{MRT,W}}$ [°C]	$\Delta T_{\mathrm{MRT,W}}$ [°C]	$T_{\mathrm{MRT,E}}$ [°C]	$\Delta T_{\mathrm{MRT,E}}$ [°C]
Winter (DJF)	16.6	-0.1	21.1	0.6	34.2	1.7	27.9	1.0	28.2	0.9
Spring (MAM)	19.2	0.0	36.9	0.7	41.1	1.0	38.5	1.2	38.0	1.0
Summer (JJA)	25.8	0.0	46.9	0.6	47.7	0.7	46.7	1.1	45.6	0.9
Autumn (SON)	22.2	-0.1	31.5	0.6	41.8	1.4	37.0	1.1	36.9	1.0
Year	21.3	0.0	35.2	0.6	41.7	1.2	38.3	1.1	37.9	0.9

Table 9. Analog of Table 5 for single-family residence in CZ10.

	T_{can} [°C]	ΔT_{can} [°C]	$T_{\mathrm{MRT,N}}$ [°C]	$\Delta T_{\mathrm{MRT,N}}$ [°C]	$T_{\mathrm{MRT,S}}$ [°C]	$\Delta T_{\mathrm{MRT,S}}$ [°C]	$T_{\mathrm{MRT,W}}$ [°C]	$\Delta T_{\mathrm{MRT,W}}$ [°C]	$T_{\mathrm{MRT,E}}$ [°C]	$\Delta T_{\mathrm{MRT,E}}$ [°C]
Winter (DJF)	15.7	-0.1	19.0	0.7	33.7	2.0	26.5	1.1	27.2	1.1
Spring (MAM)	20.1	0.0	37.8	0.7	42.2	1.1	39.3	1.2	39.1	1.0
Summer (JJA)	28.0	0.0	48.6	0.7	49.4	0.8	47.3	1.2	47.9	1.1

Autumn (SON)	22.5	-0.1	29.7	0.6	40.2	1.4	34.9	1.1	35.4	1.0
Year	22.0	-0.1	35.0	0.7	42.0	1.3	37.8	1.1	38.2	1.0

Table 10. Analog of Table 5 for single-family residence in CZ13.

	T_{can} [°C]	ΔT_{can} [°C]	$T_{\mathrm{MRT,N}}$ [°C]	$\Delta T_{\mathrm{MRT,N}}$ [°C]	$T_{\mathrm{MRT,S}}$ [°C]	$\Delta T_{\mathrm{MRT,S}}$ [°C]	$T_{\mathrm{MRT,W}}$ [°C]	$\Delta T_{\mathrm{MRT,W}}$ [°C]	$T_{\mathrm{MRT,E}}$ [°C]	$\Delta T_{\mathrm{MRT,E}}$ [°C]
Winter (DJF)	11.3	0.0	16.2	0.6	24.6	1.3	20.6	0.8	20.9	0.8
Spring (MAM)	20.7	0.0	36.0	0.7	41.3	1.1	37.5	1.2	38.2	1.1
Summer (JJA)	31.2	0.0	48.4	0.5	49.7	0.7	47.3	1.1	47.9	1.0
Autumn (SON)	22.3	0.0	29.8	0.6	41.2	1.4	35.2	1.1	35.8	1.0
Year	22.3	0.0	34.3	0.6	40.4	1.1	36.5	1.0	37.0	1.0

Table 11. Analog of Table 5 for medium office in CZ8.

	T_{can} [°C]	ΔT_{can} [°C]	$T_{\mathrm{MRT,N}}$ [°C]	$\Delta T_{\mathrm{MRT,N}}$ [°C]	$T_{\mathrm{MRT,S}}$ [°C]	$\Delta T_{\mathrm{MRT,S}}$ [°C]	$T_{\mathrm{MRT,W}}$ [°C]	$\Delta T_{\mathrm{MRT,W}}$ [°C]	$T_{\mathrm{MRT,E}}$ [°C]	$\Delta T_{\mathrm{MRT,E}}$ [°C]
Winter (DJF)	16.9	-0.2	21.9	0.8	34.6	1.3	28.1	0.9	27.0	0.8
Spring (MAM)	19.5	-0.1	34.5	0.7	40.7	0.9	38.2	1.0	37.3	0.9
Summer (JJA)	26.2	-0.1	44.6	0.6	46.6	0.7	46.4	1.0	45.2	0.8
Autumn (SON)	22.5	-0.1	31.0	0.7	42.2	1.1	36.6	0.9	35.7	0.8
Year	21.6	-0.1	34.0	0.7	41.5	0.9	38.1	1.0	37.0	0.9

Table 12. Analog of Table 5 for medium office in CZ10.

	T_{can} [°C]	ΔT_{can} [°C]	$T_{\mathrm{MRT,N}}$ [°C]	$\Delta T_{\mathrm{MRT,N}}$ [°C]	$T_{\mathrm{MRT,S}}$ [°C]	$\Delta T_{\mathrm{MRT,S}}$ [°C]	$T_{\mathrm{MRT,W}}$ [°C]	$\Delta T_{\mathrm{MRT,W}}$ [°C]	$T_{\mathrm{MRT,E}}$ [°C]	$\Delta T_{\mathrm{MRT,E}}$ [°C]
Winter (DJF)	15.9	-0.2	20.0	0.9	34.0	1.5	26.7	1.0	25.9	0.9
Spring (MAM)	20.4	-0.1	35.4	0.7	41.9	0.9	38.9	1.0	38.6	1.0

Summer (JJA)	28.4	-0.1	46.2	0.7	48.0	0.7	47.2	1.1	47.3	1.0
Autumn (SON)	22.7	-0.1	29.2	0.7	40.6	1.1	34.3	0.9	34.3	0.8
Year	22.3	-0.1	33.8	0.7	41.7	1.0	37.6	1.0	37.4	0.9

Table 13. Analog of Table 5 for medium office in CZ13.

	T_{can} [°C]	ΔT_{can} [°C]	$T_{\mathrm{MRT,N}}$ [°C]	$\Delta T_{\mathrm{MRT,N}}$ [°C]	$T_{\mathrm{MRT,S}}$ [°C]	$\Delta T_{\mathrm{MRT,S}}$ [°C]	$T_{\mathrm{MRT,W}}$ [°C]	$\Delta T_{\mathrm{MRT,W}}$ [°C]	$T_{\mathrm{MRT,E}}$ [°C]	$\Delta T_{\mathrm{MRT,E}}$ [°C]
Winter (DJF)	11.5	-0.1	16.8	0.6	25.1	1.0	20.7	0.7	19.9	0.7
Spring (MAM)	21.0	-0.1	33.8	0.7	41.2	0.9	37.6	1.0	37.4	1.0
Summer (JJA)	31.6	-0.1	46.1	0.6	48.5	0.6	47.4	1.0	47.5	0.9
Autumn (SON)	22.6	-0.1	29.3	0.7	41.8	1.1	35.4	0.9	34.3	0.9
Year	22.6	-0.1	33.0	0.7	40.2	0.9	36.6	0.9	36.2	0.9

5.3 Canyon Air Temperature

Canopy air temperature was reported in the figures and tables in Section 5.2 together with MRT and the trends are briefly summarized here. As expected canopy air temperatures increase along the gradient from coast to inland from CZ8 to CZ10 to CZ13, and the amplitude of the seasonal cycle is also larger inland. Average yearly canopy air temperatures range from 21.3 ˚C to 22.6 ˚C. Average yearly canopy air temperatures for the conventional wall case are about 0.3 ˚C higher for the medium office building than for the residential buildings, since the larger building height for the medium office building compared to the residential buildings provides more wall surface area for solar radiation to be absorbed. Canopy air temperature then increases by convection of heat from walls.

Canopy air temperatures are up to 0.2 ˚C lower in cool wall neighborhoods compared to neighborhoods with conventional walls. The largest canopy air temperature reductions of 0.2 ˚C occur for the multi-family residence and medium office building in CZ8 during winter. All other buildings, climate zones, and seasons show cooler canyon air temperature by either 0.0 or 0.1 ˚C. Canyon air temperature differences being largest in winter is inconsistent with the fact that total irradiation received on all four walls in winter is only about half that received during summer. More wall irradiation should lead to more reflection of sunlight out of the urban canyon and a larger canyon air temperature difference for cool versus conventional walls. The reason for the discrepancy is not well understood at present.

5.4 Thermal Comfort

The thermal comfort trends during the day follow the MRT and canopy air temperature trends. SET* differences between the simulations with wall albedos of 0.25 (conventional) and 0.60 (cool) can only be due to differences in MRT and canopy air temperature because the other meteorological parameters (i.e., relative humidity and wind speed) are identical. SET* differences between the four pedestrian locations are solely explained by MRT differences as air temperature and other meteorological parameter are assumed to be constant in the domain.

Figure 7 shows SET* for the reference case (a conventional-wall multi-family residence in Fullerton) averaged over the year. At night the SET* is on average around 3 ˚C higher than the canyon air temperature (Figure 3). While the MRT is lower than the canyon air temperature cooling the pedestrian, the fact that the pedestrian produces heat through walking introduces an overall warmer thermal sensation than the canyon air temperature. During the day the SET* is up to 7 ˚C higher than the canyon air temperature; the increase is caused by (i) heat production through walking and (ii) a larger MRT. The SET* trends by pedestrian location mirror those for MRT in Figure 3. Figure 8 shows the results by season which exhibit similar trends as those for the entire year.

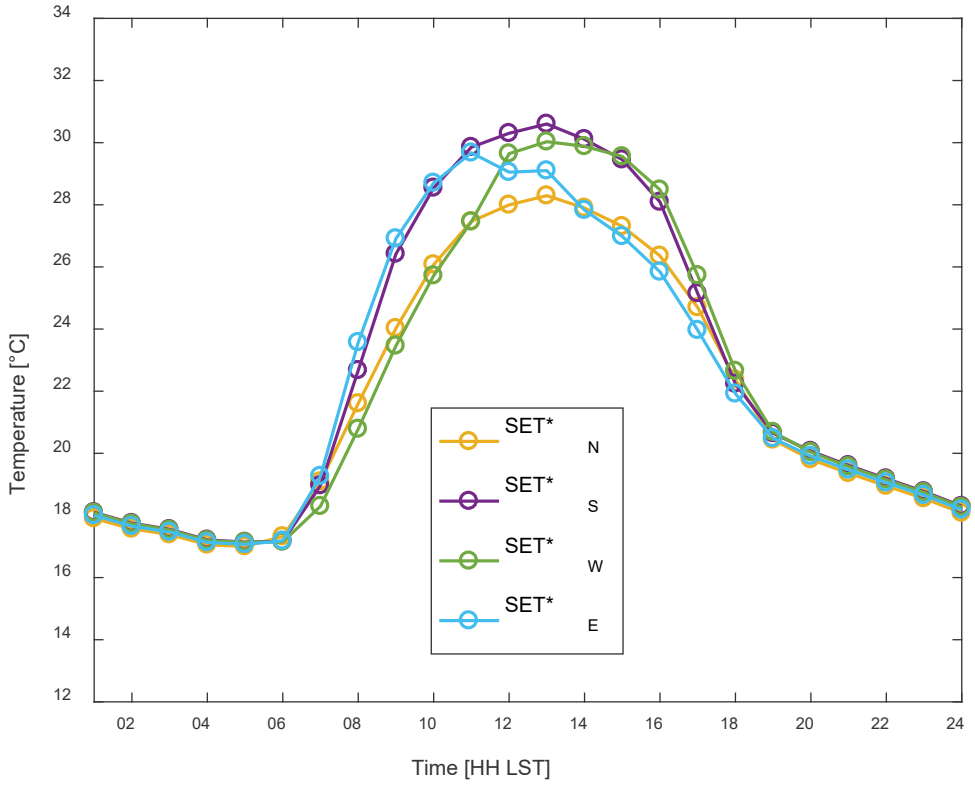

Figure 7. Average (over the year) daily cycle of SET* in four pedestrian locations for the conventional-wall multi-family residence in Fullerton (CZ8).

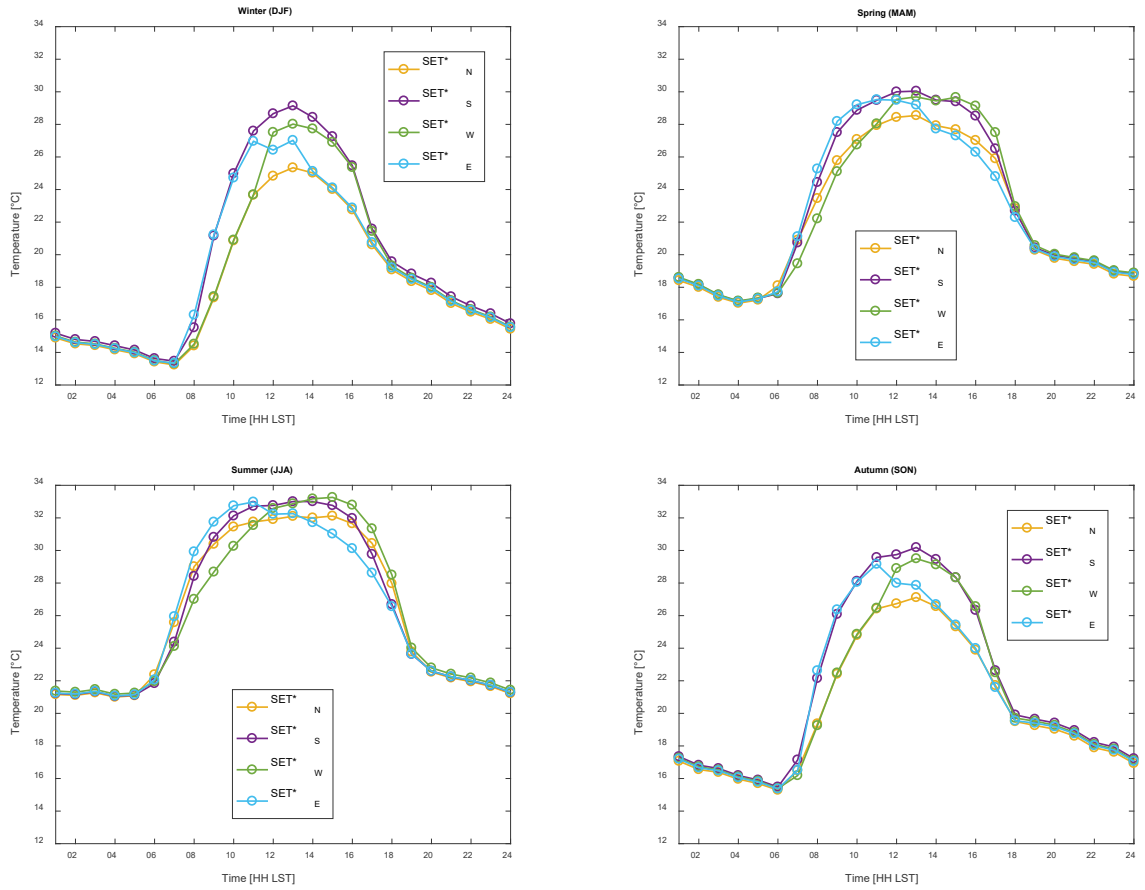

Figure 8. Seasonal analogs of Figure 7 (winter = Dec/Jan/Feb, spring = Mar/Apr/May, summer = Jun/Jul/Aug, and autumn = Sep/Oct/Nov).

As shown in Figure 9 and Figure 10 the pedestrian thermal comfort impact of cool walls is small. During daytime, cool walls increase MRT (Table 5 to Table 13), raising SET* by up to 0.5 ˚C on average over the season or year. At night, cool walls decrease MRT, lowering SET* by up to 0.3 ˚C on average over the season or year. The largest SET* effect occurs for the pedestrian near the south wall in winter since winter solar irradiation on the south wall is the most of any wall during any season. The increase in SET* is only about 0.25 ˚C per 1 ˚C increase in MRT, since the MRT increase due to the higher wall albedo is partially balanced by a decrease in canopy air temperature.

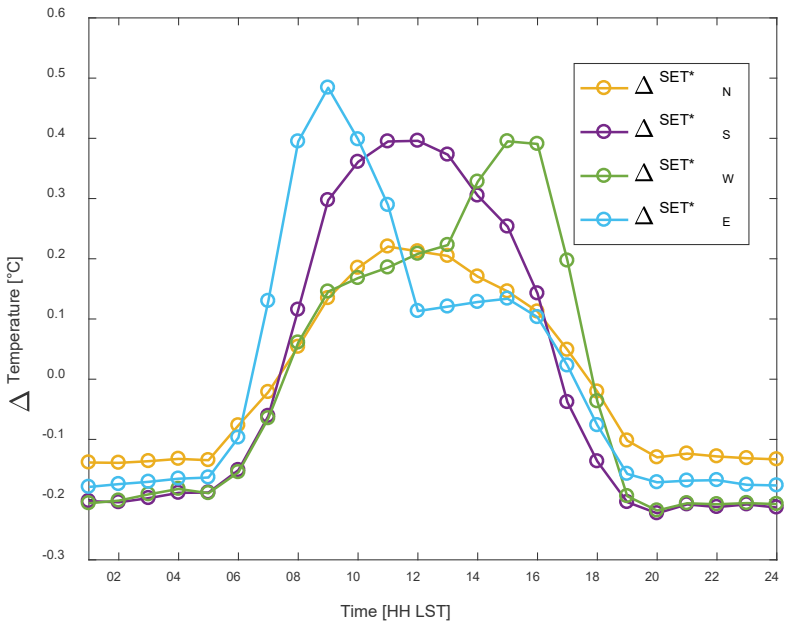

Figure 9. Average (over the year) SET* rise ΔSET^* when switching to cool walls (albedo 0.60) from conventional walls (albedo 0.25) for the multi-family residence in Fullerton (CZ8).

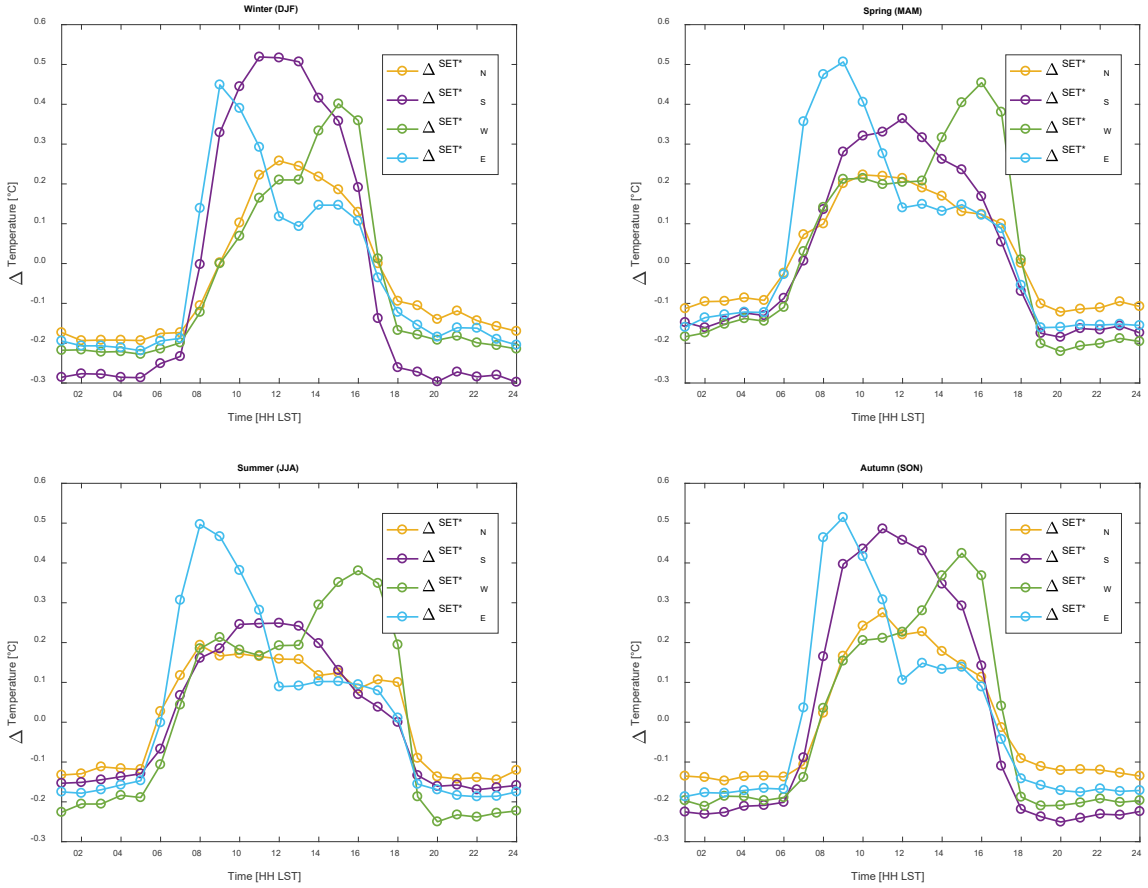

Figure 10. Seasonal analogs of Figure 9 (winter = Dec/Jan/Feb, spring = Mar/Apr/May, summer = Jun/Jul/Aug, and autumn = Sep/Oct/Nov).

For the multi-family residence in Fullerton (CZ8) and all pedestrian locations the absolute SET* difference with cool walls is less or equal to 0.2 ˚C 61% of the time (Figure 11 and Figure 12). While SET* increases over 0.5 ˚C are occasionally observed, they occur exclusively during clear winter days when the pedestrian is more likely to experience a cold sensation. In that situation the SET* increase is beneficial to pedestrian thermal comfort.

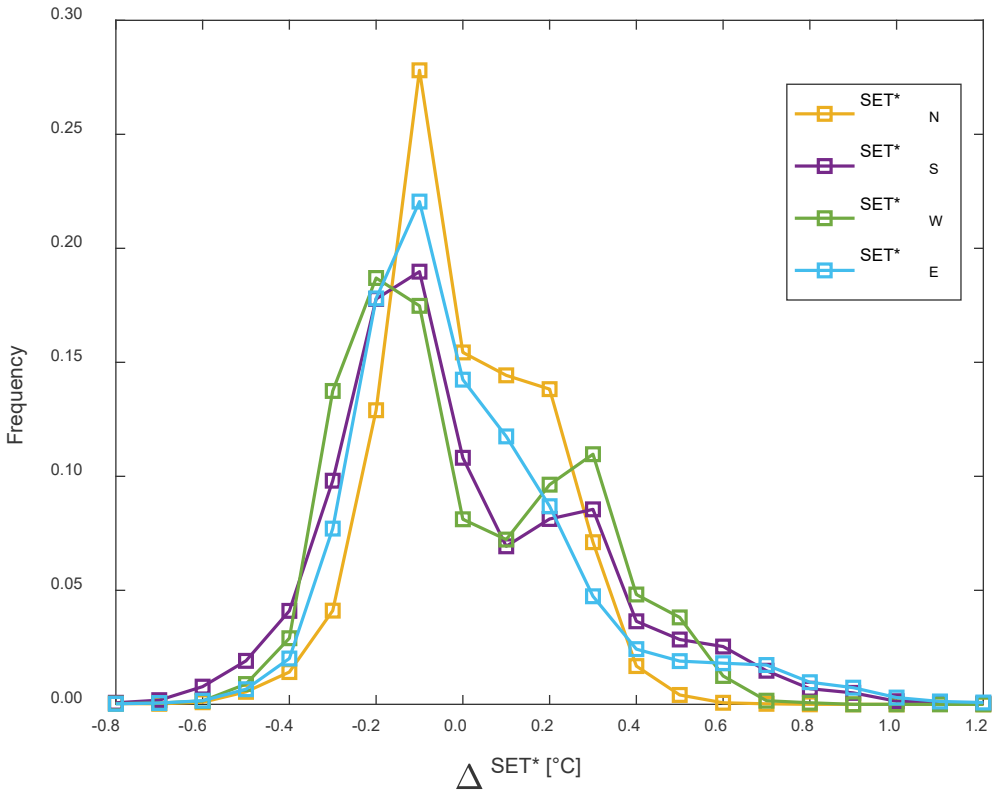

Figure 11. Frequency distribution of standard equivalent temperature (SET*) rise for pedestrians when switching to cool walls (albedo 0.60) from conventional walls (albedo 0.25). Results are for the multi-family residence in Fullerton (CZ8) and the entire year.

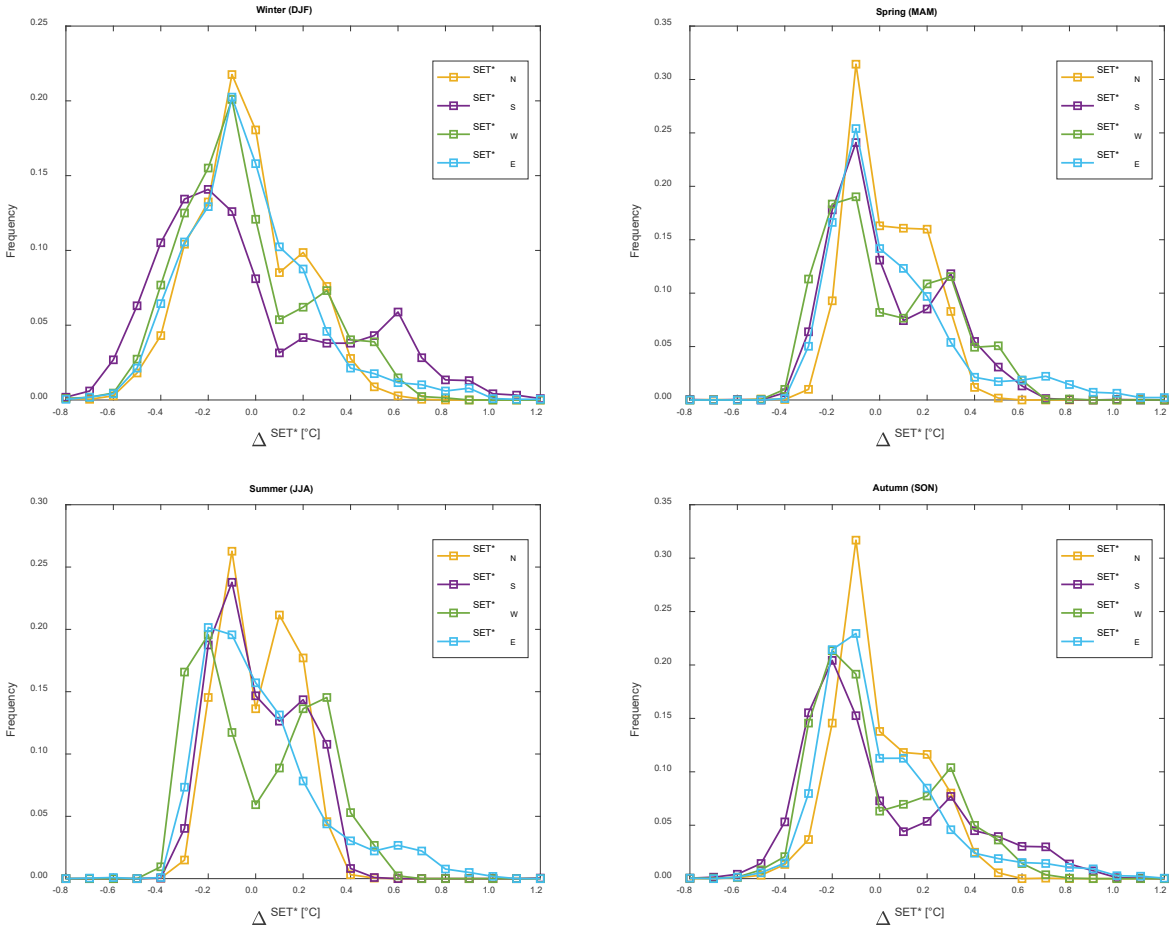

Figure 12. Seasonal analogs of Figure 11 (winter = Dec/Jan/Feb, spring = Mar/Apr/May, summer = Jun/Jul/Aug, and autumn = Sep/Oct/Nov).

As before for the MRT, the mean increase of SET* for a pedestrian near a cool wall during daytime in the entire year is reported in Table 14 through Table 22 for the different building types and climate zones. The average SET* increase ranges from 0.1 ˚C to 0.4 ˚C and is smallest for the north wall, in the summer, for the inland climate zone (CZ13), or the medium office building.

The SET* increase patterns follow the MRT trends, since MRT is an input to SET*. But SET* rises only about 0.25 ˚C per 1 ˚C increase in MRT, because SET* also depends on the canopy air temperature. Since canopy air temperature changes are 0.2˚C or less for all but two winter results, the canopy air temperature effects are less influential than the MRT effects.

Table 14. Rise in mean annual Standard Equivalent Temperature (SET*) induced by switch to cool walls from conventional walls, shown for the multi-family residence in CZ8.

	$\Delta SET^*_{\mathrm{N}}$ [°C]	$\Delta SET^*_{\mathrm{S}}$ [°C]	$\Delta SET^*_{\mathrm{W}}$ [°C]	$\Delta SET^*_{\mathrm{E}}$ [°C]
Winter (DJF)	0.1	0.3	0.2	0.2
Spring (MAM)	0.1	0.2	0.2	0.2
Summer (JJA)	0.1	0.1	0.2	0.2
Autumn (SON)	0.1	0.3	0.2	0.2
Year	0.1	0.2	0.2	0.2

Table 15. Analog of Table 14 for the multi-family residence in CZ10.

	$\Delta SET^*_{\mathrm{N}}$ [°C]	$\Delta SET^*_{\mathrm{S}}$ [°C]	$\Delta SET^*_{\mathrm{W}}$ [°C]	$\Delta SET^*_{\mathrm{E}}$ [°C]
Winter (DJF)	0.1	0.3	0.2	0.2
Spring (MAM)	0.1	0.2	0.2	0.2
Summer (JJA)	0.1	0.1	0.2	0.2
Autumn (SON)	0.1	0.2	0.2	0.2
Year	0.1	0.2	0.2	0.2

Table 16. Analog of Table 14 for the multi-family residence in CZ13.

	$\Delta SET^*_{\mathrm{N}}$ [°C]	$\Delta SET^*_{\mathrm{S}}$ [°C]	$\Delta SET^*_{\mathrm{W}}$ [°C]	$\Delta SET^*_{\mathrm{E}}$ [°C]
Winter (DJF)	0.1	0.3	0.2	0.2
Spring (MAM)	0.1	0.2	0.2	0.2
Summer (JJA)	0.1	0.1	0.1	0.2
Autumn (SON)	0.1	0.3	0.2	0.2
Year	0.1	0.2	0.2	0.2

Table 17. Analog of Table 14 for the single-family residence in CZ8.

	$\Delta SET^*_{\mathrm{N}}$ [°C]	$\Delta SET^*_{\mathrm{S}}$ [°C]	$\Delta SET^*_{\mathrm{W}}$ [°C]	$\Delta SET^*_{\mathrm{E}}$ [°C]
Winter (DJF)	0.1	0.4	0.2	0.2
Spring (MAM)	0.1	0.2	0.2	0.2
Summer (JJA)	0.1	0.1	0.2	0.2
Autumn (SON)	0.1	0.3	0.2	0.2
Year	0.1	0.2	0.2	0.2

Table 18. Analog of Table 14 for the single-family residence in CZ10.

	$\Delta SET^*_{\mathrm{N}}$ [°C]	$\Delta SET^*_{\mathrm{S}}$ [°C]	$\Delta SET^*_{\mathrm{W}}$ [°C]	$\Delta SET^*_{\mathrm{E}}$ [°C]
Winter (DJF)	0.1	0.4	0.2	0.3
Spring (MAM)	0.2	0.2	0.2	0.3
Summer (JJA)	0.1	0.1	0.2	0.2
Autumn (SON)	0.1	0.3	0.2	0.2
Year	0.1	0.3	0.2	0.2

Table 19. Analog of Table 14 for the single-family residence in CZ13.

	$\Delta SET^*_{\mathrm{N}}$ [°C]	$\Delta SET^*_{\mathrm{S}}$ [°C]	$\Delta SET^*_{\mathrm{W}}$ [°C]	$\Delta SET^*_{\mathrm{E}}$ [°C]
Winter (DJF)	0.1	0.3	0.2	0.2
Spring (MAM)	0.1	0.2	0.2	0.2
Summer (JJA)	0.1	0.1	0.1	0.2
Autumn (SON)	0.1	0.3	0.2	0.2
Year	0.1	0.2	0.2	0.2

Table 20. Analog of Table 14 for the medium office in CZ8.

	$\Delta SET^*_{\mathrm{N}}$ [°C]	$\Delta SET^*_{\mathrm{S}}$ [°C]	$\Delta SET^*_{\mathrm{W}}$ [°C]	$\Delta SET^*_{\mathrm{E}}$ [°C]
Winter (DJF)	0.1	0.2	0.1	0.1
Spring (MAM)	0.1	0.1	0.2	0.2
Summer (JJA)	0.1	0.1	0.2	0.2
Autumn (SON)	0.1	0.2	0.2	0.2
Year	0.1	0.2	0.2	0.2

Table 21. Analog of Table 14 for the medium office in CZ10.

	$\Delta SET^*_{\mathrm{N}}$ [°C]	$\Delta SET^*_{\mathrm{S}}$ [°C]	$\Delta SET^*_{\mathrm{W}}$ [°C]	$\Delta SET^*_{\mathrm{E}}$ [°C]
Winter (DJF)	0.1	0.2	0.1	0.1
Spring (MAM)	0.1	0.1	0.2	0.2
Summer (JJA)	0.1	0.1	0.2	0.2
Autumn (SON)	0.1	0.2	0.1	0.1
Year	0.1	0.2	0.1	0.2

Table 22. Analog of Table 14 for the medium office in CZ13.

	$\Delta SET^*_{\mathrm{N}}$ [°C]	$\Delta SET^*_{\mathrm{S}}$ [°C]	$\Delta SET^*_{\mathrm{W}}$ [°C]	$\Delta SET^*_{\mathrm{E}}$ [°C]
Winter (DJF)	0.1	0.2	0.1	0.1
Spring (MAM)	0.1	0.1	0.1	0.2
Summer (JJA)	0.1	0.1	0.1	0.1
Autumn (SON)	0.1	0.2	0.1	0.1
Year	0.1	0.1	0.1	0.1

5.5 Sensitivity to pedestrian shortwave absorptance

Pedestrian shortwave absorptance (α_k) is a parameter that can change considerably between persons (Table 3) due to differences in skin and clothing colors. A sensitivity analysis for MRT and thermal comfort to α_k is performed for the pedestrian near the multi-family residence in Fullerton. While α_k was 0.70 in the preceding analysis, here the project team also reports results for $\alpha_k = 0.40$ (light-colored clothing and/or skin) and $\alpha_k = 0.90$ (dark clothing and/or skin). The results are reported as the average daily cycle of MRT and SET* for the pedestrian at the south of the building. As expected pedestrian MRT is most sensitive to α_k during midday when solar radiation incident on the south wall peaks. Increase absorption of solar radiation (higher α_k) boosts the rise in MRT upon switching to cool walls. MRT differences for the light and dark-colored pedestrian with respect to the case with $\alpha_k = 0.70$ range between -1.4 ˚C and +0.8 ˚C, on

average. Notably even the light-colored pedestrian experiences a MRT increase during most of the daytime. The results by season are similar to those in Figure 6 and are not shown.

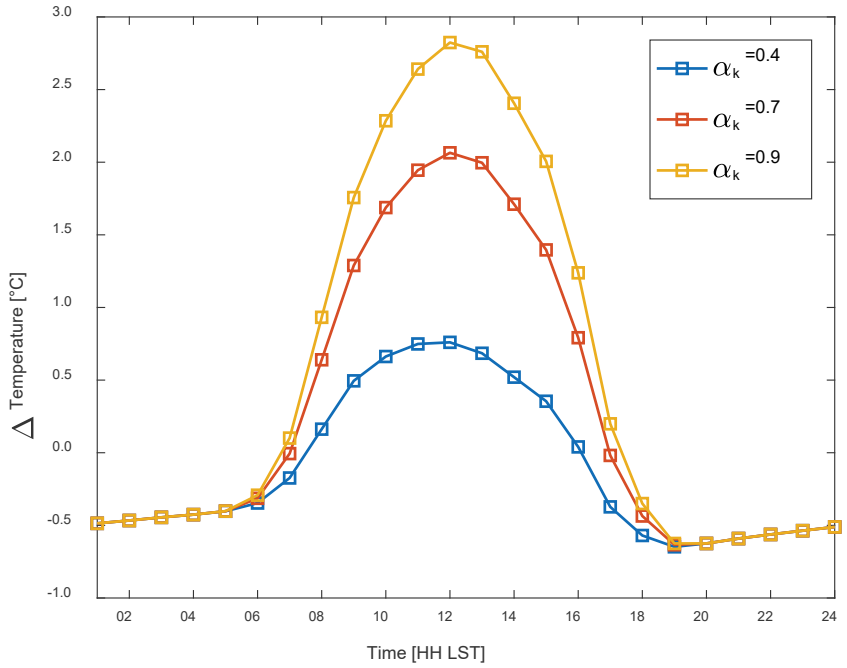

Figure 13. Average (over the year) T_{MRT} rise upon switching to cool walls (albedo 0.60) from conventional walls (albedo 0.25). Result are for the multi-family residence in Fullerton (CZ8) for a pedestrian at the south location for different values of pedestrian shortwave absorptance α_k. Refer to Figure 5 for results for the pedestrian with $\alpha_k = 0.70$ standing near the other walls.

The SET* sensitivity to α_k in Figure 14 is similar to the MRT sensitivity. The SET* sensitivity is smaller than the MRT sensitivity because the MRT is only one of the inputs to the SET* while the other inputs are unaffected by α_k. On average, relative to the pedestrian with $\alpha_k = 0.7$, SET* is up to 0.13 ˚C higher for a pedestrian with $\alpha_k = 0.90$ and up to 0.25 ˚C lower for a pedestrian with $\alpha_k = 0.40$. For the pedestrian with low solar absorptance (light-colored clothing and/or skin), the 24 h averaged effect of cool walls is a cooler thermal sensation as the daytime warmer thermal sensation is offset by a colder thermal sensation at night.

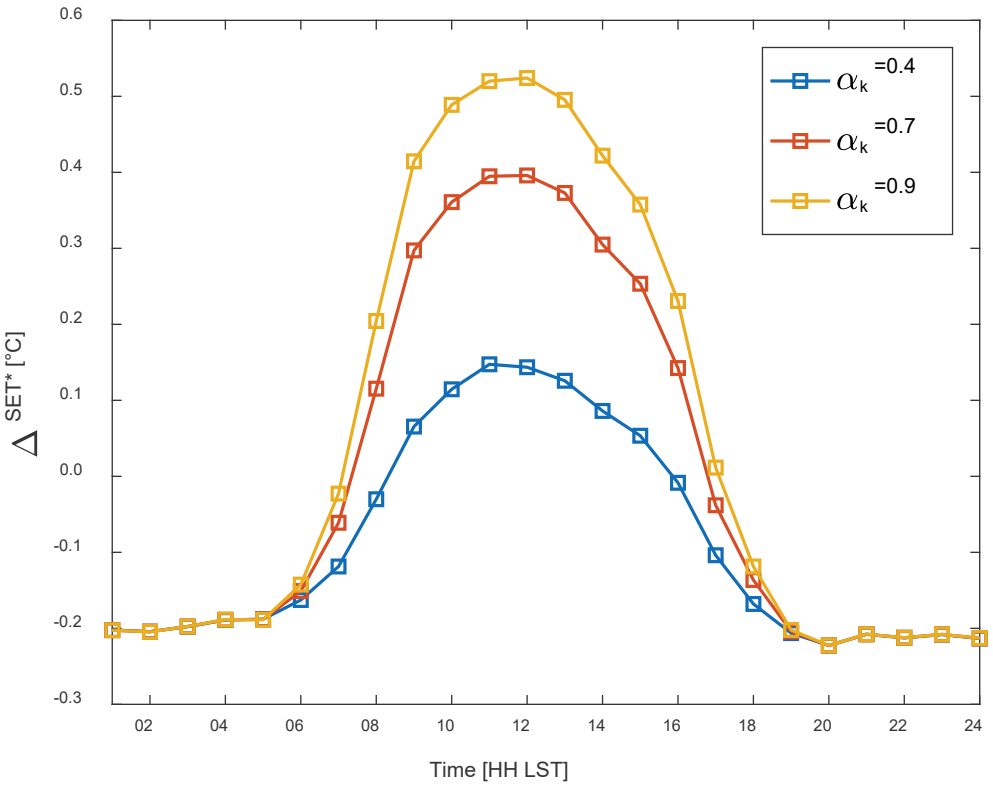

Figure 14. Average (over the year) SET* rise upon switching to cool walls (albedo 0.60) from conventional walls (albedo 0.25). Results are for the multi-family residence in Fullerton (CZ8) for a pedestrian at the south location for different α_k.

6 Conclusions and Limitations

MRT and thermal comfort were analyzed for homogeneous neighborhoods of either multi-family residences, single-family residences, or medium office buildings with cool walls. Typical meteorological year weather data is input to a neighborhood heat transfer model (TUF-IOBES) in three different California climate zones to understand impacts on a pedestrian walking 1.5 m away from walls at the four cardinal orientations. The typical daytime MRT rise near a cool wall (albedo of 0.60) versus a conventional wall (albedo of 0.25) is around 1 ˚C in most cases. Maximum rise occurred for a pedestrian near the south wall in winter and minimum rise occurred for a pedestrian near the north wall. MRT differences by building type and climate zone were negligible.

Cool walls bring about an average increase in daytime standard equivalent temperature (a measure of thermal comfort) of 0.4 ˚C or less at all pedestrian locations, building types, and climate zones. Since thermal sensation in California is generally too warm this corresponds to a

slight worsening of thermal comfort. However, the largest standard equivalent temperature increases occur in winter when a cold thermal sensation is more common. During winter, cool walls therefore improve thermal comfort. The results are sensitive to the pedestrian solar absorptance; a pedestrian with extremely small solar absorptance may even experience a cooler thermal comfort, on average over the year.

As described in Section 2, since the TUF-IOBES simulation is forced with TMY data above the urban canopy, the canopy air temperature cooling effect of cool walls is underestimated in TUF-IOBES. The project team projects that actual daytime thermal comfort temperature increases would be less than the 0.4 ˚C estimated here.

7 References

ASHRAE. 2010. Standard 55-2010: Thermal Environmental Conditions for Human Occupancy. Atlanta USA.

California Energy Commission. 2017. California Energy Maps. http://www.energy.ca.gov/maps/renewable/building_climate_zones.html. Accessed May 15, 2017.

Gagge AP, Fobelets AP, Berglund L. 1986. A standard predictive index of human response to the thermal environment. *ASHRAE Transactions* 92(2), 709-731.

Höppe P. 1992. Ein neues Verfahren zur Bestimmung der mittleren Strahlungstemperatur im Freien. *Wetter und Leben* 44(1-3), 147-151 (in German). Translation: Title: A new method for determining exterior mean radiant temperature.

Johnson GT, Watson ID. 1984. Person view-factors in the urban environment. *Meteorology and Atmospheric Physics* 34(3), 273-285. https://doi.org/10.1007/BF02265493

Nusselt, W., 1928. Grafische Bestimmung des Winkelverhaltnisses bei der Warmestrahlung. *Zeitschrift des Vereines Deutscher Ingenieure*, 72(20), p.673. Translation: Title: Graphical view factor determination in heat transfer.

Rosado, PJ. 2016. Evaluating cool impervious surfaces: application to an energy-efficient residential roof and to city pavements. Ph.D. Dissertation, University of California at Berkeley. http://escholarship.org/uc/item/6bf80485.

Underwood C R, Ward E J. 1966. The solar radiation area of man. *Ergonomics* 9(2), 155-168. http://doi.org/10.1080/00140136608964361

VDI. 2008. VDI 3787 part 2: Environmental meteorology - Methods for the human biometeorological evaluation of climate and air quality for urban and regional planning at regional level. Düsseldorf Germany. http://www.vdi.eu/nc/guidelines/vdi_3787_blatt_2-

umweltmeteorologie_methoden_zur_human_biometeorologischen_bewertung_von_klima_und_lufthy_/

Task Report Appendix A: View factors

A.1. View factors from curved side wall

A.1.1. Calculating cylinder side wall view factor from slice side wall view factors

To prepare to calculate view factors from the cylinder's side wall to building walls, sky, and ground, we divide the cylinder's side wall (surface C) of area $A_{\mathrm{C}} = 2\,\pi\,r\,H_{\mathrm{body}}$ into a series of M thin horizontal slices of thickness Δh and area $A_{\Delta \mathrm{C}} = 2\,\pi\,r\,\Delta h$.

If the view factor from some surface B (building wall, sky, or ground) to the cylinder's side wall of slice i at height h_i (surface $\Delta \mathrm{C}_i$) is $F_{\mathrm{B}\to\Delta \mathrm{C},i}$, the view factor from surface B to surface C will be

$$F_{\mathrm{B}\to\mathrm{C}} = \sum_{i=1}^{M} F_{\mathrm{B}\to\Delta \mathrm{C},i}\ . \tag{A-8}$$

Applying the view factor reciprocity relationship

$$A_{\mathrm{X}} F_{\mathrm{X}\to\mathrm{Y}} = A_{\mathrm{Y}} F_{\mathrm{Y}\to\mathrm{X}} \tag{A-9}$$

to each side of Eq. (A-8) yields

$$\frac{A_{\mathrm{C}}}{A_{\mathrm{B}}} F_{\mathrm{C}\to\mathrm{B}} = \sum_{i=1}^{M} \frac{A_{\Delta \mathrm{C}}}{A_{\mathrm{B}}} F_{\Delta \mathrm{C},i\to\mathrm{B}}\,. \tag{A-10}$$

Rearranging,

$$F_{\mathrm{C}\to\mathrm{B}} = \frac{1}{A_{\mathrm{C}}} \sum_{i=1}^{M} F_{\Delta \mathrm{C},i\to\mathrm{B}}\, A_{\Delta \mathrm{C}} = \frac{1}{2\,\pi\,r\,H_{\mathrm{body}}} \sum_{i=1}^{M} F_{\Delta \mathrm{C},i\to\mathrm{B}}\, 2\,\pi\,r\,\Delta h\ . \tag{A-11}$$

Transforming the sum to an integral,

$$F_{\mathrm{C}\to\mathrm{B}} = \frac{1}{H_{\mathrm{body}}} \sum_{i=1}^{M} F_{\Delta \mathrm{C},i\to\mathrm{B}}\, \Delta h = \frac{1}{H_{\mathrm{body}}} \int_0^{H_{\mathrm{body}}} F_{\Delta \mathrm{C}\to\mathrm{B}}(h)\, dh = \overline{F_{\Delta \mathrm{C}\to\mathrm{B}}}\ , \tag{A-12}$$

where the bar operator signifies averaging over all slices. In other words, the view factor from the side wall of the cylinder to some surface B is the average of the view factors from the side walls of its slices to surface B.

A.1.2. View factor from cylinder side wall to building wall

Now consider radiative exchange between a slice side wall ΔC and the building wall of height H shown in Figure A-1. The view factors from the cylinder's slice side wall to the portion of

the building wall above the slice ("upper building wall", or UBW), and to the portion of the building wall below the slice ("lower building wall", or LBW), are

$$F_{\Delta C \to \mathrm{UBW}} = \frac{1}{\pi^2} \int_{\gamma_1}^{\gamma_2} \int_{0}^{\omega_1} \cos^2 \phi \, d\phi \, d\theta \tag{A-13}$$

and

$$F_{\Delta C \to \mathrm{LBW}} = \frac{1}{\pi^2} \int_{\gamma_1}^{\gamma_2} \int_{\omega_2}^{0} \cos^2 \phi \, d\phi \, d\theta \,, \tag{A-14}$$

respectively. Here θ is the angle in the horizontal plane and the integration is from γ_1 to γ_2 which are the angles in the horizontal plane between the normal to the wall and the left and right edges of the wall, respectively. ϕ is the angle in the vertical plane and the integration bounds are ω_1 and ω_2, which are the angles between the horizontal plane containing ΔC and the top and bottom edge of the wall, respectively. Therefore $\omega_1 = \tan^{-1}\left(\frac{H-h}{D}\cos\theta\right)$ and $\omega_2 = -\tan^{-1}\left(\frac{h}{D}\cos\theta\right)$.

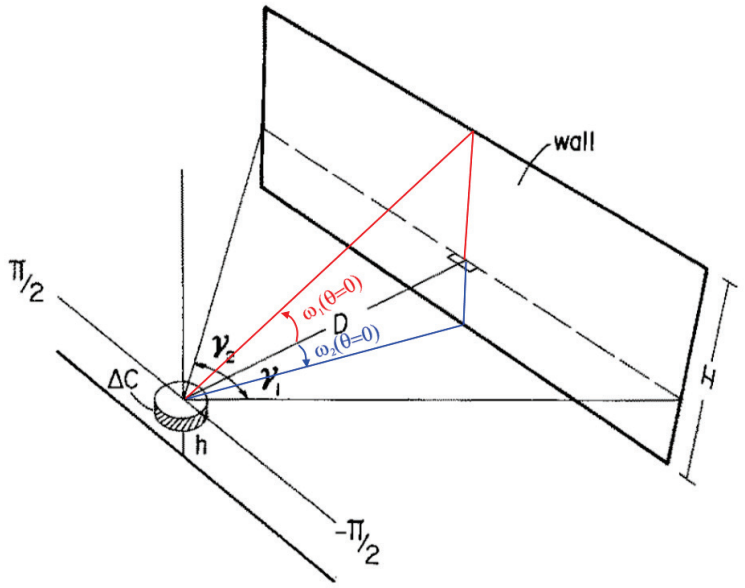

Figure A-1. Geometrical arrangement of the pedestrian (represented by a cylinder) and a building wall, showing an infinitesimal slice ΔC of the cylinder at height h above ground and at distance D from a wall of height H. Adapted from Johnson and Watson (1984).

The view factor from the slice side wall to the entire building wall (EBW) is

$$F_{\Delta C \to \mathrm{EBW}} = F_{\Delta C \to \mathrm{UBW}} + F_{\Delta C \to \mathrm{LBW}} \,. \tag{A-15}$$

Applying Eq. (A-12), the view factor from cylinder side wall to the entire building wall is

$$F_{\mathrm{C}\to\mathrm{EBW}} = \overline{F_{\Delta\mathrm{C}\to\mathrm{UBW}}} + \overline{F_{\Delta\mathrm{C}\to\mathrm{LBW}}} \,. \tag{A-16}$$

$F_{\mathrm{C}\to\mathrm{EBW}}$ is calculated for each of the 10 building walls seen by the pedestrian (Figure 2).

A.1.3. View factors from cylinder side wall to sky and ground

If the slice side wall sees N building walls, the view factors from the slice side wall to all wall regions above the slice (all UBWs) and all wall regions below the slice (all LBWs) will be

$$F_{\Delta\mathrm{C}\to\text{all UBWs}} = \sum_{j=1}^{N} F_{\Delta\mathrm{C}\to\mathrm{UBW},j} \tag{A-17}$$

and

$$F_{\Delta\mathrm{C}\to\text{all LBWs}} = \sum_{j=1}^{N} F_{\Delta\mathrm{C}\to\mathrm{LBW},j} \tag{A-18}$$

respectively, where j indexes the building walls.

The slice side wall has equal views of its upper hemisphere (UH, meaning everything above the slice) and its lower hemisphere (LH, meaning everything below the slice). Since the view factor from the slice side wall to the entire sphere is unity,

$$F_{\Delta\mathrm{C}\to\mathrm{UH}} = F_{\Delta\mathrm{C}\to\mathrm{LH}} = \tfrac{1}{2} \,. \tag{A-19}$$

The slice's upper hemisphere comprises the sky and all building wall surfaces above the slice (all UBWs), while its lower hemisphere comprises the ground and all building wall surfaces below the slice (all LBWs). Thus, the view factors from the slice side wall to the sky and to the ground are

$$F_{\Delta\mathrm{C}\to\mathrm{sky}} = F_{\Delta\mathrm{C}\to\mathrm{UH}} - F_{\Delta\mathrm{C}\to\text{all UBWs}} \tag{A-20}$$

and

$$F_{\Delta\mathrm{C}\to\mathrm{ground}} = F_{\Delta\mathrm{C}\to\mathrm{LH}} - F_{\Delta\mathrm{C}\to\text{all LBWs}} \tag{A-21}$$

respectively. Applying Eq. (A-12), the view factors from the cylinder side wall to the sky and to the ground are

$$F_{\mathrm{C}\to\mathrm{sky}} = \overline{F_{\Delta\mathrm{C}\to\mathrm{sky}}} = F_{\Delta\mathrm{C}\to\mathrm{UH}} - \overline{F_{\Delta\mathrm{C}\to\text{all UBWs}}} \tag{A-22}$$

and

$$F_{\mathrm{C}\to\mathrm{ground}} = \overline{F_{\Delta\mathrm{C}\to\mathrm{ground}}} = F_{\Delta\mathrm{C}\to\mathrm{LH}} - \overline{F_{\Delta\mathrm{C}\to\mathrm{all\ LBWs}}} \quad , \tag{A-23}$$

respectively.

A.2. View factors from top and bottom plates to wall, sky, and ground

The view factor from the top plate to one entire building wall is

$$F_{\mathrm{top\ plate}\to\mathrm{EBW}} = \frac{1}{\pi}\int_{\gamma_1}^{\gamma_2}\int_{0}^{\omega_3} \cos\phi \sin\phi \; d\phi \; d\theta \,, \tag{A-24}$$

where $\omega_3 = \tan^{-1}\left(\frac{H-H_{\mathrm{body}}}{D}\cos\theta\right)$. Since the top plate sees only the sky and the N building walls, $F_{\mathrm{top\ plate}\to\mathrm{ground}} = 0$, and the view factor from the top plate to the sky is the view factor from the top plate to the entire sphere (unity) minus the sum of its view factors to each entire building wall:

$$F_{\mathrm{top\ plate}\to\mathrm{sky}} = 1 - \sum_{j=1}^{N} F_{\mathrm{top\ plate}\to\mathrm{EBW},j} \;. \tag{A-25}$$

The cylinder's bottom plate sees only the ground, so $F_{\mathrm{bottom\ plate}\to\mathrm{ground}} = 1$, $F_{\mathrm{bottom\ plate}\to\mathrm{sky}} = 0$, and $F_{\mathrm{bottom\ plate}\to\mathrm{any\ wall}} = 0$.

A.3. View factors from entire cylinder to wall, sky, and ground

Consider a generic surface E with M elements denoted $\mathrm{E}_1 \ldots \mathrm{E}_M$. If the view factor from some surface B to element E_i is $F_{\mathrm{B}\to\mathrm{E},i}$, the view factor from surface B to surface E will be

$$F_{\mathrm{B}\to\mathrm{E}} = \sum_{i=1}^{M} F_{\mathrm{B}\to\mathrm{E},i} \,. \tag{A-26}$$

Applying view factor reciprocity [Eq. (A-9)] to each side of Eq. (A-26) and rearranging yields

$$F_{\mathrm{E}\to\mathrm{B}} = \frac{1}{A_{\mathrm{E}}}\sum_{i=1}^{M} A_{\mathrm{E},i}\, F_{\mathrm{E},i\to\mathrm{B}} \;. \tag{A-27}$$

If the body of the pedestrian is represented by the surface of the cylinder, the view factor from the body to surface B (entire wall j, sky, or ground) is

$$F_{\mathrm{body}\to\mathrm{B}} = \frac{A_{\mathrm{C}}F_{\mathrm{C}\to\mathrm{B}} + A_{\mathrm{plate}}F_{\mathrm{top\ plate}\to\mathrm{B}} + A_{\mathrm{plate}}F_{\mathrm{bottom\ plate}\to\mathrm{B}}}{A_{\mathrm{body}}} \quad , \tag{A-28}$$

where the cylinder's top and bottom plates each have surface area $A_{plate} = \pi r^2$, and the cylindrical pedestrian has surface area $A_{body} = A_C + 2 \times A_{plate}$.

Energy Research and Development Division

FINAL PROJECT REPORT

Solar-Reflective "Cool" Walls: Benefits, Technologies, and Implementation

Appendix E: Urban Climate Impacts of Cool Walls (Task 3.2 Report)

California Energy Commission
Gavin Newsom, Governor

April 2019 | CEC-500-2019-040-APE

Appendix E:
Urban climate impacts of cool walls (Task 3.2 report)

Jiachen Zhang[1], Arash Mohegh[1], Yun Li[1], Ronnen Levinson[2], George Ban-Weiss[1]

[1] Department of Civil and Environmental Engineering, University of Southern California

[2] Heat Island Group, Lawrence Berkeley National Laboratory

31 May 2018

Abstract

This study for the first time assesses the influence of employing solar reflective "cool" walls on the urban energy budget and summertime climate of the Los Angeles basin. We systematically compare the effects of cool walls to cool roofs, a heat mitigation strategy that has been widely studied and employed, using a consistent modeling framework (Weather Research and Forecasting model). Adoption of cool walls leads to increases in urban grid cell albedo that peak in the early morning and late afternoon, when the ratio of solar radiation onto vertical walls versus horizontal surfaces is at a maximum. In Los Angeles County, daily cumulative increase in grid cell reflected solar radiation from increasing whole-wall albedo (albedo of the entire wall, including its openings) by 0.80 is 783 kJ m^{-2}, 43% of that for increasing whole-roof albedo. Cool walls reduce canyon air temperatures in Los Angeles by 0.43 K (daily average), with the peak reduction (0.64 K) occurring at 09:00 LST and a secondary peak (0.53 K) at 18:00 LST. Per 0.10 whole-wall (whole-roof) albedo increase, cool walls (roofs) can reduce summertime daily average canyon air temperature by 0.048–0.054 K (0.058–0.060 K), yielding a cool-wall to cool-roof temperature reduction ratio of 83 – 90 percent.

If the albedos of windows and doors are unchanged in a cool-wall campaign, these cool-wall air temperature reductions and solar upflux increases should be multiplied by 0.83, the ratio of net wall area (gross wall area minus opening area) to gross wall area in the City of Los Angeles. In the City of Los Angeles, the whole-wall albedo increase from a cool-wall campaign that excludes windows and doors is essentially equal to the whole-roof albedo increase from a cool-roof campaign that modifies the entire roof.

Results reported here can be used to inform policies on urban heat island mitigation or climate change adaptation.

1 Introduction

The urban heat island effect (UHIE) is a phenomenon in which urban areas are warmer than surrounding rural areas, a result of urban-rural differences in land cover and population density. The UHIE can exacerbate challenges associated with high temperatures in urban areas including (a) human health impacts from extreme heat (Palecki et al., 2001), such as heat stroke, heat exhaustion rates, and premature deaths; and (b) daily total and peak air conditioning energy use during summer (Kolokotroni et al., 2006). Several important environmental processes, which are driven by the effects of urban land expansion on surface-atmosphere coupling, can aggravate or mitigate the UHIE. First, widespread application of materials with high solar absorptance (e.g., asphalt concrete and many roofing materials) in urban areas increases absorption of sunlight. Second, extensive use of materials with high heat capacity increases retention of sunlight throughout the day. Third, the geometry of urban canyons (i.e., the space between buildings and above streets) can trap both shortwave (solar) and longwave (thermal infrared) radiation (Theeuwes et al., 2014). Fourth, lack of vegetation cover in cities reduces evaporative cooling and shading of the ground surface, thereby increasing urban temperatures (Taha, 1997). Fifth, increases in soil moisture from irrigation in urban areas can increase evaporative fluxes and cool cities during the day, while at night causing increases in upward ground heat fluxes (due to the increase in soil moisture and thermal conductivity) and therefore nocturnal warming (Vahmani et al., 2016). Sixth, changes in surface roughness from urbanization can also alter wind flows and vertical mixing (Vahmani et al., 2016), with subsequent effects on temperatures that can vary by location. Finally, human activities and industrial processes contribute to releasing waste heat in cities (Fan and Sailor, 2005; Oke et al., 1991) .

To lessen the UHIE, heat mitigation strategies have been proposed and employed in some locations to alter the energy balance in cities and decrease temperatures. For example, planting trees and/or adopting vegetative roofs could increase evaporative cooling and reduce urban temperatures (Li et al., 2014). Increasing the albedo, or solar reflectance (ratio of reflected to incident sunlight) of roofs, walls, and pavements could reduce solar heat gain, lower surface temperatures, decrease heat transfer from the surface to the atmosphere, and consequently cool the outside air. Heat mitigation strategies can also influence urban climate by changing the hydrological cycle (Georgescu et al., 2014).

The effects of solar-reflective “cool” roofs on urban climate have been well studied in previous research. Large-scale implementation of cool roofs has been predicted to effectively reduce city-wide air temperatures in Athens, Greece (Synnefa et al., 2008); Sacramento (Taha, 2008); and Baltimore-Washington (Li et al., 2014). In Los Angeles, the reduction of peak air temperature induced by increasing both roof and pavement albedo was estimated to reach 1.5 K (Rosenfeld et al., 1998), while a newer study (Millstein and Menon, 2011) estimated the reduction at 13:00 local standard time (LST) in summer to be 0.5 K. In addition, Vahmani et al. (2016) concluded that widespread adoption of cool roofs could reduce Southern California summer urban air

temperatures by 0.9 K at 14:00 LST and by 0.5 K at 22:00 LST. Santamouris (2014) summarized previous literature and concluded that daily average ambient temperatures are expected to decrease linearly with average grid cell albedo increase in cities, declining 0.3 K per 0.1 albedo increase. (We note here that grid cell albedo represents a "bird's eye view" of both impervious and pervious surfaces within modeled urban regions.)

Cool pavements have been studied less than cool roofs. While they are both horizontal surfaces, temperature reductions per unit facet albedo increase can differ between them in part because cool pavements are at the bottom of the urban canyon while roofs are at the top. Mohegh et al. (2017) simulated the influence of employing cool pavements on near-surface air temperatures in Californian cities. They found that increasing pavement albedo by 0.40 could lead to annual average air temperature reductions at 14:00 LST ranging by city from 0.19 K to 0.87 K. Temperatures at 14:00 LST declined by 0.32 K per 0.10 increase in grid cell average albedo.

Despite previous studies that have examined the effects of raising albedo of horizontal surfaces in different cities, the influence of increasing the albedo of vertical surfaces (e.g., walls) on temperatures has not yet been systematically investigated. The climate effects of increasing wall albedo are expected to differ from those for cool roofs. First, increasing wall albedo and roof albedo by the same amount will influence the energy budget of the urban canopy (i.e., the urban canyon plus roof surfaces) differently for four reasons:

(a) Diurnal cycles of solar irradiance (incident radiative power per unit area) and daily solar irradiation (incident radiative energy per unit area) received by vertical walls differ from those received by (nearly) horizontal roofs. For example, in July, the north, east, south and west walls of a building in San Diego and Fullerton, CA collectively typically receive about 40% as much daily solar irradiation as its roof (See Tables A1 and A2 in Task Report Appendix A). Figure 1 in the supplemental information compares the diurnal cycle of irradiance on roofs and walls.

(b) Walls make up a different fraction of urban areas than do roofs (see Section 2.3 for more details).

(c) Walls can be shaded when sun is low, so the fraction of wall area that is illuminated varies by time. In our study, we assume that roofs are not shaded. (In the real-world, non-uniform building heights and trees can lead to roof shading, but we ignore these effects in this study.)

(d) A portion of the solar radiation that is reflected by walls is absorbed by opposing walls and pavements, and is thus trapped in the canyon. Solar radiation reflected by roofs, on the other hand, mostly escapes the canopy without being absorbed by other urban facets. Unlike cool roofs, the effect of cool walls depends of the height to width ratio of the urban canopy.

Hence, solar reflections from cool walls differ in timing and magnitude from those from cool roofs.

Second, atmospheric temperature changes induced by cool surfaces are determined not only by the change in the canyon energy budget but also by the diurnal cycle in surface-atmosphere interactions. Diurnal variations in wind speeds, planetary boundary layer (PBL) heights, and atmospheric stability can influence the relationship between changes in the surface energy budget and resulting atmospheric temperature reductions (Bonan, 2010). Cool walls and roofs induce different diurnal cycles in reflected solar radiation. Thus, the diurnal cycles in surface-atmosphere coupling contribute to differences in air temperature change. In other words, even if increases in daily reflected solar radiation were the same for cool walls and roofs, their different diurnal cycles would be expected to lead to different daily average air temperatures.

Lastly, walls are in the urban canyon whereas roofs are at the top of the canopy. This means that walls may more directly influence in-canyon air temperatures than roofs, while roofs may more directly influence above-canopy air temperatures.

In this study, we use a regional climate model, coupled to an urban canopy model, to investigate how adopting cool walls would influence albedo, reflection of sunlight, and near-surface air temperature in the Los Angeles basin. We adopt a new parameterization that diagnoses near-surface air temperature within the urban canyon, which in turn affects pedestrian thermal comfort and building energy use. A suite of additional cool roof simulations systematically compares the climate effects of cool walls to those of cool roofs within a consistent modeling framework.

2 Methodology

2.1 Model description

We use the Weather Research and Forecasting model (WRF) version 3.7 (Skamarock et al., 2008)to investigate the effects of raising wall albedo on near-surface canyon air temperatures in the Los Angeles basin. WRF is developed collaboratively by the National Center for Atmospheric Research (NCAR), the National Oceanic and Atmospheric Administration (NOAA) and other institutes, and is widely used to study regional-scale meteorology and climate.

WRF provides several parameterizations that can be used to represent processes that occur at resolutions finer than model grid cells. We summarize here the parameterizations chosen for our simulations. Physics schemes include the Rapid Radiative Transfer Model (RRTM) scheme for long-wave radiation (Mlawer et al., 1997), the Goddard shortwave scheme (Chou and Suarez, 1994) for shortwave radiation, the Yonsei University scheme (Hong et al., 2006) for the planetary boundary layer, and Lin et al. scheme for cloud microphysics (Lin et al., 1983). To simulate cumulus clouds in the middle and outer domains, the Kain-Fritsch convective parameterization is used (Kain, 2004). The Noah Land Surface Model (Chen and Dudhia, 2001)

couples the land surface and atmosphere to compute exchanges in energy (e.g., latent and sensible heat fluxes), momentum, and water. A single-layer urban canopy model (UCM) simulates the influence of urban surface-atmosphere coupling (Chen et al., 2011).. Parameterizations for physics are chosen to be consistent with our previous modeling studies for Southern California (Vahmani and Ban-Weiss, 2016a, 2016b), which were extensively evaluated by comparing to observations.

The National Land Cover Database for 2006 is used for land cover type classification in the model (Fry et al., 2011). For urban grid cells (i.e., cells dominated by urban land cover), we use impervious surface data from the National Land Cover Database (NLCD) (Wickham et al., 2013) to compute grid cell specific impervious fractions (i.e., the fraction of each grid cell covered by impervious surfaces). The urban canopy model resolves surface-atmosphere exchange for the impervious part of the grid cell, while the Noah model is used for the pervious portion of urban grid cells. Note that the Noah Land Surface model also handles non-urban grid cells. Urban land use classification and urban morphology will be discussed in Section 2.3.

Following (Vahmani and Ban-Weiss, 2016b), we have improved the default version of the WRF model by utilizing MODIS satellite observations to determine grid cell specific green vegetation fraction and leaf area index for pervious areas (i.e., for both the pervious portion of urban grid cells and for non-urban cells). Previous research has found that accounting for high resolution heterogeneity in land surface properties in urban areas can improve model simulations when comparing to observations of meteorology in Los Angeles (Vahmani et al., 2016).

2.2 Shortwave radiation calculations in the urban canopy model

In the single-layer urban canopy model (UCM) employed in WRF (Kusaka et al., 2001), the urban canopy is represented as an infinitely long street (a.k.a. ground, or canyon floor) bounded by two infinitely long buildings of identical width. That is, there is no separation between adjacent buildings on the same side of the street. Recall that we refer to the urban canopy as the canyon plus roof surfaces.

Direct (beam) and diffuse solar radiation are tracked separately in our model. At solar noon, most beam sunlight strikes horizontal surfaces (roofs and ground), rather than vertical surfaces (walls). In early morning and late afternoon, the ratio of beam vertical radiation to beam horizontal radiation is higher than that at solar noon. Buildings shade the ground when the sun is not at zenith, reducing the ground's solar irradiance and solar heat gain. Since in the canopy model all sunlight not incident on roofs strikes walls or the ground, the beam solar radiation (power) intercepted by the sun-facing wall equals beam horizontal irradiance (power/area) times the length of the ground shadow. Canyon orientation (i.e., the angle between canyon centerline and north) and solar position are considered in the calculations of ground shadow length throughout the day. Eight canyon orientations (0˚, 45˚, 90˚, 135˚, 180˚, 225˚, 270˚, 315˚) are considered, and the shadow length is averaged among the results. Ground shadows are longest

when the sun is low and shortest when the sun is high. Thus, the fraction of global horizontal irradiance that is incident on the ground peaks at solar noon, while that incident on walls reaches its minimum at solar noon and maximum at peaks in the early morning and late afternoon (Figure 2 in Task Report Appendix A).

The diffuse part of solar radiation can strike all impervious facets (roofs, walls, and ground). Downwelling diffuse solar irradiances on wall and ground surfaces are proportional to the view factors from wall to sky and from ground to sky, respectively. Each facet is assumed to reflect sunlight diffusely. The view factors from ground to wall, from wall to ground, and from sun-facing wall to sun-opposing wall influence the reception of reflected radiation by walls and ground. Note that radiation reflected twice by facets is assumed to fully escape from urban canopy. For example, absorption within the canopy of light reflected from wall to wall to ground is ignored in the model.

Note that even though WRF-UCM includes a “shadow model” that treats direct and diffuse radiation separately, as aforementioned, the default code of WRF-UCM has the “shadow model” turned off. Thus, all solar radiation is treated as diffuse and shadows casted by buildings is not considered. (See Line 853 of module_sf_urban.F in WRF3.7 where SHADOW = .false.) We turn on the shadow calculations by setting SHADOW = .true. We also add to the default shadow model wall-to-wall reflection effects following Kusaka et al. (2001).

Downward solar radiation that is not absorbed by roofs, walls, and ground is reflected out of the canopy as upwelling solar radiation. UCM calculates canopy albedo as the ratio of upwelling sunlight to downwelling sunlight at the horizontal plane bounding the top of the canopy. The changes to canopy albedo upon increasing wall albedo are computed here using the single-layer urban canopy model. Canopy albedo represents the aggregated “above-canopy” albedo of all facets in the urban portion of grid cells, not including contributions from the non-urban portion of the grid cell. Since only the urban portion of the grid cell is modified, changes in grid cell albedo are then computed as change in canopy albedo multiplied by urban fraction (Figure 1c). Note that canopy and grid cell albedo are diagnostic variables and are not used in other model calculations.

2.3 Urban land use type classification and corresponding canopy morphology

Urban morphology in the UCM is described by roof width (R), building height (H), and ground width (W). The UCM uses the urban morphology to compute (a) solar irradiance (power/area) incident onto each facet; (b) shortwave radiation (power/area) reflection and longwave radiation (power/area) transfer from each facet to other canyon facets and to the sky; and (c) area weighting factors for averaging solar absorption (power/area) and sensible heat fluxes (power/area) among facets.

Data describing spatially resolved urban morphology from the National Urban Database and Access Portal Tool (NUDAPT) are used where available. NUDAPT data (Ching et al., 2009) cover only a small portion of our domain, but include downtown Los Angeles, where unusually tall buildings are found. For grid cells where NUDAPT data are not available, we derive urban morphology as follows.

The National Land Cover Database (NLCD) for 2006 is used for land cover type classification in the model (Fry et al., 2011). NLCD includes three urban land use types: low-intensity residential, high-intensity residential, and commercial/industrial. In the WRF UCM, we define different urban morphologies for each of the three urban types.

For each urban land use type, urban canopy morphology (i.e., ground width, building height, and roof width in Table 1) is set based on two real-world datasets for Los Angeles County: LARIAC (2014) and LARIAC (2016). LARIAC (2016) provides information for every building in Los Angeles County, including ZIP Code, roof area, building height, and shape. LARIAC (2014) provides the geographical centerlines for each street in Los Angeles County. Urban morphologies in the UCM are derived satisfying (a) H/W in the UCM as the ratio between building height from LARIAC (2016) and ground width from LARIAC (2014), and (b) $2 \times H/R$ in the UCM as the ratio of gross wall area to roof area in LARIAC (2016).

Every building within each ZIP Code in Los Angeles County is classified as "low-intensity residential," "high-intensity residential," or "commercial/industrial," based on the dominant NLCD land use type (LUT) in that ZIP Code. Each building class is assigned a single representative building height H in the 2D UCM, computed as the mean building height in LARIAC (2016) for buildings in that class. Each building class is also assigned a single representative roof width R in the 2D UCM, set to match $2\,H/R$ to the median ratio of whole-building gross wall area to roof area in LARIAC (2016) for buildings in that class. Each building's roof area is set to its LARIAC (2016) footprint area, and its whole-building gross wall area is calculated as its LARIAC (2016) building height multiplied by its LARIAC (2016) building perimeter. The median ratio of gross wall area to roof area by building class is 1.95 for low-intensity residential, 1.96 for high-intensity residential, and 2.10 for commercial/industrial. Weighted by impervious area within each land use type (derived from NLCD), the mean value of these median ratios is 1.97.

Ground width W was computed by combining the building and street centerline datasets. For each road segment, we computed the distance between the street centerline in (LARIAC, 2014) and the nearest building (LARIAC, 2016). We doubled this distance to estimate ground width, then averaged ground width by ZIP Code. Finally, with knowledge of the dominant NLCD type per ZIP-Code, W was computed by taking the average of ZIP-Code level values of ground width per NLCD type.

Table 1. Two-dimensional urban morphology used in our urban canopy model (UCM), derived from LARIAC (2014) and LARIAC (2016) descriptions of the three-dimensional morphology of Los Angeles County.

Urban land use type	Building height H (m)	Roof width R (m)	Ground width W (m)
Low-intensity residential	5.8	6.0	26.6
High-intensity residential	5.3	5.4	24.3
Commercial/industrial	6.5	6.2	27.1

2.4 Canyon air temperature

For urban grid cells (i.e., grid cells dominated by urban land cover; Figure 1b), the standard WRF diagnoses and outputs canyon temperature and 2-m grid cell air temperature. Canyon temperature is effectively an aggregated skin temperature for walls and ground. This temperature is used in calculations of sensible heat flux from the canyon to the atmosphere. The calculation for the default grid cell 2-m air temperature diagnosed by WRF uses the roughness length of grass, leading to unphysical results in urban grid cells (Li and Bou-Zeid, 2014).

To better simulate the temperature near the ground level in cities, we implement the parameterization proposed by Theeuwes et al. (2014) to calculate near-surface air temperature within the urban canyon, which we refer to as canyon air temperature.

The canyon air temperature is parameterized as

$$T_{\mathrm{c}} = \frac{H_{\mathrm{c}}\, r_{2\mathrm{m}}}{\rho\, C_{\mathrm{p}}} + T_{\mathrm{a}} \tag{1}$$

where H_{c} is the total sensible heat flux (power/area) from canyon surfaces (i.e., walls and ground) to the lowest layer of the atmospheric model, C_{p} (J kg^{-1} K^{-1}) is the specific heat capacity of dry air, ρ (kg m^{-3}) is the density of air, and T_{a} (K) is the air temperature in the lowest layer of atmospheric model.

Stability correction is used to account for the influence of atmospheric stability on heat transfer based on Monin-Obukhov similarity theory. $r_{2\mathrm{m}}$ is transfer resistance that is applied between the lowest layer of the atmosphere model and two meters above ground (Theeuwes et al., 2014), computed as

$$r_{2\mathrm{m}} = \frac{1}{\kappa u_*}\left\{\ln\left(\frac{z_{\mathrm{a}}}{z_{2\mathrm{m}}}\right) - \Psi\left(\frac{z_{\mathrm{a}}}{L}\right) + \Psi\left(\frac{z_{2\mathrm{m}}}{L}\right)\right\} \tag{2}$$

where κ is the dimensionless von Kármán mixing-length constant (i.e., 0.4), u_* (m s^{-1}) is friction velocity, L (m) is the Obukhov length (i.e., the height at which turbulence kinetic energy generated by wind shear is equal to that generated by buoyancy), z_{2m} (m) is the height of 2 m, and z_a (m) is the height of the lowest atmospheric model layer (Theeuwes et al., 2014).

Ψ (unitless) is the stability correction function, which is parameterized as

$$\Psi\left(\frac{z}{L}\right) = \begin{cases} 2\ln\left\{\frac{1+(1-16\frac{z}{L})^{\frac{1}{2}}}{2}\right\} & (\frac{z}{L} < 0) \\ -5\frac{z}{L} & (\frac{z}{L} \geq 0) \end{cases} \quad (3)$$

where z is height (m).

In this study, we report changes in canyon air temperature because it is more applicable to human thermal comfort than the grid cell near-surface air temperature.

2.5 Simulation domain

Three nested domains are simulated at resolutions of 18 km, 6 km, and 2 km, respectively (Figure 1a). The outermost domain (d01) covers California; the middle domain (d02) simulates southern California; and the innermost domain (d03) encompasses the Los Angeles basin and San Diego. The domain is the same as that used in our previous modeling work (Vahmani et al., 2016; Vahmani and Ban-Weiss, 2016a; Vahmani and Ban-Weiss, 2016b). Each inner domain uses values from the adjacent outer domain as boundary conditions. The outermost domain (d1 in Figure 1a) uses the North American Regional Reanalysis (NARR) dataset (Mesinger et al., 2006) as boundary conditions. The NARR dataset has a spatial resolution of 32 km and temporal resolution of 3 hours. The atmosphere is simulated using 30 layers in the vertical. Urban areas in Los Angeles County are included in our analysis on diurnal cycles.

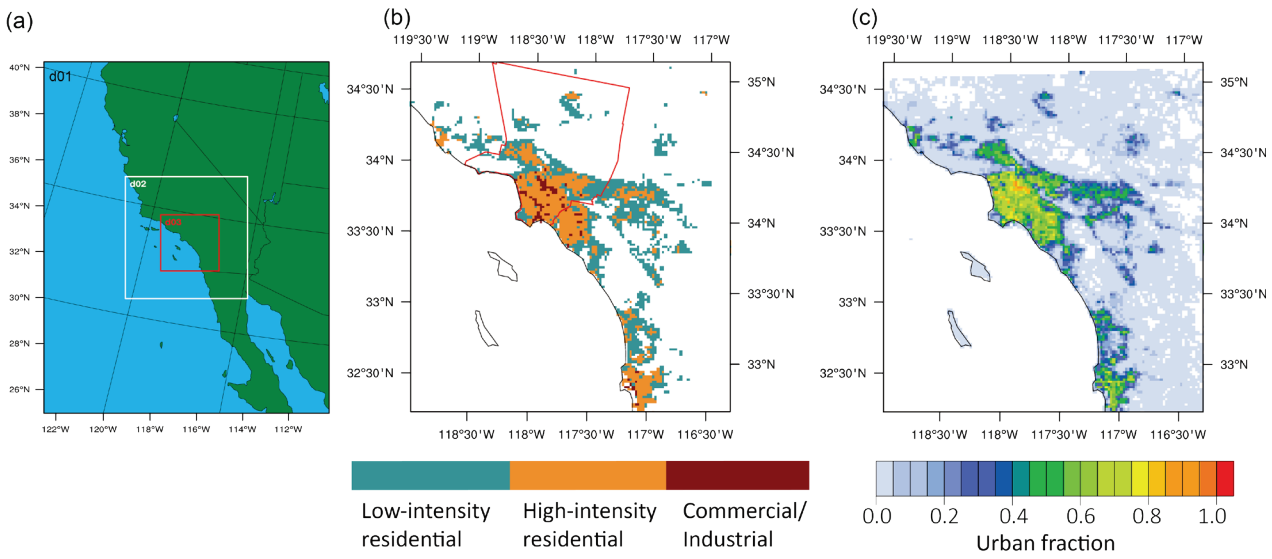

Figure 1. (a) Nested simulation domains d01 (Western United States), d02 (Central and Southern California), and d03 (Southern California). (b) Dominant urban land use types in domain d03; red outline bounds urban areas in Los Angeles County considered in our analysis of diurnal air temperatures cycles. (c) Urban fractions in domain d03.

2.6 Simulation design

Our analysis of the influence of cool walls on the climate of Southern California considers three scenarios: CONTROL, in which ground, whole-roof, and whole-wall albedos are each set to 0.10; COOL_WALL_LOW, in which whole-wall albedo is raised to 0.50; and COOL_WALL_HIGH, in which whole-wall albedo is raised to 0.90. Here whole-roof albedo is the ratio of sunlight reflected from the entire roof to that incident on the entire roof, including openings (e.g., skylights) and roof-mounted equipment, while whole-wall albedo is the ratio of sunlight reflected from the entire wall to that incident on the entire wall, including openings (windows and doors). To compare the effect of increasing whole-wall albedo to that of raising whole-roof albedo, we add two more scenarios: COOL_ROOF_LOW, in which whole-roof albedo is raised to 0.50; and COOL_ROOF_HIGH, in which whole-roof albedo is raised to 0.90 (Table 2). In this way, the whole-facet albedo increases are 0.40 for COOL_WALL_LOW and COOL_ROOF_LOW scenarios, and 0.80 for COOL_WALL_HIGH and COOL_ROOF_HIGH scenarios. The albedo values are chosen to gauge the upper bound effect of applying cool walls and roof, and to test the linearly of canyon air temperatures with increasing wall and roof albedos. Note that cool surface albedos in cases COOL_WALL_HIGH (wall albedo 0.90) and COOL_ROOF_HIGH (roof albedo 0.90) are higher than those of actual cool walls and roofs, especially after weathering and soiling. For example, the albedo of an initially bright-white roof might fall to about 0.60 - 0.70 from about 0.80 - 0.90 after several years of exposure (Sleiman et al. 2011; Berdahl et al. 2008). The initial albedo of a non-white cool surface, such as a "cool colored" roof, typically ranges from about 0.25 to about 0.50 (Levinson et al. 2007), and its albedo loss upon exposure tends to be smaller than that experienced by a bright-white roof (Sleiman et al. 2011). Note that

percentage of sunlight reflected by walls that escapes the urban canopy (Table 2) is calculated from urban morphology and wall albedo in Task Report Appendix B.

We perform three ensemble simulations per scenario to reduce the influence of model internal variability on results. The ensemble simulations are carried out by initiating the model simulations at different times (14:00 LST on 28 June 2012, 14:00 LST on 29 June 2012, and 14:00 LST on 30 June 2012). Ensemble means are reported for each scenario.

Simulations are performed for about 14 days (28 June 2012 to 11 July 2012). Due to intrinsic uncertainties in initial conditions, modeled results at the start of the simulations are unreliable (Warner, 2011). A previous study with the same model configuration discarded the first 12 simulated hours as model "spin-up" (Vahmani et al., 2016). In this study, the first three to five days are discarded as "spin-up," and only the results from 3 July 2012 to 11 July 2012 are used in our analysis of changes in canyon air temperatures and albedo.

Table 2. Wall and roof albedos in five scenarios. Ground albedo is 0.10 in each scenario.

Scenario	Wall albedo	Roof albedo	Fraction of sunlight reflected by walls that escapes urban canopy (%)
CONTROL	0.10	0.10	50
COOL_WALL_LOW	0.50	0.10	54
COOL_WALL_HIGH	0.90	0.10	59
COOL_ROOF_LOW	0.10	0.50	50
COOL_ROOF_HIGH	0.10	0.90	50

2.7 Caveats

The results later presented in this report rely on the ability of the model to accurately simulate atmospheric processes and surface-atmosphere interactions. Results may vary depending on the modeling systems employed. The climate effects of cool walls and roofs are expected to vary depending on urban morphology and impervious fraction, as well as the baseline climate of the city under investigation (Millstein and Menon, 2011; Mohegh et al., 2017).

We focus our analysis on Los Angeles County, and accordingly set the urban canopy morphology and impervious fraction based on region-specific GIS datasets.

If a cool-wall campaign does not change the albedos of doors and windows, all cool-wall air temperature reductions and solar upflux increases reported in this study should be multiplied by the ratio of net wall area (gross wall area minus area of openings) to gross wall area. We propose a ratio of 0.83, which is that computed for the City of Los Angeles (Appendix A, Table A4).

3 Results and discussion

3.1 Diurnal cycle of grid cell albedo and reflected solar radiation

Figure 2a shows the diurnal cycle of albedo changes induced by cool walls averaged over urban grid cells in Los Angeles County. Figure 2a shows that during the daytime, the urban grid cell albedo rise induced by increasing whole-wall albedo to 0.90 from 0.10 (COOL_WALL_HIGH – CONTROL) is smallest (0.02) at solar noon, and greatest (~0.10) in the early morning (06:00 LST) and late afternoon (18:00 LST) in Los Angeles County. (The average sunrise and sunset times for our analysis period are 04:48 LST and 19:07 LST, respectively.) This diurnal cycle occurs because wall albedo has its maximum influence on grid cell albedo in the early morning and late afternoon as the ratio of solar irradiance on vertical surfaces versus horizontal surfaces reaches its maximum (Figures A1 and A2 in Task Report Appendix A). On the other hand, increasing whole-roof albedo by 0.80 (COOL_ROOF_HIGH – CONTROL) will result in a constant urban grid cell albedo rise of 0.07 because the modeled roof is horizontal. Increasing whole-roof albedo, as compared to increasing whole-wall albedo by the same amount, can lead to a greater increase in average urban grid cell albedo in Los Angeles County from 07:00 to 17:00 LST.

Figure 2b shows the diurnal cycle of changes in grid cell upflux (upwelling sunlight) reflected through the horizontal plane bounding the urban canopy. The upflux is calculated as the product of downflux (global horizontal irradiance, or GHI) and grid cell albedo. GHI peaks at noon (Figure 2c). The increase in upflux induced by cool walls reaches its two greatest values at 10:00 and 15:00 LST, a result of diurnal variations of both GHI and grid cell albedo increase. Therefore, cool walls can reject more sunlight from the urban canopy in the late morning and early afternoon than in other daylight hours. The diurnal cycles of increases in reflected radiation induced by cool roofs are concave up with larger diurnal variations than for cool walls, following the trend of horizontal irradiance (Figure 2c). The increase in solar reflection reaches the maximum at solar noon, the time associated with peak horizontal irradiance.

Relative to CONTROL, the daily increase in grid cell upflux for COOL_WALL_HIGH (783 kJ m^{-2}) is 43% of that for COOL_ROOF_HIGH (1841 kJ m^{-2}) (Table 3). Three factors contribute to the difference in increased reflected solar radiation induced from cool walls versus roofs: (a) gross wall area is a factor of ~2 larger than roof area in Los Angeles County; (b) solar irradiance (W m^{-2}) onto walls and roofs differ, and daily cumulative solar irradiation (J m^{-2}) onto walls (2,857 J m^{-2}) is 38% of that onto roofs (7,575 J m^{-2}) over the analysis period (Figure A1 in Task Report Appendix A); and (c) in our model the solar radiation reflected by walls is partially (50-59%) absorbed by walls and pavements, while all solar radiation reflected by roofs escapes the canopy (Table 2).

In our simulations, the increase in whole-wall albedo for COOL_WALL_HIGH – CONTROL (0.80) is twice that for COOL_WALL_LOW – CONTROL (0.40) (Table 2). These whole-wall albedo increases lead to grid cell albedo increases at 06:00 LST and 12:00 LST that differ by a factor of ~2 (Table 3). This means that the urban increases in grid cell albedo are proportional to whole-wall albedo rises. Similarly, increase in daily cumulative reflected solar radiation scale approximately linearly with whole-wall albedo rise. These linear relationships also apply to cool roofs.

Table 3. Urban grid cell albedo, upflux (reflected solar radiation), and canyon air temperature by time of day in urban areas of Los Angeles County (shown in Figure 1b) , reporting absolute values for scenario CONTROL, and changes from CONTROL for the four remaining scenarios. [a]

Scenario	Albedo at 06:00 LST	Albedo at 12:00 LST	Daily solar upflux (kJ m^{-2})	Daily (24-hour) average canyon air temperature (K)	Canyon air temperature (K) at 14:00 LST	Canyon air temperature (K) at 20:00 LST	Daily (24-hour) average canyon air temperature (K) per 0.10 whole-facet albedo increase
CONTROL	0.143	0.148	4,339	295.2	302.0	294.5	295.2
COOL_WALL_LOW minus CONTROL	0.045	0.008	371	-0.19	-0.19	-0.18	-0.048
COOL_WALL_HIGH minus CONTROL	0.097	0.017	783	-0.43	-0.41	-0.40	-0.054
COOL_ROOF_LOW minus CONTROL	0.033	0.033	925	-0.23	-0.34	-0.18	-0.058
COOL_ROOF_HIGH minus CONTROL	0.065	0.065	1,841	-0.48	-0.72	-0.36	-0.060

[a] All values are averages from July 3 to July 12.

3.2 Spatial variation of grid cell albedo and albedo increase

Figure 3 shows spatial variations in grid cell albedo for CONTROL (Figure 3a), as well as albedo changes due to raising wall and roof albedos by 0.80 (Figure 3b,c). Spatial variability in grid cell albedo increase (Figure 3b,c) is caused by spatial variation in urban fraction (Figure 1c) and urban canyon morphologies. Urban grid cells with higher urban fraction (Figure 1c) tend to have larger albedo increases after implementing cool walls or roofs. For example, the whole-wall albedo increases for COOL_WALL_HIGH – CONTROL in downtown Los Angeles can reach as high as 0.24 at 06:00 LST, which is larger than the spatial average over urban grid cells (0.10). Consistent with Figure 2, the grid cell albedo increase from adopting cool walls is larger at 06:00 than 12:00 LST. At 06:00 LST, grid cell albedo increase induced by adopting cool walls is larger than that induced by cool roofs with the same facet albedo rise.

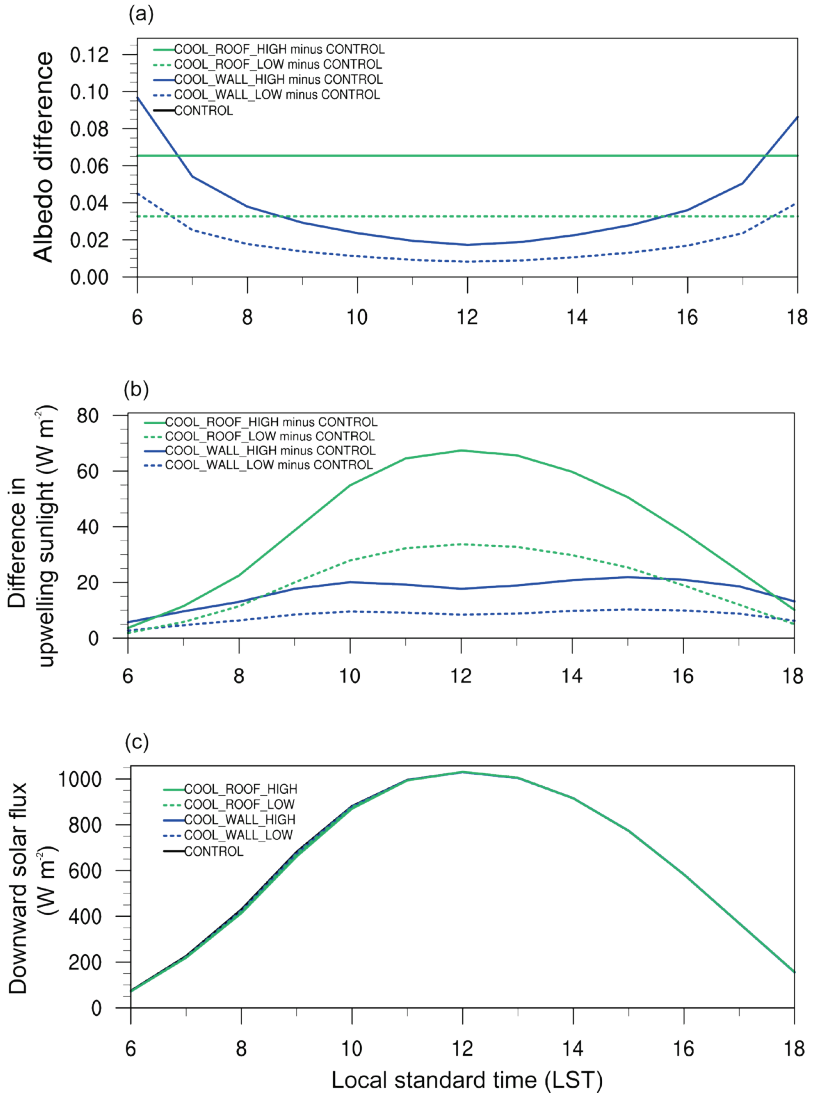

Figure 2. Diurnal cycles of difference from the CONTROL scenario for (a) grid cell albedo and (b) upwelling sunlight for the remaining scenarios COOL_ROOF_HIGH, COOL_ROOF_LOW, COOL_WALL_HIGH, and COOL_WALL_LOW; and (c) diurnal cycle of downward solar radiation (global horizontal irradiance) for the five scenarios. Values represent spatial averages in Los Angeles County (shown in Figure 1b) for urban grid cells from 00:00 LST on July 3 to 00:00 LST on July 12. We show hours of the day when downward solar flux is greater than 5 W m^{-2}.

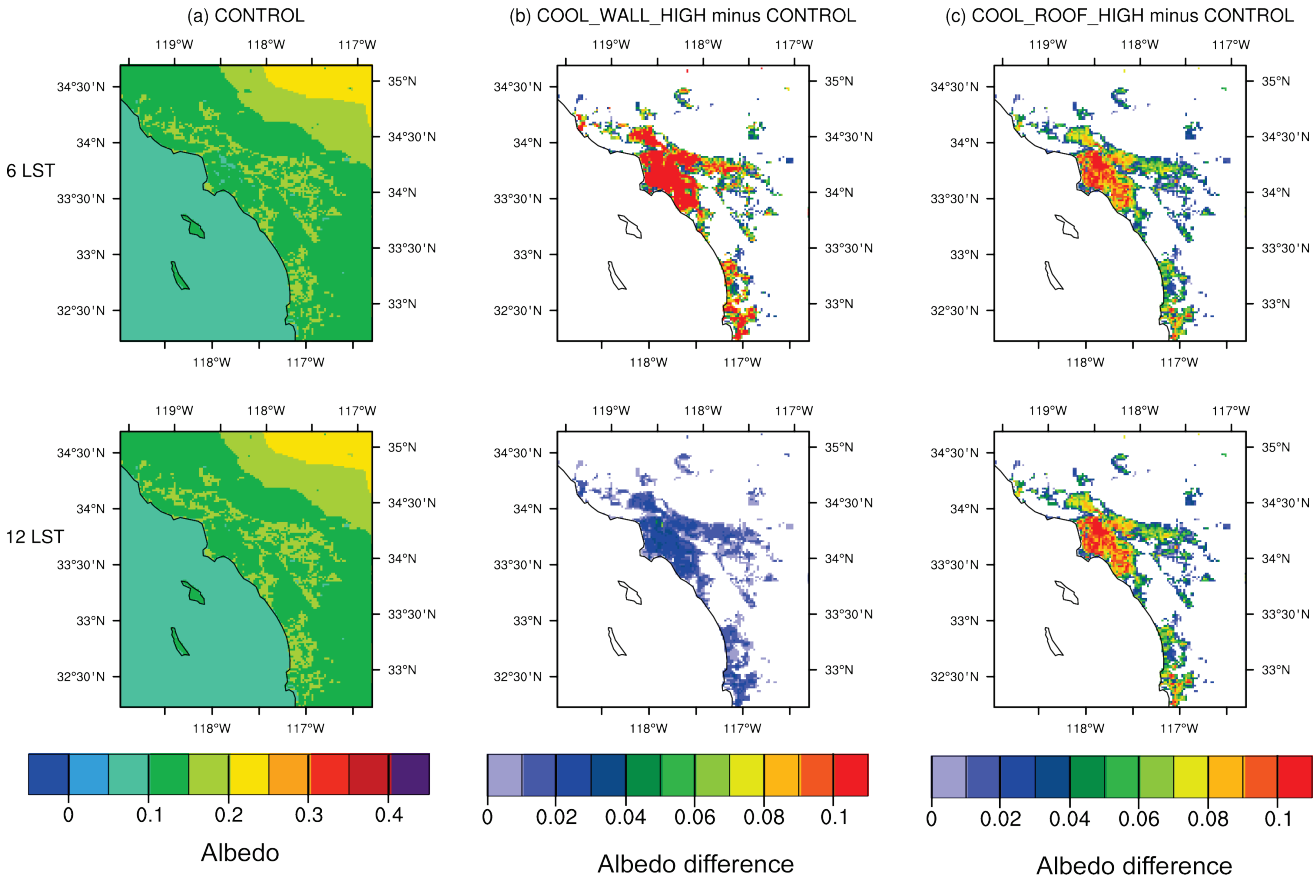

Figure 3. Simulated grid cell albedo at 06:00 LST (top) and 12:00 LST (bottom) for (a) CONTROL, as well as the albedo differences (b) COOL_WALL_HIGH – CONTROL and (c) COOL_ROOF_HIGH – CONTROL. Values are temporally averaged over the period of 00:00 LST on July 3 to 00:00 LST on July 12.

3.3 Diurnal cycle of canyon air temperatures and temperature changes

Figure 4 shows the diurnal cycle of canyon air temperatures for each simulation, and changes in temperatures upon raising whole-wall or whole-roof albedo, spatially averaged over the urban regions of Los Angeles County. Figure 4a shows that in each scenario, canyon air temperature reaches its maximum at 13:00 LST. Peak (greatest) air temperature reduction for cool walls (i.e., 0.65 K for COOL_WALL_HIGH – CONTROL and 0.28 K for COOL_WALL_LOW – CONTROL) occurs at 09:00 LST (Figure 4b). There is a second (smaller) peak in air temperature reduction observed at 18:00 LST. We hypothesize three factors contributing to the shape of the simulated diurnal cycles for canyon air temperature changes due to cool wall adoption. First, increases in reflected solar radiation and reductions in solar heat gain induced by cool walls are greatest at 10:00 and 15:00 LST (Figure 2b). Second, increasing albedo leads to solar heat gain reductions that accumulate throughout the day. Reductions in the surface temperature of thermally massive structures are related to decreases in accumulated, rather than instantaneous, solar

heat gain. Third, the height of the planetary boundary layer (PBL) has a diurnal cycle that is concave down, with a maximum occurring ~13:00 LST (Figure A3 in Task Report Appendix A). Shallower PBL heights reduce the volume of air heated by sensible heat fluxes. This means that a given reduction in sensible heat flux caused by surface temperature decreases would lead to larger reductions in atmospheric heating rate (temperature/time) in the boundary layer when PBL heights are shallow versus deep. Thus, sensible heat flux decreases from cool wall adoption are expected to have larger air temperature effects when the PBL is shallow. [Previous research has highlighted the importance of diurnal cycle in PBL height in determining urban air temperatures; higher PBL heights in urban areas relative to rural areas can contribute to a morning urban cool island (Theeuwes et al., 2015). While this study is not directly related to our research, it shows how PBL height can influence atmospheric heating and air temperature in urban areas.]

Task Report Appendix C considers how PBL height, increase in upflux, and the accumulation of solar heat gain affect diurnal cycles of canyon air temperature reduction from adopting cool walls and cool roofs. All three factors contribute to the greatest reduction in canyon air temperature induced by cool walls at 09:00 LST, which is one hour before wall irradiance peaks and a time at which the PBL height is relatively low.

For cool roofs, the peak temperature reduction of 0.88 K (COOL_ROOF_HIGH – CONTROL) occurs at 10:00 LST. This peak temperature reduction occurs later in the morning than for cool walls because of the difference in diurnal cycle of increased reflected solar radiation (Figure 2a), which reaches its maximum at solar noon for roofs rather than in the morning and afternoon for walls. A previous study on cool pavements (Mohegh et al., 2017) also found that near-surface air temperature reductions peaked in the morning and the evening. They hypothesized that it was due to the combined effects of diurnal cycles in solar irradiance, accumulated solar heat gain, and PBL height.

From 09:00 to 17:00 LST, the canyon air temperature reduction induced by cool roofs is greater than that from cool walls for equal increases in whole-facet albedo (Figure 4b). This can be attributed to the higher increase in reflected solar radiation that escapes the urban canopy from cool roofs versus walls. However, cool walls (relative to cool roofs) create higher canyon air temperature reductions per increase in reflected solar radiation from the canopy at most times of day (Figure A4 in Task Report Appendix A). This is likely because walls are in the urban canyon, so they can more directly cool canyon air than roofs. In addition, for equal increases in whole-facet albedo, cool walls lead to a greater cooling at night relative to cool roofs. The atmosphere is stable at night, meaning that there is little vertical mixing. This means that above-canopy air temperature reductions from cool roofs would undergo less mixing into the canyon, and thus have less effect on canyon air temperatures relative to cool walls at night.

As shown in Table 2, canyon air temperature reductions for COOL_WALL_HIGH relative to CONTROL at 14:00 and 22:00 LST are about the same (0.41 K and 0.40 K, respectively). The reduction at 14:00 LST is lower than that induced by cool roofs (0.72 K), while the cool-wall

reduction at 22:00 LST is higher than that induced by cool roofs (0.36 K) for equal increases in whole-facet albedo.

Increasing whole-wall albedo by 0.40 and 0.80 reduces daily average canyon air temperatures by 0.19 K and 0.43 K, respectively. The daily average canyon air temperature reductions induced by cool walls are slightly less than those induced by cool roofs with the same whole-facet albedo increase (Table 3). On the other hand, for a daily cumulative grid cell upflux increase of 1 J m^{-2}, the daily canyon temperature reduction induced by cool walls would be 0.55 μK, twice that for cool roofs (0.26 μK).

The ratio of the daily average temperature reduction for COOL_WALL_HIGH – CONTROL to that for COOL_WALL_LOW – CONTROL (0.43 K / 0.19 K = 2.3) is close to the ratio of the whole-wall albedo rises for the two scenarios (0.80 / 0.40 = 2) (Table 3), indicating that the average temperature reduction induced by cool walls is approximately proportional to increase in wall albedo. A similar linear relationship between whole-facet albedo increase and temperature reduction is also observed for cool roofs (0.48 K / 0.23 K = 2.1). Adopting cool walls (roofs) leads to 0.054 K (0.060 K) canyon air temperature reduction per 0.10 whole-facet albedo increase in the COOL_WALL_HIGH (COOL_ROOF_HIGH) - CONTROL scenario. The ratios of daily average reductions induced by cool walls to those yielded by cool roofs are 83% and 90%, respectively, for whole-facet albedo increases of 0.40 and 0.80. Note that we also did three additional ensemble simulations for the scenario COOL_ROOF_WALL_HIGH where the albedos of walls and roofs are both raised to 0.90 to test the linearity of adopting cool walls and roofs simultaneously or separately. As shown in Table A5 in the Supporting Information, the reduction in canyon air temperature in COOL_ROOF_WALL_HIGH is approximately the sum of the reductions in COOL_WALL_HIGH and COOL_ROOF_HIGH relative to CONTROL. This suggests that the effects of adopting cool walls and roofs are additive.

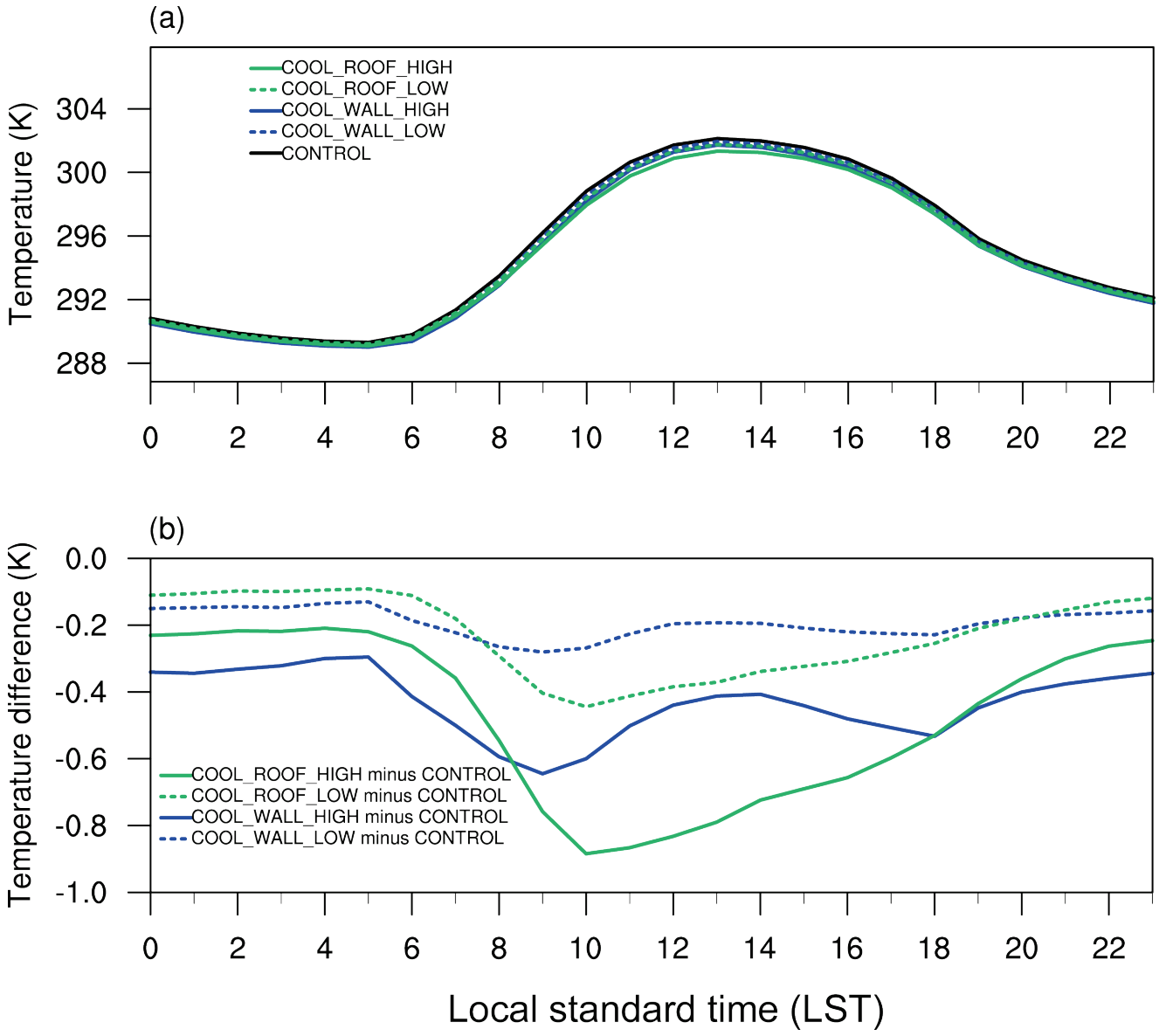

Figure 4. The diurnal cycle of (a) spatially averaged canyon air temperature (K) for CONTROL, COOL_WALL_LOW, COOL_WALL_HIGH, COOL_ROOF_LOW, and COOL_ROOF_HIGH; and (b) difference in canyon air temperatures for COOL_WALL_LOW – CONTROL, COOL_WALL_HIGH – CONTROL, COOL_ROOF_LOW – CONTROL, and COOL_ROOF_HIGH – CONTROL. Values represent spatial averages in Los Angeles County (i.e., shown in Figure 1b) for urban grid cells from 00:00 LST on July 3 to 00:00 LST on July 12.

3.4 Spatial variation of canyon air temperature

Figure 5 shows spatial variation in canyon air temperatures for the control, cool wall, and cool roof simulations at 14:00 LST and 20:00 LST. In CONTROL, desert regions and the eastern portion of the Los Angeles basin are hotter than the coastal regions, as expected. Employing cool walls and cool roofs reduces temperatures in the urban portions of the domain. Air

temperature decreases in inland urban areas are larger than those in coastal area. This is likely because the effects of cool walls and roofs accumulate as winds (which in Los Angeles are primarily due to sea breeze) advect air downstream from west to east. Cool walls lead to similar canyon air temperature reductions at 14:00 LST and 20:00 LST, while cool roofs cause larger temperature reductions at 14:00 LST than at 20:00 LST. Adopting cool walls shows a greater cooling effect than cool roofs with the same albedo rise relative to CONTROL at 20:00 LST, but a lesser cooling effect at 14:00 LST (Figure 5 and Table 3).

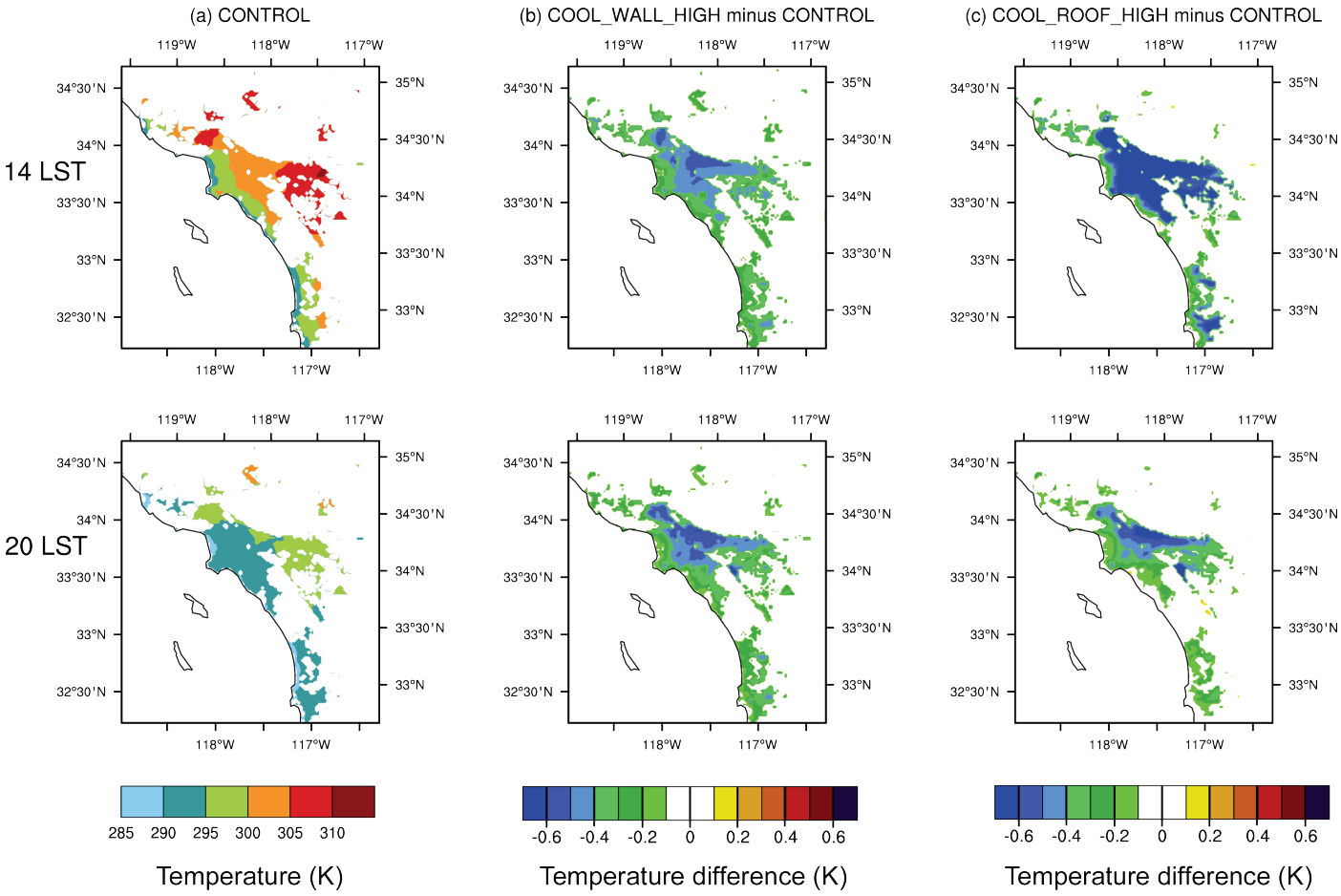

Figure 5. Simulated canyon air temperature (K) at 14:00 LST (top) and 20:00 LST (bottom) for (a) CONTROL, as well as the temperature differences for (b) COOL_WALL_HIGH – CONTROL, and (c) COOL_ROOF_HIGH – CONTROL. Values are temporally averaged over the period of 00:00 LST on July 3 to 00:00 LST on July 12.

3.5 Estimating whole-facet albedo increases from cool surface campaigns in Los Angeles

Assume that single-family homes and fast-food restaurants have high-slope roofs, and that all other buildings have low-slope roofs. From Table A4, there is 18.8M m² of low-slope roof area

and 22.7M m² of high-slope roof area in the City of Los Angeles. If a cool roof campaign in the City of Los Angeles modifies all gross roof area, raising the albedo of low-slope roofs by 0.40 (to aged albedo 0.60 from aged albedo 0.20) and the albedo of high-slope roofs by 0.15 (to aged albedo 0.25 from aged albedo 0.10), area weighting yields a city-mean whole-roof albedo rise of 0.26.

The citywide ratio of net wall area to gross wall area is 83% (Table A4). Levinson et al. (2018) found that 12 to 18 months of natural exposure lowers by only a few percentage points the albedo of a light-colored wall with initial albedo 0.60. If a cool wall campaign in LA excludes windows and doors, raising the albedo of the net wall areas by 0.33 (to aged albedo 0.58 from aged albedo 0.25), the city-mean rise in whole-wall albedo will be 83% × 0.33 = 0.27. Thus, the whole-wall albedo rise in the cool-wall campaign will be essentially equal to the whole-roof albedo rise in the cool-roof campaign.

4 Conclusions

Using the WRF model, we conduct simulations for July 2012 for three scenarios (CONTROL, COOL_WALL_LOW, and COOL_WALL_HIGH) to assess the influence of employing cool walls on albedo and climate. Three ensemble members per scenario are simulated to reduce the influence of model internal variability on simulated temperature changes. Whole-wall albedo increases for COOL_WALL_LOW and COOL_WALL_HIGH relative to CONTROL are 0.40 and 0.80, respectively. Urban grid cell albedo increases induced by cool walls peak in the early morning and late afternoon when the ratio of solar radiation onto vertical walls versus horizontal surfaces is at a maximum. On the other hand, downward solar radiation reaches its maximum at noon. Thus, the increase in reflected solar radiation (grid cell albedo increase multiplied by baseline downward solar radiation) induced by cool walls reaches its maximum at 10:00 and 15:00 LST. Daily cumulative increase in reflected solar radiation for COOL_WALL_HIGH relative to CONTROL is 783 kJ m^{-2}, or 43% of that for COOL_ROOF_HIGH (1,840 kJ m^{-2}). Factors that make the upflux increase resulting from raising whole-wall albedo differ from that caused by raising whole-roof albedo in the UCM include (a) the ratio of gross wall area to roof area (1.97); (b) the ratio of vertical (wall) to horizontal (roof) solar irradiance (power per unit area; ratio 0.38 over the analysis period); and (c) our assumption that all sunlight reflected by roofs escapes the urban canopy, while only 50 - 59% of that reflected by walls does so, because some is absorbed by the ground or opposing walls (Task Report Appendix B).

Increasing whole-wall albedo by 0.80 is simulated to reduce the spatial mean canyon air temperature in Los Angeles County by 0.43 K (daily average), with the peak reduction (0.64 K) occurring at 09:00 LST and a secondary local peak (0.53 K) at 18:00 LST. Temperature reduction peaks at 09:00 LST and 18:00 LST because of (a) high values of increased reflected solar radiation from the canopy and irradiance on vertical wall surfaces; and (b) low atmospheric mixing heights, which cause changes in surface albedo to have larger air temperature effects relative to when the planetary boundary layer is deeper. Average temperature reductions at

14:00 LST and 20:00 LST are 0.41 K and 0.40 K, respectively. Comparing temperature reductions for COOL_WALL_HIGH – CONTROL versus COOL_WALL_LOW – CONTROL show that the simulated air temperature reductions are nearly linearly related to cool wall albedo increase.

In this study, we also simulate the climate effects of employing cool roofs to systematically compare cool roofs to cool walls within a consistent modeling framework. In contrast to cool walls, cool roofs lead to a constant urban grid cell albedo rise throughout the day. During most times of day (besides early morning and late afternoon when solar zenith angle is high), the grid cell albedo and reflected solar radiation increases from implementing cool roofs are higher than cool walls, even for the same whole-facet albedo increases. The daily average canyon air temperature reduction induced by increasing whole-roof albedo by 0.80 is 0.48 K, slightly higher than that induced by cool walls (0.43 K) for equal increase in whole-wall albedo. Temperature reductions after implementing cool roofs at 14:00 and 22:00 LST are 0.72 K and 0.36 K, respectively. The peak temperature reduction from cool roofs (0.88 K) occurs at 10:00 LST due to the high solar irradiance and a relatively shallow planetary boundary layer.

Widespread adoption of cool walls (roofs) in Los Angeles County can reduce summertime daily average canyon air temperature by 0.048–0.054 K (0.058–0.060 K) per 0.10 increase in whole-wall (whole-roof) albedo. For equal increase in whole-facet albedo, the ratio of cool wall daily average canyon air temperature reduction induced by cool walls to that yielded by cool roofs is 83–90%. The temperature reductions induced by cool walls are larger at night and smaller during the day compared to cool roofs with the same whole-facet albedo increases. On the other hand, per 1 J m^{-2} increase in daily upflux, the daily-average canyon air temperature reduction induced by cool walls (0.55 μK) is twice that induced by cool roofs (0.26 μK).

Cool-wall air temperature reductions and solar upflux increases reported in this study should be multiplied by 0.83, the ratio of net wall area to gross wall area in the City of Los Angeles, if the albedos of windows and doors are unchanged in a cool-wall campaign. Finally, we estimate that in the City of Los Angeles, the whole-wall albedo increase from a cool-wall campaign that excludes windows and doors is essentially equal to the whole-roof albedo increase from a cool-roof campaign that modifies the entire roof.

5 Acknowledgements

Computation for the work described in this paper was supported by the University of Southern California's Center for High-Performance Computing (hpc.usc.edu). We thank Pablo Rosado for providing calculations on solar irradiance incident to surfaces with different orientations. We also thank Gert-Jan Steeneveld, Pouya Vahmani, Dan Li, Ravan Ahmadov, Stu McKeen, Trevor Krasowsky, Mo Chen, Mohammad Taleghani, Wei Tao, Joachim Fallmann, Haley Gilbert, and Junfeng Liu for their helpful suggestions.

References

Berdahl P, Akbari H, Levinson R, Miller WA. 2008. Weathering of roofing materials—An overview. Construction and Building Materials 22(4), 423-433. https://doi.org/10.1016/j.conbuildmat.2006.10.015

Bonan, G. B.: Ecological Climatology: Concepts and Applications, 2nd Edition., 2010.

Chen, F. and Dudhia, J.: Coupling an Advanced Land Surface–Hydrology Model with the Penn State–NCAR MM5 Modeling System. Part II: Preliminary Model Validation, Mon. Weather Rev., 129(4), 587–604, https://doi.org/10.1175/1520-0493(2001)129<0587:CAALSH>2.0.CO;2, 2001.

Chen, F., Kusaka, H., Bornstein, R., Ching, J., Grimmond, C. S. B., Grossman-Clarke, S., Loridan, T., Manning, K. W., Martilli, A., Miao, S., Sailor, D., Salamanca, F. P., Taha, H., Tewari, M., Wang, X., Wyszogrodzki, A. A. and Zhang, C.: The integrated WRF/urban modelling system: Development, evaluation, and applications to urban environmental problems, *Int. J. Climatol.*, 31(2), 273–288, https://doi.org/10.1002/joc.2158, 2011.

Ching, J., Brown, M., Burian, S., Chen, F., Cionco, R., Hanna, A., Hultgren, T., McPherson, T., Sailor, D., Taha. H., and Williams, D.: National urban database and access portal tool, *Bull. Am. Meteorol.* Soc., 90(8), 1157–1168, https://doi.org/10.1175/2009BAMS2675.1, 2009.

Chou, M-D., and M. J. Suarez, 1994: An efficient thermal infrared radiation parameterization for use in general circulation models. NASA Tech. Memo. 104606, http://citeseerx.ist.psu.edu/viewdoc/download?doi=10.1.1.26.4850&rep=rep1&type=pdf.

Duffie JA, Beckman WA. 2006. *Solar Engineering of Thermal Processes*, 3rd ed. Wiley.

Fan, H. and Sailor, D. J.: Modeling the impacts of anthropogenic heating on the urban climate of Philadelphia: A comparison of implementations in two PBL schemes, *Atmos. Environ.*, 39(1), 73–84, https://doi.org/10.1016/j.atmosenv.2004.09.031, 2005.

Fry, J. A., Xian, G., Jin, S., Dewitz, J. A., Homer, C. G., Yang, L., Barnes, C. A., Herold, N. D. and Wickham, J. D.: Completion of the 2006 National Land Cover Database for the conterminous United States, *Photogramm. Eng. Remote Sensing*, 77, 858–566, 2011.

Georgescu, M., Morefield, P. E., Bierwagen, B. G. and Weaver, C. P.: Urban adaptation can roll back warming of emerging megapolitan regions, *Proc. Natl. Acad. Sci.*, 111(8), 2909–2914, https://doi.org/10.1073/pnas.1322280111, 2014.

Hong, S.-Y., Noh, Y. and Dudhia, J.: A New Vertical Diffusion Package with an Explicit Treatment of Entrainment Processes, *Mon. Weather Rev.*, 134(9), 2318–2341, https://doi.org/10.1175/MWR3199.1, 2006.

Kain, J. S.: The Kain–Fritsch Convective Parameterization: An Update, *J. Appl. Meteorol.*, 43(1), 170–181, https://doi.org/10.1175/1520-0450(2004)043<0170:TKCPAU>2.0.CO;2, 2004.

Kolokotroni, M., Giannitsaris, I. and Watkins, R.: The effect of the London urban heat island on building summer cooling demand and night ventilation strategies, *Sol. Energy*, 80(4), 383–392, https://doi.org/10.1016/j.solener.2005.03.010, 2006.

Kusaka, H., Kondo, H., Kikegawa, Y. and Kimura, F.: A simple single-layer urban canopy model for atmospheric models: Comparison with multi-layer and slab models, *Boundary-Layer Meteorol.*, 101(3), 329–358, https://doi.org/10.1023/A:1019207923078, 2001.

LARIAC: LA County Street & Address File, [online] Available from: https://egis3.lacounty.gov/dataportal/2014/06/16/2011-la-county-street-centerline-street-address-file (Accessed 3 August 2017), 2014.

LARIAC: Countywide Building Outlines, [online] Available from: https://egis3.lacounty.gov/dataportal/lariac/ (Accessed 11 July 2017), 2016.

Levinson R, et al. 2018. Solar-reflective “cool” walls: Benefits, technologies, and implementation. California Energy Commission. Publication Number: CEC-XXX-201X-XXX. Draft online at http://goo.gl/kPqjeu .

Levinson R, Berdahl P, Akbari H, Miller W, Joedicke I, Reilly J, Suzuki Y, Vondran M. 2007. Methods of creating solar-reflective nonwhite surfaces and their application to residential roofing materials. *Solar Energy Materials & Solar Cells* 91, 304-314. https://doi.org/10.1016/j.solmat.2006.06.062

Li, D. and Bou-Zeid, E.: Quality and sensitivity of high-resolution numerical simulation of urban heat islands, *Environ. Res. Lett.*, 9(5), https://doi.org/10.1088/1748-9326/9/5/055001, 2014.

Li, D., Bou-Zeid, E. and Oppenheimer, M.: The effectiveness of cool and green roofs as urban heat island mitigation strategies, *Environ. Res. Lett.*, 9(5), https://doi.org/10.1088/1748-9326/9/5/055002, 2014.

Lin, Y.-L., Farley, R. D. and Orville, H. D.: Bulk Parameterization of the Snow Field in a Cloud Model, *J. Clim. Appl. Meteorol.*, 22(6), 1065–1092, https://doi.org/10.1175/1520-0450(1983)022<1065:BPOTSF>2.0.CO;2, 1983.

Mesinger, F., DiMego, G., Kalnay, E., Mitchell, K., Shafran, P. C., Ebisuzaki, W., Jović, D., Woollen, J., Rogers, E., Berbery, E. H., Ek, M. B., Fan, Y., Grumbine, R., Higgins, W., Li, H., Lin, Y., Manikin, G., Parrish, D. and Shi, W.: North American regional reanalysis, *Bull. Am. Meteorol. Soc.*, 87(3), 343–360, https://doi.org/10.1175/BAMS-87-3-343, 2006.

Millstein, D. and Menon, S.: Regional climate consequences of large-scale cool roof and photovoltaic array deployment, *Environ. Res. Lett.*, 6(3), https://doi.org/10.1088/1748-9326/6/3/034001, 2011.

Mlawer, E. J., Taubman, S. J., Brown, P. D., Iacono, M. J. and Clough, S. A.: Radiative transfer for inhomogeneous atmospheres: RRTM, a validated correlated-k model for the longwave, J. *Geophys. Res. Atmos.*, 102(D14), 16663–16682, https://doi.org/10.1029/97JD00237, 1997.

Mohegh, A., Rosado, P., Jin, L., Millstein, D., Levinson, R. and Ban-Weiss, G.: Modeling the climate impacts of deploying solar reflective cool pavements in California cities, *J. Geophys. Res.*, 122(13), 6798–6817, https://doi.org/10.1002/2017JD026845, 2017.

NREL. 2017. PVWatts Calculator Model. National Renewable Energy Laboratory (NREL). http://pvwatts.nrel.gov .

Oke, T. R., Johnson, G. T., Steyn, D. G. and Watson, I. D.: Simulation of surface urban heat islands under "ideal" conditions at night part 2: Diagnosis of causation, *Boundary-Layer Meteorol.*, 56(4), 339–358, https://doi.org/10.1007/BF00119211, 1991.

Palecki, M. A., Changnon, S. A. and Kunkel, K. E.: The nature and impacts of the July 1999 heat wave in the midwestern United States: Learning from the lessons of 1995, *Bull. Am. Meteorol.* Soc., 82(7), 1353–1367, https://doi.org/10.1175/1520-0477(2001)082<1353:TNAIOT>2.3.CO;2, 2001.

Rosado, P. J.: Evaluating Cool Impervious Surfaces: Application to an Energy-Efficient Residential Roof and to City Pavements, University of California, Berkeley. [online] Available from: https://escholarship.org/uc/item/6bf80485.

Rosenfeld, A. H., Akbari, H., Romm, J. J. and Pomerantz, M.: Cool communities: Strategies for heat island mitigation and smog reduction, *Energy Build.*, 28(1), 51–62, https://doi.org/10.1016/S0378-7788(97)00063-7, 1998.

Santamouris, M.: Cooling the cities - A review of reflective and green roof mitigation technologies to fight heat island and improve comfort in urban environments, *Sol. Energy*, 103, 682–703, https://doi.org/10.1016/j.solener.2012.07.003, 2014.

Skamarock, W. C., Klemp, J. B., Dudhi, J., Gill, D. O., Barker, D. M., Duda, M. G., Huang, X.-Y., Wang, W. and Powers, J. G.: A Description of the Advanced Research WRF Version 3, NCAR Tech. Note, (June), 113, https://doi.org/10.5065/D6DZ069T, 2008.

Sleiman M, Ban-Weiss G, Gilbert HE, Francois D, Berdahl P, Kirchstetter TW, Destaillats H, Levinson R. 2011. Soiling of building envelope surfaces and its effect on solar reflectance—Part I: Analysis of roofing product databases. Solar Energy Materials & Solar Cells 95, 3385-3399. https://doi.org/10.1016/j.solmat.2013.11.028

Synnefa, A., Dandou, A., Santamouris, M., Tombrou, M. and Soulakellis, N.: On the use of cool materials as a heat island mitigation strategy, *J. Appl. Meteorol. Climatol.*, 47(11), 2846–2856, https://doi.org/10.1175/2008JAMC1830.1, 2008.

Taha, H.: Urban climates and heat islands: albedo, evapotranspiration, and anthropogenic heat, *Energy Build.*, 25(2), 99–103, https://doi.org/10.1016/S0378-7788(96)00999-1, 1997.

Taha, H.: Meso-urban meteorological and photochemical modeling of heat island mitigation, *Atmos. Environ.*, 42(38), 8795–8809, https://doi.org/10.1016/j.atmosenv.2008.06.036, 2008.

Theeuwes, N. E., Steeneveld, G. J., Ronda, R. J., Heusinkveld, B. G., van Hove, L. W. A. and Holtslag, A. A. M.: Seasonal dependence of the urban heat island on the street canyon aspect ratio, *Q. J. R. Meteorol. Soc.,* 140(684), 2197–2210, https://doi.org/10.1002/qj.2289, 2014.

Theeuwes, N. E., Steeneveld, G. J., Ronda, R. J., Rotach, M. W. and Holtslag, A. A. M.: Cool city mornings by urban heat, *Environ. Res. Lett.,* 10(11), https://doi.org/10.1088/1748-9326/10/11/114022, 2015.

Vahmani, P. and Ban-Weiss, G.: Climatic consequences of adopting drought-tolerant vegetation over Los Angeles as a response to California drought, *Geophys. Res. Lett.*, 43(15), 8240–8249, https://doi.org/10.1002/2016GL069658, 2016a.

Vahmani, P. and Ban-Weiss, G.: Impact of Remotely Sensed Albedo and Vegetation Fraction on Simulation of Urban Climate in WRF-UCM: A Case Study of the Urban Heat Island in Los Angeles, *J. Geophys. Res. Atmos.*, 121(4), 1511–1531, https://doi.org/10.1002/2015JD023718, 2016b.

Vahmani, P., Sun, F., Hall, A. and Ban-Weiss, G.: Investigating the climate impacts of urbanization and the potential for cool roofs to counter future climate change in Southern California, *Environ. Res. Lett.*, 11(12), https://doi.org/10.1088/1748-9326/11/12/124027, 2016.

Warner, T. T.: *Numerical Weather and Climate Prediction.*, Cambridge, 2011.

Wickham, J. D., Stehman, S. V., Gass, L., Dewitz, J., Fry, J. A. and Wade, T. G.: Accuracy assessment of NLCD 2006 land cover and impervious surface, *Remote Sens. Environ.*, 130, 294–304, https://doi.org/10.1016/j.rse.2012.12.001, 2013.

Task Report Appendix A

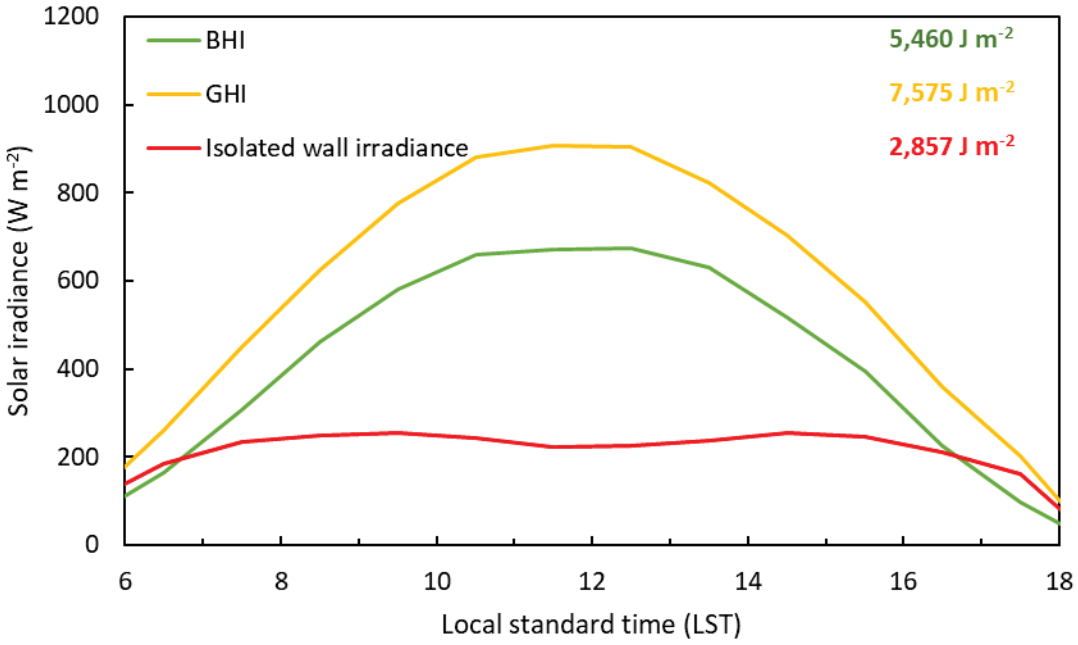

Figure A1. Diurnal cycles of beam horizontal irradiance (BHI), global horizontal irradiance (GHI), and isolated wall irradiance in Burbank, CA, averaged by hour of day in July. BHI and GHI are obtained from the typical meteorological year 3 (TMY3) file for station 722880 (Burbank-Glendale-Pasadena AP); isolated wall irradiance is the average of global tilt irradiances for north, east, south, and west walls without neighbors, computed with the standard isotropic sky model (Duffie and Beckman 2006) and assuming a ground albedo of 0.10. Daily beam horizontal irradiation (energy per unit area), global horizontal irradiation, and isolated wall irradiation are tabulated in the upper right corner.

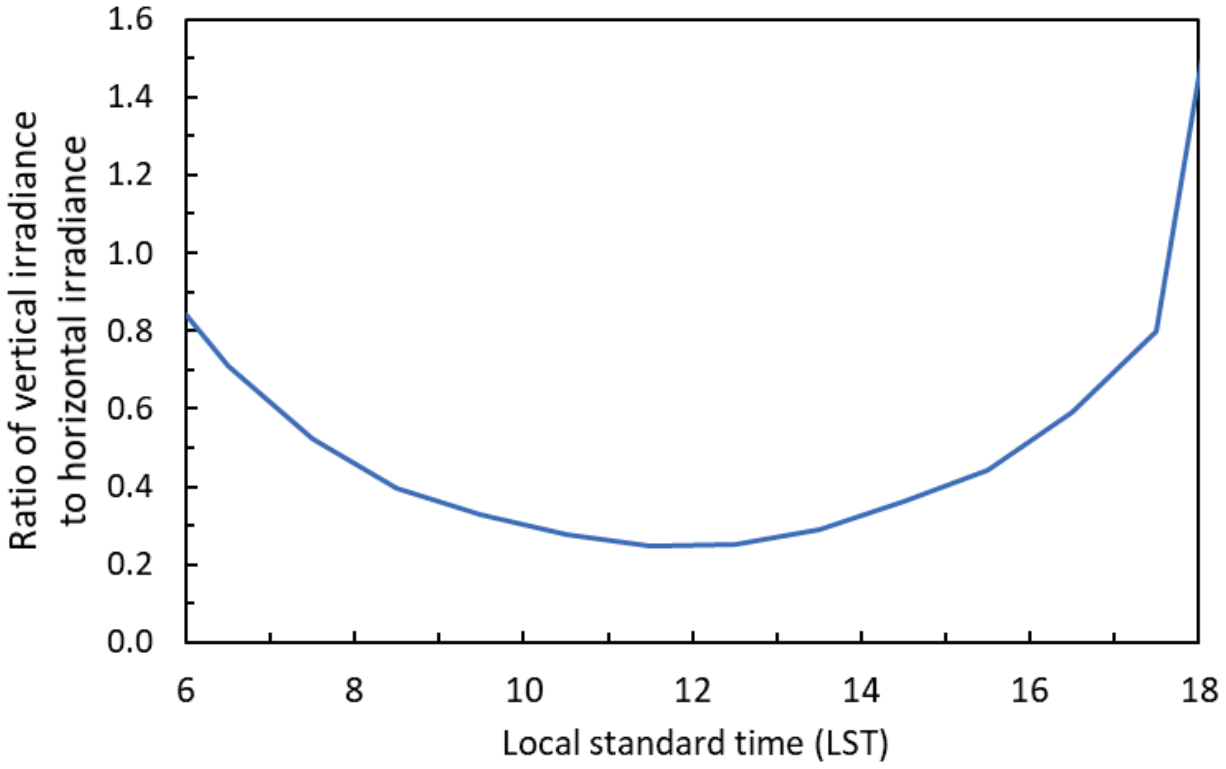

Figure A2. Diurnal cycle of the ratio between the isolated wall irradiance (vertical irradiance) and the global horizontal irradiance (GHI) shown in Figure A1.

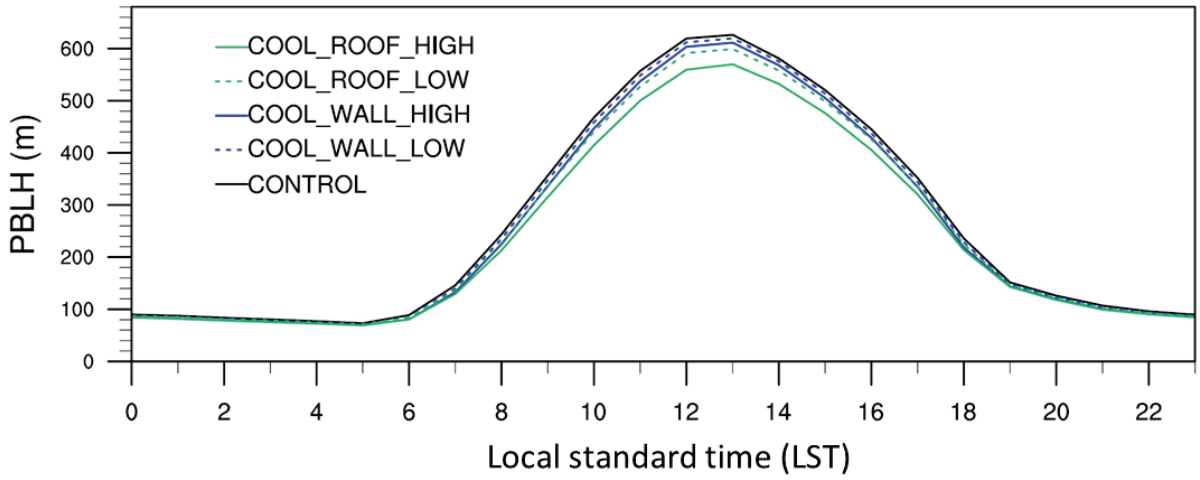

Figure A3. The diurnal cycle of spatially averaged planetary boundary layer height (PBLH) for CONTROL, COOL_WALL_LOW, COOL_WALL_HIGH, COOL_ROOF_LOW, and COOL_ROOF_HIGH. Values represent spatial averages in Los Angeles County (main article Figure1b) for urban grid cells from 00:00 LST on July 3 to 00:00 LST on July 12.

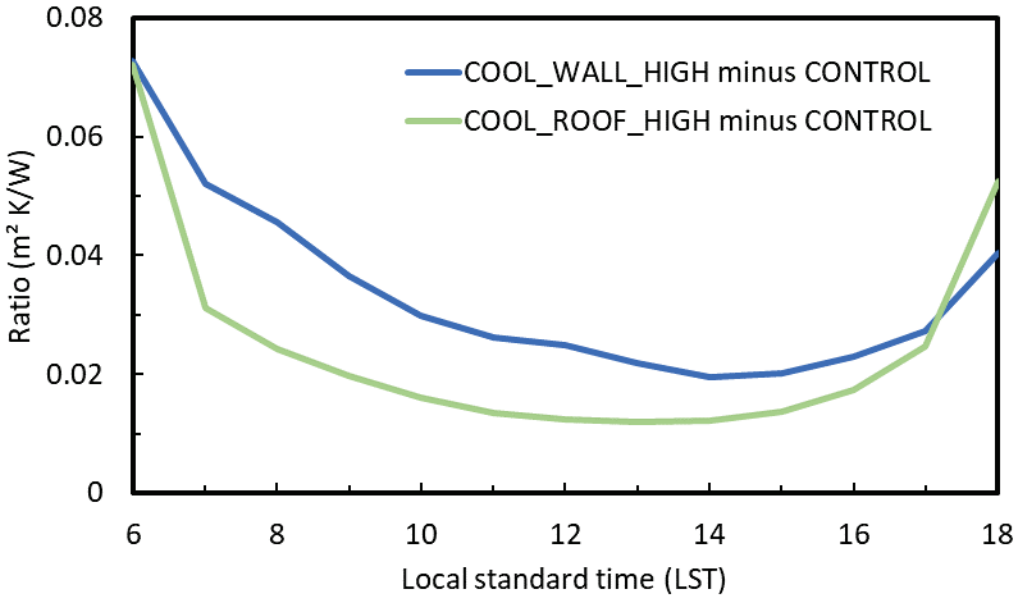

Figure A4. Increases (COOL_WALL_HIGH – CONTROL and COOL_ROOF_HIGH – CONTROL) in the ratio of canyon air temperature reduction (K) to increase in reflected solar radiation (W m^{-2}).

Table A1. Monthly and seasonal daily solar irradiation in Burbank, California (TMY3 station 722880), computed with PVWatts (NREL 2017).

		Solar Radiation [kWh/m²·day]						
		Horizontal (H)	North wall (N)	East wall (E)	South wall (S)	West wall (W)	Four-wall average (NESW)	Ratio of NESW to H
Month	January	**2.97**	**0.65**	**1.96**	**4.56**	**1.81**	**2.25**	**76%**
	February	**3.19**	**0.81**	**1.82**	**3.33**	**1.88**	**1.96**	**61%**
	March	**4.99**	**0.99**	**2.68**	**3.76**	**2.81**	**2.56**	**51%**
	April	**6.42**	**1.26**	**3.28**	**3.06**	**3.59**	**2.80**	**44%**
	May	**6.74**	**1.70**	**3.53**	**2.30**	**3.62**	**2.79**	**41%**
	June	**7.79**	**1.90**	**3.70**	**2.17**	**4.06**	**2.96**	**38%**
	July	**7.60**	**1.91**	**4.14**	**2.43**	**3.98**	**3.11**	**41%**
	August	**7.23**	**1.51**	**3.92**	**3.26**	**4.05**	**3.19**	**44%**
	September	**5.36**	**1.22**	**3.11**	**3.77**	**3.28**	**2.84**	**53%**
	October	**3.90**	**0.96**	**2.47**	**4.02**	**2.24**	**2.42**	**62%**
	November	**3.56**	**0.79**	**2.23**	**5.15**	**2.38**	**2.64**	**74%**
	December	**2.66**	**0.67**	**1.79**	**4.41**	**1.84**	**2.18**	**82%**
Season	Winter (DJF)	**2.94**	**0.71**	**1.86**	**4.10**	**1.84**	**2.13**	**72%**
	Spring (MAM)	**6.05**	**1.31**	**3.17**	**3.04**	**3.34**	**2.71**	**45%**
	Summer (JJA)	**7.54**	**1.77**	**3.92**	**2.62**	**4.03**	**3.09**	**41%**
	Fall (SON)	**4.27**	**0.99**	**2.60**	**4.31**	**2.63**	**2.63**	**62%**
Ratio	Winter / Summer	**39%**	**40%**	**47%**	**157%**	**46%**	**69%**	

Table A2. Same as Table A1, but for Riverside, California (TMY3 station 722880).

		Solar Radiation [kWh/m²·day]						
		Horizontal (H)	North wall (N)	East wall (E)	South wall (S)	West wall (W)	Four-wall average (NESW)	Ratio of NESW to H
Month	January	**3.09**	**0.75**	**1.87**	**4.62**	**2.06**	**2.33**	**75%**
	February	**3.51**	**0.92**	**2.14**	**3.93**	**2.21**	**2.30**	**66%**
	March	**4.87**	**1.07**	**2.42**	**3.69**	**2.96**	**2.54**	**52%**
	April	**6.17**	**1.39**	**3.46**	**3.15**	**3.38**	**2.84**	**46%**
	May	**6.91**	**1.77**	**3.36**	**2.45**	**3.89**	**2.87**	**41%**
	June	**7.92**	**2.02**	**3.76**	**2.26**	**4.24**	**3.07**	**39%**
	July	**7.61**	**1.98**	**4.14**	**2.46**	**4.04**	**3.16**	**41%**
	August	**7.12**	**1.59**	**3.96**	**3.24**	**3.93**	**3.18**	**45%**
	September	**4.93**	**1.22**	**2.90**	**3.42**	**2.95**	**2.62**	**53%**
	October	**3.83**	**0.99**	**2.28**	**3.84**	**2.27**	**2.34**	**61%**
	November	**3.55**	**0.82**	**2.20**	**5.06**	**2.34**	**2.60**	**73%**
	December	**2.94**	**0.73**	**2.02**	**4.95**	**1.98**	**2.42**	**82%**
Season	Winter (DJF)	**3.18**	**0.80**	**2.01**	**4.50**	**2.09**	**2.35**	**74%**
	Spring (MAM)	**5.98**	**1.41**	**3.08**	**3.10**	**3.41**	**2.75**	**46%**
	Summer (JJA)	**7.55**	**1.86**	**3.95**	**2.65**	**4.07**	**3.14**	**42%**
	Fall (SON)	**4.10**	**1.01**	**2.46**	**4.11**	**2.52**	**2.52**	**62%**
Ratio	Winter / Summer	**42%**	**43%**	**51%**	**169%**	**51%**	**75%**	

Table A3. Number of buildings included in LARIAC (2016) dataset for the three urban land use types and corresponding mean roof area and mean gross wall area.

Urban land use type	Number of buildings	Mean roof area (m^2)	Mean gross wall area (m^2)
Low-intensity residential	243,098	5,274	9,094
High-intensity residential	1,854,746	4,474	7,481
Commercial and industrial	111,187	8,726	13,094

Table A4. Conditioned floor area, roof area, net wall area, and gross wall area for DOE building prototypes reported by Levinson et al. (2018), and total floor areas in the City of Los Angeles attributed to each building category (Rosado 2016). Total roof, net wall, or gross wall area in the city by building category is calculated as total floor area times the ratio of prototype roof, net wall, or gross wall area to prototype conditioned floor area.

Building category	Prototype conditioned floor area (m^2)	Prototype roof area (m^2)	Prototype net wall area (m^2)	Prototype gross wall area (m^2)	Total floor area in city (m^2)	Total roof area in city (m^2)	Total net wall area in city (m^2)	Total gross wall area in city (m^2)	Ratio of total net wall area to total gross wall area in city
Single-family home	223	112	184	221	45,530,404	22,772,286	37,594,855	45,160,276	0.83
Apartment building	2,010	669	1,174	1,421	38,504,750	12,819,748	22,492,230	27,223,469	0.83
Small office	511	511	222	282	NA	N/A	NA	NA	NA
Medium office	4,980	1,661	1,325	1,978	3,727,395	1,243,011	991,592	1,480,225	0.67
Large office	46,300	3,563	6,953	11,590	2,261,120	174,009	339,577	565,990	0.60
Large hotel	11,400	1,979	2,812	4,026	1,223,986	212,452	301,911	432,262	0.70
Retail stand-alone	2,290	2,264	1,093	1,177	381,447	377,159	182,075	196,057	0.93
Retail strip mall	2,090	2,072	1,060	1,184	3,589,683	3,559,591	1,820,347	2,033,822	0.90
Fast-food restaurant	232	232	160	186	612	613	422	490	0.86
Sit-down restaurant	511	511	229	276	461,927	462,063	206,593	249,242	0.83
LA sum or ratio					95,681,324	41,620,933	63,929,602	77,341,834	0.83

Table A5. Urban grid cell albedo, upflux (reflected solar radiation) [a], and canyon air temperature at different times of day in Los Angeles County (shown in Figure 1b), including absolute values for CONTROL, changes relative to CONTROL for the five perturbation scenarios, and the sum of COOL_WALL_HIGH minus CONTROL and COOL_ROOF_HIGH minus CONTROL. [b]

Scenario	Albedo at 06:00 LST	Albedo at 12:00 LST	Daily average solar upflux (W m^{-2})	Daily (24-hour) average canyon air temperature (K)	Canyon air temperature (K) at 14:00 LST	Canyon air temperature (K) at 20:00 LST
CONTROL	0.143	0.148	50.2	295.2	302	294.5
COOL_WALL_LOW minus CONTROL	0.045	0.008	4.3	-0.19	-0.19	-0.18
COOL_WALL_HIGH minus CONTROL	0.097	0.017	9.1	-0.43	-0.41	-0.4
COOL_ROOF_LOW minus CONTROL	0.033	0.033	10.7	-0.23	-0.34	-0.18
COOL_ROOF_HIGH minus CONTROL	0.065	0.065	21.3	-0.48	-0.72	-0.36
COOL_ROOF_WALL_HIGH minus CONTROL	0.162	0.083	30.1	-0.95	-1.17	-0.78
COOL_WALL_HIGH minus CONTROL + COOL_ROOF_HIGH minus CONTROL	0.162	0.082	30.4	-0.91	-1.13	-0.76

[a] Daily average solar upflux (W m^{-2}) multiplied by 86,400 seconds (24 hours) is equal to daily cumulative solar upflux (J m^{-2}).

[b] All values are averages for July 3 to 12.

Task Report Appendix B

We define variables as follows.

$F_{W\to S}$ is view factor from wall to sky.

$F_{G\to S}$ is view factor from ground to sky.

$F_{W\to W}$ is view factor from wall to wall.

$F_{W\to G}$ is view factor from wall to ground.

$\propto_G$ is ground albedo ($\propto_G = 0.10$).

$\propto_W$ is wall albedo.

$$\propto_W = \begin{cases} 0.10 & \text{(CONTROL)} \\ 0.50 & \text{(COOL\_WALL\_LOW)} \\ 0.90 & \text{(COOL\_WALL\_HIGH)} \end{cases}$$

f is the fraction of solar radiation reflected by walls that escapes the canopy.

Table 1 in main article shows urban morphology configuration for grid cells where NLCD land use types are not used. View factors are calculated based on the morphology for each land use type.

The WRF model approximates f by

$$f_{WRF} = F_{W\to S} + F_{W\to W} \times \propto_W + F_{W\to G} \times \propto_G \quad \text{(B-1)}$$

Table B1 reports f_{WRF} in the control scenario and the two cool wall scenarios.

f_{WRF} overestimates f because its calculation assumes that all wall-reflected light subsequently reflected by the wall or ground will escape the canopy. That is, it neglects absorption of this light by wall or ground.

We develop a lower bound estimate for f, denoted f_L (Table B2), that assumes that of the wall-reflected light subsequently reflected by wall or ground, only that portion immediately reflected toward the sky will escape the canopy:

$$f_L = F_{W\to S} + F_{W\to W} \times \propto_W \times F_{W\to S} + F_{W\to G} \times \propto_G \times F_{G\to S} \quad \text{(B-2)}$$

Thus f lies between f_L and f_{WRF}. For example, the true fraction of wall-reflected light that escapes the canopy in the low-intensity residential region is in the range 0.48 – 0.50 for CONTROL, 0.50 – 0.54 for COOL_WALL_LOW, and 0.54 – 0.59 for COOL_WALL_HIGH. The WRF model assumes $f = f_{WRF}$ (i.e., 0.50, 0.54, or 0.59) in these three scenarios.

If needed, one can either add 3rd (and 4th) reflections in the model code or use a wall albedo that corrects for the lack of 3rd (and 4th) reflections.

Table B1. View factors and fraction f_{WRF} of wall-reflected light that escapes the canopy in the WRF urban canopy model, shown by urban land use type for the control scenario and the two cool wall scenarios.

Urban land use type	View factor from wall to ground	View factor from wall to sky	View factor from wall to wall	Fraction of solar radiation reflected by walls that escapes canopy (CONTROL)	Fraction of solar radiation reflected by walls that escapes canopy (COOL_WALL_LOW)	Fraction of solar radiation reflected by walls that escapes canopy (COOL_WALL_HIGH)
Low-intensity residential	**0.45**	**0.45**	**0.11**	**0.50**	**0.54**	**0.59**
High-intensity residential	**0.45**	**0.45**	**0.11**	**0.50**	**0.54**	**0.59**
Commercial/ industrial	**0.44**	**0.44**	**0.12**	**0.50**	**0.54**	**0.59**

Table B2. Same as Table B1, but reporting lower-bound f_{L} to the fraction of wall-reflected light that escapes the canopy.

Urban land use type	View factor from wall to ground	View factor from wall to sky	View factor from wall to wall	Fraction of solar radiation reflected by walls that escapes canopy (CONTROL)	Fraction of solar radiation reflected by walls that escapes canopy (COOL_WALL_LOW)	Fraction of solar radiation reflected by walls that escapes canopy (COOL_WALL_HIGH)
Low-intensity residential	**0.45**	**0.45**	**0.11**	**0.48**	**0.50**	**0.54**
High-intensity residential	**0.45**	**0.45**	**0.11**	**0.48**	**0.50**	**0.54**
Commercial/ industrial	**0.44**	**0.44**	**0.12**	**0.47**	**0.51**	**0.55**

Task Report Appendix C

Figure C1 shows that the relationship between reduction in canyon air temperature (K) and the ratio of increase in upflux (W m^{-2}) to PBLH (m) is approximately linear for cool roofs, but not for cool walls. However, if we exclude two outliers at 06:00 and 07:00 LST (Figure C2), reduction in canyon air temperature per unit increase in the ratio of upflux (W m^{-2}) to PBLH (m) shows improved linearity (i.e., a higher coefficient of determination). (Note that at 06:00 and 07:00 LST, the surface has just begun to warm from solar radiation. In contrast, at later hours of day, the cooling induced by cool walls is influenced not only by instantaneous increase in upflux, but also by the accumulated reduction in absorbed solar heat gain (induced by increase in upflux) during previous hours of day.)

Figures C1 and C2 suggest that the PBLH and increase in upflux both contribute to the diurnal cycle of canyon air temperature reductions from adopting cool walls and roofs. PBLH is negatively correlated with the temperature reductions, while increase in upflux is positively correlated with the temperature reductions.

As described in the main article, we should also note that there are three competing processes contributing to the diurnal cycle of temperature reduction, and the system is more complicated than a linear model.

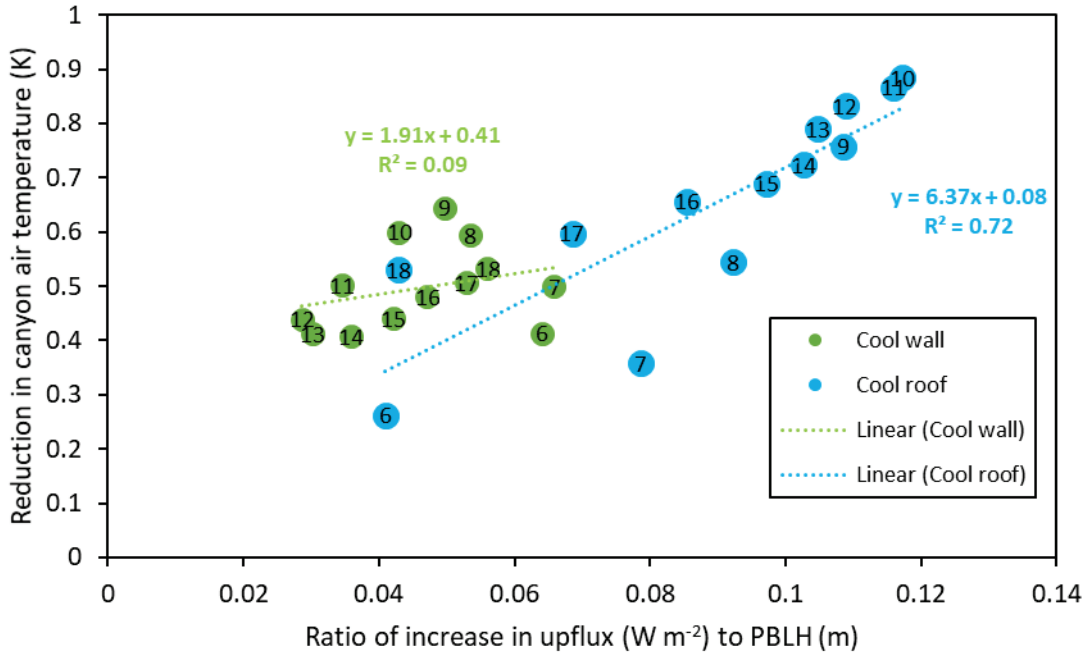

Figure C1. Scatter plot showing reductions in canyon air temperature (K) induced by cool walls (green) and cool roofs (blue) versus the ratio of increase in upflux (W m^{-2}) to PBLH height (m) in CONTROL. Numbers on dots label time of day (e.g., 6 = 06:00 LST). Least-squares linear regressions and corresponding coefficients of determination (R^2) for cool walls and roofs are also shown.

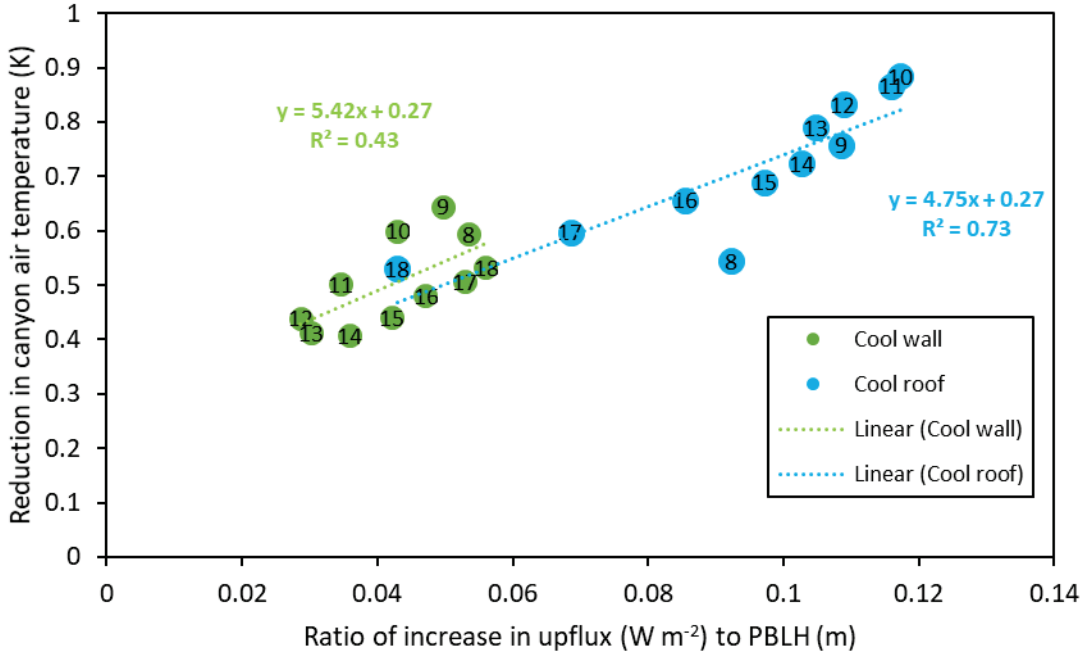

Figure C2. Same as Figure C1, but with data points corresponding to 06:00 and 07:00 LST removed.

Energy Research and Development Division

FINAL PROJECT REPORT

Solar-Reflective "Cool" Walls: Benefits, Technologies, and Implementation

Appendix F: Effect of Cool Walls on Energy-saving Benefits from Cool Pavements (Task 3.3 Report)

California Energy Commission
Gavin Newsom, Governor

April 2019 | CEC-500-2019-040-APF

Appendix F:
Effect of cool walls on energy-saving benefits from cool pavements (Task 3.3 report)

Pablo Rosado[1] and Ronnen Levinson[1]

[1] Heat Island Group, Lawrence Berkeley National Laboratory

28 February 2018

Note: This task report is a preprint of Rosado and Levinson (2015). A brief element of this report (Section 3.2: Building to roads view factors) was included in Levinson et al. (2017).

Abstract

Solar-reflective “cool” pavements are an urban heat island reduction strategy that increases pavement albedo (solar reflectance) to reduce convective heating of the outdoor air, which has the “indirect” effect of decreasing cooling loads in summer and increasing heating loads in winter. Raising pavement albedo also increases the solar flux incident on walls and windows. This “direct” effect of reflective pavement can increase cooling loads in summer and reduce heating loads in winter. In this study we focus on the direct effect of cool pavements, and quantify its impact on the annual conditioning (heating and cooling) energy uses of buildings in California, USA. The study also measures how modifying wall and window properties alter the direct effect.

We prepared nine code-compliant building prototypes with external horizontal shading surfaces that represent local roads. To quantify the direct effects of cool pavements, we simulated with EnergyPlus the annual cooling and heating energy uses of each prototype, varying the road albedo, wall absorptance, and window solar heat gain coefficient.

We present a physical model that relates each heating and cooling energy use to building properties, and to local road albedo. The results from the building simulations were used to validate the physical model, and to generate relationships that predict the direct effect of pavement albedo change on building energy use.

1 Introduction

Heat island refers to the phenomenon of having higher urban temperatures compared to the temperatures of surrounding suburban and rural areas (Santamouris 2013). In the United States, pavements cover typically up to 30% of the urban fabric (Rose et al. 2003), and as hot, dry surfaces can contribute substantially to the heat island effect.

The use of cool pavements is an urban heat island reduction strategy that increases pavement albedo (solar reflectance) to reduce convective heating of the outdoor air. This lowers the air temperature difference across the building envelope, reducing heat gain via conduction and infiltration. This "indirect" effect of reflective pavement can decrease cooling loads in summer and increase heating loads in winter. Raising pavement albedo also increases the solar flux incident on walls and windows. This "direct" effect of reflective pavement can increase cooling loads in summer and reduce heating loads in winter. The total annual changes in cooling and heating energy loads will depend on the relative magnitudes of the indirect and direct effects. This study explores only the direct effect of cool pavements for buildings in California cities.

The magnitude of the direct effect depends on the design and properties of the building's walls and windows. We prepared nine code-compliant building prototypes with external horizontal shading surfaces that represent local roads. To quantify the direct effects of cool pavements, we simulated with EnergyPlus the annual cooling and heating energy uses of each prototype, varying the road albedo, wall absorptance (1 – wall albedo), and window solar heat gain coefficient.

We present a physical model that relates each heating and cooling energy use to building properties, and to local road albedo. The results from the building simulations were used to validate the physical model, and to generate relationships that predict the direct effect of pavement albedo change on building energy use.

2 Methodology

2.1 Physical model

We derived a physical model to describe the effect of modifying building envelope properties on conditioning energy use when implementing cool pavements. This physical model describes the cooling and heating energy uses of a building from modifications to local road albedo (ρ_r), exterior wall solar absorptance (α), and window solar heat gain coefficient (σ).

Raising the local road albedo increases the reflected solar flux incident on walls and windows. Reducing the solar absorptance of the walls decreases the reflected solar flux that is absorbed and conducted through the walls and eventually heats the interior. Additionally, reducing the solar heat gain coefficient (SHGC) of windows decreases the reflected solar flux that is direct

transmitted through the window to the interior, and that is absorbed by the window and re-radiated to the interior. Thus, the change in cooling or heating energy use E by the change in the local road albedo can be described as

$$\frac{\partial E}{\partial \rho_{\mathrm{r}}} = a_2 \cdot \alpha + a_4 \cdot \sigma \ . \tag{1}$$

Similarly, the change in cooling or heating energy use by a change in the wall absorptance is described as

$$\frac{\partial E}{\partial \alpha} = a_1 + a_2 \cdot \rho_{\mathrm{r}} \tag{2}$$

The change in cooling or heating energy use by a change in window SHGC can be described as

$$\frac{\partial E}{\partial \sigma} = a_3 + a_4 \cdot \rho_r \tag{3}$$

The solutions to the differential equations of these physical models provide a way to calculate the cooling or heating energy uses as a function local road albedo building surface parameters. Combining equations (1) through (3) yields

$$E = a_0 + a_1 \cdot \alpha + a_2 \cdot \rho_{\mathrm{r}} \cdot \alpha + a_3 \cdot \sigma + a_4 \cdot \rho_{\mathrm{r}} \cdot \sigma \tag{4}$$

Equation (4) was used to obtain the solutions that describe the cooling (E_{C}) and heating (E_{H}) energy uses.

2.2 Building prototypes

The EnergyPlus prototypes include seven commercial buildings and two residential buildings. Table 1 lists the nine prototypes and summarizes their dimensions. The commercial prototypes were obtained from the California Energy Commission (CEC); the residential prototypes were obtained from the United States Department of Energy's Building Energy Codes Program (PNNL 2016a,b). All nine prototypes were modified to meet California's 2008 Title 24 commercial (CEC 2008a) and residential (CEC 2008b) building codes for: (a) wall, ground floor and ceiling thermal resistance (RSI) values; (b) window thermal transmittance, SHGC, and visible transmittance; (c) air-conditioning's SEER; and (d) heating's annual fuel utilization efficiency (AFUE).

The CEC established 16 building climate zones (hereafter, "climate zones") in the state, each representing a geographic area of a particular climate. CEC's Title 24 estipulate building construction codes for each of these 16 climate zones. For each building prototype we prepared 16 code-compliant versions, one per climate zone.

2.3 Prototype modifications

The residential and commercial prototypes were modified to include horizontal surfaces to represent local roads. Additional external vertical surfaces were included to represent the shading effect from neighboring buildings.

We obtained the minimum side and front setbacks for different building types from the street design guidelines specified for the city of Sacramento, CA in the Zoning Code of Sacramento County, ZCSC (ZCSC 2015). These setback regulations were used to define the distance between the modelled buildings and the vertical shading surfaces. We also obtained the front setbacks regulations, which we used to define the distance between the modelled buildings and the roads. Table 1 lists the front setbacks.

In average, a city block covers a surface area of 10,000 m². Hence, unless a large building occupies an entire city block, it is common to have a building facing a paved surface from only one or two sides. We estimated the number of sides each prototype faces a paved surface by comparing its footprint area to the size of a city block.

The road dimensions follow street design configurations and standards used for the city of Sacramento (DoT Sacramento 2009). We used Sacramento's street design dimensions because they are closest to the average street dimensions found in other large California cities (e.g. Los Angeles (Ryan Snyder Associates. 2011) and San Jose (DoT San Jose 2010). Hence, we classified the roads used in the modelling into three types: residential, commercial, and boulevard. The road widths are 9 m, 11 m, and 22 m, respectively. The road type added in each prototype depended on the building use. Table 1 lists the road types used.

Table 1: Summary of prototypes construction, setback distances, and road types.

Prototype building	Road type	Floors	Conditioned floor area [1000 m²]	Gross wall area [1000 m²]	Window area [1000 m²]	Window-to-wall ratio [%]	Front setback [m]	Sides facing road
Single-family home	Residential	2	0.22	0.24	0.03	14.1	10	1
Apartment complex	Residential	3	2.0	1.50	0.25	16.4	11	1
Large hotel	Boulevard, Commercial	6	11.3	4.03	1.21	30.2	15.2	2
Large office	Boulevard, Commercial	13	46.3	11.6	4.64	40.0	40, 11	2
Medium office	Commercial	3	5.0	1.98	0.65	33.0	11	1
Primary school	Residential	1	6.8	2.51	0.88	35.0	11	3
Fast-food restaurant	Commercial	1	0.23	0.19	0.03	14.0	19	1
Retail stand-alone	Boulevard	1	2.3	1.18	0.08	7.1	65	1
Retail strip mall	Boulevard, Commercial	1	2.2	1.18	0.12	10.5	65, 19	2
Sit-down restaurant	Commercial	1	0.51	0.28	0.05	17.1	19	1

Figure 1 shows the single-family home and strip mall retail prototypes. The horizontal purple surfaces are the EnergyPlus shading objects used to represent the “roads”. The single-family home also has vertical shading surfaces used to represent neighboring buildings.

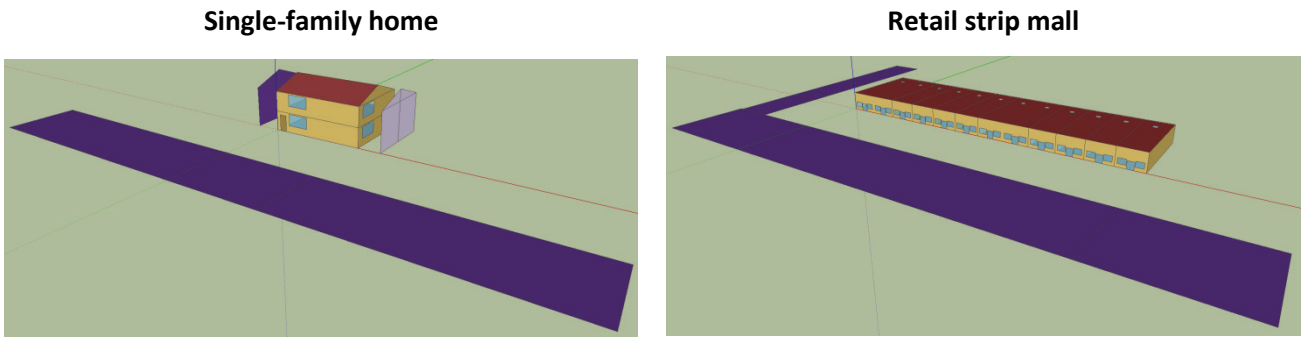

Figure 1: Modified building prototypes of the single-family home and the strip mall retail.

2.4 Weather files

The building prototypes were simulated using the most recent California weather files developed by White Box Technologies (WBT 2011) for use in Title 24 compliance calculations. They have produced 86 weather files from weather stations throughout the state of California. The files have a period of record of 12 years (1998-2009). From the 86, there are 16 weather stations that the US Department of Energy uses to demonstrate compliance with Title 24 in California's climate zones (CZ). In this study, we focused on the CZ which are most densely populated. Table 2 lists some of the major cities in each CZ.

Table 2: California's mayor cities in the represented climate zones.

Climate zone	Major cities
3	Oakland, Fremont, San Francisco
4	San Jose
7	San Diego
8	Los Angeles, Irvine, Anaheim, Santa Ana
9	Burbank, Glendale, Pasadena
10	Riverside, Rancho Cucamonga, San Bernardino
12	Sacramento
13	Fresno, Bakersfield
15	Palm Springs

2.5 EnergyPlus simulations

All simulations were run with EnergyPlus v8.1 (EnergyPlus 2003), a building energy simulation program that models cooling, heating, ventilation, and other energy flows. The time to run all simulations was reduced using the parametric simulation manager jEPlus (jEPlus 2015).

We ran simulations to perform a parametric analysis that varied the road albedo, window SHGC, and wall solar absorptance. Each prototype was modelled with six different road albedos (0.1, 0.15, 0.2, 0.4, and 0.5), four different window SHGCs (0, 0.2, 0.4, 0.6), and four different wall absorptances (0, 0.2, 0.5, and 0.8).

3 Results

3.1 Comparing contributions from walls and windows

We compared the magnitude of solar flux reflected from the roads that is incident on walls to that incident on windows. To understand the contribution through walls, we performed simulations in which the wall absorptance was either the code-compliant default or zero. These simulations were run for both low and high road albedo. We first calculated the total change in

cooling or heating energy use that results from increasing road albedo [Eq. (5)]. This is calculated with the default wall absorptance (α_d).

$$\Delta E_T = E(\rho_{high}, \alpha_d) - E(\rho_{low}, \alpha_d) \ . \quad (5)$$

Similarly, the portion of the energy change not attributed to walls was calculated with the simulations where wall absorpance was set to zero (α_0):

$$\Delta E_{non\_wall} = E(\rho_{high}, \alpha_0) - E(\rho_{low}, \alpha_0) \ . \quad (6)$$

Lastly, the portion in ΔE_T that is attributed to walls is obtained by subtracting the non-wall contribution from the total change:

$$\Delta E_{wall} = \Delta E_T - \Delta E_{non\_wall} \ . \quad (7)$$

Following the same approach described in Equations (5) through (7) but using the simulations where the windows SHGCs were set to zero, we calculated the magnitude of heat load gained through windows (ΔE_{window}).

The portions of the change in cooling or heating energy use allotted to walls and windows depend on various factors. Low wall solar absorptance decreases the heat gained through walls; similarly, lower windows SHGC reduces the cool pavements' direct effect through windows. But another factor that dictates the magnitude of the direct effect through either walls or windows is the window-to-wall ratio (window area / wall area). Large window-to-wall ratios increases the contribution through windows by increasing their surface area exposed to the incident reflected solar flux.

Since all prototypes had different window-to-wall ratios, we normalized the direct effect contributions through walls and windows by the window-to-wall ratio (largest ratio is 0.40), to allow a fair comparison of their contributions. Figure 2a,b compare the normalized cooling contribution through walls and windows, respectively to the total direct effect. From the regressions' slope, we find that windows contribute nearly 60% to the total direct effect on the cooling energy use, that is, 1.5 times the contribution through walls.

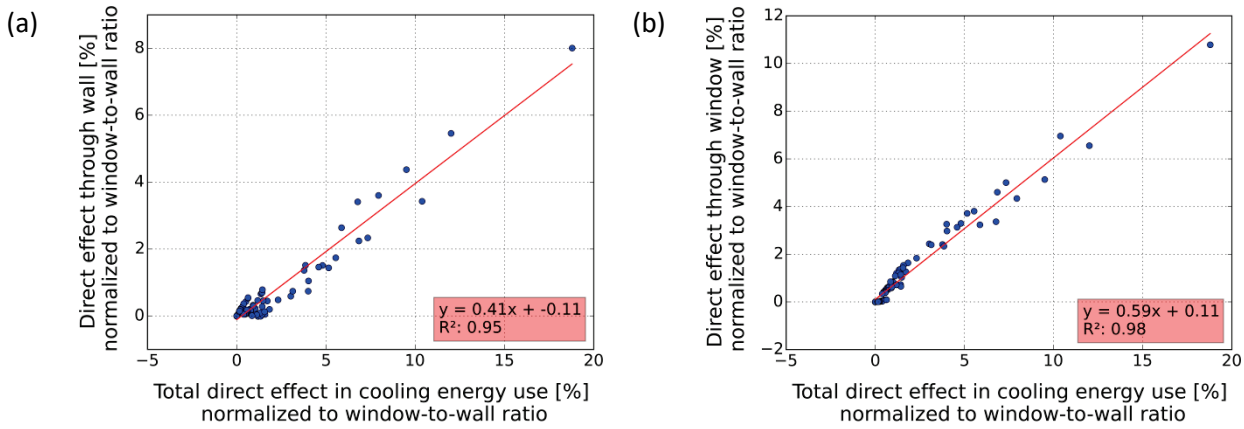

Figure 2: Comparing the fraction of the direct effect in cooling energy use that is gained (a) through the walls and (b) through the windows.

3.2 Building to roads view factors

Assuming unobstructed view from wall to road (e.g. absence of trees), we used standard radiation configurations to calculate the view factors from the prototypes to the roads. We treat the road facing walls of a building as a rectangular surface of height (H_w) and length (L_w), with a setback to the road (W_s). The road is treated as an infinitely long rectangle of width (W_r). To calculate the wall-to-road view factors ($F_{w\text{-}r}$), we employ two standard radiation configurations. One configuration was used to find the view factor from the wall to the portion of the road directly in front of the wall, which we call the central road. The second configuration was employed to calculate the view factor form the wall to the left and right wings of the road. See Figure 3 for the break out of the wall, setback, and road sections used for the view factor calculations.

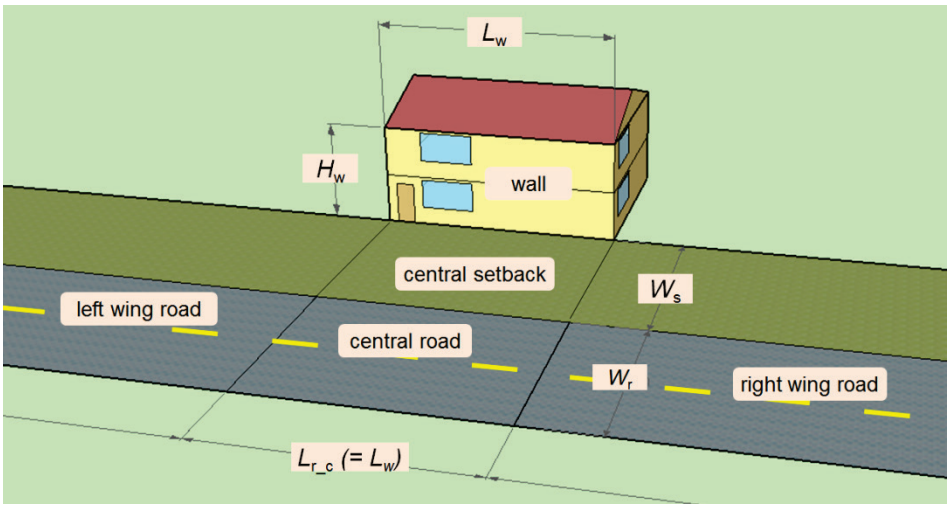

Figure 3: Diagram of single-family home with setback and road.

The first configuration (Incropera 2007) is used for two finite rectangles of same length, having one common edge, and at an angle of 90˚ of each other. Hence, the view factor from the wall to the central road portion ($F_{w\text{-}r\_c}$) was obtained by subtracting the view factor to the central setback ($F_{w\text{-}s\_c}$) from the view factor to the central setback+road ($F_{w\text{-}sr\_c}$) [Equation (8)].

$$F_{w\text{-}r\_c} = F_{w\text{-}sr\_c} - F_{w\text{-}s\_c} \tag{8}$$

The second configuration (Ehlert and Smith 1993) is commonly used for a rectangle to a rectangle in a perpendicular plane, with all boundaries being parallel or perpendicular. Thus with this configuration we obtained the view factors from the wall to the left ($F_{w\text{-}r\_l}$) and right ($F_{w\text{-}r\_r}$) wings of the road. The total wall-to-road view factor ($F_{w\text{-}r}$) was obtained as

$$F_{w\text{-}r} = F_{w\text{-}r\_c} + F_{w\text{-}r\_l} + F_{w\text{-}r\_r} \tag{9}$$

As explained in Section 4.1, the modified prototypes do not have roads at all four cardinal sides. Using the number of building sides (*N*) facing a road (Table 1), we estimated the overall building-to-road view factor F_{br} as

$$F_{b\text{-}r} = F_{w\text{-}r} \times N/4 \tag{10}$$

Table 3 lists the view factors from the wall to different portions of setback and road. These were calculated using the setback distances listed in Table 1 and the widths of the roads assigned to each prototype.

Table 3: Calculated view factors from wall to setback and road portions.

Prototype	Wall to all setback ($F_{w\text{-}s}$)	Wall to all setback + road ($F_{w\text{-}sr}$)	Wall to road ($F_{w\text{-}r}$)	Building to road ($F_{b\text{-}r}$)
Single-family home	0.373	0.430	0.057	0.014
Apartment complex	0.342	0.406	0.064	0.016
Large hotel	0.277	0.356	0.079	0.040
Large office	0.133	0.246	0.113	0.057
Medium office	0.282	0.372	0.090	0.023
Primary school	0.413	0.45	0.037	0.028
Retail stand-alone	0.422	0.46	0.038	0.010
Retail strip mall	0.434	0.462	0.028	0.014
Sit-down restaurant	0.459	0.472	0.013	0.003

Using the modelling results used for Section 5.1, we obtained a relationship that describes the change in total direct effect as a function of building to road view factor. As before, we normalized the direct effect by the window-to-wall ratio. This relationship is particular to location, which in our case we varied by climate zone. Figure 4 shows this relationship for the direct effect in cooling energy use for climate zones 9 and 12. The slope of the curve varies by climate zone, and for the effects on cooling, it ranged between 15 %/$F_{b\text{-}r}$ and 27 %/$F_{b\text{-}r}$. For the effect on heating energy use, the slopes were opposite in sign, and smaller in magnitude (-25 %/$F_{b\text{-}r}$ to -6 %/$F_{b\text{-}r}$).

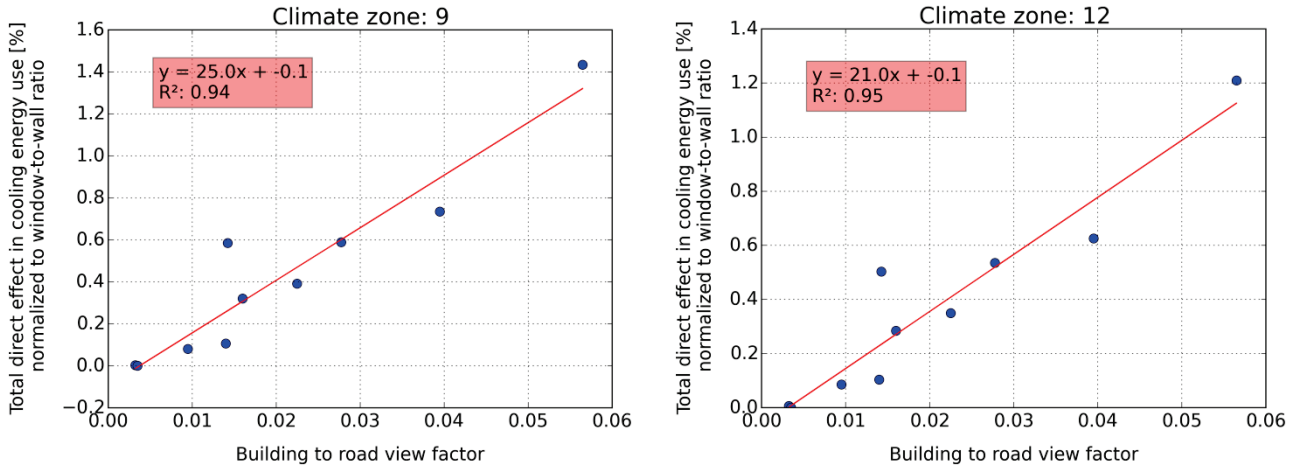

Figure 4: Direct effect in cooling energy use from cool pavements vs building to road view factors, for CZ 9 and CZ 12.

3.3 Coefficients to physical model solutions

Using multiple linear regression analysis on the EnergyPlus simulations, we calculated the coefficients to the physical model solutions described in Equation (4) for cooling and heating energy uses. The coefficients describe annual site energy uses and are particular to each prototype and to each climate zone. This leads to 81 (9 prototypes x 9 climate zones) different physical model solutions for any type of conditioning energy use. As an example, Table 4 show the cooling and heating coefficients for prototypes in climate zone 12, specifically for sit-down restaurant, retail strip mall, and single-family home. The coefficients labelled **e** represent electric energy use in units of MWh/y, and the coefficients **g** are for gas energy use in units of therms/y. Values can be converted to units of MJ by multiplying MWh × 3600, or therm × 105.5.

Table 4: Coefficients for physical model solutions for prototypes sit-down restaurant, retail strip mall, and single-family home, in CZ 12.

Prototype	Use	e0	e1	e2	e3	e4	g0	g1	g2	g3	g4
Sit-down restaurant	cooling	20.129	0.825	0.002	3.33	0.008	0	0	0	0	0
	heating	0	0	0	0	0	2725.8	-177.3	-1.428	-519.6	0.021
Retail strip mall	cooling	41.552	4.279	0.264	16.74	0.042	0	0	0	0	0
	heating	0	0	0	0	0	1510.1	-135.6	-6.982	-762.7	0.764
Single-family home	cooling	0.483	0.447	0.021	2.28	0.135	0	0	0	0	0
	heating	0	0	0	0	0	205.7	-34.8	-2.143	-168.6	-2.605

3.4 Modify wall and window to counter direct effect

Here we present how changes to wall absorptance and window SHGC can counter the direct effect of cool pavements. For purposes of the analysis, we used a road albedo of 0.10 to represent the base case, and 0.35 for the modified case; these represent typical albedo values of an aged asphalt and new standard gray cement concrete, respectively (ACPA 2002). For wall absorptance, the base case and modified case values were 0.70 and 0.45. For the windows SHGC, values were 0.35 and 0.30 respectively; these values meet the requirements in 2008 Title 24 Standards for all building climate zones and building types. Table 5 summarizes these values.

Table 5: Base case and modified case values for the varied road and building properties.

Property	Base case	Modified case
Road albedo (ρ_r)	0.10	0.35
Wall absorptance (α)	0.70	0.45
Window SHGC (σ)	0.35	0.30

3.4.1 Annual cooling site energy

Considering the case of modifying the road albedo by 0.25 while keeping the building envelope unchanged, the prototypes suffered cooling site energy penalties of no more than 1.3% of their annual use; the largest penalties occurring at climate zones with low cooling degree days at 18 ˚C (CDD18C). The penalties varied by building and location, but it averaged 0.4%.

We chose to decrease the wall absorptance by 0.25 to match (in magnitude) the road albedo increase. During the cooling season, we observed that this was generally enough to outweigh the direct cooling penalty from the cool pavements. As an example, the benefits from lower wall absorptance in the residential buildings outweigh the cool pavement penalties by more than a factor of 3 in most CZ. The single-family home and apartment complex experienced cooling savings that range between 5-19% and 2-7% respectively. These results are similar to the ones found in the commercial buildings with similar window-to-wall ratio (retail strip mall and retail stand-alone). However, lowering the wall absorptance had no effect over the cooling site energy in the prototypes with high window-to-wall ratio (medium and large office).

When considering the case of modifying the road albedo and the window SHGC, the prototypes also experienced cooling savings (average of 2.8%). Hence, the penalties from the direct effect of cool pavements during the cooling season can be far outweighed by performing small modifications to the wall absorptance and window SHGC. Figure 5 show the cooling savings from modified pavements and surface properties, as a function of CDD18C, for the single-family home and retail strip mall. The figures demonstrate how the magnitudes of the savings reduce with increasing CDD18C.

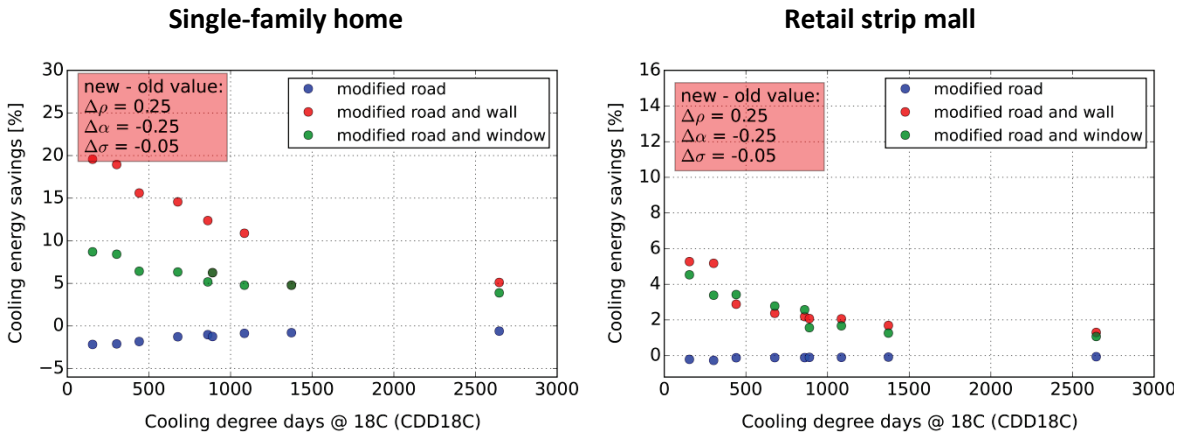

Figure 5: Cooling site energy savings vs CDD18C for single-family home and retail strip mall.

3.4.2 Annual heating site energy

As expected, the heating season experienced the opposite response from the cooling season. The single-family home experienced the largest annual heating savings from cool pavement (0.67%), but the mean savings across buildings and climate zones was 0.1%.

In magnitude, the fraction of heating penalties from modified wall absorptance and window SHGC were similar than cooling benefits. In average, modifying the roads and walls alone had a penalty of 4%. For the case of road and windows SHGC, the penalties were 3.2%.

Figure 6 show for the single-family home and retail strip mall, the heating penalties from modified pavements (negative values mean savings), walls and windows, as a function of HDD18C. In the heating season, magnitudes of the penalties did not show any obvious correlation with HDD18C.

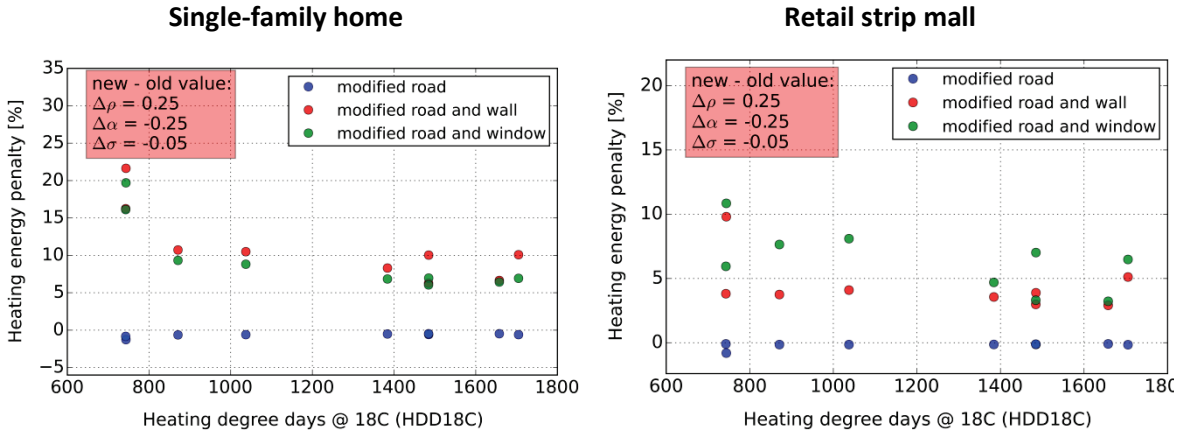

Figure 6: Heating site energy penalties vs HDD18C for single-family home and retail strip mall.

3.4.3 Annual conditioning source energy

In order to properly compare cooling and heating savings/penalties, the cooling and heating site energy uses were converted to source energy. Site energy savings are converted to source energy savings using the site-to-source conversion factors in Table 6.

Table 6: USA average source-to-site energy ratios.

	Electricity	Natural gas
Source-to-site energy ratio	3.34[a]	1.047[a]

[a] US average (EnergyStar 2013).

All buildings suffered a net conditioning source energy penalty when we only modified the road. But when combined with modified wall and windows, all prototypes experienced net source energy savings, ranging from 0.68% (sit-down restaurant) to 5.82% (apartment complex). Table 7 summarizes the base conditioning source energy intensity and the savings percent (mean savings / base) for all prototypes. Values represent the average for the nine CZ.

Table 7: Summary of conditioning source energy savings averaged over all CZ.

Prototype	Source mean conditioning (cooling + heating) energy intensity savings				
	Base [MJ/m²y]	Savings from road [%]	Savings from road + wall [%]	Savings from road + window [%]	Savings from road, wall, window [%]
Single-family home	146.5	-0.59	4.17	1.64	5.82
Apartment complex	121.6	-0.50	2.20	3.11	5.31
Large hotel	705.0	-0.40	1.14	0.68	1.82
Large office	241.5	-0.80	-0.19	2.94	2.75
Medium office	398.2	-0.29	0.35	2.58	2.93
Primary school	261.3	-0.35	0.59	2.48	3.07
Retail stand-alone	309.6	-0.07	2.00	1.59	3.60
Strip mall retail	350.2	-0.09	1.75	1.39	3.13
Sit-down restaurant	903.6	0.01	0.36	0.32	0.68

4 Summary

In this study, we focused in the direct effect of cool pavements, and quantified their impact on the annual building conditioning energy use for nine prototyped buildings in California. The prototypes were modelled varying road albedo, wall absorptance and window SHGC. The simulation results were used to generate relationships to predict the direct effect of pavement albedo change as a function of the road albedo and wall and window properties.

The study analyzed how the location and dimension of the road with respect to the building affects its direct effect on the building energy use. For this, we compared the building-to-road view factors to their direct effect. We observed a relationship in which the direct effect on cooling increases linearly with the view factor; the direct effect on heating is a linear decrease.

The direct effect from cool pavements had a slightly larger contribution through windows than walls. Their individual contributions depend heavily on the window-to-wall ratio, as well as other construction properties. In our case, the latter was similar across prototypes. Hence, after normalizing to a window-to-wall ratio of 0.40, we found windows contribute 1.5 times more to the direct effect than walls (for the base case values of wall absorptance and window SHGC).

Although increasing the pavement albedo by 0.25 caused net conditioning energy penalties that were as much as 0.80% (large office averaged over all CZ), when reducing the wall absorptance by 0.25 most prototypes experienced net conditioning energy savings (as much as 4.2%). Similarly, when window SHGC was reduced by 0.05, all prototypes experienced net conditioning energy savings ranging between 0.32% and 3.11%. Hence, the study suggests small modifications to a building's envelope can outweigh the small cooling penalties associated with the direct effect of cool pavements.

References

ACPA. 2002. American Concrete Pavement Association (ACPA), R.T., Albedo: a measure of pavement surface reflectance, 2002.

CEC. 2008a. 2008 Nonresidential compliance manual. Publication CEC-400-2008-017-CMF-REV1, California Energy Commission, Sacramento, CA. Retrieved 2016-01 from http://www.energy.ca.gov/title24/standards_archive/

CEC. 2008b. 2008 Residential compliance manual. Publication CEC-400-2008-016-CMF-REV-1, California Energy Commission, Sacramento, CA. Retrieved 2016-01 from http://www.energy.ca.gov/title24/standards_archive/

DoT Sacramento. 2009. Design and Procedures Manual: Section 15 - Street Design Standards. Department of Transportation, City of Sacramento. Retrieve 2015-12 from http://portal.cityofsacramento.org/Public-Works/Resources/Publications

DoT San Jose. 2010. Geometric Design Guidelines. Department of Transportation, City of San Jose, CA. Retrieved 2015-12-10 from https://www.sanjoseca.gov/index.aspx?NID=1882

Ehlert JR, Smith TF. 1993. View factors for perpendicular and parallel rectangular plates. *Journal of Thermophysics and Heat Transfer* 7(1), 173-175.

EnergyPlus. 2003. EnergyPlus version 8.5. Downloaded from https://energyplus.net/

EnergyStar. 2013. Portfolio Manager Technical Reference: Source Energy, 2013. Available from: http://www.energystar.gov/buildings/tools-and-resources/portfolio-manager-technical-reference-source-energy

Incropera FP. 2007. *Fundamentals of Heat and Mass Transfer, 6th Edition*. Section 13.1.1 – Radiation exchange between surfaces. Wiley & Sons.

jEPlus. 2015. jEPlus v1.6.0 – An EnergyPlus simulation manager for parametrics. Downloaded 2015-12 from http://www.jeplus.org/wiki/doku.php

Levinson RM, Gilbert HE, Jin L, Mandel BH, Millstein D, Rosado PJ, Harvey JT, Kendall A, Li H, Saboori A, Lea J, Ban-Weiss G, Mohegh A, Santero N. 2017. Life Cycle Assessment and Co-Benefits of Cool Pavements. Final report for Contract #12-314, California Air Resources Board, Sacramento, CA. https://www.arb.ca.gov/research/singleproject.php?row_id=65149 .

PNNL. 2016a. Residential Prototype Building Models. Pacific Northwest National Laboratory, Richland, WA. Retrieved 2015-10 from https://www.energycodes.gov/development/residential/iecc_models

PNNL. 2016b. Commercial Prototype Building Models. Pacific Northwest National Laboratory, Richland, WA. Retrieved 2015-10 from https://www.energycodes.gov/development/commercial/prototype_models

Rosado P, Levinson R. 2015. The direct effect of pavement albedo changes on conditioning energy use in California buildings as a function of building skin properties. *Proceedings of the 10th Energy Forum on Advanced Building Skins*, 3-4 November 2015, Bern, Switzerland, 302-311. https://abs.green/conference-proceedings .

Rose, L.S., H. Akbari, and H. Taha, Characterizing the fabric of the urban environment: A case study of Greater Houston, Texas, 2003.

Ryan Snyder Associates. 2011. Los Angeles County Model Design Manual for Living Streets. Ryan Snyder Associates, Transportation Planning for Livable Communities. Retrieved 2015-12 from http://www.modelstreetdesignmanual.com/

Santamouris, M., Using cool pavements as a mitigation strategy to fight urban heat island—A review of the actual developments. Renewable and Sustainable Energy Reviews, 2013. 26(0): p. 224-240.

WBT. 2011. White Box Technologies – weather data for energy calculations. Retrieved 2015-12-10 from http://weather.whiteboxtechnologies.com/

ZCSC. 2015. Sacramento County Zoning Code. Sacramento County, CA. Retrieved 2015-12-10 from http://www.per.saccounty.net/LandUseRegulationDocuments/Pages/Sacramento%20County%20Zoning%20Code.aspx

Energy Research and Development Division

FINAL PROJECT REPORT

Solar-Reflective "Cool" Walls: Benefits, Technologies, and Implementation

Appendix G: Effect of Wall Albedo on the Environment Inside an Unconditioned Building (Task 3.4 Report)

California Energy Commission
Gavin Newsom, Governor

April 2019 | CEC-500-2019-040-APG

Appendix G:
Effect of wall albedo on the environment inside an unconditioned building (Task 3.4 report)

Jan Kleissl[1], Matteo Pizzicotti[1], and Ronnen Levinson[2]

[1] Center for Energy Research, University of California, San Diego

[2] Heat Island Group, Lawrence Berkeley National Laboratory

28 February 2018

Abstract

Interior air temperature (IAT), mean radiant temperature (MRT) and thermal comfort were analyzed for homogeneous neighborhoods of multi-family residences with cool walls in a coastal California climate zone. The thermal environment for an occupant of a building with neither heating nor air conditioning was simulated. The typical IAT and MRT reduction inside a building with cool walls (albedo of 0.60) versus a conventional wall (albedo of 0.25) is around 0.2 to 0.5 °C in most cases. Smaller IAT and MRT reductions occur during the day and larger IAT and MRT reductions occur at night. Since thermal sensation in buildings without air conditioning is generally cold at night and warm during the day this corresponds to a slight worsening of thermal comfort at night and an improvement of thermal comfort during the day. But since homes without cooling are more common than homes without heating, in practice the comfort worsening from cool walls during nighttime would not materialize and cool walls would then only improve the thermal comfort during the day.

1 Introduction and scope

High albedo (“cool”) walls are exterior building walls with surface (usually paint) properties that increase reflection of solar radiation. Albedo is the fraction of incident sunlight reflected, or “solar reflectance”, of a material. Raising a wall’s albedo decreases its solar heat gain, which can reduce heat conducted inward through the wall on a hot day, or increase heat conducted outward on a cold day. Cool wall effects on the outdoor thermal environment of pedestrians

were examined in the Task 3.1 report: *Pedestrian mean radiant temperature and thermal comfort*. The current study examines cool wall effects on the indoor thermal environment.

The human temperature sensation is approximated through thermal comfort models. Thermal comfort depends on clothing and activity as well as environmental factors including mean radiant temperature (MRT), air temperature, and humidity. Mean radiant temperature (MRT) is defined as the uniform surface temperature of an imaginary enclosure in which the human body will exchange the same amount of radiant heat energy as in the actual non-uniform enclosure (ASHRAE Standard 55, 2010). For details on MRT see the Task 3.1 report: *Pedestrian mean radiant temperature and thermal comfort*.

In air-conditioned buildings the effect of cool walls on the indoor thermal environment is minimal as the heating, ventilation, and air conditioning (HVAC) plant removes or adds heat as needed to maintain the air temperature within the chosen setpoints. Cool walls primarily affect the indoor thermal environment through the indoor MRT (hereafter, simply "MRT"), which in turn depends on the interior wall temperature. Since wall heat storage dampens the amplitude of the interior wall temperature fluctuations compared to the exterior wall temperature fluctuations, the effect of cool walls on the MRT is small.

In buildings without air conditioning, cool walls are expected to affect the interior thermal environment more significantly. Cool walls reduce the absorption of sunlight which reduces the exterior wall temperature and the heat flux into the building. In the cooling season cool walls are expected to lead to a more comfortable (cooler) interior thermal environment, while in the heating season cool walls are expected to lead to a less comfortable (cooler) interior thermal environment.

The building outdoor and indoor thermal environment are simulated using a building-to-canopy model called TUF-IOBES (Temperature of Urban Facets – Indoor Outdoor Building Energy Simulator). TUF-IOBES simulates heat transfer in a small neighborhood of identical buildings to obtain indoor and outdoor air temperatures; interior and exterior temperatures of walls and ceiling; and radiative, convective, and conductive heat fluxes. To understand thermal impacts of cool walls on building occupants, calculations are performed for a sitting person. Calculations are performed hourly for a typical meteorological year (TMY) for a multi-family residence in CZ8 (Fullerton).

This report is structured as follows. Section 2 contains the methodology for the indoor air temperature, MRT, and thermal comfort calculation. Results are presented in Section 3 separately for MRT, indoor air temperature, and thermal comfort. Section 4 includes a discussion and concludes the report.

2 Indoor thermal environment and thermal comfort calculation

2.1 Urban and building configuration

TUF-IOBES simulates heat transfer for a 5 × 5 array of identical multi-family buildings with dimensions 27.2 by 27.2 m by 7.8 m and inter-building spacing of 31.1 m (Figure 1). Intermediate building floors and internal mass are not considered in TUF-IOBES. That is, the buildings are empty and do not store heat in the interior space. Building occupants are exposed to thermal radiation from the inside surface of exterior walls, roofs, and floor. Thermal comfort parameters are compared between simulations with wall albedo of 0.25 and wall albedo of 0.60.

The lack of internal walls and heat storage affects reductions in MRT and IAT. To simplify the discussion we define $\Delta T_{\mathrm{air}} = T_{\mathrm{air}}^{\mathrm{C25N25}} - T_{\mathrm{air}}^{\mathrm{C60N60}}$ (and a similar argument holds for ΔMRT). Lack of internal heat storage results in smaller reductions in IAT and MRT during the day when raising wall albedo, but larger reductions at night (larger ΔT_{air}). During the day, internal heat storage would result in some of the additional heat conducted through conventional walls to be stored in internal mass, rather than heating the room air, decreasing ΔT_{air}. At night, the additional stored heat in buildings with conventional walls would be convected back to the (now colder) room air, increasing ΔT_{air}. Internal walls also reduce ΔMRT, as some of the view factor from the human towards exterior walls would be replaced by view factor towards the internal wall. Since temperature differences of internal walls between C25N25 and C60N60 are smaller than temperature differences of external walls between C25N25 and C60N60 adding internal walls would reduce ΔMRT.

The lack of internal mass causes the IAT reduction curves to strongly resemble the MRT reduction curves. Since the only mass inside the building is that of the air, IAT will tend to closely follow the average wall temperature.

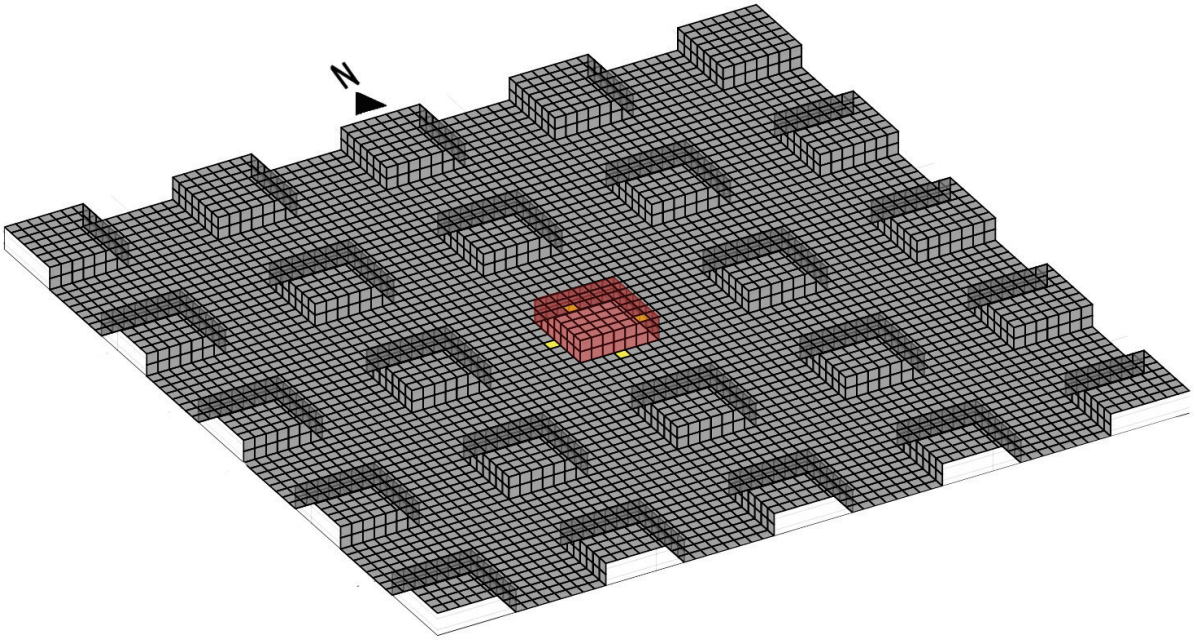

Figure 1. Calculation domain with a 5 × 5 array of multi-family residences. Results in this report refer to the central building unit highlighted in red.

Finally, while the simulations cover a building that is neither heated nor cooled, in practice buildings that are not cooled, but heated are more common. According to the 2015 Residential Energy Consumption Survey (RECS) (EIA 2015), 85% of homes in the Pacific census division (CA, OR, WA, AK, HI) use space heating (RECS Table HC6.8), while only 66% of these homes use space cooling (RECS Table HC7.8).

2.2 Air temperature

The interior air temperature (IAT) is calculated through a heat transfer model that considers heat conduction through the wall, roof, and floor; conduction and solar transmission through windows; interior heat sources, including lighting, equipment, and people; and longwave and shortwave radiative exchange between interior surfaces. The TUF-IOBES model simulates each building as a single room. Details of TUF-IOBES can be found in the Task 2.2 report: *Effect of neighboring cool walls on HVAC loads.*

2.3 Mean radiant temperature

The view factor from a person to a surface is the fraction of radiation leaving the person that strikes the surface. Since empty buildings are simulated, the human was exposed to thermal radiation from the ceiling (immediately below the roof), the insides surfaces of exterior walls, and the floor. Radiation from daylight transmitted through windows and artificial lighting is neglected in the calculation of MRT of the building occupant, but radiation from daylight transmitted through windows and artificial lighting does influence the interior surface

temperatures. The ASHRAE handbook prescribes the following equation to determine MRT from plane radiant temperature (PRT) in different directions relative to the sitting person. The equation assumes view factors from the human to the internal building surfaces that are typical and do not necessarily correspond to the simulated building dimensions.

$$\mathrm{MRT} = \frac{0.18\left(\mathrm{PRT}^{\mathrm{up}} + \mathrm{PRT}^{\mathrm{down}}\right) + 0.22\left(\mathrm{PRT}^{\mathrm{right}} + \mathrm{PRT}^{\mathrm{left}}\right) + 0.30\left(\mathrm{PRT}^{\mathrm{front}} + \mathrm{PRT}^{\mathrm{back}}\right)}{2(0.18 + 0.22 + 0.30)}$$

2.4 Thermal comfort

The ASHRAE comfort model based on Fanger's theory (Fanger, 1970) is used to compute thermal comfort considering IAT, humidity, metabolic activity, and clothing. Human comfort models attempt to emulate the typical human perception of environmental conditions through thermal comfort indices. Thermal comfort is expressed as "Predicted Mean Vote" (PMV) and "Percentage of People Dissatisfied" (PPD). PMV can take on values of -3 (cold), -2 (cool), -1 (slightly cool), 0 (neutral), 1 (slightly warm), 2 (warm), and 3 (hot). PPD ranges from 0% to 100%.

An example of the "neutral" comfort zone is given in Figure 2. To interpret this figure, note that

- 1 Clo (0.155 m²·K/W) is the thermal resistance of clothing (e.g., a business suit) needed to maintain a person in comfort sitting at rest in a room at 21°C (70 °F) with humidity less than 50%;
- 1 met (58.2 W of heat per m² of body surface area) is the heat generation by an average person seated at rest;
- operative temperature is a measure of human thermal comfort; and
- since air speed in buildings is small, operative temperature can be assumed to equal the average of indoor air temperature and indoor mean radiant temperature (ASHRAE 2009).

We assume that the person generates 1 met year-round; wears trousers and a T-shirt in summer, providing 0.57 Clo = 0.088 m²·K/W; and wears trousers and a long-sleeve shirt the rest of the year, providing 0.61 Clo = 0.095 m²·K/W.

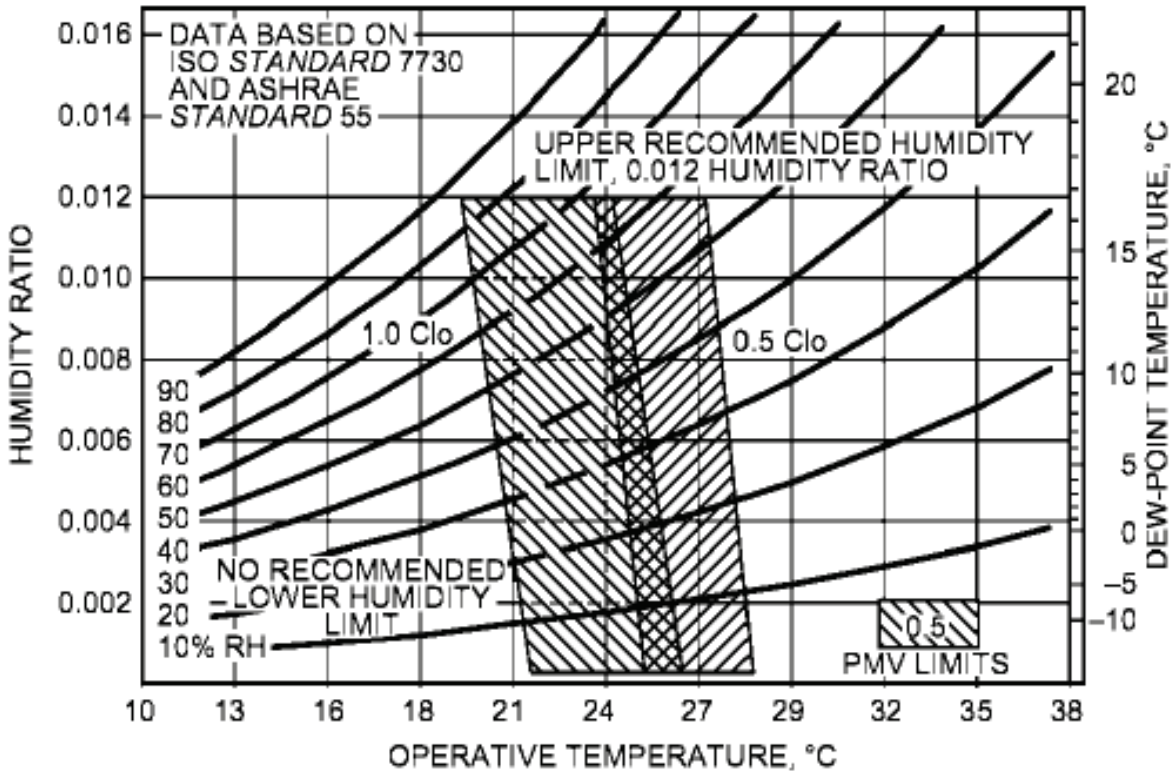

Figure 2. ASHRAE Comfort Zones: Acceptable ranges of operative temperature and humidity with air speed less than 0.2 m/s for people wearing 1.0 and 0.5 Clo clothing during primarily sedentary activity (< 1.1 met metabolic rate). Source: ASHRAE (2009).

3 Results

3.1 Interior Air Temperature (IAT)

IAT for wall albedos of 0.25 and 0.60 are compared for the multi-family residence in Fullerton, CA (California building climate zone [BCZ] 8) for the year (Figure 3) and by season (Figure 4). IATs peak around 15:00 – 16:00 local standard time (LST). The reduction in IAT with cool walls is between 0.2 °C midday and 0.5 °C at night. IATs follow the expected seasonal cycle. The reduction in IAT with cool walls is consistent across the seasons. While four-wall average solar irradiation in summer is 35% larger than in winter, the increase in four-wall solar irradiation transmitted through windows when changing wall albedo to 0.60 from 0.25 is only 0.04 kWh m^{-2} day^{-1} in summer and 0.03 kWh m^{-2} day^{-1} in winter. Cool walls raise window transmitted solar radiation only by 4% compared to conventional walls. The small effect of wall albedo on transmitted solar radiation is due to small wall-to-wall view factors.

Compared to a conventional wall, during daytime cool walls absorb a smaller fraction of incident solar radiation. This lowers the temperature of the wall's outer surface, reducing heat

flux through the wall and the air temperature in the occupied space. The daytime decrease in heat storage in cool walls causes lower wall temperatures and IAT to persist through the night.

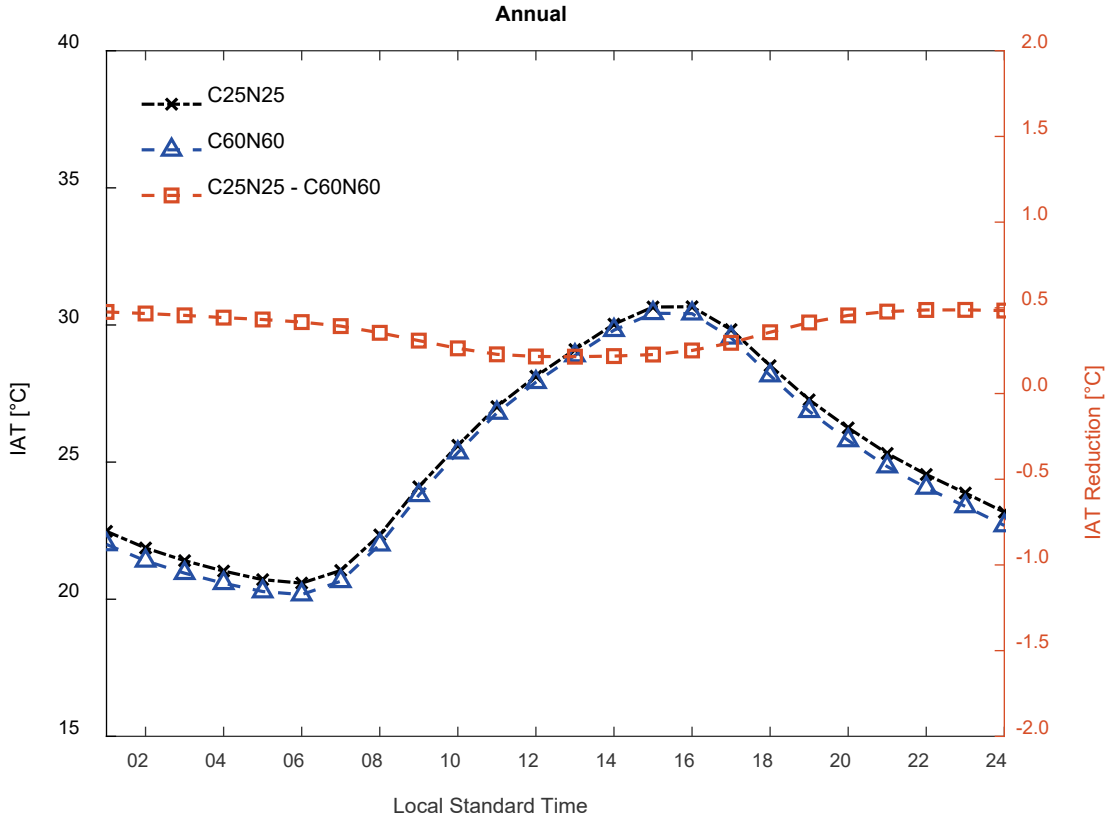

Figure 3. Average (over the year) daily cycle of interior air temperatures (IATs) for the multi-family residence in Fullerton (BCZ 8) with wall albedos equal to 0.25 (conventional wall, denoted as C25N25) and 0.60 (cool wall, denoted as C60N60). The right axis shows the IAT reduction due to cool walls.

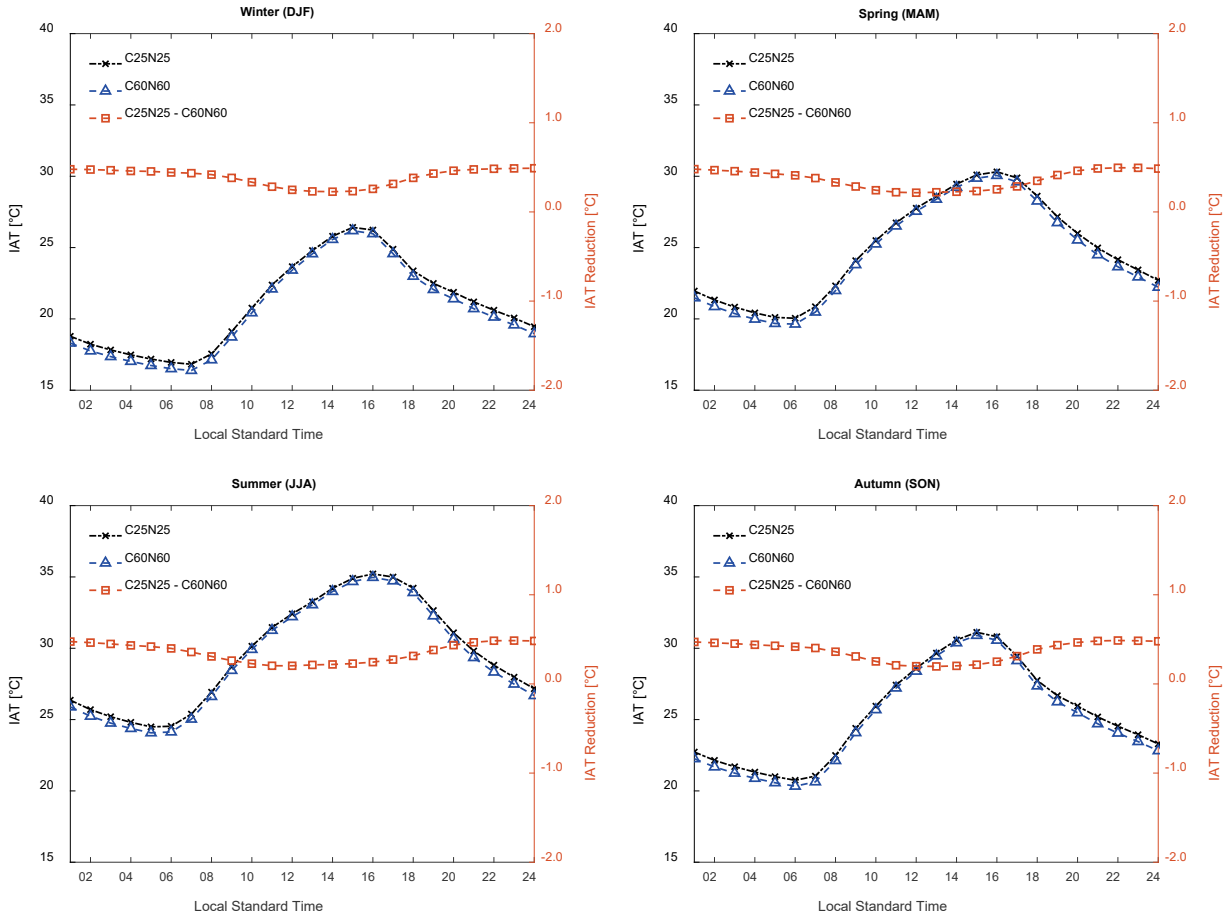

Figure 4. Seasonal analogs of Figure 3 (winter = Dec/Jan/Feb, spring = Mar/Apr/May, summer = Jun/Jul/Aug, and autumn = Sep/Oct/Nov).

3.2 Mean Radiant Temperature (MRT)

Figure 5 shows the annual average interior MRT and average rise in MRT upon switching to a cool wall (albedo 0.60) from a conventional wall (albedo 0.25). Seasonal results are presented in Figure 6. Increasing wall albedo reduces daytime MRT for the same reasons as wall albedo reduced IAT.

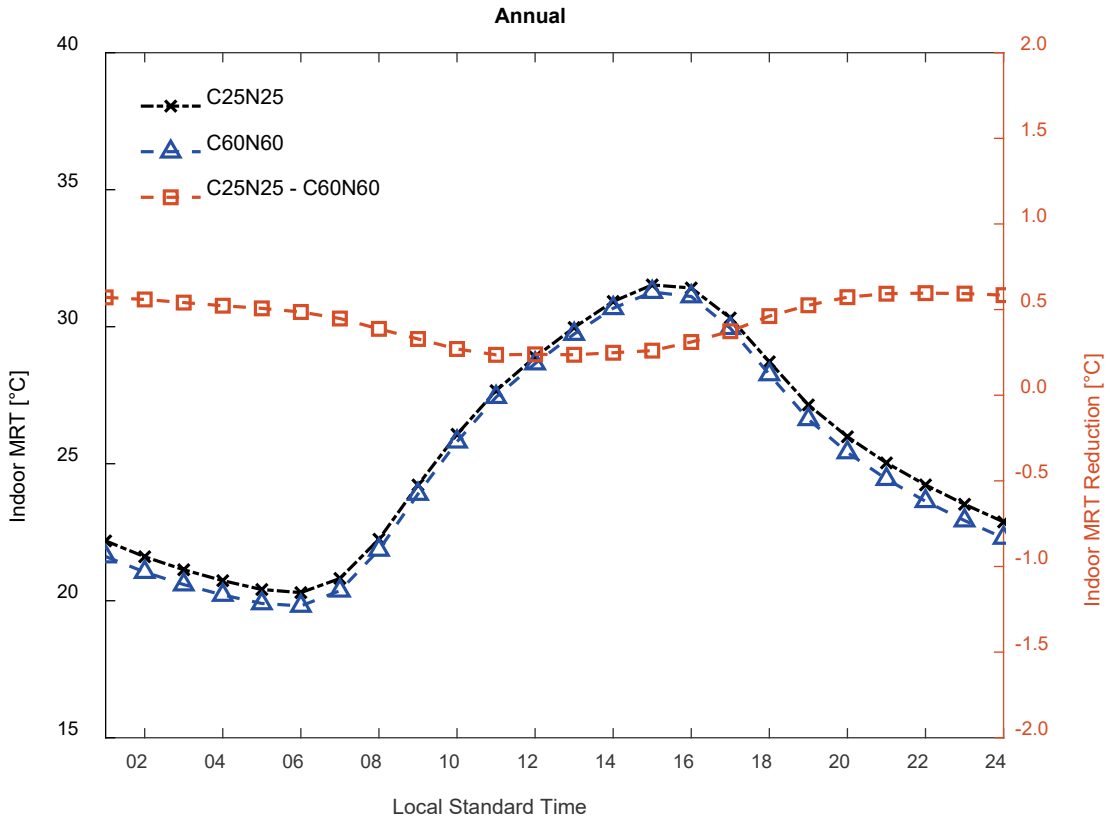

Figure 5. Average (over the year) daily cycle of mean radiant temperatures (MRTs) for the multi-family residence in Fullerton, CA (BCZ 8) with wall albedos equal to 0.25 (conventional wall denoted as C25N25) and 0.60 (cool wall denoted as C60N60). The right axis shows the MRT reduction due to raising wall albedo.

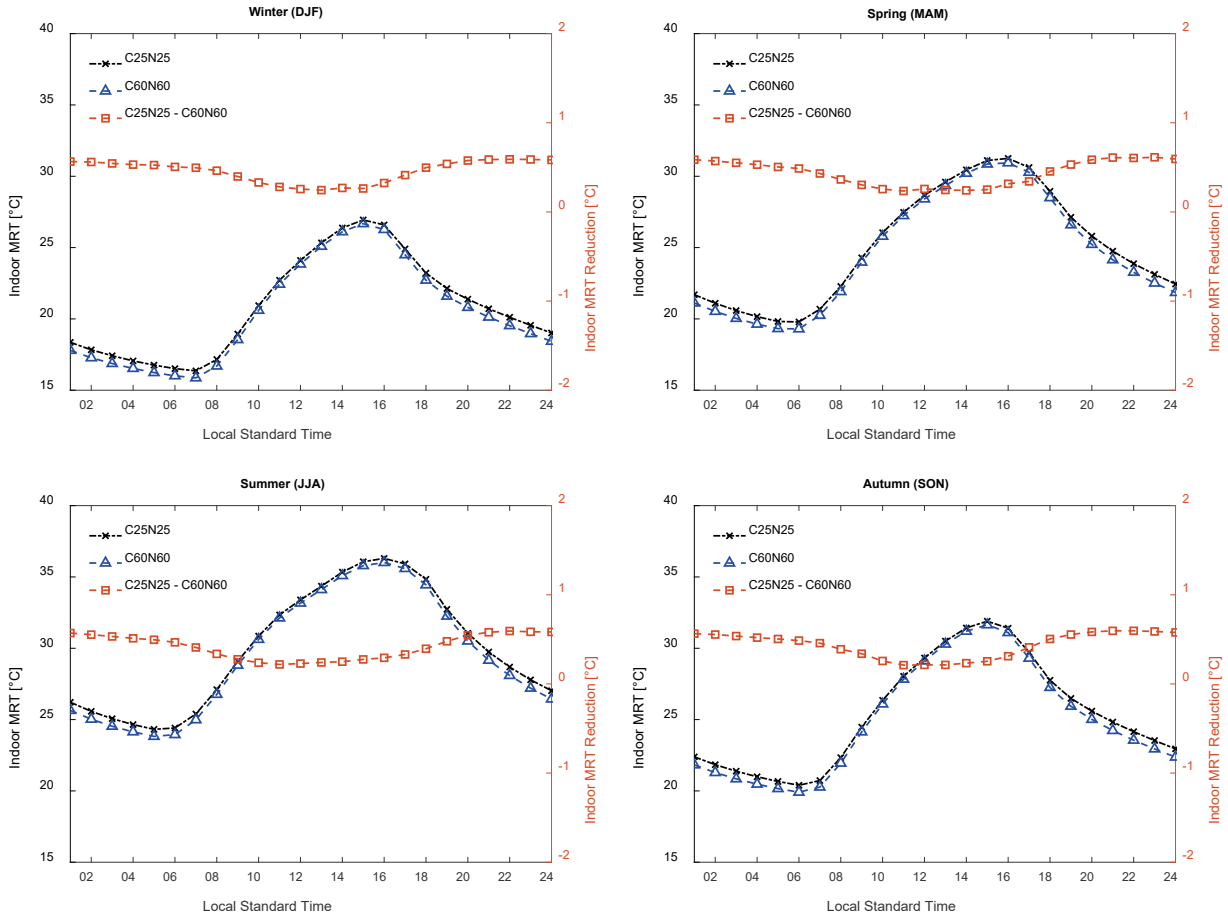

Figure 6. Seasonal analogs of (winter = Dec/Jan/Feb, spring = Mar/Apr/May, summer = Jun/Jul/Aug, and autumn = Sep/Oct/Nov).

3.3 Thermal comfort

The thermal comfort trends during the day follow the MRT and IAT trends. Since daylight and artificial light are neglected in the thermal comfort calculation, the exposition focuses on changes in thermal comfort when raising wall albedo. Figure 7 shows PMV averaged over the year. On average, the building occupant tends to be slightly cool to cool during the night and slightly warm to warm during the day. The diurnal comfort trends are expected to remain valid if daylight and artificial light were considered, because (a) daylight would further warm the occupant in daytime and (b) at night, artificial lighting impacts would be small and not reverse the cool sensation. Increasing wall albedo reduces PMV by 0.07 during midday and up to 0.17 at night. Figure 8 shows the results by season which exhibit similar trends as those for the year.

Figure 9 shows PPD averaged over the year. Figure 10 shows the results by season which exhibit similar trends as those for the entire year.

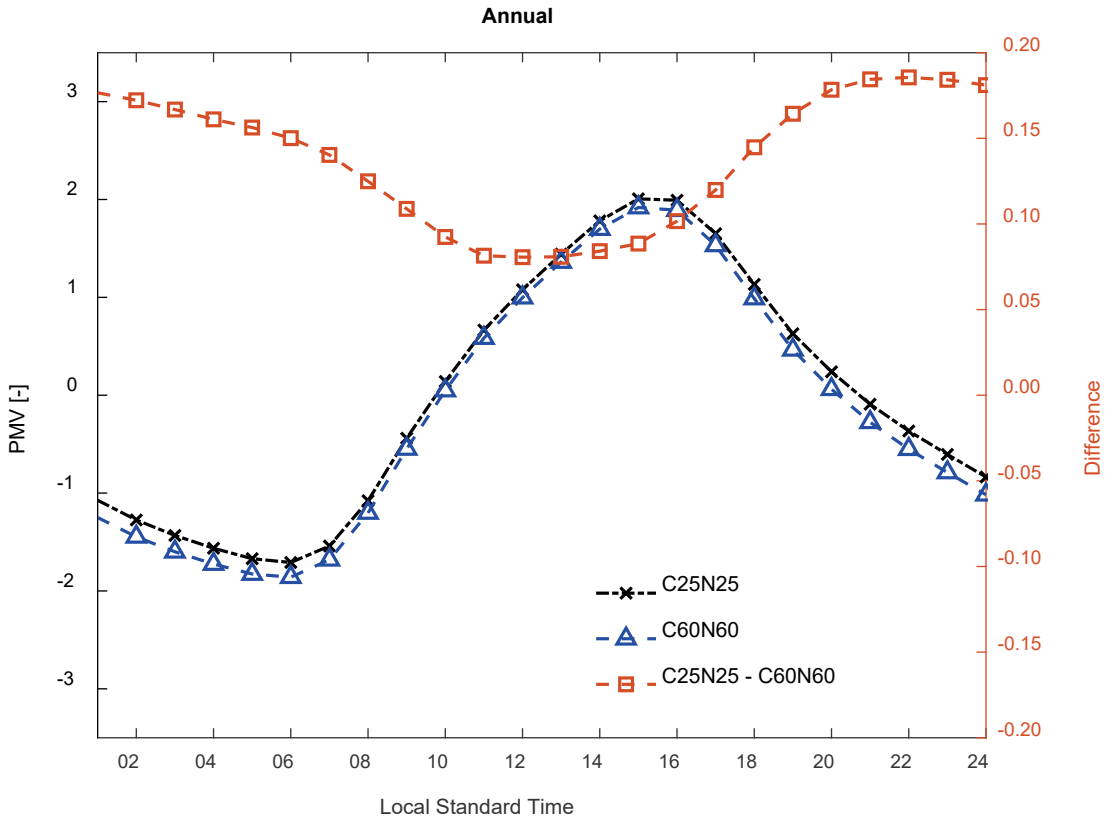

Figure 7. Average (over the year) daily cycle of predicted mean vote (PMV) for the multi-family residence in Fullerton, CA (BCZ8) with wall albedos equal to 0.25 (conventional wall denoted as C25N25) and 0.60 (cool wall denoted as C60N60). The right axis shows the PMV reduction due to raising wall albedo.

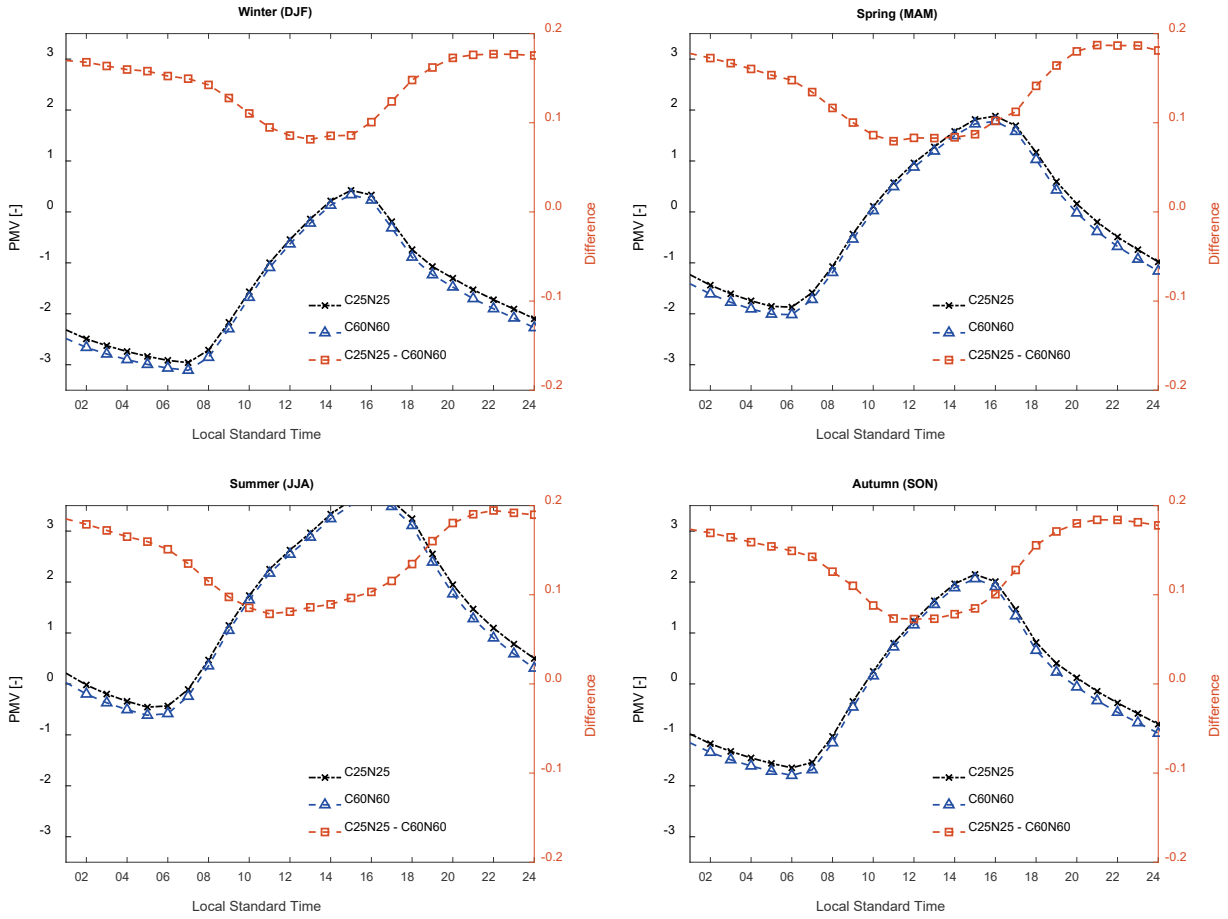

Figure 8. Seasonal analogs of Figure 7 (winter = Dec/Jan/Feb, spring = Mar/Apr/May, summer = Jun/Jul/Aug, and autumn = Sep/Oct/Nov).

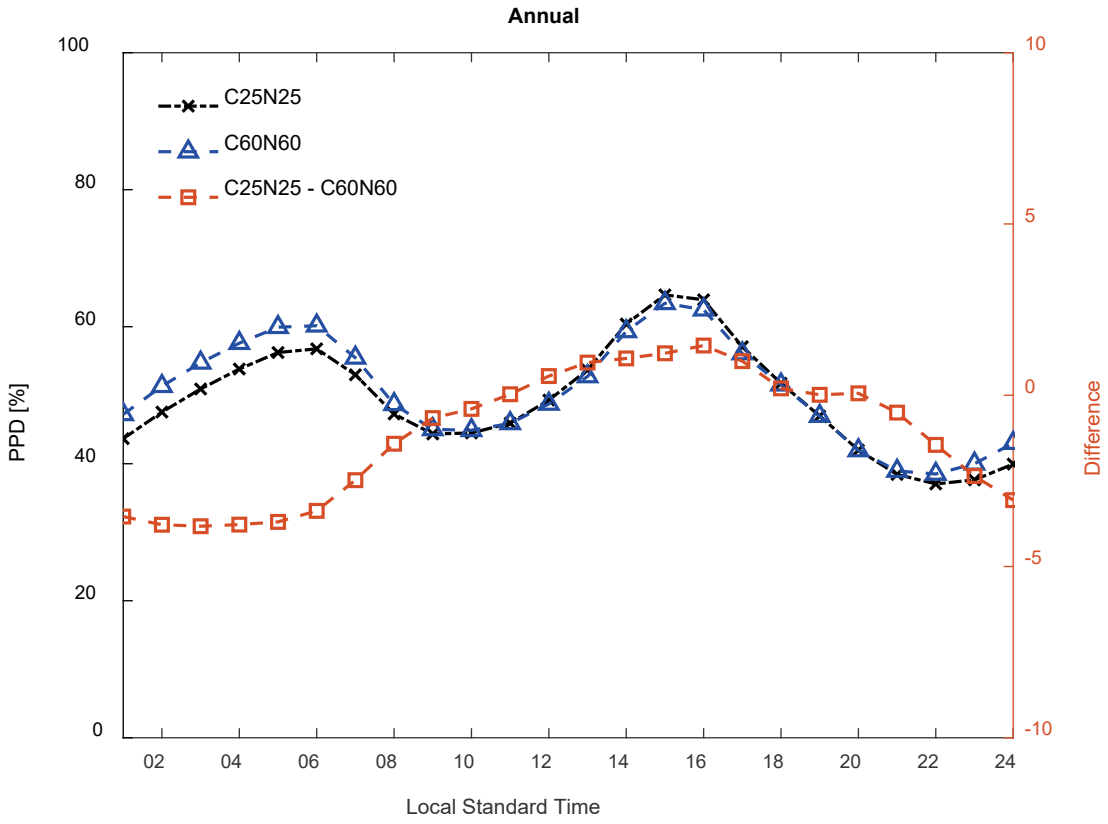

Figure 9. Average (over the year) daily cycle of percentage of persons dissatisfied (PPD) for the multi-family residence in Fullerton (CZ8) with wall albedos equal to 0.25 (conventional wall denoted as C25N25) and 0.60 (cool wall denoted as C60N60). The right axis shows the PPD reduction due to raising wall albedo.

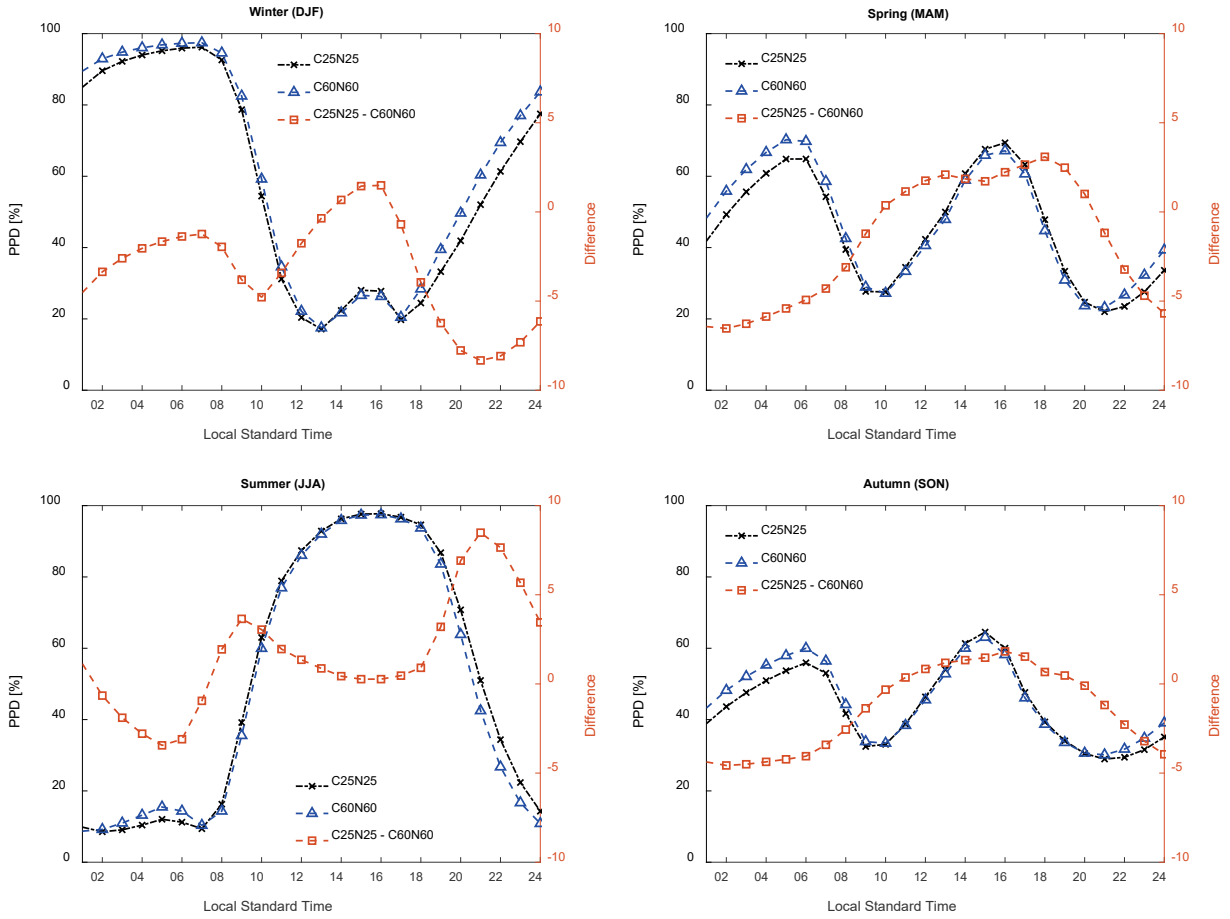

Figure 10. Seasonal analogs of Figure 9 (winter = Dec/Jan/Feb, spring = Mar/Apr/May, summer = Jun/Jul/Aug, and autumn = Sep/Oct/Nov).

4 Discussion and conclusions

Interior air temperature (IAT), mean radiant temperature (MRT) and thermal comfort were analyzed for homogeneous neighborhoods of multi-family residences with cool walls. Typical meteorological year weather data is input to a neighborhood heat transfer model (TUF-IOBES) in a coastal California climate zone to understand impacts on an occupant of a building with neither heating nor air conditioning. The typical IAT and MRT reduction inside a building with cool walls (albedo of 0.60) versus a conventional wall (albedo of 0.25) is around 0.2 to 0.5 ˚C in most cases. Smaller IAT and MRT reductions occur during the day and larger IAT and MRT reductions occur at night. The lack of internal building heat storage enhances this diurnal trend by causing smaller reductions in IAT and MRT during the day, but larger reductions at night.

Since thermal sensation in buildings without air conditioning is generally slightly cold to cold at night and slightly warm to warm during the day this corresponds to a slight worsening of

thermal comfort at night and an improvement of thermal comfort during the day. But since homes without cooling are more common than homes without heating, in practice the PPD increase from cool walls during nighttime would not materialize and cool walls would then only decrease the PPD during the day.

The variable hourly trends in the PPD reduction curves in Figure 9 are a result of the fact that PPD increases for both a too-hot and a too-cold thermal environment. Raising albedo results in a cooler building day and night. During the night, the thermal sensation of an occupant is predominantly cold. Therefore, raising wall albedo increases PPD at night. During the afternoon, the occupant thermal sensation is predominantly warm. Raising wall albedo then decreases PPD. For the rest of the day (morning and evening) too warm or too cold sensations are about equally present. Raising wall albedo increases PPD on cool days while decreasing PPD on warm days, but averaged over the year the PPD remains the same.

References

ASHRAE. 2009. *2009 Handbook: Fundamentals*. Chapter 9: Thermal Comfort. American Society of Heating, Refrigeration, and Air-Conditioning Engineers, Atlanta, GA.

EIA. 2015. 2015 Residential Energy Consumption Survey (RECS). Energy Information Administration. Retrieved 2018-01-03 from https://www.eia.gov/consumption/residential/data/2015/.

Fanger PO. 1970. *Thermal Comfort: Analysis and Applications in Environmental Engineering*. New York: McGraw Hill.

Energy Research and Development Division

FINAL PROJECT REPORT

Solar-Reflective "Cool" Walls: Benefits, Technologies, and Implementation

Appendix H: Effects of Self-cleaning Walls on Urban Air Quality (Task 3.5 Report)

California Energy Commission
Gavin Newsom, Governor

April 2019 | CEC-500-2019-040-APH

Appendix H: Effects of self-cleaning walls on urban air quality (Task 3.5 report)

Jiachen Zhang[1], Yun Li[1], Hugo Destaillats[2], Xiaochen Tang[2], Ronnen Levinson[2], and George Ban-Weiss[1]

[1] Department of Civil and Environmental Engineering, University of Southern California, Los Angeles, CA, USA

[2] Lawrence Berkeley National Laboratory, Berkeley, CA, USA

28 February 2018

Abstract

We analyze total NO_x deposition in Los Angeles County assuming a hypothetical scenario where all walls are painted with photocatalytic cool paints. We use laboratory-measured dry deposition velocities for NO_x (0.2-0.5 cm s^{-1}), and wall-to-urban land area ratios derived from a real-world building dataset. Total expected deposition is compared to recent (2012) emissions of NO_x in urban Los Angeles County to assess the magnitude of predicted deposition increases.

Daytime (05:00 LST–19:00 LST) total NO_x deposition and emissions are 6.6×10^3–1.6×10^4 mol day^{-1} and 3.3×10^6 mol day^{-1}, respectively. Therefore, daytime NO_x deposition is 0.2-0.5% of NO_x emissions in July in Los Angeles County. Thus, adopting photocatalytic cool walls is expected to have small impacts on regional air quality in Los Angeles. Note that this analysis estimates city-level NO_x deposition, and does not consider whether photocatalytic self-cleaning walls may have larger air quality benefits for near-source concentrations in urban canyons (i.e., the space between buildings and above streets). We suggest future work to estimate the impact of photocatalytic walls on near-source NO_x concentrations.

1 Introduction

Photocatalytic self-cleaning cool wall products are designed to maintain high albedos in polluted environments. Use of photoactive titanium dioxide (TiO_2) pigments in surface coatings or paints enable soiling to be oxidized under sunlight and then washed away. A possible co-benefit of these photocatalytic coatings and paints is that they can remove NO_x from ambient air, and potentially influence ambient gas- and particle-phase pollutant concentrations.

Land et al. (2009) carried out experiments to measure the deposition of NO_x onto TiO_2-impregnated surfaces. Using their upper bound measured deposition velocities and assuming that all urban surfaces in the area were impregnated with photoactive TiO_2, NO_x deposition was calculated as ~1% of total NO_x emissions in Fulton County, Georgia. Note that their estimate did not take into consideration the real-world wall area in the region.

Here we present an analysis to quantify the total NO_x deposition in Los Angeles County assuming a hypothetical scenario where all walls are painted with photocatalytic cool paints. We conduct laboratory experiments to measure dry deposition velocities of NO_x and derive wall-to-urban land area ratios from a real-world building dataset. Finally, our computed total NO_x deposition in urban Los Angeles County is compared to recent emissions (i.e., for 2012) to assess the magnitude of predicted deposition increases.

2 Methods

2.1 Measuring NO_x deposition velocities to photocatalytic surfaces in the laboratory

We conducted experiments that tested the NO_x removal abilities of two photocatalytic cool wall products, as detailed in Task Report 4.3. Measured values of the NO_x deposition velocities onto photocatalytic wall materials ranged between 0.02 to 0.05 cm s^{-1}.

2.2 Analysis approach

For a first order approximation, we assume that the deposition velocity onto cool walls is constant throughout the daytime, suggesting that the flux of UV photons is not the rate limiting factor. While this is likely not true, our goal is to quantify upper bound estimates of NO_x deposition to compare with total NO_x emissions in Los Angeles County.

The hourly averaged NO_x deposition (mol hr^{-1}) D_{NO_X} in the urban areas of Los Angeles County, induced by adopting photocatalytic walls, is computed as

$$D_{NO_X} = C_{NO_X} \times V_{NO_X} \times A_{Wall} \times k \quad (1)$$

where C_{NO_X} is NO_x concentration (ppbv) (see Section 2.3.4), V_{NO_X} is the NO_x deposition velocity onto photocatalytic walls (cm s^{-1}) derived using laboratory experiments (see Section 2.1), A_{Wall} is total wall area (m^2) in Los Angeles County (see Section 2.3.2), and k is a unit conversion factor (i.e., 1.5×10^{-6} $\frac{\text{mol s}}{\text{ppbv cm m}^2\text{ hr}}$) assuming atmospheric pressure is 1.01×10^5 Pa and temperature is 298.15 K.

E_{NO_X}, the hourly averaged NO_x emissions (mol hr^{-1}) from urban areas in Los Angeles County, is computed as,

$$E_{NO_X} = F_{NO_X} \times A_{Land} \quad (2)$$

where F_{NO_X} is the emission flux (mol m^{-2} hr^{-1}) (see Section 2.3.3) and A_{Land} is total land area (m^2) in Los Angeles County (see Section 2.3.1).

2.3 Datasets used for analysis

2.3.1 Urban land area

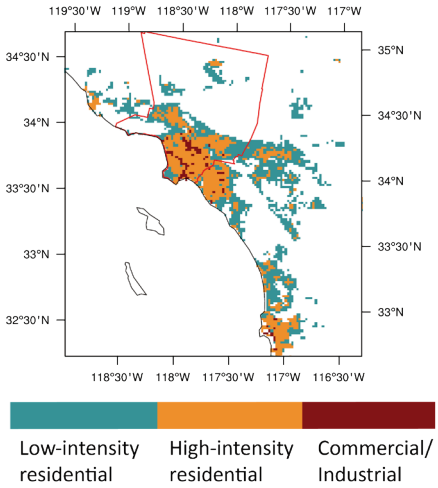

Figure 1. Map of dominant urban land use types, as defined by National Land Cover Database (NLCD). Los Angeles County is bounded by red outline.

The entire Los Angeles County (excluding Santa Catalina Island and Terminal Island) is divided into 2,650 grid cells of 2×2 km^2, where 803 grid cells are classified as urban. Figure 1 shows the land use types for urban grid cells based on National Land Cover Database (NLCD) classification. Low-intensity residential, high-intensity residential, and commercial/industrial land use types are assumed to have different urban morphological properties (e.g., roof to land area ratio and wall to land area ratio).

2.3.2 Wall to urban land area ratio

For each urban land use type, the ratio of wall area to urban land area is derived from a real-world dataset for Los Angeles County, LARIAC (2016). This dataset provides information for every building in Los Angeles County, including ZIP Code, roof area, building height, and building shape. See more details on this dataset and procedures in Section 2.3 of the Task 3.2 report: *Urban climate impacts of cool walls* (Appendix E).

2.3.3 Emission inventories

We use state-of-the-science emission inventories for 2012 from the South Coast Air Quality Management District (SCAQMD). SCAQMD provides hourly emissions for the entire year at 4-km resolution. These emissions represent all anthropogenic sources including motor vehicles, point sources such as refineries, and off-road sources. Biogenic and biomass burning emissions are not considered. The emissions data are re-gridded to 2-km resolution to match the land use classification dataset.

2.3.4 Observed NO_x concentrations

We attain NO_x concentrations for 13 monitoring stations in Los Angeles County from the Air Quality System (AQS). AQS data are collected from local, state, and federal air quality control agencies.

2.4 Caveats

The laboratory experiments reported in Task report 4.3 use a UV-A (i.e., wavelength ranging between 315-400 nm) irradiance of 11.5 W m^{-2}. In the real atmosphere, the UV intensity may differ from this laboratory UV irradiance and varies by time of day. UV irradiance may affect both hourly variation and the overall magnitude of NO_x deposition velocity. In particular, our calculations may overestimate NO_x removal during early morning and late afternoon, when UV intensity is low. For this reason, the deposition values reported here can be considered upper bounds estimates. Also note that laboratory experiments were carried out at NO_x concentrations of 300 – 1000 ppb, which is higher than typical ambient NO_x concentrations.

3 Results and discussion

3.1 The diurnal cycle NO_x concentrations

Figure 2 shows the diurnal cycle of observed NO_x concentrations. NO_x reaches its daily maximum of 26 ppbv at 06:00 LST. This can be attributed to (1) morning traffic that emits NO_x, and (2) the relatively low atmospheric boundary layer heights for early morning hours. Lower atmospheric boundary layer heights reduce the volume of air where pollutants disperse, and therefore lead to higher pollutant concentrations per emissions.

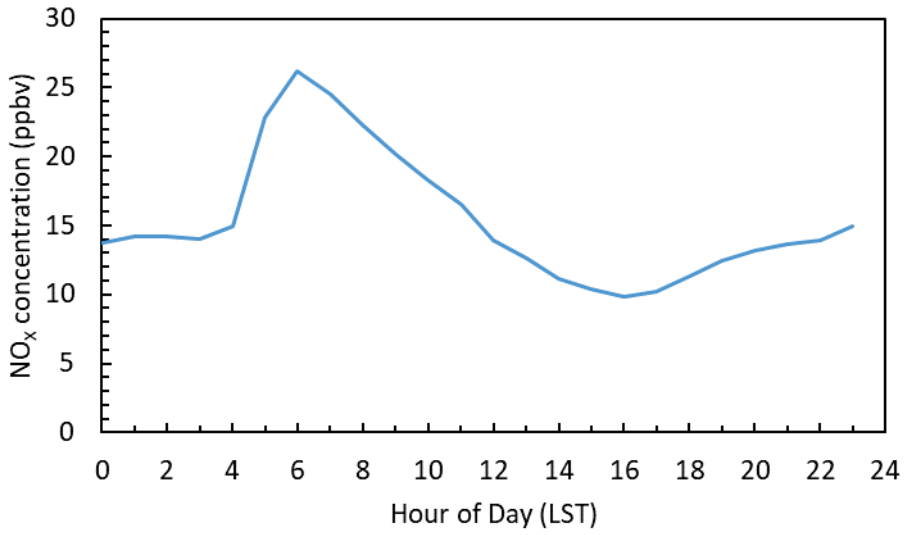

Figure 2. Diurnal cycle of observed NO_x concentrations averaged among 13 AQS sites in Los Angeles County. Each hour of day marks beginning of an hour. Values are averaged for July, 2012.

3.2 Total urban land area and wall area

Table 1 shows the urban land area and wall area for each urban land use type and other data used to compute these areas. Ratio of roof area to urban land area ($f_{R\ to\ L}$) is calculated from LARIAC (2016). Ratio of wall area (excluding windows) to roof area ($f_{W\ to\ R}$) is determined from LARIAC (2016) that provides ratio of gross wall area to roof area (detailed in Task 3.2 report) and Table 5.1 in Rosado (2016) that provides the ratio of window to wall area. Specifically, the ratio for the single-family home prototype (14.1%) is assigned to the low-intensity residential and high-intensity residential land use types, while that for retail stand-alone (7.1%) is assigned to commercial/industrial. Ratio of wall area to urban land area ($f_{W\ to\ L}$) is then calculated as $f_{R\ to\ L} \times f_{W\ to\ R}$. Total urban land area is calculated as the number of grid cells multiplied by 4 km^2. Multiplying total urban land area by $f_{W\ to\ L}$, we attain total wall area for each land use type. Total urban land area and wall area in Los Angeles County are 3,212 km^2 and 895 km^2, respectively.

Table 1. Ratios of roof to urban land area, wall to roof area, wall to urban land area, numbers of grid cells, as well as total urban area and wall area for the three NLCD urban land use types (Figure 1) in urban Los Angeles county.

Land use type	Ratio of roof area to urban land area ($f_{R\ to\ L}$)	Ratio of wall area (excluding windows) to roof area ($f_{W\ to\ R}$)	Ratio of wall area (excluding windows) to urban land area ($f_{W\ to\ L}$)	Number of grid cells	Total urban land area (km^2)	Total wall area (km^2)
Low-intensity residential	0.13	1.68	0.21	379	1,516	318
High-intensity residential	0.19	1.68	0.33	371	1,484	484
Commercial and industrial	0.23	1.95	0.44	53	212	93

3.3 NO_x deposition in July

Figure 3a shows the diurnal cycle of NO_x deposition in July. Based on the lower bound of measured NO_x dry deposition velocity (0.02 cm s^{-1}), NO_x deposition ranges from 267 – 709 mol hr^{-1}, depending on time of day. Based on the upper bound of NO_x dry deposition velocity (0.05 cm s^{-1}), NO_x deposition ranges from 668 – 1,770 mol hr^{-1}. The diurnal variability for estimated NO_x deposition follows that for ambient NO_x concentrations (see Figure 2 and Eq. 1).

(a)

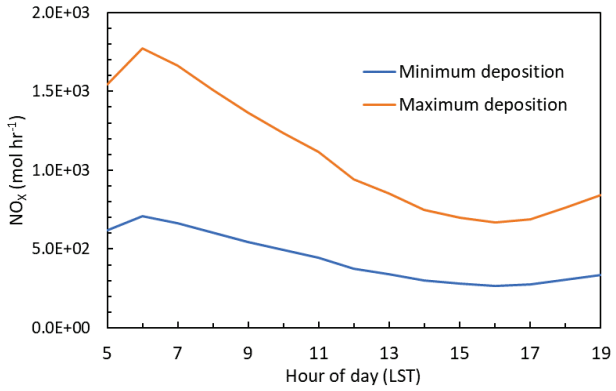

(b)

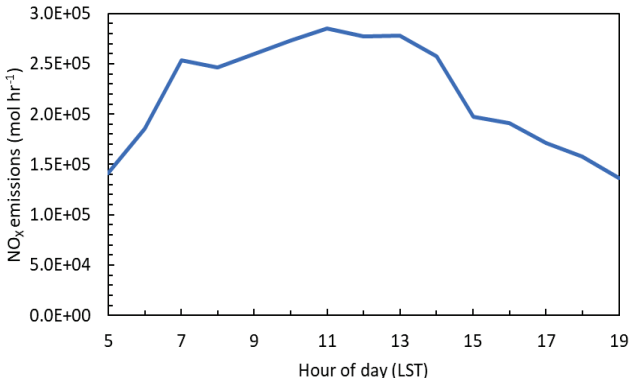

(c)

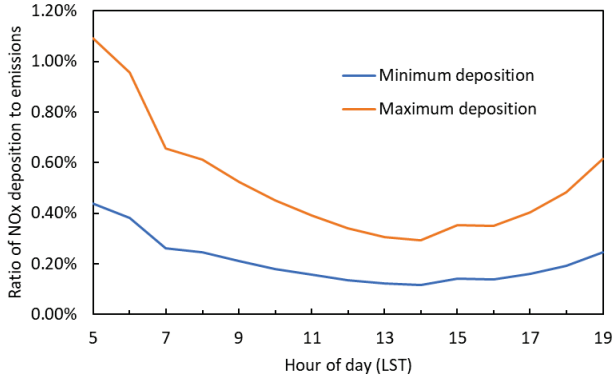

Figure 3. Diurnal cycles for urban Los Angeles County of (a) NO_x deposition (mol hr^{-1}); (b) NO_x emissions (mol hr^{-1}); and (c) the ratio of NO_x deposition to emissions. Values are averaged for July, 2012. Panels (a) and (c) show upper and lower bound estimates based on variations in measured dry deposition velocities (Section 2.1).

3.4 NO_x emissions in July

Figure 3b shows the hourly NO_x emissions during daytime averaged in July. NO_x emissions reach a maximum at 11:00 LST. NO_x emissions are in the range of $(1.3–2.8) \times 10^5$ mol hr^{-1}. The emissions start to increase with the morning traffic and peak around noon. The diurnal cycle of NO_x emissions is driven by the diurnal variations of on-road and off-road mobile sources and stationary sources (South Coast Air Quality Management District, 2013).

3.5 Discussion

Figure 3c shows the diurnal cycle of the ratio of NO_x deposition to emissions. Even when assuming the maximum deposition velocity measured in experiments, the upper bound daily maximum NO_x deposition is less than 1.1% of NO_x emissions.

Daytime (05:00 LST–19:00 LST) total NO_x deposition and emissions are 6.6×10^3–1.6×10^4 mol day^{-1} and 3.3×10^6 mol day^{-1}, respectively. Therefore, daytime NO_x deposition is 0.2-0.5% of NO_x emissions in July in LA County. Thus, adopting photocatalytic cool walls is expected to have small impacts on regional air quality in Los Angeles

This analysis estimates city-level NO_x deposition, and does not consider whether photocatalytic self-cleaning walls may have larger air quality benefits for near-source concentrations in urban canyons (i.e., the space between buildings and above streets). We suggest future work to estimate the impact of photocatalytic walls on near-source NO_x concentrations.

4 Conclusions

Using laboratory measured NO_x dry deposition velocities and wall to urban land area ratios derived from a real-world building dataset, we evaluate the total NO_x deposition from adopting photocatalytic self-cleaning cool walls in Los Angeles County. Total daytime deposition of NO_x in urban Los Angeles County for July is found to be at most 0.5% of NO_x emissions. Therefore, adopting photocatalytic cool walls is likely to have a small influence on regional air quality in Los Angeles.

References

Land, E., Bergin, M. and Huey, G.: Photocatalytic Degradation of NO_x by TOTO's Hydrotect (TiO2 Impregnated) Surfaces, 2009.
https://www.pharosproject.net/uploads/files/sources/2734/1395334647.pdf

LARIAC: Countywide Building Outlines, 2016. https://egis3.lacounty.gov/dataportal/lariac/ (Accessed 11 July 2017)

Rosado, P. J.: Evaluating Cool Impervious Surfaces: Application to an Energy-Efficient

Residential Roof and to City Pavements, University of California, Berkeley. 2016. https://escholarship.org/uc/item/6bf80485

South Coast Air Quality Management District: Air Quality Management Plan (Modeling and Attainment Demonstrations), Appendix V, 2013, http://www.aqmd.gov/docs/default-source/clean-air-plans/air-quality-management-plans/2012-air-quality-management-plan/final-2012-aqmp-(february-2013)/appendix-v-final-2012.pdf

AQS: Air Quality System, https://aqs.epa.gov/api (Accessed 30 July 2017)

Energy Research and Development Division

FINAL PROJECT REPORT

Solar-Reflective "Cool" Walls: Benefits, Technologies, and Implementation

Appendix I: Metrics and Methods to Assess Cool Wall Performance (Task 4.1 Report)

California Energy Commission
Gavin Newsom, Governor

April 2019 | CEC-500-2019-040-API

Appendix I:
Metrics and methods to assess cool wall performance (Task 4.1 report)

Ronnen Levinson[1], Hugo Destaillats[1], Sharon Chen[1], Paul Berdahl[1], and Haley Gilbert[1]

[1] Heat Island Group, Lawrence Berkeley National Laboratory

28 February 2018

1 Introduction

The ability of a wall product to stay cool in the sun depends on its solar reflectance and thermal emittance. High solar reflectance reduces solar heat gain (absorption of sunlight), while high thermal emittance helps cool the surface through long-wave radiative exchange with its environment. Wall product performance is further described by additional surface properties including solar spectral reflectance, color, soil resistance, and hydrophilicity/hydrophobicity. This report addresses the metrics and methods needed to assess the evolution of the surface properties of a wall product over its service life.

2 Properties

Here we describe each property of interest.

2.1 Solar spectral reflectance

Solar spectral reflectance (symbol r) is the variation of reflectance (fraction of incident light reflected) with wavelength over the solar spectrum. Reflectance at each wavelength ranges from 0 to 1 (or 0 to 100 percent), and can vary with the geometry of incident sunlight. Solar spectral reflectance can be used to calculate solar (0.3 to 2.5 μm), ultraviolet (0.3 – 0.4 μm), visible (0.4 – 0.7 μm), and near-infrared (NIR, 0.7 – 2.5 μm) broadband reflectances, as well as color. Colorants (pigments and dyes) and soiling agents (soot, dust, organic matter) can be identified from their spectral reflectance signatures. Solar spectral reflectance can also be used to identify "cool colored" surfaces whose solar reflectances are boosted by high NIR reflectance.

2.2 Solar reflectance

Solar reflectance (abbreviation SR; symbol ρ) is the fraction of incident sunlight reflected by a surface. The solar reflectance of a given surface can vary with the spectrum (distribution of power by wavelength) and geometry (angular distribution) of incident sunlight. Solar reflectance ranges from 0 to 1 (or 0 to 100 percent).

2.3 Color

Color is an important aesthetic property of many building envelope surfaces. Color is often identified by coordinates in a color space, such as CIELAB or HunterLAB.

2.4 Effective solar reflectance

If a surface re-emits at longer wavelengths light absorbed at shorter wavelengths, or fluoresces, it will exhibit an effective solar reflectance (abbreviation ESR; symbol ρ_{eff}) that is the fraction of incident solar power rejected by the combination of reflection and fluorescence. Like solar reflectance, effective solar reflectance ranges from 0 to 1 (or 0 to 100 percent).

2.5 Solar retroreflectance

A retroreflective surface reflects incident light to its origin. Solar retroreflectance is the fraction of incident sunlight reflected toward the sun. High solar retroreflectance could reduce both wall solar heat gain and the fraction of *wall-reflected* sunlight incident on other surfaces in the city. That is, while about 50% of global sunlight diffusely reflected from a wall, and all beam sunlight specularly reflected from a wall, will strike neighboring wall or ground surfaces, beam sunlight ideally retroreflected from a wall will return entirely to the solar disc. Ideal solar retroreflection can also minimize glare, since any path that permits the incidence of beam sunlight must be free of observers.

We address properties needed to assess solar retroreflectance in our Task 5.3 report: *Development of retroreflective materials.*

2.6 Thermal emittance

Thermal emittance (abbreviation TE; symbol ε) is the ratio of radiant energy emitted by a surface near 300 K (about 27˚C, or 80˚F) to that emitted by a black body (perfect absorber and emitter) at the same temperature. The thermal emittance of a given surface can vary with the angle at which the emitted radiation is observed. Thermal emittance ranges from 0 to 1 (or 0 to 100%).

2.7 Initial radiative properties

Initial radiative properties are those measured before exposure.

2.8 Field-exposed aged radiative properties

Natural exposure can change the radiative properties of an exterior building envelope surface over time. “Field-exposed” aged radiative properties are measured after several years of natural exposure, following a protocol that specifies the location, geometry, and duration of the exposure.

2.9 Soiling resistance

Radiative properties of building envelope surfaces change over time due to weathering and soiling. We define as weathering all physical and chemical processes associated with material degradation due to exposure to the natural environment, driven by sunlight, thermal and humidity cycles. Soiling comprises the atmospheric deposition of debris, particulates and chemical species, as well as the growth of microbia (e.g., bacteria, fungi). Collectively, weathering and soiling contribute to material aging. In highly reflective materials, losses of performance can amount to as much as 20-30% of the initial solar reflectance (Sleiman et al. 2011). These losses can be translated to significant reductions in the energy savings achieved for a given reference building stock. For this reason, roofing materials are rated using their radiative properties measured after three years of natural exposure. A similar loss of performance can be expected for many wall products. Several technologies are currently available to prevent or reduce the amount of soiling depositing on the surface of materials. Such “soil-resistant” products are likely to contribute major building energy savings.

Absolute and/or fractional changes in radiative properties (e.g., loss of solar reflectance) upon natural exposure may be evaluated to gauge the ability of a “cool” product to stay clean and maintain its high solar reflectance. “Relative” soiling resistance can be evaluated by comparing reflectance loss to that experienced by a reference product of the same initial solar reflectance. “Absolute” soiling resistance can be assessed by comparing reflectance loss to that which would be experienced if the surface were fully covered with an opaque soil layer.

2.10 Hydrophilicity/hydrophobicity

The ability of a solid surface to attract or repel water can affect its resistance to soiling. Superhydrophobic coatings with dramatically increased water contact angles can be achieved by microtexturing features that produce the “Lotus effect” and minimize the contact of surfaces with water and soiling agents. Such limited contact facilitates subsequent mechanical removal of particles and evaporation (Schaeffer et al. 2015). Superhydrophilic coatings applied primarily to self-cleaning window glass typically comprise a thin layer of a photocatalyst (anatase TiO_2). In the presence of sunlight, the TiO_2 increases the wettability of the surface, and helps form continuous water films that facilitate runoff of soiling deposits. The photocatalytic process can also remove some of the soiling agents deposited on the surface by chemical oxidation to volatile species (Chabas et al. 2014).

3 Metrics

Here we specify the metric by which each surface property is to be evaluated.

3.1 Solar spectral reflectance

We will assess near normal-hemispherical spectral reflectance over the wavelength range 250 – 2,500 nm (0.25 – 2.5 μm) at an interval of 5 nm. This reflectance is readily measurable with a UV-VIS-NIR (a.k.a. solar) benchtop spectrometer equipped with an integrating sphere. Past experience with roofing products suggests that a wavelength interval of 5 nm should provide sufficient spectral detail.

Since the spectrum 250 – 300 nm contains almost no solar energy, it is acceptable to measure solar spectral reflectance over the more limited wavelength range 300 – 2,500 nm. However, reflectance in the 250 – 300 nm portion of the UV spectrum can occasionally provide insight into material properties, and is within the measurement range of a typical solar UV-VIS-NIR spectrometer.

3.2 Solar reflectance

We will assess air mass 1.5 (AM1.5) global-hemispherical solar reflectance under the solar conditions for a sun-facing vertical surface specified by ASTM G197-14 (Standard Table for Reference Solar Spectral Distributions: Direct and Diffuse on 20° Tilted and Vertical Surfaces) (ASTM 2014). Task Report Appendix A details the process by which this particular metric, hereafter called AM1.5 global vertical (AM1.5GV) solar reflectance, was selected.

3.3 Color

We will calculate CIELAB color coordinates (L*, a*, b*) from 360 – 780 nm spectral reflectance following ASTM E308-15 (Standard Practice for Computing the Colors of Objects by Using the CIE System) (ASTM 2015c). We will select the D65 daylight illuminant and 10° observer.

3.4 Effective solar reflectance

The effective solar absorptance (abbreviation ESA; symbol α_{eff}) of a fluorescent surface is the fraction of incident solar energy that is neither reflected nor fluoresced. We will assess the ESR of an opaque fluorescent surface by subtracting its ESA from unity. We will determine the ESA of a test surface by comparing its temperature in the sun to those of non-fluorescent, opaque reference surfaces of known solar absorptance α (1 – solar reflectance ρ). That is, if T, T_1, and T_2 are the temperatures of the test surface, first reference surface, and second reference surface, respectively, and α_1 and α_2 are the solar absorptances of the two reference surfaces, then the ESA of the test surface is

$$\alpha_{eff} = \alpha_1 + (\alpha_2 - \alpha_1)\,(T - T_1) / (T_2 - T_1) \quad (1)$$

and the ESR of the test surface is

$$\rho_{eff} = 1 - \alpha_{eff}. \quad (2)$$

3.5 Solar retroreflectance

We address metrics needed to assess solar retroreflectance in our Task 5.3 report: *Development of retroreflective materials.*

3.6 Thermal emittance

We will assess hemispherical thermal emittance, the thermal emittance metric used for roofing products.

3.7 Initial radiative properties

We will assess initial radiative properties (solar spectral reflectance, solar reflectance, thermal emittance) before exposure.

3.8 Field-exposed aged radiative properties

Starting at month three, we will assess radiative properties every three months over the course of two years of field exposure. Since exposure is slated to begin in March 2016 and end in March 2018, we will include the results for the first six or seven quarters of exposure in the Cool Walls Natural Exposure task report due in December 2017, and add the results for the remaining quarter(s) to the Cool Walls Final Report due in April 2018.

3.9 Solar reflectance loss

Exposure tends to reduce the solar reflectance of a “cool” wall product. Therefore, to try to keep changes in SR positive, we will assess solar reflectance *loss*, defined as initial solar reflectance minus aged solar reflectance. Note that the solar reflectance of some products can increase over time through processes including fading, chalking, or deposition of higher-reflectance soiling matter. In that case, the solar reflectance loss would be negative.

3.10 Thermal emittance gain

Exposure tends to increase the thermal emittance of a metallic surface, and have little to no effect on that of a non-metallic surface. Therefore, to try to keep changes in TE positive, we will assess thermal emittance *gain*, defined as aged thermal emittance minus initial thermal emittance. If thermal emittance decreases, the thermal emittance gain will be negative.

3.11 Soiling resistance

By soiling resistance, we define the ability of a particular surface to retain its initial radiative performance by either avoiding the buildup of soiling, facilitating the removal of soiling, or both. Under "soiling" we include atmospheric deposition (inert inorganic species and organic materials), reactive inorganic species and their reaction byproducts, and microbial growth. The methodology does not allow for a separate analysis of each of these factors, which are usually present simultaneously.

We will assess soiling resistance with two metrics. The first metric, "relative soiling resistance" (symbol β_{rel}), compares loss of solar reflectance to that experienced by a reference material of equal initial solar reflectance ρ_i. If the test surface and the reference surface have aged solar reflectances ρ_a and $\rho_{a,ref}$, respectively, then

$$\beta_{rel} = 1 - (\rho_i - \rho_a) / (\rho_i - \rho_{a,ref}) \quad (3)$$

If β_{rel} is zero, the surface lost exactly as much solar reflectance as the reference surface. If β_{rel} is unity, the surface lost no solar reflectance. The metric β_{rel} can be less than zero (surface lost more solar reflectance than did the reference surface) or greater than one (solar reflectance increased).

The second metric, "absolute soiling resistance" (symbol β_{abs}), compares loss of solar reflectance to that which would result from covering the surface with an opaque soil layer of solar reflectance ρ_{soil}. If the test surface has initial solar reflectance ρ_i and aged solar reflectance ρ_a, respectively, then

$$\beta_{abs} = (\rho_a - \rho_{soil}) / (\rho_i - \rho_{soil}) \quad (4)$$

If β_{abs} is zero, the surface is fully soiled ($\rho_a = \rho_{soil}$); if β_{abs} is unity, the surface is unsoiled. Note that β_{abs} can not be evaluated if $\rho_i = \rho_{soil}$. We will assume $\rho_{soil} = 0.2$ based on our prior analysis of the soiling of roofing materials (Sleiman et al. 2011).

3.12 Hydrophilicity/hydrophobicity

We will assess water contact angle (abbreviation WCA; symbol θ_c), or angle at which the water-air interface meets the surface. A surface with $\theta_c < 90^\circ$ is called hydrophilic (water attracting), while one with $\theta_c > 90^\circ$ is called hydrophobic (water repelling). Water contact angle can range from 0° (water drop goes flat) for a perfectly hydrophilic surface to over 150° (water drop nearly spherical) for a superhydrophobic surface.

3.13 Solar reflectance index

Solar reflectance index (abbreviation SRI; no symbol) is a calculated "coolness" metric that relates the steady-state temperature of a well-insulated test surface in the sun to those of reference white and black surfaces. A surface that attains the same temperature as the

reference black is assigned an SRI of 0, while a surface that attains the same temperature as the reference white is assigned an SRI of 100. (Note that SRI is neither a fraction nor a percentage.) SRI typically ranges from 0 to 100, but can be lower than 0 if the surface is warmer than the reference black, or higher than 100 if the surface is cooler than the reference white.

SRI is computed from measured values of solar reflectance and thermal emittance under assumed environmental conditions. ASTM E1980-11 (Standard Practice for Calculating Solar Reflectance Index of Horizontal and Low-Sloped Opaque Surfaces) (ASTM 2011) specifies a set of environmental conditions, including solar irradiance and long-wave radiative exchange temperature, consistent with horizontal surface on a sunny summer afternoon. These environmental conditions would have to be revised to compute the SRI of a vertical surface, such as a wall. For example, incident sunlight could be based on the ASTM G197 AM1.5 global solar irradiance a sun-facing, vertical surface (about 800 W/m²), while the wall could be assumed to exchange half of its long-wave radiative exchange with the sky, and half with the ground and other walls. Wall SRI will not be calculated at this time, but could be computed if and when ASTM E1980 is extended to vertical surfaces.

4 Methods

Here we specify the method(s) by which each surface metric is to be evaluated.

4.1 Solar spectral reflectance

We will measure near normal-hemispherical solar spectral reflectance r(λ) following ASTM E903-12 (Standard Test Method for Solar Absorptance, Reflectance, and Transmittance of Materials Using Integrating Sphere) (ASTM 2012). We will use a Perkin-Elmer Lambda 900 UV-VIS-NIR benchtop spectrometer equipped with 150 mm Labsphere integrating sphere (Figure 1a-c). Three non-overlapping measurement spots will be chosen along a diagonal spanning the face of each specimen, and their results averaged.

When measuring soiled specimens, it is important to avoid contaminating the integrating sphere. An ideal but expensive and uncommon solution is to acquire a sphere with a bottom-mounted horizontal sample port. If the integrating sphere has a side-mounted vertical sample port, a quartz window should be installed over the port to prevent contamination (Figure 1d-f).

The following protocol will be used to correct spectral reflectance measurements for the effect of the window. Note that steps 1 and 2 are performed without the window installed in front of the sample port, while steps 4 through 6 are performed with the window installed in front of the spectrometer sample port.

1. Calibrate spectrometer with white calibration standard (Labsphere Spectralon SRS-99).

2. Measure spectral reflectances of void (a.k.a., light trap) [low reflectance, $r_L(\lambda)$] and white calibration standard [high reflectance, $r_H(\lambda)$].

3. Clean the window and window accessories appropriately (e.g. with glass cleaner, compressed air). Ensure these items are free of fingerprints, dust, and other contaminants.

4. Install window in front of the spectrometer sample port. <u>Do not recalibrate the spectrometer after installation.</u>

5. Re-measure spectral reflectances of void [$r_L'(\lambda)$] and white calibration standard [$r_H'(\lambda)$].

6. Measure spectral reflectance of one or more soiled specimens [$r_S'(\lambda)$].

7. Correct the spectral reflectance [$r_S'(\lambda)$] of each soiled specimen measured through the window as follows to obtain

$$r_S(\lambda) = r_L(\lambda) + [r_H(\lambda) - r_L(\lambda)] \times [r_S'(\lambda) - r_L'(\lambda)] / [r_H'(\lambda) - r_L'(\lambda)] \quad (5)$$

where

$r_S(\lambda)$ = spectral reflectance of specimen, measured through window, corrected;

$r_L(\lambda)$ = spectral reflectance of void;

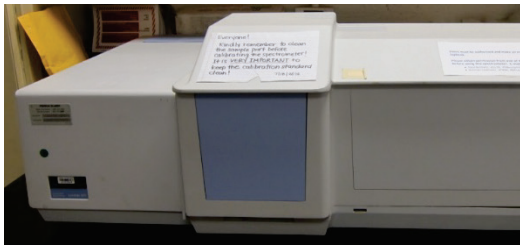

(a)

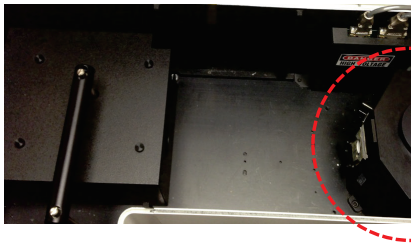

(b)

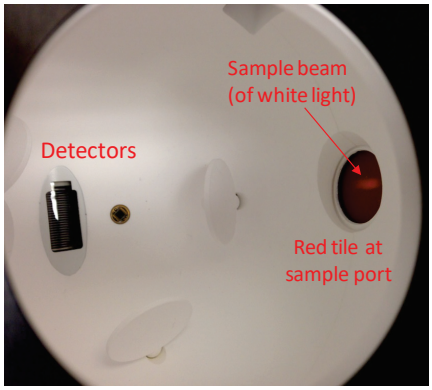

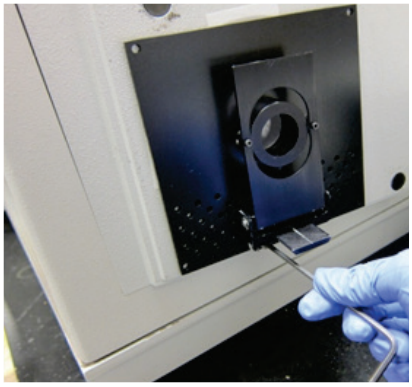

(d)

(c)

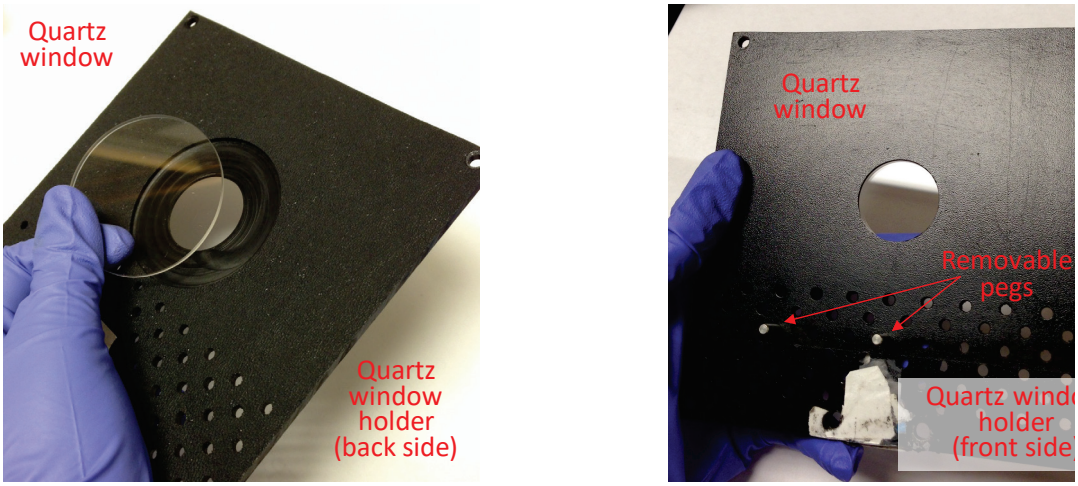

(e) (f)

Figure 1. Images of the PerkinElmer Lambda 900 UV-VIS-NIR spectrometer and its accessories, including (a) front view of closed spectrometer; (b) top view of open spectrometer, with integrating sphere accessory circled; (c) top view of open sphere; (d) side-mounted reflectance sample port fitted with quartz window; (e) window and window holder, as seen from sphere; and (f) window holder as seen from specimen.

$r_H(\lambda)$ = spectral reflectance of white calibration standard;

$r_S'(\lambda)$ = spectral reflectance of specimen, measured through window, uncorrected;

$r_L'(\lambda)$ = spectral reflectance of void, measured through window, uncorrected; and

$r_H'(\lambda)$ = spectral reflectance of white calibration standard, measured through window, uncorrected.

The uncorrected, corrected, and true solar spectral reflectances of a variety of roofing products are shown in Figure 2.

4.2 Solar reflectance

Instruments commonly used to measure solar reflectance include a UV-VIS-NIR spectrometer, a solar reflectometer, and a pyranometer (Levinson et al. 2010b).

4.2.1 Spectrometer

Following ASTM E903, we will measure near normal-hemispherical solar spectral reflectance with a UV-VIS-NIR spectrometer, then calculate AM1.5GV solar reflectance by averaging the spectral reflectance weighted by AM1.5GV solar spectral irradiance.

This “laboratory” version of AM1.5GV solar reflectance uses entirely near normal irradiance (incidence angle ~ 10°), while the “reference” AM1.5GV solar reflectance assumes that 82% of irradiance is beam light, incident at 42° from surface normal, and the remaining 18% is diffuse light. Laboratory AM1.5GV SR exactly matches reference AM1.5GV SR if the surface is perfectly matte (reflectance independent of incidence angle). If the surface is perfectly glossy (exhibiting specular “interface” reflectance that depends on incidence angle, and that is characteristic of light passing from air to a smooth surface), laboratory AM1.5GV SR will underestimate reference AM1.5GV SR by 0.002 (nonselective white) to 0.015 (nonselective black). Measurements of the magnitude of the specular component reflected by representative wall products suggest that this underestimation will not exceed 0.01.

4.2.2 Reflectometer

We will measure laboratory AM1.5GV solar reflectance following ASTM C1549-09(2014) (Standard Test Method for Determination of Solar Reflectance Near Ambient Temperature Using a Portable Solar Reflectometer) (ASTM 2009) with a Devices & Services Solar Spectrum Reflectometer, version 6 (Figure 3), once the AM1.5GV solar spectral irradiance is added to its firmware. Three non-overlapping measurement spots will be chosen along a diagonal spanning the exposure face of each specimen.

One advantage of measuring solar reflectance with a reflectometer, rather than with a spectrometer, is that the reflectometer can be kept clean simply by inverting the measurement head to face down. The instrument will be calibrated and operated in this inverted configuration.

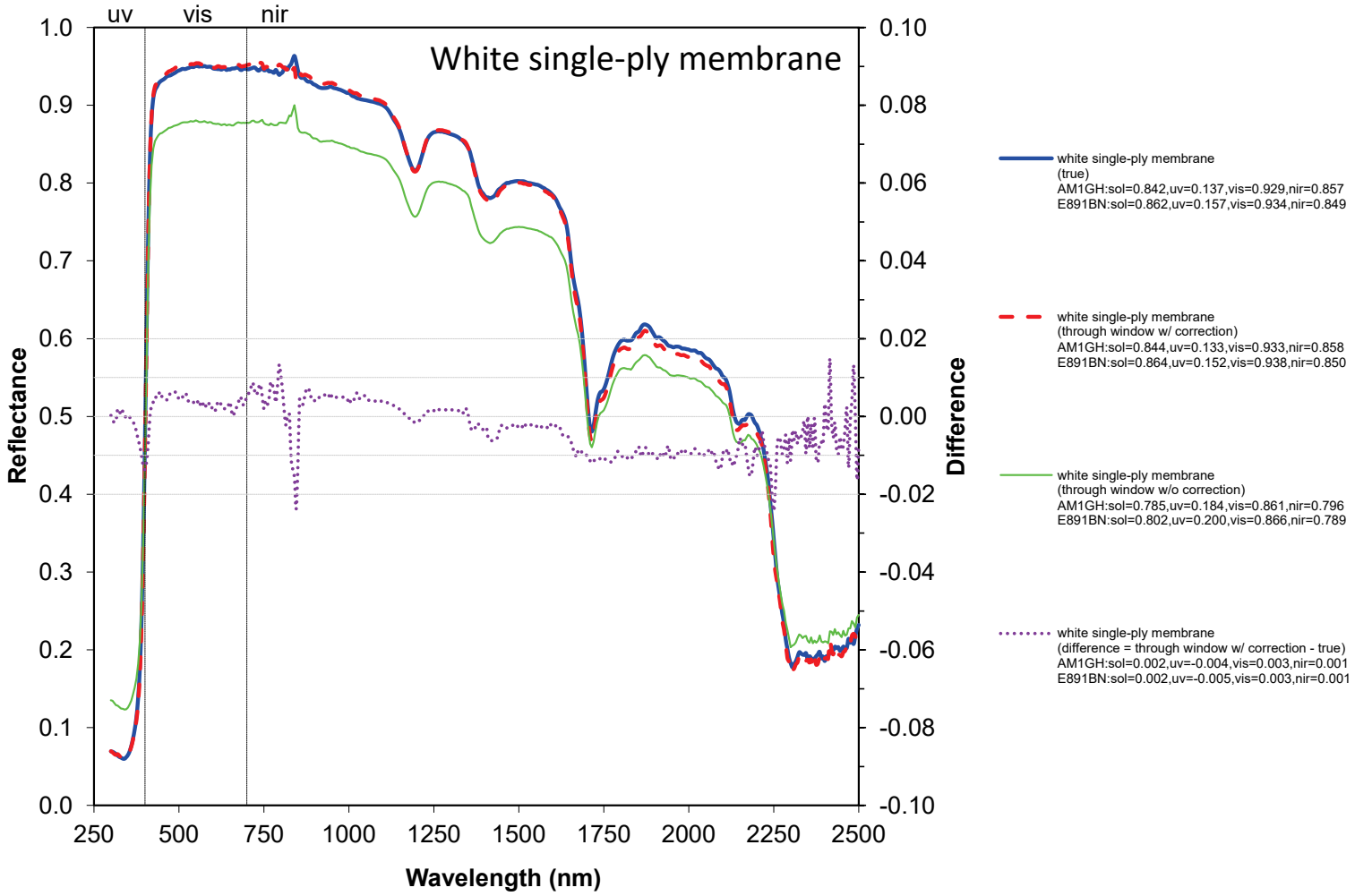

(a)

Figure 2. Solar spectral reflectances (300 – 2,500 nm @ 5 nm) of a variety of roofing products, including (a) white single-ply membrane, (b) blue single-ply membrane, (c) white painted metal (factory applied), (d) red clay tile, (e) cool green painted metal (factory applied), and (f) clear acrylic resin-coated Zincalume steel. The spectral reflectance of each specimen is shown (i) measured without a window

("true"); (ii) measured through a window, then corrected; and (iii) measured through a window, uncorrected. The difference (corrected – true) is also shown.

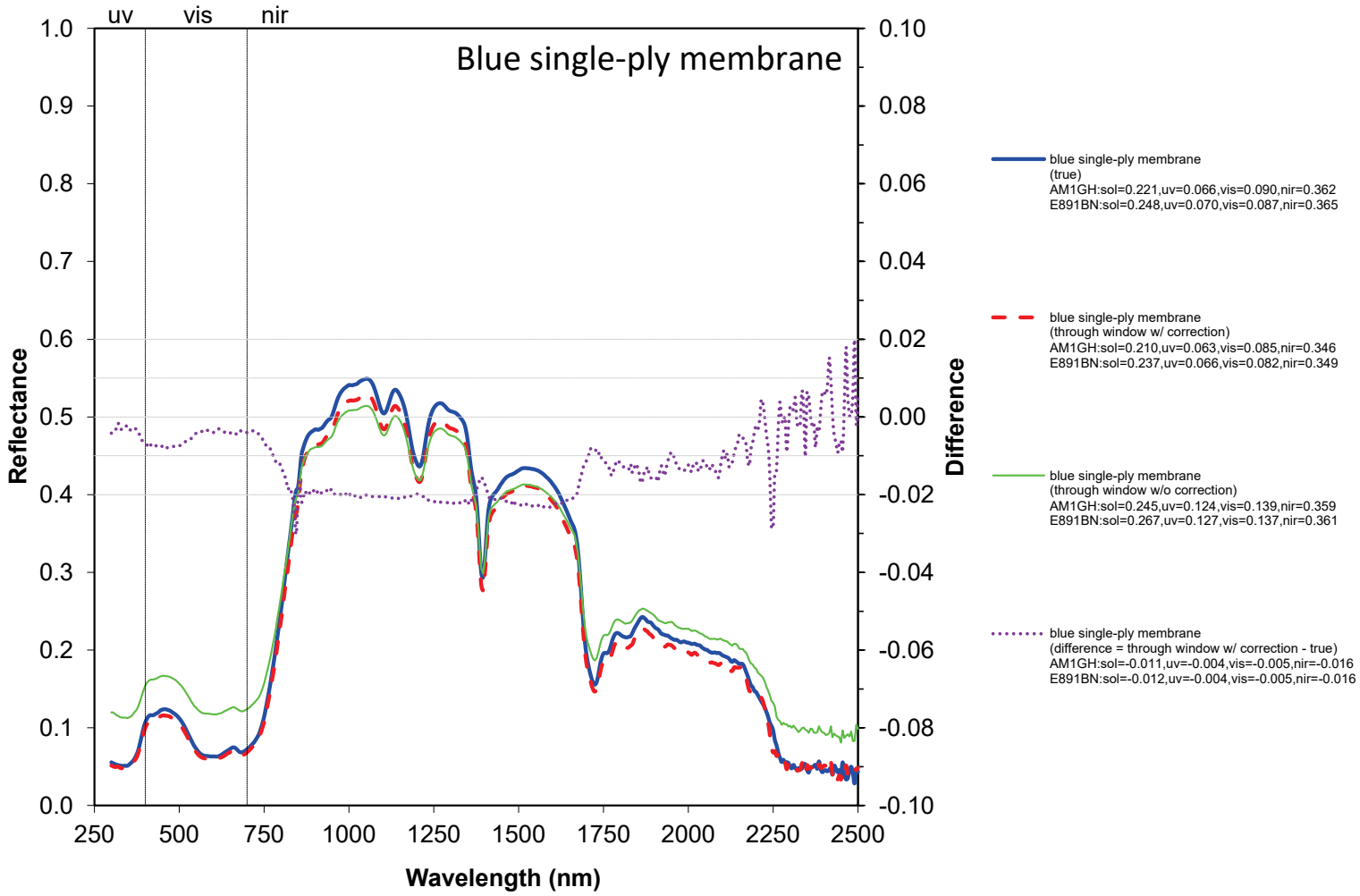

(b)

sol=300-2500 nm; uv=300-400 nm; vis=400-700nm; nir=700-2500 nm

Figure 2 (continued)

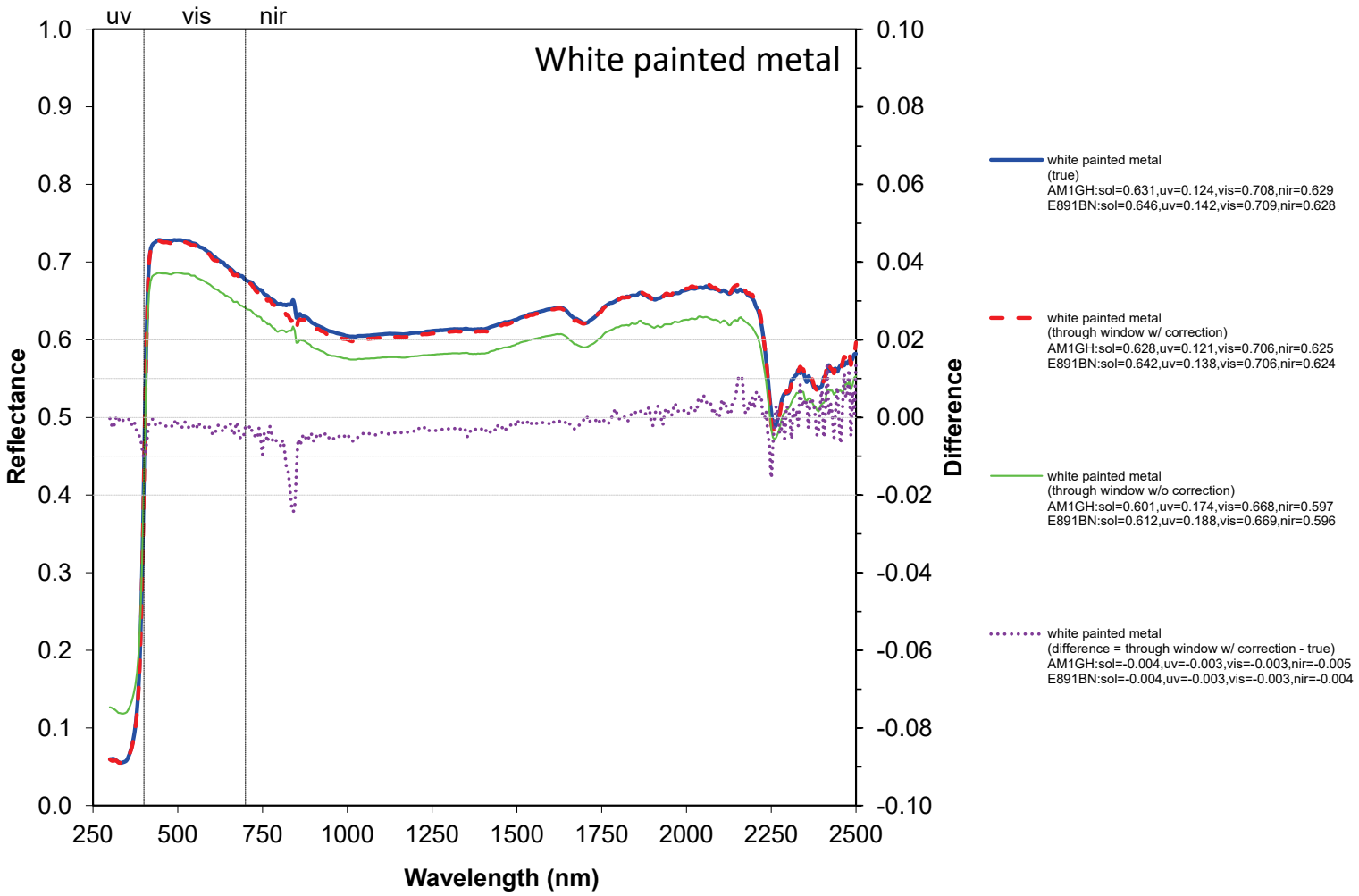

(c)

sol=300-2500 nm; uv=300-400 nm; vis=400-700nm; nir=700-2500 nm

Figure 2 (continued)

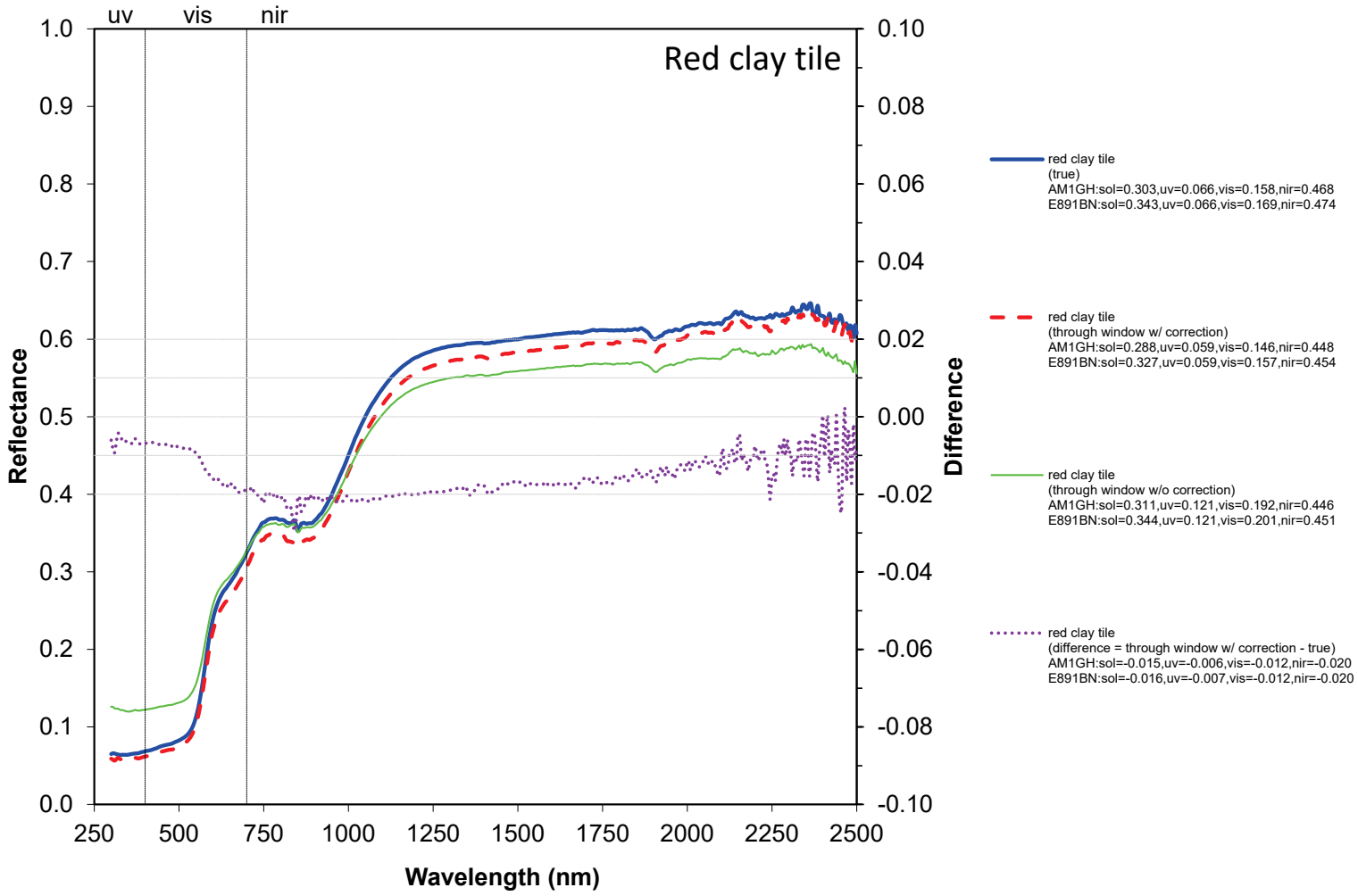

(d)

sol=300-2500 nm; uv=300-400 nm; vis=400-700nm; nir=700-2500 nm

Figure 2 (continued)

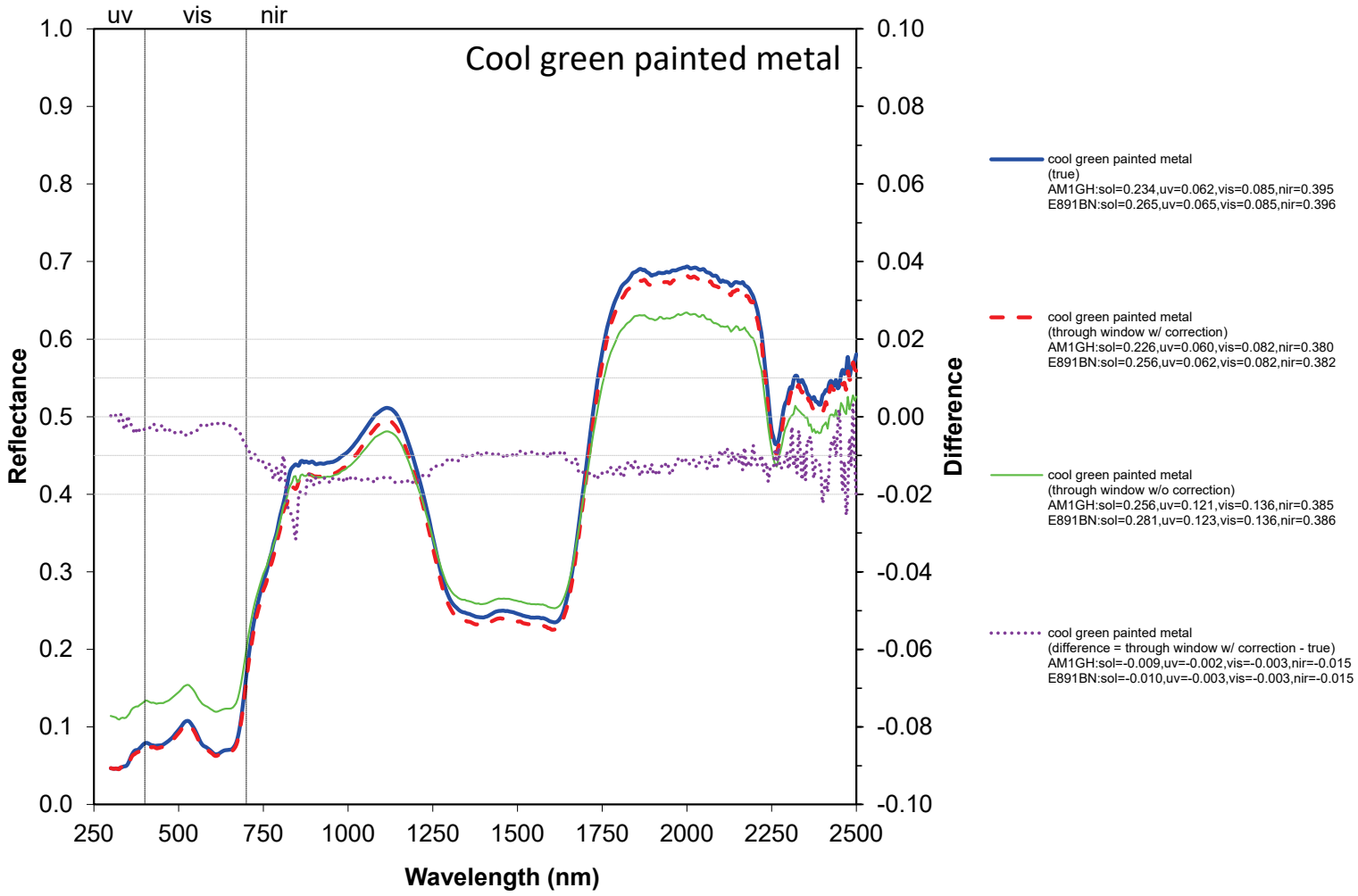

(e)

Figure 2 (continued)

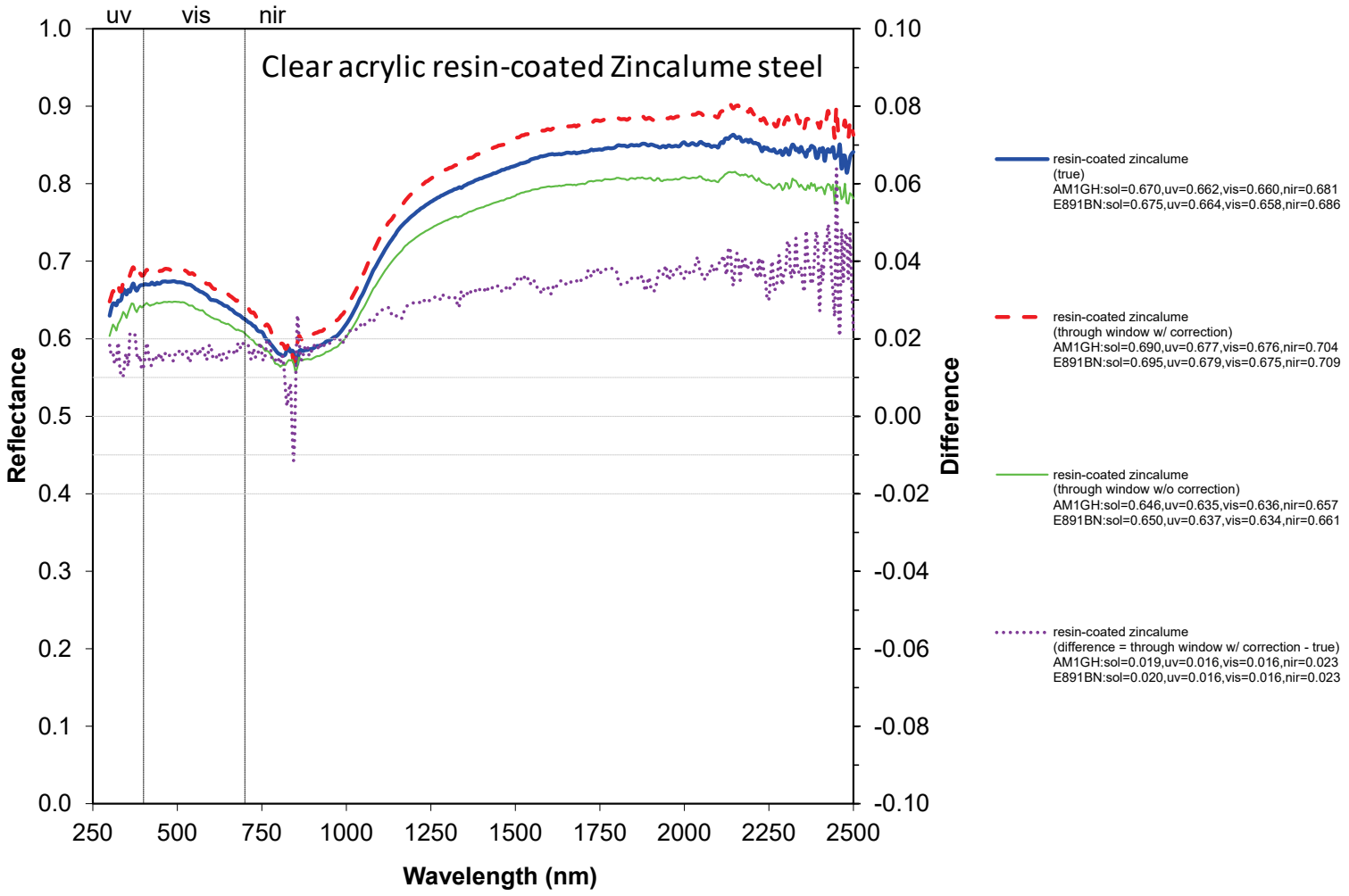

(f)

Figure 2 (continued)

4.2.3 Pyranometer

We do not at this time plan to measure wall solar reflectance with a pyranometer, because there does not yet exist a version of ASTM E1918 (Standard Test Method for Measuring Solar Reflectance of Horizontal and Low-Sloped Surfaces in the Field) (ASTM 2006) suitable for walls. Supporting, orienting, and operating a pyranometer half a meter away from a large wall surface (at least 4 m in diameter) may be tricky.

4.3 Color

CIELAB color coordinates can be calculated from solar spectral reflectance measured with a UV-VIS-NIR spectrometer, since the spectrum needed to compute color (380 – 760 nm) following ASTM E308 is a subset of the solar spectrum (300 – 2,500 nm). Another option is to use a dedicated colorimeter, such as a MiniScan EZ 4500L Spectrophotometer.

4.4 Effective solar reflectance

The measurement of effective solar reflectance is detailed by Levinson et al. (2017). A preprint of this article is presented in our Task 5.2 report: *Development of fluorescent cool pigments.*

4.5 Solar retroreflectance

The characterization of solar retroreflectance is detailed in our Task 5.3 report: *Development of retroreflective materials.*

Figure 3. Devices & Services Solar Spectrum Reflectometer, Model SSR-ER, version 6, operated with its measurement head inverted.

Figure 4. Devices & Services Portable Emissometer, Model AE1, and a multimeter.

4.6 Thermal emittance

Hemispherical thermal emittance will be measured using a Devices & Services Emissometer Model AE1 (Figure 4) with the ADP Port Adapter accessory. Specimens with high thermal conductance (> 1100 W/m²·K),[1] such as bare or painted metal panels, will be measured per ASTM C1371-15 (Standard Test Method for Determination of Emittance of Materials Near Room Temperature Using Portable Emissometers) (ASTM 2015a). All other specimens will be measured per the "Slide Method" described in Devices & Services technical note TN11-2 (Moore 2011).

The instrument will be calibrated, maintained, and operated according to manufacturer instructions, except in specific situations where doing so will irreversibly damage specimens. For example, some steps as described in the "Slide Method" technical note (such as the use of a fan, and the "sliding" action of the measurement head) will need to be modified slightly in order to minimize disturbance to field-exposed specimens.

4.7 Initial and aged solar reflectance and thermal emittance

The variation with time of the radiative properties of wall products will be measured in accordance with the practices described in the section "Natural exposure study protocol".

---

[1] Thermal conductance is the reciprocal of thermal resistance. Hence, ASTM C1371 applies only to specimens with low thermal resistance (< 0.00091 m²·K/W, or 0.0052 ft²·°F·h/BTU).

4.8 Solar reflectance loss and thermal emittance gain

Measured values of initial and aged AM1.5GV solar reflectance will be used to calculate solar reflectance loss. Similarly, measured values of initial and aged hemispherical thermal emittance will be used to calculate thermal emittance gain.

4.9 Soiling resistance

Measured values of initial and aged AM1.5GV solar reflectance will be used to calculate relative soiling resistance in accordance with Eq. (3), and to calculate absolute soiling resistance in accordance with Eq. (4).

4.10 Hydrophilicity/hydrophobicity

Surface hydrophilicity or hydrophobicity will be determined by measuring water contact angle with a goniometer, in accordance with the static sessile drop method (Figure 5). This method determines the surface energy of a surface by placing a droplet of a liquid (water) of a known surface energy. The contact angle between the drop and the surface is measured under static conditions in which the drop is sitting on the surface, rather than rolling over it. It has been found to be the most appropriate method to quantify the contact angle of porous materials such as soils and sediments (Shang et al. 2008).

Static water contact angle will be measured via the sessile drop technique using a simple manually-operated setup. It consists of a point-and-shoot digital camera with focusing lens, a micrometer syringe, and an adjustable-height horizontal specimen mounting stage backlit by a diffuse light source. The camera is positioned such that it will view the sessile drop at a slight downward angle; this facilitates visual determination of the horizon in the resultant photograph.

A droplet of deionized water (of fixed volume on the order of a few microliters) is formed at the syringe tip and subsequently deposited onto the specimen surface very carefully. It is important that the droplet does not “fall” onto the specimen as this will distort the drop shape. The sessile drop is then photographed twice in order to capture any changes in drop shape over time – the first will be taken at 2 seconds following deposition, and the second will be taken at 30 seconds following deposition.

A free drop shape analysis tool, the "LBADSA" ImageJ plug-in (http://bigwww.epfl.ch/demo/dropanalysis) developed by Stalder et al. (2010), will be used to determine the contact angle from the drop photographs. If a drop is not symmetric, both the "left" and the "right" contact angles will be measured and recorded. Each specimen will be characterized by measurements of at least three drops positioned along a diagonal spanning the exposure face.

5 Natural exposure study protocol

5.1 Specimen selection

We selected 69 wall products from 10 partners to include in the natural exposure campaign (Figure 6). This set of products covers several types of wall materials and coatings typically

(a)

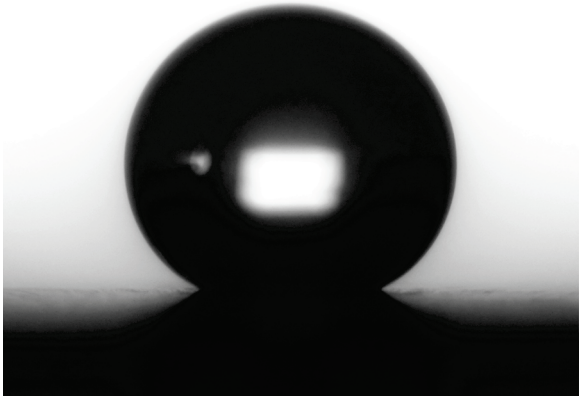

(b)

Figure 5. Sessile drop photographs produced by LBNL set-up, showing (a) a hydrophilic surface, and (b) a hydrophobic surface.

used in residential and commercial construction. It includes low-, medium-, and high-albedo products, as well as both conventional and self-cleaning products.

5.2 Specimen preparation

Partners were asked to prepare 100 replicate specimens of each product, each approximately 10 cm × 10 cm (4″ × 4″). To ensure their uniformity, we asked that these replicate specimens be cut from or produced in the same batch. Field-applied coatings were applied to appropriate substrates according to manufacturer specifications. Wood specimens were sealed on all sides in order to prevent situations where unrepresentative substrate degradation could impact true coating performance. The different categories are presented in the chart shown in Figure 6.

5.3 Specimen use

Of the 100 replicate specimens per product, 30 will be used in the initial 2 year exposure campaign in California. Exposing 10 specimens per product at each of the three California sites (Berkeley, Fresno, Los Angeles) will allow for retrieval of one specimen per product per site at the end of each of eight quarters. The remaining two specimens are spares that can be used in case of damage, or to extend the duration of exposure.

Another 18 specimens per product may be used in a parallel project to initiate a 5 year campaign at the three U.S. natural exposure sites (near Phoenix, AZ; Miami, FL, and Cleveland,

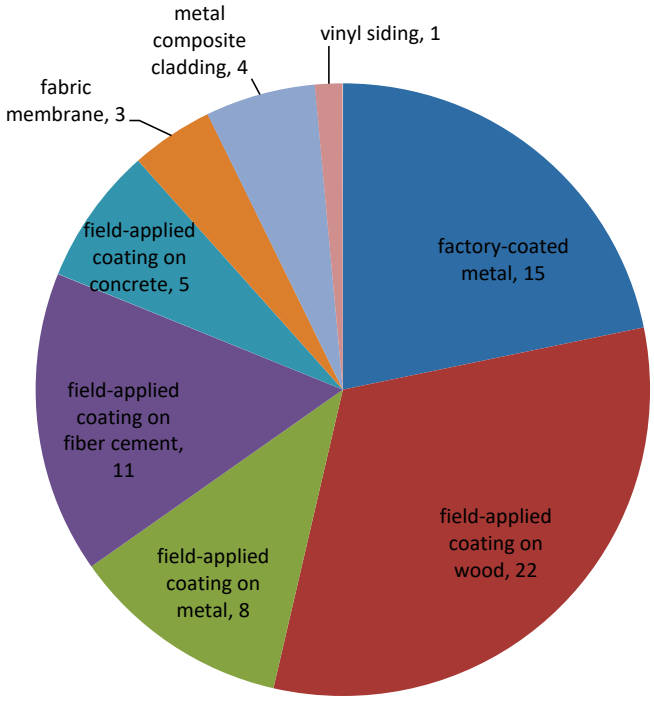

Figure 6. Distribution of cool wall products included in this study.

OH) used by the Cool Roof Rating Council for roof product rating. Exposing six specimens per product at each site will permit five annual retrievals, and provide one spare in case of damage.

Remaining specimens will be used for various laboratory tests at LBNL, including the potential development of a lab aging practice for wall products.

5.4 Specimen tracking

All information collected for each specimen—including product make and model, product manufacturer, specimen status, condition, solar reflectance, thermal emittance, and water contact angle—will be centralized and maintained in a database. Specimens are identified by a barcode asset tag attached to the back face, with a unique ID code of the format "CWXXYY", where "XX" is a 2-digit identifier (01-69) of product, and "YY" is a 2-digit identifier (00-99) of specimen replicate number (Figure 7).

5.5 Exposure practice at California sites

The wall product specimens will undergo direct natural exposure at three California locations: Lawrence Berkeley National Laboratory, in Berkeley; a PPG facility, in Fresno, and the University of Southern California, in Los Angeles. Experimental protocol will follow, as much as is possible, ASTM G7/G7M-13 (Standard Practice for Atmospheric Environmental Exposure Testing of Nonmetallic Materials) (ASTM 2013). To appropriately represent the product application, specimens will be exposed in a vertical orientation (90°) and backed by untreated marine-grade plywood. Since solar-reflective surfaces are expected to yield greatest energy savings when applied to east and west walls, and greatest peak power demand savings when applied to west

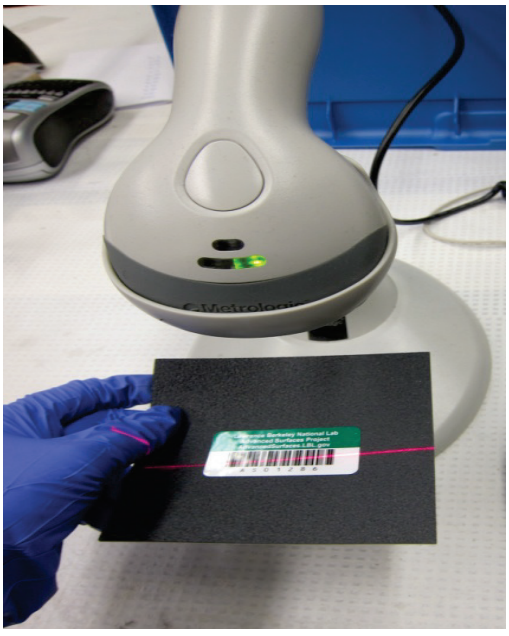

Figure 7. Example of label containing barcode (attached to back of specimen), being processed with a barcode reader.

walls, exposed specimens will face west.

Specimens will be mounted on custom-built exposure racks composed of 12 to 13 staggered rows of galvanized steel sheet metal specimen holders attached to a Unistrut frame (Figure 8). Staggering minimizes potential runoff cross-contamination between rows. Five drainage holes evenly spaced along the bottom of the specimen holders prevent water from collecting in the bottom jaws of the holders.

Each 2.1 m (7') long holder can hold up to 21 specimens, and thus can accommodate the full set of replicate specimens (10 each) for two products. This simplifies quarterly specimen retrieval, in which on-site staff need only slide one specimen from each end of the row.

5.6 Specimen characterization

At each of the eight quarters, one specimen per product per California site will be removed from the rack and sent to LBNL for characterization. The physical condition, radiative properties, and hydrophilicity/hydrophobicity of these specimens will be characterized with photographs, and with measurements of solar spectral reflectance, solar reflectance, thermal emittance, and water contact angle.

Because most measurements will to some degree disturb the soiling on naturally-exposed specimens, it will be important to order the measurement tasks starting from those with the least disturbance potential to those with the highest. The specimens will first be photographed, and then subjected to reflectometer and spectrometer measurements. Thermal emittance and water contact angle will be measured last. Retrieved specimens will be stored at LBNL after characterization.

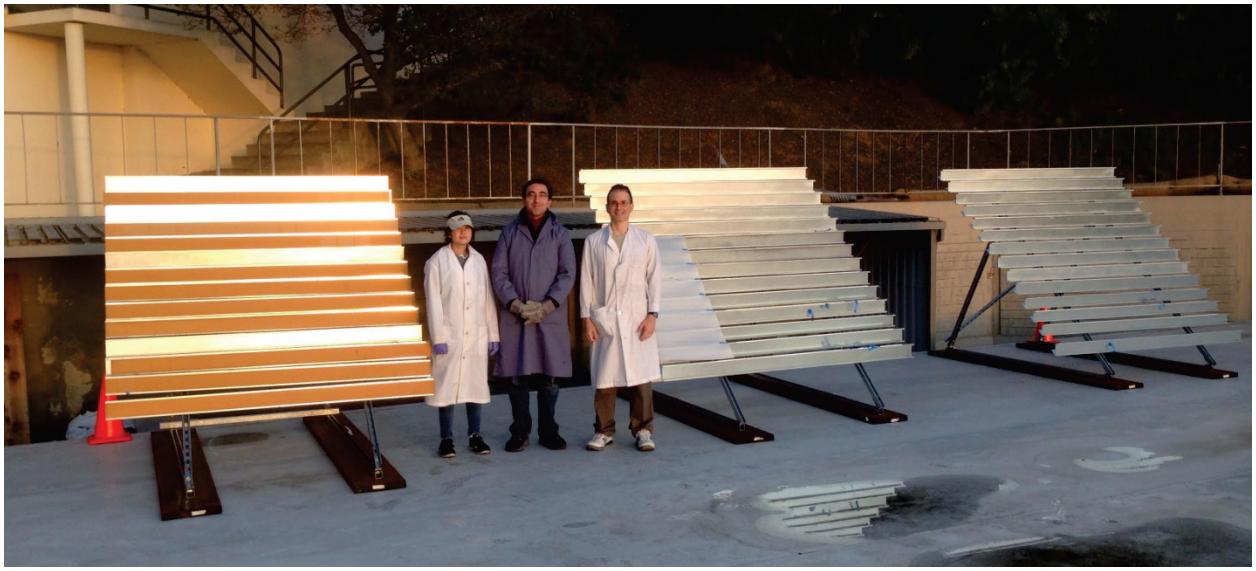

Figure 8. LBNL-designed wall product exposure racks freshly installed on a roof at Lawrence Berkeley National Laboratory (Berkeley, CA).

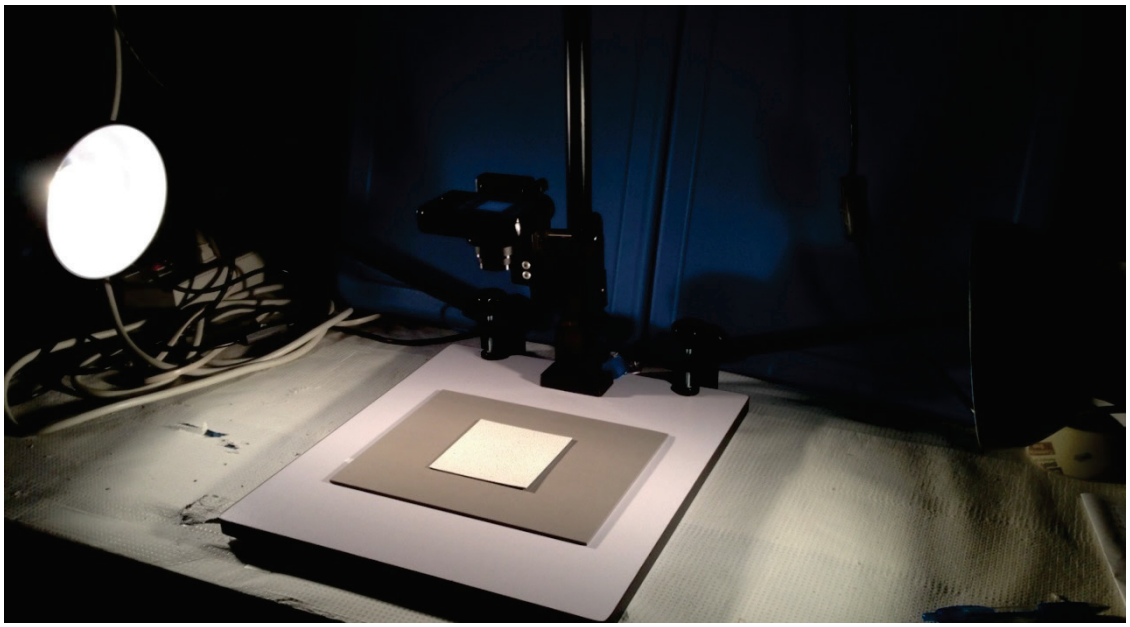

The following information will be gathered before exposure, and following quarterly specimen retrieval.

5.6.1 Image

Specimens will be photographed using a point-and-shoot digital camera mounted on a copy stand set-up that provides reproducible lighting conditions. A gray card placed in background will be helpful for white balance (Figure 9).

Figure 9. Photo copy table used to prepare specimen photos.

5.6.2 Solar spectral reflectance

Solar spectral reflectance will be measured with a UV-VIS-NIR spectrometer, as described in the Methods subsection “Solar spectral reflectance”.

Solar reflectance

Solar reflectance will be measured with a UV-VIS-NIR spectrometer, and—once the reflectometer firmware is upgraded to include the AM1.5GV solar spectral irradiance—with a Devices & Services Solar Spectrum Reflectometer. Both practices are detailed in the Methods subsection “Solar reflectance”.

5.6.3 Thermal emittance

Thermal emittance will be measured with a Devices & Services Portable Emissometer, as described in the Methods subsection “Thermal emittance”.

5.6.4 Water contact angle

Water contact angle will be measured with our custom apparatus as described in the Methods subsection “Hydrophilicity/hydrophobicity”.

5.7 Specimen storage

Because it is necessary to preserve specimen condition prior to and after measurement, each specimen will be enclosed in its own glassine paper sleeve when not undergoing exposure or measurement (Figure 10). Glassine paper was chosen for the sleeve material as it is archival-grade, non-reactive, moisture-resistant, not prone to static buildup, and semi-transparent. Storing specimens using this method prevents contamination of clean specimens as well as accidental “cleaning” of field-exposed specimens. Any debris fall-off from a field-exposed specimen will be saved by collecting the debris inside the specimen’s glassine paper sleeve. For this reason, sleeves will not be interchanged between specimens, and any damaged sleeves will be replaced accordingly.

For long periods of storage, the specimens (each inside a glassine sleeve) will additionally be placed inside a rigid waterproof secondary container. This is especially important since the glassine sleeves protecting the specimens are water-resistant, but not waterproof.

5.8 Specimen handling

Specimens need to be handled carefully in order to limit any disturbance to their condition. This involves gentle handling of both the specimen itself and its corresponding protective sleeve. The exposure face of the specimen must never be touched, scraped, or otherwise artificially contaminated by agents not representative of the exposure environment or time period. While inserting or removing specimens from their glassine sleeves, care will be taken to prevent the sleeve material from brushing against the exposure face. Likewise, the specimens will only be gripped along the side and back faces.

With field-exposed specimens there is a risk that rough handling will dislodge soiling debris that has collected on the exposure face. For this reason, it will be important to avoid violently agitating or inverting field-exposed specimens. Additionally, careful attention will be needed while specimens are being removed from the exposure racks to ensure that no damage or contamination occurs during this process. Once removed from the exposure environment and placed into glassine sleeves, these field-exposed specimens will not be handled in environments with significant levels of dust or drafts.

Many of the characterization measurements require direct contact between an instrument sample port and the specimen exposure face. In order to limit the degree of disturbance or contamination to both the specimen and the instrument, it will be necessary to clean the sample port between measurements, as well as prevent any static buildup on surfaces that come in close contact to the specimen.

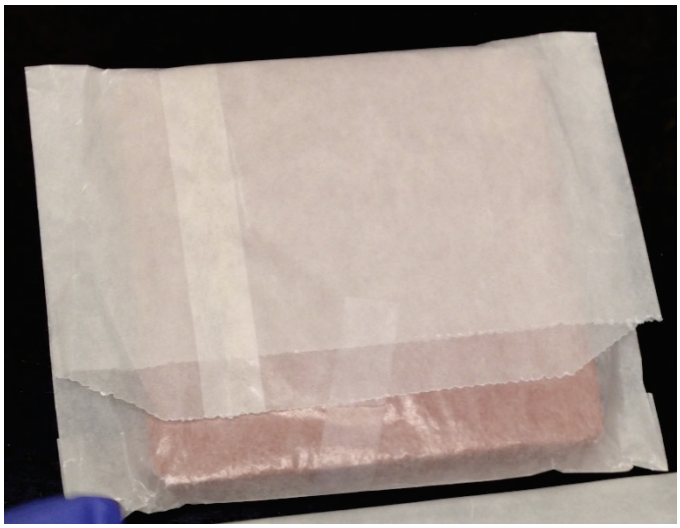

Figure 10. Specimen inside a glassine sleeve, which has been folded and taped closed.

5.9 Specimen packaging for transportation

While preparing specimens for long-distance transit via any of the typical carrier services, it is important to keep in mind that packages will be handled by personnel with no personal stake in this project. The many ways the integrity of specimens can be compromised during this process include physical damage to the specimen itself (as in breaking, chipping, scratching, or warping); disturbance of accumulated soiling; and in-package aging. Physical damage and disturbance of accumulated soiling can occur if specimens are allowed to shift around violently inside the secondary container, and/or if there is insufficient padding. In-package aging can occur if the specimens are packaged while “wet” (will leach moisture to surroundings under ambient conditions) or if the specimens become wet when package is exposed to heavy rains during transit. One specimen could soil another if packed in the same sleeve, or if a sleeve tears during transport and storage.

A proper packaging protocol will incorporate strategies that protect against the aforementioned causes of specimen damage. It will also incorporate only robust materials that will not fail during transit. Materials found to be robust include cardboard, bubble wrap, foam, and packaging tape. Materials found to be insufficient include rubber bands and copy paper.

The following describes a packaging protocol that has worked well for LBNL in the past. Each specimen is first inspected and determined to be sufficiently dry before it can be placed inside a clean glassine sleeve. The sleeve is then taped or folded over in some way to prevent the specimen inside from sliding around freely. Sleeved specimens are then arranged into a small stack, where sleeved specimens are separated from each other by buffer layers of cardboard, bubble wrap, or foam sheeting (Figure 11). Any flexible or fragile sleeved specimens are flanked by stiff material to preserve their shape. The stack of sleeved specimens is then bound tightly together such that individual specimens cannot independently move. These sleeved-specimen bundles can then be placed into a sturdy cardboard box where any voids are adequately filled with foam, bubble wrap, or air cushions. If it is expected that the box will contact water during transit, then these sleeved-specimen bundles should be wrapped in some water-resistant barrier.

Figure 11. Stacks of sleeved specimens.

6 Summary

We have developed and presented metrics and methods to characterize the solar spectral reflectance, solar reflectance, effective solar reflectance, solar retroreflectance, color, thermal emittance, soiling resistance, and hydrophilicity/hydrophobicity of wall products. We have also developed and presented a protocol for the natural exposure of wall products and California, with possible extension to three U.S. sites outside the state.

References

ASTM. 2006. ASTM E1918-06: Standard Test Method for Measuring Solar Reflectance of Horizontal and Low-Sloped Surfaces in the Field. ASTM International. http://www.astm.org/Standards/E1918.htm

ASTM. 2009. ASTM C1549-09(2014): Standard Test Method for Determination of Solar Reflectance Near Ambient Temperature Using a Portable Solar Reflectometer. http://www.astm.org/Standards/C1549.htm

ASTM. 2011. ASTM E1980-11: Standard Practice for Calculating Solar Reflectance Index of Horizontal and Low-Sloped Opaque Surfaces. ASTM International. http://www.astm.org/Standards/E1980.htm

ASTM. 2012. ASTM E903-12: Standard Test Method for Solar Absorptance, Reflectance, and Transmittance of Materials Using Integrating Sphere. ASTM International. http://www.astm.org/Standards/E903.htm

ASTM. 2013. ASTM G7/G7M-13: Standard Practice for Atmospheric Environmental Exposure Testing of Nonmetallic Materials. ASTM International. http://www.astm.org/Standards/G7.htm

ASTM. 2014. ASTM G197-14: Standard Table for Reference Solar Spectral Distributions: Direct and Diffuse on 20˚ Tilted and Vertical Surfaces. ASTM International. http://www.astm.org/Standards/G197.htm

ASTM. 2015a. ASTM C1371-15: Standard Test Method for Determination of Emittance of Materials Near Room Temperature Using Portable Emissometers. ASTM International. http://www.astm.org/Standards/C1371.htm

ASTM. 2015b. ASTM D7897-15: Standard Practice for Laboratory Soiling and Weathering of Roofing Materials to Simulate Effects of Natural Exposure on Solar Reflectance and Thermal Emittance. ASTM International. http://www.astm.org/Standards/D7897.htm

ASTM. 2015c. ASTM E308-15: Standard Practice for Computing the Colors of Objects by Using the CIE System. ASTM International. http://www.astm.org/Standards/E308.htm

Chabas A, Alfaro S, Lombardo T, Verney-Carron A, Da Silva E. Triquet S, Cachier H, Leroy E. 2014. Long term exposure of self-cleaning and reference glass in an urban environment: A comparative assessment. *Building and Environment* 79, 57-65.

Gueymard C. 2006. Simple Model of the Atmospheric Radiative Transfer of Sunshine (SMARTS) 2.9.5. http://www.nrel.gov/rredc/smarts

Levinson R, Akbari H, Berdahl P. 2010a. Measuring solar reflectance—Part I: defining a metric that accurately predicts solar heat gain. *Solar Energy* 84, 1717-1744.

Levinson R, Akbari H, Berdahl P. 2010b. Measuring solar reflectance—Part II: review of practical methods. *Solar Energy* 84, 1745-1759.

Levinson R, Chen S, Ferrari C, Berdahl P, Slack J. 2017. Methods and instrumentation to measure the effective solar reflectance of fluorescent cool surfaces. *Energy & Buildings* 152, 752-765. http://dx.doi.org/10.1016/j.enbuild.2016.11.007

Moore C. 2011. Model AE1 Emittance Measurements using a Port Adapter, Model AE-ADP. Technical Note TN11-2, Devices & Services Company, Dallas, TX. http://www.devicesandservices.com/TechNotes/TN11-2.pdf

Schaeffer DA, Polizos G, Smith DB, Lee DF, Hunter SR, Datskos PG. 2015. Optically transparent and environmentally durable superhydrophobic coating based on functionalized SiO_2 nanoparticles. *Nanotechnology* 26 (5), 055602. http://dx.doi.org/10.1088/0957-4484/26/5/055602

Shang J, Flury M, Harsh JB, Zollars RL. 2008. Comparison of different methods to measure contact angles of soil colloids. *Journal of Colloid and Interface Science* 328, 299-307.

Sleiman M, Ban-Weiss G, Gilbert HE, Francois D, Berdahl P, Kirchstetter TW, Destaillats H, Levinson R. 2011. Soiling of building envelope surfaces and its effect on solar reflectance—Part I: Analysis of roofing product databases. *Solar Energy Materials & Solar Cells* 95, 3385-3399.

Stalder AF, Melchior T, Müller M, Sage D, Blu T, Unser M. 2010. Low-bond axisymmetric drop shape analysis for surface tension and contact angle measurements of sessile drops. *Colloids and Surfaces A: Physicochemical and Engineering Aspects* 364(1-3), 72-81.

Task Report Appendix A: Development of a solar reflectance metric for walls

Motivation

If the reflectance of a surface is both "matte" (invariant with incident angle) and nonselective (invariant with wavelength), its solar reflectance will be constant. Otherwise, its solar reflectance can vary with the geometry (angular distribution) and/or spectral power distribution (power per unit wavelength, by wavelength) of incident sunlight, each of which depend on the position of the sun, the orientation of the surface, sky conditions, shading, and (unless the surface is horizontal) ground reflectance.

Spectral and solar reflectance can vary strongly with incidence angle if a surface is "glossy" (exhibits a specular "interface" reflectance characteristic of light passing from air to a smooth surface) and has low reflectance at near-normal incidence. For example, a smooth black surface may reflect 4% of light incident near normal, but 20% of light incident 70° from normal. This is evident from the images, or glare, that can be seen in smooth black surfaces when viewed from large incidence angle.

Solar reflectance can vary strongly with solar spectral irradiance if the surface's reflectance changes substantially by wavelength. For example, Levinson et al. (2010a) calculated that an ideal matte cool black horizontal surface with 0.04 reflectance in the UV and visible spectra (300 – 700 nm), and 0.90 reflectance in the NIR spectrum (700 – 2,500 nm), would exhibit a solar reflectance of 0.46 in full sun (solar irradiance 49% NIR), but only 0.27 in full shade (solar irradiance 17% NIR).

Methodology and intermediate results

The article by Levinson et al. (2010a) developed a solar reflectance metric suitable for predicting the solar heat gain of a horizontal surface, such as a flat roof or pavement, or an axisymmetric surface, such as a conical roof or the entire curved side wall of a cylinder. That study chose to evaluate solar conditions at the time of peak irradiance. That maximizes the accuracy of solar reflectance when the sun is strong, and tends to reduce errors in solar heat gain. We follow their approach to select a solar reflectance metric suited to flat walls. To wit:

1. Using the NREL SMARTS2 tool (Gueymard 2006), we calculate global, beam (direct), and diffuse (sky + ground) solar spectral irradiances under the ASTM G197 sky and ground conditions as a function of solar altitude angle and surface solar azimuth angle (solar azimuth angle – surface azimuth angle). The spectral irradiance simulation process is detailed in Section 5.1 of Levinson et al. (2010a).

2. From these spectral irradiances we calculate global solar irradiance, beam solar irradiance, diffuse solar irradiance, diffuse fraction of global solar irradiance, and NIR fraction of global solar irradiance as a function of solar position (Figure 12).

3. We determine that under G197 sky and ground conditions, a vertical surface experiences peak global solar irradiance at when the sun altitude angle is 32° and the surface solar azimuth angle is zero (surface faces the sun). This solar position is marked "P" (for peak) in Figure 12.

4. Table 1 shows that the magnitude, NIR fraction, and diffuse fraction of the peak global solar irradiance are close to those specified by ASTM G197 for an air mass 1.5 global solar irradiance on a sun-facing vertical surface (solar altitude 42°, surface solar zenith angle zero; marked "G", for G197, in Figure 12). Since the G197 air mass 1.5 global vertical (AM1.5GV) irradiance well matches the peak global solar irradiance, and is already published as an ASTM standard, we use the solar position and solar spectral irradiance associated with G197 AM1.5GV as our conditions for evaluating "reference" global solar reluctances.

5. For glossy and matte versions of several ideal surfaces (nonselective black with near-normal UV and visible reflectance r_V=0.04, and near-normal NIR reflectance r_N=0.04; nonselective gray with r_V=r_N=0.20; nonselective white with r_V=r_N=0.90; selective black with r_V=0.04, r_V=0.90; and selective gray with r_V=0.20, r_V=0.90), we calculate global solar reflectance as a function of solar position. The reflectance calculation process is detailed in Section 5.2 of Levinson et al. (2010a). Figure 13 shows the results for all surfaces that are glossy, selective, or both. (Global solar reflectance is invariant for a matte, nonselective surface.)

6. Using the NREL SOLPOS tool (https://www.nrel.gov/midc/solpos/solpos.html), we calculate the solar path (altitude and azimuth angles by time of day) the 21st day of each month, including Mar 21 (spring equinox), Jun 21 (summer solstice), Sep 21 (fall equinox), and Dec 21 (winter solstice), at latitudes 25°N (just south of Miami, FL), 37°N (mid-latitudes of mainland U.S. and California), and 45°N (Portland, OR). Solar paths at latitude 37°N are shown in Figure 14.

7. At each latitude (25°N, 37°N, 45°N), on each date (Mar 21, Jun 21, Sep 21, Dec 21), and for each cardinal wall direction (east, west, south, and north), we calculate the variation with time of day of the global solar irradiance; NIR and diffuse fractions of global solar irradiance; underestimation of global solar reflectance by reference solar reflectance; and overestimation of solar heat gain induced by substituting reference reflectance for global solar reflectance. Figure 15 shows these results at latitude 37°N. Reflectance underestimation and solar heat gain overestimation for the gray surfaces are omitted to simplify the graphs, but are similar to those for the black surfaces.

8. We calculate for each latitude, date, and wall orientation the underestimation of daily reflectance (fraction of daily solar irradiation reflected) by reference solar reflectance, and the overestimation of daily solar heat gain (daily solar irradiation absorbed) by induced by substituting reference reflectance for global solar reflectance. Table 2 shows these results at latitude 37°N.

9. Since the cooling energy savings and heating energy penalties associated with raising wall solar reflectance scale with increase in solar reflectance, we calculate the extent to which substituting reference reflectance for global solar reflectance will overestimate true rises in summer (Jun/Jul/Aug) and winter (Dec/Jan/Feb) solar reflectances. Table 3 shows results for six scenarios in which nonselective black or gray surfaces are upgraded to selective black, selective gray, or nonselective white surfaces. It omits cases in which a matte nonselective is upgraded to another matter nonselective surface, because the reflectances of matte nonselective surfaces are constant.

We extended the earlier study in at least one regard. To assess whether wall products tend to be matte or glossy, we measured the specular component of the AM1GH solar reflectance of 14 different wall products, and of 6 reference materials, with a UV-VIS-NIR spectrometer (Table 4). The procedure was to (a) open the specular reflectance port of the spectrometer's integrating sphere; (b) calibrate the instrument; (c) measure $r_1(\lambda)$, the solar spectral reflectance excluding specular component, of each specimen; (d) close the port; (e) re-calibrate the instrument; and (f) measure total solar spectral reflectance, $r_2(\lambda)$, of each specimen. The specular component of solar spectral reflectance was calculated as $r_3(\lambda) = r_2(\lambda) - r_1(\lambda)$, and weighted with AM1GH solar spectral irradiance to obtain the specular component of solar reflectance. (The solar spectrum used to weight spectral irradiance is not particularly important in this assessment of glossiness.)

Discussion

Error in solar heat gain

There are three types of error when using a fixed reference reflectance to estimate solar heat gain: (A) those due to mismatch in spectral power distribution when a surface is selective, (B) those due to mismatch in incidence angle when a surface is not matte; and (C) those that result from a combination of A and B. Here we gauge each type of error for walls at latitude 37°N (mid-mainland US, mid-California) using results presented in Table 2.

The selective black ideal surface is highly selective, and more so than any real cool color. Therefore, we can use the fractional overestimation of wall daily solar heat gain for this surface to bound type A (spectral) errors. This error ranges from -5.2% (south) to +2.5% (east and west) on Jun 21; from -8.3% (north) to +9.0% (south) on Dec 21; and from -8.5% (north) to +4.1% (east and west) on Mar 21 and Sep 21. The magnitude (absolute value) of the type A error does not exceed 9% for any cardinal direction.

We can bound type B (angular) errors by considering a glossy nonselective black surface, which exhibits maximum variation of reflectance with incidence angle. This error ranges from +2.7% (east and west) to +19.2% (south) on Jun 21; from -0.1% (south) to +5.4% (east and west) on Dec 21; and from +3.0% (east and west) to +6.2% (south) on Mar 21 and Sep 21. The magnitude of the type B error does not exceed 5.4% for east and west walls, but on Jun 21 can reach 19.2% for a south wall.

It is more challenging to bound type C (spectral + angular) errors, because type A and type B errors for a glossy selective surface can have opposite signs. However, we will consider the range of errors in for the glossy selective black and glossy selective gray, choosing the largest values. This error ranges from +5.4% (east and west) to +13.3% (north) on Jun 21; from -4.7% (north) to +14.4% (east) on Dec 21; and from -4.9% (north) to +7.5% (east and west) on Mar 21 and Sep 21. For east and west walls, the magnitude of the type C error does not exceed 7.5% on Mar, Jun, or Sep 21, but can reach 14.4% on Dec 21. For north and south walls, the magnitude of the type C error can reach 12.6% (south) to 13.3% (north) in on Jun 21, but otherwise does not exceed 8.9%.

Error in solar reflectance rise

Substituting reference reflectance for actual reflectance can induce type A, B, and C errors in estimation of solar reflectance rise when making walls cooler. The following results are evaluated at latitude 37°N (Table 3).

We bound type A (spectral) errors using scenario (e), matte nonselective black to matte selective black. For east and west walls, the overestimation of reflectance rise is -2.9% in summer and -6.6% in winter. For south walls, the error is +5.1% in summer and -6.2% in winter. For north walls, the error is +1.1% in summer and +11.2% in winter.

We bound type B (angular) errors using scenario (a), glossy nonselective black to glossy nonselective white. For east and west walls, the overestimation of reflectance rise is +2.7% in summer and +4.6% in winter; for north and south walls, the error is small in summer (+0.7% to +4.0%), but large in winter (+10.8% to +16.3).

We bound type C (spectral + angular) errors using scenario (c), glossy nonselective black to glossy selective black. For east and west walls, the overestimation of reflectance rise is -0.5% in summer and -2.6% in winter. For south walls, the error is +23.1% in summer and -5.5% in winter. For north walls, the error is +13.2% in summer and +15.8% in winter.

Note that reflectance rise errors are usually a few percentage points lower or higher if substituting laboratory reflectance, rather than reference reflectance, for the true reflectance of a glossy surface, because for a glossy surface AM1.5GV reference reflectance (based on 42° incidence) can be up to 0.015 higher than AM1.5GV laboratory reflectance (based on near-normal incidence).

Applicability of AM1.5GV solar reflectance by wall orientation

East and west walls. The preceding analysis indicates that for east and west walls, the magnitude of type A (spectral) and type B (angular) errors in solar heat gain does not exceed 9%, and the magnitude of type A and type B errors in reflectance rise does not exceed 6.6%. The magnitude of Type C error in solar heat gain can reach 14.4% in on Dec 21, but the magnitude of type C error in reflectance rise does not exceed 2.6%. This suggests that the AM1.5GV solar reflectance is suited to east and west walls.

South walls. The preceding analysis indicates that for south walls, the magnitude of type A (spectral) error in solar heat gain does not exceed 9%, and the magnitude of type A error in reflectance rise does not exceed 6.2%. The magnitude of type B (angular) error in solar heat gain can reach 19.2% on Jun 21, and the magnitude of type B error in reflectance rise can reach 16.3% in summer. The magnitude of type C (spectral + angular) error in solar heat gain can reach 12.6% on Jun 21, and the magnitude of type C error in reflectance rise can reach 23.1% in summer. The low type A and large type B and C errors in summer reflectance rise suggest that the AM1.5GV solar reflectance is suited to matte, but not glossy, south walls.

North walls. The preceding analysis indicates that for north walls, the magnitude of type A error in solar heat gain does not exceed 9%, but the magnitude of type A (spectral) error reflectance rise can be reach 11.2% in summer. The magnitude of type B (angular) error in solar heat gain can reach 12.0% on Jun 21, and the magnitude of type B error in reflectance rise can reach 10.8% in winter. The magnitude of type C (spectral + angular) error in solar heat gain can reach 13.3% on Jun 21, and the magnitude of type C error in reflectance rise can reach 15.8% in winter. The large type A, B, and C errors in reflectance rise suggest that the AM1.5GV solar reflectance may not be suited to north walls.

However, two mitigating factors may increase the applicability of AM1.5GV solar reflectance to south and north walls. First, the ideal selective black and gray surfaces are much more selective than real cool colors. For example, a real selective gray is likely to have selectance $r_N - r_V = 0.60 - 0.20 = 0.40$, which is 43% smaller than that of the ideal selective gray ($r_N - r_V = 0.90 - 0.20 = 0.70$). This suggests that type A (spectral) errors may be about 40% smaller for actual wall products. Second, Table 4 shows that the measured solar specular reflectance from even the "glossiest" wall products tested (specimens 6-9, factory applied coatings on metal) did not exceed 0.026, which is 32% smaller than that observed from the truly "glossy" black-undercoated glass surface with a 0.042 solar specular reflectance. This suggests that type B (angular) errors may be about 1/3 smaller for actual wall products.

Conclusions

We recommend the use of the AM1.5GV solar reflectance metric for east and west walls. It may also be used for matte south walls. It is not well suited to fully glossy south walls, fully glossy north walls, or highly selective north walls.

Table 1. Comparison of solar angles, solar irradiances, and solar reflectances associated with two wall solar irradiances: (a) G197-14 AM1.5 global tilt irradiance on a sun-facing wall, and (b) peak global irradiance on a sun-facing wall.

	(a) G197	(b) peak	difference (G197 - peak)
solar azimuth angle (°)	0	0	0
solar altitude angle (°)	41.8	32.0	9.76
solar beam incidence angle (°)	41.8	32.0	9.76
global tilt irradiance (W/m²)	807.	837.	-30.0
diffuse tilt irradiance (W/m²)	143.	133.	10.9
beam tilt irradiance (W/m²)	664.	704.	-40.8
NIR fraction	0.533	0.547	-0.0134
diffuse fraction	0.178	0.158	0.0193
glossy nonselective black reflectance	0.0550	0.0499	0.00510
glossy nonselective gray reflectance	0.213	0.208	0.00425
glossy nonselective white reflectance	0.902	0.901	0.000532
glossy selective black reflectance	0.507	0.516	-0.00884
glossy selective gray reflectance	0.580	0.587	-0.00710
glossy selective white reflectance	0.450	0.435	0.0145
matte nonselective black reflectance	0.0400	0.0400	0
matte nonselective gray reflectance	0.200	0.200	0
matte nonselective white reflectance	0.900	0.900	0
matte selective black reflectance	0.499	0.510	-0.0116
matte selective gray reflectance	0.573	0.583	-0.00942
matte selective white reflectance	0.441	0.430	0.0116

Table 2. Laboratory, reference, and daily solar reflectances; daily solar heat gain; underestimations by reference reflectance of instantaneous and daily solar reflectances; and underestimations by reference reflectance of instantaneous and daily solar heat gains, shown for seven ideal wall surfaces at latitude 37°N. Values are reported on (a) Mar 21, (b) Jun 21, (c) Sep 21, and (d) Dec 21 for (i) east, (ii) west, (iii) south, and (iv) north walls.

(a–i) March, east							
	glossy nonselective black	glossy nonselective gray	glossy nonselective white	glossy selective black	glossy selective gray	matte selective black	matte selective gray
laboratory reflectance	0.040	0.200	0.900	0.499	0.573	0.499	0.573
reference reflectance	0.055	0.213	0.902	0.507	0.580	0.499	0.573
daily reflectance	0.082	0.235	0.904	0.541	0.609	0.518	0.589
daily gain (kWh/m²)	516	430	53.8	258	220	271	231
underestimation of reflectance	-0.008 to 0.227	-0.006 to 0.189	-0.001 to 0.024	-0.021 to 0.295	-0.016 to 0.240	-0.042 to 0.296	-0.034 to 0.241
underestimation of daily reflectance	0.027	0.023	0.003	0.034	0.028	0.020	0.016
overestimation of gain (W/m²)	-5.2 to 59.0	-4.4 to 49.2	-0.5 to 6.2	-2.5 to 67.4	-1.9 to 54.8	-5.2 to 69.1	-4.3 to 56.3
overestimation of daily gain (kWh/m²)	15.4	12.9	1.61	19.3	16	11.1	9.01
fractional overestimation of daily gain (%)	3.0	3.0	3.0	7.5	7.3	4.1	3.9

(a–ii) March, west							
	glossy nonselective black	glossy nonselective gray	glossy nonselective white	glossy selective black	glossy selective gray	matte selective black	matte selective gray
laboratory reflectance	0.040	0.200	0.900	0.499	0.573	0.499	0.573
reference reflectance	0.055	0.213	0.902	0.507	0.580	0.499	0.573
daily reflectance	0.082	0.235	0.904	0.541	0.609	0.519	0.590
daily gain (kWh/m²)	517	431	53.9	259	221	271	231
underestimation of reflectance	-0.008 to 0.227	-0.006 to 0.189	-0.001 to 0.024	-0.021 to 0.296	-0.016 to 0.241	-0.042 to 0.297	-0.034 to 0.241
underestimation of daily reflectance	0.027	0.023	0.003	0.034	0.028	0.020	0.016
overestimation of gain (W/m²)	-5.2 to 59.1	-4.4 to 49.2	-0.5 to 6.2	-2.5 to 67.4	-1.9 to 54.8	-5.2 to 69.2	-4.3 to 56.3
overestimation of daily gain (kWh/m²)	15.4	12.8	1.61	19.3	16	11.1	9.05
fractional overestimation of daily gain (%)	3.0	3.0	3.0	7.5	7.3	4.1	3.9

(a–iii) March, south							
	glossy nonselective black	glossy nonselective gray	glossy nonselective white	glossy selective black	glossy selective gray	matte selective black	matte selective gray
laboratory reflectance	0.040	0.200	0.900	0.499	0.573	0.499	0.573
reference reflectance	0.055	0.213	0.902	0.507	0.580	0.499	0.573
daily reflectance	0.110	0.258	0.907	0.533	0.602	0.498	0.573
daily gain (kWh/m²)	658	549	68.6	346	294	371	316
underestimation of reflectance	0.016 to 0.295	0.014 to 0.246	0.002 to 0.031	0.000 to 0.157	0.001 to 0.133	-0.008 to 0.099	-0.007 to 0.081
underestimation of daily reflectance	0.055	0.046	0.006	0.026	0.022	-0.001	-0.001
overestimation of gain (W/m²)	0.4 to 40.4	0.4 to 33.7	0.0 to 4.2	0.3 to 23.4	0.5 to 19.8	-5.8 to 4.9	-4.8 to 4.0
overestimation of daily gain (kWh/m²)	40.7	33.9	4.24	19.2	16.4	-0.584	-0.475
fractional overestimation of daily gain (%)	6.2	6.2	6.2	5.5	5.6	-0.2	-0.2

(a–iv) March, north							
	glossy nonselective black	glossy nonselective gray	glossy nonselective white	glossy selective black	glossy selective gray	matte selective black	matte selective gray
laboratory reflectance	0.040	0.200	0.900	0.499	0.573	0.499	0.573
reference reflectance	0.055	0.213	0.902	0.507	0.580	0.499	0.573
daily reflectance	0.092	0.243	0.905	0.482	0.560	0.452	0.535
daily gain (kWh/m²)	153	128	16	87.4	74.1	92.4	78.3
underestimation of reflectance	0.037 to 0.088	0.031 to 0.073	0.004 to 0.009	-0.056 to 0.142	-0.045 to 0.117	-0.079 to 0.123	-0.064 to 0.100
underestimation of daily reflectance	0.037	0.031	0.004	-0.025	-0.020	-0.047	-0.038
overestimation of gain (W/m²)	0.5 to 5.1	0.4 to 4.2	0.1 to 0.5	-3.3 to 1.8	-2.6 to 1.5	-5.3 to 1.6	-4.3 to 1.3
overestimation of daily gain (kWh/m²)	6.22	5.18	0.648	-4.25	-3.34	-7.88	-6.41
fractional overestimation of daily gain (%)	4.1	4.1	4.1	-4.9	-4.5	-8.5	-8.2

(b–i) June, east							
	glossy nonselective black	glossy nonselective gray	glossy nonselective white	glossy selective black	glossy selective gray	matte selective black	matte selective gray
laboratory reflectance	0.040	0.200	0.900	0.499	0.573	0.499	0.573
reference reflectance	0.055	0.213	0.902	0.507	0.580	0.499	0.573
daily reflectance	0.080	0.233	0.904	0.533	0.602	0.511	0.584
daily gain (kWh/m²)	674	562	70.3	343	292	358	305
underestimation of reflectance	-0.007 to 0.217	-0.006 to 0.181	-0.001 to 0.023	-0.026 to 0.289	-0.020 to 0.236	-0.047 to 0.289	-0.038 to 0.236
underestimation of daily reflectance	0.025	0.021	0.003	0.026	0.022	0.012	0.010
overestimation of gain (W/m²)	-5.2 to 62.0	-4.3 to 51.7	-0.5 to 6.5	-2.3 to 61.2	-1.8 to 49.8	-7.3 to 62.7	-6.0 to 51.0
overestimation of daily gain (kWh/m²)	18.4	15.3	1.92	19	15.8	9.07	7.38
fractional overestimation of daily gain (%)	2.7	2.7	2.7	5.5	5.4	2.5	2.4

(b–ii) June, west							
	glossy nonselective black	glossy nonselective gray	glossy nonselective white	glossy selective black	glossy selective gray	matte selective black	matte selective gray
laboratory reflectance	0.040	0.200	0.900	0.499	0.573	0.499	0.573
reference reflectance	0.055	0.213	0.902	0.507	0.580	0.499	0.573
daily reflectance	0.080	0.233	0.904	0.533	0.602	0.511	0.584
daily gain (kWh/m²)	675	562	70.3	343	292	358	305
underestimation of reflectance	-0.007 to 0.217	-0.006 to 0.181	-0.001 to 0.023	-0.025 to 0.291	-0.020 to 0.237	-0.047 to 0.291	-0.038 to 0.237
underestimation of daily reflectance	0.025	0.021	0.003	0.026	0.022	0.012	0.010
overestimation of gain (W/m²)	-5.2 to 62.0	-4.3 to 51.7	-0.5 to 6.5	-2.3 to 61.4	-1.8 to 49.9	-7.3 to 62.9	-6.0 to 51.2
overestimation of daily gain (kWh/m²)	18.4	15.3	1.92	19	15.8	9.11	7.42
fractional overestimation of daily gain (%)	2.7	2.7	2.7	5.6	5.4	2.5	2.4

(b–iii) June, south							
	glossy nonselective black	glossy nonselective gray	glossy nonselective white	glossy selective black	glossy selective gray	matte selective black	matte selective gray
laboratory reflectance	0.040	0.200	0.900	0.499	0.573	0.499	0.573
reference reflectance	0.055	0.213	0.902	0.507	0.580	0.499	0.573
daily reflectance	0.207	0.339	0.917	0.561	0.627	0.471	0.551
daily gain (kWh/m²)	305	254	31.7	169	143	203	173
underestimation of reflectance	0.037 to 0.228	0.031 to 0.190	0.004 to 0.024	-0.050 to 0.098	-0.040 to 0.084	-0.072 to 0.055	-0.059 to 0.045
underestimation of daily reflectance	0.152	0.127	0.016	0.054	0.047	-0.028	-0.022
overestimation of gain (W/m²)	0.3 to 60.9	0.2 to 50.8	0.0 to 6.3	-3.6 to 26.7	-2.8 to 22.9	-7.2 to 0.4	-5.9 to 0.3
overestimation of daily gain (kWh/m²)	58.6	48.8	6.1	20.7	18	-10.6	-8.61
fractional overestimation of daily gain (%)	19.2	19.2	19.2	12.3	12.6	-5.2	-5.0

(b–iv) June, north							
	glossy nonselective black	glossy nonselective gray	glossy nonselective white	glossy selective black	glossy selective gray	matte selective black	matte selective gray
laboratory reflectance	0.040	0.200	0.900	0.499	0.573	0.499	0.573
reference reflectance	0.055	0.213	0.902	0.507	0.580	0.499	0.573
daily reflectance	0.157	0.297	0.912	0.565	0.629	0.507	0.580
daily gain (kWh/m²)	304	254	31.7	157	134	178	151
underestimation of reflectance	0.035 to 0.249	0.029 to 0.207	0.004 to 0.026	-0.025 to 0.276	-0.020 to 0.225	-0.046 to 0.272	-0.038 to 0.221
underestimation of daily reflectance	0.102	0.085	0.011	0.058	0.049	0.009	0.007
overestimation of gain (W/m²)	1.6 to 49.2	1.3 to 41.0	0.2 to 5.1	-3.1 to 31.7	-2.4 to 26.0	-5.7 to 29.0	-4.6 to 23.6
overestimation of daily gain (kWh/m²)	36.6	30.5	3.82	20.9	17.7	3.08	2.51
fractional overestimation of daily gain (%)	12.0	12.0	12.0	13.3	13.3	1.7	1.7

(c–i) September, east							
	glossy nonselective black	glossy nonselective gray	glossy nonselective white	glossy selective black	glossy selective gray	matte selective black	matte selective gray
laboratory reflectance	0.040	0.200	0.900	0.499	0.573	0.499	0.573
reference reflectance	0.055	0.213	0.902	0.507	0.580	0.499	0.573
daily reflectance	0.082	0.235	0.904	0.541	0.609	0.519	0.590
daily gain (kWh/m²)	515	429	53.6	257	219	270	230
underestimation of reflectance	-0.008 to 0.227	-0.006 to 0.189	-0.001 to 0.024	-0.021 to 0.298	-0.017 to 0.242	-0.042 to 0.298	-0.035 to 0.243
underestimation of daily reflectance	0.027	0.023	0.003	0.035	0.029	0.020	0.016
overestimation of gain (W/m²)	-5.2 to 59.0	-4.4 to 49.2	-0.5 to 6.1	-2.5 to 67.3	-1.9 to 54.7	-5.2 to 69.0	-4.3 to 56.2
overestimation of daily gain (kWh/m²)	15.4	12.8	1.6	19.4	16.1	11.2	9.09
fractional overestimation of daily gain (%)	3.0	3.0	3.0	7.5	7.3	4.1	3.9

(c–ii) September, west							
	glossy nonselective black	glossy nonselective gray	glossy nonselective white	glossy selective black	glossy selective gray	matte selective black	matte selective gray
laboratory reflectance	0.040	0.200	0.900	0.499	0.573	0.499	0.573
reference reflectance	0.055	0.213	0.902	0.507	0.580	0.499	0.573
daily reflectance	0.083	0.235	0.904	0.541	0.609	0.519	0.590
daily gain (kWh/m²)	513	428	53.5	257	219	269	230
underestimation of reflectance	-0.008 to 0.227	-0.006 to 0.189	-0.001 to 0.024	-0.021 to 0.298	-0.016 to 0.242	-0.042 to 0.298	-0.035 to 0.242
underestimation of daily reflectance	0.028	0.023	0.003	0.035	0.029	0.020	0.016
overestimation of gain (W/m²)	-5.2 to 59.0	-4.3 to 49.2	-0.5 to 6.1	-2.5 to 67.3	-1.9 to 54.7	-5.2 to 69.0	-4.3 to 56.2
overestimation of daily gain (kWh/m²)	15.4	12.8	1.61	19.3	16	11.1	9.06
fractional overestimation of daily gain (%)	3.0	3.0	3.0	7.5	7.3	4.1	3.9

(c–iii) September, south							
	glossy nonselective black	glossy nonselective gray	glossy nonselective white	glossy selective black	glossy selective gray	matte selective black	matte selective gray
laboratory reflectance	0.040	0.200	0.900	0.499	0.573	0.499	0.573
reference reflectance	0.055	0.213	0.902	0.507	0.580	0.499	0.573
daily reflectance	0.109	0.257	0.907	0.533	0.602	0.498	0.573
daily gain (kWh/m²)	663	552	69	348	296	373	317
underestimation of reflectance	0.016 to 0.295	0.013 to 0.246	0.002 to 0.031	0.000 to 0.160	0.001 to 0.136	-0.008 to 0.112	-0.007 to 0.091
underestimation of daily reflectance	0.054	0.045	0.006	0.026	0.022	-0.000	-0.000
overestimation of gain (W/m²)	0.4 to 39.9	0.3 to 33.3	0.0 to 4.2	0.2 to 23.5	0.4 to 19.9	-5.7 to 5.3	-4.7 to 4.3
overestimation of daily gain (kWh/m²)	40	33.4	4.17	19.1	16.3	-0.228	-0.186
fractional overestimation of daily gain (%)	6.0	6.0	6.0	5.5	5.5	-0.1	-0.1

(c–iv) September, north							
	glossy nonselective black	glossy nonselective gray	glossy nonselective white	glossy selective black	glossy selective gray	matte selective black	matte selective gray
laboratory reflectance	0.040	0.200	0.900	0.499	0.573	0.499	0.573
reference reflectance	0.055	0.213	0.902	0.507	0.580	0.499	0.573
daily reflectance	0.092	0.243	0.905	0.482	0.560	0.452	0.535
daily gain (kWh/m²)	152	127	15.9	87	73.8	92	78
underestimation of reflectance	0.037 to 0.073	0.031 to 0.061	0.004 to 0.008	-0.055 to 0.145	-0.044 to 0.119	-0.079 to 0.129	-0.064 to 0.105
underestimation of daily reflectance	0.037	0.031	0.004	-0.025	-0.020	-0.047	-0.038
overestimation of gain (W/m²)	0.5 to 5.1	0.4 to 4.2	0.0 to 0.5	-3.3 to 1.7	-2.6 to 1.4	-5.3 to 1.5	-4.3 to 1.3
overestimation of daily gain (kWh/m²)	6.18	5.15	0.644	-4.23	-3.33	-7.84	-6.38
fractional overestimation of daily gain (%)	4.1	4.1	4.1	-4.9	-4.5	-8.5	-8.2

(d–i) December, east							
	glossy nonselective black	glossy nonselective gray	glossy nonselective white	glossy selective black	glossy selective gray	matte selective black	matte selective gray
laboratory reflectance	0.040	0.200	0.900	0.499	0.573	0.499	0.573
reference reflectance	0.055	0.213	0.902	0.507	0.580	0.499	0.573
daily reflectance	0.103	0.253	0.907	0.569	0.632	0.537	0.604
daily gain (kWh/m²)	261	217	27.1	125	107	135	115
underestimation of reflectance	-0.004 to 0.253	-0.003 to 0.211	-0.000 to 0.026	-0.039 to 0.288	-0.031 to 0.234	-0.061 to 0.288	-0.050 to 0.234
underestimation of daily reflectance	0.048	0.040	0.005	0.062	0.051	0.038	0.031
overestimation of gain (W/m²)	-1.2 to 50.1	-1.0 to 41.7	-0.1 to 5.2	-3.7 to 55.7	-3.0 to 45.3	-5.9 to 56.6	-4.8 to 46.1
overestimation of daily gain (kWh/m²)	14.1	11.7	1.46	18	15	11	8.95
fractional overestimation of daily gain (%)	5.4	5.4	5.4	14.4	14.0	8.2	7.8

(d–ii) December, west							
	glossy nonselective black	glossy nonselective gray	glossy nonselective white	glossy selective black	glossy selective gray	matte selective black	matte selective gray
laboratory reflectance	0.040	0.200	0.900	0.499	0.573	0.499	0.573
reference reflectance	0.055	0.213	0.902	0.507	0.580	0.499	0.573
daily reflectance	0.103	0.253	0.907	0.569	0.632	0.536	0.604
daily gain (kWh/m²)	260	217	27.1	125	107	135	115
underestimation of reflectance	-0.004 to 0.253	-0.003 to 0.211	-0.000 to 0.026	-0.038 to 0.285	-0.031 to 0.232	-0.061 to 0.286	-0.049 to 0.233
underestimation of daily reflectance	0.048	0.040	0.005	0.062	0.051	0.038	0.031
overestimation of gain (W/m²)	-1.2 to 50.1	-1.0 to 41.8	-0.1 to 5.2	-3.7 to 55.6	-3.0 to 45.3	-5.9 to 56.6	-4.8 to 46.1
overestimation of daily gain (kWh/m²)	14.1	11.7	1.46	18	14.9	10.9	8.87
fractional overestimation of daily gain (%)	5.4	5.4	5.4	14.3	13.9	8.1	7.7

(d–iii) December, south							
	glossy nonselective black	glossy nonselective gray	glossy nonselective white	glossy selective black	glossy selective gray	matte selective black	matte selective gray
laboratory reflectance	0.040	0.200	0.900	0.499	0.573	0.499	0.573
reference reflectance	0.055	0.213	0.902	0.507	0.580	0.499	0.573
daily reflectance	0.054	0.212	0.901	0.547	0.613	0.540	0.607
daily gain (kWh/m²)	754	629	78.6	361	309	367	313
underestimation of reflectance	-0.006 to 0.036	-0.005 to 0.030	-0.001 to 0.004	0.013 to 0.272	0.010 to 0.222	0.016 to 0.267	0.013 to 0.217
underestimation of daily reflectance	-0.001	-0.001	-0.000	0.040	0.033	0.041	0.034
overestimation of gain (W/m²)	-4.8 to 4.6	-4.0 to 3.8	-0.5 to 0.5	10.5 to 41.0	8.4 to 33.5	13.1 to 39.8	10.6 to 32.4
overestimation of daily gain (kWh/m²)	-0.829	-0.691	-0.0864	32.1	26.1	33.1	26.9
fractional overestimation of daily gain (%)	-0.1	-0.1	-0.1	8.9	8.5	9.0	8.6

(d–iv) December, north							
	glossy nonselective black	glossy nonselective gray	glossy nonselective white	glossy selective black	glossy selective gray	matte selective black	matte selective gray
laboratory reflectance	0.040	0.200	0.900	0.499	0.573	0.499	0.573
reference reflectance	0.055	0.213	0.902	0.507	0.580	0.499	0.573
daily reflectance	0.092	0.243	0.905	0.483	0.561	0.453	0.536
daily gain (kWh/m²)	89.6	74.7	9.34	51.1	43.3	54	45.8
underestimation of reflectance	0.037 to 0.037	0.031 to 0.031	0.004 to 0.004	-0.042 to 0.043	-0.034 to 0.036	-0.065 to 0.025	-0.053 to 0.021
underestimation of daily reflectance	0.037	0.031	0.004	-0.024	-0.019	-0.046	-0.037
overestimation of gain (W/m²)	0.3 to 3.9	0.3 to 3.2	0.0 to 0.4	-2.1 to 0.4	-1.6 to 0.3	-4.2 to 0.2	-3.4 to 0.2
overestimation of daily gain (kWh/m²)	3.63	3.02	0.378	-2.39	-1.87	-4.5	-3.67
fractional overestimation of daily gain (%)	4.0	4.0	4.0	-4.7	-4.3	-8.3	-8.0

Table 3. Rises in laboratory, reference, and daily solar reflectances, and overestimations of rises in solar reflectance when substituting laboratory or reference solar reflectance for daily solar reflectance, by wall direction (E, W, S, N) and season (summer = Jun/Jul/Aug, winter = Dec/Jan/Feb), at latitude 37°N. Values are shown for upgrading a *glossy* surface (a) from nonselective black to nonselective white, (b) from nonselective gray to nonselective white, (c) from nonselective black to selective black, and (d) from nonselective gray to selective gray; and for upgrading a *matte* surface (e) from nonselective black to selective black, and (f) from nonselective gray to selective gray.

(a) glossy: nonselective black to nonselective white								
	E/summer	E/winter	W/summer	W/winter	S/summer	S/winter	N/summer	N/winter
rise in laboratory reflectance	0.860	0.860	0.860	0.860	0.860	0.860	0.860	0.860
rise in reference reflectance	0.847	0.847	0.847	0.847	0.847	0.847	0.847	0.847
rise in daily reflectance	0.824	0.809	0.824	0.809	0.728	0.841	0.764	0.814
refl. rise overestimation using lab reflectance (%)	4.3	6.3	4.3	6.3	18.2	2.3	12.5	5.7
refl. rise overestimation using ref. reflectance (%)	2.7	4.6	2.7	4.6	16.3	0.7	10.8	4.0

(b) glossy: nonselective gray to nonselective white								
	E/summer	E/winter	W/summer	W/winter	S/summer	S/winter	N/summer	N/winter
rise in laboratory reflectance	0.700	0.700	0.700	0.700	0.700	0.700	0.700	0.700
rise in reference reflectance	0.689	0.689	0.689	0.689	0.689	0.689	0.689	0.689
rise in daily reflectance	0.671	0.659	0.671	0.659	0.592	0.684	0.622	0.662
refl. rise overestimation using lab reflectance (%)	4.3	6.3	4.3	6.3	18.2	2.3	12.5	5.7
refl. rise overestimation using ref. reflectance (%)	2.7	4.6	2.7	4.6	16.3	0.7	10.8	4.0

(c) glossy: nonselective black to selective black								
	E/summer	E/winter	W/summer	W/winter	S/summer	S/winter	N/summer	N/winter
rise in laboratory reflectance	0.459	0.459	0.459	0.459	0.459	0.459	0.459	0.459
rise in reference reflectance	0.452	0.452	0.452	0.452	0.452	0.452	0.452	0.452
rise in daily reflectance	0.454	0.464	0.454	0.464	0.367	0.478	0.399	0.390
refl. rise overestimation using lab reflectance (%)	1.0	-1.1	1.1	-1.1	25.0	-4.0	15.0	17.6
refl. rise overestimation using ref. reflectance (%)	-0.5	-2.6	-0.5	-2.6	23.1	-5.5	13.2	15.8

(d) glossy: nonselective gray to selective gray								
	E/summer	E/winter	W/summer	W/winter	S/summer	S/winter	N/summer	N/winter
rise in laboratory reflectance	0.373	0.373	0.373	0.373	0.373	0.373	0.373	0.373
rise in reference reflectance	0.368	0.368	0.368	0.368	0.368	0.368	0.368	0.368
rise in daily reflectance	0.370	0.378	0.370	0.378	0.299	0.389	0.325	0.318
refl. rise overestimation using lab reflectance (%)	1.0	-1.1	1.1	-1.1	25.0	-4.0	15.0	17.6
refl. rise overestimation using ref. reflectance (%)	-0.5	-2.6	-0.5	-2.6	23.1	-5.5	13.2	15.8

(e) matte: nonselective black to selective black								
	E/summer	E/winter	W/summer	W/winter	S/summer	S/winter	N/summer	N/winter
rise in laboratory reflectance	0.459	0.459	0.459	0.459	0.459	0.459	0.459	0.459
rise in reference reflectance	0.459	0.459	0.459	0.459	0.459	0.459	0.459	0.459
rise in daily reflectance	0.473	0.491	0.472	0.491	0.436	0.489	0.454	0.413
refl. rise overestimation using lab reflectance (%)	-2.9	-6.6	-2.9	-6.6	5.1	-6.2	1.1	11.2
refl. rise overestimation using ref. reflectance (%)	-2.9	-6.6	-2.9	-6.6	5.1	-6.2	1.1	11.2

(f) matte: nonselective gray to selective gray								
	E/summer	E/winter	W/summer	W/winter	S/summer	S/winter	N/summer	N/winter
rise in laboratory reflectance	0.373	0.373	0.373	0.373	0.373	0.373	0.373	0.373
rise in reference reflectance	0.373	0.373	0.373	0.373	0.373	0.373	0.373	0.373
rise in daily reflectance	0.385	0.400	0.385	0.400	0.355	0.398	0.370	0.336
refl. rise overestimation using lab reflectance (%)	-2.9	-6.6	-2.9	-6.6	5.1	-6.2	1.1	11.2
refl. rise overestimation using ref. reflectance (%)	-2.9	-6.6	-2.9	-6.6	5.1	-6.2	1.1	11.2

Table 4. Specular solar reflectance (specular component of air mass 1 global horizontal solar reflectance) of (1) a diffuse reflectance standard; (2) a specular reflectance standard (mirror); (3) an unbacked glass microscope slide; (4) the glass slide with an opaque black undercoating; (5) the black undercoating; and (6-20) an assortment of wall products. Nominal finish comes from the product label, while LBNL assessment of finish is visual.

#	Description	Color	Coating application	Substrate	Nominal finish	LBNL assessment of finish	Specular solar reflectance
1	Spectralon SRS-99 diffuse reflectance standard	white					0.001
2	Specular reflectance standard	silver					0.888
3	Unbacked glass slide	clear					0.079
4	Glass slide with opaque black paint undercoating, glass side forward	black	field	glass			0.042
5	Glass slide with opaque black paint undercoating, painted side forward	black	field	glass		semigloss	0.004
6	(redacted)	black	factory	metal		semigloss	0.018
7	(redacted)	light gray	factory	metal		semigloss	0.016
8	(redacted)	white	factory	metal		semigloss	0.018
9	(redacted)	dark brown	factory	metal		semigloss	0.023
10	(redacted)	white	factory	metal		semigloss	0.026
11	(redacted)	dark gray-blue	field	wood	semigloss	semigloss	0.020
12	(redacted)	white	field	wood	semigloss	semigloss	0.020
13	(redacted)	light brown	field	fiber cement	semigloss	semigloss	0.005
14	(redacted)	light brown	field	fiber cement	satin	satin	0.004
15	(redacted)	white	field	fiber cement	satin	satin	0.001
16	(redacted)	dark brown	field	wood		matte	0.001
17	(redacted)	light gray-green	field	wood		matte	0.005
18	(redacted)	peach	field	wood		matte	0.006
19	(redacted)	dark gray-green	field	metal		matte	0.000
20	(redacted)	peach	field	metal		matte	0.005

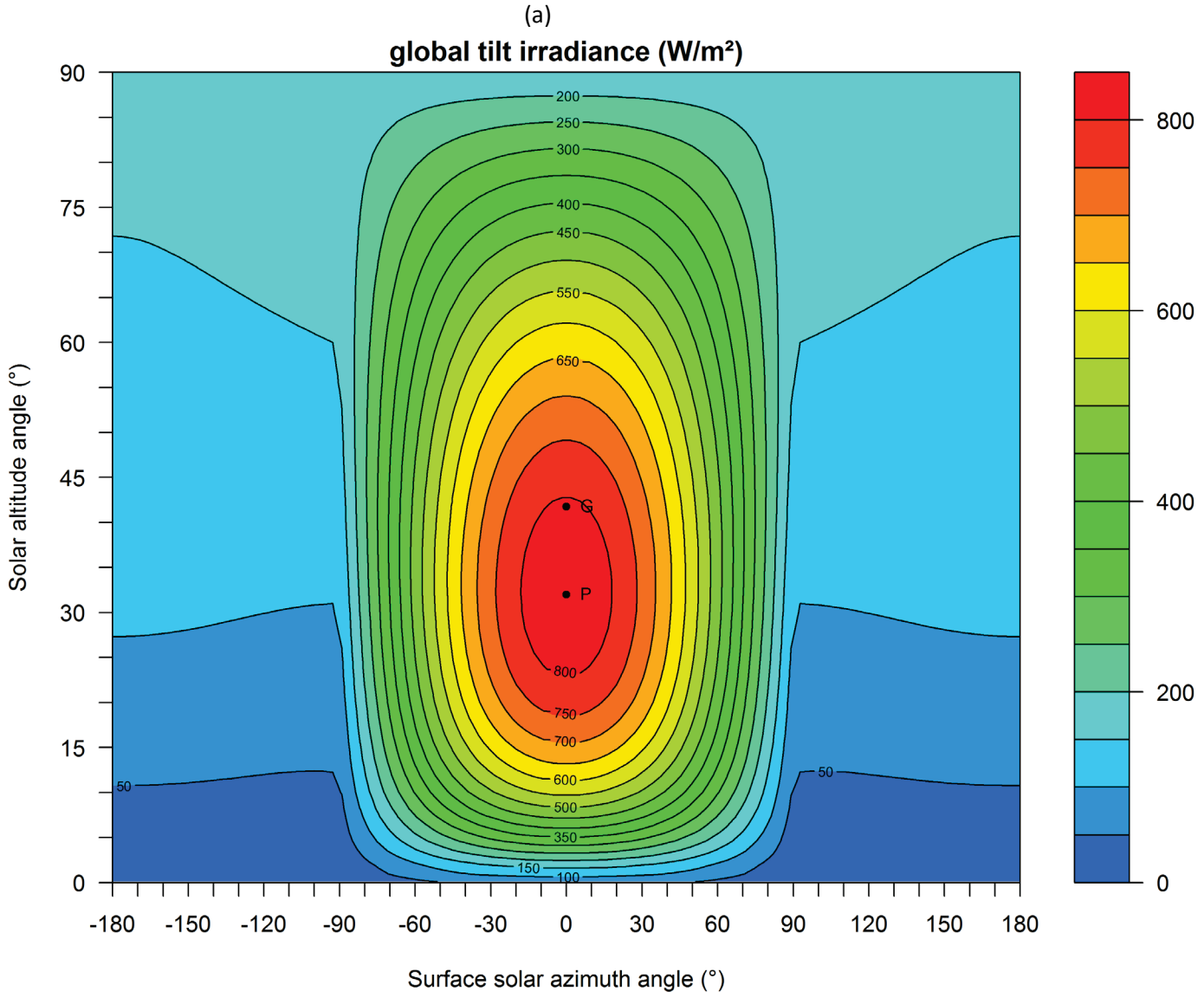

Figure 12. Variations with solar position of a wall's (a) global (beam + diffuse) tilt irradiance; (b) beam tilt irradiance; (c) diffuse tilt irradiance; (d) NIR fraction of global tilt irradiance; and (e) diffuse fraction of global tilt irradiance. Note that surface solar azimuth angle = solar azimuth angle – surface azimuth angle.

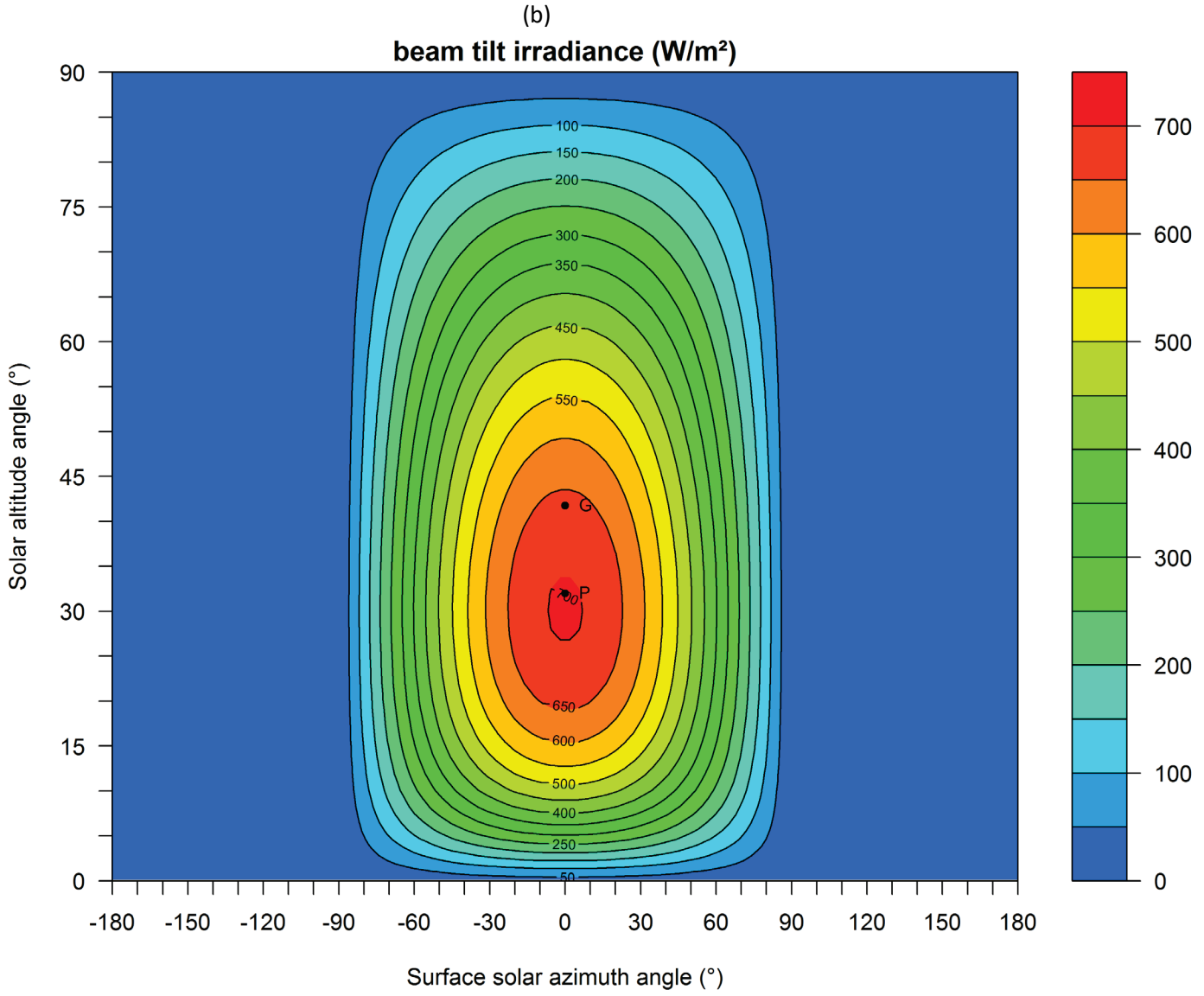

Figure 12 (continued)

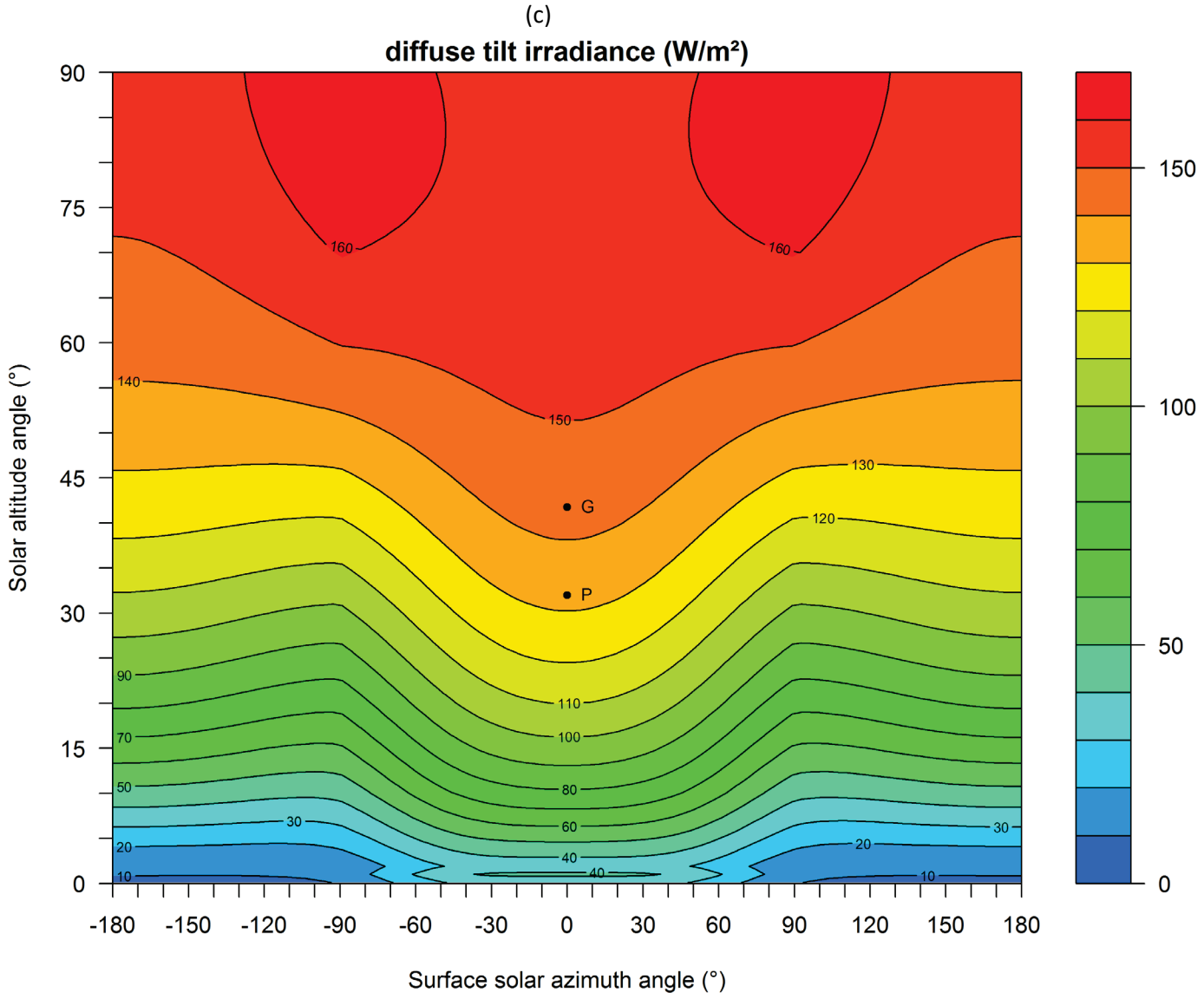

Figure 12 (continued)

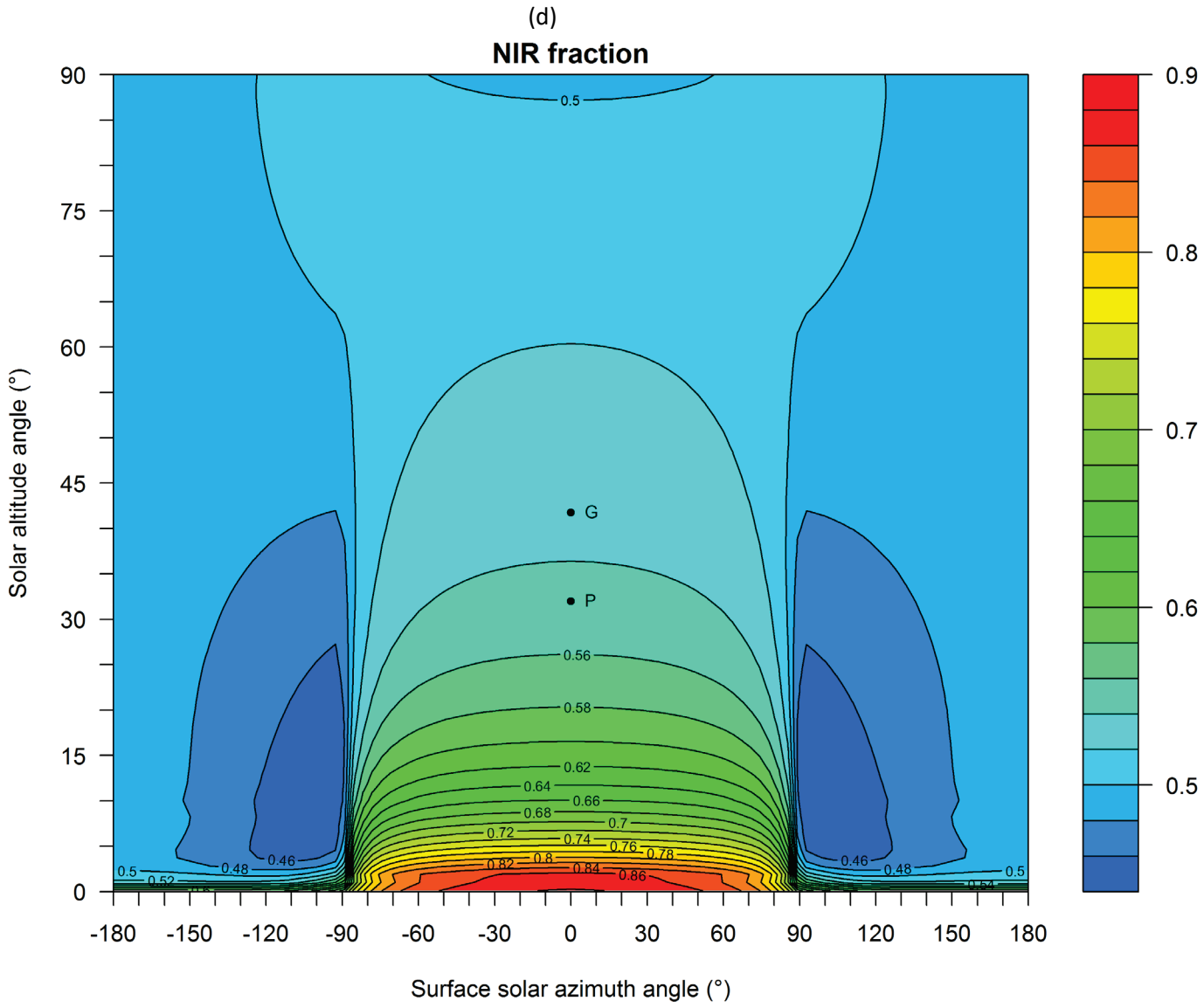

Figure 12 (continued)

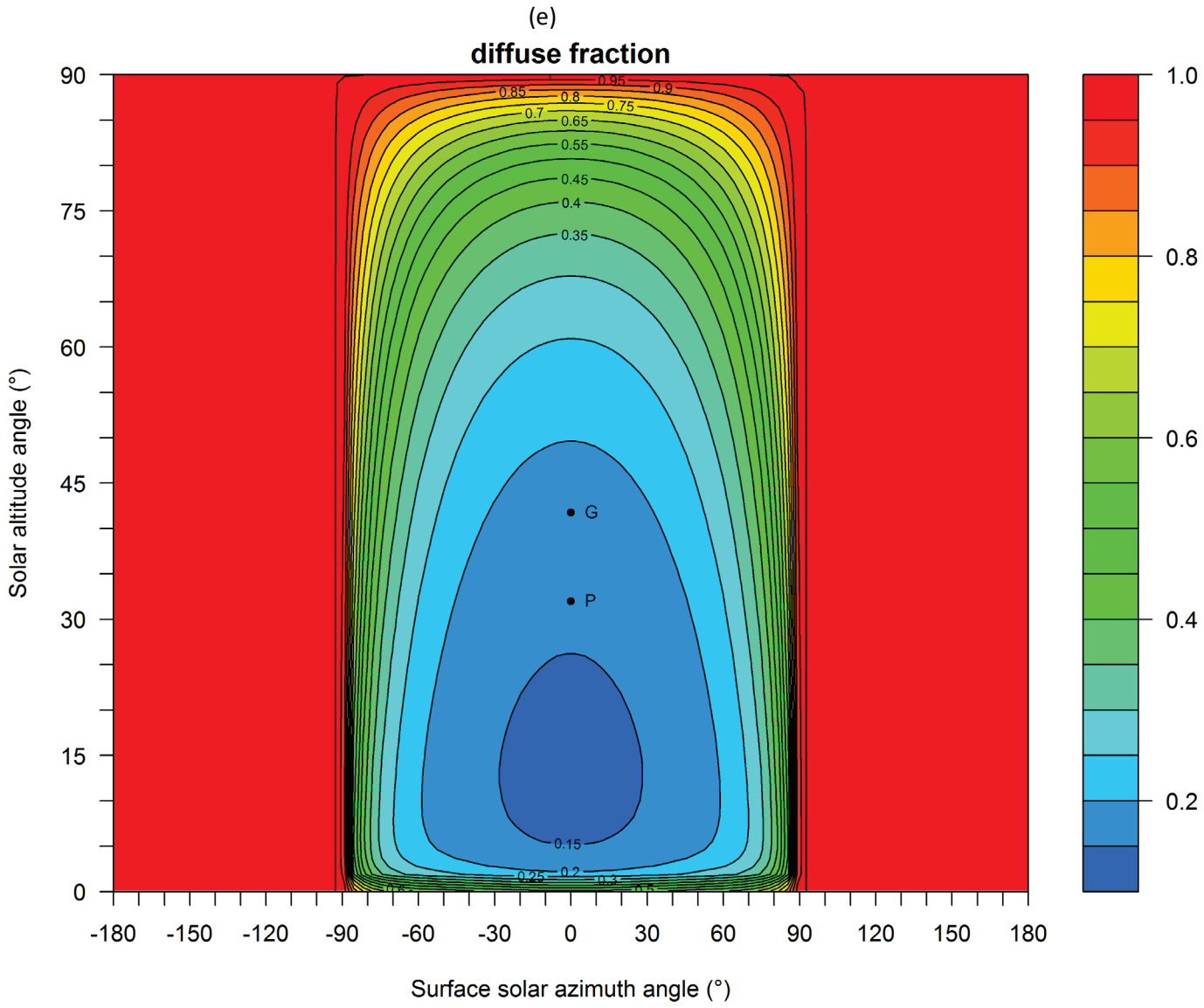

Figure 12 (continued)

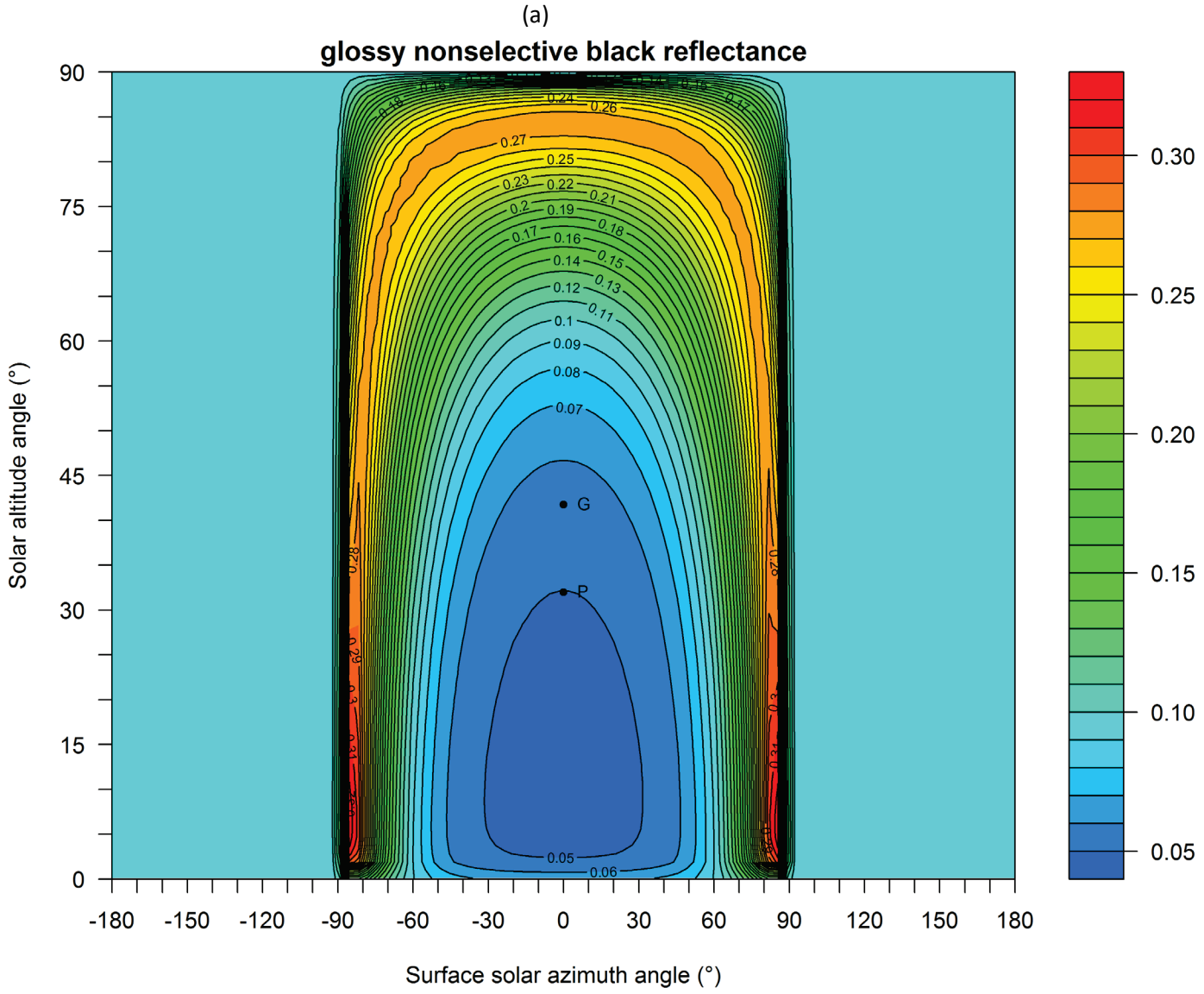

Figure 13. Variations with solar position of the global solar reflectances of seven ideal walls: (a) glossy nonselective black, (b) glossy nonselective gray; (c) glossy nonselective white; (d) glossy selective black; (e) glossy selective gray; (f) matte selective black; and (g) matte selective gray. Note that surface solar azimuth angle = solar azimuth angle – surface azimuth angle.

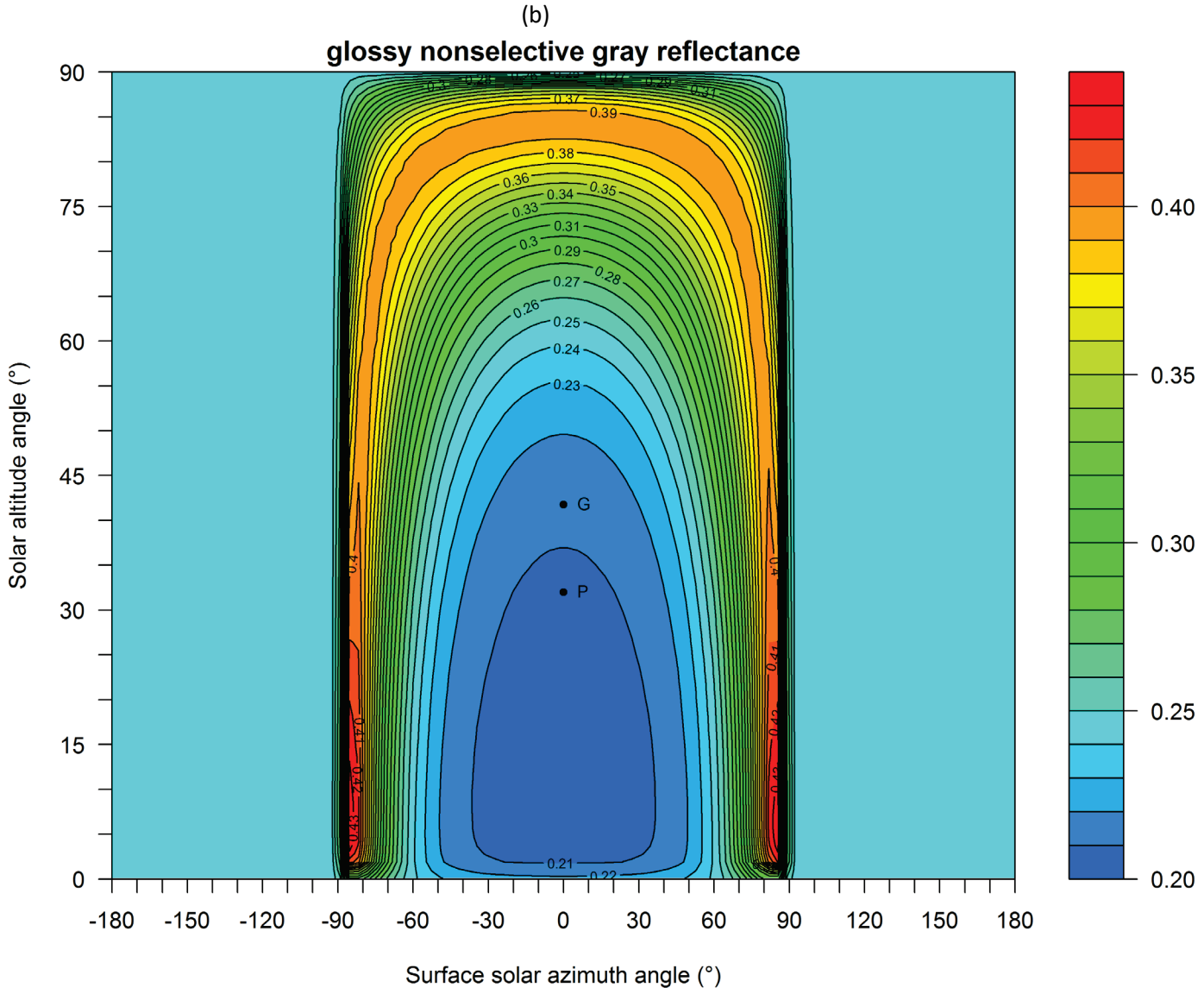

Figure 13 (continued)

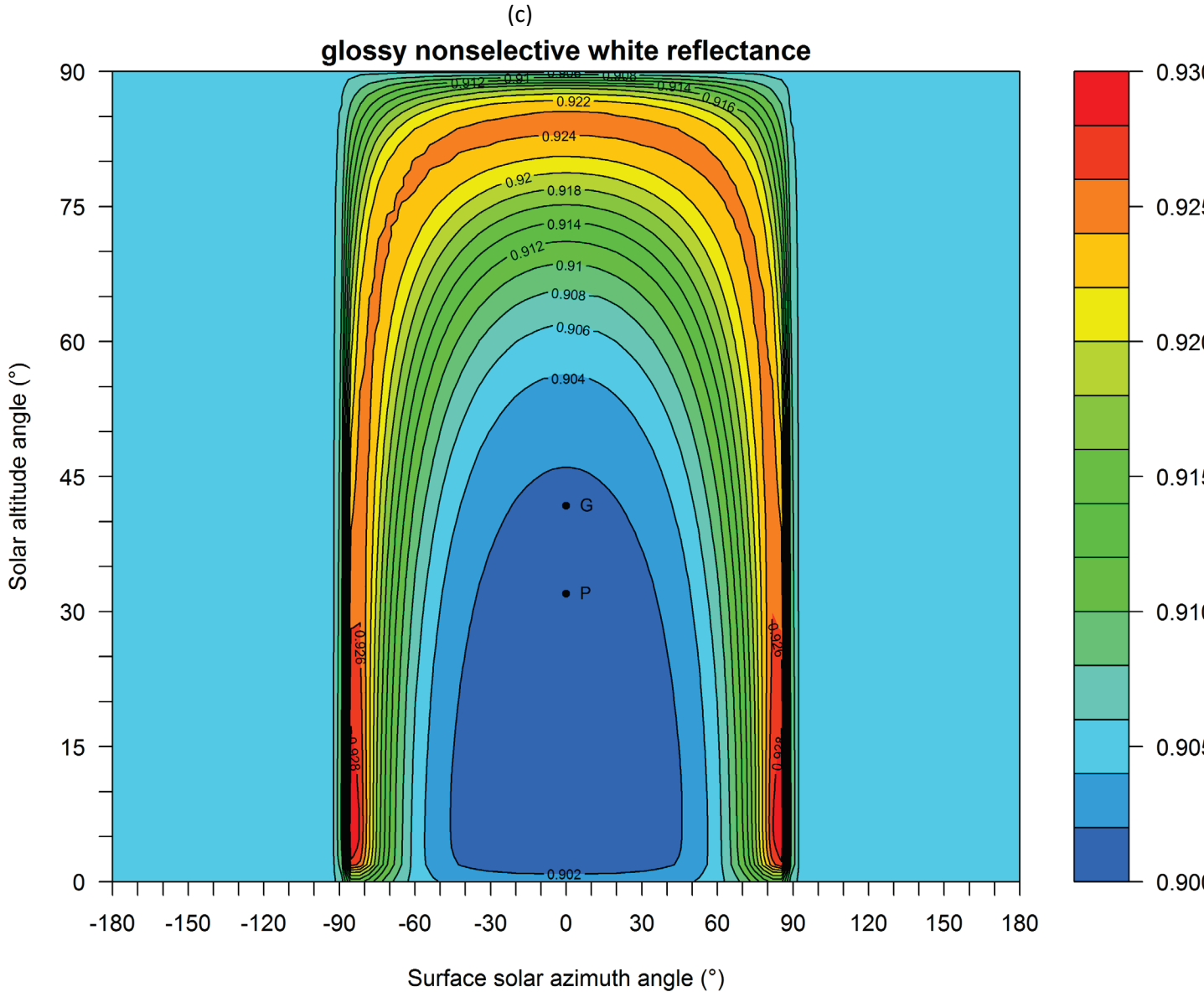

Figure 13 (continued)

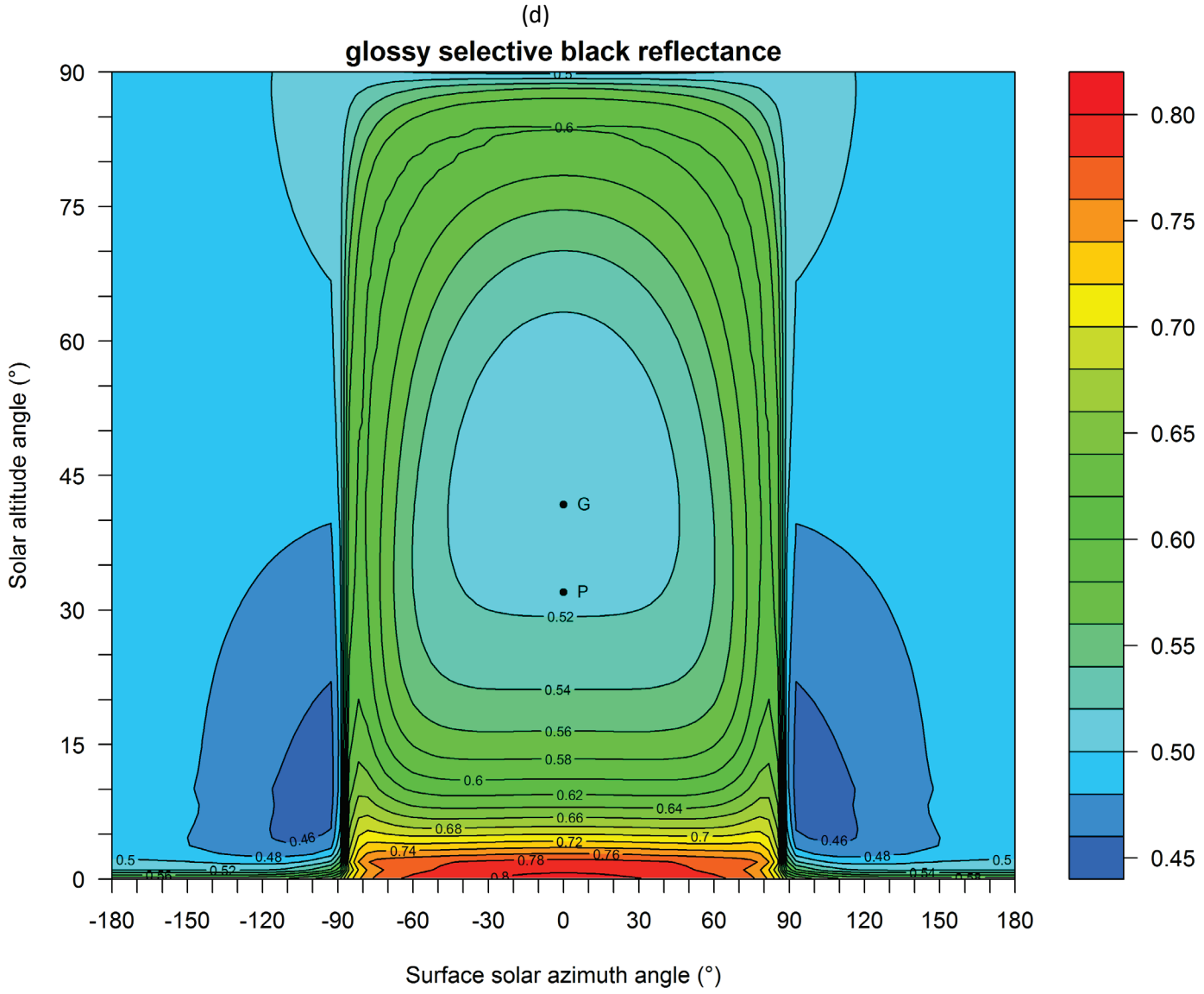

Figure 13 (continued)

(e)

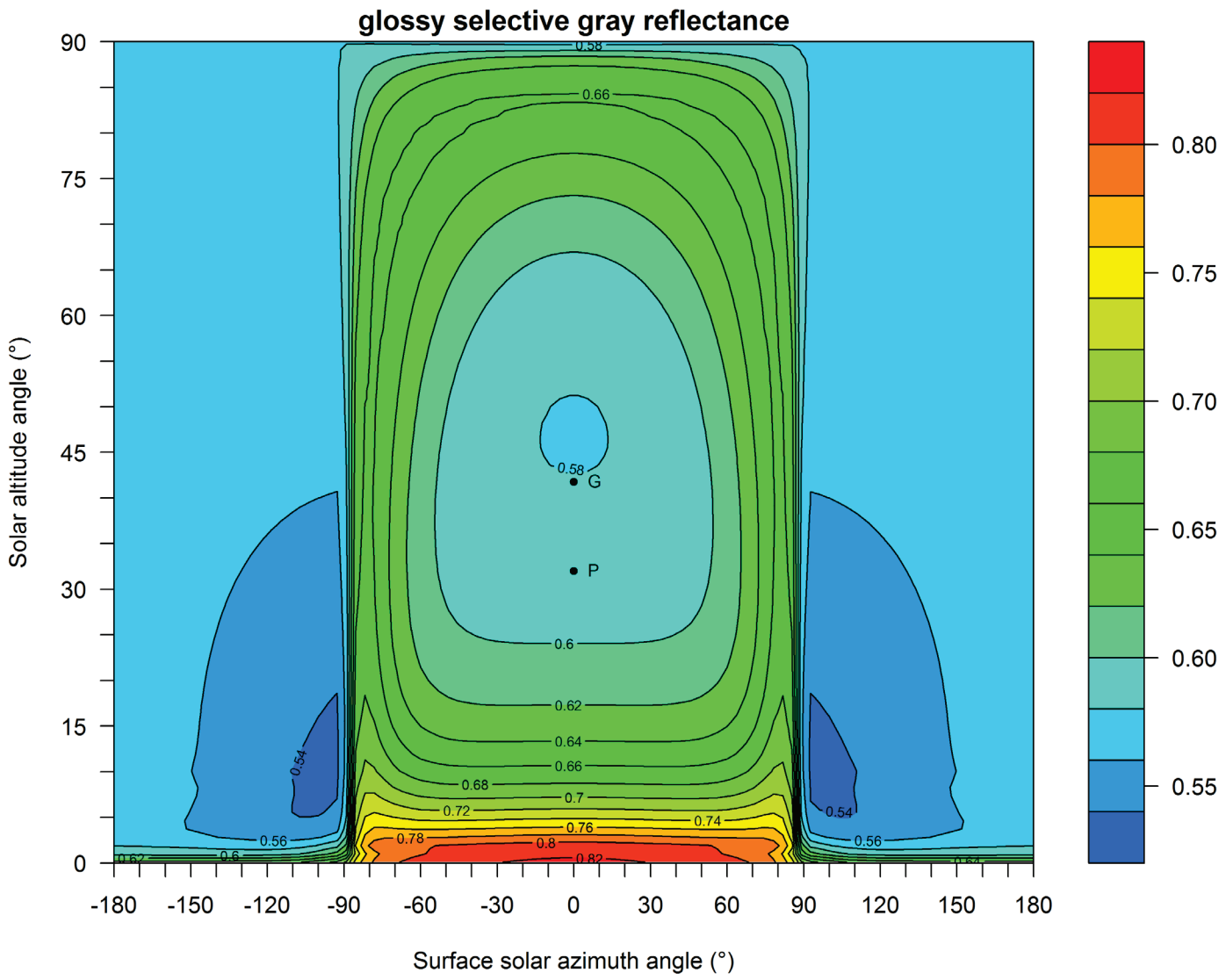

Figure 13 (continued)

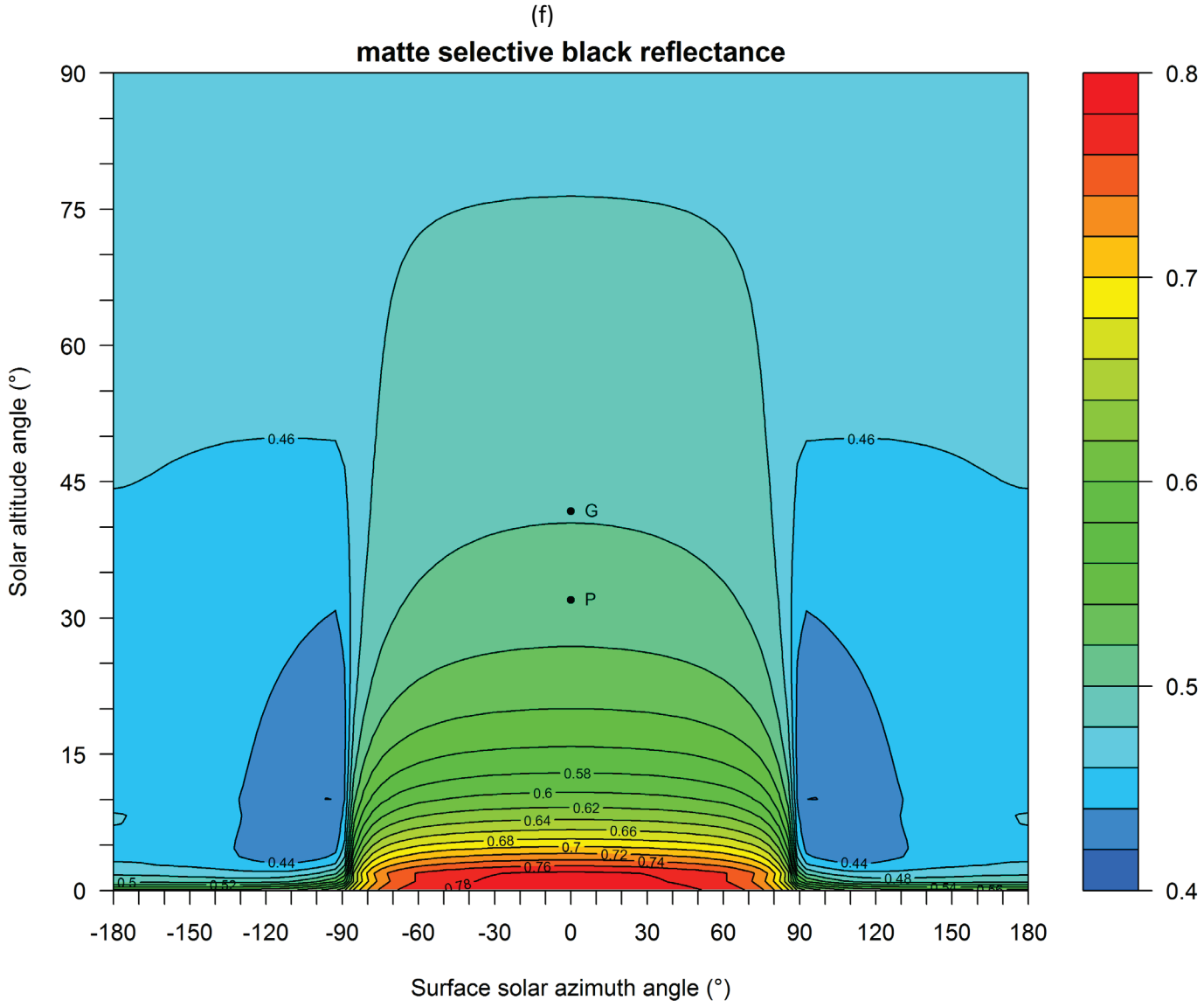

Figure 13 (continued)

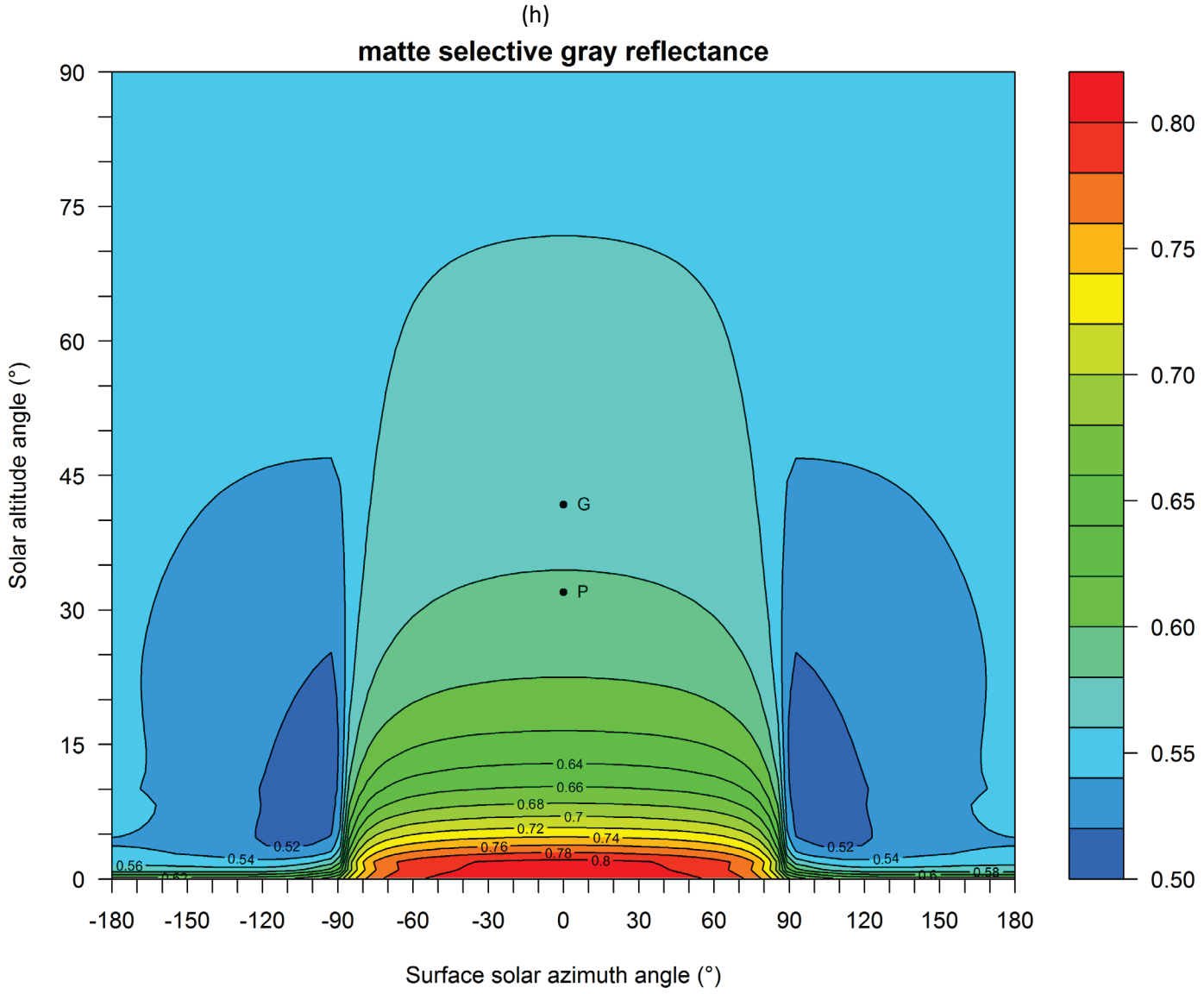

Figure 13 (continued)

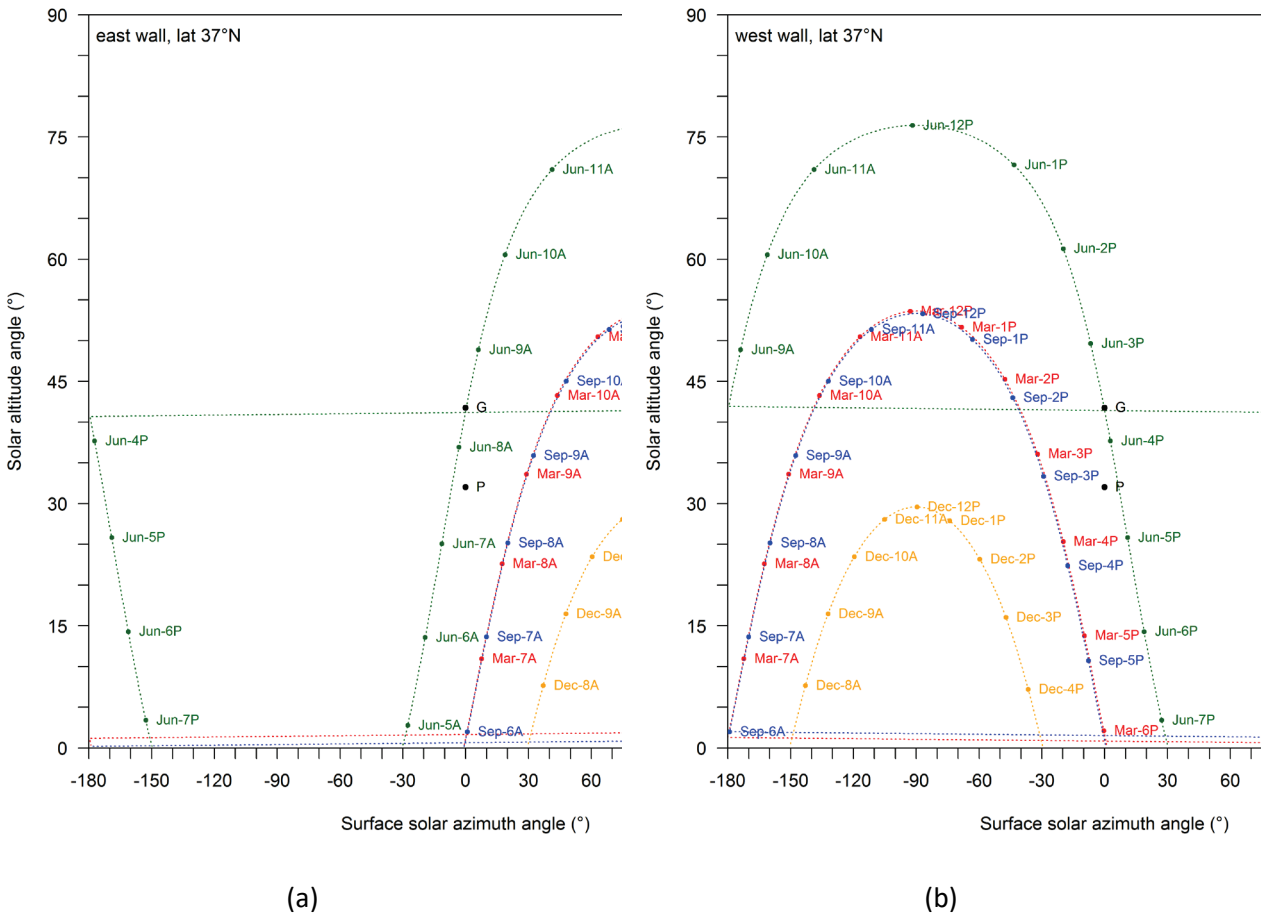

Figure 14. Solar trajectories (position versus local standard time) on Mar 21 (vernal equinox), Jun 21 (summer solstice), Sep 21 (autumnal equinox), and Dec 21 (winter solstice) across (a) east, (b) west, (c) south, and (d) north walls at latitude 37°N. Note that surface solar azimuth angle = solar azimuth angle – surface azimuth angle.

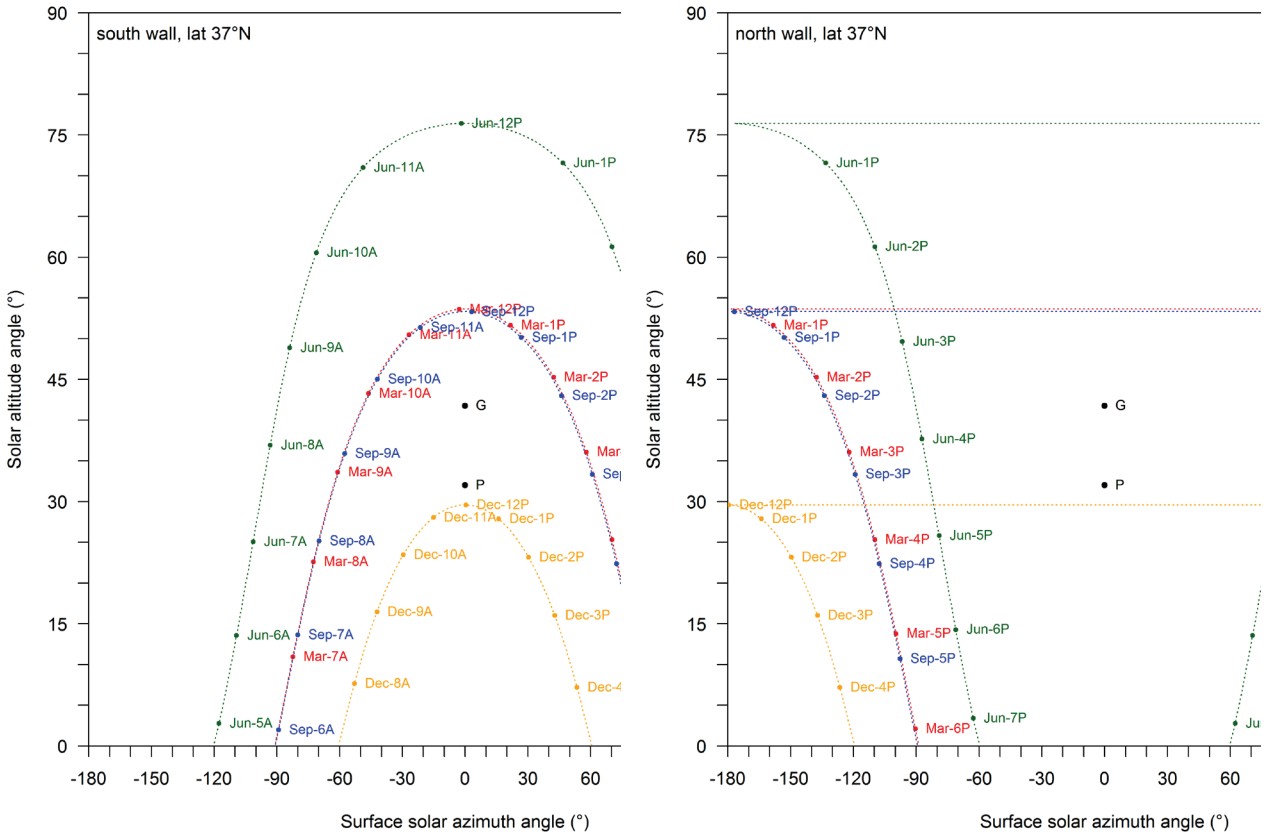

(c) (d)

Figure 14 (continued)

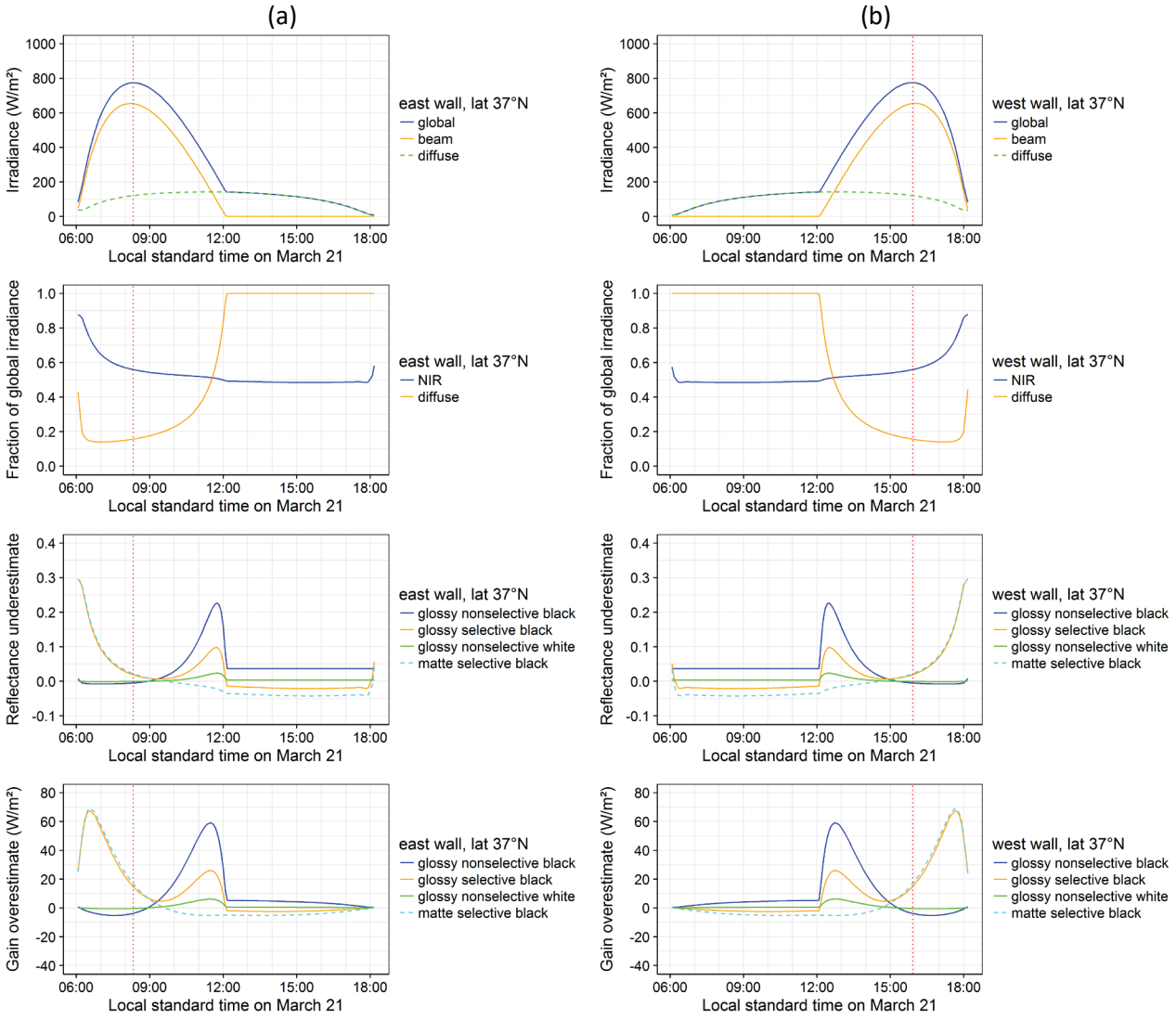

Figure 15. Top to bottom: time series on Mar 21 of global, beam, and diffuse tilt solar irradiances; NIR and diffuse fractions of global solar irradiance; underestimation of global solar reflectance, $R_g(t) – R^*$; and overestimation of solar heat gain, $I_g(t)$ [$R^* - R_g(t)$], shown for (a) east, (b) west, (c) south, and (d) north walls at latitude 37°N. Dotted red vertical line marks time of peak global solar irradiance.

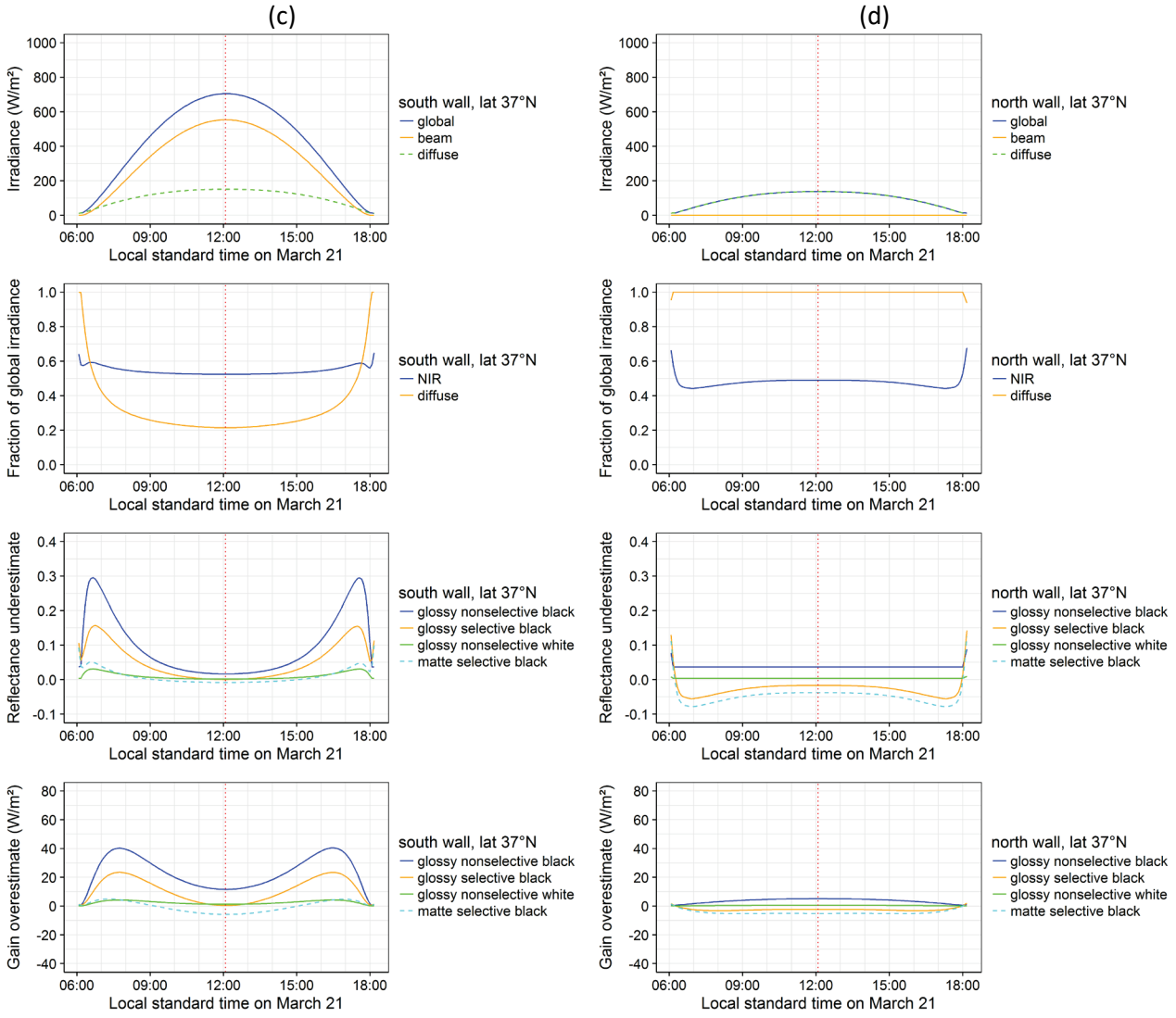

Figure 15 (continued)

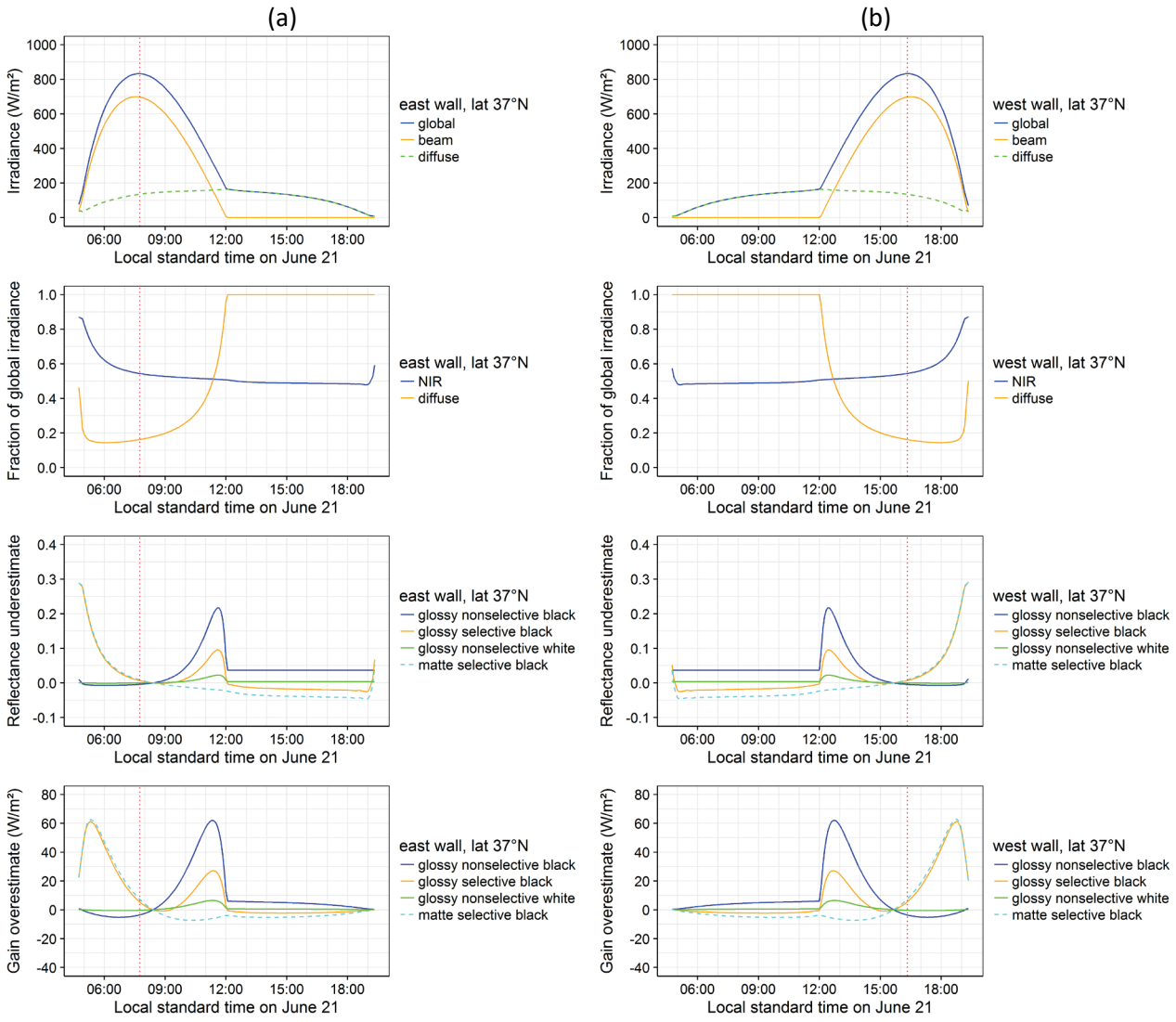

Figure 16. Time series from Figure 15 evaluated on June 21.

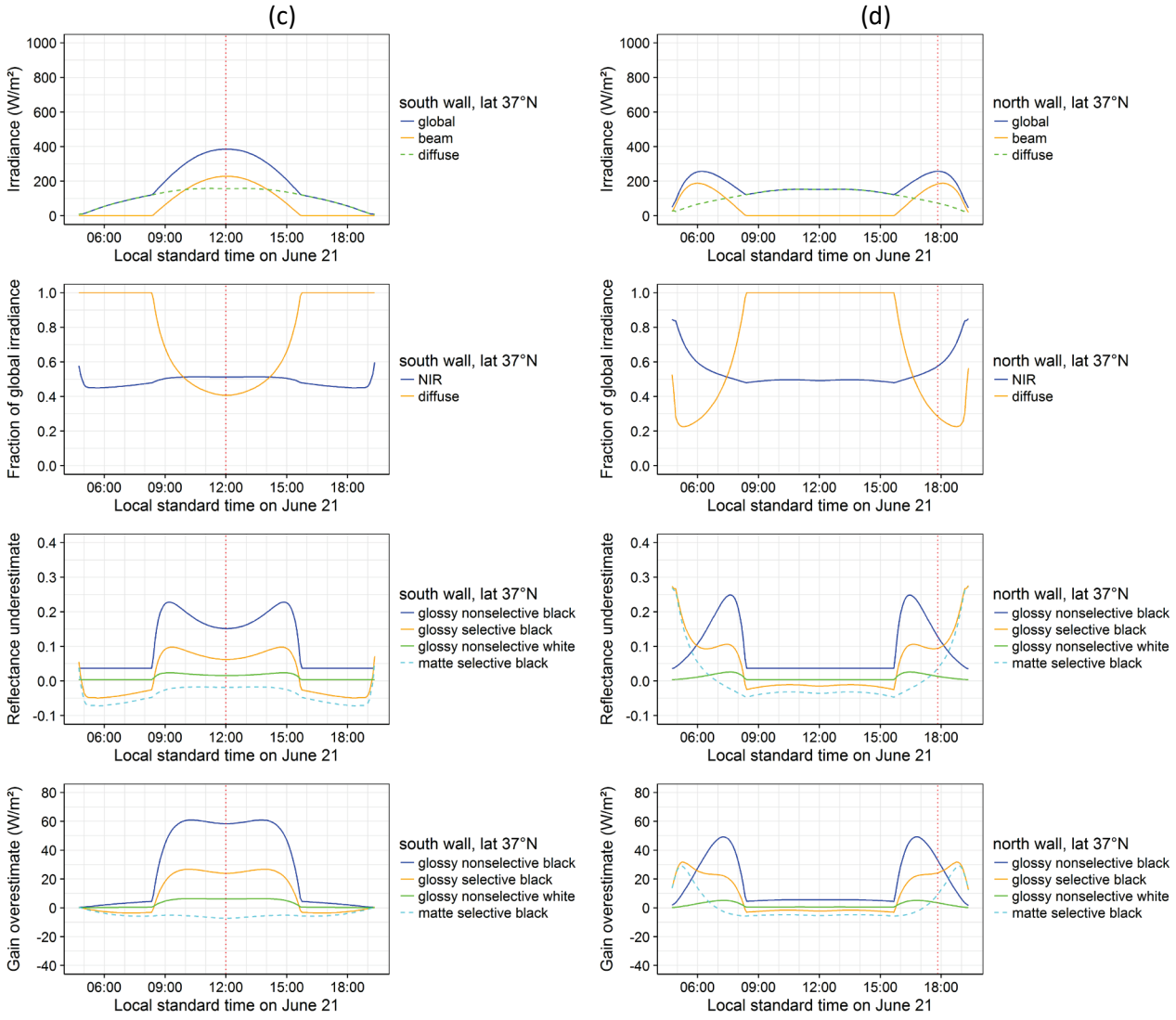

Figure 16 (continued)

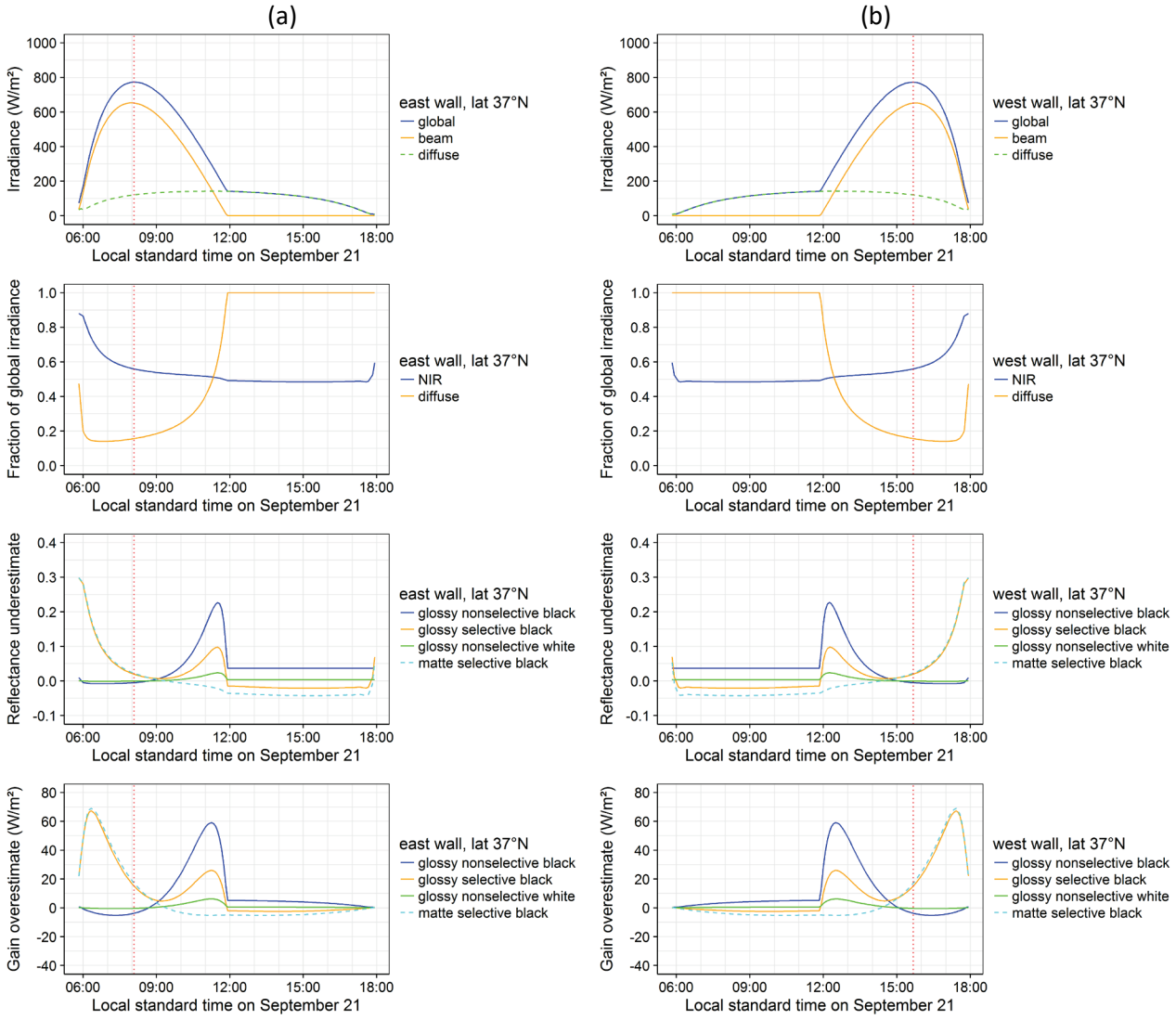

Figure 17. Time series from Figure 15 evaluated on September 21.

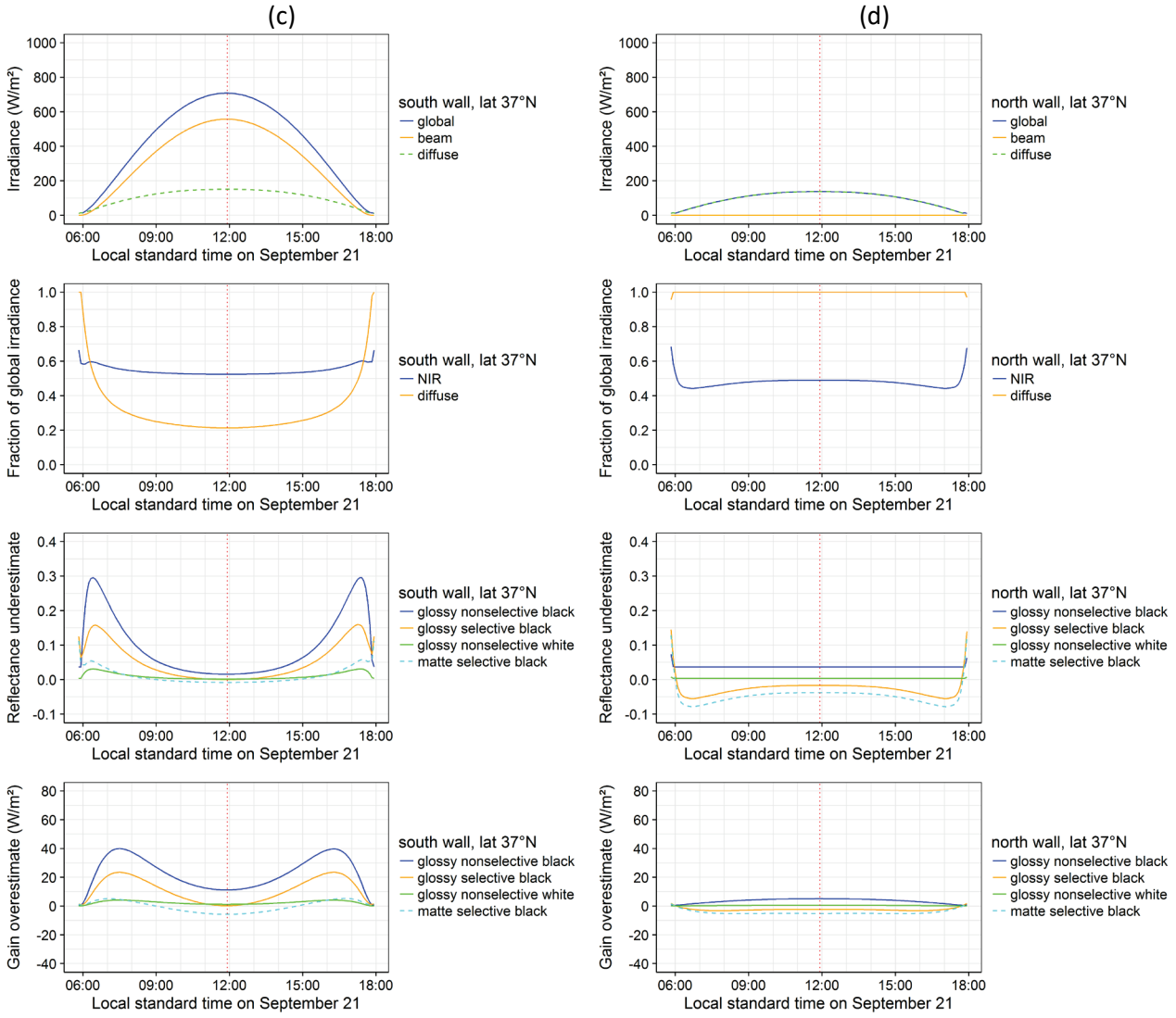

Figure 17 (continued)

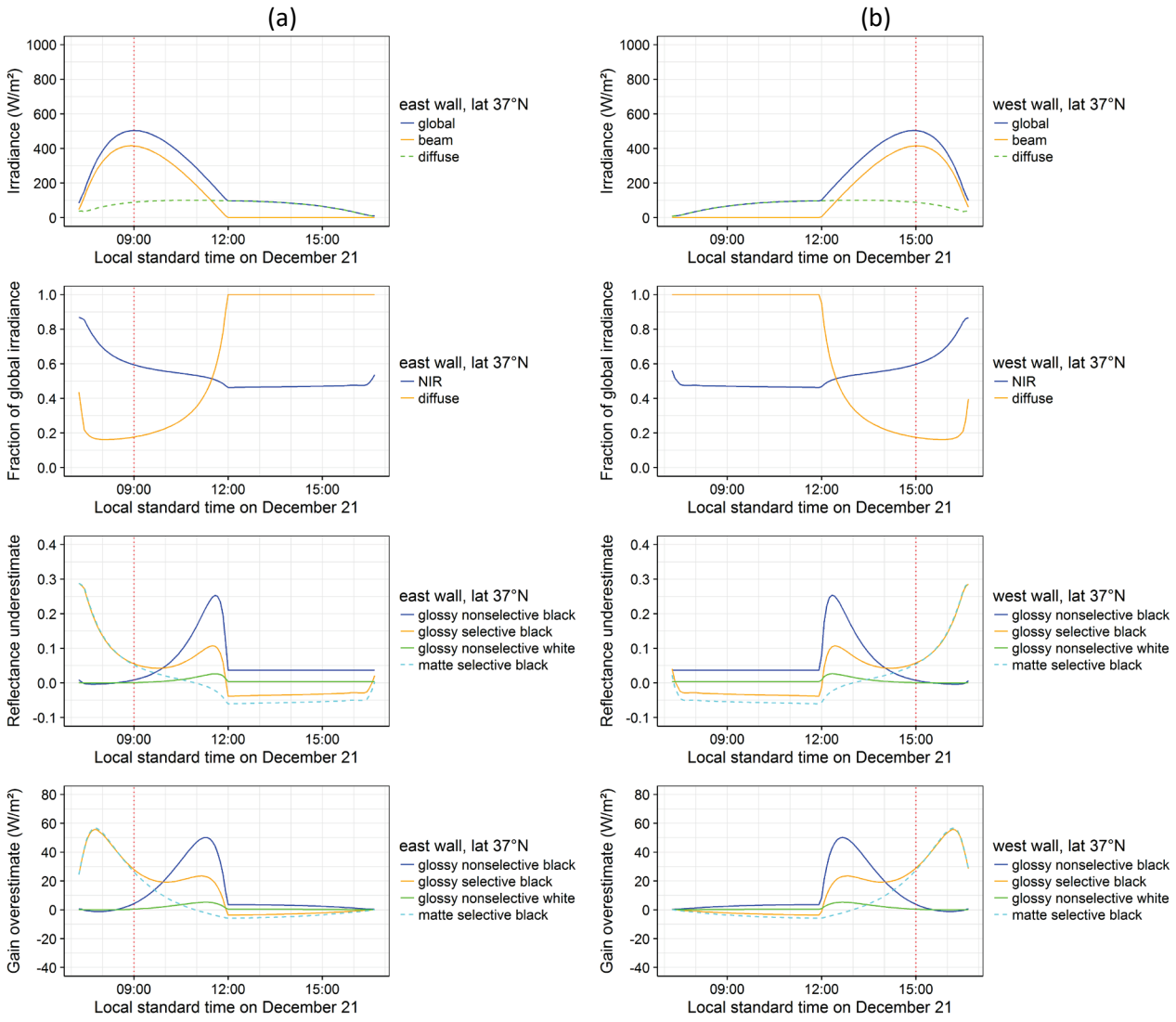

Figure 18. Time series from Figure 15 evaluated on December 21.

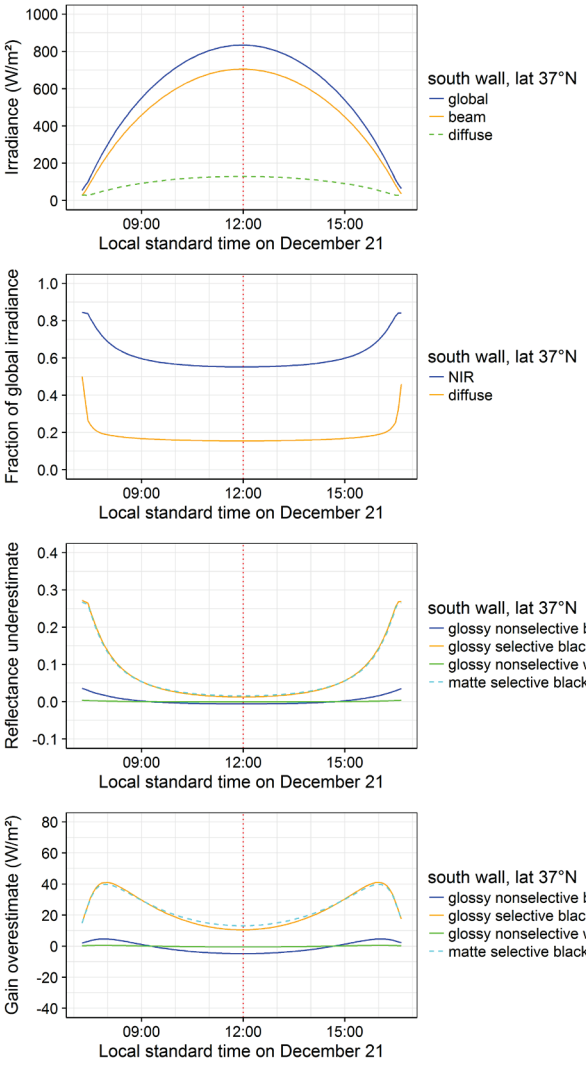

(c)

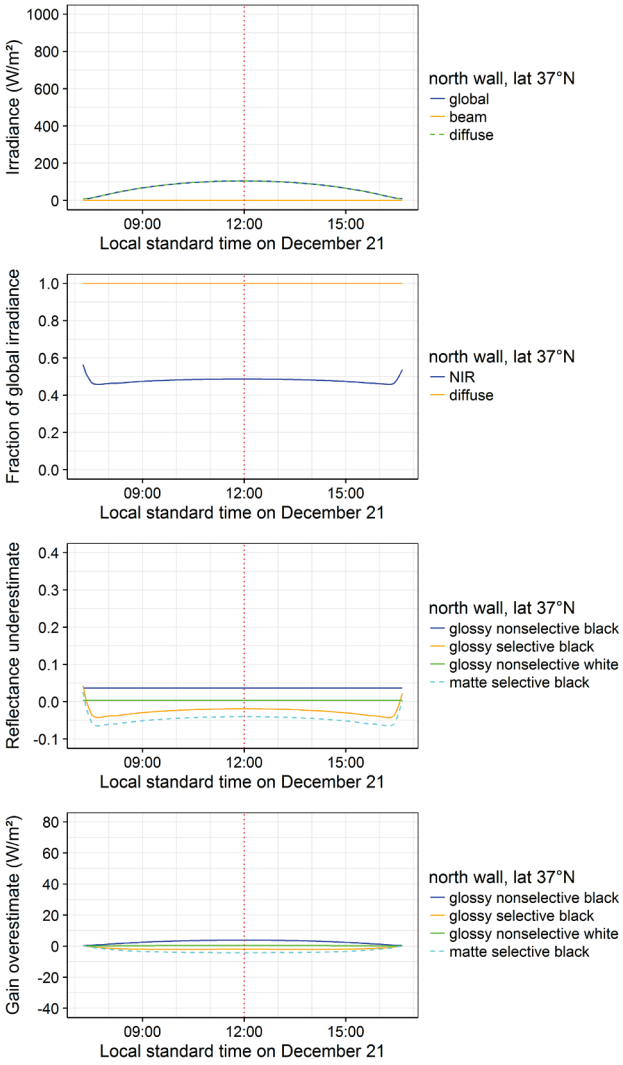

(d)

Figure 18 (continued)

Energy Research and Development Division

FINAL PROJECT REPORT

Solar-Reflective "Cool" Walls: Benefits, Technologies, and Implementation

Appendix J: Natural Exposure of Wall Products (Task 4.2 Report)

California Energy Commission
Gavin Newsom, Governor

April 2019 | CEC-500-2019-040-APJ

Appendix J:
Natural exposure of wall products (Task 4.2 report)

Sharon Chen[1], Haley Gilbert[1], Mina Truong[1], Sébastien Houzé de l'Aulnoit[1], Jiachen Zhang[2], George Ban Weiss[2], Ronnen Levinson[1], and Hugo Destaillats[1]

[1] Heat Island Group, Lawrence Berkeley National Laboratory

[2] Department of Civil and Environmental Engineering, University of Southern California

31 May 2018

Abstract

High albedo ("cool") walls that stay cool in the sun can help decrease building cooling demand and mitigate the urban heat island effect in hot and sunny climates. The magnitude of these potential benefits (or penalties) are expected to vary over time as walls weather and soil. To investigate the trend and magnitude of these changes as a function of climate, season and exposure duration, this study tracked the evolution of solar reflectance in 77 wall materials deployed for two or five years across six exposure locations in two parallel campaigns. In a two-year campaign, 69 wall materials were exposed at three California sites—Berkeley, Los Angeles, and Fresno—from spring 2016 to spring 2018, with solar reflectance tracked quarterly. In a parallel five-year campaign, 55 products are being exposed at three sites across the United States— New River, AZ (near Phoenix); Miami, FL; and Medina, OH (near Cleveland)—from summer 2016 to summer 2021, with solar reflectance tracked yearly. As of the 2-year mark in the California campaign and the 1-year mark in the U.S. campaign, observed albedo (solar reflectance) losses spanned from modest to negligible, and no material exhibited a loss exceeding 0.10. High albedo retention was categorically observed in wall products incorporating fluoropolymers or employing self-cleaning technologies.

1 Introduction

The main goal of this task was to assess the performance of commercially-available and prototype cool wall technologies. This was achieved by tracking, for a broad variety of wall products, changes in solar reflectance as a function of time exposed in the natural

environment. Protocols developed for the evaluation of these radiative properties have been described in the Task 4.1 report: *Metrics and methods to assess cool wall performance*. Specimens used in these measurements were subjected to natural exposure at three locations in California: Berkeley, Los Angeles, and Fresno. These sites represent the three most populated regions of the state and different climate zones: the San Francisco Bay Area, the South Coast Basin and the Central Valley. In addition to the three California sites, the scope of the project was later expanded in consultation with the California Energy Commission (CEC) to expose specimens at the three sites used nationally for roofing product rating: Florida, Arizona and Ohio.

This study intended to cover all the main types of wall materials and coatings typically used in residential and commercial construction in the United States. For that purpose, our team has built a strong industrial collaborative consortium comprising 11 companies that have signed CRADA agreements with LBNL and have supported the activities described below. Samples received from industrial partners are being exposed outside for 2 years at California sites and 5 years in U.S. sites to obtain a good description of initial aging processes and their effect on solar reflectance. The sample set includes products with high, medium and low initial albedos. They also include conventional products alongside advanced and innovative materials, some of which are still research prototypes.

One of the advanced technologies represented in the study's sample set is the use of dirt pick-up resistant and/or self-cleaning additives in coating formulations. Dirt-resistant coatings are formulated with fluorinated polymers or other alternatives that minimize interactions with atmospheric deposition. High surface hydrophobicity leads to water beading and runoff (also known as the "lotus effect"), which further contributes to the removal of deposited particles and chemicals.

Photocatalytic self-cleaning products can remove soiling from their surface by catalyzing the elimination of deposited soiling in the presence of sunlight. Photoactive building envelope materials represent a growing sector of the construction market, with $740M in sales in 2009, doubling by 2014 (Gagliardi, 2010). These products are used in new construction and in retrofits, and include cementitious coatings such as mortar, plaster and paint; coated metal siding; architectural fabrics; tiles; precast panels; and roofing.

The "stay-clean" properties of dirt-resistant and photoactive self-cleaning surfaces have been documented mainly in laboratory tests, and need to be quantified under real-world conditions to assess potential energy savings. A key barrier to the development of dirt-resistant and self-cleaning products has been the lack of metrics and methods to evaluate their performance.

This project applied metrics and processes to facilitate the evaluation of soiling-resistant building envelope products, by quantitatively comparing the evolution of the solar reflectance and water contact angle of "stay-clean" materials with that of baseline conventional products

through natural exposure. This approach could serve as the basis of a rating method for these materials.

2 Methodology

2.1 Selection of exposed materials

Eleven industrial partners participated in this study. In the initial phase of the project, partners were invited to submit specimens of products of interest. These products were evaluated by the LBNL team to down-select a subset of products to be exposed in the field. The selection criteria used to develop a balanced portfolio of samples sought to include

a) as many product categories as possible;

b) as many substrates for field-applied coatings (paints) as possible;

c) a wide palette of colors;

d) a variety of white and light-colored products with high initial solar reflectance (since reflective surfaces are prone to soiling); and

e) as many manufacturers as possible.

Table 1 summarizes the materials used in this study, which are also illustrated in Figure 1. The main characteristics of each material are presented in Table 2. To clarify our nomenclature:

a) We apply the term “product” as it is used by manufacturers—to identify a unique item available for purchase, or a unique prototype of an item being developed for sale.

b) A product may require a substrate for exposure and measurement (“testing”). We use the term “material” to describe a wall product in testable form. A product that does not require a substrate, such as a factory-painted metal cladding or an architectural fabric, is both a product and a material. A field-applied coating sold as liquid paint is a product, but not a material; the same coating applied to a substrate, such as a piece of wood, becomes a material.

c) Individual pieces of each material (10 cm by 10 cm) installed on exposure racks and retrieved quarterly for laboratory characterization are referred to as “specimens”.

d) Each material is labeled “CWXX”, where the prefix “CW” refers to the project name (“cool walls”) and “XX” is a two-digit anonymous code (01 – 77).

e) We abbreviate the names of the six exposure locations with the following two-letter codes: BK = Berkeley, CA; LA = Los Angeles, CA; FR = Fresno, CA; AZ = New River, AZ

(roughly 50 km north of Phoenix); FL = Miami, FL; OH = Medina, OH (roughly 40 km south of Cleveland).

Table 1. Summary of materials exposed in this study.

Product category	Substrate	Count	Colors [a]	Texture/surface finish[b]
Factory-applied coating	Metal	15	Black, dark brown, burgundy, tan, light gray, white	Smooth surface, textured surface
Field-applied coating	Metal	8	Dark green-gray, tan, peach, peach-orange	Flat finish
Field-applied coating	Concrete	5	White	Flat finish, satin finish, semi-gloss finish
Field-applied coating	Wood	24	Dark brown, dark blue-gray, dark purple-gray, peach, peach-orange, gray-green, tan, white	Flat finish, satin finish, semi-gloss finish
Field-applied coating	Fiber cement	11	Gray, tan, salmon pink, light green, white	Satin finish, flat finish
Architectural membrane	N/A	3	White	N/A
Vinyl siding	N/A	1	White	Wood grain texture
Composite metal cladding	N/A	6	Silver metallic, off-white, white	N/A
Retroreflective & reflective film	NA	4	White & metallic (pattern), mirror	N/A

[a] Color names subjectively chosen by the researchers.

[b] While most entries in this column represent manufacturer-reported properties, some were determined subjectively by LBNL research staff. A detailed breakdown can be found in Table 2.

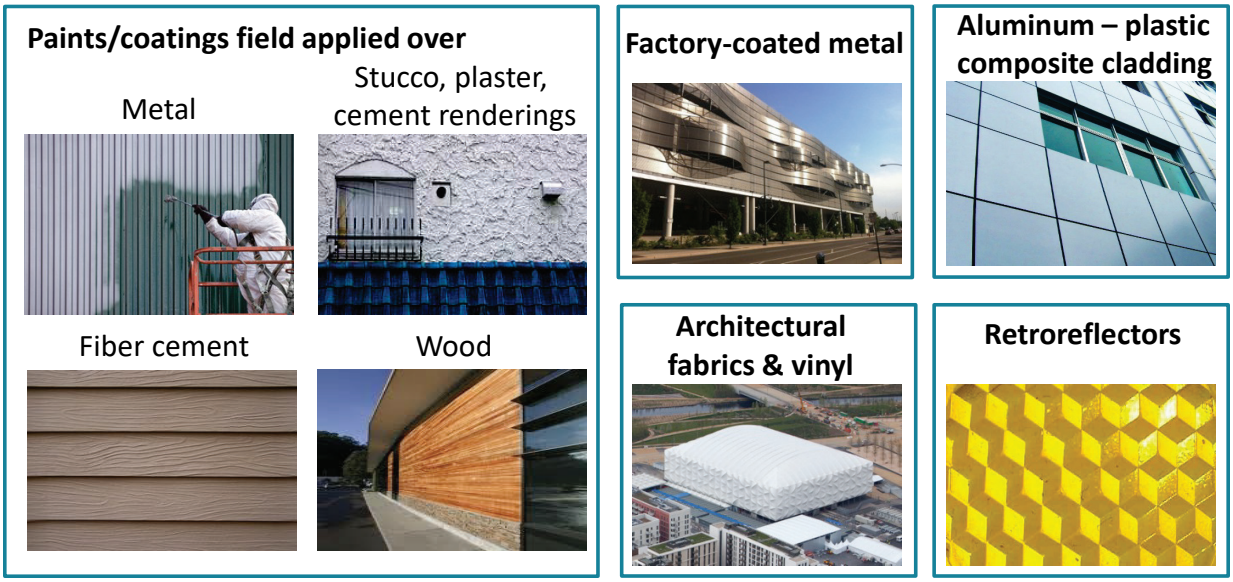

Figure 1. Examples of types of products exposed in this study.

Table 2. Description of materials used in natural exposure tests.

Code [a]	Color	Category	Description [b]	Substrate	Surface finish [c]	Commercial product (C) or experimental prototype (E)	Exposure: U.S., CA, or both
01	white	coating (factory)	fluoropolymer (PVDF) resin; smooth control for CW02	metal (aluminum)	N/A	C	CA
02	white	coating (factory)	fluoropolymer (PVDF) resin; surface texture	metal (aluminum)	N/A	C	CA
03	burgundy	coating (factory)	fluoropolymer (PVDF) resin	metal (aluminum)	N/A	C	CA
04	light gray	coating (factory)	fluoropolymer (PVDF) resin	metal (aluminum)	N/A	C	CA
05	black	coating (factory)	fluoropolymer (PVDF) resin	metal (aluminum)	N/A	C	CA
06	white	coating (factory)	fluoropolymer (PVDF) resin	metal (steel)	N/A	C	both
07	tan	coating (factory)	fluoropolymer (PVDF) resin	metal (steel)	N/A	C	both
08	dark brown	coating (factory)	fluoropolymer (PVDF) resin	metal (steel)	N/A	C	both
09	light gray	coating (factory)	fluoropolymer (PVDF) resin	metal (steel)	N/A	C	both
10	dark brown	coating (factory)	fluoropolymer (PVDF) resin	metal (steel)	N/A	C	CA
11	dark brown	coating (factory)	fluoropolymer (PVDF) resin	metal (steel)	N/A	C	CA
12	dark brown	coating (factory)	silicone-modified polyester (SMP) resin; smooth control for CW13	metal (steel)	N/A	C	CA

Code [a]	Color	Category	Description [b]	Substrate	Surface finish [c]	Commercial product (C) or experimental prototype (E)	Exposure: U.S., CA, or both
13	dark brown	coating (factory)	silicone-modified polyester (SMP) resin; surface texture	metal (steel)	N/A	C	CA
14	white	coating (factory)	polyester resin	metal (steel)	N/A	C	CA
15	white	coating (factory)	polyester resin	metal (aluminum)	N/A	C	CA
16	tan	coating (field)	non-photocatalytic control for CW17	metal (aluminum)	flat	E	CA
17	tan	coating (field)	photocatalytic	metal (aluminum)	flat	E	CA
18	dark green-gray	coating (field)	non-photocatalytic control for CW19	metal (aluminum)	flat	E	CA
19	dark green-gray	coating (field)	photocatalytic	metal (aluminum)	flat	E	CA
20	peach	coating (field)	non-photocatalytic control for CW21	metal (aluminum)	flat	E	CA
21	peach	coating (field)	photocatalytic	metal (aluminum)	flat	E	CA
22	peach-orange	coating (field)	non-photocatalytic control for CW23	metal (aluminum)	flat	E	CA
23	peach-orange	coating (field)	photocatalytic	metal (aluminum)	flat	E	CA
24	white	architectural membrane	PTFE-coated fiberglass; non-photocatalytic control for CW25/26	N/A	N/A	C	both
25	white	architectural membrane	PTFE-coated fiberglass; photocatalytic	N/A	N/A	C	both
26	white	architectural membrane	PTFE-coated fiberglass; photocatalytic	N/A	N/A	[to be disclosed]	both

Code [a]	Color	Category	Description [b]	Substrate	Surface finish [c]	Commercial product (C) or experimental prototype (E)	Exposure: U.S., CA, or both
27	white	vinyl siding	polyvinyl chloride (PVC); wood grain surface texture*	N/A	N/A	C	both
28	white	composite metal cladding	fluoropolymer (FEVE) resin	N/A	N/A	C	both
29	off-white	composite metal cladding	fluoropolymer (FEVE) resin	N/A	N/A	C	both
30	silver metallic	composite metal cladding	fluoropolymer (FEVE) resin; mica flakes	N/A	N/A	C	both
31	silver metallic	composite metal cladding	fluoropolymer (FEVE) resin; metallic flakes	N/A	N/A	C	both
32	white	coating (field)	[to be disclosed]; dirt-resistant	wood (pine; sealed)	satin*	E	both
33	white	coating (field)	[to be disclosed]; dirt-resistant	wood (pine; sealed)	flat*	E	both
34	white	coating (field)	[to be disclosed]; dirt-resistant	wood (pine; sealed)	satin*	E	both
35	white	coating (field)	[to be disclosed]; dirt-resistant	wood (pine; sealed)	flat*	E	both
36	white	coating (field)	[to be disclosed]; dirt-resistant	wood (pine; sealed)	flat*	E	both
37	white	coating (field)	[to be disclosed]; self-cleaning	concrete paver	satin*	E	both
38	white	coating (field)	[to be disclosed]; self-cleaning	concrete paver	satin*	E	both
39	white	coating (field)	[to be disclosed]; self-cleaning	concrete paver	flat*	E	both
40	white	coating (field)	[to be disclosed]; self-cleaning	concrete paver	semi-gloss*	E	both
41	white	coating (field)	[to be disclosed]; non self-cleaning control for CW37-40	concrete paver	satin*	[to be disclosed]	both
42	green	coating (field)	acrylic resin, water-based	wood (pine; sealed)	flat	C	both

Code [a]	Color	Category	Description [b]	Substrate	Surface finish [c]	Commercial product (C) or experimental prototype (E)	Exposure: U.S., CA, or both
43	peach-orange	coating (field)	acrylic resin, water-based	wood (pine; sealed)	flat	C	both
44	peach-orange	coating (field)	acrylic resin, water-based	wood (pine; sealed)	flat	C	both
45	dark brown	coating (field)	acrylic resin, water-based	wood (pine; sealed)	flat	C	both
46	dark brown	coating (field)	acrylic resin, water-based	wood (pine; sealed)	flat	C	both
47	white	coating (field)	acrylic resin; non-dirt-resistant control for CW48/49	wood (pine; sealed)	semi-gloss	C	both
48	white	coating (field)	acrylic resin; dirt pick-up resistance	wood (pine; sealed)	semi-gloss	C	both
49	white	coating (field)	acrylic resin; dirt pick-up resistance	wood (pine; sealed)	semi-gloss	E	both
50	dark blue-gray	coating (field)	acrylic resin; non-cool control for CW51	wood (pine; sealed)	semi-gloss	E	both
51	dark blue-gray	coating (field)	acrylic resin; spectrally-selective pigment	wood (pine; sealed)	semi-gloss	E	both
52	dark purple-gray	coating (field)	acrylic resin; non-cool control for CW53	wood (pine; sealed)	semi-gloss	E	both
53	dark purple-gray	coating (field)	acrylic resin; spectrally-selective pigment	wood (pine; sealed)	semi-gloss	E	both
54	white	coating (field)	fluoropolymer (PVDF) resin, water-based	fiber cement	satin	C	CA
55	white	coating (field)	fluoropolymer (PVDF) resin, water-based	fiber cement	satin	C	CA
56	light green	coating (field)	fluoropolymer (PVDF) resin, water-based	fiber cement	satin	C	both

Code [a]	Color	Category	Description [b]	Substrate	Surface finish [c]	Commercial product (C) or experimental prototype (E)	Exposure: U.S., CA, or both
57	salmon pink	coating (field)	fluoropolymer (PVDF) resin, water-based	fiber cement	satin	C	both
58	gray	coating (field)	fluoropolymer (PVDF) resin, water-based	fiber cement	satin	C	CA
59	tan	coating (field)	fluoropolymer (PVDF) resin, water-based	fiber cement	satin	C	both
60	white	coating (field)	acrylic resin, water-based; control for CW62	wood (pre-primed cedar)	flat	C	both
61	white	coating (field)	acrylic resin, water-based; control for CW63	fiber cement	flat	C	both
62	white	coating (field)	acrylic resin, water-based; improved dirt pick-up resistance	wood (pre-primed cedar)	flat	C	both
63	white	coating (field)	acrylic resin, water-based; improved dirt pick-up resistance	fiber cement	flat	C	both
64	tan	coating (field)	acrylic resin, water-based; control for CW66, 68	wood (pre-primed cedar)	flat	C	both
65	tan	coating (field)	acrylic resin, water-based; control for CW67, 69	fiber cement	flat	C	both
66	tan	coating (field)	styrene acrylic resin, water-based; spectrally-selective pigment	wood (pre-primed cedar)	flat	C	both
67	tan	coating (field)	styrene acrylic resin, water-based; spectrally-selective pigment	fiber cement	flat	C	both
68	tan	coating (field)	acrylic resin, water-based; spectrally-selective pigment; improved dirt pick-up resistance	wood (pre-primed cedar)	flat	C	both
69	tan	coating (field)	acrylic resin, water-based; spectrally-selective pigment; improved dirt pick-up resistance	fiber cement	flat	C	both
70	tan	coating (field)	acrylic resin, water-based; spectrally-selective pigment; dirt pick-up resistance	plywood (exterior-grade)	semi-gloss	C	U.S.

Code [a]	Color	Category	Description [b]	Substrate	Surface finish [c]	Commercial product (C) or experimental prototype (E)	Exposure: U.S., CA, or both
71	peach	coating (field)	acrylic resin, water-based; spectrally-selective pigment; dirt pick-up resistance	plywood (exterior-grade)	semi-gloss	C	U.S.
72	white & metallic (pattern)	plastic film	plastic film with UV-protective over-laminate; retroreflective	metal (steel)	N/A	C	U.S.
73	white & metallic (pattern)	plastic film	plastic film with UV-protective over-laminate; retroreflective	metal (steel)	N/A	C	U.S.
74	white & metallic (pattern)	plastic film	plastic film with UV-protective over-laminate; retroreflective	metal (steel)	N/A	C	U.S.
75	mirror	plastic film	plastic film with UV-protective over-laminate; reflective film	metal (steel)	N/A	C	U.S.
76	white	composite metal cladding	fluoropolymer (PVDF) resin	N/A	N/A	C	U.S.
77	silver metallic	composite metal cladding	fluoropolymer (PVDF) resin	N/A	N/A	C	U.S.

[a] For compactness, the prefix “CW” has been omitted from material labels in this column.

[b,c] Descriptions of texture or surface finishes that are followed by an asterisk (*) were determined subjectively by LBNL research staff. All other entries represent manufacturer-reported properties.

2.2 Selection and setup of exposure sites

2.2.1 Identification of sites

Three sites in California were selected to span different climates and major urban areas:

a) a building roof at the Lawrence Berkeley National Laboratory in Berkeley;

b) a parking lot at the University of Southern California, in downtown Los Angeles; and

c) a ground level concrete platform belonging to one of our industry partners in Fresno.

The Fresno site provided mostly exposure to air containing pollution associated with agricultural activity, typical of the Central Valley. The Los Angeles site was representative of pollution found in a large mega-city. The Berkeley site was cleaner, because the Laboratory is located on a hill overlooking the San Francisco Bay Area, far from highways and heavy traffic.

2.2.2 Exposure racks

Specimens were exposed vertically, facing westward. LBNL designed and built exposure racks at each of the three California exposure sites. Each rack was designed to hold a maximum of 280 specimens, arranged in 14 rows of 20 each. The rows were offset from each other to prevent contamination between vertically adjacent rows. To accommodate the complete set of specimens, three racks were required at each site, as shown in Figure 3.

As shown in Figure 2, the skeleton of each rack was assembled from hot-dip galvanized strut channels. Metal specimen holders, bent from galvanized sheet metal, formed the backbone of the 2.1 m (7')-long rows of specimens. The specimen holders were sized to accommodate both the specimens (of various thicknesses) and a 1.27 cm (0.5")-thick plywood strip (providing insulated backing for the specimens). A deeper discussion of the exposure rack design can be found in the Task 4.1 report: *Metrics and methods to assess cool wall performance*.

The final construction of the racks at each site differed in minor ways from the proposed design. At the Fresno site, the wooden sleepers at the base of the rack were foregone in favor of anchoring the rack frame directly to the concrete platform underneath. At the Berkeley site, special earthquake retrofitting attachments were required because the racks were close to a pedestrian path. At the Los Angeles site, it was determined that the racks were stable enough without wooden sleepers at the base.

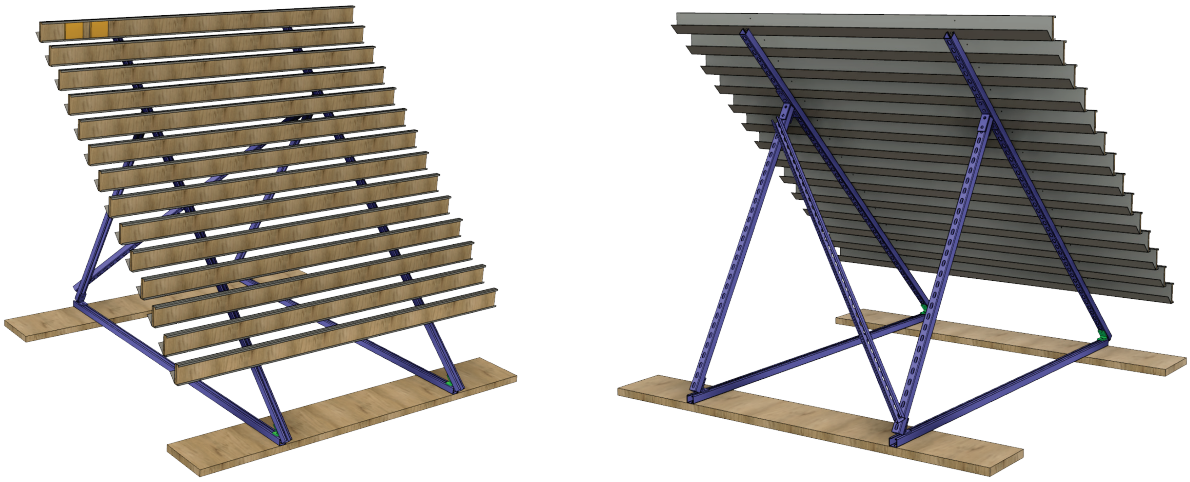

(a) (b)

Figure 2. Front-angle (a) and back-angle (b) CAD drawing views of the exposure rack design.

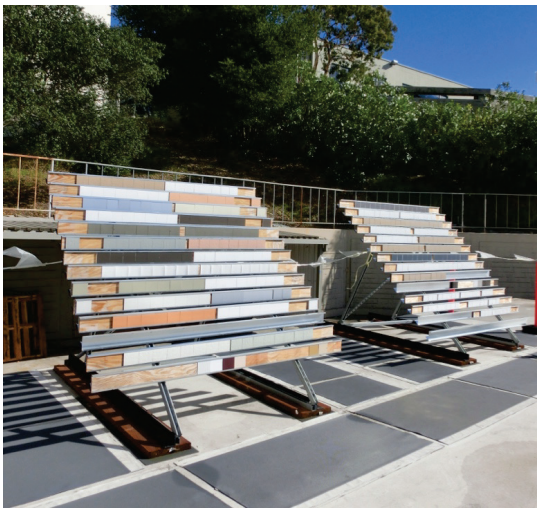

(a)

(b)

(c)

Figure 3. Newly-installed and populated exposure racks at the three California exposure sites: (a) Berkeley; (b) Fresno; and (c) Los Angeles.

2.2.3. California exposure

All three California sites were built between March and April 2016, and materials CW01 to CW69 were installed immediately after their construction. Specimens have been retrieved quarterly, following the schedule presented in Table 3. Figure 4 describes how many samples per product category have been exposed in California.

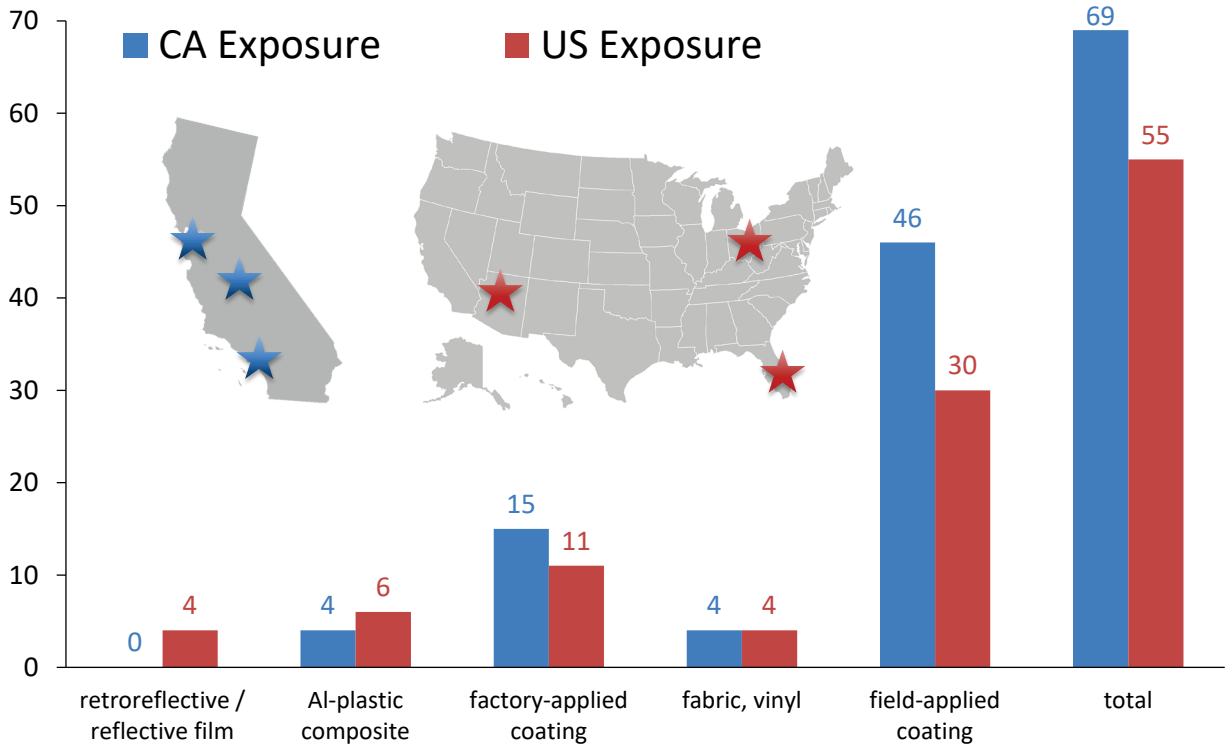

Figure 4. Location of the six exposure sites, and the number of materials per product type exposed at each site.

Table 3. Experimental schedule for California exposure.

Site	installed	3 mo	6 mo	9 mo	12 mo	15 mo	18 mo	21 mo	24 mo
BK	Mar 2016	Jul 2016	Oct 2016	Jan 2017	Apr 2017	Jul 2017	Oct 2017	Jan 2018	Apr 2018
LA	Apr 2016	Jul 2016	Oct 2016	Jan 2017	Apr 2017	Jul 2017	Oct 2017	Jan 2018	Apr 2018
FR	Mar 2016	Jun 2016	Oct 2016	Dec 2017	Apr 2017	Jul 2017	Oct 2017	Jan 2018	May 2018

2.2.4. National exposure

Once the California sites were operating, the team also secured permission from several manufacturers to expose materials at the three sites used by the Cool Roof Rating Council for roofing rating. These "U.S." exposure sites in New River, AZ; Miami, FL; and Medina, OH are operated by a commercial weathering firm that uses west-facing vertical racks such as those shown in Figure 5. In total, 55 materials from 10 partners are undergoing exposure in this campaign, 47 of which are also participating in the California campaign. The remaining 8 materials (CW70 – CW77) are exposed at U.S. national sites but not at any California sites. Exposure began in August 2016 and is scheduled to run for five years, with annual specimen retrievals occurring each summer following the schedule presented in Table 4. Figure 4 provides a count of how many materials per product category are represented in the national exposure campaign.

(a) (b)

Figure 5. Racks used in the U.S. exposure campaign. Panel (a) shows the Medina, OH racks shortly after the specimens were installed. Panel (b) shows a close-up of the rack design.

Table 4. Experimental schedule for national exposure.

Site	installed	1 yr	2 yr[a]	3 yr[a]	4 yr[a]	5 yr[a]
AZ	Aug 2016	Aug 2017	Aug 2018	Aug 2019	Aug 2020	Aug 2021
FL	Aug 2016	Aug 2017	Aug 2018	Aug 2019	Aug 2020	Aug 2021
OH	Aug 2016	Aug 2017	Aug 2018	Aug 2019	Aug 2020	Aug 2021

[a] Pending at the time this report was prepared.

2.2.5. Rainfall at each site

Monthly rainfall data at each exposure site was obtained from nearby Global Historical Climatology Network (GHCN) weather stations. The data sets were downloaded from the National Oceanic and Atmospheric Administration Climate Data Online database (NOAA, 2018). The weather stations selected for each site were

a) US1CAAL0018, in Berkeley, 3.2 km southeast of the Berkeley exposure site;

b) USW00093134, on the University of Southern California (USC) campus, 1.4 km west of the Los Angeles exposure site;

c) USW00093193, at the Fresno Yosemite International Airport, 9.9 km north of the Fresno exposure site

d) US1AZMR0416, in Anthem, AZ, 3.1 km southeast of the Arizona exposure site;

e) USC00087020, in Miami, Florida, 2.5 km northeast of the Florida exposure site; and

f) US1OHMD0002, in Brunswick, OH, 16 km northeast of the Ohio exposure site.

2.3 Experimental procedures

The general experimental procedures implemented to perform measurements in the laboratory have been described in the Task 4.1 Report *Metrics and methods to assess cool wall performance*. The key measurements are highlighted in this section.

2.3.1 Specimen retrieval, shipping and storage

Specimens exposed in California were retrieved quarterly and returned to LBNL for laboratory analysis. One specimen from the ten units exposed side-by-side for each product were retrieved

from the racks, recorded, packed and shipped to LBNL. Individual glassine envelopes were used to protect each sample from contact with the others and with packing materials. The samples were stored inside the same envelopes prior and after laboratory measurements.

2.3.2 Solar reflectance and spectral measurements

Solar reflectance was measured on all specimens with a Devices & Services Solar Spectrum Reflectometer, version 6 (Figure 6). Solar spectral reflectance (250 to 2,500 nm) was recorded for a sub-set of samples using a Perkin Elmer Lambda 900 UV-vis-NIR spectrophotometer with 150 mm Labsphere integrating sphere. The solar reflectance results are presented using the air mass 1 global horizontal (AM1GH) solar spectrum (relevant for roofs). Future analyses will report the air mass 1.5 vertical (AM1.5GV) solar reflectance (relevant for walls).

(a) (b)

Figure 6. Photography setup (a) and solar reflectometer (b) used in this study.

2.3.3 Photography of specimens

Each specimen was photographed on a copy stand using a digital point-and-shoot camera with two lamps (of color temperature similar to sunlight) providing illumination. A gray card was placed in the specimen background to control white balance.

3 Results and discussion

3.1 Rainfall recorded at each site

Rainfall at the three California sites followed similar patterns (Figure 8). Across the state we observed a dry season from April/May to October, and a rainy season through the late fall, winter and beginning of the spring. Maximum precipitation at all three sites occurred in January 2017. Berkeley was the wettest of the three locations, having experienced the most cumulative rainfall to date. One significant difference in the rain patterns was that precipitation in LA was mostly taking place during the winter months (December through February), while the other two sites showed a broader distribution, with significant levels from October through April.

Rain patterns at the national exposure sites show larger differences, as shown in Figure 9. Total precipitation was very low in Arizona (5 - 10 cm/month in winter), highest in Florida (20 - 40 cm/month in summer) and intermediate in Ohio, with consistent levels across most of the year (5 - 15 cm/month).

3.2 Performance of wall products

In this section we describe wall product performance from the perspective of how well they retain their initial albedos as they undergo natural exposure. We refer to albedo changes in terms of “losses”, calculated by subtracting the final albedo from the initial albedo. A positive albedo loss indicates that specimen reflectance *decreased* with natural exposure; a negative albedo loss indicates the specimen reflectance *increased* with natural exposure.

The data currently presented in this report covers 24 months of exposure at the three California sites and up to 1 year of exposure at the three U.S. national sites. Overall, changes in albedo, whether losses or gains, were small and, in some cases, negligible (Figure 7). At the three California sites, 24-month albedo losses of all but two materials did not exceed 0.06. At the three U.S. national sites, 1-year albedo losses of all materials did not exceed 0.05. Compared with similar results from natural exposure of roofing materials, wall materials seem to fare much better. Changes in solar reflectance of roofing materials is more marked during the first year of exposure, and in many cases that initial drop is the dominant feature over the three years required for CRRC rating (Sleiman et al, 2011; Sleiman et al, 2014).

For the same reason, we observed to date relatively little effect of seasonality, which in the case of California could be attributed primarily to rainfall.

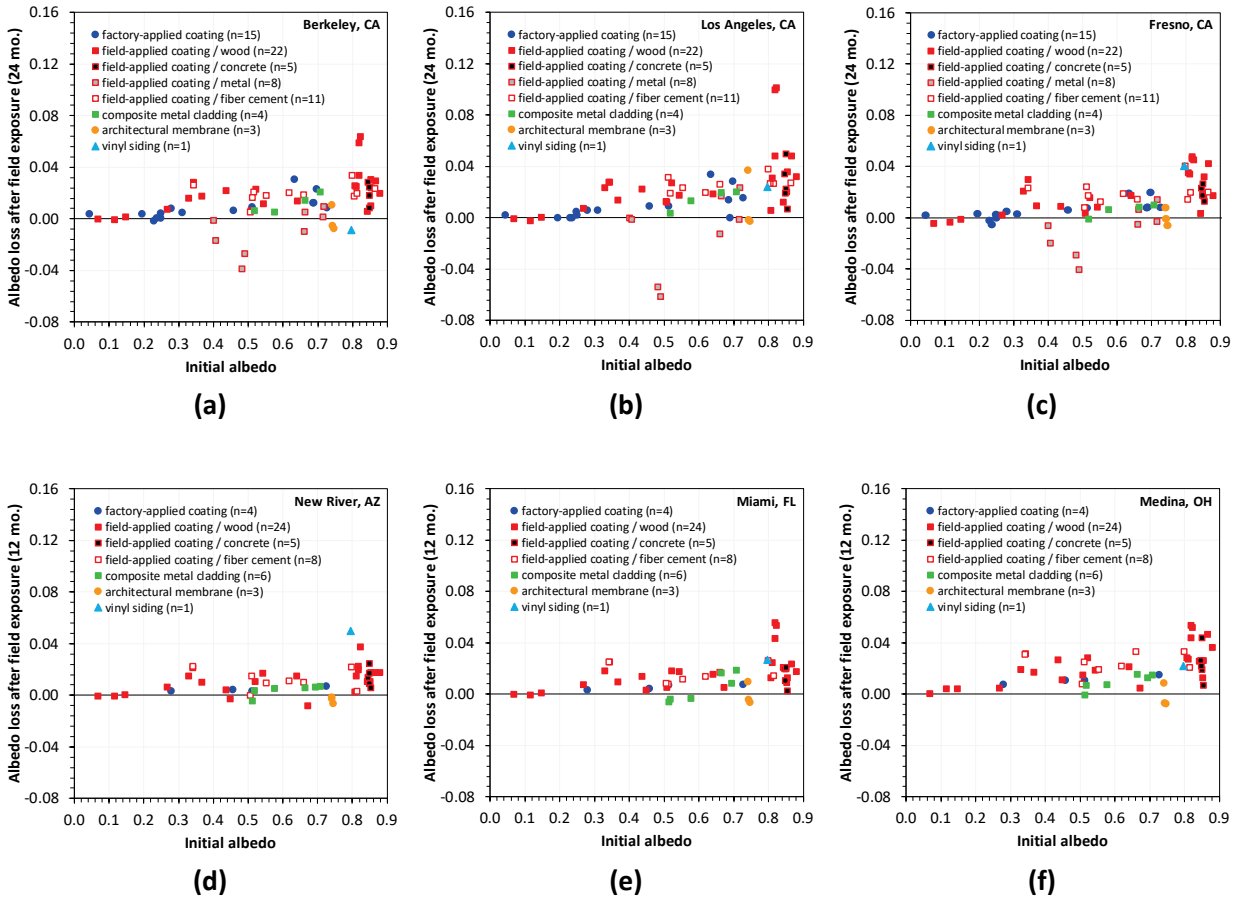

Figure 7. Summary of 24-month albedo losses of materials exposed at three California sites (panels a – c) and 12-month albedo losses of materials exposed at three U.S. national sites (panels d – f). Albedo losses observed thus far have been modest to negligible. Only three materials experienced albedo losses exceeding 0.05.

3.2.1 High performance wall products

The product categories showing highest performance were factory-applied coatings and composite metal claddings. Examples of the performance of these two categories of products are illustrated in Figure 10 for factory-applied coatings and in Figure 11 for composite metal claddings. In both cases, exposure in all six sites has not led to a significant change in solar reflectance over the course of the studied period.

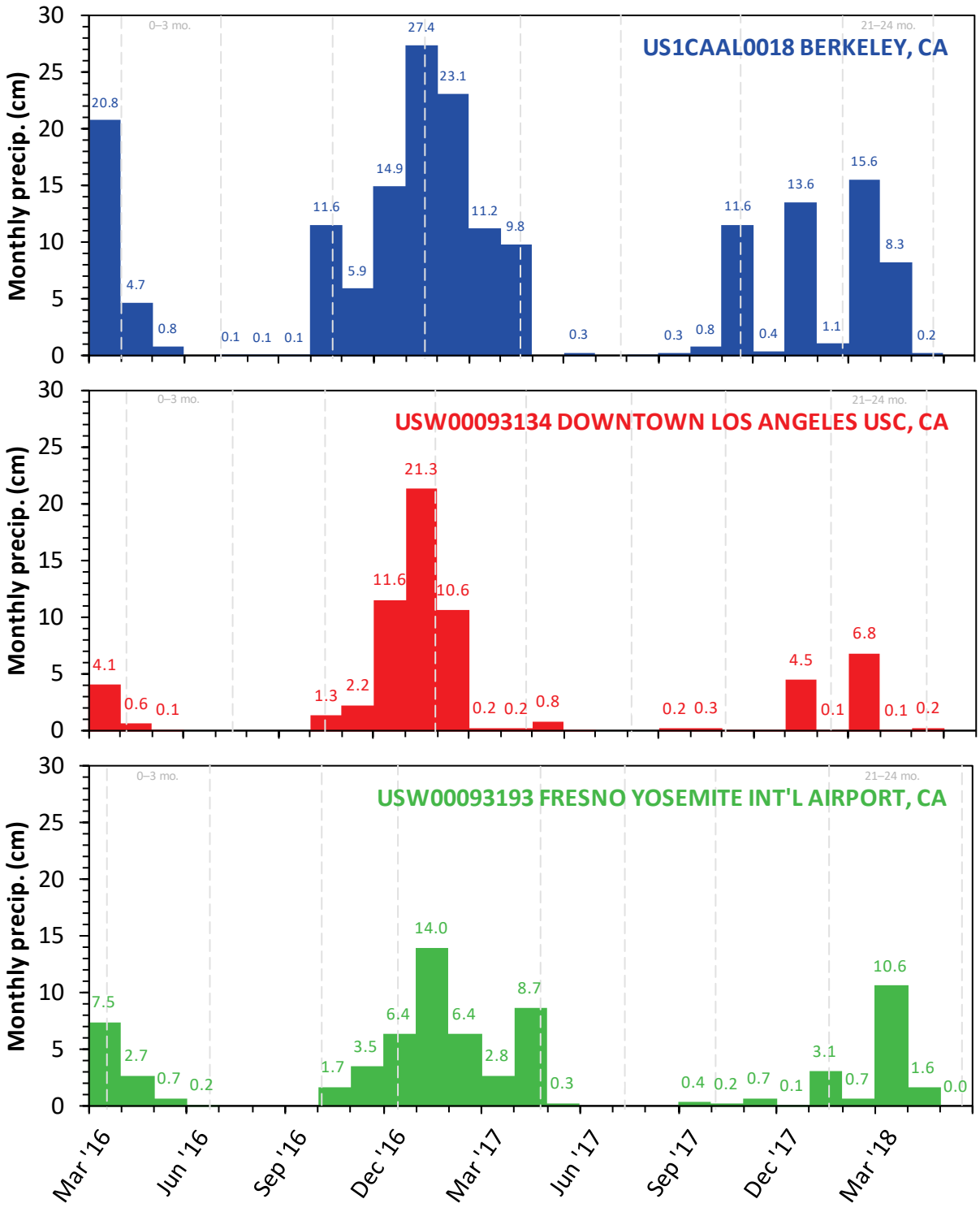

Figure 8. Rainfall patterns at the California exposure sites.

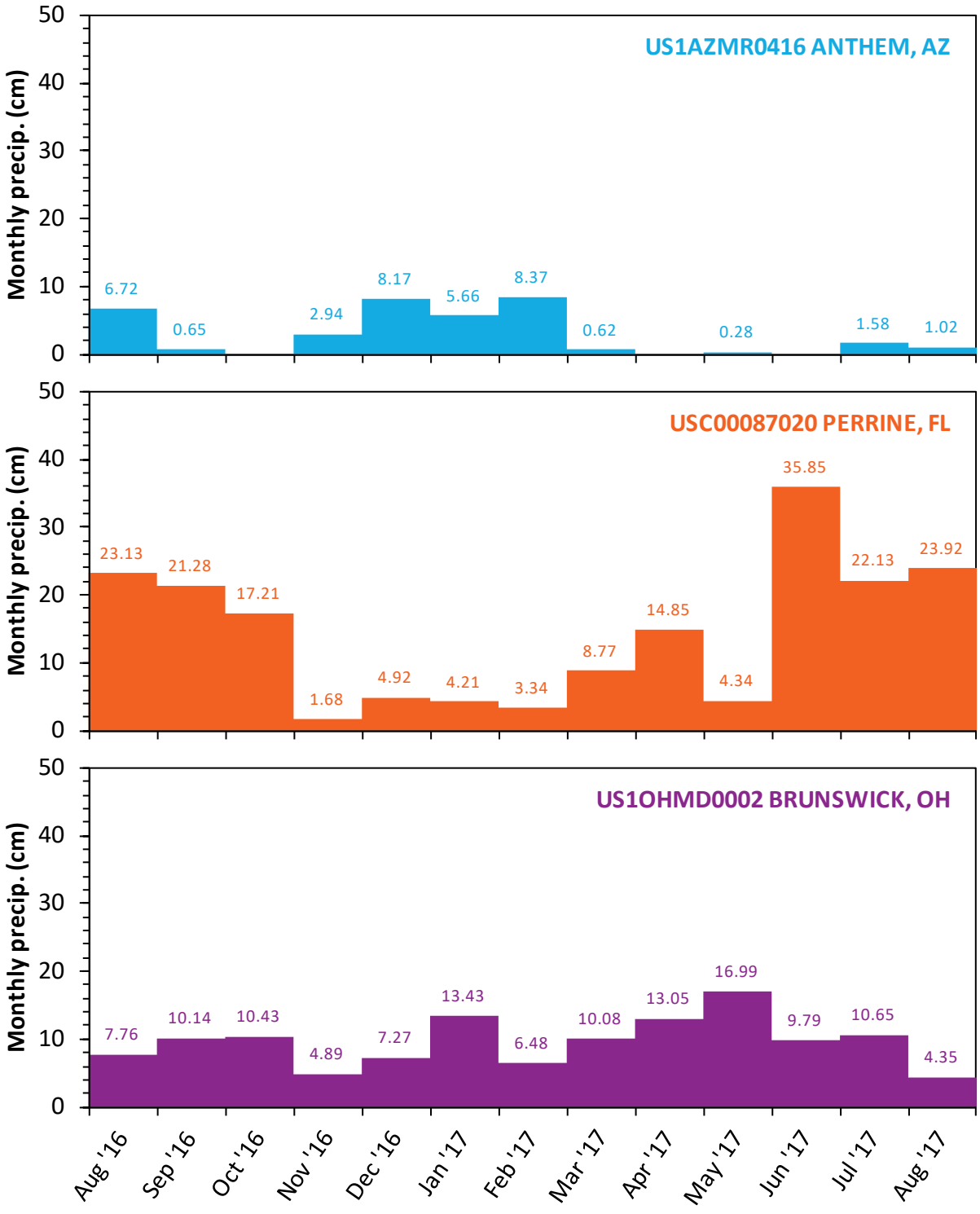

Figure 9. Rainfall patterns at the U.S. national exposure sites.

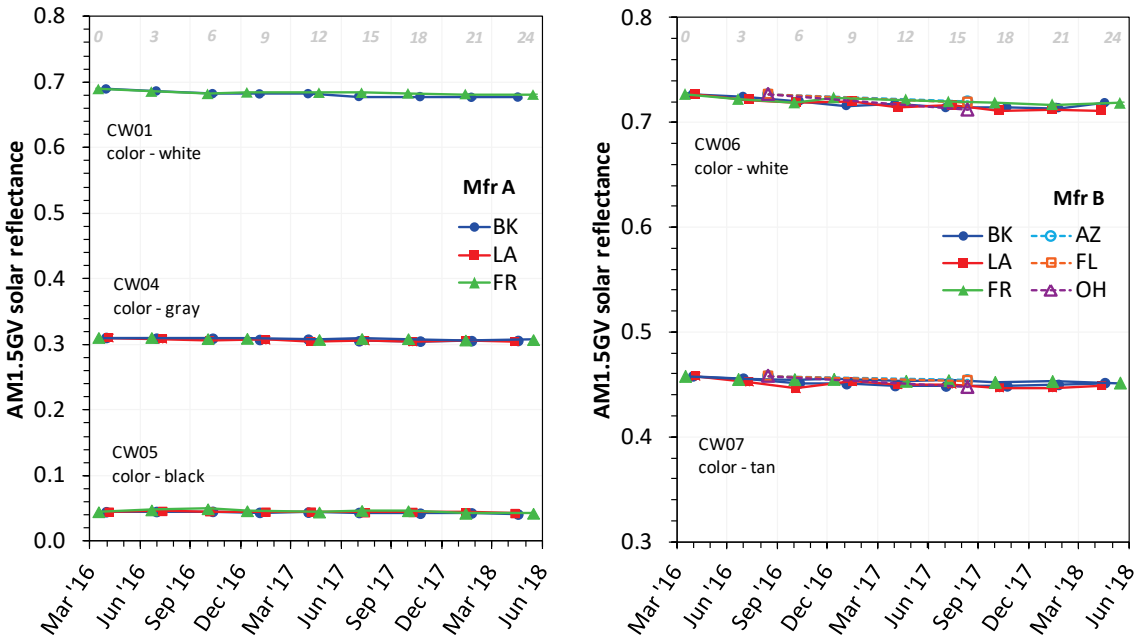

Figure 10. Solar reflectance of factory-applied products exposed in California and U.S. national sites.

Albedo losses for these products range from -0.01 to 0.03. Figure 12 shows that the largest changes are associated with initially high solar reflectances corresponding to white or light color materials, which are most affected by soiling. Negative values correspond to increases in albedo, often recorded in dark color materials as they are covered with soiling that is lighter in color. The results also suggest a site-related correlation, with Berkeley being the site in which changes are largest, and Florida, Arizona and Fresno those in which changes are of smaller magnitude.

Three different type of factory-applied coatings were tested, that included the following dirt-resistant constituents:

a) the thermoplastic polymer polyvinylidene fluoride (PVDF)

b) silicone-modified polyester

c) polyester

The first two types of products showed significantly good performance. Samples containing polyester showed the highest albedo losses, as shown in Figure 13.

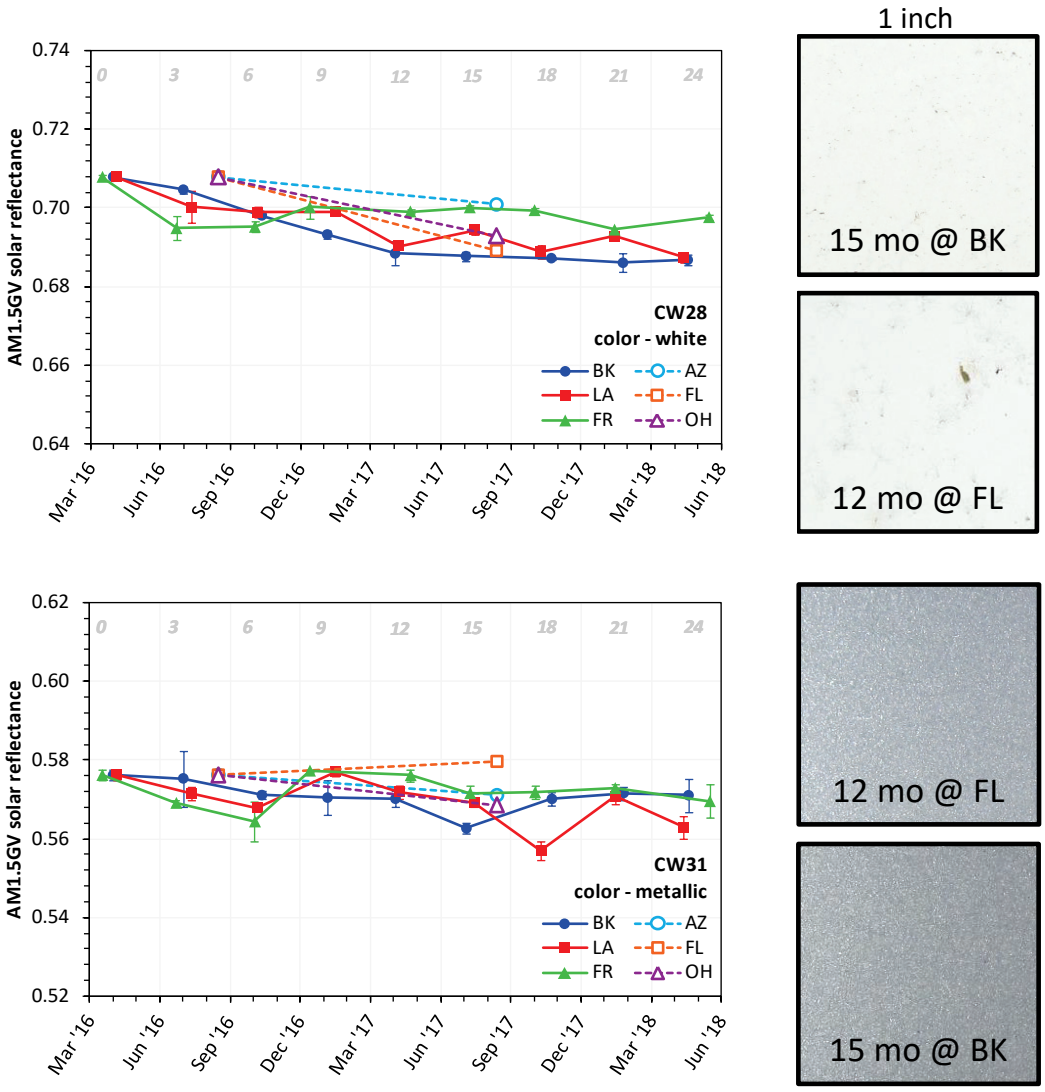

Figure 11. Solar reflectances of two different composite metal claddings exposed in California and U.S. sites.

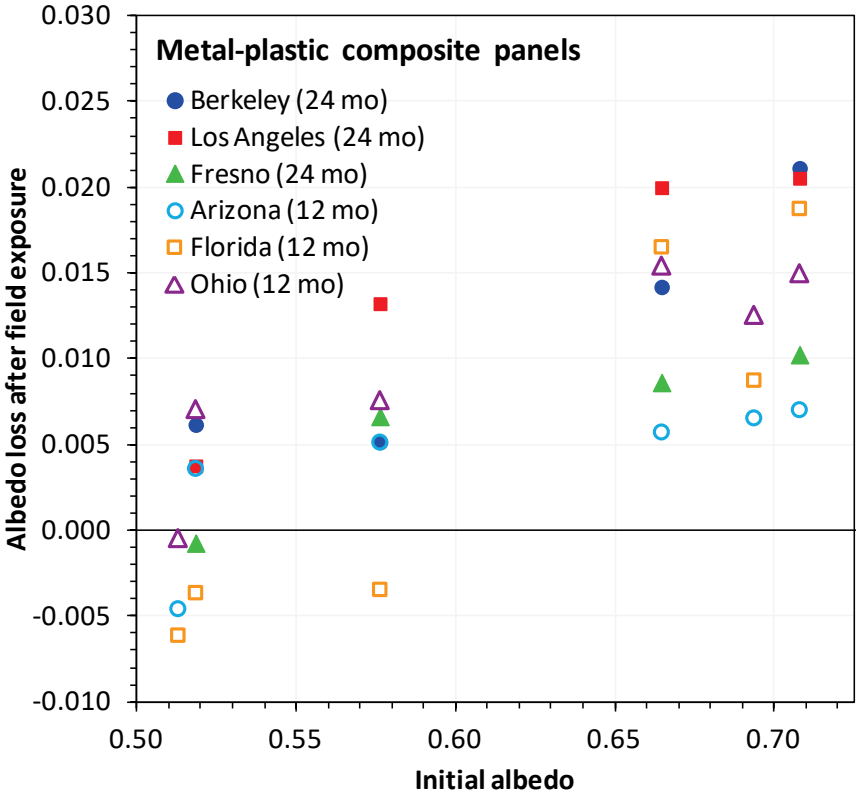

Figure 12. Changes in albedo of composite metal claddings after 24 months of exposure in California and 1 year of exposure at the U.S. national sites.

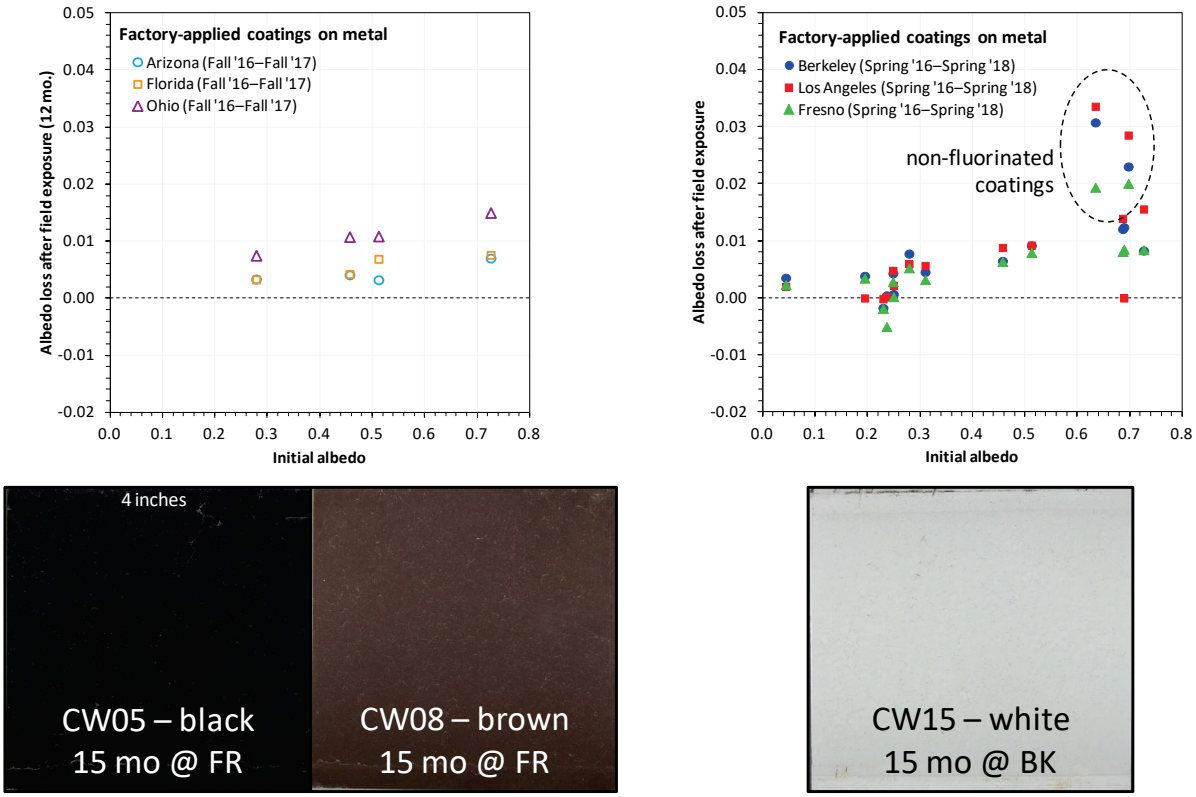

For these materials, albedo increases as materials are soiled

Soiling accumulated on CW15, a light-colored non-fluorinated coating

Figure 13. Changes in albedo of factory-applied coatings after 24 months of exposure in California and 1 year of exposure at the U.S. national sites.

3.2.1.1 Effect of surface texture

The effect of different surface textures was investigated using two different factory-applied coating products, for which we also received the equivalent smooth surface, used as control. In the first case (shown in Figure 14), the textured product had an initial albedo that was about 0.02 lower than the control sample. That gap between those two products was retained over the exposure period, in all three sites. However, a similar analysis carried out with the other textured (embossed) product and its corresponding smooth control sample did not show a significant difference between the two (Figure 15). Hence, no strong effect can be derived from these observations.

It should be noted that in Figure 15, the results for Los Angeles could not be recorded because specimens were exposed without removing their protective transparent plastic cover.

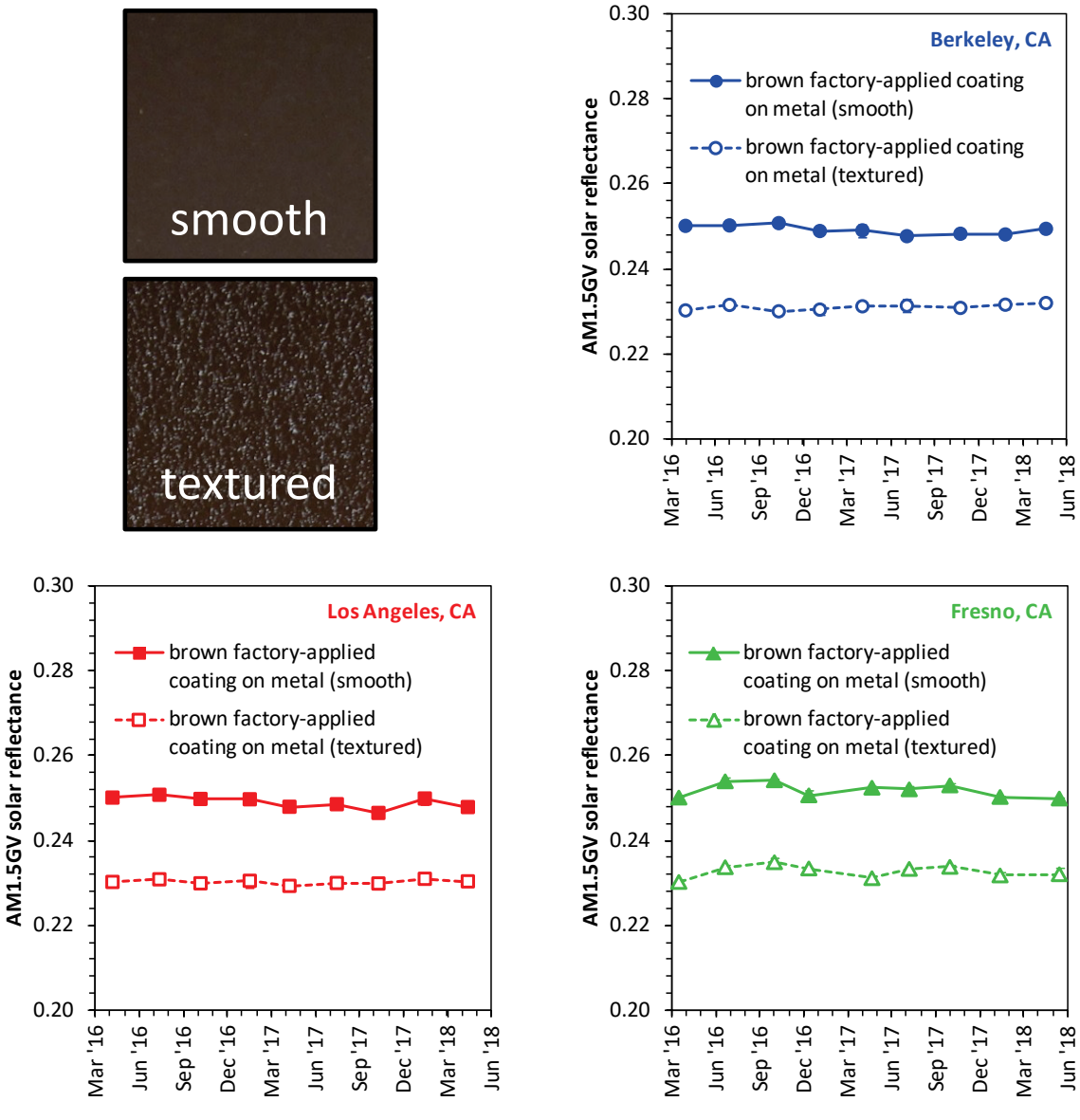

Figure 14. Comparison of solar reflectances measured for smooth and textured factory-applied coatings.

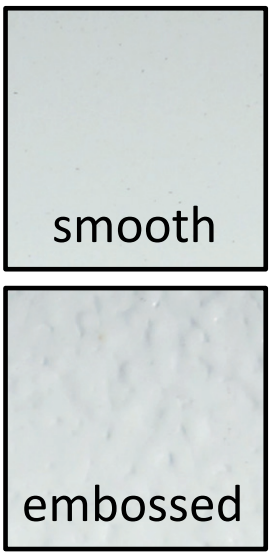

Los Angeles data not available

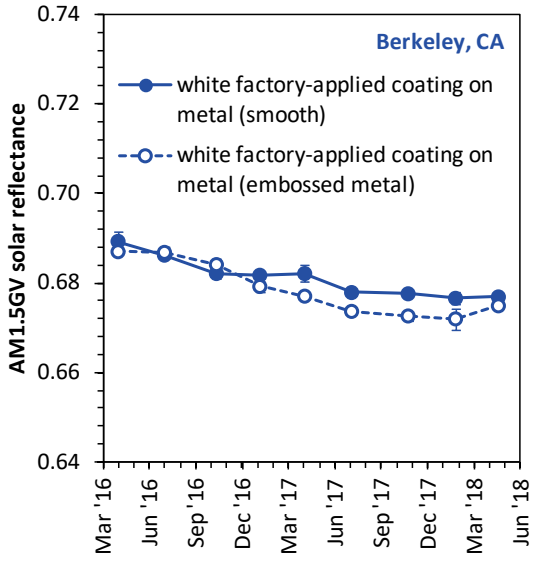

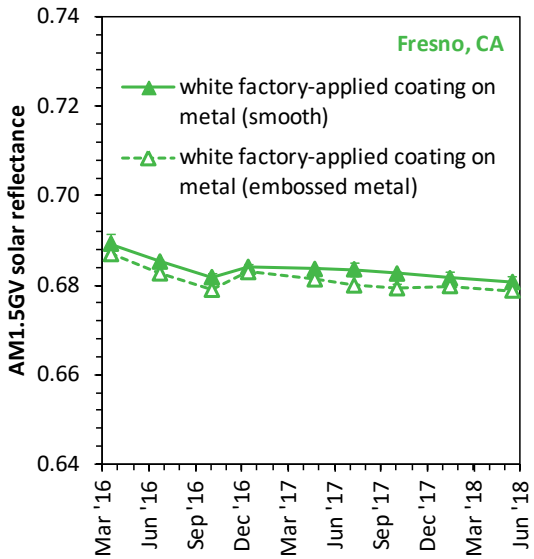

Figure 15. Comparison of solar reflectances measured for smooth and embossed factory-applied coatings.

3.2.2 Field-applied coatings

This category groups the majority of materials analyzed in this study. For that reason, the analysis was performed as a function of various other characteristics of the different products received from manufacturers.

3.2.2.1 Effect of different substrates

Field-applied coatings were evaluated on four different substrates: wood, concrete, metal, and fiber cement. Figure 16 presents the complete set of results for all products applied to all

substrates, grouped by site of exposure (California and U.S. national). There is no difference in performance (with statistical significance) between paint coatings applied over wood and fiber-cement substrates. Those applied over wood substrates seem to have slightly higher solar reflectances, possibly due to higher surface smoothness and potentially also the fact that if the coatings are not thick enough to be fully opaque, the reflectance of the substrate can modestly affect the material's albedo. In the case of the materials with concrete substrates, all of the coating products were white, and differences among the five materials could be attributed to different formulations.

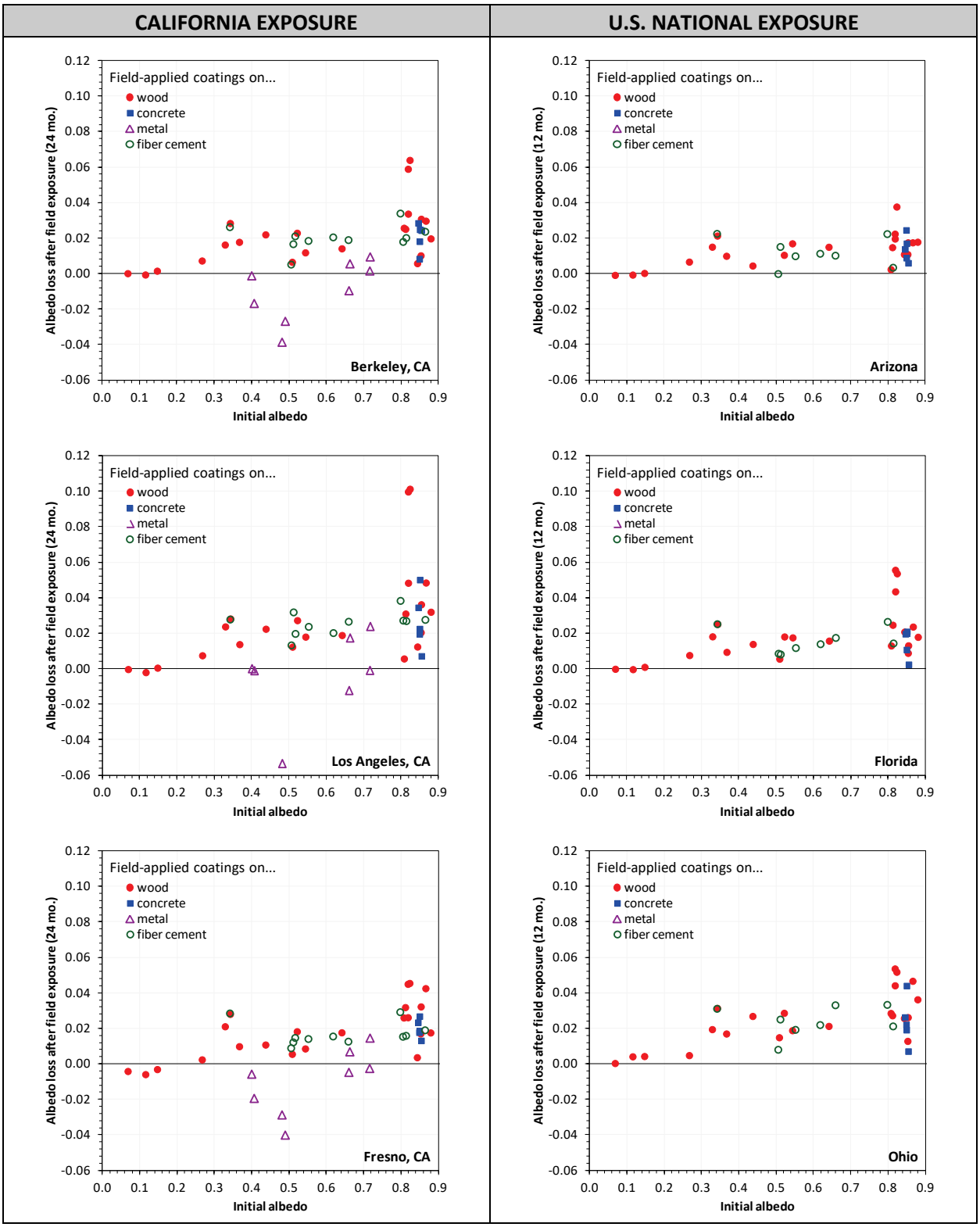

Figure 16. Changes in albedo of field-applied coatings exposed in California and U.S. national sites (all materials).

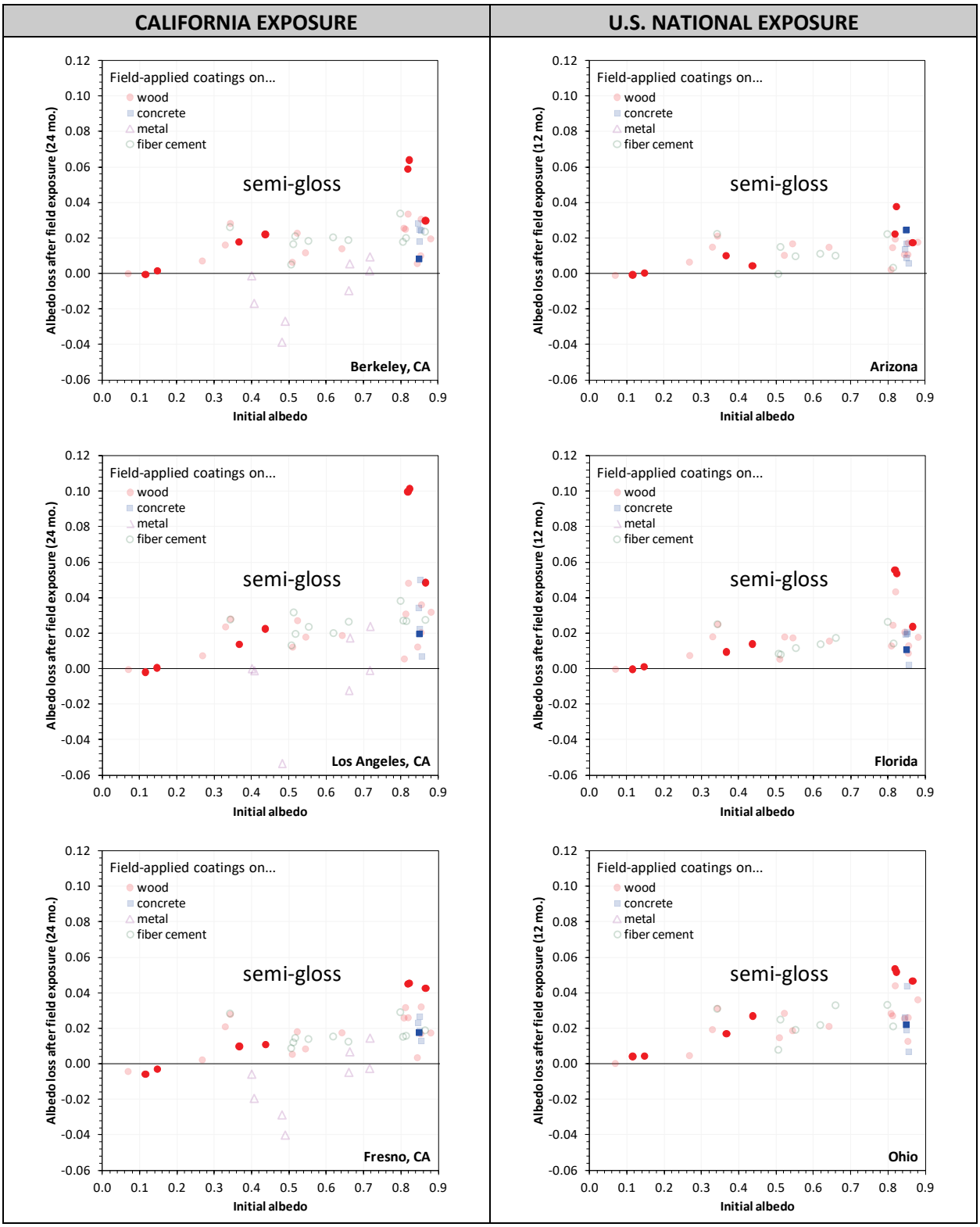

Figure 17. Changes in albedo of field-applied coatings exposed in California and U.S. national sites (semi-gloss finish).

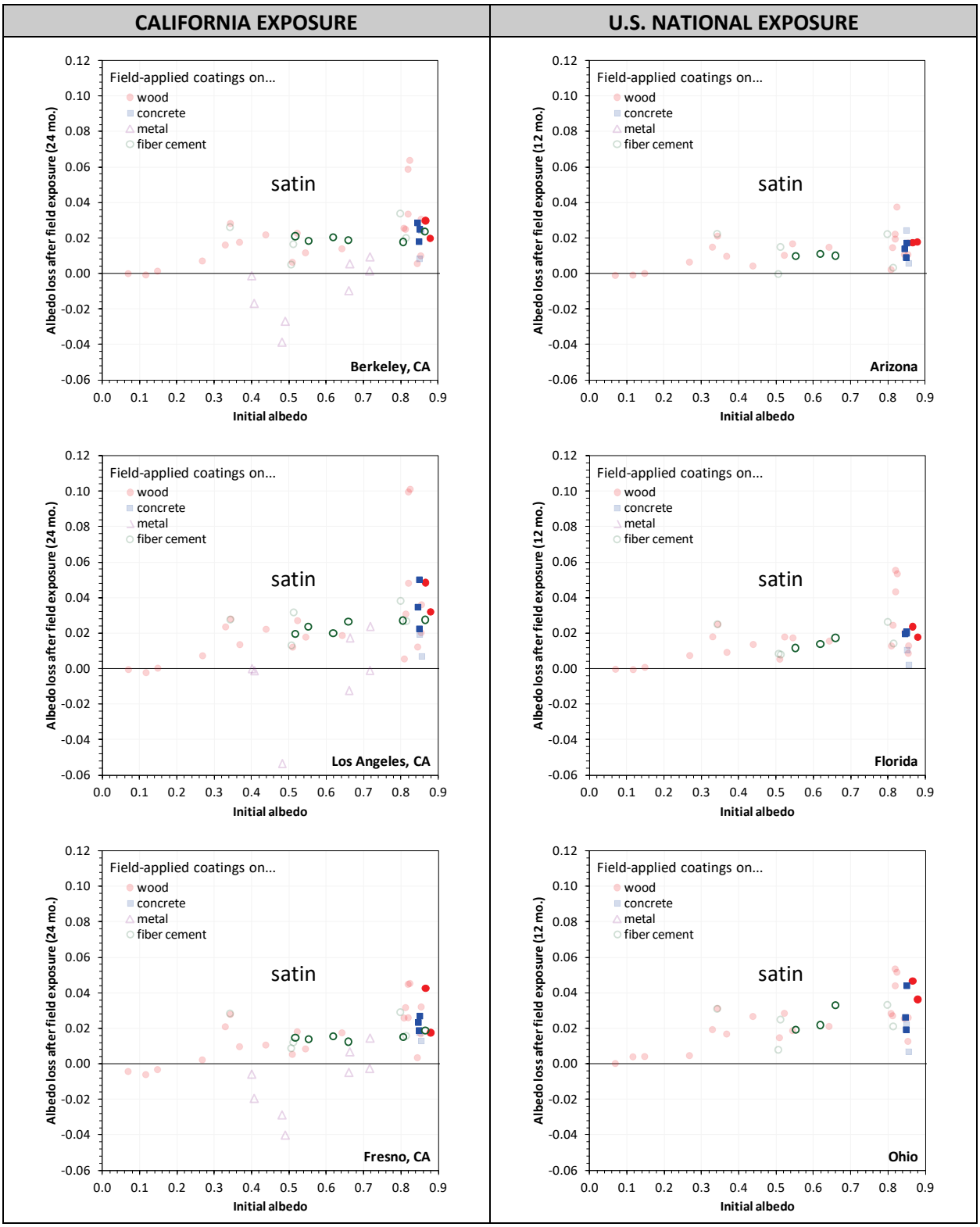

Figure 18. Changes in solar reflectance of field applied coatings exposed in California and U.S. national sites (satin finish).

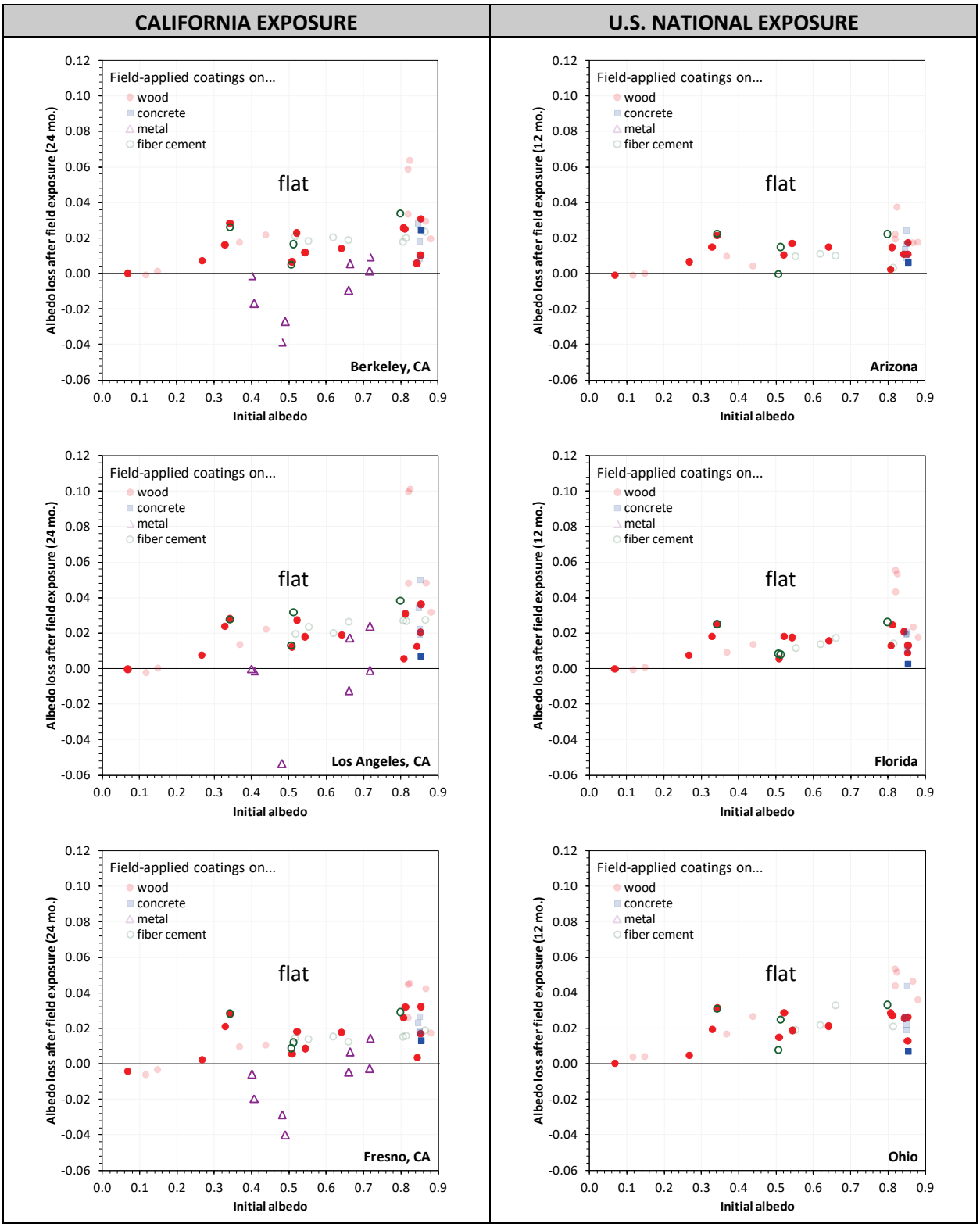

Figure 19. Changes in solar reflectance of field applied coatings exposed in California and U.S. national sites (flat finish).

3.2.2.2 Effect of surface finish

The sub-set of field-applied coating samples that corresponded to semi-gloss, satin and flat finishes, are presented in Figure 17, Figure 18 and Figure 19 respectively. Most materials fall in the latter category, and show a significant dispersion. However, for a given value of the initial albedo, the semi-gloss and satin samples tend to present a higher loss of performance than the corresponding flat material.

3.2.2.3 Effect of formulations containing cool pigments

Coloring coatings with spectrally-selective “cool color” pigments can boost albedo while providing a broad palette (Levinson et al., 2007). This enhanced performance is achieved by increasing reflectance in the near-infrared spectrum (700 – 2,500 nm), which accounts for about half of the total solar energy. Several manufacturers offer cool versions of their paint formulations and in this study we were able to compare cool paints with conventional versions of the same color used as their control samples. Figure 20, Figure 21 and Figure 22 illustrate this effect on three cool paints of different colors applied on wood. The increase in solar reflectance attributed to the use of spectrally-selective pigments over conventional pigments is in all cases between 0.2 and 0.3. Exposure at three different California sites did not significantly alter this effect.

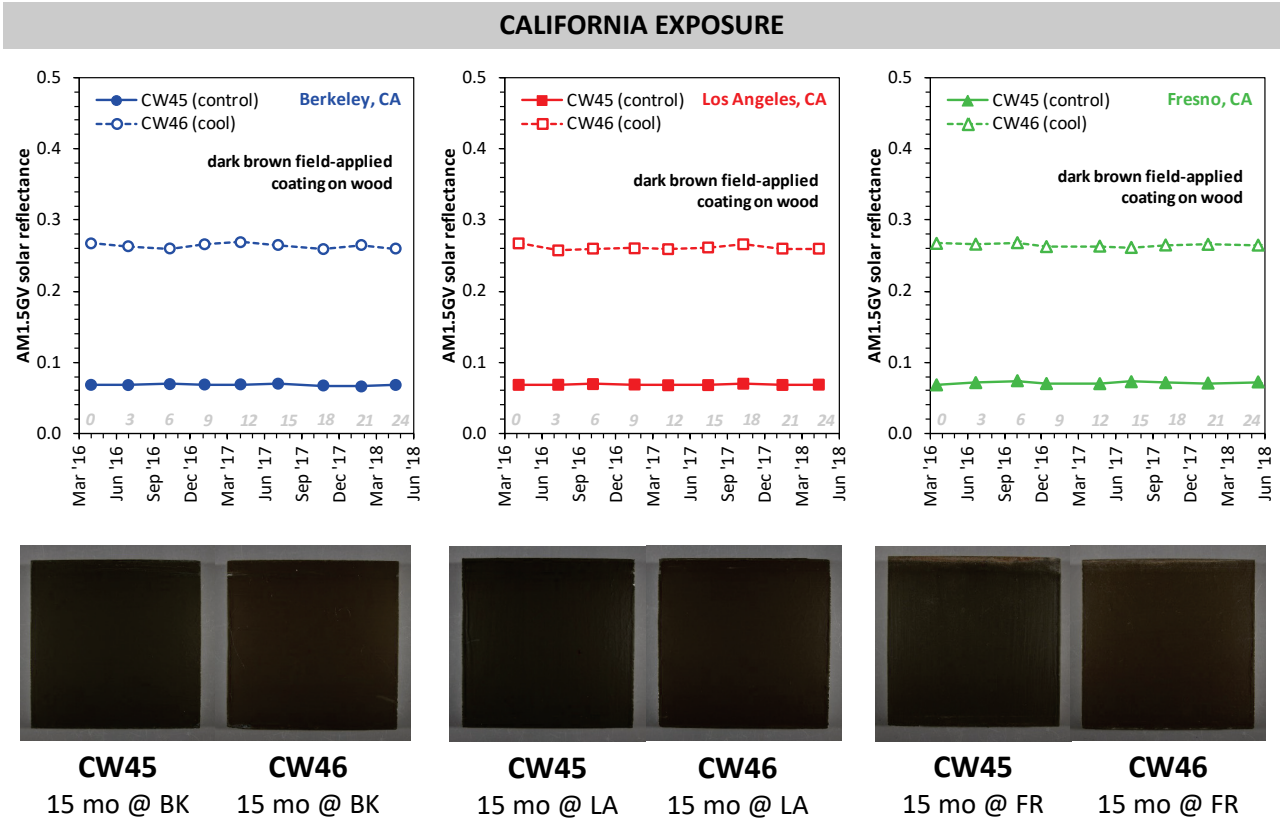

Figure 20. Solar reflectance of field applied coatings exposed in California (cool pigment vs. control).

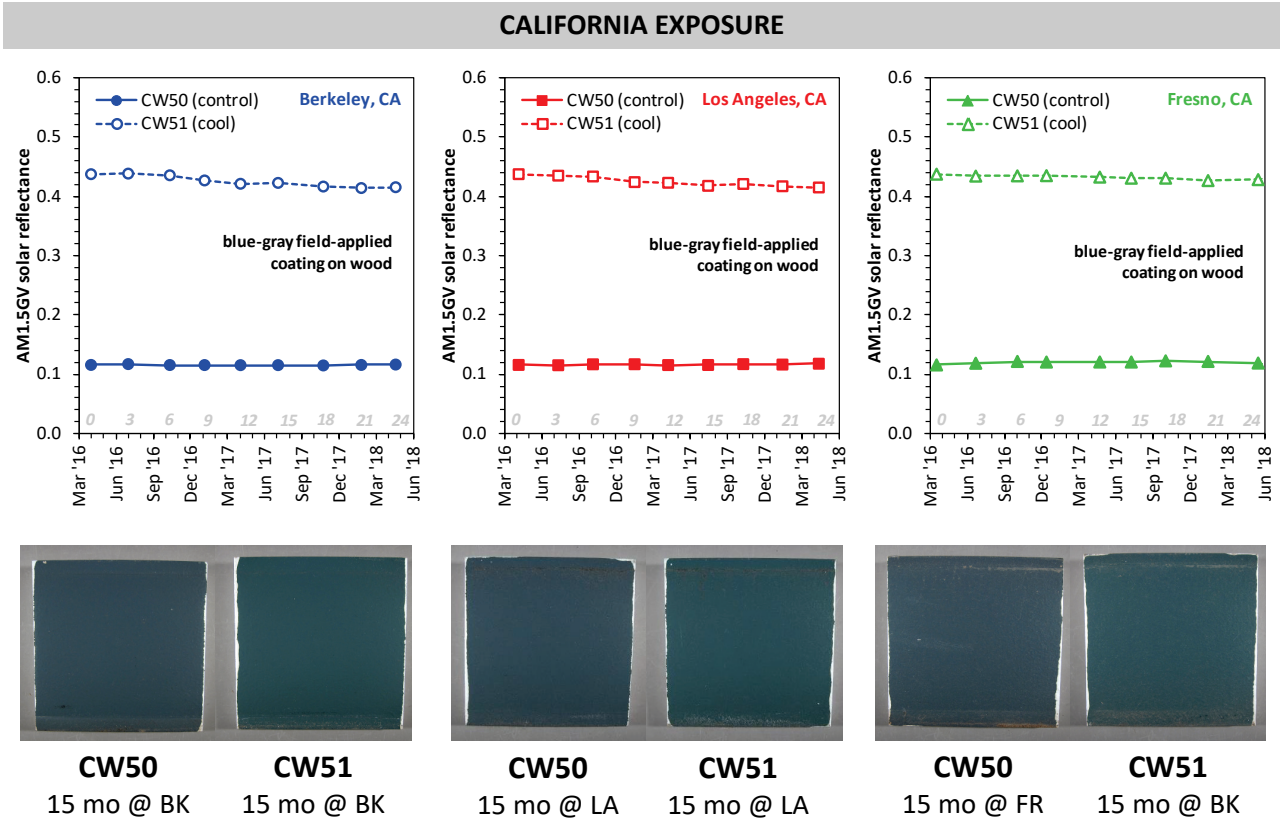

Figure 21. Solar reflectance of field applied coatings exposed in California (cool pigment vs. control).

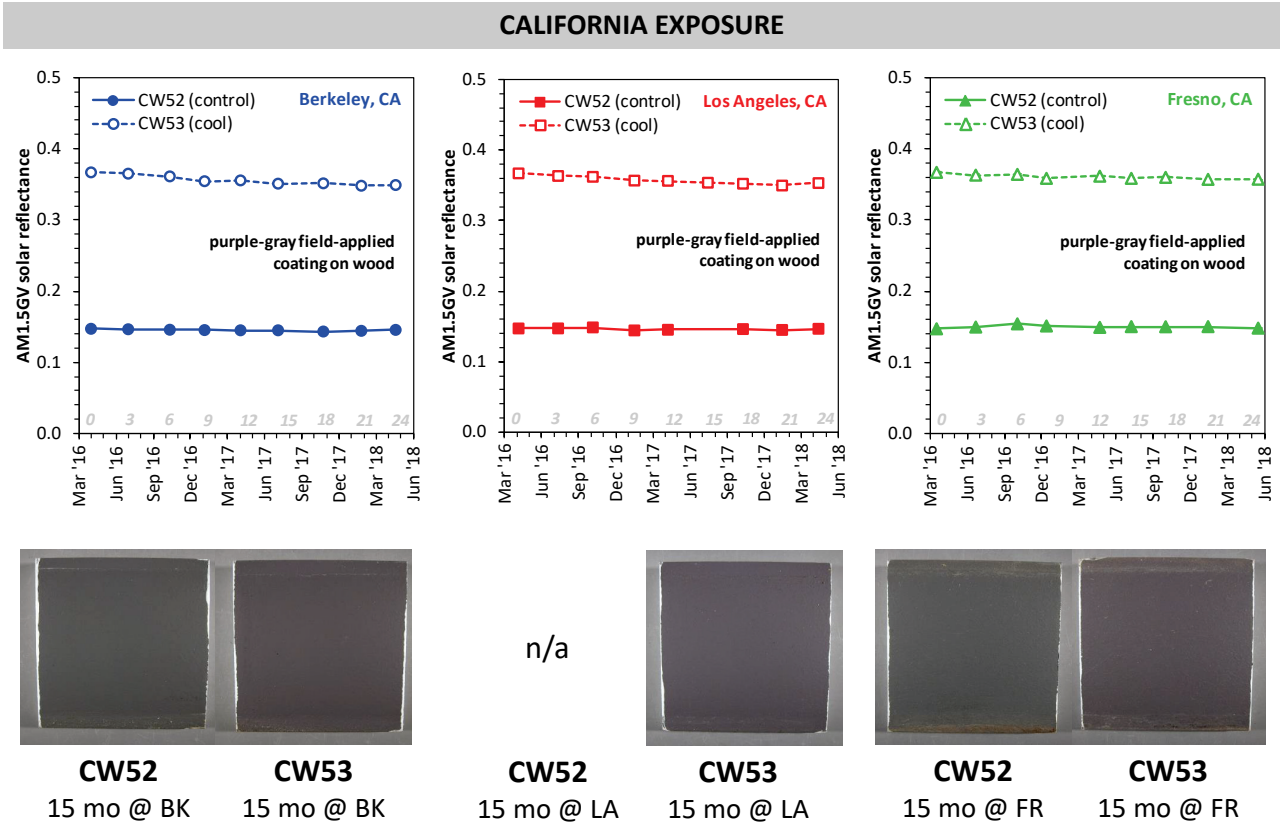

Figure 22. Solar reflectance of field applied coatings exposed in California (cool pigment vs. control).

3.2.2.4 Effect of dirt-resistant formulations

Some of the products evaluated in this study were paints formulated with dirt-resistance additives. Figure 23 illustrates the effect attributed to these additives on samples exposed in the three California sites. The control material consisted of a paint of the same general characteristics and color, but which did not have dirt-resistance additives. In all three sites, the initial solar reflectance was similar for the control and dirt-resistant samples, but a gap between them grew as a function of exposure time. This gap was less significant in Berkeley and Los Angeles than in Fresno, suggesting that the nature of soiling deposited on the surface plays an important role. Both dirt-resistant formulations seemed to perform very similarly in all three locations.

Figure 24 compares results from these same materials, corresponding to 24 months of exposure in California and 12 months in the U.S. national exposure locations. In most cases, the dirt-resistant formulation presented a smaller reduction in albedo than the controls. Photos of those same specimens are presented in Appendix 1.

Another pair of products—a white dirt-resistant paint formulation and a non-dirt-resistant paint formulation of similar type and color—were applied on two different substrates to

compare the effect of the substrate on this property (Figure 25). On all three California sites, the dirt-resistant paint applied over fiber-cement substrates showed a modest improvement in performance with respect to the non-dirt-resistant paint. In this pair, the observed albedo loss in the non-dirt-resistant formulation was 0.01 – 0.02 greater than that for the dirt-resistant formulation. When the two products were applied on wood, the difference in albedo loss between them was marginal in Berkeley and Fresno (~0.001), but modest in Los Angeles (albedo loss in the non-dirt-resistant formulation was 0.025 greater than in the dirt-resistant formulation).

Figure 26 illustrates a third set of results, corresponding to a paint formulation combining cool pigments with dirt-resistance additives. Compared to a similar non-cool and non-dirt-resistant product, the spectrally-selective pigments in this formulation boost the initial albedo by roughly 0.15. We did not observe any significant performance improvements in this dirt-resistant and cool product over a similar product with cool pigments but no additional dirt-resistant additives.

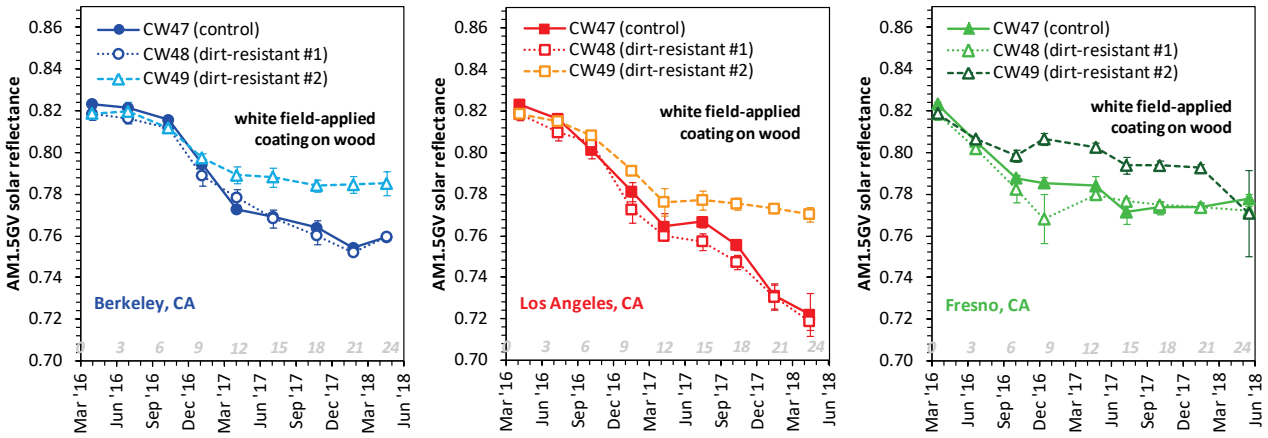

Figure 23. Solar reflectance of field applied coatings exposed in California (dirt-resistant vs. control).

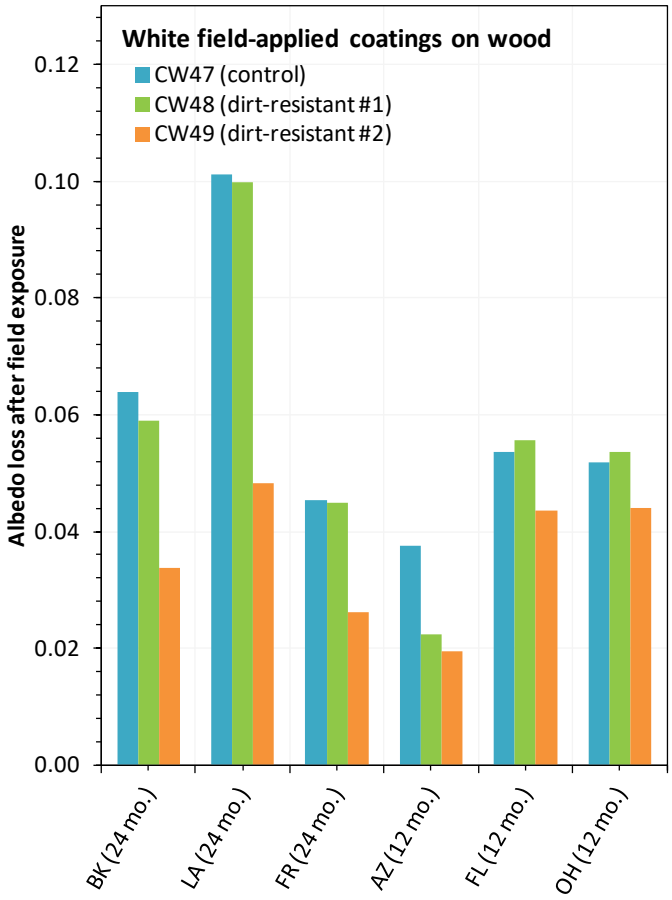

Figure 24. Change in solar reflectance of field applied coatings exposed in California and U.S. national sites (cool pigment vs. control).

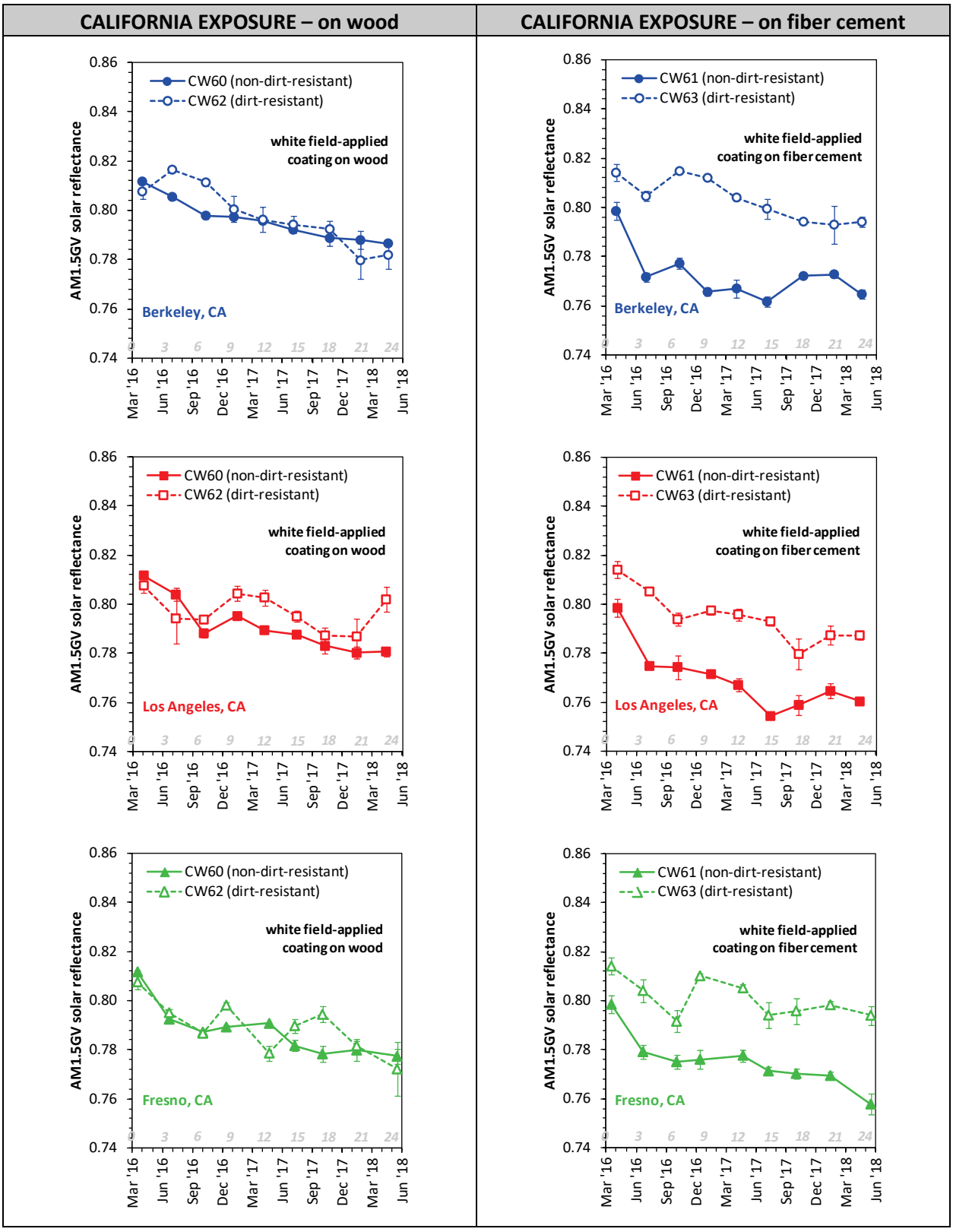

Figure 25. Solar reflectance of field applied coatings exposed in California on two different substrates (cool pigment vs. control).

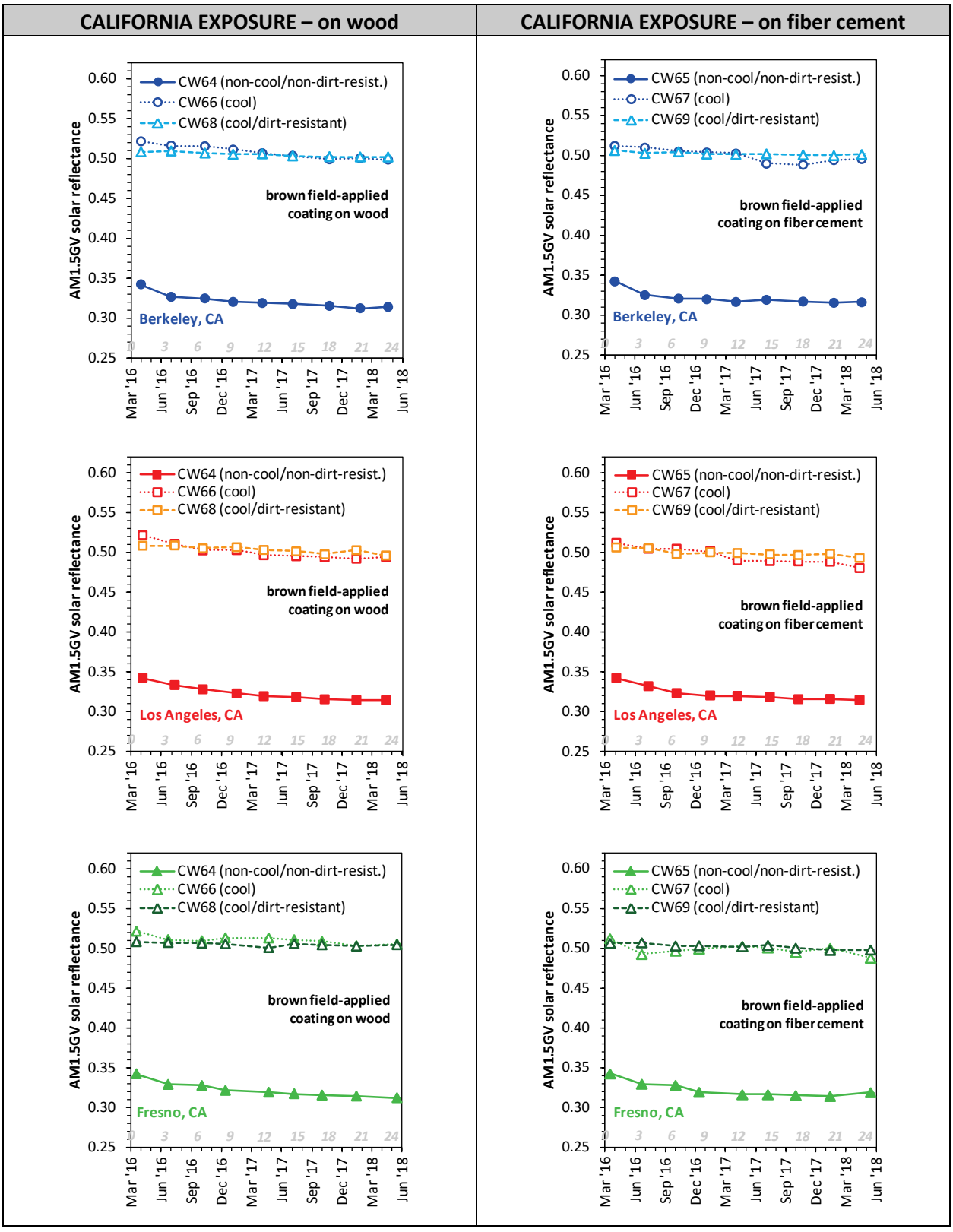

Figure 26. Solar reflectance of field applied coatings exposed in California (cool pigment + dirt-resistant vs. cool pigment vs. control).

3.2.3 Color changes due to product aging

In general, albedo loss is attributed to the presence of soiling agents such as dust deposition and microbial growth. However, in a few cases we observed a noticeable color change, which is likely the main reason for the albedo changes.

In Figure 27 and Figure 28, we illustrate the results obtained for vinyl siding specimens that were initially white, after exposure in the California and U.S. national sites. Many of the retrieved specimens had turned yellow, showing corresponding decreases in solar reflectance.

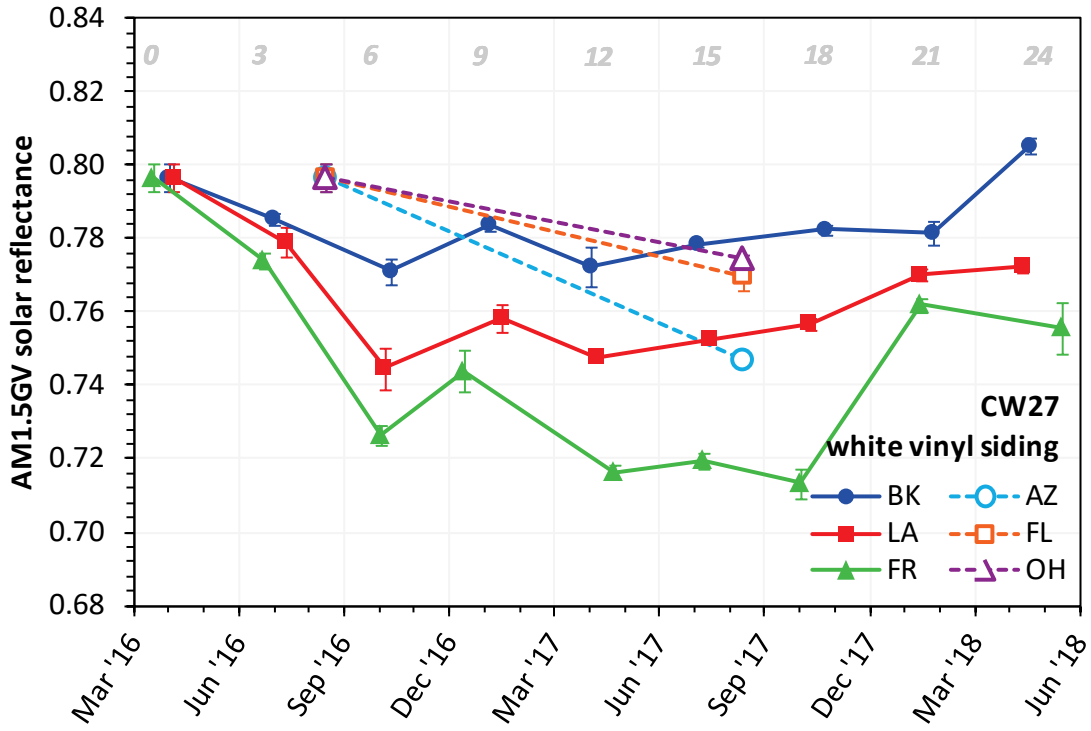

Figure 27. Solar reflectance of vinyl siding specimens exposed in California and U.S. national sites.

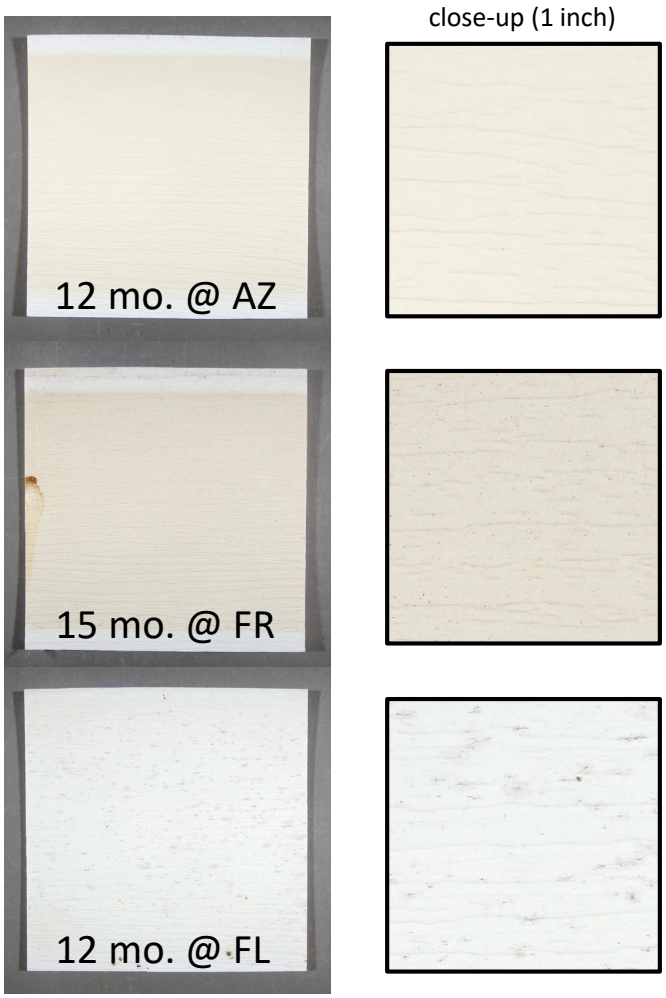

Figure 28. Images of vinyl siding specimens exposed in California sites after 12 months.

By contrast, a set of paint formulations that included photocatalytic self-cleaning pigments showed an increase in solar reflectance compared with the corresponding non-photocatalytic control, which could be attributed to the enhanced bleaching of the pigment due to the oxidative action of the photocatalyst (Figure 29).

On a similar set of products, including a photocatalytic formulation and a control, both samples showed bleaching upon exposure, with the largest effect being for the samples exposed in Los Angeles (Figure 30).

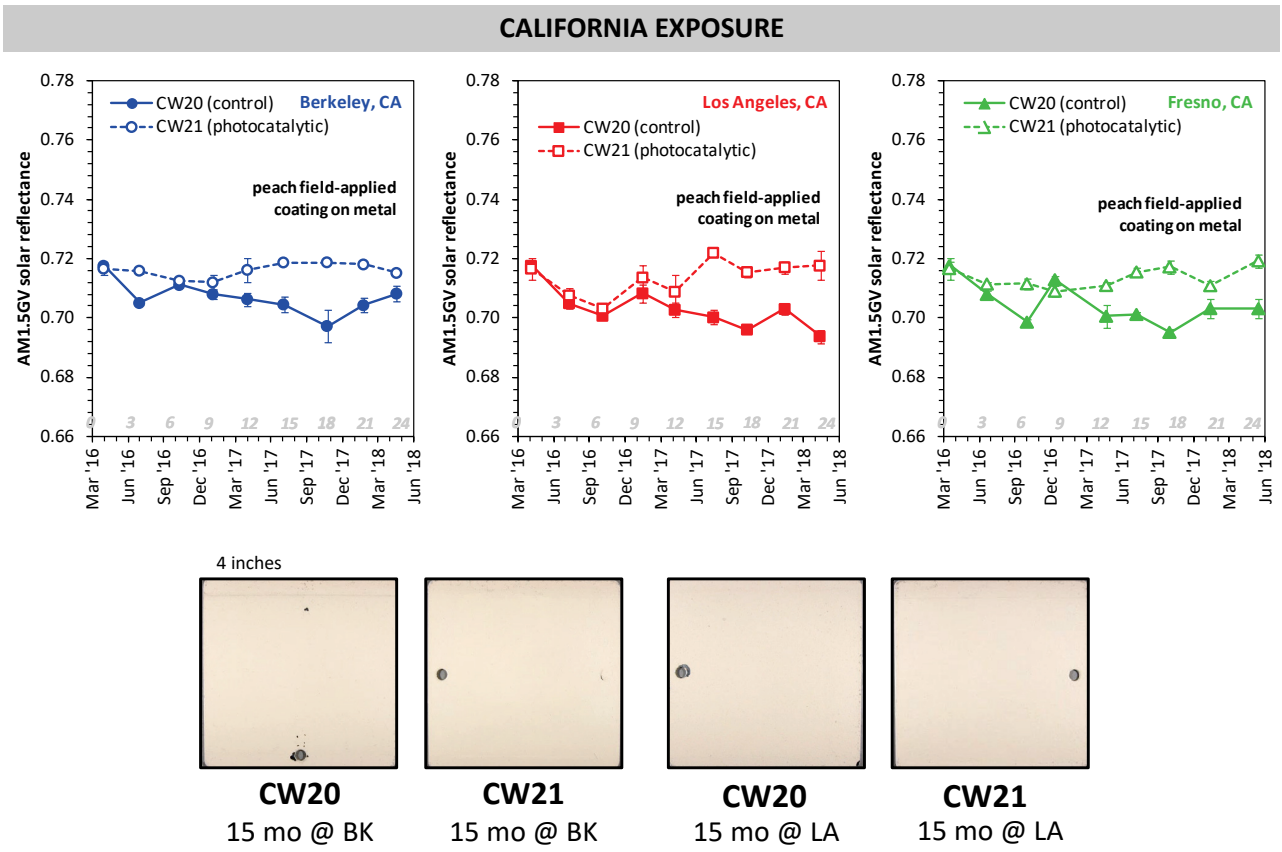

Figure 29. Solar reflectance of photocatalytic paint and their control, at the California exposure sites.

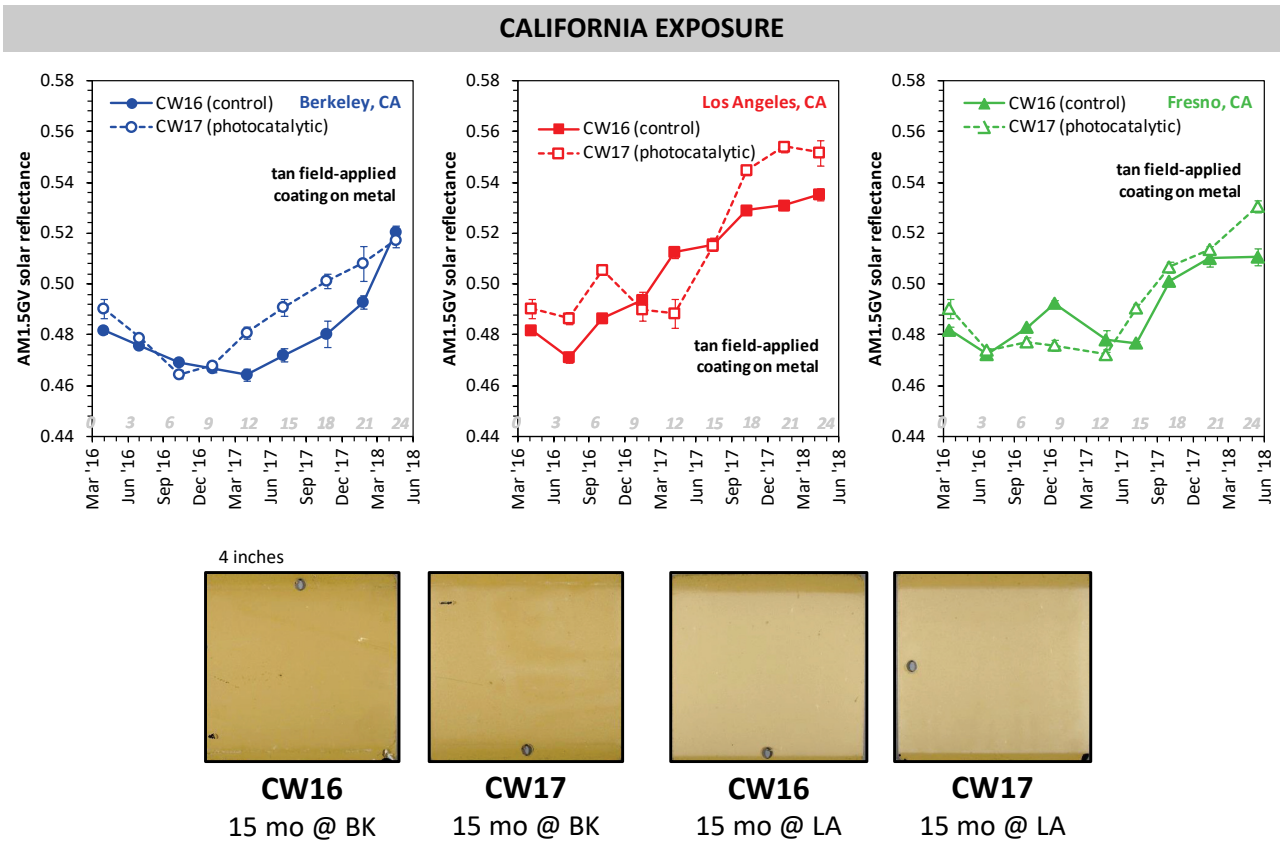

Figure 30. Solar reflectance of photocatalytic paint and their control, at the California exposure sites.

3.2.4 Self-cleaning products

Results shown in Figure 29 illustrate the effect of photoactive pigments on paint formulation. It was impossible to assess whether some of the changes in solar reflectance were due to the oxidation of soiling agents by the photocatalyst, or simply to the color change due to pigment bleaching. The results shown in Figure 30 suggest that other photocatalytic paint formulations did not have a major de-soiling effect.

Photocatalytic architectural fabrics were also investigated in detail. Those results are presented in the Task 4.3 report: *Evaluation of self-cleaning and de-polluting photocatalytic wall materials.*

4 Conclusions

Overall, the natural exposure of wall products over the course of 24 months at three California sites and 1 year at three U.S. national sites has shown modest to negligible changes in solar reflectance. Changes in albedo were caused by both soiling accumulation and color changes. We observed the highest albedo retention in factory-applied fluoropolymer coatings and varying levels of albedo retention in field-applied coatings and other products.

5 Future work

The results of this natural exposure study will be further systematized during the preparation of an archival journal article summarizing the key results. This information will also support efforts to propose implementation of cool walls rating systems.

National exposure is schedule to continue through 2021. We will coordinate with industrial partners to retrieve and measure those specimens in August of 2018, 2019, 2020, and 2021.

Acknowledgements

The authors thank Dave Speiser (Vitro) and Pablo Rosado (LBNL) for their help establishing and operating the Fresno exposure site.

References

Gagliardi M. 2010. Photocatalysts: Technology and Global Markets. BCC Research. Available online at: https://www.bccresearch.com/market-research/advanced-materials/photocatalysts-tech-markets-avm069a.html

Levinson R, Berdahl P, Akbari H, Miller W, Joedicke I, Reilly J, Suzuki Y, Vondran M. 2007. Methods of creating solar-reflective nonwhite surfaces and their application to residential roofing materials. *Solar Energy Materials & Solar Cells* 91, 304-314.

NOAA. 2018. Global Historical Climatology Network (GHCN), available through the National Oceanic and Atmospheric Administration at https://www.ncei.noaa.gov/

Sleiman M, Ban-Weiss G, Gilbert HE, Francois D, Berdahl P, Kirchstetter TW, Destaillats H, Levinson R. 2011. Soiling of building envelope surfaces and its effect on solar reflectance – Part 1: Analysis of roofing product databases. *Solar Energy Materials and Solar Cells* 95, 3385-3399.

Sleiman M, Kirchstetter TW, Berdahl P, Gilbert HE, Quelen S, Marlot L, Preble CV, Chen S, Montalbano A, Rosseler O, Akbari H, Levinson R, Destaillats H. 2011. Soiling of building envelope surfaces and its effect on solar reflectance – Part 2: Development of an accelerated aging method for roofing materials. *Solar Energy Materials and Solar Cells* 122, 271-281.

Energy Research and Development Division

FINAL PROJECT REPORT

Solar-Reflective "Cool" Walls: Benefits, Technologies, and Implementation

Appendix K: Evaluation of Self-cleaning and De-polluting Photocatalytic Wall Materials (Task 4.3 Report)

California Energy Commission
Gavin Newsom, Governor

April 2019 | CEC-500-2019-040-APK

Appendix K:
Evaluation of self-cleaning and de-polluting photocatalytic wall materials (Task 4.3 report)

Xiaochen Tang[1,2], Sharon Chen[1], Marion Russell[2], Haley Gilbert[1], Sébastien Houzé de l'Aulnoit[1], Ronnen Levinson[1], and Hugo Destaillats[1,2]

[1] Heat Island Group, Lawrence Berkeley National Laboratory

[2] Indoor Environment Group, Lawrence Berkeley National Laboratory

31 May 2018

Abstract

Photocatalytic self-cleaning materials were exposed vertically facing west for two years in three California sites. Specimens were retrieved quarterly for laboratory testing. Another set of the same materials are being exposed at other three sites in Florida, Ohio and Arizona, used for roofing rating over a period of five years, with annual retrievals. In all cases, photocatalytic materials were exposed side-by-side with non-photoactive control specimens. Photocatalytic materials exposed in California showed an excellent self-cleaning performance during all seasons. By contrast, the control material was soiled during the dry season. Photocatalytic materials also showed de-pollution effects that were sensitive to location and weather. Experiments showed nitric oxide (NO) removal and net deposition of nitrogen oxides (NO_x = NO + NO_2) in most locations and weather conditions, with fluctuations associated with atmospheric deposition and precipitation.

1 Introduction

The main goal of this task was to assess the performance of photocatalytic cool wall technologies. This was achieved by exposing these materials to the environment over a 2-year period, measuring the initial solar reflectance and its changes as a function of time. Protocols developed for the evaluation of these radiative properties have been described on the Task 4.1 Report. Specimens used in these measurements were weathered alongside the other wall products described in Task 4.2 at three locations in California: Berkeley, Los Angeles, and

Fresno. In addition, specimens were also exposed at the three sites used nationally for roofing product rating, in Florida, Arizona, and Ohio.

Photocatalytic self-cleaning products can remove soiling from their surface by catalyzing the elimination of deposited soiling in the presence of sunlight, and/or facilitating water runoff due to enhanced surface hydrophilicity. These two phenomena are illustrated in Figure 1A. Photoactive building envelope materials represent a growing sector of the construction market, with $740M in sales in 2009, doubling by 2014 (Gagliardi, 2010). These products are used in new construction and in retrofits, and include cementitious coatings such as mortar, plaster and paint; coated metal siding; architectural fabrics; tiles; precast panels; and roofing.

When these materials are exposed to sun light, photo-induced chemical processes can eliminate soiling and air pollutants adsorbed on the catalyst surface, including organic compounds and atmospheric nitrogen oxides (NO_x), as illustrated in Figure 1-B (Hoffmann et al., 1995). In the case of NO_x, photocatalytic oxidation enables a net removal of these species from the atmosphere through their irreversible conversion to the non-volatile oxidation byproducts nitrate (NO_3^-) and HNO_3. The final stable oxidation byproducts can be washed off the surface by rain or dew. Different test methods have been developed to evaluate the air purification efficiency of photocatalytic materials (Dillert et al, 2012; Mills et al, 2012; Minero et al, 2013). In this study, we adopted a commonly used approach, the ISO Standard 22197-1 “Fine ceramics (advanced ceramics, advanced technical ceramics) – test method for air-purification performance of semiconducting photocatalytic materials. Part 1. Removal of nitric oxide” (ISO, 2007).

The self-cleaning and de-polluting properties of photoactive surfaces have been documented primarily via laboratory tests. One important goal of this study is to quantify these phenomena under real-world conditions. A key barrier to the development of photocatalytic products has been the lack of metrics and methods to evaluate their performance. This study contributes with metrics and processes to facilitate the evaluation and rating of photocatalytic building envelope products.

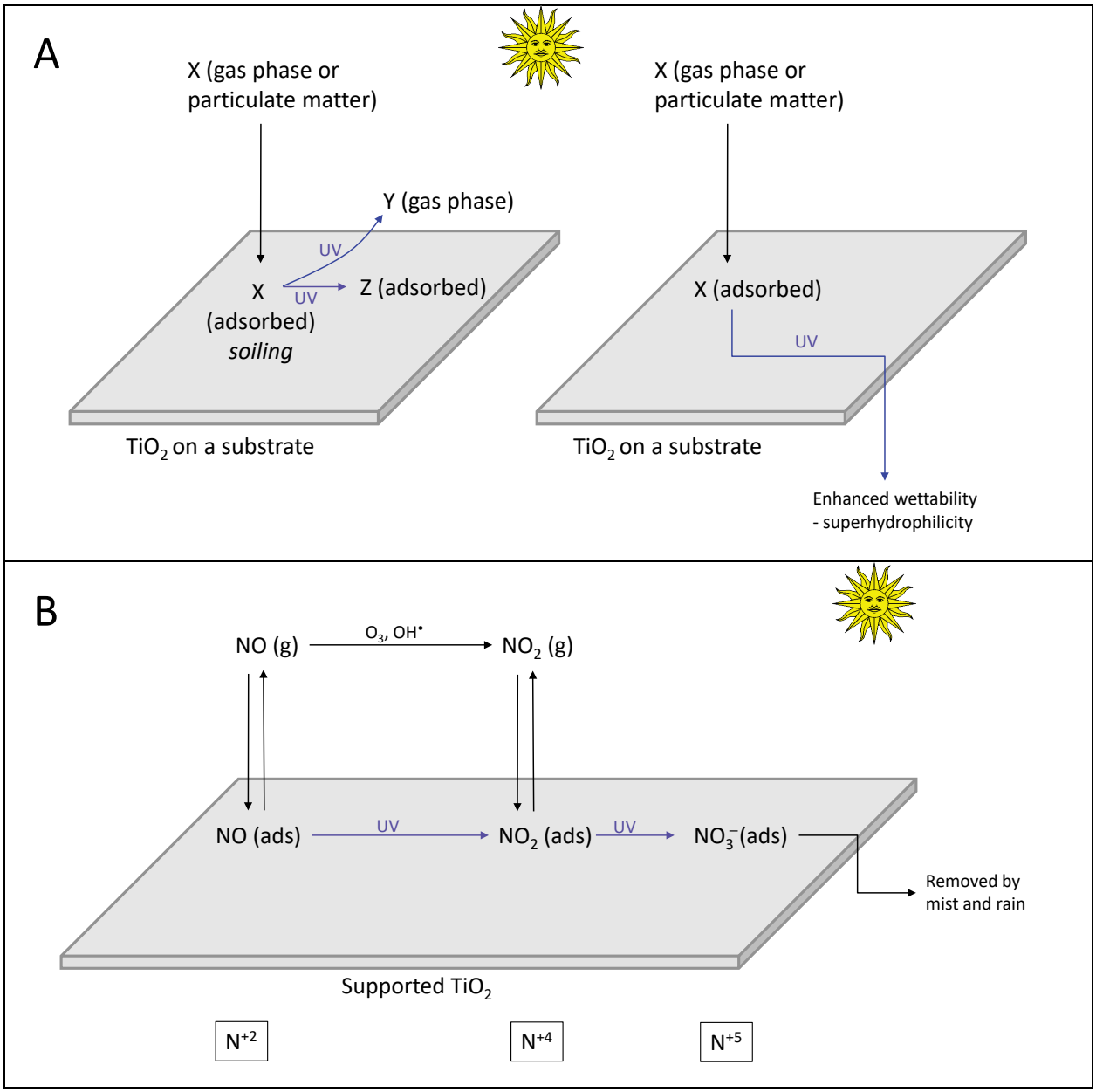

Figure 1. Illustration of (A) the self-cleaning process, and (B) the de-pollution effect of photocatalytic surfaces exposed to sun light.

2 Methodology

2.1 Selection of exposed materials

During the initial phase of the project, industrial partners were invited to submit specimens of products of interest, including specifically those that have photocatalytic additives or constituents. Despite significant efforts on our side, only two manufacturers submitted photocatalytic products. One provided photocatalytic field-applied coatings (paints); the other, architectural fabrics.

In each case, photocatalytic materials were submitted alongside their matching control samples, which were essentially products with the same characteristics but that did not have the photocatalytic functionality. Table 1 summarizes the two groups of materials, and Table 2 lists the main characteristics of each individual material. The nomenclature used in this report is the same described in Task 4.2 Report:

a) **CWXX** anonymously identifies each of the materials (where "CW" = cool walls)

b) **BK** = Berkeley, CA; **LA** = Los Angeles, CA; **FR** = Fresno, CA; **AZ** = New River, AZ; **FL** = Miami, FL; **OH** = Medina, OH.

Table 1. Summary of materials exposed in this study.

Product category	Substrate	Number of samples		Colors	Surface description
		Control	Photocatalytic		
Field-applied coating	Metal	4	4	Tan, dark green, peach	Flat
Architectural membrane	N/A	1	2	White	Textured

The photocatalytic field-applied coating samples did not exhibit de-pollution activity. Solar reflectance changes observed in those samples were attributed primarily to color changes due to bleaching, rather than soiling removal. The latter phenomenon is described in Task 4.2 Report, under section # 3.2.3 (Color changes due to product aging). For these reasons, those samples were not further evaluated in this task. Instead, this report has focused on photocatalytic architectural fabrics, which exhibited measurable de-pollution and self-cleaning performances.

Table 2. Description of materials used in natural exposure tests.

ID	Product category	Details	Commercial or experimental?	Surface sheen	Color	Substrate
CW16	coating (field)	control for CW17	experimental	flat	tan	metal
CW17	coating (field)	photocatalytic	experimental	flat	tan	metal
CW18	coating (field)	control for CW19	experimental	flat	dark green	metal
CW19	coating (field)	photocatalytic	experimental	flat	dark green	metal
CW20	coating (field)	control for CW21	experimental	flat	peach	metal
CW21	coating (field)	photocatalytic	experimental	flat	peach	metal
CW22	coating (field)	control for CW23	experimental	flat	tan	metal
CW23	coating (field)	photocatalytic	experimental	flat	tan	metal
CW24	architectural membrane	Teflon-coated fiberglass, control for CW25/26	commercial	N/A	white	N/A
CW25	architectural membrane	photocatalytic	commercial	N/A	white	N/A
CW26	architectural membrane	photocatalytic	experimental	N/A	white	N/A

2.2 Selection and setup of exposure sites

2.2.1 California sites

Three sites were selected in the State of California to expose wall materials, including the photocatalytic products and their control specimens:

a) a roof at the Lawrence Berkeley National Laboratory in Berkeley,

b) a parking lot at the University of Southern California, in downtown Los Angeles; and

c) a ground-level cement structure belonging to one of our industry partners in Fresno.

The Berkeley site was cleanest, because the Laboratory is located in a hill overlooking the San Francisco Bay Area, far from highways and heavy traffic. The Los Angeles site was representative of pollution found at a large mega-city. The Fresno site provided mostly exposure to air pollutants associated with agricultural activity, typical of the Central Valley.

Specimen holders at the three California sites were built between March and April 2016, and specimens from 69 different materials were installed immediately after their construction. Those specimens included those corresponding to the architectural fabric samples, CW24, CW25 and CW26. Specimens have been retrieved quarterly, following the schedule presented in Table 3.

Table 3. Experimental schedule for California exposure.

Site	installed	3 mo	6 mo	9 mo	12 mo	15 mo	18 mo	21 mo	24 mo
BK	Mar 2016	Jul 2016	Oct 2016	Jan 2017	Apr 2017	Jul 2017	Oct 2017	Jan 2018	Apr 2018
LA	Apr 2016	Jul 2016	Oct 2016	Jan 2017	Apr 2017	Jul 2017	Oct 2017	Jan 2018	Apr 2018
FR	Mar 2016	Jun 2016	Oct 2016	Dec 2017	Apr 2017	Jul 2017	Oct 2017	Jan 2018	May 2018

2.2.2 Exposure racks

Specimens were exposed facing west vertically (90˚ tilt) using racks specially built for this purpose. The design and construction of the racks was described in the Task 4.2 report: *Natural exposure of wall products*.

Figure 2A illustrates two of the three racks used in the Berkeley site. Figure 2B shows a photo of an individual architectural fabric specimen. Given the flexibility of this material, it was very important to keep it secured against the wood backing by clamping on the top and bottom sections.

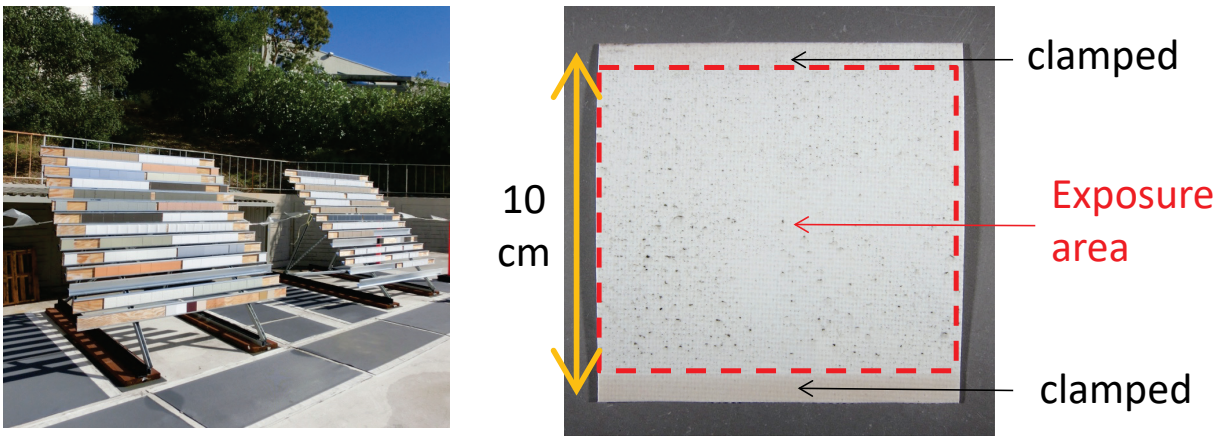

Figure 2. Exposure racks used in this study, and example of one architectural fabric specimen.

2.2.3. National exposure

In addition to the California sites, the project scope was expanded to include also the three sites used by the Cool Roof Rating Council for roofing rating. These "U.S." sites were located in New River, AZ; Miami, FL; and Medina, OH. They were operated by a commercial weathering firm that uses west-facing vertical racks. U.S. national exposure was initiated on August 2016 and is schedule to run for five years, with annual specimen retrievals each summer following the schedule presented in Table 4.

Table 4. Experimental schedule for national exposure.

Site	installed	1 yr	2 yr[a]	3 yr[a]	4 yr[a]	5 yr[a]
AZ	Aug 2016	Aug 2017	Aug 2018	Aug 2019	Aug 2020	Aug 2021
FL	Aug 2016	Aug 2017	Aug 2018	Aug 2019	Aug 2020	Aug 2021
OH	Aug 2016	Aug 2017	Aug 2018	Aug 2019	Aug 2020	Aug 2021

[a] Pending at the time this report was prepared.

2.2.4. Rainfall at each site

Monthly rainfall data at each exposure site was obtained from nearby Global Historical Climatology Network (GHCN) weather stations. The data sets were downloaded from the National Oceanic and Atmospheric Administration (NOAA, 2018). The weather stations selected for each site were:

a) US1CAAL0018, in Berkeley, 3.2 km southeast of the Berkeley exposure site;

b) USW00093134, on the University of Southern California (USC) campus, 1.4 km west of the Los Angeles exposure site;

c) USW00093193, at the Fresno Yosemite International Airport, 9.9 km north of the Fresno exposure site

d) US1AZMR0416, in Anthem, AZ, 3.1 km southeast of the Arizona exposure site;

e) USC00087020, in Miami, Florida, 2.5 km northeast of the Florida exposure site; and

f) US1OHMD0002, in Brunswick, OH, 16 km northeast of the Ohio exposure site.

2.3 Experimental procedures

The general experimental procedures implemented to perform measurements in the laboratory have been described in the Task 4.1 Report *Metrics and methods to assess cool wall performance*. The key measurements are highlighted in this section.

2.3.1 Specimen retrieval, shipping and storage

Photocatalytic specimens (and their controls) exposed in California were retrieved quarterly and sent back to LBNL for laboratory analysis along with the other materials exposed as part of Task 4.2. One specimen from the ten units exposed side-by-side for each material were retrieved from the racks, recorded, packed and shipped to LBNL in an individual glassine envelope. The samples were stored inside the same envelopes prior and after laboratory measurements. There was no exposure to sunlight after the specimens were retrieved from the racks.

2.3.2 Solar reflectance and spectral measurements

Solar reflectance was measured on all photocatalytic specimens and their control samples with a reflectometer (Devices & Services). The solar reflectance results are presented on the air mass 1 global horizontal (AM1GH) solar spectrum (relevant for roofs). After corrections to instrument outputs are finalized, future analyses will report the air mass 1.5 vertical (AM1.5GV) solar reflectance (relevant for walls). Per manufacturer's instructions, the solar reflectance of previously unexposed architectural fabrics was measured on specimens that had been pre-weathered in the laboratory by exposure to UV light. This step was necessary to remove a polymeric protective layer from the material surface.

2.3.3 Photography of specimens

The image of each specimen was obtained with a digital camera using a setup that provided good lighting conditions and a grey card used in the background.

2.3.4 Measurement of the de-pollution performance

2.3.4.1 Experimental setup

The experimental setup used to evaluate the de-pollution performance follows the conditions established by ISO Standard 22197-1 (ISO, 2017), and is described in

Figure 3. Laboratory air was pre-filtered with an activated carbon bed and a HEPA filter, and enriched with 1000 ppb nitric oxide (NO) prior to entering the exposure chamber. The relative humidity was adjusted to 50% by splitting the air flow and circulating one of the two flows through a water bubbler. In the exposure chamber, a specimen from either CW24, CW25 or CW26 was installed facing upwards in the center. A UV-A lamp with maximum intensity at ~360 nm (Model TL-D, Actinic BL, Philips, Andover, MA) was used to irradiate the specimen through a quartz window on the chamber's cover. The distance between the window and the specimen was 5 mm. The irradiance at 360 nm was measured using a digital radiometer (Model UVX, UVP LLC, Upland, CA). It was highest at the center of the sample and consistent over the exposed surface, with an average of 11.5 ± 1.5 W/m². The stability of the lamp during the experimental period was verified. Figure 4 shows a side view and a top view of the exposure chamber.
The chamber was kept at a constant temperature of 60 °C using an external circulating bath, to simulate conditions that are closer to those found in building surfaces under the sun. Air exiting the chamber was split into two flows; one of them was directed to a chemiluminescence NO_x analyzer (Model 200A, Teledyne Technologies, Thousand Oaks, CA), which was calibrated at different times during the entire studied period. The other chamber air stream was used to measure temperature and relative humidity prior to venting in a fume hood, using an in-line digital T/RH sensor (HIH6100 series, Honeywell),

Data acquisition was made in real time, with a resolution of ~5 seconds (frequency of 0.2 Hz). It comprised the NO and NO_2 concentrations at the reactor outlet, the air temperature and relative humidity, and the chamber temperature.

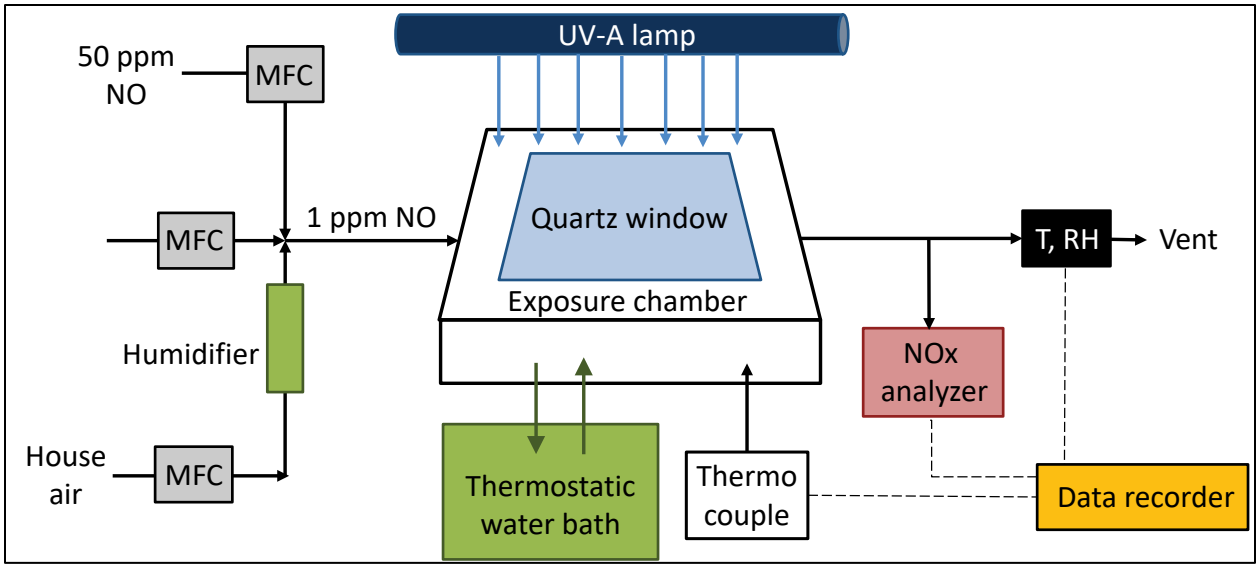

Figure 3**. Experimental setup used to evaluate the de-pollution effect**

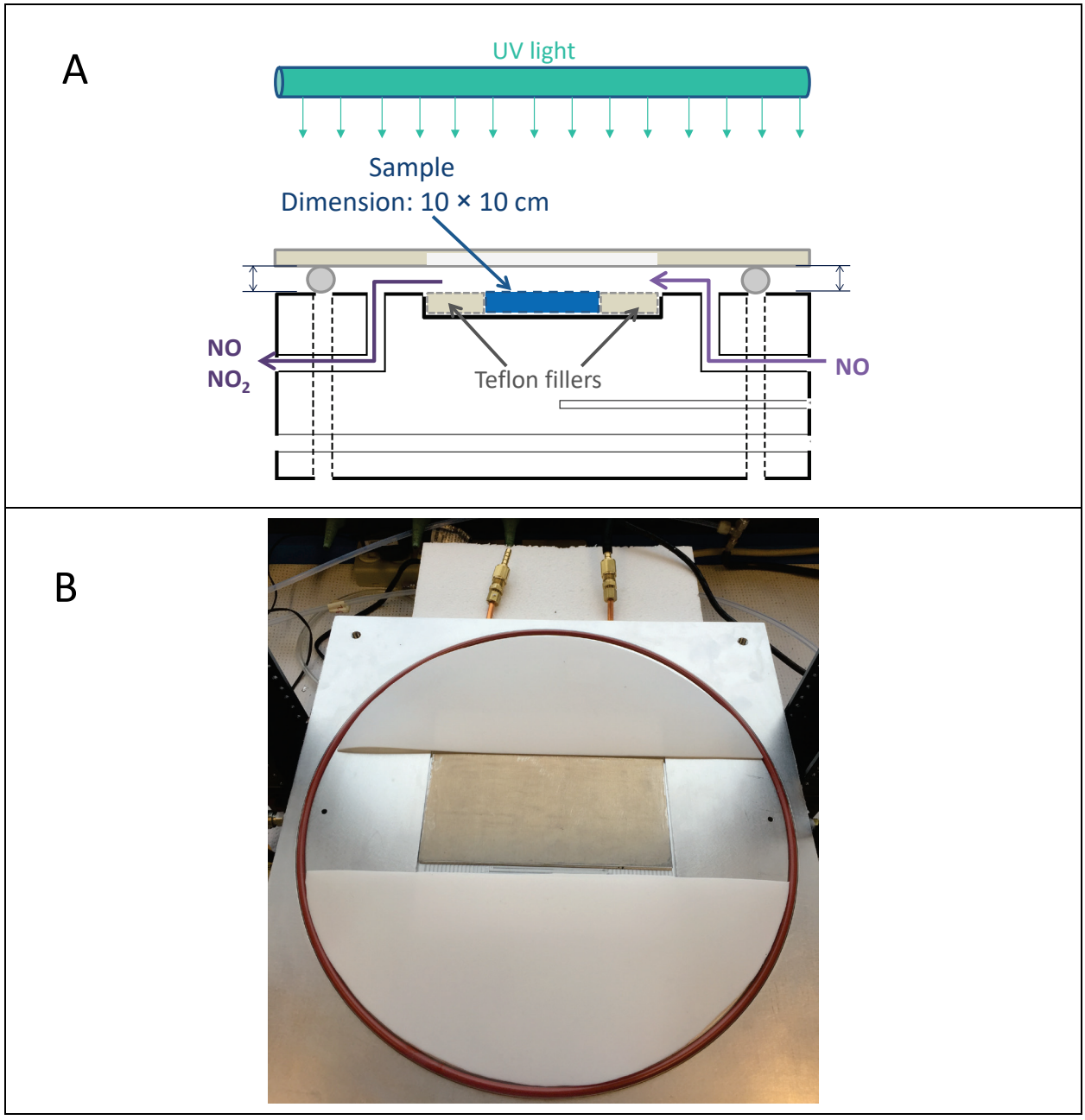

Figure 4. (A) Side view of exposure chamber; (B) Top view of exposure chamber with a reference specimen placed inside.

2.3.4.2 Experimental protocol

Tests carried out with each specimen comprised the following three segments:

a) pre-equilibration under a constant flow of NO-enriched air in the dark (~1 hour);

b) continuous UV irradiation under a constant flow of NO-enriched air (~ 6 hours), and

c) post-equilibration under a constant flow of NO-enriched air in the dark (~1 hour)

Figure 5 illustrates curves corresponding to typical NO and NO_2 traces. Removal rate of NO (r_{NO}, µmol/h) and formation rates of NO_2 (r_{NO_2}, µmol/h, from oxidation of NO) were calculated using the difference between the inlet and outlet concentrations of NO and NO_2, as follows:

$$r_{\mathrm{NO}} = \frac{\int_0^t n_{\mathrm{NO_{removed}}} dt}{t} = \frac{\int_0^t (c_{\mathrm{NO_i}} - c_{\mathrm{NO_{out}}}) dt}{t} \times \frac{Q}{V_n} \quad (1)$$

$$r_{\mathrm{NO_2}} = \frac{\int_0^t n_{\mathrm{NO_{2formed}}} dt}{t} = \frac{\int_0^t (c_{\mathrm{NO_{2out}}} - c_{\mathrm{NO_{2i}}}) dt}{t} \times \frac{Q}{V_n} \quad (2)$$

where Q and t are the flow rate and irradiation duration, and V_n is the normalized gas volume for one mole of gas at standard pressure and room temperature. This approach is illustrated in Figure 5-B. If we assume that nitrate is the only byproduct formed apart from NO_2, the rate of nitrate formation can be calculated from the difference between the values calculated with equations 1 and 2. This estimate would provide a best-case scenario prediction for the amount of nitrate that can be formed. The relative NO_2 yields (Y_{NO_2}) was determined as the ratio between the NO_2 formation rate and the NO reaction rate:

$$Y_{\mathrm{NO_2}} = \frac{r_{\mathrm{NO_2}}}{r_{\mathrm{NO}}} \quad (3)$$

The nitrate buildup rate can be predicted as the mass of nitrate formed per unit time and area ($R_{nitrate}$, mg/h· m²). Similarly, the NO_x deposition rate can be computed as the difference between NO removal and NO_2 formation rates per unit area, expressed in moles (R_{NO_x}, μmol/h·m²). The exposed surface area for each specimen was 0.01 m².

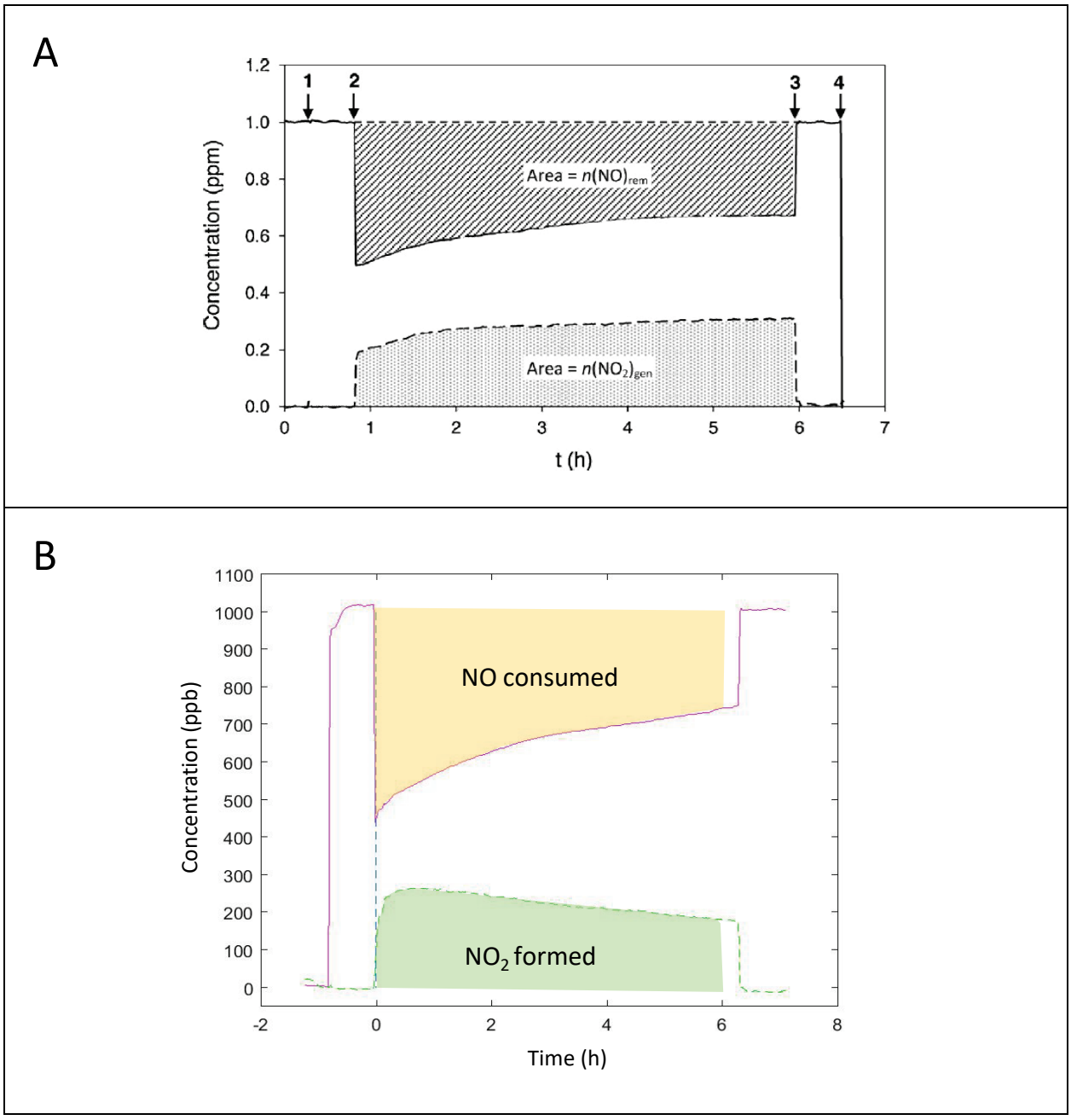

Figure 5. Examples of NO_x traces (A) adapted from Mills and Elouali (2015), and (B) recorded in this study.

3 Results and discussion

3.1 Rainfall recorded at each site

Rain patterns at the three California sites were very similar, and are presented in Figure 6. Across the State we observed a dry season from April/May to October, and a rainy season through the late fall, winter and beginning of the spring. Maximum precipitation was recorded in January 2017 in all three sites. Considering total volume of rain measured at each location, Berkeley was the site that experienced the most cumulative rainfall (approximately 160 cm through April 2018), with Los Angeles and Fresno receiving comparable lower amounts of rain (approximately 60 and 70 cm through April 2018, respectively).

One significant difference in the rain patterns was that precipitation in LA was mostly taking place during the winter months (December through February), while the other two sites showed a broader distribution, with significant levels from October through April.

3.2 Evaluation of the self-cleaning effect

3.2.1 Visual inspection

The self-cleaning effect was relatively easy to appreciate visually, as shown in the photos presented in

Figure 7. Specimens of the control material CW24 that were exposed side-by-side with the photocatalytic specimens CW25 and CW26 were much more significantly impacted by dust and soiling, leading to a visible change in color. This effect was more marked during the dry season and was significantly reduced during the rainy season.

3.2.2 Solar reflectance measurements

Measurements of solar reflectance of each specimen confirmed that, as the materials became dirtier, their albedo was reduced. Figure 9 compares the changes in solar reflectance recorded for CW25 with respect to CW24 (control). Similarly, Figure 10 makes the same comparison between the other photocatalytic product, CW26, and the control material. In both cases, the gap between photocatalytic and control materials was significant: it was higher than 0.10 at the maximum distance for specimens exposed in Los Angeles and Fresno. The gap was reduced significantly during the rainy season, in parallel to the cleaning of the control material observed visually.

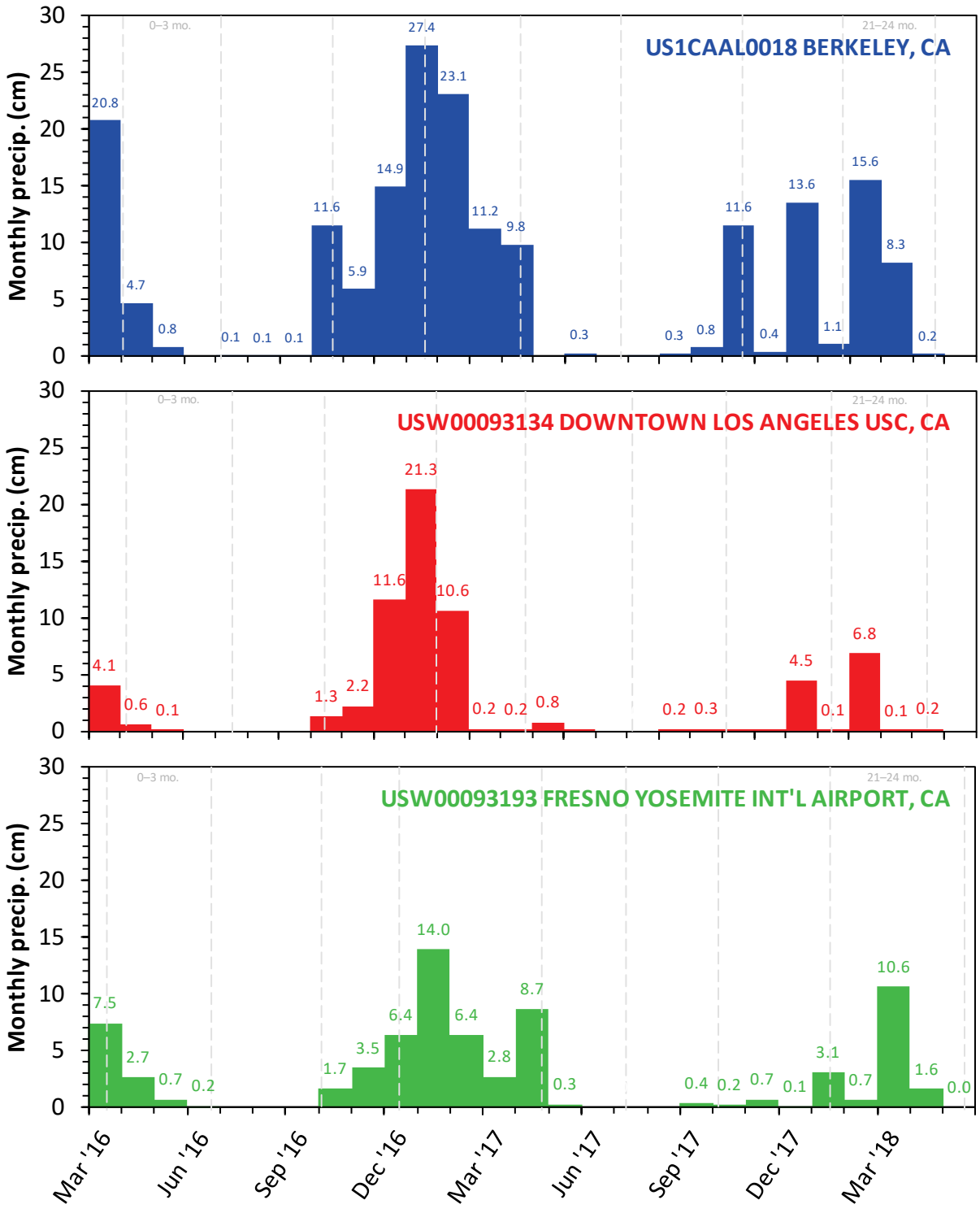

Figure 6. Rainfall patterns at the California exposure sites.

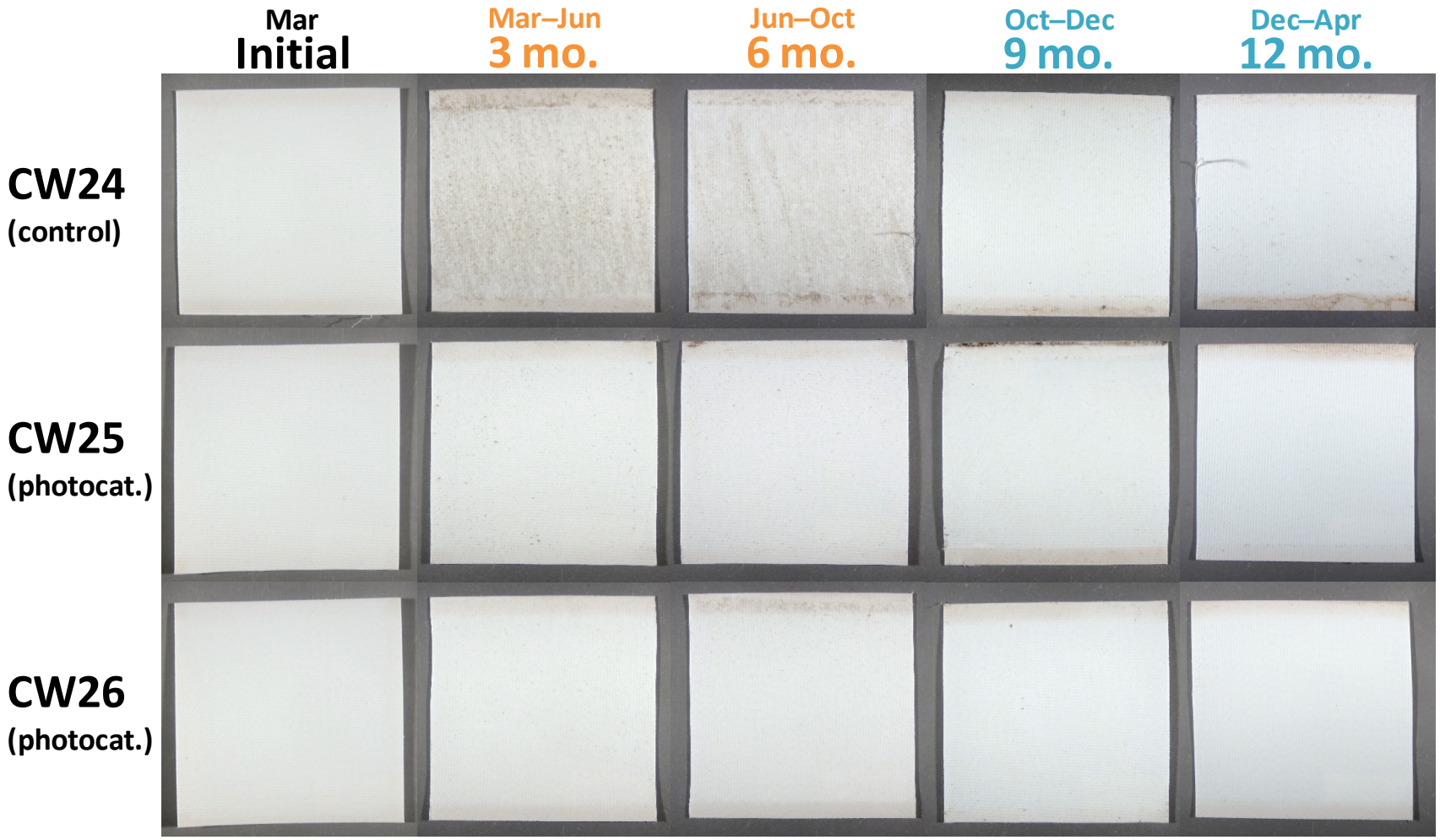

Figure 7. Images of specimens exposed in Fresno.

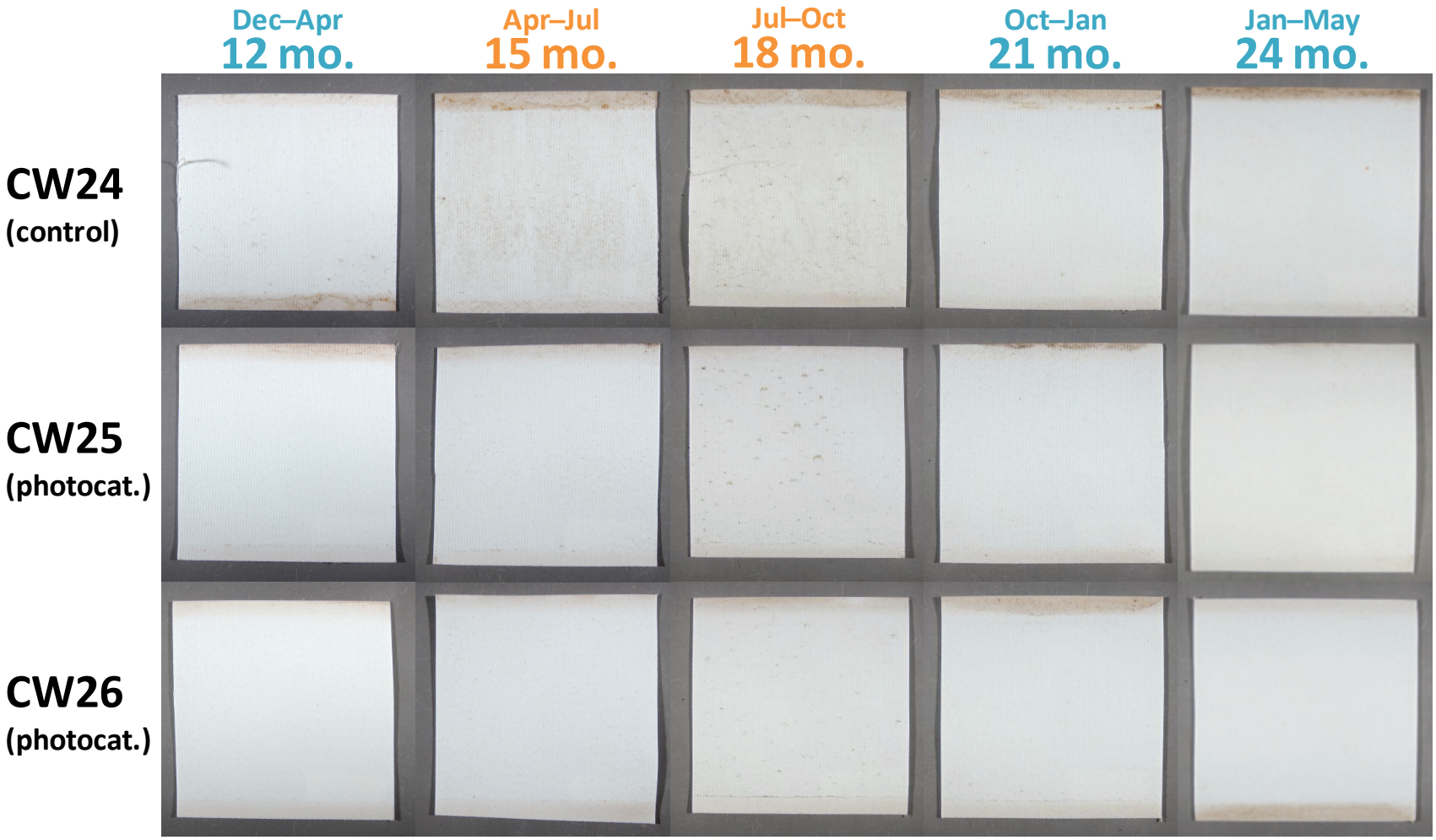

Figure 8, continued. Images of specimens exposed in Fresno.

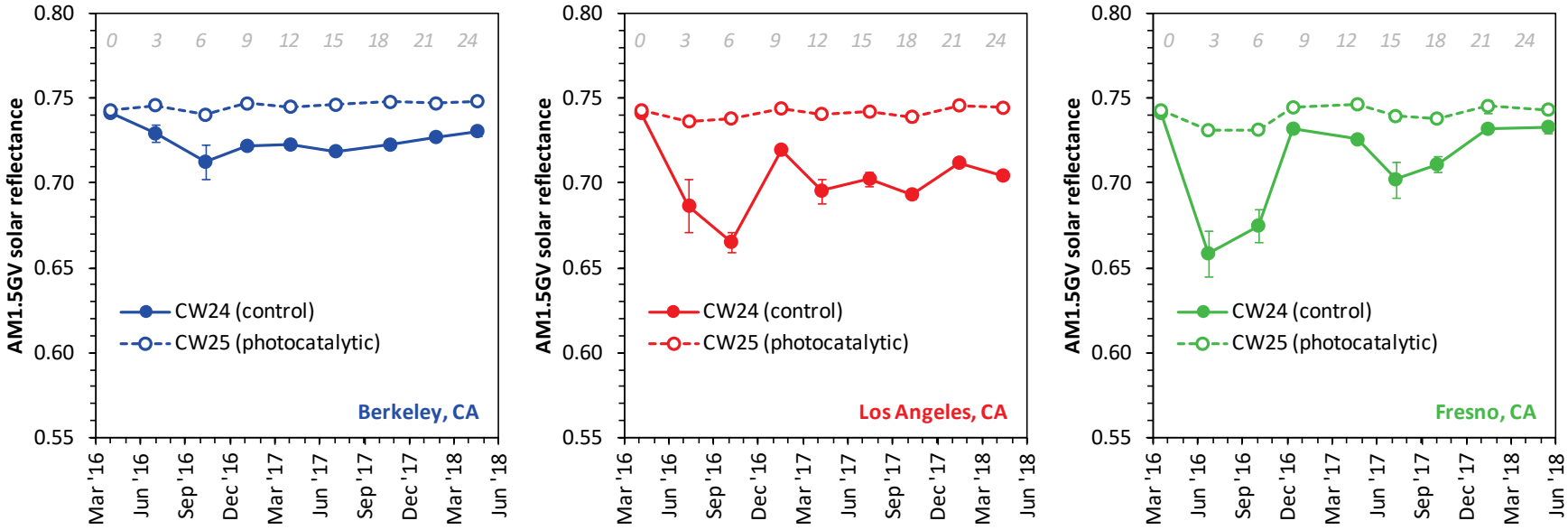

Figure 9. Solar reflectance of architectural fabrics CW24 (non-photocatalytic control) and CW25 (photocatalytic) measured in the three California sites.

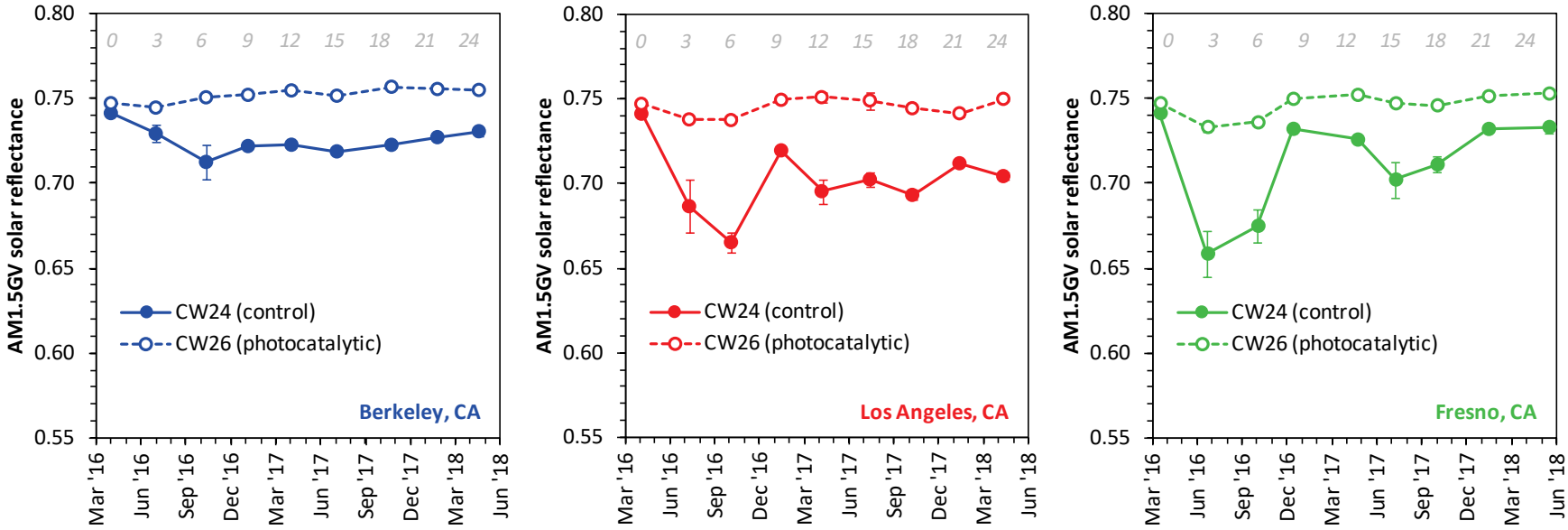

Figure 10. Solar reflectance of architectural fabrics CW24 (non-photocatalytic control) and CW26 (photocatalytic) measured in the three California sites.

3.3 Evaluation of the de-pollution effect

3.3.1 NO and NO_2 concentration profiles

Figure 11 illustrates experimental results obtained to evaluate the NO_x removal efficiency of the photocatalytic specimens and their controls. The time scale was re-zeroed at the time the UV lamp was turned on. The ~1 hour before the zero time was used to equilibrate the material with the NO_x-enriched atmosphere. When a control specimen CW24 was used, no change in NO and NO_2 concentrations was recorded, indicating that there was no reaction taking place upon irradiation alone. However, when specimens from the materials CW25 and CW26 were used, the NO and NO_2 curves showed features similar to those presented in Figure 10-B. There was an initial sharp decline in NO concentrations, accompanied by a sharp increase in NO_2 concentrations. Subsequently, NO concentrations increased asymptotically reaching a steady-state value after ~3 hours of irradiation. During the same period, NO_2 concentrations declined reaching a plateau at the same time. After six hours of irradiation, the UV lamp was turned off, and both NO and NO_2 concentrations rapidly recovered their initial values (ca. 1000 ppm and 0 ppm, respectively).

3.3.2 NO removal rates

From the integration of the curves shown in Figure 11 using equations 1 and 2, it was possible to calculate the rate of NO elimination, which is reported in Figure 12 for each specimen aged in each California site. This is the primary photocatalytic process, which leads to the formation of both NO_2 and nitrate. The material CW25 shows a significantly higher efficiency in NO elimination, as compared with CW26 in all three sites and almost all weather conditions. In Fresno and Berkeley there is a decline in performance associated with the dry season, which is reverted during the rainy season.

3.3.3 NO_x deposition rates

By subtracting the NO_2 formation rate from the NO removal rate, it was possible to determine in each case the NO_x deposition rate, which is presented in Figure 13. Overall, these rates are of lower magnitude than the primary process, the NO removal rate, due principally to the fact that a fraction of NO is converted to NO_2. However, there is a net NO_x deposition rate in most conditions. The negative values recorded in Fresno and on one occasion in Los Angeles are likely due to the presence of other nitrogen-containing species in soiling material deposited on the specimens, which can be photocatalytically converted to NO_x. This is particularly relevant for ammonia aerosols, which are commonly found in rural environments such as the one surrounding the Fresno site.

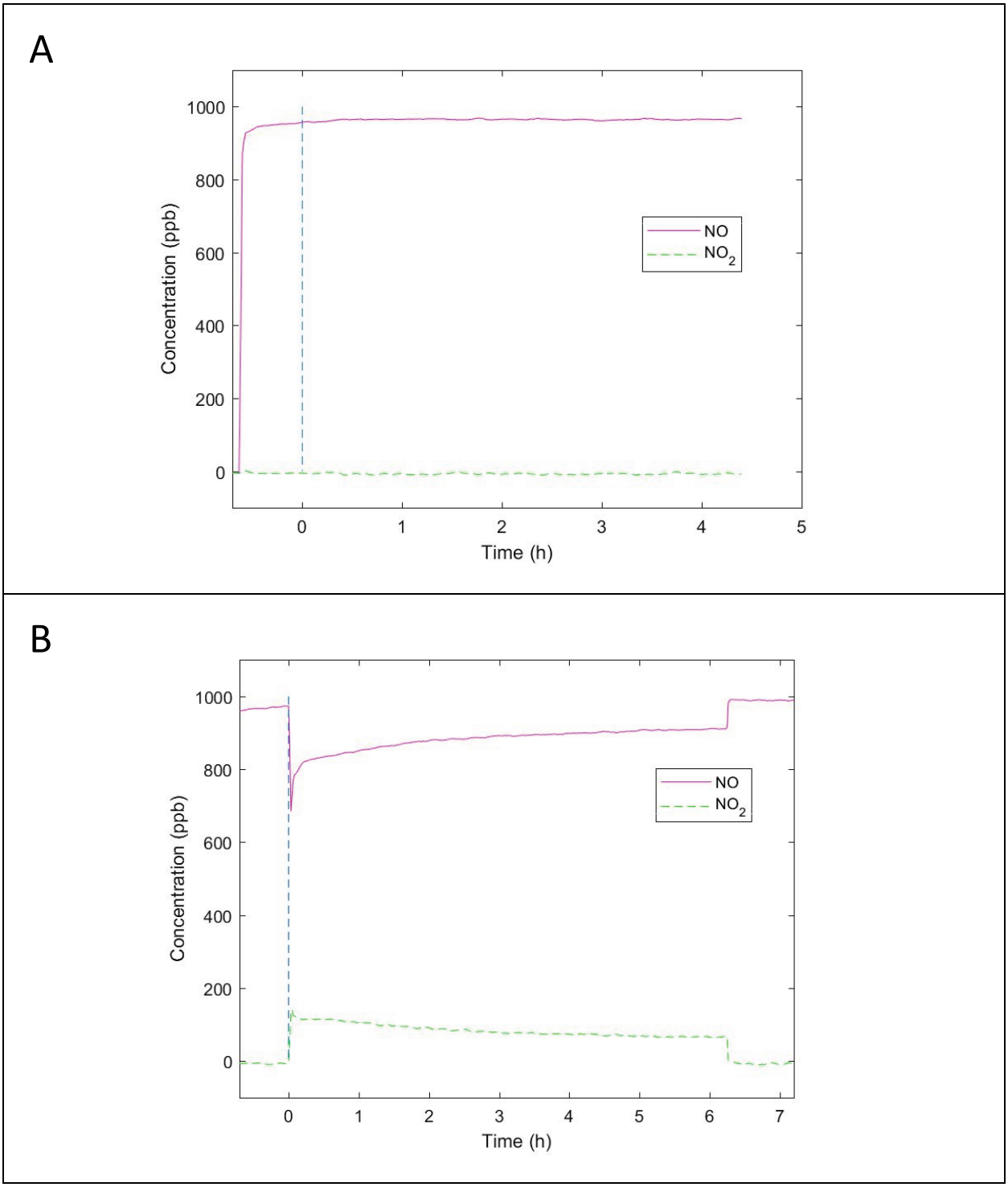

Figure 11. Typical NO and NO_2 concentration curves recorded in experiments with (A) CW24, and (B) CW25 and CW26.

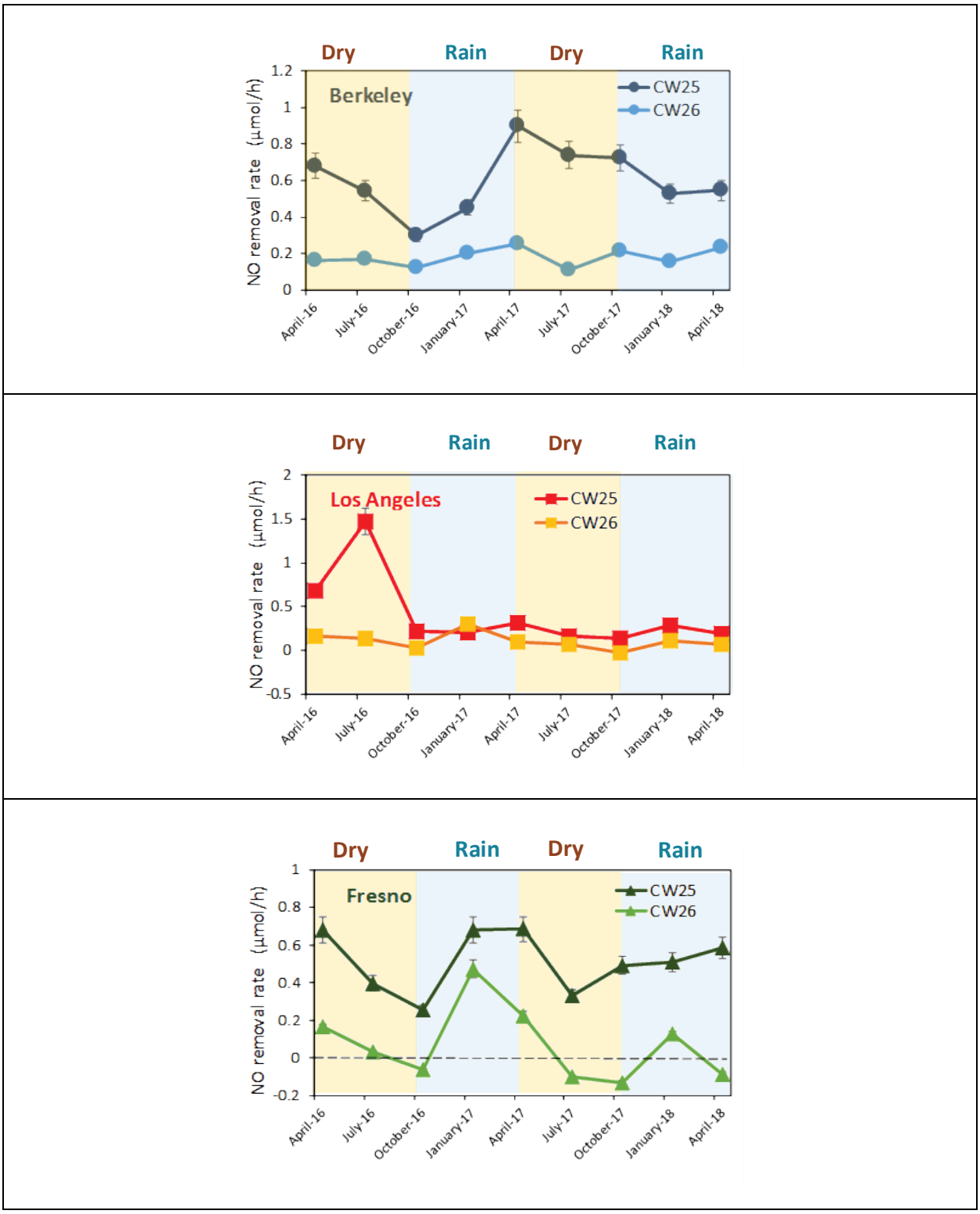

Figure 12. NO removal rate determined in each of the California sites.

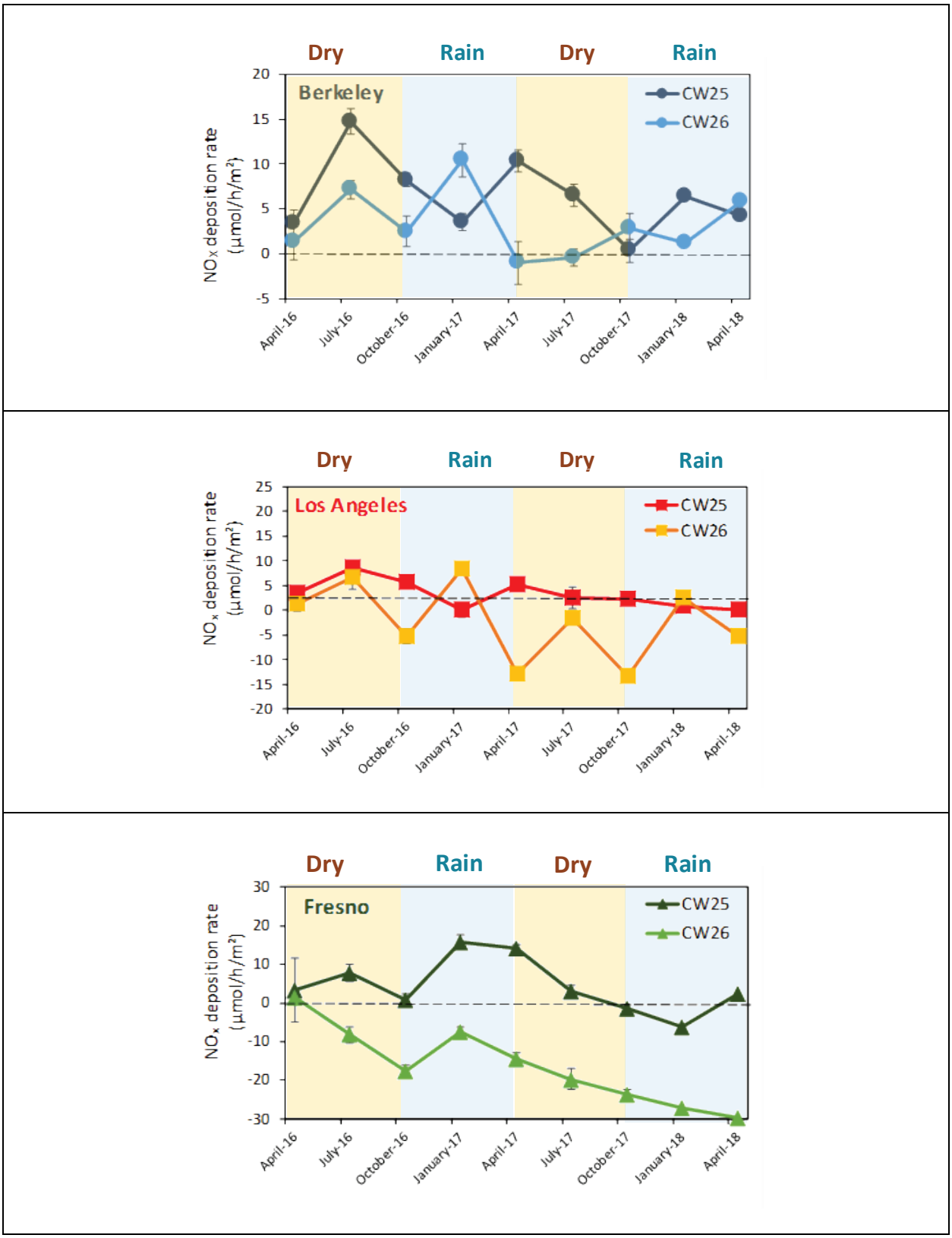

Figure 13. NO_x removal rate determined in each of the three California sites.

4 Conclusions

Results corresponding to both photocatalytic products (CW25 and CW26) show an excellent self-cleaning performance in all three California sites and during all seasons. The photocatalyst additives can successfully protect the surface from soiling buildup, preserving its original appearance.

The de-pollution effect shows a more marked effect of both location and weather. While NO removal and a net NO_x deposition were observed in most cases, there were fluctuations that were associated with the effects of atmospheric deposition and precipitation. While the materials were very effective in removing visible soiling agents, it is likely that some recalcitrant oxidation byproducts remained attached to the catalyst and may have built up over time during the dry season. Examples of those recalcitrant species are carboxylic and polycarboxylic acids, which have a low vapor pressure and are likely to remain attached to active sites, thus partially inhibiting the catalysts ability to react with NO_x and other atmospheric species. This effect can be reduced during the rainy season because while those species are not very volatile, they are water soluble and can be dissolved and removed by liquid water present on the surface.

5 Future work

The results of this project will be further systematized during the preparation of an archival journal article summarizing the key results.

National exposure is schedule to continue through 2021. We will retrieve CW24, CW25 and CW26 specimens exposed in FL, OH and AZ in August of 2018, 2019, 2020 and 2021. This information will contribute to a more complete evaluation of the self-cleaning and de-pollution performance of these materials.

References

Dillert R, Stotzner J, Engel A, Bahnemann DW. 2012. Influence of inlet concentration and lightitensity on the photocatalytic oxidation of nitrogen (II) oxide at the surface of Aeroxide ® TiO2 P25. *J. Haz. Mater.* 211, 240-246.

Gagliardi M. 2010. Photocatalysts: Technology and Global Markets. BCC Research. Available online at: https://www.bccresearch.com/market-research/advanced-materials/photocatalysts-tech-markets-avm069a.html

Hoffmann MR, Martin ST, Choi WY, Bahnemann DW. 1995. Environmental applications of semiconductor photocatalysis. *Chem. Rev.* 95, 69-96.

ISO. 2007. Fine ceramics (advanced ceramics, advanced technical ceramics) – test method for air purification performance of semiconducting photocatalytic materials. Part 1: Removal of nitric oxide. International Organization for Standardization, Standard 22187-1.

Mills A, Hill C, Robertson PKJ. 2012. Overview of the current ISO test for photocatalytic materials. *J. Photochem. Photobiol. A – Chemistry*, 237, 7-23.

Mills A, Elouali, S. 2015. The nitric oxide ISO photocatalytic reactor system: Measurement of NO_x removal activity and capacity. *J. Photochem. Photobiol. A – Chemistry* 305, 29-36.

Minero C, Bedini A, Minella M. 2013. On the standardization of the photocatalytic gas/solid tests. *Int. J. Chem. Reactor Engineering*, 11, 717.

Energy Research and Development Division

FINAL PROJECT REPORT

Solar-Reflective "Cool" Walls: Benefits, Technologies, and Implementation

Appendix L: Assessment of Existing and New Retroreflective Materials (Task 4.4 Report)

California Energy Commission
Gavin Newsom, Governor

April 2019 | CEC-500-2019-040-APL

Appendix L:
Assessment of existing and new retroreflective materials (Task 4.4 report)

28 February 2018

This activity was merged into Task 5.3.

Please see Task 5.3 report: *Development of retroreflective materials* (Appendix O).

Energy Research and Development Division

FINAL PROJECT REPORT

Solar-Reflective "Cool" Walls: Benefits, Technologies, and Implementation

Appendix M: Improvement of Self-cleaning Coatings and Claddings (Task 5.1 Report)

California Energy Commission
Gavin Newsom, Governor

April 2019 | CEC-500-2019-040-APM

Appendix M: Improvement of self-cleaning coatings and claddings (Task 5.1 report)

28 February 2018

This activity was merged into Task 4.3.

Please see Task 4.3 report: *Self-cleaning and de-polluting photocatalytic materials* (Appendix K).

Energy Research and Development Division

FINAL PROJECT REPORT

Solar-Reflective "Cool" Walls: Benefits, Technologies, and Implementation

Appendix N: Development of Fluorescent Cool Pigments (Task 5.2 Report)

California Energy Commission
Gavin Newsom, Governor

April 2019 | CEC-500-2019-040-APN

Appendix N: Development of fluorescent cool pigments (Task 5.2 report)

Paul Berdahl[1], Sharon Chen[1], and Ronnen Levinson[1]

[1] Heat Island Group, Lawrence Berkeley National Laboratory

31 May 2018

Abstract

The re-emission at longer wavelengths of light absorbed at shorter wavelengths, or fluorescence, can lower the temperature in the sun of dark surfaces. We identified and developed two classes of pigments that fluoresce in or close to the invisible near-infrared spectrum: one based on ruby (aluminum oxide doped with chromium), which we have used to formulate pink and red coatings; and another based on the Egyptian and Han blue family (calcium copper tetra-silicate, and variants replacing calcium with barium or strontium), which we have used to prepare blue, green, and blue-black coatings. Measurements made with a calorimetric apparatus developed in this study indicate that fluorescence can reject up to 15% of the sunlight incident on these coatings. Some of the fluorescent blue pigments also exhibit a quantum yield (number of emitted photons divided by the number of exciting photons that are absorbed) much higher than that previously reported. This may facilitate their use in luminescent solar concentrators for photovoltaic generation of electricity.

1 Overview

Various pigments are used to formulate desired non-white colors that stay cooler in the sun than alternatives. These cool pigments provide a high near-infrared (NIR) reflectance in the solar infrared range of 700 to 2500 nm, and also a color specified by a reflectance spectrum in the 400 to 700 nm visible range. Still cooler materials can be formulated by also utilizing the phenomenon of fluorescence (photoluminescence).

While potential fluorescent cool pigments have been screened during a prior DOE funded project with PPG Industries (Zalich and Kornish 2016), only a few pigments have demonstrated the potential for efficient fluorescence and also appear to have adequate (low) cost and durability. The first such pigment was ruby, which is composed of aluminum oxide doped with chromium. It can be used to produce red and pink colored materials. The second important

class of materials includes the ancient pigment Egyptian blue. Egyptian blue has the chemical composition of $CaCuSi_4O_{10}$—that is, calcium copper tetra-silicate. The most important other members of this class, the Egyptian blue family, have the same formula but with barium (Ba) or strontium (Sr) replacing calcium. The barium variant is also known from ancient times as Han (or Chinese) blue. The strontium variant has no common name. The best performance to date with the Egyptian blue family has been achieved with the calcium and strontium compounds. These blue pigments can also be blended with yellow pigment to achieve a green color, or with an orange pigment to obtain a blue-shade black. The blending process does not diminish the near-infrared fluorescence.

Laboratory-fabricated coatings have shown that coatings with fluorescent pigments can provide a contribution, or boost, to the Effective Solar Reflectance (ESR) of up to 0.17 above the ordinary Solar Reflectance (SR). The target for future commercial coatings is a fluorescence benefit (ESR minus SR) of 0.10 to 0.15. The energy flux of full sunlight is roughly 1,000 W m^{-2}, so we can expect that future colored fluorescence materials can reduce peak heat absorption rates by 100 to 150 W m^{-2}.

2 Measurement of effective solar reflectance

If a surface re-emits at longer wavelengths light absorbed at shorter wavelengths, or fluoresces, it will exhibit an effective solar reflectance that is the fraction of incident solar power rejected by the combination of reflection and fluorescence. Like solar reflectance, effective solar reflectance ranges from 0 to 1 (or 0 to 100 percent).

Levinson et al. (2017) detail the development and application of a calorimetric technique for the measurement of effective solar reflectance (Task Report Appendix A).

3 Ruby pigments

Even though natural rubies are quite expensive, manufactured rubies are not. The wholesale cost of cut and polished ruby gems for jewelry is about US$0.30 per carat (200 mg). A layer of manufactured rubies has a pleasing dark red color with a fluorescence benefit of 0.30! Also, ruby pigment is not difficult to manufacture; manufacturers can use the same solid-state reaction techniques they currently employ for other mixed metal oxide pigments such as Fe-Cr-O cool black. Unfortunately, prototype coatings colored with ruby pigment are not as dark as desired and have a fluorescence benefit of only 0.15. Future research may yield further improvements. In the meantime, ruby pigments can provide a dark pink color with high ESR, near 0.80. For comparison, smooth white commercial materials have SR in the range of 0.70 to 0.85—about the same as the ruby pigment. Berdahl et al. (2016) provides more details and shows photos of these materials (Task Report Appendix B).

4 Egyptian and Han blue family of pigments

These alkaline earth copper silicates usually are synthesized by solid-state reaction techniques. Briefly, oxides or carbonates of the component metals are intimately mixed and heated in air for a few hours to a temperature near 900 ˚C. After the synthesis, copper oxide (CuO), a black compound, is usually present as an impurity. If too much CuO is present, the resulting pigment is gray rather than blue. Egyptian blue is available commercially, from Kremer Pigmente. Thus, this company can control the CuO concentration to some extent. However, we have found that for fluorescent pigment applications, even more stringent limitations on CuO contamination are needed. We found that washing (leaching) the commercial pigment with hydrochloric acid (HCl) reduces but does not eliminate the CuO. In Berdahl et al. (2018), included here as a pre-print (Task Report Appendix B), we showed that the near-infrared fluorescence is enhanced by up to a factor of 2 with the HCl soak. The paper also contains color images of some of the samples.

The fluorescence benefits of the prototype materials range from about 0.08 up to 0.17. The best material is based on washed Egyptian blue, with pigment amount of 68 g m^{-2}. The visual reflectance (at 550 nm) is only 0.15, a medium dark blue, while the ESR is 0.57. The relatively small amount of pigment needed per unit area indicates that it is a reasonably strong pigment. The density is 3.09 g cm^{-2}. Allowing a PVC (pigment volume concentration) of up to 50%, minimum coating thickness is only about 44 μm.

The quantum yield of the fluorescence is the number of emitted photons divided by the number of exciting photons that are absorbed. With only exotic exceptions, the quantum yield must be less than 1.0, and for many fluorescence processes is much less than unity. Our most important result is that the quantum yield of the Ca and Ba variants is quite high and even approaches unity, as shown in Figure 1.

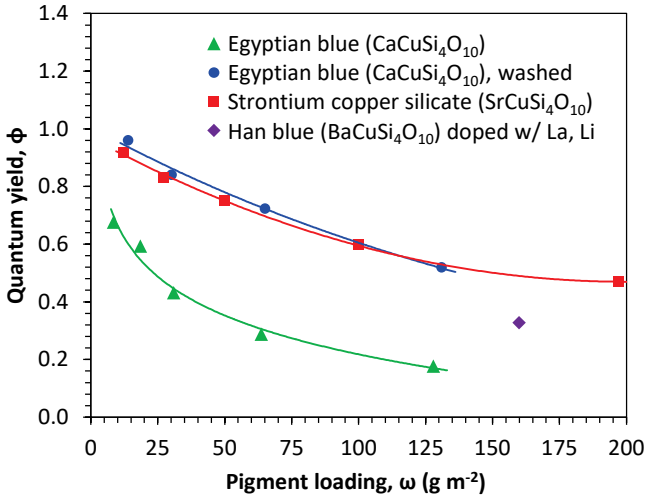

Figure 1. The quantum yield of blue alkaline earth copper silicate pigmented coatings as a function of pigment loading (areal density).

5 An unexpected result: Luminescent solar concentrator (LSC) applications

LSC technology is a strategy for concentrating solar radiation for photovoltaic generation of electricity. A large transparent plate containing a phosphor (or an organic dye) absorbs sunlight, resulting in emission of fluorescence, much of which is trapped within the plates by total internal reflection. The trapped energy emerges from the edges of the plate in concentrated form and is then converted to electricity by a photovoltaic cell. The 900 nm fluorescence from Egyptian blue family phosphors is well matched to conventional silicon photovoltaic cells.

It was only recently, in this project, that accurate quantum yield numbers became available. Prior literature indicates that the yield for Egyptian blue is only about 10% and is even lower for the other compounds. Now we know that if the CuO contamination issue is addressed, the quantum yield is high and can even approach unity. For additional detail, see Berdahl et al. (2018) (Task Report Appendix C).

References

Berdahl P, Boocock SK, Chan GC-Y, Chen SS, Levinson RM, Zalich MA. 2018. High quantum yield of the Egyptian blue family of infrared phosphors ($MCuSi_4O_{10}$, M = Ca, Sr, Ba). *J. Applied Physics* 123, 193103 (11 pp). https://doi.org/10.1063/1.5019808

Berdahl P, Chen SS, Destaillats H, Kirchstetter TW, Levinson RM, Zalich MA. 2016. Fluorescent cooling of objects exposed to sunlight – The ruby example. *Solar Energy Materials & Solar Cells* 157, 312-317. http://doi.org/10.1016/j.solmat.2016.05.058

Levinson R, Chen S, Ferrari C, Berdahl P, Slack J. 2017. Methods and instrumentation to measure the effective solar reflectance of fluorescent cool surfaces. *Energy & Buildings* 152, 752-765. http://dx.doi.org/10.1016/j.enbuild.2016.11.007

Zalich M, Kornish B. 2016. Fluorescent pigments for high-performance cool roofing and facades, DOE project report, Contract No. DE-EE0006347. http://osti.gov

Task Report Appendix A:
Preprint of ESR measurement article (Levinson et al. 2017)

Methods and instrumentation to measure the effective solar reflectance of fluorescent cool surfaces

Ronnen Levinson[1,*], Sharon Chen[1], Chiara Ferrari[3], Paul Berdahl[1], and Jonathan Slack[1]

[1] Heat Island Group, Lawrence Berkeley National Laboratory

[2] University of Modena and Reggio Emilia, Modena, Italy

[*] Corresponding author, RML27@cornell.edu

Abstract

Fluorescent cool dark surfaces stay cool in the sun by reflecting near-infrared (NIR) irradiance and by actively emitting in the NIR spectrum some of the energy absorbed from visible sunlight. The fraction of incident solar energy rejected by reflection and fluorescence is the “effective solar reflectance”, or ESR, of the surface.

It is challenging to measure ESR with a solar spectrometer or a solar reflectometer, the radiometric instruments most commonly used to measure the solar reflectance (SR) of specimens in the laboratory. We have tested a variety of calorimetric techniques for using temperature in the sun to interpolate the effective solar absorptance (1 – ESR) of a fluorescent test specimen from the known solar absorptances of non-fluorescent reference specimens. Our experiments show that averaging out noise in the temperature signal induced by variations in convection is key.

We developed a computer-controlled rotary apparatus that compares the temperatures in the sun of up to six specimens. Trials on six different fluorescent specimens indicate that it can measure ESR with a repeatability of about 0.02. To maximize the ratio of signal to noise in temperature determination, and to facilitate calculation of the fluorescence benefit (ESR - SR), measurements should be performed with specimens facing the sun.

1 Introduction

High solar reflectance can help keep a roof or wall cool in the sun. The coolest building envelope surfaces are bright white, reflecting about 90% of incident sunlight (spectrum 300 – 2,500 nm) when new and unsoiled (CRRC, 2016). In recent decades, cool surface designers have broadened their product color palettes by offering "cool colored" surfaces that pair low reflectance in the visible spectrum (400 – 700 nm) with high reflectance in the near-infrared (NIR) spectrum (700 – 2,500 nm). A high-performance dark cool colored surface available today, such as a natural red clay tile, may reflect about 20% of visible light, and about 60% of NIR light, to attain a solar reflectance (SR) near 0.40 [1].

The temperature in the sun of a non-white surface can be further reduced without affecting color if the surface rapidly re-emits some of the absorbed ultraviolet (UV; 300 – 400 nm) or visible sunlight as invisible NIR radiation. These "fluorescent" cool surfaces can reject sunlight by both reflection (light leaves at the wavelength of incidence) and fluorescence (light leaves at a longer wavelength). Recent collaboration among Lawrence Berkeley National Laboratory (LBNL; Berkeley, CA, USA), PPG Industries, Inc. (Allison Park, PA, USA), and the Shepherd Color Company (West Chester, OH, USA) has yielded fluorescent cool pigments, such as ruby (Al_2O_3:Cr), that could be used to make cool dark architectural coatings [2] [3].

The fraction of incident sunlight rejected by the combination of reflection and fluorescence is called "effective solar reflectance," or ESR. If a surface is opaque, its effective solar absorptance (ESA) α_e is one minus its effective solar reflectance ρ_e. Of course, if a surface does not fluoresce, its effective solar reflectance equals its pure solar reflectance (SR) ρ, and its effective solar absorptance equals its pure solar absorptance (SA) α.

This study examines various laboratory and field methods for measurement of ESR. We are particularly interested in techniques suited to characterize small coated specimens, on the order of 100 cm^2, that can be made from limited quantities of prototype cool fluorescent pigments.

We can classify ESR measurement techniques as radiometric (based on measuring radiation) or calorimetric (based on measuring temperature). We note that the idea of relating the solar reflectance of an opaque surface to its temperature in the sun is not new. For example, Berdahl and Bretz [4] showed a close correlation between temperature in the sun and laboratory spectrometer measurement of solar reflectance. Also, Yuan, Emura, & Farnham [5] used surface temperature measurements to estimate the solar reflectance of 50 cm by 50 cm samples of retroreflective building envelope materials.

2 Theory

2.1 Calorimetric calculation of ESA and ESR

Using a standard linearization of long-wave radiative exchange, the steady-state temperature T of an adiabatic surface in the sun is governed by the energy balance

$$\alpha_e I = h_c (T - T_a) + h_r (T - T_r) , \quad (1)$$

where I is global solar irradiance (incident solar power per area); T_a is air temperature; T_r is long-wave radiative exchange temperature (equal to sky temperature, if the surface sees only the sky); and h_c is the convective heat transfer coefficient. The radiative heat transfer coefficient h_r is approximated as

$$h_r \approx 4 \varepsilon \sigma T_a^3 \quad (2)$$

where ε is surface thermal emittance and σ is the Stefan-Boltzmann constant. Solving Eq. (1) for surface temperature yields

$$T = (\alpha_e I + h_c T_a + h_r T_r) / (h_c + h_r). \quad (3)$$

This indicates that neglecting the weak temperature dependences of h_c and h_r, surface temperature will scale linearly with ESA (or with pure SA, if the surface does not fluoresce).

Note that while the relationship between surface temperature and ESA varies with h_c and h_r, ESA itself is a short-wave radiative property independent of convection and long-wave radiation.

Consider three specimens on a common platform. If a test specimen of unknown ESA $\alpha_{e,3}$ experiences the same solar irradiance, convective heat transfer coefficient, radiative heat transfer coefficient, air temperature, and radiative exchange temperature as nearby non-fluorescent reference specimens of known pure SAs α_1 and α_2, the ESA of the test specimen can be related to the pure SAs of the reference specimens by temperature interpolation:

$$\alpha_{e,3} = \alpha_1 + (\alpha_2 - \alpha_1) (T_3 - T_1) / (T_2 - T_1) . \quad (4)$$

The ESA of a test specimen can also be determined by fitting a line of the form

$$T = m \alpha + b \quad (5)$$

to the temperatures and pure SAs of the non-fluorescent reference specimens, then computing

$$\alpha_{e,3} = (T_3 - b) / m . \quad (6)$$

If the test specimen is opaque, its ESR will be

$$\rho_{e,3} = 1 - \alpha_{e,3} . \quad (7)$$

2.2 Variations with specimen position of convective heat transfer coefficient

Error in calorimetric determination of ESA via Eq. (4) may be induced by specimen-to-specimen variations in solar irradiance, thermal emittance, or convective heat transfer coefficient. Differences in solar irradiance can be minimized by keeping specimens parallel and avoiding shadows, while thermal emittance can be made consistent through choice of material. However, the forced component of the convective heat transfer coefficient can depend strongly on the distance from leading edge of the platform to leading edge of specimen. Let local Reynold's number

$$\mathrm{Re}_x = U\,x\,/\,\nu \tag{8}$$

where U is free-stream wind speed, x is distance from edge of plate (platform), and ν is the kinematic viscosity of air. The local forced convective heat transfer coefficient

$$h_x = k\,\mathrm{Nu}_x\,/\,x \tag{9}$$

where k is the thermal conductivity of air and Nu_x is the local Nusselt number. If the flow over the plate is laminar ($\mathrm{Re}_x < 500{,}000$),

$$\mathrm{Nu}_x = 0.332\,\mathrm{Re}_x^{(1/2)}\,\mathrm{Pr}^{(1/3)}\,/\,[1-(\xi\,/\,x)^{(3/4)}]^{(1/3)} \tag{10}$$

where Pr is the Prandtl number of air and ξ is the unheated starting length (Ref. [6], Eq. 6.98). If the flow over the plate is turbulent ($\mathrm{Re}_x > 500{,}000$), then

$$\mathrm{Nu}_x = (\mathrm{Nu}_x)_{\xi=0}\,/\,[1-(\xi\,/\,x)^{(9/10)}]^{(1/9)} \tag{11}$$

where

$$(\mathrm{Nu}_x)_{\xi=0} = 0.0296\,\mathrm{Re}_x^{(4/5)}\,\mathrm{Pr}^{(1/3)} \tag{12}$$

(Ref. [6], Eqs. 6.99 and 6.92).

Figure 1 shows variations with distance from leading edge of plate of laminar and turbulent local forced convective heat transfer coefficients, calculated for a free-stream wind speed of 2 m/s and zero unheated starting length. At that speed, flow is laminar ($\mathrm{Re}_x < 500{,}000$) for the first 400 cm. The laminar convective heat transfer coefficient drops rapidly from 28 W/m²·K at 1 cm, to 9 W/m²·K at 10 cm, and to 6 W/m²·K at 20 cm. This indicates that unless the specimens are centered on a large platform (say, 1 m by 1 m), variations in distance from platform edge may induce substantial specimen-to-specimen differences in temperature, and thus introduce error in calculation of ESA from measured temperatures.

2.3 Uncertainty in ESA

We can use Eq. (1) to approximate the ratio s of the uncertainty in computed ESA, $\Delta\alpha_e$, to uncertainty in measured surface temperature, ΔT, as

$$s \equiv \Delta\alpha_e\,/\,\Delta T \approx d\alpha_e\,/\,\mathrm{dT} = (h_c + h_r)\,/\,\mathrm{I}. \tag{13}$$

The reciprocal of this sensitivity, (1/s), can be estimated by measuring the variation with solar absorptance of the surface temperatures of non-fluorescent materials, then calculating the slope of the best linear fit to T vs. α.

3 Test and reference specimens

This study uses six ruby-based fluorescent test specimens prepared by some of the authors in earlier work [3], and 11 non-fluorescent reference specimens.

The thermal emittance of each test and reference specimen was measured with a Devices & Services Portable Emissometer following ASTM C1371-15: Standard Test Method for Determination of Emittance of Materials Near Room Temperature Using Portable Emissometers [7].

The solar spectral reflectance of each reference specimen was measured with a PerkinElmer Lambda 900 UV-VIS-NIR spectrometer with 150 mm Labsphere integrating sphere, following ASTM E903-12: Standard Test Method for Solar Absorptance, Reflectance, and Transmittance of Materials Using Integrating Spheres [8]. Each specimen was mounted at the sphere's reflectance port in the conventional manner to measure "without window" solar spectral reflectance. In some cases, it was also measured with a quartz window between the port and the specimen to determine "with window" solar spectral reflectance. Each solar spectral reflectance was weighted with an air mass 1 global horizontal (AM1GH) solar spectral irradiance to calculate AM1GH solar reflectance [9] [10].

The pure solar reflectance of each test specimen was measured in accordance with Section 4.2, below.

3.1 Fluorescent test specimens

The first test specimen, "ruby crystal clear", is a clear-coated ruby crystal array on a white substrate (Figure 2b). Each crystal is a square pyramid, approximately 5 mm by 5 mm by 2.6 mm. The clear acrylic increases the thermal emittance of this specimen to 0.875 from 0.765 for uncoated crystals.

The remaining five fluorescent test specimens are ruby-pigment coatings (Figure 3). Each coating was prepared by mixing ruby pigment (alumina doped with chromium oxide) into clear acrylic, then applying the pigmented acrylic to a bright white substrate (an aluminum panel painted white). The ruby-pigment coatings are labelled 0.2%, 1%, 2%, 3%, and 4% according to the weight fraction of chromium oxide (Cr_2O_3) present in the alumina (Al_2O_3) pigment. Their thermal emittances range from 0.876 to 0.885 (Table 1).

3.2 Non-fluorescent reference specimens

We prepared 11 non-fluorescent reference specimens, each 75 mm by 75 mm (Table 2). References specimens A1 – A9 are aluminum panels hand painted with two layers of titanium oxide white, then overcoated with titanium oxide white and/or bone black to create a white, gray, or black surface (Figure 4). Their thermal emittances range from 0.886 to 0.926.

Reference specimen A10, “ruby crystal white”, is an aluminum panel with a ruby crystal array, overpainted white (Figure 2c); reference specimen A11, “ruby crystal gray”, is the analog of specimen A10, but overpainted gray, rather than white (Figure 2a). Their thermal emittances are 0.911 and 0.912, respectively. Ruby crystal white and ruby crystal gray each have essentially the same shape and thermal properties as ruby crystal clear.

4 Radiometric measurement of ESR

4.1 Spectrofluorometer

Absolute and complete spectral fluorescence measurements are not routine, so complete calibrated measurements are uncommon. However, measurement of spectral emission intensity (arbitrary units) is essential for optimizing fluorescent materials. One can compare emission from various samples under the same conditions to find the spectral distributions and even small differences in intensity.

LBNL adapted equipment formerly used to determine the albedo of polluted snow [11] to make a spectrofluorometer that measures fluorescence over the spectrum 500 – 1,100 nm. The apparatus includes a tungsten lamp (with xenon gas fill), a high-quality short-pass filter (optical density 4) to block wavelengths that would interfere with observation of the fluorescence emission, a 150 mm Labsphere integrating sphere, and a spectrophotometer. The incident light passes through the integrating sphere to strike the fluorescent sample, and the diffuse emission is collected by the integrating sphere. An optical fiber port on the sphere passes the fluorescence to the input fiber of a compact Ocean Optics S2000 spectrometer with a fixed diffraction grating and a silicon array detector. The fluorescence spectra of several ruby coatings are shown range at full scale in Figure 5 and with greater detail in ESM Figure A-1.

PPG purchased a PTI (Photon Technology International) QM-500 spectrofluorometer that uses an InGaAs detector (500 – 1,700 nm). The instrument determines the excitation wavelength with an input monochromator and the emission wavelength with an output monochromator, and can thus determine both excitation and emission spectra. This arrangement is more sensitive at longer wavelengths, while the LBNL fluorescence instrumentation, using a silicon array detector, is insensitive to radiation beyond about 1,100 nm.

Since measurements from each spectrofluorometer are reported in arbitrary units, neither instrument can be used as configured to assess effective spectral reflectance (ratio of emitted +

reflected power to excitation power, as a function of excitation wavelength). However, it may be possible to adapt the PTI QM-500 spectrofluorometer to measure effective spectral reflectance by calibrating its input (excitation) and output powers, and adding an integrating sphere. The same adapted spectrofluorometer could also be used to measure pure spectral reflectance by measuring output power only at the excitation wavelength.

4.2 Spectrophotometer

Using a UV-VIS-NIR spectrophotometer with integrating sphere to measure effective spectral reflectance is not feasible, because the instrument's calibration protocol assumes that the wavelength of detected light is the same as that of incident light. The effective reflectance spectrum will be inaccurate if instrument response at emission wavelengths differs from that at excitation wavelengths. However, this apparatus can be used to measure the pure spectral reflectance of a fluorescent surface by selectively filtering its detector(s). Pure spectral reflectance can be used to calculate pure solar reflectance, which in turn can be subtracted from ESR to assess the portion of ESR attributable to fluorescence.

For example, ruby emits in the spectrum 650 – 800 nm, with strong peaks near 694 nm (edge of visible spectrum). Covering the photomultiplier used to detect 250 – 900 nm radiation with a filter that blocks this emission (ESM Figure A-2) permits measurement of pure spectral reflectance from 250 to 650 nm. Pure spectral reflectance over the remainder of the solar spectrum (650 – 2,500 nm) can be measured without a filter, since incident radiation at these wavelengths does not excite ruby. Figure 6 shows the apparent solar spectral effective reflectance (blue curve) and the solar spectral pure reflectance (red curve) of ruby crystal clear. Using an air mass 1 global horizontal (AM1GH) solar spectral irradiance to compute broadband properties [9] [10], the apparent difference between apparent effective solar reflectance (0.452) and pure solar reflectance (0.434) is only 0.017. We will later demonstrate that the true ESR of this specimen is about 0.74, indicating that the apparent ESR assessed by spectrophotometer was about 0.28 low.

4.3 Reflectometer

Using the Solar Spectrum Reflectometer (Devices & Services, Dallas, TX, USA) to measure ESR presents a similar challenge, because its calibration protocol also assumes that the wavelength of detected light is the same as that of incident light. For example, using version 6 of this instrument to measure the AM1GH ("G1") solar reflectance of ruby crystal clear yields 0.508, or about 0.22 below true ESR. We also note that the incandescent lamp in this reflectometer may not generate enough UV light to excite certain fluorescent pigments.

4.4 Pyranometer

The ESR of a very large specimen (at least 4 m by 4 m) could be measured with a first-class pyranometer following ASTM E1918-06(2015): Standard Test Method for Measuring Solar

Reflectance of Horizontal and Low-Sloped Surfaces in the Field [12]. Specifically, E1918 could yield ESR as the ratio of the reflected and fluoresced upflux measured by a downward-facing pyranometer to the solar irradiance measured by an upward-facing pyranometer.

The ESR of a large specimen (about 1 m by 1 m) could be measured with a first-class pyranometer following non-ASTM method E1918A [13] [10]. The E1918A technique exactly covers a test surface with a stacked pair of opaque, non-fluorescent masks of known solar reflectance. The lower mask is black and the upper mask is white. A downward-facing pyranometer first measures upflux with the white mask exposed. The white mask is removed, and upflux is remeasured with the black mask exposed. The black mask is removed, and the upflux is measured a third time with the test surface exposed. The ESR of the test surface can be interpolated from the SRs of the white and black masks by comparing the upflux with test surface exposed to the upfluxes with white and black masks exposed.

Since neither E1918 nor E1918A can determine the ESR of a small test specimen (about 10 cm by 10 cm), these techniques will be more useful when fluorescent cool envelope materials are available in large quantities.

4.5 Pyrheliometer plus pyranometer

The ESR of a small test specimen could be measured by using a pyrheliometer to measure reflected plus fluoresced upflux, and a pyranometer to measure downflux (solar irradiance). ESR could then be calculated as the ratio of the measured upflux to the product of the measured irradiance and the view factor from the pyrheliometer to the portion of the test surface that it sees.

The challenge is that since a pyrheliometer has a narrow field of view, it would measure a very small upflux from a test surface whose reflection and fluorescence are diffuse. For example, a vertical pyrheliometer with a 38 mm diameter collimating tube and a 1° “slope” angle that is placed 100 mm above a test surface would see a target of diameter 41 mm. The view factor from the detector tube opening to the target would be 0.039. If the test surface receives an irradiance of 1000 W/m² and has an ESR of 0.50, the pyrheliometer would measure an upflux of 19.5 W/m². Raising ESR by 0.05 would increase the measured upflux by only 2 W/m², suggesting that the signal to noise ratio of ESR measurement could be small.

As an aside, it would be reasonable to consider the use of a pyranometer or pyrheliometer plus pyranometer to determine ESR as calorimetric, since each instrument measures radiance with a thermopile. We choose to classify them as radiometric because these methods calculate ESR from radiances, rather than temperatures.

5 Experiments to design calorimetric apparatus

The following series of experiments was used to design and refine techniques for calorimetric assessment of ESR in accordance with Eqs. (4) through (7). Readers uninterested in the preliminary designs may skip ahead to Section 5.6.

5.1 Experiment 0A: Measuring ESA of ruby crystal clear exposed on reclining chair

The temperature in the sun of ruby crystal clear was compared to those of three reference specimens: A10 (ruby crystal white), A1 (white), and A2 (gray#1). The support was the adjustable back of a reclining chair facing directly into the sun. A light beige towel was placed under the samples and over the chair's upholstered pad (ESM Figure A-3). The four specimens were laid out with 25 mm gaps along the width of the pad (560 mm), leaving about 90 mm of pad on each side of the array.

The temperature of the back of each specimen was measured with a thermistor and recorded with a data logger, as detailed in ESM Table A-1. The trial began about 13:00 local daylight time (LDT) on 2015-06-23 in Walnut Creek, CA, USA (clear sky, air temperature 31.6 ˚C, slight breeze). After a 15 minute warm up, an 11 minute period with fairly steady temperatures was chosen for analysis.

Two determinations of ESA for the ruby crystal sample were performed. Simple temperature interpolation with A1 (white) and A2 (gray #1) yielded an ESA of 0.262, which is close to that of A2 (0.267). However, since the convective heat transfer coefficient over the ruby crystal array might differ from that over a smooth painted metal panel, the ESA of the test specimen was also extrapolated from that of ruby crystal white, as follows. The ruby crystal sample was about 2.4 ˚C warmer than ruby crystal white (SA 0.231). We calculated the convective heat transfer coefficient over the ruby crystal white specimen by assuming I = 1050 W/m², h_r = 6 W/m²·K, and $T_r = T_a$ – 12 ˚C, then solving Eq. (1) to obtain h_c = 9 W/m²·K. Using this convective heat transfer coefficient for ruby crystal clear, Eq. (1) was solved to find ρ_e = 0.264. The mean of the two determinations was 0.263, and thus the ESR is 0.737.

5.2 Experiment 0B: Assessing linearity of surface temperature vs. ESA with nine reference specimens exposed on reclining chair

To test the linear relationship between surface temperature and ESA required for use of Eq. (4), the temperatures of the nine painted metal reference specimens (A1 – A9) were measured at the same site and using the same support (reclining chair back plus towel) used in Experiment 0A. The nine specimens were arranged in a three by three array with about 2.5 cm spacing. The top

three samples were A1 – A3, with A4 – A6 in the middle, and A7 – A9 at bottom. The left and right margins were each about 14 cm.

On 2015-07-28 at 13:45 LDT (clear sky, air temperature 40 to 40.5 ˚C, calm), the specimens were placed on the support to warm up for 25 min. Their upper surface temperatures were then measured with an infrared thermometer eight times over the next 30 min, as detailed in ESM Table A-1. Median surface temperature varied nearly linearly with solar absorptance (Figure 7), supporting use of Eq. (4). The slight downward curvature in this plot is likely due to slight increases in the radiative and convective heat transfer coefficients with increasing temperature.

5.3 Experiment 1: Measuring ESA of ruby crystal panel exposed on three-specimen platform

With the goal of creating a simple portable apparatus for reproducible calorimetric measurement of ESA, we built a 15 cm by 30 cm by 5 cm platform from white foam board (lightweight moisture-resistant low density polystyrene) with three specimen cavities, each 76 mm by 76 mm (Figure 8). Each cavity can support an optional quartz window (100 mm by 100 mm by 1.6 mm) above the specimen to reduce wind noise. A silicon pyranometer measures solar irradiance, while a handheld vane anemometer is used to measure wind speed. Thermistors were affixed to the back of each specimen with thermal paste and aluminum tape, as detailed in ESM Table A-1.

We made three versions of this platform, each with a uniform cavity depth of 6 mm (0.25”), 13 mm (0.5”), or 19 mm (0.75”). Trials were conducted at LBNL at various times between 10:50 and 15:40 LDT on sunny days in September 2015. In each trial, the test specimen was ruby crystal clear. One reference specimen was always A1 (white), and the second was either A2 (gray#1) or A3 (gray#2). The platform was oriented to face the sun (surface normal parallel to solar beam).

Figure 9 shows five different trials in which test specimen ESA was calculated from Eq. (4). The horizontal line shows the ESA measured in Experiment 0A (0.263). Trial 1A, using no window and the shallowest (6 mm) cavity, yielded an ESA only about 0.01 lower than that found in Experiment 0A, but with noticeable wind noise. Adding windows (Trial 1B) further lowered the estimate of ESA by about 0.06 without reducing noise. Retaining windows while increasing cavity depth to 13 mm (Trials 1C and 1E) or 19 mm (Trial 1F) eliminated window noise, but yielded ESAs about 0.02 to 0.03 lower than found in Experiment 0A.

Each quartz window is nonselective in the solar spectrum, with minimal absorption (absorptance < 0.01 from 300 to 2,500 nm) and essentially constant near normal-hemispherical solar spectral reflectance (0.06 ± 0.01). However, reflections at the air-window interfaces make the solar reflectance of a specimen measured through a quartz window differ from that observed without a quartz window (Levinson, Berdahl, & Akbari 2005). For example, for reference specimens A1 – A9 (Table 2),

$$\rho_{\text{with window}} = 0.82\ \rho_{\text{without window}} + 0.06 \quad (14)$$

with coefficient of determination $R^2 > 0.99$; differences ($\rho_{\text{with window}} - \rho_{\text{without window}}$) range from about -0.06 to +0.08.

It may be possible to compensate for window reflectance by using Eq. (4) to compute the with-window ESA of the test specimen from the with-window SAs of the reference specimens, then calculating the without-window ESR of the test specimen by assuming that Eq. (14) applies to ESR. This approach would yield with-window ESAs of 0.27 to 0.32, with-window ESRs of 0.68 to 0.73, and without-window ESRs of 0.75 to 0.82 for ruby crystal clear in Trials 1B, 1C, 1E, and 1F. These ESRs are 0.01 to 0.08 higher than those found in Experiment 0A (ruby crystal clear on a reclining chair).

Windows can alter in other ways the relationship between SR (or ESR) and specimen temperature. For example, the coefficient of free convection over each specimen is a function of the difference between the temperature of the specimen and that of the air in the cavity [6]. The absence of forced convection over the specimen when a window seals the cavity makes the total (forced + free) convective coefficient h_c more dependent on specimen SA (or ESA) and temperature. This weakens the assumption underlying Eq. (4) that h_c is the same for all specimens. To minimize errors induced by variations in h_c, one would have to use reference specimens whose SAs closely bound the ESA of the test specimen.

5.4 Experiment 2: Measuring surface temperatures of non-fluorescent specimens on five-specimen platform

To explore the effects of wind-induced surface temperature fluctuations measured without protective windows, we measured the temperatures of non-fluorescent metal specimens on several different platforms. Six trials, 2A – 2F, were conducted at LBNL on sunny but often windy days in October 2015, between 11:40 and 16:00 LDT. Trials 2A – 2C exposed a set of five duplicate 50 mm by 50 mm green specimens (SA 0.88), while Trials 2D – 2F tested a set of five different 50 mm by 50 mm specimens (SAs 0.72, 0.73, 0.77, 0.88, 0.96).

Trial 2A arranged the five duplicate specimens in two rows at the center of a 36 cm by 38 cm by 2.5 cm foam board; Trial 2B arranged them in one row on a 20 cm by 61 cm by 2.5 cm foam board; and Trial 2C set them in a cavity array (9 cm by 9 cm, 25 mm deep). Trial 2D exposed the five different specimens as in Trial 2B; Trial 2E added a parapet-style wind break (25 mm height, 5 cm from the specimen row) to the Trial 2D setup; and Trial 2F exposed these five different specimens exposed as in Trial 2C (ESM Figure A-4).

The platform was oriented to face the sun. After a 10 minute warm up, specimen temperatures were recorded every 10 seconds for a period of 20 minutes.

Trials 2A – 2C yielded temperature range (max – min) values of about 1 to 2 ˚C. Trials 2D – 2F yielded surface temperatures that generally increased with solar absorptance, but with much more noise and less linearity than observed on a calm day in Experiment 0B (Figure 7).

The slopes of the lines fit to T vs. α in Figure 7 range from 31.4 to 42.1 ˚C per unit change in solar absorptance. We can use these slopes to relate error in ESA to error in measured surface temperature. For example, in Experiment 0B or Experiment 2D, an error of 1 ˚C would change ESA by 0.027.

5.5 Experiment 3: Measuring surface temperatures of non-fluorescent specimens on rotating apparata (early versions)

Since specimen placement, especially distance from leading edge of platform to specimen, is expected to affect convective heat transfer coefficient, surface temperature, and finally estimation of ESA, we tried symmetrically arranging duplicate specimens on a rotating platform to make convection more uniform.

Our first approach manually rotated the square platform (33 cm by 33 cm by 2.5 cm) shown in ESM Figure A-5, which faced the sun. Trials 3A and 3B were conducted at LBNL on sunny afternoons in November 2015. Following a 10 minute warm up, each trial rotated the platform a quarter turn every 5 min for 20 minutes, with a data logger recording specimen temperatures every 10 seconds. At the end of Trial 3A, the time-averaged temperature range was 1.1 ˚C; at the end of Trial 3B, it was 0.4 ˚C (ESM Figure A-6).

Our second approach installed a circular platform of diameter 30 cm on the platter of a phonographic turntable (Figure 10). The platform was horizontal and revolved at 0.55 Hz (33 RPM). As in previous trials, the specimens were allowed a 10 minute warm up period. In Trial 3C, conducted at LBNL on a sunny, calm late morning in January 2016, the time-averaged temperature range over a 6 minute measurement period was 0.4 ˚C (Figure 11).

5.6 Experiment 4: Measuring surface temperatures of non-fluorescent specimens on first programmable rotating platter

We built a rotating platter that holds six specimens, and positions each in turn under a fixed infrared thermometer. The first version of this programmable apparatus measured the temperature of each specimen for several seconds, recorded the final value, then quickly rotated the platter to bring the next specimen into the thermometer's narrow field of view.

The platter, a 5.1 cm thick, 45 cm diameter slab of expanded polystyrene (EPS) foam adhered to a thin aluminum plate, was rotated by a computer-controlled electric stepper motor. The angular position of the platter was continuously measured with a shaft-mounted goniometer to

provide closed-loop control of platter rotation. Up to six specimens, each 50 to 75 mm on a side, could be placed at 60° intervals on the surface of the platter, which in turn was faced into the sun (ESM Figure A-7). The operator could specify (a) the duration and speed of pre-measurement "spin-up" revolutions; (b) the number of measurement revolutions; (c) the duration of each temperature measurement; and (d) the speed with which to rotate the platter to bring the next specimen under the thermometer.

We conducted four trials, 4A – 4D, in April 2016. In each trial, the platter was spun at 30 RPM for 10 minutes to minimize any pre-trial differences in specimen temperature that might result from spatial variations in convection coefficient or solar irradiance. Next, over a series of 20 to 40 revolutions, the platter was rotated in increments of 60° to bring each specimen under the thermometer. Specimen temperature was recorded after 4 to 5 seconds of measurement. The platter was then rotated for about 2 sec to bring the next specimen into view.

Trials 4A and 4B exposed six duplicate green specimens—the same as those used in Experiments 2 and 3—on April 15 (sunny) and April 18 (intermittently cloudy, and windier), respectively. Trial 4B temperature and solar irradiance time series are shown in ESM Figure A-8. Trial 4A yielded time-averaged temperatures with a range of 0.18 °C after 40 revolutions, while Trial 4B yielded a range of 0.74 °C after 35 revolutions (ESM Figure A-9).

Trials 4C and 4D exposed reference specimens A1 (white), A2 (gray #1), A3 (gray #2), A4 (gray #3), A7 (gray #6), and A9 (black) on April 15 and April 18, respectively. Trial 4D temperature and solar irradiance time series are shown in Figure 12. While instantaneous temperatures fluctuated over the course of each trial, time-averaged surface temperatures varied linearly with solar absorptance (Figure 13).

5.7 Upgrading the programmable rotating platter to create final apparatus

After Experiment 4, we improved the capabilities and performance of the programmable rotating platter by changing its drive motor, expanding its suite of local weather sensors, and upgrading its electronics and control software. These improvements made it substantially easier to operate the apparatus and to use its measurements to assess ESR.

First, we smoothed the rotation of the platter by replacing its stepper motor drive with a variable-speed DC motor drive. This reduced the tendency of the platter to vibrate when its motion is halted, and increased the accuracy with which each specimen can be positioned below the IR thermometer. Second, we added a three-cup anemometer to measure local wind speed, and a shaded thermistor to measure ambient air temperature. Third, we replaced the handheld data logger with a computer-controllable, multifunction data acquisition (DAQ) device. This increased the accuracy of sensor signal digitization and made all measurements immediately available to the apparatus control software. Fourth, we upgraded the control software (Python code executed on a Windows PC) to (a) better regulate the motion of the platter; (b) capture

specimen temperature, weather, and platter angle at the end of each specimen measurement; and (c) record to a file the time-stamped instantaneous specimen temperature and weather measurements, along with cumulative mean specimen temperatures, as they are captured.

The final apparatus is shown in Figure 14 and detailed in ESM Table A-1. A video of the platter motion is presented in the Electronic Supplementary Material.

6 Measurement of ESR with final apparatus

In Experiment 5 (September 2016), we used the final apparatus to measure the ESRs of ruby crystal clear and the five fluorescent ruby-pigment coatings.

6.1 Methodology

We conducted 30 trials at LBNL with the upgraded apparatus in late September 2016. The fluorescent specimens were grouped with non-fluorescent reference specimens to form four test sets (A – D). Set A compared the 0.2%, 1%, and 2% coatings to references A1 (white), A2 (gray#1), and A3 (gray#2), while Set B compared the fluorescent 2%, 3%, and 4% coatings to the same three references. Note that the 2% coating was present in both Set A and Set B.

Set C compared ruby crystal clear to references A10 (ruby crystal white) and A11 (ruby crystal gray). Set D was Set C plus the 2% coating and references A1 (white) and A2 (gray#1) (Figure 15). Set E, comprised of references A1 (white), A2 (gray#1), A3 (gray#2), A4 (gray#3), A7 (gray#6), and A9 (black) was measured to verify that the reference temperatures varied linearly with solar absorptance.

Sets A, B, and C were tested facing the sun in Trials 5A – 5C, 5D – 5F, and 5G – 5I, respectively, then tested horizontally with solar elevation angles of 45 to 52˚ in Trials 5J – 5L, 5M – 5O, and 5P – 5R. Set D was tested horizontally in extended Trial 5S, a series of 10 subtrials (5S/i through 5S/x) in which the solar elevation angle ranged from 18˚ to 49˚. Set E temperatures were measured facing the sun in Trial 5T, then horizontally in Trial 5U.

Each trial included a 10 min spin up at about 8 RPM, except in extended Trial 5S, where spin-up time was reduced to 1 min when the gap between consecutive subtrials was less than 10 min. With the exception of Trial 5U, which was briefer, each trial (or subtrial) included about 25 to 50 measurement revolutions (Table 3). In the measurement phase, the apparatus held each specimen under the IR thermometer for 5 seconds before spinning the platter at about 6 RPM to bring the next specimen into view.

The ESA and ESR of each specimen was calculated following Eqs. (5) through (7). Its fluorescence benefit (ESR – SR) was calculated by subtracting its AM1GH solar reflectance from its sun-facing ESR.

6.2 Results

Figure 16 illustrates the output of the apparatus with the time series of solar irradiance, wind speed, air temperature, and instantaneous and cumulative mean specimen temperatures measured in Trial 5C.

Figure 17 shows how the ESA of each fluorescent test specimen in Trials 5D – 5F was determined by locating its final mean temperature on a line fit through the final mean temperatures and pure SAs of the non-fluorescent references. Similar plots for all trials involving fluorescent specimens (5A – 5R) are presented in ESM Figure A-10.

Specimen ESRs are reported by trial in Table 3 and summarized in Table 4. Mean ESR measured horizontally was 0.047 higher than mean ESR measured facing the sun for ruby crystal clear, and 0.021 to 0.031 higher for the coatings. For a given specimen and orientation, ESR sample standard deviation ranged from 0.002 to 0.023.

The variations with solar beam incidence angle of the ESRs of the 2% coating and of ruby crystal clear are shown in Figure 18.

The linear variation with pure SA of the final mean temperatures of non-fluorescent reference specimens is shown in ESM Figure A-11.

7 Discussion

7.1 Radiometric measurement techniques

Two of the radiometric ESR measurement techniques (pyranometer methods E1918, requiring a sample at least 4 m by 4 m; and E1918A, requiring a sample about 1 m by 1 m) are promising for rating commercial products once available at large scale, but not for measuring the ESR of small prototype specimens (about 10 cm by 10 cm). The combination of a pyrheliometer and pyranometer may work to characterize small specimens if the ratio of signal to noise can be improved.

It may be possible to calibrate the input and output of a spectrofluorometer to provide absolute measurement of the effective spectral reflectance of a small specimen. Such an instrument would not have to cover the entire solar spectrum so long as it includes all excitation and emission wavelengths. Pure reflectance at non-excitation wavelengths could be assessed with a traditional spectrophotometer.

7.2 Calorimetric measurement techniques

From the calorimetric measurement design experiments we have made the following observations.

1. The temperatures of stationary reference specimens varied nearly linearly with SA on a calm, sunny day, validating the calculation of ESA by temperature interpolation of known SA values (Experiment 0B).

2. ESA can be measured in calm, sunny conditions (Experiment 0A).

3. Wind can induce variations of about 2 ˚C in duplicate specimen surface temperature if the specimens are stationary and unshielded (Experiment 2).

4. Shielding specimens with a window removes convection noise, but yields ESA different from that measured with unshielded specimens on a calm, sunny day (Experiment 1). Further heat transfer analysis would be required to correct for the radiative and convective influences of the windows.

5. Rotating the specimen platform and averaging the time series of specimen temperature measurements mitigates convection noise (Experiments 3 through 5).

Experiments 3 through 5 identified two useful rotary techniques: (a) continuous measurement of the temperature of each specimen with a contact thermometer, such as a thermistor, thermally connected to its back; and (b) intermittent measurement of the temperature of each specimen with a single IR thermometer that sees the face of each specimen in turn. Each has practical advantages and disadvantages.

Continuous measurements can be recorded with a small, standalone logger, so long as the logger can revolve with the platter. No computer control is required, since the platter can spin at a constant speed. Weather measurements can be collected with a second logger. The primary disadvantages to this method are that (a) the temperature sensors must be cross calibrated, ideally before each trial; (b) the temperature sensors must be joined to specimens with thermal paste to minimize thermal resistance; (c) this thermal resistance may grow if the sensor is dislodged; and (d) a standalone logger that can record and process thermistor and pyranometer signals tends to be expensive (about US$1K). The first three issues can be managed. For example, one could use thermal epoxy, rather than thermal paste, to permanently bond an accurate but inexpensive thermistor (example: US Sensor KS103G2, 0.1 ˚C interchangeability, US$5) to the back of each specimen, then cross-calibrate the sensors by measuring specimen temperatures when rotated in a dark room. As for the last issue, we note that the labor savings associated with this simple design may offset the investment in data logging equipment.

Intermittent measurements can be performed with a single, non-contact IR thermometer, removing the needs to cross calibrate multiple temperature sensors and thermally bond them to the specimens. This makes it easy to change specimens. Computer control of platter motion and data collection makes the system programmable and versatile, allowing systematic investigation of geometric and dynamic factors that may influence results. Analysis features built into the control software also reduce the need to post-process temperature measurements. On the other hand, even when the broadband thermal emittances of specimens

are matched, the use of an IR thermometer can complicate assessment of surface temperature if there are specimen-to-specimen variations in spectral emittance within the portion of the thermal IR detected by the sensor [14].

The intermittent-measurement apparatus is more complicated than that needed for continuous measurement. Substantial effort was required to design and build the electronics and software needed to intermittently rotate the platter, synchronize temperature measurements to platter motion, and communicate with the DAQ hardware. We note in particular that early attempts to use an inexpensive hobbyist microcontroller with integrated analog and digital I/O uncovered serious limitations in these microcontrollers, including limited range and resolution of analog input; lack of basic functionality, such as a battery powered clock to maintain system time; and incomplete, unsupported application program interfaces for both the microcontroller and its accessories, such as external analog-to-digital conversion integrated circuits. Most vexing of all, we discovered that some dedicated-function integrated circuits failed randomly. We resolved these problems by switching to a more expensive, but more robust, scientific-grade DAQ device.

7.3 ESR measurement repeatability and technique

The Experiment 5 trials indicate that the final apparatus measures the ESR of a given specimen, in a given orientation, with a repeatability (sample standard deviation) of about 0.02.

In our earliest experiments with a clear-coated ruby array with sun normal to the sample, we found ESR = 0.737. At the conclusion of the present work we have ESR = 0.764. The difference, 0.027, is within the combined uncertainties of the two measurements and is indicative of the current state of the art. On the other hand, under favorable circumstances, the standard deviations (repeatability) obtained with the current apparatus is as small as 0.002, so there is room for further improvement.

The ESR of the ruby crystal clear was about 0.05 higher measured horizontally (solar incidence angle around 50°) than when measured facing the sun. This may result from variations with beam incidence angle in specular reflectance from the clear-coated crystals. (The white- and gray-coated crystals appear matte.) A normally incident photon must be reflected twice before leaving the pyramid surface of the ruby crystal array, reducing net reflectance. For example, if the sloping top surface reflectance of a ruby crystal is 0.07, the net surface reflectance for a normally incident photon is only $0.07 \times 0.07 = 0.0049$. For incidence angles well away from normal the surface reflectance should be comparable to 0.07.

The ESR of the coatings was about 0.02 higher measured horizontally (solar incidence angle around 50°) than when measured facing the sun. The reason for this variation is unclear, but is not surprising since reflectance often increases with incidence angle (Appendix A of Ref. [9]).

We recommend measuring ESR with specimens facing the sun, for three reasons. First, since pure solar reflectance is typically measured at near-normal incidence, measuring ESR at normal

(or near normal) incidence makes it easier to compute the fluorescence benefit (ESR – pure SR). Second, facing the sun provides a consistent incidence angle. Third, facing the sun maximizes the incident solar flux, increasing the ratio of signal (temperature rise induced by solar heat gain) to noise (temperature fluctuations induced by variations in convection).

If measuring ESR with specimens facing the sun, it may be desirable to compute the SRs of each spectrally selective surface with a sun-facing solar spectral irradiance, rather than with AM1GH. However, the difference in spectral power distribution between the sun-facing irradiance and the AM1GH irradiance, and the associated error in pure SR, may be small so long as the sun is not very low in the sky. For example, the near-infrared fraction of the ASTM Standard G173 air mass 1.5 global tilt solar spectral irradiance on a 37° surface rotated toward the sun (G173GT; solar altitude angle 41.8°, solar beam incidence angle 4.8°) is 0.518, which is only 0.031 (6.4%) greater than the 0.487 near-infrared fraction of AM1GH [9]. If the NIR reflectance of a highly selective surface exceeds its UV/visible reflectance by 0.40, its G173GT solar reflectance will be only 0.012 higher than its AM1GH solar reflectance.

7.4 Other applications

Our calorimetric technique could also be applied to other special surfaces, including directionally selective reflectors (DSRs) used as cool envelope materials. The solar reflectance of a DSR, such as a retroreflector, or a roofing product that looks white from the sky and dark from ground level, is inconvenient to measure with a conventionally configured spectrophotometer that provides only near-normal irradiance. It could be measured at any solar incidence angle using our calorimetric technique, though measurement at incident angles approaching 90° may substantially reduce the ratio of signal to noise.

8 Summary

Test methods are needed to evaluate the abilities of surfaces colored with fluorescent cool pigments to reject incident sunlight by the combination of reflection and fluorescence. Our review of radiometric techniques for the measurement of effective solar reflectance suggests that two pyranometer methods (E1918A, E1918) could be applied to large or very large specimens, and that a suitably calibrated spectrofluorometer fitted with an integrating sphere could measure the effective spectral reflectance of a small specimen.

We have tested a variety of calorimetric techniques for using temperature in the sun to interpolate the effective solar absorptance of a test specimen from the known solar absorptances of non-fluorescent reference specimens. Our experiments showed that averaging out noise in the temperature signal induced by variations in convection is key.

We have developed a computer-controlled rotary apparatus that compares the temperatures in the sun of up to six specimens. Trials on six different fluorescent specimens indicate that it can measure ESR with a repeatability of about 0.02. To maximize the ratio of signal to noise in

temperature determination, and to facilitate calculation of the fluorescence benefit, measurements should be performed with specimens facing the sun.

This apparatus could also be used to assess the solar reflectance of directionally selective reflectors that are difficult to characterize with conventional laboratory instruments.

Acknowledgements

This work was supported by the Assistant Secretary for Energy Efficiency and Renewable Energy, Office of Building Technology, State, and Community Programs, of the U.S. Department of Energy under Contract No. DE-AC02-05CH11231; and by the California Energy Commission (CEC) through its Electric Program Investment Charge (EPIC). We also wish to thank Howdy Goudy of Lawrence Berkeley National Laboratory for assistance with electronics; Katerina Tsou of Michigan State University for her contributions to measurements; and Victor Cassella of Kipp & Zonen for loan of an SP Lite2 pyranometer.

References

[1] R. Levinson, P. Berdahl, H. Akbari, W. Miller, I. Joedicke, J. Reilly, Y. Suzuki and M. Vondran, "Methods of creating solar-reflective nonwhite surfaces and their application to residential roofing materials," *Solar Energy Materials & Solar Cells,* vol. 91, pp. 304-314, 2007.

[2] M. Zalich and B. Kornish, "Fluorescent pigments for high-performance cool roofing and facades," 2016.

[3] P. Berdahl, S. Chen, H. Destaillats, T. Kirchstetter, R. Levinson and M. Zalich, "Fluorescent cooling of objects exposed to sunlight – the ruby example," *Solar Energy Materials & Solar Cells,* vol. 15, p. 312–317, 2016.

[4] P. Berdahl and S. Bretz, "Preliminary survey of the solar reflectance of cool roofing materials," *Energy & Buildings,* vol. 25, pp. 149-158 (Figures 11, 12), 1997.

[5] J. Yuan, K. Emura and C. Farnham, "A method to measure retro-reflectance and durability of retro-reflective materials for building outer walls," *Journal of Building Physics,* vol. 38, no. 6, p. 500–516, 2015.

[6] F. White, Heat and Mass Transfer, Addison-Wesley, 1988.

[7] ASTM, ASTM C1371-15: Standard Test Method for Determination of Emittance of Materials Near Room Temperature Using Portable Emissometers, ASTM International, 2015.

[8] ASTM, ASTM E903-12: Standard Test Method for Solar Absorptance, Reflectance, and Transmittance of Materials Using Integrating Spheres, ASTM International, 2012.

[9] R. Levinson, H. Akbari and P. Berdahl, "Measuring solar reflectance—Part I: defining a metric that accurately predicts solar heat gain," *Solar Energy,* vol. 84, pp. 1717-1744.

[10] R. Levinson, H. Akbari and P. Berdahl, "Measuring solar reflectance—Part II: review of practical methods. Solar Energy," *Solar Energy,* vol. 84, pp. 1745-1759, 2010.

[11] O. Hadley and T. Kirchstetter, "Black-carbon reduction of snow albedo," *Nature Climate Change,* vol. 2, no. 6, pp. 437-440, 2012.

[12] ASTM, ASTM E1918-06(2015): Standard Test Method for Measuring Solar Reflectance of Horizontal and Low-Sloped Surfaces in the Field, ASTM International, 2015.

[13] H. Akbari, R. Levinson and S. Stern, "Procedure for measuring the solar reflectance of flat or curved roofing assemblies," *Solar Energy,* vol. 82, pp. 648-655, 2008.

[14] Micro-Epsilon, "Basics of Non Contact Temperature Measurement," 2016. [Online]. Available: http://www.micro-epsilon.com/download/products/dat--infrared-basics--en-us.pdf. [Accessed 3 October 2016].

[15] ASTM, ASTM C1549-09(2014): Standard Test Method for Determination of Solar Reflectance Near Ambient Temperature Using a Portable Solar Reflectometer, ASTM International, 2014.

[16] CRRC, "Rated Products Directory," Cool Roofing Rating Council, Oakland, CA, USA, 2016. [Online]. Available: http://coolroofs.org.

[17] R. Levinson, P. Berdahl and H. Akbari, "Solar spectral optical properties of pigments, part I: Model for deriving scattering and absorption coefficients from transmittance and reflectance measurements," *Solar Energy Materials & Solar Cells,* vol. 89, pp. 319-349, 2005.

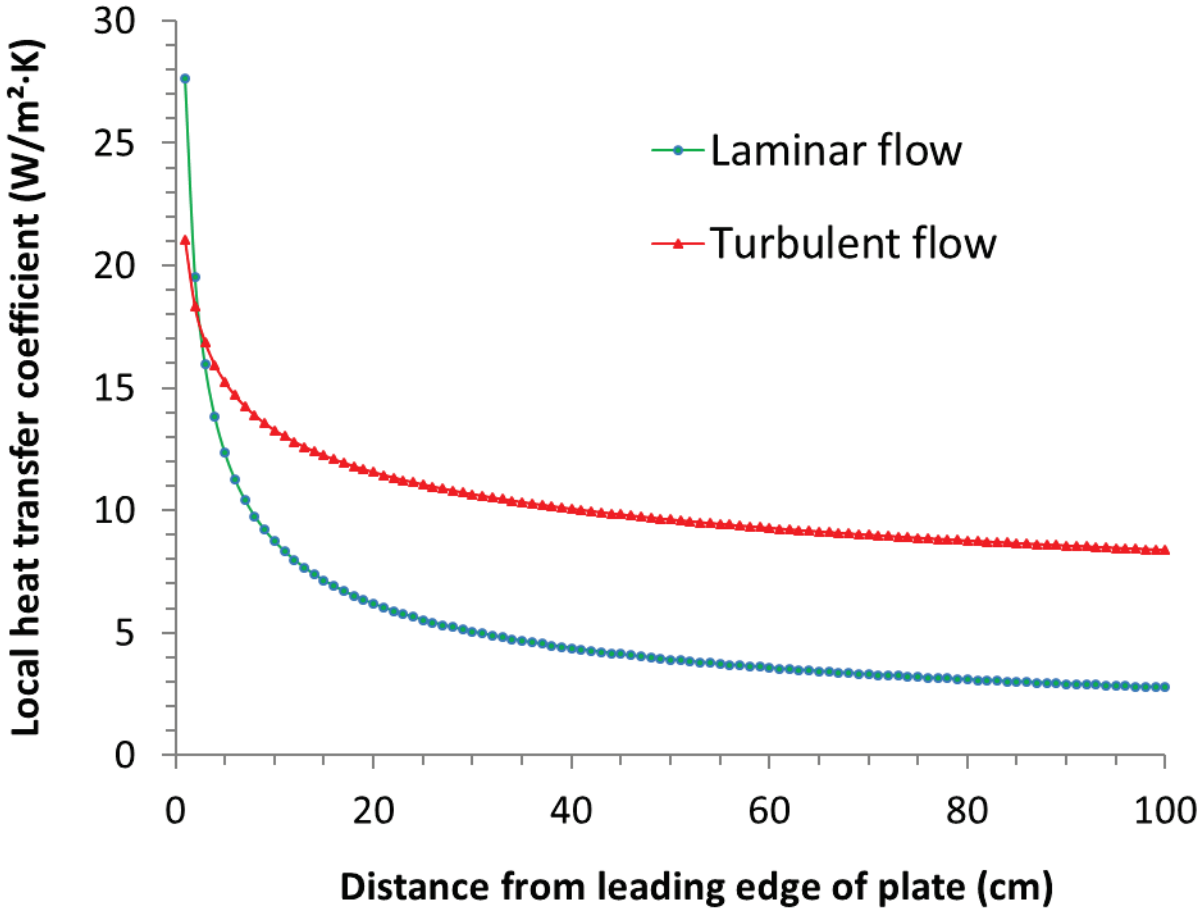

Figure 1. Variations with distance from leading edge of plate of laminar and turbulent local forced convective heat transfer coefficients, calculated for a free-stream wind speed of 2 m/s. At that speed, flow is laminar (local Reynold's number < 500,000) for the first 400 cm.

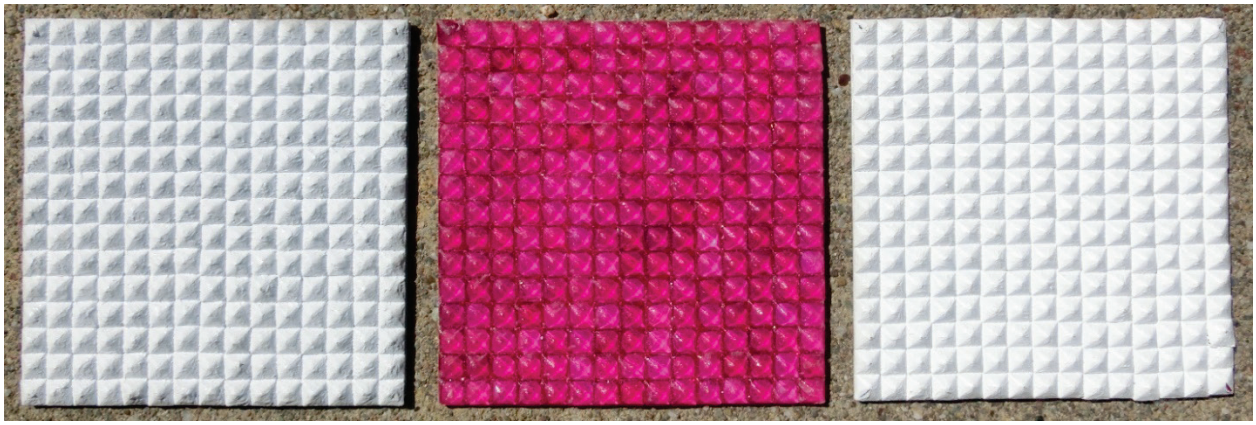

(a) (b) (c)

Figure 2. Images of 75 mm by 75 mm ruby crystal specimens overcoated with (a) gray acrylic paint ("ruby crystal gray"), (b) clear acrylic paint ("ruby crystal clear"), or (c) white acrylic paint ("ruby crystal white"). The gems are set in a thick layer of bright white artist paint on an aluminum substrate.

0.2% 1% 2% 3% 4%

Figure 3. Images of 75 mm by 75 mm ruby-pigment coatings with 0.2%, 1%, 2%, 3%, or 4% weight fractions of chromium oxide present in the alumina pigment.

A1 (white) A2 (gray#1) A3 (gray#2) A4 (gray#3) A7 (gray#6) A9 (black)

Figure 4. Images of six of the painted metal panels (A1 – A9) used as non-fluorescent reference specimens: A1 (white), A2 (gray#1), A3 (gray#2), A4 (gray#3), A7 (gray#6), and A9 (black). Each panel is 75 mm by 75 mm.

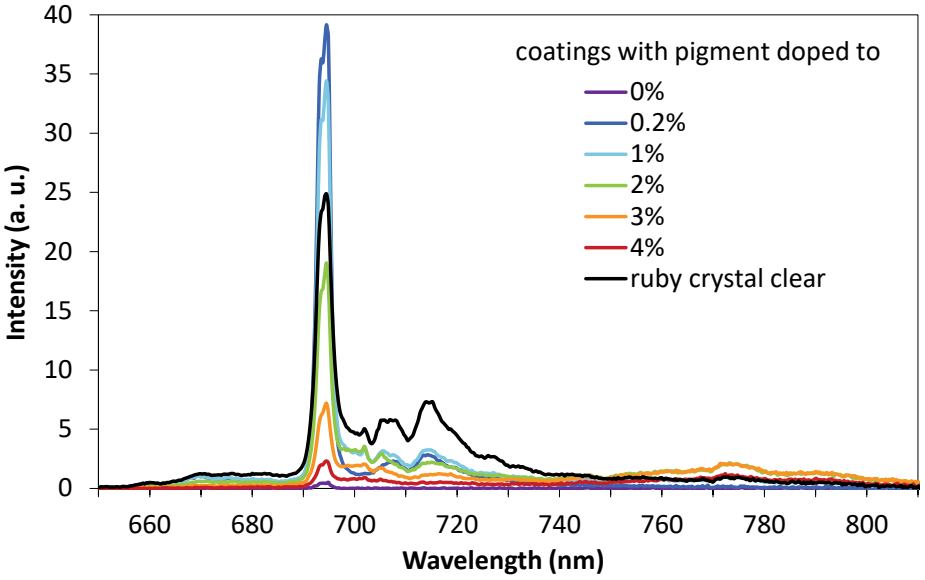

Figure 5. Fluorescence spectra obtained with the LBNL spectrofluorometer of highly-pigmented ruby coatings with ~500 g m^{-2} of 0 to 4 wt% Cr_2O_3-doped Al_2O_3, and of the ruby crystal clear.

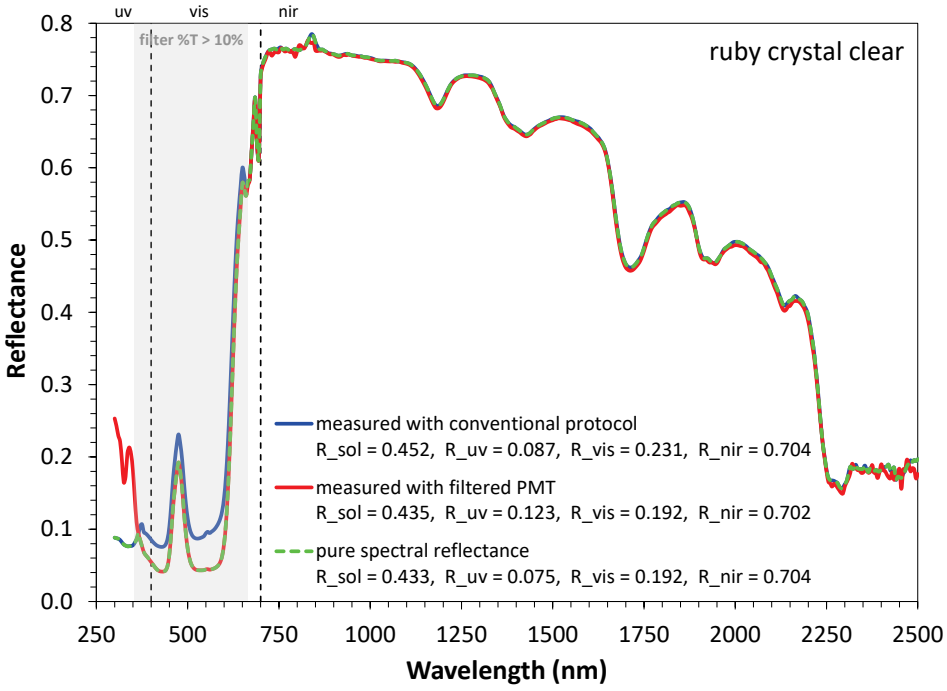

Figure 6. Solar spectral "effective" reflectance (blue curve, measured without correction) and solar spectral reflectance (red curve, measured by filtering emission) of ruby crystal clear. Pure spectral reflectance (dashed green curve) uses filtered data where filter transmittance exceeds 10%, and non-filtered data at other wavelengths. Each spectrum was obtained with a UV-vis-NIR spectrophotometer with integrating sphere. The effective reflectance spectrum will be inaccurate if instrument response at emission wavelengths differs from that at excitation wavelengths.

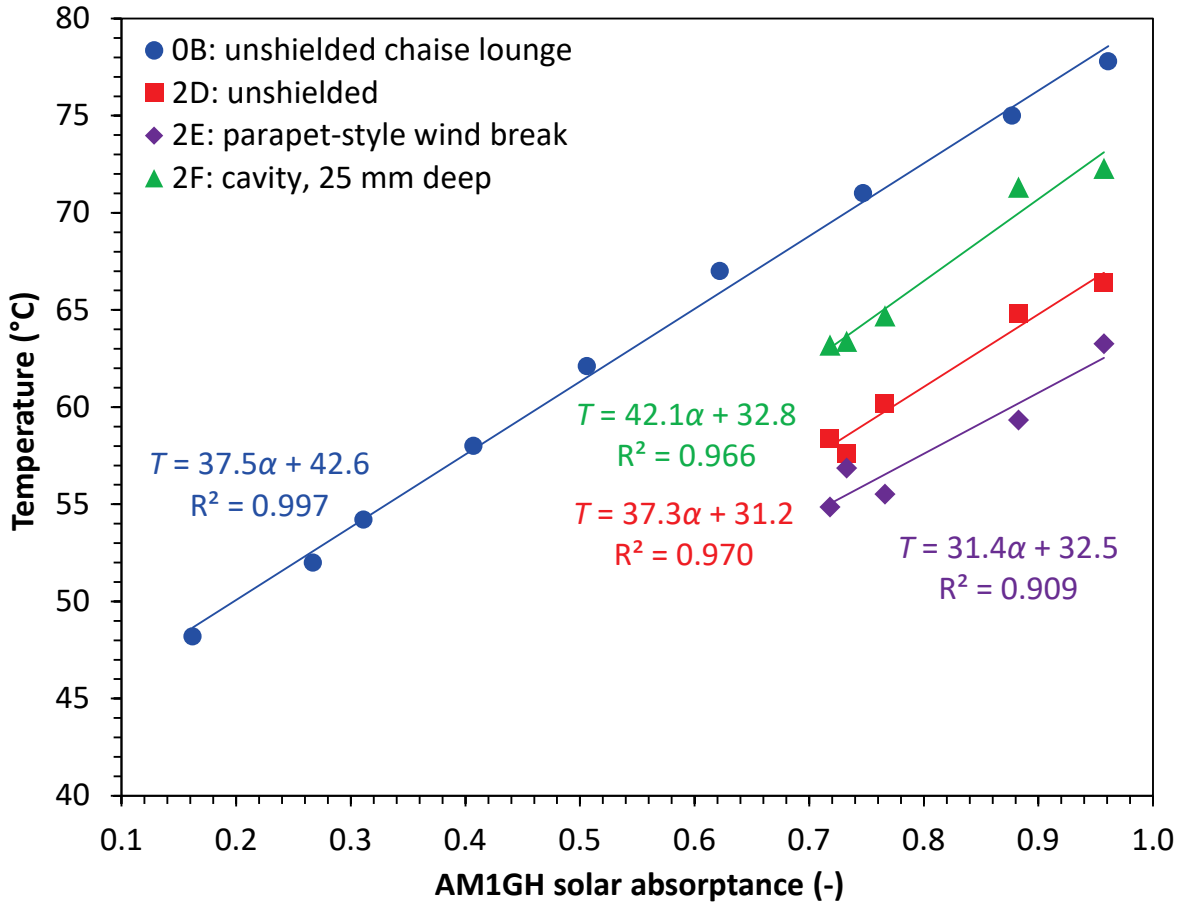

Figure 7. In experiment 0B, the median surface temperatures of nine non-fluorescent painted metal panels (reference specimens A1 – A9) varied nearly linearly with solar absorptance on a sunny, calm afternoon in July 2015. Also shown are variation of time-averaged surface temperature with solar absorptance of non-fluorescent specimens tested in Experiment 2, Trials 2D – 2F, conducted on sunny days in October 2015.

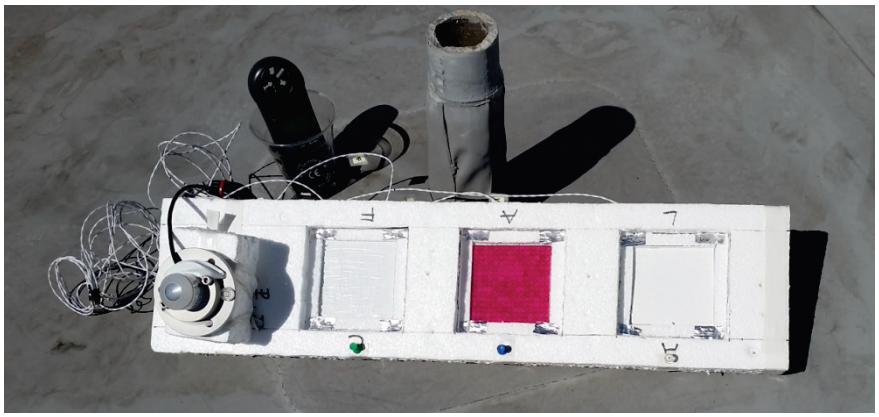

Figure 8. Three-cavity insulated apparatus used to measure the ESA of ruby crystal clear (center cavity). Image also shows the pyranometer and anemometer used to measure solar irradiance and wind speed.

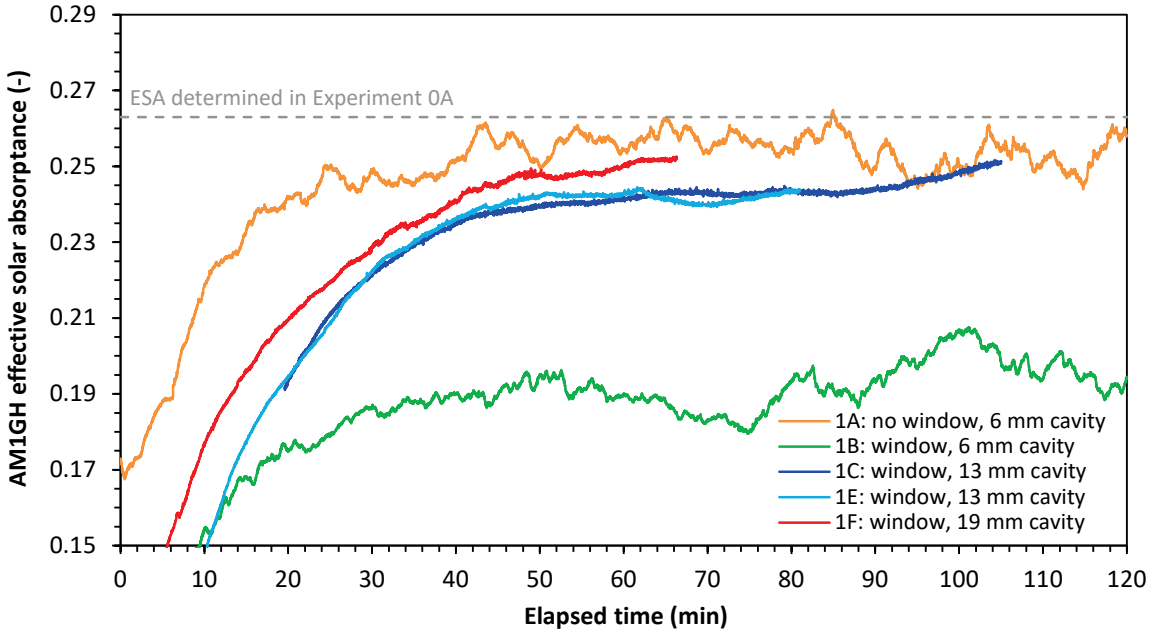

Figure 9. Effective solar absorptance of ruby crystal clear interpolated from solar absorptances of white (A1) and either gray#1 (A2) or gray#2 (A3) reference specimens, using temperatures measured with several versions of the Experiment 1 apparatus.

(a)

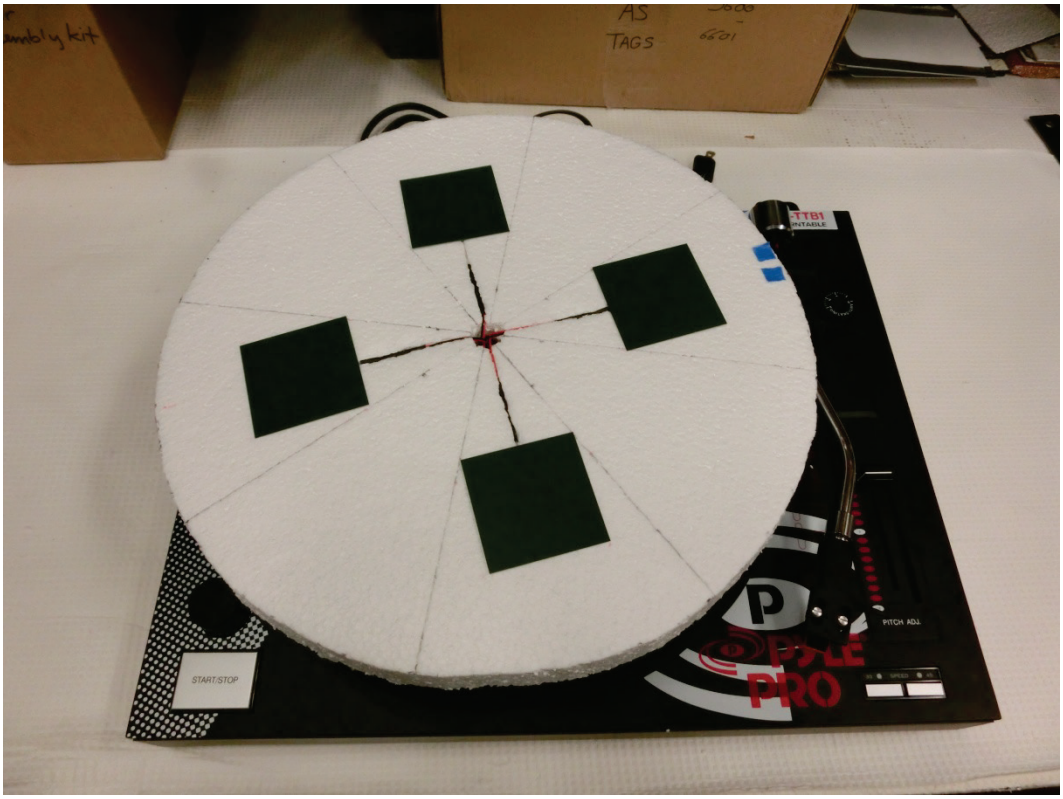

(b)

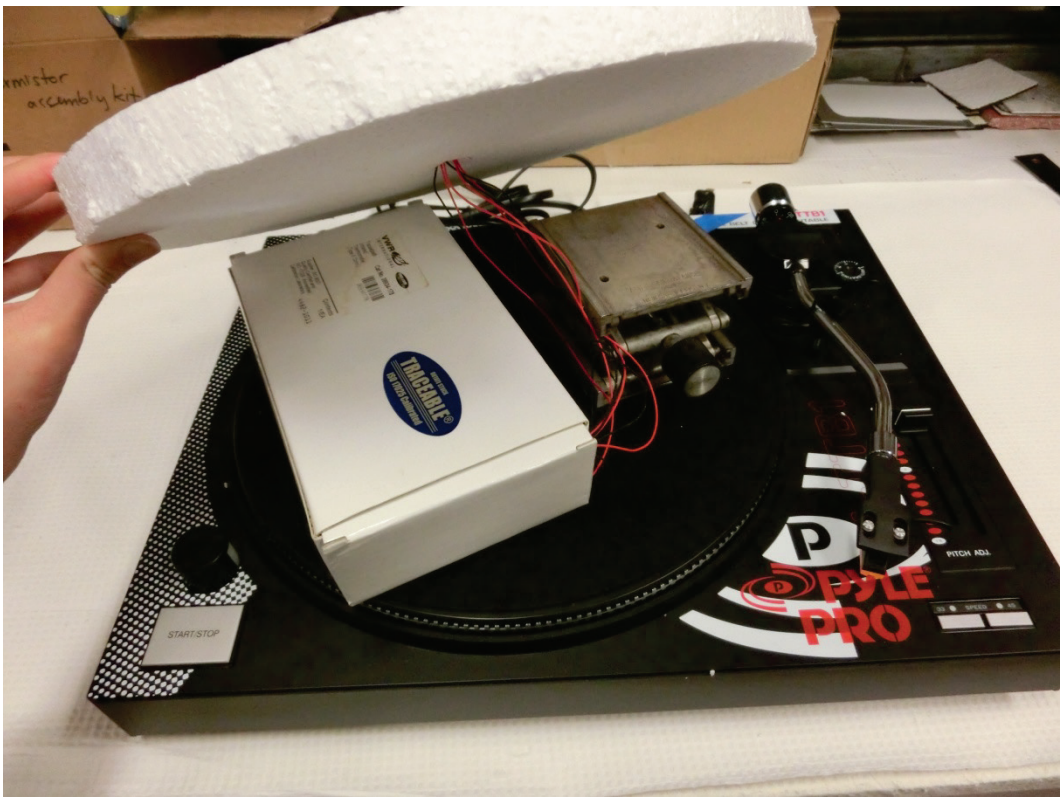

Figure 10. Images of a continuously rotating platform on a phonographic turntable, including (a) a top view showing four duplicate specimens, and (b) a look under the hood. The four specimens are spaced 5 cm from each other, and 3.8 cm from the platform edge.

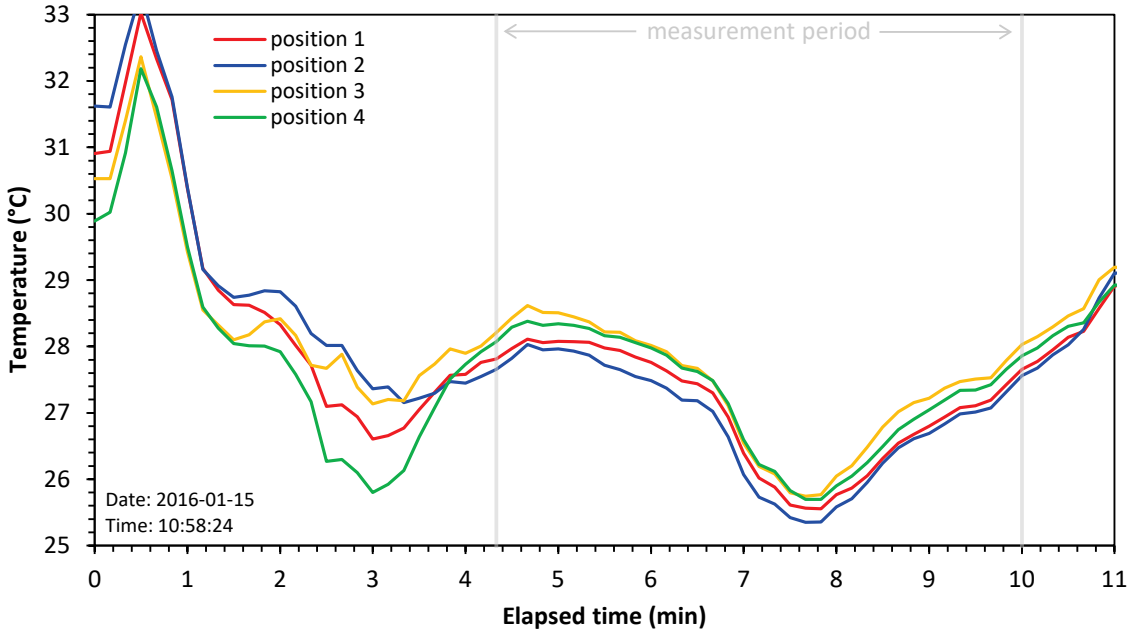

Figure 11. Surface temperatures of duplicate non-fluorescent specimens measured on a platform revolving at 33 RPM, measured in Trial 3C of Experiment 3. Outside air temperature was about 18 °C.

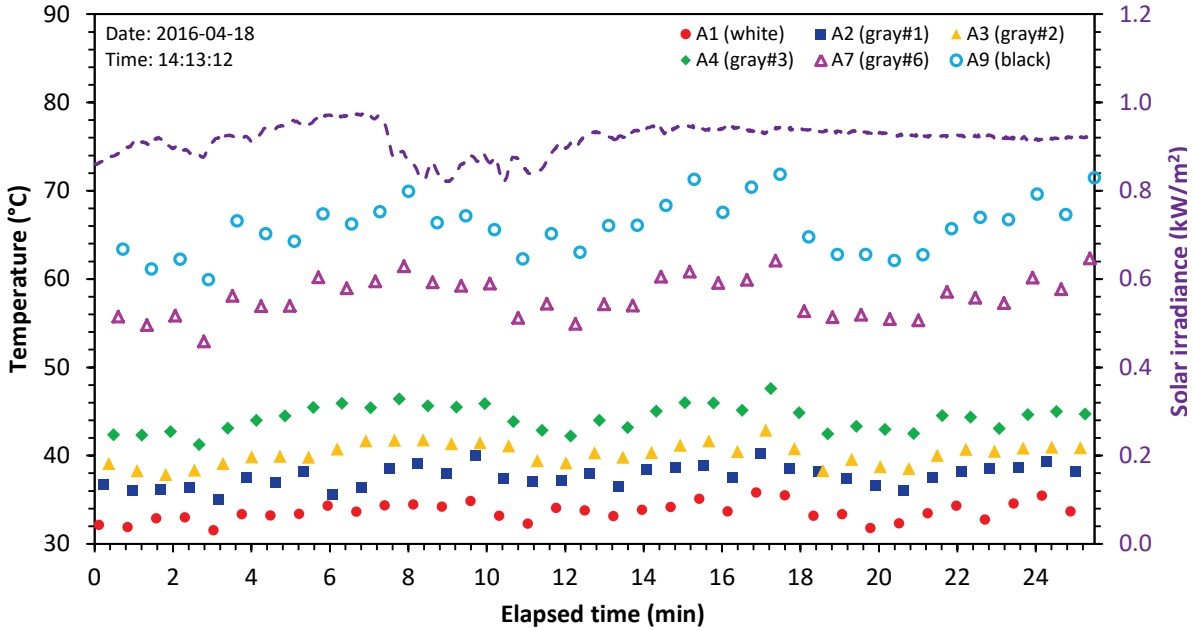

Figure 12. Instantaneous surface temperatures of six non-fluorescent reference specimens measured with the initial programmable rotary apparatus in Trial 4D. Also shown is global horizontal solar irradiance.

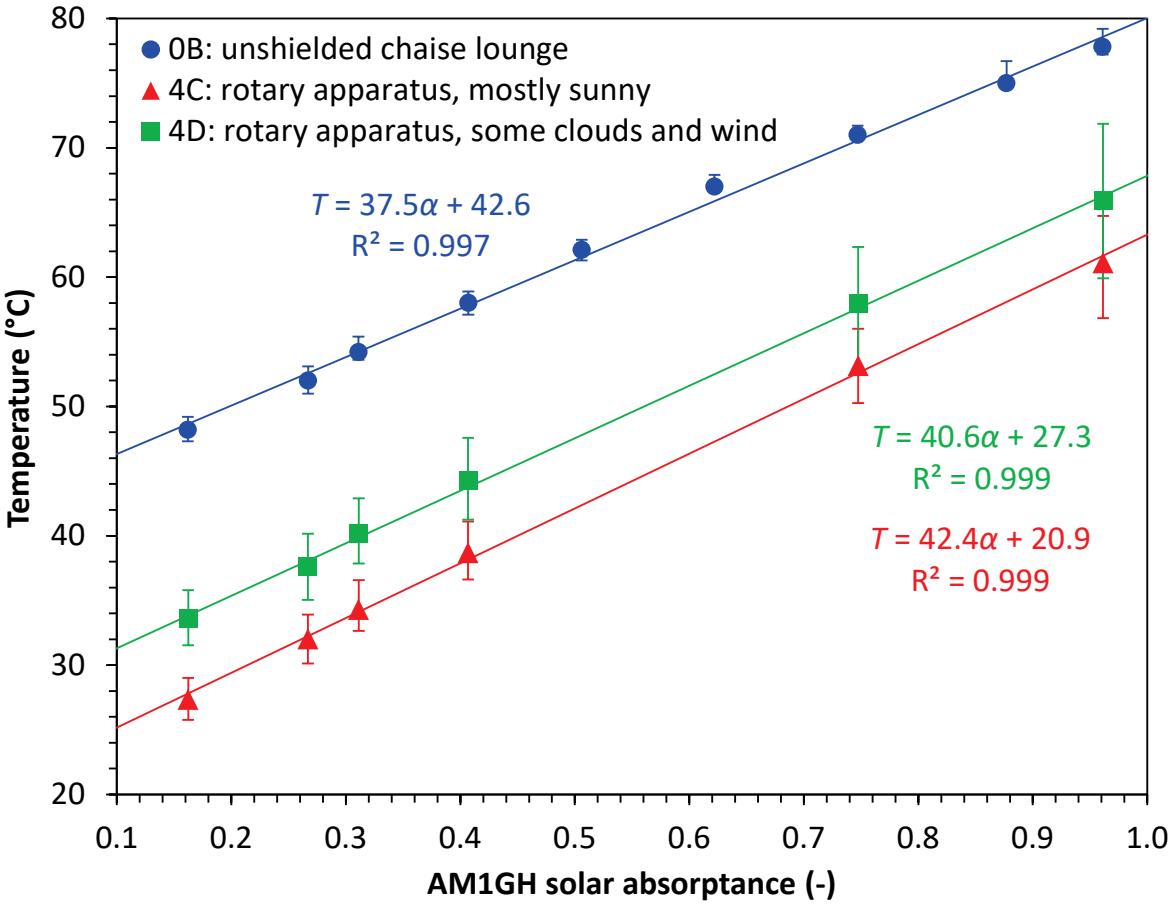

Figure 13. Variation with solar absorptance of the time-averaged temperatures of six gray-scale reference specimens (L to R: A1, A2, A3, A4, A7, and A9) measured with the initial programmable rotary apparatus in Trials 4C and 4D (April 2016). Also shown for comparison are the temperatures of all nine gray-scale reference specimens (L to R: A1 – A9) in Trial 0B (June 2015). Error bars bound low and high values.

Figure 14. Photo of final apparatus, including rotating platter, IR thermometer (upper right), anemometer (lower left), pyranometer (on same board as anemometer), and control electronics (underneath tripod). The air temperature sensor is hidden below the platter.

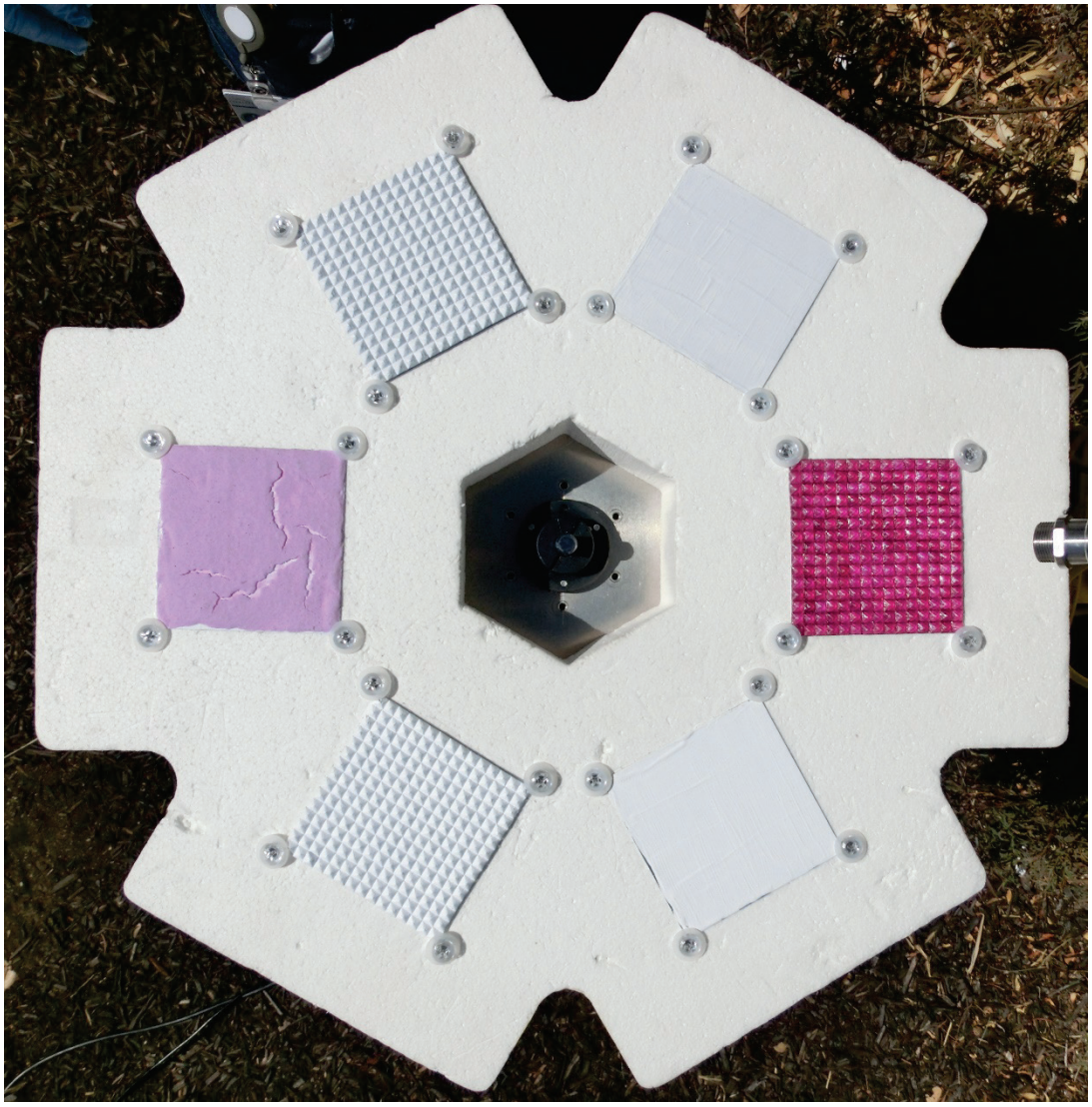

Figure 15. Top view of Set D on the platter. Clockwise from left: 2% coating, ruby crystal gray, A2 (gray#1), ruby crystal clear, A1 (white), and ruby crystal white.

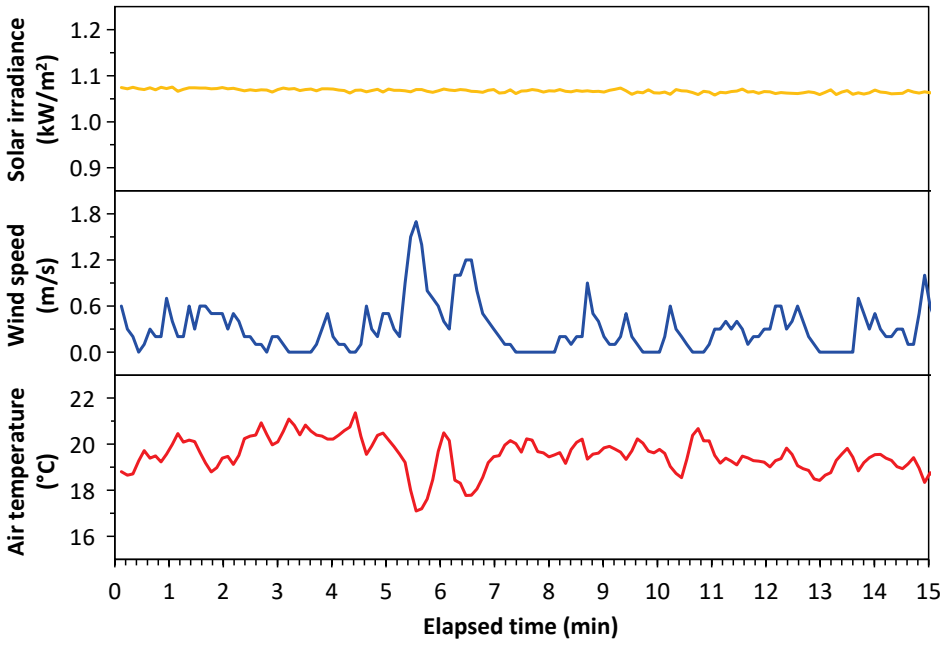

(a)

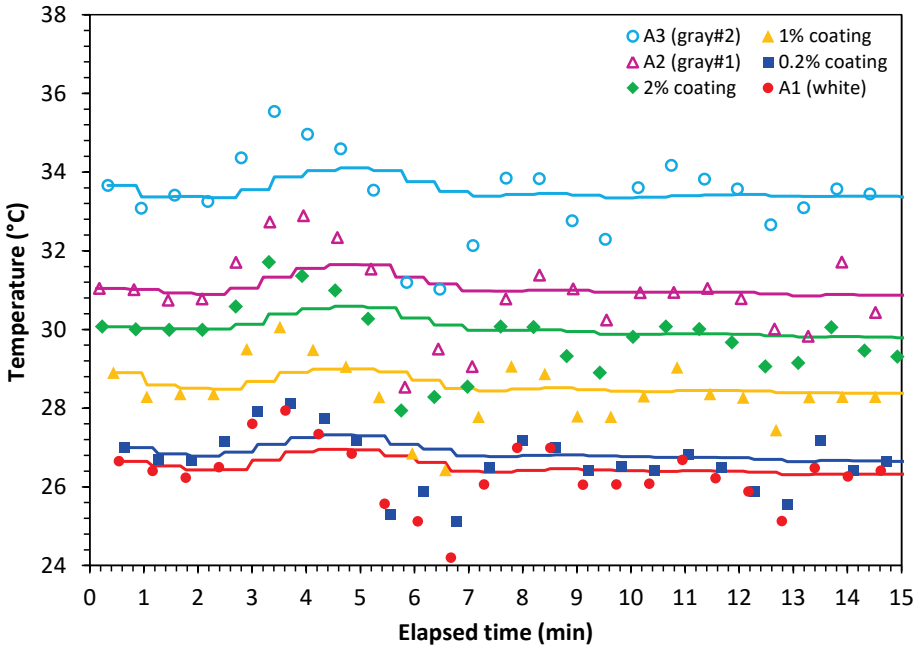

(b)

Figure 16. Time series of (a) weather and (b) specimen temperatures measured during Trial 5C. In panel b, symbols are instantaneous values and lines are cumulative means.

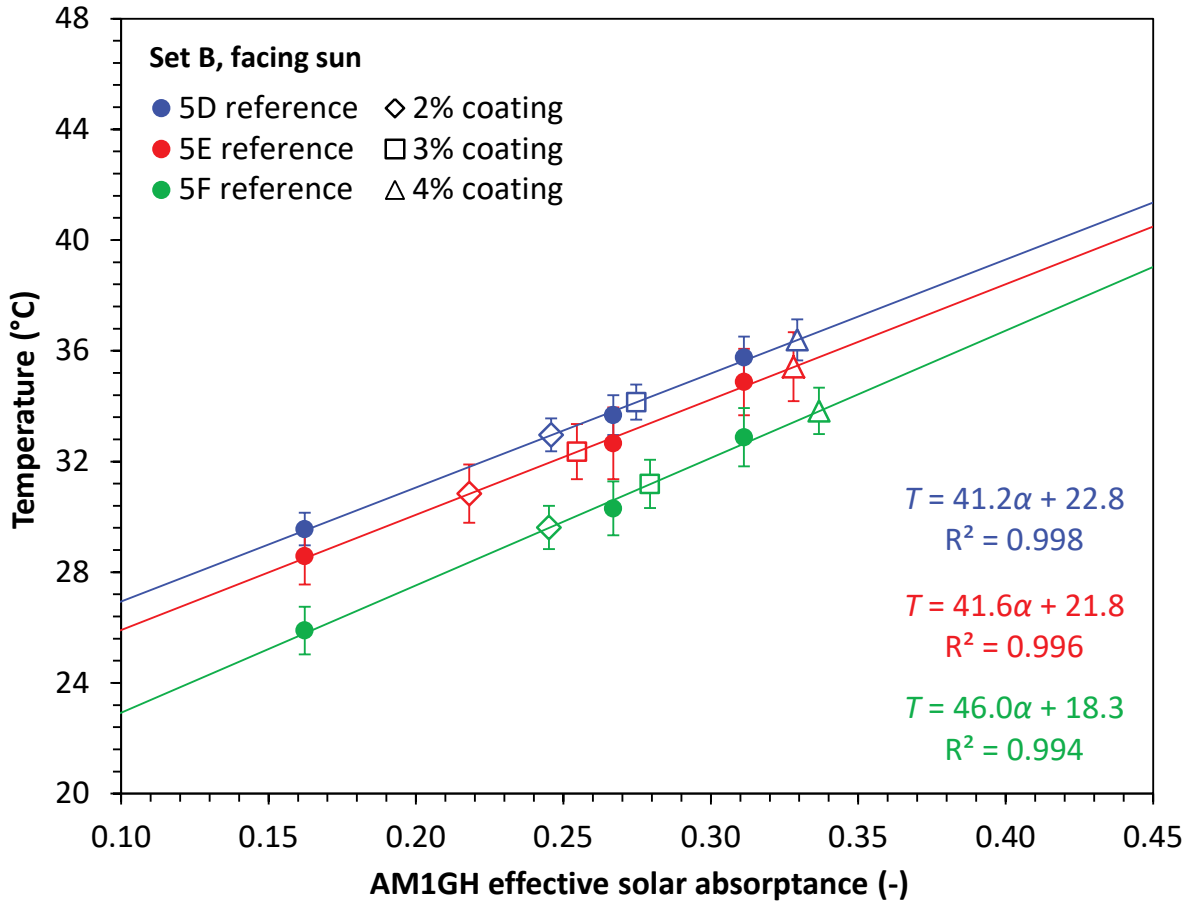

Figure 17. Determination of test specimen ESA from final mean temperatures of test and reference specimens, shown for Trials 5D – 5F (Set B, facing sun).

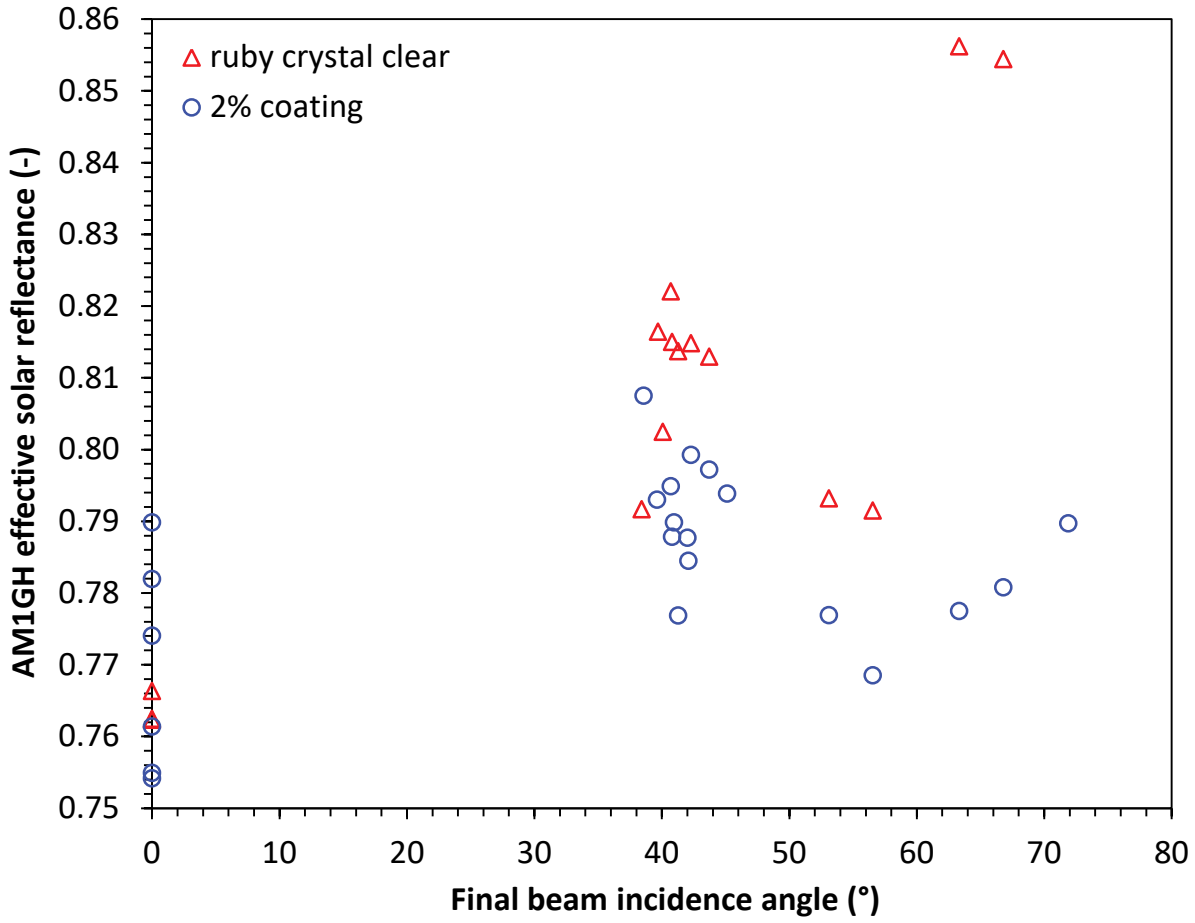

Figure 18. Variation of ESR with solar beam incidence angle for ruby crystal clear and 2% ruby coating.

Table 1. Radiative properties of fluorescent test specimens.

Description	Specimen thickness (mm)	Thermal emittance	Pure AM1GH solar reflectance w/o window
0.2% coating	1.4	0.885	0.732
1% coating	1.6	0.876	0.679
2% coating	1.6	0.880	0.640
3% coating	1.7	0.884	0.626
4% coating	1.6	0.885	0.588
ruby crystal clear	4	0.875	0.434

Table 2. Radiative properties of non-fluorescent reference specimens, including solar reflectances measured without and with a quartz window over the spectrophotometer's reflectance port. Each specimen is 75 mm by 75 mm.

Code	Description	Coating dry film thickness (μm)	Specimen thickness (mm)	Thermal emittance	AM1GH solar reflectance w/o window	AM1GH solar reflectance w/ window
A1	white	120	1.1	0.888	0.838	0.762
A2	gray #1	108	1.1	0.888	0.733	0.665
A3	gray #2	169	1.2	0.895	0.689	0.615
A4	gray #3	248	1.2	0.886	0.593	0.547
A5	gray #4	214	1.2	0.900	0.494	0.463
A6	gray #5	214	1.2	0.897	0.378	0.366
A7	gray #6	174	1.2	0.905	0.253	0.264
A8	gray #7	217	1.2	0.918	0.123	0.165
A9	black	106	1.1	0.926	0.039	0.102
A10	ruby crystal white		4	0.911	0.769	
A11	ruby crystal gray		4	0.912	0.638	

Table 3. Conditions and outcomes of Trials in Experiment 5 (i/iii).

Trial	5A	5B	5C	5D	5E	5F	5G	5H	5I
specimen set	A	A	A	B	B	B	C	C	C
specimen orientation [a]	FS	FS	FS	FS	FS	FS	FS	FS	FS
date (2016-MM-DD)	09-27	09-28	09-28	09-27	09-28	09-28	09-27	09-27	09-28
measurement start (LDT)	13:43	12:35	15:17	17:34	12:00	16:21	14:36	15:51	13:16
spin-up time (min)	10	10	10	10	10	10	10	10	10
measurement time (min)	15.5	15.5	15.3	15.3	15.6	15.5	15.5	15.4	15.7
measurement revolutions	25	25	25	25	25	25	25	25	25
initial solar elevation (°)	48.8	49.3	38.6	15.3	47.5	28.5	44.2	33.7	49.5
final solar elevation (°)	47.8	49.7	36.4	12.4	48.5	25.8	42.3	31.2	49.0
final beam incidence angle (°)	0	0	0	0	0	0	0	0	0
mean solar irradiance (kW/m^2)	1.063	1.049	1.067	0.862	1.043	0.984	0.976	0.920	1.069
s.d.	0.009	0.004	0.004	0.019	0.003	0.007	0.145	0.129	0.003
mean wind speed (m/s)	0.16	0.33	0.31	0.00	0.22	0.14	0.11	0.02	0.27
s.d.	0.17	0.22	0.32	0.02	0.15	0.14	0.18	0.06	0.21
mean air temperature (°C)	27.8	19.1	19.5	24.7	19.4	18.4	32.5	32.8	19.5
s.d.	0.49	0.89	0.77	0.35	0.96	0.66	2.94	0.79	0.81
ruby crystal clear ESR							0.762	0.766	0.762
0.2% coating ESR	0.826	0.824	0.829						
1% coating ESR	0.838	0.825	0.792						
2% coating ESR	0.790	0.774	0.761	0.754	0.782	0.755			
3% coating ESR				0.725	0.745	0.721			
4% coating ESR				0.671	0.672	0.663			

[a] FS = facing sun; H = horizontal.

Table 3 (continued, ii/iii).

Trial	5J	5K	5L	5M	5N	5O	5P	5Q	5R
specimen set	A	A	A	B	B	B	C	C	C
specimen orientation [a]	H	H	H	H	H	H	H	H	H
date (2016-MM-DD)	09-21	09-24	09-26	09-22	09-26	09-27	09-23	09-26	09-27
measurement start (LDT)	14:16	11:17	12:32	11:59	13:31	11:46	12:38	13:01	12:28
spin-up time (min)	10	10	10	10	10	10	10	10	10
measurement time (min)	33.5	32.7	15.5	32.7	15.5	15.3	33.0	15.4	15.5
measurement revolutions	50	50	25	50	25	25	50	25	25
initial solar elevation (°)	48.6	44.6	50.0	49.4	49.8	46.7	51.3	50.5	49.5
final solar elevation (°)	44.9	48.0	50.4	51.4	49.0	47.9	51.6	50.3	49.9
final beam incidence angle (°)	45.1	42.0	39.6	38.6	41.0	42.1	38.4	39.7	40.1
mean solar irradiance (kW/m^2)	0.807	0.783	0.861	0.895	0.819	0.906	0.876	0.861	0.895
s.d.	0.040	0.015	0.003	0.008	0.042	0.004	0.003	0.003	0.010
mean wind speed (m/s)	0.33	0.14	0.25	0.36	0.16	0.02	0.36	0.22	0.08
s.d.	0.33	0.19	0.25	0.33	0.22	0.07	0.33	0.25	0.11
mean air temperature (°C)	21.5	24.6	32.7	20.3	33.6	28.3	22.4	33.5	28.6
s.d.	1.21	0.86	0.82	1.16	0.83	0.78	0.99	0.76	0.62
ruby crystal clear ESR							0.792	0.816	0.802
0.2% coating ESR	0.851	0.854	0.861						
1% coating ESR	0.844	0.841	0.838						
2% coating ESR	0.794	0.788	0.793	0.807	0.790	0.784			
3% coating ESR				0.776	0.761	0.747			
4% coating ESR				0.704	0.682	0.683			

Table 3 (continued, iii/iii).

Trial	5S/i	5S/ii	5S/iii	5S/iv	5S/v	5S/vi	5S/vii	5S/viii	5S/ix	5S/x	5T	5U
specimen set	D	D	D	D	D	D	D	D	D	D	E	E
specimen orientation [a]	H	H	H	H	H	H	H	H	H	H	FS	H
date (2016-MM-DD)	09-29	09-29	09-29	09-29	09-29	09-29	09-29	09-29	09-29	09-29	09-28	09-26
measurement start (LDT)	12:38	12:56	13:13	13:33	13:52	15:10	15:33	16:13	16:33	17:00	14:10	10:56
spin-up time (min)	10	1	1	1	1	10	1	10	1	5	10	10
measurement time (min)	15.7	15.7	15.7	15.7	15.8	15.7	15.7	15.7	15.6	16.3	15.4	9.5
measurement revolutions	25	25	25	25	25	25	25	25	25	25	25	15
initial solar elevation (°)	49.1	49.3	49.2	48.6	47.5	39.2	35.9	29.4	26.0	21.1	46.5	41.4
final solar elevation (°)	49.3	49.2	48.7	47.7	46.3	36.9	33.5	26.7	23.2	18.1	45.0	42.6
final beam incidence angle (°)	40.7	40.8	41.3	42.3	43.7	53.1	56.6	63.3	66.8	71.9	0	47.4
mean solar irradiance (kW/m^2)	0.850	0.853	0.848	0.833	0.814	0.649	0.584	0.534	0.468	0.322	1.043	0.759
s.d.	0.003	0.003	0.003	0.005	0.006	0.011	0.014	0.014	0.016	0.055	0.003	0.005
mean wind speed (m/s)	0.20	0.12	0.18	0.13	0.14	0.24	0.17	0.16	0.07	0.16	0.16	0.28
s.d.	0.17	0.15	0.25	0.18	0.18	0.26	0.22	0.17	0.14	0.18	0.18	0.20
mean air temperature (°C)	18.0	18.6	18.6	18.4	18.2	19.4	19.2	19.0	19.7	17.9	20.1	28.8
s.d.	1.16	1.26	1.34	1.21	1.09	1.42	1.04	1.16	0.89	0.84	0.84	0.51
ruby crystal clear ESR	0.822	0.815	0.814	0.815	0.813	0.793	0.792	0.856	0.854	0.910		
0.2% coating ESR												
1% coating ESR												
2% coating ESR	0.795	0.788	0.777	0.799	0.797	0.777	0.768	0.777	0.781	0.790		
3% coating ESR												
4% coating ESR												

Table 4. ESRs of fluorescent specimens by measurement orientation, showing sample count, mean, and standard deviation. Horizontal measurements include only those in which the final solar elevation angle was at least 40°. Also shown are pure SR and fluorescence benefit (ESR facing sun – pure SR).

effective solar reflectance	ESR facing sun count	ESR facing sun mean	ESR facing sun s.d.	ESR horizontal count	ESR horizontal mean	ESR horizontal s.d.	ESR horizontal – ESR facing sun	AM1GH pure SR	fluorescence benefit (ESR facing sun – AM1GH pure SR)
ruby crystal clear	3	0.764	0.002	8	0.811	0.010	0.047	0.434	0.330
0.2% coating	3	0.826	0.002	3	0.855	0.005	0.029	0.732	0.095
1% coating	3	0.818	0.023	3	0.841	0.003	0.023	0.679	0.140
2% coating	6	0.769	0.015	11	0.792	0.008	0.023	0.640	0.130
3% coating	3	0.730	0.013	3	0.761	0.015	0.031	0.626	0.104
4% coating	3	0.669	0.005	3	0.689	0.012	0.021	0.588	0.081

A. Electronic Supplementary Material

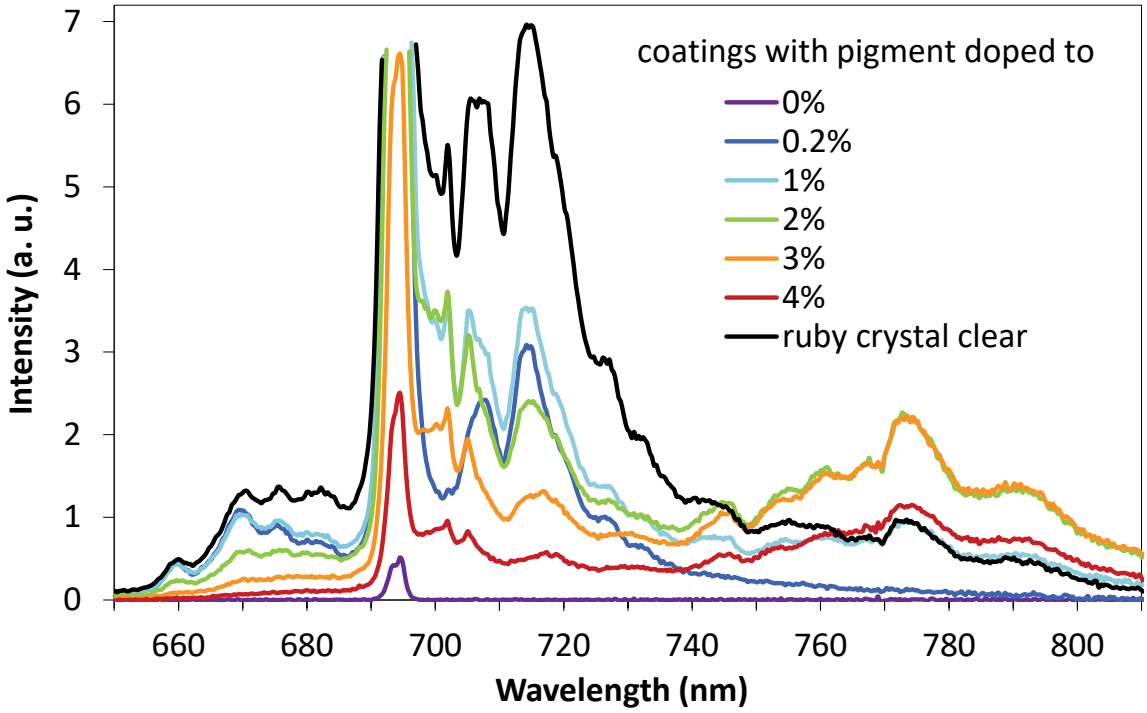

ESM Figure A-1. More detail of the spectra in Figure 5. Note that the nominal 0% pigment must contain a trace of Cr, since a double peak is visible near 694 nm.

(a) (b) (c)

ESM Figure A-2. Photomultiplier tube sensor (250 – 900 nm) in the integrating sphere of a UV-VIS-NIR spectrophotometer (a) exposed and (b) covered with a removable filter. The filter (c) is mounted in a paper cup that has been painted bright white. It passes 90 to 95% of light from 400 to 650 nm, and reflects nearly 100% of light from 650 to 865 nm.

ESM Figure A-3. Reclining chair with towel used to support specimens in Experiment 0. Note that this photo shows a set of specimens different from that used in Experiment 0.

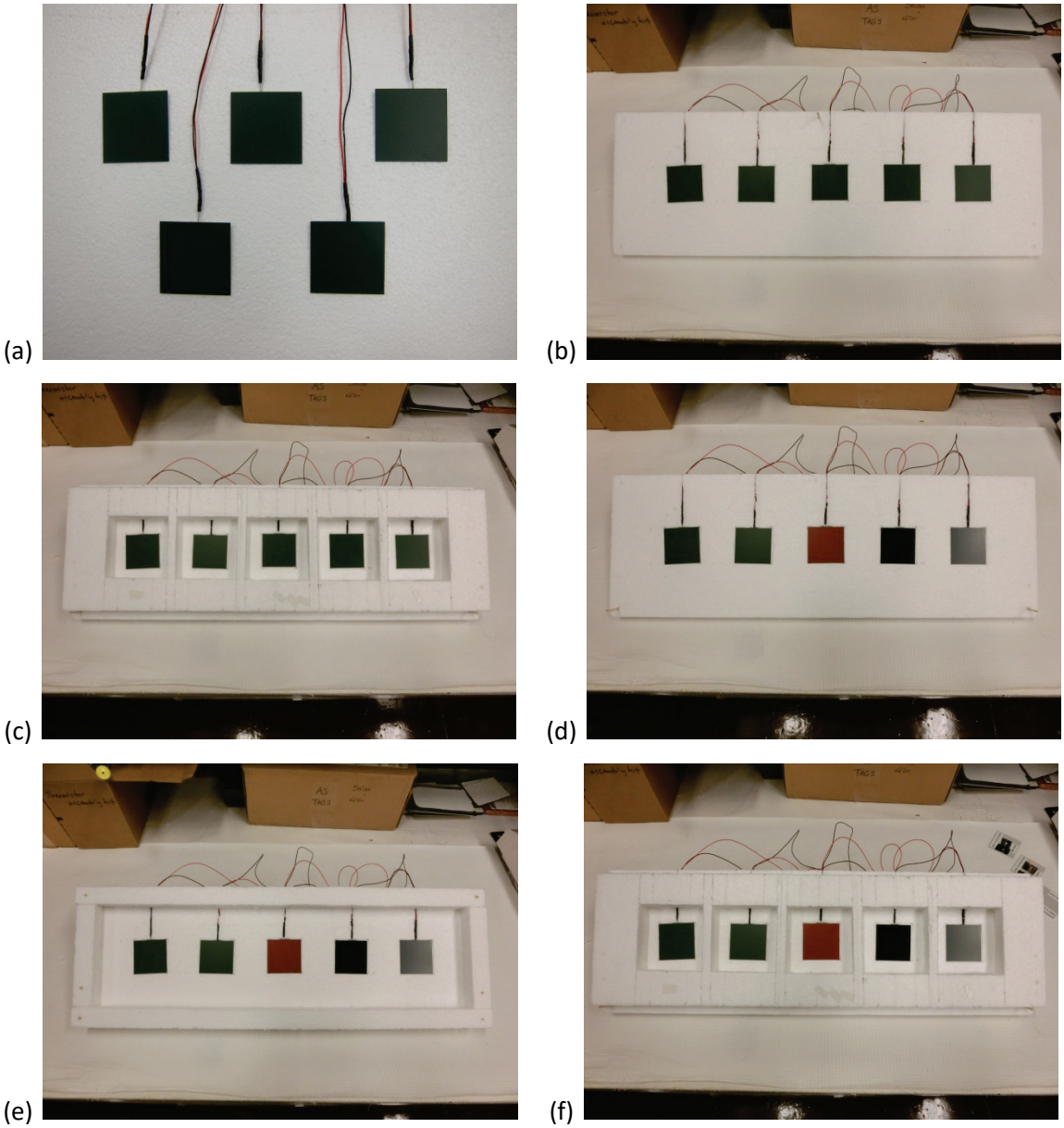

ESM Figure A-4. Apparata and specimens (50 mm by 50 mm) used in Experiment 2, including (a) Trial 2A, five duplicate specimens arranged in two rows at the center of a 36 cm by 38 cm by 2.5 cm foam board; (b) Trial 2B, the five duplicates arranged in one row on a 20 cm by 61 cm by 2.5 cm foam board; (c) Trial 2C, the five duplicates in a cavity array (9 cm by 9 cm, 25 mm deep); (d) Trial 2D, five different specimens exposed as in 2B; (e) Trial 2E, adding a parapet-style wind break (25 mm height, 5 cm from the specimen row) to the 2D setup; and (f) Trial 2F, five different specimens exposed as in 2C.

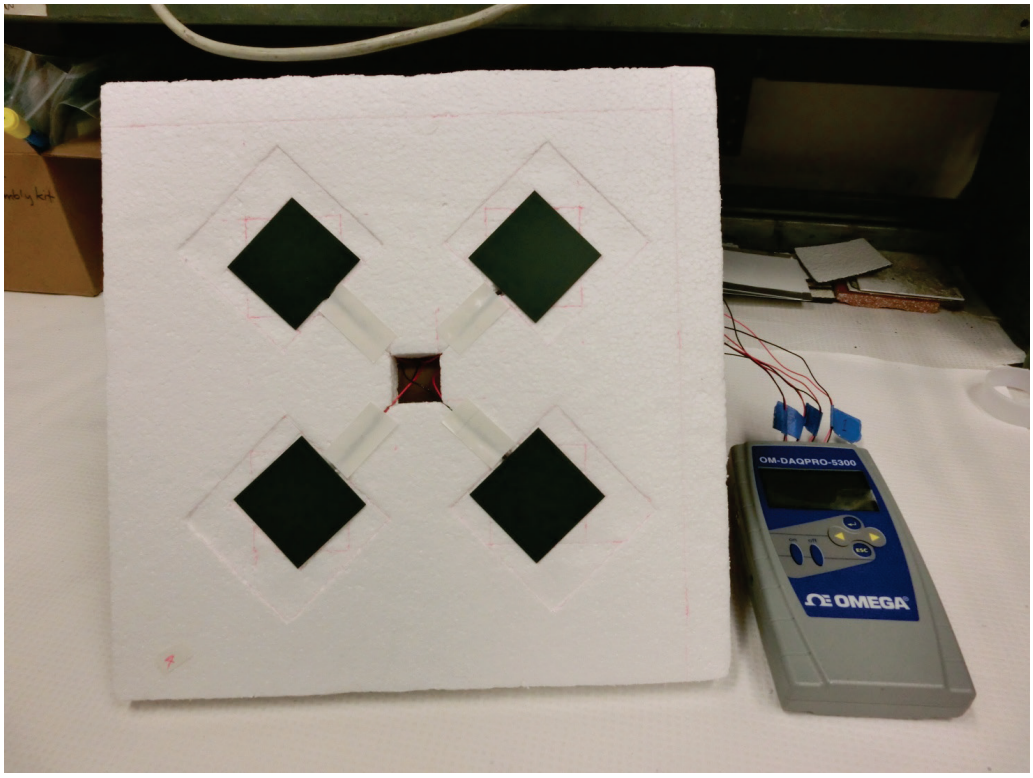

ESM Figure A-5. Duplicate non-fluorescent specimens on a manually rotated platform with four very shallow cavities. The specimens are arranged in a two by two array on a 33 by 33 by 2.5 cm foam board, with 5 cm spacing. The margin on each side is 6.4 cm.

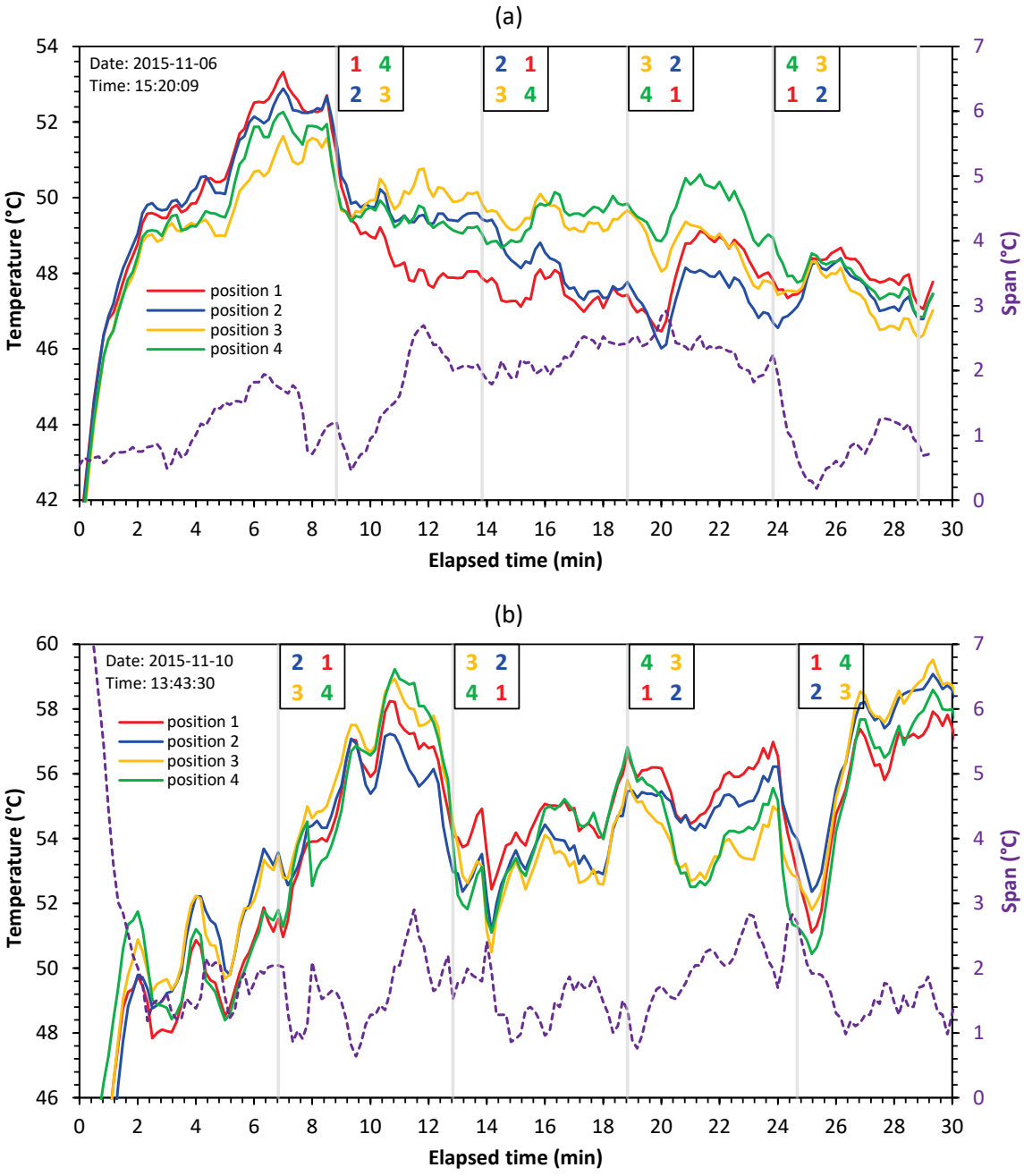

ESM Figure A-6. Surface temperatures and surface temperature range of duplicate non-fluorescent specimens measured on a manually rotated platform, measured in (a) Trial 3A and (b) Trial 3B of Experiment 3.

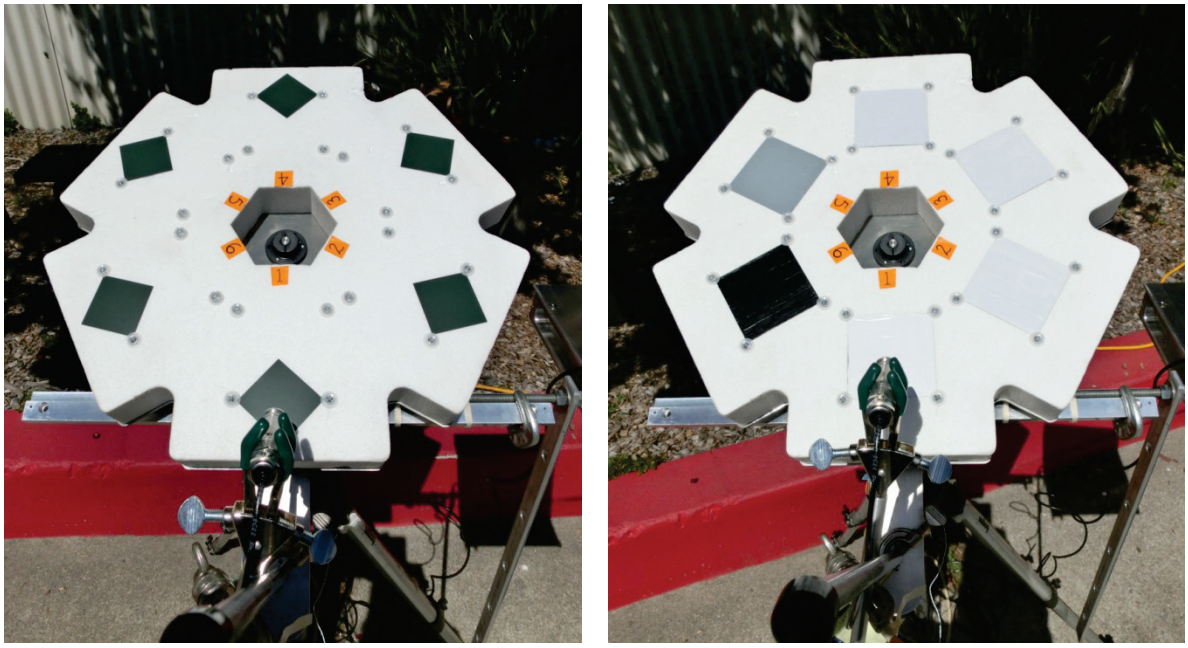

(a) (b)

ESM Figure A-7. Images of the initial programmable rotary apparatus configured for (a) Trials 4A and 4B (six duplicate green specimens) and (b) Trials 4C and 4D (six gray-scale reference specimens). The fixed-position infrared thermometer is shown in foreground.

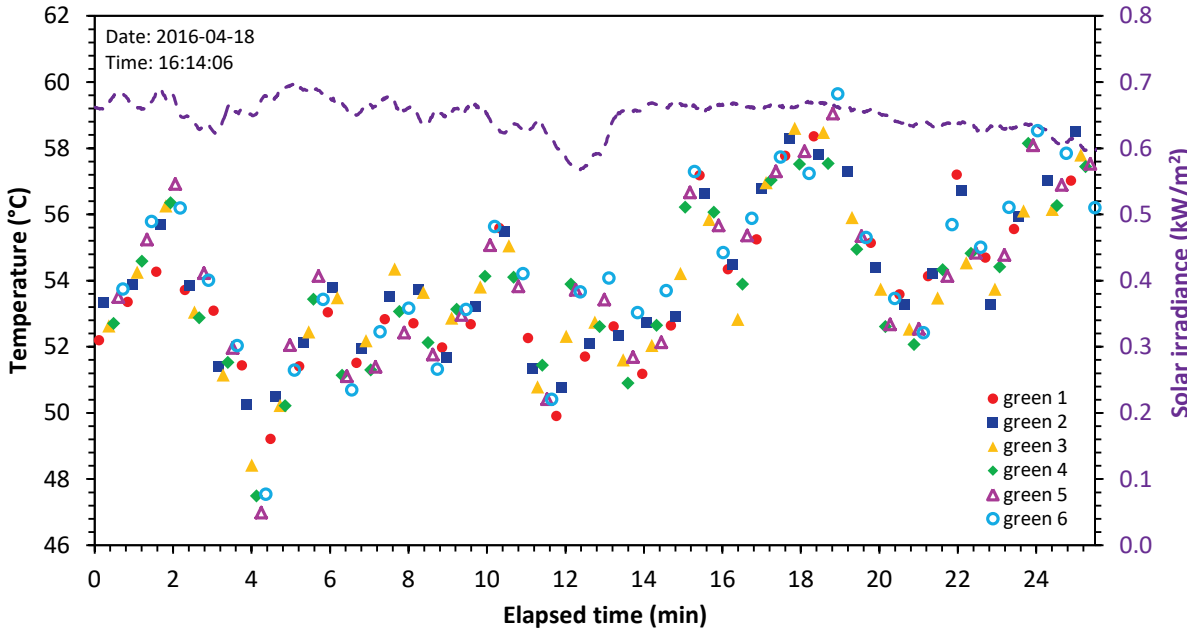

ESM Figure A-8. Instantaneous surface temperatures of six duplicate green specimens measured with the initial programmable rotary apparatus in Trial 4B. Also shown is global horizontal solar irradiance.

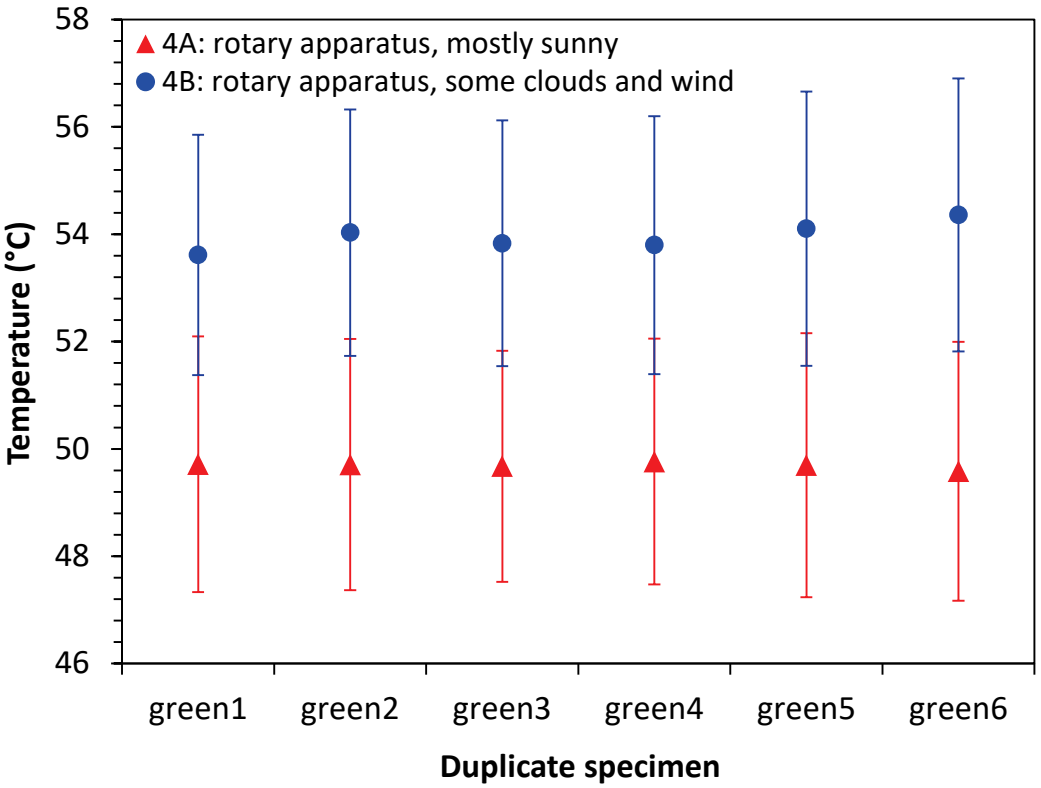

ESM Figure A-9. Means and standard deviations of duplicate green specimen temperatures measured with the initial programmable rotary apparatus in Trials 4A and 4B.

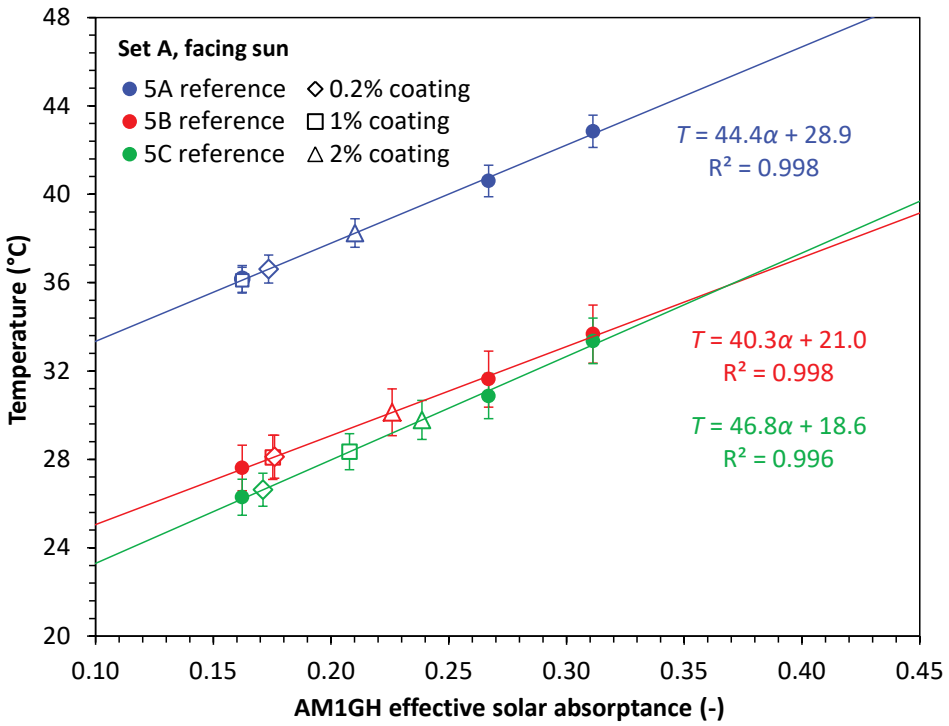

(a)

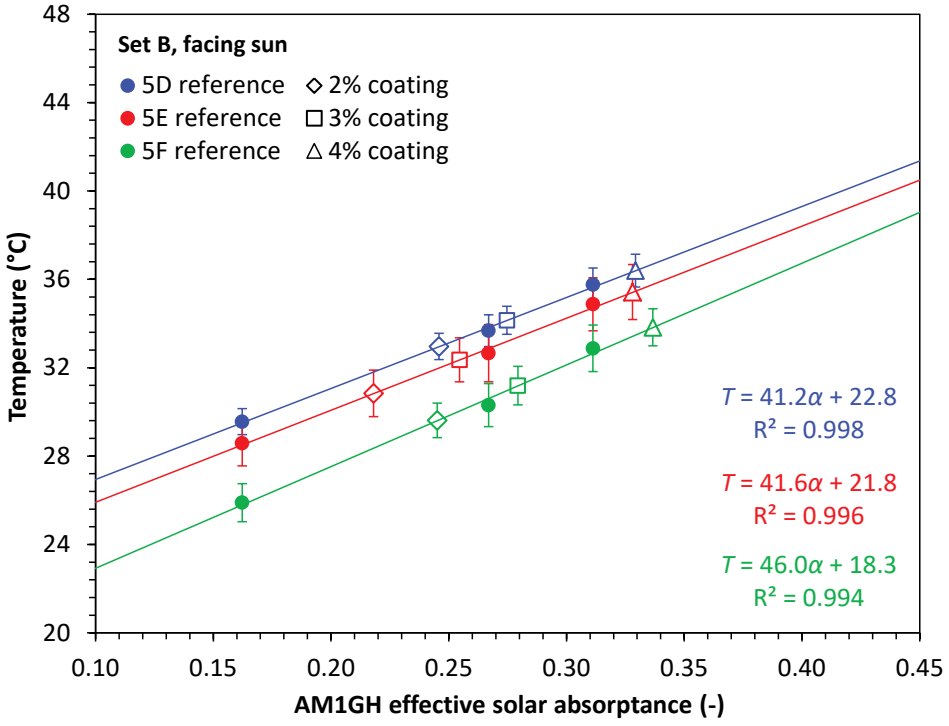

(b)

ESM Figure A-10. Determination of test specimen ESA from final mean temperatures of test and reference specimens, shown for (a) Trials 5A – 5C (Set A, facing sun); (b) Trials 5D – 5F (Set B, facing sun); (c) Trials 5G – 5I (Set C, facing sun); (d) Trials 5J – 5L (Set A, horizontal); (e) Trials 5M – 5O (Set B, horizontal); and (f) Trials 5P – 5R (Set C, horizontal. Note that Trial 5M used reference A4 (gray#3) in place of reference A3 (gray#2).

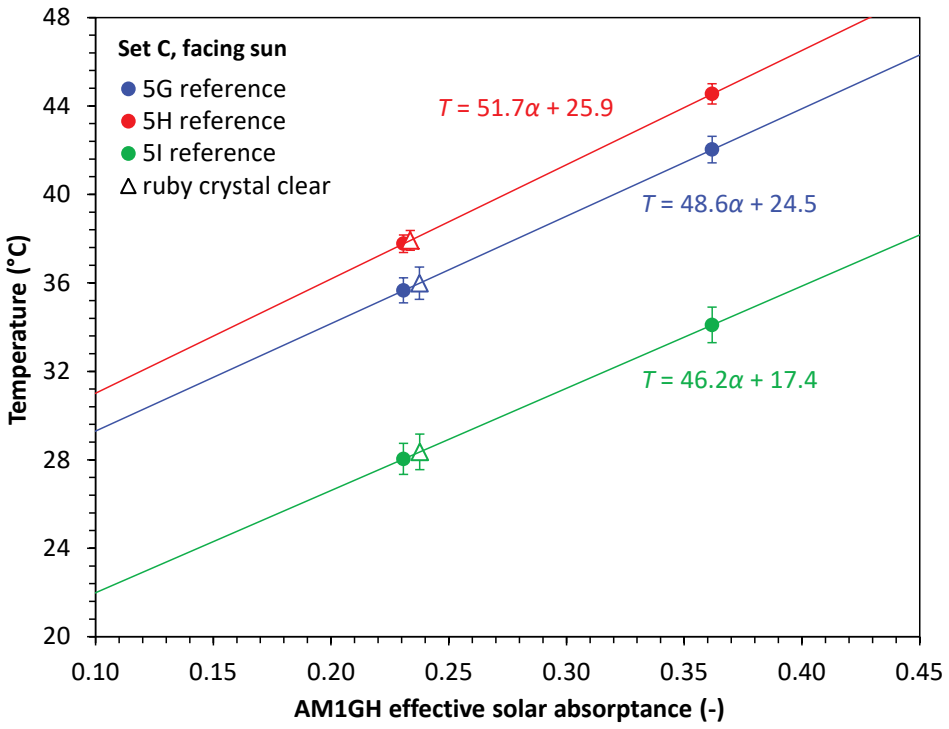

(c)

ESM Figure A-10 (continued)

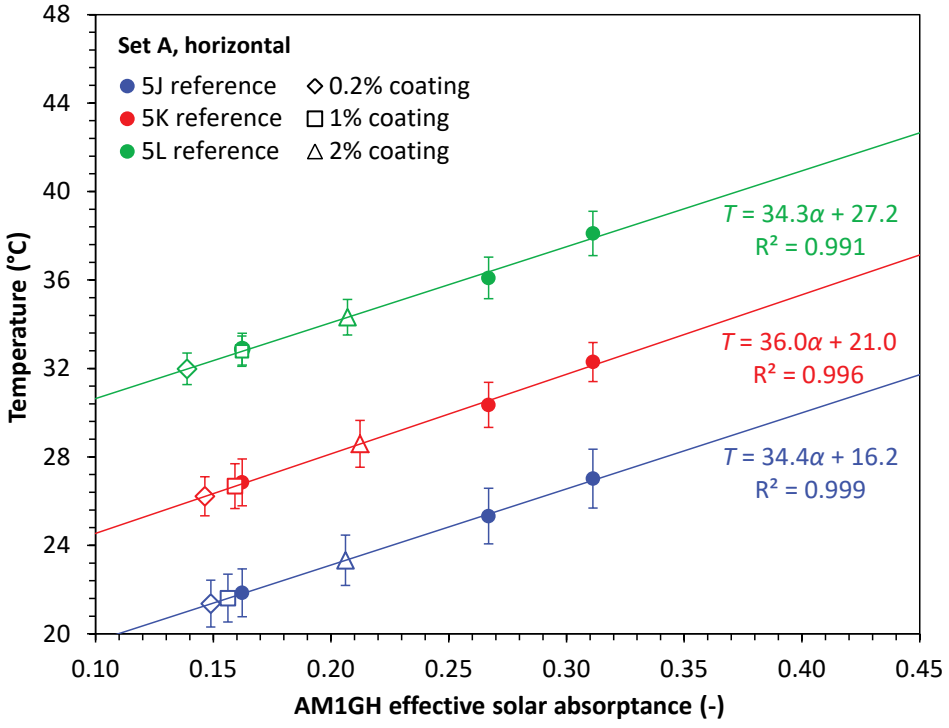

(d)

ESM Figure A-10 (continued)

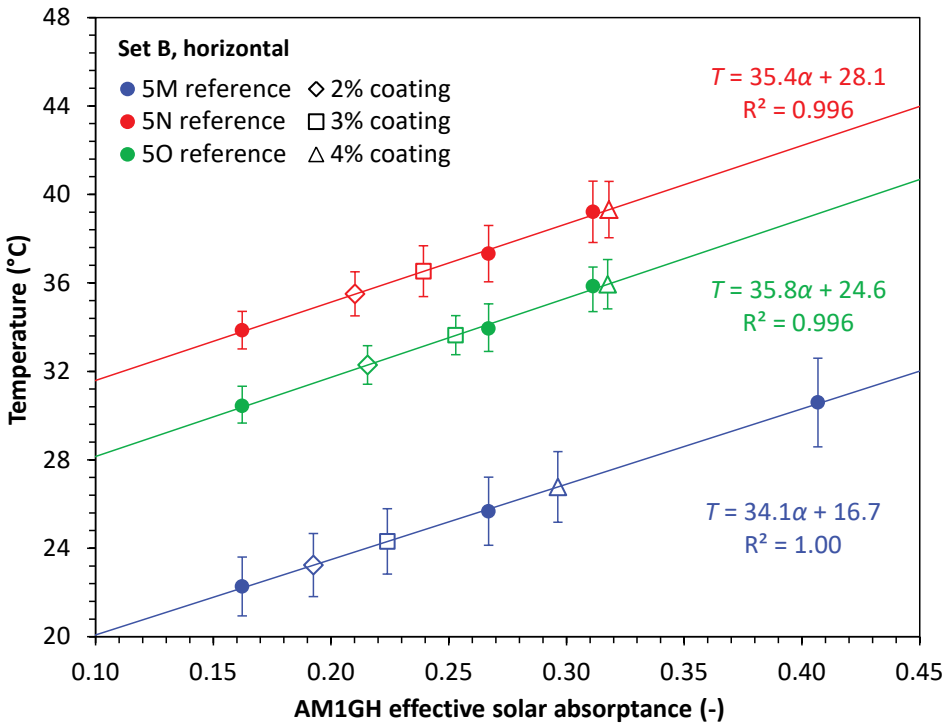

(e)

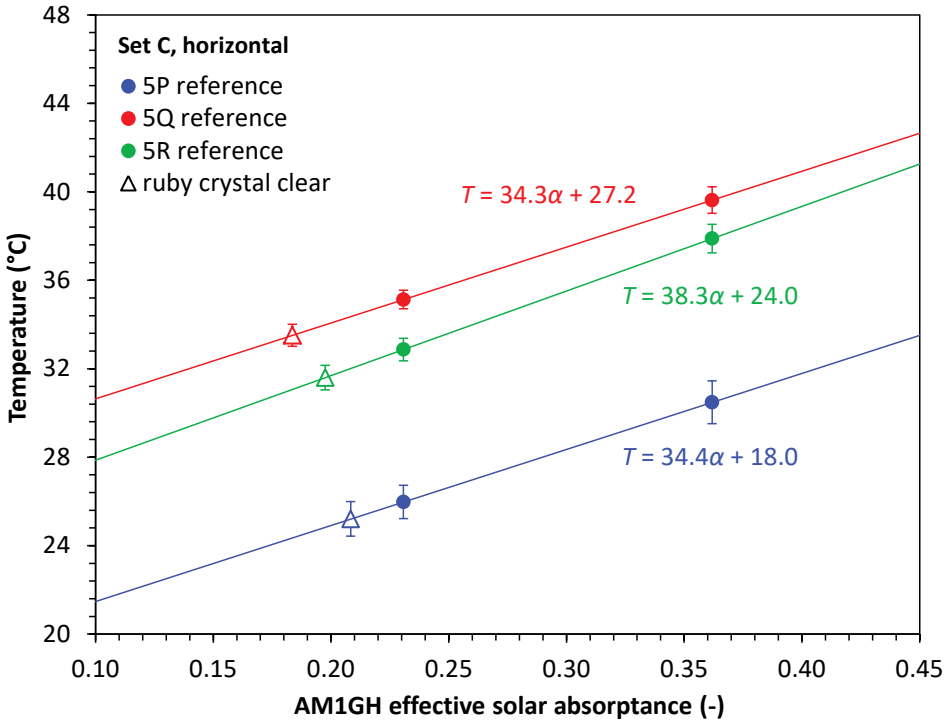

(f)

ESM Figure A-10 (continued)

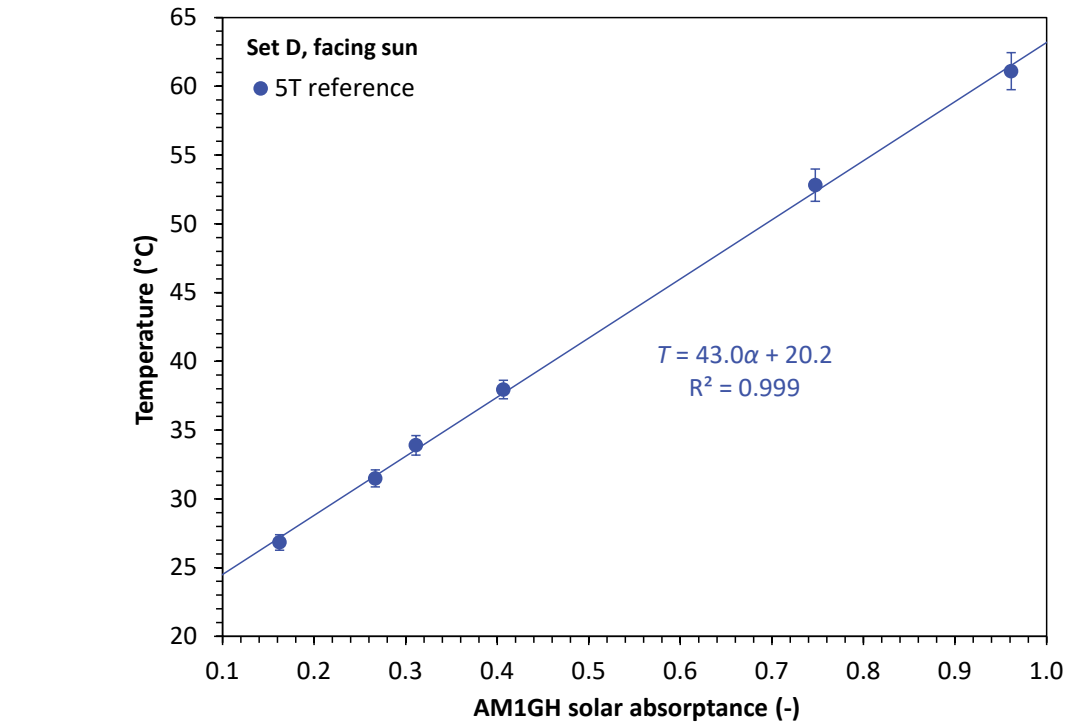

(a)

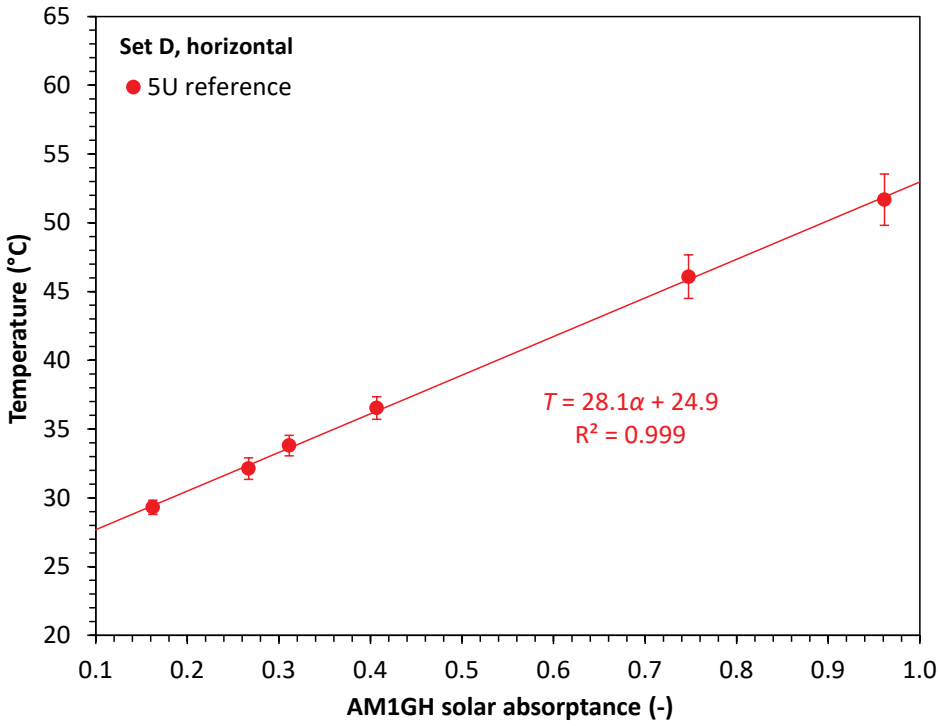

(b)

ESM Figure A-11. Final mean temperature versus pure SA for non-fluorescent reference specimens, shown for (a) Trial 5T (Set E, facing sun) and (b) Trial 5U (Set E, horizontal).

ESM Table A-1. Measurement sensors and protocols used in calorimetric experiments.

	Experiment 0A	Experiment 0B	Experiment 1	Experiment 2	Experiment 3	Experiment 4	Experiment 5 (final apparatus)
Specimen surface temperature							
Sensor type	Thermistor, NTC 10K ohm	Handheld infrared thermometer	Thermistor, NTC 10K ohm	Thermistor, NTC 10K ohm	Thermistor, NTC 10K ohm	Fixed-mount infrared thermometer	Same as Experiment 4
Sensor make and model	Omega 44006	VWR Traceable Infrared Thermometer (Cat. No. 36934-178)	Omega 44006	US Sensor PR103J2	US Sensor PR103J2	Omega OS151-MT	Same as Experiment 4
Sensor range	-80 to 120 °C	-60 to 500 °C	-80 to 120 °C	-55 to 80 °C	-55 to 80 °C	0 to 250°C	Same as Experiment 4
Sensor accuracy (nominal)	unknown	±(2% + 1 °C) %	unknown	±0.05 °C	±0.05 °C	±1% of reading or ±1°C, whichever is greater	Same as Experiment 4
Sensor repeatability (nominal)	unknown	unknown	unknown	unknown	unknown	±0.5% of reading or ±0.5°C, whichever is greater	Same as Experiment 4
Sensor interchangeability	±0.2 °C (0 to 70 °C)	—	±0.2 °C (0 to 70 °C)	±0.05 °C (0 to 50 °C)	±0.05 °C (0 to 50 °C)	unknown	Same as Experiment 4
Sensor features		adjustable emissivity				15:1 field of view;	Same as Experiment 4

	Experiment 0A	Experiment 0B	Experiment 1	Experiment 2	Experiment 3	Experiment 4	Experiment 5 (final apparatus)
						emissivity fixed at 0.95	
Protocol	Sensors attached to back of specimen with aluminum tape; 9 measurements logged over a period of 11 min	Instrument held briefly above each of 9 specimens; 8 measurement sets performed over a period of 30 min	Sensor attached to back of specimen with thermal paste and aluminum tape; measurements logged every 1 sec over a period of 1-2 hrs	Sensor attached to back of specimen with thermal paste and aluminum tape; measurements logged every 10 sec over a period of 20 min	Sensor attached to back of specimen with thermal paste and aluminum tape; measurements logged every 10 sec over a period of 20 min (3A and 3B) or 6 min (3C)	To reduce shadows, sensor mounted ~3.8 cm from center of specimen, with 55-65° angle between sensor axis and specimen plane; waited 4-5 sec for reading to stabilize	Sensor mounted 2.5 cm (along line of sight) from center of specimen, with 45° angle between sensor axis and specimen plane.
Ambient air temperature							
Sensor type	Old-style bulb thermometer	Same as Experiment 0A	Thermistor, NTC 10K ohm	Same as Experiment 1	Same as Experiment 1	None	Thermistor, NTC 10K ohm
Sensor make and model			Omega 44006	Same as Experiment 1	Same as Experiment 1		US Sensor KS103G2
Sensor range	-30 to 50 °C	Same as Experiment 0A	-80 to 120 °C	Same as Experiment 1	Same as Experiment 1		-80 to 135 °C
Sensor accuracy	± 0.5 °C	Same as Experiment 0A	Unknown	Same as Experiment 1	Same as Experiment 1		see interchangeability
Sensor interchangeability			±0.2 °C (0 to 70 °C)	Same as Experiment 1	Same as Experiment 1		±0.1 °C (0 to 70 °C)

	Experiment 0A	Experiment 0B	Experiment 1	Experiment 2	Experiment 3	Experiment 4	Experiment 5 (final apparatus)
Sensor features							
Protocol	Measurements before and after experiment. Sensor in shade, height 1.5 m	Measurements before, at midpoint, and after experiment. Sensor in shade, height 1.5 m	Sensor installed on the back side of apparatus; measurements logged every 1 sec over a period of 1 to 2 hours	Sensor installed on the back side of apparatus; measurements logged every 10 sec over a period of 20 min	Sensor installed on the back side of apparatus; measurements logged every 10 sec over a period of 20 min (3A and 3B) or 6 min (3C)		Sensor mounted on the underside of the specimen platter, shaded from sunlight.
Solar irradiance							
Sensor type	None	None	Silicon pyranometer	Same as Experiment 1	None	Same as Experiment 1	Same as Experiment 1
Sensor make and model			Kipp & Zonen SP Lite2	Same as Experiment 1		Same as Experiment 1	Same as Experiment 1
Sensor spectral range			400 to 1100 nm	Same as Experiment 1		Same as Experiment 1	Same as Experiment 1
Sensor max irradiance			2000 W/m²	Same as Experiment 1		Same as Experiment 1	Same as Experiment 1
Sensor accuracy			Unknown	Same as Experiment 1		Same as Experiment 1	Same as Experiment 1
Protocol			Sensor mounted on the front face of	Sensor placed immediately adjacent to		Sensor placed within 2 m of apparatus, in	Sensor placed on the ground within 1 m of apparatus. Sensor

	Experiment 0A	Experiment 0B	Experiment 1	Experiment 2	Experiment 3	Experiment 4	Experiment 5 (final apparatus)
			apparatus; measurements logged every 1 sec over a period of 1 to 2 hours	apparatus and tilted equivalently; measurements logged every 10 sec over a period of 20 min		horizontal plane	orientation (horizontal or tilted facing the sun) for each trial matched that of the specimens.
Wind speed							
Sensor type	None	None	Handheld vane anemometer	None	None	None	3-cup anemometer
Sensor make and model			PCE Instruments Anemometer PCE-AM 81				Adafruit product 1733
Sensor range			0.4 to 30 m/s				0.5 to 32 m/s
Sensor accuracy			±3% full scale (<20 m/s); ±4% full scale (>20 m/s)				resolution 0.1 m/s; worst-case accuracy 1 m/s
Protocol	Low wind speed required (a cloth on apparatus must not move)	Low wind speed required (a cloth on apparatus must not move)	Sensor placed behind apparatus with propeller oriented for measuring airflow parallel				Sensor placed on the ground within 1 m of apparatus

	Experiment 0A	Experiment 0B	Experiment 1	Experiment 2	Experiment 3	Experiment 4	Experiment 5 (final apparatus)
			to apparatus; recorded maximum wind speed over experiment duration				
Data acquisition system							
Instrument type	Portable handheld data logger	None (measurements recorded manually)	Portable handheld data logger	Portable handheld data logger	Portable handheld data logger	Portable handheld data logger	Multifunction data acquisition device with Python application programming interface
Instrument make and model	Omega OM-DAQPRO-5300		Omega OM-DAQPRO-5300	Omega OM-DAQPRO-5300	Omega OM-DAQPRO-5300	Omega OM-DAQPRO-5300	`LabJack T7`

Task Report Appendix B:
Pre-print of ruby pigment article (Berdahl et al. 2016)

Fluorescent cooling of objects exposed to sunlight – the ruby example

Paul Berdahl[1*], Sharon S. Chen[1] , Hugo Destaillats[1], Thomas W. Kirchstetter[1], Ronnen M. Levinson[1], and Michael A. Zalich[2]

[1] Heat Island Group, Lawrence Berkeley National Laboratory

[2] PPG Industries, Inc., Coatings Innovation Center, Allison Park, PA 15101, USA

[*]Corresponding author, paul.berdahl@gmail.com

Abstract

Particularly in hot climates, various pigments are used to formulate desired non-white colors that stay cooler in the sun than alternatives. These cool pigments provide a high near-infrared (NIR) reflectance in the solar infrared range of 700 to 2500 nm, and also a color specified by a reflectance spectrum in the 400 to 700 nm visible range. Still cooler materials can be formulated by also utilizing the phenomenon of fluorescence (photoluminescence). Ruby, Al_2O_3:Cr, is a prime example, with efficient emission in the deep red (~694 nm) and near infrared (700-800 nm). A layer of synthetic ruby crystals on a white surface having an attractive red color can remain cooler in the sun than conventional red materials. Ruby particles can also be used as a red/pink pigment. Increasing the Cr:Al ratio produces a stronger (darker) pigment but doping above ~3 wt % Cr_2O_3 causes concentration quenching of the fluorescence. The system quantum efficiency for lightly doped ruby-pigmented coatings over white is high, 0.83 ± 0.10.

1. Introduction

The purpose of this paper is to introduce a novel method for reducing the temperature of (non-white) colored materials exposed to sunlight, by utilizing the phenomenon of fluorescence. In order to illustrate the principle, we use the example of chromium-doped aluminum oxide, i.e., ruby. Of course, it is well known that fluorescent emission transports radiant energy, but its application to reduce the temperature of objects exposed to sunlight is novel.

There are a number of applications in which it is desirable to reject solar heat. These include building envelopes (roofs, walls, etc.) to reduce air conditioning energy use [1-4]. A similar need occurs if materials such as vinyl plastics can be damaged by excessive heat. Automobiles in hot

climates likewise benefit from minimizing solar heating [5]. Further uses are cooling instrumentation enclosures and storage tanks, and cooling ships and military vehicles to reduce their thermal radiation signature [6)]. Cool roofing is a key application and a focus of this paper.

In maintaining sunlit objects at low temperatures, high solar reflectance is of course quite beneficial. If some of the solar flux cannot be reflected, then high thermal-infrared emittance and efficient convective cooling are desired. White coatings have suitable solar reflectance and thermal emittance properties, and are appropriate for many applications. On the other hand for aesthetic reasons (or for camouflage) white or other light colors may not be suitable. Building energy codes may require cool roofing. However, manufacturers of roofing materials are then faced with a palette of mostly pastel colors not attractive for their customers. For this reason "cool" colors are needed.

Over the past several decades, cool colored roofing has increased in popularity. For the materials designers, the problem has been to match a desired color (spectral reflectance in the 400 to 700 nm visible range) while maximizing solar reflectance. This has been done mainly by minimizing absorption in the solar near-infrared range (NIR, *ca.* 700 to 2500 nm) [7,8]. Thus non-selective blacks such as carbon black and iron oxide magnetite black are omitted from recipes, and selective blacks such as mixed metal oxides of iron and chromium are used. In the NIR, the selective blacks have lower absorptance and also fairly high reflectance. Durable and cool pigments are available in a variety of colors, mainly based on inorganic mixed oxides containing transition metals. Some organic pigments are also useful and produce vivid colors. However the cost and durability of organics are limitations.

The modern strategy of color combined with high-NIR reflectance is effective but *passive*. Even higher performance is possible by utilizing the *active* phenomenon of fluorescence. Absorbed photons will not only produce heat but also cause fluorescence.

A prototypical fluorescent material is ruby, aluminum oxide doped with chromium. When lightly doped ruby is excited with ultraviolet (UV) or visible light, it fluoresces at 692.9 and 694.3 nm, a doublet called the R-lines [9]. The absorption strength is weak in the red part of the spectrum, and also weak in the blue. Thus the color of ruby varies from pink at low doping to a bluish red as more chromium is added. At high concentrations of chromium (*ca.* 1%), an additional emission spectrum extending from about 655 to beyond 800 nm is particularly apparent [10-13]. The 700-800 nm emission is thought to be due to neighboring pairs and possibly other clusters, of Cr^{3+} ions. At higher doping, first the R-lines are extinguished (concentration quenching), and then the additional spectrum also fades away.

Ruby certainly has remarkable optical properties. The first optical laser was fabricated from a lightly doped ruby crystal with silvered end faces, exposed to the light from a flash lamp [9]. Also, the spectral shift of the fluorescent R lines is used to measure pressure [14] and the brightness and decay time can be used to measure temperature [15].

As a first experiment to verify the cooling due to ruby fluorescence, inexpensive commercial synthetic ruby gems were employed. An array of square pyramidal crystals was attached to a bright white substrate (TiO_2 pigmented coating) using a transparent acrylic overcoat. An off-white sample with a calibrated solar reflectance of 0.65 was used for comparison. Both samples were mounted on an insulating substrate and exposed to full sunlight on a clear day. The reference sample's temperature was 21.3 ˚C above air temperature whereas the ruby-covered sample was only 14.8 ˚C above air temperature. Therefore the effective solar reflectance (ESR) (corrected for some exposed substrate) was larger than 0.65, and estimated to be about 0.71. (Effective solar reflectance is the fraction of incident solar energy that is rejected by reflectance *and* fluorescence. Additional, more complete, measurements on another ruby-crystal-covered substrate are reported below.) Thus the concept of utilizing chromium-doped alumina to provide reddish colors that are cool in the sun seemed worthy of further investigation.

2. Performance of array of synthetic ruby crystals

Polished ruby crystals intended for the jewelry industry were purchased from a commercial supplier. The cost was about 60 USD per lot of 200 crystals. The footprint of each crystal is a 5 mm x 5 mm square with a chamfered pyramidal shape about 2.6 mm high. A 75 mm square aluminum substrate was coated with 3 layers of an acrylic white paint. The crystals were arranged in a square array to cover the substrate and coated with two coats of clear acrylic. The white underlay enhances absorption of excitation light that may pass through the ruby and also reflects fluorescent emission that strikes the substrate. The clear acrylic coating holds the crystals in place and also raises the thermal emittance to 0.89 from 0.71. Figure 1(A) shows the appearance of the crystal array in full sun; the red color is dark, having reflectance in the center of the visual range at 550 nm of only 0.044. The fluorescence is not visible in Fig. 1(A) because the camera (and eye) is not very sensitive at 694 nm and is completely insensitive in the 700 to 800 NIR range. Fig. 1 (B) shows the glow of the array at 694 (and 655 -700) nm when excited by UV in the dark. The fluorescence tends to emerge from the edges of the crystals.

Temperature measurements in full sun were used to estimate the effective solar absorptance of the crystal array and, by subtracting from unity, its effective solar reflectance. Temperature rise in the sun is roughly proportional to solar absorptance. Calibrated non-fluorescent gray and white samples were used for comparison, as was a reference ruby array over-coated with an opaque white paint. The white array was used to check that convective cooling was not unduly enhanced by surface roughness. A first estimate, made by interpolating between calibrated gray and white samples, yielded an effective absorptance of 0.262. A second estimate used the white-coated ruby crystal array as a reference, and employed estimates of the solar flux (1050 W m^{-2}) and of the longwave radiative cooling of a blackbody emitter, referred to ambient air temperature (70 W m^{-2}), to infer the sum of the radiative and convective heat transfer coefficients of $h_r + h_c = 14.7$ W m^{-2} K^{-1}. These coefficients were then used to compute the effective solar absorptance of the ruby crystal array as 0.264. Averaging the two estimates of

absorptance and subtracting from unity yields ESR = 0.737 ± 0.010. Spectrometer measurement, excluding the fluorescence, yields solar reflectance SR = 0.434. Thus the fluorescence contribution ("boost"), the difference ESR-SR, is about 0.30; the fluorescent energy flux is over 300 W m^{-2}. The ruby array is as cool in the sun as typical white commercial materials with SR in the range of [0.65, 0.85], but is quite visually dark.

3. Combustion synthesis of ruby powder

The combustion synthesis method of Kingsley and Patil [16] was chosen as a convenient method for synthesizing small quantities of ruby powder with various chromium concentrations. Briefly, hydrated nitrates of aluminum and chromium are dissolved in water, as is sufficient urea (fuel) for a combustion reaction. A glass beaker containing the solution is placed in a 500 ˚C furnace. After boiling for several minutes, the dehydrated solution ignites for several seconds. What remains in the beaker is a fluffy pink product consisting of Al_2O_3:Cr. The yield is ~ 95% crystalline α-phase alumina with γ-phase alumina as a second phase. The Cr doped γ phase is easily identified as its color is not pink. Depending on the Cr concentration, this phase is green, yellow or white [17]. The unwanted γ phase was physically removed, although we also verified that annealing it at 1200 ˚C for two hours in air can convert it to the α phase.

In preparing various ruby powders, we found that some excess fuel improved preparation of larger lots. Further, higher furnace temperatures were beneficial for higher Cr doping. The combustion process is more rapid at higher furnace temperatures, though if it is too fast the product is dispersed inside the furnace.

X-ray fluorescence (XRF) verified the expected chromium concentration for two of the samples (1%, 3%). (In this paper, we express the doping by means of *w*, the weight fraction of Cr_2O_3 in Al_2O_3. A common alternative is to use *x*, the ratio of numbers of Cr to Al atoms; $x = 0.67\ w$.). BET-measured surface area varied considerably from run to run, with typical values of 1 m^2g^{-1}, ranging up to 11 m^2g^{-1} with higher furnace temperatures. Electron micrographs (Fig. 2) show slab-like particles with typical thickness of 2 to 5 μm. The morphology is likely a replica of the walls of foam just prior to combustion. After each synthesis a small UV lamp was used to visually check for the expected red fluorescence. X-ray diffraction also was used to verify that the observed peaks are those of the α phase of alumina.

To measure optical properties, the powders were mixed with a transparent acrylic paint using a spatula on a smooth glass surface, and spread as a ~500 μm coating onto a white substrate (75 mm square of aluminum with three coats of an artists' titanium dioxide white). This process is crude but simple. About 3 g of pigment was used in each coating. In what follows, the coatings are identified by the weight fraction of chromium oxide in the alumina pigment: 0.0% 0.2%, 1%, 2%, 3%, and 4%.

4. Spectral fluorescence and Effective Solar Reflectance (ESR)

The optical setup included a 6 V lamp (tungsten filament, xenon gas fill), a filter to block excitation light in the spectral range of emission, a 150 mm integrating sphere, and an Ocean Optics spectrometer with silicon array detector. The spectrometer was calibrated using the tungsten lamp filament as a reference at an assumed temperature of 3000 K.

Figure 3 shows the spectral emission of the ruby-pigmented coatings and the crystal array. Comparable data for two ruby crystals may be found in [12]. The sharp peak at 694 nm is highest in the low concentration samples (0.2%, 1%) and diminishes monotonically with higher doping. Particularly at higher doping, emission ranges all the way from 655 to ~800 nm.

ESR measurements were performed on each of the 75 mm square samples by placing them on a thermally insulating substrate in full sunlight, next to calibrated non-fluorescent white and light gray samples of known solar reflectance (SR). Thermistors underneath the samples determined the temperatures, and the ESR values were then determined by interpolation. For comparison, the regular SR was determined with a Perkin Elmer Lambda 900 spectrometer fitted with a 150 mm integrating sphere. A standard solar spectrum for clear sky conditions with the sun high in the sky was used as a weighting function [18]. The short-wave part of the spectrum was detected with a photomultiplier tube (out to ~ 860 nm), and the long-wave part was detected with a PbS semiconductor detector. Now, the ruby fluorescence interferes slightly with the reflectance measurement since, for example, when the sample is illuminated with blue light it reflects blue light but also glows with red and near-infrared light detected by the phototube. For this reason, we used an interference filter placed over the phototube to greatly reduce its sensitivity to red and near infrared light. This filter allowed us to measure the reflectance spectrum excluding the fluorescence. Measurements without the filter then allowed us to evaluate the reflectance correction needed to account for fluorescence. This correction had the spectral shape of the well-known ruby excitation spectrum [9] and was largest at 0.081 at 560 nm for the 1% sample. The ESR results for the ruby pigmented coatings are shown in Fig. 4, along with SR measurements and reflectance at 550 nm. These coatings are not as dark as the ruby crystal array but nonetheless exhibit a fluorescence contribution (ESR-SR) of up to 0.16.

5. Determination of quantum efficiency

It is assumed that all of the photons not reflected in the UV and the 400 to 700 nm visible range are absorbed by Cr^{3+} ions. This approximation is based on the idea that other weak absorption centers present, for example in the undoped Al_2O_3 sample, are not able to successfully compete for photons with the chromium ions. Particularly in the 650 to 700 nm

range the Cr^{3+} absorption may be slightly overestimated. Beyond 700 nm, there is still some absorption but it is relatively weak and will be neglected (Fig. 5).

The reflectance spectra in Fig. 5 show the two sharp absorption dips corresponding to the main ruby emission lines, and also some features at longer wavelength. This structure is a consequence of time reversal invariance, in that photon emission processes can proceed in reverse, causing absorption. Also, it is interesting that the baselines in this figure are lower with higher doping. We do not understand the reasons for this absorption but note that a similar phenomenon has been observed in a multiple scattering environment by another group [19].

The number of fluoresced photons can be estimated based on the energy content in the ESR-SR fluorescent contribution and the wavelength distribution in Fig. 4. Division by the number of photons absorbed then yields the quantum efficiency data shown in Table 1. The typical Cr_2O_3 content of the ruby crystals was determined by X-ray fluorescence to be 0.9%; analysis of the very lightest and darkest crystals showed a range of 0.6% to 1.8%.

Table 1**. Performance of eight samples. Visual reflectance, ESR, ESR-SR, energy efficiency, and quantum efficiency.**

Sample	Cr_2O_3 content (wt % in Al_2O_3)	Reflectance at 550 nm	Effective Solar Reflectance (ESR)	Fluorescence Contribution, (ESR-SR)	Energy efficiency	Quantum efficiency
Crystal array 1	~ 0.9	0.04	0.706	0.293	0.70	0.95
Crystal array 2	~ 0.9	0.044	0.737	0.303	0.72	0.98
Coating	0.0	0.923	0.828	0.00	0	0
Coating	0.2	0.540	0.824	0.092	0.56	0.93
Coating	1	0.366	0.807	0.128	0.55	0.74
Coating	2	0.301	0.805	0.165	0.62	0.83
Coating	3	0.261	0.780	0.154	0.56	0.74
Coating	4	0.203	0.637	0.049	0.16	0.21

The white substrate has a reflectance of about 0.933 at 700 nm. Since half of the photons are emitted toward the substrate, the highest possible system quantum efficiency is about 0.97. Thus the crystal arrays have very high quantum efficiencies, and the films pigmented with ruby are in the range of 0.83 ± 0.10 for doping ≤ 3%. The relatively large uncertainty in the quantum efficiency is believed to reflect experimental errors in ESR of roughly 0.01. By 4%, the quantum efficiency decreases dramatically to 0.21.

6. Limitations of ruby powder as a red pigment

We have shown that doping above 3% of Cr_2O_3 leads to much reduced fluorescence. If we elect to use 3% or less dopant, the absorption strength of the pigment is limited. The average optical absorption cross section of the Cr^{3+} ion in the portion of the solar spectrum absorbed by ruby is roughly 1×10^{19} cm^{-2} [9]. The concentration of ions at 3% is ~ 6×10^{20} cm^{-3}. For the product of these numbers and the layer thickness d to be unity, $d \sim 160$ µm. Now some commercial coatings (paints) are as thin as 20 µm, so it is clear that the ruby pigments are "weak." In commercial coatings applications, maximum pigment volume concentrations are on the order of 50 %, which would require twice the film thickness. On the other hand, efficient use of the fluorescence requires a reflective underlayer, which halves the needed thickness. Further, introduction of some scattering may enhance absorption efficiency at the expense of a lighter color. However, the main point is that the limited pigment tinting strength is an issue in applications in which film thickness is constrained.

The color of the coatings studied here range from light red to pink, in contrast to the darker array of ruby crystals. The reason is light scattering due to the difference in ruby refractive index (~1.76) and that of the polymer medium (~1.5). Reduction of light scattering can be obtained by using larger particles, with fewer interfaces per unit volume, or by using nanoparticles with diameters well below 100 nm. Also, the medium can possibly be engineered to have a high and matching refractive index (scattering is proportional to the square of the difference in refractive indices).

Finally, we point out that aluminum oxide particles are hard and abrasive, so care is required to avoid damage to coating manufacturing equipment.

7. Fluorescent pigments other than ruby

While the fluorescence of ruby is remarkable, with high quantum efficiency, our example is not unique. Other solid-state laser materials like Nd-doped YAG (yttrium aluminum garnet) are obvious possibilities. The study of IR fluorescence in historical pigments [20] has shown that the cadmium pigments CdS, CdSe and their alloys fluoresce [21], as do some alkali earth copper silicates [22, 23] such as Egyptian blue ($CaCuSi_4O_{10}$) and Han blue ($BaCuSi_4O_{10}$). Decades of research on phosphors for color television, for mercury-vapor fluorescent lamps, and more recently for light emitting diodes, has led to a wide variety of efficient compounds that fluoresce in the visible [24, 25]. Doubtless some of these compounds can be modified for emission in the near infrared. Further candidate materials for NIR fluorescence may be found in sister applications. These include pigments for labeling, including nanoparticles for biological applications, direct-bandgap semiconductors considered for photovoltaics, and chromophores for application in fluorescent solar concentrators [26, 27].

For applications to cooling of sunlit materials, beyond fluorescence, we need interesting color, compatibility with high NIR reflectance, durability, and minimal toxicity.

8. Summary

In summary, we have introduced the idea of utilizing fluorescence to reduce the temperature of objects in sunlight, using ruby as an example. We have also used temperature measurements in sunlight, together with spectral measurements of reflectance and fluorescence, to determine the quantum efficiency of the fluorescence process.

Acknowledgments

M. L. Shiao pointed out to P. B. that innovation in cool roofing materials is needed. Colleagues at Shepherd Color (S. Boocock, J. Peake) advised us on solid-state synthesis of mixed metal oxide pigments. We thank M. Levitus of Arizona State University for assistance with early fluorescence measurements, X. Song of the LBNL electrochemistry group for assistance with

BET measurements, N. Bronstein of University of California at Berkeley for bringing Refs. 26 and 27 to our attention, and D. McHenry of PPG Industries for XRF measurements.
This work was supported by the Assistant Secretary for Energy Efficiency and Renewable Energy, Building Technologies Office of the US Department of Energy under Contract No. DE-AC02-05CH11231. Additional support was provided by the California Energy Commission under Agreement EPC-14-010.

References

1. J. A. Reagan and D. M. Acklam, Solar reflectivity of common building materials and its influence on the roof heat gain of typical southwestern USA residences, *Energy & Buildings* **2**, 237-248 (1979).

2. A. H. Rosenfeld, H. Akbari, J. J. Romm, and M. Pomerantz, Cool communities: strategies for heat island mitigation and smog reduction, *Energy & Buildings* **28**, 51-62 (1998).

3. M. Pomerantz, H. Akbari, P. Berdahl, S. J. Konopacki, H. Taha, and A. H. Rosenfeld, Reflective surfaces for cooler buildings and cities, *Philosophical Magazine Part B* **79**, 1457-1476 (1999).

4. H. Akbari, R. Levinson, L. Rainer, Monitoring the energy-use effects of cool roofs on California commercial buildings, *Energy & Buildings* **37**, 1007-1016 (2005).

5. R. Levinson, H. Pan, G. Ban-Weiss, P. Rosado, R. Paolini, and H. Akbari, Potential benefits of solar reflective car shells: cooler cabins, fuel savings and emission reductions, *Applied Energy* **88**, 4343-4357 (2011).

6. R. F. Brady and L. V. Wake, Principles and formulations for organic coatings with tailored infrared properties, *Prog. in Organic Coatings* **20**, 1-25 (1992).

7. R. Levinson, P. Berdahl, H. Akbari, W. Miller, I. Joedicke, J. Reilly, Y. Suzuki, and M. Vondran, Methods of creating solar-reflective nonwhite surfaces and their applications to residential roofing materials, *Solar Energy Materials and Solar Cells* **91**, 304-314 (2007).

8. R. Levinson, P. Berdahl, and H. Akbari, Solar spectral optical properties of pigments, Parts I and II, *Solar Energy Materials and Solar Cells* **89**, 319-349 and 351-389 (2005).

9. T. H. Maiman, R. H. Hoskins, I. J. D'Haenens, C. K. Asawa, and V. Evtuhov, Stimulated optical emission in fluorescent solids. II. Spectroscopy and stimulated emission in ruby, *Phys. Rev.* **123**, 1151–1157 (1961).

10. N. A. Tolstoi, Liu Shun'-fu, and M. E. Lapidus, The luminescence kinetics of chromium luminophors. III. Ruby, O*ptics & Spectroscopy* **13**, #2, 133-136 (1962).

11. A. L. Schawlow, D. L. Wood, and A. M. Clogston, Electronic spectra of exchange-coupled ion pairs in crystals, *Phys. Rev. Lett.* **3**, 271-273 (1959).

12. R. C. Powell, B. DiBartolo, B. Birang and C. S. Naiman, Fluorescence studies of energy transfer between single and pair Cr^{3+} systems in Al_2O_3, Phys. Rev. 155, 299-308 (1967).

13. R. C. Powell and B. DiBartolo, Optical properties of heavily doped ruby, *Phys. Stat. Sol. (a)* **10**, 315-357 (1972).

14. J. D. Barnett, S. Block, and G. J. Piermarini, An optical fluorescence system for quantitative pressure measurement in the diamond-anvil cell, *Rev. Sci. Instruments* **44**, 1-9 (1973).

15. C. Pflitsch, R. A. Siddiqui, and B. Atakan, Phosphorescence properties of sol-gel derived ruby measured as functions of temperature and Cr^{3+} content, *Appl. Phys. A* **90**, 527-532 (2008).

16. J. J. Kingsley and K. C. Patil, A novel combustion process for the synthesis of fine particle α-alumina and related oxide materials, *Materials Letters* **6**, 427-432 (1988).

17. S. Cava, R. Beninca, S. M. Tebcherani, I. A. Souza, C. A. Paskocimas, E. Longo, and J. A. Varela, Structural and spectroscopic characterization of $Al_{2-x}Cr_xO_3$ powders obtained by polymeric precursor method, *J. Sol-Gel Sci. Techn.* **43**, 131-136 (2007).

18. R. Levinson, H. Akbari, P. Berdahl, Measuring solar reflectance – part I: defining a metric that accurately predicts solar heat gain, *Solar Energy* **84**, 1717-1744 (2010).

19. C. Wang and Z Zhao, Transparent polycrystalline ruby ceramic by spark plasma sintering, *Materials Research Bulletin* **45**, 1127-1131 (2010).

20. A. Romani, C. Clementi, C. Miliani, and G. Favaro, Fluorescence spectroscopy: a powerful technique for noninvasive characterization of artwork, *Accounts of Chemical Research* **43**, 837-846 (2010).

21. M. Thoury, J. K. Delaney, E. Rene de la Rie, M. Palmer, K. Morales, and J. Krueger, Near-infrared luminescence of cadmium pigments: in situ identification and mapping in paintings, *Appl. Spectroscopy* **65**, 939-951 (2011).

22. G. Pozza, D. Ajo, G. Chiari, F. De Zuane, and M. Favaro, Photoluminescence of the inorganic pigments, Egyptian Blue, Han blue, and Han purple, *J. of Cultural Heritage* **1**, 393-398 (2000).

23. G. Accorsi, G. Verri, M. Bolognesi, N. Armaroli, C. Clementi, and Aldo Romani, The exceptional near-infrared luminescence properties of cuprorivaite (Egyptian blue), *Chem. Commun.* 3392-3394 (2009).

24. W. M. Yen and M. J Weber, *Inorganic phosphors: compositions, preparation, and optical properties*, CRC Press, Boca Raton, Florida 33487 USA (2004)

25. W. M. Yen, S. Shionoya, and H. Yamamoto, eds., *Fundamentals of phosphors*, CRC Press, Taylor and Francis Group, Boca Raton, Florida 33487 USA (2007).

26. P. S. Friedman and C. R. Parent, Luminescent solar concentrator development, project report SERI/STR-211-3149 for the Solar Energy Research Institute (1087).

27. M. G. Devije and P. P. C. Verbunt, Thirty years of luminescent solar concentrator research: solar energy for the built environment, *Adv. Energy Mater.* **2**, 12-35 (2012).

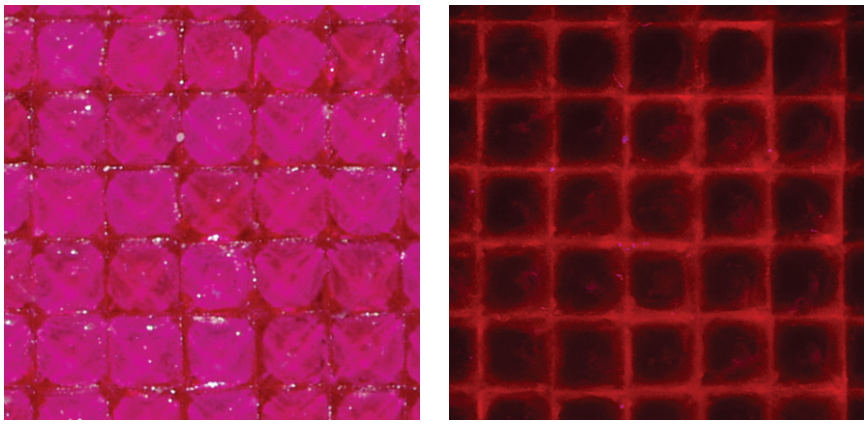

(A) **(B)**

Fig. 1**. Photographs of a portion of the ruby crystal array** (A) **in sunlight** (B) **when illuminated by ultraviolet radiation in the dark.**

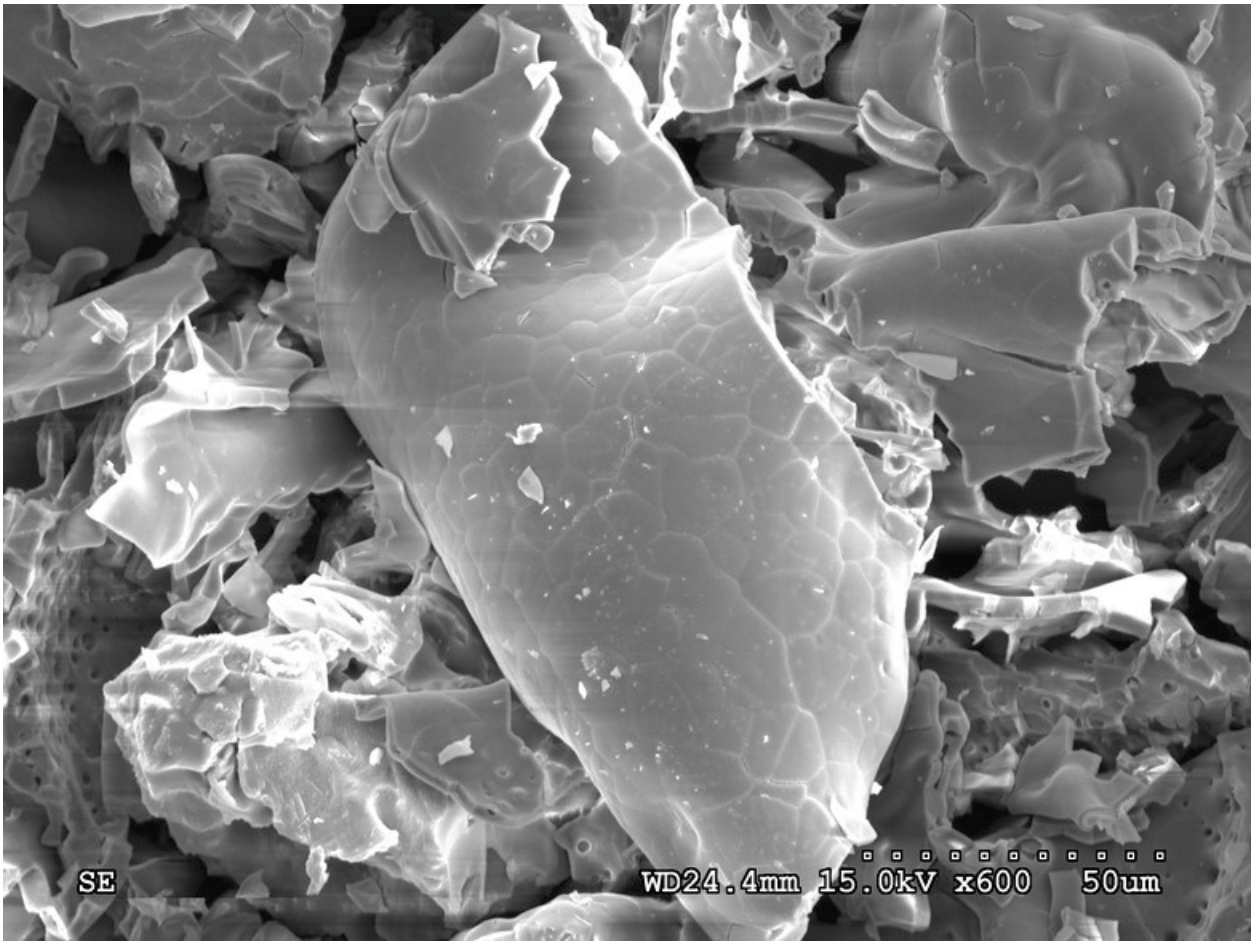

Fig. 2. (A) **Low-resolution scanning electron micrograph of Al_2O_3:Cr combustion product.**

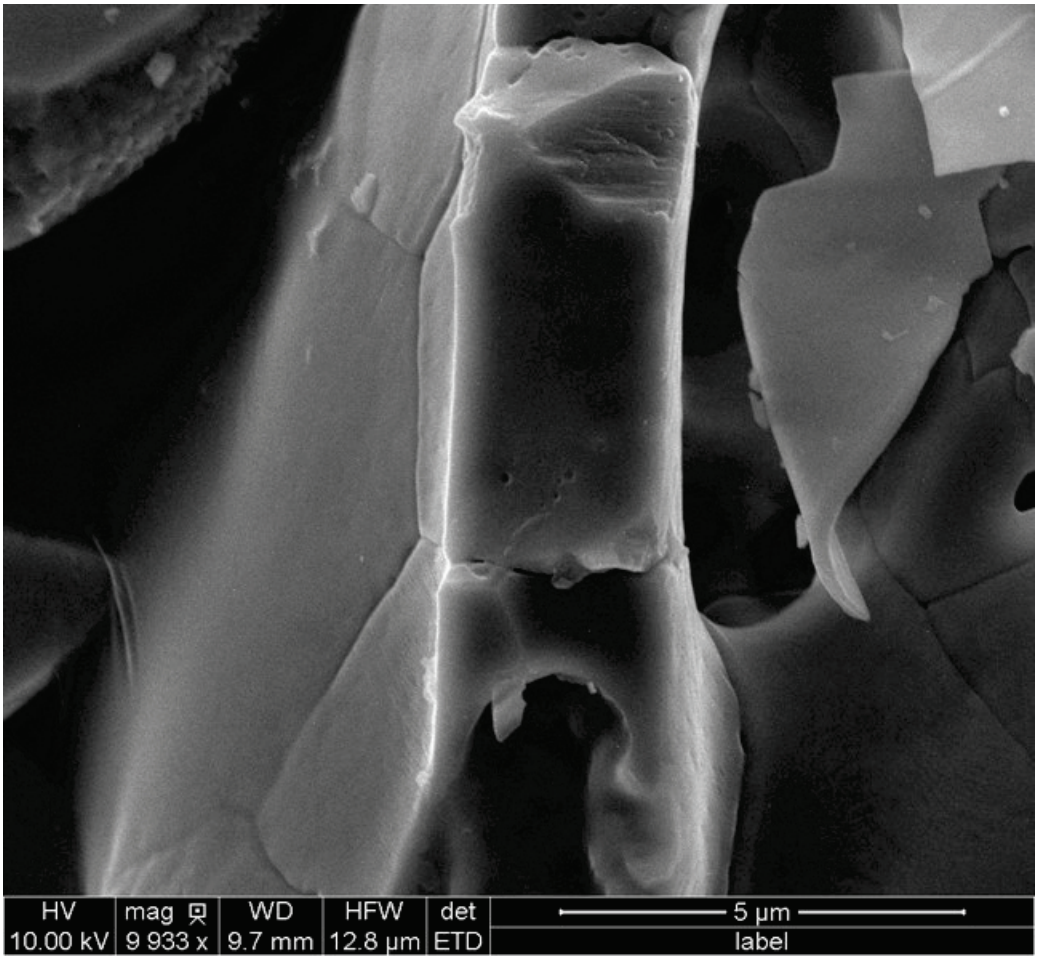

Fig. 2 (B) **Scanning electron micrograph of Al_2O_3:Cr combustion product.**

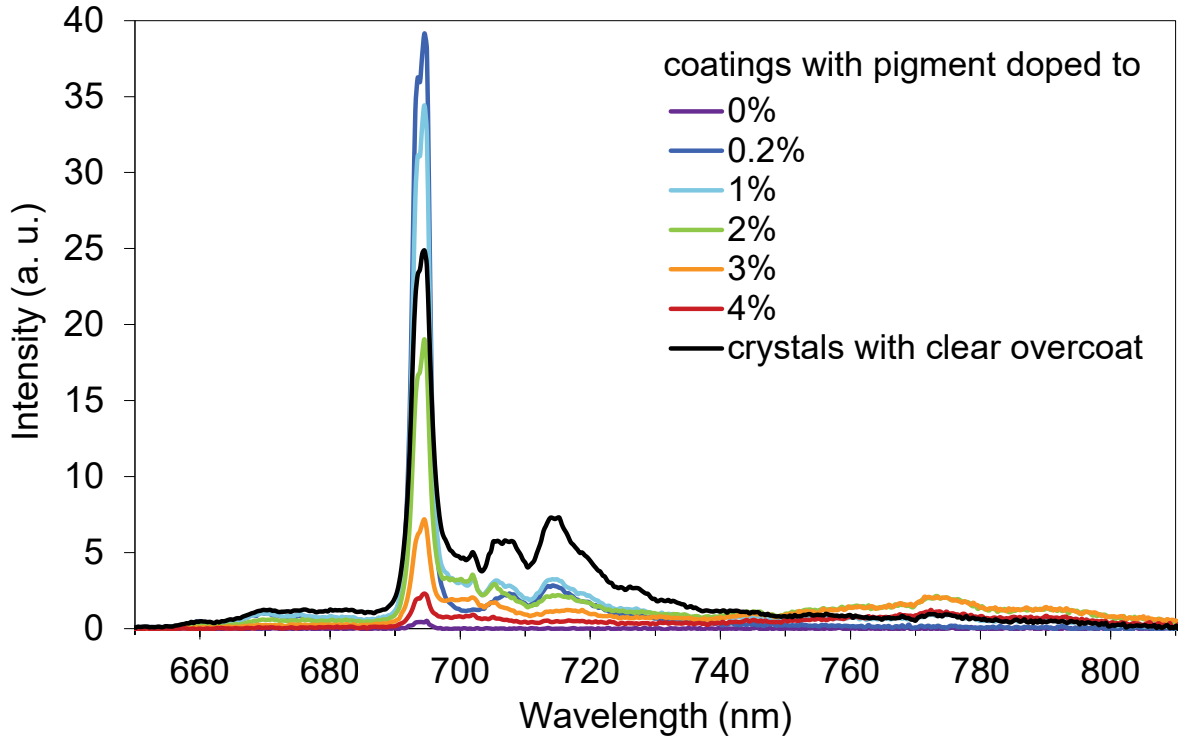

Fig. 3 (A) **Spectral fluorescence of our samples. Percentages are the weight percent of Cr_2O_3 in the pigments.**

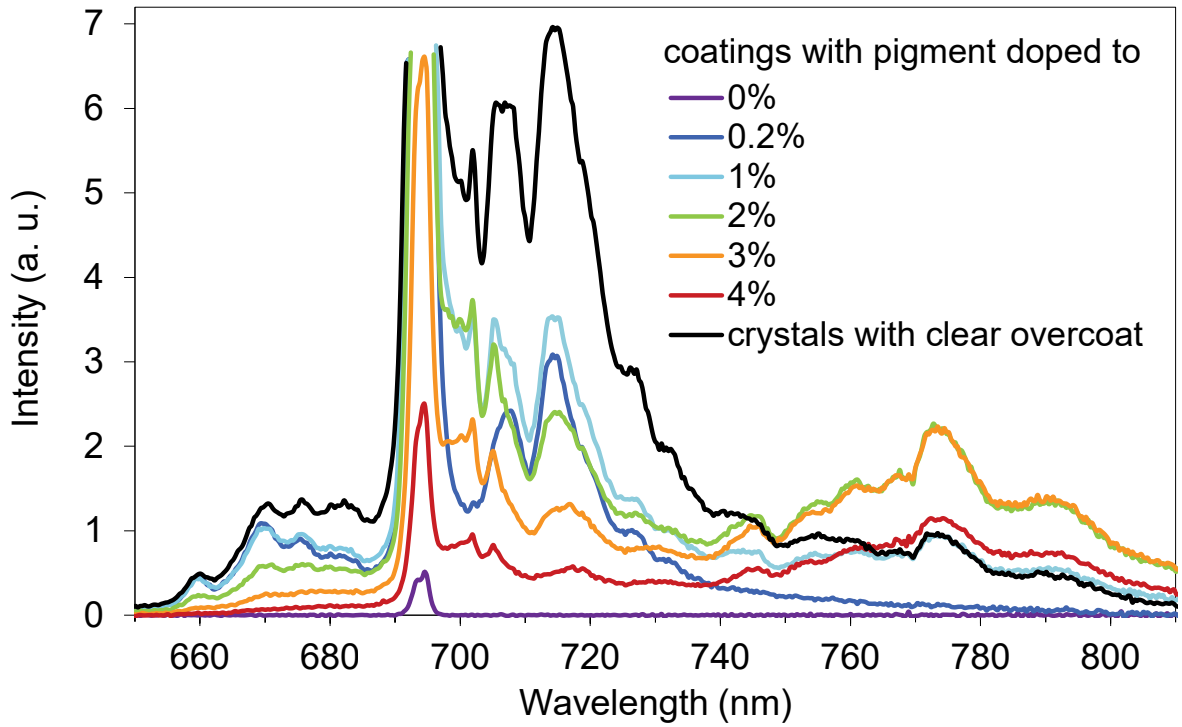

Fig. 3 (B) **Details of fluorescence shown in Fig. 3** (A).

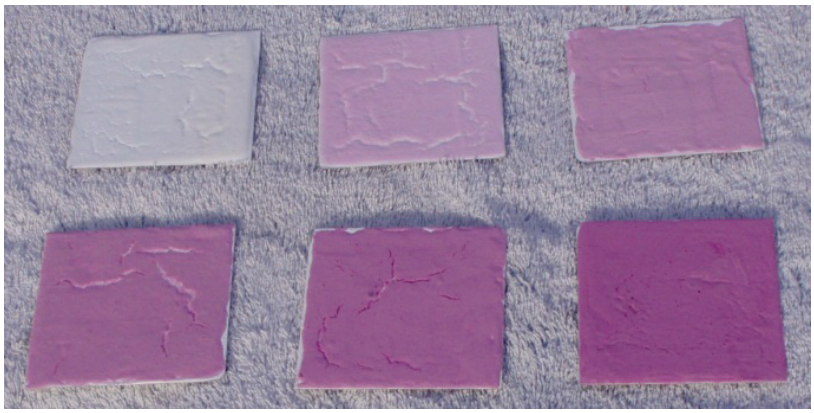

Fig. 4 (A) **Coatings containing ruby powders with 0, 0.2, 1, 2, 3, and 4% doping. The darker coatings contain pigments with more chromium.**

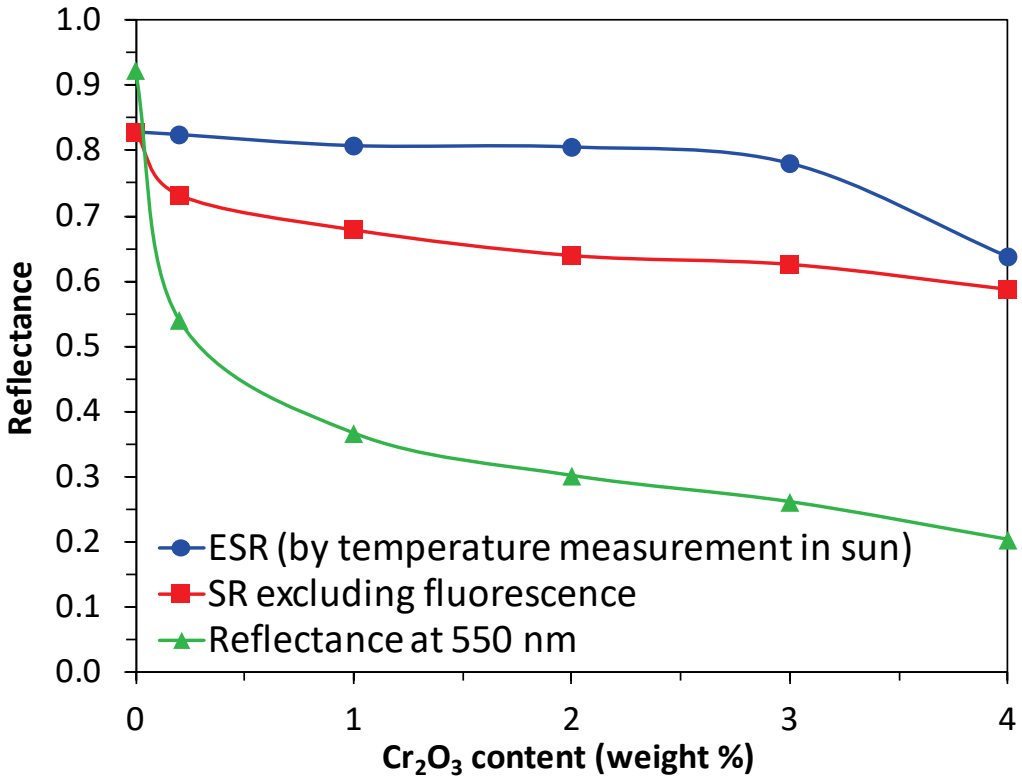

Fig. 4 (B**) Effective Solar Reflectance (ESR), Solar Reflectance (SR) and visual brightness: reflectance at 550 nm.**

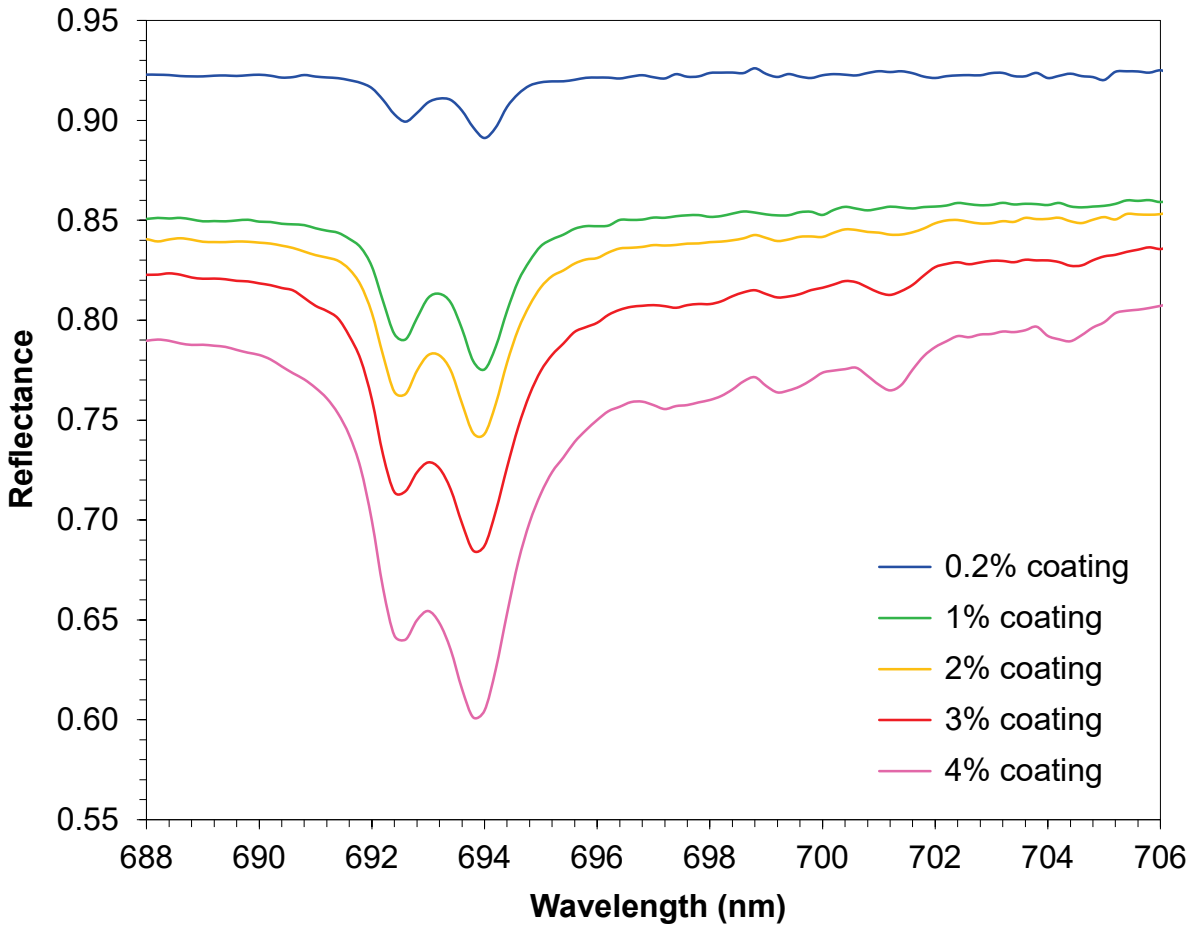

Fig. 5 **High resolution reflectance spectra near the R-lines. In addition to spectral features, broadband absorption is present that increases with doping.**

Task Report Appendix C:
Pre-print of blue pigment article (Berdahl et al. 2018)

High Quantum Yield of the Egyptian Blue Family of Infrared Phosphors ($MCuSi_4O_{10}$, M = Ca, Sr, Ba)

Paul Berdahl[a *], Simon K. Boocock[b], George C-Y Chan[a], Sharon S. Chen[a], Ronnen M. Levinson[a], and Michael A. Zalich[c]

[a] Heat Island Group, Lawrence Berkeley National Laboratory

[b] Shepherd Color Company, Cincinnati, OH 45246

[c] PPG, Coatings Innovation Center, Allison Park, PA 15101

[*] Corresponding author, paul.berdahl@gmail.com

Abstract

The alkaline earth copper tetra-silicates, blue pigments, are interesting infrared phosphors. The Ca, Sr, and Ba variants fluoresce in the near-infrared at 909, 914, and 948 nm, respectively, with spectral widths on the order of 120 nm. The highest quantum yield ϕ reported thus far is ca. 10%. We use temperature measurements in sunlight to determine this parameter. The yield depends on the pigment loading (mass per unit area) ω with values approaching 100% as $\omega \rightarrow 0$ for the Ca and Sr variants. Although maximum quantum yield occurs near $\omega = 0$, maximum fluorescence occurs near $\omega = 70$ g m^{-2}, at which $\phi = 0.7$. The better samples show fluorescence decay times in the range of 130 to 160 μs. The absorbing impurity CuO is often present. Good phosphor performance requires long fluorescence decay times and *very* low levels of parasitic absorption. The strong fluorescence enhances prospects for energy applications such as cooling of sunlit surfaces (to reduce air conditioning requirements) and luminescent solar concentrators.

1 Introduction

Egyptian blue, $CaCuSi_4O_{10}$, and Han blue, $BaCuSi_4O_{10}$, have been utilized as important blue pigments for literally thousands of years.[1] The strontium variant, $SrCuSi_4O_{10}$, is less well known but is a similar blue pigment.[2] Accorsi et al.[3] provided an early description of the fluorescence of Egyptian blue and its application to artworks from ancient Egypt. The fluorescent emission spectra of the Ca and Sr compounds are very similar, whereas the Ba compound emits at slightly longer wavelength and with a broader spectrum. An important recent paper by Borisov

et al.[4] displays excitation and emission spectra for the three compounds. For Egyptian blue, they also reported that the decay time τ is about 159 μs for their solid-state synthesized material. Grinding to reduce the particle size yields shorter decay time of 126 μs, which they attributed to the introduction of defects by mechanical stress during grinding. This behavior is typical for phosphors.[5,6] Borisov et al. also found τ = 139 μs for Kremer Pigmente's Egyptian blue, in agreement with the value to be reported here of 137 (± 4) μs.[4]

Applications of the near-infrared fluorescence of these blue compounds include optical chemosensors.[4,7] In these sensors excitation of two or more phosphors can produce fluorescent signals which when ratioed can be used to determine parameters such as pH. Biological labeling applications can be found in which the larger penetration depth of near-infrared vs. visible light is an advantage.[8] Near-infrared fluorescence also has application in optical electronics such as lasers.[9]

Energy applications of the alkaline earth copper silicate phosphors now look increasingly attractive due to high quantum yield. The application that motivates the current research is energy conservation by reducing the temperature of sunlit objects. Current technology for this purpose relies on high near-infrared reflectance.[10] If an architect specifies blue or another dark color for a roof rather than white, the roof can be cooler in sunlight (saving air conditioning energy) if it efficiently rejects the invisible near-infrared component of sunlight. This paper addresses the additional advantage gained if the roof also fluoresces in the deep red or near-infrared.[11] For luminescent solar concentrator (LSC) applications, a large thin transparent plate absorbs sunlight and then fluoresces near-infrared energy that eventually emerges from the edges of the plate for photovoltaic conversion to electricity.[12,13]

Long radiative lifetimes are desirable as they indicate the relative weakness of competing non-radiative relaxation mechanisms and therefore lead to higher quantum yield (efficiency) of the fluorescence process. However, long lifetimes are not sufficient for high quantum yield because parasitic absorption can lead to mere heating without fluorescence. Parasitic absorption can interfere with the excitation process, and with the emission process. Thus, both corresponding spectral ranges are important. For the specific impurity CuO, important for the present work, parasitic absorption occurs both in the excitation and in the emission spectra. If a parasitic impurity is added to (or not removed from) a fluorescent phosphor, we expect a diminished quantum yield but an unchanged decay time.

Measurements of fluorescence intensity can be used to determine the quantum yield of phosphors. However, the emitted light need not have a simple angular distribution, so an integrating sphere is needed to collect the fluorescence. Also, calibrated spectrometers are needed. Thus, complete quantum yield measurements are not convenient, and are less available in the literature than fluorescence decay lifetimes. The method of De Mello et al.[14] has been employed. Based on this method, the quantum yield of Kremer Egyptian blue is reported as 10.5%.[3] For the Sr and Ba analogs fabricated by hydrothermal synthesis, quantum yields are reported to be 8.5% and 6.9%, respectively.[15]

In this work, we use a novel method for determination of quantum yield, namely temperature measurements in full sunlight.[11] This approach is motivated by the “cool roof” application, in which we want to know how much the sunlit roof (or other facade) is cooled by its fluorescence. Test sample temperatures are compared in full sunlight with calibrated non-fluorescent gray samples, to determine the effective solar reflectance (ESR). The solar reflectance (SR) is determined in the usual way based on spectral solar reflectance (excluding fluorescence) and a standard solar spectrum. The difference ESR – SR represents the fluorescence contribution to the ESR. From this contribution, and by knowing the spectrum of the fluorescence, we can determine the number of photons emitted. The number of incident solar photons absorbed in the excitation spectral range is determined from the spectral reflectance. Finally, the quantum yield is the ratio of fluoresced to absorbed numbers of photons. We find that the pigment loading ω (pigment mass per unit area, in g m^{-2}) affects the quantum yield ϕ with larger concentrations having lower ϕ; this effect is attributed primarily to parasitic absorption. Peak values of the quantum yield thus occur at low values of ω, below 10 g m^{-2}. On the other hand, for a given amount of excitation radiation, peak values of fluorescence occur for ω in the range of 20 to 100 g m^{-2}, with the larger values corresponding to situations in which parasitic absorption is less important.

6 Experimental and theoretical details

6.1 Synthesis

The barium and strontium copper silicate blue pigments were synthesized at Shepherd Color using traditional ceramic techniques. Starting raw materials, in appropriate proportions, were mixed together intimately using intensive dry blending. The dry mixtures were homogenized by screening through fine brass cloth mesh, then administered to ceramic crucibles for firing. For a source of alkali-earth the corresponding carbonate was used, barium or strontium as appropriate. For copper, finely ground copper (II) oxide was chosen, while silica was furnished as finely ground amorphous silica, free of alkali. Lanthanum was introduced as the lanthanum (III) carbonate, and was always accompanied by an equimolar amount of lithium carbonate to maintain charge balance.[16]

All pigments were built to a parent stoichiometry of $M(Cu)Si_4O_{10}$, or $M_y(La)_x(Li)_x(Cu)_ySi_4O_{10}$, where M is either Ba or Sr, and the coefficients x and y sum to unity. The mixed powders were calcined in air at 850 ˚C, with a soak no shorter than five hours. The resulting fired products were coarse ground in a mortar and pestle, then fine ground once on a jet-mill, or wet-ground with fine zirconia beads in DI water to a tractable size.

Elemental composition was determined by x-ray fluorescence, which found levels of all elements (excepting lithium and oxygen) to be consistent with the target compositions.

The crystal phase of each finished pigment was confirmed by x-ray powder diffraction, by reference to patterns for parent phases found in the ICDD (International Centre for Diffraction

Data) PDF-4+ database. The barium copper tetra silicate, with equimolar lanthanum and lithium substitution for copper and barium, reported as Effenbergite, $BaCuSi_4O_{10}$, having powder pattern 04-007-5484. The unsubstituted strontium copper silicate analog to Han blue reported as Wesseltite, pattern 04-009-5401. The median particle sizes of the barium and the strontium compound powders were 1.3 and 49 µm, respectively.

6.2 **Instrumentation**

Fluorescence measurements conducted at Lawrence Berkeley National Laboratory (Berkeley Lab) used a compact Ocean Optics S2000 spectrometer fitted with a 150 mm Labsphere integrating sphere. (We use the term fluorescence as a general synonym for photoluminescence, and avoid the term phosphorescence.) The light source is a tungsten incandescent lamp with xenon gas fill. The incident light is directed through a port on the top of the integrating sphere onto the sample at a port on the bottom of the sphere. A 725 nm short-pass filter with optical density 4 (attenuation better than 10^{-4} in the stop band) blocks excitation light that would otherwise overlap with the fluorescence spectrum. The spectrometer receives light from the integrating sphere by means of an optical fiber and uses a diffraction grating to disperse the spectrum on a silicon array detector. The silicon detector covers a spectral range of about 500 – 1,100 nm.

Pulsed fluorescence measurements used an in-house fabricated pulse generator to drive three red light emitting diodes (620 nm) each with 1 ampere, 10 µs pulses with ~1 ms pulse repetition interval. The fluoresced light was passed through a 695 nm long-pass filter and focused onto a Thorlabs DET 200 fast (ns) photodiode. The photodiode output was processed by an SRS 570 low noise current preamplifier and then acquired by a Tektronix 3054 digital oscilloscope. The $1/e$ response time of the whole detection system is approximately 3.4 µs.

Diffuse spectral reflectance measurements were made with a Perkin-Elmer Lambda 900 UV-VIS-NIR spectrometer fitted with a 150 mm Labsphere integrating sphere. A photomultiplier tube serves as detector from 250 to 860 nm; at longer wavelengths up to 2,500 nm, a PbS photoconductive detector is employed. The standard solar spectral irradiance used to compute solar averages (AM1GH, air-mass 1 global horizontal) represents the radiation received by a horizontal surface with the sun overhead on a clear day, summing to 1,090 W m^{-2}.[17]

6.3 **Sample preparation**

Phosphor powders are useful for screening materials. However, loose powders can introduce variability in repeated experiments depending on how the powder is packed or otherwise arranged. Powders suspended (dispersed) into a coating offer the advantage of durability, and reference samples can be used repeatedly. The phosphors have a tetragonal structure with refractive indices of 1.63 (ordinary ray, electric field perpendicular to the c-axis) and 1.59 (extraordinary ray).[2, 18, 19] Since the acrylic polymer has an index of ~1.5, scattering is reduced relative to a powder in air, and the color is a darker blue. All the pigmented coating samples used in the current work were prepared at Berkeley Lab by hand-dispersing pigments into a

transparent acrylic base (Liquitex gloss medium & varnish) with a spatula, which does not lead to an ideal dispersion. These coatings crack upon drying (and are patched to fill cracks), and do not resemble commercial coatings. Coatings are applied with a spatula over a white substrate which is itself composed of three brushed layers of an acrylic artist's white coating (total dry film thickness about 150 μm) on an aluminum panel. This white substrate has a reflectance of ~ 0.9 from 500 to 1,000 nm, and serves to reflect excitation radiation that passes through the test coating, enhancing absorption by the phosphor. Additionally, the diffuse fluoresced emission is directed outward from the coating by the white substrate.

7 Theoretical considerations

It would be useful to have a complete numerical radiative transfer model for phosphor particles suspended in a medium above a white or black substrate. However, modeling the radiative performance of even non-fluorescent coatings is complex.[20,21] If the incident light is collimated, one needs to keep track of how the diffuse radiation field develops due to scattering. One also needs to know the differential scattering cross section of the particles. The treatment of scattering needs to be approximated unless complete solutions of the Boltzmann-type photon transport equation are to be found. Further, there are interface reflectances that depend on photon incidence angle and polarization; total internal reflection at the top interface is particularly important. Such a code is certainly achievable, but we leave this problem to others. We resort to qualitative and semi-quantitative analysis supported by experimental data.

Consider a thin phosphor-pigmented layer (coating) supported by either a white or black substrate, illuminated with excitation radiation by a beam at normal incidence. Here thin means that the phosphor only absorbs a small fraction of the incident radiation. Also, for simplicity, assume that the black and white layers are perfect, with reflectances of 0 and 1. Scattering by the phosphor is neglected. If the absorption coefficient (with units of inverse length) is α and the layer thickness h, then the fraction of incident radiation absorbed by the black-backed layer is αh. For the white-backed layer additional absorption is caused by the diffusely reflected radiation. As an approximation, the typical path length of the reflected radiation is increased by a factor of two. (The factor of two is exact in the limit $\alpha h \to 0$, but slightly smaller factors will apply in realistic situations.) Thus, the total absorbed fraction of the white-backed layer is roughly $3 \alpha h$. Even this value is an underestimate, due to the large reflectance for diffuse radiation (~0.6) at the underside of the top interface, due total internal reflection.[20] See Figure 19.

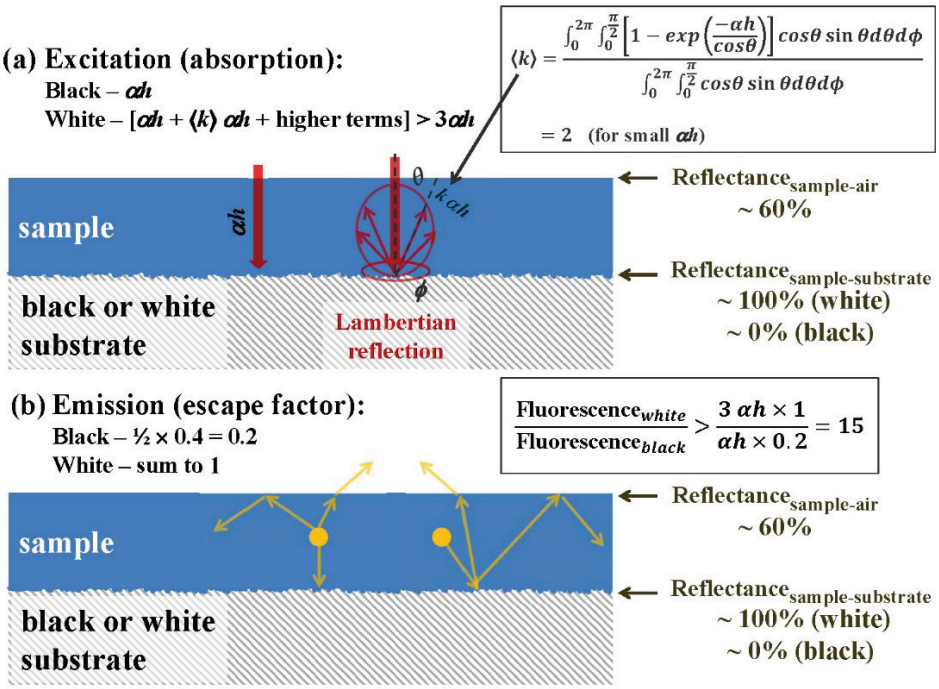

Figure 19. Schematic depiction of radiation transport in thin blue fluorescent coatings over ideal white or black substrates. (a) Absorption of normally incident excitation radiation. (b) Emission of near-infrared fluorescence.

Almost all of the fluoresced radiation emerges from the white-backed layer whereas only about one fifth of the radiation emerges from the black-backed layer. (Of the upward-emitted radiation, only 2/5 is transmitted by the upper interface.) Therefore, we expect the white-backed layer to fluoresce with about 15 times the intensity of the black-backed layer. In one experiment, with a coating containing 12 g m^{-2} of strontium copper silicate ($SrCuSi_4O_{10}$) phosphor on a microscope slide, we found that the fluorescent intensity with a white surface below the slide was like that of a coating applied directly to a white substrate. Replacing the white surface below the slide with black electrical tape adhered underneath the slide yielded a fluorescent intensity that was smaller by a factor of 17. Thus, a reflective underlayer greatly enhances fluorescence.

As already mentioned long fluorescence decay times are desired. From the literature on phosphors generally,[5,6] and from Borisov et al.,[4] we note that larger crystalline particles, free from deleterious impurities, strain, and other defects are desirable. If small particles must be produced by grinding, reducing the decay time, post annealing may be helpful. Long decay times are indicative of the weakness of deleterious non-radiative relaxation processes and are required for high quantum yields. Of course, parasitic absorption can interfere with high

quantum yields, but it is helpful that long decay times can be measured even in the presence of parasitic absorption.

7.1 Determination of quantum yield

In classical measurements of quantum yield one wavelength near the center of the excitation range is used and the emission spectrum is integrated to determine the number of emitted photons. In the case at hand, the total emitted energy is determined from the ESR (effective solar reflectance) calorimetric measurement of temperature in sunlight. The fluorescence contribution to the ESR is then determined by subtracting the conventional spectrometer-measured SR (solar reflectance). (In general, the conventional SR measurement may require filters to exclude fluorescence,[11] but for this paper they are not needed.) The spectrum of emission is determined separately. Since the spectral distribution is known, the emitted photon flux can be determined from the energy flux.

Accounting for the number of excitation photons absorbed is more subtle. The spectral absorptance A of a sample is compared with that of a sample with no pigment, A_o. If the coating layer is optically thin, then the absorptance of the pigment can be approximated by $A - A_o$. If, on the other hand, the layer is optically thick, with A approaching unity, then the absorption of the substrate is nearly zero. With acceptable accuracy for our problem, in which A_o is small, we perform a linear interpolation for A', the pigment absorption, as

$$A' = (A\text{-}A_o)/(1\text{-}\ A_o). \qquad (1)$$

Thus $A' = 0$ when $A = A_o$, and $A' = 1$ when $A = 1$. For the integration over wavelength, we multiply by the spectral photon flux of our standard solar spectrum and, for convenience, take the ends of the excitation spectrum as the points at which the excitation strength falls to 5% of its peak value, based on the spectra shown by Borisov et al.[4]

Also, we wish to determine the fraction of the fluoresced photons which are absorbed by the substrate with $A_o = 0.1$ rather than emitted by the layer. If A_o were zero, this fraction would be 0%. For a downward-directed photon, the absorption probability is approximately A_o. Such a photon may be reflected several times between the white substrate and the top of the coating; the resulting absorption probability is nevertheless A_o. An upward-directed photon is either transmitted by the top interface, with 40% probability, or reflected with 60% probability. On being reflected, it is now downward directed and consequently has probability A_o for absorption. Summing the possible outcomes, we find that the overall probability of absorption is $0.8\ A_o$. Thus, we conclude that 8% of the fluoresced photons are absorbed by the imperfect white substrate.

The state of the art of ESR measurements is still not very well developed; however, work is being conducted to improve the technique.[22] This latest technique uses a rotating sample stage to ensure that identical specimens will attain equal temperatures. The basic measurement

difficulty is temperature fluctuation caused by wind. Convective heat transfer is temporally and spatially irregular due to atmospheric turbulence. Measuring only during periods of low wind speed is helpful but not a panacea. The effective solar absorptance, ESA = 1 – ESR tends to have errors on the order of 5% of ESA. Thus, for example, if ESA = 0.40 (ESR = 0.60), the uncertainty is roughly ± 0.02. Now the fluorescence contribution to ESR may be on the order of 0.10, or even smaller, so that experimental error can be undesirably large. This difficulty is ameliorated by utilizing ESR measurements only in favorable circumstances. Most fluorescence measurements are performed on a relative basis, comparing unknown samples to a “bright” reference sample, which is in turn calibrated by the ESR technique.

8 Optical measurements

8.1 Fluorescence

After a process of screening pigment powders[23] for bright near-infrared fluorescence two promising materials were found to be $SrCuSi_4O_{10}$ and a variant[16] of Han blue ($BaCuSi_4O_{10}$) which is co-doped with La and Li. These pigments were synthesized by the solid-state reaction technique at Shepherd Color and initially screened at PPG. Selected samples were forwarded to Berkeley Lab for additional study.

Figure 20a shows fluorescence curves for five acrylic coatings pigmented with $SrCuSi_4O_{10}$ powder. The dips at 880 and 945 nm are merely artifacts of the spectrometer system. Further, the silicon array detector has diminished sensitivity at longer wavelengths. Thus, the central wavelength in these spectra is a slightly less than 900 nm, whereas calibrated spectrometer measurements[4] find a nearly symmetrical broad peak at 914 nm. Despite the limitations of the spectrometer, one can see that progressing from low to high pigment concentration, the spectrum shifts slightly to longer wavelengths. One likely explanation is that the intrinsic absorption of the strontium copper silicate compound extends from shorter excitation wavelengths to the 880 nm region and thereby encroaches on the left side of the fluorescence spectrum. Additionally, we suggest that this red shift is partly due to small amounts of the black absorbing impurity CuO. CuO is a semiconductor with band edge in the 900 nm region which becomes less absorptive with increasing wavelength in the 900 nm region.[24, 25] Stated another way, CuO selectively attenuates the shorter wavelengths and thereby causes a small red shift.

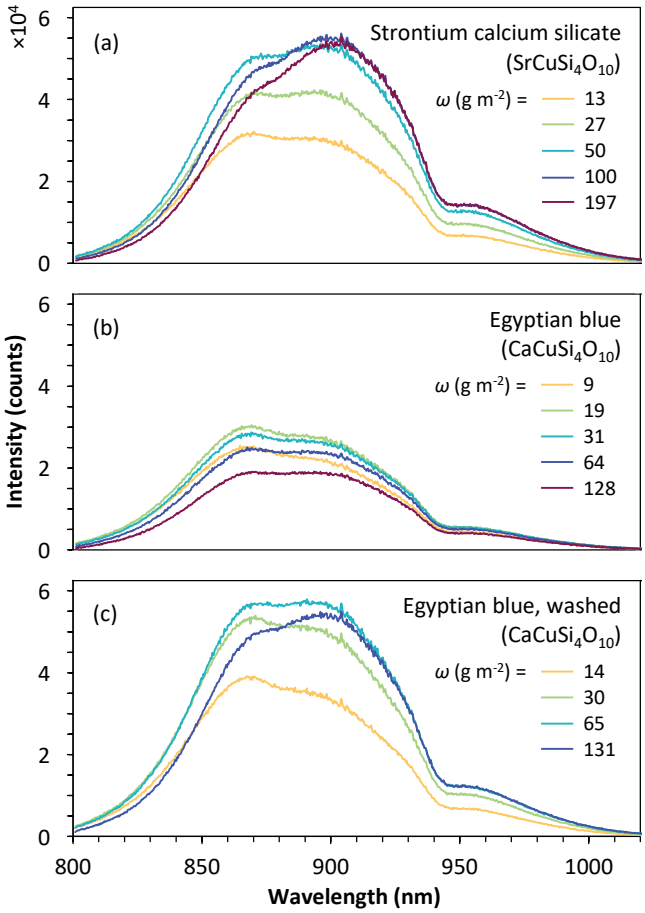

Figure 20. Measured spectral fluorescent intensities of (a) five coatings pigmented with strontium calcium silicate; (b) five coatings with commercial Egyptian blue pigment from Kremer Pigmente; and (c) four coatings with the same commercial Egyptian blue pigment, that has been treated with HCl to reduce the amount of CuO. Each coating was applied to a white substrate.

Figure 20b shows analogous fluorescence data, acquired as in Figure 20a, but for commercially available $CaCuSi_4O_{10}$ (Egyptian blue from Kremer). Clearly, the Egyptian blue pigment is less fluorescent than the Sr compound. However, Figure 20c shows fluorescence data for Egyptian blue pigment that has been soaked in 0.3 M HCl for 12 hours ("washed") to dissolve small amounts of CuO. The fluorescence of the purified Egyptian blue pigment is then quite comparable to that of $SrCuSi_4O_{10}$ (strontium calcium silicate).

Decay time measurements are summarized in Figure 21. The curves are normalized to unity at zero time, then displaced vertically by 10% from one another for clarity. The top three curves are linear on the logarithmic plots, for which the experimental uncertainties are about ± 4 μs. The La and Li doped Han blue ($BaCuSi_4O_{10}$) data deviate from a straight line. One possible explanation is the presence of an additional, shorter time constant. It is tempting to think that it might contain some Han purple ($BaCuSi_2O_6$), as this has a short time constant of 20 μs. However, x-ray diffraction shows only a minor second phase of $BaSiO_3$ which, lacking copper,

seems unlikely to be the source of the short time constant. The Han purple sample is comparably bright with the other materials at ~10 µs, but due to its short time constant the total number of photons is smaller by a factor of about seven. Our lifetime measurements are in good agreement with Fig. 5 of Ref. 4 for $SrCuSi_4O_{10}$ and for Egyptian blue. For Han blue, there are some differences which are understandable since our sample is doped with La and Li, and there is a lack of a simple exponential decay. The time constants of the original and washed Egyptian blue are very similar—equal within experimental uncertainty—even though the HCl washed sample exhibits much stronger fluorescence.

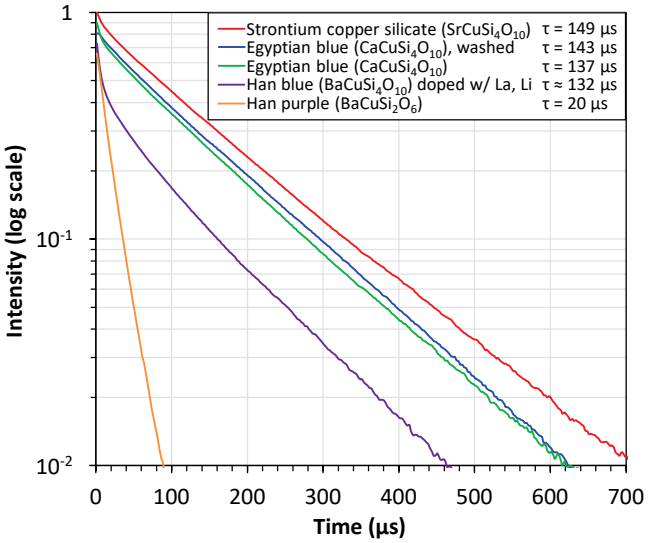

Figure 21. Fluorescence decay curves. For the top three curves, the interval 25 to 300 µs was used to extract the time constant τ. The Han blue (La, Li doped $BaCuSi_4O_{10}$) sample shows evidence of more than one decay; the longer decay was estimated based on the 125 to 400 µs period. For Han purple ($BaCuSi_2O_6$), the 25 to 100 µs interval was used.

Comparisons with the literature indicate that samples synthesized by hydrothermal methods generally have larger surface area and shorter decay time than those made by the solid-state method. For example, Ref. 15 gives 16 and 33 µs for the Sr and Ba compounds whereas Figure 21 lists 149 and 132 µs. Also, for Han (Chinese) purple, Ref. 26 gives 6.4 µs whereas we have obtained 20 µs for a commercial sample from Kremer. For Egyptian blue manufactured by Kremer, we have obtained 137 µs, which as already mentioned, agrees well with Borisov et al.[4] Borisov et al. also found 159 µs for unground samples by solid-state synthesis. Additional values reported for Egyptian blue by solid-state synthesis are 107 µs,[3], 142 µs,[27] and about 160 µs.[28]

The fluorescence measurements presented in Figure 20 are summarized in Figure 22, which shows the area under each peak, relative to the area of the reference sample of $SrCuSi_4O_{10}$ with pigment loading ω = 100 g m^{-2}. This reference sample has an effective solar reflectance (ESR) of

0.544, a spectrometer determined solar reflectance (SR) of 0.410, and therefore a fluorescence contribution of 0.134. Given the 1,090 W m^{-2} energy content of our reference solar spectrum, the fluorescence energy flux in full sun is 146 W m^{-2}. Further, the central photon wavelength is 914 nm, which allows us to estimate the photon flux as 6.73 x 10^{20} m^{-2} s^{-1}. Now we turn to the issue of determining the number of exciting photons that are absorbed.

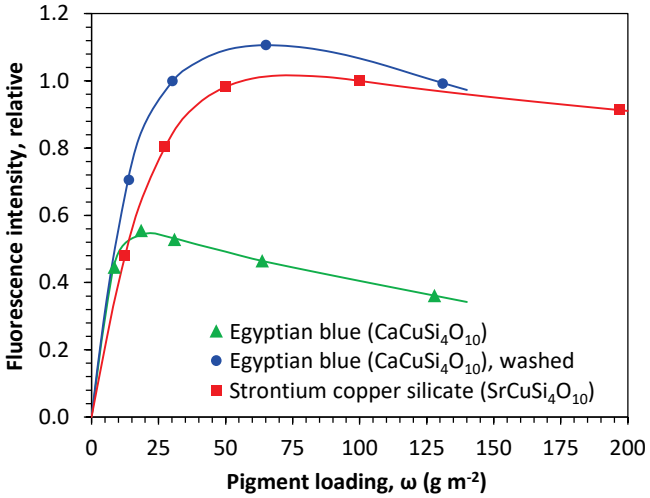

Figure 22. Intensity of fluorescence, integrated over wavelength, as a function of pigment loading, based on the data in Figure 20. The sample at ω = 100 g m^{-2} was used for reference and assigned the value 1.0.

9 Spectral reflectance measurements

Figure 23a shows spectral reflectance data for the five samples presented in Figure 20a. The top curve represents a sample with no pigment, i.e., a transparent acrylic coating over a white substrate. Comparing with the curves below, one can see that $SrCuSi_4O_{10}$ absorbs from about 475 to 880 nm, which is the excitation region. There is only weak absorption between 880 and 1100 nm. Reflectance data for Egyptian blue appears in Figure 5b for the untreated pigment and Figure 5c for the Egyptian blue pigment washed with HCl. The untreated Egyptian blue shows much more absorption in the 880 to 1,100 nm region compared to the same washed pigment and the Sr pigment. It also shows less peak-to-valley variation in the visible region. Both characteristics can be attributed to parasitic absorption by CuO.

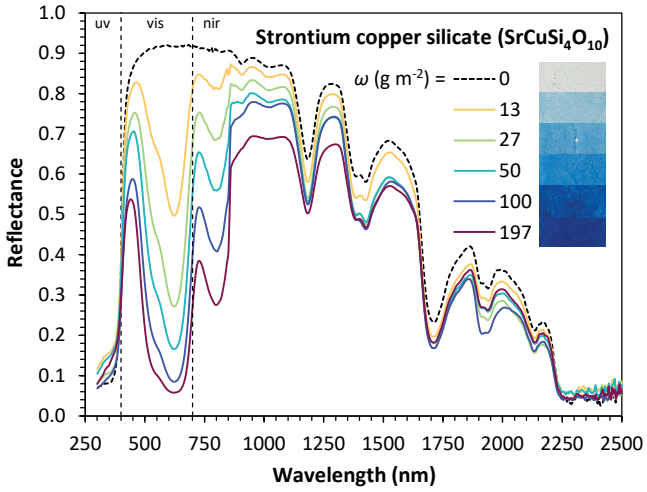

Figure 23a. Measured spectral reflectance of the coatings of Figure 20a and of one transparent coating with no pigment. Inset shows colors.

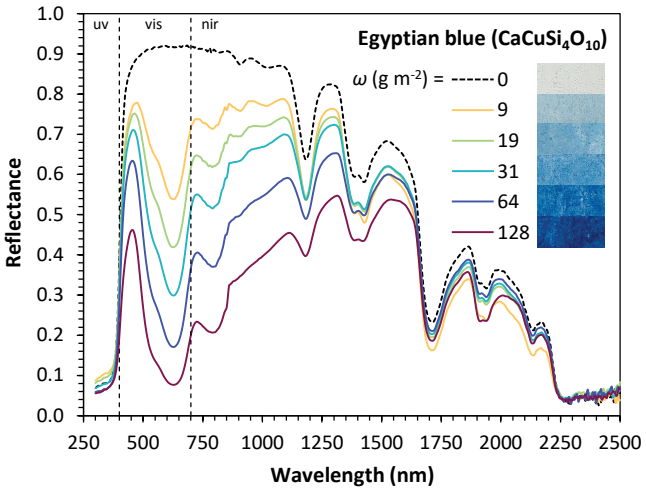

Figure 5b. Spectral reflectance and images of the coatings of Figure 20b (as received Egyptian blue).

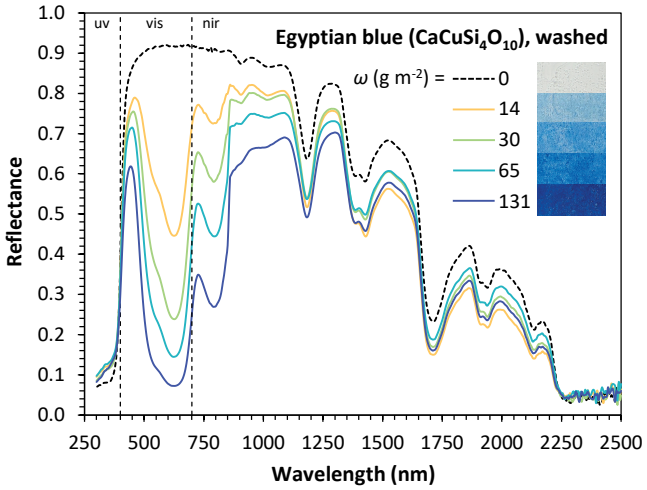

Figure 5c. Spectral reflectance and images of the coatings of Figure 20c (Egyptian blue washed with HCl).

X-ray diffraction data in Figure 24, for the as-received and washed Egyptian blue powders, show small peaks at 35.5˚ due to CuO. The peak is smaller in the washed sample but still present. The optical reflectance data of Figs. 5 b, c are consistent: the parasitic absorption in the 880 to 1,100 nm region is reduced but not eliminated by washing. The visible region reflectance indicates that all samples are blue as shown in the insets, with high blue reflectance (400 to 500 nm) and low reflectance in the 500 to 700 nm region. The peak-to-valley distance of the untreated Egyptian blue is enhanced by the reduction of the CuO impurity.

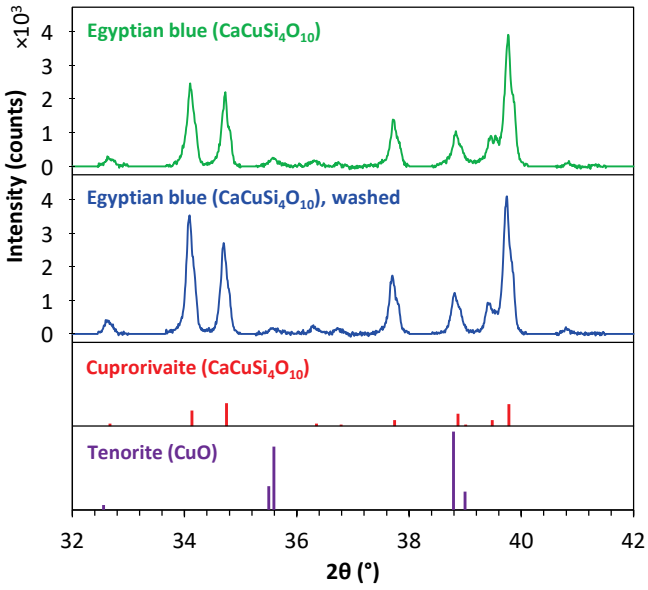

Figure 24. X-ray diffraction data vs. scattering angle 2θ for Egyptian blue, washed with HCl, and as received from Kremer. Both samples have some CuO (tenorite, small peak at 35.5°), and there is less in the washed sample.

The rate of photon absorption by the pigments is computed from the reflectance curves with and without pigments shown in Figure 23. As detailed earlier, the absorptance of the substrate is reduced to account for photons not striking the substrate due to absorptance by the pigment. The excitation region is taken to be 475 to 880 nm; photons outside this range are assumed not to excite the pigment. Figure 25 summarizes the rate of photon absorption.

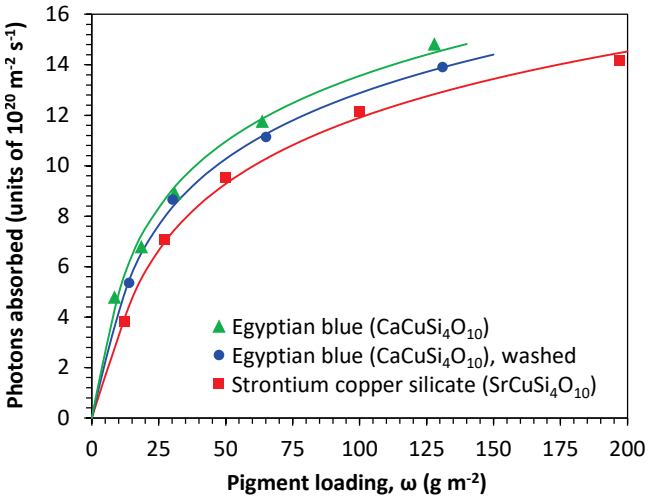

Figure 25. Rate of photon absorption by the pigments between 475 and 880 nm in full sun computed from the spectral reflectance, the spectral reflectance of a sample with no pigment, and a standard solar spectrum.[17]

9.1 Quantum yield

The quantum yield is now readily computed and is displayed in Figure 26. Most notably, the quantum yield ϕ varies with the pigment loading ω (mass per unit area) and, for small ω, approaches unity for the $SrCuSi_4O_{10}$ and $CaCuSi_4O_{10}$ compounds. Due to the limited measurement accuracy of the ESR measurement for the 100 g m^{-2} $SrCuSi_4O_{10}$ calibration sample, the values of ϕ are uncertain by ca. ± 20%. Nevertheless, the trends and overall high values are clear. Figure 22 shows that the fluorescence is maximum near 70 g m^{-2} for the better Sr and Ca compounds. Figure 26 then shows that at that maximum the quantum yield is ca. 0.70 (± 0.15). It seems likely, that if the impurity concentration of CuO can be further reduced, even higher performance may be feasible.

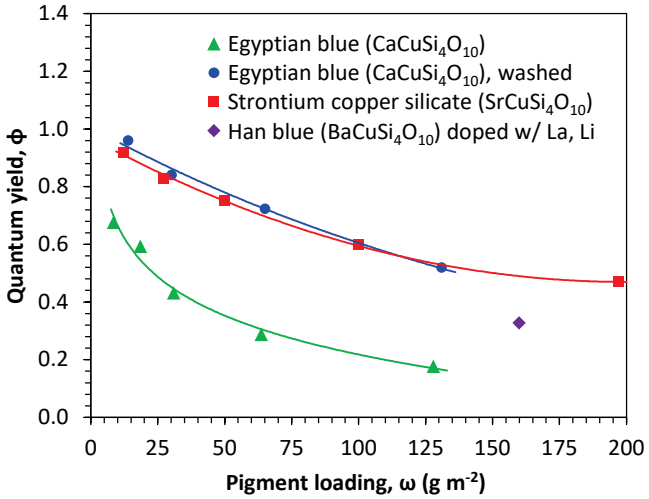

Figure 26. The quantum yield of the pigmented coatings as a function of pigment loading (areal density), based on the data in Figure 22 and Figure 25. The single data point for the Han blue pigment is based on a separate ESR measurement, required by the longer wavelength of fluorescence.

The quantum yield of the Han blue ($BaCuSi_4O_{10}$) compound doped with La and Li is based on a separate ESR measurement, subject to its own 20 % uncertainty, but it seems clear that this specific sample does not perform quite as well as its Sr and Ca counterparts.

In evaluating the quantum yield, we computed the number of excitation photons absorbed by the pigment, as distinct from the substrate. Also, we corrected for the fact that 8% of the fluoresced photons were absorbed by the imperfect white substrate.

10 Two energy applications

10.1 Cool roofing and facades

The efficient blue fluorescent pigments, calcium and strontium copper tetra-silicates, are suitable for fabricating blue-colored surfaces that stay cooler in the sun than non-fluorescent blues. The amount of fluorescent cooling can be more than 150 W m^{-2} in full sun. Attention still must be paid to provide coating formulations that provide high near-infrared reflectance.

For the ruby pigments studied earlier[10] the use of colored co-pigments will reduce fluorescent performance because the excitation range covers the entire visible spectrum (except for the end of the red region in which fluorescence occurs). The currently investigated blue pigments do not absorb blue light. Consequently, a co-pigment can introduce absorption in the short wavelength part of the visible spectrum without impairing fluorescence. For example, a yellow co-pigment can be added to blue provide a green color. Further, an orange pigment can be added to obtain a cool black. Figure 27 shows four images of a coating with $SrCuSi_4O_{10}$ pigment

by itself (blue), mixed with either of two yellow pigments to make green, and coated over orange to make a blue-shade black. Table 1 tabulates the performance of these samples.

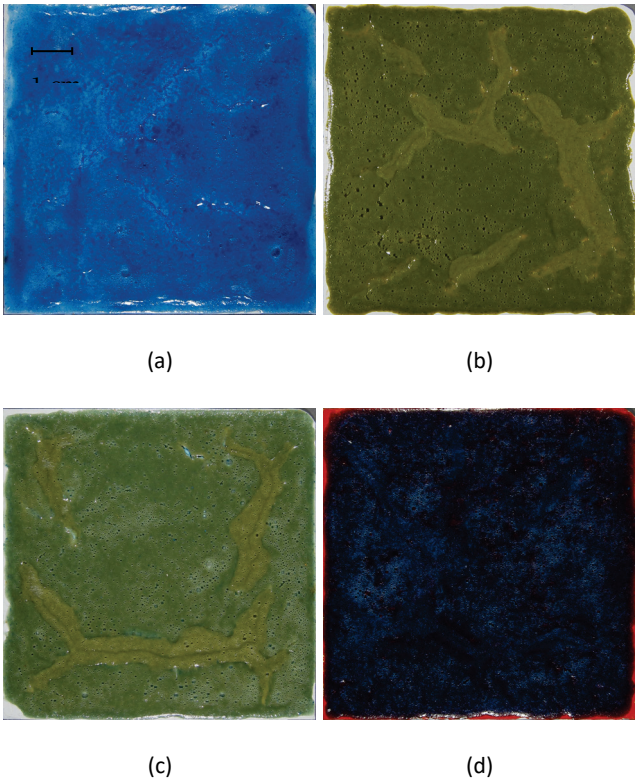

Figure 27. Coating samples with the $SrCuSi_4O_{10}$ pigment with a bright white undercoat. (a) blue pigment alone (b) blue mixed with azo yellow (Diarylide yellow, PY83 HR70) (c) blue mixed with Shepherd yellow 193 (A mixed oxide of Cr, Sb, Ti). Discoloration on green panels is caused by attempts to patch cracks that occurred during drying. (d) Coating sample, a blue-shade black in color, using the pigment over an orange coating, over white. The orange was Liquitex cadmium light red hue (imitation), one brushed coating. The spectrometer reflectance was 0.14 in the blue at 450 nm, 0.08 in the center of the visible (green) at 550 nm and 0.10 in the red at 650 nm. Thus, this sample is nearly black.

Table 5. Optical and thermal performance of the four coatings with $SrCuSi_4O_{10}$ blue pigment shown in Figure 27. The reflectance at 550 nm is included as an indication of visual brightness.

Co-pigment	Fluorescent pigment loading (g m^{-2})	Visual reflectance (550 nm)	Solar reflectance (SR)	Effective solar reflectance (ESR)	Fluorescence contribution (ESR-SR)
none	100	0.17	0.410	0.544	0.134
Shepherd 193 yellow	90	0.23	0.384	0.507	0.123
Azo yellow	130	0.26	0.350	0.475	0.125
Organic orange underlayer	130	0.08	0.330	0.469	0.139

Table 6 shows information on several additional samples that were characterized by ESR measurements. Of special note is the first sample with fluorescence contribution of 0.175, the largest value observed with the alkaline earth copper silicates. It utilized the washed Egyptian blue, with nearly optimum pigment amount, and was very well dispersed. It absorbed and emitted about 17% more photons than the sample with $\omega = 65$ g m^{-2} in Figure 26, with the result that the quantum yield ϕ was the same, at 0.72.

Table 6. Five auxiliary samples for which optical and thermal performance data were obtained.

Pigment(s)	Fluorescent pigment loading (g m^{-2})	Visual reflectance (550 nm)	Solar reflectance (SR)	Effective solar reflectance (ESR)	Fluorescence contribution (ESR-SR)
Washed Egyptian blue (EB)	68	0.15	0.394	0.569	0.175
Washed EB, with organic orange underlayer	60	0.06	0.263	0.388	0.126
Washed EB, mixed with azo yellow	128	0.16	0.196	0.304	0.108
As received EB (not purified)	128	0.14	0.268	0.360	0.092
$Ba(La,Li)CuSi_4O_{10}$	160	0.19	0.363	0.438	0.075

If the yellow or orange co-pigments mentioned above can also fluoresce, an additional cooling effect can be obtained. For example, phosphors are used in some white LEDs to absorb blue light and emit yellow. One such compound is YAG:Ce^{3+} ($Y_3Al_5O_{12}$:Ce^{3+}) which absorbs between

420 and 500 nm and emits between 500 and 650 nm.[29] Another possibility is a dye with similar absorption and emission properties. A dye would also minimize scattering. The use of such supplementary phosphors can further excite the alkaline earth copper silicate phosphor and enhance the NIR emission.

10.2 **Luminescent solar concentrators (LSC)**

LSC devices utilize phosphors to absorb sunlight and emit fluorescence that can be trapped by total internal reflection and delivered to photovoltaic cells positioned at the edges of a large plastic or glass sheet. The total area of expensive photovoltaic cells can thereby be minimized. While these devices have great potential, obstacles have delayed implementation. Part of the diffuse fluorescence is nearly normal to the sheet and therefore not trapped. In some designs, a selective dielectric interference filter helps confine the fluorescence. Absorption of the fluorescence can occur before it reaches the sheet edge. The Stokes shift is a double-edged sword: energy is lost due to the redshift of wavelength, but a large Stokes shift also reduces re-absorption losses. Finally, the quantum yield of the phosphor is important. Current reviews[13, 30, 31, 32] indicate that an important class of prospective phosphors is organic dyes of which Ref. 13 gives 20 examples. Another class of phosphors is “quantum dots” such as nanoparticles of CdSe with shells of CdS that can absorb over an extended short-wave spectrum and emit fluorescence in a narrow long-wave band.[33] Other inorganic phosphors have not received close recent attention for LSC applications. Ruby, $Al_2O_3:Cr^{3+}$, is one possibility.[11, 12, 34] And now, with adequate quantum yield, the $MCuSi_4O_{10}$ (M = Ca, Sr, Ba) infrared phosphors should be investigated as well.

Li et al.[27] advocated the use of Egyptian blue phosphor for LSC applications. They noted that performance declines only slightly at elevated temperatures, and envisage that a polymer with nanoparticles or a specially formulated glass could host the blue particles in a transparent matrix with matching refractive index. However, a maximum quantum yield of 10.5 % is not acceptable for energy applications.[3] For various other applications such as temperature measurements using fluorescence, high efficiency is welcome, but not essential, provided the signal-to-noise ratio is acceptable. Our observation of quantum yields exceeding 70%, using these durable inorganic phosphors, may open a path for further LSC development.

Discussion

In view of the much smaller quantum yield based on the sparse measurements reported in the literature[3,15] for the alkaline earth copper tetra-silicates, and in view of the relative novelty of our procedure for measurements of this yield, we briefly review the technique. Instead of employing a single wavelength for excitation, we use natural sunlight. The spectral absorption of the phosphor is deduced from spectral reflectance measurements, as is the overall solar reflectance (excluding fluorescence). The determination of the fluorescent intensity is based on *temperature measurements in sunlight*, in comparison with calibrated non-fluorescent gray

reference samples. The difference between the effective solar reflectance determined from temperature measurements in sunlight and the ordinary spectrometer-determined solar reflectance gives the fraction of the incident solar flux which is re-radiated by fluorescence. (That fraction varies from 0.075 to 0.175 in Table 2, for example.) Then, the number of fluoresced photons can be computed based on the known fluorescence spectrum. The quantum yield is thus an average over the components in sunlight that are absorbed by the phosphor.

The present technique for determining quantum yield using temperature measurements in sunlight has been employed once before.[11] The fluorescent pigment studied was ruby, the α-phase of Al_2O_3:Cr. For doping levels up to 3 wt % Cr_2O_3, the quantum yield of a coating with ruby powder was found to be 0.83 ± 0.10. Some of the best work on this well-known material was done around the time of the demonstration of the first laser, see Maiman et al. (1961).[35] They studied a single crystal with light doping (0.05 wt % Cr_2O_3) and found that the quantum efficiency varied with excitation wavelength in the range of 0.57 – 0.79. They concluded that the average value was 0.70 ± 0.05. Details preclude a precise comparison with Maiman et al. – single crystal vs. powder in a coating, anisotropy of ruby, dependence of emission spectrum with doping[11], etc. – but their results provide evidence that measurements in sunlight can provide quantum yield values not greatly different from more traditional measurements.

A straightforward alternative approach to the determination of quantum yield could rely entirely on laboratory measurements using a lamp with monochromator for excitation. After such measurements, the question would remain: what is the performance in the sun? The present approach merely answers this last question first, and then works backward to deduce what the quantum yield must be.

11 Concluding remarks

Future applications of infrared fluorescence are enhanced by the high quantum yields of the alkaline earth copper tetra-silicates. It remains to be seen if the barium compound can match the very high performance of the calcium and strontium compounds.

Non-white coatings with high ESR (effective solar reflectance) are useful for energy conservation applications (e.g., to reduce air conditioning needs). Pigments used should have decay times >140 μs and contain as little CuO as possible. Coating systems should have a highly reflective backplane, optionally include near-infrared reflective pigments, and include a well-dispersed layer of $MCuSi_4O_{10}$ (M = Ca, Sr, or Ba) near-infrared phosphor.

In addition to medium and dark blue colors, green and even black materials can be achieved by adding co-pigments. A blue-shade black with ESR exceeding 0.5 appears likely in the near term.

12 Acknowledgements

At Berkeley Lab, T. Kirchstetter and X. L. Mao provided advice and equipment. At PPG, initiation of the work was catalyzed by S. Hellring, J. Kulfan, C. Balliet, and I. Schwendeman, and ongoing support was provided by B. Kornish, J. Stalker, and M. Baxter. At Shepherd Color, W. Yuhasz and S. Davis synthesized samples of barium- and strontium-bearing alkali-earth copper silicate blues and other IR-fluorescing pigments used for evaluation.

This work was supported by the Assistant Secretary for Energy Efficiency and Renewable Energy, Building Technologies Office of the U. S. Department of Energy under Contract nos. DE-AC02- 05CH11231 and DE-EE0006347. Support was also provided by the California Energy Commission under Agreement EPC-14-010.

References

(1) Berke, H., The invention of blue and purple pigments in ancient times, *Chem. Soc. Rev.,* **2007**, 36, 15-30.

(2) Giester, G. and Rieck, B., Wesselsite, $SrCu[Si_4O_{10}]$, a further new gillespite-group mineral from the Kalahari Manganese Field, South Africa, *Mineral. Mag.*, **1996**, 60, 795-798.

(3) Accorsi, G.; Verri, G.; Bolognesi, M.; Armaroli, N.; Clementi, C.; Miliani, C.; Romani, A., The exceptional near-infrared luminescence properties of cuprorivaite (Egyptian blue), *Chem. Commun.*, **2009**, 3392-3394

(4) Borisov, S. M.; Wurth, C.; Resch-Genger, U.; Klimant, I., New life of ancient pigments: applications in high-performance optical sensing materials, *Anal. Chem.* **2013**, 85, 9371-9377.

(5) Yen, W. M.; Weber, M. J., eds*., Inorganic phosphors: composition, preparation, and optical properties*, CRC Press **2004**, p. 334, prepared by L. S. Rohrer.

(6) Tilley, R. J. D., *Colour and the optical properties of materials*, John Wiley & Son **2011**, p. 378.

(7) McDonagh, C.; Burke, C. S.; MaxCraith, B. D.; Optical Chemical Sensors, *Chem Rev*. **2013**, 108, 400-422.

(8) Werts, M. H. V.; Woudenberg, R. H.; Emmerink, P. G.; van Gassel, R.; Hofstraat, J. W.; Verhoeven, J. W.; A near-infrared luminescent label based on Yb^{III} ions and its application in a fluoroimmunoassay, *Angew. Chem. Int. Ed.* **2000**, 39, No. 24, 4542-4544.

(9) Kuck, S., Laser-related spectroscopy of ion-doped crystals for tunable solid-state lasers, *Appl. Phys. B*, **2001**, 72, 515-562.

(10) Levinson, R.; Berdahl, P.; Akbari, H; Miller, W.; Joedicke, I.;Reily, J.; Suzuki, Y.;, Vondran, M., Methods of creating solar-reflective nonwhite surfaces and their application to residential roofing materials, *Sol. En. Mat. & Sol. Cells*, **2007**, 91, 304-314.

(11) Berdahl, P.; Chen, S. S.; Destaillats, H.; Kirchstetter, T. W.; Levinson, R. M.; Zalich, M. A.; Fluorescent cooling of objects exposed to sunlight – the ruby example, *Sol. En. Mat. & Sol. Cells*, **2016**, 157, 312-317.

(12) Friedman, P. S.; Parent, C. R., Luminescent solar concentrator development, Project Report SERI/STR-211-3149 for the Solar Energy Research Institute, **1987**.

(13) Devije, M. G.; Verbunt, P. P. C., Thirty years of luminescent solar concentrator research: solar energy for the built environment, *Adv. Energy Mater.,* **2012**, 2, 12-35.

(14) de Mello, J. C.; Wittmann, H. F.; Friend, R. H., An improved experimental determination of external photoluminescence quantum efficiency, *Adv. Mater.*, **1997**, 9 No.3, 230-232.

(15) Chen, Y; Shang, M.; Wu, X.; Feng, S., Hydrothermal synthesis, hierarchical structures and properties of blue pigments $SrCuSi_4O_{10}$ and $BaCuSi_4O_{10}$, *CrystEngComm*, **2014**, 16, 5418-5423.

(16) Jose, S.; Reddy, L., Lanthanum-strontium copper silicates as intense blue inorganic pigments with high near-infrared reflectance, *Dyes and Pigments* **2013**, 98, 540-546.

(17) Levinson, R; Akbari, H.; Berdahl, P., Measuring solar reflectance – part I: defining a metric that accurately predicts solar heat gain, *Solar Energy,* **2010**, 84, 1717-1744.

(18) Mazzi, F.; Pabst, Reexamination of cuprorivaite, *Amer. Mineral.* **1962**, 47, 409-411.

(19) Giester, G.; Rieck, B., Effenbergerite, BaCu[Si4O10], a new mineral from the Kalahari Manganese Field, South Africa: description and crystal structure, *Mineralogical Magazine,* **1994**, 58, 663-670.

(20) Levinson, R.; Berdahl, P.; Akbari, H., Solar spectral optical properties of pigments – Part I: model for deriving scattering and absorption coefficients from transmittance and reflectance measurements, *Solar Energy Materials & Solar Cells,* **2005**, 89, 319-349.

(21) Levinson, R.; Berdahl, P.; Akbari, H., Solar spectral optical properties of pigments – Part II: survey of common colorants, *Solar Energy Materials & Solar Cells*, **2005**, 89, 351-389.

(22) Levinson, R.; Chen, S.; Ferrari, C.; Berdahl, P.; Slack, J., Methods and instrumentation to measure the effective solar reflectance of fluorescent cool surfaces, *Energy & Buildings*, **2017**, 752-765. https://doi.org/10.1016/j.enbuild.2016.11.007

(23) M. Zalich, B. Kornish, Fluorescent pigments for high-performance cool roofing and facades, **2016**, Project report, contract no. DE-EE0006347, http://osti.gov.

(24) E.D. Palik, ed., *Handbook of Optical Constants of Solids*, **1998**, Academic Press.

(25) Cheng, Q.; Chai, J.; Zhang, Z., Investigation of double-layer coating with CuO particles of different concentrations on aesthetic and thermal aspects, *Int. J. Thermal Sciences,* **2016**, 105, 36-44.

(26) Chen, Y.; Zhang, Y.; Feng, S., Hydrothermal synthesis and properties of pigments Chinese purple $BaCuSi_2O_6$ and dark blue $BaCu_2Si_2O_7$, *Dyes and Pigments*, **2014**, 105, 167-173.

(27) Li, Y. J.; Ye, S.; Wang, C. H.; Wang X. M.; Zhang, Q. Y., Temperature-dependent near-infrared emission of highly concentrated Cu^{2+} in $CaCuSi_4O_{10}$ phosphor, *J. Mater. Chem. C*, **2014**, 2, 10395-10402.

(28) Zhuang, Y.; Tanabe, S., Forward and back energy transfer between Cu^{2+} and Yb^{3+} in $Ca_{1-x}CuSi_4O_{10}$:Yb_x crystals, *J. Appl. Phys.,* **2012**, 112, 093521.

(29) Kim, Y.; Shim, K. B.; Wu, M.; Jung, H. K., Monodispersed spherical YAG:Ce^{3+} phosphor particles by one-pot synthesis, *J. of Alloys and Compounds,* **2017**, 693, 40-47.

(30) van Sark, W. G. H. M., Luminescent solar concentrators – A low cost alternative, *Renewable Energy*, **2013**, 49, 207-210.

(31) Assadi, M. K.; Hanaei, H.; Mohamed, N. M.; Saidur, S. B.; Bashiri, R.; Moayedfar, M., Enhancing the efficiency of luminescent solar concentrators (LSCs), *Appl. Phys. A*, **2016**, 122, 821, 1-12.

(32) Tummeltshammer, C.; Taylor, A.; Kenyon, A. J.; Papakonstantinou, I., Losses in luminescent solar concentrators unveiled, *Solar Energy Materials & Solar Cells*, **2016**, 144, 40-47.

(33) Bronstein, N. D.; Yao, Y.; Xu, L.; O'Brien, E.; Powers, A. S.; Ferry, V. E.; Alivisatos, A. P.; Nuzzo, R. G., Quantum dot luminescent concentrator cavity exhibiting 30-fold concentration, *ACS Photonics*, **2015**, 2, 1576-1583.

(34) Hovel, H. J.; Hodgson, R. T.; Woodall, J. M., The effect of fluorescent wavelength shifting on solar cell spectral response, *Solar Energy Materials*, **1979**, 2, 19-29.

(35) Maiman, T. H.; Hoskins, R. H.; D'Haenens, I. J.; Asawa, C. K.; Evtuhov, V., Stimulated optical emission in fluorescent solids. II. Spectroscopy and stimulated emission in ruby, *Phys. Rev.*, **1961**, 123, 1151-1157.

Energy Research and Development Division

FINAL PROJECT REPORT

Solar-Reflective "Cool" Walls: Benefits, Technologies, and Implementation

Appendix O: Development of Retroreflective Materials (Task 5.3 Report)

California Energy Commission
Gavin Newsom, Governor

April 2019 | CEC-500-2019-040-APO

Appendix O: Development of retroreflective materials (Task 5.3 report)

Ronnen Levinson[1], Sharon Chen[1], Jonathan Slack[1], Howdy Goudey[1], and Paul Berdahl[1]

[1] Heat Island Group, Lawrence Berkeley National Laboratory

29 June 2018

Abstract

Raising a city's albedo increases the fraction of incident sunlight returned to outer space, cooling cities and their buildings. Retroreflective cool walls could improve upon diffusely reflecting cool walls by reflecting incoming beam radiation to the solar disc (if the retroreflection is three dimensional and ideal) or at least upwards (if the retroreflection is two dimensional and/or imperfect). The greatest challenge in retroreflective wall design appears to be the need to operate at large incidence angles to reflect a substantial portion of incident sunlight. First-principle physics, ray tracing simulations, and solar spectral bi-directional reflectance intensity measurements suggest that it will be difficult to achieve this with surfaces that rely on total internal reflection.

Attempts to produce a two-surface retroreflector with orthogonal mirror grooves by cutting and polishing an aluminum block indicate that residual surface roughness impedes retroreflection. Ongoing efforts focus on shaping aluminized Mylar film, a material with very high specular reflectance across the solar spectrum.

1 Introduction

Raising a city's albedo increases the fraction of incident sunlight returned to outer space, cooling cities and their buildings. "Cool" horizontal surfaces with high solar reflectance, such as white roofs and light-colored pavements, are ideal solutions for a low-density city with short buildings, in which most of the sunlight is intercepted by roofs and pavements. However, in a densely populated urban area with many tall buildings, more sunlight falls on walls than on roofs or pavements. A large fraction of light that is diffusely reflected from a vertical surface can strike neighboring buildings, pavements, or pedestrians.

Figure 1 illustrates three idealized reflections: specular (perfectly mirrorlike), Lambertian (perfectly diffuse), and retro (back to source). We can increase the effective albedo of urban areas, and prevent heating of neighboring buildings, by making building walls retroreflective. A retroreflector, such as a cube-corner (Figure 2a), orthogonal groove (Figure 2b), or cat's eye (Figure 3) can return light toward its source. Retroreflective cool walls could improve upon diffusely reflecting cool walls by reflecting incoming beam radiation to the solar disc (if the retroreflection is three dimensional and ideal) or at least upwards (if the retroreflection is two dimensional and/or imperfect). This can increase the fraction of sunlight reflected out of the urban canyon formed by the walls of neighboring buildings and the ground between them.

Today, corner-cube and cat's eye retroreflectors are widely used for traffic safety, remote sensing, and optical communication. Here we consider the application of retroreflectors to exterior walls.

For example, consider an isolated building with 0.60 wall albedo and 0.20 ground albedo, each surface a Lambertian reflector. About 36% of the sunlight incident on the wall would return to the sky [0.60 wall albedo × (0.5 sky view factor + 0.5 ground view factor × 0.20 ground albedo)] (Figure 4a). If the wall were instead covered with a retroreflector of equal albedo—say, orthogonal mirror pairs, each surface of albedo 0.775, with a two-bounce albedo of 0.775^2 = 0.60 (Figure 2b)—it would reflect upward 60% of incident beam sunlight, and about 30% of the incident diffuse sunlight (of the 60% of diffuse light that is reflected, half will go up, and half will go down). If 20% of the incident sunlight is diffuse, the final fraction returned to the sky would be 80% × 0.60 wall solar retroreflectance + 20% × [0.60 wall solar diffuse reflectance × (0.5 sky view factor + 0.5 ground view factor × 0.20 ground albedo)] = 55% (Figure 4b).

A Lambertian wall would have to reflect 92% of incident sunlight to return 55% of incident sunlight to the sky [0.92 wall albedo × (0.5 sky view factor + 0.5 ground view factor × 0.20 ground albedo)] (Figure 4c).

Introducing a neighboring building reduces wall and ground sky view factors, but does not impede retroreflection. Hence the boost in skyward reflection offered by substituting a retroreflective wall for a Lambertian wall will be even greater for a wall within the urban canyon.

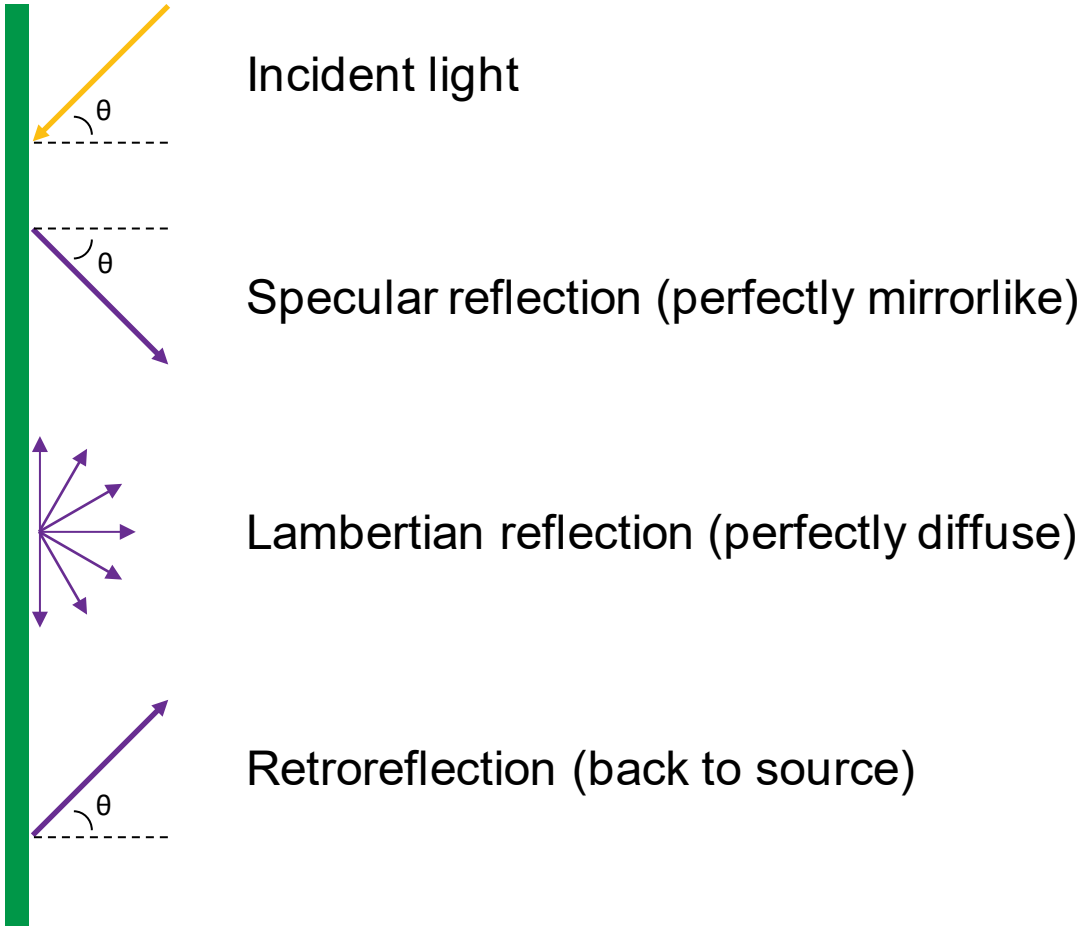

Figure 1. Specular, Lambertian, and retro reflection of beam light striking a vertical surface.

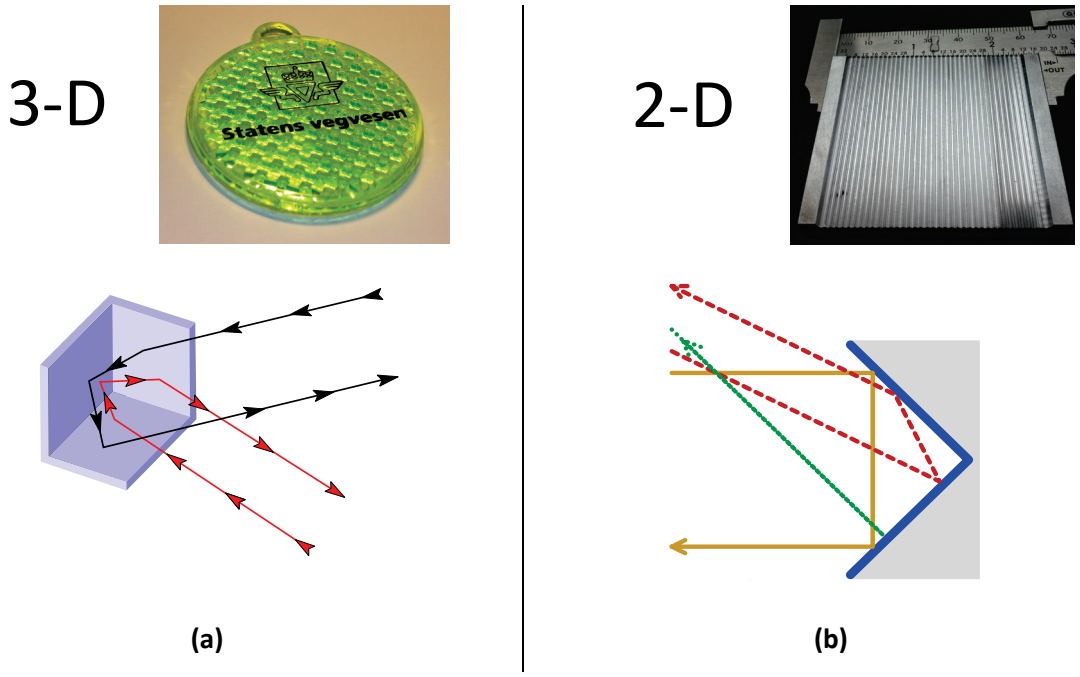

Figure 2. A retroreflector uses up to three orthogonal mirrors to return light to its source. Panel (a) shows a bicycle reflector comprised of three-mirror "cube corners" that will perfectly retroreflect any beam, while panel (b) shows a groove aluminum block comprised of two-mirror orthogonal groove that, if oriented with the block vertical and the grooves horizontal, will retroreflect about the horizontal plane and specularly reflect about the vertical plane.

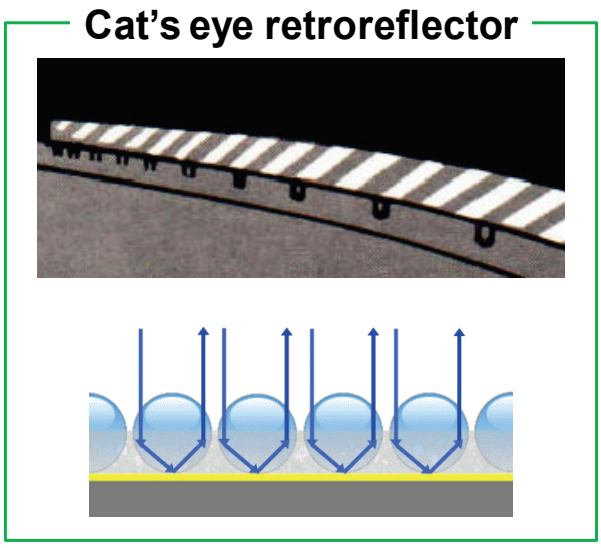

Figure 3. A cat's eye retroreflector, such as this safety paint, uses spheres of high real refractive index in a lower-index binder to provide three reflections that return light to its source.

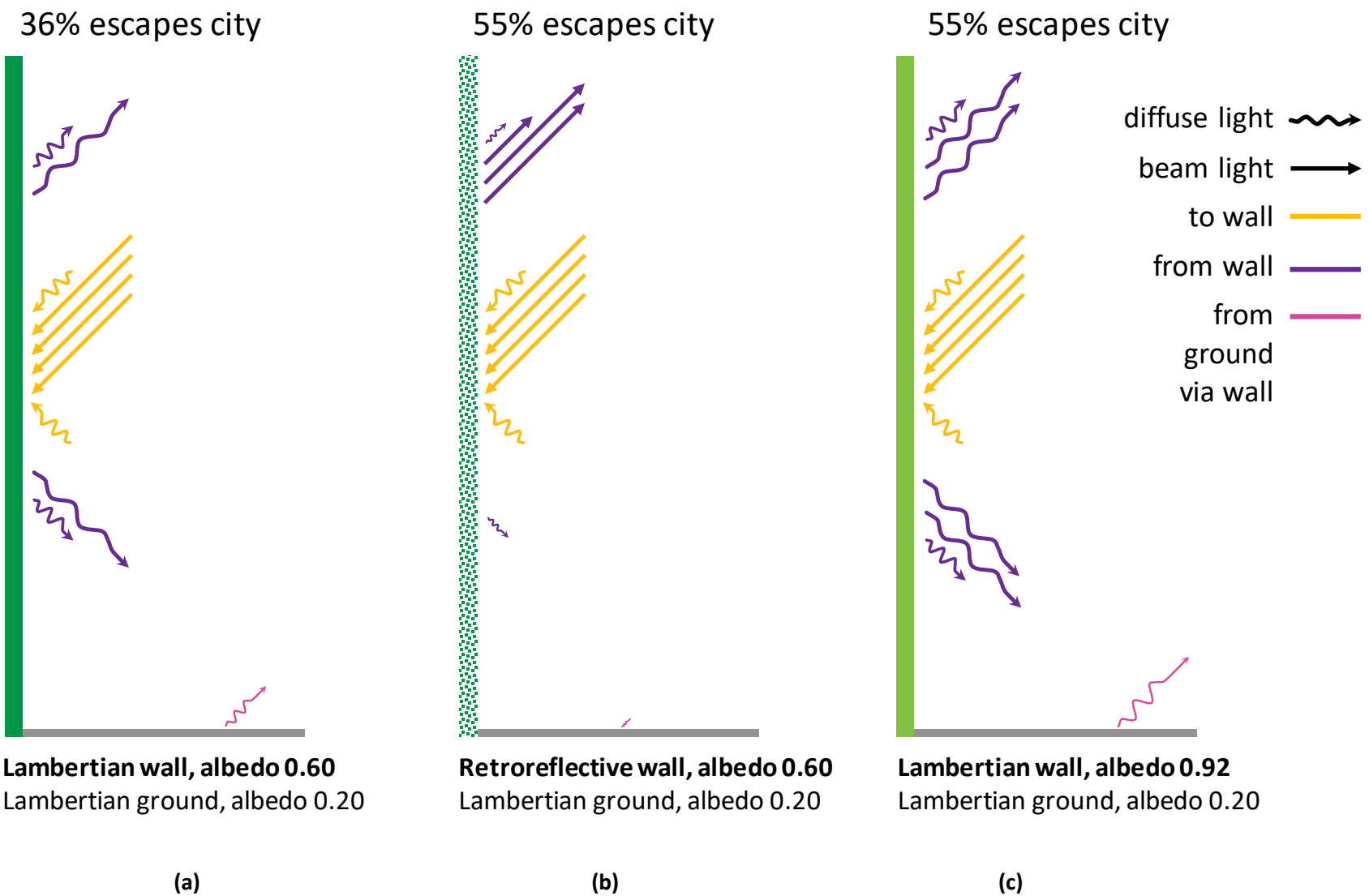

Figure 4. Retroreflective cool surfaces can help sunlight that strikes walls escape the city.

2 Design considerations

A safety retroreflector makes a sign easier to read in low light (e.g., at night, or in a tunnel) by reflecting vehicle headlamp illumination to the driver. If the sign is far away, making the path from sign to driver nearly parallel to that from headlamp to sign, modest retroreflection of headlamp light arriving at near-normal incidence will suffice. Only visible light (0.4 – 0.7 μm) need be reflected (ASTM 2017).

To reduce the solar heat gain of the building and its surroundings, a *wall* retroreflector must reflect a large fraction of incident sunlight. Sunlight will strike the wall over a wide range of incidence angles, and about half the radiative energy in sunlight arrives in the invisible near-infrared spectrum (0.7 – 2.5 μm) (Levinson et al. 2010). Thus, the design requirements for a wall retroreflector differ significantly from those for a safety retroreflector (Figure 5).

2.1 Solar spectral reflectance of mirrorlike surfaces

In principle, a transparent surface exhibiting total internal reflection (TIR) or a metal mirror can provide strong specular reflection over most or all of the solar spectrum (0.3 – 2.5 μm). Examples:

- Crown glass (e.g., Schott N-BK7) has a narrow range of real refractive index (n=1.48 – 1.56) over the entire solar spectrum. Its internal transmittance is greater than 0.99 from 0.4 to 1.5 μm, greater than 0.93 from 1.5 to 2.0 μm, and 0.66 to 0.93 at wavelengths longer than 2.0 μm (Polyanskiy 2018).

- An optical-grade mirror can specularly reflect nearly 90% of incident sunlight (curve C in Figure 6).

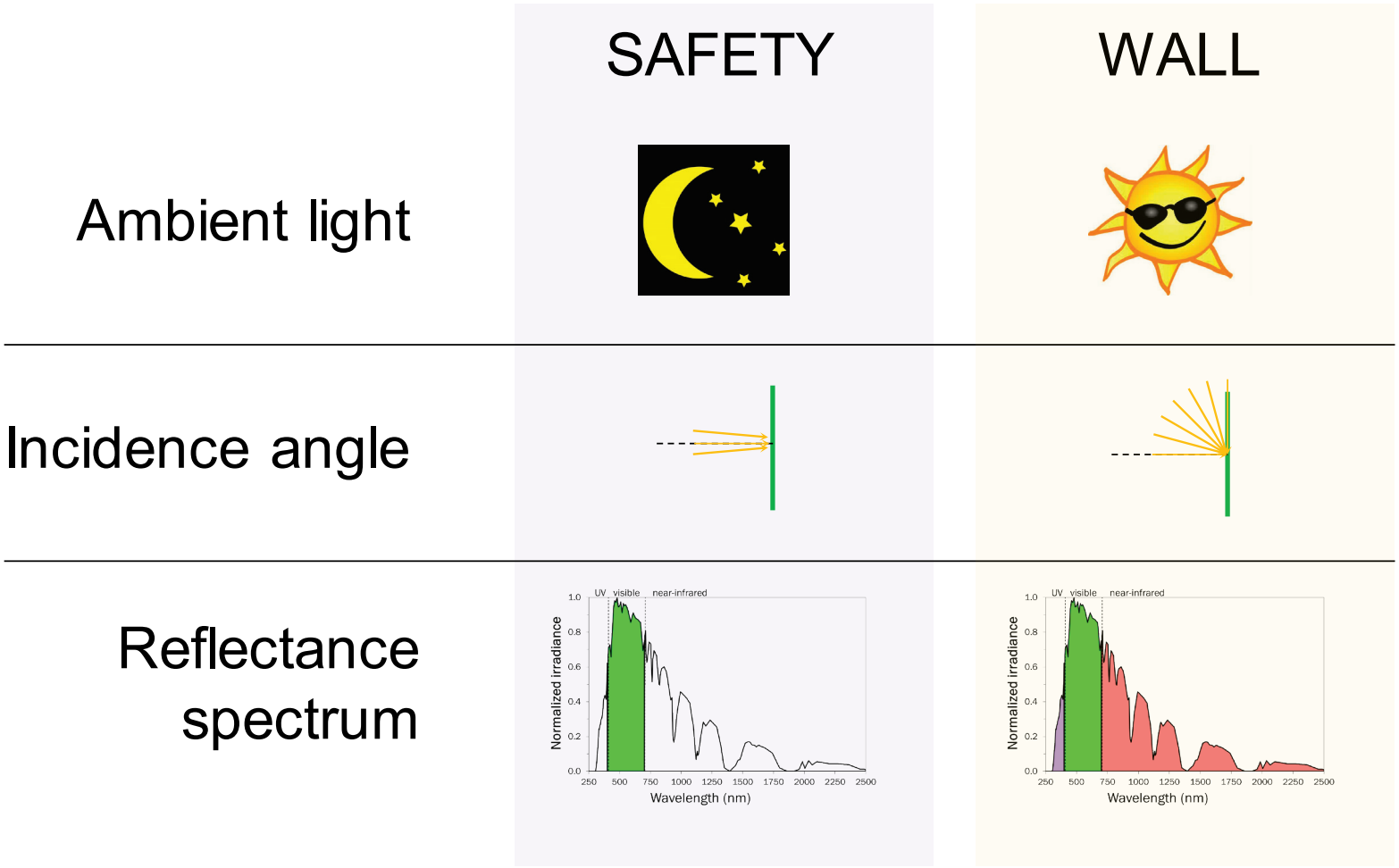

Figure 5. Compared to safety retroreflectors, wall retroreflectors must reflect a larger fraction of incident sunlight, over a wide range of incidence angles and wavelengths.

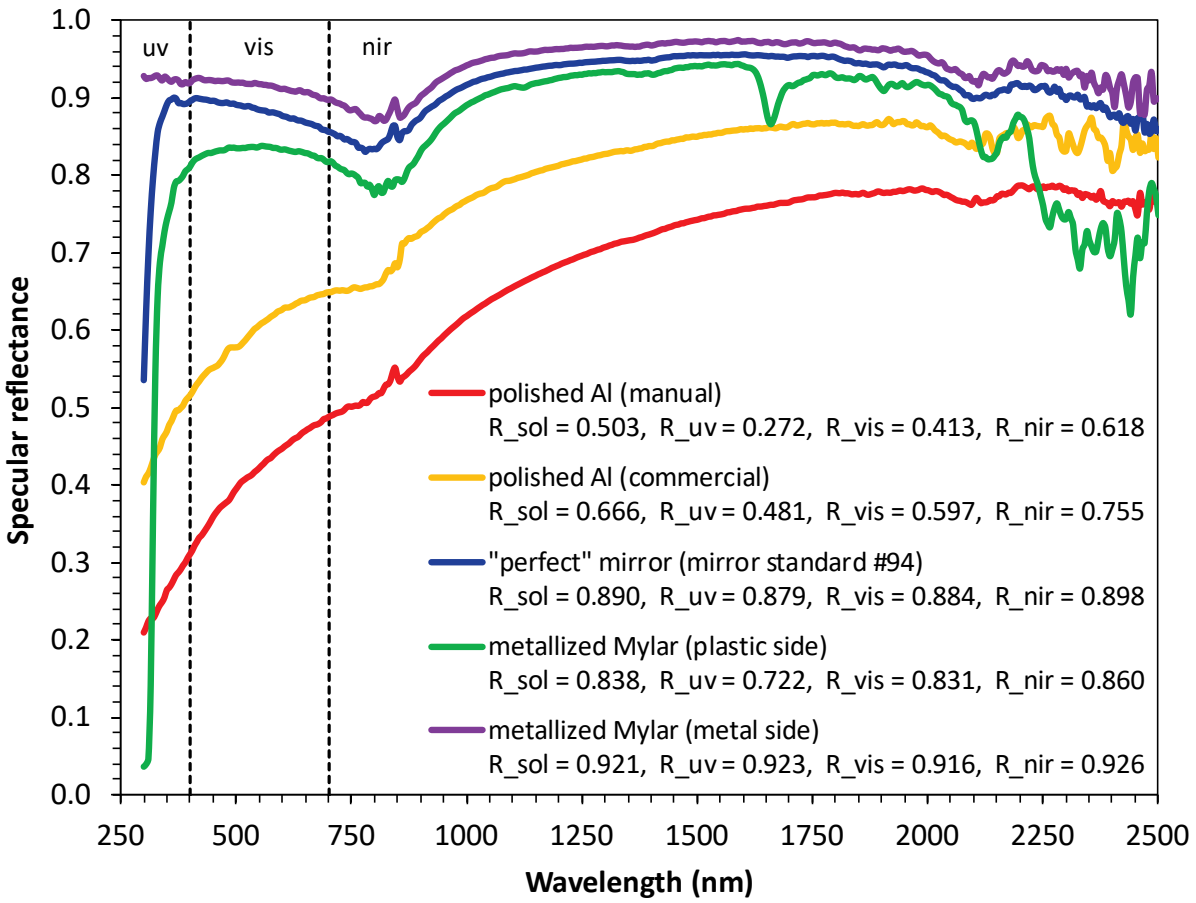

Figure 6. Specular components of solar spectral reflectances of five mirrorlike systems, including a manually polished block of aluminum (curve B); a mirror calibration standard (curve C); a commercially polished aluminum sheet (curve D); the metal face of aluminized Mylar (curve E); and the plastic face of aluminized Mylar (curve F).

2.2 Angular distribution of solar irradiation

To explore the distribution of angles at which beam sunlight strikes walls, we computed hourly solar positions and hourly beam irradiances on isolated walls following the procedure detailed in the Task 2.3 report: *Using solar availability to scale HVAC savings*. That is, we calculated beam tilt irradiance with the standard isotropic sky model (Duffie and Beckman 2006), using as inputs (a) global horizontal and diffuse horizontal hourly solar irradiation values from Typical Meteorological Year 3 (TMY3) weather files (NREL 2018b) and (b) mid-hour solar positions computed with the Measurement and Information Data Center Solar Position and Intensity (MIDC SOLPOS) Calculator provided by the National Renewable Energy Laboratory (NREL 2018a). Ground albedo was set to 0.20. We then calculated in each season (e.g., summer = June/July/August) the variation with solar altitude of the cumulative fraction of wall-incident solar energy.

To illustrate, consider summer sunlight in Fresno, CA. About 85%, 37%, 35%, and 1% of the beam radiation incident on a north, east, west, or south wall arrives when the solar altitude angle is less than or equal to 30˚ (Figure 7). Since the incidence angle of beam radiation striking a wall will always equal or exceed the solar altitude angle, less than 37% of the beam radiation striking the east or west wall, and essentially none of that striking the south wall, will do so at an incidence angle less than or equal to 30˚.

Table 1 summarizes by U.S. climates (Figure 8) and wall direction the distribution with solar altitude angle of beam sunlight incident in summer.

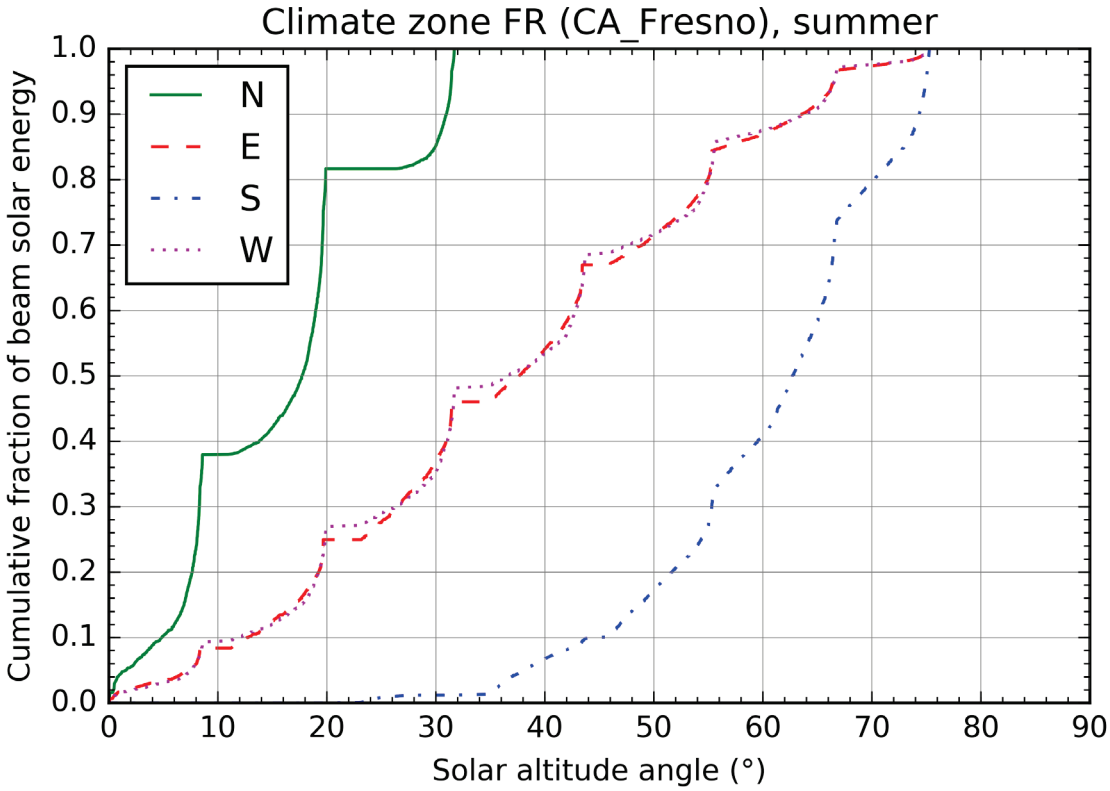

Figure 7. Variation with solar altitude angle of the cumulative fraction of beam solar energy incident on an isolated north (N), east (E), south (S), or west (W) wall in Fresno, CA during the summer months (June/July/August).

Table 1. Percentage of beam sunlight incident on an isolated north, east, south, or west wall in summer at solar altitude angles up to 5, 15, 30, 45, 60, or 75°, reported for the climates shown in Figure 8.

	(a) north						(b) east						(c) south						(d) west					
Climate	**5°**	**15°**	**30°**	**45°**	**60°**	**75°**	**5°**	**15°**	**30°**	**45°**	**60°**	**75°**	**5°**	**15°**	**30°**	**45°**	**60°**	**75°**	**5°**	**15°**	**30°**	**45°**	**60°**	**75°**
1A	0	22	62	88	99	100	0	9	30	54	78	95	0	0	1	6	27	73	1	4	22	49	73	97
2A	5	37	78	98	100	100	2	10	32	56	82	97	0	0	1	7	30	80	0	9	31	53	79	99
2B	30	60	90	100	100	100	6	18	37	62	84	100	0	0	0	10	32	90	6	15	36	60	82	100
3A	9	34	81	100	100	100	2	9	33	63	85	98	0	0	1	9	40	86	2	9	31	65	86	98
3B	3	28	82	99	100	100	1	8	40	62	83	97	0	0	1	7	30	80	1	9	28	61	85	98
BU	8	26	84	100	100	100	2	9	34	65	85	98	0	0	1	8	36	85	2	5	33	62	84	97
FR	10	42	85	100	100	100	3	12	37	67	87	99	0	0	1	10	41	95	3	12	35	69	87	99
3C	23	51	94	100	100	100	3	9	35	59	84	100	0	0	1	10	42	97	5	13	33	63	89	100
4A	21	51	93	100	100	100	1	8	36	64	87	100	0	0	1	11	45	100	6	15	35	70	88	100
4B	17	45	92	100	100	100	6	15	45	65	86	98	0	0	1	7	35	86	3	12	31	61	85	98
4C	28	71	99	100	100	100	3	13	37	68	96	100	0	0	2	20	74	100	4	16	40	75	94	100
5A	11	48	92	100	100	100	2	11	36	70	90	100	0	0	1	15	52	100	1	9	36	67	88	100
5B	17	59	100	100	100	100	4	16	41	69	93	100	0	0	2	16	62	100	3	13	46	70	92	100
6A	35	68	97	100	100	100	5	15	39	73	92	100	0	0	2	19	64	100	7	17	41	73	92	100
6B	16	55	100	100	100	100	3	15	45	71	96	100	0	0	2	18	71	100	3	12	44	69	96	100
7	22	67	99	100	100	100	2	14	42	70	96	100	0	0	2	20	72	100	4	17	39	75	94	100
8	50	89	100	100	100	100	14	38	69	97	100	100	0	0	12	77	100	100	1	7	51	93	100	100

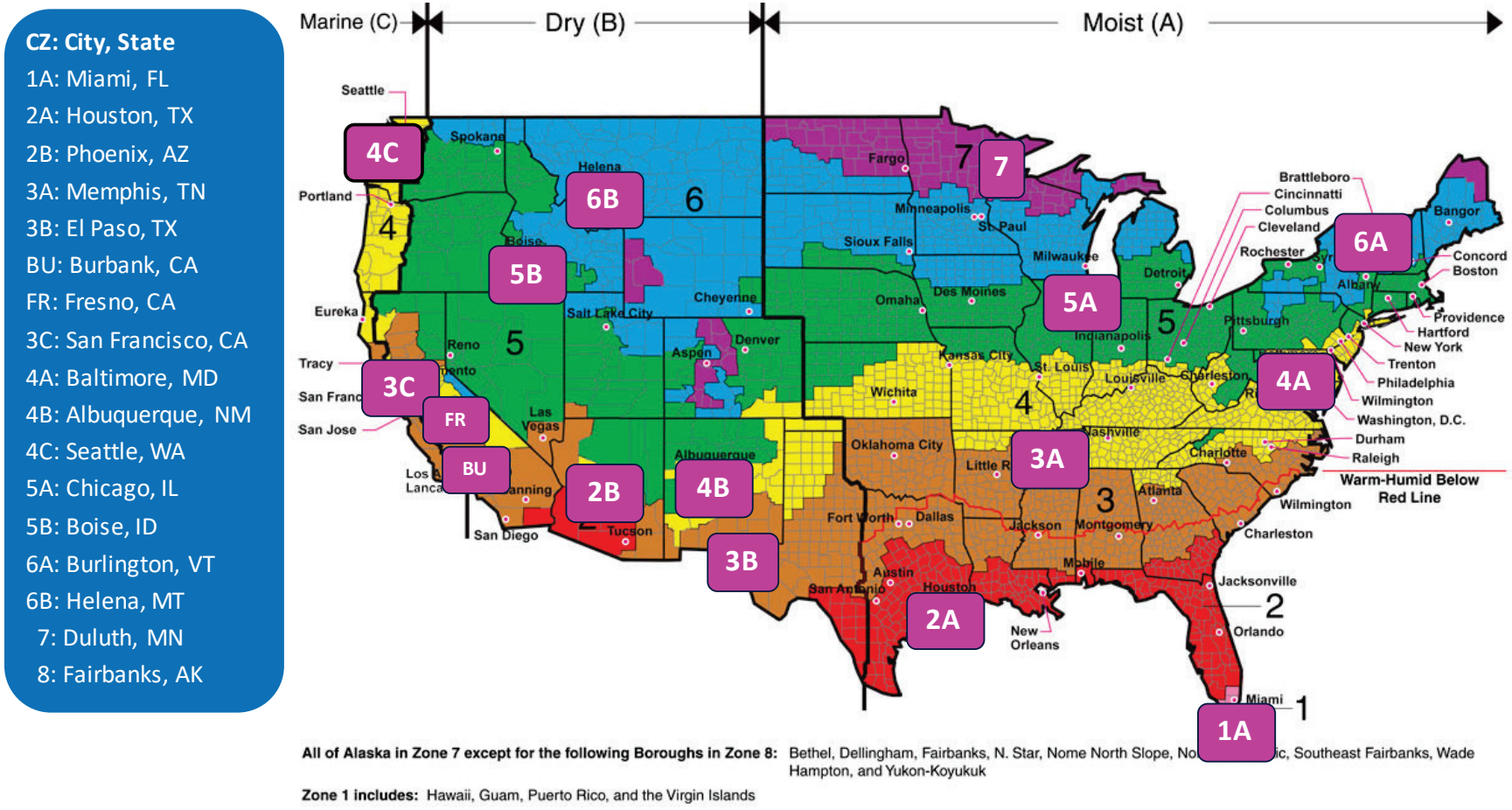

Figure 8. Map of U.S cities representing ASHRAE climate zones (CZ) 1 – 8, plus two California cities (Burbank and Fresno). Adapted from Briggs et al. (2003a,b).

2.3 Vertical surface retroreflection vs. solar altitude angle

The preceding analysis indicates that systems that retroreflect only near-normal light may not work well when applied to south, east, and west walls.

Consider beam sunlight incident on the vertical symmetric two-surface retroreflector shown in Figure 9. A beam of altitude angle $\alpha < 45°$ in the plane of page will strike face 1 at incidence angle $\theta_1 = \alpha + \gamma = \alpha + (90° - \beta) = 45° + \alpha$. The beam reflected from face 1 will strike face 2 at incidence angle $\theta_2 = 180° - 90° - \theta_1 = 45° - \alpha$. The beam reflected from face 2 will be anti-parallel to original solar beam, completing the retroreflection.

2.3.1 Case 1: Metal mirror faces

If each surface is metal mirror, the system will retroreflect beam sunlight incident on face 1 when $\alpha < 45°$; retroreflect beam sunlight originally incident on face 2 when $\alpha = 45°$; and reflect specularly upward, but not to its origin, beam sunlight originally incident on face 2 when $\alpha \neq 45°$. The latter flux will go directly to the sky when $\alpha < 45°$, or to the sky via face 1 when $\alpha > 45°$.

2.3.2 Case 2: Transparent faces

If each surface is made of the same transparent material with $n \geq 1.5$, face 1 will exhibit TIR for $\alpha < 45°$ because the beam incidence angle $\theta_1 = 45° + \alpha$ will always exceed the material's critical angle in air, θ_c (Figure 10). However, the beam reflected from face 1 will be reflected by face 2 only if $\theta_2 = 45° - \alpha$ exceeds θ_c. The maximum solar altitude α_{max} at which face 2 will total internally reflect the beam from face 1 beam ranges from 3.2° for low-index glass (n=1.5) to 20.4° for diamond (n=2.4) (Table 2). When $\alpha_{max} < \alpha < 45°$, beam light reflected from face 1 will pass through face 2. Meanwhile, beam sunlight originally incident on face 2 will strike at angle $\theta_2 = 45° - \alpha$. If $\theta_2 < \theta_c$, it will pass through face 2. Otherwise, it will be reflected specularly upward, in some cases striking face 1. Reflected light that strikes face 1 will be reflected to the sky since $\theta_1 = 45° + \alpha > \theta_c$. Thus, beam sunlight incident originally incident on either face 1 or face 2 will pass through face 2 when $\theta_2 = 45° - \alpha \leq \theta_c$, or $\alpha \geq 45° - \theta_c$.

Inspection of the 5° altitude columns in Table 1(b-d) indicates that if made of low-index glass or plastic (n = 1.5, θ_c = 3.2°), this system will transmit, rather than retroreflect, nearly all beam sunlight incident on an east, south, or west wall in summer.

Table 2. Real refractive indices and critical angles of some transparent materials.

Material	Real refractive index	Critical angle in air (°)	Maximum solar altitude yielding total internal reflection at face 2 (°)
Low-index glass [a]	1.5	41.8	3.2
High-index glass [b]	2.0	30.0	15.0
Cubic zirconia	2.2	27.0	18.0
Diamond	2.4	24.6	20.4

[a] Such as Schott N-BK7 crown glass (Polyanskiy 2018).

[b] Such as Ohara Glass lanthanum S-LaH79 (Polyanskiy 2018).

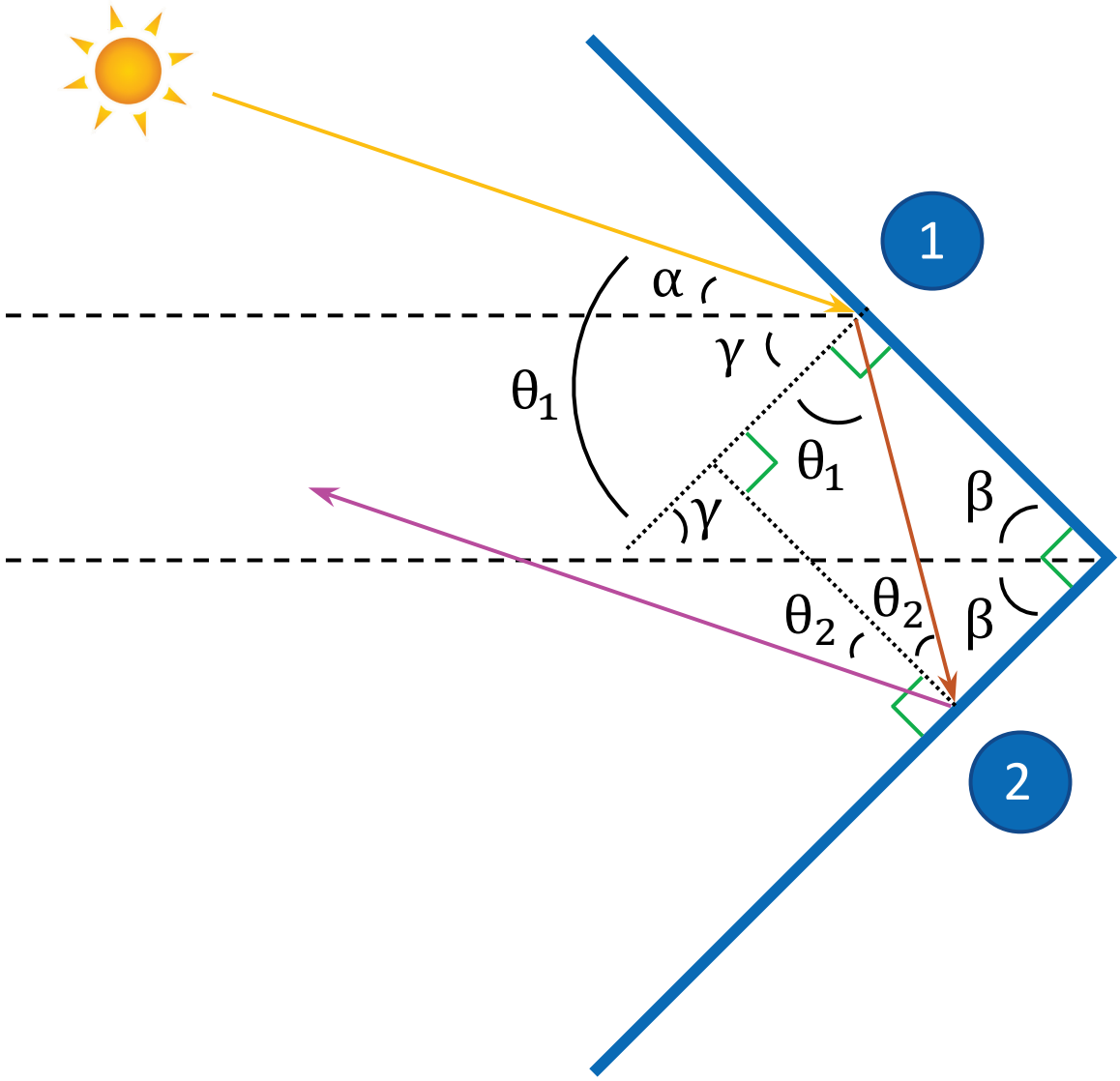

Figure 9. Angles of incidence and reflectance at faces of a vertical symmetric two-surface retroreflector (isosceles right triangle formed by orthogonal faces 1 and 2 and their undrawn vertical hypotenuse; β=45°).

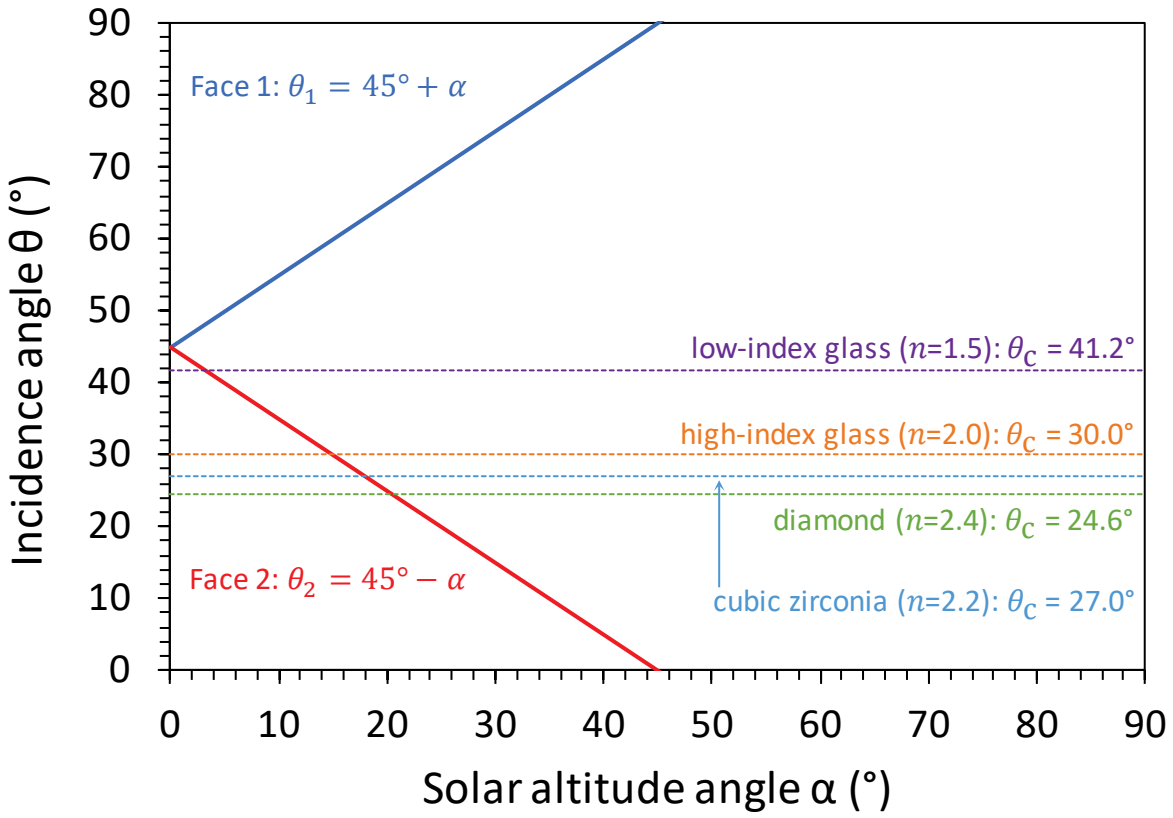

Figure 10. Angles of incidence on when downwelling beam sunlight strikes face 1, and beam-light reflected from face 1 strikes face 2, in the vertical retroreflector system drawn in Figure 9. Shown for reference are the critical angles for various clear windows in air.

3 Ray-tracing simulations

We used the open-source Ray Optics Simulation web application (Tu 2018) to simulate a variety of 2-D vertical retroreflectors.

3.1 Designs

Each “symmetric” design comprises an array of pairs of equal length faces forming an isosceles right triangle with a vertical hypotenuse and 45° acute angles. Each “asymmetric” design comprises an array of pairs of unequal length faces (upper face length 5, lower face length 3.3) forming a right triangle with a vertical hypotenuse and acute angles of 33.5° (top) and 56.5° (bottom). Low and high-index glasses follow the specifications of Table 2.

a) Symmetric empty mirrors, where light passes from air to ideal metal mirrors.

b) Symmetric empty mirrors behind a low-index glass vertical window, to keep the mirrors clean.

c) Asymmetric empty mirrors.

d) Asymmetric empty mirrors behind a low-index glass vertical window.

e) Symmetric low-index glass right triangular prisms.

f) Symmetric low-index glass right triangular prisms with ideal metal mirror backing replacing the glass-air interface.

g) Asymmetric low-index glass right triangular prisms.

h) Asymmetric low-index glass right triangular prisms with ideal metal mirror backing.

i) Symmetric high-index glass right triangular prisms.

j) Symmetric high-index glass right triangular prisms with ideal metal mirror backing.

k) Asymmetric high-index glass right triangular prisms.

l) Asymmetric high-index glass right triangular prisms with ideal metal mirror backing.

3.2 Results

Figure 11 shows the paths of beams incident from altitudes of α = 0, 15, 30, 45, 60, and 75°. The following observations are limited to the six altitudes simulated.

3.2.1 Prisms

- As predicted in Section 2.3.2, design *e* retroreflects only at $\alpha = 0^{\circ}$ and design *i* retroreflects only at $\alpha = 0$, 15, and 30˚. The retroreflection at $\alpha = 30^{\circ}$ by design *i* is simply specular reflection.
- Design *g* does not work.
- Design *k* fares poorly at $\alpha = 0^{\circ}$, provides mixed results at $\alpha = 30^{\circ}$, and works well at $\alpha > 30^{\circ}$.
- Mirror backings (designs *f*, *h*, *j*, and *l*) help a bit, but reflect some light downward.

3.2.2 Empty mirrors

- Design *a* provides a combination of retroreflection and not-to-origin upward reflection.
- Design *c* fares poorly at $\alpha = 0^{\circ}$, provides mixed results at $\alpha = 30^{\circ}$, and works well at $\alpha > 30^{\circ}$.
- Placing the mirrors behind a vertical window (designs *b* and *d*) has little effect.

From these analyses we conclude that design *a* (symmetric empty mirrors) is the logical starting point for prototype fabrication, and that it can kept clean behind a low-index window (design *b*) without performance penalty.

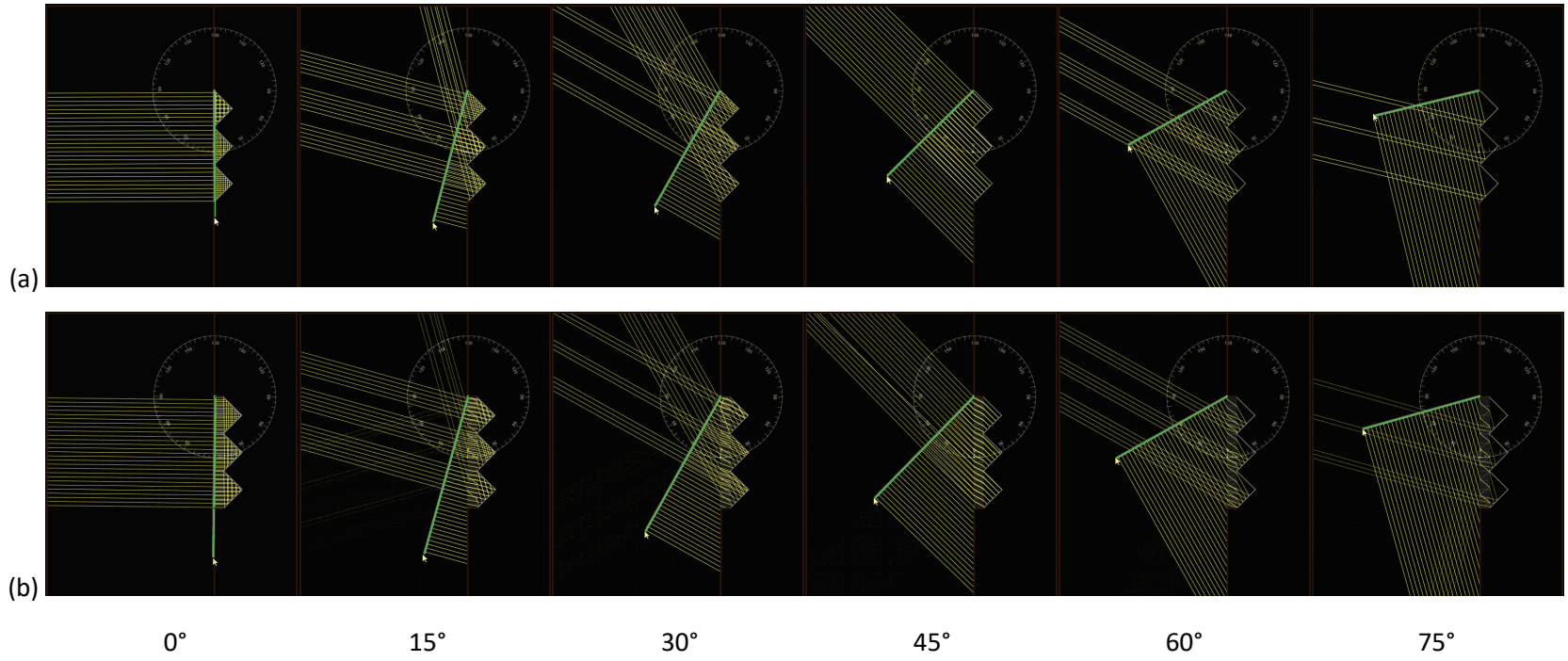

Figure 11. Reflection of beam light as a function of beam altitude angle, shown for a variety of two-surface retroreflectors. Shown here: (a) symmetric empty mirrors; (b) symmetric empty mirrors behind a low-index glass window (n=1.5).

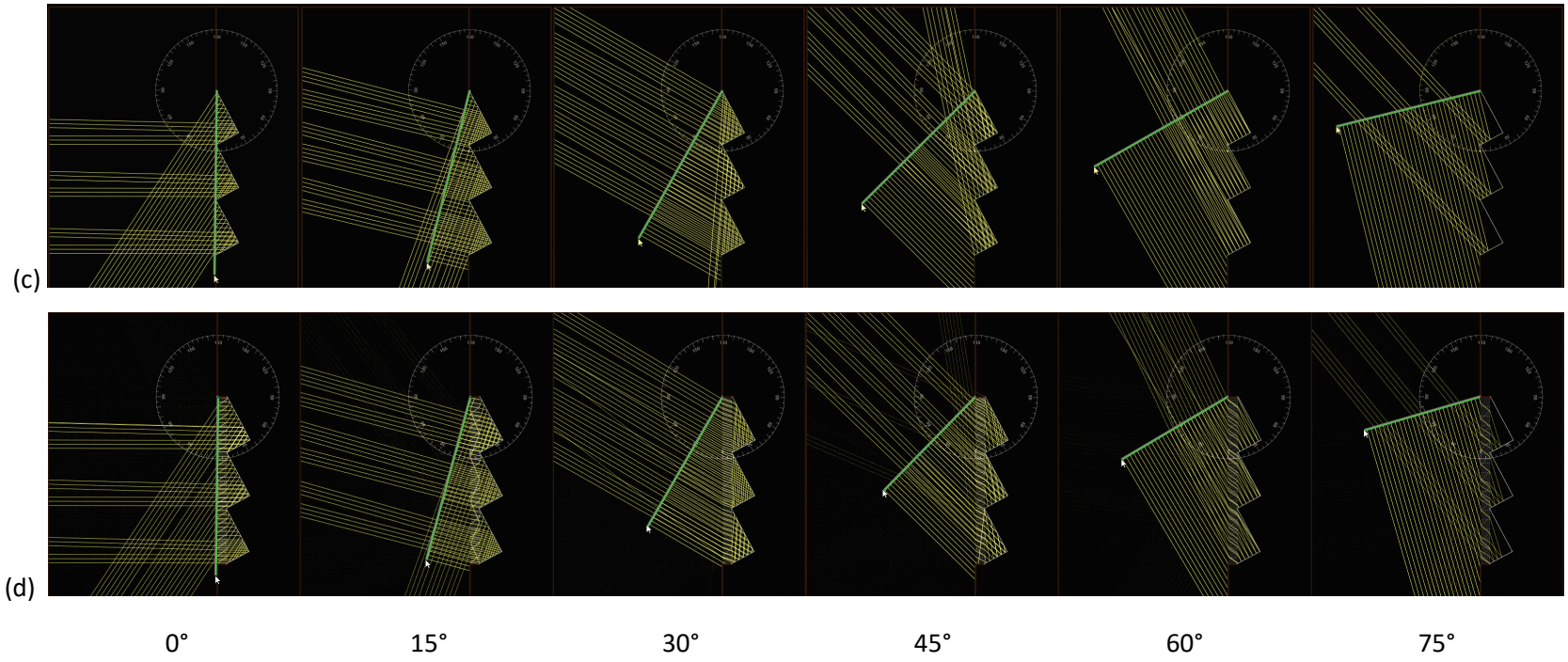

Figure 11 (continued). Shown here: (c) asymmetric empty mirrors; (d) asymmetric empty mirrors behind a low-index glass window (*n*=1.5).

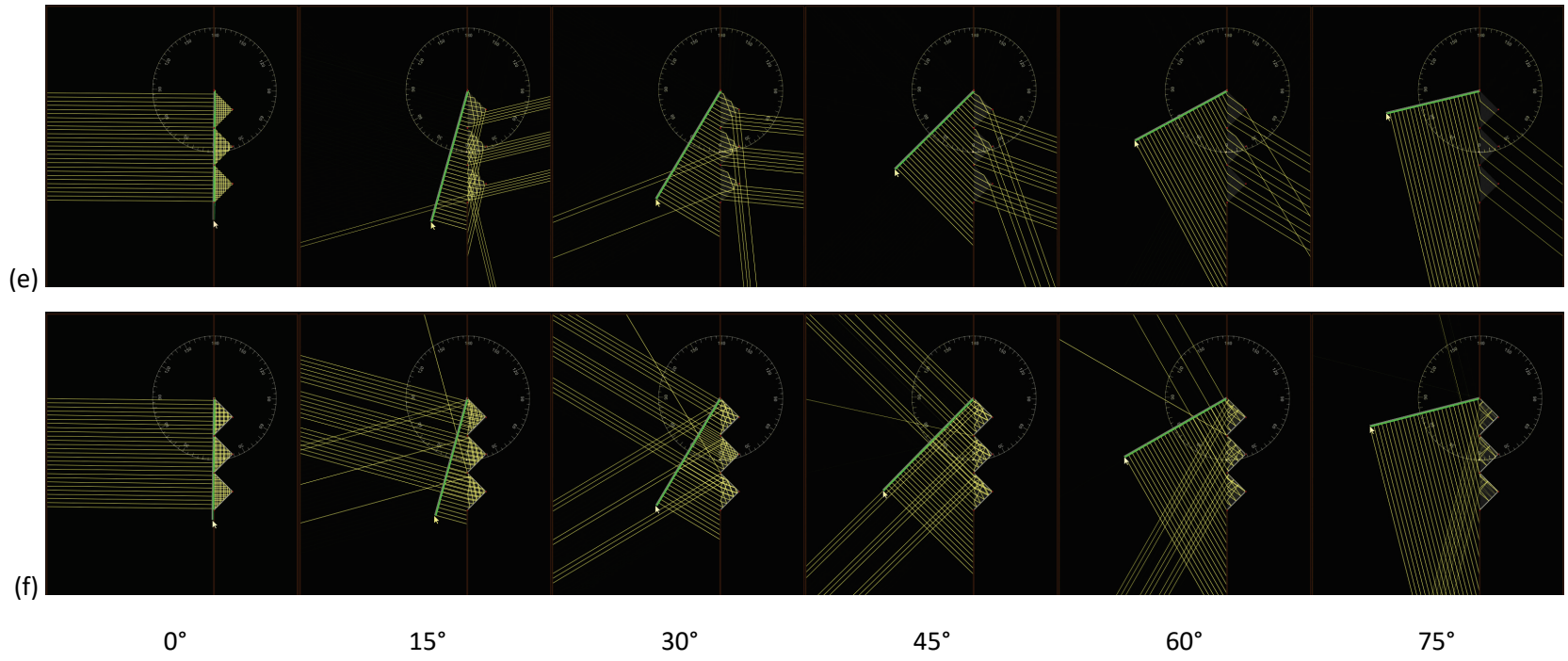

Figure 11 (continued). Shown here: (e) symmetric low-index glass (n=1.5) right triangular prisms; (f) system *e* plus mirror backing.

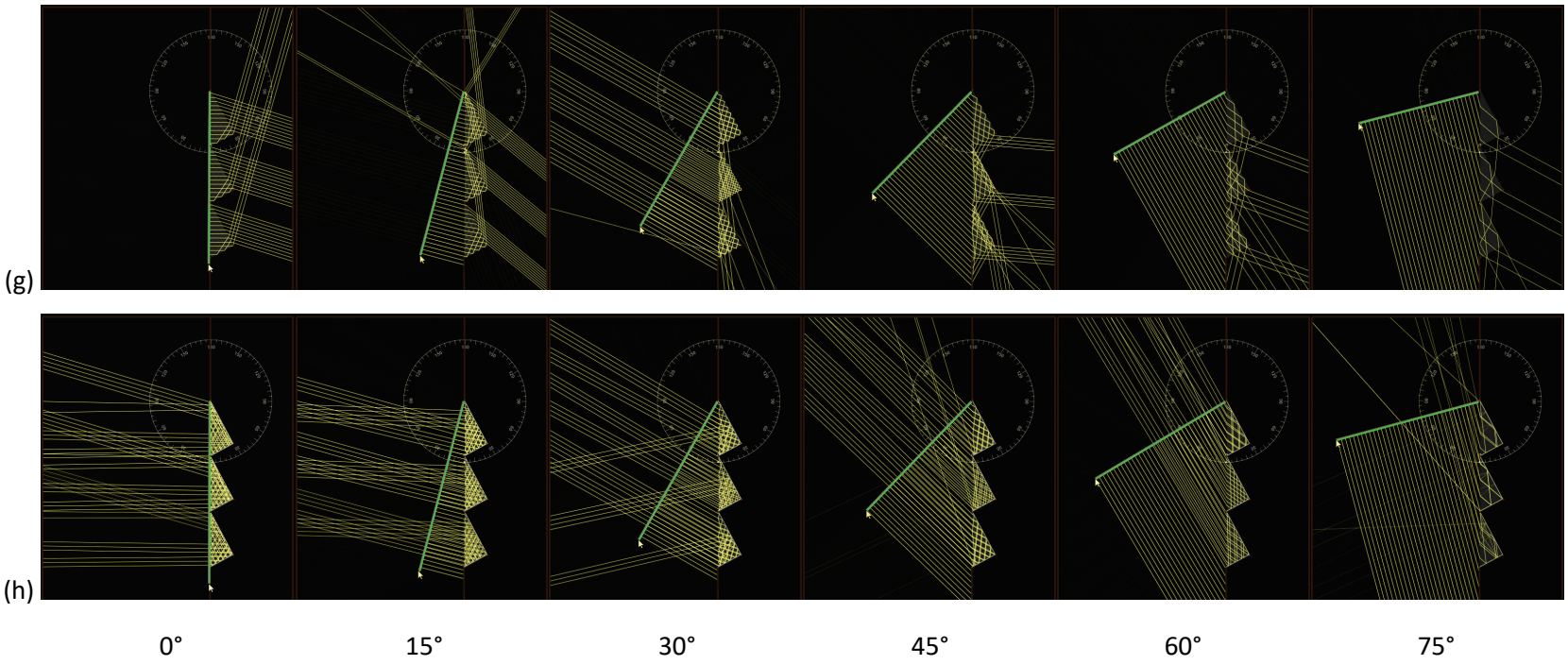

Figure 11 (continued). Shown here: (g) asymmetric low-index glass (n=1.5) right triangular prisms; (h) system *g* plus mirror backing.

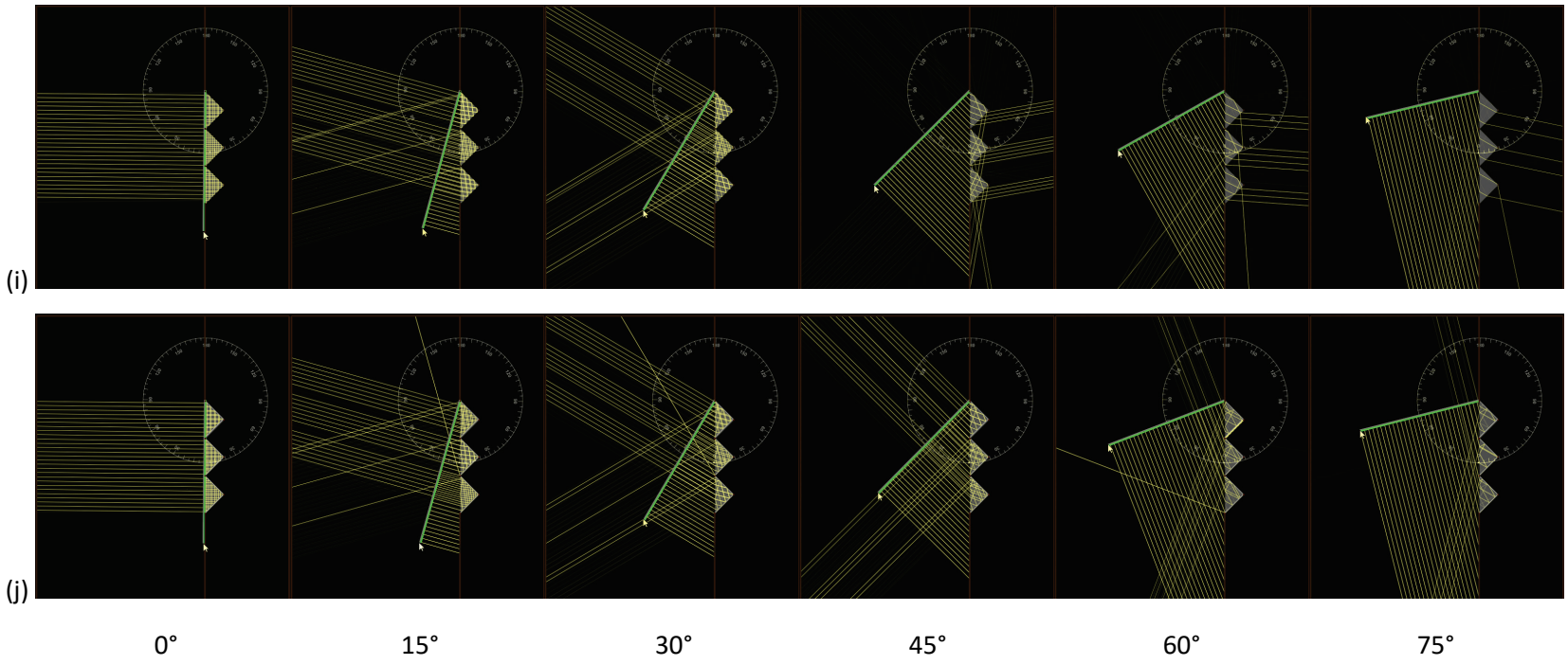

Figure 11 (continued). Shown here: (i) symmetric high-index glass (n=2.0) right triangular prisms; (j) system *i* plus mirror backing.

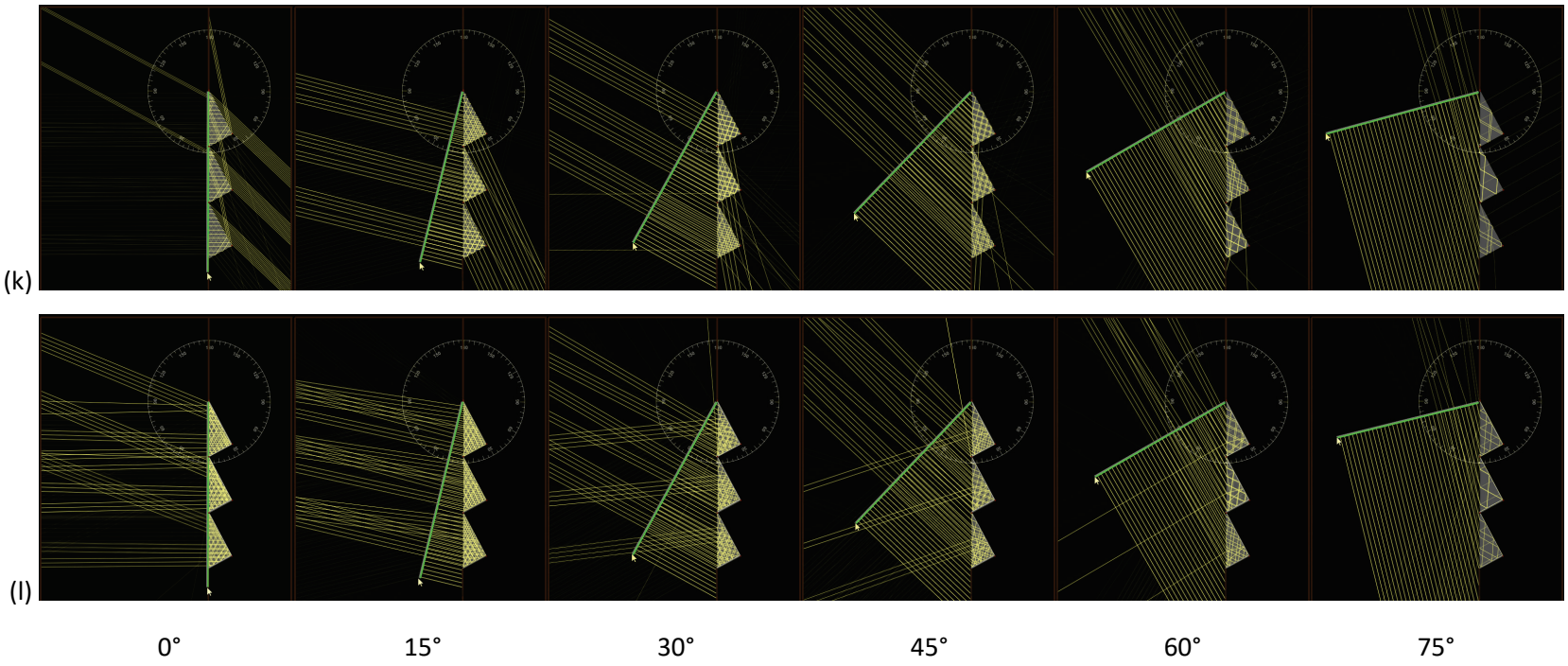

Figure 11 (continued). Shown here: (k) asymmetric high-index glass (*n*=2.0) right triangular prisms; (l) system *k* plus mirror backing.

4 Instrumentation

We assessed retroreflection with two instruments: a simple, monochromatic goniometer that we built in-house, and a sophisticated solar spectral gonionometer designed and operated by Dexerials, a project partner.

4.1 Simple goniometer

The simple goniometer comprises a vertical laser (violet[1], wavelength 405 nm) that shines upward through a small (~ 2 mm) central hole in a hole in a cardboard box. The box is lined with a printed sheet of paper bearing a series of concentric rings that mark the angle (5° to 75° in 5° increments) at which light is reflected from a specimen mounted on a turnable spit. A camera looking down on the box can records images of the light patterns formed within the rings (Figure 12).

The angle of Fresnel (first-surface) reflection equals the angle of incidence on the specimen. The intensity of the retroreflection (if any) can be compared to that of Fresnel reflection (Table 3).

Table 3. Fresnel reflectances of p (parallel)-polarized light (R_p), s (perpendicular)-polarized light (R_s), and unpolarized light ($\bar{R}$) in air striking a surface of real refractive index 1.5 at incidence angle θ, computed following Georgia State University (2005).

θ (°)	5	10	15	20	25	30	35	40	45	50	55	60	65	70	75
R_p	0.04	0.04	0.04	0.03	0.03	0.03	0.02	0.01	0.01	0.00	0.00	0.00	0.01	0.04	0.11
R_s	0.04	0.04	0.04	0.05	0.05	0.06	0.07	0.08	0.09	0.11	0.14	0.18	0.23	0.30	0.40
$\bar{R}$	0.04	0.04	0.04	0.04	0.04	0.04	0.04	0.05	0.05	0.06	0.07	0.09	0.12	0.17	0.25

Patterns of light reflection from the three specimens shown in Figure 13—a mirror calibration standard, a polished aluminum panel with brush marks, and a white retroreflective safety film—can be seen in Figure 14.

As expected, each specimen yields a specular (Fresnel) reflection, but only the safety film exhibits retroreflection. The intensity of this retroreflection can be compared to that of the Fresnel reflection at 70°, which ranges from 0.04 to 0.30 if the laser beam is polarized, or is 0.17 if the laser beam is unpolarized (Table 3).

We recommend rotating a linearly polarized laser beam to orient its electric field perpendicular to the plane of incidence (that containing the surface normal and incident ray). This will raise

[1] There was no special reason to use a violet laser; we simply had one available.

its Fresnel reflectance to its maximum (s-polarized) value R_s, making it easier to compare retroreflection to Fresnel reflection. The upper and lower images in Figure 14c show maximum and minimum specular reflectances observed when rotating the incident laser beam. The rotations corresponding to these two images were approximately 90˚ apart.

4.2 Advanced goniometer

Dexerials' advanced spectro-goniometer (Figure 15) measures solar spectral bi-directional reflectance from 0.350 to 2.350 µm. Its design and operation are detailed by Harima and Nagahama (2017).

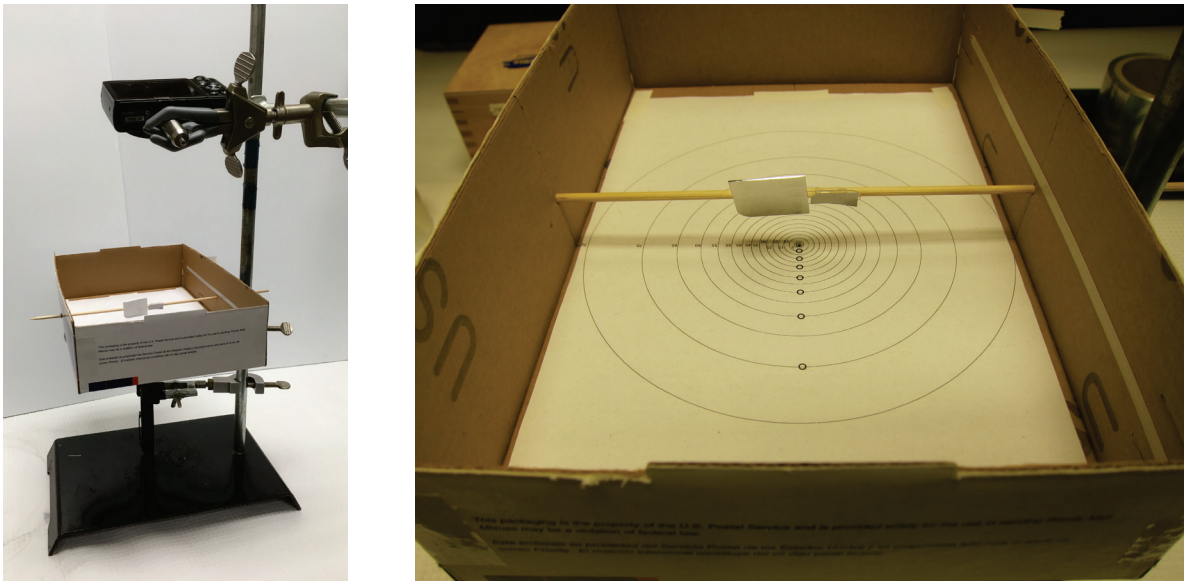

(a) (b)

Figure 12. We built a simple goniometer to compare retroreflection to specular reflection (~ 5%). (a) side view of goniometer with laser pointer shining up and camera looking down; (b) top view of goniometer, showing specimens (aluminum panel at left; white retroreflective safety film at right) mounted on rotatable spit, central hole admitting laser beam, and concentric rings (5° to 75° in 5° increments) marking angle of reflection.

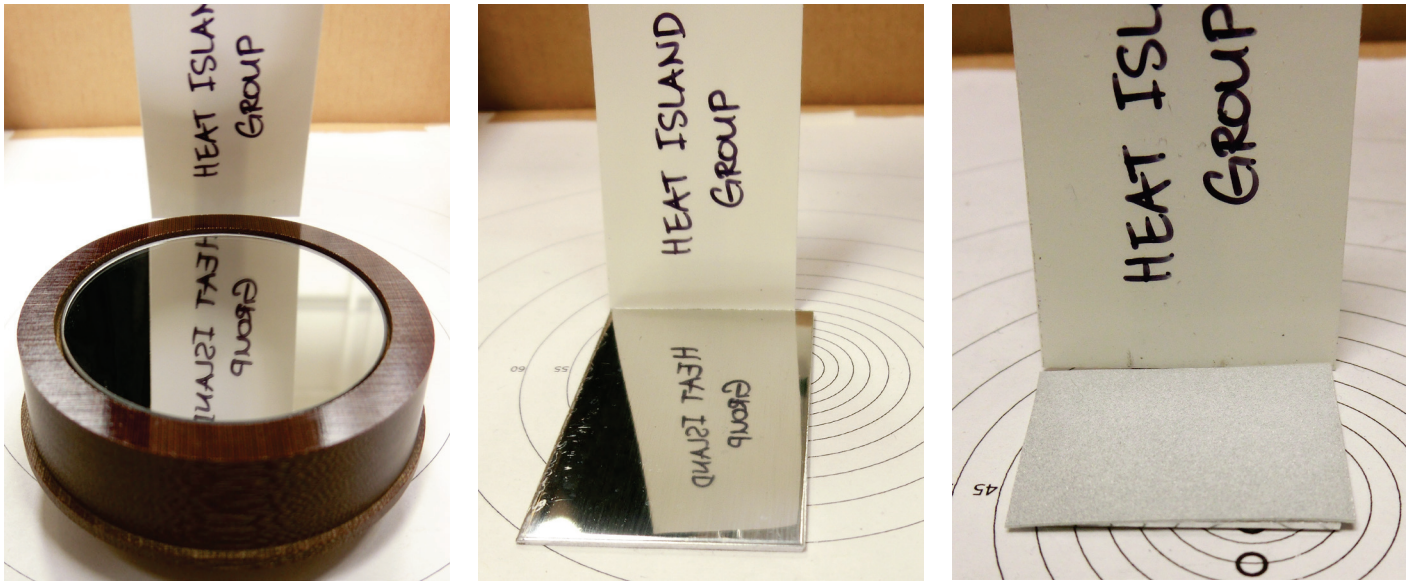

(a) (b) (c)

Figure 13. Three surfaces tested in the simple goniometer: (a) mirror calibration standard; (b) polished aluminum panel with brush marks; and (c) white retroreflective safety film.

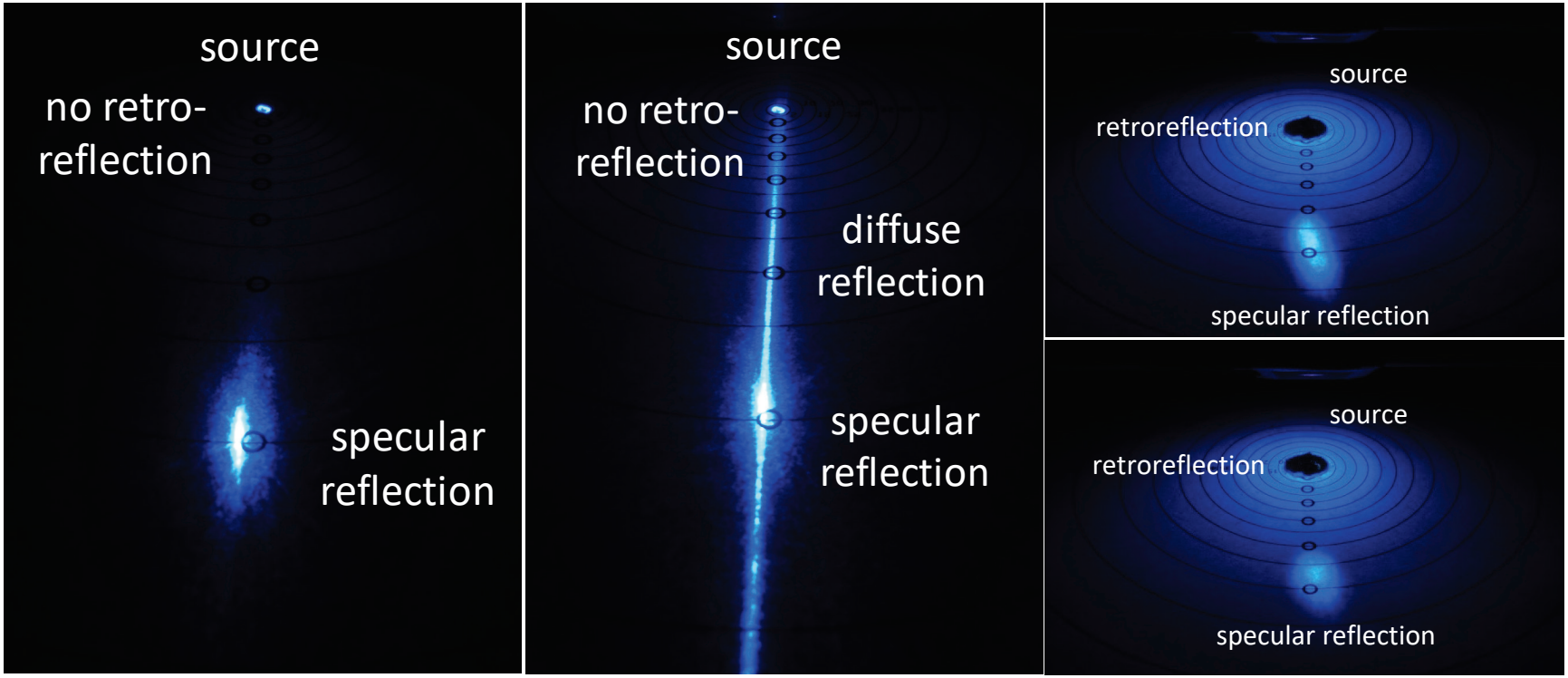

(a) (b) (c)

Figure 14. Simple goniometer images of laser light at 70° incidence reflected from (a) mirror calibration standard, exhibiting purely specular reflection; (b) polished aluminum panel, exhibiting specular and diffuse reflections; and (c) a white retroreflective safety film, exhibiting specular reflection and retroreflection. Upper and lower images in panel (c) show maximum and minimum specular reflectances observed when rotating incident laser beam.

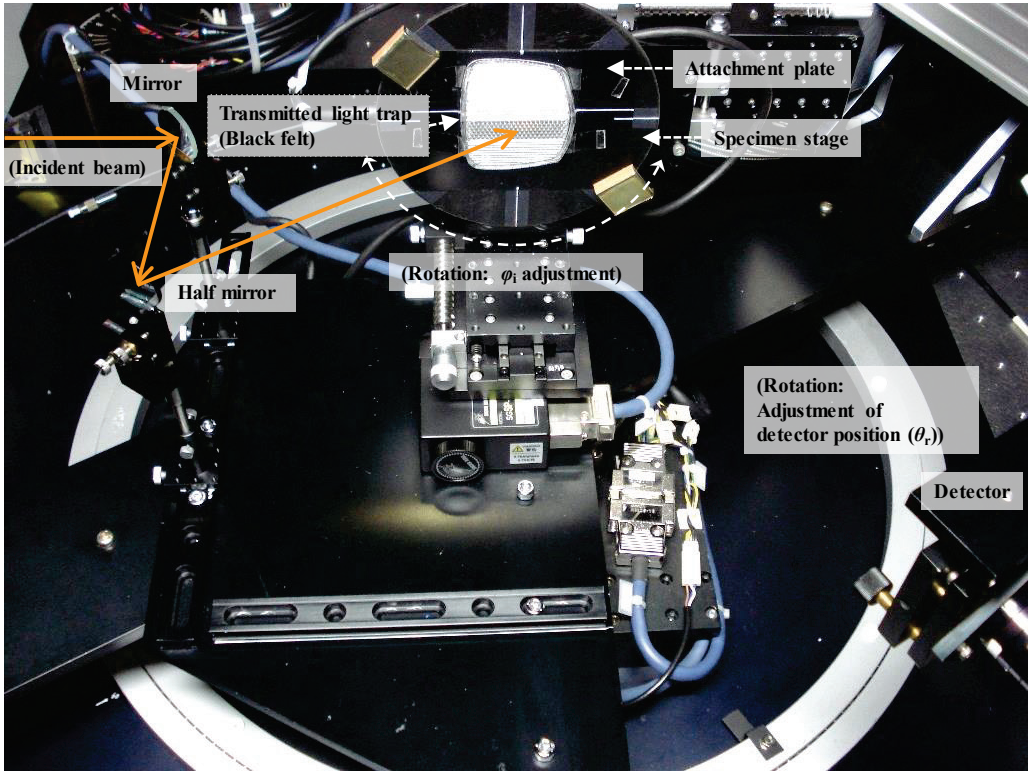

(a)

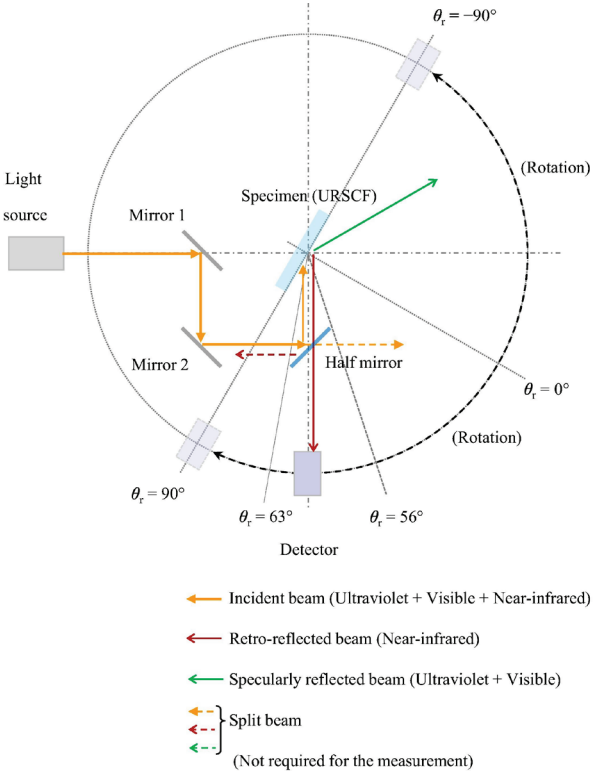

(b)

Figure 15. Dexerials' advanced spectro-goniometer measures solar spectral bi-directional reflectance. Source: Harima and Nagahama (2017)

5 Prototype development and evaluation

5.1 Safety films

Examination in the simple goniometer of retroreflections and Fresnel reflections from several safety films (e.g., the white film in Figure 13c and Figure 14c) showed that the retroreflection was often weaker than the Fresnel reflectance, which we in turn estimated to be about 0.04 to 0.17 (Table 3).

5.2 Bicycle retroreflector

We tested the retroreflectance of several specimens of a clear prismatic bicycle reflectors in three conditions:

a) bare (Figure 16, left and middle segments in each photo);

b) with a third of the rear coated with LO/MIT low-E radiative barrier paint (Figure 16, right segment in each photo); and

c) with about 0.4 μm of aluminum sputtered on the rear (Figure 17).

Specimen *b* was abandoned after inspection with the simple goniometer indicated that the LO/MIT coating did not enhance retroreflection. We measured the near normal-hemispherical solar spectral reflectances of the two remaining two specimens (*a* and *c*) with a Perkin-Elmer Lambda 900 UV-vis-NIR spectrometer equipped with 150 mm Labsphere integrating sphere (Figure 18). We then sent them to Dexerials for characterization in the advanced goniometer.

Figure 19 shows the visible and near-infrared (NIR) bi-directional reflectance intensities of the bare reflector (panel a) and the aluminum coated reflector (panel b). Retroreflection from each specimen is evident at incidence angles of 15 and 30˚, with a small hint of retroreflection at 45˚ from the coated specimen. In each case the magnitudes of the visible and NIR retroreflectors are similar, and diminish as incidence angle increases. The aluminum coating increased Fresnel reflection and reduced retroreflection. Since retroreflection essentially vanishes at incidence angles exceeding 30˚, these specimens do not seem promising for wall application.

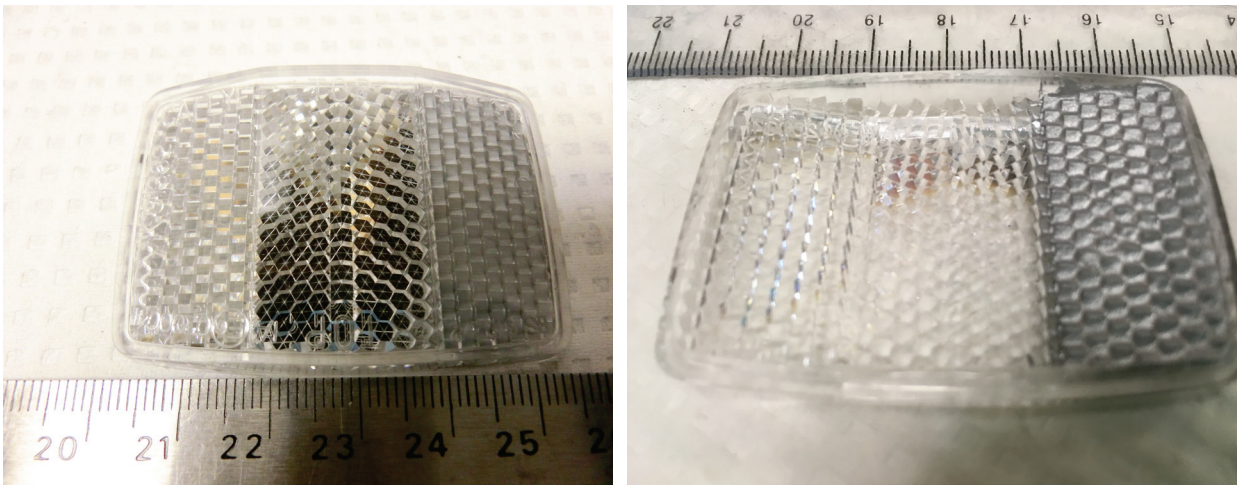

(a) front (b) back

Figure 16. Front and rear faces of a clear plastic bicycle retroreflector showing right third of back surface coated with LO/MIT low-E radiative barrier paint. Rulers are marked in centimeters.

(a) front (b) back

Figure 17. Front and rear faces of another clear plastic bicycle reflector with about 0.4 μm of aluminum sputtered on its rear.

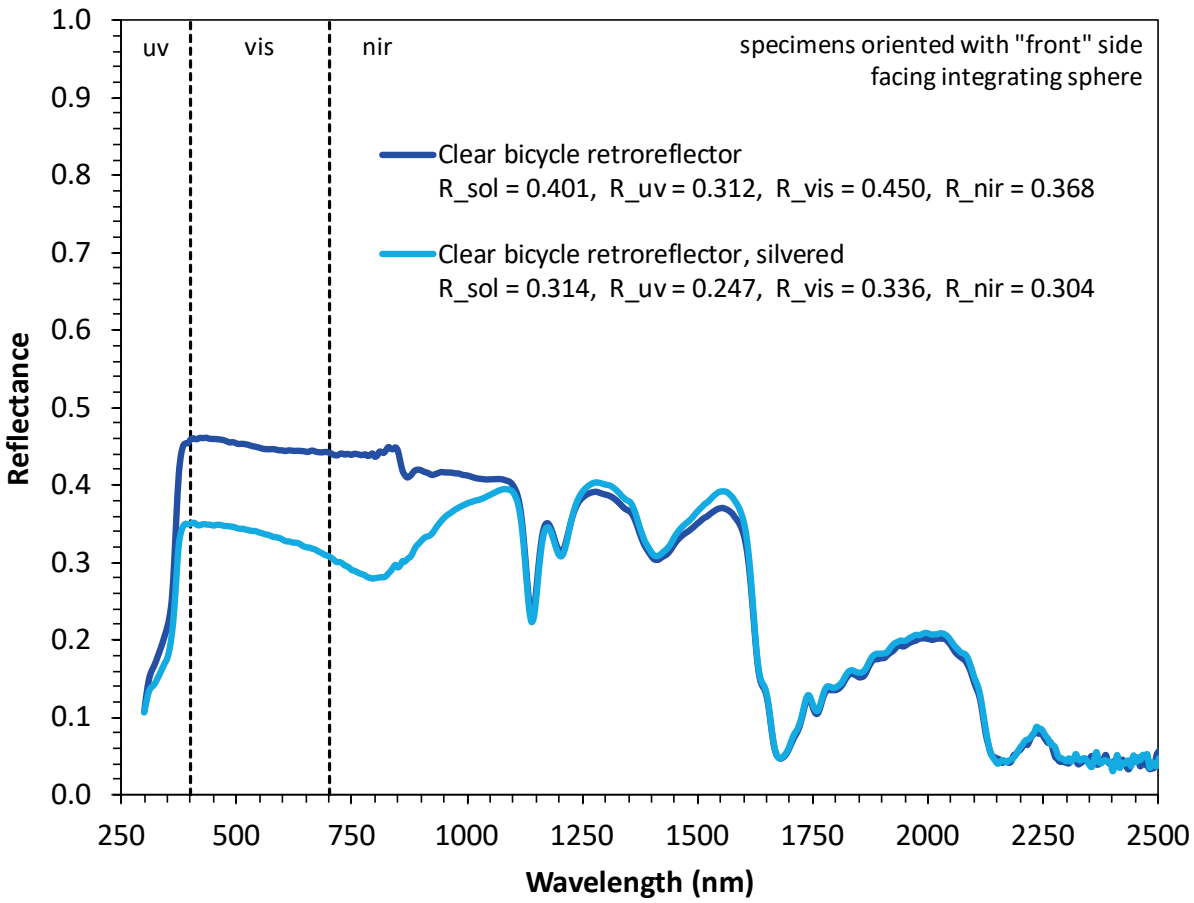

Figure 18. Near normal-hemispherical solar spectral reflectance of front of bicycle retroreflector before and after sputtering aluminum on its back surface.

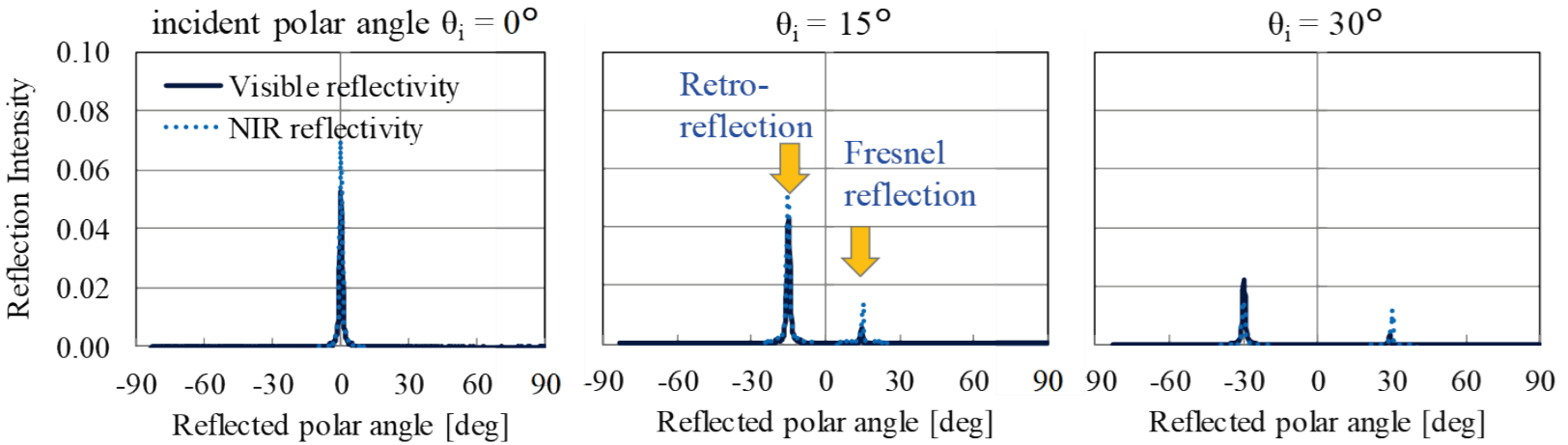

(a)

Figure 19. Bi-directional reflectance intensities of (a) bare bicycle retroreflector and (b) aluminum-coated bicycle retroreflector, courtesy Dexerials.

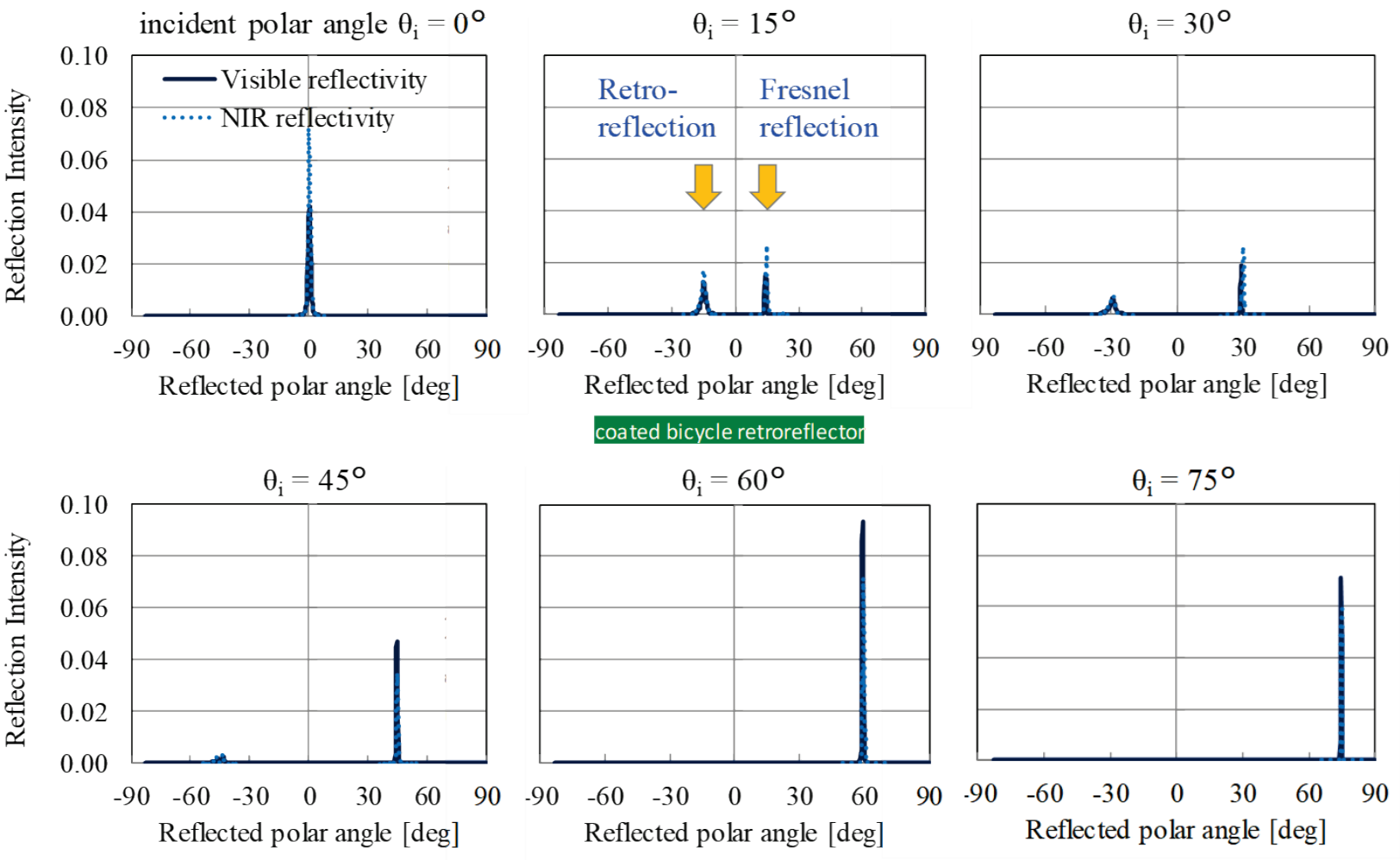

(b)

Figure 19 (continued).

5.3 ABS plastic groove retroflector

We hired a 3-D printing service to fabricate ABS plastic pieces with orthogonal grooves, onto which we planned to sputter a thin coating aluminum following the same process used to coat the bicycle reflector. However, stairsteps found in the groove faces—an issue that we tried, but failed, to avoid by printing the pieces standing tall—suggested that a thin aluminum coating would also be jagged, and unlikely to provide the specular reflections needed for retroreflection.

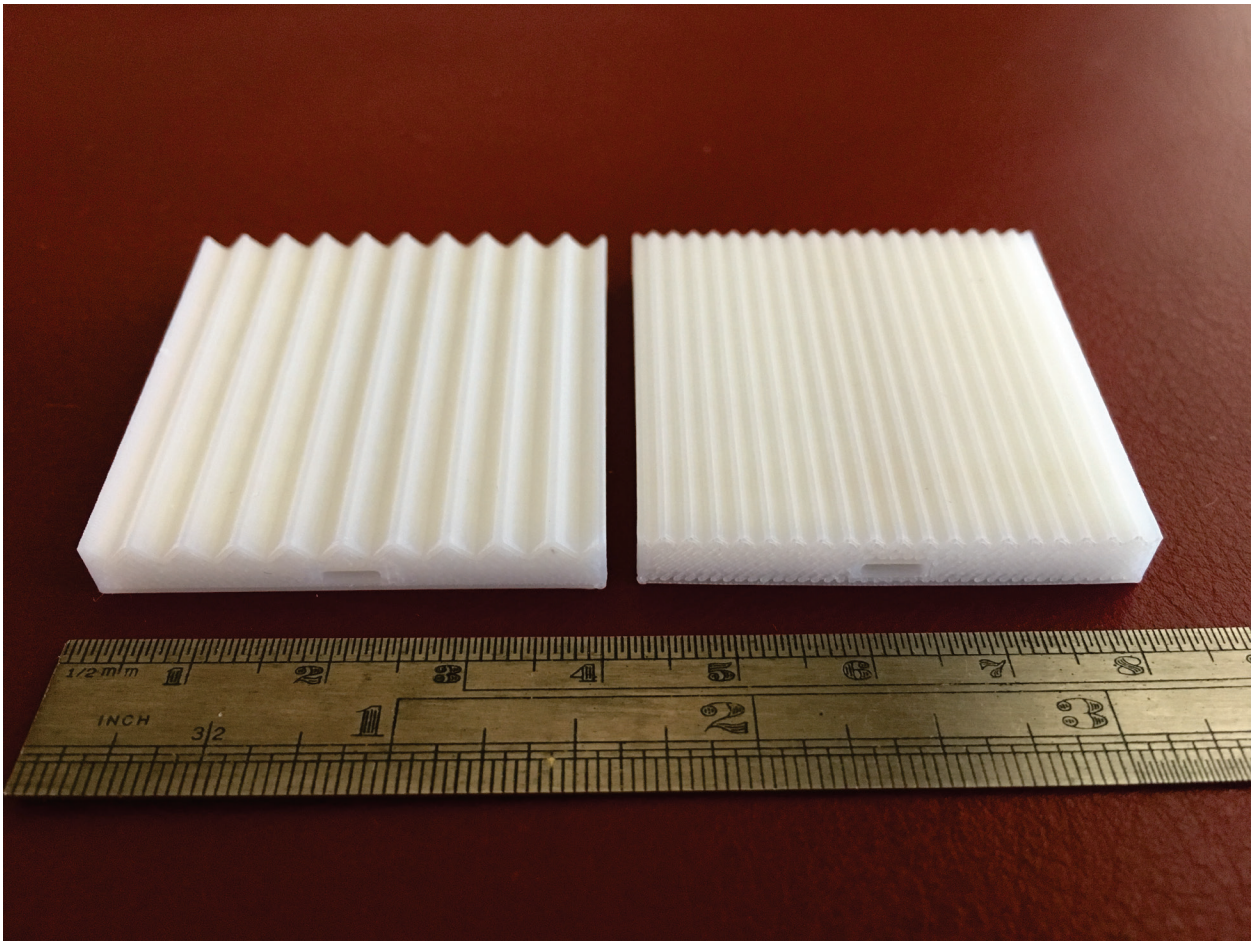

Figure 20. Right-angles grooves 3D printed in ABS plastic. Left: 4-mm pitch; right: 2-mm pitch.

5.4 Grooved aluminum block

We used a computer numeric control (CNC) milling machine to cut 2 mm pitch orthogonal grooves in an aluminum block (Figure 21). The grooves exhibited no retroreflection, so we manually polished them with a buffing wheel and paste (Figure 22). We also polished the rear of the block with the same tool and paste (Figure 22c, right image) to compare its specular spectral reflectance to that of a mirror standard (curves B and C in Figure 6).

We imaged the front and rear of the aluminum block, and the mirror standard, in the simple goniometer (Figure 23). It was hard to see retroreflection of the 405 nm violet laser beam from the polished grooves, possibly because at this wavelength the specular near-normal hemispherical reflectance of the polished block (as gauged by that of its rear) is about 0.31, making its two-bounce reflectance only $0.31^2 = 0.096$.

The simple goniometer allows for a comparative assessment of retroreflection by examining the brightness of light reflected towards the pinhole source. For flat surfaces, this assessment is more relevant at high incidence angles. The results from the mirror calibration standard (top row of Figure 23) provide an example of what we would see with a purely specular and non-retroreflective surface. The results from the hand-polished flat aluminum surface provide an example of what we would see with a non-retroreflective surface that reflects both specularly and diffusely. With these two samples as comparison, we interpret the hand-polished retroreflector prototype's more pronounced light intensities around the pinhole source at incidence angles greater than 50° to be evidence of some retroreflection (bottom row of Figure 23). Ultimately, however, the prototype reflects light at a wide range of angles over a wide range of incidence angles, so its performance in its current state is rather poor.

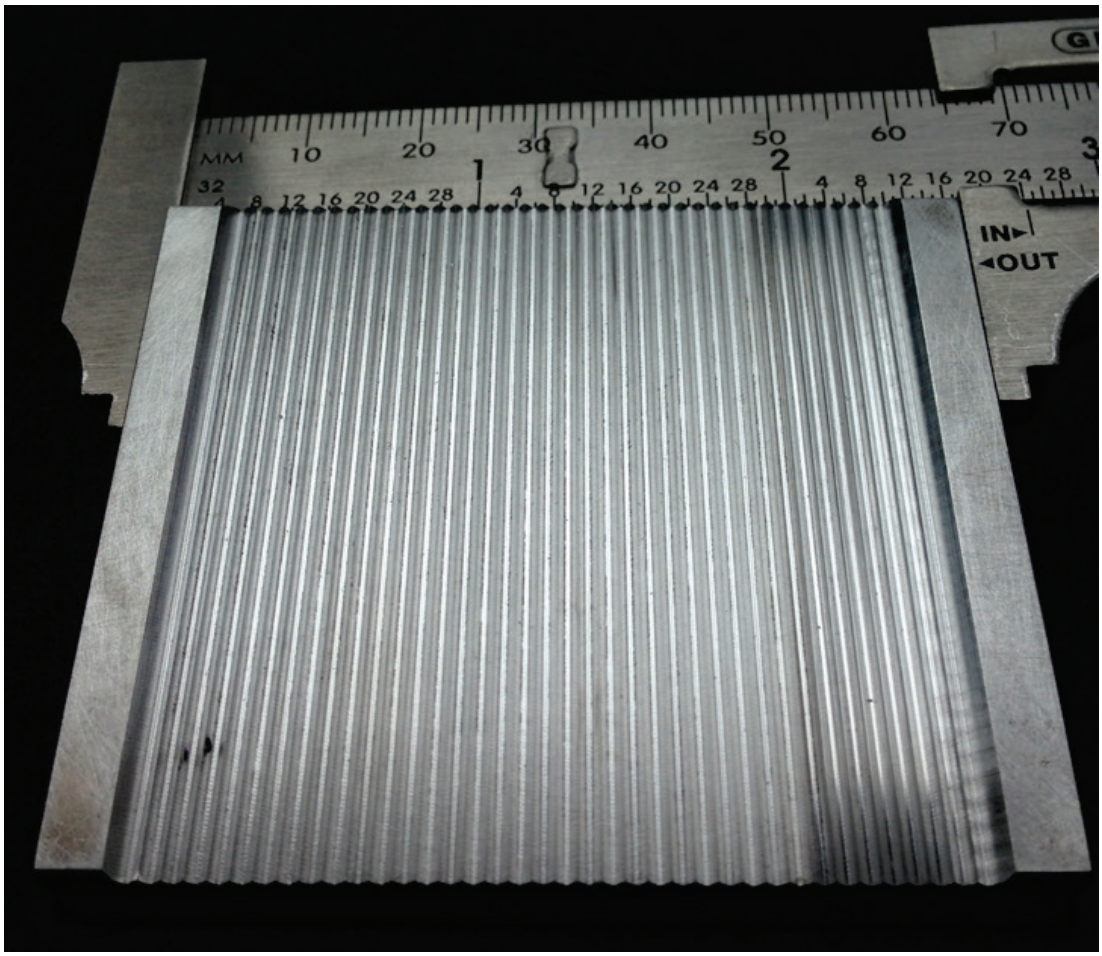

Figure 21. Unpolished aluminum block with 2-mm pitch right-angle grooves.

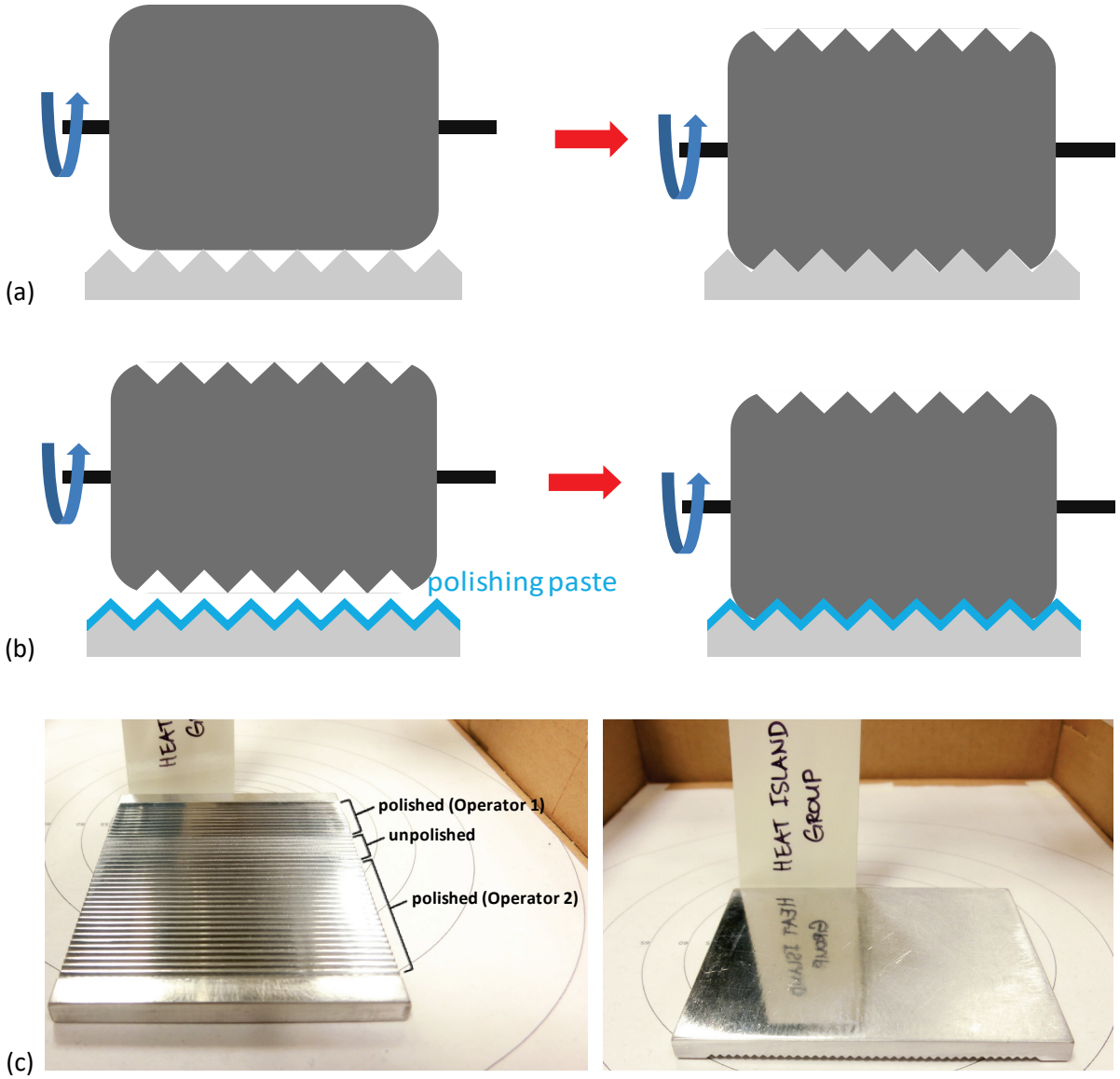

Figure 22. Polishing of right-angle groove aluminum block, showing (a) shaping of the buffing wheel; (b) polishing with paste; and (c) sections of the groove face polished by two different operators (left) and the back face smoothed by one of the operators (right).

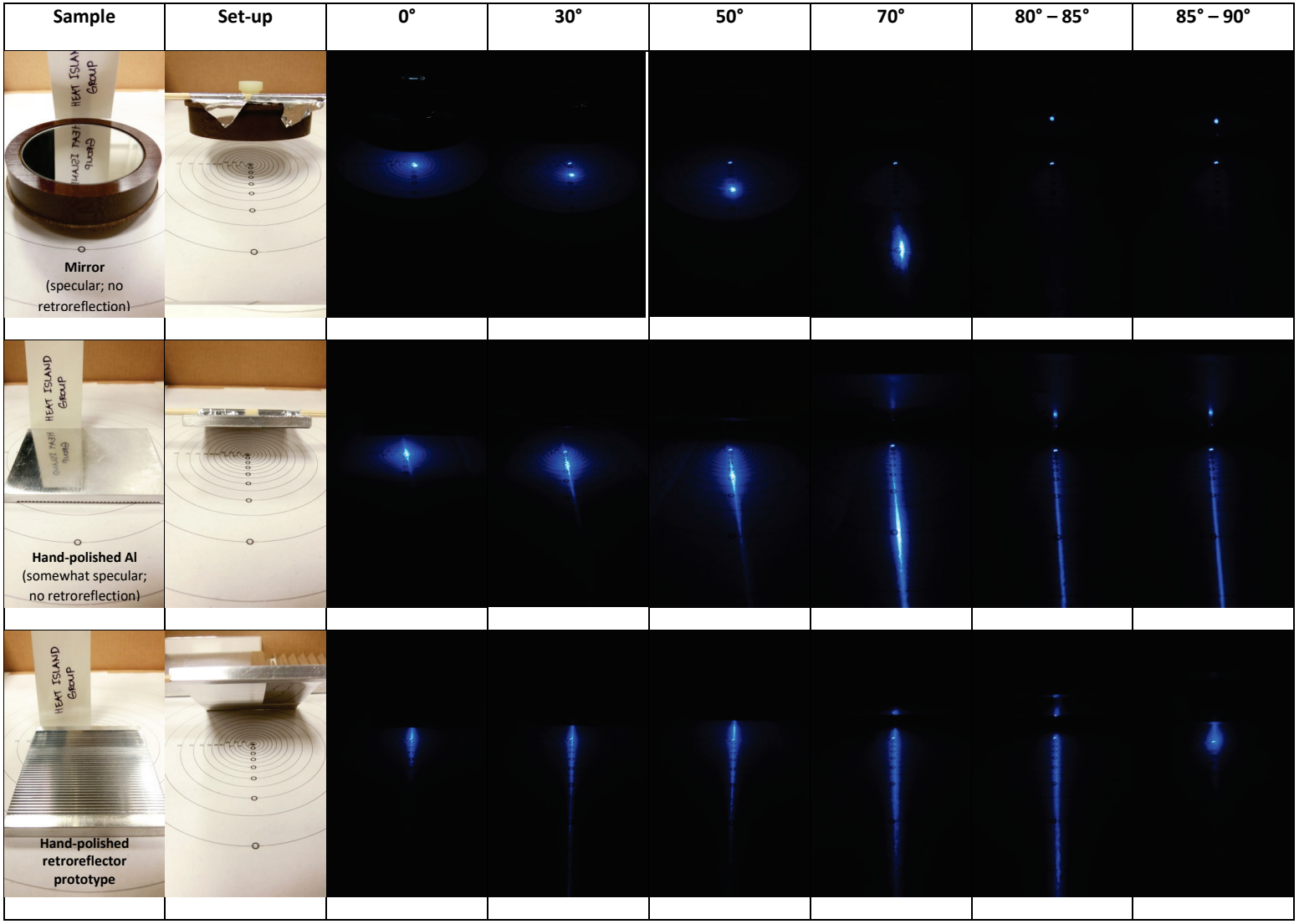

Figure 23. Reflections from three metal surfaces—a mirror reflectance standard, top row; the hand-polished rear face of the aluminum block, middle row; and the hand-polished grooved face of the aluminum block—imaged at incidence angles of 0 to nearly 90° in the simple goniometer.

5.5 Aluminized Mylar film

Aluminized Mylar film has very high specular reflectance across the solar spectrum, with a metal-face specular solar reflectance of about 0.92, and a plastic-face specular solar reflectance of about 0.84 (curves E and F in Figure 6). With the metal face forward, the two-bounce albedo could be $0.92^2 = 0.83$; with the plastic face forward, it could be $0.83^2 = 0.69$. The primary challenges appear to be forming orthogonal folds in the film and keeping the film flat. We are experimenting with creasing the film, stamping the film in a die, and even gluing or taping it to a smooth grooved surface (Figure 24).

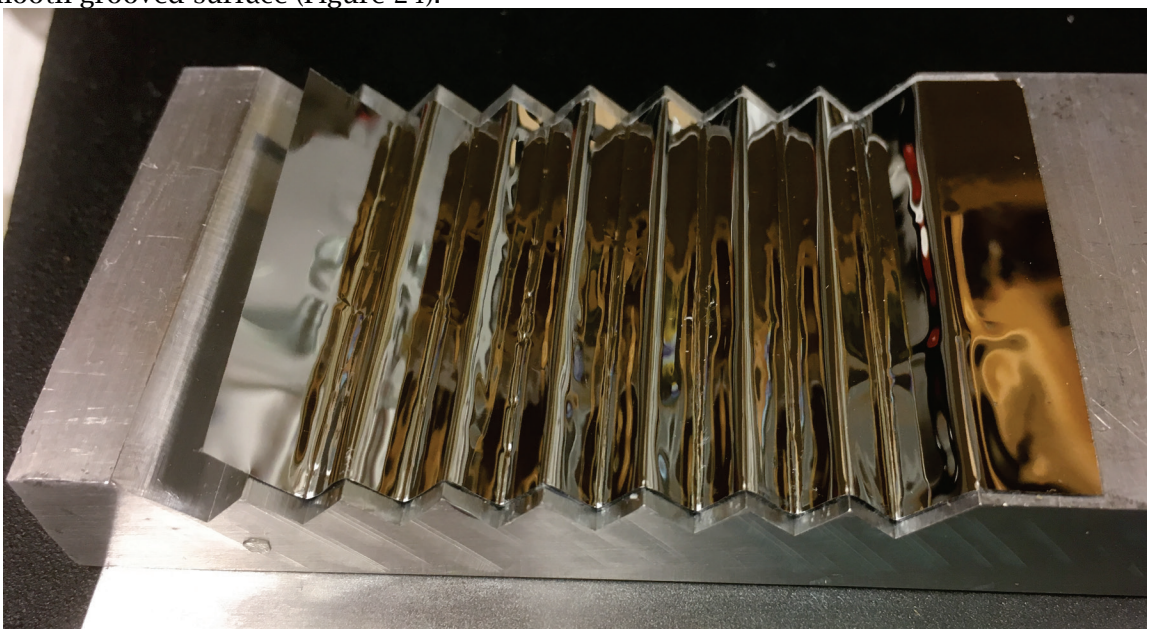

Figure 24. Aluminized Mylar adhered with double-sided tape to aluminum block with 7-mm pitch orthogonal grooves.

6 Summary

Raising a city's albedo increases the fraction of incident sunlight returned to outer space, cooling cities and their buildings. Retroreflective cool walls could improve upon diffusely reflecting cool walls by reflecting incoming beam radiation to the solar disc (if the retroreflection is three dimensional and ideal) or at least upwards (if the retroreflection is two dimensional and/or imperfect). For example, a retroreflective wall with albedo 0.60 could reflect 55% of incident sunlight to the sky, while a Lambertian wall of the same albedo would reflect only 36% of this light skyward.

The greatest challenge in retroreflective wall design appears to be the need to operate at large incidence angles to reflect a substantial portion of incident sunlight. First-principle physics and ray tracing simulations suggest that it will be difficult to achieve this with surfaces that rely on total internal reflection; this appears to be confirmed by solar spectral bi-directional reflectance

intensity measurements made on a prismatic bicycle reflector, and by comparison in a simple goniometer of the intensities of the Fresnel and retro reflections from prismatic retroreflective safety films.

Attempts to produce a two-surface retroreflector with orthogonal mirror grooves by cutting and polishing an aluminum block indicate that residual surface roughness impedes retroreflection. Ongoing efforts focus on shaping aluminized film Mylar, a material with very high specular reflectance across the solar spectrum.

Acknowledgements

We thank Dexerials for measuring the solar spectral bidirectional reflectance intensities of prototype retroreflectors.

References

ASTM. 2017. ASTM D4956-17: Standard Specification for Retroreflective Sheeting for Traffic Control. ASTM International. https://doi.org/10.1520/D4956-17

Duffie JA, Beckman WA. 2006. *Solar Engineering of Thermal Processes*, 3rd ed. Wiley.

Georgia State University. 2005. Hyperphysics tutorial: Fresnel's equations. http://hyperphysics.phy-astr.gsu.edu/hbase/phyopt/freseq.html#c1

Harima T, Nagahama T. 2017. Evaluation methods for retroreflectors and quantitative analysis of near-infrared upward reflective solar control window film — Part I: Theory and evaluation methods. *Solar Energy* 148, 177-192.

Levinson R, Akbari H, Berdahl P. 2010. Measuring solar reflectance—Part I: defining a metric that accurately predicts solar heat gain. *Solar Energy* 84, 1717-1744.

NREL. 2018a. Measurement and Information Data Center Solar Position and Intensity (MIDC SOLPOS) Calculator. National Renewable Energy Laboratory. https://midcdmz.nrel.gov/solpos/solpos.html .

NREL. 2018b. National Solar Radiation Data Base, 1991- 2005 Update: Typical Meteorological Year 3. National Renewable Energy Laboratory. http://rredc.nrel.gov/solar/old_data/nsrdb/1991-2005/tmy3

Polyanskiy MN. 2018. Refractive index database. http://refractiveindex.info

Tu R. 2018. Ray Optics Simulation web application. http://ricktu288.github.io/ray-optics

Energy Research and Development Division

FINAL PROJECT REPORT

Solar-Reflective "Cool" Walls: Benefits, Technologies, and Implementation

Appendix P: Cool Wall Application Guidelines
(Task 6.1 Report)

California Energy Commission
Gavin Newsom, Governor

April 2019 | CEC-500-2019-040-APP

Appendix P:
Cool wall application guidelines (Task 6.1 report)

Ronnen Levinson[1], Pablo Rosado[1], Sharon Chen[1], Hugo Destaillats[1], Haley Gilbert[1], George Ban-Weiss[2], Jiachen Zhang[2], Jan Kleissl[3], Matteo Pizzicotti[3]

[1] Heat Island Group, Lawrence Berkeley National Laboratory

[2] Department of Civil and Environmental Engineering, University of South California

[3] Center for Energy Research, University of California at San Diego

29 June 2018

Abstract

This document introduces the concept of solar-reflective "cool" walls, and provides guidelines for their building- and climate-appropriate use to conserve energy and reduce emissions of greenhouse gases and criteria pollutants across California and the United States. First, it explores the nature of cool walls by answering basic questions, such as what is a cool wall, why choose a cool wall, and where do cool walls save energy. Second, it provides a simple guide to cool wall effects by detailing the energy cost savings (or penalties) that arise from increasing wall reflectance in three common building categories—single-family home, medium office, and retail stand-alone. This includes identification of building vintage, calculating energy cost savings, and gauging cost effectiveness, with worked examples. Third, it provides a detailed guide to these effects by describing the operation and application of the Cool Surface Savings Explorer, a database tool that can report the cool wall and cool roof energy, energy cost, peak power demand, and emission savings simulated for many building categories. Fourth, it discusses how to adjust cool walls savings and penalties to account for shading and reflection by neighboring buildings by applying a "solar availability factor".

1 Introduction

This document introduces the concept of solar-reflective "cool" walls, and provides guidelines for their building- and climate-appropriate use to conserve energy and reduce emissions of greenhouse gases and criteria pollutants across California and the United States. First, it

explores the nature of cool walls through a series of questions & answers. Second, it provides a simple guide to cool wall effects by detailing the energy cost savings (or penalties) that arise from increasing wall reflectance in three common building categories—single-family home, medium office, and retail stand-alone. Third, it provides a detailed guide to these effects by describing the operation and application of the Cool Surface Savings Explorer, a database tool that can report the cool wall and cool roof energy, energy cost, peak power demand, and emission savings simulated for many building categories. Fourth, it discusses how to adjust cool walls savings and penalties to account for shading and reflection by neighboring buildings.

Note that the term “wall” means “exterior wall” throughout this document.

2 Cool wall questions and answers

2.1 What is a cool wall?

A “cool” wall is a wall surface that stays cool in the sun by reflecting sunlight, and by efficiently emitting thermal infrared radiation. Reflective walls and roofs have long been used to cool buildings in hot, sunny climates. For example, Figure 1 shows building walls in Santorini, Greece that have been white-washed (coated with a solution of powdered lime) for high reflectance.

A cool wall exhibits high solar reflectance (fraction of incident sunlight that is reflected; also known as “albedo”) and high thermal emittance (ratio of radiative power emitted by a surface near 300 K [27 ˚C, or 80 ˚F] to that emitted by a black body at the same temperature). High solar reflectance is most important to staying cool in the sun.

Figure 1. Buildings with white-washed walls in Santorini, Greece.

Heat flow through walls can be reduced with insulation, and the warming and cooling of walls can be dampened with massive construction (e.g., thick concrete). Walls can also be cooled by shading. However, we use the term “cool wall” to refer exclusively to an exterior wall surface that employs high solar reflectance to reduce solar heat gain (absorption of sunlight), and high thermal emittance to efficiently reject through emission of thermal infrared radiation some of the solar energy that is absorbed.

2.2 Why choose a cool wall?

Raising wall albedo lowers its surface temperature in the sun, reducing daytime heat flow into the building’s occupied space. In the cooling season, this can save energy in an air-conditioned building, or make an uncooled building more comfortable. In the heating season, increasing wall albedo can also increase heating energy use, or make an unheated building less comfortable.

Depending on building construction, operation, and location, raising wall albedo can either reduce or increase annual energy use, energy cost, and emissions of greenhouse gases, such as carbon dioxide, and criteria pollutants, such as nitrogen oxides (NO_x) and sulfur dioxide (SO_2). It can also decrease peak power demand. Sections 3 and 4 of this document explore these savings (or penalties).

Raising wall albedo also slightly increases the amount reflected to neighboring buildings. This effect is addressed in Section 5.

Making walls more reflective increases the fraction of sunlight incident on urban surfaces that escapes the city, reducing citywide solar heat gain, lowering urban air temperature, and mitigating the urban heat island effect[1]. The urban cooling benefit is explored in the Task 3.2 report: Urban climate impacts of cool walls.

The research team is working to develop incentives for the building- and climate-appropriate use of cool walls. The goal is to recognize cool walls in building standards, such as California's Title 24 and ASHRAE 90.1; green building codes, such as CalGreen, ASHRAE 189.1, and LEED; EPA EnergyStar; and/or utility energy-efficiency rebate programs. These efforts are detailed in the Task 6.3 report: *Advancements in infrastructure development: building standards and incentive programs*.

2.3 Where do cool walls save energy?

Cool walls reduce annual HVAC (heating, ventilation, and air conditioning) energy cost in all California building climate zones (Figure 2) and in U.S. climate zones 1 – 4 (Figure 3). Please see Section 3 for details.

2.4 Is a cool wall like a cool roof?

Yes—a cool wall is the analog of a cool roof. However, the timing and amount of sunlight incident on a wall (vertical) varies by direction, and differs from that on a roof (closer to horizontal); see Table 1 (California) and Table 2 (United States). Walls also tend to be less insulated than roofs, with roughly 50% less resistance to heat flow. The combination of lower insolation (incident solar radiation) and lower thermal resistance tends to make the annual energy cost savings intensity (energy cost savings per unit area of surface modified) upon raising the albedo of all four walls (north, south east, and west) comparable to that from raising roof albedo. This is explored further in Section 3.

[1] The urban heat island effect is the elevation of urban air temperature over that in surrounding rural areas. It is driven in part by the prevalence of dark, dry surfaces in cities.

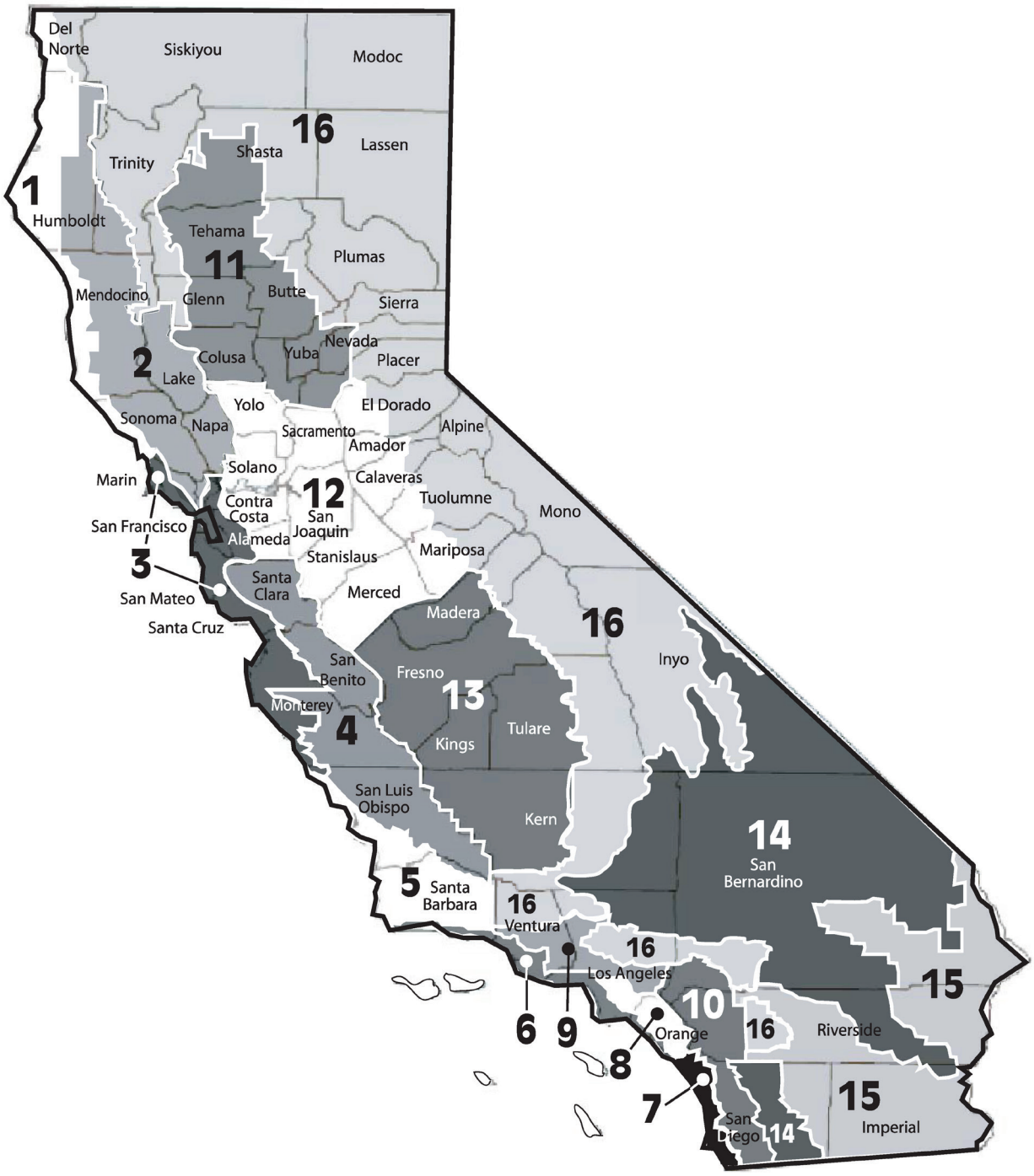

Figure 2. Map of California building climate zones (BCZs), showing zones (1 – 16) and counties.

CZ: City, State

1A: Miami, FL
2A: Houston, TX
2B: Phoenix, AZ
3A: Memphis, TN
3B: El Paso, TX
BU: Burbank, CA
FR: Fresno, CA
3C: San Francisco, CA
4A: Baltimore, MD
4B: Albuquerque, NM
4C: Seattle, WA
5A: Chicago, IL
5B: Boise, ID
6A: Burlington, VT
6B: Helena, MT
7: Duluth, MN
8: Fairbanks, AK

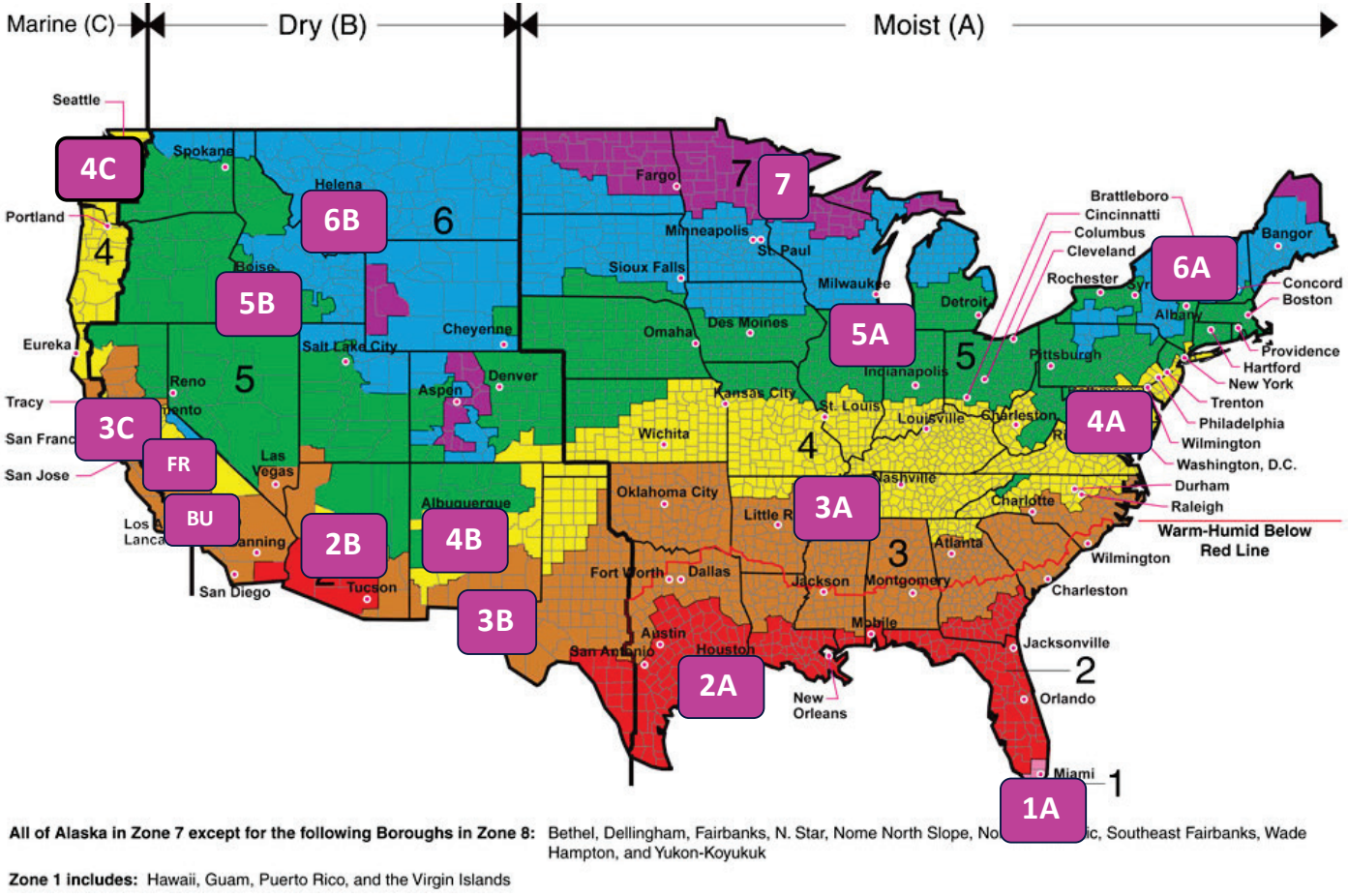

Figure 3. Map of U.S cities representing ASHRAE climate zones 1 – 8, plus two California cities (Burbank and Fresno). Adapted from Briggs et al. (2003a,b).

Table 1. Ratios of daily sunlight over a surface facing north (N), east (E), south (S), or west (W) to daily sunlight over a horizontal (H) roof. The table includes ratios computed for summer days and winter days in the cities representing each California building climate zone (Figure 2).

City or town in California	CACZ	Summer (Jun, Jul, and Aug)				Winter (Dec, Jan, and Feb)			
		N-to-H ratio	E-to-H ratio	S-to-H ratio	W-to-H ratio	N-to-H ratio	E-to-H ratio	S-to-H ratio	W-to-H ratio
Arcata	1	31%	44%	46%	65%	32%	68%	148%	66%
Santa Rosa	2	23%	49%	40%	55%	32%	64%	136%	66%
Oakland	3	24%	45%	40%	55%	29%	61%	139%	65%
San Jose	4	23%	51%	39%	54%	28%	66%	146%	67%
Santa Maria	5	24%	42%	37%	59%	24%	65%	144%	65%
Long Beach	6	25%	43%	36%	59%	25%	59%	134%	62%
San Diego	7	24%	43%	34%	56%	22%	60%	138%	63%
Fullerton	8	25%	47%	36%	56%	26%	61%	137%	64%
Burbank	9	24%	52%	35%	53%	24%	63%	139%	63%
Riverside	10	25%	52%	35%	54%	25%	63%	141%	66%
Beale (for Red bluff) [a]	11	24%	56%	41%	54%	31%	63%	144%	69%
Sacramento	12	23%	57%	39%	54%	32%	61%	139%	68%
Fresno	13	24%	56%	37%	56%	32%	64%	129%	64%
China Lake	14	23%	58%	34%	55%	23%	71%	158%	69%
Palm Springs (for Imperial) [a]	15	26%	57%	34%	57%	24%	66%	148%	68%
Montague (for Mount Shasta) [a]	16	23%	58%	42%	55%	26%	67%	169%	75%
Minimum		**23%**	**43%**	**34%**	**53%**	**22%**	**59%**	**129%**	**62%**
Maximum		**31%**	**58%**	**46%**	**65%**	**32%**	**71%**	**169%**	**75%**

[a] Calculated for town that is near the climate zone's representative city.

Table 2. Ratios of daily sunlight over a surface facing north (N), east (E), south (S), or west (W) to daily sunlight over a horizontal (H) roof. The table includes ratios computed for summer days and winter days in each of the U.S. representative cities (Figure 3).

City, State	USCZ	Summer (Jun, Jul, and Aug)				Winter (Dec, Jan, and Feb)			
		N-to-H ratio	E-to-H ratio	S-to-H ratio	W-to-H ratio	N-to-H ratio	E-to-H ratio	S-to-H ratio	W-to-H ratio
Miami, FL	1A	31%	52%	31%	48%	25%	58%	107%	58%
Houston, TX	2A	29%	54%	33%	50%	29%	57%	114%	64%
Phoenix, AZ	2B	25%	54%	34%	54%	23%	65%	144%	68%
Memphis, TN	3A	27%	53%	39%	54%	27%	64%	136%	64%
El Paso, TX	3B	25%	54%	32%	52%	24%	66%	138%	64%
San Francisco, CA	3C	25%	49%	40%	56%	29%	64%	144%	66%
Baltimore, MD	4A	29%	56%	43%	53%	29%	69%	150%	67%
Albuquerque, NM	4B	26%	58%	36%	50%	22%	65%	153%	69%
Salem, OR	4C	28%	56%	50%	61%	36%	65%	144%	70%
Seattle, WA	4C	28%	55%	53%	57%	37%	68%	157%	70%
Chicago, IL	5A	31%	57%	48%	56%	33%	67%	152%	68%
Peoria, IL	5A	19%	46%	36%	46%	21%	59%	141%	56%
Boise, ID	5B	25%	58%	46%	57%	32%	68%	159%	71%
Burlington, VT	6A	31%	58%	51%	58%	34%	68%	147%	66%
Helena, MT	6B	28%	62%	52%	57%	36%	79%	195%	86%
Duluth, MN	7	28%	55%	51%	58%	32%	72%	176%	72%
Fairbanks, AK	8	42%	79%	77%	61%	38%	131%	323%	69%
Minimum [a]		**19%**	**46%**	**31%**	**46%**	**21%**	**57%**	**107%**	**56%**
Maximum [a]		**31%**	**62%**	**53%**	**61%**	**37%**	**79%**	**195%**	**86%**

[a] Excluding USCZ 8 (Fairbanks, AK).

2.5 Do cool walls help mitigate the urban heat island effect?

Yes. Simulations predict that increasing wall albedo throughout Los Angeles County by 0.4 would lower daily average outside air temperature in the "urban canyon" between buildings by about 0.2 ˚C (0.4 ˚F) in July. This is comparable to (about 84% of) the air temperature reduction provided by the same countywide increase in roof albedo. For details, please see the Task 3.2 report: *Urban climate impacts of cool walls.*

2.6 How do cool walls affect pedestrian comfort?

Simulations predict that in Los Angeles, the mean radiant temperature (MRT)[2] experienced when walking beside a cool wall (albedo 0.60) is about 1 ˚C (1.8 ˚F) higher than that experienced when walking beside a conventional wall (albedo 0.25). The pedestrian's average increase in daytime standard equivalent temperature (SET*)[3] is about 0.4 ˚C (0.7 ˚F). Please see the Task 3.1 report: *Pedestrian mean radiant temperature and thermal comfort* for details.

2.7 Are there specifications for cool walls?

Cool walls are an emerging measure in modern building energy efficiency standards. Cool wall specifications vary substantially across the few standards in which they appear. To wit:

- ASHRAE 90.1-2016: Energy Standard for Buildings Except Low-Rise Residential Buildings (ASHRAE 2016) permits east and west walls to be unshaded in ASHRAE climate zone 0 (hot & tropical) if they have a solar reflectance index (SRI) not less than 29, which would typically correspond to an albedo of at least 0.28.[4]

- 2011 and later editions of ASHRAE 189.1: Standard for the Design of High-Performance Green Buildings (ASHRAE 2011) have for east walls in climate zones 0 – 4 and west walls in climate zones 0 – 6 cool wall provisions similar to those in ASHRAE 90.1-2016.

- Several recent Chinese building energy efficiency standards assign extra thermal resistance to reflective walls, reducing the need for physical wall insulation. Some offer this trade-off only for very high wall albedos (at least 0.80), while others provide a thermal resistance benefit that scales with wall albedo (Ge and Levinson 2016).

As a starting point for discussion, we offer the following observations about wall reflectance and wall albedo. First, in North America, walls come in a wide color palette, from dark to light.

---

[2] Mean radiant temperature (MRT) is defined as the uniform surface temperature of an imaginary enclosure in which the human body will exchange the same amount of radiant heat energy as in the actual non-uniform enclosure.

[3] SET* is defined as the air and radiant temperature of a standard isothermal environment that would cause the same thermal stress to the human body as the test environment.

[4] SRI is an artificial temperature index that compares the surface temperature of a test roof to that of black roof (solar reflectance 0.05, thermal emittance 0.90, SRI 0) and that of a bright-white roof (solar reflectance 0.80, thermal emittance 0.90, SRI 100) (ASTM 2011). It is designed for a wall-insulated horizontal surface, and should not be applied to walls. However, under the medium wind speed conditions commonly used to compute SRI, a well-insulated horizontal surface with solar reflectance 0.28 and thermal emittance 0.90 would have an SRI of 29.

For example, Figure 5 shows a recently completed apartment complex in Berkeley, CA with both white walls and dark brown walls. That said, black walls and bright-white walls seem uncommon to the authors. Second, despite entertaining reports of their abilities to toast passersby (Schiler and Valmont 2005), shiny bare-metal walls, such as that shown in Figure 6, are also unusual.

Third, Table 3 combines wall product albedo measurements made at Berkeley Lab (Figure 4) with our engineering judgement to crudely relate albedo to color. It suggests that after rounding albedos to the nearest 0.05, conventionally pigmented dark and dark-to-medium colors will have albedos 0.10 to 0.40; intermediate-performance, "cool" versions of these colors that use spectrally selective pigments[5] will have albedos 0.30 to 0.60; a conventionally pigmented off white or dull white surface will have albedo 0.60; and a conventionally pigmented bright white surface will have albedo 0.80.

[5] More about the design of spectrally selective, "cool colored" surfaces can be found in Levinson et al. (2007).

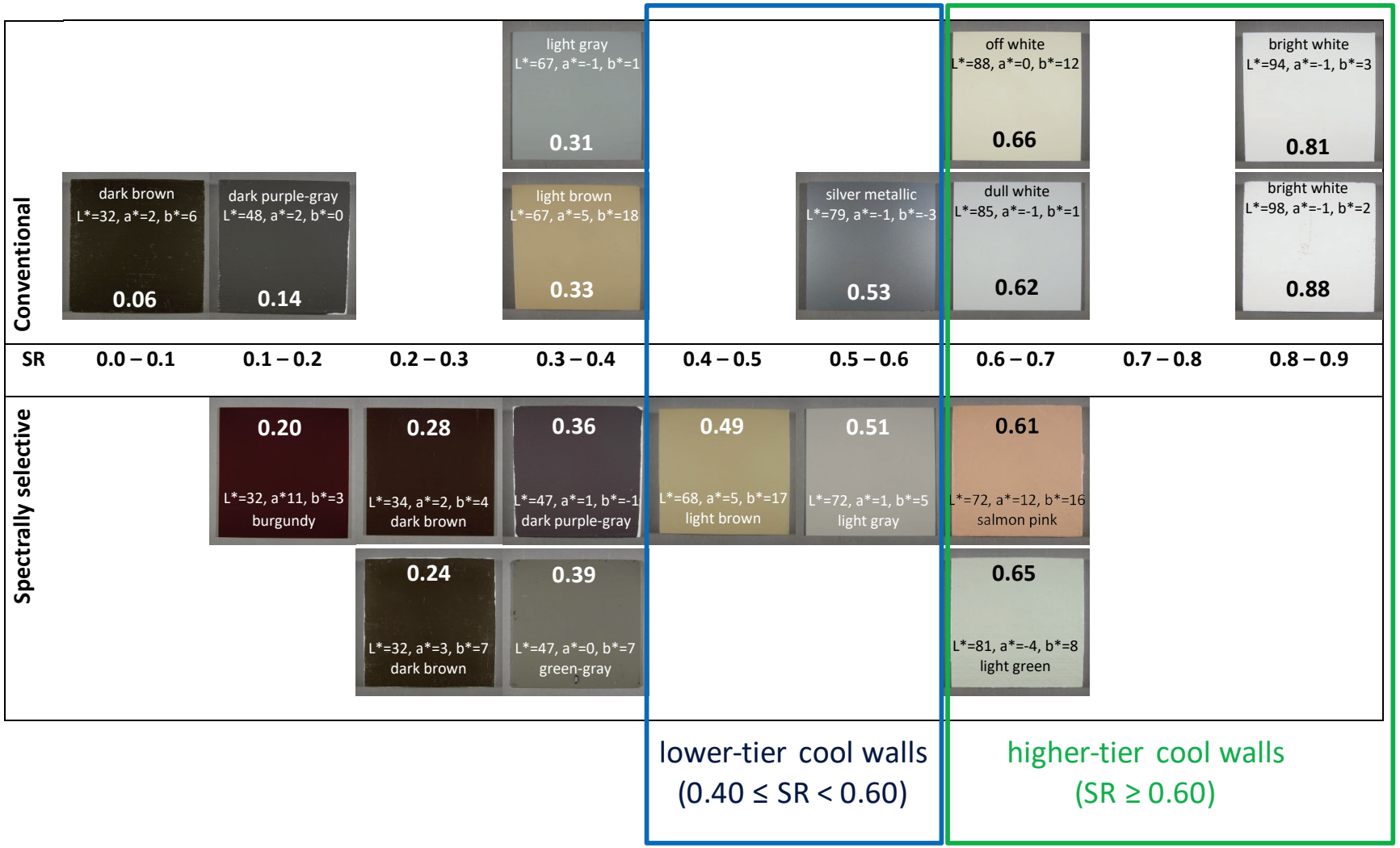

Figure 4. Initial images and radiative properties of some wall products characterized by LBNL, including AM1.5GV (air mass 1.5 global vertical) solar reflectance (SR) and CIELAB color coordinates (L*, a*, b*) computed with D65 illuminant and 10° observer. Specimens in upper group are colored with conventional pigments, while those in the lower group are colored with spectrally selective pigments ("cool colors").

Table 3. Approximate relationship between color and albedo of wall products, assuming that half of sunlight arrives in the near-infrared spectrum. Values serve only to provide general guidance and should not be quoted to more than one decimal place.

Color	Albedo with conventional pigmentation[a]	Albedo with intermediate-performance "cool color" pigmentation[b]	Albedo with high-performance "cool color" pigmentation[c]
Black	0.05	0.28	0.40
Dark	0.10 to 0.20	0.30 to 0.35	0.43 to 0.48
Dark-to-medium	0.20 to 0.40	0.35 to 0.45	0.48 to 0.58
Medium-to-light	0.40 to 0.50	0.45 to 0.50	0.58 to 0.63
Light (off white or dull white)	0.60	NA [d]	0.68
Bright white	0.80	NA	NA

[a] Assumes broadband reflectance N in the near-infrared spectrum (0.7 – 2.5 μm) is equal to broadband reflectance V in the visible spectrum (0.4 – 0.7 μm).

[b] Assumes N = 0.50.

[c] Assumes N = 0.80 for bright-white and N = 0.75 for all other colors.

[d] Not applicable (NA) because the near-infrared reflectance in the conventional formulation exceeds that in the cool-color formulation.

From these observations, we could generate typical wall albedos as follows:

- A black wall is assigned an albedo of 0.05.
- A conventionally colored wall (dark or dark-to-medium color; conventional pigmentation) is assigned an albedo of 0.25 (midway between 0.10 and 0.40).
- A cool colored wall (dark or dark-to-medium color; intermediate-performance cool-color pigmentation) is assigned an albedo of 0.40 (a bit past midway between 0.30 and 0.45).
- A light-colored wall (off white or dull white) is assigned an albedo of 0.60.
- A bright-white wall is assigned an albedo of 0.80.

Assuming that few walls will be black, bright white, or bare metal, we propose the following conventional and cool wall specifications for modeling cool wall effects.

- A warm wall (baseline scenario) is assigned albedo 0.25 (conventionally colored) and thermal emittance 0.90.

- A lower-tier cool wall (lower-performance cool wall scenario) is assigned albedo 0.40 (cool colored) and thermal emittance 0.90.

- A higher-tier cool wall (higher-performance cool wall scenario) is assigned albedo 0.60 (light colored) and thermal emittance 0.90.

We further propose that in building energy efficiency standards, green building programs, and utility incentive programs, a product with an aged thermal emittance of at least 0.75 (meaning not bare metal) could qualify as a lower-tier cool wall with aged albedo $0.40 \leq \rho < 0.60$, and as a higher-tier cool wall with aged albedo $\rho \geq 0.60$.

Figure 5. White walls and dark brown walls on apartment buildings in Berkeley, CA.

Figure 6. White wall (left) and bare stainless-steel wall (right) on the Berkeley Art Museum and Pacific Film Archive in Berkeley, CA.

2.8 How can I find a cool wall product?

Appearance is a reasonable first indicator of albedo, in the sense that when conventionally pigmented, dark surfaces tend to have lower albedo and light surfaces tend to have higher albedo. Light-colored exterior wall paints are widely available.

However, about half of the radiation in sunlight arrives as invisible near-infrared (NIR) light. Near-infrared reflectance can deviate strongly from visible reflectance. For example, a natural red clay roofing tile typically reflects about 20% of visible sunlight, 60% of NIR sunlight, and about 40% of all sunlight. Therefore, a cool wall product rating system analogous to the cool roof product rating system provided by the Cool Roof Rating Council (CRRC) is needed.

2.9 How might a cool wall rating system compare to the

existing cool roof rating system?

The process for rating wall products could closely mirror that for roofing products, with four minor differences. First, wall products would be oriented vertically, rather than at a 5° or 45° tilt, during the natural exposure period. Second, the three-year natural exposure period used for roofing products may or may not be ideal for wall products; ongoing natural exposure testing at the CRRC's three test sites will help determine the optimal duration. (See the Task 4.2 report: *Natural exposure of wall products*, for details.)

Third, wall-product solar reflectance should be measured using a solar spectral irradiance representative of that incident on a vertical wall. The Task 4.1 report: *Metrics and methods to assess cool wall performance* identifies a suitable irradiance, and a solar reflectance based on this irradiance can be measured with the Devices & Services Solar Spectrum Reflectometer, version 6, following a minor upload to its firmware. Fourth, the laboratory aging practice at the heart of the CRRC's Rapid Ratings program has yet to be adapted to wall products. Thus, Rapid Ratings would not be immediately available.

2.10 Will cool walls lose reflectance over time?

Early results indicate that walls soil less than roofs. The research team has been naturally exposing wall materials at three sites in California (Berkeley, Fresno, and Los Angeles) since March 2016, and at three sites across the U.S. (Phoenix, AZ; Cleveland, OH; and Miami, FL) since August 2016 (Figure 7). After 24 months of California exposure and 12 months of U.S. exposure, the albedos of a majority of the tested materials fell by about 0.00 - 0.05 (Figure 8). A prior study found that field-applied *roof* coatings on near-horizontal substrates experienced first-year albedo losses of up to about 0.25.

California exposure will continue through April 2018 (2 years), while U.S. exposure will continue through August 2021 (5 years). More detail is available in the Task 4.2 report: *Natural exposure of wall products*.

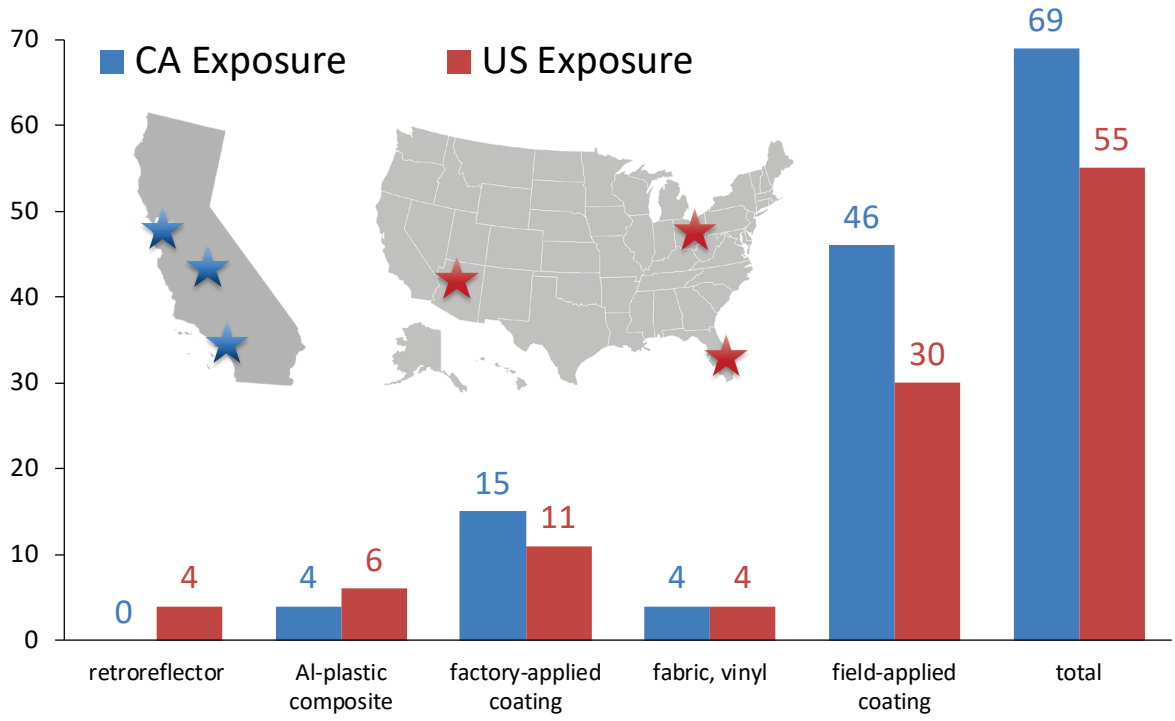

Figure 7. Distribution by type of wall materials being exposed across California (CA) and the United States (US).

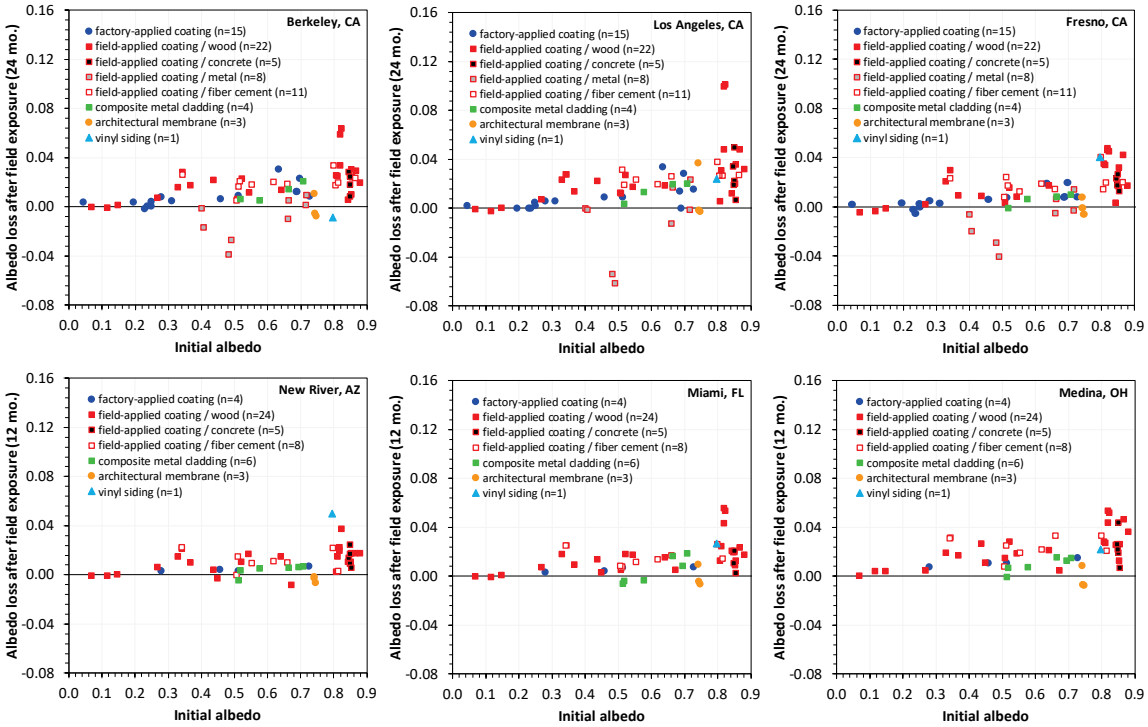

Figure 8. Decreases in albedos of tested materials exposed for 24 months across California (top row) and for 12 months across the U.S. (bottom row).

2.11 Do cool walls products cost more than conventional wall products?

Since color does not appear to affect the price of conventionally pigmented paints, it should be possible to choose a higher-tier, light-colored cool paint instead of a warm paint at no extra cost. We do not yet have data on the cost premium for substituting a lower-tier, spectrally selective (cool) dark paint for a warm paint. However, we estimate the premium as follows.

The median wet-film pigment volume concentration (PVC) in commercial artist paints surveyed by Levinson et al. (2005) was 7% (range 3 to 22%). The median density of their pigments was 3.3 g/mL (range 1.4 to 5.2 g/mL). Using these median values, 1 L of wet paint would contain 1000 mL × 7% × 3.3 g/mL = 231 g of pigment, and a U.S. gallon (3.79 L) of wet paint would contain 0.875 kg of pigment.

The median price of spectrally selective (cool) red, green, brown, and black inorganic pigments used by Levinson et al. (2016) to color roofing granules was US$18.6 per kg (range $7.3 to $30.4 per kg), while the cost of a nonselective (conventional) inorganic pigment was $1 per kg. Relative to the conventional pigment, the cost premium for the median-price cool pigment would be $17.6 per kg. At 0.875 kg of pigment per gallon, the cost premium per gallon of paint using the median-price cool pigment would be $15.4. The premium for a gallon of paint based on the lowest values of PVC (3%), pigment density (1.4), and pigment cost premium ($6.3/kg) would be $2.2, while that based on the highest values of PVC (22%), pigment density (5.2 g/mL), and pigment cost premium would be $60.2. Thus, substituting spectrally selective pigments for conventional pigments in paint would yield a median cost premium per gallon of about $15, with a range of about $2 to $60.

3 Simple guide to cool-wall effects on an isolated building

Raising wall albedo can reduce the need for space cooling and increase the need for space heating over the course of the year. One way to assess the net annual benefit (or penalty) of raising wall albedo is to simulate a building's annual heating, ventilation (a.k.a. fan), and air conditioning (HVAC) site energy uses with a conventional wall (base case), and then again with a cool wall (test case).

3.1 Identifying vintage

This section focuses on energy costs savings for three vintages (new, older, oldest) of three common categories of buildings: single-family home, medium, office and retail stand-alone (Figure 9). In the California simulations, new buildings comply with the 2016 edition of California's Title 24 building energy efficiency standards; older buildings meet 1998 Title 24; and oldest buildings follow pre-1978 construction practices. In the U.S. simulations, new

buildings comply with the International Energy Conservation Code (IECC) (residential) or ASHRAE 90.1 (commercial) building energy efficiency standards in effect in each state as of 2016; older and oldest residential buildings follow 1980s and pre-1980 construction practices, respectively; older commercial buildings comply with ASHRAE 90.1-1989; and oldest commercial buildings follow pre-1980 construction practices. Prototypes and simulations are detailed in the Task 2.1 report: *Simulated HVAC energy savings in an isolated building.*

Single-family home (2 floors; footprint 110 m²)	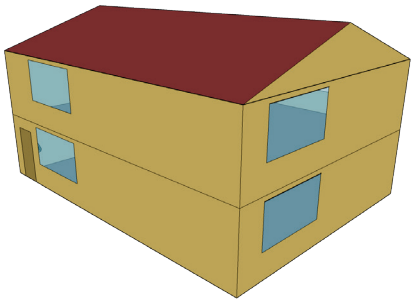
Medium office (3 floors; footprint 1,660 m²)	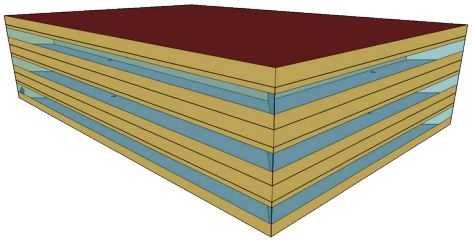
Retail stand-alone (1 floor; footprint 2,290 m²)	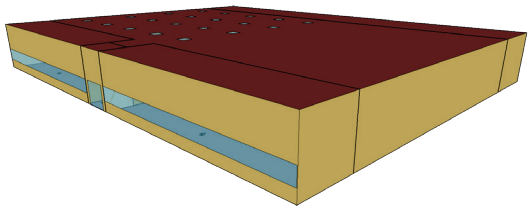

Figure 9. Sketches of the single-family home, medium office, and retail stand-alone building prototypes.

The cities representing the California and U.S. climate zones are listed in Table 4 and Table 5, respectively. A list of California building climate zones by ZIP code is available in reference CEC (2018).

Table 4. Cities or towns in California used to represent its 16 building climate zones.

City or town	CACZ		City or town	CACZ
Arcata	1		Burbank	9
Santa Rosa	2		Riverside	10

Oakland	3		Red Bluff	11
San Jose	4		Sacramento	12
Santa Maria	5		Fresno	13
Long Beach	6		China Lake	14
San Diego	7		Imperial	15
Fullerton	8		Mount Shasta	16

Table 5. Cities in United States used to represent ASHRAE climate zones.

City	State	ASHRAE CZ
Miami	Florida	1A
Houston	Texas	2A
Phoenix	Arizona	2B
Memphis	Tennessee	3A
El Paso	Texas	3B
San Francisco	California	3C
Baltimore	Maryland	4A
Albuquerque	New Mexico	4B
Salem [a]	Oregon	4C
Seattle [b]	Washington	4C
Chicago [a]	Illinois	5A
Peoria [b]	Illinois	5A
Boise	Idaho	5B
Burlington	Vermont	6A
Helena	Montana	6B
Duluth	Minnesota	7
Fairbanks	Alaska	8

[a] For commercial prototypes only.

[b] For residential prototypes only.

3.2 Calculating energy cost savings

Whole-building absolute energy saving are obtained by subtracting test-case energy use from base-case energy use. The cooling energy savings will be positive (or zero, if cooling is never needed); heating energy savings will be negative (or zero, if heating is never needed); and fan energy savings can have any sign. Negative heating savings can also be expressed as a positive heating penalty.

The heating gas savings (if gas heat is used) can be multiplied by the local price of natural gas to calculate heating gas energy cost savings, while each electricity savings (for electric cooling, ventilation, and/or electric heating) can be multiplied by the local price of electricity to compute the corresponding electricity cost savings.

Normalizing whole-building annual energy cost savings ($) to the wall area modified (m²) yields annual energy cost savings intensity ($/m²). This value can be used to estimate whole-building annual energy cost savings for an arbitrary modified wall area, or to assess the cost effectiveness of a cool wall product. Figure 10 shows annual HVAC energy cost savings intensities attained by raising the albedo of all walls, or raising the albedo of the roof, in new, older, and oldest vintages of single-family home, medium, office and retail stand-alone buildings across California. Figure 11 shows the same results across the United States.

Dividing the whole-building annual energy cost savings ($) by the whole-building base-case annual energy cost ($) yields the whole-building annual energy cost savings fraction (dimensionless). The whole-building annual HVAC energy cost savings fraction gauges the extent to which raising wall albedo reduces HVAC energy expenditure. Figure 12 and Figure 13 show whole-building annual energy cost savings fractions across California and the United States, respectively.

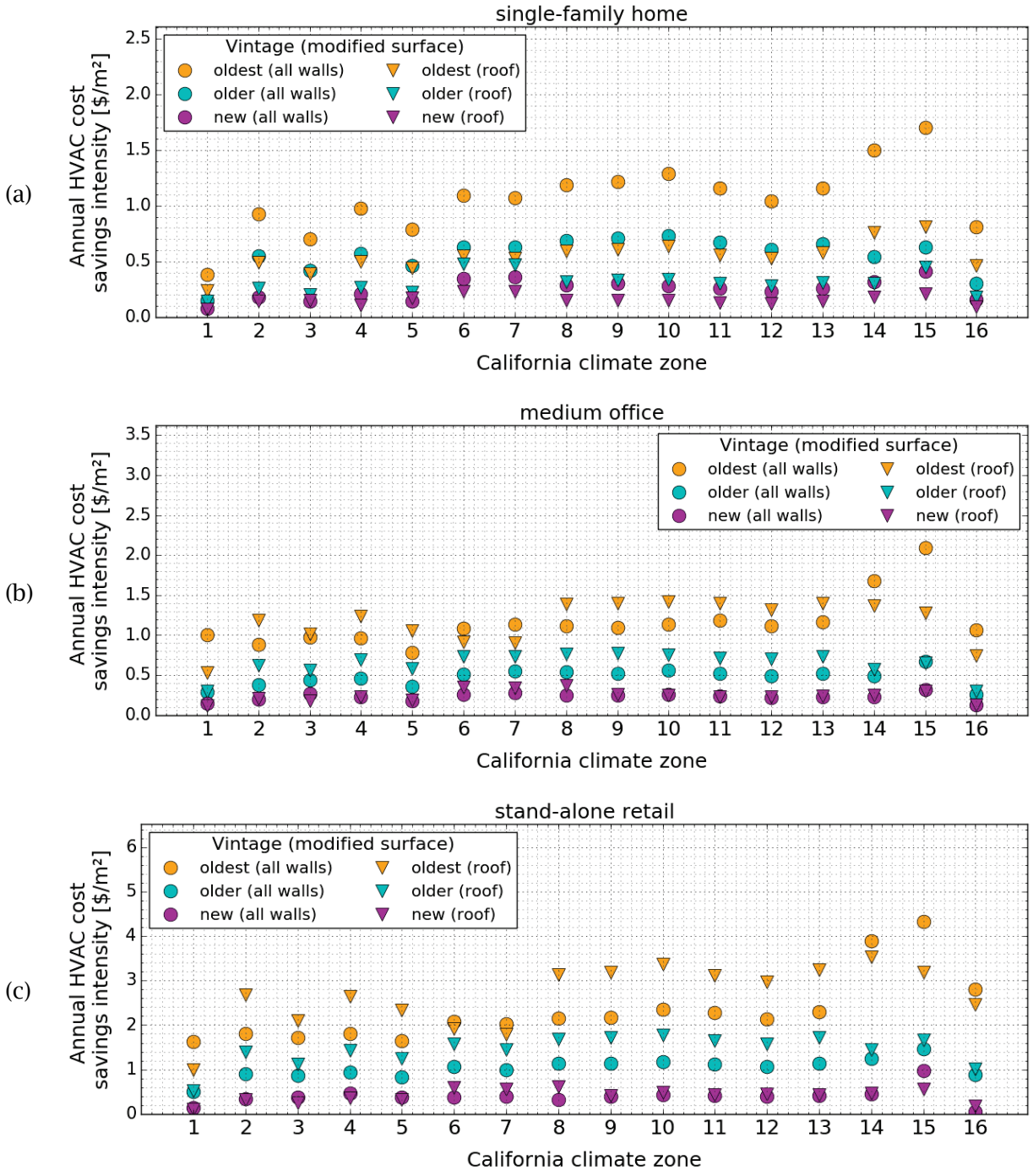

Figure 10. Annual HVAC energy cost savings intensity by vintage and by *California climate zone* for the (a) single-family home, (b) medium office, and (c) retail stand-alone. The plots compare the savings intensity from increasing the albedo of all walls by 0.35 to the savings intensity from increasing the roof albedo by 0.30 (residential) or 0.40 (commercial).

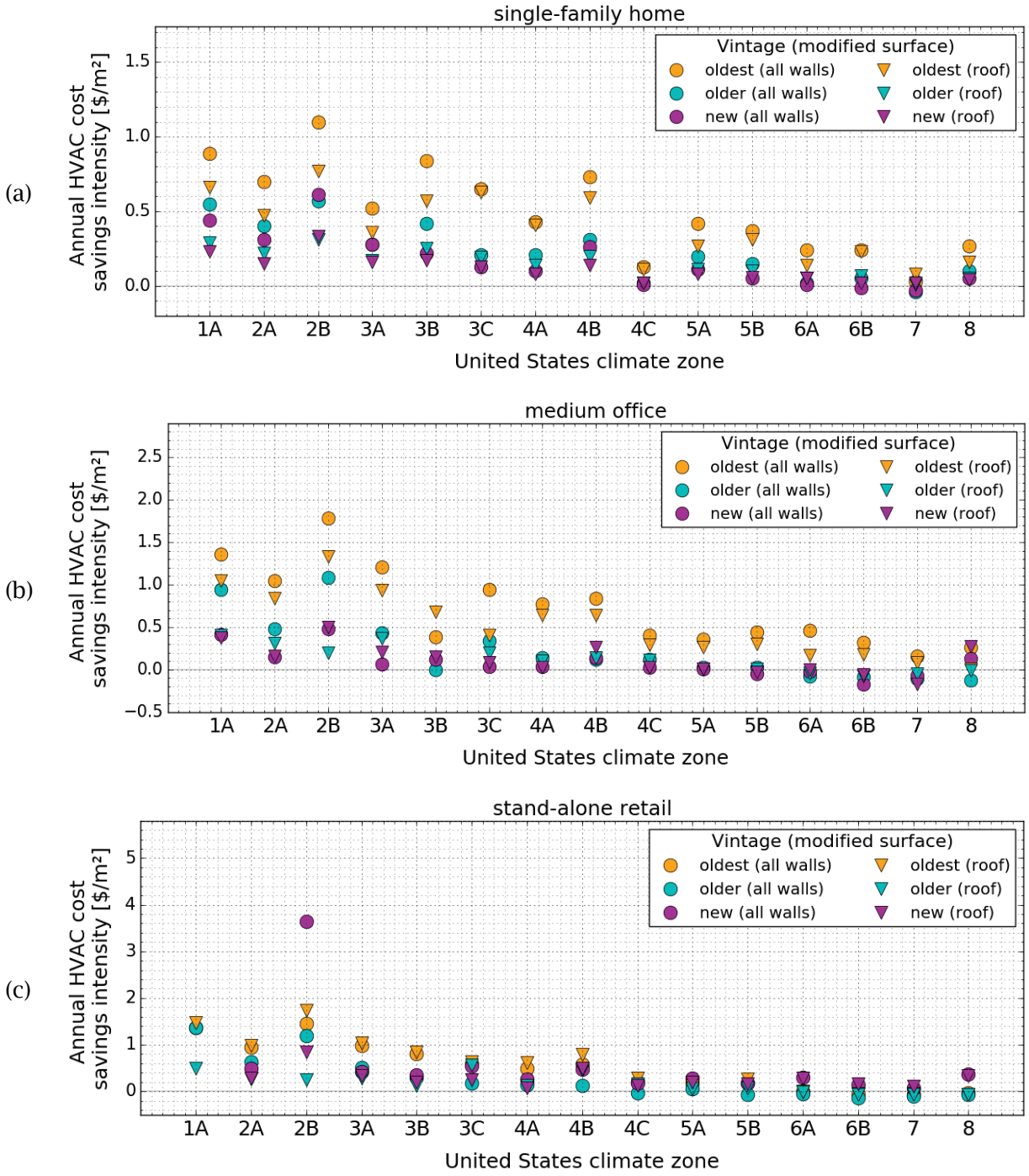

Figure 11. Annual HVAC energy cost savings intensity by vintage and by U.S. climate zone for the (a) single-family home, (b) medium office, and (c) retail stand-alone. The plots compare the savings intensity from increasing the albedo of all walls by 0.35 to the savings intensity from increasing the roof albedo by 0.30 (residential) or 0.40 (commercial). Panel (c) omits savings for new retail stand-alone in USCZ 1A (Miami) because modifying the albedo of its back wall yielded unrealistically large changes in annual fan energy use.

(a)

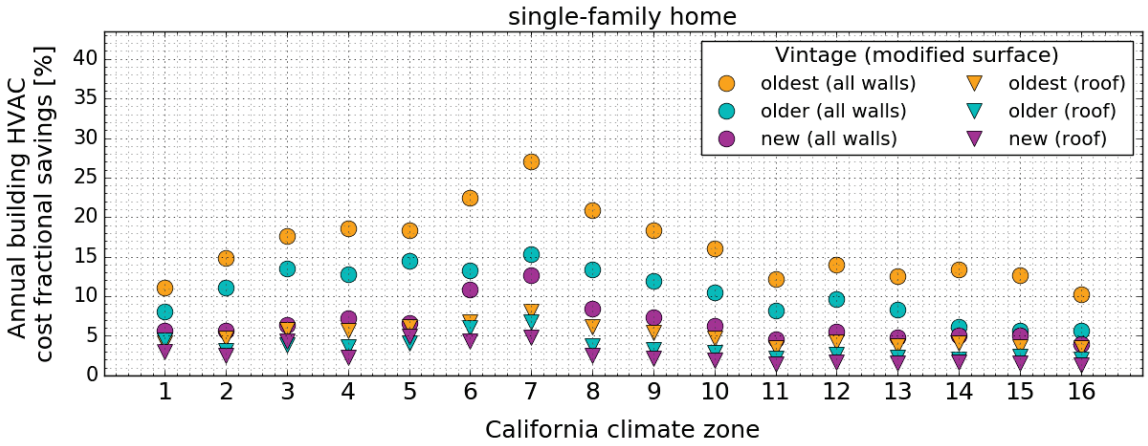

(b)

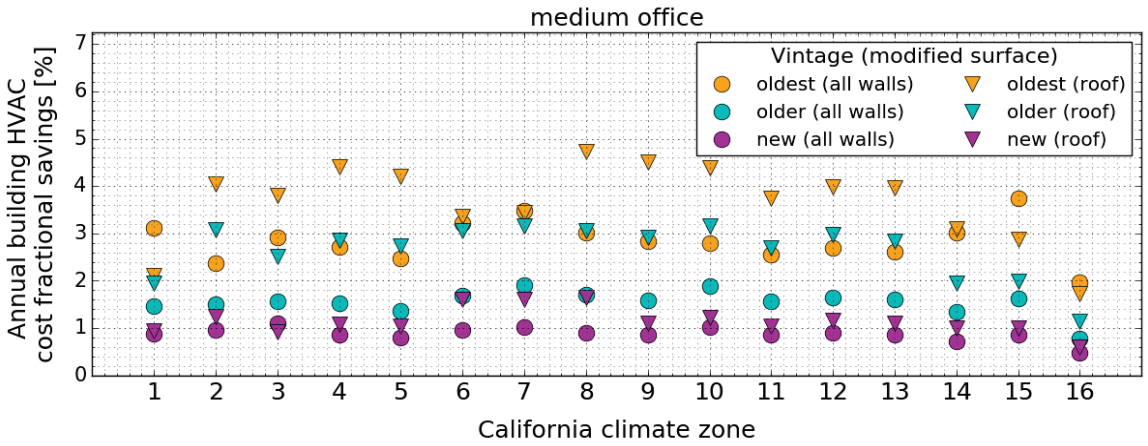

(c)

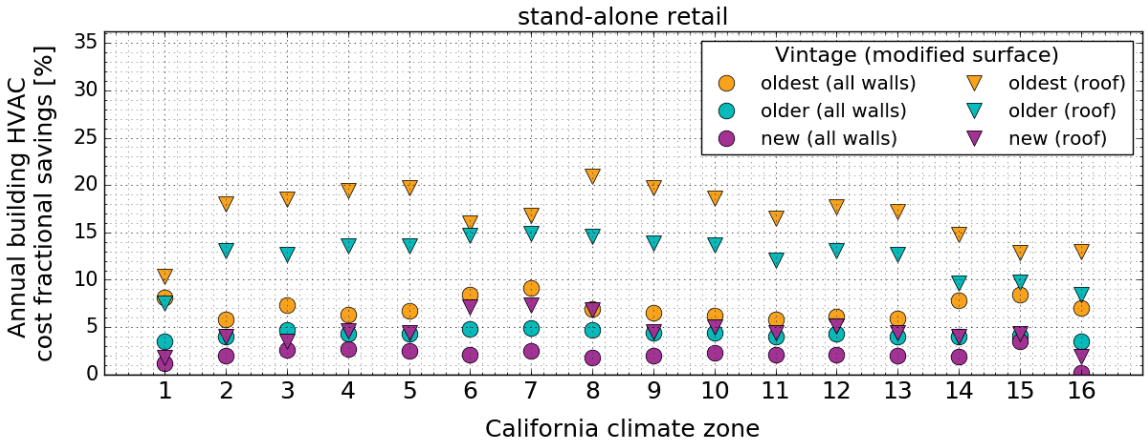

Figure 12. Annual HVAC energy cost fractional savings by vintage and by California climate zone for the (a) single-family home, (b) medium office, and (c) retail stand-alone. The plots compare the savings intensity from increasing the albedo of all walls by 0.35 to the savings intensity from increasing the roof albedo by 0.30 (residential) or 0.40 (commercial).

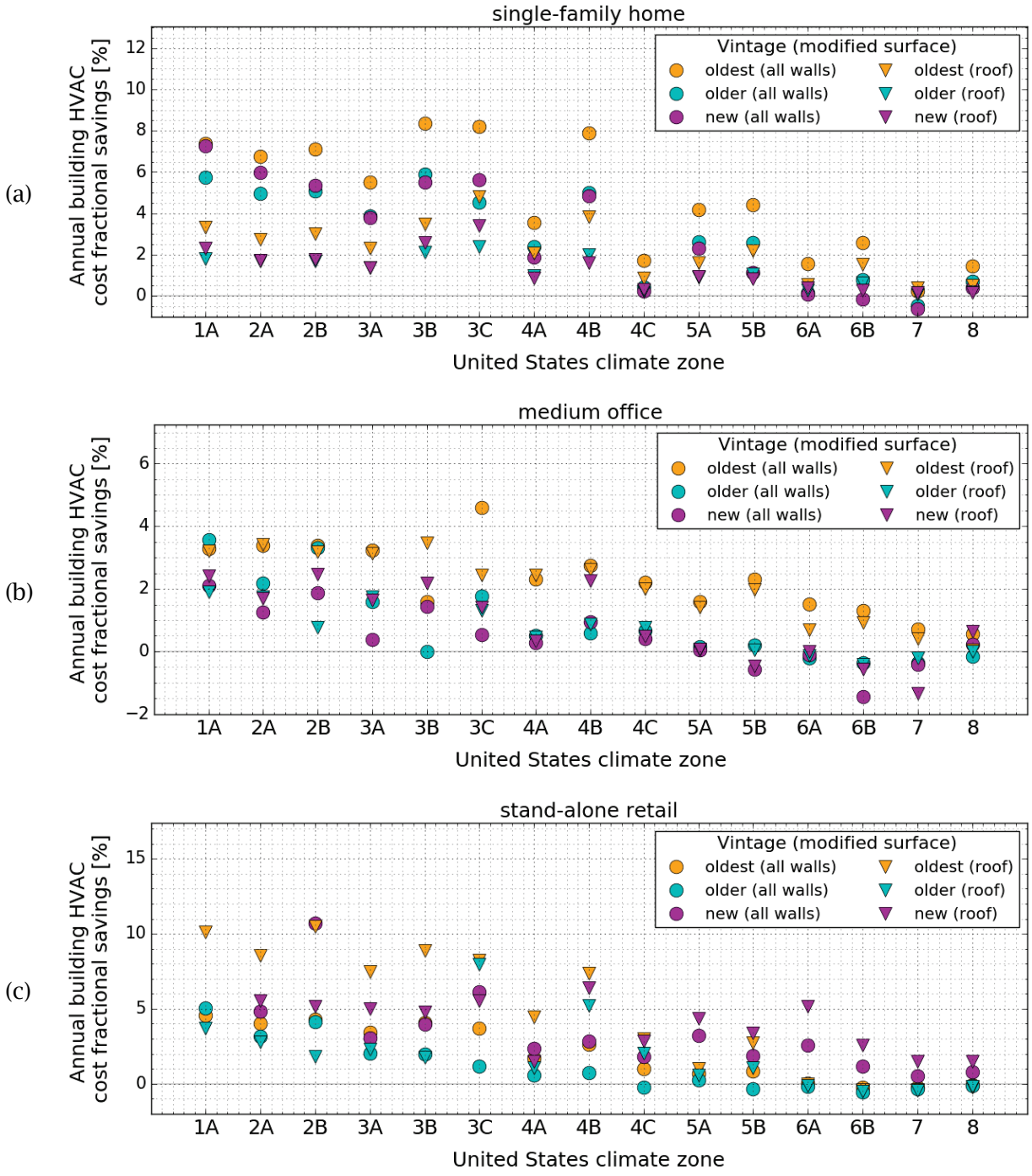

Figure 13. Annual HVAC energy cost fractional savings by vintage and by U.S. climate zone for the (a) single-family home, (b) medium office, and (c) retail stand-alone. The plots compare the savings intensity from increasing the albedo of all walls by 0.35 to the savings intensity from increasing the roof albedo by 0.30 (residential) or 0.40 (commercial). Panel (c) omits savings for new retail stand-alone in USCZ 1A (Miami) because modifying the albedo of its back wall yielded unrealistically large changes in annual fan energy use.

3.3 Gauging cost effectiveness

Annual HVAC (cooling + heating + fan) energy cost savings intensity can be used to evaluate the cost effectiveness of selecting a cool wall product instead of a conventional wall product. Two common gauges of cost effectiveness are

- simple payback time, or ratio of product cost premium per unit area to annual energy cost savings intensity; and
- life-cycle cost savings intensity, or present value (PV) of annual energy cost savings intensity over the product's service life minus initial product cost premium per unit area.

If the product cost premium is zero, the simple payback time will be zero, and the life-cycle cost savings intensity will be more helpful. Both gauges apply if the cool product costs more than the conventional product.

Given a real (inflation-adjusted) annual rate of return r, the PV of N years of constant annual energy cost savings intensity c is $b \times c$, where PV multiplier

$$b \equiv \sum_{i=1}^{N}(1+r)^{-i} = [1-(1+r)^{-N}]. \quad (1)$$

(Levinson and Akbari 2010). The PV multiplier b increases with service life N, and decreases with real rate of return r (Table 6).

Table 6. Present value multiplier b (ratio of present value of lifetime energy cost savings) computed from Eq. (1) for various combinations of product service life N (years) and real (inflation-adjusted) annual rate of return r.

N (years)	r=1%	r=3%	r=5%	r=7%
5	4.9	4.6	4.3	4.1
10	9.5	8.5	7.7	7.0
15	13.9	11.9	10.4	9.1
20	18.0	14.9	12.5	10.6
25	22.0	17.4	14.1	11.7
30	25.8	19.6	15.4	12.4

3.4 Applying the savings tables

Table 7 details annual HVAC energy cost savings intensity ($/m²) in each California climate zone (Figure 2) by building category, vintage, and surface modified, while Table 8 does the same for annual whole-building HVAC energy cost savings fraction (%). Annual HVAC energy cost

savings intensity and annual whole-building HVAC energy cost savings fraction in U.S. climates (Figure 3) are detailed in Table 9 and Table 10, respectively.[6]

These tables present cool wall savings from increasing wall albedo by 0.35 (to 0.60 from 0.25) in both residential and commercial buildings, and cool roof savings from increasing roof albedo by 0.30 (to 0.40 from 0.10) in residential buildings and by 0.40 (to 0.60 from 0.20) in commercial buildings. Results average the savings obtained when the long-axis of the building runs east-west with those calculated when the axis runs north-west.[7]

[6] San Francisco represents U.S. climate zone 3C, but also lies within California climate zone 3. Since the state's Title 24 standards supersede the ASHRAE and IECC standards, we recommend using the California climate zone 3 for this city.

[7] Readers interested in results based on a single orientation of the building's long axis (east-west or north-south) should use instead the Cool Surface Savings Explorer (Section 4).

Table 7. Annual HVAC energy cost savings intensity ($/m²) by California climate zone (CACZ 01 – 16), building vintage (new, older, oldest), and surface(s) modified (R = roof; N = north wall; E = east wall; S = south wall; W = west wall; N E S W = all four walls), tabulated for (a) single-family home, (b) medium office, and (c) retail standalone buildings. Results are mean of values for N-S and E-W orientations of the building's long axis.

(a) Single-family home annual HVAC energy cost savings intensity ($/m²).

	new						older						oldest					
	R	**N**	**E**	**S**	**W**	**N E S W**	**R**	**N**	**E**	**S**	**W**	**N E S W**	**R**	**N**	**E**	**S**	**W**	**N E S W**
CACZ_01	0.12	0.05	0.14	0.10	0.07	0.08	0.25	0.09	0.24	0.22	0.13	0.16	0.41	0.20	0.44	0.69	0.49	0.39
CACZ_02	0.24	0.11	0.28	0.22	0.18	0.19	0.45	0.31	0.68	0.72	0.58	0.56	0.85	0.53	1.03	1.29	1.16	0.95
CACZ_03	0.27	0.07	0.22	0.18	0.11	0.14	0.35	0.22	0.56	0.61	0.41	0.43	0.67	0.36	0.82	1.09	0.80	0.71
CACZ_04	0.19	0.11	0.30	0.27	0.20	0.22	0.46	0.29	0.73	0.81	0.58	0.58	0.87	0.49	1.13	1.45	1.11	1.00
CACZ_05	0.29	0.07	0.23	0.19	0.10	0.14	0.39	0.22	0.60	0.71	0.43	0.47	0.76	0.38	0.89	1.29	0.88	0.80
CACZ_06	0.40	0.20	0.42	0.47	0.37	0.36	0.84	0.36	0.74	0.85	0.67	0.64	0.96	0.62	1.20	1.51	1.26	1.12
CACZ_07	0.40	0.19	0.43	0.49	0.39	0.37	0.81	0.34	0.74	0.87	0.67	0.64	0.92	0.57	1.19	1.52	1.24	1.09
CACZ_08	0.26	0.18	0.36	0.37	0.31	0.30	0.56	0.40	0.80	0.92	0.76	0.71	1.03	0.69	1.30	1.61	1.39	1.21
CACZ_09	0.26	0.18	0.37	0.37	0.31	0.30	0.57	0.41	0.82	0.93	0.78	0.73	1.05	0.70	1.33	1.63	1.45	1.24
CACZ_10	0.26	0.15	0.39	0.36	0.28	0.29	0.58	0.37	0.89	0.99	0.76	0.74	1.11	0.66	1.47	1.79	1.48	1.32
CACZ_11	0.23	0.15	0.35	0.30	0.27	0.26	0.53	0.36	0.79	0.86	0.75	0.68	0.99	0.63	1.28	1.53	1.45	1.19
CACZ_12	0.21	0.14	0.34	0.26	0.23	0.24	0.50	0.35	0.79	0.75	0.65	0.62	0.92	0.59	1.24	1.33	1.26	1.07
CACZ_13	0.24	0.15	0.37	0.30	0.27	0.27	0.54	0.36	0.84	0.82	0.72	0.68	1.01	0.63	1.38	1.45	1.37	1.18
CACZ_14	0.30	0.19	0.46	0.37	0.33	0.33	0.53	0.31	0.73	0.64	0.55	0.55	1.31	0.84	1.78	1.89	1.78	1.53
CACZ_15	0.36	0.22	0.52	0.50	0.44	0.42	0.78	0.34	0.79	0.79	0.69	0.65	1.42	0.90	1.93	2.14	2.03	1.73
CACZ_16	0.16	0.10	0.27	0.16	0.16	0.16	0.31	0.17	0.44	0.34	0.30	0.30	0.79	0.44	0.97	1.06	1.10	0.83

Table 7 (continued)

(b) Medium office annual HVAC energy cost savings intensity ($/m²).

	new						older						oldest					
	R	**N**	**E**	**S**	**W**	**N E S W**	**R**	**N**	**E**	**S**	**W**	**N E S W**	**R**	**N**	**E**	**S**	**W**	**N E S W**
CACZ_01	0.12	0.04	0.14	0.17	0.25	0.15	0.30	0.03	0.29	0.32	0.48	0.29	0.53	-0.08	1.40	1.05	1.65	1.00
CACZ_02	0.21	0.09	0.21	0.22	0.29	0.20	0.62	0.16	0.41	0.35	0.61	0.38	1.19	0.26	1.17	0.82	1.33	0.88
CACZ_03	0.18	0.06	0.29	0.40	0.34	0.27	0.56	0.09	0.51	0.65	0.55	0.44	1.01	0.13	1.15	1.43	1.21	0.97
CACZ_04	0.23	0.07	0.26	0.29	0.30	0.23	0.69	0.14	0.59	0.53	0.62	0.46	1.24	0.22	1.24	1.14	1.27	0.96
CACZ_05	0.19	0.06	0.21	0.22	0.25	0.18	0.58	0.08	0.45	0.40	0.50	0.36	1.06	0.13	1.09	0.87	1.10	0.78
CACZ_06	0.35	0.11	0.30	0.28	0.34	0.26	0.73	0.19	0.59	0.57	0.68	0.51	0.91	0.36	1.37	1.23	1.40	1.09
CACZ_07	0.34	0.12	0.29	0.33	0.35	0.28	0.73	0.21	0.70	0.63	0.69	0.55	0.90	0.39	1.40	1.33	1.43	1.14
CACZ_08	0.37	0.11	0.28	0.29	0.32	0.25	0.77	0.22	0.62	0.59	0.68	0.54	1.39	0.39	1.40	1.25	1.42	1.12
CACZ_09	0.26	0.12	0.28	0.28	0.33	0.25	0.77	0.23	0.60	0.58	0.70	0.53	1.40	0.41	1.28	1.26	1.49	1.10
CACZ_10	0.25	0.12	0.31	0.33	0.32	0.27	0.75	0.23	0.66	0.70	0.68	0.56	1.42	0.38	1.42	1.29	1.46	1.14
CACZ_11	0.23	0.10	0.29	0.24	0.32	0.24	0.71	0.22	0.60	0.52	0.77	0.52	1.40	0.36	1.50	1.25	1.71	1.19
CACZ_12	0.23	0.10	0.26	0.21	0.32	0.22	0.70	0.18	0.58	0.41	0.73	0.49	1.32	0.33	1.57	1.03	1.65	1.13
CACZ_13	0.24	0.11	0.29	0.24	0.31	0.23	0.73	0.23	0.67	0.51	0.75	0.52	1.40	0.40	1.59	1.12	1.59	1.17
CACZ_14	0.25	0.13	0.27	0.20	0.30	0.23	0.57	0.31	0.62	0.42	0.68	0.49	1.37	0.78	2.17	1.34	2.45	1.68
CACZ_15	0.30	0.17	0.35	0.37	0.39	0.32	0.65	0.36	0.75	0.74	0.85	0.67	1.28	0.97	2.38	2.06	2.95	2.09
CACZ_16	0.13	0.04	0.18	0.08	0.23	0.13	0.30	0.07	0.30	0.14	0.55	0.26	0.74	0.16	1.59	0.57	2.13	1.07

Table 7 (continued)

(c) Retail stand-alone annual HVAC energy cost savings intensity ($/m²).

	new						older						oldest					
	R	**N**	**E**	**S**	**W**	**N E S W**	**R**	**N**	**E**	**S**	**W**	**N E S W**	**R**	**N**	**E**	**S**	**W**	**N E S W**
CACZ_01	0.11	0.02	0.21	0.29	0.06	0.15	0.52	0.12	0.63	0.87	0.52	0.50	0.99	0.30	1.87	2.62	2.17	1.63
CACZ_02	0.33	0.18	0.38	0.40	0.42	0.34	1.40	0.46	0.90	1.14	1.16	0.90	2.68	0.85	1.92	2.22	2.39	1.81
CACZ_03	0.25	0.11	0.43	0.63	0.48	0.39	1.12	0.29	0.96	1.38	0.94	0.86	2.09	0.60	1.86	2.65	2.01	1.71
CACZ_04	0.37	0.16	0.76	0.48	0.35	0.46	1.42	0.36	1.05	1.30	1.11	0.93	2.65	0.65	2.03	2.58	2.15	1.80
CACZ_05	0.32	0.11	0.65	0.43	0.27	0.37	1.24	0.31	0.92	1.13	1.00	0.83	2.34	0.65	1.80	2.22	2.11	1.65
CACZ_06	0.60	0.23	0.23	0.58	0.61	0.37	1.57	0.48	1.15	1.37	1.29	1.07	1.91	0.93	2.23	2.68	2.69	2.08
CACZ_07	0.57	0.17	0.48	0.54	0.40	0.40	1.44	0.45	0.98	1.34	1.30	0.99	1.79	0.85	2.23	2.62	2.64	2.03
CACZ_08	0.62	0.21	0.16	0.53	0.54	0.33	1.68	0.55	1.26	1.45	1.42	1.14	3.14	0.98	2.31	2.80	2.69	2.16
CACZ_09	0.42	0.22	0.46	0.53	0.42	0.39	1.72	0.56	1.23	1.46	1.41	1.14	3.18	0.98	2.33	2.78	2.82	2.18
CACZ_10	0.48	0.21	0.47	0.55	0.58	0.45	1.78	0.54	1.24	1.55	1.51	1.18	3.36	1.02	2.46	3.02	3.07	2.35
CACZ_11	0.44	0.22	0.49	0.51	0.51	0.42	1.64	0.54	1.11	1.46	1.44	1.12	3.12	1.02	2.49	2.90	2.99	2.28
CACZ_12	0.45	0.20	0.45	0.43	0.49	0.39	1.58	0.52	1.20	1.32	1.35	1.07	2.96	0.95	2.38	2.57	2.80	2.14
CACZ_13	0.43	0.24	0.49	0.47	0.51	0.42	1.72	0.58	1.22	1.41	1.46	1.14	3.24	1.07	2.58	2.68	3.05	2.30
CACZ_14	0.47	0.27	0.52	0.48	0.59	0.45	1.45	0.67	1.23	1.42	1.74	1.24	3.53	1.87	4.06	4.19	5.68	3.89
CACZ_15	0.56	0.30	2.23	0.59	0.55	0.98	1.67	0.77	1.48	1.70	2.00	1.46	3.18	2.10	4.34	4.78	6.47	4.32
CACZ_16	0.18	-0.80	0.40	0.37	0.37	0.05	1.02	0.30	0.95	1.17	1.22	0.88	2.47	1.04	2.99	3.34	4.38	2.80

Table 8. Analog of Table 7 for annual whole-building HVAC energy cost saving fraction (%).

(a) Single-family home annual whole-building HVAC energy cost saving fraction (%).

	new						older						oldest					
	R	**N**	**E**	**S**	**W**	**N E S W**	**R**	**N**	**E**	**S**	**W**	**N E S W**	**R**	**N**	**E**	**S**	**W**	**N E S W**
CACZ_01	5.17	0.90	2.40	1.81	1.16	5.70	7.71	1.18	3.03	2.88	1.68	8.13	7.08	1.41	3.10	4.89	3.46	11.07
CACZ_02	4.44	0.84	2.09	1.66	1.33	5.69	5.42	1.54	3.36	3.57	2.86	11.03	8.10	2.08	4.02	5.05	4.54	14.86
CACZ_03	7.43	0.84	2.50	2.02	1.30	6.34	6.62	1.71	4.34	4.77	3.20	13.46	10.00	2.24	5.07	6.72	4.95	17.63
CACZ_04	3.85	0.95	2.57	2.32	1.68	7.27	6.16	1.59	3.98	4.47	3.16	12.81	9.81	2.27	5.24	6.74	5.15	18.55
CACZ_05	8.47	0.87	2.69	2.23	1.22	6.60	7.20	1.73	4.65	5.45	3.31	14.45	10.45	2.18	2.18	7.37	5.03	18.34
CACZ_06	7.42	1.55	3.20	3.56	2.80	10.89	10.50	1.87	3.81	4.42	3.46	13.30	11.66	3.14	6.05	7.63	6.33	22.44
CACZ_07	8.29	1.66	3.70	4.23	3.31	12.62	11.76	2.01	4.40	5.21	4.02	15.32	13.83	3.53	7.41	9.48	7.69	27.10
CACZ_08	4.42	1.23	2.50	2.63	2.19	8.41	6.36	1.91	3.77	4.35	3.57	13.40	10.74	2.95	5.58	6.92	5.95	20.85
CACZ_09	3.87	1.07	2.25	2.25	1.91	7.36	5.65	1.69	3.39	3.81	3.21	11.93	9.44	2.59	4.93	6.05	5.35	18.39
CACZ_10	3.32	0.82	2.08	1.94	1.51	6.20	5.00	1.33	3.15	3.50	2.70	10.50	8.20	2.01	4.47	5.45	4.51	16.01
CACZ_11	2.45	0.63	1.53	1.32	1.17	4.56	3.84	1.07	2.36	2.55	2.24	8.15	6.17	1.62	3.28	3.94	3.74	12.22
CACZ_12	2.90	0.79	1.99	1.51	1.32	5.48	4.65	1.35	3.06	2.93	2.53	9.67	7.30	1.95	4.06	4.39	4.14	13.98
CACZ_13	2.64	0.66	1.68	1.36	1.21	4.82	4.02	1.11	2.58	2.50	2.21	8.30	6.49	1.68	3.67	3.85	3.65	12.54
CACZ_14	2.79	0.73	1.77	1.40	1.25	5.05	3.59	0.87	2.06	1.79	1.54	6.16	6.93	1.83	3.90	4.15	3.89	13.41
CACZ_15	2.66	0.67	1.57	1.53	1.33	5.06	4.11	0.76	1.72	1.73	1.50	5.66	6.30	1.67	3.54	3.94	3.73	12.73
CACZ_16	2.32	0.59	1.59	0.96	0.97	3.95	3.47	0.78	2.06	1.59	1.41	5.67	5.91	1.38	3.00	3.30	3.41	10.29

Table 8 (continued)

(b) Medium office annual whole-building HVAC energy cost saving fraction (%).

	new						older						oldest					
	R	**N**	**E**	**S**	**W**	**N E S W**	**R**	**N**	**E**	**S**	**W**	**N E S W**	**R**	**N**	**E**	**S**	**W**	**N E S W**
CACZ_01	0.94	0.06	0.20	0.26	0.38	0.89	1.94	0.04	0.38	0.42	0.61	1.47	2.11	-0.07	1.10	0.84	1.29	3.13
CACZ_02	1.24	0.11	0.24	0.26	0.34	0.97	3.09	0.16	0.40	0.35	0.60	1.50	4.05	0.18	0.79	0.56	0.90	2.38
CACZ_03	0.92	0.06	0.29	0.41	0.34	1.10	2.52	0.08	0.45	0.59	0.49	1.57	3.81	0.10	0.86	1.08	0.91	2.93
CACZ_04	1.09	0.07	0.25	0.27	0.28	0.87	2.86	0.12	0.49	0.45	0.52	1.53	4.40	0.16	0.87	0.81	0.89	2.73
CACZ_05	1.04	0.07	0.23	0.24	0.27	0.80	2.74	0.08	0.42	0.38	0.47	1.36	4.21	0.11	0.86	0.70	0.87	2.48
CACZ_06	1.60	0.11	0.27	0.27	0.31	0.97	3.06	0.17	0.49	0.48	0.56	1.69	3.36	0.27	1.01	0.92	1.03	3.23
CACZ_07	1.61	0.11	0.27	0.32	0.33	1.04	3.15	0.19	0.60	0.55	0.59	1.91	3.45	0.30	1.07	1.03	1.09	3.49
CACZ_08	1.64	0.10	0.25	0.26	0.28	0.90	3.06	0.18	0.49	0.48	0.54	1.71	4.73	0.27	0.95	0.85	0.96	3.02
CACZ_09	1.11	0.10	0.24	0.24	0.28	0.86	2.91	0.18	0.45	0.44	0.53	1.59	4.51	0.26	0.82	0.82	0.96	2.83
CACZ_10	1.23	0.12	0.30	0.32	0.31	1.02	3.15	0.19	0.55	0.60	0.56	1.88	4.38	0.24	0.87	0.80	0.89	2.79
CACZ_11	1.04	0.10	0.26	0.22	0.29	0.87	2.70	0.17	0.45	0.40	0.58	1.57	3.75	0.20	0.80	0.67	0.91	2.55
CACZ_12	1.16	0.11	0.26	0.22	0.32	0.90	2.97	0.16	0.49	0.35	0.62	1.65	3.98	0.20	0.94	0.63	0.99	2.70
CACZ_13	1.10	0.10	0.27	0.23	0.28	0.86	2.83	0.18	0.52	0.40	0.58	1.60	3.96	0.23	0.89	0.64	0.89	2.62
CACZ_14	1.00	0.11	0.22	0.16	0.24	0.72	1.94	0.21	0.42	0.29	0.46	1.34	3.10	0.35	0.98	0.61	1.10	3.02
CACZ_15	1.00	0.11	0.24	0.25	0.27	0.86	1.98	0.22	0.45	0.45	0.52	1.62	2.88	0.44	1.06	0.93	1.32	3.75
CACZ_16	0.60	0.04	0.17	0.07	0.22	0.48	1.15	0.05	0.23	0.11	0.42	0.79	1.72	0.08	0.73	0.26	0.97	1.97

Table 8 (continued)

(c) Retail stand-alone annual whole-building HVAC energy cost saving fraction (%).

	new						older						oldest					
	R	**N**	**E**	**S**	**W**	**N E S W**	**R**	**N**	**E**	**S**	**W**	**N E S W**	**R**	**N**	**E**	**S**	**W**	**N E S W**
CACZ_01	1.79	0.05	0.46	0.55	0.11	1.17	7.55	0.22	1.19	1.41	0.84	3.47	10.30	0.40	2.52	3.06	2.50	8.15
CACZ_02	4.00	0.29	0.61	0.55	0.58	2.02	13.06	0.56	1.09	1.19	1.20	4.04	18.00	0.74	1.67	1.67	1.78	5.86
CACZ_03	3.48	0.21	0.79	0.98	0.75	2.61	12.67	0.43	1.41	1.73	1.19	4.71	18.48	0.69	2.15	2.61	1.98	7.31
CACZ_04	4.57	0.27	1.20	0.68	0.48	2.72	13.54	0.45	1.29	1.38	1.18	4.27	19.41	0.63	1.93	2.11	1.75	6.35
CACZ_05	4.43	0.20	1.16	0.66	0.42	2.45	13.56	0.45	1.31	1.38	1.21	4.35	19.71	0.72	1.97	2.08	1.97	6.69
CACZ_06	7.09	0.36	0.37	0.78	0.80	2.10	14.71	0.59	1.39	1.43	1.34	4.82	15.96	1.01	2.41	2.51	2.50	8.40
CACZ_07	7.33	0.29	0.81	0.80	0.58	2.49	14.93	0.61	1.32	1.56	1.50	4.96	16.80	1.04	2.71	2.75	2.73	9.14
CACZ_08	6.87	0.31	0.24	0.66	0.67	1.75	14.56	0.62	1.41	1.40	1.37	4.74	20.92	0.85	2.00	2.08	1.99	6.93
CACZ_09	4.49	0.30	0.64	0.63	0.51	2.03	13.84	0.59	1.29	1.31	1.26	4.41	19.73	0.79	1.87	1.92	1.94	6.51
CACZ_10	5.06	0.29	0.64	0.65	0.68	2.25	13.69	0.54	1.24	1.33	1.29	4.38	18.63	0.73	1.77	1.87	1.89	6.27
CACZ_11	4.40	0.30	0.64	0.58	0.57	2.07	12.07	0.51	1.06	1.21	1.18	3.98	16.53	0.71	1.70	1.72	1.76	5.83
CACZ_12	5.09	0.31	0.66	0.55	0.61	2.14	13.11	0.56	1.30	1.22	1.25	4.30	17.70	0.74	1.84	1.71	1.85	6.15
CACZ_13	4.39	0.32	0.65	0.55	0.57	2.04	12.68	0.56	1.17	1.16	1.20	4.05	17.25	0.74	1.78	1.60	1.80	5.89
CACZ_14	4.03	0.31	0.58	0.47	0.56	1.89	9.67	0.58	1.07	1.06	1.29	4.00	14.78	1.02	2.20	1.96	2.64	7.83
CACZ_15	4.26	0.30	2.16	0.50	0.46	3.54	9.75	0.59	1.12	1.11	1.30	4.12	12.83	1.10	2.27	2.15	2.90	8.40
CACZ_16	1.87	-1.14	0.54	0.44	0.42	0.19	8.48	0.32	1.02	1.09	1.12	3.49	12.94	0.72	2.02	1.96	2.53	7.04

Table 9. Annual HVAC energy cost savings intensity ($/m²) by U.S. climate zone (1A - 8), building vintage (new, older, oldest), and surface(s) modified (R = roof; N = north wall; E = east wall; S = south wall; W = west wall; N E S W = all four walls), tabulated for (a) single-family home, (b) medium office, and (c) retail standalone buildings. Results are mean of values for N-S and E-W orientations of the building's long axis.

(a) Single-family home annual HVAC energy cost savings intensity ($/m²).

	new						older						oldest					
	R	**N**	**E**	**S**	**W**	**N E S W**	**R**	**N**	**E**	**S**	**W**	**N E S W**	**R**	**N**	**E**	**S**	**W**	**N E S W**
USCZ_1A	0.40	0.28	0.48	0.49	0.52	0.44	0.49	0.35	0.60	0.61	0.64	0.55	1.14	0.56	0.94	0.99	1.07	0.89
USCZ_2A	0.26	0.22	0.37	0.33	0.36	0.31	0.39	0.28	0.47	0.42	0.45	0.40	0.80	0.47	0.78	0.78	0.81	0.70
USCZ_2B	0.58	0.33	0.76	0.76	0.65	0.61	0.54	0.31	0.71	0.71	0.60	0.57	1.33	0.57	1.27	1.39	1.21	1.10
USCZ_3A	0.28	0.19	0.35	0.27	0.31	0.28	0.29	0.20	0.36	0.28	0.31	0.28	0.62	0.34	0.62	0.57	0.60	0.52
USCZ_3B	0.30	0.14	0.33	0.23	0.23	0.22	0.44	0.26	0.57	0.47	0.45	0.42	0.99	0.48	1.03	1.01	0.91	0.84
USCZ_3C	0.21	0.07	0.25	0.17	0.09	0.13	0.31	0.11	0.41	0.33	0.12	0.21	1.07	0.31	0.90	1.01	0.53	0.65
USCZ_4A	0.13	0.09	0.17	0.05	0.11	0.10	0.25	0.16	0.30	0.16	0.25	0.21	0.70	0.30	0.56	0.42	0.51	0.43
USCZ_4B	0.24	0.17	0.40	0.26	0.26	0.26	0.35	0.20	0.47	0.31	0.30	0.31	1.01	0.42	0.97	0.91	0.75	0.73
USCZ_4C	0.03	0.00	0.05	0.00	0.00	0.01	0.04	0.01	0.07	0.03	0.03	0.02	0.18	0.06	0.20	0.20	0.14	0.13
USCZ_5A	0.13	0.08	0.17	0.08	0.12	0.11	0.19	0.15	0.27	0.17	0.24	0.20	0.47	0.28	0.52	0.44	0.52	0.42
USCZ_5B	0.11	0.03	0.13	0.04	0.04	0.05	0.17	0.09	0.24	0.16	0.15	0.15	0.52	0.19	0.51	0.47	0.39	0.37
USCZ_6A	0.08	0.03	0.07	-0.06	0.01	0.01	0.09	0.05	0.10	-0.07	0.03	0.02	0.24	0.21	0.32	0.19	0.36	0.24
USCZ_6B	0.04	0.02	0.07	-0.04	-0.01	-0.01	0.11	0.05	0.16	0.05	0.07	0.05	0.39	0.14	0.36	0.27	0.26	0.24
USCZ_7	0.02	0.01	0.02	-0.08	-0.02	-0.03	0.02	-0.00	0.01	-0.10	-0.05	-0.04	0.14	0.06	0.12	-0.04	0.06	0.03
USCZ_8	0.06	0.07	0.13	0.01	0.03	0.05	0.09	0.11	0.20	0.09	0.09	0.10	0.28	0.21	0.42	0.31	0.26	0.27

Table 9 (continued)

(b) Medium office annual HVAC energy cost savings intensity ($/m²).

	new						older						oldest					
	R	**N**	**E**	**S**	**W**	**N E S W**	**R**	**N**	**E**	**S**	**W**	**N E S W**	**R**	**N**	**E**	**S**	**W**	**N E S W**
USCZ_1A	0.38	0.21	0.49	0.45	0.51	0.41	0.40	0.47	1.16	0.93	1.18	0.94	1.05	0.74	1.74	1.28	1.64	1.36
USCZ_2A	0.16	0.08	0.21	0.11	0.18	0.15	0.31	0.22	0.65	0.36	0.65	0.48	0.84	0.55	1.36	1.01	1.29	1.05
USCZ_2B	0.50	0.26	0.60	0.50	0.54	0.48	0.20	0.48	1.38	1.02	1.44	1.08	1.33	0.80	2.24	1.97	2.13	1.78
USCZ_3A	0.21	0.10	0.22	0.11	0.23	0.06	0.37	0.20	0.60	0.27	0.64	0.43	0.93	0.59	1.56	1.25	1.47	1.21
USCZ_3B	0.15	0.07	0.17	0.11	0.15	0.12	0.08	0.17	0.50	0.10	0.55	0.32	0.68	0.16	1.10	0.90	1.06	0.82
USCZ_3C	0.08	-0.03	0.09	0.03	0.11	0.04	0.20	-0.03	0.52	0.27	0.62	0.34	0.40	0.28	1.28	0.90	1.26	0.94
USCZ_4A	0.03	0.00	0.08	-0.02	0.08	0.04	0.10	0.07	0.19	0.00	0.28	0.14	0.64	0.34	1.02	0.80	0.95	0.77
USCZ_4B	0.26	0.10	0.20	0.11	0.17	0.14	0.15	0.09	0.23	-0.09	0.29	0.12	0.64	0.43	1.16	0.74	1.08	0.84
USCZ_4C	0.03	-0.02	0.07	0.03	0.08	0.03	0.11	-0.02	0.16	0.12	0.22	0.12	0.29	0.09	0.50	0.45	0.61	0.40
USCZ_5A	0.01	-0.02	0.04	-0.03	0.05	0.01	0.01	0.01	0.07	-0.08	0.13	0.03	0.26	0.10	0.57	0.23	0.56	0.37
USCZ_5B	-0.03	-0.29	-0.22	-0.28	-0.23	-0.05	0.01	0.01	0.07	-0.06	0.13	0.03	0.30	0.13	0.67	0.42	0.53	0.44
USCZ_6A	0.00	-0.05	0.01	-0.07	0.04	-0.02	-0.04	-0.08	-0.07	-0.22	0.04	-0.08	0.17	0.06	0.74	0.26	0.75	0.46
USCZ_6B	-0.06	-0.06	-0.01	-0.60	-0.00	-0.17	-0.08	-0.08	-0.06	-0.24	0.02	-0.09	0.18	0.08	0.67	0.14	0.53	0.32
USCZ_7	-0.17	-0.09	-0.03	-0.14	-0.01	-0.07	-0.05	-0.06	-0.11	-0.23	-0.03	-0.11	0.08	0.02	0.25	-0.03	0.39	0.16
USCZ_8	0.27	0.08	0.21	-0.01	0.26	0.13	-0.01	-0.08	-0.14	-0.27	-0.02	-0.13	0.01	0.08	0.36	0.29	0.31	0.26

Table 9 (continued)

(c) Retail stand-alone annual HVAC energy cost savings intensity ($/m²).

	new						older						oldest					
	R	**N**	**E**	**S**	**W**	**N E S W**	**R**	**N**	**E**	**S**	**W**	**N E S W**	**R**	**N**	**E**	**S**	**W**	**N E S W**
USCZ_1A*	NA	NA	NA	NA	NA	NA	0.49	0.82	1.42	1.45	1.85	1.36	1.47	0.74	1.34	1.32	2.15	1.37
USCZ_2A	0.28	0.14	0.59	0.80	0.98	0.51	0.27	0.38	0.88	0.78	0.72	0.64	0.98	0.49	1.01	1.06	1.42	0.95
USCZ_2B	0.85	1.72	3.54	4.15	5.11	3.65	0.25	0.60	1.48	1.40	1.55	1.20	1.73	0.68	1.43	1.73	2.20	1.47
USCZ_3A	0.33	0.15	0.52	0.43	0.53	0.42	0.28	0.19	0.74	0.64	0.48	0.51	1.04	0.31	1.00	1.21	1.45	0.99
USCZ_3B	0.21	0.18	0.32	0.42	0.54	0.35	0.13	0.14	0.44	0.30	0.34	0.30	0.85	0.38	0.77	0.95	1.27	0.81
USCZ_3C	0.24	-0.24	0.72	0.72	-0.07	0.54	0.56	-0.12	0.88	0.46	-0.44	0.17	0.64	-0.24	0.56	1.31	0.81	0.59
USCZ_4A	0.08	-0.45	-0.34	0.27	0.28	0.26	0.13	0.06	0.25	0.13	0.08	0.14	0.61	0.13	0.66	0.74	0.43	0.49
USCZ_4B	0.50	0.27	0.57	0.43	0.61	0.47	0.46	0.04	0.37	0.06	0.01	0.13	0.79	0.11	0.69	0.78	0.79	0.58
USCZ_4C	0.13	0.09	0.17	0.22	0.31	0.17	0.16	-0.06	0.05	-0.04	-0.15	-0.04	0.28	-0.08	0.21	0.50	0.16	0.19
USCZ_5A	0.19	0.43	0.61	0.22	0.61	0.29	0.06	0.02	0.11	0.03	0.09	0.05	0.12	0.07	0.13	0.25	0.29	0.17
USCZ_5B	0.16	0.07	0.21	0.15	0.24	0.18	0.08	-0.05	0.05	-0.14	-0.12	-0.06	0.26	0.01	0.12	0.38	0.20	0.17
USCZ_6A	0.29	0.08	0.38	0.20	0.34	0.30	-0.02	-0.04	-0.04	-0.09	-0.06	-0.05	-0.00	-0.07	0.07	0.04	-0.04	0.01
USCZ_6B	0.16	0.08	0.13	0.10	0.27	0.15	-0.06	-0.07	-0.10	-0.26	-0.18	-0.14	-0.05	-0.09	-0.11	-0.03	-0.05	-0.07
USCZ_7	0.11	2.26	0.07	2.90	0.22	0.07	-0.06	-0.04	-0.09	-0.15	-0.11	-0.10	-0.05	-0.04	-0.06	-0.06	-0.08	-0.07
USCZ_8	0.33	0.27	0.63	0.36	0.32	0.37	-0.06	-0.05	-0.07	-0.15	-0.05	-0.07	-0.07	-0.08	-0.06	0.10	-0.10	-0.04

* We have omitted all results for the new stand-alone retail building in USCZ 1A (Miami) because modifying the albedo of its back wall yielded unrealistically large changes in annual fan energy use.

Table 10. Analog of Table 9 for annual whole-building HVAC energy cost saving fraction (%).

(a) Single-family home annual whole-building HVAC energy cost saving fraction (%).

	new						older						oldest					
	R	**N**	**E**	**S**	**W**	**N E S W**	**R**	**N**	**E**	**S**	**W**	**N E S W**	**R**	**N**	**E**	**S**	**W**	**N E S W**
USCZ_1A	4.00	1.16	1.98	2.04	2.13	7.28	3.11	0.92	1.57	1.61	1.68	5.74	5.73	1.16	1.95	2.06	2.23	7.39
USCZ_2A	2.96	1.06	1.74	1.55	1.71	5.96	2.91	0.87	1.46	1.31	1.38	4.96	4.68	1.13	1.87	1.88	1.96	6.77
USCZ_2B	3.05	0.72	1.66	1.67	1.41	5.36	2.90	0.69	1.59	1.58	1.33	5.09	5.21	0.93	2.06	2.25	1.95	7.10
USCZ_3A	2.38	0.67	1.22	0.95	1.06	3.81	2.39	0.67	1.23	0.96	1.08	3.86	3.98	0.90	1.64	1.50	1.60	5.49
USCZ_3B	4.43	0.89	2.04	1.44	1.41	5.52	3.68	0.91	1.99	1.64	1.57	5.88	5.98	1.20	2.58	2.53	2.27	8.35
USCZ_3C	5.71	0.81	2.80	1.94	0.99	5.62	4.02	0.59	2.17	1.77	0.66	4.55	8.15	0.98	2.84	3.20	1.68	8.22
USCZ_4A	1.49	0.40	0.81	0.23	0.53	1.86	1.71	0.46	0.85	0.44	0.72	2.37	3.56	0.62	1.17	0.87	1.07	3.57
USCZ_4B	2.75	0.82	1.87	1.24	1.22	4.86	3.41	0.83	1.90	1.28	1.23	5.00	6.56	1.14	2.60	2.46	2.02	7.90
USCZ_4C	0.49	0.03	0.40	-0.01	0.02	0.24	0.40	0.04	0.33	0.16	0.13	0.45	1.46	0.20	0.66	0.65	0.46	1.73
USCZ_5A	1.66	0.43	0.87	0.44	0.65	2.29	1.53	0.47	0.88	0.57	0.78	2.63	2.77	0.70	1.27	1.08	1.27	4.17
USCZ_5B	1.40	0.19	0.69	0.19	0.20	1.14	1.82	0.37	1.06	0.70	0.64	2.60	3.78	0.57	1.51	1.40	1.17	4.42
USCZ_6A	0.67	0.11	0.24	-0.21	0.03	0.09	0.44	0.11	0.19	-0.15	0.06	0.16	0.94	0.33	0.51	0.30	0.58	1.57
USCZ_6B	0.43	0.07	0.34	-0.18	-0.06	-0.16	0.97	0.20	0.60	0.18	0.27	0.79	2.57	0.39	0.98	0.73	0.71	2.59
USCZ_7	0.21	0.04	0.11	-0.37	-0.10	-0.63	0.11	-0.01	0.02	-0.29	-0.13	-0.46	0.67	0.12	0.25	-0.09	0.12	0.25
USCZ_8	0.29	0.13	0.24	0.03	0.06	0.39	0.37	0.19	0.34	0.14	0.16	0.70	0.89	0.28	0.57	0.41	0.34	1.45

Table 10 (continued)

(b) Medium office annual whole-building HVAC energy cost saving fraction (%).

	new						older						oldest					
	R	**N**	**E**	**S**	**W**	**N E S W**	**R**	**N**	**E**	**S**	**W**	**N E S W**	**R**	**N**	**E**	**S**	**W**	**N E S W**
USCZ_1A	2.41	0.28	0.62	0.58	0.66	2.11	1.91	0.45	1.11	0.89	1.12	3.58	3.20	0.46	1.05	0.78	0.99	3.29
USCZ_2A	1.69	0.18	0.44	0.23	0.39	1.25	1.75	0.25	0.74	0.42	0.74	2.18	3.42	0.44	1.09	0.82	1.04	3.38
USCZ_2B	2.47	0.25	0.59	0.50	0.52	1.87	0.79	0.38	1.06	0.79	1.11	3.31	3.18	0.39	1.07	0.95	1.02	3.39
USCZ_3A	1.64	0.16	0.34	0.18	0.36	0.39	1.75	0.18	0.56	0.25	0.60	1.60	3.14	0.40	1.04	0.85	0.99	3.25
USCZ_3B	2.17	0.22	0.49	0.33	0.44	1.44	0.55	0.24	0.69	0.14	0.76	1.79	3.46	0.17	1.11	0.92	1.07	3.30
USCZ_3C	1.40	-0.09	0.30	0.10	0.35	0.55	1.32	-0.04	0.67	0.36	0.80	1.76	2.44	0.36	1.58	1.12	1.50	4.60
USCZ_4A	0.33	0.01	0.16	-0.04	0.16	0.29	0.47	0.07	0.17	0.01	0.26	0.50	2.43	0.25	0.76	0.61	0.71	2.31
USCZ_4B	2.26	0.17	0.35	0.20	0.30	0.95	0.87	0.10	0.27	-0.11	0.35	0.58	2.61	0.36	0.94	0.61	0.88	2.75
USCZ_4C	0.48	-0.07	0.22	0.10	0.24	0.40	0.77	-0.03	0.22	0.18	0.31	0.67	2.00	0.13	0.69	0.63	0.84	2.22
USCZ_5A	0.09	-0.05	0.08	-0.05	0.10	0.07	0.05	0.02	0.07	-0.08	0.13	0.14	1.43	0.11	0.62	0.26	0.62	1.60
USCZ_5B	-0.46	-0.82	-0.63	-0.80	-0.65	-0.58	0.05	0.01	0.10	-0.09	0.20	0.20	1.97	0.18	0.88	0.55	0.70	2.30
USCZ_6A	0.01	-0.08	0.02	-0.10	0.06	-0.11	-0.12	-0.05	-0.04	-0.15	0.03	-0.21	0.71	0.05	0.62	0.22	0.63	1.52
USCZ_6B	-0.56	-0.13	-0.02	-1.25	-0.01	-1.44	-0.41	-0.08	-0.06	-0.24	0.02	-0.36	0.92	0.08	0.69	0.15	0.55	1.32
USCZ_7	-1.35	-0.14	-0.05	-0.22	-0.02	-0.43	-0.21	-0.05	-0.09	-0.19	-0.03	-0.35	0.42	0.03	0.29	-0.04	0.43	0.73
USCZ_8	0.65	0.04	0.10	-0.01	0.12	0.25	-0.01	-0.03	-0.04	-0.08	-0.01	-0.15	0.04	0.05	0.20	0.16	0.17	0.57

Table 10 (continued)

(c) Retail stand-alone annual whole-building HVAC energy cost saving fraction (%).

	new						older						oldest					
	R	**N**	**E**	**S**	**W**	**N E S W**	**R**	**N**	**E**	**S**	**W**	**N E S W**	**R**	**N**	**E**	**S**	**W**	**N E S W**
USCZ_1A*	NA	NA	NA	NA	NA	NA	3.73	0.82	1.42	1.24	1.58	5.03	10.12	0.67	1.20	1.02	1.65	4.54
USCZ_2A	5.55	0.37	1.53	1.78	2.17	4.84	2.78	0.51	1.18	0.90	0.83	3.17	8.56	0.55	1.14	1.02	1.38	4.00
USCZ_2B	5.18	1.36	2.81	2.81	3.47	10.72	1.80	0.56	1.38	1.12	1.24	4.15	10.48	0.54	1.12	1.17	1.48	4.28
USCZ_3A	5.02	0.28	1.03	0.74	0.88	3.04	2.28	0.21	0.80	0.59	0.44	2.05	7.48	0.29	0.94	0.97	1.17	3.44
USCZ_3B	4.76	0.54	0.96	1.09	1.39	3.95	1.78	0.25	0.78	0.45	0.51	1.99	8.85	0.52	1.05	1.10	1.47	4.07
USCZ_3C	5.55	-0.72	2.19	1.89	-0.19	6.13	7.99	-0.20	1.64	0.72	-0.73	1.17	8.25	-0.39	0.95	1.88	1.16	3.68
USCZ_4A	1.48	-1.17	-0.88	0.58	0.59	2.37	1.06	0.07	0.28	0.12	0.07	0.57	4.43	0.12	0.62	0.60	0.35	1.70
USCZ_4B	6.38	0.45	0.94	0.61	0.85	2.86	5.23	0.05	0.55	0.08	0.01	0.71	7.36	0.14	0.83	0.80	0.82	2.62
USCZ_4C	2.83	0.28	0.50	0.55	0.76	1.85	2.05	-0.10	0.08	-0.06	-0.22	-0.24	3.00	-0.11	0.30	0.61	0.19	0.98
USCZ_5A	4.33	1.27	1.81	0.58	1.53	3.24	0.59	0.03	0.14	0.04	0.09	0.25	1.01	0.08	0.14	0.23	0.27	0.69
USCZ_5B	3.36	0.19	0.58	0.37	0.58	1.85	1.04	-0.09	0.08	-0.20	-0.17	-0.35	2.71	0.01	0.17	0.45	0.24	0.86
USCZ_6A	5.14	0.19	0.85	0.39	0.67	2.58	-0.10	-0.03	-0.03	-0.07	-0.05	-0.16	-0.03	-0.06	0.06	0.03	-0.03	0.02
USCZ_6B	2.59	0.17	0.27	0.19	0.49	1.16	-0.49	-0.08	-0.12	-0.25	-0.17	-0.55	-0.38	-0.09	-0.11	-0.03	-0.04	-0.25
USCZ_7	1.47	4.36	0.13	4.80	0.15	0.54	-0.47	-0.04	-0.09	-0.12	-0.10	-0.35	-0.38	-0.04	-0.05	-0.05	-0.07	-0.23
USCZ_8	1.47	0.16	0.36	0.18	0.16	0.79	-0.21	-0.03	-0.04	-0.06	-0.02	-0.13	-0.24	-0.04	-0.03	0.04	-0.04	-0.07

* We have omitted all results for the new stand-alone retail building in USCZ 1A (Miami) because modifying the albedo of its back wall yielded unrealistically large changes in annual fan energy use.

The following examples illustrate how to use the savings tables.

3.4.1 Example 1: Cool walls on an isolated 30-year-old single-family home in Fresno, CA

The city of Fresno is within California building climate zone 13 (Table 1 or Figure 2), and a home built 30 years ago (in 1988) is best represented by the "older" vintage (Section 3.1). From Table 7a we obtain the annual HVAC energy cost savings intensity c ($/m²) for an older single-family home in this climate (CACZ_13):

Table 11. Annual HVAC energy cost savings intensity ($/m²) in Example 1. Savings in the first four columns (N, E, S, W) result from modifying walls individually, while those in the last column (N E S W) result from modifying all walls simultaneously.

N	E	S	W	N E S W
0.36	0.84	0.82	0.72	0.68

Assume that

- the house is due to be painted;
- the new paint will last for N=10 years;
- the real rate of return is r=3%
- one gallon of paint coats 400 ft²;
- we will apply two coats; and
- we wish to decide whether to choose a light-colored paint (higher-tied cool wall with aged albedo 0.60) or a darker conventional paint (warm wall with aged albedo 0.25).

Table 6 indicates that the PV multiplier for N=10 years and r=3% is b=8.5. The life-cycle HVAC energy cost savings intensity is $b \times c$:

Table 12. Life-cycle HVAC energy cost savings intensity ($/m²) in Example 1.

N	E	S	W	N E S W
3.06	7.14	6.97	6.12	5.78

We consider two scenarios: (A) the cool paint costs the same as the warm paint, or (B) the cost premium for the cool paint is $15/gallon.

In Scenario A (or Example 1A), the simple payback time is zero because the cost premium is zero. However, we can still compute life-cycle cost savings intensity.

With zero cost premium, the life-cycle cost savings intensity equals the life-cycle HVAC energy cost savings intensity (Table 12):

Table 13. Life-cycle cost savings intensity ($/m²) in Example 1A.

N	E	S	W	N E S W
3.06	7.14	6.97	6.12	5.78

To obtain savings per ft², divide by 10.76 ft²/m²:

Table 14. Life-cycle cost savings intensity ($/ft²) in Example 1A.

N	E	S	W	N E S W
0.28	0.66	0.65	0.57	0.54

In Scenario B (or Example 1B), the cost premium of $15/gallon yields a two-coat material cost premium of 2 × $15/gallon × 1 gallon/400 ft² × 10.76 ft²/m² = $0.81/m². Dividing this cost premium by the annual HVAC energy cost savings intensity ($/m²) provides the simple payback time in years:

Table 15. Simple payback time (y) in Example 1B.

N	E	S	W	N E S W
2.3	0.96	0.99	1.1	1.2

The life-cycle cost savings is the life-cycle HVAC energy cost savings intensity (Table 12) minus the material cost premium:

Table 16. Life-cycle cost savings intensity ($/m²) in Example 1B.

N	E	S	W	N E S W
2.25	6.33	6.16	5.31	4.97

If you prefer IP units, divide by 10.76 ft²/m²:

Table 17. Life-cycle cost savings intensity ($/ft²) in Example 1B.

N	E	S	W	N E S W
0.21	0.59	0.57	0.49	0.46

Hence, choosing the more reflective paint will be cost effective in either scenario, with zero simple payback time in Scenario A (no cost premium), and a 1 - 2 y simple payback time in Scenario B ($15/gal cost premium).

We can use the wall-specific life-cycle cost savings intensity to estimate the whole-building life cycle cost savings. Say the home is 15 m long (north-south), 10 m wide (east-west), and 6 m high, with a 2 m² door and 15 m² of windows each on the east and west facades, and 10 m² of

windows each on the north and south facades. The net wall area (gross wall area minus openings) on the will be 15 m × 6 m – 2 m² - 15 m² = 73 m² on the east façade and on the west façade, and 10 m × 6 m – 10 m² = 50 m² on the north façade and on the south façade.

Table 18. Net wall area (m²) in Example 1.

N	E	S	W	N E S W
50	73	50	73	246

Multiplying each façade's life-cycle cost savings intensity (Table 14 for Scenario A; Table 16 for Scenario B) by its net wall area (Table 18) yields its life-cycle cost savings. In Scenario A, we get

Table 19. Life-cycle cost savings ($) in Example 1A.

N	E	S	W	N E S W
153	521	349	447	1,422

while in Scenario B we get

Table 20. Life-cycle cost savings ($) in Example 1B.

N	E	S	W	N E S W
113	462	308	388	1,223

Note that in each scenario the sum of individual wall savings (N + E + S + W) differs by about 3% from the savings based on the four-wall (N E S W) intensity because the distribution of net wall area in this example does not exactly match that in the modeled prototype.

Rounding to the near $100, the whole-building life-cycle cost savings are $1,400 in Scenario A and $1,200 in Scenario B.

We can find in Table 8 the fraction by which cool roof and cool walls reduce our annual whole-building HVAC energy cost:

Table 21. Annual whole-building HVAC energy cost saving fraction (%) in Example 1.

N	E	S	W	N E S W
1.11	2.58	2.5	2.21	8.3

This result is specific to the geometry of the prototype, and does not consider the net wall area of each façade on the actual home. However, it does indicate that making all four walls cool will lower the building's annual HVAC energy cost by about 8%.

3.4.2 Example 2: Adding neighbors to the home in Example 1

Assume the 6-m tall home in Example 1 is on the west side of a residential street, with its front neighbor across the street (30 m east), its rear neighbor across a pair of back yards (6 m west), and its side neighbors across narrow side yards (3 m north and 3 m south) (Figure 14).

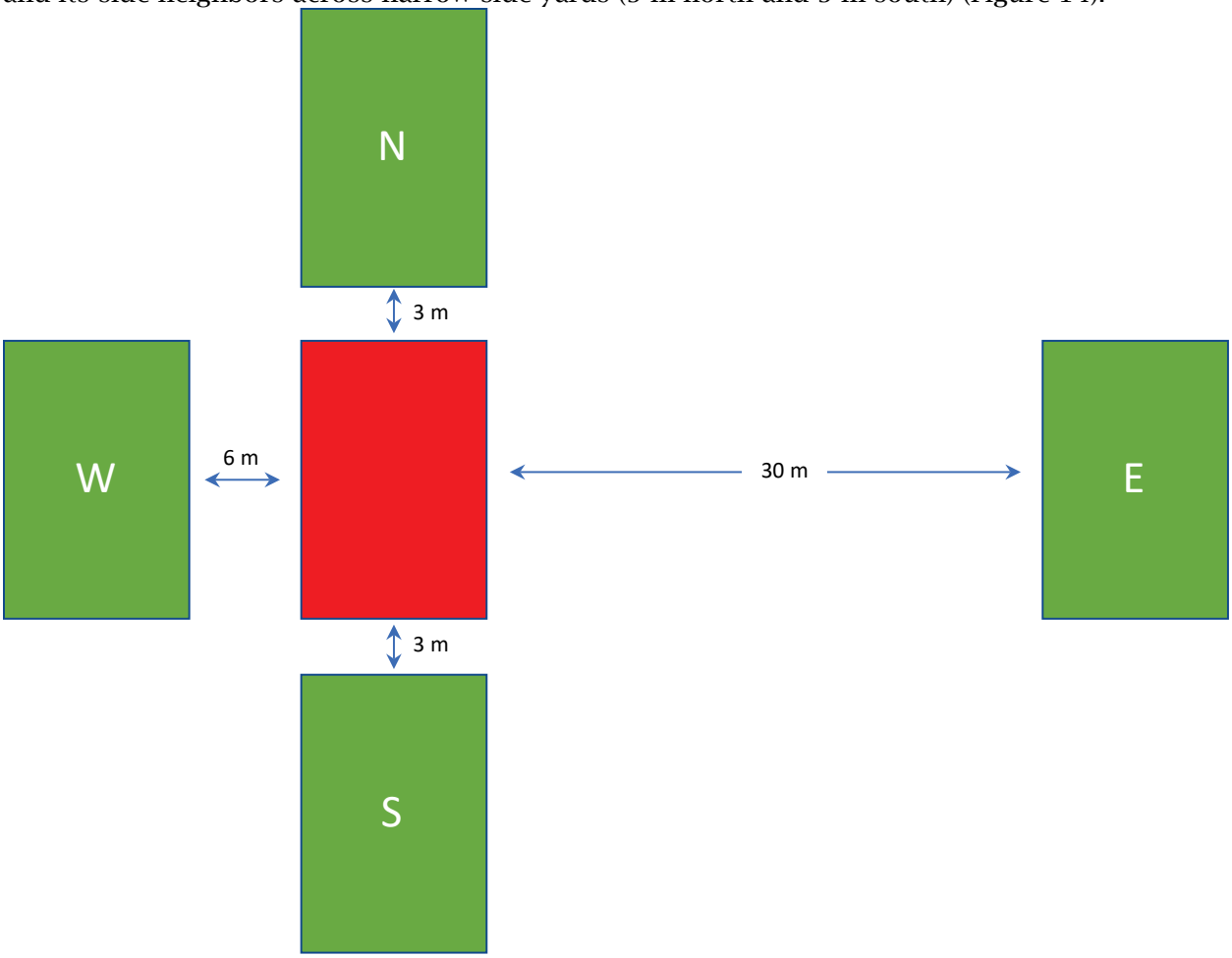

Figure 14. A single-family home (central building, in red) surrounded by its neighbors (in green). Each building is 10 m wide, 15 m long, and 6 m high.

We will show in Section 5 that the shading and reflection by these neighboring buildings will scale the sunlight incident on the walls of the central (modeled) building by the following "solar availability factors" (SAFs):

Table 22. Solar availability factors in Example 2.

N	E	S	W
0.47	0.92	0.50	0.63

Since cool wall savings are proportional to incident sunlight, we multiply each wall's isolated building annual HVAC energy cost savings intensity (Table 11) by its SAF (Table 22) to get its adjusted annual HVAC energy cost savings intensity:

Table 23. Annual HVAC energy cost savings intensity ($/m²) in Example 2.

N	E	S	W
0.17	0.77	0.41	0.45

Note that we do not try to scale the savings intensity in the four-wall case (N E S W).

We can then recalculate the life-cycle HVAC energy cost savings intensity, life-cycle cost savings intensity, and other values evaluated in Example 1, yielding

Table 24. Life-cycle HVAC energy cost savings intensity ($/m²) in Example 2.

N	E	S	W
1.44	6.57	3.49	3.86

Table 25. Life-cycle cost savings intensity ($/m²) in Example 2A.

N	E	S	W
1.44	6.57	3.49	3.86

Table 26. Life-cycle cost savings intensity ($/m²) in Example 2B.

N	E	S	W
0.63	5.76	2.68	3.05

Table 27. Simple payback time (y) in Example 2B.

N	E	S	W
4.8	1.0	2.0	1.8

While the life-cycle cost savings remains positive for all four walls, the Scenario B simple payback time for the north wall has grown to 4.8 y, or nearly half the assumed service life of the paint.

Using the net wall areas computed in Example 1 (Table 18), we get

Table 28. Life-cycle cost savings ($) in Example 2A.

N	E	S	W
72	480	175	282

Table 29. Life-cycle cost savings ($) in Example 2B.

N	E	S	W

32	420	134	223

Interactions with the neighboring buildings reduce the whole building life cycle cost savings by roughly $400, to about $1,000 in Scenario A and $800 in Scenario B.

Finally, we can use the SAFs to adjust the annual whole-building HVAC energy cost saving fraction. Total savings from the four cool walls is reduced to about 5.5% from about 8%.

Table 30. Annual whole-building HVAC energy cost saving fraction (%) in Example 2.

N	E	S	W
0.52	2.37	1.25	1.39

4 Detailed guide to cool-wall effects on an isolated building

Energy cost savings is only one measure of energy efficiency benefit. A wider list of properties related to energy use includes

- site energy (here, electricity or gas) consumed at the building;
- source energy (a.k.a. primary energy) required to produce the site energy;
- energy cost;
- peak power demand, or electric power demand averaged over peak demand hours (e.g., summer afternoons, noon to 6 pm local time); and
- emissions of carbon dioxide (CO_2), carbon dioxide equivalent (CO_2e), nitrogen oxides (NO_x), and sulfur dioxide (SO_2).

Annual savings in each of these properties depends on building category, location, vintage, and orientation, and can be disaggregated by surface(s) modified and by HVAC component (cooling, heating, or fan). There are also four metrics per property: baseline value, whole building absolute savings, whole building fractional savings, and savings intensity.

Since it is impractical to tabulate all these results within this document, we have prepared the Cool Surface Savings Explorer, or "Explorer" for short. The Explorer is an Excel[8] tool that parses the Cool Surface Savings Database, a comma separated value (CSV) text file containing the results of all simulations and calculations performed in Task 2.1 (energy savings for an isolated building).

[8] The tool runs in Excel for Windows, but not in Excel for Mac OS.

Note that the Explorer is *not* a general-purpose simulation tool or savings calculator. It simply extracts previously computed results from the Database.

Note also that our analysis has focused on the most common building categories, such as single-family home, medium office, and retail stand-alone. Results for some highly complex building prototypes, such as large office and large hotel, have not been fully vetted.

4.1 Installing the Explorer

The tool and database are available in a ZIP archive online at http://bit.ly/2Kwvtpu . To install, copy these two files to a local folder.

4.2 Operating the Explorer

Launching the Explorer will open the database and display a "Simulation selector" (hereafter, "Selector") window (Figure 15).

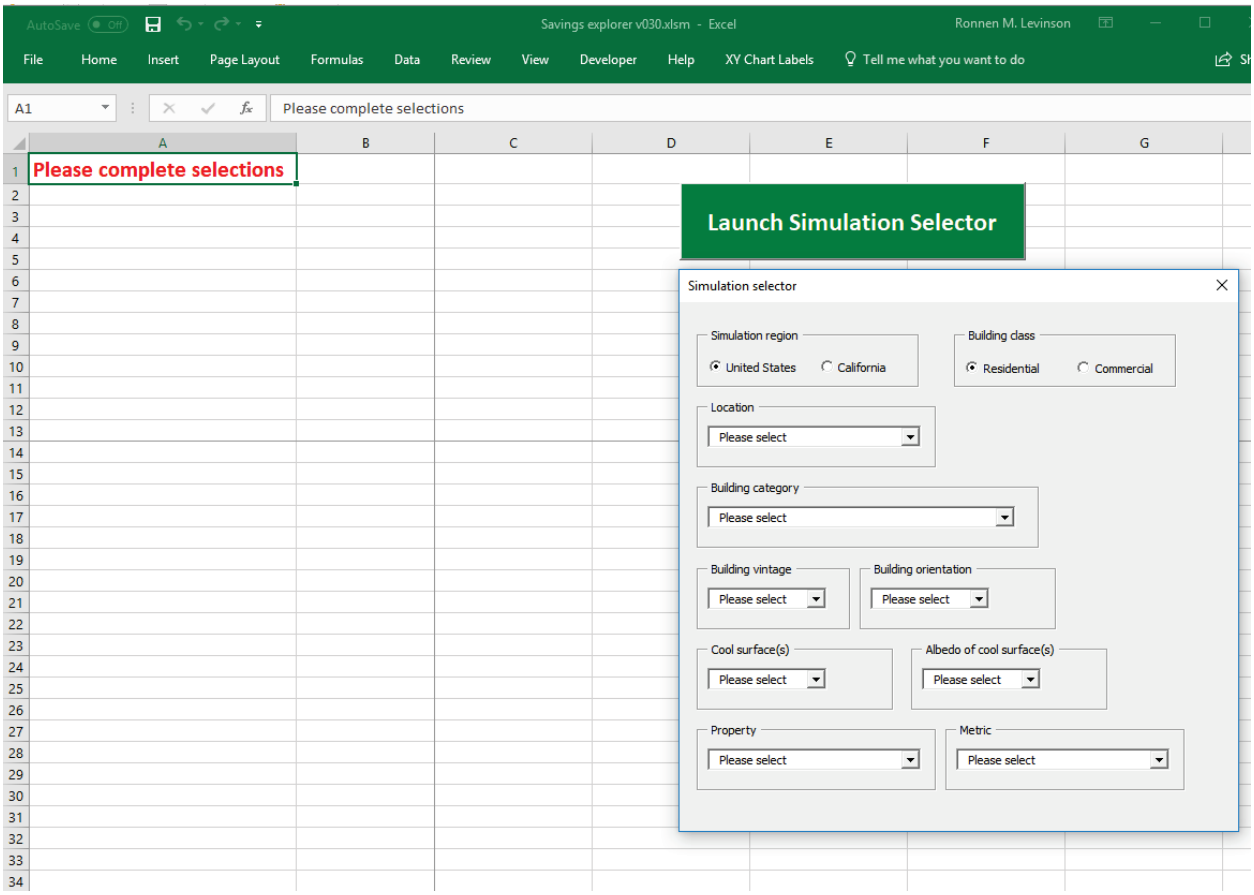

Figure 15. Initial appearance of the Explorer, with Simulation selector window at right (Figure 16).

Within the Selector:

1. Choose the simulation region (United State or California) and the building class (residential or commercial) (Figure 16). Changing the region or class may reset the location or building category to “Please select” because options for location and category depend on region and class.

2. Choose the location. Options vary with simulation region and building class (Figure 17 to Figure 19).

3. Choose the building category. Options vary with simulation region and building class (Figure 20 to Figure 23).

4. Choose the building vintage (Figure 24).

5. Choose the building orientation (Figure 25).

6. Choose the surface(s) to be made cool (Figure 26).

7. Choose the albedo to be assigned to the cool surface(s) (Figure 27).

8. Choose the property to be reported (Figure 28).

9. Choose the metric to be reported (Figure 29).

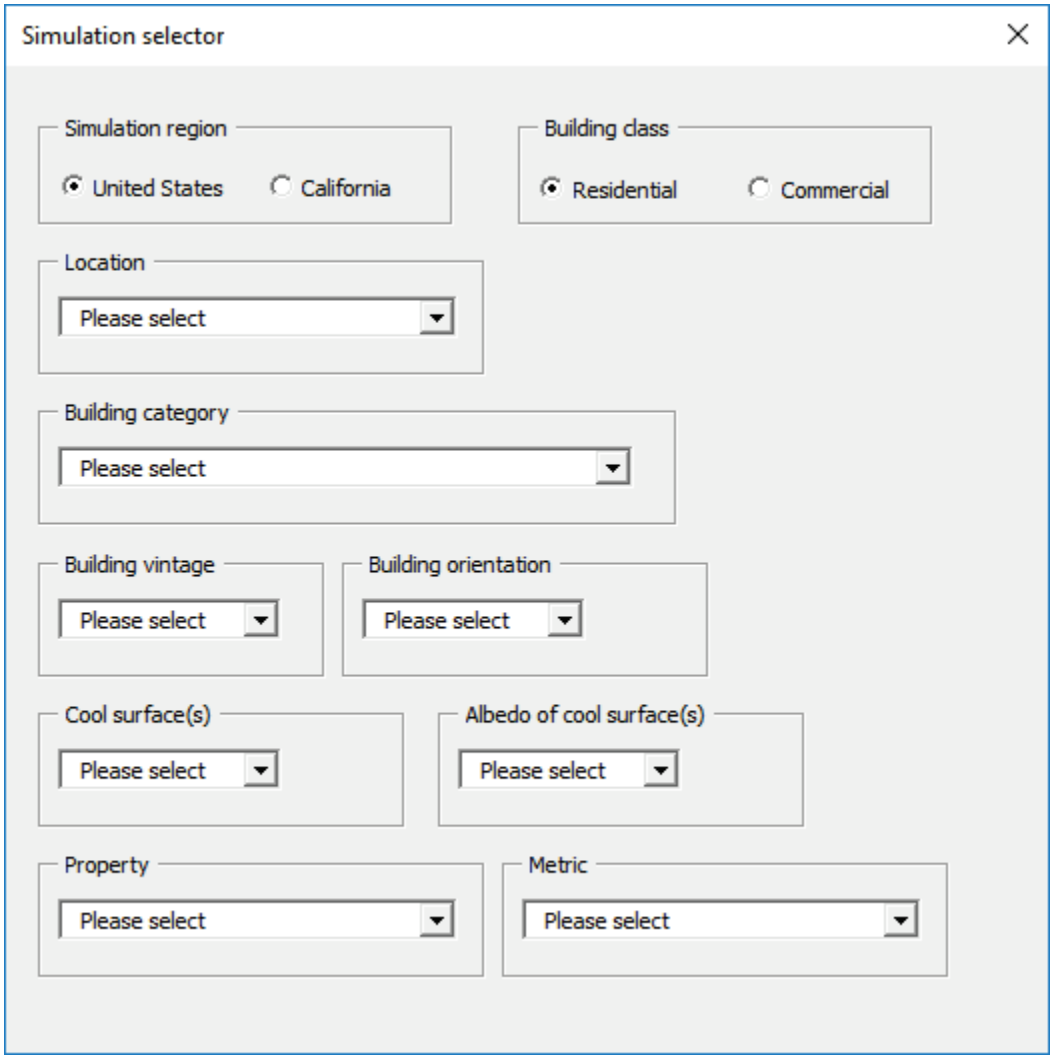

Figure 16. Initial appearance of Simulation selection window. Simulation region defaults to "United States" and building class defaults to "Residential", while all other inputs default to "Please select".

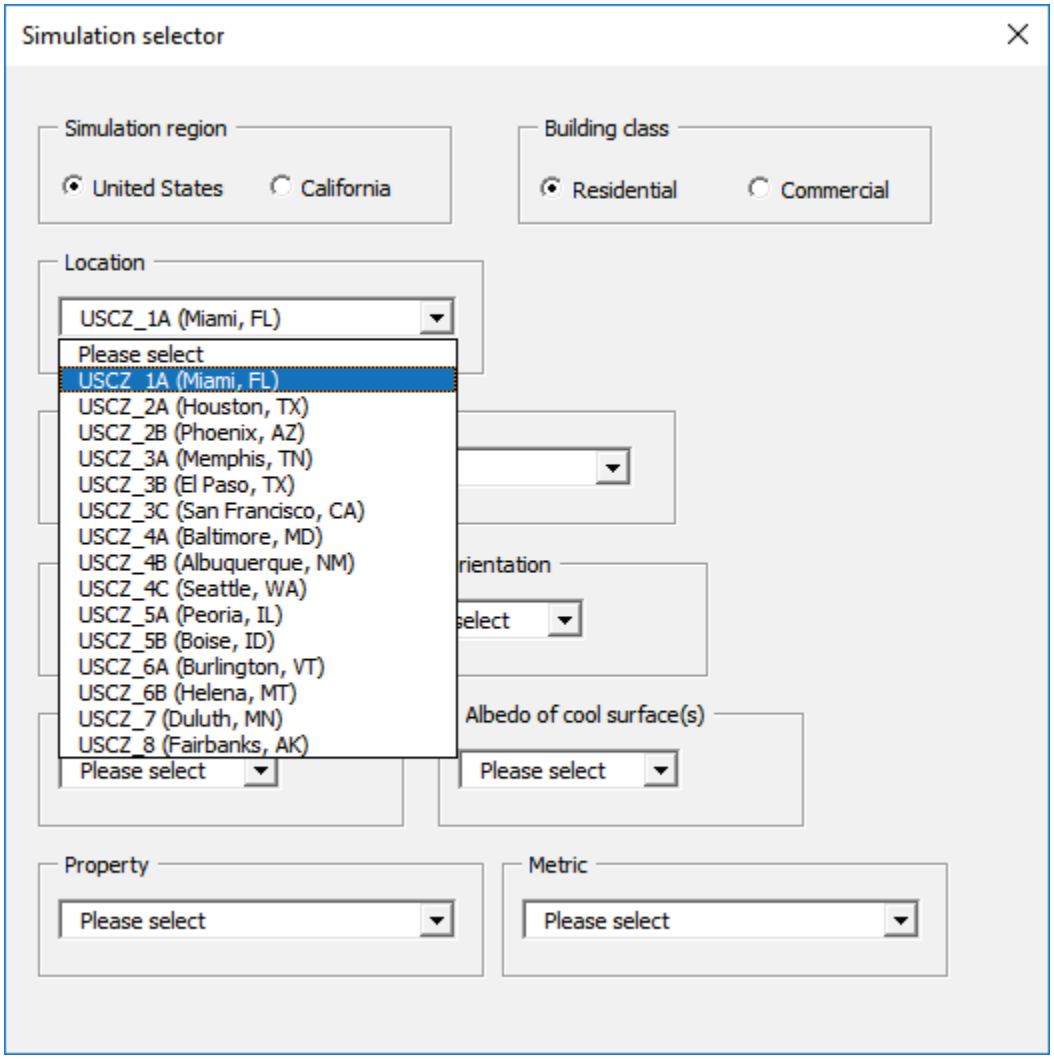

Figure 17. U.S. residential building locations.

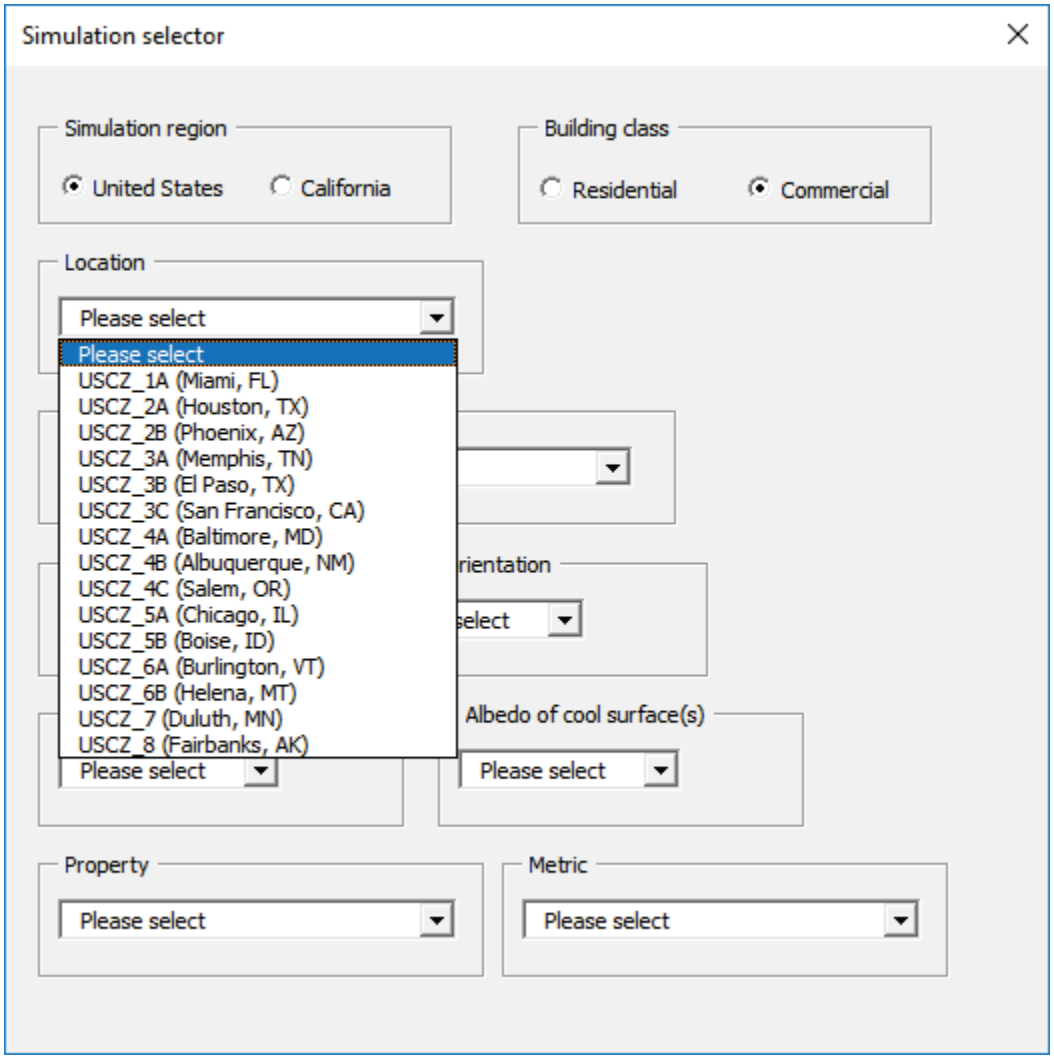

Figure 18. U.S. commercial buildings locations.

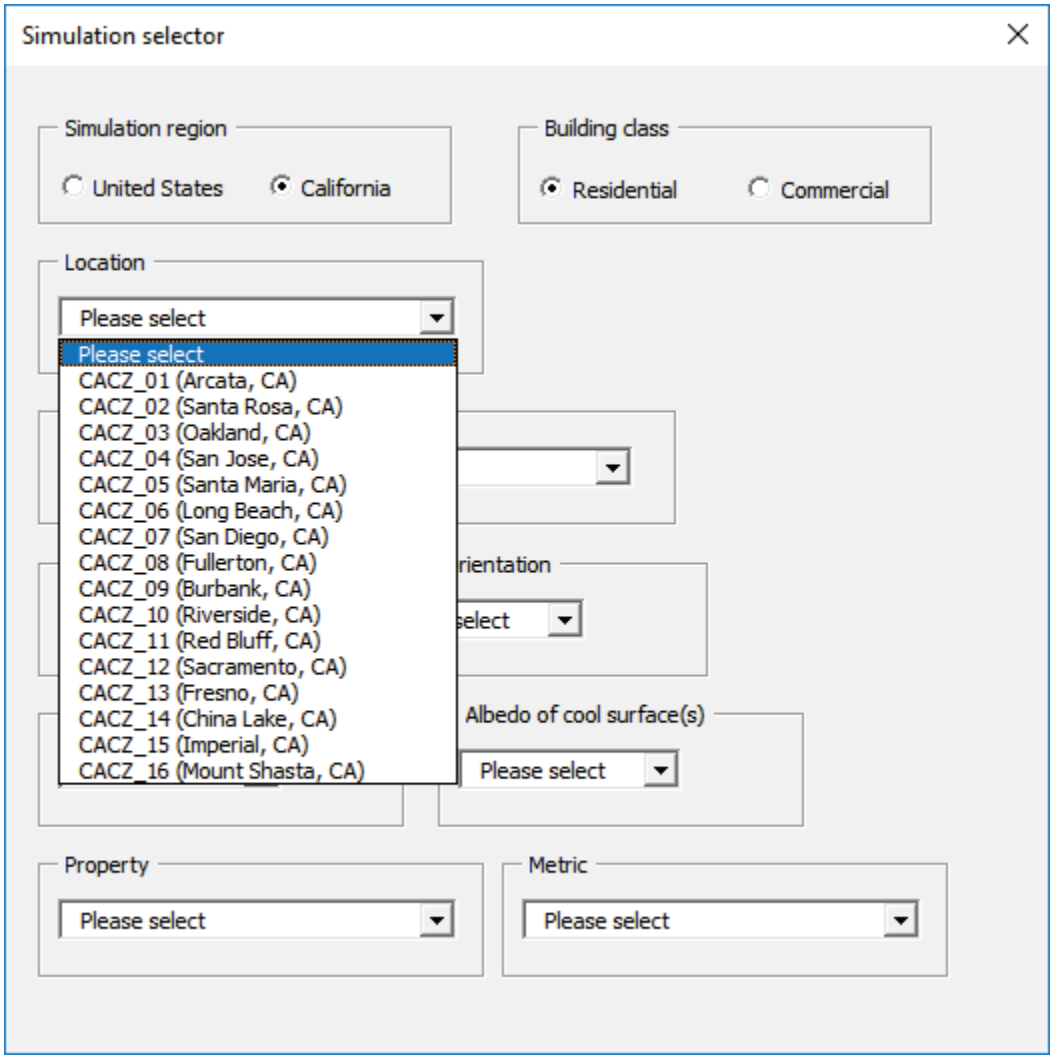

Figure 19. California residential (and commercial) building locations.

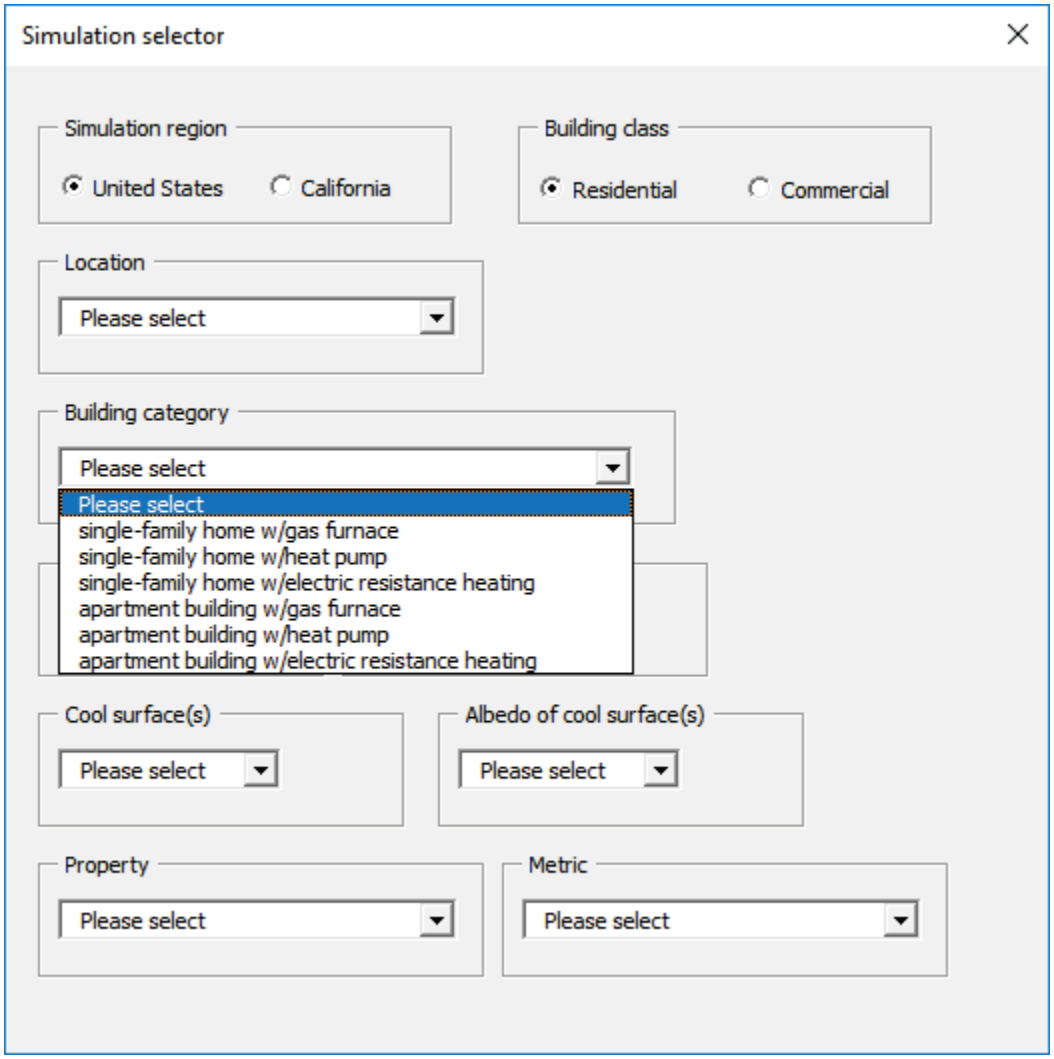

Figure 20. U.S. residential building categories.

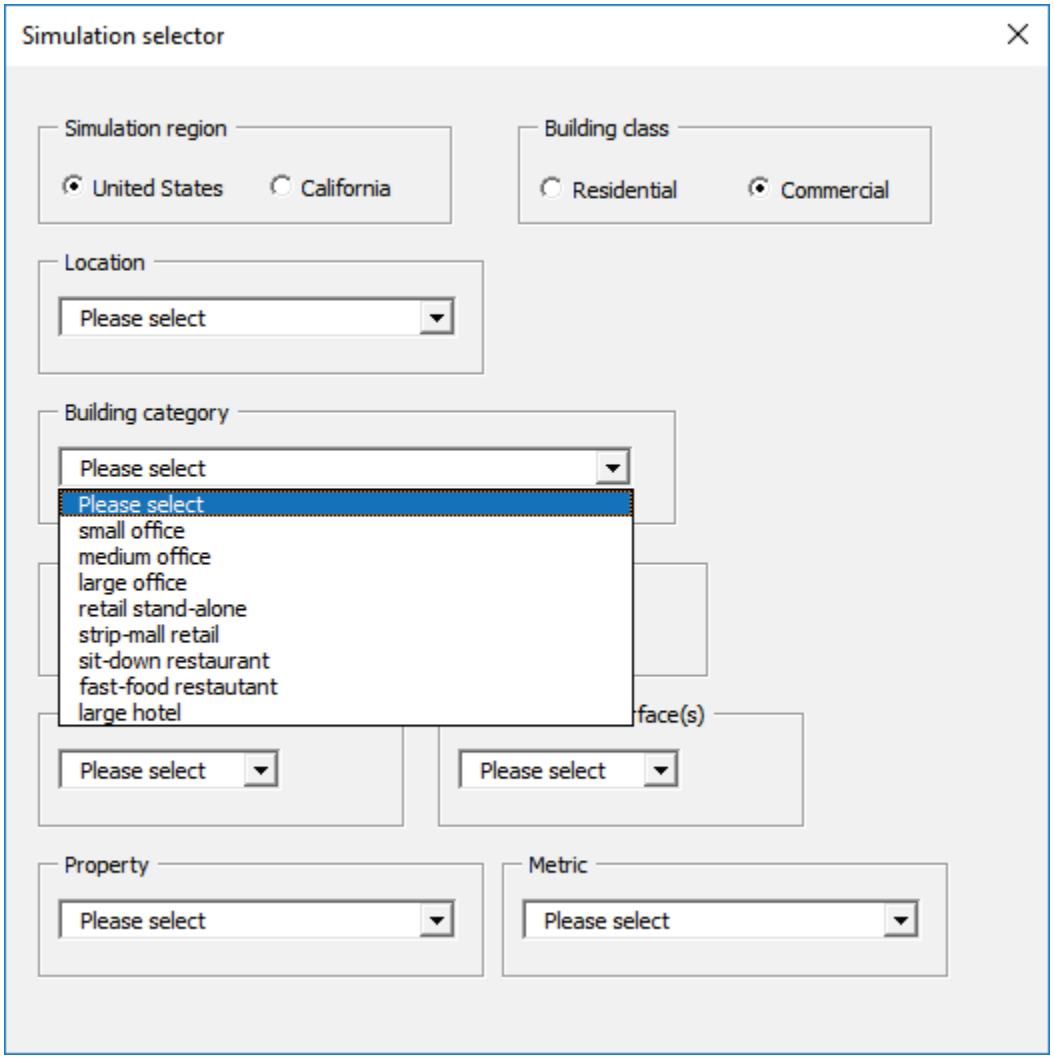

Figure 21. U.S. commercial building categories.

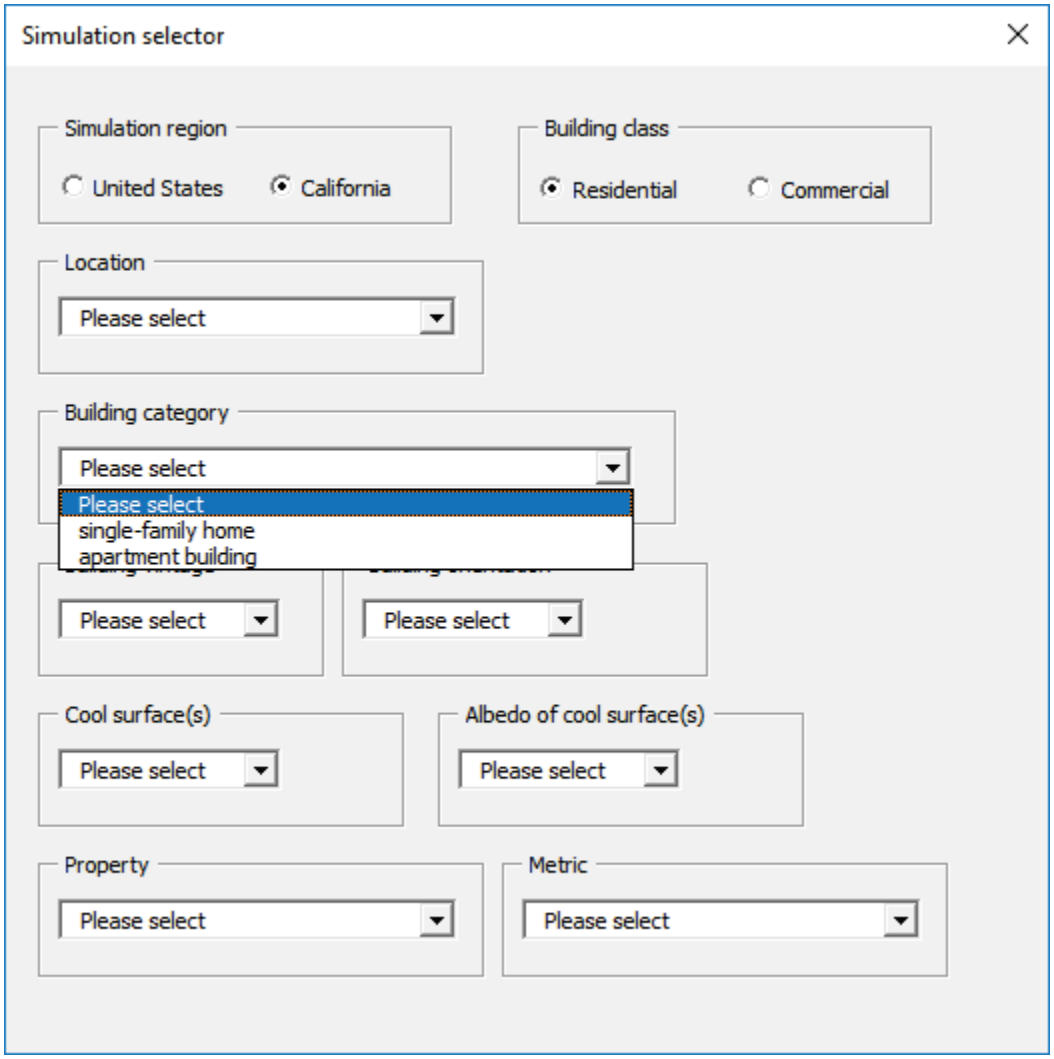

Figure 22. California residential building categories.

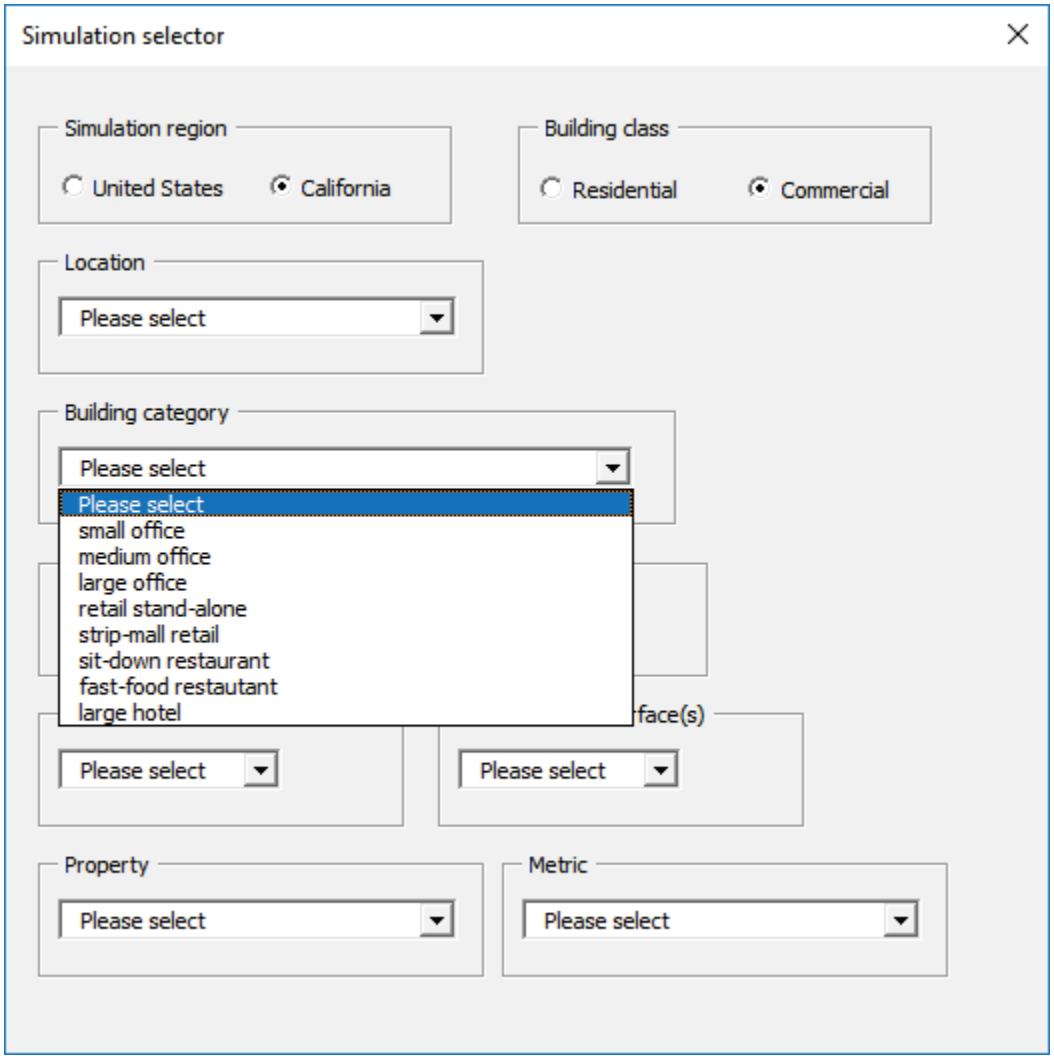

Figure 23. California commercial building categories.

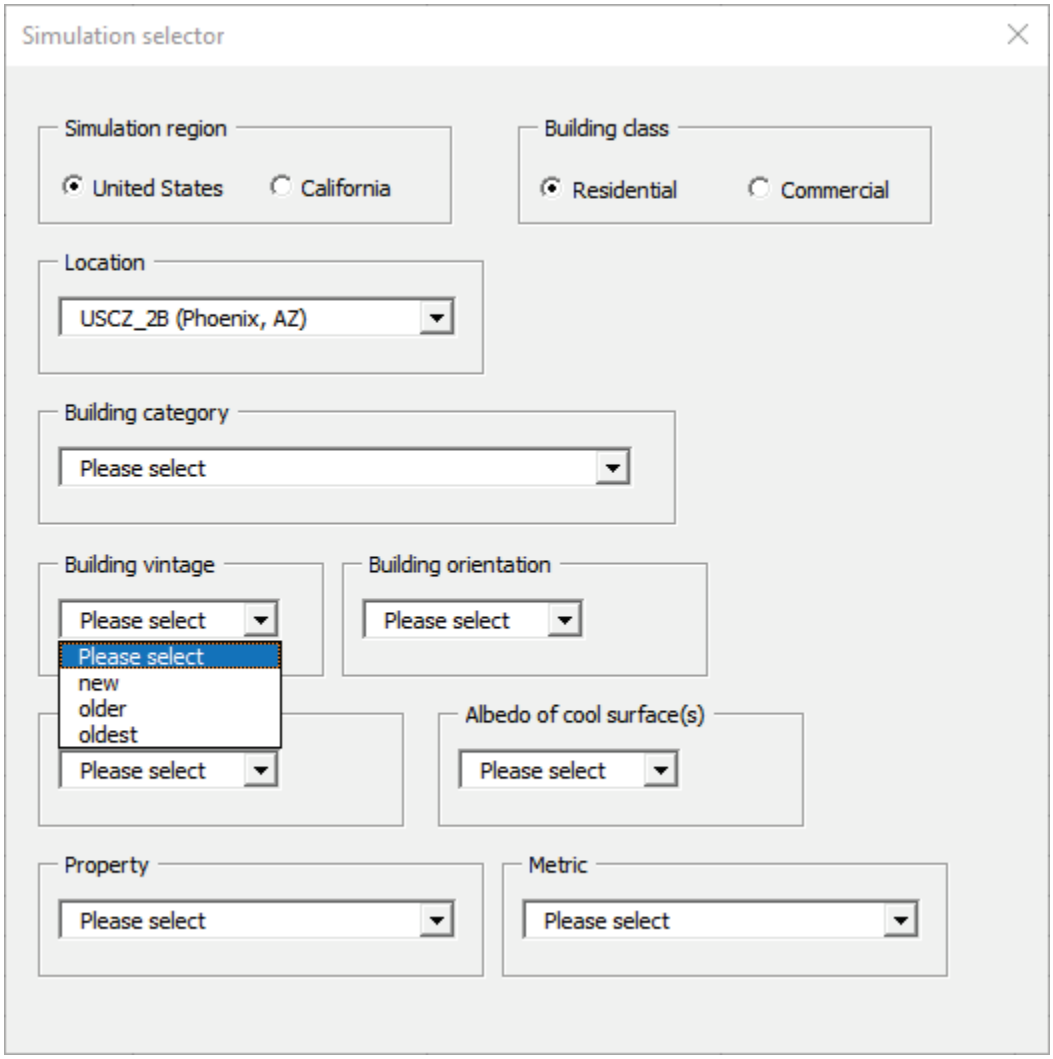

Figure 24. Building vintages.

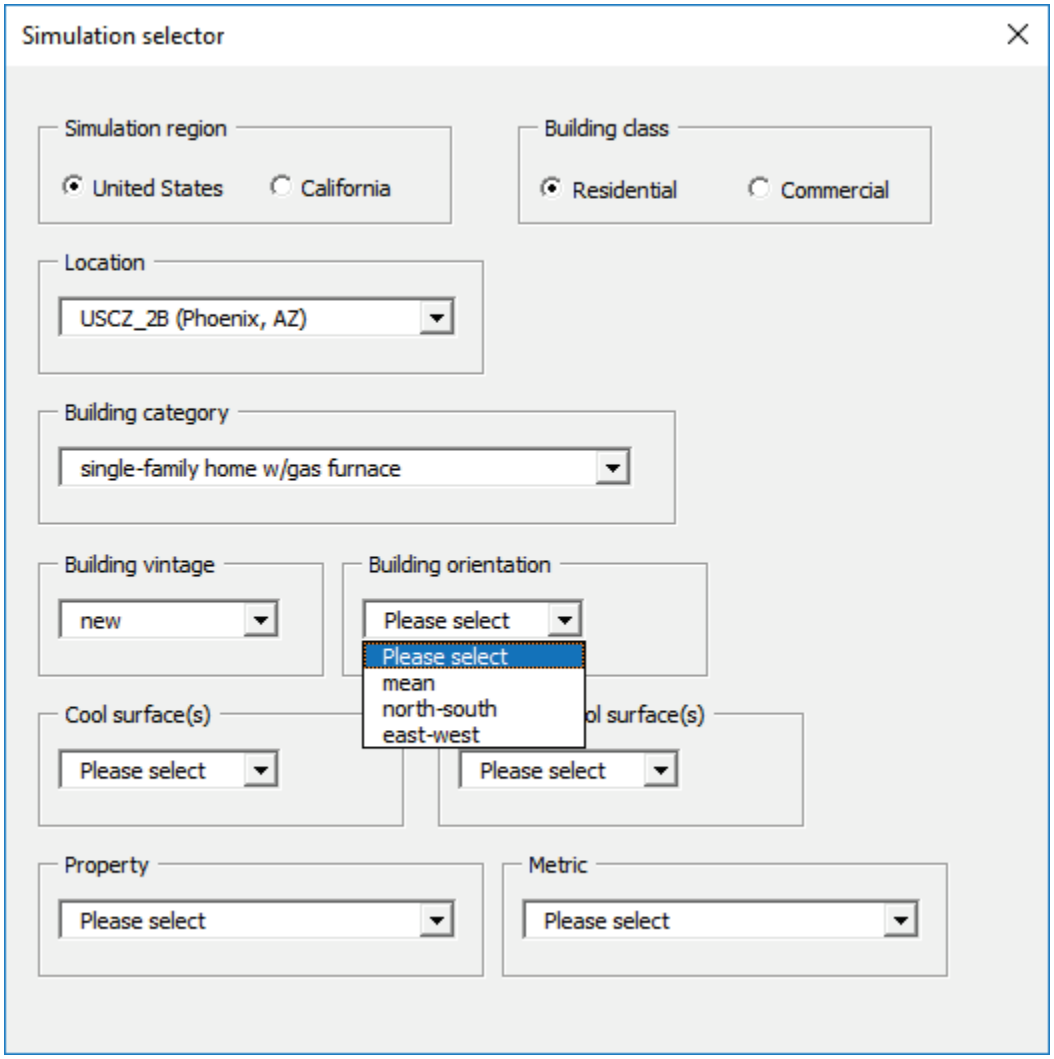

Figure 25. Building orientations.

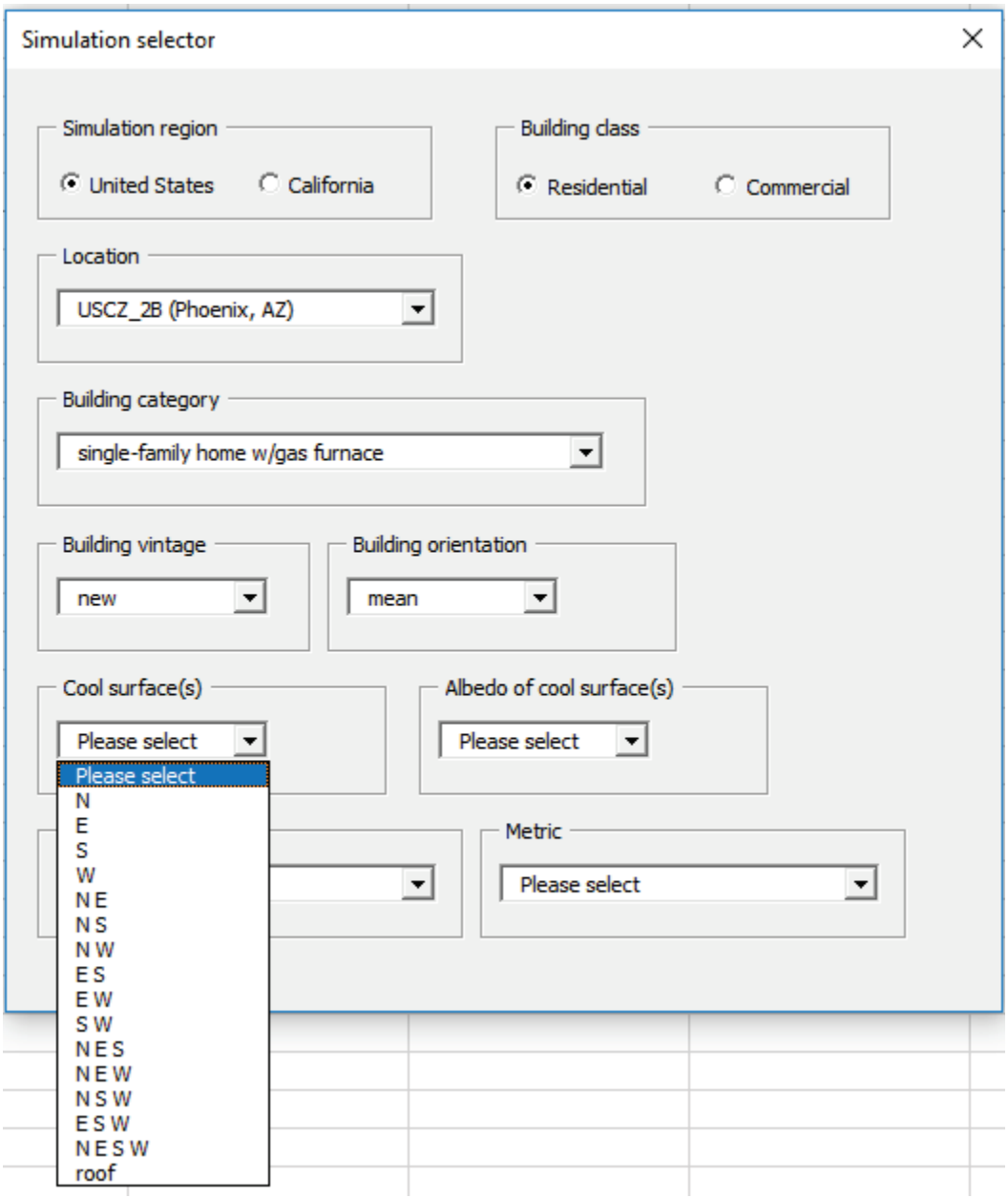

Figure 26. Surfaces that can be made cool.

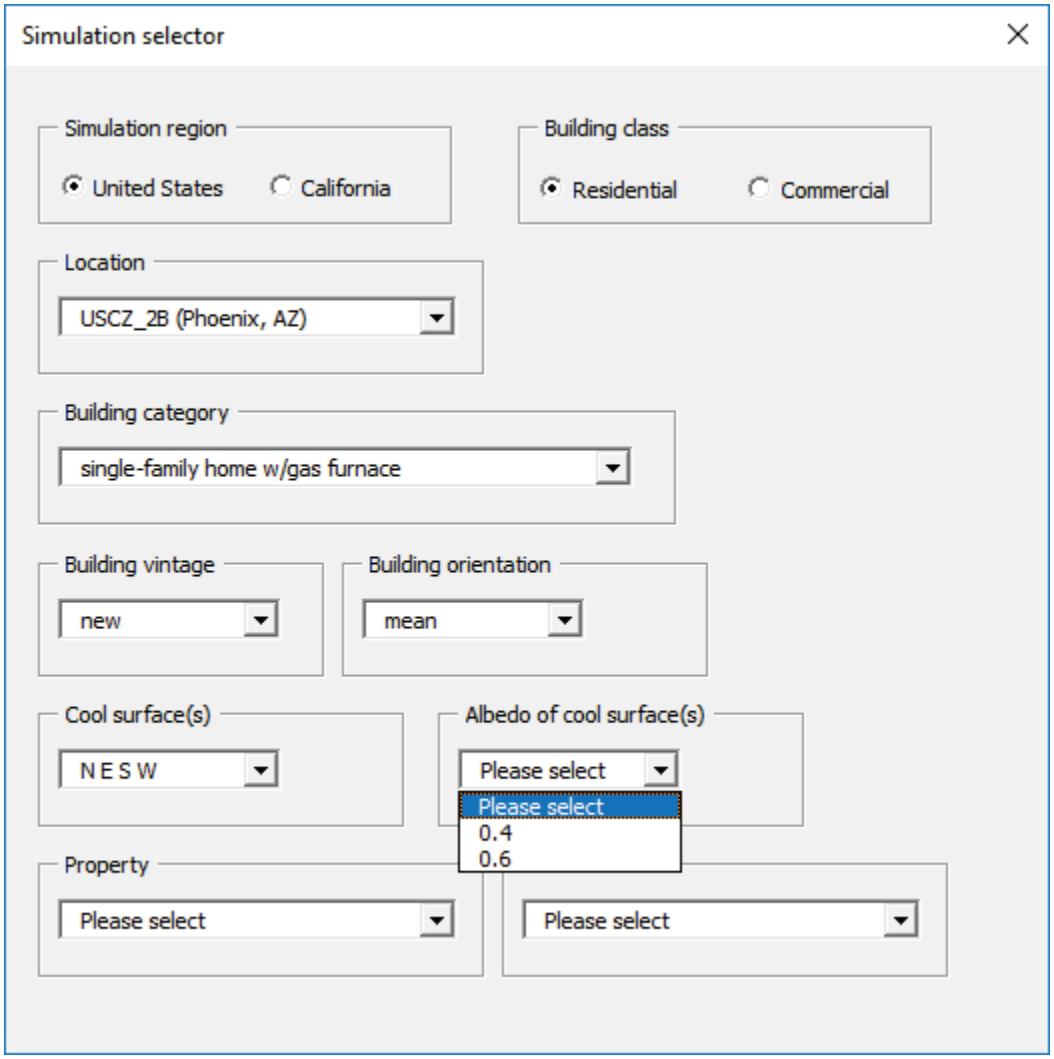

Figure 27. Albedos that can be assigned to the cool surface(s).

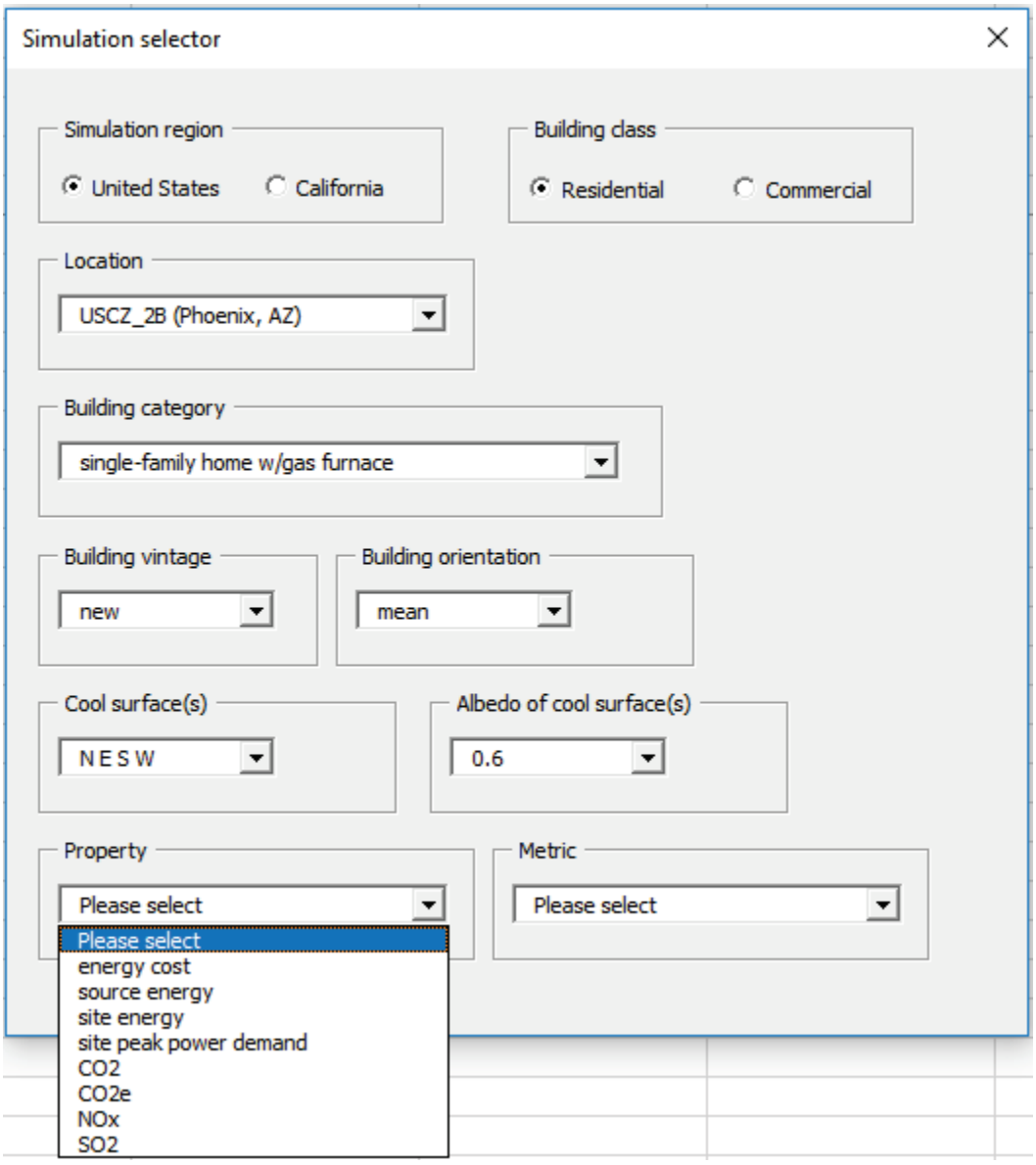

Figure 28. Properties that can be reported.

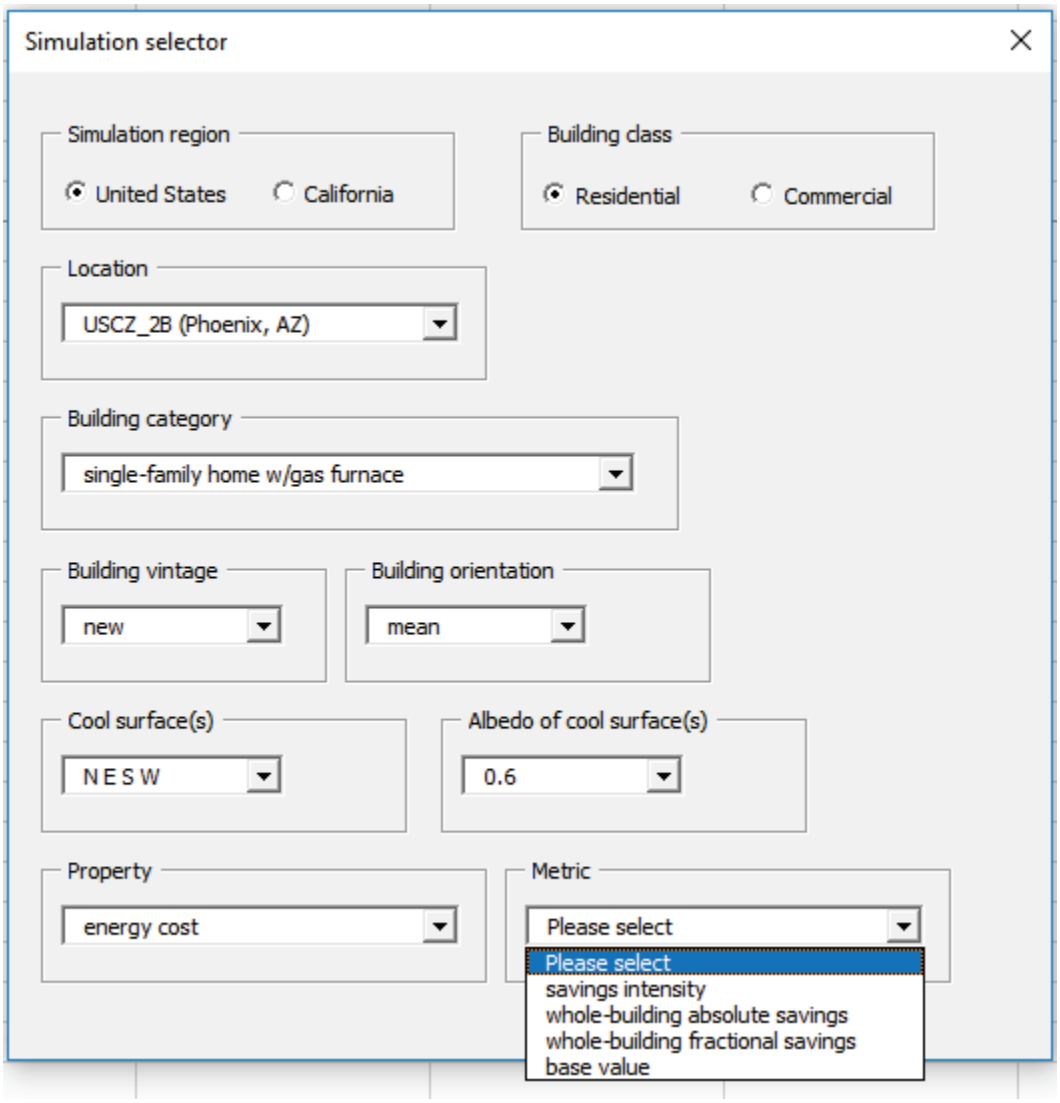

Figure 29. Metrics that can be reported.

Once all selections are complete, the Explorer will then filter the Database and copy simulation parameters and results to columns A and B of the Explorer sheet (Figure 30).

Revising choices within the Selector will update the parameters and results shown in columns A and B. Clearing any selection—i.e., directly or indirectly changing it to "Please select"—will clear the parameters and results displayed in columns A and B.

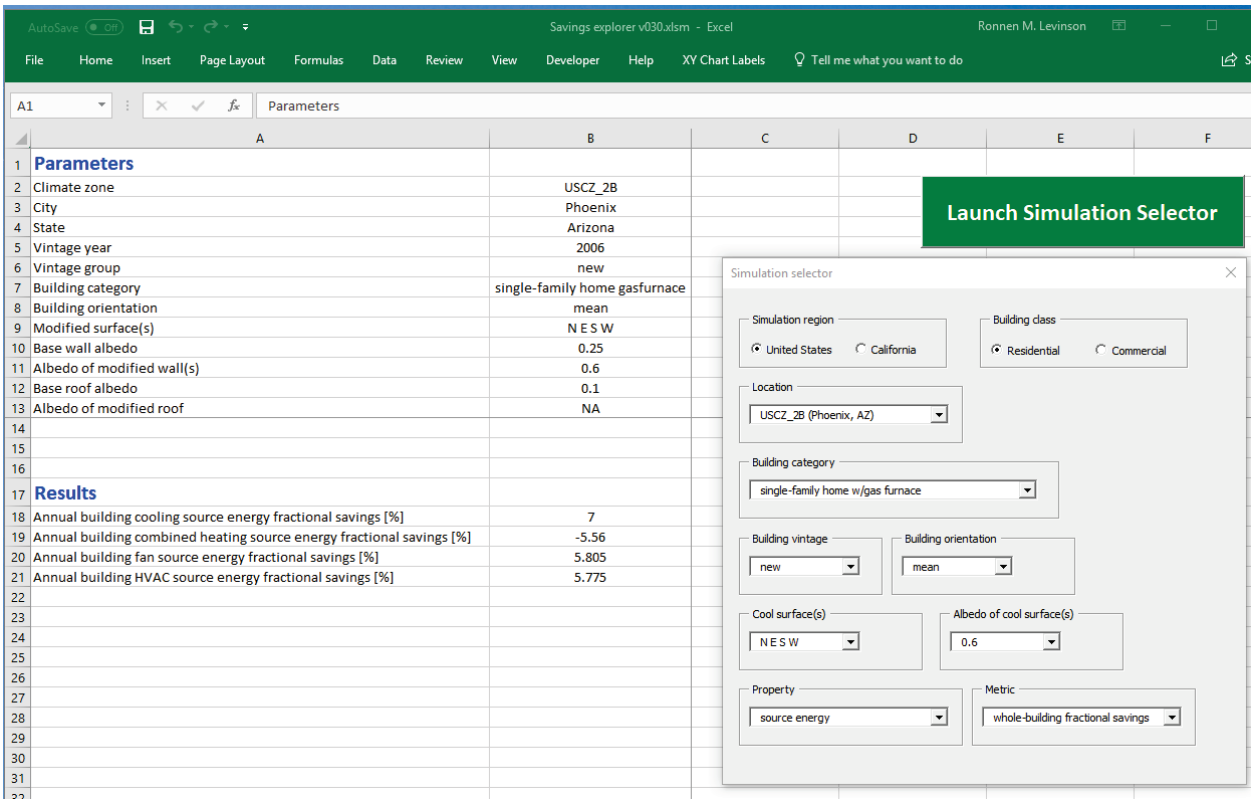

Figure 30. Explorer window displays database entries in columns A and B after parameter selection is complete.

4.2.1 Example 1: Whole-building source energy savings fractions for a new single-family home w/gas furnace in Phoenix, AZ, upon raising albedos of all four walls to 0.60 from 0.25

Configuring the Selector as shown in Figure 31 returns the whole-building energy saving fractions shown in cells A18 – B21 of Figure 32.

Observe that the simulation parameters listed in cells A1 – B13 include some not explicitly specified within the Selector, including vintage year (2006), which is set according to vintage group (new) and state (Arizona); base wall albedo (0.25), which is universal; base roof albedo (0.1), which is set according to building class (residential); and albedo of modified roof (NA), which is not applicable here because the roof's albedo was not modified in this simulation.

Raising wall albedo lowers whole-building cooling, heating, fan, and HVAC (cooling + heating + fan) annual source energy uses by 7.0%, -5.6%, 5.8%, and 5.8%, respectively. Note that "combined heating" sums all modes of heating used in the building (gas and/or electric).

4.2.2 Example 2: Site energy savings intensities for the building considered in Example 1

A useful application of the Explorer is to retrieve the site energy savings, which can be used to calculate energy cost, source energy, or emission savings for energy prices, source energy factors, or emission factors other than those assumed in our study.

Configuring the Selector as shown in Figure 33 returns the site energy savings intensities shown in cells A18 – B21 of Figure 34.

Raising wall albedo yields cooling, gas heating, electric heating, and fan annual site energy savings intensities of 4.791 kWh/m², -0.043 therms/m², 0 kWh/m², and 0.875 kWh/m².

To compute new energy cost, source energy, or emission savings, it is convenient to sum the component annual site electricity savings (cooling, electric heating, and fan) to obtain HVAC annual site electricity savings. Here the HVAC annual electricity savings intensity is 4.791 (cooling) + 0 (electric heating) + 0.875 (fan) = 5.666 kWh/m², and the HVAC annual site gas savings intensity is (gas heating) are -0.043 therms/m².

To obtain annual energy cost savings intensity, we sum the product of the annual site electricity savings intensity and the local electricity price and the product of the annual site gas savings intensity and the local gas price. If electricity costs $0.12/kWh and gas costs $1.50/therm, the HVAC annual energy cost savings intensity will be 5.666 kWh/m² × 0.12/kWh – 0.043 therms/m² × $1.50/therm = $0.615/m².

Computing source energy or emission savings from site energy savings is analogous. Please see the Task 2.1 report: *Simulated HVAC energy savings in an isolated building* for information about energy prices, source energy factors, and emission factors.

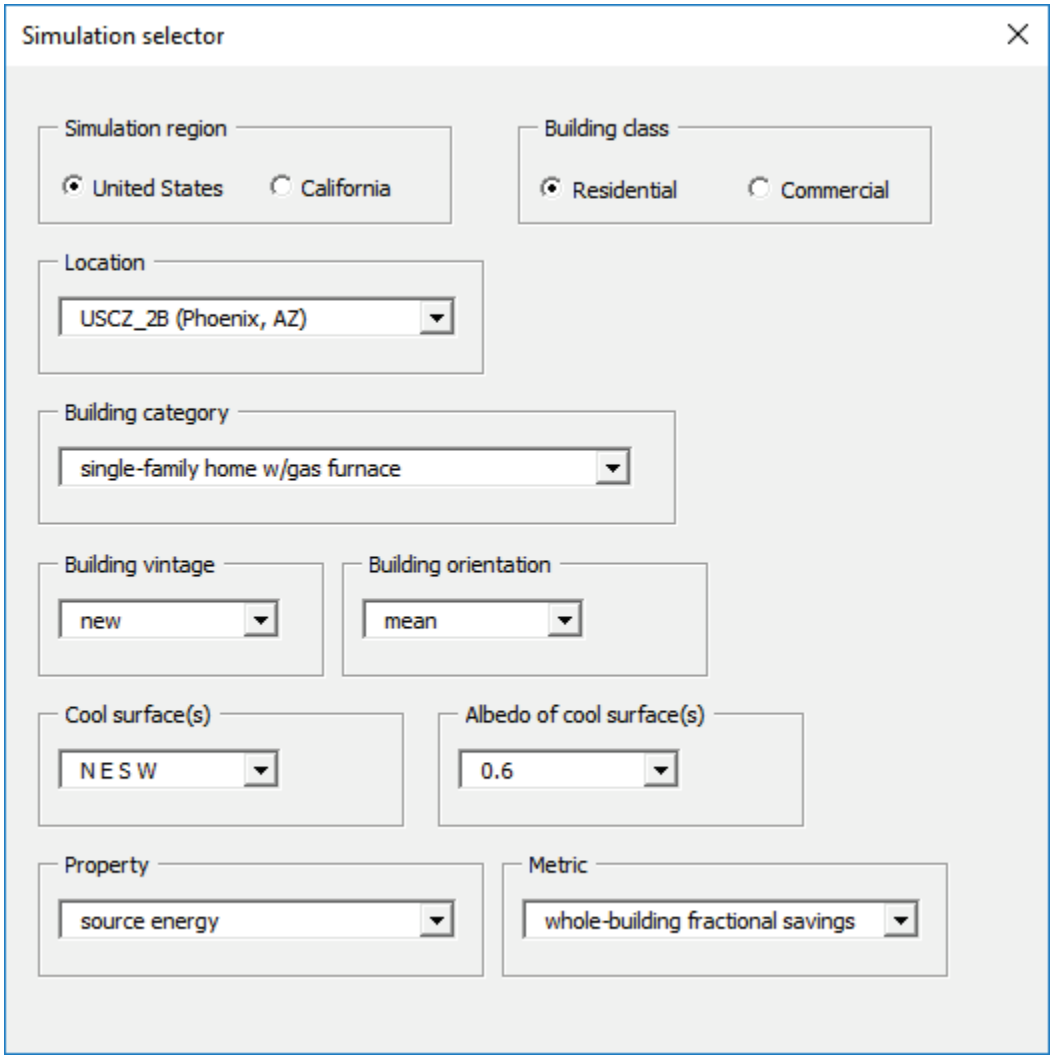

Figure 31. Close-up of Figure 30 showing Selector settings used to obtain whole-building source energy fractional savings for a new single-family home w/gas furnace in Phoenix, AZ (U.S. climate 2B) upon raising the albedo of all walls to 0.60 from the baseline of 0.25. Choosing "mean" building orientation averages results obtained for north-south and east-west orientations of the building's long axis.

	A	B
1	**Parameters**	
2	Climate zone	USCZ_2B
3	City	Phoenix
4	State	Arizona
5	Vintage year	2006
6	Vintage group	new
7	Building category	single-family home gasfurnace
8	Building orientation	mean
9	Modified surface(s)	N E S W
10	Base wall albedo	0.25
11	Albedo of modified wall(s)	0.6
12	Base roof albedo	0.1
13	Albedo of modified roof	NA
14		
15		
16		
17	**Results**	
18	Annual building cooling source energy fractional savings [%]	7
19	Annual building combined heating source energy fractional savings [%]	-5.56
20	Annual building fan source energy fractional savings [%]	5.805
21	Annual building HVAC source energy fractional savings [%]	5.775

Figure 32. Close-up of Figure 30 showing whole-building source energy fractional savings for a new single-family home w/gas furnace in Phoenix, AZ (U.S. climate 2B) upon raising the albedo of all walls to 0.60 from the baseline of 0.25.

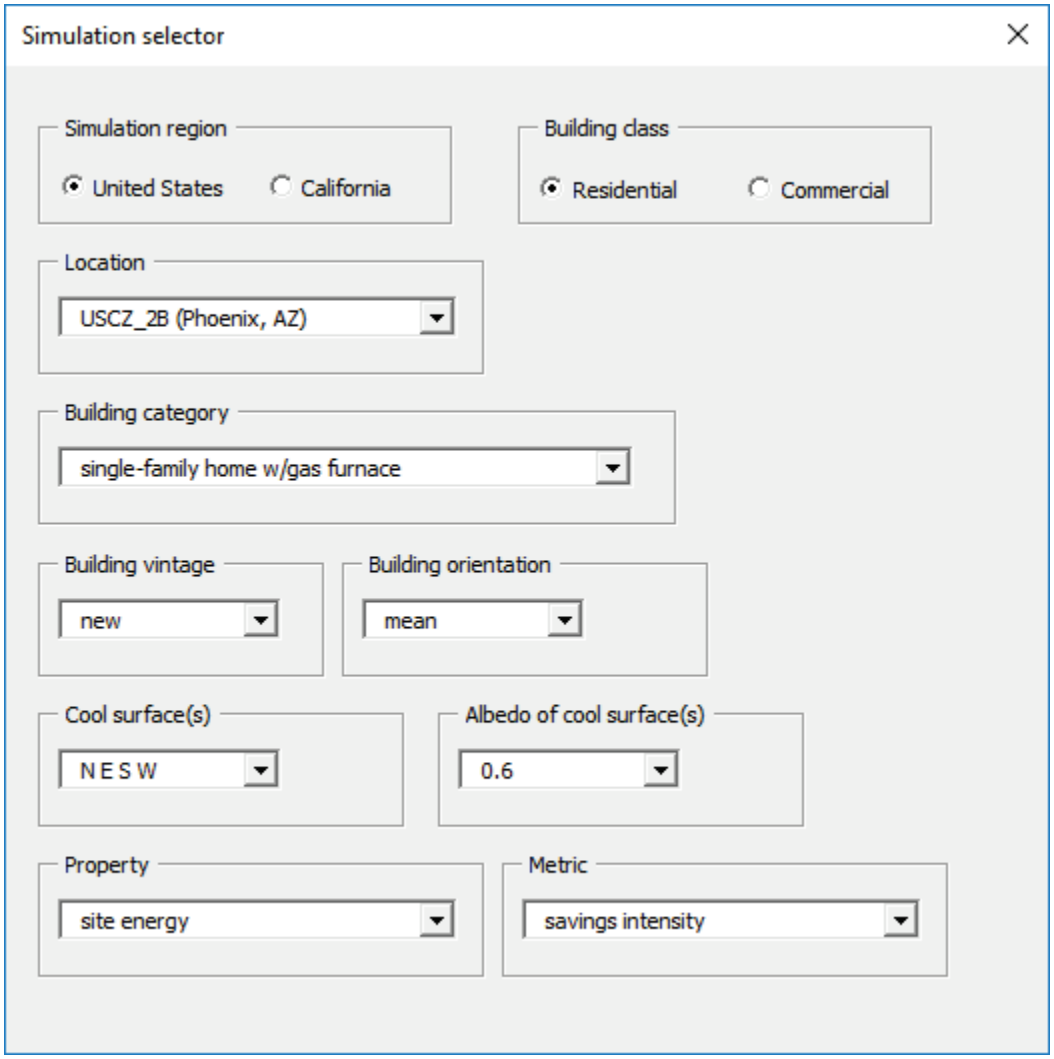

Figure 33. Selector settings to obtain site energy savings intensities for a new single-family home w/gas furnace in Phoenix, AZ (U.S. climate 2B) upon raising the albedo of all walls to 0.60 from the baseline of 0.25.

	A	B
1	**Parameters**	
2	Climate zone	USCZ_2B
3	City	Phoenix
4	State	Arizona
5	Vintage year	2006
6	Vintage group	new
7	Building category	single-family home gasfurnace
8	Building orientation	mean
9	Modified surface(s)	N E S W
10	Base wall albedo	0.25
11	Albedo of modified wall(s)	0.6
12	Base roof albedo	0.1
13	Albedo of modified roof	NA
14		
15		
16		
17	**Results**	
18	Annual cooling site energy absolute savings intensity [kWh/m2]	4.791
19	Annual gas heating site energy absolute savings intensity [therms/m2]	-0.043
20	Annual electric heating site energy absolute savings intensity [kWh/m2]	0
21	Annual fan site energy absolute savings intensity [kWh/m2]	0.875

Figure 34. Site energy savings intensities for a single-family home w/gas furnace in Phoenix, AZ (U.S. climate 2B) upon raising the albedo of all walls to 0.60 from the baseline of 0.25.

5 Adjusting cool wall effects to account for neighboring buildings

The solar availability (incident solar radiation) for a central (modeled) building can be reduced by shadows cast by neighboring buildings, and increased by sunlight reflected from neighboring buildings. The solar availability factor (SAF) of a central building wall, defined as the ratio of sunlight incident on the central building wall in the presence of the neighboring wall to that incident in the absence of the neighboring wall, can be used to scale the cool-wall savings simulated for an isolated central building (no neighbors).

This approach emphasizes simplicity, so that its results can be applied knowing only the canyon aspect ratio R (ratio of building height H to building separation W), city, and month. It assumes that the central building and its neighbors are of equal height, and does not consider shading or reflection by surfaces other than neighboring walls, such as trees. The theory and calculation of SAF is detailed in the Task 2.3 report: *Using solar availability to adjust HVAC energy savings.*

To obtain the solar availability factor for a central wall, first calculate its canyon aspect ratio $R = H/W$. Our guidelines focus on results for the four aspect ratios drawn to scale in Figure 35:

- R=0.2, representing two-story single-family homes across a residential street (H=6 m, W=30 m);
- R=1, representing two-story single-family across small back yards (H=6 m, W=6 m);
- R=2, representing adjacent two-story single-family homes on the same side of a street (H=6 m, W=3 m); and
- R=10, representing adjacent 10-story office buildings on the same side of the street (H=30 m, W=3 m).

Figure 35. Canyon aspect ratio $R = H/W$ = 0.2, 1, 2, or 10.

Figure 36 illustrates variation with central wall orientation (N, E, S, or W) and aspect ratio (0.2, 1, 2, or 10) of monthly SAF in Fresno, CA when the central and neighboring walls each have albedo 0.25. For greatest accuracy, we would apply the cooling-season mean SAF to cooling energy savings, the heating-season mean SAF to heating energy savings, and the annual mean SAF to fan energy savings. However, that requires inspection of the polar plots and details of the local heating and cooling season.

We can trade accuracy for simplicity by applying the annual average SAF to all savings. This strategy works best when monthly SAF varies little over the course of the year, and less well if there are strong seasonal variations.

Table 31 reports for all 17 climates shown in Figure 18 the annual mean, minimum, maximum, and range (maximum – minimum) values of monthly SAF for conventional central and neighboring walls by climate, central wall orientation, and aspect ratio.

For the Fresno single-family home scenario in Section 3.4.2, we take the annual mean SAF for the east wall (R = 0.2) from Table 31a; the annual mean SAF for the west wall (R = 1) from Table 31b; and the annual mean SAFs for north and south walls (R = 2) from Table 31c. The application of SAF to scale savings is worked in Section 3.4.2.

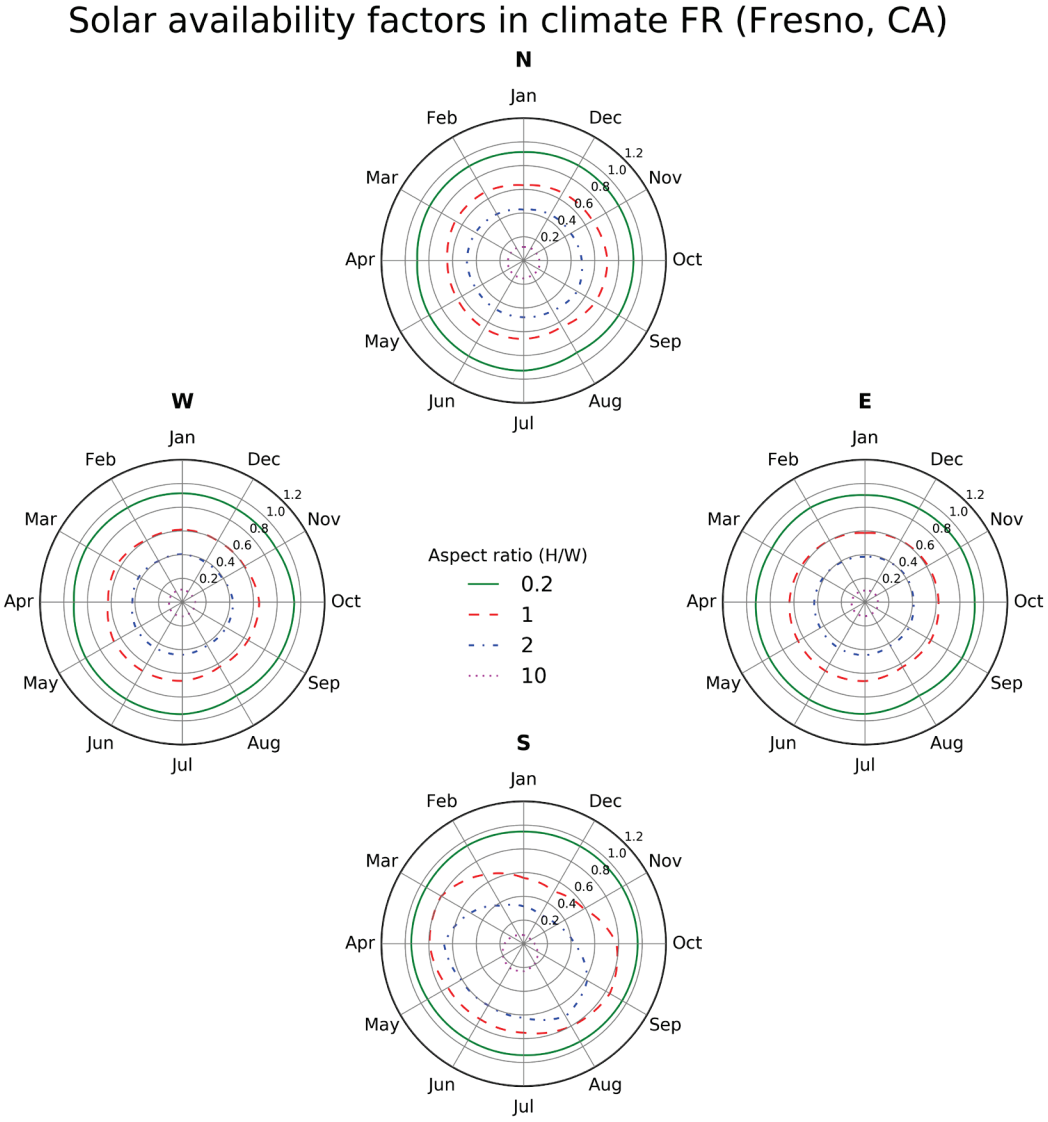

Figure 36. Monthly SAFs for a north (N), east (E), south (S), or west (W) conventional central wall (ρ=0.25) with conventional neighboring wall (ρ=0.25). Results shown for aspect ratios 0.2, 1, 2, and 10 in Fresno, CA.

Table 31. Annual mean, minimum, maximum, and range (maximum – minimum) values of monthly SAF for a north (N), east (E), south (S), or west (W) conventional central wall (ρ=0.25) with a conventional neighboring wall (ρ=0.25). Results shown by climate for aspect ratios of (a) R=0.2, (b) R=1, (c) R=2, and (d) R=10.

(a) aspect ratio R=0.2

	N				E				S				W			
	mean	min	max	range	mean	min	max	range	mean	min	max	range	mean	min	max	range
1A (Miami, FL)	0.91	0.91	0.92	0.02	0.92	0.89	0.94	0.05	0.93	0.91	0.96	0.05	0.91	0.84	0.94	0.10
2A (Houston, TX)	0.91	0.89	0.92	0.03	0.91	0.86	0.94	0.07	0.93	0.91	0.95	0.04	0.91	0.86	0.93	0.07
2B (Phoenix, AZ)	0.92	0.86	0.95	0.09	0.91	0.87	0.95	0.08	0.95	0.93	0.97	0.04	0.92	0.88	0.95	0.06
3A (Memphis, TN)	0.92	0.90	0.93	0.03	0.92	0.85	0.94	0.08	0.94	0.92	0.96	0.04	0.91	0.84	0.94	0.10
3B (El Paso, TX)	0.93	0.91	0.95	0.04	0.94	0.88	0.96	0.07	0.95	0.93	0.97	0.04	0.93	0.90	0.94	0.04
BU (Burbank, CA)	0.92	0.91	0.94	0.03	0.93	0.89	0.94	0.06	0.95	0.93	0.96	0.04	0.93	0.90	0.95	0.05
FR (Fresno, CA)	0.92	0.90	0.93	0.03	0.92	0.90	0.95	0.04	0.95	0.94	0.96	0.03	0.93	0.91	0.95	0.04
3C (San Francisco, CA)	0.91	0.88	0.94	0.06	0.92	0.87	0.94	0.07	0.95	0.93	0.96	0.03	0.92	0.89	0.94	0.05
4A (Baltimore, MD)	0.91	0.88	0.93	0.06	0.90	0.74	0.94	0.19	0.94	0.91	0.96	0.05	0.90	0.83	0.93	0.10
4B (Albuquerque, NM)	0.93	0.88	0.97	0.09	0.92	0.87	0.95	0.08	0.95	0.93	0.97	0.03	0.92	0.89	0.95	0.06
4C (Seattle, WA)	0.91	0.90	0.92	0.03	0.91	0.85	0.94	0.08	0.94	0.91	0.96	0.05	0.90	0.82	0.93	0.12
5A (Chicago, IL)	0.91	0.91	0.93	0.02	0.91	0.86	0.94	0.08	0.94	0.92	0.95	0.03	0.91	0.84	0.94	0.10
5B (Boise, ID)	0.92	0.90	0.94	0.03	0.91	0.86	0.94	0.08	0.95	0.92	0.96	0.04	0.91	0.86	0.95	0.09
6A (Burlington, VT)	0.91	0.87	0.93	0.06	0.90	0.82	0.93	0.11	0.94	0.90	0.95	0.05	0.90	0.85	0.93	0.08
6B (Helena, MT)	0.92	0.88	0.94	0.06	0.91	0.86	0.94	0.08	0.95	0.91	0.96	0.05	0.90	0.80	0.95	0.15
7 (Duluth, MN)	0.91	0.86	0.93	0.07	0.90	0.83	0.94	0.11	0.94	0.91	0.96	0.05	0.90	0.84	0.94	0.10
8 (Fairbanks, AK)	0.88	0.77	0.94	0.16	0.77	0.56	0.92	0.36	0.79	0.24	0.96	0.72	0.91	0.70	0.94	0.24

Table 31 (continued)

(b) aspect ratio R=1

	N				E				S				W			
	mean	min	max	range	mean	min	max	range	mean	min	max	range	mean	min	max	range
1A (Miami, FL)	0.65	0.62	0.69	0.08	0.63	0.59	0.66	0.07	0.70	0.61	0.80	0.19	0.63	0.57	0.66	0.09
2A (Houston, TX)	0.65	0.61	0.69	0.07	0.62	0.57	0.66	0.09	0.70	0.59	0.80	0.21	0.62	0.57	0.66	0.09
2B (Phoenix, AZ)	0.68	0.61	0.75	0.14	0.61	0.56	0.65	0.09	0.72	0.54	0.83	0.30	0.62	0.57	0.67	0.10
3A (Memphis, TN)	0.66	0.63	0.69	0.06	0.62	0.56	0.67	0.10	0.69	0.50	0.80	0.29	0.61	0.55	0.67	0.12
3B (El Paso, TX)	0.69	0.65	0.75	0.10	0.64	0.60	0.69	0.09	0.73	0.57	0.82	0.26	0.63	0.58	0.69	0.11
BU (Burbank, CA)	0.68	0.64	0.72	0.08	0.63	0.59	0.68	0.10	0.71	0.53	0.82	0.29	0.64	0.58	0.69	0.11
FR (Fresno, CA)	0.66	0.63	0.71	0.07	0.63	0.58	0.67	0.09	0.71	0.51	0.84	0.33	0.63	0.60	0.67	0.07
3C (San Francisco, CA)	0.66	0.62	0.69	0.07	0.63	0.56	0.68	0.12	0.70	0.47	0.83	0.36	0.63	0.58	0.66	0.09
4A (Baltimore, MD)	0.65	0.61	0.69	0.08	0.60	0.47	0.65	0.19	0.67	0.44	0.81	0.36	0.60	0.54	0.65	0.12
4B (Albuquerque, NM)	0.70	0.62	0.77	0.15	0.61	0.55	0.67	0.11	0.71	0.51	0.83	0.32	0.62	0.56	0.69	0.13
4C (Seattle, WA)	0.64	0.62	0.67	0.05	0.60	0.55	0.65	0.11	0.64	0.37	0.80	0.42	0.59	0.51	0.65	0.14
5A (Chicago, IL)	0.64	0.63	0.67	0.04	0.60	0.53	0.64	0.12	0.65	0.42	0.80	0.38	0.61	0.53	0.65	0.12
5B (Boise, ID)	0.67	0.64	0.72	0.08	0.59	0.51	0.65	0.13	0.68	0.39	0.85	0.46	0.60	0.53	0.66	0.14
6A (Burlington, VT)	0.63	0.59	0.66	0.07	0.59	0.52	0.64	0.12	0.65	0.39	0.78	0.40	0.59	0.53	0.64	0.11
6B (Helena, MT)	0.66	0.63	0.70	0.06	0.59	0.51	0.64	0.14	0.64	0.34	0.82	0.48	0.58	0.47	0.65	0.18
7 (Duluth, MN)	0.64	0.59	0.67	0.08	0.58	0.50	0.64	0.13	0.63	0.35	0.80	0.45	0.58	0.52	0.63	0.12
8 (Fairbanks, AK)	0.60	0.49	0.66	0.17	0.42	0.25	0.56	0.31	0.47	0.10	0.79	0.69	0.58	0.36	0.64	0.27

Table 31 (continued)

(c) aspect ratio R=2

	N				E				S				W			
	mean	min	max	range	mean	min	max	range	mean	min	max	range	mean	min	max	range
1A (Miami, FL)	0.45	0.43	0.48	0.05	0.42	0.39	0.44	0.06	0.48	0.36	0.62	0.26	0.42	0.38	0.45	0.07
2A (Houston, TX)	0.45	0.43	0.48	0.06	0.42	0.38	0.44	0.07	0.47	0.32	0.63	0.31	0.41	0.37	0.45	0.07
2B (Phoenix, AZ)	0.49	0.44	0.52	0.08	0.41	0.37	0.44	0.07	0.51	0.28	0.70	0.42	0.41	0.36	0.45	0.09
3A (Memphis, TN)	0.46	0.44	0.48	0.03	0.41	0.37	0.45	0.08	0.47	0.27	0.63	0.36	0.41	0.36	0.45	0.10
3B (El Paso, TX)	0.50	0.46	0.53	0.07	0.42	0.39	0.46	0.07	0.51	0.30	0.68	0.38	0.42	0.38	0.47	0.09
BU (Burbank, CA)	0.48	0.45	0.50	0.05	0.42	0.38	0.47	0.08	0.50	0.28	0.67	0.39	0.43	0.38	0.47	0.09
FR (Fresno, CA)	0.47	0.43	0.52	0.09	0.42	0.38	0.45	0.07	0.50	0.28	0.71	0.43	0.42	0.39	0.45	0.06
3C (San Francisco, CA)	0.46	0.44	0.50	0.06	0.42	0.36	0.47	0.11	0.48	0.26	0.66	0.41	0.42	0.37	0.45	0.07
4A (Baltimore, MD)	0.46	0.43	0.47	0.05	0.40	0.30	0.44	0.14	0.45	0.24	0.62	0.38	0.40	0.34	0.44	0.10
4B (Albuquerque, NM)	0.50	0.45	0.54	0.09	0.41	0.36	0.45	0.09	0.50	0.26	0.68	0.42	0.41	0.36	0.47	0.11
4C (Seattle, WA)	0.44	0.42	0.46	0.04	0.40	0.35	0.44	0.09	0.43	0.21	0.65	0.44	0.39	0.33	0.44	0.11
5A (Chicago, IL)	0.45	0.43	0.46	0.02	0.40	0.34	0.43	0.09	0.44	0.23	0.60	0.37	0.40	0.34	0.44	0.10
5B (Boise, ID)	0.47	0.43	0.52	0.09	0.39	0.33	0.43	0.10	0.47	0.21	0.69	0.48	0.39	0.34	0.45	0.10
6A (Burlington, VT)	0.44	0.42	0.46	0.04	0.39	0.33	0.42	0.09	0.44	0.22	0.60	0.38	0.39	0.34	0.43	0.08
6B (Helena, MT)	0.46	0.44	0.49	0.04	0.38	0.32	0.42	0.10	0.44	0.18	0.69	0.50	0.37	0.29	0.43	0.14
7 (Duluth, MN)	0.45	0.43	0.47	0.04	0.38	0.32	0.42	0.10	0.43	0.20	0.63	0.43	0.38	0.33	0.42	0.09
8 (Fairbanks, AK)	0.40	0.33	0.45	0.12	0.26	0.15	0.36	0.20	0.28	0.06	0.51	0.45	0.38	0.23	0.42	0.19

Table 31 (continued)

(d) aspect ratio R=10

	N				E				S				W			
	mean	min	max	range	mean	min	max	range	mean	min	max	range	mean	min	max	range
1A (Miami, FL)	0.13	0.12	0.13	0.01	0.11	0.10	0.11	0.02	0.13	0.08	0.19	0.11	0.11	0.10	0.12	0.02
2A (Houston, TX)	0.13	0.12	0.13	0.01	0.11	0.09	0.11	0.02	0.13	0.07	0.18	0.11	0.11	0.09	0.11	0.02
2B (Phoenix, AZ)	0.14	0.14	0.14	0.01	0.10	0.09	0.11	0.02	0.14	0.06	0.25	0.19	0.10	0.09	0.11	0.03
3A (Memphis, TN)	0.13	0.12	0.13	0.01	0.11	0.10	0.12	0.03	0.13	0.06	0.19	0.13	0.11	0.09	0.12	0.03
3B (El Paso, TX)	0.14	0.14	0.16	0.02	0.11	0.10	0.12	0.03	0.15	0.06	0.25	0.18	0.11	0.10	0.13	0.03
BU (Burbank, CA)	0.14	0.12	0.15	0.02	0.11	0.10	0.13	0.03	0.14	0.06	0.23	0.17	0.11	0.09	0.12	0.03
FR (Fresno, CA)	0.13	0.11	0.15	0.04	0.11	0.10	0.12	0.02	0.14	0.06	0.24	0.17	0.11	0.10	0.12	0.02
3C (San Francisco, CA)	0.13	0.12	0.14	0.02	0.11	0.09	0.12	0.03	0.13	0.06	0.21	0.16	0.11	0.10	0.12	0.02
4A (Baltimore, MD)	0.13	0.12	0.13	0.01	0.10	0.07	0.11	0.04	0.12	0.05	0.19	0.14	0.10	0.09	0.12	0.03
4B (Albuquerque, NM)	0.14	0.13	0.15	0.02	0.10	0.09	0.12	0.03	0.14	0.06	0.25	0.19	0.11	0.09	0.13	0.04
4C (Seattle, WA)	0.12	0.11	0.13	0.02	0.10	0.09	0.11	0.03	0.10	0.05	0.16	0.11	0.10	0.09	0.12	0.03
5A (Chicago, IL)	0.12	0.11	0.13	0.01	0.10	0.09	0.11	0.03	0.11	0.05	0.18	0.13	0.10	0.09	0.12	0.03
5B (Boise, ID)	0.13	0.11	0.14	0.03	0.10	0.09	0.11	0.03	0.11	0.05	0.20	0.15	0.10	0.08	0.12	0.03
6A (Burlington, VT)	0.12	0.11	0.12	0.01	0.10	0.09	0.11	0.03	0.11	0.05	0.16	0.11	0.10	0.08	0.11	0.03
6B (Helena, MT)	0.13	0.12	0.14	0.02	0.09	0.08	0.10	0.02	0.10	0.04	0.18	0.14	0.09	0.08	0.11	0.03
7 (Duluth, MN)	0.12	0.11	0.13	0.01	0.10	0.08	0.11	0.03	0.10	0.04	0.16	0.12	0.10	0.08	0.11	0.03
8 (Fairbanks, AK)	0.11	0.09	0.12	0.03	0.06	0.04	0.09	0.05	0.06	0.02	0.12	0.10	0.10	0.06	0.11	0.05

References

ASHRAE. 2011. *ANSI/ASHRAE/IES/USGBC Standard 189.1-2011—Standard for the Design of High-Performance Green Buildings*. American Society of Heating, Refrigerating, and Air-Conditioning Engineers. Atlanta, GA.

ASHRAE. 2016. *ANSI/ASHRAE/IES Standard 90.1-2016—Energy Standard for Buildings Except Low-Rise Residential Buildings*. American Society of Heating, Refrigerating, and Air-Conditioning Engineers. Atlanta, GA.

ASTM. 2011. *ASTM E1980: Standard Practice for Calculating Solar Reflectance Index of Horizontal and Low-Sloped Opaque Surfaces*. ASTM International, West Conshohocken, PA, 2001, https://doi.org/10.1520/E1980-11 .

Briggs RL, Lucas RG, Taylor ZT. 2003a. Climate Classification for Building Energy Codes and Standards: Part 1—Development Process. *ASHRAE Transactions* 109(1).

Briggs RL, Lucas RG, Taylor ZT. 2003b. Climate Classification for Building Energy Codes and Standards: Part 2—Zone Definitions, Maps, and Comparisons. *ASHRAE Transactions* 109(2).

CEC. 2018. Energy maps of California: List of climate zones areas by ZIP code. California Energy Commission. http://www.energy.ca.gov/maps/renewable/building_climate_zones.html

Ge J, Levinson RM. 2016. The advancement of cool standards in China from 2010 to 2015. Report LBNL-1007007, Lawrence Berkeley National Laboratory, Berkeley, CA. https://doi.org/10.2172/1361499

Levinson R, Akbari H. 2010. Potential benefits of cool roofs on commercial buildings: conserving energy, saving money, and reducing emission of greenhouse gases and air pollutants. *Energy Efficiency* 3 (1), 53-109.

Levinson R, Berdahl P, Akbari H. 2005. Solar spectral optical properties of pigments, part II: Survey of common colorants, *Solar Energy Materials & Solar Cells* 89, 351-389.

Levinson R, Berdahl P, Akbari H, Miller W, Joedicke I, Reilly J, Suzuki Y, Vondran M. 2007. Methods of creating solar-reflective nonwhite surfaces and their application to residential roofing materials. *Solar Energy Materials & Solar Cells* 91, 304-314.

Levinson RM, Chen SS, Ban-Weiss GA, Gilbert HE, Berdahl PH, Rosado PJ, Destaillats H, Sleiman M, Kirchstetter TW. 2016. Next-generation factory-produced cool asphalt shingles: Phase 1 final report. Report LBNL-2001007, Lawrence Berkeley National Laboratory, Berkeley, CA. http://escholarship.org/uc/item/2t3602nt

Schiler M, Valmont E. 2005. Microclimatic impact: glare around the Walt Disney Concert Hall. Proceedings of the Solar World Congress 2005 Joint American Solar Energy Society / International Solar Energy Society Conference, Orlando, August 6-12. http://www.sbse.org/awards/docs/2005/1187.pdf

Energy Research and Development Division

FINAL PROJECT REPORT

Solar-Reflective "Cool" Walls: Benefits, Technologies, and Implementation

Appendix Q: Cool Wall Workshop Proceedings
(Task 6.2 Report)

California Energy Commission
Gavin Newsom, Governor

April 2019 | CEC-500-2019-040-APQ

Appendix Q:
Cool wall workshop proceedings (Task 6.2 report)

Haley Gilbert[1] and Sharon Chen[1]

[1] Heat Island Group, Lawrence Berkeley National Laboratory

28 February 2018

Abstract

The research team hosted a Cool Wall workshop on 25 October 2017 to review and discuss its research portfolio with interested parties. This one-day event at Lawrence Berkeley National Laboratory was attended by industry, state government, federal government, utility, and building code stakeholders. There were 42 in-person and 6 remote participants. Presentations from the research team addressed energy and emission savings, changes to the urban environment, product aging, novel technologies, and infrastructure. These proceedings document the presentations and ensuing discussions.

LBNL Heat Island Group

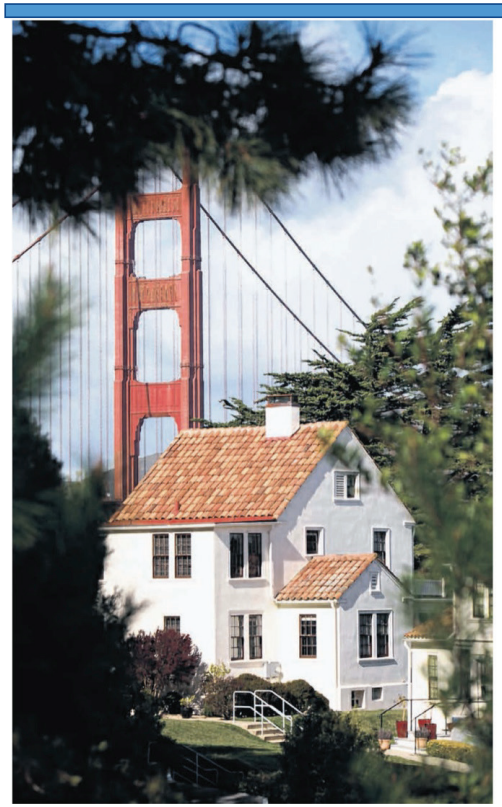

Source: Lea Suzuki, San Francisco Chronicle, 10 February 2013

Solar Reflective "Cool" Walls: Benefits, Technologies, and Implementation

Workshop Proceedings

25 October 2017

1 Agenda

8:30 am – 5:00 pm Pacific Time • October 25, 2017
Building 15, Room 253 • Lawrence Berkeley National Laboratory • Berkeley, CA

Hosted by Lawrence Berkeley National Laboratory (LBNL) in partnership with University of Southern California (USC) and University of California, San Diego (UCSD)

Workshop and research supported by the California Energy Commission (CEC)

8:30 – 9:00	**Check-in & breakfast**	
9:00 – 9:15	Introductions, agenda and logistics	Ronnen Levinson, LBNL
9:15 – 10:00	CW Benefits 1: Simulated HVAC energy savings in an isolated building (Task 2.1)	Ronnen Levinson, LBNL
10:00 – 10:15	CW Benefits 2: Effect of neighboring cool walls on HVAC loads (Task 2.2)	Jan Kleissl, UCSD
10:15 – 10:40	**Discussion**	**Facilitated by Ronnen Levinson and Haley Gilbert, LBNL**
10:40 – 11:00	**Morning break**	
11:00 – 11:30	CW Co-Benefits 1: Pedestrian mean radiant temperature and thermal comfort (Task 3.1)	Jan Kleissl, UCSD
11:30 – 12:00	CW Co-Benefits 2: Urban climate impacts of cool walls (Task 3.2)	George Ban-Weiss, USC
12:00 – 12:30	**Discussion**	**Facilitated by Ronnen Levinson and Haley Gilbert, LBNL**
12:30 – 12:40	**Grab lunch**	
12:40 – 1:00	Overview of California's Electric Program Investment Charge (EPIC)	David Hungerford, CEC
1:00 – 1:30	**Lunch break**	
1:30 – 2:00	CW Technologies 1: Natural exposure of wall products (Task 4.1)	Hugo Destaillats, LBNL
2:00 – 2:30	CW Technologies 2: Self-cleaning and de-polluting photocatalytic materials (Tasks 4.2 and 3.3)	Xiaochen Tang, LBNL Jiachen Zhang, USC
2:30 – 3:00	CW Technologies 3: Fluorescent cool pigments (Task 5.1)	Paul Berdahl, LBNL
3:00 – 3:30	**Discussion**	**Facilitated by Hugo Destaillats and Haley Gilbert, LBNL**
3:30 – 3:40	**Afternoon break**	
3:40 – 4:00	CW Technologies 4: Retroreflective materials (Task 5.2)	Ronnen Levinson, LBNL
4:00 – 4:30	Advancing cool wall adoption through standards, incentive programs, and application guidelines (Task 6.1)	Haley Gilbert, LBNL Ronnen Levinson, LBNL
4:30 – 5:00	**Discussion & wrap-up**	**Facilitated by Ronnen Levinson and Haley Gilbert, LBNL**
5:00	**Adjourn**	

2 In-person participants

First Name	Last Name	Title	Organization
George	Ban-Weiss	Professor	University of Southern California
Paul	Berdahl	Staff Physicist (retired)	LBNL Heat Island Group
Brandon	Bethke	Vice President	Tempo Chemicals & Solutions
Paul	Bethke	Business Manager	Tempo Chemicals & Solutions
Michael	Biel	Vice President	The Ultimate Coatings Company
Chris	Boyce	Technical Formulator	ESI Tec
Sharon	Chen	Principal Research Associate	LBNL Heat Island Group
William	Dean	Climate Change Advisor	California Environmental Protection Agency
Hugo	Destaillats	Staff Scientist	LBNL Heat Island Group
Hannah	Erickson	Student	NA
Matthew	Eschenauer	Staff Scientist	Sherwin-Williams Company
Marlene	Garrow	Group Leader	Sherwin-Williams Company / Valspar
Haley	Gilbert	Principal Research Associate	LBNL Heat Island Group
Kathleen	Gisser	Staff Scientist	Sherwin-Williams Company
Timothy	Hebrink	Staff Scientist	3M Company
David	Hungerford	Senior Scientist	California Energy Commission
Timothy	Hyer	Vice President of Digital	Gardner-Gibson
Jan	Kleissl	Professor	University of California, San Diego
David	Lamouranne	Captain	GreenStar Smart Roof
Ronnen	Levinson	Staff Scientist	LBNL Heat Island Group
Victoria	Ludwig	Heat Island Reduction Program Manager	U.S. Environmental Protection Agency
Robert	Martuch	Program Manager, Formulation Technology	Sherwin-Williams Company
James	Moses	Technical Services Manager	Mitsubishi Chemical Composites America
Tsutomu	Nagahama	Deputy General Manager	Dexerials Corporation
Hiroko	Furumi (Nakagawa)	Marketing Manager	Dexerials Corporation
Daisuke	Narumi	Professor	Yokohama National University
Olivier	Rosseler	Principal Scientist	Saint-Gobain
Gregory	Sarnecki	Senior Scientist	Behr Process
Erica	Sherman	Senior Research Associate	GAF
Michael	Shewmaker	Energy Specialist	California Energy Commission
Ginger (Jinzhen)	Shi	Section Manager, R&D	Behr Process Corporation
Ming	Shiao	Principal Scientist	GAF Materials Corporation
Morgan	Sibbald	Program Manager, Government Initiatives	Sherwin-Williams Company

Xiaochen	Tang	Postdoctoral Researcher	LBNL Heat Island Group
Peter	Turnbull	Principal, Zero Net Energy Program	Pacific Gas and Electric Company
Jerry (Jingting)	Wu	Applications Engineer	Dexerials Corporation
Jiachen	Zhang	PhD Candidate	USC

3 Remote participants

First Name	Last Name	Title	Organization
Craig	Tranby	Environmental specialist	Los Angeles Department of Water and Power
Dave	Sailor	Professor	Arizona State University
Martha	VanGeem	Principal Engineer	VanGeem Consulting
Howard	Wiig	Energy analyst	Hawaii State Energy Office
Gary	Ilalaole	Homeowner	NA
Scott	Kriner	Consultant	Metal Construction Association

4 Presentations, summaries, and notes

Key: Q = Question, A = Answer, D = Discussion

CW Benefits 1: Simulated HVAC energy savings in an isolated building (Task 2.1)
Ronnen Levinson, LBNL
9:15 – 10:00 am
(Link to presentation) (Link to 2-page summary)

Q: (Manufacturer) What was base case SR [solar reflectance] for building energy simulations?

A: (Ronnen Levinson, LBNL) 0.25 for walls, 0.10 for [residential] roofs.

Q: (Manufacturer) Why did you select these solar reflectances chosen for walls and the roof?

A: (Ronnen Levinson, LBNL) The cool-wall albedo for residential buildings assumed an off-white color, because most homes will not use bright-white walls. For residential roofs the increase from albedo 0.10 [base roof] to albedo 0.40 [cool roof] is actually greater than what Title 24 requires. These results can be scaled by albedo increase. It is easier to find cool options for walls than for asphalt shingle roofing.

Q: (Unknown) Is it easier to find and use cool wall products vs. cool-colored roofs for residences today?

A: (Ronnen Levinson, LBNL) Yes, it is easy to find white/off-white cool wall products today while cool-colored high-slope roofing products are less common.

Q: (Unknown) What is the size/dimension of the residential building prototype?

A: (Ronnen Levinson, LBNL) The single-family home has two floors with a total area of 220 m² (about 2,400 ft²). The apartment building has three floors with a total area of 2,010 m² (about 22,000 ft²).

Q: (Manufacturer) How do these [energy cost savings intensities] relate to energy cost savings for a household?

A: (Ronnen Levinson, LBNL) This slide reports annual energy cost savings per square meter of surface modified. You can multiply this value by the wall area to be made cool.

4.1 CW Benefits 2: Effect of neighboring cool walls on HVAC loads (Task 2.2)
Jan Kleissl, UCSD
10:00 – 10:15 am

(Link to presentation) (Link to 2-page summary)

Q: (Manufacturer) Did you take into account effective humidity?

A: (Jan Kleissl, UCSD) No, we did not but it's a good factor to consider.

Q: (Manufacturer) Is a 0.25 wall albedo for the base case a good value to use?

A: (Ronnen Levinson, LBNL) It is reasonable, and based on default values specified in the performance-compliance paths of building energy efficiency standards. Existing walls come in all different colors and albedos.

Q: (Manufacturer) Does the model take into account the convection changes?

A: (Jan Kleissl, UCSD) No we don't do fluids modeling. However, we factor in convection coefficients based on differences in surface/wall temperature versus air temperature.

Q: (Manufacturer) What do you assume is the building-to-building reflection interaction—diffuse or specular?

A: (Jan Kleissl, UCSD) Diffuse.

Q: (Manufacturer) This is still the result on the central building, right?

A: (Jan Kleissl, UCSD) Yes.

Q: (Christian Koehler, LBNL) Have you compared your results with Ronnen's SAF [solar availability factor] results? Do they match?

A: (Jan Kleissl, UCSD) The results from this modeling activity (Task 2.2) are generally lower than those reported in Task 2.1.

Q: (Manufacturer) How does the albedo of the street affect the model?

A: (Jan Kleissl, UCSD) Higher pavement albedo will generally enhance the effects. California neighborhoods usually consist of closely spaced buildings, with big roads (for cars), generally the view factor from wall to neighboring wall is much smaller than wall to pavement. Higher pavement albedo would enhance secondary reflections from neighboring cool wall to pavement to central building wall.

Q: (Manufacturer) Did you take into account all of the radiation exchanges between buildings, pavement, etc.?

A: (Jan Kleissl, UCSD) Yes.

Q: (Manufacturer) If you are an early adopter in Fullerton, let's say, and you get savings from your cool walls, then your neighbors decide they want cool walls too—are your savings reduced?

A: (Jan Kleissl, UCSD) It depends on how close your neighbors are, but generally yes.

Q: (Manufacturer) Have you calculated the savings based on distance between you and your neighbor?

A: (Jan Kleissl, UCSD) We used an inter-building spacing of 23 m = 70', which is a typical distance for a neighbor across the street in a residential neighborhood. SAFs [solar availability factors] in Ronnen's presentation can be used to analyze the effects of building spacing.

A: (Ronnen Levinson, LBNL) No matter what distance we choose, we'll be wrong—people must do this kind of modeling for their specific building.

Q: (Manufacturer) You didn't talk about factoring in emissivity.

A: (Ronnen Levinson, LBNL) We assume a thermal emissivity of 0.90, which is pretty accurate so long as the material does not have a bare metal surface.

Q: (Manufacturer) What about the reduction of community wide air temperature from deploying cool walls?

A: (Ronnen Levinson, LBNL) This will be presented during an upcoming presentation (Task 3.2).

Q: (Manufacturer) If I park my car next to a cool house—does my car warm up?

A: (Jan Kleissl, UCSD) Depends on orientation, time of day, and climate but it could.

Q: (Bill Dean, CalEPA) Does the TUF-IOBES model take into account light that reflects off the wall to the ground, etc?

A: (Ronnen Levinson, LBNL) Yes.

4.2 Morning discussion section
Facilitated by Ronnen Levinson and Haley Gilbert, LBNL
10:15 – 10:40 am

D: (Manufacturer) For cool walls there doesn't have to be a cost increase. Therefore, it becomes more of a marketing dilemma to convince the consumer that light-colored walls are also "cool" to have.

D: (Manufacturer) If you do a survey of wall products on the market, 60-70% of products are already light colors. Therefore, the projected benefit of this work would be smaller since you are only improving the remaining 30-40%, right? Also, color choice is important. If we tell people to change from a nice dark cedar siding to white cedar siding in order to save 5% on energy. That value is not enough to convince consumers, so we need to remember to respect color.

Q: (Manufacturer) Is there an inherent cost premium associated with cool pigments? Is the cost something where if you scale-up the manufacturing of the product, the pigments costs can decrease?

A: (Manufacturer) With these things we first need to start small and see how amenable people are to adopting them. We also need to introduce incentives to help drive the market in this direction.

A: (Manufacturer) I can provide a commercial viewpoint. One of the problems with life cycle cost analysis (LCCA) is that the people who construct the building are never the same as those who operate it. So the life cycle costs occur to different people at different stages. We see this again and again where studies are done but things never get adopted. The builder has a responsibility to be economical, and so anything new is going to be a hard sell if it is based on any type of increased [up-front] cost. All manufacturers have gone through these LCCA tools and found that it has very little impact on the actual construction of the structure.

Q: (Ronnen Levinson, LBNL) What is the actual cost [of cool pigments]?

A: (Manufacturer) It's about three times the cost versus conventional [pigments], generally speaking.

Q: (Ronnen Levinson, LBNL) What fraction of the coating is pigment?

A: (Manufacturer) Depends on the tone [of the color]—for a deep brown it might be 7-18%.

A: (Ronnen Levinson, LBNL) In roofing the specialty pigments are in the ballpark of 10% or so of the total [material] cost. So if 90% of the coating cost relates to other things, a 3X pigment cost increase is not actually as much as it initially sounds.

D: (Manufacturer) Don't forget that the biggest cost difference has to do with the painting application. You can have inefficient and efficient methods and everything in between. So if

you have an efficient coating system (like coil coating), the cost difference will be very different from an inefficient method (like powder coating).

Q: (Manufacturer) I would think it is easier to adopt light-colored walls. Where do you think the market is going now? Let's say that if people are trending towards light colors; then doesn't that mean cool dark pigments represent going in a different direction?

A: (Manufacturer) Yes, most exterior wall coatings [currently] are light colors.

A: (Manufacturer) In Europe, brighter deeper colors are actually pretty common but still the vast majority are light colors.

Q: (Unknown) So does this mean that we don't need special pigment technology since light colors are already popular?

Q: (Bill Dean, CalEPA) In California, can we make [cool wall] regulations and still offer the same color range [customers find today]?

A: (Manufacturer) We would need to know what the required SR would be.

A: (Ronnen Levinson, LBNL) Let's say 60%.

A: (Manufacturer) We also need to know about longevity requirements and durability too.

4.3 CW Co-Benefits 1: Pedestrian mean radiant temperature and thermal comfort (Task 3.1)
Jan Kleissl, UCSD
11:00 – 11:30 am

(Link to presentation) (Link to 2-page summary)

Q: (Manufacturer) What about the aspect ratio/view factor?

A: (Jan Kleissl, UCSD) Not much effect—there is 0.5 view factor with a multi-family residence.

Q: (Manufacturer) What about the interaction with ground albedo?

A: (Jan Kleissl, UCSD) In these simulations, we assume ground albedo of 0.10.

A: (Ronnen Levinson, LBNL) If I make a wall more reflective it lowers the wall's temperature. More sunlight is reflected from the wall, but the wall is cooler and emits less thermal radiation. It's not an equal balance, though; the decrease in emitted longwave radiation is not as great as the increase in reflected sunlight. As the pedestrian becomes more reflective, the effect [of raising wall albedo on pedestrian comfort] decreases.

Q: (Victoria Ludwig, EPA) Have you looked at internal thermal comfort [that inside unconditioned buildings]?

A: (Jan Kleissl, UCSD) We will be looking at that soon. We are currently running simulations. It'll be interesting to look at what happens in indoor environments where you don't have air conditioning.

Q: (Manufacturer) How do the effects presented here compare to heat island effects [in magnitude]?

A: (Ronnen Levinson, LBNL) Wait for George's presentation (Task 3.2) coming up next.

Q: (Manufacturer) Do you account for high performance technologies in windows? I expect the answer is no, but will you eventually incorporate things like 3M's IR reflective window film?

A: (Jan Kleissl, UCSD) We haven't done it but you can get applicable results by changing the reflectance, and emission inputs accordingly.

A: (Ronnen Levinson, LBNL) If interested, I can introduce you to Christian Kohler of the Windows and Daylighting Group.

4.4 CW Co-Benefits 2: Urban climate impacts of cool walls (Task 3.2)
George Ban-Weiss, USC
11:30 am – 12:00 pm
(Link to presentation)

Q: (Manufacturer) What is the albedo of rooftop PV?

A: (George Ban-Weiss, USC) There is an "effective albedo" of 0.40 albedo from an efficient PV system which is similar in albedo to cool-colored roofing products.

Q: (Unknown) If you made all buildings in a city with cool walls and cool roofs—how much change could you expect?

A: (George Ban-Weiss, USC) Depends on albedo increase, but if you're looking at peak temperature reductions, I would say a ballpark value of peak canyon air temperature reduction is 1˚ C. Note that you can't scale based on spatial adoption though you can scale by albedo increase.

Q: (Unknown) What is the impact of June gloom on the calculations?

A: (George Ban-Weiss, USC) If you don't know, this is a phenomenon where in June the waters off the shore are cold and the land is warmer; therefore, a marine layer forms in June. You can look at results on mostly cloudy days though to get the answer, and I would expect to see smaller reductions on those days.

Q: (Manufacturer) So how does all of this affect air pollution—ozone in particular?

A: (George Ban-Weiss, USC) I defer to Jiachen's presentation (Task 3.3) later today, and also note that the full research on this topic isn't yet completed. But if I were a betting man I

would think that ozone will decrease since the temperature effect will outweigh the dispersion effect of slowing down the removal of ozone.

Q: (Manufacturer) But isn't there another study that talks about increase in ozone from an increase UV reflectance?

A: (George Ban-Weiss, USC) I am a co-author on that paper. Note that in these simulations [those in the current study] we assume UV reflectance remains unchanged in the cool roof and cool wall scenarios.

Q: (Ronnen Levinson, LBNL) So you mentioned that there's less sunlight on walls than on roofs—about half—is it right to say that we see these cool wall temperature reductions because there are more walls than roofs?

A: (George Ban-Weiss, USC) It's two things: 1) canyon air temperature—if you increase wall albedo, which is much closer to the urban canyon than roofs are, you can imagine that changing walls has a much larger relative impact than changing roofs; and 2) yes you are right there is more wall area than roof area.

Q: (Manufacturer) Cooling the land reduces sea breeze—does this model take this effect into account [the reduced sea breeze]?

A: (George Ban-Weiss, USC) Yes. We note that sea breeze dampens the effect of cool walls, but doesn't completely eliminate the effect.

Q: (Manufacturer) Can you relate the magnitude of your results with the magnitude of Jan's results? I'm speaking in a thermal comfort sense. It seems negligible.

A: (George Ban-Weiss, USC) So it's difficult to compare—scale is one of the differences between our research. I am looking at the spatial scale dependence of cool wall adoption while Jan is looking at neighborhood scale. I am looking at a megacity so there is an important accumulation effect [that you don't really see at a smaller scale]. Because of the spatial scale effects like this you can't really scale linearly between our models. From a thermal comfort point of view maybe you won't see much effect, but from an urban heat island mitigation viewpoint these numbers are not negligible.

Q: (Ronnen Levinson, LBNL) Can you compare these reductions with expected summer average temperature increase due to climate change?

A: (George Ban-Weiss, USC) Those projections are on the order of 4 °C; these reductions are on the order of a tenth of that. [Cool surfaces] will not reverse effects of climate change, but it's not negligible. Also, I will mention here that I did a study a while ago on this topic but for cool roofs in Los Angeles. For the mid-century results, cool roofs can partially reverse climate change in residential areas and in industrial areas it can almost fully reverse it since you can have very high albedos on horizontal roofs. But by the end of the century, climate change dominates. Therefore, it's more like a near-term solution but certainly not a long-term answer to climate change.

Q: (Haley Gilbert, LBNL) Did you evaluate temperature reductions on extreme heat days currently and under future climate change scenarios?

A: (George Ban-Weiss, USC) Baseline meteorology affects extreme heat days. On a hot day you see lots of stagnation, which would probably be similar on an extreme heat day, though not exactly the same. Jiachen's simulation data actually includes an extreme heat period and we can look at those three days compared to what we see in the whole month. But talking in terms of predicting future events we need to know things like how climate change affects wind speed which is not well known right now. And that is why research into how climate change affects air pollution is super uncertain.

Q: (Manufacturer) Can cool wall reductions in greenhouse gases impact the temperatures of Los Angeles?

A: (George Ban-Weiss, USC) Only by a tiny amount, and we don't include these effects in our modeling. You could reduce greenhouse gases in Los Angeles to zero and it wouldn't really affect the climate of Los Angeles. This is because climate change is a global phenomenon. If everyone had electric cars in Los Angeles, you still wouldn't see much difference! Basically, it is not local.

Q: (Manufacturer) What about PV panels on rooftops?

A: (George Ban-Weiss, USC) This relates to my previous study looking at effects of cool roofs on climate change. If a PV cell is 10% reflective and let's assume that conversion efficiency is the upper end of what is achievable like 30%, then you could say the effective albedo is 40% and that's roughly equal to a high-performance cool-color residential roof. Therefore, the same cooling benefits apply here. You can use effective albedo as a way to look at how PVs will affect climate. So if we say that efficiency was 20% and that the effective albedo is 30%, then you can say the PV has albedo equivalent to cool-colored residential roofs. But neither will be as good as a white commercial cool roof.

A: (Ronnen Levinson, LBNL) Of the sunlight that arrives on the surface of a PV panel, some gets reflected, some is converted, and some is absorbed. The fraction gets absorbed without conversion is what matters. Air flow under roofing tiles or PV panels does affect the extent to which the building heats up but doesn't affect the urban system.

Q: (Bill Dean, CalEPA) Regarding semi-volatiles in gas vs particle phase—if I breathe them in, what are the differences when it comes to health effects?

A: (George Ban-Weiss, USC) The accumulation mode particles are the ones that persist in the atmosphere the most. Size is 100 - 1000 nm. Due to the size, they don't deposit very quickly. When you breathe gas it diffuses quickly and it would be taken up in the nasopharyngeal area. Same as really small particles. The semivolatiles are usually in accumulation mode, so too big to diffuse quickly and too small to settle by gravity, so they make it deeper into airways, so then can translocate into different parts of the body. Therefore, where the pollution deposits in the body matters for health reasons.

Q: (Manufacturer) Anybody studying energy storage at nighttime?

A: (Paul Berdahl, LBNL) Short answer is no—there's a common strategy of nighttime ventilation and you can use that to store energy temporarily but I don't think there is any widespread systems examination that's going on. In its simplest form, you just open your windows at night, then close up the house during the heat of the day. There are also strategies where nighttime cold water is produced by radiative cooling panels, or by refrigeration, and circulated to produce cooling during the day. Commenting on PVs—it's great that you can have a reduced heat load because you're converting solar energy to electricity. In a building consider though that the electricity is being used to power appliances and that heat will go back into the environment. This is in comparison to the cool roof where the roof has an advantage as it just reflects back into space and also cools the interior space.

Q: (Manufacturer) Los Angeles was the basis for this study, how do you extrapolate to Phoenix or some other city?

A: (George Ban-Weiss, USC) You can't—the temperature impacts of increasing albedo don't really translate from one city to another unfortunately so things like differences in baseline temperature, wind speed especially, evolution of boundary layer mixing heights. You can make rough extrapolations but I would hesitate to extrapolate results to another city. You can instead run the simulations in another city and then see how they differ.

D: (Victoria Ludwig, USEPA) The discussion questions on the back of the paper you gave us, align with the trouble we run into with cities as well. Like how these results would be received by cities. Cities would need someone to translate this research into laymen's terms and we do try to do this but it's hard. Local officials come to me and say well I can't implement all mitigation strategies, and I can't do cool roofs alongside cool walls and vegetation—so which one do I do? If I want to do cool walls, well then what policy incentives would work for the non-municipal buildings which the city doesn't have direct control over. The officials will ask me who has studied this and how can they communicate results to their elected officials. They would also want to know what other cities are implementing these strategies and to what success. This type of information would be very helpful for me.

4.5 Overview of California's Electric Program Investment Charge (EPIC)
David Hungerford, CEC
12:40 – 1:00 pm
(Link to presentation)

Q: (Manufacturer) Is there a limit on percent renewable energy for the grid to manage?

A: (David Hungerford, CEC) I'm not qualified to answer that. The general answer would be yes, but we don't know what that is. I've read recent estimates that put it at a very high number. It depends on what you want the system to look like. We started 120 years ago and up until the [19]70s had a grid design that said load should be met by supply and it was all about how to build supply to meet the load and also keep stability. System operations, utilities,

transmission organizations functioned like they are an accelerator with no brake pedal. That was their goal. If we instead have a system where power is available sometimes and less available at other times, or less available in a low carbon sense, at that point consumption is going to have to shift. If we keep consumption at current levels and try to store renewable energy, well that would be expensive. But how do you match the consumption behavior to the available load—that's the question. If everyone was willing to live that way [because some people do live off the grid] then we'd have no problem. So it's a matter of willingness to adapt. How much can you do without having to change behavior? Well that's going to be a lower number.

4.6 CW Technologies 1: Natural exposure of wall products (Task 4.1)
Hugo Destaillats, LBNL
1:30 – 2:00 pm
(Link to presentation) (Link to 2-page summary)

Q: (Manufacturer) When you did your measurements, what's the spot size that you measure, and is it large enough to capture the differences in soiling?

A: (Hugo Destaillats, LBNL) 1" spots and three spots per specimen. So yes.

Q: (Unknown) Do you discriminate between microbial growth and soiling?

A: (Hugo Destaillats, LBNL) We don't analyze what's on the surface, only the effect whatever is on the surface has on the solar reflectance. I would say in humid areas the soiling would probably be more microbial related, depending on the specific products we're talking about [especially for porous clay tiles, you may not see it on other types of materials].

Q: (Manufacturer) What is the resolution of the images? Can you see soiling particles in these photographs?

A: (Sharon Chen, LBNL) I don't know; we just use a point-and-shoot camera.

Q: (Manufacturer) Have you measured how hot the samples get?

A: (Hugo Destaillats, LBNL) No, we haven't measured that. But we could.

Q: (Manufacturer) Did you measure color L, a, b?

A: (Hugo Destaillats, LBNL) We will eventually do so for some products using spectrometer measurements.

Q: (Manufacturer) Why do you report solar reflectance instead of temperature under the sun?

A: (Hugo Destaillats, LBNL) We only report solar reflectance, since temperature will ultimately be affected by other factors [like wind].

Q: (Manufacturer) There are a number of industry standards for durability and longevity of paint. What are the durability ratings for these products?

A: (Hugo Destaillats, LBNL) We don't know. The manufacturers will know, but the products in this set that are commercial will probably have passed those tests but we won't know unless the manufacturers tell us more about these products.

D: (Manufacturer) Testing those parameters would be a very important step for acceptance in the coating industry.

Q: (Manufacturer) When you made the reflectance measurements after soiling, did you wash and return [specimens] to the racks?

A: (Hugo Destaillats, LBNL) No.

4.7 CW Technologies 2: Self-cleaning and de-polluting photocatalytic materials (Tasks 4.2 and 3.3) Xiaochen Tang, LBNL and Jiachen Zhang, USC 2:00 – 2:30 pm

(Link to presentation) (Link to 2-page summary)

Q: (Manufacturer) The cool roofing model shows an increase in pollution, why?

A: (Jiachen Zhang, USC) The increase in particulate matter (PM) concentration is reported in the modeling work of Epstein et al., (2017). They suggested that cool roofs will reduce temperatures and lower planetary boundary layer (PBL) height, and thus suppress pollutant dispersion. [See http://www.pnas.org/content/114/34/8991.abstract]

A: (Haley Gilbert, LBNL) Let me remind the group that these effects are site-specific, and slight differences from site to site may affect which one of the pathways dominates, leading to either an increase or decrease in pollution.

Q: (Manufacturer) You're looking at NO_x deposition and the ability to "react that away" and also how that affects ozone and PM. Are you thinking at all about what other things in the air might be affecting these reaction sites?

A: (Hugo Destaillats, LBNL) The catalysts are on the surface and will react with whatever is there. Let's say the coating formulation is inert and physically covered by a soiling layer—then the reaction is totally blocked. You saw in the dry season the NO_x removal decreased and later increased when it was cleaned. This represents a physical barrier preventing the reaction from occurring.

Q: (Manufacturer) I was wondering specifically about VOCs or other things in the air that could be competing for those sites on the surface as well.

A: (Hugo Destaillats, LBNL) We can look at concentration and reactivity. NO_x is pretty reactive, and there's a lot of it. But you're right so I'll emphasize here that this is a test that is done to characterize the material and not to predict how it will react in the environment.

4.8 CW Technologies 3: Fluorescent cool pigments (Task 5.1)
Paul Berdahl, LBNL
2:30 – 3:00 pm
([Link to presentation]) ([Link to 2-page summary])

Q: (Unknown) Did you run six identical samples to test whether the [ESR measurement] apparatus worked?

A: (Paul Berdahl, LBNL) Yes.

Q: (Manufacturer) Do you check the emissivity of the samples?

A: (Paul Berdahl, LBNL) Yes, we did. We also checked the apparatus results by running with thermistors. For the crystals the thermal emissivity was a bit low, so we coated the sample with a transparent acrylic layer to bring it up to 0.90.

Q: (Manufacturer) What was the substrate with the rubies? I wasn't clear what you were putting the ruby over.

A: (Paul Berdahl, LBNL) We put the pigment into a clear base. We have a standard white substrate that is an aluminum panel with 3 coats of brushed white. If you use a black substrate you get a factor of 17 less performance. You need a good white substrate.

4.9 CW Technologies 4: Retroreflective materials (Task 5.2)
Ronnen Levinson, LBNL
3:40 – 4:00 pm
([Link to presentation]) ([Link to 2-page summary])

D: (Unknown) In residential construction, lap siding already has an upward tilt so that geometry could be accommodating to the retroreflector geometry you propose.

Q: (Unknown) Did you measure retroreflection with different sun angles?

A: (Ronnen Levinson, LBNL) The measurements performed by Dexerials included various incidence angles. They illuminated the samples at varying incidence angles and the detector moves around to detect retroreflection.

Q: (Manufacturer) Did you give any thought to flecks in the paint? Metallic flakes, mica flakes?

A: (Ronnen Levinson, LBNL) Not sure how they can be used for retroreflection.

D: (Manufacturer) In a coating they tend to be used all facing one angle

D: (Ronnen Levinson, LBNL) Let's talk about this afterwards.

4.10 Advancing cool wall adoption through standards, incentive programs, and application guidelines (Task 6.1)
Haley Gilbert, LBNL and Ronnen Levinson, LBNL
4:00 – 4:30 pm
(Link to presentation) (Link to 2-page summary)

Q: (Manufacturer) With a wall we have multiple products: windows from one company and shutters from another; one side of house has a stone wall but the other side is something else. So how do we write building code language for a cool wall when there's so much going on?

A: (Ronnen Levinson, LBNL) For us, "wall" just means net wall—no windows, no doors. Anything that's a shutter is not in the purview of this. We care about SR and TE, much as we do for roofs. There are lots of different types of wall materials, but you set requirements independently of the materials. Maybe you can have different requirements based on wall direction just like there are different requirements based on roof slope.

A: (Jan Kleissl, UCSD) Maybe we could do something like have standards incorporating area-weighting of reflectance.

Q: (Manufacturer) With regards to the amount of work to get to those requirements, some of the legwork has already been done with roofs so do you think the process will be as long as with roofs?

A: (Haley Gilbert, LBNL) I think it may be shortened but success will depend on the level of interest.

D: (Manufacturer) You can look at roof/attic systems as a monolithic structure. For the residential wall market, it's similar, where there's wall and windows and you can generalize what % of the surface is wall or window. But when you're looking at a commercial product, there is more variety. You can't just expect that you can approximate these exterior surfaces as just X% walls and X% windows. You have great variety of construction, for example storefronts, curtain walls, etc., where there's a lesser percentage of wall vs. other parts. Let's say in a storefront 25% of the surface is wall, and now I've just made it cooler! In the real world this doesn't really mean much [because the cool wall makes up a small fraction of the storefront]. My thought on this is that you need to break down your timeline of adoption between the residential sector where I think there's a good chance of adoption and the commercial sector where I think it would be much harder to get support for a variety of reasons.

D: (Code consultant) In ASHRAE 90.1 what we did, as you recall in the very beginning with Ronnen's presentation, is to separate things by building type. There are already some commercial prototypes that have a low wall-to-window ratio so because the analyses here have accounted for that, I don't think it's a lost cause to do cool walls in the commercial realm. Also, I want to mention here that Climate Zone 0 encompasses a band including central South America, Africa, Indonesia, etc., and while none of these areas happen to be in U.S. they include major population centers. I want to add that I know solar reflective index (SRI) is for horizontal surfaces but we used it because it is referenced in LEED, however we can definitely go back to solar reflectance.

D: (Utility) I think we need some real-world field measurements [as we did for cool roofs]. We don't really know what's going to happen in the field so impacts should be validated by field measurements.

Q: (Ronnen Levinson, LBNL) Could this be funded by the next three-year phase of the EPIC program?

A: (David Hungerford, CEC) The initiatives have not been written yet. And so certainly funding is a possibility.

D: (Haley Gilbert, LBNL) It is tricky to do field work with these new technologies. It's hard to tease out the impact of a specific technology when in the field you see a combination of all these different technologies put together. So you need is isolated studies that can be easily controlled.

D: (David Hungerford, CEC) There are categories of research that deal with demonstration and development. What you're talking about falls more under applied research. Within a longer-term project or larger proposal there could be a component of applied research alongside a demonstration effort.

D: (Manufacturer) I want to offer a word of caution. You've touched on the fact that wall geometry is more complicated than a roof with effects from other surfaces. It just seems so difficult to come up with a simple narrative you can tell a consumer about what sort of benefit they can see. If a given magnitude of benefit is so dependent on specific conditions, what if they come back to us as manufacturers and say, "Well we didn't see the benefit you claimed!". What we sell is a base paint. That base paint can then be tinted as the customer pleases at our various locations. So we test the base paint and report the results. But ultimately the customer can come in and add color tints to it in the store.

D: (Unknown) Also remember that with these cool colors you need to be careful about mixing different incompatible kinds of pigment! It can drop the SR!

D: (Manufacturer) I'll tell you I didn't hear anything about the cost part of the equation today. The cost is a big factor in whether something will be adopted. A method towards adoption with existing products [that have no cost premium] might be moving towards white walls.

But home owner associations might not like this limited choice/color. Until the cost issue is sorted out I don't see a clear path towards adoption.

D: (Ronnen Levinson, LBNL) Spectrally selective pigments may be three times the cost, but that is for the pigment only right? If the pigment represents only, let's say, 10% of the cost, then that "three times" figure [offered by the Ultimate Coatings rep] doesn't necessarily represent the total cost increase of incorporating cool pigments.

D: (Manufacturer) If we talk about conservative adoption with realistic [SR] numbers, and do not include the realm of "Martha Stewart great vibrant colors great prices"—we're talking about modest colors and then I think we can definitely keep costs in line.

D: (Manufacturer) I want to remind everyone that when GAF cool roof shingles first came out they were very expensive. But then now everyone makes them and the prices have gone down a lot. So we have to recognize that there is an educational curve here in the industry too. My background is in the trades, and I can tell you that the cost of labor is the preponderance of the cost of an installed roof/wall. We get stuck in this conversation about cool walls being so expensive, but [the magnitude of] that cost doesn't even touch the labor cost.

D: (Unknown) So let's say that we're not considering cool pigments—let's talk about white pigments. Can we use white paint as the cool wall case?

D: (Manufacturer) Look, consumers are paying extra for energy-saving products. Therefore, manufacturers need compelling energy savings information to share with consumers. However, if we sell a cool roof, the manufacturer has to substantiate the energy savings claim—well if you buy this you can save this much. Manufacturers are liable in a legal sense for the claims we make. [Lots of agreement from attendees.] So we are looking for whatever support this group can offer us in terms of demonstrating concrete benefits.

D: (Manufacturer) When I buy a roof, I don't paint it—I buy some roofing material that was already painted. I don't know what it cost manufacturers to produce the cool product, I just buy the complete product. On the other hand, a large percentage of walls in the residential sector are painted in the field by somebody who went to a big box store and bought a 5-gallon bucket of paint to paint a house. So the owner's going to know what the cost is—that is the cost of that bucket of paint. The labor is going to be exactly the same for painting houses, so you don't get the benefit from efficiencies in painting [application]. What it costs to get that paint will be what is important to the owner. In the commercial sector, the cladding comes pre-finished so any cost increases can be absorbed into the cost of the product, which may be a bit more.

D: (Manufacturer) I think the three-year aged value is very important. With this value, you can see there is a real difference between all these options. I like to tell people that all white paints are not created equal. If you go to the Cool Roof Rating Council (CRRC) website you can see how different the three-year aged values are for the different [white] products. So

you can sell high-end premium paint and point to the aged values to show how it doesn't soil as quickly. The aged cool wall SR values will be helpful to know and share.

D: (Manufacturer) Color is very personal. Don't mess with the color space of your offerings. Whatever new technology that is introduced needs to be able to accommodate all the color choices that people want. It doesn't matter if the customer is only buying one of your products, they want to see that they have hundreds of options to choose from. It doesn't matter if you don't like [this particular shade of brown]; there is a customer out there that really does want [the particular shade of brown]. I don't want to introduce cool walls here if that is something that will limit the color space of what we sell.

D: (Ronnen Levinson, LBNL) Well we only intend to try this in areas where it's beneficial.

D: (Manufacturer) Look you have to understand that where California goes, so goes the nation. [Lots of agreement from audience.] So if you're really going to be that restrictive, know that it will affect the national market.

D: (Ronnen Levinson, LBNL) In cool roofing, the codes are climate zone specific.

D: (Manufacturer) All the large paint companies will sell paint that says Title 24 compliant no matter where you are. It's just not cost-effective for manufacturers to sell different products based on geography.

D: (Manufacturer) Look, codes are political documents. And those political entities don't always align with your climate zones. So if cool walls are adopted into building codes and they become prescriptive, know that it's going to end up being enforced on someone who doesn't need it.

D: (Haley Gilbert, LBNL) One way to address that is to tailor the language so that it's not an imposition, but more like an option. Or incentivize, rather than prescribe.

D: (Manufacturer) Providing incentives is basically giving someone something for nothing. That's what I like about white walls as a pathway of adoption. It's easy to find in the market and already used. Once it's accepted, maybe then you start adding things like cool colors.

D: (Manufacturer) I just wanted to add that in terms of starting small, I don't think I would go adding on all these extra technologies like self-cleaning, retroreflectors, or fluorescence right at the very beginning.

D: (Manufacturer) There are lots of things premium paints do that consumers don't know about. We match our standards to the Master Painter's Institute, which has standards about washability, etc. But as a consumer you have no idea. We could do something like that with cool walls. It doesn't go on the label, but it will be inherent. You can accomplish this working with those organizations to get these standards in, working with general contractors saying well you have to use paints that have these characteristics.

Q: (Manufacturer) Have you looked at what Europe is doing when it comes to energy efficiency?

A: (Haley Gilbert, LBNL) With regards to cool walls/roofs research, the UK building stock is older and lacks cooling systems. So they are evaluating cool walls/roofs as a way to mitigate future climate change warming effects since they don't have infrastructure like air conditioning and people are not acclimated to hot weather.

Post workshop feedback (via email)

Code consultant:

Consider the point of entry: in most regions of the country, walls are not painted, even residential walls. Brick, stone, or Hardie board [fiber-cement siding] are used. If the point of entry could allow a range of preferable color choices in products that manufacturers already have, this would be best. However, I realize that the analysis was done for 0.6 [solar reflectance] which is very white.

A map of world climate zones is shown in Figure Annex1-3, on page 379 of ASHRAE 90.1-2016. There are also tables in Annex1-3 that list international cities in various climate zones. It might be that half of the world population lives in climate zones 0 and 1.

Howard Wiig, Hawaii State Energy Office:

Martha asked question regarding color selection. Each paint company has color blades of seven colors each. When I selected the lightest two, the lowest common denominator was 0.64—hence my number. Very scientific.

The addition of a white primer or underlayment increases reflective efficacy by 17 times? If so, that should be the primer of choice—can be inexpensive acrylic as it won't weather and acrylic has good adherence properties. [Note from Ronnen: the 17X increase mentioned by Paul Berdahl referred specifically to the performance of *fluorescent* cool pigments.]

I tuned in late, but I didn't hear mention of Stanford (maybe that explains it) studies in reflective wavelengths exiting the atmosphere, presumably unhindered by atmospheric elements.

The fact that reduced reflectance potential of walls is practically offset by walls occupying more space than windows.

Thanks so much for giving Hawaii full billing! The photos you showed were Laie Elementary school. I will check to see if good monitoring was done.

I spoke with Energy Star regarding their minimum roof reflectance values. They admitted that they hadn't paid much attention to this element. I and others agree that the new minimum should be 0.80 initial solar reflectance and 0.65 aged—and that's conservative.

I agree with Martha that commercial roofs like warehouses and Big Boxes are excellent candidates for cool walls.

The [building simulation] results showed that in Climate Zones 1-3, cool walls have excellent performance and payback time (if, indeed, there's a cost premium for cool walls.)

Manufacturer:

When we talk about co-benefits of cool walls, I am also thinking about extended product durability. Lowering the wall temperature will slow down the degradation kinetics (typically increasing the temperature by 10 ˚C doubles the reaction rate). This would have a positive impact on cost as coatings or cladding materials would require less maintenance.

Similarly, reducing the heat build would enable more cladding options in warm climates. Vinyl and polypropylene siding cannot be used in warm climates as they soften with too much heat (around 150-170 ˚F for vinyl if I remember correctly).

Occupant comfort is another added benefit (although more difficult to quantify and market). We have a team in France dedicated to occupant comfort and quantifying it. Maybe we can involve them at some point.

I will present the photocatalytic work to the business units and discuss publishing the results.

Energy Research and Development Division

FINAL PROJECT REPORT

Solar-Reflective "Cool" Walls: Benefits, Technologies, and Implementation

Appendix R: Advancements in Infrastructure Development - Building Standards and Incentive Programs (Task 6.3 Report)

California Energy Commission
Gavin Newsom, Governor

April 2019 | CEC-500-2019-040-APR

Appendix R: Advancements in infrastructure development: building standards and incentive programs (Task 6.3 report)

Haley Gilbert[1] and Ronnen Levinson[1]

[1] Heat Island Group, Lawrence Berkeley National Laboratory

31 May 2018

Abstract

This report describes our efforts to advance the infrastructure needed to promote the appropriate use of cool wall technologies. Following the model successfully used for cool roofs, our activities included developing guidelines, pursuing development of a product rating program, encouraging utility rebates, investigating ENERGY STAR label qualification, and pursuing credits/requirements in building energy standards and energy-efficiency programs (e.g., Title 24, ASHRAE 90.1, LEED). We began our efforts by searching for all existing references to cool walls in building energy standards and incentive programs. We also formed a Working Group of key cool wall stakeholders to support and contribute to the activities.

1 Introduction

Cool roofs can be found on rooftops across the United States. They are included in many city, state, and federal building codes/standards. To advance the adoption of cool walls, we can follow and learn from the cool roof adoption model. Cool roofs were first incorporated in many codes/standards as credits and later transitioned to prescriptions. The timeline in Figure 1shows how the adoption of cool roofs took time and was also accompanied by incentives, such as ENERGY STAR certification and utility rebates. The process was aided by the establishment of the Cool Roof Rating Council (CRRC). The CRRC is an independent organization that has developed methods for evaluating and labeling roofing products for reference by codes, standards, and rebates. It has also propagated the cool roof concept and its rating program.

Following the model successfully used for cool roofs, we set out to develop the infrastructure needed to advance the appropriate use of cool walls. Our activities included

- preparation of Cool Wall Application Guidelines;
- initiation of a product rating program;
- initiation of a utility rebate program;
- initiation an ENERGY STAR program for cool walls;
- support for the development of cool wall credits in California, U.S., and international building energy standards/programs (e.g., Title 24, ASHRAE 90.1, LEED); and
- coordination of project results workshop.

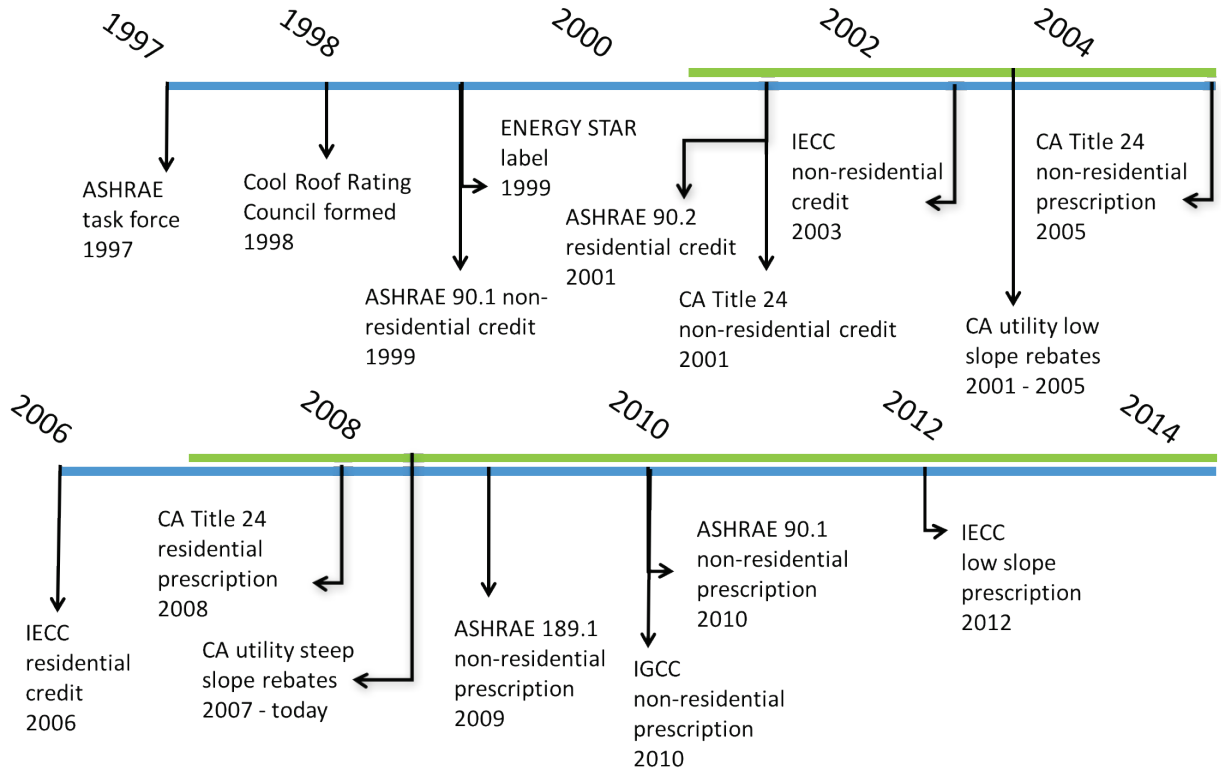

Figure 1. A timeline of the inclusion of cool roofs in major building codes/standards and other milestones (Akbari & Levinson, 2008).

We began our efforts by searching for all existing references to cool walls in building energy standards and incentive programs. We also formed a Working Group of key cool wall stakeholders to support and contribute to the activities.

We drew upon the data and results from the reports of Task 2 (*Quantify Cooling, Heating, and Lighting Energy Use Savings*) Task 3 (*Quantify the Environmental and Energy Co-benefits of Cool Walls*) to support our activities to advance cool wall adoption.

2 Current references in building standards and incentive programs

One of our initial activities was to investigate existing references to cool walls in building standards, green building programs, and incentive programs. We needed to understand where cool walls were currently referenced to know where and how to focus our efforts.

2.1 Building standards and green building programs

While cool wall references in building standards and green building programs are not prevalent, we found references in *ANSI/ASHRAE/IES Standard 90.1-2016—Energy Standard for Buildings Except Low-Rise Residential Buildings* (ASHRAE 90.1)*; ANSI/ASHRAE/IES/USGBC Standard for the Design of High-Performance Green Buildings 189.1-2014, Standard for the Design of High-Performance Green Buildings* (ASHRAE 189.1); California Green Building Standards Code; Green Building Initiative's Green Building Assessment Protocol for Commercial Buildings; and in Hawaii's State Energy Conservation Code (Hawaii Energy Code, 2015).

New to ASHRAE 90.1-2016 was the inclusion of a cool wall measure in ASHRAE climate zone 0, which is found in hot and tropical regions outside of the United States (e.g., Hyderabad, India). This measure is found in Section 5.5.3.2 of the building envelope chapter. In addition to the above-ground wall insulation requirements, in ASHRAE climate zone 0, above-grade walls need to either be "cool" walls with solar reflectance index (SRI) greater than or equal to 29 on 75% of East and West walls; or 30% of East and West walls should be shaded (ASHRAE 90.1). The previous version, ASHRAE 90.1-2013, did not include this measure.

ASHRAE 189.1-2014 also includes a cool wall exception for shading on East and West walls. This measure is in the Site Sustainability section under the mitigation of urban heat island effect sub-section (Section 5.3.5.2). ASHRAE 189.1 is a high-performance green building code, therefore includes measures that provide a range of environmental benefits—not just energy savings. The exception, adopted in 2011, allows for 75% of East and West walls to have an SRI greater than or equal to 29, in place of the 30% East and West wall shading requirement (ASHRAE 189.1).

Similar to ASHRAE 189.1 is the California Green Building Standards Code (CALGreen). This statewide mandatory green building standard features provisions to "reduce energy, water, waste, and transportation impacts while protecting the environment and public health" (Papke, 2015). Beyond the mandatory measures, the code includes three levels of reach standards that California cities can voluntarily adopt (Papke, 2015). It includes an elective reflective wall

measure under the Site Development section for exterior wall shading (Section A5.106.7.2). The exterior wall shading provision can be met by either (1) shading the building's fenestration, or (2) surfacing 75% of walls to have an SRI greater than or equal to 29. However, the requirement for opaque walls areas can also be met with shading provided by vegetation (CBSC, 2016).

The voluntary Green Building Initiative's (GBI) Green Building Assessment Protocol for Commercial Buildings includes a provision for reflective walls in their Mitigating Heat Island Effect section (7.3.4.3). This is a rating program similar to U.S. Green Building Council's Leadership in Energy and Environmental Design (LEED). The provision states that 75% of East, West, and South wall surfaces should have an SRI greater than or equal to 29 or be covered with vegetation. This provision is not applicable for ASHRAE climate zones 6 through 8 and is worth 3 points in their rating program (GBI, 2017).

We also contacted Howard Wiig of Hawaii's State Energy Office to learn more about the cool wall exception in Hawaii's State Energy Conservation Code. Hawaii adopted the 2015 International Energy Conservation Code (IECC) in 2015 but included several amendments. The 2015 IECC does not include any references to cool walls. However, they amended 2015 IECC to include an exception for continuous wall insulation for wood or metal framed buildings when walls either have a visible reflectance value greater than or equal to 0.64, or overhangs that shade the walls (Wiig and Makela, 2015).

The presence of several existing cool wall references in building standards and green building programs is very helpful to further increase cool wall adoption. While the existing references are not ideal, we have found it easier to edit and update existing references than to develop new language for adoption. We have begun to work with our contacts involved in these various codes, standards, and programs to share our project results and resources, and discuss how we can improve and strengthen these existing references. Our efforts are further described in Section 8.

2.2 Incentive programs

We also looked for cool wall references in utility rebate programs, U.S. EPA ENERGY STAR, and other building energy efficiency incentive programs. Incentive programs can be critical to helping new building energy efficiency technologies gain market share. Incentives can help defray the cost premium (if any) of a new energy efficiency technology, and advertise its benefits to consumers.

One incentive program to increase building energy efficiency in existing building is Property Assessed Clean Energy (PACE) financing programs. PACE programs can now be found across the United States but need to be authorized by state law. PACE financing was initiated in California in 2007 with the passage of California Assembly Bill 811 (Contractual Assessments: energy efficiency improvements, 2007), which amended the state's existing laws to allow PACE financing for renewable energy and energy efficiency improvements to homes and businesses.

PACE program availability varies by city and county across the California. PACE financing allows property owners to fund energy efficiency, water efficiency and renewable energy projects. The financing covers the cost of the materials/product and installation. Property owners can finance up to 100% of their project and pay it back over time through their existing property tax bill as a voluntary property tax assessment (Center for Sustainable Energy, 2018).

There are 12 PACE financing programs in California for residential and commercial buildings (Table 1). The PACE programs often restrict funding to eligible products that have been vetted by the organization to provide the intended energy and water benefits. Many of the PACE programs provide the list of eligible products on their websites. We found that three PACE programs available in California include cool walls as eligible products (Table 1). The three programs are the Home Energy Renovation Opportunity (HERO) program, PACE Funding, and Energy Efficient Equity. The HERO program is offered by Renovate America in partnership with the Western Riverside Council of Government and is one of the most popular PACE loan programs offered in California (Matasci, 2017). The specifications for cool wall product eligibility are listed in Table 2. Therefore, a homeowner can pay for and install an eligible cool wall product with PACE financing.

Table 1. PACE financing programs for residential and commercial buildings in California. The table indicates whether the program includes a cool walls measure.

Program	Building Type (Residential/Commercial/Both)	Cool Walls Measure
AllianceNRG Program (https://www.alliancenrg.com/retail/)	Both	Noa
California First (https://renewfinancial.com/product/californiafirst)	Both	Noa
Energy Efficient Equity (https://www.energyefficientequity.com/)	Residential	Yes
FigTree Financing (http://www.figtreefinancing.com/)	Commercial	Noa
Green Finance San Francisco (https://sfenvironment.org/residentialpace)	Commercial	Noa
Home Energy Renovation Opportunity (HERO) Program (https://heroprogram.com/)	Residential	Yes
LA County Commercial PACE Program (http://lapace.org/commercial.html)	Commercial	Noa
MPower (http://www.mpowerplacer.org/)	Both	Noa
PACE Funding (http://www.pacefunding.com/homeowner/)	Residential	Yes
Samas Capital PACE (http://samas-pace.com/)	Commercial	Noa
Sonoma County Energy Independence Program (SCEIP) (http://sonomacountyenergy.org/)	Both	Noa
Ygrene (https://ygreneworks.com/)	Both	Noa

[a] The program websites did not offer enough information on specific eligible products or the program accepts custom measures not listed.

Table 2. The PACE program specifications for cool wall product eligibility.

PACE program	Cool wall eligibility specifications
HERO program (https://heroprogram.com/products)	Product must have a solar reflectance rating greater than 0.5 as tested by a recognized third-party laboratory using the ASTM C1549-09 standard test method or equivalent standard. Product manufacturer, brand, and model must be a pre-approved HERO Cool Wall Coating. Product primary application surface must be exterior wall surfaces of conditioned (heating and/or cooled) buildings. Trim, soffit, and/or fascia may also be included as secondary work scope items, as applicable. Product is only eligible for properties located within California Energy Commission building climate zones 4 through 10 and 12 through 15. Product is not eligible for properties located within CEC building climate zones 1 through 3, 11, and 16.
PACE Funding (http://www.pacefunding.com/homeowner/)	Product must be included on PACE Funding Cool Wall Eligible Product List. Product must have solar reflectance ≥ 0.5 as tested by recognized third-party laboratory to ASTM C1549-09 standard. Product is only eligible to be installed on properties located within California building climate zones 4-10 and 12-15. Installed per manufacturer specs.

3 Application guidelines

Since the benefits of cool walls can vary by building type, vintage, and location, the Task 6.1 report: *Cool wall application guidelines* provides guidance for their building- and climate-appropriate use to conserve energy and reduce emissions of greenhouse gases and criteria pollutants across California and the United States. First, it explores the nature of cool walls through a series of questions & answers. Second, it provides a simple guide to cool wall effects by detailing the energy cost savings (or penalties) that arise from increasing wall reflectance in three common building categories—single-family home, medium office, and retail stand-alone. Third, it provides a detailed guide to these effects by describing the operation and application of the Cool Surface Savings Explorer, a database tool that can report the cool wall and cool roof energy, energy cost, peak power demand, and emission savings simulated for many building categories. Fourth, it discusses how to adjust cool walls savings and penalties to account for shading and reflection by neighboring buildings.

4 Stakeholder working group

The Cool Walls Working Group is comprised of research team members and other cool wall stakeholders. It was formed in Fall 2017 to advance the appropriate adoption of cool walls by incorporating the technology into building codes and incentive programs. Group members are expected to meet quarterly, collaborate on activities, and help communicate activities/results to other stakeholders. The timeline of the formation of the Working Group and its first year of meetings is shown in Figure 1.

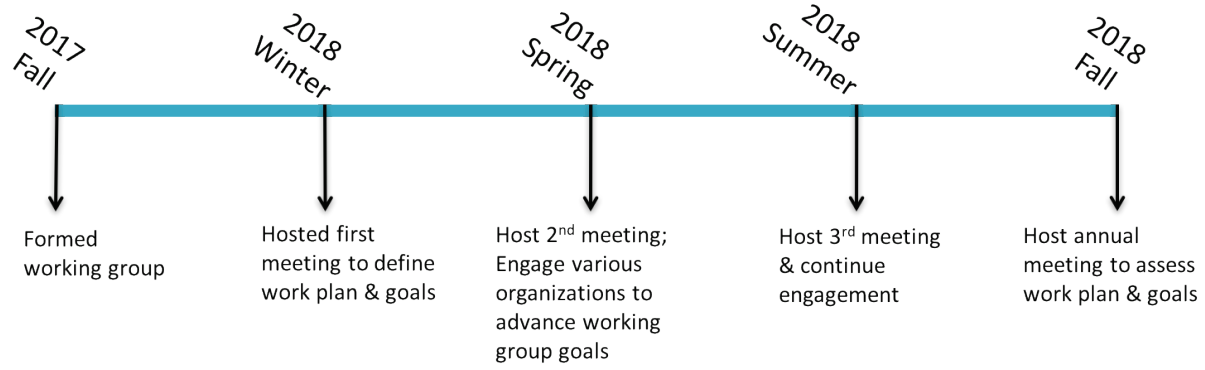

Figure 2. The Cool Walls Working Group was announced at the project workshop in October 2017. As the timeline depicts, the Group will meet quarterly.

Given the composition of the Working Group, we are positioned to provide a diverse perspective on how best to increase cool wall adoption, and also be able to provide information needed regarding the science, benefits, market and use of cool wall products. This will be extremely helpful when working on cool wall measures for building codes/standards and cool wall incentive programs.

One of the Cool Walls project objectives was to initiate the development of cool wall infrastructure. The Cool Walls project period is not long enough to cover the full implementation of cool wall infrastructure, therefore the Working Group will also be critical in providing continued support for cool walls in the absence of project support.

The Working Group participants include manufacturers, California utilities, rating organization, state building code official, California and national environmental program officials, and researchers. Current Working Group members are listed in Table 3. The Working Group consists of 24 members and three observers from 18 organizations. Membership is open allowing us to continually recruit key new members as we pursue different activities.

This project initiated and investigated cool wall measure inclusion for many building codes and standards, green building programs, and incentives. The research team identified current cool wall references upon which to build, and researched the processes to establish new and revise

existing cool wall measures. The research team connected with key staff and stakeholders in the various organizations who will be critical when pursuing the development of cool wall measures. The information and contacts that the research team gathered will be the shared with the Working Group to aid future activities.

Table 3. There are 24 members (two observers not listed) in the Cool Walls Working Group.

Name	Organization	Name	Organization
Bill Dean	California Environmental Protection Agency	Jerry Wu	Dexerials
Bill Yanetti	Mitsubishi Chemical Composites America	Jim Moses	Mitsubishi Chemical Composites America
Brandon Bethke	Tempo Chemicals & Solutions	Michael Biel	Ultimate Coatings
Craig Tranby	Los Angeles Department of Water and Power	Olivier Rosseler	Saint Gobain
David Story	PPG	Peter Turnbull	Pacific Gas & Electric
Gary Ilalaole	Homeowner	Rich Wipfler	Eastman Chemical
Gen Minase	Eastman Chemical	Ronnen Levinson	LBNL Heat Island Group
Haley Gilbert	LBNL Heat Island Group	Tim Hebrink	3M
Hiroko Furumi	Dexerials	Tim Hyer	Gardner-Gibson
Howard Wiig	State of Hawai'i	Tsutomu Nagahama	Dexerials
Hugo Destaillats	LBNL Heat Island Group	Victoria Ludwig	U.S. Environmental Protection Agency
Jeff Steuben	Cool Roof Rating Council	Yisheng Dai	Eastman Chemical

One of the first efforts of the Working Group is to establish a work plan that prioritizes our activities and focuses our resources. To help develop the work plan, a poll was shared with all the Working Group members to identify initial priorities. The poll listed potential activities brainstormed during the Working Group's kick-off call in December 2017. Members were directed to select up to five choices. The results of the poll (Figure 2) clearly indicate a strong interest from members to prioritize the development a cool wall product rating system.

A work plan is now under development using the results of the poll. The work plan will also take into account available resources, impact of the activity, and timing. Many of the activities that are described in Sections 5 through 8 of this report will be included in the work plan. The Working Group will leverage the resources and findings from the research team to successfully pursue and implement cool wall measures in codes, standards, and incentive programs. A draft work plan will be circulated for comments to all the Group members ahead of the Fall 2018

meeting. The final work plan will be presented to the Working Group during the Fall 2018 meeting.

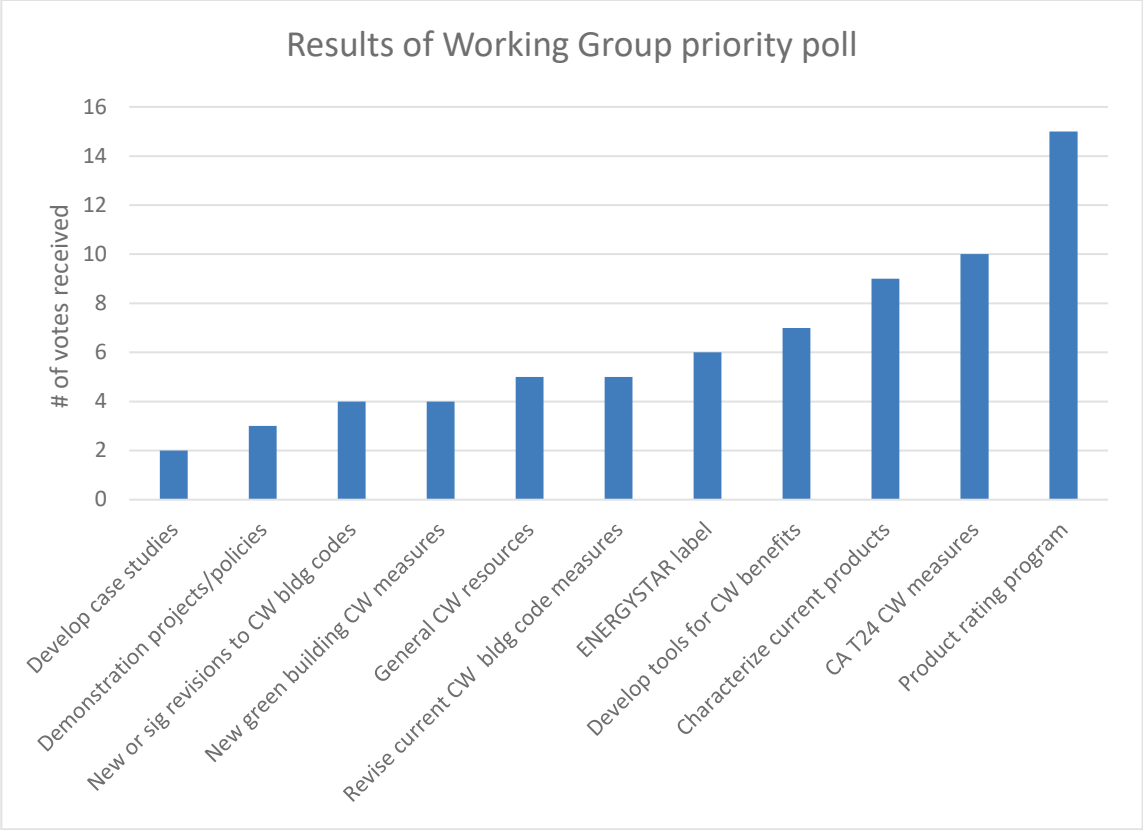

Figure 3. The most popular activities identified in the Working Group priority poll were the development of a product rating program followed by interest in California Title 24 cool wall ("CA T24 CW") measures and characterization of currently available cool wall products.

5 Product rating program

To increase the adoption of cool wall measures in building codes, standards, and green building programs, a third-party rating system will need to be developed. An independent rating system will give confidence to these organizations that products meet the specified property requirements. A rating system would involve the development of a credible method to evaluate and label the radiative properties of wall products.

Cool roof adoption provides a helpful model. The Cool Roof Rating Council (CRRC) was established in 1998. Its mission is to develop methods to measure and label the radiative properties of roofing products. The CRRC administers a product rating program that provides strict guidelines for the measurement, reporting, and labeling of products submitted by manufacturers for evaluation. It enables the use of cool roof codes, standards, incentives, and specifications by providing third party verified data on radiative properties which can be referenced (CRRC, 2018). The CRRC ANSI/CRRC 100 standard developed and followed by CRRC

is now referenced in ASHRAE 90.1, ASHRAE 90.2, ASHRAE 189.1, IECC, and International Green Construction Code (IgCC)). The CRRC program manual (CRRC-1) is referenced in California's Building Energy Efficiency Standards (T24) and ENERGY STAR (Ms. S Schneider 2018, pers.comm., 23 January).

There are two options for establishing a cool wall rating system: develop a new organization modeled on existing and successful programs, like the CRRC; or expand the scope of an existing organization to include wall products. We have decided to pursue the latter option first because it is more time and resource efficient. We identified the CRRC as the first organization to approach because a cool wall rating organization would operate similarly, and the CRRC has evaluation methods and metrics closely aligned to those required for cool wall products. Dating back to 2009, the CRRC's strategic plan included a measure to expand their scope to rate wall products. In addition, there is overlap among cool roof and cool wall manufacturers. We found that there are nine CRRC Class A (commercial) members and/or licensees that are participants in our cool walls project. We also identified a further 19 members and/or licensees that produce or have an interest in wall products.

To advance the idea of expanding the scope of the CRRC to include wall products, we have presented project updates to the CRRC's board of directors (November 2015 and January 2018), technical committee (October 2015 and August 2017), and membership (CRRC newsletter article, January 2016; membership meeting, June 2016). During the board of directors meeting in January 2018, we presented final project results and proposed that CRRC develop in 2018 an actionable plan to begin rating wall products in 2019. In response, the board of directors created a task group that is to prepare a cool walls expansion plan that includes technical measures and a financial analysis. The plan was discussed with the technical committee and presented to the membership in spring 2018. It will be voted on by the board of directors in fall 2018. The CRRC will issue in February 2018 a memorandum outlining this effort.

6 Utility incentives

Utility incentives can be designed to encourage the use of building energy efficiency technologies by spurring development and sales. Utility rebates were offered for cool roofs in California before they were prescribed in the California's Title 24 building energy efficiency standards (Akbari and Levinson 2008). Something similar for cool walls would help increase the adoption of these technologies. Thus, one of our activities was to initiate utility incentive programs in California.

In California, there are investor owned utilities (IOUs) and publicly owned utilities (POUs). The major IOUs in California include Pacific Gas and Electric (PG&E), Southern California Edison (SCE) and San Diego Gas and Electric (SDG&E). These three comprise approximately 75% of electricity supply in California. There are more than 40 POUs in the state and the largest one, Los Angeles Department of Water and Power (LADWP) services 3.9 million customers. (CEC, 2018).

To initiate a utility incentive program for cool wall products, we reached out to PG&E and LADWP. California IOUs are mandated by CPUC to develop and offer similar rebates . LADWP is a POU and therefore designs its rebate programs independently of the IOUs (Mr. C Tranby 2018, pers.comm., 9 January). By contacting both organizations, we can learn about the rebate development process for California IOUs and POUs.

6.1 Los Angeles Department of Water and Power

We spoke with Craig Tranby of LADWP's Environmental Affairs Department in January 2018. He expressed great interest in exploring the feasibility of offering a cool wall utility rebate. LADWP has offered a cool roof rebate since 2011 (LADWP, 2014), therefore are supportive of solar reflective building products.

We discussed several cool wall incentive options: downstream, upstream, and direct install. Downstream incentives are offered to consumers in the form of rebates when they purchase and install an energy efficient product. Upstream incentives are for manufacturers or distributors to off-set any price premiums in the manufacture and/or distribution of these products. Direct install programs are run by utilities. They staff crews that survey buildings, assess which energy efficiency products are good options, and install the products free of cost to the building owner. These programs typically operate in income-targeted communities (Mr. C Tranby 2018, pers.comm., 9 January).

Cool roofs were supported with downstream incentives in the form of rebates to consumers when they purchased and installed the qualifying cool roof products. These rebates require the customer to complete an application specifying address, proof of purchase, approved building permit, and installation contract. The rebate processing team will sometimes use aerial imagery to confirm the size of the rooftop. It also reserves the right to conduct a post-installation visit. This could be a good option for cool walls but a bit trickier to enforce since many homeowners chose to paint their exterior on their own and do not hire a licensed contractor. Pre- and post-installation photos might be required to verify installation. It would also be important to have develop clearly labeled cool wall products to aid consumer identification This might prove challenging since there is not yet a rating program or ENERGY STAR label. However, we have are working to develop both a rating program and ENERGY STAR label as part of Task 6 activities. A consumer rebate could be trialed during a seasonal promotion period—during late spring in preparation for summer months—with extra outreach to see if consumers were interested (Mr. C Tranby 2018, pers.comm., 9 January).

In addition to downstream incentives, we also discussed the feasibility of an upstream incentive for manufacturers. These incentives would be designed to off-set any price premiums for cool walls products. For example, this type of incentive might work well for cool-colored wall products that are formulated with special pigments that often cost more than traditional pigments. Incentives to manufacturers can sometimes be smaller than consumer rebates because the incremental cost for manufacturers to produce the product is less than the cost

premium for consumers to buy the product. There is also precedent for energy efficiency program administrators working with manufacturers to increase the availability of energy-efficiency products in a region, like California. We would need to identify which manufacturers to target.

Lastly, we discussed the idea of including cool walls as one of the upgrades offered in LADWP's direct install program. They have crews that are sent out to income-targeted communities to assess and install free energy efficiency upgrades. The crew could easily assess the existing color of the home and paint the exterior if it is in need of replacement and is a dark color (Mr. C Tranby 2018, pers.comm., 9 January).

For these cool wall incentive options, Tranby will be discussing the ideas with his management. We will also share our cool wall application guidelines with LADWP and highlight the benefits of using cool walls in the LADWP service area climate zones. These resources help justify the incentives, and also inform the type and amount of any incentives that can be offered.

In addition to incentives programs, LADWP offered to help communicate the idea of cool walls to its client base and to other local POUs. For example, LADWP has an active Twitter account that can link to stories or resources on cool walls. Since LADWP is the largest POU in California, other local POUs, like Pasadena Water and Power, often consult LADWP for guidance and direction on energy efficiency programs. Pasadena Water and Power followed LADWP's lead and now offers cool roof rebates (Mr. C Tranby 2018, pers.comm., 9 January).

6.2 Pacific Gas and Electric

We have not yet had an opportunity to connect with PG&E. We continue to reach out to PG&E through our existing network of contacts but have not contacted staff knowledgeable about the rebate program process. We will continue through various means and contacts to learn more about their incentive program process and potential options for cool wall incentives.

7 U.S. EPA ENERGY STAR label

The U.S. Environmental Protection Agency (EPA) ENERGY STAR's label is widely recognized by consumers nationwide. ENERGY STAR labeled products are the same or better than standard products but benefit consumers by using less energy and saving money. Typical ENERGY STAR certified products for appliances, HVAC equipment, lighting, and other product types reduce energy costs by 30% or more (U.S. EPA, 2018b). There have been ENERGY STAR certified roof products since 1999 establishing a precedent for certifying cool building envelope products (Akbari and Levinson 2008).

U.S. EPA has established the following criteria for ENERGY STAR certification (U.S. EPA, 2018c), which we quote here:

- Product categories must contribute significant energy savings nationwide.

- Certified products must deliver the features and performance demanded by consumers, in addition to increased energy efficiency.
- If the certified product costs more than a conventional, less-efficient counterpart, purchasers will recover their investment in increased energy efficiency through utility bill savings, within a reasonable period of time.
- Energy efficiency can be achieved through broadly available, non-proprietary technologies offered by more than one manufacturer.
- Product energy consumption and performance can be measured and verified with testing.
- Labeling would effectively differentiate products and be visible for purchasers.

The specification development cycle for ENERGY STAR certification is illustrated in Figure 3. The first steps are to pull information together about

- Product features & functions (overview of technology)
- Consumer perspectives
- Industry overview and market analysis
- Testing & performance metrics
- Energy efficiency potential
- Energy cost savings & consumer payback
- Related voluntary & regulatory measures
- Related utility incentives, activities, and education programs

This collection of data normally involves various stakeholders but the there is also ample opportunity throughout the specification process to receive feedback during workshops or public comment periods (U.S. EPA, 2018a).

Our project results from Task 2 *Quantify Cooling, Heating, and Lighting Energy Use Savings* reports will help provide the information needed to establish energy efficiency potential and energy cost savings. However, we will need to work with industry stakeholders to conduct a market analysis and to collect consumer perspectives.

We have been in touch with U.S. EPA staff to learn more about the process and the prospects of initiating a new cool wall ENERGY STAR specification. We met with U.S. EPA ENERGYSTAR management in January 2018 to share our findings and to solicit their support. We will share the final project deliverables in February 2018 and host a follow-up call to review in detail the energy-saving benefit calculations.

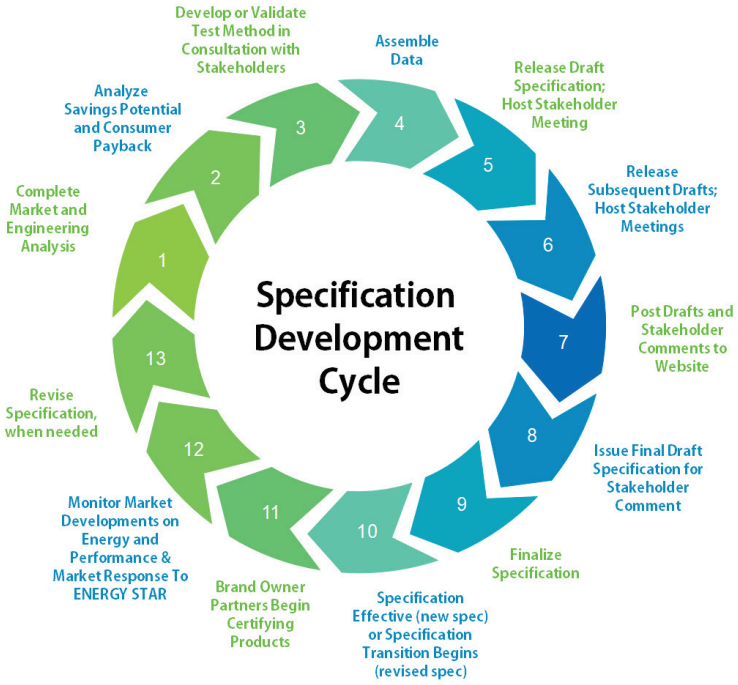

Figure 4. The U.S. EPA ENERGY STAR specification development cycle (U.S. EPA, 2018a).

8 Measures in building energy standards and green building programs

We set out to develop language to introduce and/or improve cool wall measures in building energy codes and standards as well as in green building programs. We investigated ASHRAE 90.1, ASHRAE 189.1, California Title 24, CALGreen, and U.S. Green Building Council's Leadership in Energy and Environmental Design (LEED). We prioritized our efforts to take advantage of the timing of code cycles, build upon current cool wall measures, and focus on California standards and other widely referenced standards and programs.

The activities initiated by the research team will be continued by the Cool Walls Working Group.

8.1 ASHRAE standards

8.1.1 ASHRAE 90.1

There are existing cool wall measures in the 2016 version of ASHRAE 90.1. However, we would like to improve the measures by clarifying the language and extending the measures to U.S. ASHRAE climate zones 1 through 3.

First, we would like to replace specification of Solar Reflectance Index (SRI) by specification of solar reflectance (SR) and thermal emittance (TE). SRI is determined from the summer-afternoon

energy balance of a well-insulated horizontal or low-slope surface, such as a roof. It is not appropriate for a wall because the solar and thermal infrared radiations received by a vertical surface differ from those incident on a horizontal surface. Wall convection coefficients may also differ from those for a roof.

Second, we would like to extend the cool wall measures from ASHRAE climate zone 0, a hot and humid climate not found in the U.S., to ASHRAE climate zones 1 through 3 (Figure 4). We found that there are building energy cost saving benefits that extend through climate zone 4 in our Task 2: *Quantify Cooling, Heating, and Lighting Energy Use Savings* analysis. To initiate these changes, we are fortunate to be in touch with key members of ASHRAE—Martha Van Geem, an independent code consultant, and Rahul Athalye, a research engineer at Pacific Northwest National Laboratory. We have had early conversations with Martha and Rahul to discuss these changes and to share findings from our draft project reports and tools. Martha and Rahul will be drafting revised language to share with the sub-committee chair in January 2018. We will meet with them again to share additional project resources and updates in February 2018.

These changes would be introduced to ASHRAE as amendments to the current (2016) version. An amendment is used to incorporate changes during times outside of the three-year revision cycle. The amendment would still go through two public review periods to solicit comments and would be voted on by ASHRAE for final approval and inclusion.

8.1.2 ASHRAE 189.1

There are existing cool wall measures in ASHRAE 189.1 that could be strengthened and expanded. First, it should specify values of solar reflectance and thermal emittance, rather than SRI. Second, we would like the language to specify that 75% of the east, west, and *south* walls meet the SR requirement. Third, we would like to raise the minimum solar reflectance from about 0.28[1] to 0.40 to increase its environmental benefits.

[1] Under the medium wind speed conditions commonly used to compute SRI, a well-insulated horizontal surface with solar reflectance 0.28 and thermal emittance 0.90 would have an SRI of 29.

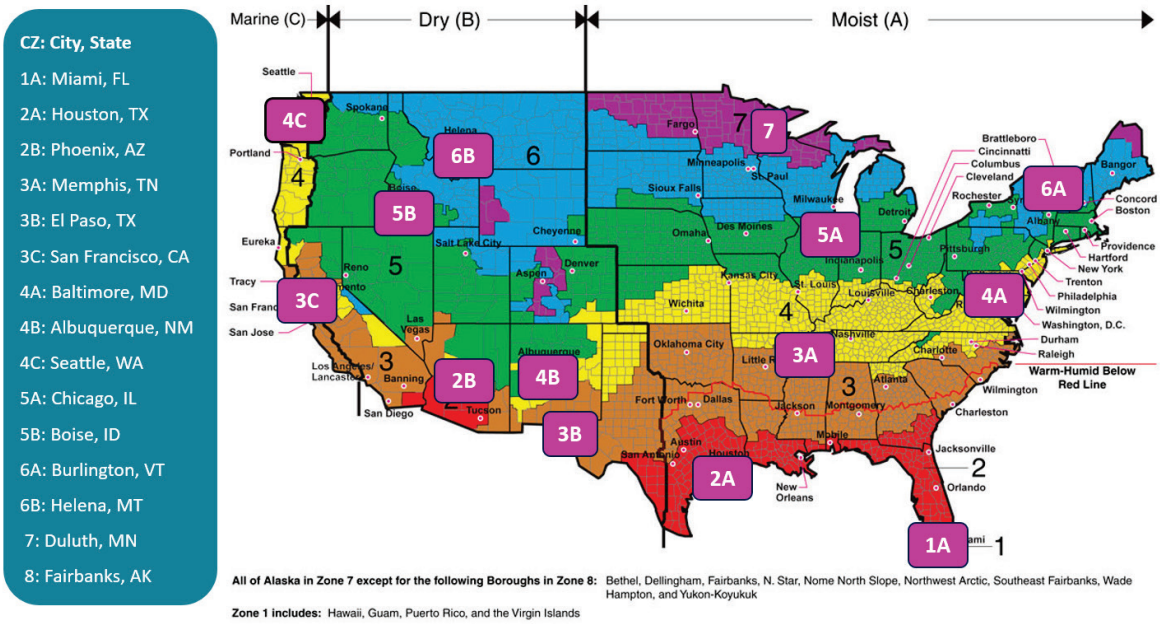

Figure 5. Map of ASHRAE climate zones in the United States, locating representative cities. Adapted from Briggs et al. (2003a,b).

8.2 California Building Energy Efficiency Standards

There are no references to cool walls in the current 2016 California Building Energy Efficiency Standards (Title 24) nor any under consideration for the 2019 update. We are targeting the 2022 edition for inclusion of cool wall measures.

We have been communicating with staff in the California Energy Commission (CEC), Building Standards Office, Efficiency Division—Payam Bozorgchami and Michael Shewmaker—to learn more about the process of including new measures. We have shared our project findings and they agree that cool walls inclusion would be worth further investigation via a Codes and Standards Enhancement (CASE) initiative. The CEC uses a Codes and Standards Enhancement (CASE) process to develop and vet changes to the standards. A CASE initiative for cool walls would build upon the current cool wall research. It would require re-simulating building energy savings with CEC-approved software and completing a market assessment to evaluate the cost-effectiveness of cool walls on residential and non-residential buildings across California climate zones. It would also propose specific language to include in Title 24.

CEC staff will meet with the California IOUs in Winter 2018 to brainstorm a list of potential new measures for 2022 CA T24. The list will be narrowed and several measures will be selected for CASE initiatives. We will work with CEC staff to support the selection of cool walls for a CASE initiative.

8.3 California Green Building Standards

There is an elective voluntary measure for cool walls for nonresidential buildings in the California Green Building Standards (CALGreen). CALGreen is on a triennial code cycle similar to California Title 24. However, unlike CA T24, it features mandatory provisions as well as defines three levels of reach standards that California cities can voluntarily adopt. More than 100 local governments have adopted standards that go beyond the 2013 CALGreen mandatory provisions (Papke, 2015).

Cool roof and cool pavement measures are found in the voluntary Tier 1 and Tier 2 levels that exceed the baseline code. Cool walls are noted in the exterior wall shading measures as a voluntary elective. All three are included as urban heat island countermeasures. Since they are voluntary, they can be adopted by local governments. For example, the City of Los Angeles has adopted a cool roof ordinance that meets the Tier 1 requirement and exceeds the cool roof requirements from CA T24 (City of Los Angeles, 2013).

We would like to see the language improved for the cool wall measure, and included as a provision in Tier 1 and Tier 2. First, we would like to replace specification of Solar Reflectance Index (SRI) by specification of solar reflectance (SR) and thermal emittance (TE) for the reasons identified above. In addition, we would like to see the cool wall measure separated from fenestration measure in the exterior wall shading section. These are both good measures and provide very different benefits to the building occupants and environment. The standard could require both, rather than one or the other. Or, the standard could separate the fenestration and wall requirements into two provisions. We would also like to move the cool wall measure from an "elective" provision to one that is listed in Tier 1 and Tier 2 so it can be easily adopted by local governments. We also would like to increase the SR requirement since these are designed as reach code provisions. Tier 1 requirements could include cool wall products with SR greater than or equal to 0.40 and less than 0.60. Tier 2 could include products with SR greater than or equal to 0.60. These two tiers of SR requirements are described in more detail in the Task 6.1 report: *Cool wall application guidelines*.

We are in contact with California Air Resources Board (CARB) regarding improvements to the cool wall measures in CALGreen since they have led other standard changes. The California Buildings and Standards Commission must accept state agency input on revisions and/or new provisions to CALGreen. However, similar to California Title 24, a report needs to be completed to develop and vet changes to the standards. This analysis is based on broader environmental benefits since CALGreen refers to California Building Energy Efficiency Standards for all energy-related measures (Ms. D Papke 2015, pers.comm., 17 November). Unfortunately, this is a resource-intensive effort so finding funds to invest in a standard change will be challenging. We will be in contact with ARB to present and share our final project deliverables.

8.4 U.S. Green Building Council's Leadership in Energy and

Environmental Design

U.S. Green Building Council's Leadership in Energy and Environmental Design (LEED) is the most widely used green building rating system in the world (USGBC, 2018). LEED is available for all building types and is divided into nine measurements to address wide-ranging environmental impacts of building construction and operations. LEED includes a heat island reduction credit under its Sustainable Sites section with measures for roofs and nonroofs (LEED v4, 2016).

Levinson served on LEED's Sustainable Sites (SS) Technical Advisory Group (TAG) from 2013 to 2017. As a member of the SS TAG he was (and still is) consulted on improvements to the heat island reduction credit. He presented an overview of the cool walls project to the SS TAG during the USGBC's *Convergence* meeting held in June 2016, and was invited to develop a cool walls pilot credit. All pilot credit submissions require an application that presents the intent of the credit, provides background information to justify the credit, and lists the applicable rating systems and project phase impacts. Levinson will be working to draft the cool pilot credit for submission in spring/summer 2018.

While there are other codes, standards, and green building programs, like the IECC, International Green Conservation Code (IgCC) and the GBI Green Building Assessment Protocol for Commercial Buildings, we will focus our near-term efforts on those presented here. We hope to reevaluate cool wall prospects in these other codes, standards and programs pending interest and resources from the Working Group.

9 Project results workshop

We hosted our Cool Walls results workshop on 25 October 2017 with 38 in-person and six remote participants from government, utilities, manufacturers and university sectors. The one-day workshop featured 10 presentations and several discussion sections to get feedback from participants on the research and results. The Cool Walls project results workshop proceedings can be found in the Task 6.2 report: *Cool wall workshop proceedings*.

10 Summary

We accomplished our goals this activity. We completed the cool wall application guidelines to provide guidance for their building- and climate-appropriate use to conserve energy and reduce emissions of greenhouse gases and criteria pollutants across California and the United States. We hosted a workshop to share our project results and solicit feedback from key stakeholder. We are in touch with key staff at ENERGY STAR and California utilities to develop cool wall incentives, such as an ENERGY STAR label and consumer rebate program. We are in contact with several building energy standard/code organizations and green building programs to introduce new cool wall measures or improve cool wall measures where they existed previously. This includes efforts to engage with the California Energy Commission and California utilities

to complete a CASE initiative to develop and vet new cool wall specifications for Title 24. Under our guidance, the Cool Roof Rating Council announced the formation of a task group that will prepare a cool walls expansion plan tentatively scheduled for a board-of-directors vote in fall 2018.

There is a need for continued effort and support for cool wall infrastructure after this project concludes so we convened a Cool Walls Working Group comprised of key stakeholders. The Group will build upon the research team efforts to see many of these activities through to completion.

References

Akbari H, Levinson R. 2008. Evolution of Cool-Roof Standards in the United States. *Advances in Building Energy Research* 2(1), 1-32. http://doi.org/10.3763/aber.2008.0201

ASHRAE 189.1. 2014. *ANSI/ASHRAE/IES/USGBC Standard for the Design of High-Performance Green Buildings 189.1-2014, Standard for the Design of High-Performance Green Buildings*. American Society of Heating, Refrigerating, and Air-Conditioning Engineers. Atlanta, GA.

ASHRAE 90.1. 2016. *ANSI/ASHRAE/IES Standard 90.1-2016—Energy Standard for Buildings Except Low-Rise Residential Buildings*. American Society of Heating, Refrigerating, and Air-Conditioning Engineers. Atlanta, GA.

Briggs RL, Lucas RG, Taylor ZT. 2003a. Climate Classification for Building Energy Codes and Standards: Part 1—Development Process. ASHRAE Transactions, 109(1).

Briggs RL, Lucas RG, Taylor ZT. 2003b. Climate Classification for Building Energy Codes and Standards: Part 2—Zone Definitions, Maps, and Comparisons. ASHRAE Transactions 109(2).

CBSC. 2016. Guide to the 2016 California Green Building Standards Code. California Building Standards Commission, Sacramento, CA. Retrieved 2018-01-31 from https://www.documents.dgs.ca.gov/bsc/CALGreen/CALGreen-Guide-2016-FINAL.pdf

CEC. 2018. Differences Between Publicly and Investor-Owned Utilities. California Energy Commission, Sacramento, CA. Retrieved 2018-01-31 from http://www.energy.ca.gov/pou_reporting/background/difference_pou_iou.html

Center for Sustainable Energy. 2018. Property Assessed Clean Energy (PACE) Programs. Center for Sustainable Energy, San Diego, CA. Retrieved 2018-01-15 from http://energycenter.org/policy/property-assessed-clean-energy-pace

City of Los Angeles. 2014. 2014 Los Angeles Green Building Code Ordinance no. 183149. Los Angeles Municipal Code § 99.01.101.3 and 99.04.106.5 Article 9, Chapter IX. Retrieved 2018-01-

27 from https://www.ladbs.org/docs/default-source/publications/ordinances/cool-roof-ordinance-183149.pdf?sfvrsn=11

Contractual Assessments: energy efficiency improvements. 2007. California Assembly Bill 811. Streets and Highways Code § 5898.

CRRC. 2018. CRRC Overview. Cool Roof Rating Council, Portland, OR. Retrieved 2018-01-31 from http://coolroofs.org/about-crrc/overview

GBI. 2017. Green Building Assessment Protocol for Commercial Buildings Public Comment Draft 3. Green Building Initiative, Portland, OR. Retrieved 2018-01-31 from https://www.thegbi.org/content/misc/BSR_GBI01-201X_Third_Public_Comment_Draft_10-20-17_final.pdf

Hawaii Energy Code. 2015. State Energy Conservation Code. Hawaii State Energy Office, Honolulu, HI. Retrieved 2018-01-15 from http://energy.hawaii.gov/hawaii-energy-building-code/2015-iecc-update

LADWP. 2014. LADWP's 'Cool Roof' Rebates Reduce Costs and Save Energy. Los Angeles Department of Water and Power 16 January 2014. Retrieved 2018-01-31 from http://www.ladwpnews.com/ladwps-cool-roof-rebates-reduce-costs-and-save-energy/

LEED v4. 2016. Leadership in Energy and Environmental Design. U.S. Green Building Council, Washington, DC. Retrieved 2018-01-31 from https://www.usgbc.org/credits/new-construction-core-and-shell-schools-new-construction-retail-new-construction-hospitali-1

Matasci S. 2017. HERO Solar Program: Loan Interest Rates, Terms, Pros and Cons. EnergySage blog. Retrieved 2018-01-31 from https://news.energysage.com/hero-loan-program-interest-rates-terms/

Papke D. 2015. An Overview of the Process to Develop the Green Building Standards Code: A California Air Resources Board Briefing Paper. California Air Resources Board, Sacramento, CA.

U.S. EPA. 2018a. ENERGY STAR Partner Resources. ENERGY STAR Product Specification Development Process. U.S. Environmental Protection Agency, Washington, DC. Retrieved 2018-01-31 from https://www.energystar.gov/partner_resources/product_specification_development_process

U.S. EPA. 2018b. Frequently Asked Questions. U.S. Environmental Protection Agency, Washington, DC. Retrieved 2018-01-31 from https://www.energystar.gov/index.cfm?c=roof_prods.pr_roof_faqs

U.S. EPA. 2018c. How a Product Earns the ENERGY STAR Label. U.S. Environmental Protection Agency, Washington, DC. Retrieved 2018-01-31 from https://www.energystar.gov/products/how-product-earns-energy-star-label

USGBC. 2018. What is LEED?. U.S. Green Building Council, Washington, DC. Retrieved 2018-01-31 from https://www.usgbc.org/help/what-leedhttps://www.ladbs.org/docs/default-source/publications/ordinances/cool-roof-ordinance-183149.pdf?sfvrsn=11

Wiig H, Makela E. 2015. 2015 IECC with Hawaii Amendments. Presentation. Hawaii State Energy Office and Cadmus. Retrieved 2018-01-15 from https://energy.hawaii.gov/wp-content/uploads/2016/07/2015-IECC-with-Hawaii-Amendments.pdf